Wireless Communications and Mobile Computing

Decentralization and Security Issues in Blockchain Enabled Internet of Things

Lead Guest Editor: Hongju Cheng
Guest Editors: Ling Yuan and Naixue Xiong

Decentralization and Security Issues in Blockchain Enabled Internet of Things

Wireless Communications and Mobile Computing

Decentralization and Security Issues in Blockchain Enabled Internet of Things

Lead Guest Editor: Hongju Cheng
Guest Editors: Ling Yuan and Naixue Xiong

Copyright © 2023 Hindawi Limited. All rights reserved.

This is a special issue published in “Wireless Communications and Mobile Computing.” All articles are open access articles distributed under the Creative Commons Attribution License, which permits unrestricted use, distribution, and reproduction in any medium, provided the original work is properly cited.

Chief Editor

Zhipeng Cai, USA

Associate Editors

Ke Guan, China
Jaime Lloret, Spain
Maode Ma, Singapore

Academic Editors

Muhammad Inam Abbasi, Malaysia
Ghufran Ahmed, Pakistan
Hamza Mohammed Ridha Al-Khafaji, Iraq
Abdullah Alamoodi, Malaysia
Marica Amadeo, Italy
Sandhya Aneja, USA
Mohd Dilshad Ansari, India
Eva Antonino-Daviu, Spain
Mehmet Emin Aydin, United Kingdom
Parameshachari B. D., India
Kalapraveen Bagadi, India
Ashish Bagwari, India
Dr. Abdul Basit, Pakistan
Alessandro Bazzi, Italy
Zdenek Becvar, Czech Republic
Nabil Benamar, Morocco
Olivier Berder, France
Petros S. Bithas, Greece
Dario Bruneo, Italy
Jun Cai, Canada
Xuesong Cai, Denmark
Gerardo Canfora, Italy
Rolando Carrasco, United Kingdom
Vicente Casares-Giner, Spain
Brijesh Chaurasia, India
Lin Chen, France
Xianfu Chen, Finland
Hui Cheng, United Kingdom
Hsin-Hung Cho, Taiwan
Ernestina Cianca, Italy
Marta Cimitile, Italy
Riccardo Colella, Italy
Mario Collotta, Italy
Massimo Condoluci, Sweden
Antonino Crivello, Italy
Antonio De Domenico, France
Floriano De Rango, Italy
Antonio De la Oliva, Spain
Margot Deruyck, Belgium
Liang Dong, USA
Praveen Kumar Donta, Austria
Zhuojun Duan, USA
Mohammed El-Hajjar, United Kingdom
Oscar Esparza, Spain
Maria Fazio, Italy
Mauro Femminella, Italy
Manuel Fernandez-Veiga, Spain
Gianluigi Ferrari, Italy
Luca Foschini, Italy
Alexandros G. Fragkiadakis, Greece
Ivan Ganchev, Bulgaria
Óscar García, Spain
Manuel García Sánchez, Spain
L. J. García Villalba, Spain
Miguel Garcia-Pineda, Spain
Piedad Garrido, Spain
Michele Girolami, Italy
Mariusz Glabowski, Poland
Carles Gomez, Spain
Antonio Guerrieri, Italy
Barbara Guidi, Italy
Rami Hamdi, Qatar
Tao Han, USA
Sherief Hashima, Egypt
Mahmoud Hassaballah, Egypt
Yejun He, China
Yixin He, China
Andrej Hrovat, Slovenia
Chunqiang Hu, China
Xuexian Hu, China
Zhenghua Huang, China
Xiaohong Jiang, Japan
Vicente Julian, Spain
Rajesh Kaluri, India
Dimitrios Katsaros, Greece
Muhammad Asghar Khan, Pakistan
Rahim Khan, Pakistan
Ahmed Khattab, Egypt
Hasan Ali Khattak, Pakistan
Mario Kolberg, United Kingdom
Meet Kumari, India
Wen-Cheng Lai, Taiwan

Jose M. Lanza-Gutierrez, Spain
Pavlos I. Lazaridis, United Kingdom
Kim-Hung Le, Vietnam
Tuan Anh Le, United Kingdom
Xianfu Lei, China
Jianfeng Li, China
Xiangxue Li, China
Yaguang Lin, China
Zhi Lin, China
Liu Liu, China
Mingqian Liu, China
Zhi Liu, Japan
Miguel López-Benítez, United Kingdom
Chuanwen Luo, China
Lu Lv, China
Basem M. ElHalawany, Egypt
Imadeldin Mahgoub, USA
Rajesh Manoharan, India
Davide Mattera, Italy
Michael McGuire, Canada
Weizhi Meng, Denmark
Klaus Moessner, United Kingdom
Simone Morosi, Italy
Amrit Mukherjee, Czech Republic
Shahid Mumtaz, Portugal
Giovanni Nardini, Italy
Tuan M. Nguyen, Vietnam
Petros Nicopolitidis, Greece
Rajendran Parthiban, Malaysia
Giovanni Pau, Italy
Matteo Petracca, Italy
Marco Picone, Italy
Daniele Pinchera, Italy
Giuseppe Piro, Italy
Javier Prieto, Spain
Umair Rafique, Finland
Maheswar Rajagopal, India
Sujan Rajbhandari, United Kingdom
Rajib Rana, Australia
Luca Reggiani, Italy
Daniel G. Reina, Spain
Bo Rong, Canada
Mangal Sain, Republic of Korea
Praneet Saurabh, India
Hans Schotten, Germany
Patrick Seeling, USA
Muhammad Shafiq, China
Zaffar Ahmed Shaikh, Pakistan
Vishal Sharma, United Kingdom
Kaize Shi, Australia
Chakchai So-In, Thailand
Enrique Stevens-Navarro, Mexico
Sangeetha Subbaraj, India
Tien-Wen Sung, Taiwan
Suhua Tang, Japan
Pan Tang, China
Pierre-Martin Tardif, Canada
Sreenath Reddy Thummaluru, India
Tran Trung Duy, Vietnam
Fan-Hsun Tseng, Taiwan
S Velliangiri, India
Quoc-Tuan Vien, United Kingdom
Enrico M. Vitucci, Italy
Shaohua Wan, China
Dawei Wang, China
Huaqun Wang, China
Pengfei Wang, China
Dapeng Wu, China
Huaming Wu, China
Ding Xu, China
YAN YAO, China
Jie Yang, USA
Long Yang, China
Qiang Ye, Canada
Changyan Yi, China
Ya-Ju Yu, Taiwan
Marat V. Yuldashev, Finland
Sherali Zeadally, USA
Hong-Hai Zhang, USA
Jiliang Zhang, China
Lei Zhang, Spain
Wence Zhang, China
Yushu Zhang, China
Kechen Zheng, China
Fuhui Zhou, USA
Meiling Zhu, United Kingdom
Zhengyu Zhu, China

Contents

Contents

Contents

Hindawi
Wireless Communications and Mobile Computing
Volume 2023, Article ID 9825851, 1 page
https://doi.org/10.1155/2023/9825851

Retraction

Retracted: Image Classification Model Based on Deep Learning in Internet of Things

Wireless Communications and Mobile Computing

Received 8 August 2023; Accepted 8 August 2023; Published 9 August 2023

Copyright © 2023 Wireless Communications and Mobile Computing. This is an open access article distributed under the Creative Commons Attribution License, which permits unrestricted use, distribution, and reproduction in any medium, provided the original work is properly cited.

This article has been retracted by Hindawi following an investigation undertaken by the publisher [1]. This investigation has uncovered evidence of one or more of the following indicators of systematic manipulation of the publication process:

(1) Discrepancies in scope
(2) Discrepancies in the description of the research reported
(3) Discrepancies between the availability of data and the research described
(4) Inappropriate citations
(5) Incoherent, meaningless and/or irrelevant content included in the article
(6) Peer-review manipulation

The presence of these indicators undermines our confidence in the integrity of the article's content and we cannot, therefore, vouch for its reliability. Please note that this notice is intended solely to alert readers that the content of this article is unreliable. We have not investigated whether authors were aware of or involved in the systematic manipulation of the publication process.

Wiley and Hindawi regrets that the usual quality checks did not identify these issues before publication and have since put additional measures in place to safeguard research integrity.

We wish to credit our own Research Integrity and Research Publishing teams and anonymous and named external researchers and research integrity experts for contributing to this investigation.

The corresponding author, as the representative of all authors, has been given the opportunity to register their agreement or disagreement to this retraction. We have kept a record of any response received.

References

[1] S. Zou, W. Chen, and H. Chen, "Image Classification Model Based on Deep Learning in Internet of Things," *Wireless Communications and Mobile Computing*, vol. 2020, Article ID 6677907, 16 pages, 2020.

Hindawi
Wireless Communications and Mobile Computing
Volume 2023, Article ID 9819036, 1 page
https://doi.org/10.1155/2023/9819036

Retraction

Retracted: A Real-Time Garbage Truck Supervision and Data Statistics Method Based on Object Detection

Wireless Communications and Mobile Computing

Received 8 August 2023; Accepted 8 August 2023; Published 9 August 2023

Copyright © 2023 Wireless Communications and Mobile Computing. This is an open access article distributed under the Creative Commons Attribution License, which permits unrestricted use, distribution, and reproduction in any medium, provided the original work is properly cited.

This article has been retracted by Hindawi following an investigation undertaken by the publisher [1]. This investigation has uncovered evidence of one or more of the following indicators of systematic manipulation of the publication process:

(1) Discrepancies in scope
(2) Discrepancies in the description of the research reported
(3) Discrepancies between the availability of data and the research described
(4) Inappropriate citations
(5) Incoherent, meaningless and/or irrelevant content included in the article
(6) Peer-review manipulation

The presence of these indicators undermines our confidence in the integrity of the article's content and we cannot, therefore, vouch for its reliability. Please note that this notice is intended solely to alert readers that the content of this article is unreliable. We have not investigated whether authors were aware of or involved in the systematic manipulation of the publication process.

Wiley and Hindawi regrets that the usual quality checks did not identify these issues before publication and have since put additional measures in place to safeguard research integrity.

We wish to credit our own Research Integrity and Research Publishing teams and anonymous and named external researchers and research integrity experts for contributing to this investigation.

The corresponding author, as the representative of all authors, has been given the opportunity to register their agreement or disagreement to this retraction. We have kept a record of any response received.

References

[1] X. Zhang, Y. Gao, G. Xiao, B. Feng, and W. Chen, "A Real-Time Garbage Truck Supervision and Data Statistics Method Based on Object Detection," *Wireless Communications and Mobile Computing*, vol. 2020, Article ID 8827310, 9 pages, 2020.

Hindawi
Wireless Communications and Mobile Computing
Volume 2023, Article ID 9785610, 1 page
https://doi.org/10.1155/2023/9785610

Retraction

Retracted: Physarum-Inspired Autonomous Optimized Routing Protocol for Coal Mine MANET

Wireless Communications and Mobile Computing

Received 8 August 2023; Accepted 8 August 2023; Published 9 August 2023

Copyright © 2023 Wireless Communications and Mobile Computing. This is an open access article distributed under the Creative Commons Attribution License, which permits unrestricted use, distribution, and reproduction in any medium, provided the original work is properly cited.

This article has been retracted by Hindawi following an investigation undertaken by the publisher [1]. This investigation has uncovered evidence of one or more of the following indicators of systematic manipulation of the publication process:

(1) Discrepancies in scope
(2) Discrepancies in the description of the research reported
(3) Discrepancies between the availability of data and the research described
(4) Inappropriate citations
(5) Incoherent, meaningless and/or irrelevant content included in the article
(6) Peer-review manipulation

The presence of these indicators undermines our confidence in the integrity of the article's content and we cannot, therefore, vouch for its reliability. Please note that this notice is intended solely to alert readers that the content of this article is unreliable. We have not investigated whether authors were aware of or involved in the systematic manipulation of the publication process.

Wiley and Hindawi regrets that the usual quality checks did not identify these issues before publication and have since put additional measures in place to safeguard research integrity.

We wish to credit our own Research Integrity and Research Publishing teams and anonymous and named external researchers and research integrity experts for contributing to this investigation.

The corresponding author, as the representative of all authors, has been given the opportunity to register their agreement or disagreement to this retraction. We have kept a record of any response received.

References

[1] H. Jiang, X. Liu, S. Xiao, C. Tang, and W. Chen, "Physarum-Inspired Autonomous Optimized Routing Protocol for Coal Mine MANET," *Wireless Communications and Mobile Computing*, vol. 2020, Article ID 8816718, 14 pages, 2020.

Hindawi
Wireless Communications and Mobile Computing
Volume 2021, Article ID 8881631, 7 pages
https://doi.org/10.1155/2021/8881631

Research Article

Application of Feature Extraction Algorithm in the Construction of Interactive English Chinese Translation Mode

Guangjun Dong,[1] Youchao Yang,[2] and Qiankun Zhang[3]

[1]*Anhui Vocational College of Electronics & Information Technology, Bengbu 233000, China*
[2]*Anhui University of Finance and Economics, Bengbu 233030, China*
[3]*Anhui Audit College, Hefei 230001, China*

Correspondence should be addressed to Youchao Yang; 120081279@aufe.edu.cn

Received 19 August 2020; Revised 20 September 2020; Accepted 27 October 2020; Published 17 April 2021

Academic Editor: Hongju Cheng

Copyright © 2021 Guangjun Dong et al. This is an open access article distributed under the Creative Commons Attribution License, which permits unrestricted use, distribution, and reproduction in any medium, provided the original work is properly cited.

In the process of English translation, traditional interactive English translation system is not obvious in English semantic context. The optimal feature selection process does not achieve the optimal translation solution, and the translation accuracy is low. Based on this, this paper designs an interactive English Chinese translation system based on a feature extraction algorithm. By introducing the feature extraction algorithm, the optimal translation solution is selected, and the semantic mapping model is constructed to translate the best translation into English Chinese translation. The real experiment results show that the interactive English Chinese translation system based on feature extraction algorithm can get the best solution.

1. Introduction

In the process of daily English translation, an interactive English translation system is usually used for English Chinese translation [1, 2]. However, the traditional interactive English translation system does not have the best feature context selection in the process of translation feature semantics and context extraction, resulting in the low accuracy of translation [3].

In view of the above situation, this paper designs an interactive English Chinese translation system based on the feature extraction algorithm. The feature extraction algorithm is introduced to select the feature semantics, and the semantic ontology mapping model is established [4, 5]. The optimal solution is selected for the interactive English Chinese translation process, and the English Chinese translation process is finally realized through coding. In order to ensure the effectiveness of the interactive English Chinese translation system based on the feature extraction algorithm, a comparative simulation experiment is designed. The experimental data show that the interactive English-Chinese translation system based on the feature extraction algorithm in this paper can effectively carry out interactive translation between English and Chinese and solve the selection process of the optimal feature context [6, 7].

2. An Overview of Text Classification

With the development of electronic information technology, how to classify data accurately, efficiently, and quickly has become a hot topic at present. The feature word set is generated by multifeature extraction algorithm, the text feature vector is generated by the TF-IDF frequency algorithm, and the text classification is classified by the support vector machine (SVM) classifier model [8, 9]. And the corresponding calling interface is designed for the classification system, which ensures the usability of the classification module. At the same time, a Classified Thesaurus is designed to preserve the unique feature words of each category and to prioritize the categories of documents to be classified [10].

2.1. Two Methods of Text Representation. The vector space model of Salton is also called the word bag representation of text. The way to express text in bag words usually includes participle, taking root, removing function words, statistical

word frequency, selecting features, vectorization, and normalization [11, 12].

(1) Participle: according to certain rules, the text composed of strings is decomposed into a set of different words. By segmenting the training samples, a set of text representation Dictionary of all the different words in the training sample is obtained [13, 14]. (2) Take synonyms: there are many synonyms in Chinese documents, which express the same meaning and merge these synonyms into one word. (3) Functional words: pronouns, prepositions, auxiliary words, etc. are called functional words. Because functional words generally do not contain effective classification information, they can be eliminated from the dictionary of text representation. (4) Statistical word frequency: the frequency of every word root in a text representation dictionary in each text document. (5) Selection feature: select some words that contain significant category information in text representation dictionary. (6) Vectorization: vector models are used to represent each text in the form of vectors [15].

The classification system based on dictionary segmentation is influenced by the completeness of dictionaries and the segmentation algorithm. Aiming at the drawback of dictionary classification system, a text feature extraction technology based on N-gram information is proposed. It makes the text data classification system free from the dependence on the complex word segmentation processing program and the large word library and realizes the domain independence and time independence of the Chinese text data classification [16, 17]. The concept of N-gram information is a string proposed by the founder of information theory, Chesaning, in the study of source code, which is often used to represent the continuous n characters of the source output. Shannon has used it to study the statistical characteristics of characters or strings in English text, that is, the entropy of information. Then, N-gram information is widely used in the fields of text compression, character recognition, and error correction. It is a direct code-oriented technology [18, 19]. Classifier of Naive Baye is shown in Figure 1.

N-gram according to the byte stream to use the length of N of the window segmentation, such as People's Republic of China, according to $N = 4$ sliding window segmentation called China, the people, Republic, country, such 5 grams. Because in Chinese, the two-word phrase has the greatest probability of occurrence, two words for four bytes, so N usually takes 4 [20].

In the VSM model, there are many ways to calculate the weight of entry TK. According to its value type, it can be divided into two kinds: the first Boolean type and its calculation method are to use all the entries of training documents as a complete set. If an entry TK appears in the document, its weight is 1; otherwise, it is set to 0. The second is the real number: the weight of the document is calculated according to the weight formula of the characteristic word [21, 22].

2.2. Commonly Used Classification Methods. The KNN method, one of the most famous pattern recognition statistics methods, has been used for more than 40 years and has been used in text classification research early. It is an example that is based on text classification method. For a test text, calculate

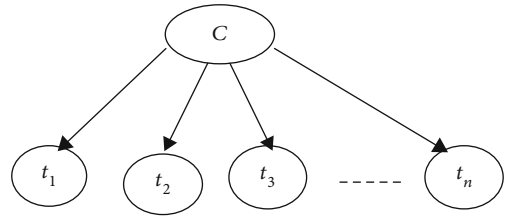

Figure 1: Classifier of Naive Baye.

the similarity between each text and its training set, and find the most similar K training texts based on text similarity. Then, each text class is scored based on the sum of documents similarity between the text and the test text in K training documents. Sort by value and specify the type of test text according to the score [23].

If we use all the sample points in the class as the representative points of the class, we call them the nearest neighbour method. It was proposed by Cover and Hart in 1968, and it is an important nonparametric method in pattern recognition [24]. The nearest neighbour method calculates the distance from the sample to all the representative points, and classifications are classified into categories belonging to the nearest representative point. In order to overcome the defects of the nearest neighbour method, the nearest neighbour is generalized to the k-nearest neighbour. It selects the nearest K representative point from the sample to be categorized to see which category of the K representative points belongs to the class and puts the test sample into the class. Linear separable schematic diagram is shown in Figure 2.

It can also be said that given a test document to be classified, the system finds the most similar k-nearest neighbours in the training set and gives the candidate category of the document based on the category of the nearest neighbour [25, 26]. The similarity between neighbour document and test document can be used as the class weight of the document in the nearest neighbour class. If some of the documents in the k-nearest neighbour belong to the same class, the sum of the class weights of each neighbour in the classification is the similarity between the category and the test document. By sorting the candidate class scores and giving a threshold, the categories of test documents can be determined [27].

Support vector machine, SVM, is a machine learning technology developed by Vapnik and its team led by Baer laboratories. The theoretical basis of SVM comes from the statistical learning theory put forward by Vapnik et al. The basic idea is that for a given learning task with a limited number of training samples, how to compromise the accuracy (for a given set of training sets), and the capacity of the machine (the machine can learn the ability of any training set without error) to get the best promotion performance. He adopted the principle of Structural Risk Minimization [28]. The SVM algorithm not only has a solid theoretical foundation but also achieves good results when applied to text categorization. If a vector of a training set can be linearly segmented by a hyperplane, and the distance between the nearest vector of the hyperplane is maximum, the hyperplane is called the best hyperplane. The closest point to the hyperplane is called

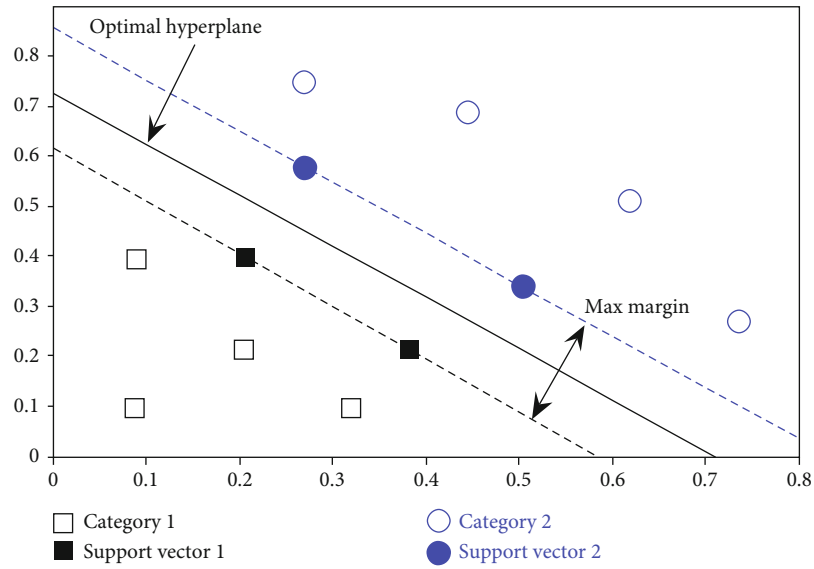

Figure 2: Linear separable schematic diagram.

support vector. The point at which the decision surface is designed is called support vector (SV) [29].

Simple Bias classification is one of the commonly used methods in machine learning. The simple Bias classification method divides training instance I into feature vector W and decision category variable C. The simple Bias classification assumes that the components of the eigenvectors are relatively independent relative to the decision variables, that is, each feature is independent of the category, which is the characteristic independence hypothesis [30]. For text categorization, it assumes that each word is independent between T_i and T_j.

3. Feature Extraction

Feature extraction is a concept in computer vision and image processing. It refers to using a computer to extract image information and decide whether each image's point belongs to an image feature. The result of feature extraction is to divide the points on the image into different subsets. These subsets often belong to isolated points, continuous curves, or continuous regions [31]. A method of transforming a set of measured values of a pattern to highlight the representational characteristics of the pattern. Image analysis and transformation are used to extract the required features [32]. Feature extraction refers to the method and process of extracting characteristic information from images by computer.

3.1. Basic Concepts. There is no universal and precise definition of the features so far. The precise definition of characteristics is often determined by questions or application types. Feature is an interesting part of a digital image. It is the starting point of many computer image analysis algorithms. Therefore, the success of an algorithm is often determined by the characteristics that it uses and defines. Therefore, one of the most important features of feature extraction is "repeatability:" the features extracted from different images of the same scene should be the same [33].

Feature extraction is a primary operation in image processing, that is to say, it is the first arithmetic processing of an image [34]. It checks each pixel to determine whether the pixel represents a feature. If it is part of a larger algorithm, the algorithm usually checks only the feature area of the image. As a precondition for feature extraction, input images are smoothed in scale space through Gauss fuzzy kernel. After that, one or more features of the image can be calculated by local derivative operation [35].

Sometimes, if feature extraction requires a lot of computing time, and the time that can be used is limited, a high-level algorithm can be used to control the feature extraction class, so only the part of the image is used to find the feature. Because many computer image algorithms use feature extraction as its primary computing step, a large number of feature extraction algorithms have been developed, and their extraction features are varied, and their computational complexity and repeatability are very different [36].

3.2. Characteristic Type. The edge is a pixel that forms the boundary between the two image regions. Generally, the shape of an edge can be arbitrary and may include intersection points. In practice, the edge is generally defined as a subset of points with large gradients in the image. Some commonly used algorithms will also link high gradient points to form a more perfect description of edges. These algorithms may also impose restrictions on edges. Locally, the edge is a one-dimensional structure.

Corner is a point-like feature in an image, and it has a two-dimensional structure in part. In the early algorithm, edge detection was first carried out; then, the trend of the edge was analysed to find the sudden turning angle of the edge. The algorithm developed later does not require the edge detection step. Instead, it can directly search for high curvature in the image gradient. Later, it was found that sometimes

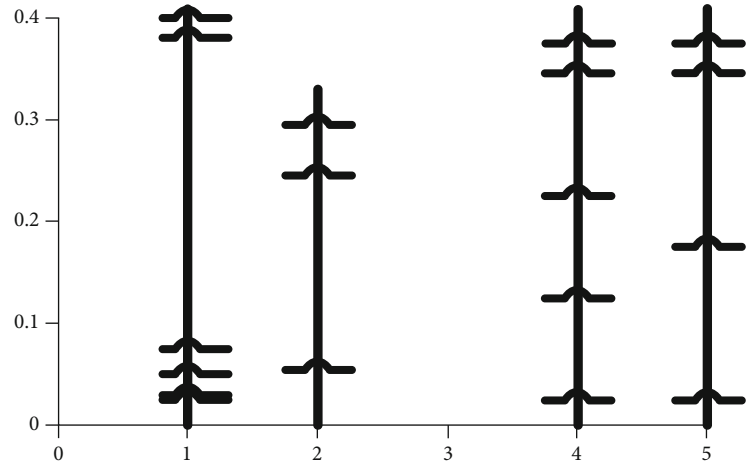

Figure 3: Results of comparison test.

a region with the same angular features could be found in the original image without corners.

Unlike angles, the region describes a regional structure in an image, but the region may also consist of only one pixel, so many regional tests can also be used to detect angles. A regional monitor detects a region that is too smooth for the angle monitor in the image. Area detection can be imagined as narrowing an image and then corner detection on a reduced image. Results of comparison test are shown in Figure 3.

Long striped objects are called ridges. In practice, the ridge can be regarded as a one-dimensional curve representing the symmetry axis, and the local needle has a ridge width for each ridge pixel. Extracting ridges from Gray gradient images is more difficult than extracting edges, corners, and regions. In aerial photography, ridges are often used to distinguish roads. In medical images, they are used to distinguish vessels.

3.3. Feature Extraction Step. Chi-square test: (1) the total number of documents in the statistical sample is N. (2) The frequency of positive documents (A), the frequency of negative documents (B), the frequency of positive documents, and the frequency of negative documents are calculated. (3) Calculating the square value of each word. (4) Each word is sorted according to the chi-square value from large to small, and the first k word is taken as the feature, and K is the feature dimension.

Information gain: (1) the number of documents in statistical positive and negative classifications: N1 and N2. (2) The frequency of positive documents (A), the frequency of negative documents (B), the frequency of positive documents, and the frequency of negative documents are calculated. (3) Computational information entropy. (4) Calculating the information gain of each word. (5) Each word is sorted according to the information gain value from large to small, and the first k word is taken as the feature, and K is the feature dimension.

3.4. Text Feature Extraction. Many machine learning problems involve Natural Language Processing (NLP) and must deal with text information. Text must be transformed into quantifiable feature vectors. Next, we will introduce the most commonly used method of text representation: the Bag-of-words model.

Thesaurus model is the most commonly used method of text modelling. For a document, ignoring its word order, grammar, and syntax, it is only regarded as a collection of words or a combination of words. The appearance of each word in the document is independent, does not depend on the appearance of other words, or when the author of the article chooses a word in any place is independent of the influence of the preceding sentence. The lexicon model can be regarded as an extension of the single thermal encoding, which sets an eigenvalue for each word. The lexicon model is based on similar words. Thesaurus model can achieve effective document classification and retrieval through limited coding information.

4. The Construction of Interactive English Chinese Translation Model

4.1. Introduction of Feature Extraction Algorithm. In this paper, the feature extraction algorithm is introduced, and the mapping of the best context is extracted to the translation process by the feature extraction algorithm, and the standard extraction of the feature context is completed. The optimal context is described by the semantic ontology mapping model. In the process of translation, there are N translation contexts, including K class semantic translation, and the number of translation contexts is N_i $(i = 1, 2, \cdots, K)$. The probability of K class semantic translation is $X_i = \{X_{i1}, X_{i2}, \cdots, X_{\mathrm{iN}}\}$, $X_{ij} = \{i = 1, 2, \cdots, K\,; J = 1, 2, \cdots, Ni\}$; it is a directional n-dimensional vector result. Translation can be achieved by defining the process and translating the context into formula (1).

$$\alpha_i = \frac{1}{N_i} \sum_{j=1}^{N_i} x_{ij}. \tag{1}$$

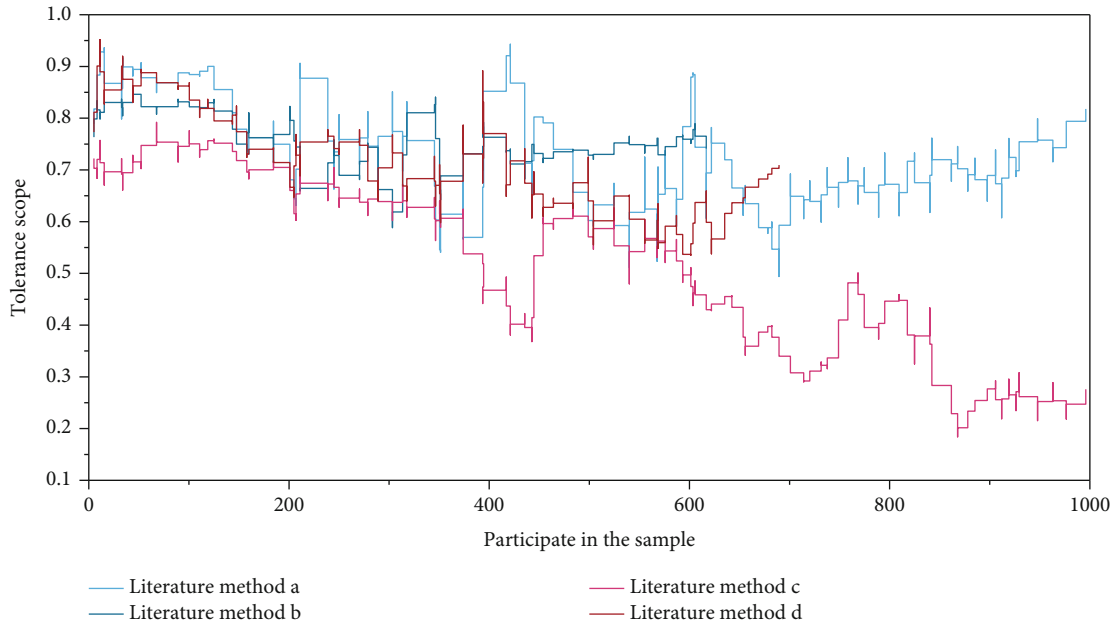

Figure 4: Comparison of feature extraction algorithms in different references.

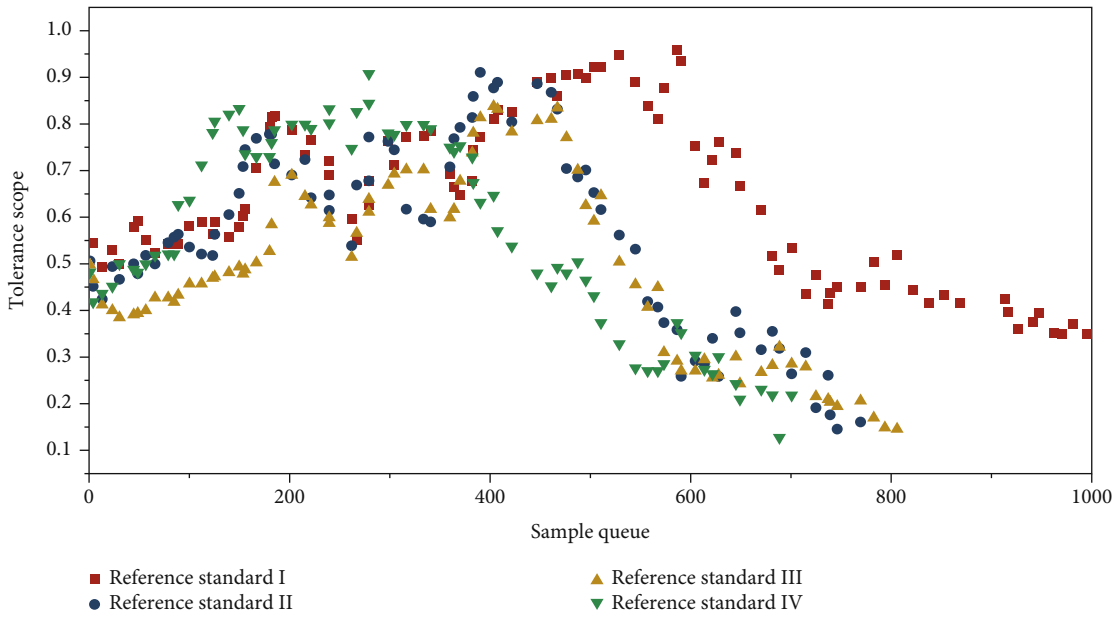

Figure 5: Performance comparison of feature extraction algorithms under different standards.

In the formula, the alpha I is able to translate into the semantic translation context, and the best context alpha selection process is formula (2).

$$\alpha = \frac{1}{K}\sum_{i=1}^{N_i} \alpha_{ij}. \tag{2}$$

4.2. The Design of the Language Processing Module of English Chinese Translation. Before conducting Interactive English Chinese translation, we first need to analyze the semantic transformation in English and Chinese translation and the word cover distortion components. In the process of English-Chinese translation, for example, as an example of the English word "image," the English Chinese translation of the word may be a picture, but its synonyms are "image" and "picture." Therefore, the three words have semantic fuzziness in a certain environment. In the process of English and Chinese translation, the semantic similarity and the possible semantic mapping of synonyms are described as formula (3).

$$\theta : S \longrightarrow S \times [-0.5, 0.5]. \tag{3}$$

In the form of theta, theta is an approximate semantic in the process of English-Chinese translation; S is a language

mapping in the process of English-Chinese translation; this article is an interactive English Chinese translation, and the degree of revision of semantic mapping is beyond the [-0.5,0.5]. In this paper, the mapping relation between English and Chinese translation semantics is used to solve the problem of selection and correction of ambiguity. Comparison of feature extraction algorithms in different references is shown in Figure 4.

The high-order replacement expression of the English Chinese translation semantics is Mountain [0, T], and the translation semantics of the literal translation semantics in the English Chinese translation process is represented by the matching translation set after the conceptual analysis. In which T represents the context judgment set of interactive translation semantics. By definition above, the analytic point in English Chinese translation sentence can be expressed by function Delta.

$$\Delta : [0, T] \to S \times [-0.5, 0.5). \tag{4}$$

We use interactive English Chinese translation statements to translate the content two times, such as formula (5).

$$\Delta(\beta) = \begin{cases} S_E, & K = \text{round}(\beta), \\ \alpha_E = \beta - K, & \alpha_E \in [-0.5, 0.5). \end{cases} \tag{5}$$

In the form of α_E, alpha E is the substitution expression coefficient in English Chinese translation; S_E is an interactive semantic substitution of information code, and round is a language information integration operator in the process of English Chinese Translation.

4.3. Result Analysis. Figure 2 is an interactive English Chinese translation system based on feature extraction algorithm and a traditional interactive English Chinese translation system. In the process of translation, the number of points in the control points and the control chart on the left side of the translation process are shown. On the right, the traditional Chinese English-Chinese translation system has a controlled distribution.

The node control distribution can reflect the semantic and contextual relevance of the translation system. The distribution is loosely illustrated, but the translation is correct but lack of contextual coherence. Performance comparison of feature extraction algorithms under different standards is shown in Figure 5.

By analysing Figure 5, it can be concluded that the interactive English-Chinese translation system based on the feature extraction algorithm designed in this paper has achieved good test results in other algorithms and tests under different standards. Therefore, we believe that the establishment of this model is highly efficient and can provide some reference and reference for English-Chinese translators.

5. Conclusions

This paper designs an interactive English Chinese translation system based on feature extraction algorithm. The feature extraction algorithm is introduced to select the feature semantics and establish the semantic ontology mapping model. The optimal solution of the interactive English Chinese translation process is selected, and the English Chinese translation process is finally realized through coding. It is hoped that this study will enable accurate translation in the process of English Chinese translation.

Data Availability

All the data can be obtained from the author.

Conflicts of Interest

The authors declare that they have no competing interests.

Acknowledgments

Key Research Projects of Humanities and Social Sciences in Anhui Universities in 2017 “A Study of Professional Development of EOP Teachers Based on Students’ Occupational Competence” (No. SK2017A0735).

References

[1] S. Desroches, A. Lapointe, J. Marin et al., “Environmental Scan on Canadian Interactive Knowledge Translation Tools to Prevent Diabetes Complications in Patients With Diabetes,” *Canadian Journal of Diabetes*, vol. 45, no. 2, pp. 97–104.e2, 2021.

[2] F. Ragep, M. Jamil, and F. Taro, “On astronomia: an arabic critical edition and english translation of epistle 3,” *Journal for the History of Astronomy*, vol. 5, 2016.

[3] M. Forcada, F. J. Ragep, and T. Mimura, “Astronomy in tenth-century Islamic encyclopaedism,” *Journal for the History of Astronomy*, vol. 47, no. 3, pp. 346-347, 2016.

[4] D. Raynaud, S. Gessner, and B. Mota, “Andalò di negro's de compositione astrolabii: a critical edition with english translation and notes,” *Archive for History of Exact Sciences*, vol. 73, no. 6, pp. 551–617, 2019.

[5] P. Kormanik, “Using Google Translate (Tm) for Non-native English Translation of Breast Cancer Treatment Summaries,” *Oncology Nursing Forum*, vol. 43, 2016.

[6] A. Tzouma and L. C. Triarhou, “The cerebellar system and what it signifies from a biological perspective, by professor christofredo jakob (english translation),” *The Cerebellum*, vol. 15, no. 4, pp. 395–416, 2016.

[7] S. Bi, “Intelligent system for English translation using automated knowledge base,” *Journal of Intelligent & Fuzzy Systems*, vol. 39, no. 4, pp. 5057–5066, 2020.

[8] Q. Guan, H. An, X. Gao, S. Huang, and H. Li, “Estimating potential trade links in the international crude oil trade: A link prediction approach,” *Energy*, vol. 102, no. 1, pp. 406–415, 2016.

[9] C. Y. Read, C. E. Ricciardi, A. Gruhl, L. Williams, and K. M. Vandiver, “Building genetic competence through partnerships and interactive models,” *Journal of Nursing Education*, vol. 55, no. 5, pp. 300–303, 2016.

[10] O. Texler, D. Futschik, M. Kučera et al., “Interactive video stylization using few-shot patch-based training,” *ACM Transactions on Graphics*, vol. 39, no. 4, 2020.

[11] J. Smith, I. Pike, M. Brussoni et al., "Mixed methods study exploring parent engagement in child health research in British Columbia," *BMJ Open*, vol. 9, no. 5, article e025404, 2019.

[12] C. Valmohammadi and S. Dashti, "Using interpretive structural modeling and fuzzy analytical process to identify and prioritize the interactive barriers of e-commerce implementation," *Information & Management*, vol. 53, no. 2, pp. 157–168, 2016.

[13] A. Tsimicalis, S. Le May, J. Stinson et al., "Linguistic validation of an interactive communication tool to help french-speaking children express their cancer symptoms," *Journal of Pediatric Oncology Nursing*, vol. 34, pp. 98–105, 2016.

[14] J. Reimand, T. Arak, P. Adler et al., "G:profiler—a web server for functional interpretation of gene lists (2016 update)," *Nucleic Acids Research*, vol. 44, no. W1, pp. W83–W89, 2016.

[15] A. Shook and V. Marian, "The influence of native-language tones on lexical access in the second language," *Journal of the Acoustical Society of America*, vol. 139, no. 6, pp. 3102–3109, 2016.

[16] U. R. Charrondiere, D. Rittenschober, V. Nowak, C. Nicodemi, P. Bruggeling, and C. Petracchi, "Fao/infoods e-learning course on food composition data," *Food Chemistry*, vol. 193, pp. 6–11, 2016.

[17] X. Chen, K. Naehrer, and T. J. Applegate, "Interactive effects of dietary protein concentration and aflatoxin b_1 on performance, nutrient digestibility, and gut health in broiler chicks," *Poultry Science*, vol. 95, no. 6, pp. 1312–1325, 2016.

[18] M. Weniger, F. Kapp, and P. Friederichs, "Spatial verification using wavelet transforms: a review," *Quarterly Journal of the Royal Meteorological Society.*, vol. 143, no. 702, pp. 120–136, 2017.

[19] L. Kane and P. Khanna, "Vision-based mid-air unistroke character input using polar signatures," *IEEE Transactions on Human-Machine Systems*, vol. 47, no. 6, pp. 1077–1088, 2017.

[20] C. Poncelet and F. Jacquemard, "Model-based testing for building reliable realtime interactive music systems," *Science of Computer Programming*, vol. 132, pp. 143–172, 2016.

[21] N. Wang, D. Mo, Z. Song, R. Wang, and Y. Wu, "Feature extraction algorithm of a precession target based on a doppler frequency profile of dual-aspect observation," *Applied Optics*, vol. 58, no. 17, pp. 4695–4700, 2019.

[22] J. Xu and Z.-H. Mao, "Multilabel Feature Extraction Algorithm Via Maximizing Approximated and Symmetrized Normalized Cross-Covariance Operator," *IEEE Transactions on Cybernetics*, vol. 11, pp. 1–14, 2019.

[23] G. P. Wang, J. X. Yang, and R. Li, "Ufklda: an unsupervised feature extraction algorithm for anomaly detection under cloud environment," *ETRI Journal*, vol. 41, no. 5, pp. 684–695, 2019.

[24] U. Ozgunalp, "Robust lane-detection algorithm based on improved symmetrical local threshold for feature extraction and inverse perspective mapping," *IET Image Processing*, vol. 13, no. 6, pp. 975–982, 2019.

[25] A. J. Heitmann and R. S. Gardiner-Garden, "A robust feature extraction and parameterized fitting algorithm for bottomside oblique and vertical incidence ionograms," *Radio Science*, vol. 54, no. 1, pp. 115–134, 2019.

[26] H. O. Awa, O. U. Ojiabo, and B. C. Emecheta, "Integrating TAM, TPB and TOE frameworks and expanding their characteristic constructs for e-commerce adoption by SMEs," *Journal of Science & Technology Policy Management*, vol. 6, no. 1, pp. 76–94, 2015.

[27] Z. Ju and S.-Y. Wang, "Predicting lysine lipoylation sites using bi-profile bayes feature extraction and fuzzy support vector machine algorithm," *Analytical Biochemistry*, vol. 561-562, pp. 11–17, 2018.

[28] X. Liu and H. Zhao, "Hierarchical feature extraction based on discriminant analysis," *Applied Intelligence*, vol. 49, no. 7, pp. 2780–2792, 2019.

[29] W. Jujie and L. Yaning, "Multi-step ahead wind speed prediction based on optimal feature extraction, long short term memory neural network and error correction strategy," *Applied Energy*, vol. 230, pp. 429–443, 2018.

[30] Y. Xue, Y. Wang, and B. Sun, "Asymmetric probability distribution function-based distillation curve reconstruction and feature extraction for industrial oil-refining processes," *Energy & Fuels*, vol. 34, no. 2, pp. 2533–2544, 2020.

[31] Y. Liu, M. Ma, X. Liu, N. Xiong, A. Liu, and Y. Zhu, "Design and analysis of probing route to defense sink-hole attacks for Internet of Things security," *IEEE Transactions on Network Science and Engineering*, vol. 7, no. 1, pp. 356–372, 2020.

[32] F. Long, N. Xiong, A. V. Vasilakos, L. T. Yang, and F. Sun, "A sustainable heuristic QoS routing algorithm for pervasive multi-layered satellite wireless networks," *Wireless Networks*, vol. 16, no. 6, pp. 1657–1673, 2010.

[33] Y. Zhou, D. Zhang, and N. Xiong, "Post-cloud computing paradigms: a survey and comparison," *Tsinghua Science and Technology*, vol. 22, no. 6, pp. 714–732, 2017.

[34] W. Pan and C. Chai, "Measuring software stability based on complex networks in software," *Cluster Computing*, vol. 22, Supplement 2, pp. 2589–S2598, 2019.

[35] W. Pan and C. Chai, "Structure-aware Mashup service clustering for cloud-based Internet of Things using genetic algorithm based clustering algorithm," *Future Generation Computer Systems*, vol. 87, pp. 267–277, 2018.

[36] G. Yang, Q. Yang, and H. Jin, "A novel trust recommendation model for mobile social network based on user motivation," *Electronic Commerce Research*, vol. 14, 2019.

Hindawi
Wireless Communications and Mobile Computing
Volume 2021, Article ID 6656498, 10 pages
https://doi.org/10.1155/2021/6656498

Research Article

TS-PADM: Anomaly Detection Model of Wireless Sensors Based on Spatial-Temporal Feature Points

Fengjiao Wang,[1,2] **Ruixing Li**,[1,2] **Hua Wang**,[1,2] **Hengliang Zhu**,[1] **and Naixue Xiong**[3]

[1]*Department of Computer, Min Jiang Teachers College, Fuzhou Fujian, China*
[2]*Fujian University Applied Engineering Centre for Internet of Things, Fuzhou, Fujian, China*
[3]*Northeastern State University, Oklahoma, USA*

Correspondence should be addressed to Fengjiao Wang; wangfengjiao@fzmjtc.cn

Received 20 October 2020; Revised 15 November 2020; Accepted 14 March 2021; Published 12 April 2021

Academic Editor: Alessandro Bazzi

Copyright © 2021 Fengjiao Wang et al. This is an open access article distributed under the Creative Commons Attribution License, which permits unrestricted use, distribution, and reproduction in any medium, provided the original work is properly cited.

In the practical application, sensor data collection is an essential means for the system to perceive the intrinsic features of data. The anomaly detection of data points can improve data quality and explore the potential information of data. The anomaly detection can be classified as two basic types, that is, classification and clustering. Those methods usually depend on the spatial correlation of data and have high computation complexity, so they are not suitable for the smart home and another mini-Internet of Things (IoT) environment. To overcome these problems, we propose a novel method for anomaly detection. In this paper, we first define the temporal and spatial feature of data flows; then, a time series denoising autoencoder (TSDA) is proposed to extract the discriminative high-dimensional characteristics to represent the data points. Moreover, a probability statistics-based anomaly detection model (PADM) was proposed for identifying the abnormal data. Extensive experimental results demonstrated that our method has fewer parameters and is easy to adjust and optimize. More importantly, our approach has higher precision and recall rate than the gradient boosted decision tree and XGBoot.

1. Introduction

Anomaly points are also called outliers or inconsistent points in the data mining and statistical analysis, and the anomaly point detection is a process to find the abnormal points whose behaviours are different from others. The development of IoT and sensor technologies makes smart home richer and more prosperous in the monitoring field [1]. Due to the uncertainty of the sensor deployment area and the limitation of equipment resources, the sensor data is easily interfered with and broken by external factors, so there is a widespread problem of sensor data unreliability. Therefore, it is urgent to solve the problem of ensuring and improving the quality of sensor data. Anomaly detection is a hot research topic in academia and industry, such as disease recognition in the medical system, network intrusion detection in the security field, credit card antifraud in the financial field, and anomaly detection in urban traffic management [2]. Besides, under the age of big data, there is the abuse of false data in monitoring data, so detecting these outliers has also become a new focus.

Traditional anomaly detection methods mainly include hierarchical clustering, partition-based clustering, density-based clustering, and fuzzy clustering. The clustering algorithms are widely applied, such as the Gaussian mixture model (GMM), *K*-means clustering, and fuzzy clustering analysis [3]. However, when these methods are applied to small IoT environments, such as smart homes or smart buildings, the detection based on spatial correlation can increase the algorithm's complexity. On the other hand, because the number of same-type sensor nodes deployed in the environment is small and the spatial correlation of data is insufficient, so the detection results of these algorithms are usually unsatisfactory. Also, the high dimension of data is a massive challenge for anomaly detection, and traditional methods usually utilize the nearest neighbour or neighbourhood information to search the nearest data points. However, the data in a high-dimensional space tends to be sparser than

in the lower dimensions, and the distance among the data points is no longer intuitive [4]. Therefore, by the temporal correlation and statistical features of data, in this paper, we creatively propose a novel model for anomaly point detection, which employs the spatial-temporal features and probability statistics (TS-PADM). We also propose a time series denoising autoencoder (TSDA) network to compress high-dimensional monitoring data, which can be used to represent the temporal and spatial feature of detection points.

Furthermore, a Gaussian model is introduced into the anomaly detection. In this model, we use the auxiliary target variables to gain the anomaly points by the objective function of region partitioning. Here, the EM algorithm is used to determine the target solution, and then, the anomaly points are detected. Experimental results show that the method proposed in this paper achieves better performance than random forest (RF) [5], gradient boosted decision tree algorithm (GBDT) [6], and XGBoot algorithm [7] in terms of accuracy.

This paper's structure is organized as follows: Section 2 discusses the relevant research work of the anomaly detection method. Section 3 introduces the representation of data spatial-temporal features based on time series denoising autoencoder in detail. Section 4 elaborates on the new anomaly detection algorithm of this paper. Section 5 shows the experimental results and verification. Finally, Section 6 summarizes the paper.

2. Relation Work

The anomaly detection methods in wireless sensor networks are divided into a statistics-based method, distance-based method, classification-based method, and cluster-based method. Literature [8] proposed the abnormal data detection through the variable-width histogram of computational data; i.e., the dynamic data in the technical network of data fusion were aggregated into a variable-width histogram to detect the anomaly data. Liu et al. [9] proposed an isolation forest algorithm which built anomaly indexes according to the path length from leaf node to root node, with good detection results for the global outliers but bad results for dealing with local sparser points. Wang et al. [10] proposed gradient boosted decision tree, which combined weaker learners into a stronger learner through iteration and reduced residual errors in successive iterations, thus generating trees deepened lengthwise. This method has the advantages of high prediction accuracy and strong robustness to outliers [11, 12].

Chen et al. [13] proposed the extreme gradient boosting tree algorithm, which took a step in the negative gradient of the loss function but conducted second-order Taylor series expansion of empirical errors and added some standard terms to make the loss function expandable. However, this algorithm had too many parameters, and the using effect relies too heavily on parameter tuning results. Literature [14] proposed an anomaly detection method based on presumptive mathematical statistics model and kernel density function but required the prior knowledge of sensor data distribution and relied on a definite mathematical model, so it had the features of limitations and weak universality. Literature [15] proposed an anomaly detection algorithm based on support vector machines (SVM), which learned a classification model with a training dataset and classified data instance into the class learned. In this algorithm, when the class has less data or the data did not belong to any class, such data were regarded as anomaly data. This algorithm required larger data samples to be training sets, so the number of samples would become its bottleneck, and the effect of anomaly detection was unsatisfactory. Literature [16] proposed an anomaly detection algorithm based on the K-means algorithm, which classified similar data instances into the data families with similar behaviours to achieve anomaly detection. This method did not introduce and utilize data streams' statistical features based on the data's spatial correlation. Literature [17] proposed an anomaly detection algorithm based on combining the K-means algorithm and the FP growth algorithm, which first conducted data modelling and then detected abnormal data. The cluster centre location and number selection of this method greatly impacted detection results, so its detection effects were not stable, and its complexity was very high [18]. Literature [19, 20] proposed an anomaly detection method based on distributed computation, which had sound detection effects in the large distributed environment. However, it was complicated and not easy to be achieved, so it was not suitable for the wireless sensor networks deployed in the home environment. Also, its data anomaly detection was achieved by the temporal and spatial correlation among detection data [21, 22].

In the specific environment of IoT, the same type of sensor nodes is insufficient in the number, so using the features of the time series of the data stream will have better detection effects [23]. This paper adapts autoencoder to extract the temporal-spatial features of detection points specific to this environment and the defects of existing methods. Considering the correlation of the spatial position of detection points and the change law of time series, auxiliary distribution variables were introduced to optimize the objective function of deep clustering. According to space-time features, detection points were clustered, and a multivariate Gaussian model based on probability statistics is designed to detect the anomaly data. Compared with the literature [24], our method does not need additional sensor nodes to provide data and saves the cost of communication, storage, and computation. The detection in standard scenarios such as causing the equidistant change of data stream when the equipment was turned on reduced the false alarm rate. Data anomaly can be effectively and accurately detected under the environment of a single sensor data stream [25].

3. Spatial-Temporal Features

3.1. Feature Description. Suppose that the total number of the sensor detection points included in the smart equipment is n, and define all detection point sets as $X = \{x_i = i|1, \cdots, n\}$, where $x_i \in dx$ refers to the physical quantity features of detection points, including air quality, temperature, illumination, heart rate, and noise. d_x refers to the number of dimensions of spatial-temporal features. The original features are mapped to the latent feature space by feature mapping

$\varphi : x \longrightarrow Z$ to gain the original features of time series and space, so it can be expressed as $Z = \{z_i \mid i = 1, \cdots, n\}$. Based on latent feature data z_i, the probability p_{ij} of detection point x_i belonging to the region r_j is calculated by feature mapping $f_\theta : z \longrightarrow P$, where θ refers to parameter set.

Most spatial features that are original data features of the sensor have dynamic properties, and time series data is highly dimensional and continuously variable. The code mapping of $\varphi : x \longrightarrow Z$ can reduce time series data and feature representation. Latent feature data is $z_i \in Z$, and feature dimensions are $d_x * dz$, where z_i consists of the features of time series and space of detection points. The model realizes dimension reduction and compression of time series data and uses normalization method to process spatial feature data of detection points.

3.2. Representation of Features of Time Series. A time series denoising autoencoder (TSDA) is proposed in this paper for the time series data of the detection points with high dimensionality and much noise. Random noise data were added into the sample dataset in the training process in order to enhance the antinoise property of TSDA. Convolutional layers (Conv2D) and maximum pooling layers (MaxPooling2D) were used in the encoding phase to achieve the feature extraction representation of time series data; the convolutional layers opposed to the encoding process and upsampling layers (UpSampling2D) were used in the decoding phase to reconstruct extraction representation into primitive input. TSDA has the same input and output, and its objective function is reconstruction error to optimize encoder and decoder.

(1) Series input: the time series (normalized) $T_{xi} = [t_1, t_2, \cdots, t_\gamma]$ with a length of γ in the detection point x_i is selected. In order to facilitate the subsequent operations such as convolution, pooling, and upsampling, $\mathrm{T}(x_i)$ is converted into two-dimensional matrix $\mathrm{T}'(x_i)$ by reshaping; meanwhile, Gaussian random noise was added into $\mathrm{T}''(x_i)$ to gain TSDA input

(2) Encoding phase: multiple convolutional layers and maximum pooling layers are alternately stacked to compress input data to gain the feature representation

(3) Decoding phase: multiple convolutional layers and upsampling layers are alternately stacked to restore the data feature representation to reconstruction input

(4) Objective function: the error between the primitive input and the reconstruction input is taken as the loss function

Weight was saved after TSDA training, and only the encoder is used to complete the feature extraction representation of time series.

Suppose feature of time series $YT(x_i)$ of x_i as $YT(x_i) = [yt_1, yt_2, \cdots, yt_x]$, where t_x refers to the number of dimensions of the feature of time series.

3.3. Representation of Spatial Features. The spatial features of detection points included coordinate position information, degree of importance of detection points, and instrument type, which were processed with the normalization method. Suppose the spatial features (YS) of x_i (YS) as $YS(x_i) = [ys_1, ys_2, \cdots ys_x]$, where s_x refers to the feature dimension.

The coordinate values determined the primitive spatial position of the detection points in the measuring coordinate system. When the dimensional units were different and the numerical values are significantly differentiated, it is not easy to give the relative position relation an accurate description among the detection points with specific quantities. Therefore, removing the influence of dimension and large values could effectively retain the relative position information of detection points and improve the convergence rate of subsequent training. The detailed practice is as follows:

(1) Unified dimension: the dimension units of coordinate values were unified through the unit conversion in the coordinate system (the unit is usually unified as meter)

(2) Nonlinear normalization: the extensive space range occupied by the structural body causes broadly differentiated position coordinate data of each detection point [26]. The function

$$y = \operatorname{sgn}(x) \frac{\ln(|x|)}{\ln(\max|x|)} \tag{1}$$

Function (1) is used for conversion, where $\operatorname{sgn}(x)$ is a mathematical formula that avoids negative coordinate values caused by different origins of coordinates selected in some coordinate systems.

4. Anomaly Detection Algorithm Based on Spatial-Temporal Features

4.1. Data Partitioning. The data partitioning problem can be equivalent to the problem that n detection points are partitioned into m regions. Suppose the region set finally partitioned as $R = \{r_j \mid j = 1, \cdots, m\}$. Formula (2) is used to calculate the possibility p_{ij} of the detection point z_i in the region $r_i, i = 1, \cdots, n$.

$$p_{ij} = f(z_i, \theta) = \frac{e^{\theta_j^T z_i}}{\sum_{j=1}^{m} r_j e^{\theta_j^T z_i}}. \tag{2}$$

The softmax activation function $(f_\Theta = e^{x_i} / \sum e^{x_i})$ is adopted to calculate the possibility, where $\Theta = [\theta_1, \theta_2, \cdots, \theta_m] \in d_z \times m$, and then, the gradient descent method is used to optimize the parameters. When, i.e., $p_{ij'} = \max\{p_{ij} \mid j = 1, \cdots, m\}$, when $p_{ij'}$ is the maximum possibility, the detection point x_i is partitioned into the region $r_{j'}$ [27].

4.2. Iterative Solution. Suppose the time series features as $YT(x_i) = [yt_1, yt_2, \cdots, y_x]$, where t_x refers to the dimensions

of features of time series. Suppose space as $YS(x_i) = [ys_1, ys_2, \cdots, ys_x]$, where s_x refers to the dimensions of features that is the normalized parameter X. It is a training set containing m data, in which each sample is an n-dimension datum:

$$X = \left[x^{(1)}, x^{(2)}, \cdots, x^{(m)}\right],$$
$$x^{(i)} = \begin{bmatrix} x_1^{(1)} \\ x_1^{(2)} \\ \vdots \\ x_n^{(i)} \end{bmatrix}. \tag{3}$$

It can be judged whether a sample is abnormal or not through the following function:

$$p\left(x^{(j)}; \mu, \sigma^2\right) = \prod_{i=1}^{n} p\left(x_i^{(j)}, u_i, \sigma^2\right) < \varepsilon. \tag{4}$$

We aim to acquire μ and σ according to the training set to gain a definite multivariate regular distribution model. Specifically, the following conclusion can be obtained from the maximum likelihood estimators:

$$\mu = \frac{1}{m}\sum_{j=1}^{m} x^{(j)},$$
$$\sum = \frac{1}{m}(X-\mu)(X-\mu)^T, \tag{5}$$

where Σ is a covariance diagonal matrix, and the multivariate regular distribution model finally acquired can be written as

$$p\left(x^{(j)}; \mu, \sigma^2\right) = p\left(x : \mu, \sum\right) = (2\pi)^{-(n/2)}\left|\sum\right|^{-(1/2)} \cdot \exp\left(-\frac{1}{2}(x-\mu)^T\sum^{-1}\right)(x-\mu). \tag{6}$$

The expectation maximum (EM) algorithm is used to find the maximum likelihood estimation of parameters or the maximum posterior estimation in the probabilistic model. The probabilistic model relies on the unobservable latent variables.

The expectation maximum algorithm is used for alternate calculation in three steps:

(1) Calculation of expectation (E): the existing estimated values of the probabilistic model parameters are used to calculate the expectation of latent variables

(2) Maximization (M): the expectation of latent variables acquired in the above E step is used to perform the parameter model's maximum likelihood estimation

(3) E step

The latent variable $y_{t,k}$ is introduced into the existing sample set $Y = (y_1, y_2, \cdots, y_T)$, and the data can be expanded as perfect numbers, where $t = 1, 2, 3, \cdots, T$.

The latent variable $y_{t,k}$ refers to the detection point of the sample coming from the kth smart device. The likelihood function of perfect numbers

$$\begin{aligned} P(y, y \mid \mu, \varepsilon, \pi) &= \prod_{t=1}^{\pi}\left(y_t, y_{t,1}, y_{t,2}, y_{t,3}, \cdots, y_{t,k}\right) \\ &= \prod_{t=1}^{T}\prod_{k=1}^{k}\left(\pi_k N\left(y_t; \mu_k * \varepsilon_k\right)\right)^{y_{t,k}} \\ &= \prod_{k=1}^{k}\pi_k \varepsilon_{t=1}^{T} y_{t,k} \prod_{t=1}^{T}\left(\pi_k \mathrm{N}\left(y_t; \mu_k * \varepsilon_k\right)\right)^{y_{t,k}}. \end{aligned} \tag{7}$$

The log-likelihood function of perfect numbers is R:

$$\ln p(y, y \mid \mu, \varepsilon, \pi) = \sum_{k=1}^{K}\left\{\left(\sum_{t=1}^{T}\gamma_{t,k}\right)\ln \pi_k + \sum_{t=1}^{T}\gamma_{t,k}[-\ln(2\pi) - 0.5 \ln |\Sigma_k|]\right. \tag{8}$$

4.3. Description of TS-PADM Algorithm. A feature set of wireless sensors $X = \{x_i = i | 1, \cdots, n\}$ is taken as the input parameters of the TS-PADM algorithm, and the probability distribution $\{p_{ij} | i = 1, \cdots, n; j = 1, \cdots, t\}$ of detection points in various regions is taken as the output. The hyperparameters requiring manual setting in the algorithm include training batches, maximum number of iterations, and threshold of iteration errors. During the classification of detection points, the space and time of detection points are used for unsupervised clustering, and the number of regions t need not be designated. See the details in Algorithm 1.

Feature mapping $\varphi : x \longrightarrow Z$ represents the features of time series of detection points through the denoising compression of time series and represents the spatial features with the normalization method, that is, mapping the primitive features of detection points to the latent feature space. Generally, the results of a clustering algorithm (such as K-means and Gaussian mixture model) are selected to initialize the target distribution R, avoiding the uncertainty of random initialization and speeding up the convergence process. Because R is the actual possibility distribution of detection points in their regions, the initialization by different clustering algorithms does not affect it. The EM method is used for iterative solution. As the target distribution R has been initialized, the EM method is used in line 4 to update the parameter ε and the possibility distribution P and then to fix the parameter to update the target distribution R. The algorithm finally gets the abnormal detection points back.

Input: a feature set of detection points $X = \{x_i = i | 1 \cdots, n\}$
Output: the probability of detection points in various regions $\{p_{ij} | i = 1, \cdots, n ; j = 1, \cdots t\}$
1. Map the primitive features of detection points to the latent feature space, $f_\theta : z \longrightarrow P$,
2. Use a clustering algorithm to initialize the target distribution R
3. WHILE NOT converged:
4. Fix the target distribution $\min_y R$ *and update the parameter* ε
5. Calculate the possibility of the detection points in the region $p_{ij} = f(z_i, \Theta)$ *and update P*
6. Fix the parameters and calculate $\gamma_{ij} = \varphi(p_{ij}, \varepsilon)$ *to update target distribution R*
7. END WHILE
8. RETURN $\{p_{ij} | i = 1, \cdots, n ; j = 1, \cdots t\}$

Algorithm 1: Anomaly detection algorithm based on spatial-temporal features.

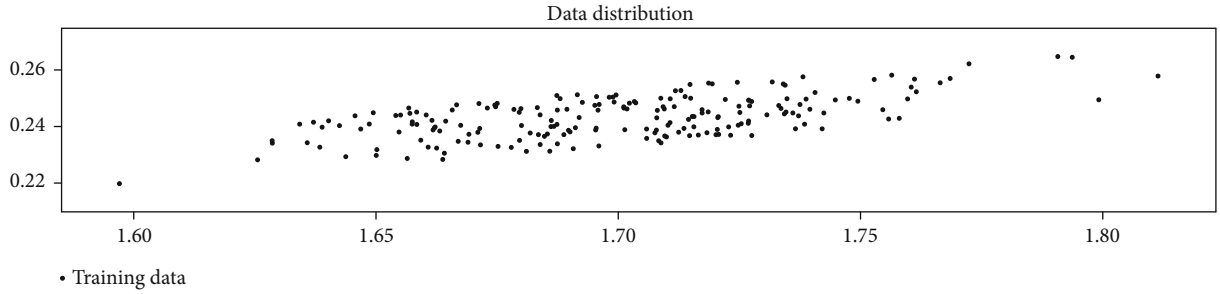

Figure 1: Test distribution of data samples.

5. Experimental Results and Verification

5.1. Data Sample Structure. Numerous sensors and smart devices in the smart home environment generate a large amount of data at all times, and conversely, those data provide a basis for altogether mining user behaviours and realizing smart control of home devices. Smart home environment data usually include monitoring data and smart device status. The monitoring data can be divided into two parts. The first part is environmental monitoring data of temperature, humidity, time, weather, brightness, etc., which are generally acquired through sensors and network information; the second part is user information involving user's position, status, and movement, which are acquired through indoor positioning technology and wearable devices. The status of a smart device refers to its current work status and parameter settings.

On the one hand, the status becomes some input dimension of decision-making by the Bayesian model as equipment information. On the other hand, it is also the decision-making objectives of the Bayesian model. The model is used for decision-making based on the current environmental data to achieve intelligent control of home devices by modifying the device status. There are distributed and multichannel methods to collect the smart home's environmental data, so the integration of scattered data is an essential prerequisite for the decision-making of device control. An expression specification of the home environment's data samples is proposed in this thesis: the current home environment data are sampled every 30 seconds and sorted into a data sample structured as in Figure 1. It is a modelling representation of the current home environment's sensor data, forming a primitive dataset. For the detailed derivative processes of maximum likelihood estimator, covariance matrix, and the maximum likelihood estimation of the multivariate normal distribution, please refer to literature [28].

(1) Data generation. Partial log data of sensor is input to test the algorithm model in this paper. The Gaussian model in the experiment had a mean value of [0,1], a covariance of [[0.3,0],[0,0.1]], and 30 data samples; the Gaussian model has a mean value of [1, 2], a covariance of [[0.2,0],[0,0.3]], and 30 data sample

(2) Data preprocessing. The algorithm in this paper is used to preprocess the points of the sample set as a decomposition time series feature set $YT(x_i) = [yt_1, yt_2, \cdots, yt_x]$ and an actual spatial feature set $YS(x_i) = [ys_1, ys_2, \cdots, ys_x]$. The data need to be preprocessed before applying the EM algorithm of the Gaussian mixture model to the samples. That is, all the sample values are scaled to between 0 and 1. In literature [29], Mikalsen et al. proposed a method of calculating the distance between data objects for anomaly detection. It defines the data anomaly as a case that in the dataset X, the number of data objects existing in the circle in the range of R is less than ρ for a data object 0. On this basis, the features of time series and spatial-temporal features are creatively decomposed. Data partitioning of the feature set is applied to the comprehensive utilization of time correlation and the data stream's statistical features. The data

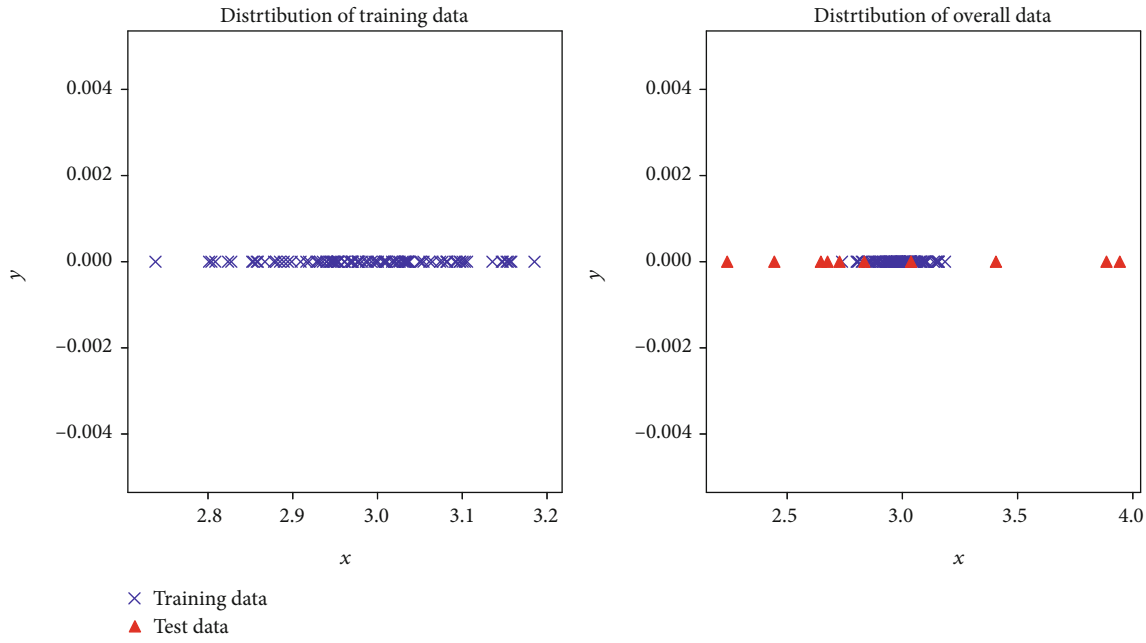

Figure 2: Test distribution of data samples.

samples from the dataset are trained for the model, and the results are obtained as shown in Figure 2

5.2. Experiment Preparation

5.2.1. Measured Dataset. The measured data are about 100,000 data records of detection points obtained from an environmental monitoring platform's processed monitoring data from April 1, 2019, to June 1, 2019. Nine hundred sixty-four measuring points are involved, and the observed physical quantity includes air quality, temperature, illumination, pollutants, and noise.

5.3. Benchmark Methods. The most commonly used K-means clustering and Gaussian mixture model are selected as benchmark methods based on a probability statistics-based anomaly detection model (PADM).

On the measured dataset, the model in this paper (TS-PADM) was used to extract features and modify K-means and GMM.

5.4. Evaluation Index. Experiments are performed with the above methods: K-means, GMM, and TS-PADM are used in the experiment on the dataset, and Silhouette Coefficient (SC) and Rand Index (RI) are adopted to evaluate the region partitioning performance.

The evaluation index SC is used to quantify the distribution of detection points. $SC \in [-1, 0)$ indicates that region partitioning performance is basically wrong, 0 indicates that it is involved into the locally optimal solution, and $SC \in [-1, 0)$ indicates that the more the value, the more reasonable and uniform the distribution of detection points. The RI index is used to measure the cohesion degree of the region. The more the value, the higher the cohesion degree [30].

For the accuracy rate, the models are used to classify the test set; it refers to the proportion of the number of samples correctly classified in total samples shown as follows [31]:

$$\text{Accuracy} = \frac{N_{\text{correct}}}{N_{\text{total}}}. \tag{9}$$

For the recall rate, it refers to the proportion of the true-positive (TP) samples truly classified in all positive samples (TP + TN), where TN (true negative) refers to the data falsely classified as follows:

$$\text{Recall} = \frac{\text{TP}}{\text{TP} + \text{TN}}. \tag{10}$$

5.5. Experimental Results of Measured Dataset. To make it simple, we suppose that all the data in *X_train* are normal data. In this way, fit (*X_train*) refers to the calculated model parameters of multivariate normal distribution, and Gaussian (*X_test*) refers to the density value of multivariate normal distribution calculated according to the objective function.

All the samples in X are detected by predict(X) and returned to the list of detection results corresponding to X. The elements in the list are a two-tuple. The first element records whether x_i is normal data, and the second element records $p\ (x_i\ ; \mu, \Sigma)$. Since we have assumed that all the data in *X_train* are normal data, the smallest density value in *X_train* is selected as ε here.

20 test data in *X_test* are possible abnormal samples. A large number of samples are needed by the intelligent detection program to train a function model. Perhaps, we firstly consider to label the samples as "normal" and "abnormal" like supervised learning and then train the model through classification algorithm. Suppose that xtest is a data sample, and predict (xtest) is used to judge whether xtest is a qualified

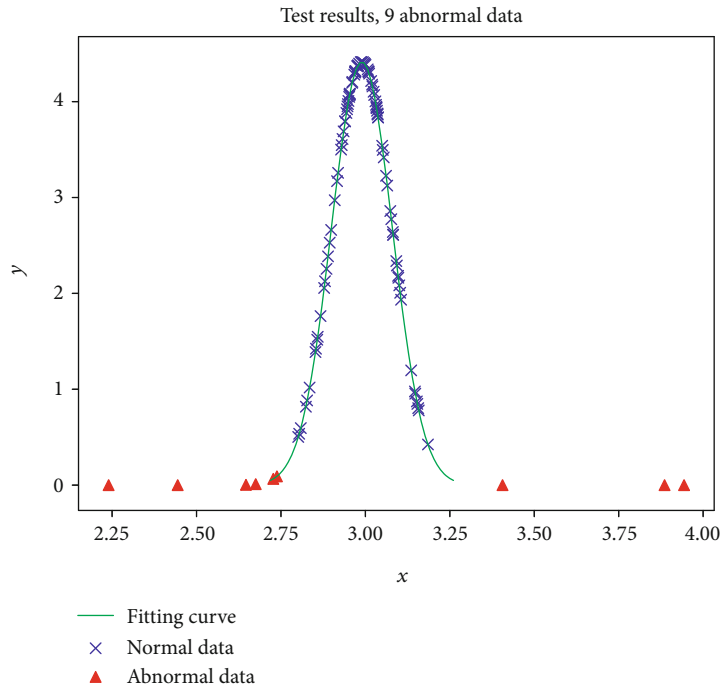

Figure 3: Detection results.

sample. From this, it can be seen that most of the training data are concentrated in the mean area of normal distribution, while the abnormal data are deviated towards both ends of the "reverse clock." Next, the anomaly detection model is trained by fit method, and the results are $\mu = 2.98961537626059$ and $\sigma^2 = 0.008178221946938589$. After the model parameters are obtained, the objective function can be used to predict the data. Gussian (X) realizes the density function of normal distribution, while predict (X) detects all samples in X and returns to the list of detection results corresponding to X. Its visualization results are shown in Figure 3 as follows.

5.6. Experimental Control and Conclusions. The index factor SC was used to quantify the abnormal situation of measuring points, and RI index was used to measure the cohesion degree of region. The larger the values, the better the corresponding performance [32]. The average SC and RI indexes of K-means, GMM, and TS-PADM are calculated as shown in Table 1.

As shown in Table 1, SC and RI indexes of TS-PADM were significantly higher than those of K-means and GMM. The air quality coefficients of the three methods were within the interval, and the SC of TS-PADM was 44.3% and 37.6% higher than that of K-means and GMM, respectively, indicating that TS-PADM had better region partitioning results. TS-PADM preceded K-means and GMM in the RI index by 36.8% and 21.8%, respectively, indicating that its areas partitioned had a higher cohesion degree, higher correlation of detection point single domain, and lower correlation among single domains. TS-PADM was superior to K-means and GMM in regional cohesion and distribution of measuring points.

Table 1: K-means, GMM, and TSPADM test results.

Indicators	K-means	GMM	TS-PADM
SC	0.532	0.558	0.768
RI	590.7	731.1	935.3

The accuracy rate and recall rate of the proposed algorithm were compared with those of the random forest (RF) algorithm [33], gradient boosted decision tree (GBDT) algorithm [5], and XGBoot algorithm [6]. The compared results of different algorithms on dataset are calculated as shown in Table 2.

From the analysis of the experimental results, it can be found that the detection effect of the proposed method was equivalent to that of XGBoot when anomaly classification was simulated on the dataset; TS-PADM has a higher accuracy rate and recall rate than the other methods and shows good anomaly classification performance. The experimental results show that the proposed method's effect is better than that of the GBDT algorithm and the RF algorithm. In practical problems, XGBoot has many hyperparameters that are complicated to adjust and optimize. The method proposed in this thesis based on feature segmentation and cascaded random forest has fewer hyperparameters and better practicability, so it is of better research and application value in the field of future outlier detection.

Although the TS-PADM algorithm performs well in the measured dataset in this paper, it may not also show such

Table 2: Compared results of different algorithms on dataset.

Algorithms	Accuracy	Recall
TS-PADM	0.9812	0.9867
RF	0.9623	0.9423
GBDT	0.9451	0.9532
XGBoot	0.9634	0.9654

Table 3: Characteristics of experimental dataset.

Dataset	Total instances	Outliers	Features
Heart disease	303	120	75
WPBC	198	47	34
Parkinson	197	48	23
Internet ads	3279	454	1558

WPBC is Breast Cancer Wisconsin (Prognostic) Dataset.

Table 4: Compared results of different algorithms on Heart disease.

Algorithms	Accuracy	Recall
TS-PADM	0.9417	0.9502
RF	0.9515	0.9412
GBDT	0.8762	0.9121
XGBoot	0.9192	0.9234

The RF algorithm is comparable to TS-PADM.

Table 5: Compared results of different algorithms on WPBC.

Algorithms	Accuracy	Recall
TS-PADM	0.9452	0.9562
RF	0.9411	0.9318
GBDT	0.8642	0.8579
XGBoot	0.9327	0.9236

The TS-PADM algorithm performs best and is stable.

good accuracy and recall rate with the amount of data and feature data increasing.

5.7. Control Experiment and Analytical Results. In order to verify the effectiveness of the method proposed in this paper, tests were conducted on the four datasets shown in Table 3. These datasets were obtained from the UCI [34] open resource. The UCI currently maintains 559 datasets as a service to the machine learning community. The tenfold cross-validation method is used on all the experimental datasets, with 80% for training and 20% for validation.

Tables 4–7 present the comparison results obtained by different outlier detection algorithms.

Analysis of the experimental results shows that the algorithm in this paper is comparable to the RF algorithm when the amount of data is similar. As the number of data instances increased, the method outperformed the other three algorithms in accuracy and had a higher recall on the Internet ad datasets.

Table 6: Compared results of different algorithms on Parkinson.

Algorithms	Accuracy	Recall
TS-PADM	0.9445	0.9552
RF	0.9423	0.9123
GBDT	0.8478	0.8636
XGBoot	0.9122	0.8356

The WPBC and Parkinson have similar data volume, and the TS-PADM algorithm performs best.

Table 7: Compared results of different algorithms on Internet ads.

Algorithms	Accuracy	Recall
TS-PADM	0.9745	0.9612
RF	0.9411	0.9378
GBDT	0.8778	0.8832
XGBoot	0.8423	0.8356

With the increasing number of Internet ad data instances, TS-PADM has outstanding advantages.

Combining the above data shows that the TS-PADM performs a slight disadvantage on heart disease. But it does not perform as consistently as TS-PADM on high-dimensional datasets with many features. TS-PADM achieves high recall on both high- and low-dimensional datasets while ensuring accuracy in the anomaly classification task, and the performance advantage is even more pronounced on high-dimensional datasets.

6. Conclusions

In this paper, the anomaly detection model of wireless sensors based on temporal-spatial feature points (TS-PADM) is proposed to compress high-dimensional monitoring data to represent the detection points' temporal-spatial features. On this basis, an anomaly point model based on probability statistics is adopted, and auxiliary target variables are introduced to optimize the objective function of region partitioning. The detection data obtained by sensors achieve better results in anomaly detection modelling. Extensive experiments show that the proposed TS-PADM algorithm can obtain relatively superior detection results and respond to the abnormal data changes of smart equipment in time. In future work, we will exploit deep learning methods to extract high-level semantic features of anomaly data to improve the prediction of anomaly detection.

Data Availability

The measured data which are about 100,000 data records used to support the findings of this study are available from the corresponding author upon request. And the four

datasets shown in Table 3 were obtained from the UCI (http://archive.ics.uci.edu/ml/index.php.) open resource.

Conflicts of Interest

The authors declare that there is no conflict of interest regarding the publication of this paper.

Acknowledgments

The financial support for this work provided by the Fundamental Research Funds for Department of Education, Fujian Province (No. JZ180635) is gratefully acknowledged.

References

[1] C. Wang, Z. Liu, H. Gao, and Y. Fu, "Applying anomaly pattern score for outlier detection," *IEEE Access*, vol. 7, pp. 16008–16020, 2019.

[2] M. Li, R. Kashef, and A. Ibrahim, "Multi-level clustering-based outlier's detection (MCOD) using self-organizing maps," *Big Data and Cognitive Computing*, vol. 4, no. 4, p. 24, 2020.

[3] M. Ahmed, A. N. Mahmood, and M. R. Islam, "A survey of anomaly detection techniques in financial domain," *Future Generation Computer Systems*, vol. 55, no. 6, pp. 278–288, 2016.

[4] Y. Djenouri and A. Zimek, "Outlier detection in urban traffic data," in *Proceedings of the 8th International Conference on Web Intelligence, Mining and Semantics*, pp. 1–12, Novi Sad, Serbia, 2018.

[5] Z. H. Gong, J. N. Wang, and C. A. Su, "Weighted Deep Forest Algorithm," *Computer Applications and Software*, vol. 36, no. 2, pp. 274–278, 2019.

[6] K. Guo, D. Liu, Y. Peng, and X. Peng, "Data-driven anomaly detection using OCSVM with boundary optimization," in *2018 Prongs tics and System Health Management Conference IEEE*, pp. 244–248, Chongqing, China, 2018.

[7] T. Chen and C. Guestrin, "XGBboost: a scalable tree boosting system," in *Proceedings of the 22nd ACM Sigkdd International Conference on Knowledge Discovery and Data Mining*, pp. 785–794, San Francisco, CA, USA, 2016.

[8] H. Zhang and Z. Li, "Anomaly detection approach for urban sensing based on credibility and time-series analysis optimization model," *IEEE Access*, vol. 7, pp. 49102–49110, 2019.

[9] F. T. Liu, K. M. Ting, and Z. H. Zhou, "Isolation- based anomaly detection," *ACM Transactions on Knowledge Discovery from Data (TKDD)*, vol. 6, no. 1, pp. 1–39, 2012.

[10] H. Wang, M. J. Bah, and M. Hammad, "Progress in outlier detection techniques: a survey," *IEEE Access*, vol. 7, pp. 107964–108000, 2019.

[11] Y. Yang, N. Xiong, N. Y. Chong, and X. Défago, "A decentralized and adaptive flocking algorithm for autonomous mobile robots," in *2008 The 3rd International Conference on Grid and Pervasive Computing - Workshops*, Kunming, China, 2008.

[12] A. Shahzad, M. Lee, Y. K. Lee et al., "Real time MODBUS transmissions and cryptography security designs and enhancements of protocol sensitive information," *Symmetry*, vol. 7, no. 3, pp. 1176–1210, 2015.

[13] B. Chen, T. Hu, Z. Huang, and C. Fang, "A spatio-temporal clustering and diagnosis method for concrete arch dams using deformation monitoring data," *Structural Health Monitoring*, vol. 18, no. 5-6, pp. 1355–1371, 2018.

[14] Y. Yu, X. Liu, E.-Z. Wang, K. Fang, and L. Huang, "Dam safety evaluation based on multiple linear regression and numerical simulation," *Rock Mechanics and Rock Engineering*, vol. 51, no. 8, pp. 2451–2467, 2018.

[15] D. Dua and C. Graff, *UCI Machine Learning Repository*, University of California, School of Information and Computer Science, Irvine, CA, 2019, http://archive.ics.uci.edu/ml.

[16] V. K. Samparthi and H. K. Verma, "Outlier detection of data in wireless sensor networks using kernel density estimation," *International Journal of Computer Applications*, vol. 5, no. 6, pp. 28–32, 2010.

[17] V. Nalina, A. S. Sandesh, R. D. Sequiera, and P. Jayarekha, "Cloud computing based vehicle tracking information system," in *2015 IEEE International Advance Computing Conference (IACC)*, vol. 2, Banglore, India, 2011no. 1.

[18] S. Misra, A. Singh, S. Chatterjee, and M. S. Obaidat, "Mils-Cloud: a sensor-cloud-based architecture for the integration of military tri-services operations and decision making," *IEEE Systems Journal*, vol. 10, no. 2, pp. 628–636, 2016.

[19] C. Srimathi, S. Park, and N. Rajesh, "Proposed framework for underwater sensor cloud for environmental monitoring," in *2013 Fifth International Conference on Ubiquitous and Future Networks (ICUFN)*, pp. 104–109, Da Nang, Vietnam, 2013.

[20] H. Paulheim and R. Meusel, "A decomposition of the outlier detection problem into a set of supervised learning problems," *Machine Learning*, vol. 100, no. 2-3, pp. 509–531, 2015.

[21] Q. Zhang, C. Zhou, N. Xiong, Y. Qin, X. Li, and S. Huang, "Multimodel-based incident prediction and risk assessment in dynamic cybersecurity protection for industrial control systems," *IEEE Transactions on Systems, Man, and Cybernetics: Systems*, vol. 46, no. 10, pp. 1429–1444, 2016.

[22] K. Huang, Q. Zhang, C. Zhou, N. Xiong, and Y. Qin, "An efficient intrusion detection approach for visual sensor networks based on traffic pattern learning," *IEEE Transactions on Systems, Man, and Cybernetics: Systems*, vol. 47, no. 10, pp. 2704–2713, 2017.

[23] W. Wu, N. Xiong, and C. Wu, "Improved clustering algorithm based on energy consumption in wireless sensor networks," *IET Networks*, vol. 6, no. 3, pp. 47–53, 2017.

[24] O. Ghorbel, W. Ayedi, H. Snoussi, and M. Abid, "Fast and efficient outlier detection method in wireless sensor networks," *IEEE Sensors Journal*, vol. 15, no. 6, pp. 3403–3411, 2015.

[25] Y. Zhang, N. Meratnia, and P. J. M. Havinga, "Distributed online outlier detection in wireless sensor networks using ellipsoidal support vector machine," *Ad Hoc Networks*, vol. 11, no. 3, pp. 1062–1074, 2013.

[26] F. Elijorde, S. Kim, and J. Lee, "A wind turbine fault detection approach based on cluster analysis and frequent pattern mining," *KSII Transactions on Internet and Information Systems*, vol. 8, no. 2, pp. 664–677, 2014.

[27] I. A. Klampanos, A. Davvetas, S. Andronopoulos, C. Pappas, A. Ikonomopoulos, and V. Karkaletsis, "Autoencoder-driven weather clustering for source estimation during nuclear events," *Environmental Modelling & Software*, vol. 102, pp. 84–93, 2018.

[28] K. G. Dizaji, A. Herandi, C. Deng, W. Cai, and H. Huang, "Deep clustering via joint convolutional autoencoder embedding and relative entropy minimization," in *2017 IEEE*

International Conference on Computer Vision (ICCV), pp. 1–13, Venice, Italy, 2017.

[29] K. Ø. Mikalsen, F. M. Bianchi, C. Soguero-Ruiz, and R. Jenssen, "Time series cluster kernel for learning similarities between multivariate time series with missing data," *Pattern Recognition*, vol. 76, pp. 569–581, 2018.

[30] J. R. Hershey, Z. Chen, J. Le Roux, and S. Watanabe, "Deep clustering: discriminative embeddings for segmentation and separation," in *2016 IEEE International Conference on Acoustics, Speech and Signal Processing (ICASSP)*, pp. 31–35, Shanghai, China, 2016.

[31] J. W. Branch, C. Giannella, B. Szymanski, R. Wolff, and H. Kargupta, "In-network outlier detection in wireless sensor networks," *Knowledge and Information Systems*, vol. 34, no. 1, pp. 23–54, 2013.

[32] H. Su, J. Ren, and Z. Wen, "An approach using Dempster–Shafer evidence theory to fuse multi-source observations for dam safety estimation," *Soft Computing*, vol. 23, no. 14, pp. 5633–5644, 2019.

[33] B. Wei, D. Yuan, H. Li, and Z. Xu, "Combination forecast model for concrete dam displacement considering residual correction," *Structural Health Monitoring*, vol. 18, no. 1, pp. 232–244, 2019.

[34] D. Dua and C. Graff, *UCI Machine Learning Repository*, 2019, http://archive.ics.uci.edu/ml/index.php.

Hindawi
Wireless Communications and Mobile Computing
Volume 2021, Article ID 8872689, 10 pages
https://doi.org/10.1155/2021/8872689

Research Article

Research on the Operation of e-Commerce Enterprises Based on Blockchain Technology and Bilateral Platforms

Xiaoye Ma,[1] Weina Li,[2] and Jun Wu[1]

[1]*Guilin University of Electronic Technology, Guilin 541000, China*
[2]*Tangshan Normal University, Tangshan 063000, China*

Correspondence should be addressed to Weina Li; yuna-ada@hotmail.com

Received 20 August 2020; Revised 23 September 2020; Accepted 24 February 2021; Published 15 March 2021

Academic Editor: Hongju Cheng

Copyright © 2021 Xiaoye Ma et al. This is an open access article distributed under the Creative Commons Attribution License, which permits unrestricted use, distribution, and reproduction in any medium, provided the original work is properly cited.

E-commerce platform enterprises have typical bilateral market characteristics. The e-commerce platform provides real-time communication services for buyers and sellers. Different buyers and sellers form crossnetwork characteristics. The formulation and implementation of bilateral strategies affect both the merchants and consumers' choice of platform and registration transactions. This impact will directly lead to the transaction value of the platform. Then, the article builds an econometric model and empirically analyses the impact of e-commerce platforms. The e-commerce chain is a complex structure that consists of logistics, information flow, and capital flow and connects suppliers, manufacturers, distributors, and users in the industry together. Blockchain technology can be used as a large-scale collaboration tool to adapt to supply chain management, the main factor that drives the market power of the enterprise. The research results show that the input costs of advertising, research and development, and employee training and the impact of long-term investment and taxation on market forces are quite different in different industries, both positive and negative, and subsidies, inventory, and state-owned holdings have a negative impact on the market power of companies in all industries. Finally, the competition strategy of e-commerce platform enterprises is summarized. On the basis of the conclusions of the theory and case study, the paper puts forward specific suggestions and countermeasures for the competition strategy of e-commerce platform enterprises in the bilateral network environment.

1. Introduction

The bilateral market theory is a broad concern of the economics community since the 21st century. It is based on the multiproduct theory and the network external protection theory and the emerging market theory with the network market as the main research position. Whether it is emerging online shopping, online payment, "computer industry, or traditional intermediary or media industry, there are significant bilateral market characteristics." The existing basic research analysis shows that, for companies in this type of industry, such as product quantity, price positioning and compatibility positioning, quality positioning, etc., the government's policies and regulations on these contents are difficult to explain with traditional market analysis theories [1].

The bilateral market provides a place and opportunity for both parties to complete the transaction theme. The platform is the core of the bilateral market. The platform provides unique products for the transaction entity to achieve an effective contact with the transaction entity, complete the transaction, and obtain the transaction from the transaction entity.

1.1. Profit. The traditional unilateral market only includes buyers and sellers of commodity transactions, but the bilateral market is different from it. To form a bilateral market, one must meet three conditions: first, the transaction subject must be different and there are two or more groups. Second, there is an effective association between different entities or the implementation of coordinated externalities [2]. Third, there is an institution that transforms the externalities created by a group of subjects into internalized ones [3].

Platform enterprises play an important role in networked market economy and trade activities. These platform

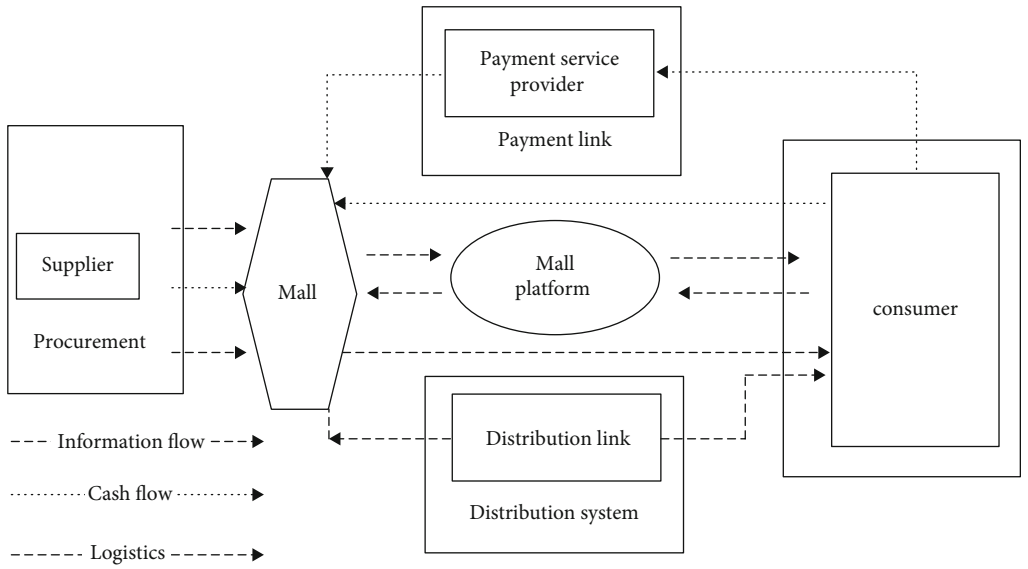

Figure 1: Schematic diagram of bilateral market characteristics.

enterprises provide targeted products or services to both parties of the transaction or to multiple users of the transaction. Through differentiated pricing strategies, different users can implement commodity delivery through the platform which has the characteristics of a bilateral market. By definition, it can be concluded that the bilateral market has obvious market characteristics compared with the unilateral market [4].

The so-called "network externality" means that the utility of one side of the main body on both sides of the platform provider will increase as the number of the other side body increases. Network externalities are an important indicator of whether a market is a bilateral market [5, 6]. We can easily associate with the fact that the more that small businesses involved in the surrounding area provide related products and services to a large enterprise at the same time, the higher the information sensitivity between them and the versatility of parts and services. The more that users use a certain kind of resource sharing software, the more valuable shared resources can serve more users and thus more valuable resources will be available for users; for the software value, the software value and utility are constantly improving [7, 8]. From the perspective of the bilateral market, compared with the network externality existing between the same users, the network externality formed based on the bilateral users of the platform is more critical and the crossnetwork externality can be embodied. The quantity will act on the bilateral users of the platform, which will affect the transaction volume. The transaction volume and quantity of bilateral users will have a greater impact. Crossnetworking plays a very important role in establishing a bilateral market [9].

Based on the transaction process of the bilateral market, the formation of a transaction requires the buyer and the seller and the platform enterprise to participate in the transaction process. The platform enterprise provides services for the good delivery between the buyer and the seller in the transaction process. Therefore, the platform enterprise has a separate allocation to the bilateral purchase and sale [10].

1.2. The Cost of the Fee. The formula for calculating the amount that the platform enterprise collects from both parties or unilateral parties is $P = \mathrm{Pb} + \mathrm{Ps}$ (Pb is the price of the buyer user and Ps is the price of the seller user). The amount charged is related to the trading volume of the platform users and the revenue of the platform. More importantly, this total price should be reasonably distributed among the bilateral users in the market [11].

The so-called "dependency" means that only when the entities located on both sides of the platform provider have a demand for the products or services provided by the platform vendors that the products or services must have the value provided by the platform vendors, or else, the platforms may be different. The theme of the product is not for the purpose of providing products and services, so these products and services cannot reflect their value. Products and services provided by companies in the bilateral market show high filling and interdependence when driving users on both sides of the market to complete a transaction. The existence of a demand becomes a prerequisite for another demand, and mutual dependence and complementarity are reflected [12]. A schematic diagram of the characteristics of the bilateral market is shown in Figure 1 [13, 14].

2. Estimation of Market Power of e-Commerce Enterprises

For the e-commerce platform, from the perspective of network externality, there is a positive crossnetwork externality between the platform, users, and vendors, that is, the platform will gather popularity and scale effects by a large number of users or vendors [15], to attract the other users to join and ultimately reach the stability of users on both sides of the platform. At the same time, users will also have network externalities, especially in the presale model of goods, with the aggregation of users, thus forming a dominant advantage and controlling the price of the transaction. The externalities between vendors are different due to the different effects in

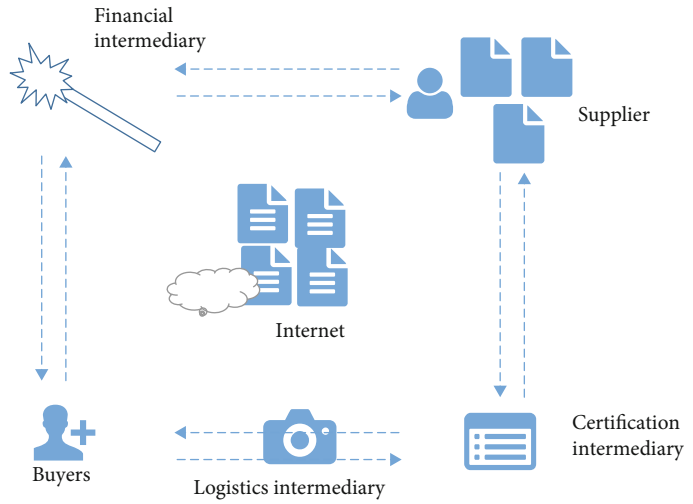

Figure 2: E-commerce system structure.

different environments [16]. The externality of the network can be positive or negative. For example, for merchants offering the same kind of goods or services, the greater the number, the more intense the competition and the profit. The more difficult it will be, the lower the willingness of merchants to enter the platform and the negative network externality. For the manufacturers that provide different goods or services, the more manufacturers that join, the stronger the platform will be and the consumption will meet different needs [17]. The ability of the person is stronger, seeing the potential of user purchase, making the manufacturer more willing to enter the platform, which is the positive network externality. Based on the above analysis, we set a parameter t before the parameters of the intragroup network externality between users in the following discussion, in order to specifically consider the C2B which is mainly based on the presale mode and involves the internal and externalities of the user group. The pricing of the e-commerce model is negligible for intergroup network externalities between vendors. The construction of the e-commerce model can be seen in Figure 2 [18].

From the perspective of real experience, manufacturers with seller market power face a large number of consumers in the downstream and can obtain monopoly profits by limiting production and increasing product prices. Consumers can also weaken the vendor's market power by, to a certain extent, freely choosing the purchase channel. In the upstream factor market, manufacturers with buyer market power mainly obtain monopoly profits by lowering factor prices. A large number of scattered sellers make it impossible to choose a transaction object, because consumers have the right to choose merchants. On the other hand, the product storage and transportation costs are high and many products have very strong specialty, which has no other use than selling to the company. Therefore, companies often have stronger market power in the raw material purchase market. Although this empirical inference is logically established, there is currently no empirical analysis by scholars in domestic academic circles.

2.1. Model Construction. Estimating the size of each company's market power is the first step in analyzing the formation of market forces. Traditional estimation methods, including the NEIO model, Solow residual method, and nonparametric method, can only estimate the industry's average Lerner index value, which is obviously inappropriate as a dependent variable, so market forces should be reconsidered.

2.1.1. The Estimation Method. From the current research progress in this area, a more feasible solution is to estimate the Lerner index by estimating the cost function and marginal cost function of the enterprise and combining the output price of the enterprise. Specifically, the cost function is first constructed to estimate the relevant parameters, and then, the marginal cost function is obtained by derivation and the estimated parameter value of the cost function is substituted into the marginal cost function to estimate the Lerner index of each enterprise.

2.1.2. The Index Value. Such a treatment method can reflect the difference in market power of different enterprises and can be used as a dependent variable to analyze the formation factors of market forces.

The stochastic boundary cost function is currently the most widely used form of function for the cost function. Based on the random boundary production function, Sclunidt and Lovell constructed the corresponding stochastic boundary cost function. Many scholars have applied the stochastic boundary cost function to study the market power-related issues. According to the special situation of China's food industry, this paper constructs a random boundary cost function as follows:

$$\begin{aligned}\ln cit = {} & \sum \gamma h \ln whit + \gamma q \ln qit + \frac{1}{2}\sum\sum \gamma hj \ln whit \ln wjit \\ & + \frac{1}{2}\gamma qq(\ln qit)^2 + \sum \gamma hq \ln whit \ln qjit + \rho tT \\ & + \rho qT \ln qjit + \sum \rho hT \ln whit + \ln ui + \ln vi.\end{aligned} \tag{1}$$

In which, $c$it is the total cost and $q$it is the total output of enterprise 1, $w$hit is the factor price of the enterprise (including raw materials, labour, and capital), and T is the time trend item, which represents technological progress. By calculating the yield qi, the formula for calculating the marginal cost can be obtained.

$$mc\text{it} = \left(\gamma q + \gamma qq \ln \text{qjt} + \sum \gamma hq \ln \text{whit} + \rho qT\right) \frac{c\text{it}}{q\text{it}}. \quad (2)$$

Thus, the Lerner index ($l = (p - mc)/p$) of the firm can be further estimated.

According to the "structure-behavior-performance" paradigm, the factors affecting market power can be roughly divided into two categories; one is the industry structure, including the number of buyers and sellers, product differentiation, diversification, manufacturer size, barriers to entry, and vertical integration and second is vendor behavior, including pricing, research and development, collusion, mergers, advertising, and investment. However, in addition to these two factors, government policies often affect the market power of enterprises. Especially in China, state-owned enterprises often have strong market power by virtue of government asylum. Government policies mainly include regulation, antitrust, taxation and subsidies, government procurement, investment incentives, employment incentives, and research and development support.

Among all these variables, only a few are quantifiable, which means that most of the variables affecting market forces cannot be included in the econometric model for empirical analysis, such as product differentiation and barriers to entry, which are formed by the market forces of manufacturers. But because the data is not available, important factors can only be used in qualitative analysis.

Combined with the data acquisition situation, this paper selects seven relatively important and energized indicators from the above variables as the explanatory variables of the model and one control variable and constructs the measurement model as follows:

$$\begin{aligned} \ln L\text{it} = {} & a + \beta 1 \ln \text{ADVit} + \beta 2 \ln \text{RDit} + \beta 3 \ln \text{EDUit} \\ & + \beta 4 \ln \text{LIit} \beta 5 \ln \text{TAXit} + \beta 6 \ln \text{SUBit} \\ & + \beta 7 \ln \text{INVit} + \beta 8 \text{Dit} + \varepsilon \text{it}. \end{aligned} \quad (3)$$

Respectively represent the company's market power, advertising investment, R&D investment, personnel training costs, long-term investment, taxes, subsidies, inventory, taxes, subsidies, and dummy variables.Dit presents the external environment of the enterprise; in the virtual variable representing the nature of the property rights of the enterprise, in the paid-in capital of the enterprise, when the proportion of state-owned capital exceeds the proportion of nonstate-owned capital, $D = 1$; otherwise, $D = 0$; $D = 1$ means the enterprise is state controlled, which is a control variable used to observe whether state-owned enterprises have obvious advantages in the formation of market forces.

It is true that the model misses some important explanatory variables, but the purpose of this paper is not to use the model for prediction but mainly to analyze the impact of each variable on market forces. Therefore, under the condition that the data is not available, this is a suboptimal choice.

2.2. Data Description. The variables selected when estimating the random boundary cost function and the marginal cost are basically the same. Some variables were added in estimating the formation of market forces, including advertising inputs, R&D investment, staff training costs, long-term investments, taxes, subsidies, inventory, and virtual variables of the nature of corporate property rights. The dummy variables of the nature of enterprise property rights are derived from the composition of the paid-in capital of enterprises published in the "China Industrial Enterprise Database". The paid-in capital in the original data is divided into six categories, namely state-owned capital, collective capital and corporate capital, gold, personal capital, capital from Hong Kong, Macao and Taiwan, and foreign capital. First, calculate the proportion of various types of capital in the paid-in capital, and then, compare the sum of the proportion of the national capital and the proportion of the other five types of capital; the former is greater than the latter and vice versa. The average values of the main variables that affect the formation of market power are shown in Table 1.

The remaining data on variables such as advertising investment and R&D investment are obtained directly from the China Industrial Enterprise Database. Since many companies invest very little or even zero investment in these areas, the explanatory power of individual variables on market forces is relatively weak. See the results of the analysis below.

Table 1 shows the average investment value of enterprises in different industries in advertising, research and development, etc. It can be seen that the tobacco processing enterprises' investment in various indicators is far greater than other industries. In other industries except tobacco, processing enterprises are significantly more expensive than other companies in terms of advertising investment, and the processing investment of processing enterprises is also the largest among all enterprises. These reflect the behavior characteristics of companies in different industries.

3. Results Analysis

By using the stochastic boundary cost function analysis method in the Stata 12.1 software to regress the model, the cost function of the enterprise can be estimated, as shown in Table 2. It is not difficult to find from the table that except for the automobile processing industry, the parameter estimation of the cost function of other industries is mostly significant, indicating that the fitting effect of the model is better. The best model fitting results are in the tobacco, food, and garment processing industries. As can be seen from the table, the cost function coefficients of these three industries are mostly significant. In industries other than tobacco, multicollinearity problems may exist between the intersection of time-trend items and other variables and certain variables in the model and are therefore eliminated when estimating the model.

Table 1: Mean of the main variables affecting the formation of market forces.

Industry	ADV	RD	EDU	LI	TAX	SUB	INV
Tobacco	3030000	10400000	1578855	16500000	91900000	7361961	545000000
Automobile industry	202452	23997	16338	1578228	5327519	237776	59900000
Foodstuffs	15857	19085	93515	5761954	1080000	211211	20400000
Clothing	13479	73224	6309	26413	912358	37938	2721520
Electronic product	31886	3349	6229	404361	808828	128833	9175943

Table 2: Parameter estimation of random boundary cost function.

Ln c	Tobacco		Automobile industry		Foodstuffs		Clothing		Electronic product	
	Coefficient	Standard deviation	Coefficient	Standard deviation	Coefficient	Standard deviation	Coefficient	Standard deviation	Coefficient	Standard deviation
γh	219.64	88.164	-41.99	42.14	9.283	4.609	−5.766	4.142	17.868	7.445
γhj	−30.55	14.27	6.604	7.010	0.499	0.999	−1.432	0.520	2.508	0.918
γq	121.79	42.04	1.134	14.095	−98.03	16.00	169.7	15.4	−78.884	16.416
γqq	0.053	0.010	−7.064	15.711	17.53	2.868	−27.33	2.643	3.579	3.414
γhq	−0.228	0.041	3.101	10.010	3.712	1.240	0.018	1.069	8.938	2.046
ρt	0.102	0.032	−0.009	0.158	0.023	0.027	−0.065	0.001	0.096	0.002
ρq	−0.111	0.045	−0.097	0.074	0.151	0.012	−0.115	0.018	0.055	0.043
ρh	0.016	0.007	0.007	0.108	0.055	0.010	0.032	0.011	−0.035	0.013
CONS	64.35	317.34	87.979	199.128	−274	46	544	42.14	126.3	57.0
σ^2	0.118	0.037	0.148	0.1008	0.054	0.043	0.145	0.050	11.627	0.131
γ	0.424	0.007	0.784		0.971	0.002	0.947	0.015	0.933	0.001

After estimating the cost function, the relevant coefficient is substituted into the marginal cost function to estimate the marginal cost of the enterprise, thereby further estimating the market power of the enterprise. Finally, by regression model, the main results affecting market forces can be obtained, as shown in Table 3. Due to the lack of data in some variables (such as advertising and R&D) and the possible omission of important explanatory variables, the model's goodness of fit (R^2) is not high, especially in soybean oil, rapeseed oil, and rice. In the pork and beef processing industries, the expansion is less than 0.1, which is the biggest flaw in this study. The parameter estimates of the random boundary cost function are shown in Table 2.

3.1. Corporate Behavior and Market Power. According to the "structure-behavior-performance" paradigm, corporate behavior is the decisive factor in shaping market forces. In a market economy environment, companies generally use a variety of means to achieve their business objectives of minimizing costs and maximizing profits.

3.1.1. Advertising and R&D. Advertising and R&D are the most important means for enterprises, and they are also the most common business strategy. The former has a significant effect on maintaining product prices and promoting product sales, while the latter is a key means to maintain product quality and diversity and enhance the core competitiveness of enterprises. In the food industry, product brand awareness, reputation, quality and safety, diversification, packaging, quality, taste, and other aspects of improvement, to promote and enhance product prices, have a great role in promoting. Therefore, there is reason to believe that advertising and R&D investments are likely to be important factors in promoting the formation of corporate market forces.

Due to the data published in the "China Industrial Enterprise Database", the lack of data on corporate advertising and R&D is more serious. In addition, many food companies in China have invested little or even zero investment in this area. Therefore, in the estimation results of the model, the coefficients of these two variables are not significant. Despite that, in some industries with large sample sizes, some better estimates are still available. Among them, the advertising investment of tobacco and garment processing enterprises has a significant positive impact on their respective market forces, but the impact is very small. The former has an elasticity value of 0.1 and the latter has only 0.02. The advertising investment of automobile processing enterprises has a significant negative impact on its market power, and the impact is also very small, at 0.02, which is inconsistent with empirical judgment. Although the coefficient of advertising investment in other industries is not significant, the coefficient values are mostly positive, which confirms the promotion of advertising to market power to a certain extent. Among the estimated coefficients of R&D investment, the coefficient value is 0.1 to 0.06, which indicates that in these two processing industries, the market power will increase by 0.1% and 0.06% for

Table 3: ADF test results.

Variable	Level	First order difference	Number of unit roots
RPt	−1.93	−7.55	RP$t \sim I(1)$
RBt	−1.69	−5.47	RB$t \sim I(1)$
RLt	−1.41	−7.20	RL$t \sim I(1)$
RCt	−2.65	−9.87	RC$t \sim I(1)$
PPt	0.30	−7.36	PP$t \sim I(1)$
Lt	4.10	−0.39	$Lt \sim I(1)$
NWt	−2.62	−13.20	NW$t \sim I(1)$
EX1	−2.87	−8.28	EX1 $\sim I(1)$
EX2	−3.34	−9.81	EX2 $\sim I(1)$
EX3	−2.62	−9.81	EX3 $\sim I(1)$
EX4	−2.41	−16.41	EX4 $\sim I(1)$

every 1% increase in R&D investment. As with the ad input variable, although the coefficient of R&D investment in most industries is not significant, the estimates are mostly positive.

3.1.2. Government Policies and Market Forces. Government policy is an important factor influencing market forces and has become a consensus in the academic community. However, in China, the influence of government policies on the market power of enterprises varies greatly depending on the nature of the industry and it has a decisive influence on the formation of market forces in certain special industries (such as state-owned monopoly industries and cutting-edge technology industries). The impact on market forces in the general industry may be relatively small.

The impact of government policies on market forces is very complex. Because the data used in this paper is enterprise-level panel data, it may affect the market power of each company, and there are not many government policy variables that can be quantified. This paper selects two indicators, tax and subsidy, both of which can be obtained directly from the database.

3.1.3. The Nature of Corporate Property Rights and Market Forces. For a long time, state-owned enterprises have suffered from various diseases in the monopoly and management efficiency. In the eyes of many people, state-owned enterprises have even become synonymous with monopoly and inefficiency. Regardless of whether this view is too extreme, it is well known that state-owned enterprises, with their own superior position, have more favorable treatment than private enterprises in many aspects and fields such as industry access, bank loans, and administrative examination and approval. Does state-owned capital holdings have a significant impact on the market power of enterprises? From the current research progress, the answer to this question is only at the level of empirical judgment or simple data analysis. There is no strong evidence to support both the positive and the negative. .

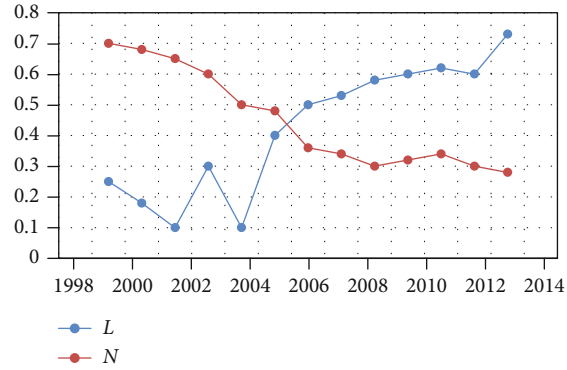

Figure 3: Trends in the number and market power of tobacco processing enterprises in China.

3.1.4. The Market Structure. First, there is often a relationship between the number of firms in an industry and the average market power of firms. In general, The smaller the number of enterprises, the higher the concentration, the larger the average size of the enterprise, and the stronger the average market power of the enterprise. In China's food industry, the structure of certain industries has undergone earth-shaking changes since the reform and opening up. Through mergers and acquisitions between enterprises, the production capacity is quickly concentrated to enterprises with high production efficiency and good management efficiency. Compared with the previously dispersed small enterprises, the large-scale enterprises after the merger and reorganization have more prominent economies of scale and the integration of horizontal and vertical chains is also higher, which is why it is easy to produce the so-called scope economy and economies of scale. These are all beneficial to the company to save production costs, control product prices, and thus increase the market volume of enterprises.

Taking the tobacco processing industry as an example, since 1999, China's tobacco processing industry has implemented a merger and reorganization policy with "Guanxiao-Fuda" as its main strategy, and the number of tobacco processing enterprises and cigarette brands has declined rapidly. The number of cigarette industrial enterprises with legal person qualification decreased from 143 in 2001 to 30 in 2011, and the average production scale of cigarettes per enterprise increased from 240000 to 1.61 million; the number of cigarette brands decreased from 1049 in 2001 to 2004 nearly 210 brands were reduced each year. At the same time, the market power of tobacco companies as a whole is rising, especially after 2003; the value of the Lerner index rose rapidly from 0.1 to 0.7 in 2011, as shown in Figure 2. It shows that there is a clear reverse trend between the number of tobacco processing enterprises in China and the market forces. This result is basically consistent with the previous judgment. Under the influence of these policies, the number of cigarette companies and the number of brands have been greatly reduced. Figure 3 shows the trend of the number of Chinese tobacco processing companies and market strength.

However, in the strict sense, the exact causal relationship between the two is far more than that simple. In the absence of scientific theoretical methods, it can only be inferred from

the existing data, as well as experience and logic that the reduction in the number of firms may lead to an increase in market power, and it cannot be assumed that such a relationship exists between the two. At least, changes in market power are also affected by many other factors.

4. Adjustment of Market Power

4.1. The Impact of Market Forces on Price Transmission. The price transfer between vertically related markets often shows a certain asymmetry, mainly including two situations: first, the speed and amplitude of the transmission between the upstream and downstream prices in the industrial chain are asymmetrical, that is, the price of the upper (lower) tour changes. The grid does not change at the same time or at the same extent, and the second is that the price of the lower (upper) tour does not respond to the price increase and decline of the upper (lower) tour. Symmetrically, when the price of the upper (lower) tour is more fully or quickly transferred to the lower (upper) tour price than the fall, it is "positive" asymmetric price transfer and vice versa is a "negative" asymmetric price transfer.

In real life, many economic variables do not function in one direction but often influence each other and jointly promote the operation of the entire economic system. At the same time, time series variables generally have their own and cross-span effects, that is, the current observations of endogenous variables are affected by the value of the variable itself and other endogenous variables [16]. The effects of these aspects are traditional single-equation models, and even the simultaneous equation model is difficult to reveal effectively. Until 1980, Sims proposed a vector autoregressive (VAR) model to make this problem reasonable. Therefore, a large number of scholars try to use the VAR model to study the price transfer problem. Although there are some differences in the selection of variables or specific functional forms, the main ideas are developed under the framework of the VAR model.

Based on the VAR model, Engle and Granger combine the counteraction theory with the error correction model and propose a vector error correction (VEC) model. The VEC model can basically eliminate the possible trend of the variables by using the first-order difference and avoid the "pseudoregression" problem to some extent. At the same time, the error correction term retains the important information of the variable level value, so it is used by some scholars to analyze the price. Pass the question, most of the relevant empirical researches in China fall into this category, that is, using VAR or VEC models, focusing on the analysis of price transfer between vertically related markets from the perspective of the statistical relationship of time series data. In general, such models biased toward econometric theory and techniques have strong advantages in empirical analysis and can overcome the drawbacks of pure theoretical models that are difficult to regress with data. At the same time, this kind of measurement model is gradually improved in the continuous development and the reliability of the model is increasingly enhanced. The biggest shortcoming lies in the lack of theoretical foundations, especially when the causal relationship between variables is not clear and the conclusions drawn are easily questioned.

4.2. The Measurement Model. A large number of studies have shown that the VAR model has certain advantages in analyzing time series data, which can not only avoid the "pseudoregression" problem caused by the traditional method due to data instability but also better fit the dynamic relationship between variables. The VAR(p) constructed in this paper is

$$Xt = \Phi 1Xt - 1 + \Phi 2Xt - 2 + \cdots + \Phi pXt - p + \Psi wt + \varepsilon t, \quad t = 1, 2, \cdots, T. \tag{4}$$

Among them, Xt is the kxl dimension endogenous variable, wt is the price of pork and its substitutes in this article, p is a dxl dimension exogenous variable, that is, the supply and demand shock of pork, P is the lag order, and T is the sample size. The estimated coefficients are kxk dimensional matrices. And Φp is the kXd dimensional matrix Ψ, and εt is a kXl dimensional perturbation vector, which can be correlated with each other but cannot be related to its own hysteresis value. The εt covariance matrix is $\sum$ which a kXk dimensional positive definite matrix.

When the time series data is nonstationary, the VEC model can obtain effective estimation and test results. Thus, the model can be converted to

$$\Delta Xt = \alpha\beta' Xt - p + \sum_{i=1}^{p-1} \gamma i \Delta Xt - 1 + \Psi wt + \varepsilon t, \quad t = 1, 2, \cdots, T. \tag{5}$$

In which, β is the rxk dimension vector representing the counteraction relationship between endogenous variables, that is, the long-term equilibrium relationship between retail and production prices and the retail price of substitutes, which determines the number and form of counteraction relations; k_{xr} represents the dimension vector a. The error correction coefficient represents the speed at which the equilibrium relationship between prices is adjusted to the equilibrium state when it deviates from the long-term equilibrium state. After analyzing the counteraction relationship between the variables, this paper uses the generalized impulse response function to further estimate how the impact of the supply and demand affects the price and its transmission when a food safety incident occurs. At the same time, this method can also test whether market forces will affect the asymmetric transmission of food prices in the production and retail sectors.

4.3. Data Description. The data used in this paper are monthly time series data, and the sample period is from January 1 to December 2010 for a total of 120 months. RP_t, RB_t, RL_t, and RC_t represent the retail prices of food 1, food 2, food 3, and food 4, respectively, and the latter three are the substitute prices of food 1; PP_i is the purchase price. L_t is the average monthly salary of employees in manufacturing urban units. Since the relevant departments in China only announces quarterly wage levels, L_t is based on quarterly

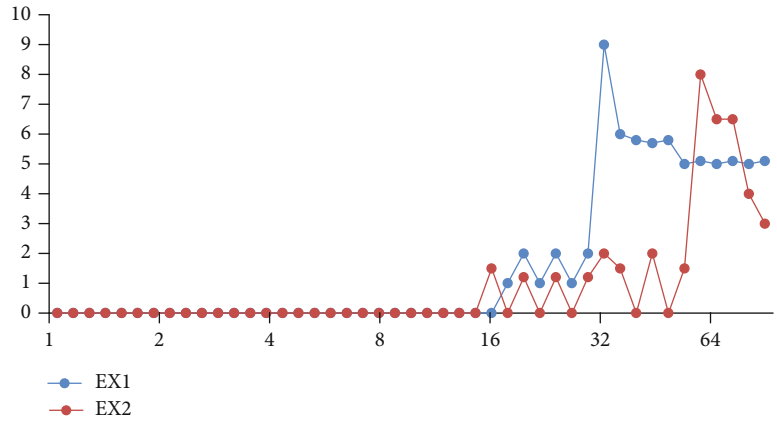

Figure 4: About the number of negative news reports.

Table 4: The results of counteraction analysis.

Explained variable	Explanatory variables
RPt	32.78 + 2.44RBt − 5.38R$L t$ + 3.2RCt + 4.1EX1 − 0.15NWt (3.21) (−5.69) (3.97) (6.67) (-5.72)
	5.78 + 1.33RBt − 1.72RLt + 1.54RCt + 0.48EX1 − 0.04NWt (5.10) (−5.32) (5.91) (3.79) (−5.25)
	6.65 + 1.35RBt − 0.33RLt + 0.44RCt + 1.36EX1 − 0.06NWt (2.06) (−0.47) (0.7) (−3.10) (−3.42)
	5.37 − 0.16RBt − 0.52RLt + 0.76RCt + 0.02EX1 + 0.44NWt (−0.29) (1.26) (1.61) (0.08) (2.95)
RPt − PPt	15.78 + 0.98RBt − 2.30RLt + 1.11RCt + 1.98EX1 − 0.07NWt (2.49) (−5.00) (2.88) (6.58) (−5.34)
	3.78 + 0.23RBt − 0.25RLt + 0.19RCt + 0.14EX1 − 0.01NWt (2.06) (−1.74) (1.68) (2.49) (−1.73)
	1.58 + 0.36RBt + 0.28RLt − 0.33RCt + 1.36EX1 − 0.06NWt (1.00) (0.73) (−0.95) (−3.18) (4.39)
	2.37 − 0.16RBt − 3.45RLt + 3.76RCt + 0.89EX1 + 0.02NWt (−2.03) (3.13) (−0.12) (0.74) (3.84)

salary conversion and the accuracy is poor. NWt is the net export (export-import) quantity, which represents the supply shock of food.

When a food safety incident occurs, the net export volume tends to change accordingly. The change in the volume of imports and exports will inevitably have a full impact on the supply of domestic food. Therefore, it is a better choice to use the net export of pork as a substitute for supply shock. EXl, EX2, EX3, and EX4 represent the media exposure index of the event impact variable. After the natural logarithmic transformation, the measurement model is introduced. This paper is called the media exposure index.

In empirical research, these impact variables are difficult to quantify. Because the time span of the impact cannot be accurately evaluated, the method of dummy variables is not necessarily the most effective. This article selects the number of news stories for each type of event as a surrogate variable for these shocks. From the perspective of knives and demand, news reports are the most important source of consumer confidence and access. The negative reports of food safety incidents will hurt the consumer confidence of the people and affect their consumption of food 1; from the perspective of supply, when the epidemic broke out, the relevant news reports were overwhelming, and as the epidemic gradually eased, the number of reports also corresponded accordingly. Therefore, it is a relatively good choice to replace these variables with the number of news reports. Figure 4 shows the number of negative news reports.

4.3.1. Estimated Results. Since time series data often exhibits nonstationary characteristics, it is necessary to perform a smooth test on the data before performing the metering regression; otherwise, a "pseudoregression" problem will occur. This paper uses the ADF (augmented Dickey-Fuller) method; the test results are shown in Table 3.

It can be seen from the test results in Table 3 that except L , which is a two-order difference stationary (that is, there are two unit roots), the other variable is the first-order difference. Therefore, in addition to L, the remaining variables can be constructed into VAR and VEC models for further quantitative analysis.

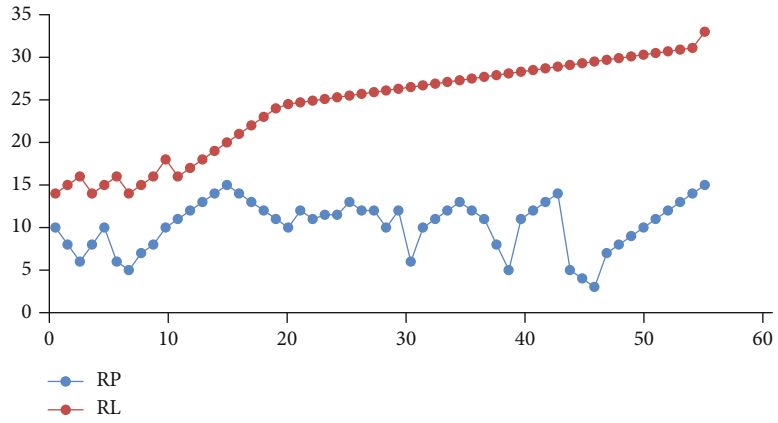

Figure 5: Changes in retail prices of food 1 and substitute.

4.3.2. Counteraction Analysis. This paper introduces four types of negative event shocks into different models, on the one hand, to distinguish the four types of impacts. The impact of food prices on supply and demand and the direction of the impact are different; on the other hand, considering the placement of four shock variables in the model, there may be an obvious collinearity problem [13]. That is, some events may occur at the same time. If they are placed in the same model, it is impossible to distinguish which impact variable from which the effect is derived. The results of the countermeasure analysis are shown in Table 4.

In the absence of food safety incidents, the increase in net exports (NWt) will reduce the supply of food in the domestic market, causing food prices to rise, which creates a "positive effect", as shown in Figure 5; at the time of food supply, since the decrease in net exports (increased net imports) is negligible compared to the reduction in supply due to news, its "positive effect" on prices is relatively weak; at the same time, consumers will compete to purchase relatively reliable imported foods. This raises the price of imported food and produces a more significant "negative effect." At this time, the supply of domestic food was originally in short supply and the price of food increased. Therefore, in many cases, the reduction in net out days will lead to a huge increase in food prices in the event of a negative news outbreak.

The price of substitutes has a positive impact on the price transfer of the pork industry in most cases, that is, the price increase of substitutes will lead to an increase in pork prices and the price of live pigs does not increase rapidly or equally, thus expanding pork retail and production. The changes in retail prices of food and substitutes are shown in Figure 5.

5. Conclusion

This paper uses monthly time series data to study the impact of food safety incidents of e-commerce food companies on prices and their transmission in vertical associated markets and analyses the role of market forces in them. Research indicates that first, there is a clear asymmetry in the price transfer of China's food industry. The impact of food safety incidents on the retail price of food is greater than its impact on the purchase price. Second, China's food retailers have a certain market power, which is an important reason for the asymmetric transmission of food industry prices. Although we cannot deny that the gap between food retail and production prices is related to other marketing or regulatory costs, the test results show that market forces do have an impact on the difference between the two prices. Third, the impact of different types of security incidents on pork prices and their transmission is not consistent. Some have a significant positive impact on food prices, while also increasing the gap between food retail prices and production prices, while others have the opposite effect, not only causing food retail prices to fall but also shrinking retail and the gap in production prices. And fourth, in different food safety incidents, the net export of food and food (supply shock) has different effects on pork prices and their transmission. At the same time, in the price transfer model, net exports will offset the impact of some negative news to narrow the gap between food retail and production prices; conversely, net exports will increase the impact of negative news events on price transmission.

Data Availability

All author information is available from the author.

Conflicts of Interest

We declare that there is no conflict of interest regarding the publication of this article.

References

[1] E. T. Nwaeze, "The adjustment process of accruals: empirical evidence and implication for accrual research," *Review of Quantitative Finance & Accounting*, vol. 17, no. 2, pp. 187–211, 2001.

[2] C. Proa, "Gradual wage-price adjustments, labor market frictions and monetary policy," *Journal of Economic Behavior & Organization*, vol. 82, no. 1, pp. 220–235, 2012.

[3] S. Bauer, S. Lazarev, A. Molinari et al., "The power of in situ pulsed laser deposition synchrotron characterization for the detection of domain formation during growth of

Ba0.5Sr0.5TiO3 on MgO," *Journal of Synchrotron Radiation*, vol. 21, no. 2, pp. 386–394, 2014.

[4] T. S. H. Teo, S. Lin, and K. H. Lai, "Adopters and non-adopters of e-procurement in Singapore: an empirical study," *Omega*, vol. 37, no. 5, pp. 972–987, 2009.

[5] Y.-R. Lee, X. Jin, and H.-J. Kim, "Node localization based on neural network using semi-supervised learning in wireless sensor networks," *The Journal of Korean Institute of Communications and Information Sciences*, vol. 44, no. 3, pp. 517–527, 2019.

[6] I. Černý, A. Veverková, M. Kovár, V. Pačuta, and J. Molnárová, "Influence of temperature and moisture conditions of locality on the yield formation of sunflower (Helianthus annuus L.)," *Acta Universitatis Agriculturae Et Silviculturae Mendelianae Brunensis*, vol. 59, no. 6, pp. 99–104, 2014.

[7] O. Hassan, K. Salahddine, K. Khaoula, E. Lahoucine, and K. Salah-Ddine, "Secure data for wireless sensor network using detection malcious node method," *Test Engineering and Management*, vol. 82, no. 1-2, pp. 4968–4982, 2020.

[8] J. P. V. Pinheiro, E. Ahlke, U. Nowak-Göttl et al., "Pharmacokinetic dose adjustment of Erwiniaasparaginase in protocol II of the paediatric ALL/NHL-BFM treatment protocols," *British Journal of Haematology*, vol. 104, no. 2, pp. 313–320, 2015.

[9] L. Wang, Q. Guo, and J. G. Liu, "Measuring node importance based on weighted nonlinear method," *Application Research of Computers*, vol. 35, no. 5, pp. 1426–1428, 2018.

[10] Y. Cheng, Q. Liu, J. Wang, S. Wan, and T. Umer, "Distributed fault detection for wireless sensor networks based on support vector regression," *Wireless Communications and Mobile Computing*, no. 5, pp. 1–8, 2018.

[11] S. Dolha, P. Negirla, F. Alexa, and I. Silea, "Considerations about the signal level measurement in wireless sensor networks for node position estimation," *Sensors*, vol. 19, no. 19, pp. 41–79, 2019.

[12] G. Y. Liu, S. Tang, D. Li, and J. Hu, "Self-adjustment of calcium phosphate coating on micro-arc oxidized magnesium and its influence on the corrosion behaviour in simulated body fluids," *Corrosion Science*, vol. 79, no. 3, pp. 206–214, 2014.

[13] I. Černý, "Veverková, Alexandra, Kovár, Marek, et al. Influence of temperature and moisture conditions of locality on the yield formation of sunflower (Helianthus annuus L.)," *Acta Universitatis Agriculturae Et Silviculturae Mendelianae Brunensis*, vol. 59, no. 6, pp. 99–104, 2014.

[14] J. M. Barros Neto, E. A. Anjos, S. E. Silva, C. M. Tavares, and A. N. Pedro, "The formation of the professional nurse and the labor market today," *Revista Gestãoe& Saúde*, vol. 5, no. 1, pp. 176–193, 2014.

[15] J. P. Vieira Pinheiro, E. Ahlke, U. Nowak-Göttl et al., "Pharmacokinetic dose adjustment of Erwinia asparaginase in protocol II of the paediatric ALL/NHL-BFM treatment protocols," *British Journal of Haematology*, vol. 104, no. 2, pp. 313–320, 2015.

[16] A. Gavrin, B. N. Kaiser, D. Geiger et al., "Adjustment of host cells for accommodation of symbiotic bacteria: vacuole defunctionalization, HOPS suppression, and TIP1g retargeting in Medicago," *Plant Cell*, vol. 26, no. 9, pp. 3809–3822, 2014.

[17] Y. Guangyou, X. Chenbo, G. Xiong, and Z. Tuo, "Energy efficient node deployment optimization for cts based on cooperative beamforming in single-hop wireless sensor networks," *Automatic Control and Computer Sciences*, vol. 54, no. 2, pp. 147–155, 2020.

[18] Y. F. Badir and G. C. O'Connor, "The formation of tie strength in a strategic alliance's first new product development project: the influence of project and partners' characteristics," *Journal of Product Innovation Management*, vol. 32, no. 1, pp. 154–169, 2015.

Hindawi
Wireless Communications and Mobile Computing
Volume 2021, Article ID 6626480, 11 pages
https://doi.org/10.1155/2021/6626480

Research Article

Analysis of Customization Strategy for E-Commerce Operation Based on Big Data

Su Chen

School of International Trade and Economics, Ningbo University of Finance and Economics, Ningbo 315175, China

Correspondence should be addressed to Su Chen; suchen@nbufe.edu.cn

Received 3 October 2020; Revised 20 October 2020; Accepted 5 February 2021; Published 26 February 2021

Academic Editor: Hongju Cheng

Copyright © 2021 Su Chen. This is an open access article distributed under the Creative Commons Attribution License, which permits unrestricted use, distribution, and reproduction in any medium, provided the original work is properly cited.

In order to improve the efficiency of customization and reduce the cost of customization under Big data environment, this paper uses cost-sharing contract, pricing mechanism, Hotelling model, and game theory tools and research methods, for C2B Electronic Commerce (e-commerce) mode of Supply Chain Pricing Strategy for in-depth discussion. This paper first gives the architecture of the customization service system based on big data. The paper studies the game equilibrium of supply chain members under four scenarios: centralized decision-making, decentralized decision-making, C2B-dominated decision-making, and traditional enterprise-dominated decision-making in a supply chain composed of a supplier and C2B e-commerce enterprises with horizontal price competition, and examines the cross-price. Important parameters such as impact coefficient, impact coefficient of effort degree of personalized customization, and so on have an impact on variables such as effort degree of personalized customization, retail price, and profit of supply chain members of C2B e-commerce enterprises. Research shows that with the increase of cross-price impact coefficient, C2B e-commerce will enhance its personalized customization efforts in different situations in order to pursue higher profits.

1. Introduction

With the continuous development and popularization of Internet technology, e-commerce has begun to challenge the traditional business transaction model and become an important market force, affecting the development process of the world economy [1, 2]. E-commerce is a new business model based on the Internet as a trading platform. Since its appearance in the 1990s, its development momentum has been very rapid. Under the circumstance of making full use of Internet resources, e-commerce has incomparable advantages over the traditional business model [3, 4]. It can realize cross-regional and all-weather business, with a complete range of goods, easy retrieval, low cost, and can provide personalized services for consumers. All these are the unique features of electronic commerce born on the Internet [5].

C2B module customization: this C2B model is mainly to meet the personalized needs of specific groups formed a model, with a strong market target orientation; usually, the success rate of marketing will be relatively large [6]. Typically, such as Haier Home Appliances Customization Service, Blue Orange Mobile Phone, etc. are trying this kind of service. Consumers choose and combine the performance of the components according to their own needs when placing an order, and then, the manufacturer produces according to the combination requirements in the order [7]. However, the C2B mode of this module combination requires higher production efficiency of the enterprise production line, and this so-called function combination cannot really integrate the opinions of consumers. Consumers' choice is just to arrange and combine the existing functions within the range given by the manufacturer [8]. Restrictions on objective conditions of the needs of consumers [9, 10]. Mass customization refers to the new mode of production produced by enterprises in order to adapt to the new market environment. With the diversification and customization of products aggravating economic value and strategic advantages, the demand of consumer personalized customization needs to be urgently met [11]. The realization of mass customization is facilitated. Mass customization is an important way to enhance the competitiveness of enterprises, so more and more supply chain enterprises also realize the importance

of pricing in the case of mass customization. Some researchers study the product pricing problem of mass customizer and distributor under the condition that product price and lead time affect demand and analyze the lead time strategy and optimal pricing strategy of supply chain enterprises under centralized decision, decentralized decision, and mass customizer-led decision. Based on this, a commission contract is proposed. It can effectively coordinate the lead time and pricing problem of mass customization supply chain. Literature investigates the product pricing problem under mass customization and analyzes the time problem of price change from the perspective of internal operation decision-making in order to achieve the goal of maximizing profit [12]. Under the condition of certain mass customization capability, how to analyze the individual demand of consumers and determine the degree of customization effort of products are discussed. E-commerce refers to the use of any information and communication technology for any form of business or management operations or information exchange. The relationship between enterprise income and customer satisfaction and customization degree is discussed. The model and algorithm of optimizing output are established, and the optimum degree of customization is determined to maximize profits [13].

In order to improve the efficiency of customization and reduce the cost of customization under Big data environment, this paper uses cost-sharing contract, pricing mechanism, Hotelling model, and game theory tools and research methods, for C2B Electronic Commerce (e-commerce) mode of Supply Chain Pricing Strategy for in-depth discussion. This paper first gives the architecture of the customization service system based on big data. The paper studies the game equilibrium of supply chain members under four scenarios: centralized decision-making, decentralized decision-making, C2B-dominated decision-making, and traditional enterprise-dominated decision-making in a supply chain composed of a supplier and C2B e-commerce enterprises with horizontal price competition, and examines the cross-price. Important parameters such as impact coefficient, impact coefficient of effort degree of personalized customization, and so on have an impact on variables such as effort degree of personalized customization, retail price, and profit of supply chain members of C2B e-commerce enterprises. Research shows that with the increase of cross-price impact coefficient, C2B e-commerce will enhance its personalized customization efforts in different situations in order to pursue higher profits [14].

2. Electronic Commerce's Customization System Based on Network Big Data

2.1. The Big Data Platform for Electronic Commerce. The implementation of C2B customization mode requires the active participation of consumers, but the participation of consumers requires enterprises to spend more energy to achieve, which will inevitably cause a burden on the cost of enterprises. However, under the influence of the big data era, we can make full use of the collected large data to realize the "big data customization" C2B mode [15]. This mode is actually based on the full analysis of the collected massive data, mining valuable information for enterprises, usually consumers' consumption habits. Methods and characteristics, and then the integration of various social resources based on large data extracted from useful information for product production. The intelligent tourism system architecture based on big data technology is shown in Figure 1.

The data that can be used in the personalization of e-commerce are mainly click traffic data of website and mobile device data. In our daily life, we can also integrate the personal data of e-commerce users through some records with the characteristics of identifying users to form a complete set of personalized e-commerce recommendation data. For effective marketing and promotion, every click and its time on the Internet are recorded, and with this data, service providers can carefully analyze user access patterns to provide more targeted services. User personalized behaviour data mainly include social network, logged-in sites, page stay and news, search keywords, mobile phone click applications, and LBS-based user behaviour data.

E-commerce data is becoming more and more huge, traditional databases will have query bottlenecks, whether in storage or inquiry, there are performance bottlenecks, user applications and analysis results show a trend of integration, real-time and response time requirements are getting higher and higher, the model used is becoming more and more complex, and the amount of calculation increases exponentially, traditional skills. Unable to deal with large data: mobile customer data volume to TB level; Oracle database SQL statements can get results, but hope to further improve efficiency.

According to the existing personalized recommendation structure, the improved E-commerce can be divided into four modules: data integration, data preprocessing, model algorithm, and online recommendation of products. Starting from the data integration, the user's personal information is collected from all aspects, and the user's personalized data is fully grasped from the data source. Then, the formatted data are stored in the database through data preprocessing, and the effective analysis data are extracted by e-commerce. Using e-commerce personalized recommendation technology, by matching the existing recommendation patterns, a certain rule is stored in the database. When the user browses the relevant information in the e-commerce website, the recommendation information is returned to the client through the current session to complete an effective e-commerce personalized recommendation activity.

2.2. CBR Architecture of Customization Service in Electronic Commence. CBR architecture of customization service in electronic commerce is shown in Figure 2.

The theory of customization service is to adjust the information organization mode to provide the best service according to the specific consumption mode of each user. But the convergence of the crowd consumption shows that it is feasible to divide the consumption behaviour mode according to the user group. For large-scale e-commerce service providers, it does not reduce the quality of customized service. On the premise of quantity, this partition can greatly reduce information load. CBR is precisely an idea to solve new problems

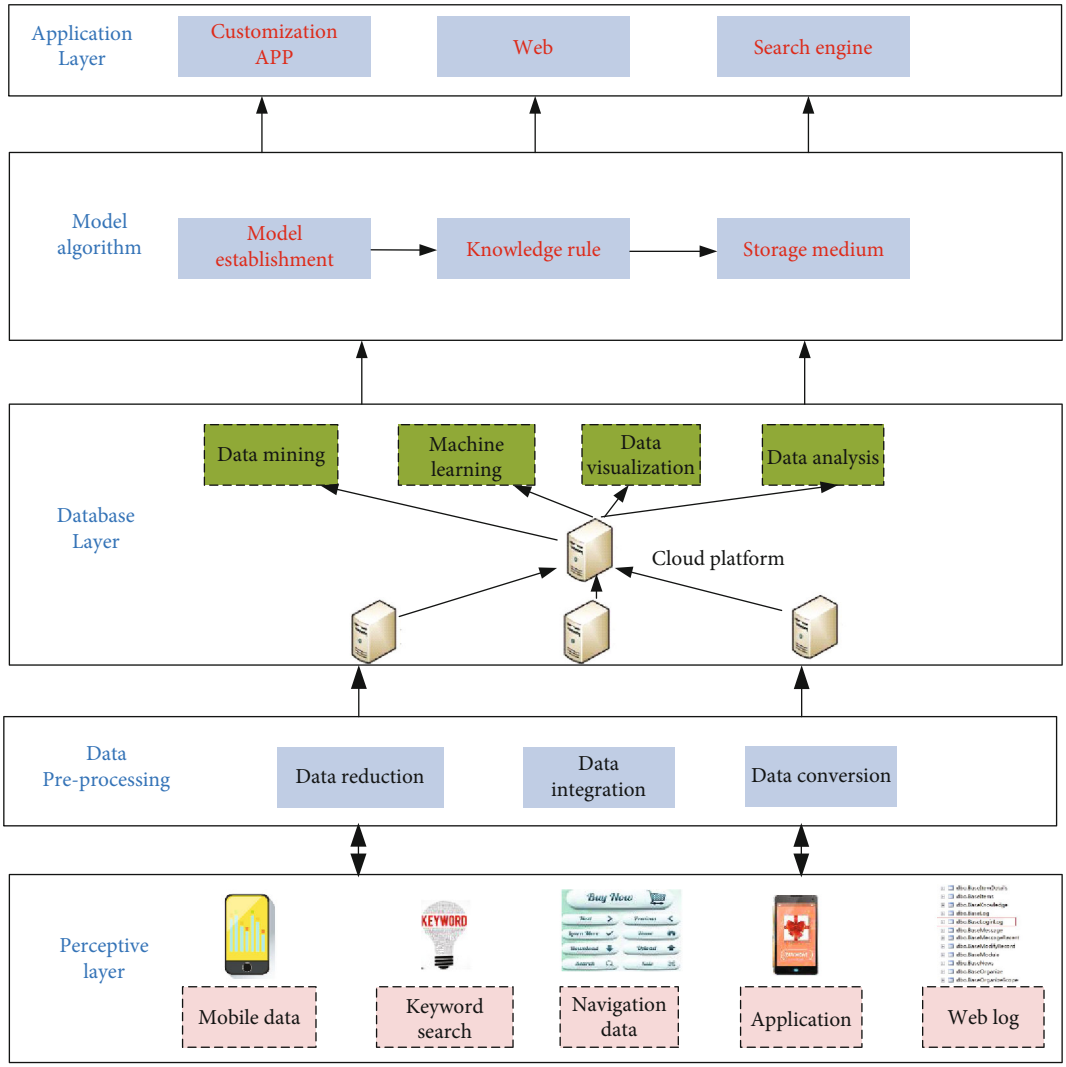

Figure 1: The intelligent tourism system architecture based on Big data technology.

with the help of past experience. It is embodied in customized services, that is, to provide a single user with the information services necessary to complete network consumption behaviour by using the known classification of consumer behaviour patterns. The mature CBR technology provides a complete set of solutions for the realization of customized services in e-commerce environment. On this basis, we give the client/server structure of customized service CBR, as shown in Figure 2. The "customization" is the abbreviation of customization service, and the algorithm is the abbreviation of rewriting algorithm.

Due to the uncertainty of the number of online customers, the scalability of the system becomes very important. The client/server architecture is used to meet this need. The client is a plug-in (such as Java Applet) that can run on a standard WWW browser, and the server includes two server modules, the control centre and the customized service (corresponding to the retrieval and rewriting of the traditional CBR, respectively), which can be distributed on multiple computers. The typical customization service process is as follows: the client application starts, establishes a connection between the customized client and the case control centre, requests the product customization service, a control centre for customer verification, and returns the product information. The customized client submits the product information to the customized server and requests the case to rewrite the customized server. According to the product information, the algorithm server chooses the corresponding mechanism from the algorithm library to rewrite. The customized client interacts with the customized client repeatedly until the user stops the loop by accepting or rejecting the result of rewriting. The customized client returns the final result recognized by the user to the control centre for restarting.

3. C2B Electronic Commerce Pricing Strategy considering Customized Effort

In today's information economy era, customers need personalized products and services more and more. However, some enterprises set the same price instead of charging different consumers different prices according to their perceived consumption value, thus losing a lot of potential benefits. In fact,

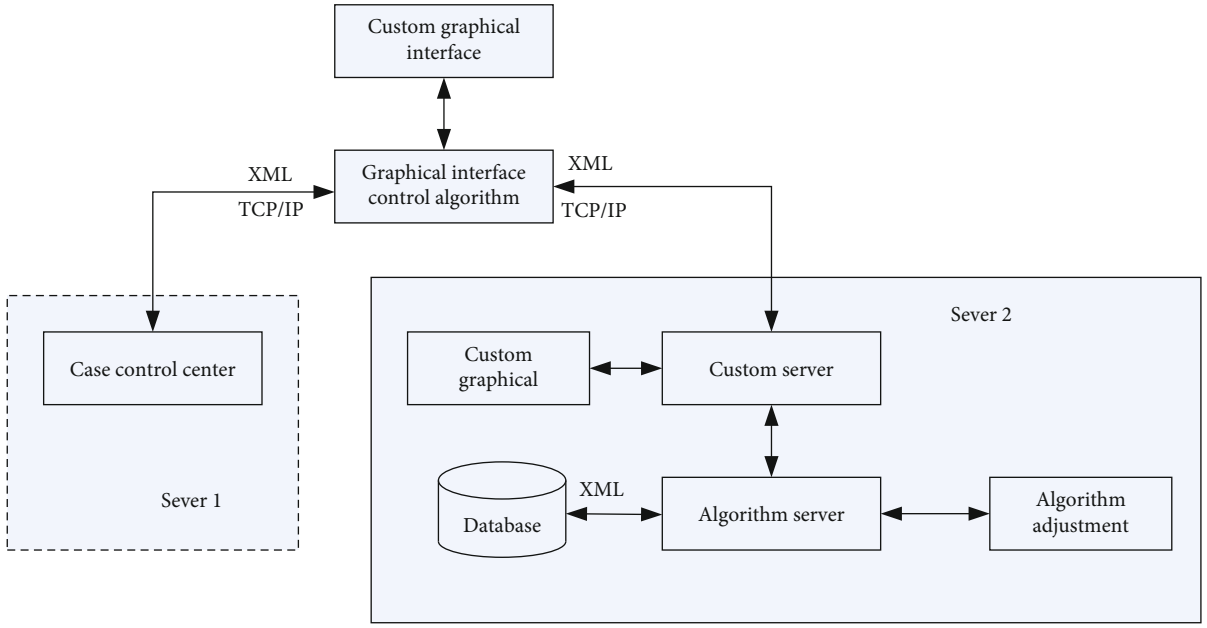

Figure 2: CBR architecture of customization service in electronic commerce.

different customers have a variety of needs, C2B electronic commerce (e-commerce) enterprises should adopt personalized customized pricing strategy according to actual needs; in order to improve consumer value, further expand market demand, thus greatly improving economic benefits.

Most of the traditional supply chain enterprises are affected by other supply chain members. By pricing and inventory flow, suppliers always dominate the supply chain. But with the rapid development of the economy, manufacturers and retailers are shifting their positions in the transaction, leading retailers like Carrefour, Best Buy, and Wal-Mart are rising, and their power structure in the supply chain will change accordingly. In order to survive and develop in the fierce competition, supply chain enterprises must analyze the behaviour of their competitors and make reasonable decisions according to the actual situation in order to win a place for themselves.

3.1. Mathematical Strategy Model Analysis and Symbol Description. Consider a two-echelon supply chain structure model consisting of a supplier and two manufacturers with horizontal price competition (a C2B e-commerce enterprise and a traditional enterprise). The supplier and C2B e-commerce enterprises as well as the traditional enterprises are risk-neutral, and the market demand and cost parameters are also their common information. The supplier provides general parts to C2B e-commerce enterprises and traditional enterprises at wholesale price w. The C2B e-commerce enterprises deliver the products to customers after individualized customization. The traditional enterprises assemble the general parts into standard products and then ship them. The retail price of individualized customized products is p_c, and the market needs it. Quantity is D_c, the retail price of standardized products is p_s, and the market demand is D_s, D_c and D_s which constitute the whole consumer market. Suppose $w < p_c, p_s$, otherwise, the profits of suppliers and C2B business enterprises and traditional enterprises will be zero. The C2B pricing model is shown in Figure 3.

In the demand function constructed in this paper, the market demand is fixed. The retail price p_c of customized products has a negative impact on the demand D_c of personalized products, a positive impact on the demand D_s of standardized products, a negative impact on the demand D_s of standardized products, a positive impact on the demand D_c of personalized products, and a positive impact on the personality of products. The degree of customization effort e has a positive impact on the demand for customized products and a negative impact on the demand for standardized products. The following demand functions is built as

$$\begin{cases} D_c = 1 - p_c + \theta p_s + \gamma e \\ D_s = 1 - p_s + \theta p_c - \gamma e \end{cases}. \tag{1}$$

In which, $\theta \in (0, 1)$ represents the cross-price influence coefficient, and $\gamma \in (0, 1)$ is the individualized customization effort influence coefficient. From the above demand function, we can see that the market demand D_c is positively correlated with the degree of customization effort e and the retail price p_s of standardized products, and negatively correlated with the retail price p_c of customized products. Market demand D_s is positively correlated with the degree of customization effort e and retail price p_c of customized products but negatively correlated with the retail price p_s of standardized products. The cost function of C2B business enterprise customization effort degree is

$$c_k = \frac{k}{2} e^2. \tag{2}$$

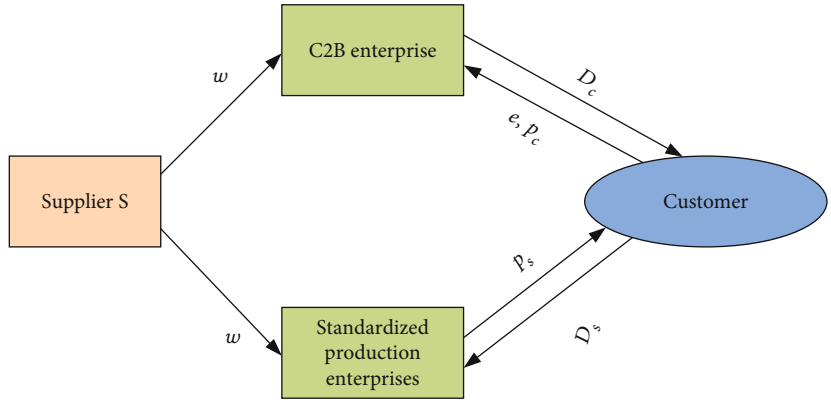

Figure 3: C2B pricing model.

In which, $k > 0$, c_k for personalized customization effort cost parameter. $\partial c_k/\partial e > 0$, $\partial^2 c_k/\partial^2 e > 0$.

3.2. Pricing Model under Centralized Decision and Its Solution. Members of the supply chain want to achieve the goal of maximizing the profit of the supply chain. When the supply chain adopts the centralized decision-making mode, the decision-maker sets the optimal degree of customization effort from the angle of maximizing the profit of the whole supply chain and, then, determines the retail price of C2B e-commerce enterprises and traditional enterprises. The total profit function of C2B supply chain is as follows:

$$\begin{aligned}\pi = {} & (p_c - w)(1 - p_c + \theta p_s + \gamma e) \\ & + (p_s - w)(1 - p_s + \theta p_c - \gamma e) - \frac{k}{2}e^2.\end{aligned} \tag{3}$$

The first derivative p_c and p_s can be obtained:

$$\begin{cases} 1\text{-}2p_c + 2\theta p_s + (1-\theta)w + \gamma e = 0 \\ 1\text{-}2p_s + 2\theta p_c + (1-\theta)w - \gamma e = 0 \end{cases}. \tag{4}$$

In the centralized decision-making situation, the optimal pricing p_c^{cd} and p_s^{cd} of C2B supply chain and the optimal degree of customization effort e^{cd} are as follows:

$$\begin{cases} p_c^{cd} = \dfrac{1}{2(1-\theta)} + \dfrac{1}{2}w \\ p_s^{cd} = \dfrac{1}{2(1-\theta)} + \dfrac{1}{2}w \\ e^{cd} = 0 \end{cases}. \tag{5}$$

In the centralized situation, the decision-maker has no incentive to improve the profit of the whole supply chain through the strategy of individualized customization effort. Although the profit of the whole supply chain has been maximized, consumers cannot buy customized products. In addition, we can conclude that the greater the cross-price influence coefficient, the higher the final pricing of C2B e-commerce enterprises and traditional enterprises. Secondly, there is a positive correlation between the price of products and the wholesale price of suppliers. This is because the higher the wholesale price of suppliers, the higher the purchasing cost of C2B e-commerce enterprises and traditional enterprises will be, so the supply chain enterprises will increase the price in order to achieve considerable profits. In the sense of management, C2B supply chain enterprises should not only meet the individual needs of consumers but also make the cost control of enterprises within a certain range, so as to ensure the necessary profits.

$$\begin{cases} D_c^{cd} = \dfrac{1}{2} + \dfrac{1}{2}w(\theta - 1) \\ D_s^{cd} = \dfrac{1}{2} + \dfrac{1}{2}w(\theta - 1) \\ \pi^{cd} = \dfrac{1}{2}\left(\dfrac{1}{1-\theta} - w\right)([1 + w(\theta - 1)]) \end{cases}. \tag{6}$$

It shows that the market demand of individualized customized products is the same as that of standardized products when the centralized decision-making model is adopted. The market demand is positively correlated with wholesale price, and the influence coefficient of cross-price is also positively correlated. When the influence coefficient of cross-price rises, the market demand of products will increase. The profit of a supply chain is increased.

3.3. Pricing Model and Solution under Decentralized Decision-Making. When decentralized decisions are made, supply chain members are independent individuals. Different from centralized decision-making, C2B e-commerce enterprises and traditional enterprises have different interests in decentralized decision-making. C2B e-commerce enterprises first determine the degree of individual customization effort e , and then, the two enterprises determine the retail prices of two different products p_s and p_c at the same time. In this case, it can be concluded that the profit function of C2B business enterprise and traditional enterprise are

$$\begin{cases} \pi_c^{nl} = (p_c - w)(1 - p_c + \theta p_s + \gamma e) - \dfrac{k}{2}e^2 \\ \pi_s^{nl} = (p_s - w)(1 - p_s + \theta p_c - \gamma e) \end{cases}. \quad (7)$$

Under the independent and simultaneous decision-making of C2B e-commerce enterprises and traditional enterprises, the optimal pricing p_c^{nl} and p_s^{nl} of supply chain members and the optimal degree of customization effort e^{nl} are as follows:

$$\begin{cases} p_c^{nl} = \dfrac{(w+1)\left[k(2+\theta)^2 - 2\gamma\right] + 2\gamma^2(1 + \theta w - w)}{(2-\theta)\left[k(2+\theta)^2 - 2\gamma\right]} \\ p_s^{nl} = \dfrac{(w+1)\left[k(2+\theta)^2 - 2\gamma\right] - 2\gamma^2(1 + \theta w - w)}{(2-\theta)\left[k(2+\theta)^2 - 2\gamma\right]} \\ e^{nl} = \dfrac{2\gamma(1 + \theta w - w)(2+\theta)}{(2-\theta)\left[k(2+\theta)^2 - 2\gamma\right]} \end{cases}. \quad (8)$$

3.4. Pricing Model and Solution of C2B Business Enterprise Dominated Decision-Making. Considering that C2B e-commerce enterprises which provide customized products play a dominant role, they make decisions first, while traditional enterprises which provide standardized products to consumers follow suit, and the two enterprises make decisions individually. In the model of this section, C2B e-commerce enterprises and traditional enterprises constitute a three-stage sequential game model. In the first stage, C2B e-commerce enterprises determine the degree of effort to customize the product personalized in the second stage, C2B e-commerce enterprises according to the actual situation to determine the price of customized products p_c; in the third stage, traditional enterprises determine the price of standardized products p_s. From this, we get the pricing decision timing of the C2B supply chain. In this case, it can be concluded that the profit function of C2B business enterprise and traditional enterprise are

$$\begin{cases} \pi_c^{cs} = (p_c - w)(1 - p_c + \theta p_s + \gamma e) - \dfrac{k}{2}e^2 \\ \pi_s^{cs} = (p_s - w)(1 - p_s + \theta p_c - \gamma e) \end{cases}. \quad (9)$$

C2B e-commerce enterprises first determine the degree of personalized effort of the product e^{cs}, and then according to the actual situation to determine the price of personalized customized products p_c, and finally the traditional enterprise to determine the price of standardized products to consumers p_s. In this paper, the C2B supply chain model is solved by the inverse induction method of dynamic game. The following conclusions can be drawn. Under the dominant decision-making of C2B business enterprises, the degree of individualized customization of supply chain members is

$$e^{cs} = \frac{(2-\theta)[2 + \theta(w+1)]\gamma - w(2-\theta)\left(2-\theta^2\right)\gamma}{4k\left(2-\theta^2\right) - (2-\theta)^2\gamma}. \quad (10)$$

3.5. The Pricing Model and Solution of Traditional Enterprise Dominated Decision-Making. Considering the dominance of traditional enterprises providing standardized products, C2B e-commerce enterprises that provide customized products to consumers first make decisions, and then, the two enterprises make decisions individually. In the model of this section, C2B e-commerce enterprises and traditional enterprises constitute a three-stage sequential game model. In the first stage, C2B enterprises determine the degree of individualized effort e; in the second stage, the traditional enterprises determine the price PS of standardized products; in the third stage, C2B e-commerce enterprises determine the price PC of personalized customized products according to the actual situation.

In this case, it can be concluded that the profit function of C2B business enterprise and traditional enterprise are

$$\begin{cases} \pi_c^{ts} = (p_c - w)(1 - p_c + \theta p_s + \gamma e) - \dfrac{k}{2}e^2 \\ \pi_s^{ts} = (p_s - w)(1 - p_s + \theta p_c - \gamma e) \end{cases}. \quad (11)$$

Firstly, C2B e-commerce enterprises determine the degree of individual effort e^{ts}; then, the traditional enterprises determine the price p_s of standardized products they provide to consumers, and finally, C2B e-commerce enterprises determine the price p_c of customized products according to the actual situation. Reverse induction is still used to solve the C2B supply chain model.

The customization effort e^{ts} of supply chain members can be expressed as

$$e^{ts} = \frac{2US\gamma + (\theta - 2)w\gamma ST}{4kT^2 - 2S^2\gamma^2}, \quad (12)$$

where $S = -\theta^2 - 2\theta + 4$, $T = 4 - 2\theta^2$, $U = -\theta^2 + 2\theta + 4 + \theta^2 w$.

4. Simulation Results and Discussion

Because the expression of equilibrium decision of supply chain members is very complicated in some situations, it is difficult to get intuitive conclusions. In order to further analyze the relationship between the variables, this section simplifies the model by assuming that the degree of customization effort e is a parameter. Comparing four different decision situations of supply chain members under C2B scenario is conducted in this section.

4.1. The Influence of Cross-Price Influence Coefficient on Decision Equilibrium. Based on the basic model proposed in this paper, the simulation is carried out in the subsection. Considering e as the decision variable, the parameters are assigned as follows according to the actual situation of the enterprise: $w = 0.5$, $\gamma = 1$, and $k = 1$.

The study did not affect the degree of customization effort e. Figure 4 shows that in three different scenarios, with no increase, that is, the more intense price competition, C2B e-commerce enterprises personalized customization

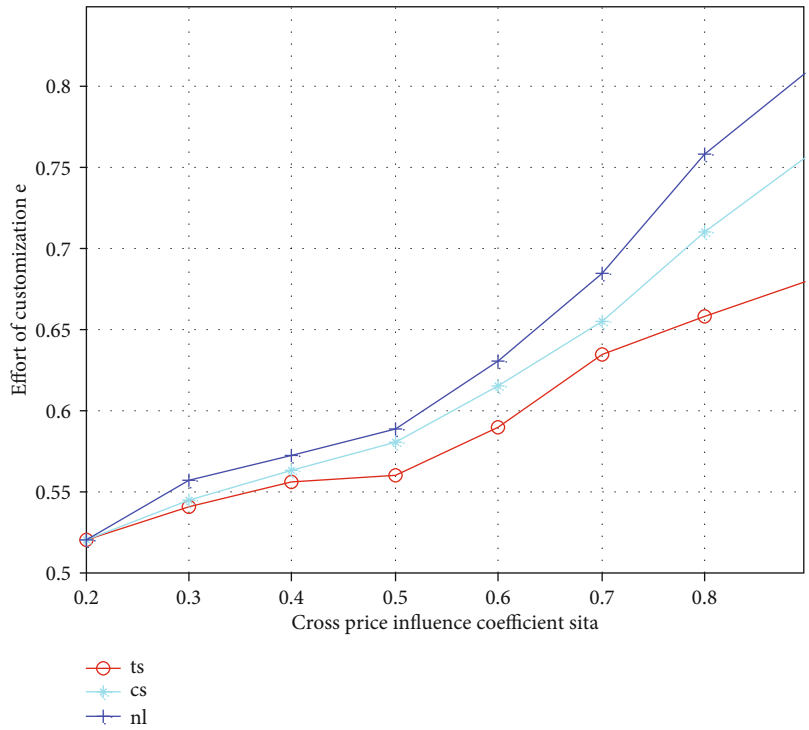

Figure 4: Influence of cross-price influence coefficient θon decision equilibrium.

efforts have increased. This is very understandable, C2B e-commerce enterprises perceive fierce price competition, will set a higher degree of customization efforts to achieve product differentiation, in order to obtain customer orders. It is worth noting that under the C2B e-commerce-dominated situation, C2B e-commerce enterprise personalized customization efforts to improve faster, because in this situation, C2B e-commerce enterprises have the dominant power in price competition, which can better use personalized customization to win the favour of customers.

4.2. The Impact of θ on Standardized Price and Customization Price. Consider the impact of θ on product prices. From Figures 5 to 6, we can see that the price of customized products and standardized products will increase with the increase of cross-price impact coefficient. There is no positive correlation between the price of the product and the increase in the price of θ. The price of standardized products under centralized decision-making mode is the highest, and the price under decentralized decision-making and e-commerce-led mode is higher than that under traditional enterprise-led mode, respectively. The price of standardized products is the lowest under traditional enterprise-dominated situation. The reason for this phenomenon may be that traditional enterprises want to take advantage of their dominant advantages and adopt low price. The competitive strategy of price marketing has won the favour of more consumers.

4.3. The Impact of θ on Standardized Demand and Customization Demand. Consider the impact of θ on product demand. From Figures 7 to 8, we can see that with the increase of cross-price impact coefficient, the demand for personalized customized products and standardized products will increase. From Figure 7, we can see that the demand of customized products is the biggest when traditional enterprises are dominant. The demand of products increases with the increase of θ. The larger θ, the faster the demand is rising. From Figure 8, we can see that the demand for standardized products is the smallest when traditional enterprises are dominant and the demand for standardized products increases slowly when centralized decision-making is taken. This shows that the change of 0 at this time has a weak impact on product demand. When the cross-price influence coefficient is higher than a certain threshold ($\theta > 0.425$), the demand for products in decentralized decision-making scenario is the largest, and when it is not in a certain interval ($0 < \theta < 0.425$), the demand for products in centralized decision-making scenario is the largest. When it is higher than a certain threshold ($\theta > 0.67$), when C2B e-commerce enterprises dominate, the market demand of standardized products is larger than that of centralized decision-making situation, which shows that θ has a greater driving force for product demand in this context.

4.4. The Impact of θ on Profit of e-Commerce Enterprises and Traditional Enterprises. As shown in Figure 9, with the increase of x, the profits of C2B e-commerce enterprises grow rapidly in three different situations, but they are the most profitable under the traditional enterprise-led situation, which is very interesting. This shows that, although C2B e-commerce enterprises cannot bring high profits by dominating price competition, they are more profitable to become followers in pricing. This is because, although the price of

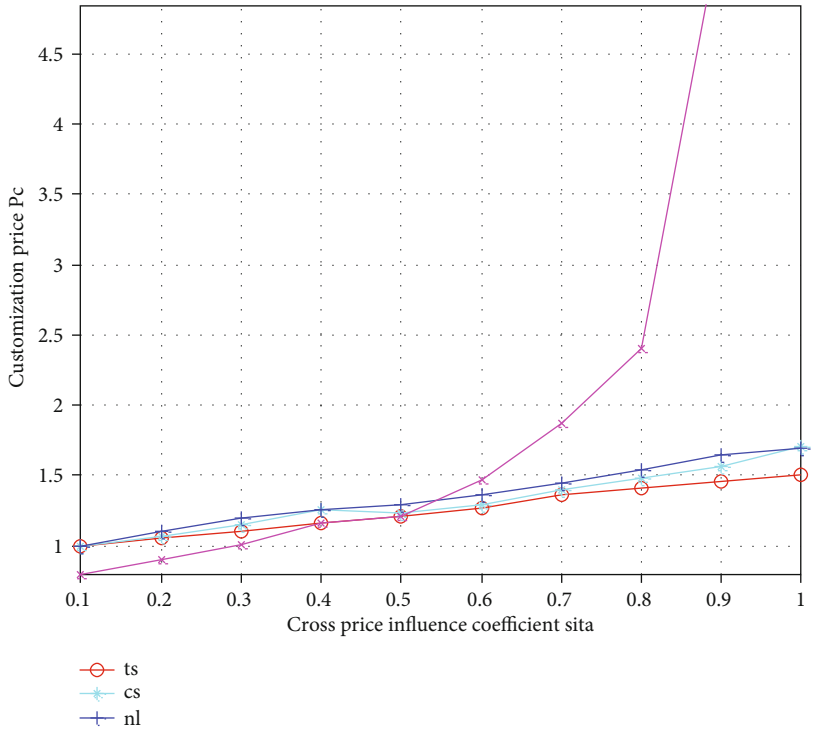

Figure 5: The impact of θ on standardized price.

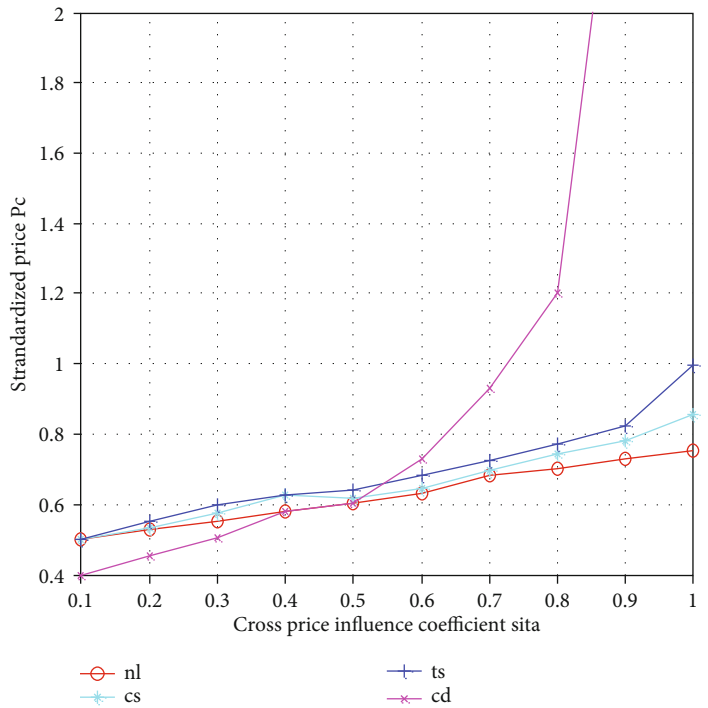

Figure 6: The impact of θ on the price of customization price.

personalized products is higher and the unit profit is increased under the C2B-dominated situation, the demand falls greatly, so the profit is smaller than that under the traditional enterprise-dominated situation.

As is shown in Figure 10, the profit of traditional enterprises is positively correlated with X. When traditional enterprises are dominant, the profit of standardized products is the largest, while the profit of traditional enterprises is the

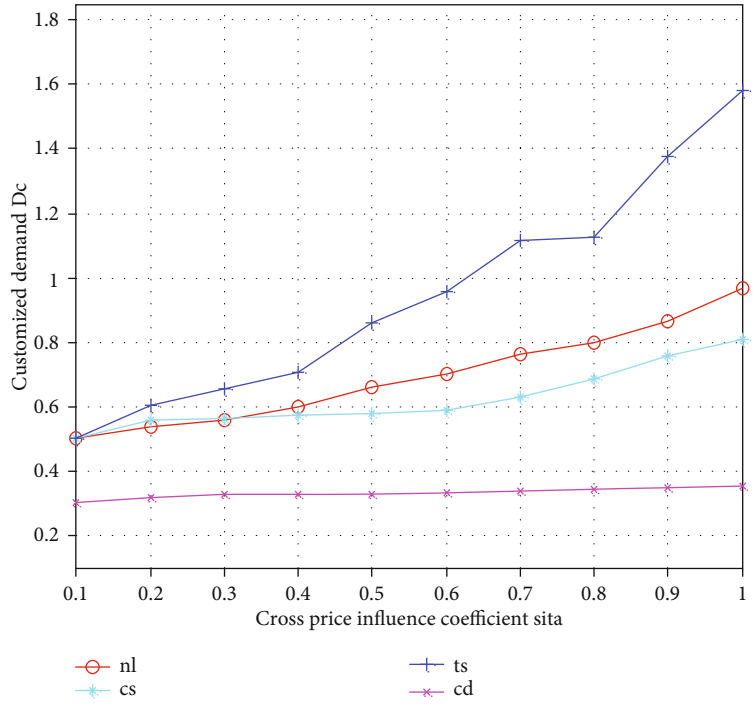

Figure 7: The impact of θ on standardized demand.

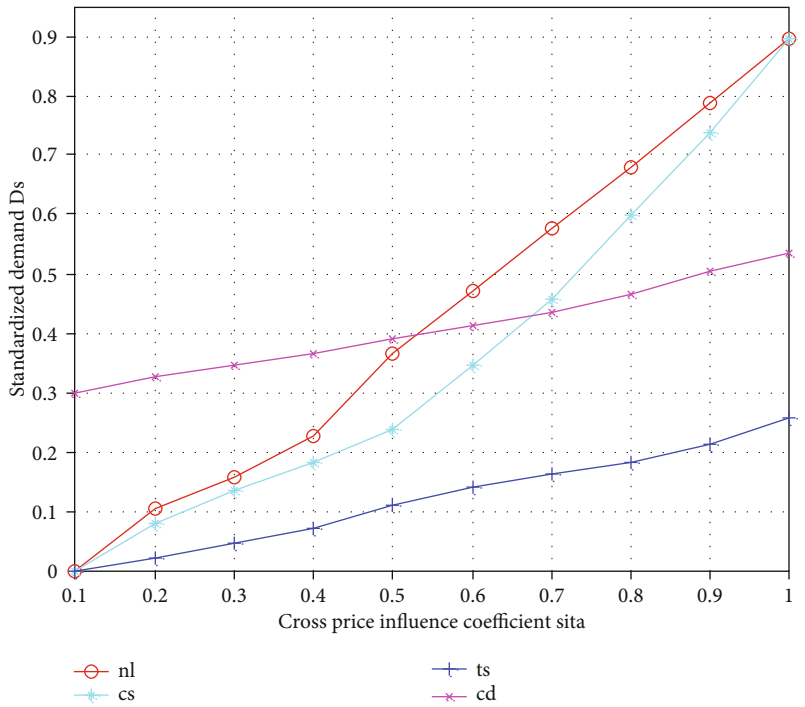

Figure 8: The impact of θ on the price of customization demand.

lowest under decentralized decision-making. And the bigger the X, the more profitable it will be to promote the growth of traditional business profits.

It is worth noting that, compared with other scenarios, the profits of C2B e-commerce enterprises and traditional enterprises are lower in both independent and simultaneous decision-making scenarios, which show that when choosing reasonable pricing strategies, enterprises should also pay attention to cooperation and competition, rather than relying solely on their own single enterprise to compete with many enterprises. After all, in the fierce market competition, the dominant situation on one side will not last long. In order

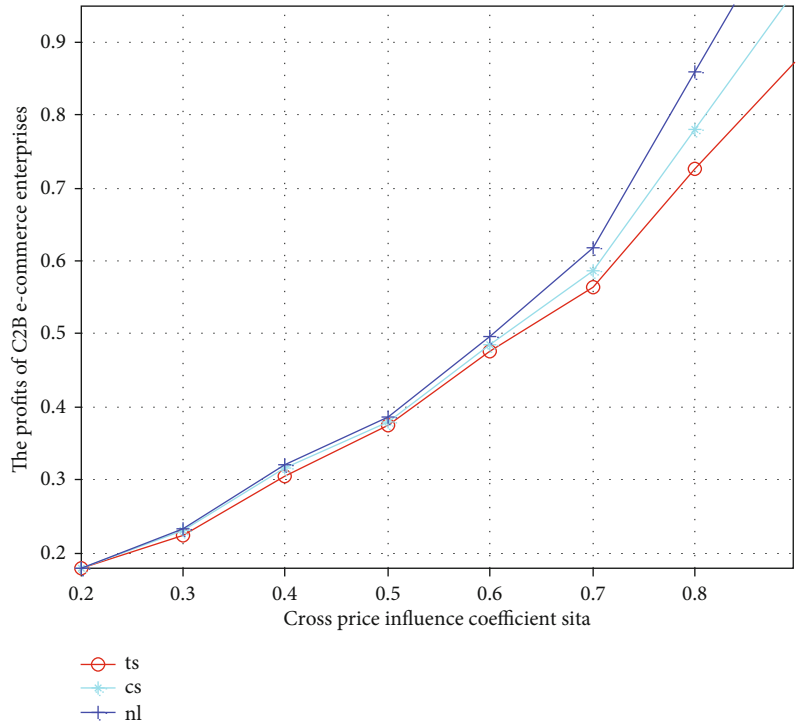

Figure 9: The impact of θ on the profits of C2B e-commerce enterprises.

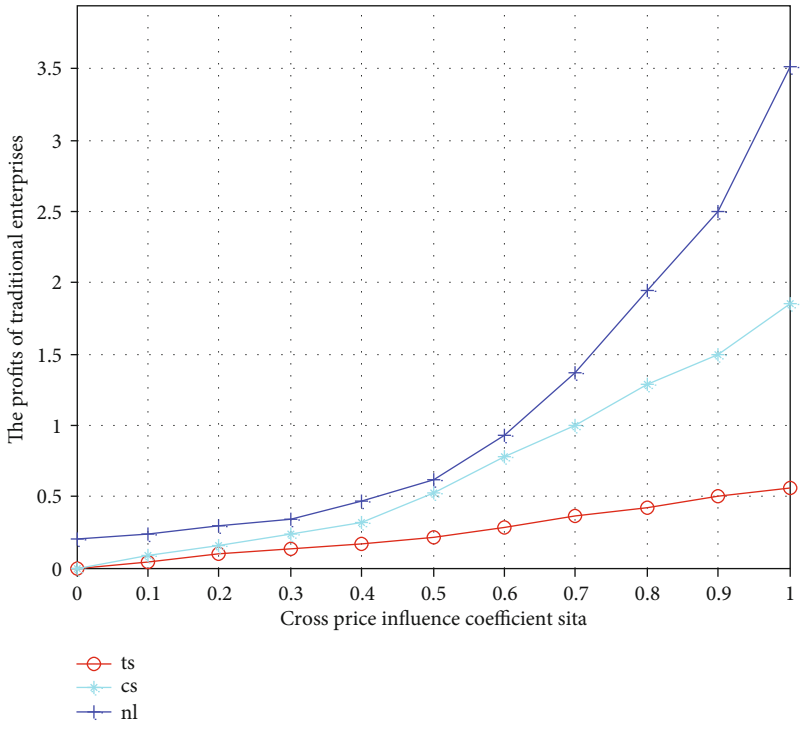

Figure 10: The impact of θ on the profits of traditional enterprises.

to remain invincible in the cruel competition, enterprises and competitors should maintain the spirit of both competition and mutual learning and cooperation, and constantly innovate to meet the needs of more consumers.

5. Conclusion

The continuous development and expansion of e-commerce market has brought many business opportunities to the

market, and also brought different degrees of negative impact. In an age of computer development is very rapid, large data network technology to every aspect of life brings a lot of change, this article discussed the electronic commerce strategy research based on the technology of network data, through the study of game balance four members of the supply chain scenario: centralized decision-making and decentralized decision-making, C2B-dominated decision-making, and traditional enterprise-dominated in the enterprise applications; finally, it is concluded that the e-commerce market of big data based on Internet can develop healthier, whether the data storage and analysis of the research can be more efficient. This method can bring important development function to the electronic commerce market.

Data Availability

All data are true and reliable, and all data can be obtained by contacting the author.

Conflicts of Interest

The authors declare that they have no conflicts of interest.

References

[1] W. Liu, Y. Yang, S. Wang, and E. Bai, "A scheduling model of logistics service supply chain based on the time windows of the FLSP's operation and customer requirement," *Annals of Operations Research*, vol. 257, no. 1-2, pp. 183–206, 2017.

[2] Q. Tu, M. A. Vonderembse, and T. S. Ragu-Nathan, "The impact of time-based manufacturing practices on mass customization and value to customer," *Journal of Operations Management*, vol. 19, no. 2, pp. 201–217, 2001.

[3] Y. Wang, E. Zio, X. Wei, D. Zhang, and B. Wu, "A resilience perspective on water transport systems: the case of eastern star," *International Journal of Disaster Risk Reduction*, vol. 33, no. 1, pp. 343–354, 2019.

[4] Z. Chen, Y. Zhang, C. Wu, and B. Ran, "Understanding individualization driving states via latent Dirichlet allocation model," *IEEE Intelligent Transportation Systems Magazine*, vol. 11, no. 2, pp. 41–53, 2019.

[5] R. Aron, A. Sundararajan, and S. Viswanathan, "Intelligent agents in electronic markets for information goods: customization, preference revelation and pricing," *Decision Support Systems*, vol. 41, no. 4, pp. 764–786, 2006.

[6] Y. Wang and D. Li, "Testing the moderating effects of toolkits and user communities in personalization: the case of social networking service," *Decision Support Systems*, vol. 55, no. 1, pp. 31–42, 2013.

[7] S. Rosaci and G. M. L. Sarné, "Recommending multimedia web services in a multi-device environment," *Information Systems*, vol. 38, no. 2, pp. 198–212, 2013.

[8] Z. Ning, X. Kong, F. Xia, W. Hou, and X. Wang, "Green and sustainable cloud of things: enabling collaborative edge computing," *IEEE Communications Magazine*, vol. 57, no. 1, pp. 72–78, 2018.

[9] S. Afshin Mansouri, D. Gallear, and M. H. Askariazad, "Decision support for build-to-order supply chain management through multiobjective optimization," *International Journal of Production Economics*, vol. 135, no. 1, pp. 24–36, 2012.

[10] J. H. Park and S. C. Park, "Agent-based merchandise management in business-to-business electronic commerce," *Decision Support Systems*, vol. 35, no. 3, pp. 311–333, 2003.

[11] K. Li and T. C. Du, "Building a targeted mobile advertising system for location-based services," *Decision Support Systems*, vol. 54, no. 1, pp. 1–8, 2012.

[12] S. Kortmann, C. Gelhard, C. Zimmermann, and F. T. Piller, "Linking strategic flexibility and operational efficiency: the mediating role of ambidextrous operational capabilities," *Journal of Operations Management*, vol. 32, no. 7-8, pp. 475–490, 2014.

[13] I. G. Dino and R. Stouffs, "Evaluation of reference modeling for building performance assessment," *Automation in Construction*, vol. 40, no. 4, pp. 44–59, 2014.

[14] M. Zhang, D. Zhang, F. Goerlandt, X. Yan, and P. Kujala, "Use of HFACS and fault tree model for collision risk factors analysis of icebreaker assistance in ice-covered waters," *Safety Science*, vol. 111, pp. 128–143, 2019.

[15] T. Yuan and O. Joon, "Research on credit scoring of Chinese listed SMEs based on DEA method," *Credit*, vol. 32, no. 6, pp. 52–56, 2014.

Hindawi
Wireless Communications and Mobile Computing
Volume 2021, Article ID 6666236, 10 pages
https://doi.org/10.1155/2021/6666236

Research Article

To Delay Instantiation of a Smart Contract to Save Calculation Resources in IoT

Hong Su,[1] Bing Guo,[1] Yan Shen,[2] Zhen Zhang,[1] and Chaoxia Qin[1]

[1]*College of Computer Science, Sichuan University, Chengdu 610041, China*
[2]*Control Engineering College, Chengdu University of Information Technology, Chengdu 610041, China*

Correspondence should be addressed to Bing Guo; guobing@scu.edu.cn

Received 20 October 2020; Revised 10 January 2021; Accepted 4 February 2021; Published 18 February 2021

Academic Editor: Hongju Cheng

Copyright © 2021 Hong Su et al. This is an open access article distributed under the Creative Commons Attribution License, which permits unrestricted use, distribution, and reproduction in any medium, provided the original work is properly cited.

Smart contracts are required to be instantiated in the predeployed stage, which consumes computation resources from then on. It is a big waste in the blockchain whose nodes are composed of IoT devices, as those devices often have limited resources (such as limited power supplies or a limited number of processes to run). Meanwhile, IoT devices are heterogeneous and different smart contracts are required. If those smart contracts are instantiated previously, numerous meaningless addresses are required. In this paper, we propose to delay the instantiation of a smart contract when used and terminate it when not used, which is similar to the life cycle of a variable. Then, a new kind of variable (the wrapping variable) is used to hide details of the instantiation and the address. The smart contract is instantiated in the construction function of the wrapping variable, or even it is delayed to the time when there are requests for it. The smart contract terminates when the variable is out of its scope. Then, different instantiation methods are proposed. Finally, we perform the qualitative comparison between the proposed approach and the predeployment method, and it demonstrates that the proposed methods optimize the life cycle of the smart contract and save calculation resources.

1. Introduction

Smart contracts are widely used in the cooperation between blockchains and IoT devices, with the aim of achieving reliability, security, and trust [1, 2]. To manage numerous IoT devices, smart contracts are used to control and configure IoT devices in a secure way [3]. For the efficient data aggregation [4] in IoT, [5] proposes an aggregation way with privacy preserved. As intrusion detection is important in IoT [6, 7], a collaborative intrusion detection based on smart contracts is proposed [8]. For the interaction with the nonblockchain system (like IoT), [9] proposes a direct interaction way without an oracle [10].

Currently, smart contracts are required to be deployed previously [11], which preinstantiates the smart contracts [12, 13]. The instance of a smart contract occupies calculation resources (including the memory, CPU, or disk space) of blockchain nodes. Even when there is no request for a smart contract, its instance is not terminated and the resources are occupied. This is suitable in the blockchain whose nodes have external power supplies (such as a PC or a server), while blockchain nodes may be composed of IoT devices [14]. The resources of IoT devices are often limited [15, 16], such as limited power supply or a limited number of processes to run. Then, it is fatal to delay or reduce requests for a smart contract to save power.

Meanwhile, a unique address [17, 18] or identifier is required to access a smart contract in the predeployment method. IoT devices are of big amount (more than 30 billion in 2020 (https://www.statista.com/statistics/471264/iot-number-of-connected-devices-worldwide/)) and various types, which results in various smart contracts. If we instantiate those smart contracts previously, users have to use numerous meaningless addresses to interact with blockchains. Some deployment tools [19] or platforms [20, 21] facilitate the deployment process. However, this process

Figure 1: Current process of smart contracts. The smart contract is instantiated previously, and an address is returned. The caller interacts with the smart contract by the address. In this way, a smart contract exists even if there is no request.

makes the instantiation details being exposed to the callers (smart contract author or its user) and forces the callers to use the addresses of smart contracts. Figure 1 shows an example.

In this paper, we propose the methods to delay the instantiation of a smart contract after the smart contract has been deployed and to perform the destruction of a smart contract timely to save calculation resources. This way is similar to the life cycle management of a local variable. Then, we propose to use variables to wrap the instantiation steps of smart contracts. The details of the deployment of a smart contract are not exposed to the caller, which is performed in the background.

The major contributions of this paper are as follows.

(1) We propose to create a smart contract instance when there are requests for it and terminate the instance when it is not used (out of its usage scope), which is similar to a local variable. It is aimed at delaying the instantiation of a smart contract and terminating a smart contract in time

(2) We propose to adopt a new kind of variable to hide the details of the instantiation and termination. This kind of variety is called the wrapping variable. The caller only needs to create a wrapping variable, and in its construction, the smart contract is instantiated. When the variable is out of its scope, the smart contract terminates. It only needs to control a variable to optimize the life cycle of a smart contract. This method also facilitates one smart contract to invoke another smart contract, in which the latter is a local variable

(3) We propose two instantiation methods: instant instantiation and postinstantiation. Instant instantiation creates a smart contract instance when its wrapping variable is created. Postinstantiation creates the smart contract instance when there are real invocations to the wrapping variable

The rest of this paper is organized as follows. Section 2 describes different instantiation methods. Section 3 shows the simulation results and the corresponding analysis. Section 4 gives the summary and concludes the paper.

2. Instantiation Methods

2.1. Motivation. Currently, the smart contract instantiation is done before the execution, and this procedure is called deployment. It has some disadvantages as described in Introduction. However, a smart contract can be used as the way that a variable is used—it is dynamically instantiated and terminated. It shortens the runtime of a smart contract. In this method, the instantiation is performed when there are invocations of a smart contract. When it is not used or out of its usage scope, the termination of a smart contract is performed. It also facilitates the usage of a smart contract to use a variable instead of the global address of the deployed smart contract.

2.2. Different Instantiation Methods. We can instantiate an instance beforehand or delay the instantiation when there is a function call (invocation) to the smart contract. Figure 2 shows three possible instantiation methods.

2.2.1. Preinstantiation Method. This is the currently used method, in which the instantiation is performed before the real execution. The instance is associated with an address (or other unique identifiers), which is used to look up the smart contract instance and dispatch corresponding invocations to it. However, this instance may run without any invocation for a long time (in a waiting state). When there are no invocations, the smart contract still resides in the memory until it has been obviously been terminated. It is shown in the "preinstantiation" part of Figure 2.

2.2.2. Instant Instantiation. In this method, a smart contract is instantiated when it has been called by another smart contract or a user. (1) If smart contract T is invoked by smart contract S, S creates a variable V which wraps T. Variable V instantiates smart contract T in its constructor. Successive access to the instance of T is through variable V. (2) If it is called by a user, the instantiation is triggered by the blockchain platform when its user sends a transaction to trigger its function. Then, the request is passed to the newly created instance. In both cases, there is no need to give an address to the caller. Then, a new kind of variety is proposed to access the smart contract instance. In this paper, we define a new class (Java class) to stand for this kind of variable.

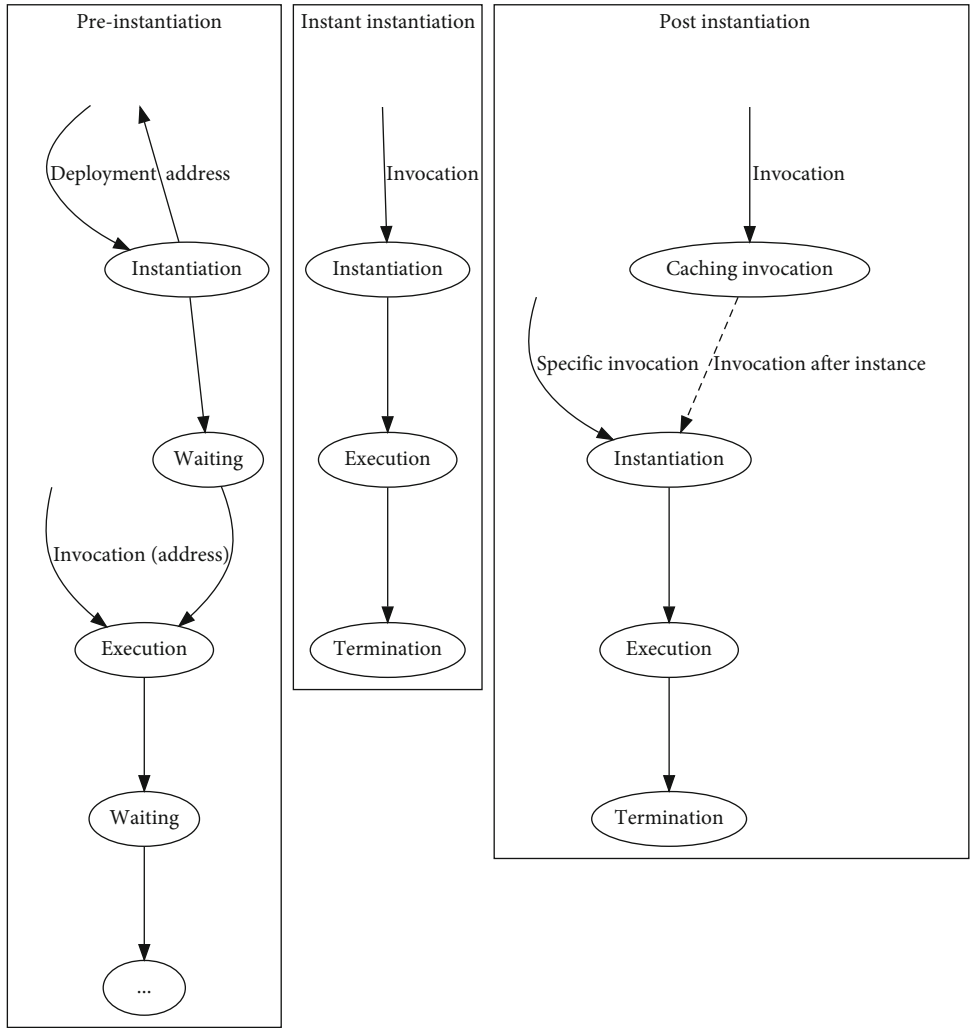

Figure 2: Different instantiation methods.

The instance is terminated when the variable is not required; either the calling smart contract exits or the variable is out of its scope. The scope of a variable further shortens the runtime of a smart contract instance. If we put the variable into a smaller scope, the variable lives only in this scope. There is a difference between the normal variable termination and the variable for the smart contract. The latter one requires that the execution results of the smart contract have been confirmed in the blockchain. After the confirmation, the blockchain consensus protocol enforces the correctness of this smart contract [14].

For other methods of the smart contract, the corresponding variable forwards it to the smart contract. As the smart contract is running in a different process, the method invocation is done by the interprocess communication (IPC) on each node, while this is hidden in the implementation of the variable. Figure 3 shows the relationship between the variable and the smart contract.

Instant instantiation facilitates the invocation of different smart contracts. The caller does not need to care about the instantiation and termination of a smart contract. Further, the caller is not required to access a smart contract by a string of meaningless numbers (the address of a smart contract in the predeployment method). Algorithm 1 is an example.

From Algorithm 1, we know that instances of smart contracts SCA and SCB are created and sealed in variables at lines 12 and 16, and then, their methods are accessed by those two variables. Those variables are automatically deconstructed at the end of this scope (line 18).

2.2.3. Postinstantiation (Lazy Instantiation). When some methods of a smart contract are invoked, the instance of the smart contract does not have to be created. For example, a caller updates a value to a smart contract continuously and no users retrieve this value. During this time, it is not necessary to have an instance. We can cache those updating methods in the variable and only instantiate the smart contract when a user tries to get the value. Figure 4 shows this process.

Postinstantiation is that a smart contract is instantiated when there is a request that its instance has to be created. The corresponding request is called the instantiation must request or method (IMR), and other requests are called the instantiation unnecessary request or method (IUR).

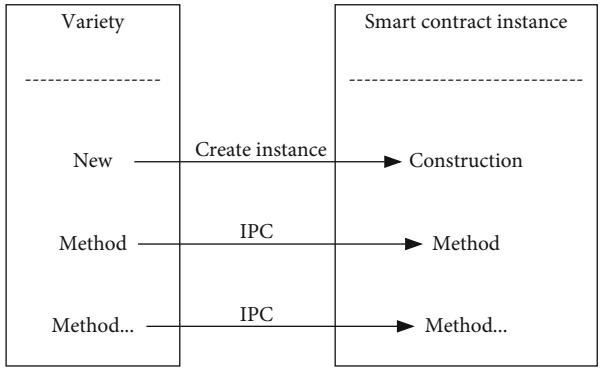

Figure 3: The relationship between the variable and the smart contract instance. The interaction among the variable and the smart contract instance is the IPC (interprocess communication) method.

Postinstantiation is aimed at delaying the instantiation of the smart contract. IUR requests sent before IMR are cached. Those logics are inside the variable, which is illustrated in Algorithm 2.

The postinstantiation delays the instantiation before IMR. And if the user has not sent any IMR, the instance can even be avoided. In this case, it is still traceable, as the transaction to invoke the smart contract is stored in the blockchain.

2.3. Resource Analysis. In this section, we analyze the resources (CPU and memory) saved by the dynamical instantiation and termination. We regard a smart contract (S) as a collection of smart contract copies (s) running on different nodes. The notation of s_i denotes the smart contract copy (s) on different node i shown as follows.

$$S = [s_1, \cdots, s_k, \cdots]. \tag{1}$$

When the smart contract is instantiated, it occupies corresponding resources, such as memory and CPU. We use rs_i to denote its resources on node i.

$$rs_i = [\text{memory}, \text{CPU}, \cdots]. \tag{2}$$

Node resources are occupied during the time from the instantiation to the termination. We use $rs_i^{-}t_j$ to denote the resources occupied at time t_j; t_0 is the time of the instantiation, and t_n is the time of the termination. The resources over time are shown in

$$rs_{it} = \left[rs_{it_0}, \cdots, rs_{it_j}, \cdots, rs_{it_n}\right]. \tag{3}$$

Suppose the time of the first invocation is tv_{start} and the time of the last invocation is tv_{end}. Then, the relationship between the invocation time and the resource occupation time is shown in

$$t_0 < tv_{\text{start}} \&\& t_n > tv_{\text{end}}, \quad \text{if preinstantiation,} \tag{4}$$

$$t_0 \approx tv_{\text{start}} \&\& t_n \approx tv_{\text{end}}, \quad \text{if instant instantiation,} \tag{5}$$

$$t_0 \geq tv_{\text{start}} \&\& t_n \approx tv_{\text{end}}, \quad \text{if postinstantiation.} \tag{6}$$

For the preinstantiated method, this may be a very long time or even there is no invocation after the smart contract has been instantiated. It occupies resources longer than the instant instantiation. The postinstantiation has the least resource occupation time, as its instantiation time (t_0) is not earlier than the time of the first IMR invocation, shown in (6). Then, we get the conclusion that the instant instantiation and the postinstantiation occupy the resource in less time than the predeployment method.

We define a variable t_s to measure the time saved by different instantiation methods, which is shown in (7). If its value is positive, it saves the waiting time, which is the postinstantiation case. If it is close to 0, the runtime of the smart contract instance is approximately equal to the invocation last time, which is the instant instantiation case. If its value is negative, it spends time waiting for requests, which is the predeployment case.

$$t_s = (tv_{\text{start}} - t_0) + (tv_{\text{end}} - t_n). \tag{7}$$

The total runtime saved (TS) is the summarization of all nodes which run the smart contract, shown in (8). Thus, it saves more resources in the larger blockchain networks as their node number n is more.

$$\text{TS} = \sum t_s. \tag{8}$$

3. Verification

In this section, we show our simulation results of different instantiation methods. As the smart contracts are required to be preinstantiated in currently available blockchains, we develop a blockchain that supports different instantiation types. It removes the requirement to preinstantiate a smart contract and keeps the procedure to put the code of a smart contract to the blockchain in the predeployment stage.

The smart contract language is Java. There are two reasons. (1) The blockchain platform is developed by Java, and all nodes have the JRE (Java runtime environment) to run the Java code. Then, it saves the steps to provide an extra runtime environment for another language. (2) It is convenient to invoke smart contracts by the reflection mechanism of Java. User-defined smart contracts can be simply invoked in this way.

We provide a class as the variable to wrap the smart contract instance. It wraps behaviors that are required for different instantiation methods. The instantiation type is set in the configuration file of the smart contract. If the instantiation type is preinstantiation, its instance is created in the code putting procedure. If it is the instant instantiation, the instance is created when its creation function is called. If it is the postinstantiation, the instance is created when the specific methods are called. Those methods have calls to a platform function call which creates the instances.

```
1: Define smart contract SCA
2: …
3: End Define
4:
5: Define smart contract SCB
6: …
7: End Define
8:
9: Define smart contract SCC
10: //scope begin {
11: // create an instance (new process) of SCA
12: Variable sca = new Variable("SCA");
13: invoking method of sca
14: …
15: // create an instance (new process) of SCB
16: Variable scb = new Variable("SCB");
17: invoking method of scb
18: //scope end } - sca and scb are ready to terminate (condition a), and those two smart contract instances terminate after their states have been confirmed in blockchain (condition b)
19: End Define
```

Algorithm 1. Smart contract invocation by a variable.

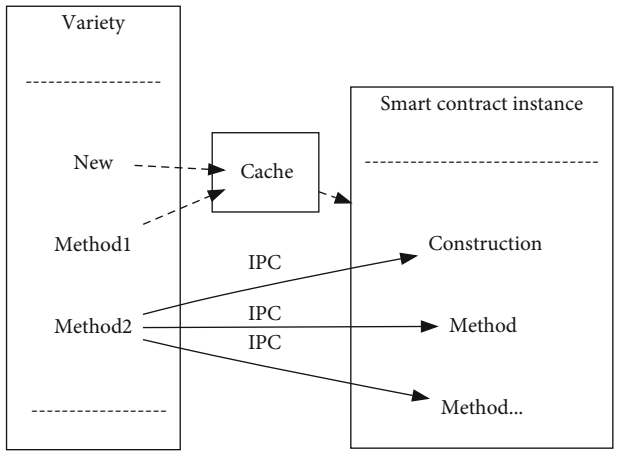

Figure 4: The relationship between the variable and the smart contract instance in the postinstantiation method. The instantiation of a smart contract can be delayed to the invocation of specific methods, and other methods are cached before the instantiation.

```
1: Process(Request r)
2: …
3: if r is IMR then
4:    create instance
5:    forward cached requests and r to instance
6: end if
7: if r is IUR then
8:    if instance is not created then
9:       cache r
10:   else
11:      forward r to instance
12:   end if
13: end if
```

Algorithm 2. Handling for IMR and IUR.

There is special handling for the termination of a variable. When a variable is out of its (definition and usage) scope, the compiler can add the corresponding code there. As we do not want to change the Java compiler, we directly put a function to terminate the smart contract instance at the end of its scope. Meanwhile, the termination function calls a function (the final checking function or FCF) which checks whether the key states of a smart contract have been sealed in the blockchain. If not sealed, FCF waits and checks. Otherwise, it exits and the smart contract destructs to release resources.

We use the file method as the interprocess communication between the process of the wrapping variable and smart contract instance as they run in different processes. The variable passes the function name and its parameters to corresponding request files, and the smart contract instance reads from those files continuously. The smart instance invokes the corresponding functions by a Java reflect mechanism.

Two kinds of verifications are carried out. (1) We perform the comparative verification between the proposed method and the preinstantiation method. It is aimed at showing the benefit of the proposed instantiation methods. (2) We also perform the verification of different instantiation methods proposed in this paper to demonstrate the advantages of different methods.

3.1. Comparison between the Preinstantiation Method and Proposed Method. We adopt the runtime of smart contracts to compare those two methods. The proposed instantiation is triggered by a transaction when the first request is sent from the user. In the preinstantiation method, the smart contract is preinstantiated in the predeployment stage and its instance keeps running from then on. Requests for both

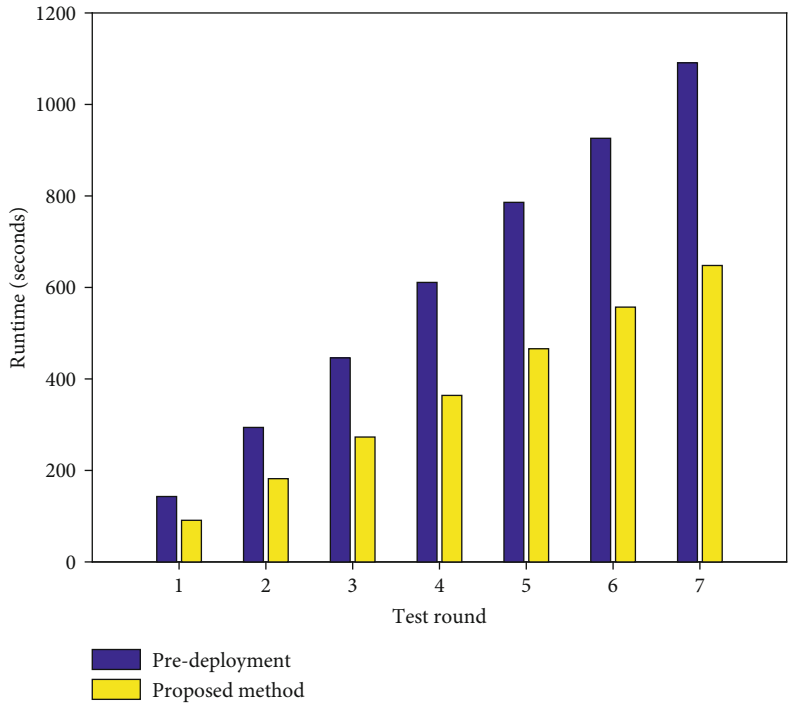

Figure 5: The accumulated runtime comparison between the proposed method and the preinstantiation method.

methods are sent out by a script in a random interval (the interval changes from 40 seconds to 80 seconds).

Figure 5 shows the accumulated runtime (t_{runAcc}) of those two methods. The accumulated runtime is the summarization of the runtime of all instances, as shown in (9). In the proposed method, there may be several instances during a test round and thus t_{runAcc} is the summarization of the runtime of all instances. In the preinstantiation method, there is only one instance and t_{runAcc} is equal to the runtime of that instance. The runtime (t_{run_i}) of instance i is from the moment of its instantiation to the moment of its termination, which contains the code execution time (t_{exec_i}) and the waiting time (t_{waiting_i}), as shown in (10).

$$t_{\text{runAcc}} = \sum t_{\text{run}\_i}, \tag{9}$$

$$t_{\text{run}\_i} = t_{\text{exec}\_i} + t_{\text{waiting}\_i}. \tag{10}$$

From Figure 5, we see that the preinstantiation method takes more runtime than the proposed method. The reason is as follows. In (10), time t_{waiting_i} of the proposed method is less than that of the preinstantiation method, because the waiting time is saved as each instance of the proposed method is terminated when not used. However, time t_{exec_i} of the proposed method is more, as it instantiates a smart contract several times, while time t_{waiting_i} is much bigger than time t_{exec_i} in this verification.

At the first invocation, the preinstantiation method has taken 52 seconds more. This value is the interval between the first invocation and the preinstantiation. As there are intervals among invocations, the additional runtime taken by the preinstantiation increases. In fact, the runtime of the preinstantiation method is the time after it has been instantiated. The instance in the proposed method is only created when there is request, and it does not occupy the interval time between different smart contract instances.

Table 1: Different kinds of optimization of SCX.

Instantiation type	Postinstantiation	Local variable	Comment
A	No	No	SCY-A
B	Yes	No	SCY-B
C	No	Yes	SCY-C
D	Yes	Yes	SCY-D

3.2. Different Instantiation Methods. In this section, we verify two optimizations for the proposed methods. One is the postinstantiation, and another one is to define the variable of the smart contract instance in a smaller scope (a local variable). We combine those two optimizations and get four kinds of possible instantiation optimization, shown in Table 1.

The according codes are shown in Algorithm 3. Two smart contracts are used: smart contracts SCX and SCY. SCY does different instantiations of SCX as shown in Table 1. It results in four subtypes of SCY: SCY-A, SCY-B, SCY-C, and SCY-D. SCX has two subtypes: SCXI and SCX-Post, and the latter one is the postinstantiated. And SCX provides two methods: the first one is not an instantiation must method and the second is an instantiation must method.

We have performed 28 test rounds. In those test rounds, verifications of combinations A, B, C, and D are tested in turn. The test results are shown in Figure 6. From it, we see that smart contract SCX in type A has the longest runtime,

```
1: Define smart contract SCXI
2: …
3: End Define
4:
5: Define smart contract SCX-Post
6: …
7: End Define
8:
9: Define smart contract SCY-A
10: do other action
11: Variable scx = new Variable(”SCXI”);
12: invoking method1 of scx
13: do other action
14: invoke method2 of scx;
15: do other action
16: End Define
17:
18: Define smart contract SCY-B
19: do other action
20: Variable scx = new Variable(”SCX-Post”);
21: invoking method1 of scx; // Method1 is cached
22: do other action
23: invoke method2 of scx; // Method2 requires to have a real SCX smart contract instance
24: do other action
25: End Define
26:
27: Define smart contract SCY-C
28: do other action
29: //scope begin {
30: Variable scx = new Variable(”SCXI”);
31: invoking method of scx
32: do other action
33: invoke method of scx;
34: //scope end }
35: do other action
36: End Define
37:
38: Define smart contract SCY-D
39: do other action
40: //scope begin {
41: Variable scx = new Variable(”SCX-Post”);
42: invoking method1 of scx; // Method1 is cached
43: do other action
44: invoke method2 of scx; // Method2 requires to have a real SCA smart contract instance
45: //scope end }
46: do other action
47: End Define
```

Algorithm 3. Different instantiation combinations.

which is shown in the first part of Figure 6. SCX is created when its according variable is created and lives until SCY-A terminates. SCX in SCY-D has the shortest runtime, which is shown in the last part of Figure 6. The reason is that SCX is created until its second method is created (the instantiation must method), and it is defined in a smaller scope, which makes it terminate early.

The other two methods take less time than the first one and more time than the last one. The second one delays the instantiation time of smart contract SCX, and the third one defines smart contract SCY in a smaller scope. Then, both save the runtime.

We also demonstrate the accumulated runtime in Figure 6, which is the summarization of the runtime of the instances in previous test rounds. From it, we can see that the accumulated runtime of SCX and SCY is very close in case A, which indicates that SCX lives along with SCY. On the other hand, the curve of the accumulated runtime of SCX and SCY forms a big angle in case D, which indicates that the execution time of SCX is shorter than that of SCY

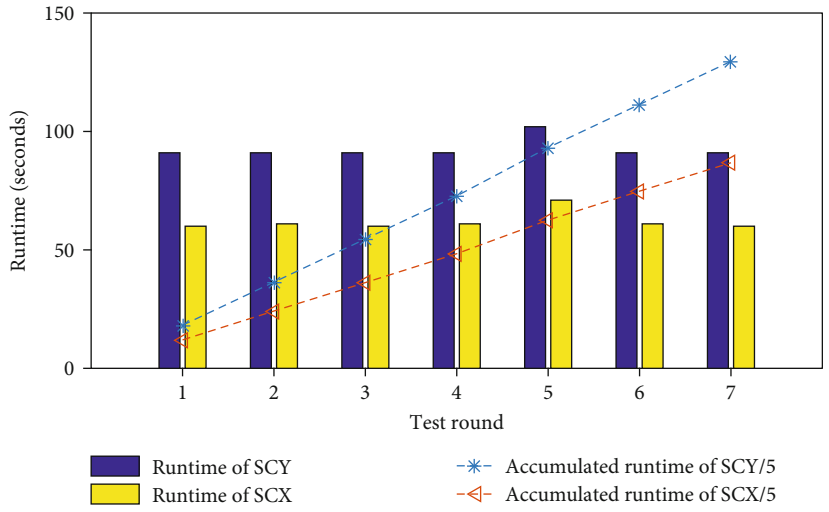

(a)

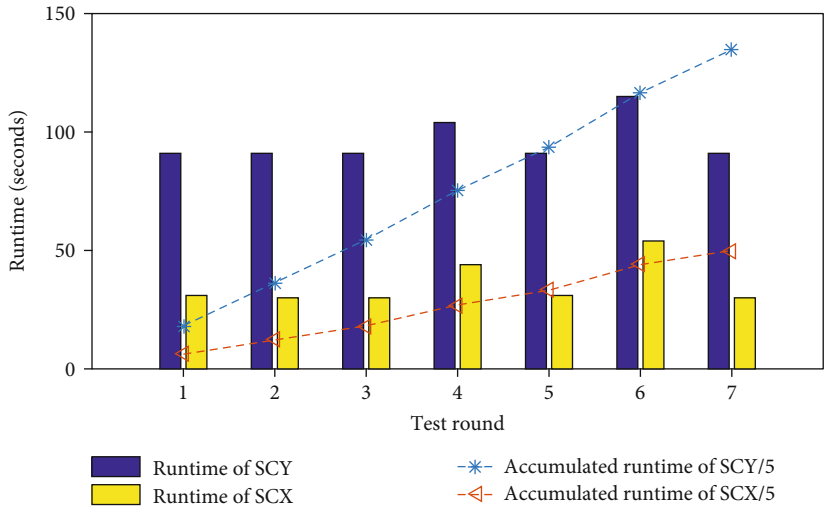

(b)

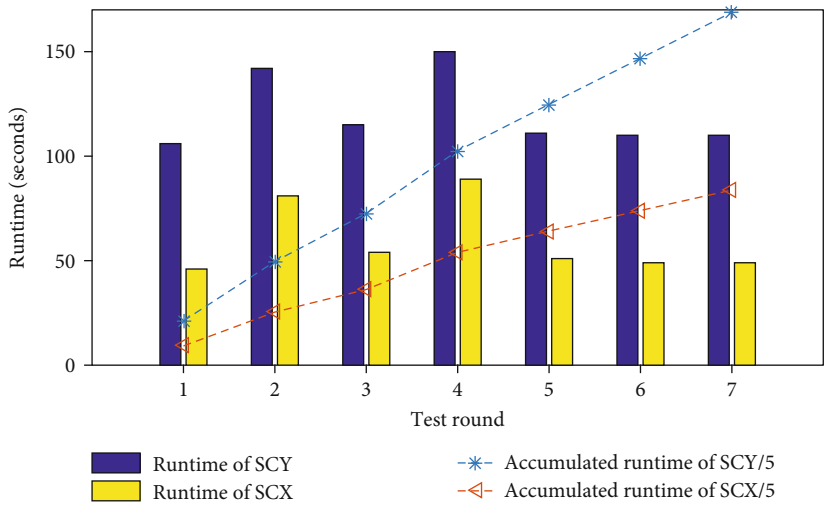

(c)

Figure 6: Continued.

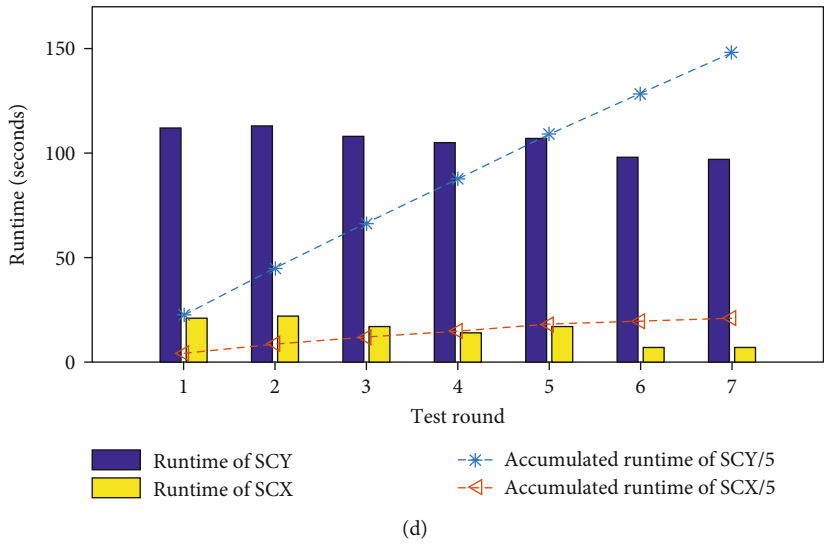

(d)

Figure 6: The runtime of smart contracts in different instantiation cases (A, B, C, and D from (a) to (d)). Accumulated runtime is the summarization of the runtime in the previous test run, and to make it suitable to the diagram, its value has been divided by 5.

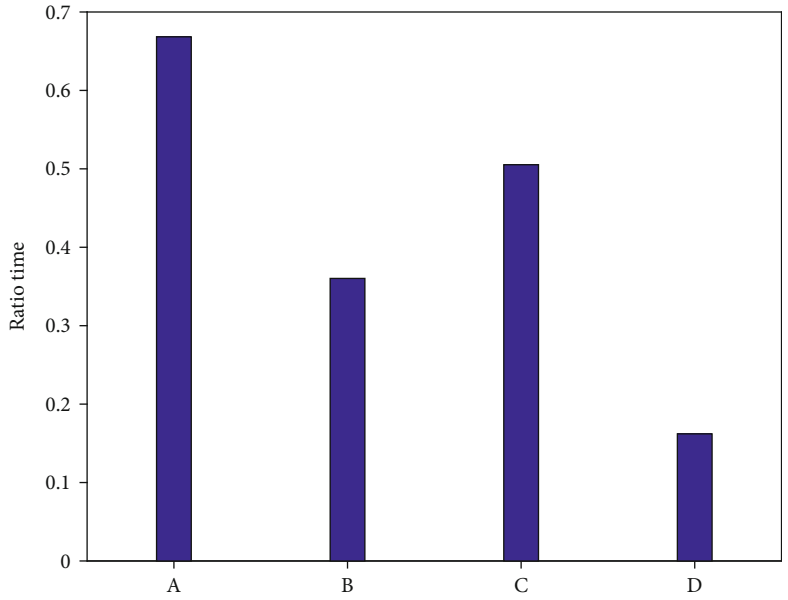

Figure 7: The runtime of the smart contract SCX to the runtime of smart contract SCY (ratioTime) in different instantiation cases (A, B, C, and D).

and it is optimized to save the additional resource occupation time.

As the time SCY also changes with time, and to have a more comparison of how the proportion of the runtime is saved, we use another measurement, ratioTime, which is the ratio of the runtime of the smart contract SCX to the runtime of smart contract SCY, referring to (11). The result is shown in Figure 7.

$$\text{ratioTime} = \frac{\text{runtime}(X)}{\text{runtime}(Y)}. \tag{11}$$

From Figure 7, we also see the same optimization results. In method A, SCX runs at the most time when SCY runs and has the highest ratioTime, and method D has the lowest ratioTime. The two left methods have the medium ratioTime.

4. Conclusion

In this paper, we address the preinstantiation issues of smart contracts for IoT scenarios, in which blockchain nodes are composed of resource-limited IoT devices. We propose different instantiation methods to optimize the instantiation

of a smart contract, with the aim of solving the issues of the preinstantiation (it occupies computation resources even if there is no request and requires a global address). We adopt a new kind of variable to wrap the instantiation and termination of a smart contract. The smart contract instantiates when its wrapping variable is created, and it can even delay the instantiation to the moment when an instance is a must. The termination of a smart contract is performed when the variable is out of scope. At last, we perform the corresponding verifications, which show that our proposed methods occupy fewer resources (measured by the runtime). More resources can be saved if we combined different instantiation methods.

Data Availability

No data were used to support this study.

Conflicts of Interest

The authors declare that they have no conflicts of interest.

Acknowledgments

This work was supported in part by the National Natural Science Foundation of China under Grant No. 61772352; the National Key Research and Development Project under Grant Nos. 2020YFB1711800 and 2020YFB1707900; the Science and Technology Project of Sichuan Province under Grant Nos. 2019YFG0400, 2020YFG0479, and 2020YFG0322; and the R&D Project of Chengdu City under Grant No. 2019-YF05-01790-GX.

References

[1] L. Hang and D. H. Kim, "Reliable task management based on a smart contract for runtime verification of sensing and actuating tasks in IoT environments," *Sensors*, vol. 20, no. 4, p. 1207, 2020.

[2] R. Xu, Y. Chen, E. Blasch, and G. Chen, "Blendcac: a smart contract enabled decentralized capability-based access control mechanism for the IoT," *Computers*, vol. 7, no. 3, p. 39, 2018.

[3] S. Huh, S. Cho, and S. Kim, "Managing IoT devices using blockchain platform," in *2017 19th international conference on advanced communication technology (ICACT)*, pp. 464–467, Bongpyeong, South Korea, 2017.

[4] H. Cheng, Y. Chen, N. Xiong, and F. Li, "Layer-based data aggregation and performance analysis in wireless sensor networks," *Journal of Applied Mathematics*, vol. 2013, 12 pages, 2013.

[5] Z. Guan, G. Si, X. Zhang et al., "Privacy-preserving and efficient aggregation based on blockchain for power grid communications in smart communities," *IEEE Communications Magazine*, vol. 56, no. 7, pp. 82–88, 2018.

[6] Q. Zhang, C. Zhou, N. Xiong, Y. Qin, X. Li, and S. Huang, "Multimodel-based incident prediction and risk assessment in dynamic cybersecurity protection for industrial control systems," *IEEE Transactions on Systems, Man, and Cybernetics: Systems*, vol. 46, no. 10, pp. 1429–1444, 2015.

[7] K. Huang, Q. Zhang, C. Zhou, N. Xiong, and Y. Qin, "An efficient intrusion detection approach for visual sensor networks based on traffic pattern learning," *IEEE Transactions on Systems, Man, and Cybernetics: Systems*, vol. 47, no. 10, pp. 2704–2713, 2017.

[8] O. Alkadi, N. Moustafa, B. Turnbull, and K. R. Choo, "A deep blockchain framework-enabled collaborative intrusion detection for protecting IoT and cloud networks," *IEEE Internet of Things Journal*, 2020.

[9] H. Su, B. Guo, Y. Shen, T. Li, C. Qing, and Z. Zhang, "A solution for state conflicts of smart contract in interaction with non-blockchain," in *IEEE INFOCOM 2020-IEEE conference on computer communications workshops (INFOCOM WKSHPS)*, pp. 382–387, Toronto, ON, Canada, Canada, 2020.

[10] G. Caldarelli, "Understanding the blockchain oracle problem: a call for action," *Information*, vol. 11, no. 11, p. 509, 2020.

[11] G. Destefanis, M. Marchesi, M. Ortu, R. Tonelli, A. Bracciali, and R. Hierons, "Smart contracts vulnerabilities: a call for blockchain software engineering?," in *2018 international workshop on Blockchain oriented software engineering (IWBOSE)*, pp. 19–25, Campobasso, Italy, 2018.

[12] Y. Liu, Q. Lu, X. Xu, L. Zhu, and H. Yao, "Applying design patterns in smart contracts," in *International Conference on Blockchain*, pp. 92–106, Cham, 2018.

[13] T. Chen, X. Li, X. Luo, and X. Zhang, "Under-optimized smart contracts devour your money," in *2017 IEEE 24th international conference on software analysis, evolution and reengineering (SANER)*, pp. 442–446, Klagenfurt, Austria, 2017.

[14] A. Reyna, "On blockchain and its integration with IoT. Challenges and opportunities," *Future Generation Computer Systems*, vol. 88, pp. 173–190, 2018.

[15] W. Wu, N. Xiong, and C. Wu, "Improved clustering algorithm based on energy consumption in wireless sensor networks," *IET Networks*, vol. 6, no. 3, pp. 47–53, 2017.

[16] I. Kuzminykh, A. Carlsson, M. Yevdokymenko, and V. Sokolov, "Investigation of the IoT device lifetime with secure data transmission," in *Internet of Things, Smart Spaces, and Next Generation Networks and Systems*, pp. 16–27, Springer, Cham, 2019.

[17] A. Bahga and V. Madisetti, "Blockchain platform for industrial Internet of things," *Journal of Software Engineering and Applications*, vol. 9, no. 10, pp. 533–546, 2016.

[18] X. Li, P. Jiang, T. Chen, X. Luo, and Q. Wen, "A survey on the security of blockchain systems," *Future Generation Computer Systems*, vol. 107, 2017.

[19] M. Knecht and B. Stiller, "SmartDEMAP: a smart contract deployment and management platform," in *IFIP international conference on autonomous infrastructure, management and security*, pp. 159–164, Cham, 2017.

[20] C. F. Liao, C. J. Cheng, K. Chen, C. H. Lai, T. Chiu, and C. Wu-Lee, "Toward a service platform for developing smart contracts on blockchain in BDD and TDD styles," in *2017 IEEE 10th Conference on Service-Oriented Computing and Applications (SOCA)*, pp. 133–140, Kanazawa, Japan, 2017.

[21] C. Sillaber and B. Waltl, "Life cycle of smart contracts in blockchain ecosystems," *Datenschutz Und Datensicherheit Dud*, vol. 41, no. 8, pp. 497–500, 2017.

Hindawi
Wireless Communications and Mobile Computing
Volume 2021, Article ID 8871150, 11 pages
https://doi.org/10.1155/2021/8871150

Research Article

Transaction Prediction in Blockchain: A Negative Link Prediction Algorithm Based on the Sentiment Analysis and Balance Theory

Ling Yuan[1], **JiaLi Bin**[1], **YinZhen Wei**[2], **Zhihua Hu**[2] **and Ping Sun**[2]

[1]*School of Computer Science, Huazhong University of Science and Technology, 430074, China*
[2]*Huanggang Normal University, 438000, China*

Correspondence should be addressed to YinZhen Wei; wyz_gs@163.com

Received 25 July 2020; Revised 19 December 2020; Accepted 1 February 2021; Published 16 February 2021

Academic Editor: Miguel López-Benítez

Copyright © 2021 Ling Yuan et al. This is an open access article distributed under the Creative Commons Attribution License, which permits unrestricted use, distribution, and reproduction in any medium, provided the original work is properly cited.

User relationship prediction in the transaction of Blockchain is to predict whether a transaction will occur between two users in the future, which can be abstracted into the link prediction problem. The link prediction can be categorized into the positive one and the negative one. However, the existing negative link prediction algorithms mainly consider the number of negative user interactions and lack the full use of emotion characteristics in user interactions. To solve this problem, this paper proposes a negative link prediction algorithm based on the sentiment analysis and balance theory. Firstly, the user interaction matrix is constructed based on calculating the intensity of emotion polarity for social network texts, and a reliability weight matrix (noted as RW-matrix) is constructed based on the user interaction matrix to measure the reliability of negative links. Secondly, with the RW-matrix, a negative link prediction algorithm is proposed based on the structural balance theory by constructing negative link sample sets and extracting sample features. To evaluate the performance of the negative link prediction algorithm proposed, the variable management method is used to analyze the influence of negative sample control error and other parameters on the accuracy of it. Compared with the existing prediction benchmark algorithms, the experimental results demonstrate that the proposed negative link prediction algorithm can improve the accuracy of prediction significantly and deliver good performances.

1. Introduction

Everything in our lives has been digitized with the network technologies including the wireless mesh network with the topology preservation [1] and the wireless sensor networks using the Markov random field [2], both of which assist in providing the last mile Internet access for users. Moreover, with the development of the Blockchain, the technology behind the Bitcoin cryptocurrency system [3], many kinds of cryptocurrencies have been used in digital transactions. The link prediction algorithms can be used to predict whether a cryptocurrency transaction relationship will occur between the users. Tanevski et al. [4] use the Bitcoin OTC network to predict whenever a possible transaction will be made between two users in the network. In the transactions of Blockchain, the node represents a user, and the link represents the trust degree or the ratings or the assessments of the users given to each other after they made a transaction; the value of the link can be either numbers or texts. Thus, the link prediction algorithm, which is based on the information of user relations and user attributes in various networks, will provide more information and support for the decision-making of users who make transactions based on Blockchain technology.

Link prediction is mainly divided into the user similarity matrix [5] and the machine learning-based method [6]. In the user similarity matrix, the value represents the similarity between two nodes, and when the value is greater, the possibility of the existence of links between nodes is greater. The machine learning-based method is to create a model with a set of adjustable parameters. The optimal parameter value is found by the optimization strategy, so the obtained model can reproduce the real network structures and relationship characteristics better. In addition, Yuan and Pradeep found that adding emotional features can improve the accuracy of link prediction [7]. According to the user's emotional

features extracted from different topics, the more likely the two users have common emotional tendencies, the more likely they are to be friends.

However, most platforms prefer to exhibit the positive sentiments and conceal the negative ones. For example, the users can express their positive sentiments with the thumbs-up icon or other functions directly. In contrast, if users want to express negative sentiments, they can only leave messages in the comments section. Hence, most social platforms ignore the negative data; the importance of negative link prediction is underestimated and underutilized [8]. Fortunately, researchers found that the negative link is a good complement to the positive link [9]. The negative link prediction can use the positive link and the interactions of users in the network to predict the possible negative relationships among users, where the interaction among users includes the number of interactions, interaction tendency, and interaction intensity [10]. The existing negative link prediction algorithms mainly focus on the number of negative interactions of users and lack the full utilization of the emotional features in the interaction of users which can improve the accuracy of link prediction [11].

Therefore, this paper proposes a negative link prediction algorithm based on the sentiment analysis. Firstly, with the combination of the sentiment analysis method and the social network, this paper proposes a method to calculate the intensity of the emotional polarity for social network texts. On this basis, we propose a method to construct the user interaction relationship matrix. Based on the user interaction relationship matrix, we construct a reliability weight matrix (noted as RW-matrix) for measuring the reliability of negative links. Secondly, we construct a negative link sample set based on the interactions of users and extract the sample features. Then, the paper proposes a negative link prediction algorithm with the structural balance theory (noted as SABT-NLP).

The remainder of this paper is organized as follows. Section 2 discusses the related work. Section 3 introduces the preliminaries of negative link prediction, and Section 4 describes the details of the proposed methodology. Section 5 presents the experimental evaluation, and finally, Section 6 gives the conclusion.

2. Related Work

Link prediction can use the existing network topology and other information contained in the network to predict the possibility of future connections in the network which have not yet been connected in the network. Symbol networks are one of the most representative methods used in link prediction [12, 13]. Symbol networks are networks with positive and negative signs. For example, YouTube allows users to utilize some of the features to express their opinions about whether they like a video or not. Epinions allows users to rate other users' contents. Such functions in social networks contribute to the development of the symbol network.

Liben-Nowell and Kleinberg [14] proposed a link prediction model and pointed out that the link prediction mainly depends on the similarity between nodes. The more similar the two nodes are, the more likely that a link exists, which can be determined based on the common neighbor method and common path method. However, such methodology is not so suitable for large-scale social networks because of the high costs caused by computing feature values. Song et al. [15] proposed a matrix decomposition method to solve the problem of node similarity in online social networks, which can be applied to large-scale social networks. However, it raises a trick problem; i.e., online social networks do not completely correspond to offline social relationships. Then, Fire et al. [16] proposed a prediction algorithm for the cases lacking some offline friends. Such proposed algorithm can adapt to large-scale social networks as well. Moreover, this methodology can help online social network users to explicitly find people who either know each other or have similar interests with them.

In addition to the analysis of the node similarity to help the link prediction, the attributes like vertices and edges can also be extracted in different scenarios to improve the prediction performance. Benchettara et al. [17] proposed a link prediction algorithm for bipartite social networks based on the extracted attributes of vertices and edges.

Link prediction includes not only the positive one but also the negative one. Leskovec et al. [18] pointed out that the information contained in the negative link can effectively improve the prediction accuracy. Kunegis et al. [19] also confirmed that the negative link prediction can have added value to the social network analysis. Nevertheless, the existing negative link prediction algorithms mainly consider the number of negative interactions among users [18, 19], lacking the full utilization of the sentiment features in the interaction between users. Yuan and Pradeep [7] pointed out that adding emotional features can improve the accuracy of link prediction. Therefore, our paper mainly focuses on how to combine the user interaction information and sentiment analysis to solve the negative prediction problem.

3. Preliminaries

To better understand how to utilize the user interaction information and the positive link to predict the negative link, the basic definition is as follows.

First, a relation network g_p is given that contains the positive link, A is the user content relation matrix, O is the user opinion relation matrix, and then a predictor f is generated by g_p, A, and O, which can predict the negative relation network. Before illustrating our proposed method about the negative link prediction, the meanings of symbols which will be used are shown in Table 1.

3.1. Sentiment Polarity Intensity Quantification. In social networks, texts have the following characteristics: huge in volume, short in length, disorganized in words, and freely expressed in grammar. To perform sentiment analysis and quantification of network texts, we design a method for the short text of the social networks by using polarity intensity quantification. The intensity of the text is quantified based on the polarity intensity of each sentiment word.

Table 1: The meanings of symbols in the paper.

Symbol	Meaning
$\mathcal{G}_p$	A set of positive links known in the network
A	$R^{m\times M}$, user content matrix: the relationship matrix of users and contents
O	$R^{m\times M}$, user opinion matrix: the relationship matrix of users and opinions
Q (quantity)	$R^{m\times M}$, user opinion number matrix: the relationship matrix of users and the number of opinions
S	$R^{m\times M}$, user opinion intensity matrix: the relationship matrix of users and the sentiment intensity of opinions
C (count)	$R^{m\times m}$, user interaction number matrix: the relationship matrix of the number of user interactions
E (emotion)	$R^{m\times m}$, user interaction intensity matrix: the relationship matrix of the sentiment intensity of user interactions
NC (negative count)	$R^{m\times m}$, user negative interaction number matrix: the relationship matrix of the number of negative user interactions
NE (negative emotion)	$R^{m\times m}$, user negative interaction intensity matrix: the relationship matrix of the sentiment intensity of negative user interactions
N (nexus)	$R^{m\times m}$, user interaction matrix: the relationship matrix of user interactions
NN (negative nexus)	$R^{m\times m}$, user negative interaction matrix: the relationship matrix of negative user interactions
Senti	The polarity intensity quantification method

The sentiment words can be divided into basic sentiment words and compound sentiment words. The polarity of the basic sentiment words is based on the SentiWordNet annotation of the sentiment dictionary. The polarity intensity calculation of the compound sentiment words is complicated, which can be determined by the following semantic rules:

(1) Degree Modifiers+Basic Sentiment Words. Degree modifiers give different weights such as $(0.5, 0.7, 0.9, 1.1, 1.3, 1.5)$ depending on the intensity of action. For example, the weight 1.5 represents the sentiment intensity of "super," the weight 1.3 represents the sentiment intensity of "very," the weight 1.1 represents the sentiment intensity of "a little," and the weight 0.5 represents the sentiment intensity of "little." The polarity intensity of this type of compound words is the product of the intensity of the degree modifier and the intensity of the basic sentiment word. If the product exceeds the interval $[-1, 1]$, its boundary is used as the polarity of the compound word.

(2) Repeated Degree Modifiers. For example, the sentiment intensity of "really really like" is stronger than that of "really like." The weight of two "really" needs to be multiplied on the basis of the "like" weight. If the product exceeds the interval $[-1, 1]$, its boundary is used as the polarity of the compound words.

(3) Negatives+Basic Sentiment Words. Such compound words only need to reverse the polarity of the original emotional words. For example, the sentiment intensity of "not good" is the reverse of the intensity of "good."

(4) Negatives, Degree Modifiers, and Basic Sentiment Words Occur Continuously. The combination of such compound words is complicated. Moreover, the different order of appearance of the negatives and degree modifiers will produce the opposite sentiment tendency. If the degree modifiers appear in the middle between the negative and the basic sentiment word, the polarity is the same as that of the basic sentiment word, and the intensity is equal to the negation of the degree modifier. However, if the degree modifier appears before the negative and the basic sentiment word, the polarity of the compound word should be inverted on the polarity of the basic sentiment word, and the intensity should be multiplied by the weight of the degree modifier based on the basic sentiment word. If the product exceeds the interval $[-1, 1]$, the boundary is used as the polarity intensity of the compound word.

(5) Emoticons. Emoticons are one of the popular paradigms for users to express their emotional tendency with graphic animations. In order to express richer emotions, we add emoticons to the sentiment dictionary.

Based on the above semantic rules and the sentiment dictionary, we can compute the polarity and intensity of each sentiment word, which is shown as Equation (1) below:

$$\text{Senti}(t) = \begin{cases} \text{sign}\,(a_1) * \max\,(|a_1|, |a_n|), & \text{if } a_1 \times a_n > 0, \\ a_1 + a_n, & \text{if } a_1 \times a_n < 0, \end{cases} \tag{1}$$

where $\text{Senti}(t)$ represents the sentiment polarity and intensity of the text, t is the text to be quantified, and $a_1, a_2, a_3, \cdots, a_n$ is a sequence of all emotional words in the text t after sorted from large to small with the intensity. If $\text{Senti}(t)$ is positive, the larger the $\text{Senti}(t)$ is, and the stronger the positive sentiment of the text t is. However, if $\text{Senti}(t)$ is negative, the smaller the $\text{Senti}(t)$ is, and the stronger the negative sentiment of the text t is.

3.2. User Interaction Matrix Construction. The user interaction matrix is a comprehensive description to fully express the relationship between users. The interaction between users mainly includes point of praise, point stepping, forwarding,

and comment. The user interaction matrix is constructed as follows:

(1) Initializing the user opinion number matrix Q, user opinion intensity matrix S, user interaction number matrix C, user interaction intensity matrix E, user negative interaction number matrix NC, and user negative interaction intensity matrix NE, all of the elements in this matrix are initialized to 0

(2) In the user opinion relation matrix O, O_{ij} represents the comments that the user u_i gives the opinion P_j. With the polarity intensity quantification method in Section 3.1, we can calculate $\text{Senti}(O_{ij})$. If $\text{Senti}(O_{ij}) < 0$, we can set $O_{ij} = -1$, $S_{ij} = Q_{ij}$, which means that the opinion has negative emotion. On the contrary, If $\text{Senti}(O_{ij}) > 0$, we can set $O_{ij} = 1$, $S_{ij} = Q_{ij}$, which means that the opinion has positive emotion

(3) We set $C = A \times Q^T$, which matches the number of user interactions with the users to represent the number of the user interaction. We calculate $\text{NC} = A \times ((Q - |Q|)/2)^T$ to represent the number of negative user interaction

(4) We set $E = A \times S^T$, which matches the intensity of user opinions with the users to represent the emotional intensity of user interaction. We calculate $\text{NE} = A \times ((S - |S|)/2)^T$ to represent the negative emotional intensity of user interaction

(5) For each element C_{ij} in the user interaction number matrix C, if $C_{ij} = 0$, then $N_{ij} = 0$. Otherwise, $N_{ij} = (C_{ij} \times E_{ij})/\text{MAX}\{E_{ik}\}_{k=1,\cdots,m}$, where N_{ij} represents the interaction intensity between the users u_i and u_j. We can see that the more interactive times between users, the more intense the user interaction. The denominator of this formula is the max value of user emotional interaction to all other users, which is used to normalize the formula

(6) For each element NC_{ij} in the user negative interaction number matrix NC, if $\text{NC}_{ij} = 0$, then $\text{NN}_{ij} = 0$. Otherwise, $\text{NN}_{ij} = (\text{NC}_{ij} \times \text{NE}_{ij})/\text{MAX}\{\text{NE}_{ik}\}_{k=1,\cdots,m}$, where NN_{ij} represents the negative interaction intensity between users u_i and u_j

3.3. Reliability Weight Matrix Construction. The $U = \{u_1, u_2, \cdots, u_m\}$ represents the set of users in the network, where m represents the number of users. A symbol network can be divided into a positive network subgraph $g_{\text{p}}(U, E_{\text{p}})$ and a negative one $g_{\text{n}}(U, E_{\text{n}})$, where E_{p} and E_{n} represent the pair of users with a positive link and a negative one, respectively. E_{o} indicates the pair of users without the links, and the negative link prediction needs to construct the negative link sample from the unlabeled $E_{\text{n}} \cup E_{\text{o}}$. $P = \{p_1, p_2, \cdots, p_M\}$ represents a collection of content published by users, and M represents the number of content.

Based on the related user interaction matrix constructed in Section 3.2, the reliability weight matrix W is defined as Equation (2) below:

$$W_{ij} = \begin{cases} f\left(\dfrac{\text{NC}_{ij} \times \text{NE}_{ij}}{\text{MAX}\{\text{NE}_{ik}\}_{k=1,\cdots,m}}\right), & \text{NC}_{ij} \neq 0, \\ r, & \text{NC}_{ij} = 0. \end{cases} \tag{2}$$

3.4. Structural Balance Theory Equation. The basis of the symbol network is the structural balance theory. The balance theory examines the relationship of a triple, which considers that only "the friend's friend is my friend, the enemy's enemy is my friend" is a balanced relationship, and the other is unbalanced. Only the balanced relationship is stable, and the unbalanced relationship has the tendency to transform into a balanced relationship. The triple of the balance theory model is represented as a triangle with three edges, where the plus sign (+) is used to represent the positive relation on an edge, and the minus sign (-) is used to represent the negative one on an edge. The balance of the triangle structure can be determined by the product of three edges. If the product is positive, the structure is balanced. If the product is negative, the structure is unbalanced.

For example, suppose that s_{ij} indicates the relationship between the users u_i and u_j, which can be considered an edge in a triangle. If $s_{ij} = 1$, it indicates that there is a positive relationship between u_i and u_j. In contrast, if $s_{ij} = -1$, it indicates that there is a negative relationship between u_i and u_j. For example, the triple $\langle u_i, u_j, u_k \rangle$ could be balanced when: $s_{ij} = 1$, $s_{jk} = 1$, and $s_{ik} = 1$ or $s_{ij} = -1$, $s_{jk} = -1$, and $s_{ik} = 1$.

For the negative candidate users, we utilize a triple, $\langle u_i, u_j, u_k \rangle$, to determine whether they are the real, active, and existing users. The process is performed as follows: suppose that there are two users, saying u_i and u_k. If there is a third user u_j that is located in the middle of the users u_i and u_k, the triple is constructed. If the production of three edges in such triple does not meet the requirements of the structural balance theory, then we consider that the negative link is unstable and excluded from the negative link candidate set.

To make generalization better, we specify a matrix B. The x_h and x_l represent links $\langle u_i, u_k \rangle$ and $\langle u_j, u_k \rangle$, respectively. If the $\langle u_i, u_j \rangle$ is a positive link, both x_h and x_l are available, then $B_{hl} = 1$. Otherwise, if both x_h and x_l are unavailable, then $B_{hl} = 0$. According to the structural balance theory, if $B_{hl} = 1$, then the x_h and x_l must be the same type of link. Therefore, the balance theory equation is computed as Equation (3) below:

$$\min \frac{1}{2} \sum_{h,l} B_{hl} \left(w^T x_h - w^T x_l\right)^2 = w^T X \ell X^T w, \tag{3}$$

where ℓ is the Laplacian matrix on B. Equation (3) will be inferred in the negative link prediction algorithm of Section 4.3.

4. Negative Link Prediction Algorithm

The link prediction algorithm can be regarded as a classification problem, and the existing links are used as labels to extract features. Unlike the traditional positive link prediction problems, because many online social networks only open positive links to the public, it is necessary to build negative link sample sets firstly, and the accuracy of the sample sets would directly affect the accuracy of negative link prediction. This section firstly describes the construction algorithm of the negative link sample set and then introduces the feature extraction of the negative link. Finally, a negative link prediction algorithm is proposed.

4.1. Negative Link Sample Set Construction Algorithm. In this section, a negative link prediction sample set construction algorithm is proposed based on the methods presented in Section 3 of the sentiment polarity intensity quantification, the user interaction matrix construction, the RW-matrix construction, and the structural balance theory equation.

The basic idea of constructing the negative link sample set is to select negative interaction user pairs as negative link candidate sets from the negative interaction matrix and then use the structural balance theory and RW-matrix to further filter the candidate set to obtain highly reliable negative link samples.

The process of this proposed algorithm is described as follows:

(1) Initialization of the negative link sample set NS

(2) For each element of a negative user interaction matrix NN_{ij}, if the number of user negative interactions is not 0, that is $\mathrm{NN}_{ij} \neq 0$, add such user pair to the negative link sample candidate setNS

(3) The positive link subgraph g_{p} in the network and the negative link in the candidate set NS form a symbol network g; then, the structural balance theory is used to filter the edges in g

(4) For each user pair $\langle u_i, u_j \rangle$ in the candidate set NSand any useru_k which can form a triple set $\langle u_i, u_j, u_k \rangle$, if this triple set cannot satisfy the structural balance theory, $\langle u_i, u_j \rangle$ will be removed from the candidate set NS

(5) For each user pair $\langle u_i, u_j \rangle$ in the candidate set NSand any useru_k which can form a triple set $\langle u_i, u_j, u_k \rangle$, if this triple set can satisfy the structural balance theory, $\langle u_i, u_j \rangle$ will be preserved in the candidate set NS

(6) For each user pair $\langle u_i, u_j \rangle$ in the candidate set NS, if $(\mathrm{NE}_{ij}/\mathrm{MAX}\{\mathrm{NE}_{ik}\}_{k=1,\cdots,m}) < 0.5$ which indicates that the negative sentiment intensity of the user u_i to u_j is less than half of the maximum negative emotional intensity of the user u_i, to all other users, $\langle u_i, u_j \rangle$ will be removed from the candidate set NS

So far, we can obtain highly reliable negative link samples.

4.2. Feature Extraction of the Negative Link. From the negative link samples, we can extract features. The features of the negative links can be divided into the following categories: user features, user-user pair features, and symbol features. We explain such features in detail.

(1) User Features. It is extracted from each user node. The features of the user u_i include the following information: the in-degree or out-degree of the positive link, the number of the triples which contain the user u_i, the amount of content published by the user u_i, the positive or negative opinions to the content published by the user u_i, and the opinions that the user$u_i$have to other users.

(2) User-User Pair Features. It is used for extracting features from each pair of users $\langle u_i, u_j \rangle$. The extracted features include the following: the number of positive or negative interactions between u_i and u_j and between u_j and u_i, the Jaccard coefficient of the in-degree or out-degree between u_i and u_j, the shortest path between u_i and u_j, and the average value in respect to the sentiment intensity of positive or negative interactions between u_i and u_j.

(3) Symbol Features. The symbol network g is composed of the positive link subgraph g_{p} and the negative link sample set NS, where the weight of the positive link is 1. The weight of the negative link is obtained from the reliability weight matrix. The symbol features for each pair of users include the following: the weighted in-degree or weighted out-degree of the negative links of u_i and u_j, the Jaccard coefficient of the in-degree or out-degree of the negative links of u_i and u_j, and the features of 16 weighted triples proposed by Leskovec et al. [18].

These three types of features are represented by F1, F2, and F3, respectively. In order to obtain the influence of different features on the accuracy of prediction, the importance of each feature can be determined by gradually increasing the feature and by observing the change of the accuracy rate after the new features are added to the original feature set. The detailed experiment data is analyzed in Section 5.3.

4.3. Negative Link Prediction Algorithm. Previously, we obtain a highly reliable negative link sample set by selecting users with negative interactions from the user interaction matrix and utilizing structural balance theory and reliability matrix to filter out useless candidate sets. Meanwhile, feature extraction identifies the features required for the classification. Next, we should select the appropriate classifier to carry out the negative link prediction. Since some noises would be introduced to the construction of a negative link sample, the classifier should have the ability to tolerate noise. Here, the soft interval support vector machine is chosen as the classifier, which is proved to have better noise tolerance. Since the soft interval support vector machine (SVM) has the ability to tolerate noise, we introduce the SVM as the classifier.

Let $\chi = \{x_1, x_2, \cdots, x_N\}$ be a collection of pairs of users in $E_{\mathrm{n}} \in E_{\mathrm{o}}$, where X_i represents the feature vector of the user x_i,

E_n represents the pair of users with the negative link, and E_o indicates the pair of users without the link. The SVM in its standard form in the negative link prediction is given as Equation (4) below:

$$\begin{aligned} &\min_{w,b,\varepsilon} \frac{1}{2} PwP^2 + C \sum_{x_i \in \mathrm{PS} \cup \mathrm{NS}}^{N} \varepsilon_i \\ &\text{s.t.} \quad y_i\left(w^T x_i + b\right) \geq 1 - \varepsilon_i, \quad x_i \in \mathrm{PS} \cup \mathrm{NS} \\ &\varepsilon_i \geq 0, \end{aligned} \tag{4}$$

where ε_i, a slack variable, represents the noise tolerance of the training samples, and C is the penalty parameter ($C > 0$). Notice that the larger the penalty parameter C, the more the errors obtained in the classification penalty, and vice versa. In the negative link prediction algorithm, the noise levels of the positive and negative link samples are different because the positive link sample is trusted in the network and the negative is not, which is inferred from the prediction. Therefore, the slack variables C_p and C_n are introduced in the positive and negative links, respectively, to control the noise. Since the reliability of the negative link is measured by its reliability weight matrix, we introduce the slack variable c_j and set the negative link of $\langle u_i, u_j \rangle$ as x_i. When the c_j is used to control the noise of x_i, Equation (4) is updated to Equation (5) as follows:

$$\begin{aligned} &\min_{w,b,\varepsilon} \frac{1}{2} PwP^2 + C_p \sum_{x_i \in \mathrm{PS}}^{N} \varepsilon_i + C_n \sum_{x_i \in \mathrm{NS}}^{N} c_j \varepsilon_j \\ &\text{s.t.} \quad y_i\left(w^T x_i + b\right) \geq 1 - \varepsilon_i, \quad x_i \in \mathrm{PS} \\ &\qquad y_j\left(w^T x_j + b\right) \geq 1 - \varepsilon_j, \quad x_j \in \mathrm{NS} \\ &\varepsilon_i \geq 0, \quad \varepsilon_j \geq 0. \end{aligned} \tag{5}$$

The balance theory Equation (3) is introduced into the negative link prediction, and the slack variable C_b is given to the balance theory equation to control the error. Then, we can get the updated Equation (6) as follows:

$$\begin{aligned} &\min_{w,b,\varepsilon} \frac{1}{2} PwP^2 + C_p \sum_{x_i \in \mathrm{PS}}^{N} \varepsilon_i + C_n \sum_{x_i \in \mathrm{NS}}^{N} c_j \varepsilon_j + \frac{C_b}{2} w^T X 1 X^T w \\ &\text{s.t.} \quad y_i\left(w^T x_i + b\right) \geq 1 - \varepsilon_i, \quad x_i \in \mathrm{PS} \\ &\qquad y_j\left(w^T x_j + b\right) \geq 1 - \varepsilon_j, \quad x_j \in \mathrm{NS} \\ &\varepsilon_i \geq 0, \quad \varepsilon_j \geq 0. \end{aligned} \tag{6}$$

Equation (6) is an optimization problem with respect to the inequality constraints. We can transform such optimization problem into a dual form. Since w can be represented as $w^* = \sum a_i K(x_i, x)$ by the inner production of eigenvectors,

Table 2: The statistical result of the Epinions dataset.

Category	Number
Number of users	14765
Number of positive links	272513
Number of negative links	52704
Total number of texts	612321
Number of positive comments on the text	6937986
Number of negative comments on the text	163502

Equation (6) can be updated to Equation (7) as follows:

$$\begin{aligned} &\min_{a,b,\varepsilon} \frac{1}{2} a^T K a + C_p \sum_{x_i \in \mathrm{PS}}^{N} \varepsilon_i + C_n \sum_{x_i \in \mathrm{NS}}^{N} c_j \varepsilon_j + \frac{C_b}{2} a^T K \ell K^T a \\ &\text{s.t.} \quad y_i(a_k K(x_k x_i) + b) \geq 1 - \varepsilon_i, \quad u_i \in \mathrm{PS} \\ &\qquad y_j\left(a_k K\left(x_k, x_j\right) + b\right) \geq 1 - \varepsilon_j, \quad u_j \in \mathrm{NS} \\ &\varepsilon_i \geq 0, \quad \varepsilon_j \geq 0. \end{aligned} \tag{7}$$

In Equation (7), K is the Gram matrix of the samples. If we set S_i as Equation (8), we have

$$S_i = \begin{cases} C_p, & x_i \in \mathrm{PS}, \\ C_n c_i, & x_i \in \mathrm{NS}. \end{cases} \tag{8}$$

Then, when the Lagrange multipliers β and γ are factored into consideration, the Lagrange function of Equation (7) is expressed as Equation (9) below:

$$\begin{aligned} L(w, b, \varepsilon, a, \gamma) = {} & \frac{1}{2} a^T \left(K + C_b K \ell K^T\right) a + \sum_{i=1}^{l} s_i \varepsilon_i - \sum_{i=1}^{l} \beta_i \\ & \cdot \left[y_i \left(\sum_k a_k K(x_k, x_i) + b \right) - 1 + \varepsilon_i \right] - \sum_{i=1}^{l} r_i \varepsilon_i. \end{aligned} \tag{9}$$

Take the derivative of b and ε, respectively, to get Equation (10) as follows:

$$L(a, \beta) = \frac{1}{2} a^T \left(K + C_b K \ell K^T\right) a - a^T K J^T Y \beta + \sum_{i=1}^{l} \beta_i. \tag{10}$$

where $J = [I, 0]$, Y is a diagonal matrix of $l \times l$, and l is composed of positive and negative link samples.

When we compute the derivative of a and substitute Equation (10), the optimization problem is transformed into a

Table 3: The meaning and testing value setting of key parameters in the experiment.

	Meaning	Value
C_n	Error control for the negative sample	0, 0.001, 0.01, 0.05, *0.10*, 0.50, 1.0
c_j	Error control for the negative sample X_j	$f(x) = \begin{cases} 0, 0.01, 0.05, 0.10, 0.25 \\ 0.5, 0.75, 1, 1 - 1/\log(1+x) \end{cases}$
C_b	Regularization error control for the balance theory	0, 0.001, 0.01, 0.05, *0.10*, 0.50, 1.0

Lagrange function as Equation (11) below:

$$\max_{\beta} \sum_{i=1}^{l} \beta_i - \frac{1}{2}\beta^T Q \beta$$
$$\text{s.t.} \quad \sum_{i=1}^{l} \beta_i y_i = 0 \tag{11}$$
$$0 \le \beta_i \le s_i,$$

where $Q = YJK(I + C_b \ell K^T)^{-1} J^T Y$.

The process of the negative link prediction is illustrated as follows:

(1) Choose the SVM as the classifier, with Equation (4)

(2) Considering the noise control of positive and negative samples, different error control variables, C_p and C_n, are assigned to the positive and negative samples, respectively

(3) For the negative link sample x_i, a variable c_j is introduced to further control the error. $C_j = W_{ik}$ and W is the RW-matrix, with Equation (5)

(4) The structural balance theory is introduced into the negative link prediction, where the slack variable C_b is given to the balance theory equation to control the error, with Equation (6)

(5) With a series of deduction, an optimization problem is transformed into a Lagrange function following Equations (7)–(10), finally obtaining the negative link prediction model as Equation (11)

5. Results and Analysis

We present an in-depth discussion of our proposed negative link prediction algorithm. Section 5.1 describes the dataset used in the experiments, Section 5.2 explains the experimental platform, and Section 5.3 analyzes the experimental results.

5.1. Experimental Dataset. The Epinions is used as a dataset for experimental evaluation. It is an open commodity review website, which allows users to evaluate the commodity, make comments on statements from other users, and rate the trust or distrust of users. In addition, it also contains the following relationships: positive-negative relationship, users-content attributions relationship, and users-user rates relationship.

Table 4: Classification results of different feature sets under different classifiers.

Feature set	Classifier	Accuracy	Recall ratio	F1 score
F1	SVM	0.20	0.19	0.0195
	Naive Bayes	0.18	0.17	0.175
F1+F2	SVM	0.22	0.22	0.22
	Naive Bayes	0.20	0.20	0.20
F1+F2+F3	SVM	0.25	0.24	0.245
	Naive Bayes	0.22	0.21	0.215

The statistical results of the Epinions dataset are shown in Table 2.

For the data in Table 2, they need to be processed and filtered, and the users who have no positive or negative interactions with others need to be removed. By the way, the data quality indicators [20], such as accuracy, timeliness, completeness, and consistency, are a good choice for evaluating the quality of data for experimental data. Meanwhile, it should be noted that the negative link in Table 2 is only used as an experimental result analysis and for comparison, not for the training and classification of the negative link prediction model.

5.2. Experimental Setting. We mainly evaluate our proposed negative link prediction algorithm with three key parameters involved in the negative link prediction algorithm: C_n, c_j, and C_b. When testing one parameter, the remaining parameters are kept as default values. The detailed information with respect to each parameter is presented in Table 3, where the italicized data is the default value.

In order to evaluate the significance of our proposed algorithm, we choose four groups of baseline algorithms for comparisons, which are described as follows:

(1) Random Algorithm. This is the baseline algorithm in the general link prediction. The links in the network are randomly marked as negative, which indicates that the sampling set of the negative link is generated at random.

(2) The Shortest Path Algorithm. The shorter the shortest path between nodes in the network, the more likely there is a link. In addition, it might have a connection for the nodes with a distance of less than threshold 2. The algorithm considers the nodes as candidates when these nodes do not have a link or the shortest distance threshold is not greater than 2. Nodes in the candidate set are marked as negative links.

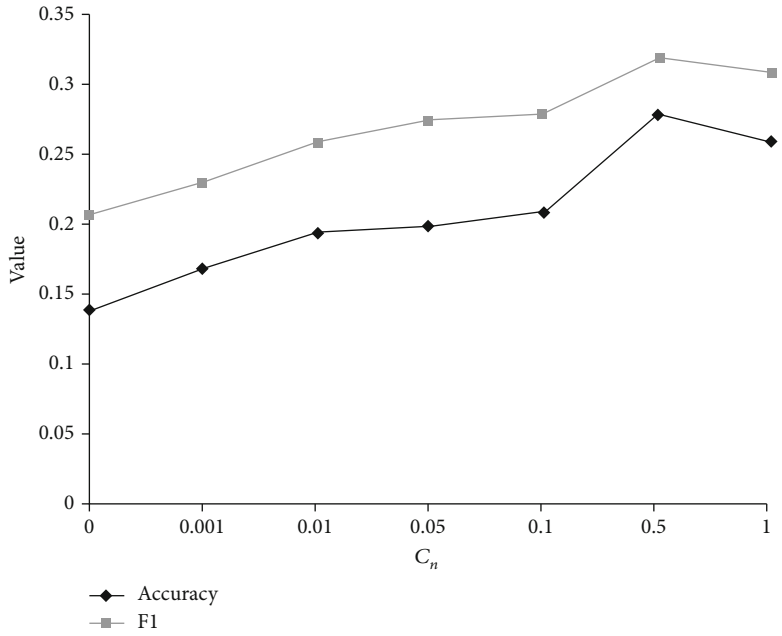

Figure 1: Influence of C_n on the predictive performance.

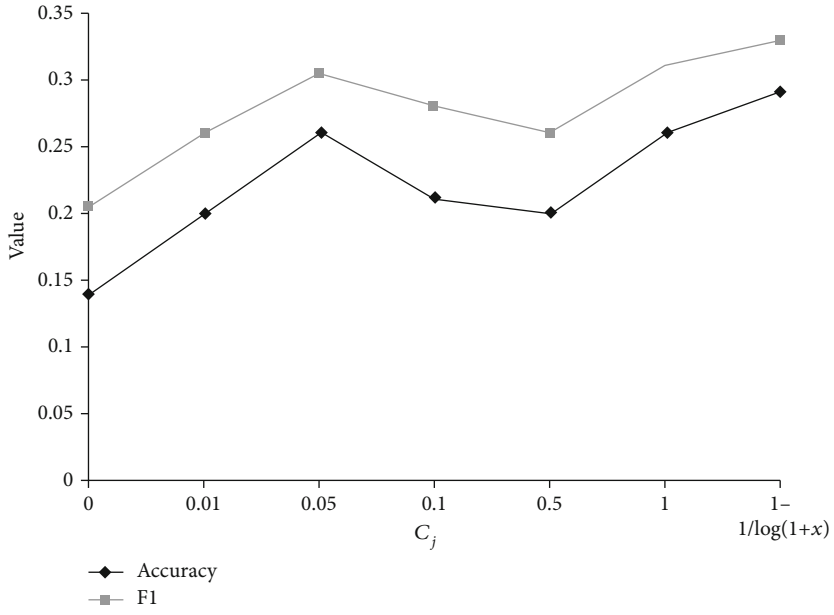

Figure 2: Influence of c_j on the predictive performance.

(3) Negative Interaction Determination Algorithm. Since there is a strong positive relationship between negative user interactions, the nodes are joined into the negative link candidate set when they have negative interactions. Then, nodes in the candidate set are marked as negative links when they are in pairs.

(4) Balanced Negative Interaction Determination Algorithm. Based on the negative interaction determination algorithm, the balance theory is introduced to filter out useless users. In other words, if the nodes do not meet the requirements of the balance theory, they will be dropped. Otherwise, they are added to the negative link candidate set. Then, nodes in pairs are marked as negative links.

5.3. Experimental Analysis

5.3.1. Experiment of Negative Link Feature Set Classification. Three types of features, viz., user features, user-user pair features, and symbol features, are represented as F1, F2, and F3, respectively. The meanings of these features are illustrated in Section 4.2.

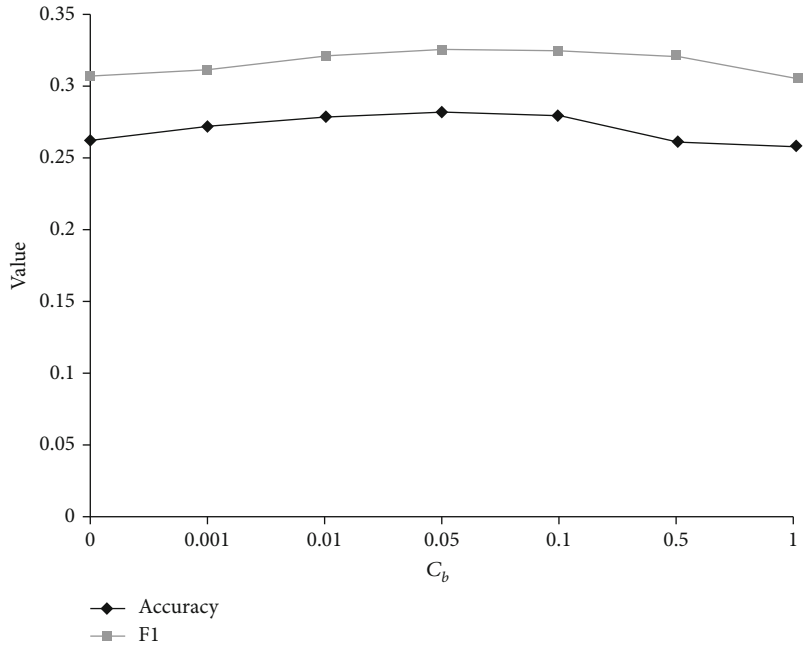

Figure 3: Influence of C_b on the predictive performance.

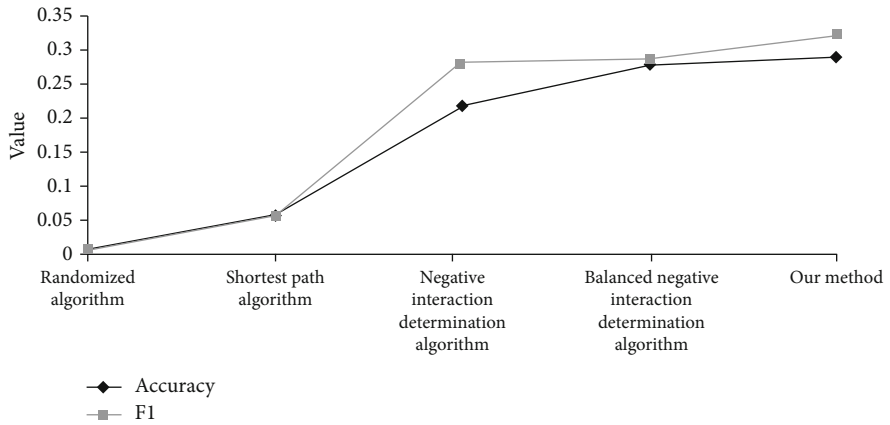

Figure 4: Comparison of the negative link prediction algorithm and the prediction reference methods.

In order to obtain the influence of different features on the prediction accuracy, w adopts a stepwise increasing feature method. For example, the first feature set (F1) contains only user features. The second feature set (F1+F2) contains user features and user-user pair features. And the third feature set (F1+F2+F3) contains all the features. By adding the new features to the original feature set, we can observe the changes in the classification accuracy to determine the importance of each feature.

We use SVM and Naive Bayes as the classifiers. The classification results on the real Epinions dataset are shown in Table 4.

From Table 4, we can find that SVM can achieve higher accuracy, which indicates that the SVM classifier is more suitable for negative link prediction. Furthermore, on each classifier, the F1 value increases consecutively as the feature increases, which indicates that these three types of features are helpful in the classification. More specifically, the F1 value has the fastest growth when adding the symbol features. It means that the symbol features play a crucial role in the classification results in the negative link prediction. The experimental analysis demonstrates that the RW-matrix proposed in our algorithm is reasonable and feasible.

5.3.2. Experiment of Key Parameters in the Negative Link Prediction Algorithm. We use C_n, c_j, and C_b as the key parameters to evaluate the algorithm. The experiment is performed by using the control variable method. When one parameter is tested, the other parameters are kept as the default values.

(1) Negative Sample Error Control Parameter Cn. The experimental results are shown in Figure 1. With the change of C_n, the accuracy rate and the F1 value are with a process that first

rises, gradually stabilizes, and then decreases. The peak value is reached when $C_n = 0.5$. When $C_n = 1$, the positive sample error control parameter should be $C_p = 1$; then, the positive samples and negative samples are the same as error control coefficients. The decreases in the accuracy rate and F1 value indicate that the negative sample should be given a different error control coefficient.

(2) Error Control Parameter cj for the Negative Sample xj. The negative link $\langle u_i, u_j \rangle$ is recorded as a negative sample x_j, $c_j = W_{ij}$ is the error control parameter of x_j, and W is the reliability weight matrix (RW-matrix). The experimental results are shown in Figure 2, and $c_i = f(x) = 1 - (1/\log(1 + x))$ is a better function identified by the previous researchers, which has also achieved higher accuracy in this experiment. Due to a direct relationship between the number of negative interactions and the number of negative links, when $c_j = 0$, the negative link prediction without considering the number of negative interactions is much less accurate. When x_j takes other constants, the accuracy rate decreases to a certain degree compared with $c_i = f(x) = 1 - (1/\log(1 + x))$. This indicates that the RW-matrix can really reflect the reliability of the negative link.

(3) Regularization Error Control Parameter Cb of the Structural Balance Theory. The experimental results are shown in Figure 3. With the change of C_b, the accuracy rate and the F1 value both rise firstly and gradually decrease afterwards. $C_b = 0$ to $C_b = 0.001$ is a significant improvement in accuracy, indicating that the regularization equation of the structural balance theory can improve the performance of negative link prediction. The middle segment remains relatively stable, and the accuracy gradually decreases with the increase of C_b. Such results indicate that the weights should be selected appropriately; otherwise, too large weights would reduce the accuracy rate.

5.3.3. Experiment of the RWSBT-NLP Algorithm and Baseline Algorithm Comparison. The negative link prediction algorithm is compared with four prediction reference methods, illustrated in Section 5.2. The experimental results are shown in Figure 4. The performance of the random algorithm is the worst since the negative link accounts for a small proportion of the overall network. The shortest path algorithm has a larger improvement than the random algorithm, which indicates that the negative link is more likely to exist in the network at a very close distance. The accuracy of the negative interaction determination algorithm has increased dramatically, which indicates that there is a strong link between negative interactions and negative links. The balanced negative interaction determination algorithm improves the accuracy rate compared to the negative interaction determination algorithm, which means that the balance theory does improve the accuracy rate by removing some points that do not meet the balance theory. The accuracy of our proposed negative link prediction algorithm is slightly higher than that of the balanced negative interaction determination algorithm. It indicates that when the negative link prediction algorithms take the sentiment characteristics into account, they can improve the accuracy of the prediction and have a good performance.

6. Conclusions

This paper focuses on the problem of negative link prediction in symbol networks. We propose a negative link prediction algorithm by using the sentiment analysis and structural balance theory. The sentiment analysis is mainly embodied in the construction of the user interaction matrix based on the calculation of the sentiment intensity of social network texts. Based on the user interaction matrix, we construct the reliability weight matrix (RW-matrix). Then, based on the structural balance theory and constructed RW-matrix, we propose the negative link prediction algorithm by building the negative link sample set and extracting the features. With the experiments and conductions with the real dataset, the influence of each parameter on the accuracy of the prediction results has been analyzed based on the control variable method. Compared with the existing predictive algorithms, the proposed negative link prediction algorithm can improve the accuracy of prediction dramatically with good performances.

Data Availability

The Epinions dataset used to support the findings of this study can be available from http://www.trustlet.org/epinions.html.

Conflicts of Interest

The authors declare that there is no conflict of interest regarding the publication of this paper.

Acknowledgments

Thanks are due to QuanFeng YAO, Xiang HU, and JiWei HU for their help. This work was supported by the Social Science Fund Planning Project of the Ministry of Education of the People's Republic of China "Research on Data Service and Guarantee for the Fourth Paradigm of Social Science" (20YJA870017).

References

[1] H. Cheng, N. Xiong, A. V. Vasilakos, L. Tianruo Yang, G. Chen, and X. Zhuang, "Nodes organization for channel assignment with topology preservation in multi- radio wireless mesh networks," *Ad Hoc Networks*, vol. 10, no. 5, pp. 760–773, 2012.

[2] H. Cheng, Z. Su, N. Xiong, and Y. Xiao, "Energy-efficient node scheduling algorithms for wireless sensor networks using Markov random field model," *Information Sciences*, vol. 329, pp. 461–477, 2016.

[3] M. H. Miraz and M. Ali, "Applications of blockchain technology beyond cryptocurrency," 2018, https://arxiv.org/abs/1801.03528.

[4] O. Tanevski, I. Mishkovski, and M. Mirchev, "Link prediction on Bitcoin OTC network," 2020.

[5] B. Jeong, J. Lee, and H. Cho, "Improving memory-based collaborative filtering via similarity updating and prediction modulation," *Information Sciences*, vol. 180, no. 5, pp. 602–612, 2010.

[6] J. Tang, H. Gao, X. Hu, and H. Liu, "Exploiting homophily effect for trust prediction," in *Proceedings of the Sixth ACM International Conference on Web Search and Data Mining*, pp. 53–62, New York, 2013.

[7] G. Yuan and K. Pradeep, "Exploiting sentiment homophily for link prediction," in *Proceedings of the 8th ACM Conference on Recommender Systems*, pp. 17–24, New York, 2014.

[8] J. Tang, X. Hu, Y. Chang, and H. Liu, "Predictability of distrust with inter-action data," in *Proceedings of the 23rd ACM International conference on Conference on Information and Knowledge Management*, pp. 181–190, New York, 2014.

[9] H. Ma, M. Lyu, and I. King, "Learning to recommend with trust and distrust relationships," in *Proceedings of the Third ACM Conference on Recommender Systems*, pp. 189–196, New York, 2009.

[10] J. Cho, "The mechanism of trust and distrust formation and their relational outcomes," *Journal of Retailing*, vol. 82, no. 1, pp. 25–35, 2006.

[11] P. Sharma, U. K. Singh, T. V. Sharma, and D. Das, "Algorithm for prediction of links using sentiment analysis in social networks," in *Proceedings of the 7th International Conference on Computing Communication and Networking Technologies*, pp. 110–116, New York, 2016.

[12] K. Jérôme, A. Lommatzsch, and C. Bauckhage, "The Slashdot Zoo: mining a social network with negative edges," in *Proceedings of the 18th International Conference on World Wide Web*, pp. 741–750, New York, 2009.

[13] K. Y. Chiang, C. J. Hsieh, N. Natarajan, I. S. Dhillon, and A. Tewari, "Prediction and cluster-ing in signed networks: a local to global perspective," *Journal of Machine Learning Research*, vol. 15, no. 1, pp. 1177–1213, 2013.

[14] D. Liben-Nowell and J. Kleinberg, "The link-prediction problem for social networks," in *Proceedings of the Twelfth International Conference on Information and Knowledge Management*, pp. 556–559, New York, 2009.

[15] H. H. Song, T. W. Cho, V. Dave, Y. Zhang, and L. Qiu, "Scalable proximity estimation and link prediction in online social networks," in *Proceedings of the 9th ACM SIGCOMM Conference on Internet Measurement*, pp. 322–335, New York, 2009.

[16] M. Fire, L. Tenenboim, O. Lesser, R. Puzis, L. Rokach, and Y. Elovici, "Link prediction in social networks using computationally efficient topological features," in *2011 IEEE Third International Conference on Social Computing*, pp. 73–80, New York, 2011.

[17] N. Benchettara, R. Kanawati, and C. Rouveirol, "Supervised machine learning applied to link prediction in bipartite social networks," in *Proceedings of the 2010 International Conference on Advances in Social Networks Analysis and Mining*, pp. 326–330, New York, 2010.

[18] J. Leskovec, D. Huttenlocher, and J. Kleinberg, "Predicting positive and negative links in online social networks," in *Proceedings of the 19th International Conference on World Wide Web*, pp. 641–650, New York, 2010.

[19] J. Kunegis, J. Preusse, and F. Schwagereit, "What is the added value of negative links in online social networks?," in *Proceedings of the 22nd International Conference on World Wide Web*, pp. 727–736, New York, 2013.

[20] H. Cheng, D. Feng, X. Shi, and C. Chen, "Data quality analysis and cleaning strategy for wireless sensor networks," *EURASIP Journal on Wireless Communications and Networking*, vol. 2018, no. 1, 11 pages, 2018.

Hindawi
Wireless Communications and Mobile Computing
Volume 2021, Article ID 6620236, 20 pages
https://doi.org/10.1155/2021/6620236

Research Article

Blockchain-Based DNS Root Zone Management Decentralization for Internet of Things

Yu Zhang, Wenfeng Liu, Zhongda Xia, Zhongze Wang, Lu Liu, Weizhe Zhang, Hongli Zhang, and Binxing Fang

Harbin Institute of Technology, Harbin, China

Correspondence should be addressed to Wenfeng Liu; 15b903031@hit.edu.cn

Received 23 October 2020; Revised 23 December 2020; Accepted 19 January 2021; Published 8 February 2021

Academic Editor: Hongju Cheng

Copyright © 2021 Yu Zhang et al. This is an open access article distributed under the Creative Commons Attribution License, which permits unrestricted use, distribution, and reproduction in any medium, provided the original work is properly cited.

Domain Name System (DNS) is a widely used infrastructure for remote control and batch management of IoT devices. As a critical Internet infrastructure, DNS is structured as a tree-like hierarchy with single root zone authority at the top, which puts the operation of DNS at risk from single point of failure. The current root zone management is lack of transparency and accountability, since only the root zone file is published as the final outcome of operations inside the root zone authority. Towards distributed root zone operation in DNS, this paper presents a blockchain-based root operation architecture—RootChain, composed of multiple root servers. On the basis of maintaining the single root authority for top-level domain (TLD), RootChain decentralizes TLD data publication by empowering delegated TLD authorities to publish authenticated data directly. The transparency and accountability of root zone operation are attained by smart-contracting the whole life cycle of TLD operation and logging all operations on the chain. RootChain is transparent to recursive/stub resolver and DNS/DNSSEC-compatible. A proof-of-concept prototype of RootChain has been implemented with Hyperledger Fabric and evaluated by experiments.

1. Introduction

The rapidly developing Internet of Things devices have touched every corner of our life. Nowadays, remotely controlling IoT devices and acquiring data from IoT devices are the popular requirements. In order to efficiently manage a large number of IoT devices across platforms and scenarios, it is currently a feasible method to allocate a DNS name to each device as a globally unique identifier.

Users resolve the domain name of the IoT device through the DNS infrastructure to obtain the IP address required for further communication. Throughout the whole interaction process with IoT devices, the reliability and availability of the DNS domain name, especially the root domain name as the name resolution starting point, is the prerequisites.

DNS is structured as a tree-like hierarchy with a single root at the top. Currently, under the functions of Internet Assigned Numbers Authority (IANA), the operation and maintenance of root zone are performed by Public Technical Identifiers (PTI) as the root zone operator and Verisign as the root zone maintainer, respectively, on behalf of the IANA function operator—Internet Corporation for Assigned Names and Numbers (ICANN). Although there are 13 root servers with hundreds of root server mirrors, the centralization of root zone management puts the DNS at risk from single point of failure (SPOF). The root zone management is lack of transparency and accountability, since only the root zone file is released as the result of the management process, the management process is like a black-box, implemented through the collaboration of several inner root zone management partners.

In order to reduce the single point of failure of DNS root, there have been some typical and widely used blockchain-based DNS decentralization solutions. Unfortunately, they all have compatibility issues with the current DNS, which makes it difficult to be further widespread used. Namecoin

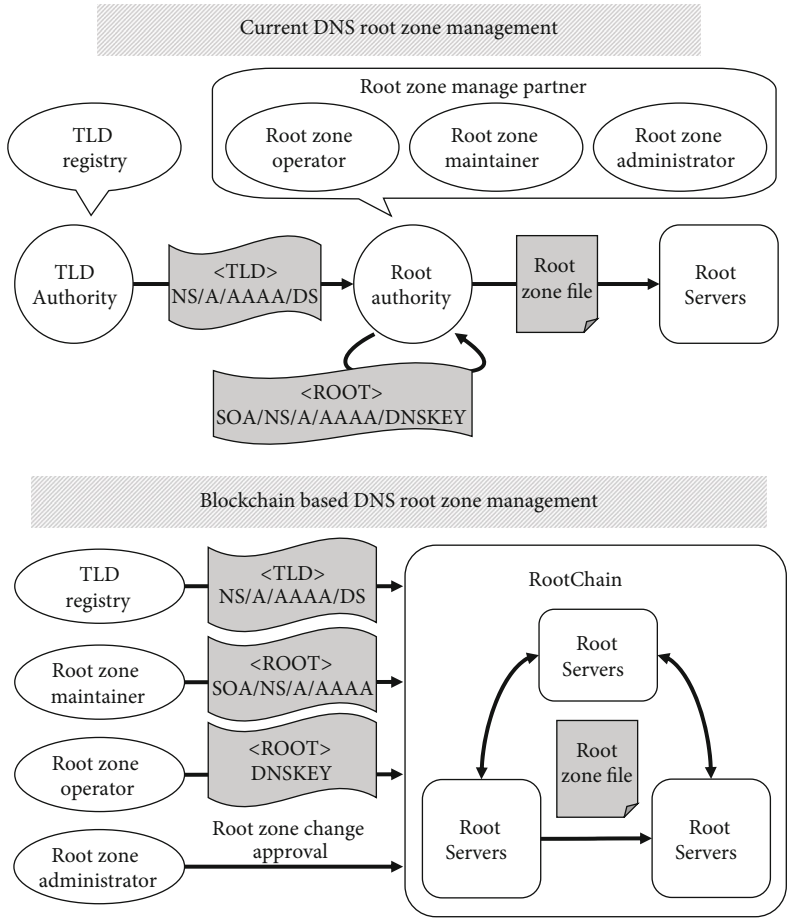

Figure 1: Comparison of the root zone data publication process between DNS and RootChain.

[1] and its successor Blockstack [2] are two notable solutions that have been deployed, which provided decentralized name registration and resolution service based on blockchain. Blockstack creates a new namespace independent from the current DNS, leading to namespace split. In Blockstack, domain names are registered in a first-come-first-serve manner, which is vulnerable to cybersquatting.

To help DNS improve operation transparency and reduce the risk of single point of failure, we propose RootChain, a systematical design for distributed DNS root zone management based on blockchain, which achieves the following goals:

(i) *Goal 1: Uniform Global Namespace*. Retaining a uniform global namespace with the single root authority of current DNS, so to avoid namespace split and cybersquatting.

(ii) *Goal 2: Anti-SPOF Risk*. Distributing root zone operation cross multiple physical nodes under different operators, so to avoid the single point of failure.

(iii) *Goal 3: Transparency and Accountability*. Supporting the operation of the entire TLD life cycle management, so to provide the transparency and accountability of root zone management process.

(iv) *Goal 4: Compatibility*. Be transparent to recursive resolver and compatible with DNS/DNSSEC at protocol level.

RootChain builds a permissioned blockchain that run by current root server operators. To reduce SPOF risk, RootChain decentralizes root zone management while still retaining a single root authority to maintain uniform global namespace; the key idea of RootChain is to separate delegation and data publication from the root zone management process; the root authority is responsible for TLD delegation, and each TLD authority publishes data for its own TLD through RootChain. The root authority and TLD authorities contribute data to the root zone file together via RootChain. Such cooperation among multiple stakeholders effectively mitigates the SPOF risk in current root zone management. With the operations recorded and publicized on RootChain, the inherent consensus and tamper-proof characteristics of blockchain significantly improve the transparency and accountability of root zone management. A comparison between current root zone management and RootChain (blockchain-based) root zone management is illustrated in Figure 1.

The key contributions are as follows:

(i) Propose a blockchain-based architecture for distributed root zone management, realizing a cooperation

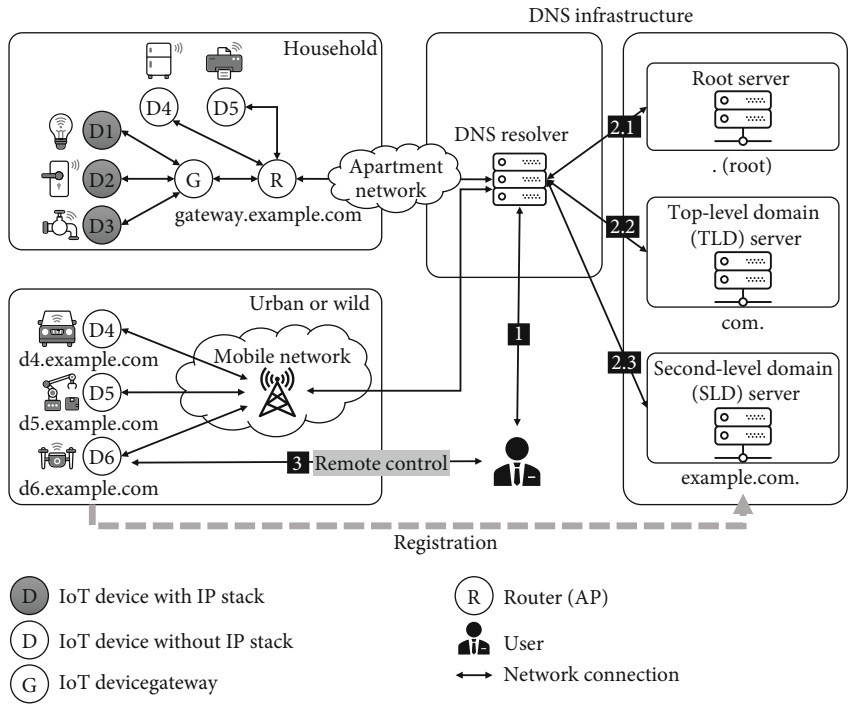

Figure 2: Example scenes of the relationship between DNS and IoT devices. Users identify the network location of the IoT devices by using its domain name of through DNS.

framework for multiple root zone management partners, which is compatible with the current DNS

(ii) Design smart contracts for supporting the operation of the entire TLD life cycle management. We propose a flexible and configurable TLD delegation strategy based on a state machine for different types of TLDs and different business models

(iii) Design, implement, and evaluate a proof-of-concept prototype of RootChain based on Hyperledger Fabric [3]. To the best of our knowledge, RootChain is the first distributed and DNS-compatible system for root zone management

The remainder of this paper is structured as follows. Section 2 introduces the background, including the interaction logic between DNS and IoT as well as the current DNS root zone management model. Section 3 explains the potential risks in the current root zone management model. Section 4 presents the RootChain architecture. Section 5 designs smart contracts. Section 6 discusses the properties of RootChain. Section 7 explains the implementation details. Section 8 evaluates RootChain. Section 9 introduces related work. Section 10 concludes the paper.

2. Background

2.1. The Interactions between IoT and DNS. As shown in Figure 2, we define the model of IoT as a combination of devices that sense and act on the physical environment and provide remote services based on the Internet. There are usually big differences between IoT devices, including differences in hardware architecture, operating systems, and network functions.

From the perspective of the development trend of IoT devices, IoT devices have at least one thing in common, that is, they need to store the current state of the device to a remote server and accept control command from remote users via the Internet. In other words, practical development experiences show that IoT devices usually rely on some centralized cloud services to better interact with users, and users usually interact with IoT devices through cloud servers. The interaction between IoT devices and DNS infrastructure is mainly reflected in the following two typical scenes:

Scene 1. IoT devices collect environmental data through the carried sensors and upload the data to the data server for users to pull and use. In this scenario, IoT devices initiate DNS queries to resolve the IP address of the remote data server.

Scene 2. Users send a control command to the IoT device through the control server to make the device take a series of actions. In this scenario, IoT devices register the domain name used for identifying itself in the authoritative server in advance.

Typical IoT applications, such as indoor smart locks, smart water and electricity equipment, outdoor smart cars, and mechanical equipment, need to uniquely name the device object and then use name resolution system to uniquely identify the device on the network.

Figure 2 shows that the user identifies the network location (IP address) of the IoT device by using the domain name of the IoT device through DNS. The user needs to control the drone through the network for cruise and photography task. The domain name of the drone is identified as http://d6

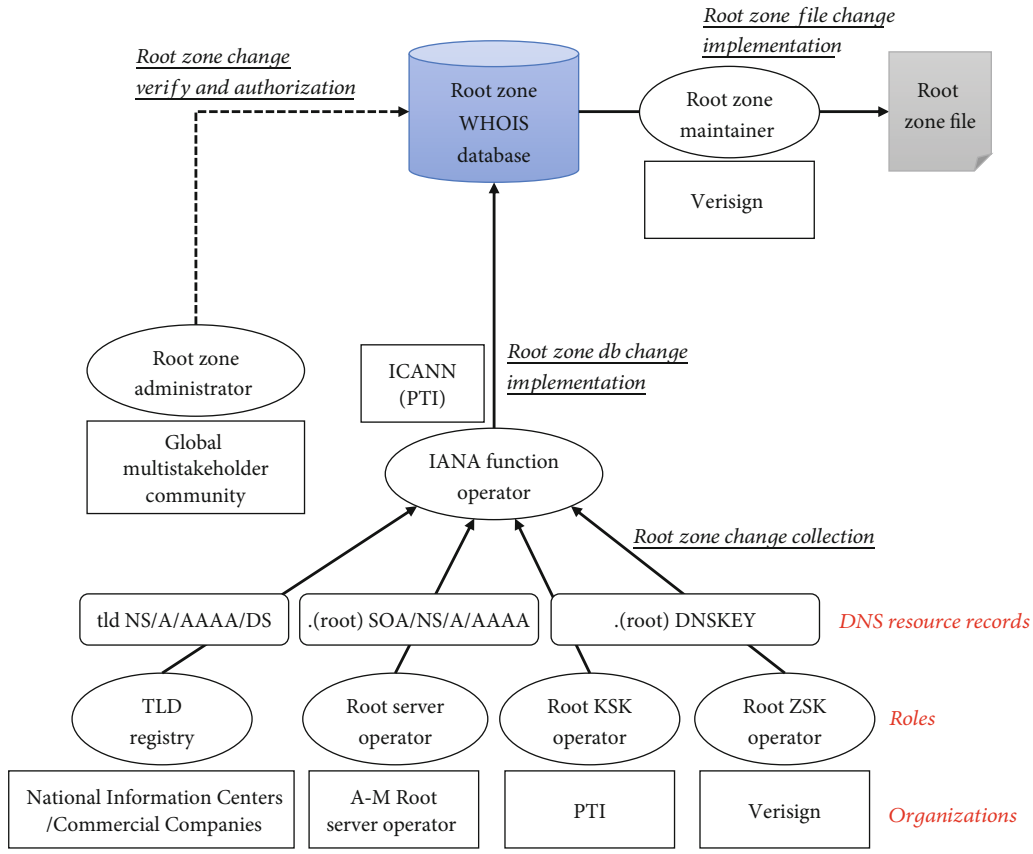

Figure 3: DNS root zone management model—roles and organizations.

.example.com/, and the name is registered in the service application and DNS server in advance.

When remotely controlling the drone to perform a task, the user needs to acquire the IP address of the drone named http://d6.example.com/ through hierarchical structured DNS. DNS root server is the starting point for domain name resolution. The user first queries the root server for the IP address of the top-level domain (TLD) authoritative server of the domain name—com—and then queries the TLD authoritative server for the IP address of the second-level domain (SLD) authoritative server of the domain name—http://example.com/, which is managed by the application service provider. Finally, query the current IP address of the drone from the SLD authoritative server. After the user obtains the IP address of the drone device, they can transmit task commands to the drone device via the Internet.

2.2. DNS Root Zone Management Model. Root zone management involves the processes by which changes are made to the root zone resource records. There are three main roles involved in managing the root zone (Figure 3): IANA function operator, root zone maintainer, and root zone administrator. The IANA function operator is responsible for collecting and processing requests for changes to the root zone data from all participating parties and implementing changes to the root zone database (WHOIS database [4]). The root zone maintainer is responsible for implementing changes to the root zone files based on the root zone database. The root zone administrator verifies whether the above two roles follow the established procedures and policies during the operation process and authorizes the implementation of root zone database changes and implementation of root zone file changes.

The three roles of IANA function operator, root zone maintainer, and root zone manager are performed by different organizations. The ICANN organization (performed by its affiliate PTI) plays the role of the IANA function operator, and ICANN legally obtains the right to exercise the function by signing the IANA function contract [5]. IANA has several key functions [6], and we mainly focus on its DNS root zone management functions in this paper. Verisign performs the role of root zone maintainer by signing a root zone maintenance service agreement (RZMA) [7] with ICANN. The role of root zone manager has been performed by the US Commerce Department's National Telecommunications and Information Administration (NTIA) since 2000. In 2016, NTIA signed a withdrawal contract [8] and announced that this role would be subsequently transferred to the ICANN board of directors composed of global multistakeholders.

The IANA function operator is responsible for collecting root zone changes from the downstream roles that provide root zone data and submitting them to the root zone database after summarizing them. From the perspective of the data provider, the root zone data includes three types: (1) top-level domain data (tld NS-Records, A/AAAA-Records, and DS-Records), (2) root server data (root NS-Records,

A/AAAA-Records, and SOA-Records), and (3) root key data (root DNSKEY-Records). The role of providing top-level domain data is TLD registry, which is usually played by national information centers (ccTLDs) or commercial companies (gTLDs). The role of providing root server data is the root server operator, played by current 12 root server operators [9] around the world. The roles that provide root key data are root KSK operator and root ZSK operator, played by PTI and Verisign, respectively.

3. Problem Description

3.1. Threat Modeling for DNS Root Zone Management. By analyzing the current DNS root zone management model introduced above (Section 2.2), we can find that there are two main potential threats in the root zone management process.

Single point of failure risk. Related roles (TLD registry, root server operator, root KSK/ZSK operator), respectively, submit part of the root zone data that they are responsible for, but all submitted data need to be aggregated to the role of IANA function operator before it can be written to the root zone database according to predetermined procedures and strategies. This means that IANA function operator is the bottleneck of the entire root zone management process. When IANA function operator has an availability failure or misconfiguration, it will cause subsequent name resolution failure of hundreds of root servers that rely on this piece of root zone data file.

Lack of transparency and accountability. Root zone management details inside the root zone management partners are mostly hidden to the public. Only the root zone file is published as the final management outcome. The management process includes the interaction between multiple roles. For example, the IANA function operator needs to verify the authenticity of its identity before receiving the root zone changes submitted by the TLD registry, all root zone data changes need to be reviewed by the root zone administrator before they can be updated to the root zone database. The root zone maintainer can only use the data reviewed by administrator to generate root zone files. However, the root zone file does not contain the records of the above interaction process, which means when the root zone data has misconfiguration, and the public cannot understand at which step the root zone data problem occurs. The lack of transparency has further led to a lack of accountability of root zone management. When there is a problem with the root zone data, you can only rely on the self-correction and self-examination between root zone management partners, which creates a space for shirking responsibility to a certain extent.

3.2. Assumption. This paper assumes that only the IANA function operator role can authorize top-level domains to ensure a globally unique DNS namespace, and all root server operators and all users admit the TLD delegation decisions made by IANA function operator.

This paper assumes that the root management partners may provide service in an arbitrary and unpredictable way. This may be a result of compromised server, misoperation/-misconfiguration, software/hardware failure, etc.

4. System Design

4.1. Architecture of RootChain. RootChain is a permissioned blockchain system comprised of root servers running blockchain nodes. By separating the delegation of TLDs from the data publication of TLDs, RootChain distributes DNS root zone operation while retaining a single root authority. The transactions of root zone operation are submitted to RootChain by the root authority and TLD authorities and are recorded in the blockchain ledger cross all root servers. The root zone file can be derived from the blockchain ledger consisting of transactions of root zone operation. As shown in Figure 4, there are four major roles in RootChain:

Root authority. There is only one single root authority in RootChain. The root authority here covers the 3 roles of IANA function operator, root zone maintainer, and root zone administrator in current DNS. Besides publishing root domain data, the root authority delegates a TLD to a TLD authority and transfers and revokes existing TLD delegations according to contracts signed among the root authority and TLD authorities.

TLD authority. The TLD authority in RootChain refers to the role of TLD registry in DNS. A TLD is delegated to a TLD authority by the root authority through submitting TLD delegation transaction to RootChain. TLD authority publishes the data of authoritative servers for the delegated TLD, renews the delegated TLD before the delegation expires, redeems the delegated TLD after the delegation expires, and performs operations according to the delegation contract signed with the root authority.

Root server operator. A root server operator is responsible for managing root servers. Besides providing name resolution service as authoritative name servers, root servers in RootChain are also responsible for the root zone management according to the blockchain transactions. Root server operators guarantee the physical security and constant availability of root servers, ensure that root servers continue to participate in RootChain, and provide nondiscriminatory name resolution service to users.

User. A user of RootChain corresponds to a recursive resolver and stub resolver in the current DNS, which sends a standard DNS query to any root server to obtain the NS and A/AAAA records of TLDs.

4.2. Root Zone Operation for TLDs. There are three types of root zone operations for TLDs in RootChain, as shown in Figure 5.

Delegation operations. The root authority delegates TLD to TLD authorities with *delegation publication* operations, by binding TLDs to the public keys of TLD authorities. The root authority may transition or revoke TLDs with *delegation transition* operations or *delegation revocation* operations; TLD authorities may renew and redeem the delegation of TLDs with *delegation renewal* operations and *delegation redemption* operations.

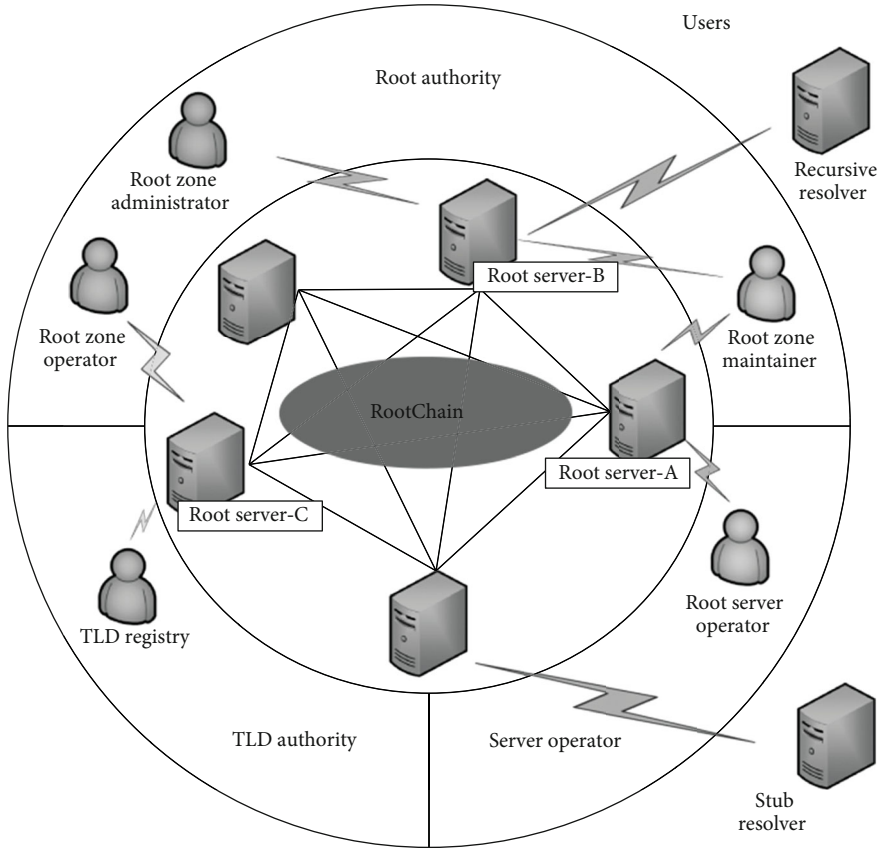

Figure 4: RootChain architecture.

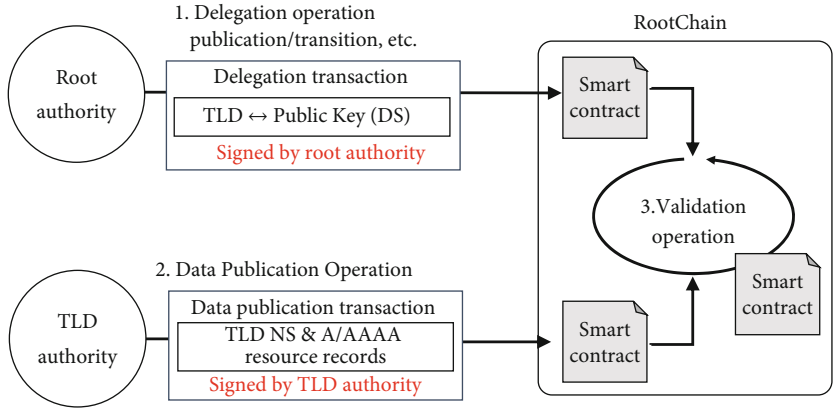

Figure 5: Root zone operation for TLDs.

The smart contracts that determine the *delegation policy* are specified in the corresponding delegation operation. It should be noted that a delegation operation may not always take effect immediately, and certain operations need to wait for confirmations from other authorities to take effect, which we will be explained further in Section 4.3.

Data publication operations. A TLD authority publishes the NS/A/AAAA resource records for the delegated TLD by sending signed data publication operations to RootChain. A data publication operation is valid and will be used as part of the root zone file only if it carries the proper signature signed by the corresponding TLD authority. Note that a new data publication operation for a TLD will overwrite the previously published data.

Validation operations. Root servers validate the effectiveness of the delegation operation and the data publication operation by executing smart contracts in the validation operation. Smart contracts enforce the root authority and all TLD authorities to only act in accordance with established policies. More details on smart contracts will be presented in Section 5.

4.3. Delegation Policies. A delegation policy is specified in a TLD delegation publication operation and determines how

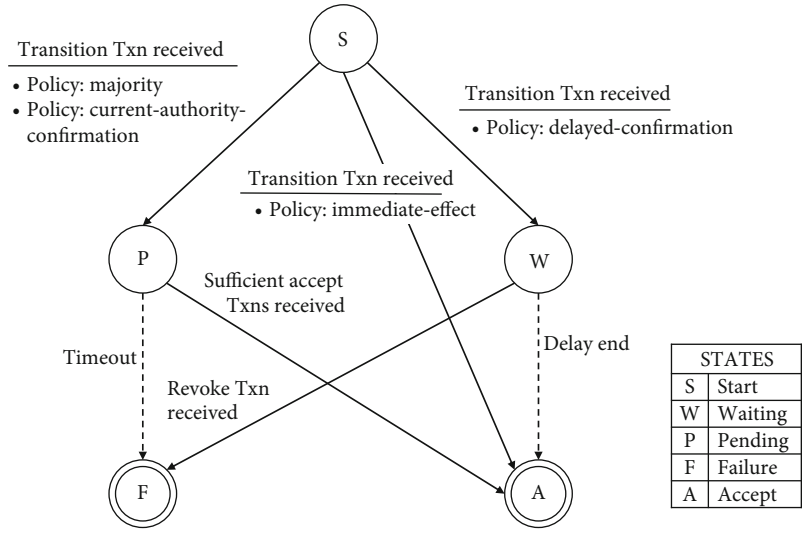

Figure 6: State transition diagram of TLD delegation operations.

the delegation of the TLD may be later operated. We have defined four delegation policies:

Delayed-confirmation policy: an operation will take effect only if no objections are received within a grace period. This policy is usually used in scenarios where disputes and frictions occur between root and TLD authorities; delayed acknowledgement brings a grace period to the delegation operation; during the grace period, the dispute may be resolved through offline negotiations among the authorities.

Majority policy: an operation takes effect only if confirmations are received from more than half of the TLD authorities in RootChain. This policy applies to scenarios that require more democratic and collective decision-making.

Current-authority-confirmation policy: when a TLD has been delegated to an TLD authority, subsequent operations such as delegation transition and revocations must be approved by the current TLD authority. This policy focuses on protecting the rights of the delegated TLD authority.

Immediate-effect policy: an operation submitted by an authority may immediately take effect. This policy applies to delegation operations accepted by default; for example, the former authority of a TLD is generally considered to have the right to redeem the TLD preferentially during a grace period.

The above four delegation strategies are the expression of different degrees of trust relationship between members in different situations. The majority policy applies to situations that require collective decision-making and need to be resolved when the authorization of a top-level domain name is disputed, but a single entity's interests may be damaged by collective decision-making. Delayed-confirmation policy is used in situations of high mutual trust among members. Delegation operations that have been initiated take effect automatically for a certain period. This strategy reduces the process of interaction, but when there are a few of destroyer in the environment, the management process would be confused. The current-authority-confirmation and immediate-effect policy are applied to situations that require a high degree of protection for delegated entity, who have full control over the top-level domains delegated to them. This strategy makes root domain management more distributed and weakens the root authority's control over the top-level domain authority.

RootChain implements the above policies through smart contracts. Different from the current DNS without the concept of delegation policy in the DNS protocol specifications, RootChain can flexibly express more rich and finer-grained delegation policies according to the real-world scenarios. This is one significant advantage of RootChain over the current DNS.

Figure 6 shows the state transition of a TLD in RootChain resulting from the execution of TLD delegation operations under different policies. Take the delegation transition operation as an example, the TLD is in the S state before a coming delegation transition operation, indicating that the current TLD delegation information is in effect. When RootChain receives the delegation transition operation, the state of the TLD begins to change:

(i) The TLD enters the W state, if a TLD uses the delayed-confirmation policy in the corresponding delegation publication operation. If RootChain does not receive any objection to the delegation transition during the grace period, the delegation transition will automatically enter the "accept" state after the grace time expires, and the delegation transition operation takes effect. If the RootChain receives the root authority's objection during the grace period, the TLD delegation transition operation immediately enters the "failure" state, and the delegation status of the TLD remains unchanged

(ii) The TLD enters the P state, if the TLD uses the majority policy. If RootChain receives confirmations from more than half of all TLD authorities during the delegation transition window, the delegation transition operation takes effect. If RootChain fails to receive enough confirmations within the window

period, the delegation transition operation enters the "failure" state, and the delegation status of the TLD remains unchanged

(iii) If the TLD uses the current-authority-confirmation policy, then same as the majority policy, the TLD name also enters the P state. If RootChain receives a confirmation from the current authority of the TLD during the timeout period, the operation takes effect. Conversely, if the RootChain fails to receive such a confirmation within the timeout period, the delegation transition operation enters the "failure" state, and the delegation status of the TLD remains unchanged

(iv) If the TLD uses the immediate-effect policy, the delegation change will take effect immediately without the need for any confirmation after the root authority initiates the delegation transition

4.4. Transactions. Delegation operations and data publication operations are stored in RootChain in the form of *transactions*. There are two types of transactions.

Delegation transaction: the delegation transaction is stored in the "DelegationTxn" data structure (Table 1). The "Previous Txn" field stores the index of the transaction containing the preceding operation associated with this delegation operation. The type of the delegation operation is stored in the "Operation Type" field. There are five types of delegation operations: publication, revocation, transition, renewal, and redemption. The publication operation binds a TLD "Auth Name" with a public key "Auth Key." According to different business scenarios, different TLD delegation transition, revocation, and redemption policies may be specified, and the specific policies are all stored as fields of "DelegationTxn," with each field named with the "Policy" suffix. RootChain currently supports four delegation policies, as described in Section 4.3. The validity period of the publication operation starts from "Valid From" and ends at "Valid To." If the delegated TLD exceeds the validity period, the authority will need to extend the validity period of the TLD by sending a renewal transaction. The renewal window is within "Renewal Grace Period" days since the "Valid To" date. If the renewal fails or is absent, the TLD will enter the redemption state, and the authority needs to redeem the TLD by following the redemption policy within "Redemption Grace Period". Beyond the redemption window, the root authority will send a revocation transaction, and the transaction is received and verified by RootChain, eventually marking the TLD to be revoked. "Signature" is the signature of the entire delegation transaction, being signed using the private key of the appropriate authority to provide the authenticity and integrity of the delegation transaction.

Data publication transaction: the data publication transaction is stored in the "DomainTxn" data structure (Table 2), and the "Previous Txn" field stores the index of the transaction containing the preceding delegation operation associated with this data operation. The type of data operation is stored in the "Operation Type" field, and there are two types including data publication and data deletion. A resource record "(NAME, TTL, CLASS, TYPE, RDATA)" is a 5-tuple representing domain name data, which is consistent with the DNS protocol. The "RRSIG" field is a digital signature for the resource record, which is consistent with the DNSSEC protocol. "Signature" is the signature of the entire data publication transaction, using the private key of the appropriate authority.

Table 1: Definitions of TLD delegation transaction.

DelegationTxn	
PrevTxn	Associated preceding transaction
OperationType	Type of delegation operation
DomainName	Delegated domain name
DelegatedKey	Delegated public key
ValidFrom	Start of validity period
ValidTo	End of validity period
TransitionPolicy	Delegation transition policy
TransitionWindow	Delegation transition window
RenewalGracePeriod	Delegation renewal grace period
RevocationPolicy	Delegation revocation policy
RedemptionPolicy	Delegation redemption policy
RedemptionGracePeriod	Delegation redemption grace period
TimeStamp	Timestamp of transaction creation
TxnSignature	Signature on the transaction

Table 2: Definitions of TLD data publication transaction.

DomainTxn	
PrevTxn	Associated preceding transaction
OperationType	Type of delegation operation
NAME	TLD name
TTL	Time-to-live (DNS protocol)
CLASS	Record class (DNS protocol)
TYPE	Record type (DNS protocol)
RDATA	Record data sets (DNS protocol)
RRSIG	Signature of the resource record (DNSSEC protocol))
TimeStamp	Timestamp of transaction creation
TxnSignature	Signature on the transaction

5. Smart Contracts

5.1. Overview. As shown in Table 3, a smart contract describes operations involved in the three phases described in Section 4.2, including delegation operations (publication, transition, revocation, renewal, and redemption), data publication operations, and validation operation. Delegation operation means the binding of a top-level domain to an entity; after the binding operation, the entity becomes the registry of that top-level domain, also known as the authority of that top-level domain. The data publication operation binds the delegated top-level domain to its authoritative server. The binding information includes the name and IP address of

Table 3: Semantics of RootChain smart contract.

RootChain operation	
Smart contract	Example Initiator → Output
DelegationPublication	RA → <TLD,TAPubKey>RA
DelegationTransition	TA → <TLD,TAPubKey>TA
DelegationRevocation	RA → <TLD,∅>RA
DelegationRenewal	TA → <TLD,ValidTo>TA
DelegationRedemption	TA → <TLD,TAPubKey>TA
DataPublication	TA/RA → <ZoneData>(TA/RA)
DelegationValidation	RootChain → true/false
DataValidation	RootChain → true/false
RevokeOP	RA/TA → <TLD,OP-ID>(RA/TA)
ConfirmOP	RA/TA → <TLD,OP-ID>(RA/TA)

the authoritative server. The verification operations are primarily used to verify the legitimacy of delegation operations and data publication operations.

There are two additional operations involved in the execution of smart contracts, namely, the *revoke* operation (RevokeOP) and confirmation operation (ConfirmOP). A revoke operation is submitted by the initiator of another operation to revoke the previously initiated operation, and such a revoke operation is submitted as a result of objections from other authorities to the submitted operation. A confirmation operation stands for the confirmation on a submitted operation, and an authority conducts a signed confirmation operation for a submitted operation that requires confirmation from other authorities to take effect.

5.2. Delegation Smart Contract. Delegation smart contracts are implemented by the function *DelegationOperation()* as described by Algorithm 1. The delegation publication operation is initiated by the root authority (RA in Table 3) specifying the TLD ("AuthName") to be delegated and the authoritative public key ("AuthKey") bound to the TLD. The delegation publication operation also needs to specify the validity period (from "ValidFrom" to "ValidTo"), the authoritative transition policy ("TransitionPolicy"), and the policies for subsequent delegation operations that may be submitted after the current delegation of the TLD expires. The delegation transition operation is initiated by the current TLD authority ("TA" in Table 3) and is implemented by changing the authoritative public key bound to the TLD ("AuthKey"). The delegation revocation operation resets the authoritative public key bound to the TLD ("AuthKey" = ∅). The delegation renewal operation extends the authoritative TLD valid period by resetting the end of valid period date of the delegated TLD ("ValidTo"). Delegation redemption operation rebinds the TLD with the previous public key ("AuthKey"), if the TLD's authoritative public key has been reset within a certain period ("RedemptionPolicy").

5.3. Data Publication Smart Contract. Data publication smart contract is implemented by the function *DataPublicationOperation()* as described by Algorithm 3. The data publishing operation publishes various types of domain name data including NS records and A/AAAA records. Domain data is stored in NAME, TTL, CLASS, TYPE, and RDATA fields, and the signature is stored in the RRSIG field, corresponding to the fields with the same names in DNS/DNSSEC protocol specifications.

5.4. Validation Smart Contract. Validation smart contracts check the validity of submitted transactions. There are currently two types: DelegationValidation and DataValidation smart contract. Two forms of checks are performed to determine the validity of a transaction: transaction format check and transaction effectiveness check. To pass the transaction format check, the value filled in each field needs to conform to the specifications. For example, the timestamp of a transaction must be within the valid period, and the digital signature of the transaction should match the transaction content. To pass the transaction effectiveness check, i.e., to determine whether the operation in this transaction should take effect, the preceding transaction must be valid, and the current transaction must satisfy the policy set in the preceding transaction. A preceding transaction is the transaction whose outcome directly influences the operation in this transaction. For example, the delegation publication transaction of a TLD is the preceding transaction of a delegation transition transaction of the TLD if no other delegation transactions are submitted in-between, and in this case, only when the delegation publication transaction of the TLD is valid and the TLD is in the validity period, it is possible for the subsequent delegation transition transaction to pass the effectiveness check. Generally speaking, the transaction effectiveness check performs association checks on the validity of all transactions in the partial order set formed by transaction dependencies.

The smart contract that verifies the validity of delegation transactions is implemented by the function *DelegateVerification()* (Algorithm 2), and the smart contract that verifies the validity of a data publication transaction is implemented by the function *DataValidation()* (Algorithm 4). For the format check on data publication transactions, in addition to meeting the requirements already mentioned, all data fields inherited from the DNS protocol and the DNSSEC protocol must also conform to the corresponding protocol specifications. Also, note that in both functions, the effectiveness check is implemented by invoking the smart contract in the preceding delegation transaction.

5.5. A Detailed Example: Life Cycle of One TLD. The life cycle of a TLD includes three major phases: delegation phase, data publication phase, and name resolution phase. Figure 7 shows how the full life cycle of a TLD is managed using smart contracts. In this example, ICANN is the root authority, the TLD registry represents a TLD authority, and the user is a user of the RootChain name resolution service.

In delegation phase (step 1), the root authority delegates the TLD to a certain TLD registry. To initiate this phase, the TLD authority sends a delegation publication request to RootChain (step 1.1), and the root server that receives this request executes the smart contract (Algorithm 1) to validate

```
Input:
    op_type, auth_name, auth_key, valid_from, valid to,
    trans_policy, redempt_policy, revoke_policy, prev_txn
Output:
    DelegationTxn
1: DelegationTxn.OperationType == op_type
2: if op_type != publication then
3:     DelegationTxn.PrevTxn = prev_txn
4: end if
5: if op_type == publication then
6:     DelegationTxn.AuthName = auth name
7:     DelegationTxn.AuthKey = auth key
8:     DelegationTxn.ValidFrom = valid from
9:     DelegationTxn.ValidTo = valid to
10:    DelegationTxn.TransitionPolicy = trans policy
11:    DelegationTxn.RevocationPolicy = revoke policy
12:    DelegationTxn.RedemptionPolicy = redempt policy
13: end if
14: if op_type == transformation then
15:    if DelegationTxn.ValidTo < CurrentTime() then
16:        DelegationTxn.AuthKey = auth_key.
17:    end if
18: end if
19: if op_type == Revocation then
20:    DelegationTxn.AuthKey =∅
21: end if
22: if op_type == Renewal then
23:    DelegationTxn.ValidTo = Valid_to
24: end if
25: if op type == Redemption then
26:    if auth_key == DelegationTxn.PrevTxn.AuthKey then
27:        DelegationTxn.AuthKey = auth_key
28:        Auth.ValidFrom = valid_from
29:        Auth.ValidTo = valid_to
30:    end if
31: end if
32: DelegationTxn.TimeStamp = CurrentTime()
33: DelegationTxn.Signature = GenSig()
34: return DelegationTxn
```

Algorithm 1. DelegateOperation().

the contents of the request and then generate the delegation publication transaction (DelegationTxn in step 1.2). The transaction is then handed over to the ordering server to reach a global consensus (steps 1.3 and 1.4) and packaged into data blocks (step 1.5). The consensus server sends the already wrapped data block containing the delegation publication transaction to root servers who store the block in the ledger database (step 1.6).

In data publication phase (step 2), a TLD authority publishes the domain name data for its TLD. Since only the resource record of a delegated TLD published by the TLD authority may take effect, step 2 must take place after step 1 for the same TLD. In this phase, the TLD authority sends a data publication request to the RootChain (step 2.1), and the root server that receives the request executes a data publication smart contract (Algorithm 3) to validate the contents of the request and generate a data publication transaction DomainTxn (step 2.2) which is then passed to ordering nodes where consensus is reached (steps 2.3 and 2.4). Subsequent operations (step 2.5 and step 2.6) are the same as those in step 1 and will not be described here. For compatibility reasons, each root server operator periodically checks the validity of the committed domain name data (step 2.7) by executing the validation smart contract (Algorithm 4). Root server operators read verified data publication transactions from RootChain that contain root zone data (including root DNSKEY resource records, NS resource records, and A, AAAA resource records associated with NS) and TLD data (TLD DS resource records, NS resource records, and A, AAAA resource records related to NS records). Then, root server operators write the validated root domain data and the TLD data into the root zone file (step 2.8). The format of the zone file is compatible with the current mainstream authoritative server software.

In name resolution phase (step 3), a user resolves a published TLD name by sending a DNS query. The user obtains

```
Input:
    CurDelegationTxn
Output:
    bool
1: if CurDelegationTxn has invalid field value then
2:     return false
3: end if
4: if prevtx !=; then
5:     verify_key = prevtx.AuthKey
6:     sig = CurDelegationTxn.Signature
7:     if VeriSig(verify_key, sig) != true then
8:         return false
9:     end if
10:    /* validity period of prevtx needs to cover the validity period of CurDelegationTxn */
11:    if prevtx.ValidFrom < CurDelegationTxn.ValidFrom or prevtx.ValidTo > CurDelegationTxn.ValidTo then
12:        return false
13:    end if
14:    if op_type == Transition or Revocation then
15:        if ConfirmOPs of CurDelegationTxn do not satisfy prevtx.TransitionPolicy/RevocationPolicy then
16:        return false
17:        end if
18:    end if
19:    if op_type == RenewalPolicy then
20:        if CurDelegationTxn.TimeStamp - prevtx.TimeStamp > prevtx.RenewalGracePeriod then
21:            return false
22: end if
23: end if
24: if op_type == RedemptionPolicy then
25:            if (ConfirmOPs of CurDelegationTxn do not satisfy prevtx.RedemptionPolicy) or (CurDelegationTxn.TimeStamp - pre-
vtx.TimeStamp > prevtx.RedemptionGracePeriod) then
26:            return false
27:        end if
28:    end if
29:    DelegationVerification(prevtx)
30: end if
31: return true
```

Algorithm 2. DelegateVerification().

```
Input:
    op_type; name, ttl, type, rdata_sets; rrsig, prev_txn
Output:
    DomainTxn
1: DomainTxn.OperationType == op_type
2: DomainTxn.PrevTxn == prev_txn
3: if op_type == publication then
4:     DomainTxn.NAME = name
5:     DomainTxn.TTL = ttl
6:     DomainTxn.TYPE = type
7: end if
8: DomainTxn.RDATA = rdata_sets
9: DomainTxn.RRSIG = rrsig
10: if op_type == deletion then
11:     DomainTxn.NAME =∅
12: end if
13: DomainTxn.TimeStamp = CurrentTime()
14: DomainTxn.Signature = GenSig()
15: return DomainTxn
```

Algorithm 3. DataPublicationOperation().

the TLD name resource record that has been committed on the RootChain by initiating a standard DNS query to the root server. In Figure 7, the user queries the NS record of the TLD (step 3.1). After the root server receives the query, the data validity check (Algorithm 4) is performed according to the smart contract. Only the resource record in transactions that pass the validity check is returned to the user in the form of DNS reply (step 3.2).

6. Discussions

6.1. Architecture Features. RootChain improves the operation transparency and accountability of the root zone by smart-contracting the whole life cycle of TLD operation and logging all operations on the RootChain blockchain ledger. RootChain reduces the risk of single point of failure in the root zone data publication and distribution process by allowing delegated TLD authorities to publish the authoritative data for delegated TLDs directly through the RootChain. Meanwhile, RootChain retains the single root authority (ICANN) as the single trust anchor, ensuring compatibility with the current

```
Input:
    CurDomainTxn
Output:
    bool
1: if A certain field in CurDomainTxn has an invalid value
then
2:      return false
3: end if
4: /* check if the values conform to DNS/DNSSEC protocol */
5: if CurDomainTxn.[NAME/CLASS/TTL/TYPE/RDATA] do not conform to DNS protocol specification then
6:      return false
7: end if
8: if CurDomainTxn.RRSIG do not conform to DNSSEC protocol specification then
9:      return false
10: end if
11: DelegationTxn = CurDomainTxn.PrevTxn
12: /* check signature of CurDomainTxn */
13: if DelegationTxn!=∅; then
14:      verify_key = DelegationTxn.AuthKey
15:      sig = CurDomainTxn.TxnSignature
16:      if VeriSig(verify_key, sig) != true then
17:          return false
18:      end if
19:      if DelegateVerification(DelegationTxn) == false then
20:          return false
21:      end if
22: end if
23: return true
```

Algorithm 4. DataValidation().

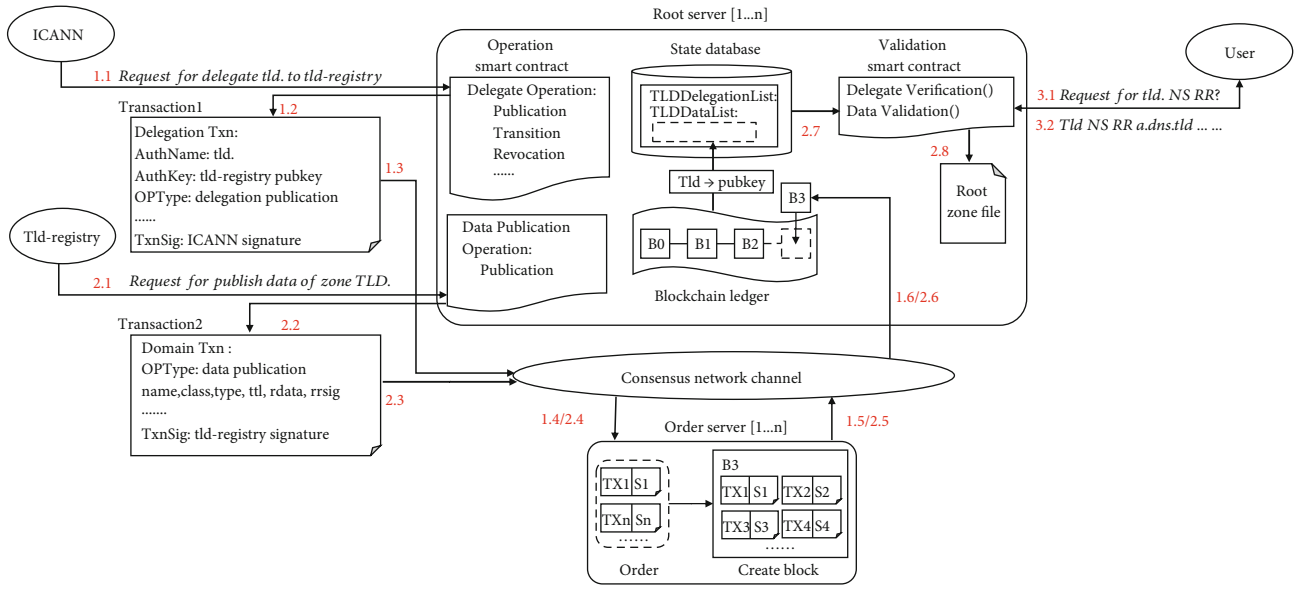

Figure 7: A demonstration of the life cycle of a TLD managed with operations that depend on smart contracts. (1) The root authority delegates a TLD. (2) A TLD authority publishes TLD domain data. (3) A user resolves a delegated TLD.

DNS. Corresponding to the four goals introduced in Section 1, the RootChain system has reached the following four features:

One global namespace with a single root authority. RootChain keeps ICANN as the *single* root authority, which is crucial for the compatibility with the current DNS. In RootChain, all TLD delegation transactions must be initiated by the root authority to guarantee the uniformity of namespace. This feature of RootChain avoids namespace split and cybersquatting.

Distributed root zone operation. RootChain realizes root zone operation decentralization in two aspects: (1) root zone data publication decentralization: in RootChain, root zone data is published through a blockchain network. The data for each TLD is published directly by the corresponding TLD authority, instead of through the root authority in the current DNS. (2) Root zone data distribution decentralization: each node with access to the RootChain blockchain ledger may obtain a complete and accurate copy of the root zone file by examining the operations and data stored in RootChain, instead of by retrieving the root zone file published by the single point of source—the root authority in the current DNS.

Management of the entire TLD life cycle. RootChain supports the management of the entire life cycle of a TLD through the use of smart contracts. The life cycle of a TLD mainly includes delegation phase, data publication phase, and name resolution phase. In delegation phase, the TLD is delegated to a TLD authority, and the policies for subsequent operations are determined; in data publication phase, the domain name data of a TLD is published by and only by the TLD authority; in name resolution phase, the latest effective domain name data is returned to resolvers as DNS reply.

Be transparent to recursive/stub resolvers. RootChain is compatible with DNS/DNSSEC in terms of protocol specifications. RootChain stores domain name data according to DNS/DNSSEC protocol specifications (i.e., in the form of NS/A/AAAA/DS/RRSIG records etc.), from which a complete and accurate root zone file can be composed, and users can receive name resolution service in a DNS/DNSSEC-compliant way.

6.2. Potential Risks. RootChain is a permissioned blockchain architecture. The characteristic of the permissioned blockchain is that all nodes know each other's identity (by their certificates), so there are some certain amount of underlying trusts between nodes. All nodes need to be confirmed by the access control mechanism before they can enter the blockchain network and invoke operations. Therefore, RootChain is insufficient to guard against clients that have already permitted to the blockchain network from maliciously disrupting the system, e.g., clients write large amounts of garbage data to blockchain network. For such a malicious client node, RootChain can ensure that the client node can only have a limited malicious impact on the blockchain network by limiting the invoke rate of each node. RootChain can also identify abnormal behavior through transaction listening mechanisms and then deny access to invoke operations within the blockchain network through access control mechanisms.

6.3. Interoperability Influence. DNS, as Internet infrastructure, interacts with many other systems, such as CDN. The RootChain only deals with the management process of the DNS root zone and does not affect the operation of the DNS system components. Therefore, other protocols or services that interact with DNS components are not affected by RootChain. Besides, DNS has some related security mechanisms, such as DNSSEC and DNS encryption (DoT and DoH). For DNSSEC, RootChain can meet DNSSEC requirements by adding DNSSEC-related resource records in the zone management process, such as DS resource records and DNSKEY resource records to data publication operations. For DNS encryption, DNS encryption is worked for the communication link between the DNS stub resolver and the DNS recursive resolver. RootChain works for the management process of the root zone, which is used for the DNS authoritative server. Thus, RootChain does not affect DNS encryption mechanisms.

7. System Implementation

We implemented RootChain based on the open source project Hyperledger Fabric (version 1.4) [3]. Fabric is a widely used open source blockchain infrastructure project led by IBM that provides common components for blockchain-based application development, such as peer-to-peer (P2P) networking overlay and consensus algorithms. Figure 8 shows the implementation architecture of RootChain. Three main modules provide the basic functionalities:

Blockchain ledger module. The blockchain ledger module provides storage and access to all the transactions issued by authorities, including transactions that contain approved policies, and built-in smart contracts for performing delegation and data validity verification. Each transaction stored on the RootChain is signed by its publisher's private key; hence, any attempt to tamper with stored data can be detected.

Consensus module. The consensus module builds a decentralized network composed of root servers that facilitate the execution of consensus algorithms among all root servers. The consensus network nodes, i.e., root servers, communicate with each other over a peer-to-peer (P2P) network. All nodes execute the same consensus algorithm to ensure global consistency on a public transaction sequence, i.e., a public blockchain ledger.

Identity module. The identity module manages the identity information of all the root servers in the consensus network. This module registers and issues X.509 certificates to valid root servers (also operators) and root zone management partners. The identity module also provides access control service to the consensus network, granting access only to root servers with valid certificates. The access control policy ensures the authenticity and integrity of the data exchanged in RootChain-related internode communications.

On top of the main modules, the modules of root chain provide services related to root zone management. <Delegation Module> and <Data Publication Module> provide root zone operation services to the root authority and TLD authorities. <Domain Resolution Module> provides name resolution service to users. <Validation Module> provides delegation and domain data validation service to the Domain Resolution Module.

8. Evaluation

The root zone management service provided by RootChain is mainly implemented by combining four basic smart

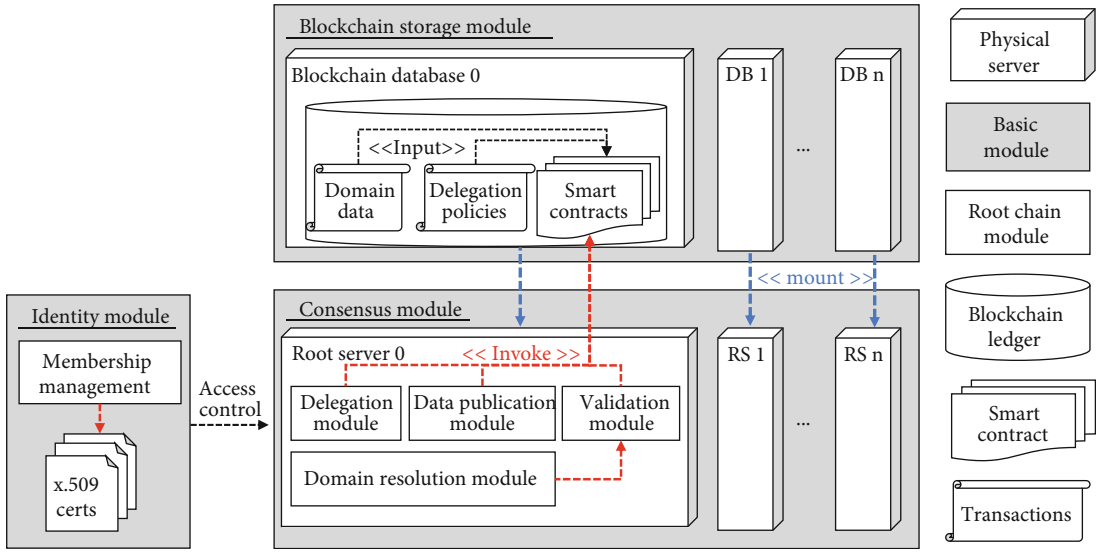

Figure 8: Architecture of system implementation.

contracts (designed in Section 5). Four basic smart contracts are as follows: write delegation (publish delegation), read delegation, write data (publish domain data), and read data. In this section, we will evaluate the execution efficiency and resource consumption of the four basic smart contracts during the operation process of the RootChain system.

8.1. Test Tools and Test Environment. We use the open source blockchain benchmark tool Caliper [10] to evaluate RootChain prototype system. Caliper allows testers to customize test cases to measure the performance of various blockchain implementations. RootChain runs in a small network composed of 5 physical machines, uses an additional machine to run the Caliper client to initiate smart contract invoke request to the RootChain network, and collects benchmark test results. Each machine that runs RootChain is allocated 32 vCPUs of Intel Xeon(R) CPU E5-2620 v4 at 2.10 GHz and 32 GB of memory. The client machines used to generate requests are allocated with 12 vCPUs and 32 GB of memory. All nodes are connected to a local network with 1000 Mbps bandwidth.

8.2. Latency and Throughput. Figure 9(a) comprehensively shows the change trend of the average delay and throughput of the 4 basic smart contracts under different transaction arrival rates. The results show that the type of smart contract does not affect the changing trend of latency and throughput. Therefore, all subsequent tests use a single smart contract to display the evaluation results.

Figure 9(a) shows that the latency increases with the transaction arrival rate, and after passing the critical point, the latency starts to increase rapidly. Combining Figures 9(a)–9(c), it can be found that the arrival of the critical point is affected by two factors, transaction arrival rate (TAR) and network scale. The result of Figure 9(b) shows that when the TAR gradually increases, the larger the network scale, the easier it is to usher in the critical point. For example, when the number of network nodes is 6, the critical point is at 150 tps, and when the number of network nodes is 10, the critical point is at 75 tps. Similarly, the results of Figure 9(c) show that as the number of networks increases, the value of TAR that reaches critical becomes smaller. In addition, the delay fluctuation is affected by the type of smart contract, and the measurement results in Figure 9(d) show that the delay fluctuation range of the write type smart contract is larger than that of the read-type smart contract.

Figure 9(a) shows that throughput gradually increases with the growth of TAR, beginning to show a linear growth trend, but the throughput of write-type smart contract stops growing when the transaction arrival rate hits the range of 175-200 tps. Beyond this range, the transaction queue begins to block, and the average waiting time per transaction becomes longer, causing the average throughput to decrease slowly. Throughput results for read-type smart contract show the same trend as those for write type. Since read operations require relatively fewer computational resources, the average throughput reaches the critical point when the transaction arrival rate reaches a higher rate of about 225 tps. In combination with Figures 9(e) and 9(f), the critical interval that leads to a decrease in transaction throughput is also affected by TAR and network scale. Figure 9(e) shows that the larger the network scale, the earlier the critical interval will come. For example, when the number of nodes is 4, the critical interval is 175-200 tps, but when the number of nodes is 10, the critical interval is 125-150 tps. What is more, Figure 9(f) shows that when the TAR is below the critical point, the transaction throughput is largely independent of the number of nodes. Beyond the critical point, as the number of nodes increases, transaction throughput decreases, and the rate of decline decreases as the number of nodes grows bigger.

Practicality analysis. The evaluation results show that RootChain's prototype system has a minimum of 150 tps and a maximum of 200 tps at a scale of 10 nodes. This means that RootChain can process at least 150 secondary root zone data change requests per second. Currently, there are 1504

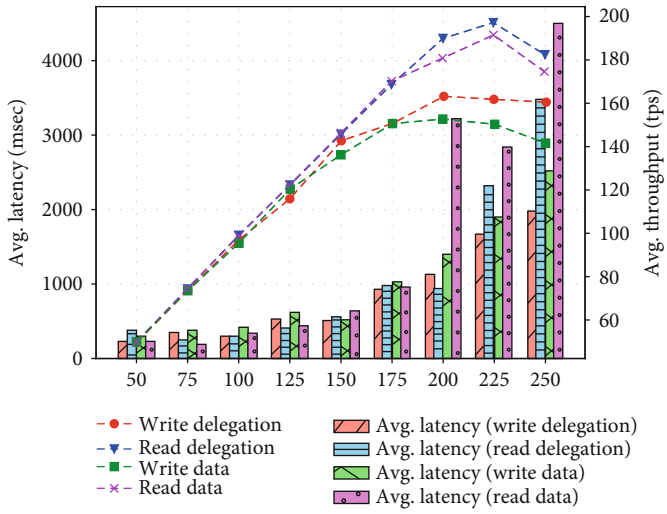

(a) Average latency/throughput vs. transaction arrival rate

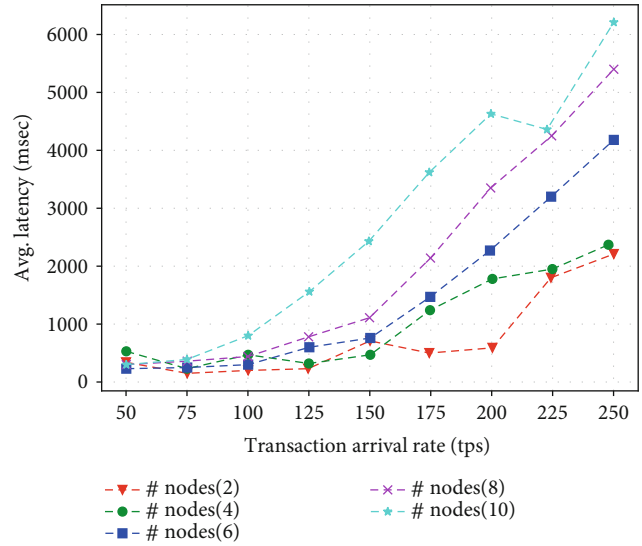

(b) Average latency vs. transaction arrival rate in different number of nodes

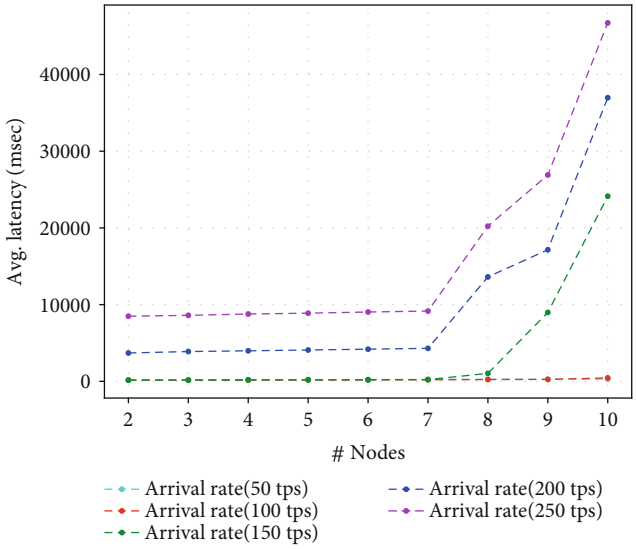

(c) Average latency vs. number of nodes in different transaction arrival rates

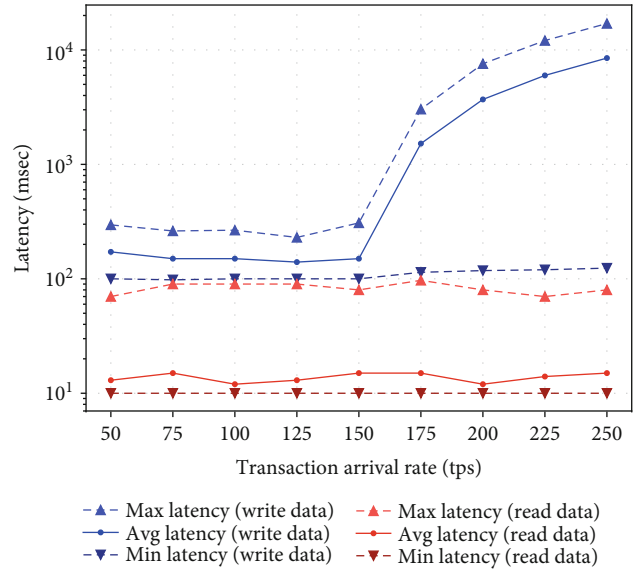

(d) Max/Min/Avg. latency vs. transaction arrival rate

Figure 9: Continued.

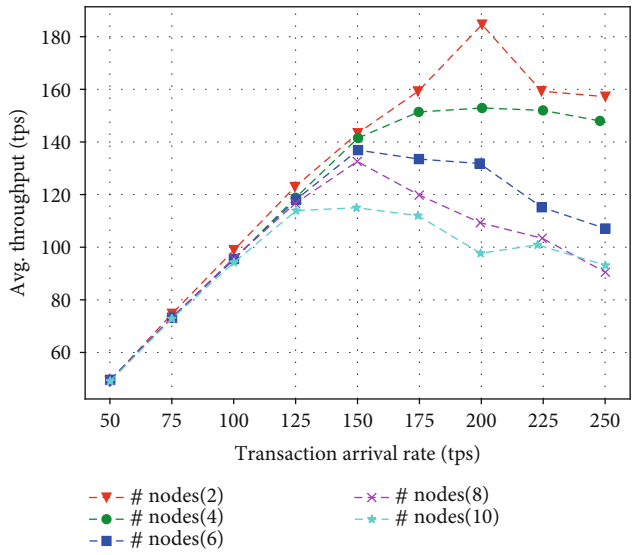

(e) Average throughput vs. transaction arrival rate in different number of nodes

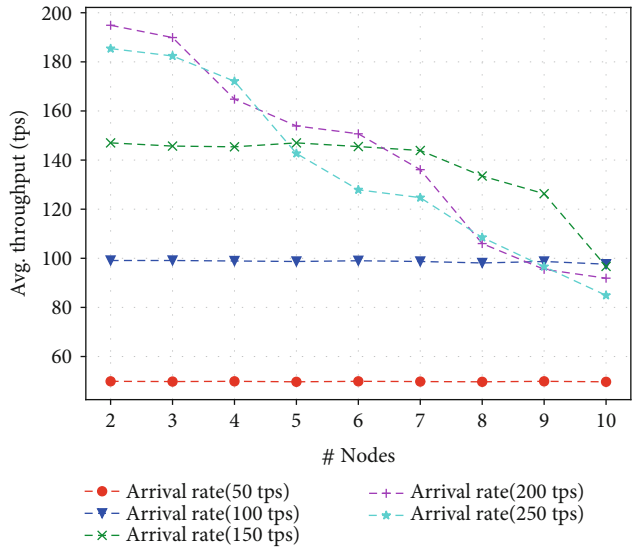

(f) Average throughput vs. number of nodes in different transaction arrival rate

Figure 9: Evaluation results of the execution performance of the RootChain prototype system.

top-level domains registered in the root zone database published by IANA [11]. Therefore, our system supports each top-level domain to submit 8,617 (150*3600*24/1504) change requests to the RootChain system every day. This value far exceeds the daily update frequency of the top-level domain registry. From the perspective of delay, when tps reaches 150, the processing delay of each transaction is between 2 s and 4 s, so the second-level delay is acceptable to users.

8.3. Resource Consumption. Figure 10(a) shows the relationship between CPU usage and transaction arrival rate. Observation shows that CPU usage first increases linearly with TAR and then reaches a certain critical point, and the growth trend slows down until it stops increasing. This is because the number of transactions that the network can process per second is limited. When the transaction rate exceeds the critical point, the excess transactions will be discarded. After that, the number of transactions processed by the network per second remains unchanged, so the CPU usage rate tends to a certain fixed value. Combined with the analysis of Figure 10(d), it can be found that the higher the transaction arrival rate, the smaller the network scale when the CPU usage reaches the upper limit. When the transaction arrival rate is 250 tps, the critical number of network node is 7, and when the transaction arrival rate is 150 tps, the critical number of network node is 8.

Figures 10(b) and 10(e) show the relationship between memory usage and transaction arrival rate. From the test results, memory usage increases linearly with transaction arrival rate. Although there is an upper limit on the number of transactions processed per second in the RootChain network, unprocessed transactions will be cached in the pending transaction queue of the RootChain network, so the memory usage increases linearly with the transaction arrival rate, unlike the CPU usage, which has a critical point in the trend of change.

Figures 10(c) and 10(f) show the relationship between the total network traffic and the transaction arrival rate. Since the duration of the test process is fixed, the total transaction volume tested has a linear relationship with the transaction arrival rate. The total transaction volume determines the communication traffic within the network, so there is also a linear relationship between communication traffic and transaction arrival rate.

9. Related Work

Distributed security is an important research direction in the field of IoT [12].

9.1. Traditional DNS Decentralization Solutions. In 2000, Kangasharju and Ross proposed a new decentralized DNS data management scheme [13], which changed the storage of DNS data from a hierarchical structure to a flat structure. The scheme proposed to replace all the secondary authoritative servers with the new authoritative servers—replicated name servers (RNSs). RNSs are interconnected by using multicast and synchronizing their database with each other. RootChain does not change the storage of root zone data inside root servers, but decentralizes root zone operation for TLDs.

The ORSN project [14] maintains a set of independent open root servers to prevent users from being monitored and controlled by government agencies when resolving domain names. The scheme implements root server operation decentralization in the form of community spontaneous organization, but the dependency on the root zone file provided by ICANN is the limitation of the scheme. RootChain realizes decentralization of root zone operation, removing this limitation.

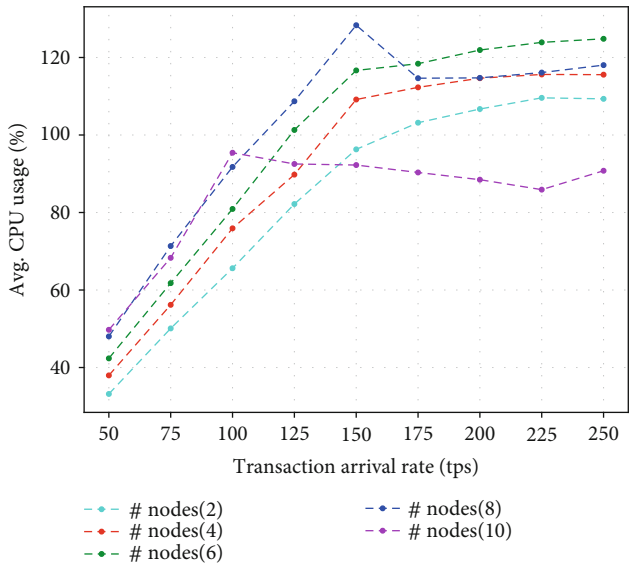

(a) Average CPU usage vs. transaction arrival rate in different number of nodes

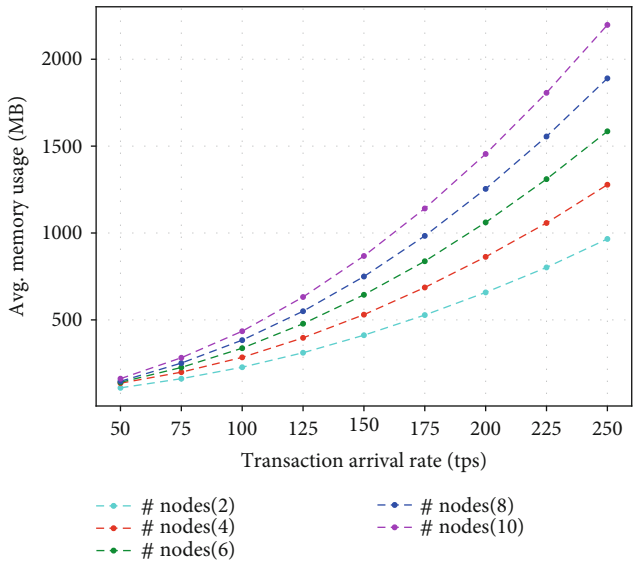

(b) Average memory usage vs. transaction arrival rate in different number of nodes

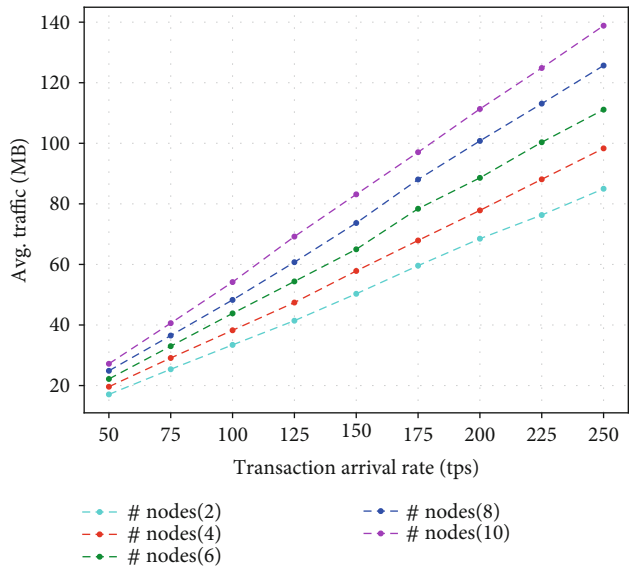

(c) Average Traffic vs. transaction arrival rate in different number of nodes

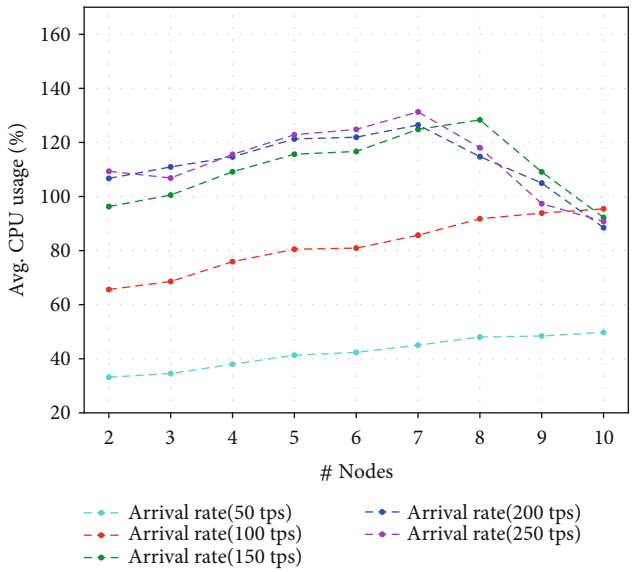

(d) Average CPU usage vs. number of nodes in different transaction arrival rate

Figure 10: Continued.

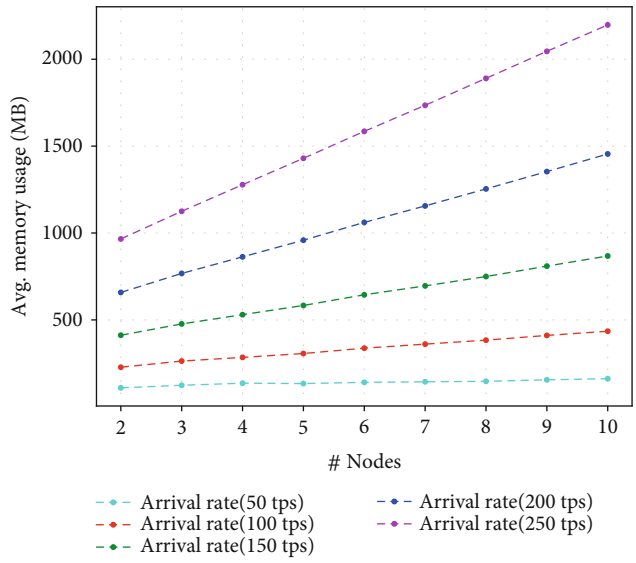

(e) Average memory usage vs. number of nodes in different transaction arrival rate

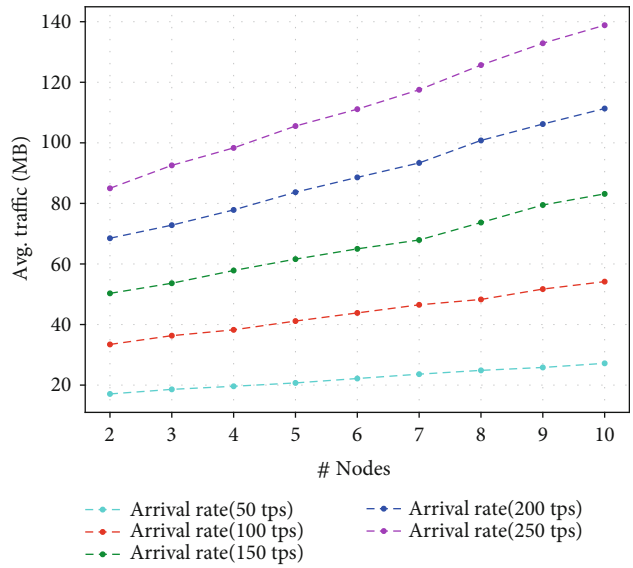

(f) Average Traffic vs. number of nodes in different transaction arrival rate

Figure 10: Evaluation results of the resource consumption of the RootChain prototype system.

The UnifiedRoot [15] project and the Public-Root [16] project have established a new DNS that is completely independent of the current DNS, which uses a new namespace parallel to the current one, leading to namespace split. Those solutions are completely isolate from the current DNS ecosystem and essentially only transfer the control from one center to another. RootChain retains the current DNS namespace and does not change the root zone authority for TLD delegation.

9.2. Blockchain-Based DNS Decentralization Solutions. Namecoin [1] is a distributed naming system based on blockchain, without any name registration authority. Instead, Namecoin adopts the "first come, first served" manner for obtaining domain names under the ".bit" domain. As Namecoin provides name resolution service by sharing domain name data over a peer-to-peer network, there is no single-point-of-failure issue. But the following issues remain unsolved with Namecoin: (1) there is no root zone; thus, no TLD authority, which is not compatible with the current DNS ecosystem. (2) Proof-of-Work (PoW) [17] is adopted for global consensus over name data, which means that Namecoin is vulnerable to attacks from major mining pools of Bitcoin. In fact, there has been cases when a single mining pool controlled over 50% of the overall computing power [18].

The BlockStack Naming Service (BNS) [2] is a global naming and storage system based on Bitcoin, which binds names to off-chain state. Blockstack extends the functionality of Bitcoin by adding a middle layer "virtualchain" on top of Bitcoin, enabling any data storage with a name as the key. Blockstack has the following problems: (1) TLD names are still acquired by bidding, and as with Namecoin, malicious squatting behavior cannot be avoided. (2) Blockstack is developed on top of Bitcoin, and its security and efficiency are inevitably determined by Bitcoin. The PoW consensus mechanism adopted by Bitcoin has already shown security vulnerabilities [19]. Bitcoin's slow transaction committing speed and long confirmation time have also be inherited and not been properly resolved in Blockstack.

Compared to Namecoin and Blockstack, RootChain retains the current DNS root zone authority for TLD delegation, so there is no risk of namespace split nor malicious squatting. Within the system, participants make an agreement in a "one person, one vote" fashion, gathering all root server operators into the root zone data operation, making sure that the system will not be compromised by a single participant. The PoW consensus algorithm has a lot of computational waste and is proved to be not efficient. RootChain adopts a PBFT-like [20] consensus scheme to eliminate the unnecessary resource waste [21–25]. Use blockchain technique to design a trust enhancement mechanism or security data management scheme for DNS.

9.3. Other IoT-Related Decentralized Security Solutions. Yang et al. [12] propose a decentralized and adaptive flocking algorithm for autonomous mobile robots. Shahzad et al. [26] propose a real-time transmission encryption security protocol for industrial IoT devices. Lu et al. [27] propose an IoT security solution based on authentication mechanism. Zhang et al. [28] propose multimodel incident prediction and risk assessment methods for dynamic network security in industrial IoT control devices. Huang et al. [29] propose a network intrusion detection method for sensor devices. Wu et al. [30] propose an energy optimization method for wireless sensor networks composed of IoT devices. [31–35] propose enhanced solutions for Internet of Things security.

DePET [36] is a decentralized privacy-preserving energy trading scheme for vehicular energy network via blockchain. CertCoin [37] is a blockchain-based identity authentication system alternative to PKI. EthIKS [38] is a blockchain-based key verification service system on the Ethereum

platform, eliminating the need for a trusted third party. Wang et al. [39] and Yakubov et al. [40] also introduced blockchain-based PKI certificate management systems. BGP Coin [41] is a blockchain-based Internet resource management solution for IP address prefixes and AS numbers through smart contracts. Those solutions share the similar spirit with RootChain in distributing infrastructures through blockchain, but for different systems.

In summary, different from previous solutions, RootChain distributes DNS root zone operation through blockchain while retaining a single root authority, by separating the delegation of TLDs from the data publication of TLDs.

10. Conclusion

In this paper, we have proposed a blockchain-based root operation architecture—RootChain. By decoupling TLD data publication from TLD delegation, RootChain distributes root zone operation across multiple root servers while maintaining the single root authority. The root zone data is authenticated and published by delegated TLD authorities directly into the ledger of RootChain. To improve the transparency and accountability of root zone operation, we designed smart contracts for the whole lifetime of TLD from delegation to revocation, including some abuse-proof mechanisms for TLD transition. The prototype of RootChain has been implemented with Hyperledger Fabric and evaluated by experiments. We take RootChain as the first step towards distributed root zone operation in DNS. Our future work includes (1) the quantitive comparison between RootChain and other proposals for DNS decentralization, (2) the design of distributed consensus mechanism for RootChain under the assumption without a single trust anchor, and (3) extending the design of RootChain to other Internet infrastructures with single root authority, such as RPKI.

Data Availability

The data used to support the finding of this study are available from the corresponding author upon request.

Conflicts of Interest

The authors declare that they have no conflicts of interest.

Acknowledgments

This work is partially supported by the National Key Research and Development Program of China (Grant No. 2018YFB1800702).

References

[1] A. Loibl and J. Naab, *Namecoin*, 2014, http://namecoin.info.

[2] M. Ali, J. Nelson, R. Shea, and M. J. Freedman, "Blockstack: a global naming and storage system secured by blockchains," in *2016 USENIX Annual Technical Conference (USENIX ATC 16)*, pp. 181–194, Denver, CO, 2016.

[3] *The Hyperledger Fabric project*March 2019, https://www.hyperledger.org/projects/fabric.

[4] *Root Zone Database*October 2020, https://www.iana.org/domains/root/db.

[5] *Iana naming function contract*October 2020, https://www.icann.org/en/system/files/files/iana-namingfunction-agreement-revised-to-address-comments-15sep16-en.pdf.

[6] *An introduction to the internet assigned numbers authority (iana) functions*October 2020, https://www.icann.org/en/system/files/files/ianafunctions-15jun15-en.pdf.

[7] *Root zone maintainer service agreement*October 2020, https://www.icann.org/ianaimpdocs/129-root-zonemaintainer-service-agreement-v-28sep16.

[8] *National telecommunications and information administration (ntia) close-out contract*October 2020, https://www.ntia.doc.gov/files/ntia/publications/sa1301-12-cn-0035001-10212016.pdf.

[9] *List of root server operators*October 2020, https://www.iana.org/domains/root/servers.

[10] *The Hyperledger Caliper project*March 2019, https://www.hyperledger.org/projects/caliper.

[11] *IANA Root Zone Database*October 2020, https://www.iana.org/domains/root/db.

[12] Y. Yang, N. Xiong, N. Y. Chong, and X. Defago, "A decentralized and adaptive flocking algorithm for autonomous mobile robots," in *International Conference on Grid Pervasive Computing Workshops*, Kunming, 2008.

[13] J. Kangasharju and K. W. Ross, "A replicated architecture for the domain name system," in *Proceedings IEEE INFOCOM 2000. Conference on Computer Communications. Nineteenth Annual Joint Conference of the IEEE Computer and Communications Societies (Cat. No. 00CH37064)*, vol. 2, pp. 660–669, Tel Aviv, Israel, Israel, 2000.

[14] *The Open Root Server Network (ORSN) project*March 2019, https://www.orsn.org.

[15] *The UnifiedRoot project*March 2019, http://www.unifiedroot.com.

[16] *The Public-Root project*March 2019, http://public-root.com/.

[17] M. Jakobsson and A. Juels, "Proofs of work and bread pudding protocols," *Secure Information Networks*, pp. 258–272, 1999.

[18] H. A. Kalodner, M. Carlsten, P. Ellenbogen, J. Bonneau, and A. Narayanan, "An empirical study of Namecoin and lessons for decentralized namespace design," *WEIS*, 2015.

[19] S. Feng, W. Wang, Z. Xiong, D. Niyato, P. Wang, and S. S. Wang, "On cyber risk management of blockchain networks: a game theoretic approach," *IEEE Transactions on Services Computing*, p. 1, 2018.

[20] M. Castro and B. Liskov, "Practical byzantine fault tolerance," *OSDI*, vol. 99, pp. 173–186, 1999.

[21] Z. Yu, D. Xue, J. Fan, and C. Guo, "Dnstsm: DNS cache resources trusted sharing model based on consortium blockchain," *IEEE Access*, vol. 8, pp. 13640–13650, 2020.

[22] J. Zhang, J. Zhai, R. Yang, and S. Liu, "Research on enterprise DNS security scheme based on blockchain technology," in *International Conference on Blockchain and Trustworthy Systems*, pp. 690–701, Singapore, 2019.

[23] W. Wang, N. Hu, and X. Liu, "Blockzone: a blockchain-based dns storage and retrieval scheme," in *International Conference on Artificial Intelligence and Security*, pp. 155–166, Cham, 2019.

[24] S. Gourley and H. Tewari, "Blockchain backed dnssec," in *International Conference on Business Information Systems*, pp. 173–184, Cham, 2018.

[25] G. He, W. Su, S. Gao, and J. Yue, "TD-Root: a trustworthy decentralized DNS root management architecture based on permissioned blockchain," *Future Generation Computer Systems*, vol. 102, pp. 912–924, 2020.

[26] S. Aamir, L. Malrey, L. Young-Keun et al., "Real time MODBUS transmissions and cryptography security designs and enhancements of protocol sensitive information," *Symmetry*, vol. 7, no. 3, pp. 1176–1210, 2015.

[27] Y. Lu, S. Wu, Z. Fang, N. Xiong, S. Yoon, and D. S. Park, "Exploring finger vein based personal authentication for secure IoT," *Future Generation Computer Systems*, vol. 77, pp. 149–160, 2017.

[28] Q. Zhang, C. Zhou, N. Xiong, Y. Qin, X. Li, and S. Huang, "Multimodel-based incident prediction and risk assessment in dynamic cybersecurity protection for industrial control systems," *IEEE Transactions on Systems Man Cybernetics Systems*, vol. 46, no. 10, pp. 1429–1444, 2017.

[29] H. Kaixing, Z. Qi, Z. Chunjie, X. Naixue, and Q. Yuanqing, "An efficient intrusion detection approach for visual sensor networks based on traffic pattern learning," *IEEE Transactions on Systems, Man, and Cybernetics: Systems*, vol. 47, no. 10, pp. 2704–2713, 2017.

[30] W. Wu, N. Xiong, and C. Wu, "Improved clustering algorithm based on energy consumption in wireless sensor networks," *IET Networks*, vol. 6, no. 3, pp. 47–53, 2017.

[31] Y. Liu, M. Ma, X. Liu, N. Xiong, A. Liu, and Y. Zhu, "Design and analysis of probing route to defense sink-hole attacks for Internet of Things Security," *IEEE Transactions on Network Science and Engineering*, 2018.

[32] Z. Pan, C.-N. Yang, V. S. Sheng, N. Xiong, and W. Meng, "Machine learning for wireless multimedia data security," *Security and Communication Networks*, vol. 2019, 2 pages, 2019.

[33] A. Shahzad, M. Lee, C. Lee et al., "The protocol design and new approach for scada security enhancement during sensors broadcasting system," *Multimedia Tools and Applications*, vol. 75, no. 22, pp. 14641–14668, 2016.

[34] A. Shahzad, R. Landry, M. Lee, N. Xiong, J. Lee, and C. Lee, "A new cellular architecture for information retrieval from sensor networks through embedded service and security protocols," *Sensors*, vol. 16, no. 6, p. 821, 2016.

[35] N. Xiong, J. He, J. H. Park, D. H. Cooley, and Y. Li, "A neural network based vehicle classification system for pervasive smart road security," *The Journal of Universal Computer Science*, vol. 15, no. 5, pp. 1119–1142, 2009.

[36] Y. Long, Y. Chen, W. Ren, H. Dou, and N. N. Xiong, "Depet: a decentralized privacy-preserving energy trading scheme for vehicular energy network via blockchain and k-anonymity," *IEEE Access*, vol. 8, pp. 192587–192596, 2020.

[37] C. Fromknecht, D. Velicanu, and S. Yakoubov, *Certcoin: A Namecoin Based Decentralized Authentication System*, vol. 6, Massachusetts Institute of Technology, Cambridge, MA, USA, 2014.

[38] M. S. Melara, A. Blankstein, J. Bonneau, E. W. Felten, and M. J. Freedman, "Coniks: bringing key transparency to end users," *24th USENIX Security Symposium (USENIX Security 15)*, pp. 383–398, 2015.

[39] Z. Wang, J. Lin, Q. Cai, Q. Wang, D. Zha, and J. Jing, "Blockchain-based certificate transparency and revocation transparency," *IEEE Transactions on Dependable and Secure Computing*, 2020.

[40] A. Yakubov, W. Shbair, A. Wallbom, and D. Sanda, "A blockchainbased pki management framework," in *The First IEEE/IFIP InternationalWorkshop on Managing and Managed by Blockchain (Man2Block) colocated with IEEE/IFIP NOMS 2018*, Tapei, Tawain, 2018.

[41] Q. Xing, B. Wang, and X. Wang, "Poster: Bgpcoin: a trustworthy blockchain-based resource management solution for bgp security," in *Proceedings of the 2017 ACM SIGSAC Conference on Computer and Communications Security*, pp. 2591–2593, Dallas, TX, USA, 2017.

Hindawi
Wireless Communications and Mobile Computing
Volume 2021, Article ID 6679654, 14 pages
https://doi.org/10.1155/2021/6679654

Research Article

An Atomic Cross-Chain Swap-Based Management System in Vehicular Ad Hoc Networks

Chenkai Tan[1], **Shaoyi Bei**[1], **Zhengjun Jing**[1,2] and **Neal Xiong**[3]

[1]*School of Vehicle and Traffic Engineering, Jiangsu University of Technology, Changzhou 213001, China*
[2]*School of Computer Engineering, Jiangsu University of Technology, Changzhou 213001, China*
[3]*Department of Mathematics and Computer Science, Northeastern State University, Tahlequah, OK 74464, USA*

Correspondence should be addressed to Zhengjun Jing; zhengjun_jing@163.com

Received 20 October 2020; Revised 9 December 2020; Accepted 9 January 2021; Published 29 January 2021

Academic Editor: Hongju Cheng

Copyright © 2021 Chenkai Tan et al. This is an open access article distributed under the Creative Commons Attribution License, which permits unrestricted use, distribution, and reproduction in any medium, provided the original work is properly cited.

The blockchain-based management system has been regarded as a novel way to improve the efficiency and safety of Vehicular Ad Hoc Networks (VANETs). A blockchain-based scheme's performance depends on blockchain nodes' computing power composed from the road-side unit (RSU). However, the throughput of blockchain-based application in VANETs is limited by the network bandwidth. A single blockchain cannot record large-scale VANETs' data. In this paper, we design an atomic cross-chain swap-based management system (ACSMS) to boost the scalability of blockchain-based application in VANETs. The blockchain-based public-key encryption with keyword search is further introduced to protect user privacy. The analysis shows that ACSMS achieves cross-chain swap without loss of CAV security privacy. The simulation results show that our method can realize multiple blockchain-based applications in VANETs.

1. Introduction

Nowadays, connected autonomous vehicles (CAVs) equip with the on-board unit (OBU) that enables vehicle ad hoc networks (VANETs [1]) to be formed. By C-V2X and DSRC communication, VANETs could improve traffic efficiency [2] and road safety [3]. With the VANET development [4], CAVs not only need safely and efficiently communicate to other CAVs [5–7] but also need to decide the trustworthiness of other CAVs' messages. There are many attacks and challenges [8–11] in VANETs, which may be solved by blockchain technology. For example, blockchain-based VANET schemes have been designed to provide security key transfers [12] and decentralized trust management [13].

Blockchain is a novel tamper-resistance and decentralization ledger-based storage method, which is useful in VANETs. However, the throughput of blockchain is limited by the blockchain consensus algorithms and network bandwidth. For example, the throughput on Ethereum [14] is 10-30 TPS. Simultaneously, the number of CAVs around the world will reach 2 billion in the next 10-20 years [15]. Therefore, Shrestha et al. [16] proposed that administrator divide multiple blockchains according to geographical location to enhance application scalability.

There are three categories of existing blockchain-based VANET schemes: the blockchain-based PEKS [17], the blockchain-based dynamic key management system [12] (BKM), and the blockchain-based trust management system [13] (BTM). First, the blockchain-based PEKS integrates blockchain technology and PEKS. The blockchain technology supports the data tamper resistance, and PEKS supports verifiable searching simultaneously. Second, BKM could prevent an unregistered user from accessing VANETs illegally. However, BKM uses pseudo-ID to achieve conditional privacy. Without revealing CAVs' identities, the user will lack the motivation to deliver information. Therefore, BTM was proposed to build trust in the communications of CAVs and incentive users to forward announcements.

Toward enhancing the flexibility of the blockchain-based scheme in VANETs, we integrate multiple blockchain-based

applications into the single blockchain. Then, we use the atomic cross-chain protocol to connect blockchain. The main contributions of this article are summarized as follows:

(i) In VANETs, network size can be geographically unbounded and very scalable, but nodes in VANETs have geographical relevancy. We partition country maps into regions, and each region maintains an independent blockchain, which will reduce blockchain scalability issues. We develop ACSMS to connect multiple blockchain systems while maintaining the property of trust and integrity built by individual blockchains. Therefore, the ACSMS can enhance interoperability between chains

(ii) We also introduce the blockchain-based PEKS [18] as the data-sharing scheme. In blockchain-based PEKS, CAVs use the public key to encrypt the data and the corresponding keywords. The ciphertext signature is provided in the blockchain, and the ciphertexts are stored in the TA server. Thus, the blockchain-based PEKS support verifies of ciphertexts

(iii) Furthermore, we attempt to integrate the blockchain-based PEKS, BKM, and BTM into ACSMS, such that CAVs could use multiple blockchain-based applications with a single blockchain account. Compared with other reference schemes, ACSMS achieves more functionality

The remainder of this paper is organized as follows. The related works are briefly introduced in Section 2. In Section 3, we give the model overview and details of ACSMS. Then, the security analysis of our scheme is presented in Section 4. In Section 5, we make a performance evaluation of ACSMS. In Section 6, we give the conclusions of the paper.

2. Related Work

2.1. Blockchain-Based PEKS. Since Boneth et al. [19] first posed PEKS, numerous schemes about PEKS have been put forward. There are four polynomial-time algorithms of PEKS: KeyGen, Trapdoor, PEKS, and Test. If the user sends a trapdoor to the server, the server can locate all ciphertexts containing keywords through PEKS. Significantly, blockchain-based PEKS for VANETs [17] allows users to detect any unauthorized manipulation. The blockchain-based PEKS schemes [17, 18, 20] avoid the centralized malicious attacks [21]. The oblivious protocol between users and blockchain servers can thwart off-line KGA (keyword guessing attacks).

2.2. BKM. Lei et al. [12] proposed a novel key management scheme based on blockchain to transfer key within the decentralized VANETs securely. Similarly, Ma et al. [22] developed an efficient BKM scheme that supports key updates and revocation. Furthermore, a lightweight mutual authentication protocol for BKM is proposed in [22]. Shrestha et al. [16] also employed blockchain technology to disseminate information in VANETs. Unlike Lei et al. and Ma et al., Shrestha et al. divided the map into blockchain regions according to the density of CAVs. However, Shrestha et al. did not use cross-chain technology to connect the different regions.

As shown in Figure 1, the basic structure of the blockchain [23] consists of a series of various blocks that has a block header and a block body. The block header is used to identify a particular block, and a block header consists of blockchain version, the previous block's hash (PreHash), MerkleRoot, Timestamp (TS), nonce, and difficulty target. The block body is used to record transactions, and a block body consists of transactions and a Merkle hash tree formed by the hash value of transactions. Each block has a difficulty target related to the previous block; a chain structure is formed. If a miner first finds the nonce and broadcast correct block into the network, this block's validity will be acknowledged by other blockchain nodes.

2.3. BTM. The decentralized BTM schemes are introduced to determine the trustworthiness of CAVs. Yang et al. [13] proposed a BTM to query neighbours' trust values and then verify the received messages. Similarly, Lu et al. [24] investigated an anonymous BTM to break the linkability between real identities and the public keys. Furthermore, Lu et al. used the TA and RSU to provide BTM. Zhao et al. [25] employed blockchain technology to associate resource allocation with the trust value of CAVs. In addition, Zhao et al. introduced a novel BTM based on PBFT&PoS consensus algorithm to support cross-chain swap. But PBFT&PoS-based BTM cannot support PoW-based scheme.

3. An Atomic Cross-Chain Swap-Based Management System

3.1. System Model. As illustrated in Figure 2, three types of entities in VANETs are CAVs, RSU, and TA.

The connected autonomous vehicles (*CAVs*): each CAV, as a sender *S*, is equipped with a hardware security module (HSM) and an OBU. The feature of CAVs includes dynamic mobility, wireless communication [26], and predictable trajectory [27] [22, 28]

The roadside unit (*RSU*): the RSUs provide V2I provide V2I services by communicating with CAVs. RSU as blockchain nodes $\{KS_1, KS_2, ..., KS_n\}$ creates new blocks to maintain the blockchain in the region

The trust authority (*TA*): as a storage server *C*, the main task of TA includes the identity review of CAV users, deployment of smart contracts, and the issuance of transaction data. The TA also sends the pseudo-IDs to the CAVs. After the initial registration, TA provides every CAVs with a unique blockchain account to realize ACSMS

With different transfer protocols, CAVs can reach V2X through OBU. The concept design of the OBU [29] is illustrated in Figure 3. The OBU provides with long-range wide-area network (LoRaWAN), narrow-band internet of things (NB-IoT), and global positioning system (GPS). By LoRaWAN and NB-IoT, CAVs communicate with the TA (V2C), RSU (V2I), and other CAVs (V2V).

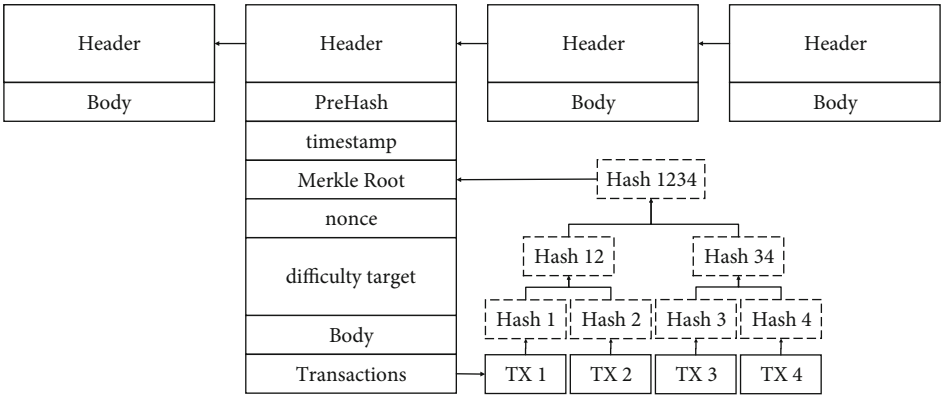

Figure 1: The basic blockchain structure.

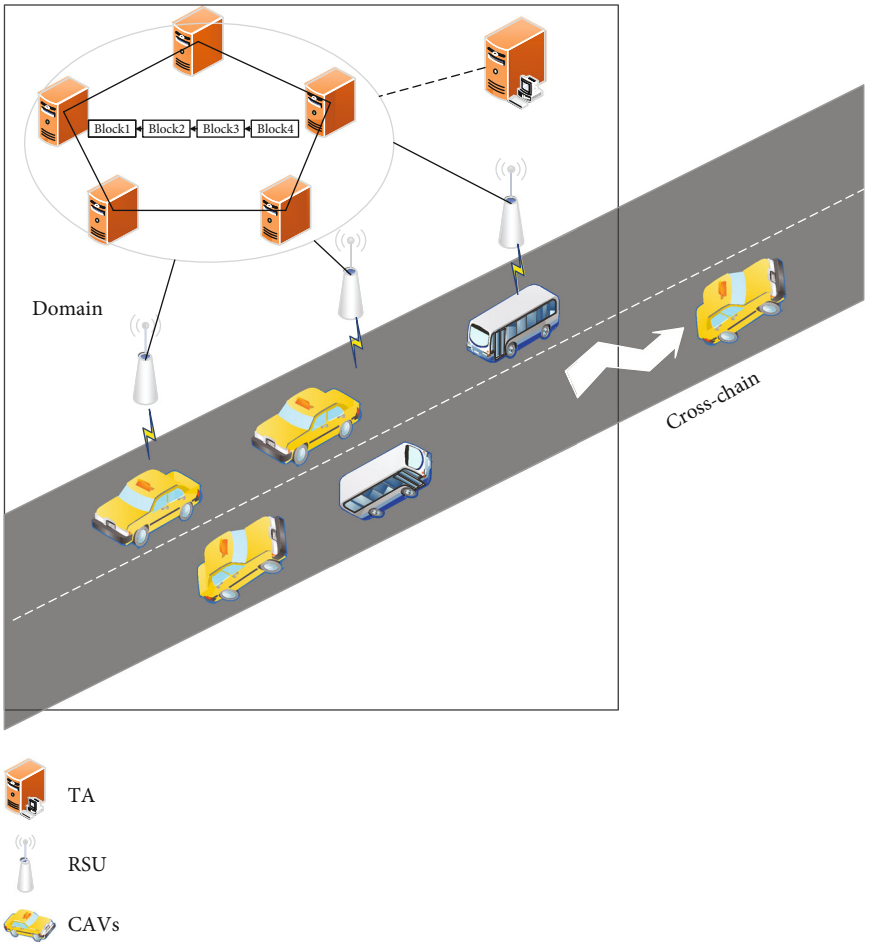

Figure 2: System model of ACSMS.

In the ACSMS, there are four primary functions: blockchain-based PEKS, BKM, BTM, and atomic-cross chain-swap. We will, respectively, present the four functions.

(a) *The blockchain-based public-key encryption with keyword search* (*PEKS*). CAVs outsource ciphertext and cypher-text signature to the TA. Then, the TA broadcasts the signature and the serial number of ciphertext into the blockchain. Finally, by TEST algorithm and the signature, the searcher can obtain correct ciphertext from the TA

(b) *The blockchain-based key management* (*BKM*). The TA registers CAVs and sends pseudo-ID to CAVs. By blockchain-based PEKS, CAVs' details (such as licence plate and driver's licence) are encrypted to protect privacy. By pseudo-ID, CAVs enable explicit mutual authentication with RSU through a handover

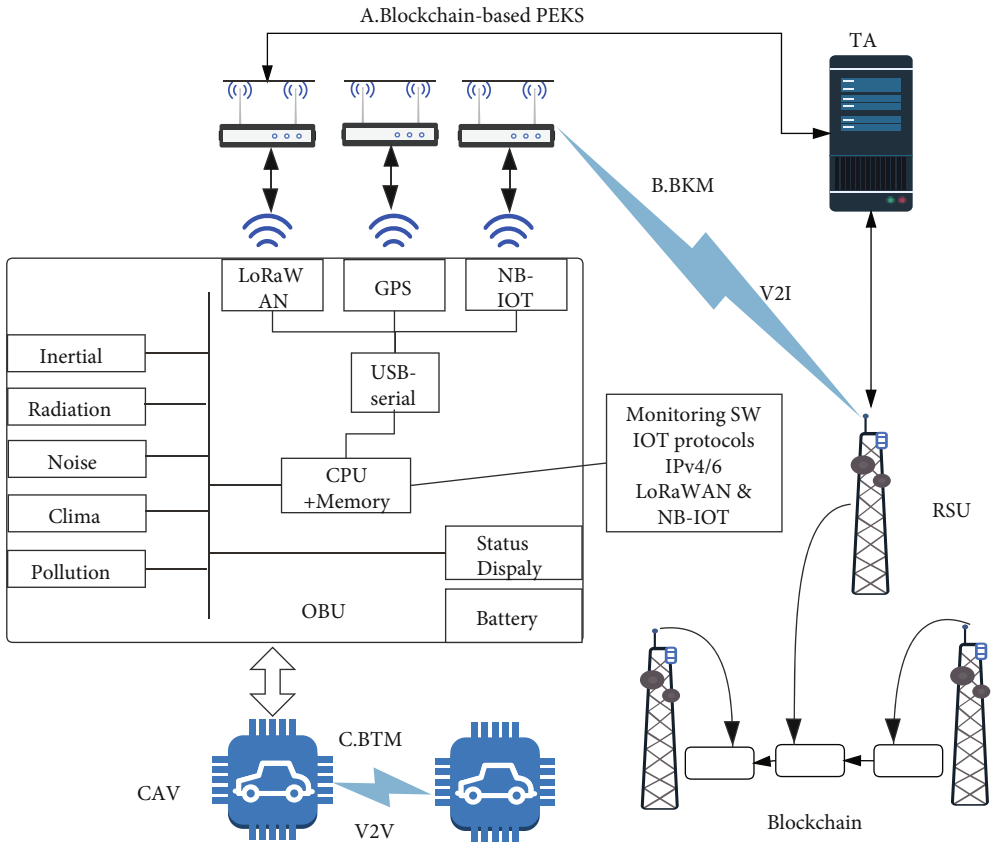

Figure 3: The structure of ACSMS.

authentication protocol [30]. Furthermore, blockchain technology provides decentralized authentication for this protocol

(c) *The blockchain-based trust management* (*BTM*). After the BKM, CAV, and RSU establish a shared symmetric key for the subsequent communication session. Then, RSU gets CAV's trust value from the blockchain. To share trust value with pseudo-ID, RSU generates an authentication code of CAVs' trust value. Other CAVs can then gain the credibility of CAVs' trust value without knowing the CAVs' real identity

(d) *The atomic-cross chain-swap*. We use an atomic-cross chain-swap algorithm [31, 32] that provides cross-chain interoperability among blockchain-based systems. Only serial number of ciphertext and CAVs' trust value are swapped across different blockchains

3.2. The Blockchain-Based PEKS. Based on the project of PEKS from bilinear pairings [17, 20, 33], we design a blockchain-based PEKS scheme for ACSMS. In the blockchain-based PEKS, the CAV (S) has a blockchain account b_{s_1} and send message (M) to the TA (C). Furthermore, the public key and private key of b_{s_1} are $(\mathrm{PK}_{b_s}, \mathrm{SK}_{b_s})$.

It should be emphasized that the PEKS construction in this work is very basic and can be extended to more complex PEKS through integrating with other technology. For example, by introducing cloud storage services [18], the CAV is able to outsource the data to the cloud storage services.

3.2.1. Setup Stage. With a security parameter λ, the system parameters $\{q, \hat{e}, \mathbb{G}_1, \mathbb{G}_2, H_1, H_2, H_3, H_4, \mu,\}$ are generated. Here, $(\mathbb{G}_1,+)$ and $(\mathbb{G}_2,\cdot)$ are two cyclic groups of prime order q. $\hat{e}$: $\mathbb{G}_1 \times \mathbb{G}_1 \longrightarrow \mathbb{G}_2$ be an admissible bilinear map, which satisfies bilinear, nondegenerate, and computable [34].

H is a cryptographic hash function, $H_1{:}\{0,1\}^* \longrightarrow \mathbb{Z}_q^*$, $\mathbb{Z}_q^* = \{\rho \mid 1 \le \rho \le q\}$. $H_2{:}\mathbb{G}_2 \longrightarrow \{0,1\}^{\log q}$. $H_3{:}\{0,1\}^* \longrightarrow \{0,1\}^h$, where h is the output length of H_3. $H_4{:}\{0,1\}^* \longrightarrow \mathbb{G}_1$. $\mu = \hat{e}(P,P)$.

3.2.2. Blockchain Stage

(i) *KeyGen*. The CAV (S) picks a random secret key S $\mathrm{k}_s = x \in \mathbb{Z}_q^*$, and corresponding public key is $\mathrm{Pk}_s = X = xP \in \mathbb{G}_1$. With same parameters, the TA (C) generates the key as $(\mathrm{Pk}_c = Y = yP \in \mathbb{G}_1, \mathrm{Sk}_c = y \in \mathbb{Z}_q^*)$.

(ii) *Trapdoor*. Take as input Sk_s and keyword w, the CAV computes the Trapdoor [33] $T_w = (H_1(w) +$

$x)^{-1}P$. Then, the CAV encrypts M through a standard public-key encryption $E(\cdot)$ [35].

(iii) *PEKS*. Take as input Pk_s, Pk_c, and w, the CAV randomly selects $r_1, r_2 \in \mathbb{Z}_q^*$. The CAV computes $A = r_1 H_1(w)P + r_1 X$, $B = r_2 P$, $V = H_2(\hat{e}(r_1 P + r_2 A, Y))$, and output $\mathrm{PEKS}(w, \mathrm{PK}_s) = (A, B, V)$ [33].

With the encrypted M and keywords $\{w_1, w_2, \cdots, w_n\}$, a list of ciphertext is got by CAV, which is $\mathrm{Ct}_s = E(M)\| \mathrm{PEKS}(w_1, \mathrm{PK}_s)\|\cdots\|\mathrm{PEKS}(w_n, \mathrm{PK}_s)$, where $\|$ indicates message concatenation operation. Then, the CAV computes the signature of Ct_s as [34] $\mathrm{Sig} = P/(H_3(Ct_s) + x)$. Finally, the CAV sends ciphertext Ct_s and Sig to the TA.

To fast search Sig, the TA generates serial number Sn_i from b_{s_1} record Sn_{i-1}, and $\mathrm{Sn}_i = \mathrm{Sn}_{i-1} + 1$. The TA broadcasts a transaction $(\mathrm{Sig}, \mathrm{Sn}_i)$ into blockchain nodes (RSU) to check data integrity and authenticate user, which the receive account is b_{s_1}. Then, RSU KS_t will broadcast $(\mathrm{Sig}, \mathrm{Sn}_i)$ into the blockchain network, when a blockchain node KS_t(RSU) finds a correct nonce.

(iv) *TEST*. Take as input Pk_s, y, (A, B, V), and T_w, test $H_2(\hat{e}(yA, T_w + B)) \stackrel{?}{=} V$, where $\stackrel{?}{=}$ operation returns true if two values are equal and false if they are not equal. With keywords $\{w_1, w_2, \cdots, w_n\}$ and TEST, the TA obtains ciphertexts of each keyword. Then, check $\hat{e}(H_3(Ct_s)P + X, \mathrm{Sig}) \stackrel{?}{=} \hat{e}(P, P)$ through blockchain. The Sig proves that the ciphertexts belong to the blockchain account b_{s_1}, when $\stackrel{?}{=}$ operation returns true

By sending trapdoors and blockchain signature to the TA, the searcher can obtain ciphertexts as follows. The CAV (S) send $(\mathrm{Pk}_s, T_w, \mathrm{Sig}_{\mathrm{searcher}}, ts, \mathrm{PK}_{b_s})$ to the searcher, which $\mathrm{Sig}_{\mathrm{searcher}} = P/(H_3(\mathrm{Pk}_s\|T_w\|ts) + \mathrm{SK}_{b_s})$. With Pk_s, y, (A, B, V), and T_w, the TA can find ciphertexts from $(\mathrm{Pk}_s, T_w, \mathrm{Sig}_{\mathrm{searcher}}, ts, \mathrm{PK}_{b_s})$. If $\hat{e}(H_3(\mathrm{Ct}_s)P + X, \mathrm{Sig}) = \hat{e}(P, P)$, the ciphertexts belong to the blockchain account b_s. If $\hat{e}(H_3(\mathrm{Pk}_s\|T_w\|ts)P + X, \mathrm{Sig}_{\mathrm{searcher}}) = \hat{e}(P, P)$, the legal searcher is consented with the CAV (S).

The correctness of the scheme is proofed as follows:

$$
\begin{aligned}
&H_2(\hat{e}(yA, T_w + B))\\
&\quad = H_2\left(\hat{e}\left[yA, (H_1(w) + x)^{-1}P + r_2 P\right]\right)\\
&\quad = H_2\left(\hat{e}\left\{yr_1 P(H_1(w) + x), P\left[H_1(w) + x\right)^{-1} + r_2\right]\right\}\Big)\\
&\quad = H_2(\hat{e}\{r_1 Y, P[1 + r_2(H_1(w) + x)]\})\\
&\quad = H_2(\hat{e}\{Y, r_1 P + r_2[r_1 P H_1(w) + r_1 X]\})\\
&\quad = H_2(\hat{e}(Y, r_1 P + r_2 A)) = H_2(\hat{e}(r_1 P + r_2 A, Y)) = V,
\end{aligned}
$$

$$
\begin{aligned}
&\hat{e}(H_3(Ct_s)P + X, Sig)\\
&\quad = \hat{e}\left\{P[H_3(Ct_s) + x], \frac{1}{H_3(Ct_s) + x}P\right\}\\
&\quad = \hat{e}(P, P)^{(H_3(Ct_s)+x)(1/(H_3(\mathrm{Ct}_s)+x))} = \hat{e}(P, P).
\end{aligned}
\tag{1}
$$

3.3. Blockchain-Based Key Management in VANETs. The design goals of the BKM are security and efficiency user authentication. The VANET performs the BKM inside the blockchain region that can decentralized record user public key [12, 22]. However, BKM [12, 22] is hard to realize key revocation and hard to support cross-chain verify. In this paper, we take the PKI-based scheme [30] to realize key agreement, public update, and revocation. The ACSMS setups stage corresponding to the BKM system setup. The ACSMS blockchain stage includes the BKM user registration, CAV authentication, and the TA management CAVs' pseudo-ID. In contrast to [30], the blockchain is used to authentication users' pseudo-ID.

3.3.1. System Setup Phase. In our system, all nodes keep loose time synchronization. The system setup phase is as follows: First, the RSU has to install a blockchain-based application. Second, based on the density of CAVs in a country, maps are partitioned into different regions. Third, TA sends a unique blockchain account to every RSU. RSU then creates new blocks to maintain the blockchain in the region. Finally, administrators apply ACSMS to these blockchains.

3.3.2. Registration Phase. To ensure legitimacy within VANET, TA must register new CAVs [22, 36] through relevant CAV information S_{info}. S_{info} is formed by phone number, licence plate, driver's ID, etc. Different from the blockchain-based PEKS, the TA will sign the S_{info}. Take as input S_{info}, TA private key y, TA computes the signature of S_{info}, $\mathrm{Sig}_{S_{\mathrm{info}}} = P/(H_3(S_{\mathrm{info}}) + y)$. By the blockchain-based PEKS, CAVs get ciphertext ($\mathrm{Ct}_{\mathrm{info}}$) of S_{info}. Then, the CAV (S) sends the ciphertext $\mathrm{Ct}_{\mathrm{info}}$ to the TA (C), and the TA generates serial number Sn_i.

The blockchain transaction of $(\mathrm{Sig}_{S_{\mathrm{info}}}, \mathrm{Sn}_i)$ is processed as follows. The TA encapsulates $(\mathrm{Sig}_{S_{\mathrm{info}}}, \mathrm{Sn}_i)$ into JSON format. Next, TA sends the transaction to the RSU, and the RSU executes the mining process; the transaction $(\mathrm{Sig}_{S_{\mathrm{info}}}, \mathrm{Sn}_i)$ is added to the block. If a miner KS_t finds a nonce, KS_t broadcasts the block into the network. The RSU gets the transaction $(\mathrm{Sig}_{S_{\mathrm{info}}}, \mathrm{Sn}_i)$ through update the blockchain.

After the TA registers CAVs, the TA chooses a set of unlinkable pseudo-IDs $\mathrm{PID} = \{\mathrm{Pid}_1, \mathrm{Pid}_2, \cdots\}$ for each CAVs. For each $\mathrm{Pid}_j \in \mathrm{PID}$, TA computes the private key s $H_4(\mathrm{Pid}_j)$, s is a random number $\in \mathbb{Z}_q^*$. Then, TA sends all tuples $(\mathrm{Pid}_j, sH_4(\mathrm{Pid}_j))$ back to the CAV (S) using a secure transmission protocol. By changing its pseudo-ID, CAV achieves conditional location privacy and identity privacy in the VANETs.

3.3.3. Authentication Phase. The authentication based on bilinear pairing [30] could ensure the security of ACSMS. We use an handover authentication protocol to ensure efficiency seamless handover over multiple access points [30].

As Figure 4 shows, when an RSU (KS_t) is within the CAV direct communication range, the protocol run of BKM is as follows:

(1) The CAV picks an unused pseudo-ID $(\mathrm{Pid}_i, sH_4(\mathrm{Pid}_i))$

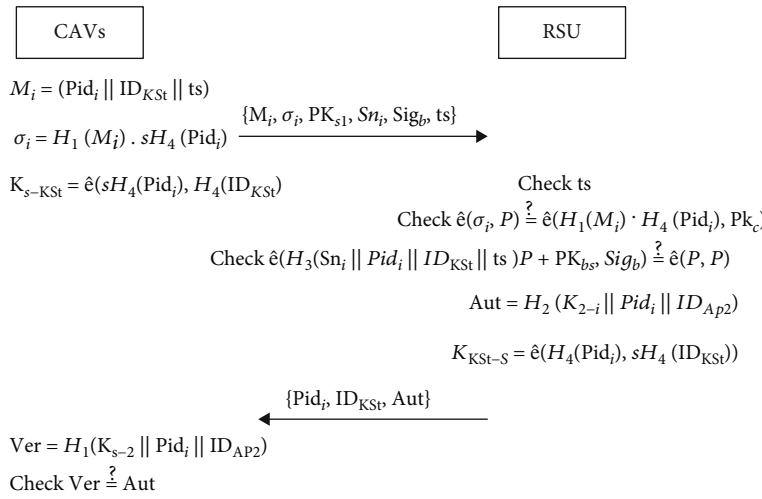

FIGURE 4: The protocol run of BKM.

(2) With message $M_i = (\mathrm{Pid}_i \| \mathrm{ID}_{\mathrm{KS}_t} \| \mathrm{ts})$ and $sH_4(\mathrm{Pid}_i)$, the CAV computes the signature $\sigma_i = H_1(\mathrm{M}_i) \cdot sH_4(\mathrm{Pid}_i)$ [30], where $\mathrm{ID}_{\mathrm{KS}_t}$ is RSU' (KS_t) identity, ts is a timestamp, and ‖ indicates the message concatenation operation

(3) The CAV computes the signature of $(\mathrm{Sig}_{S_{\mathrm{info}}}, \mathrm{Sn}_i)$ as $\mathrm{Sig}_b = P/H_3(\mathrm{Sn}_i \| \mathrm{Pid}_i \| \mathrm{ID}_{\mathrm{KS}_t} \| \mathrm{ts}) + \mathrm{SK}_{b_s}$, where SK_{b_s} is the private key of b_{s_1}

(4) The CAV sends the access request message $\{\mathrm{M}_i, \sigma_i, \mathrm{PK}_{b_s}, \mathrm{Sn}_i, \mathrm{Sig}_b, \mathrm{ts}\}$ to RSU (KS_t) through unicast, where PK_{b_s} is the public key of b_{s_1}

(5) The CAV computes the shared symmetric key with RSU (KS_t) as $K_{\mathrm{S-KS}_t} = \hat{e}(sH_4(\mathrm{Pid}_i), H_4(\mathrm{ID}_{\mathrm{KS}_t}))$ [30]

Upon receipt of $\{\mathrm{M}_i, \sigma_i, \mathrm{PK}_{b_s}, \mathrm{Sn}_i, \mathrm{Sig}_b\}$, the RSU KS_t proceeds as follows:

(1) RSU first checks ts to prevent replay attack. Then, RSU checks signature σ_i as $\hat{e}(\sigma_i, P) = \hat{e}(H_1(\mathrm{M}_i) \cdot sH_4(\mathrm{Pid}_i), P) = ^? \hat{e}(H_1(\mathrm{M}_i) \cdot H_4(\mathrm{Pid}_i), \mathrm{Pk}_c)$ [30]. Then, RSU needs to retrieve the corresponding $\{b_{s_1}, \mathrm{Sn}_i\}$ from the blockchain to ensure user legitimacy within pseudo-ID. Finally, RSU checks $\hat{e}(H_3(\mathrm{Sn}_i \| \mathrm{Pid}_i \| \mathrm{ID}_{\mathrm{KS}_t} \| \mathrm{ts})P + \mathrm{PK}_{b_s}, \mathrm{Sig}_b) = ^? \hat{e}(P, P)$. If both formula is correct, the CAV (S) is a legal vehicle, which was signed by the TA

(2) RSU further computes the shared symmetric key K_{KS_t-S}: $K_{\mathrm{KS}_t-S} = \hat{e}(H_4(\mathrm{Pid}_i), sH_4(\mathrm{ID}_{\mathrm{KS}_t})) = \hat{e}(sH_4(\mathrm{Pid}_i), H_4(\mathrm{ID}_{\mathrm{KS}_t})) = K_{\mathrm{S-KS}_t}$ [30]

(3) Then, KS_t generates an authentication code $\mathrm{Aut} = H_1(K_{\mathrm{KS}_t-S} \| \mathrm{Pid}_i \| \mathrm{ID}_{\mathrm{KS}_t})$ [30] and sends $\{\mathrm{Pid}_i, \mathrm{ID}_{\mathrm{KS}_t}, \mathrm{Aut}\}$ to the CAV (S)

Upon receipt of $\{\mathrm{Pid}_i, \mathrm{ID}_{\mathrm{KS}_t}, \mathrm{Aut}\}$, the CAV computes the verification code $\mathrm{Ver} = H_1(K_{\mathrm{KS}_t-S} \| \mathrm{Pid}_i \| \mathrm{ID}_{\mathrm{KS}_t}) = ^? \mathrm{Aut}$ [30]. If Ver matches Aut, KS_t is a legitimate RSU. The shared key between the CAV and RSU is K_{KS_t-S}.

By this protocol, CAV realizes authentication with RSU. The blockchain technology provides decentralized key authentication for the protocol. Between RSU and CAVs, a shared symmetric key K_{KS_t-S} is also established for the subsequent communication session.

If the administrator wants to find S_{info} of $\{\mathrm{M}_i, \sigma_i, \mathrm{PK}_{s_1}, \mathrm{Sn}_i, \mathrm{Sig}_b\}$, the TA first obtains T_w and Pk_s from the CAV. The TA takes as input Pk_s, y, and T_w and tests if $H_2(\hat{e}(yA, T_w + B)) = V$. With keywords $\{w_1, w_2, \cdots, w_n\}$ and TEST, the TA obtains ciphertext $\mathrm{Ct}_{\mathrm{info}}$ of each keyword. Then, the TA sends ciphertext $\mathrm{Ct}_{\mathrm{info}}$ to the CAV and CAV decryption $\mathrm{Ct}_{\mathrm{info}}$ as S_{info}'. After this, the CAV sends S_{info}' to the TA. Then, TA checks if $\hat{e}(H_3(S_{\mathrm{info}}')P + Y, \mathrm{Sig}_{S_{\mathrm{info}}}) = \hat{e}(P, P)$, where $\mathrm{Sig}_{S_{\mathrm{info}}}$ is obtained from the account b_{s_1}. If so, the correct S_{info} belongs to account b_{s_1}.

3.4. Blockchain-Based Trust Management in VANETs. The BKM uses pseudo-ID to provide conditional privacy. However, VANET is difficult to forward reliable message with an anonymous environment. Besides, the user with pseudo-ID will lack the motivation to forward announcements [37]. The BTM [13, 24, 25] was proposed to resolve these issues, which can recognize and eliminate of misbehaving vehicles. The process of the BTM is as follows. First, the CAV validates the legitimacy of received messages from neighboring CAVs. Second, based on the validated result, the rating of messages is generated by CAVs. Third, with the ratings uploaded from CAVs, the RSU gets the offsets of involved CAVs. Finally, the RSU adds the offset into the blockchain, where the offset is reflected by the CAV's blockchain account balance.

To calculate trust value, Zhao et al. [25] classify CAVs into three roles: privilege vehicles (S_1), enterprise vehicles

(S_2), and individual vehicles (S_3). Each role has different initial credibility. To share trust value with pseudo-ID, KS_t generates an authentication code of CAV's trust value OC_P as $Sig_{OC_p} = P/(H_3(Pid_i \| OC_P \| ts_1) + SK_{KS_t})$. SK_{KS_t} is the private key of the RSU (KS_t). Upon receipt of {Message, Pid$_i$, ts$_1$, Sig_{OC_p}, OC_P}, other CAV checks $\hat{e}(H_3(Pid_i \| OC_P \| ts_1)P + PK_{KS_t}, Sig_{OC_p}) = ^{?} \hat{e}(P, P)$, where PK_{KS_t} is RSU's (KS_t) public key.

A CAV receive M kinds of road-relevant events from different CAVs in a certain time. There are J CAVs in the reference set. The CAVs separate received messages into M groups as $\{g_1, g_2, \cdots, g_M\}$. g_i is one road-relevant event, which contains messages $\{W_i^1, W_i^2, \cdots, W_i^J\}$ that send by CAVs in the reference set J. According to [25], the tuple of one specific message (W_k^j [25]) is defined as

$$W_k^j = \left(d_k^j, \text{time}_k^j, OC_P\right), P \in (S_1, S_2, S_3). \tag{2}$$

The CAV receiver obtains the road-relevant event k from the neighboring CAV j. d_k^j is the distance between the location of the event k and CAV j; time_k^j is the message received time of CAV j; OC_P is the trust value of CAV j. According to [25], the credibility of specific messages (c_k^j) is calculated as:

$$c_k^j = \eta e^{\alpha d_k^j} + (1 - \eta) m_k^j + OC_p. \tag{3}$$

η is the balance coefficient between distance and time; α is a parameter to control the communication boundary; m_k^j is used to prevent replay attack. Next, t_i is the trust value of one road-relevant event g_i, which contains $\{c_1^i, c_2^i, \cdots, c_J^i\}$. t_i is calculated as (3) using Bayesian Inference [38].

$$t_i = P(e \mid g_i) = \frac{P(e) \cdot \prod_{k=1}^{J} P\left(c_i^k \mid e\right)}{P(e) \cdot \prod_{k=1}^{j} P\left(c_i^k \mid e\right) + P(\bar{e}) \cdot \prod_{k=1}^{J} P\left(c_i^k \mid \bar{e}\right)}. \tag{4}$$

$P(e)$ is the prior probability of event e; $\bar{e}$ is the complementary event of e. By comparing with threshold (Thr), the CAV j judges the event g_i. Then, CAV j generates ratings rate_i^j(i.e., +1 or -1) and sends to RSU. By weighted aggregation (4), RSU gets the offset of the trust value $\in [0, 1]$. According to [13], the sensitivity of ratings offset_i is controlled by $F(\cdot)$.

$$\text{offset}_i = \frac{F(m) \cdot m + F(n) \cdot n}{m + n}, \tag{5}$$

where m is the positive(+1) rating and n is the negative(-1) rating;

Compared offset_i with a threshold (Thr_1), if $\text{offset}_i >= \text{Thr}_1$, the offset of one CAV j is $\text{offset}_i^j = \text{rate}_i^j$. Otherwise, the offset of one CAV j is $\text{offset}_i^j = -\text{rate}_i^j$. After the event g_i, the new trust value of CAV j is $OC_p = OC_p + \text{offset}_i^j$. Finally, if a miner finds offset blocks that meet difficulty target, RSUs can share the new trust value of CAV j.

3.5. Atomic Swap-Based Cross-Chain Scheme. For now, the researcher proposed four categories cross-chain technologies [39], which include atomic cross-chain swap, multicentre witness, side chain (Ethereum 2.0), and distributed private key control. Atomic cross-chain swap [31, 32, 40, 41] is a standard method to connect multiple blockchains. Without trusted third parties, the atomic swap can realize fair cross-chain exchange.

The ACSMS can exchange the CAV's data for the blockchain-based PEKS, the BKM, and the BTM. Take as input last signature (Sig, Sn_i, data), old blockchain account (PK_{b_s1}, SK_{b_s1}), and new blockchain account (PK_{b_s2}, SK_{b_s2}). S computes the cross-chain transaction $\text{Asset}_R = \{\text{Sig}(Sn_{i+1} \| ts \| OC_p), Sn_{i+1}, ts, PK_{b_s1} \longrightarrow PK_{b_s2}, OC_p, \text{swap}\}$. The signature $\text{Sig}(Sn_{i+1} \| ts \| OC_p) = P/(H_3(Sn_{i+1} \| ts \| OC_p) + SK_{b_s1})$. After the ACSMS process, if searcher wants to find past information, then searcher uses index Si and PK_{b_s1} to find past signature (Sig), which can check data integrity and authenticate the user. The cross-chain model is illustrated in Figure 5.

The atomic swaps problem in VANETs is as follows. Assume a CAV has an account (PK_{b_s1}, PR_{b_s1}) and holds an asset $Z = (\text{Asset}_S, OC_p)$ in blockchain A. If CAV accesses blockchain B domain, the CAV creates a new blockchain account (PK_{b_s2}, PR_{b_s2}) in blockchain B. By the smart contract [32], the CAV can deal with other CAV or RSU or TA to realized cross-chain swap. Compared with other CAVs and RSU, it is more securely and efficient that CAVs deal with the TA as escrow agent [31, 32, 41]. The escrow agent to occur for the ACSMS is as follows.

4. Security Analysis

4.1. Security of Blockchain-Based PEKS. The security of blockchain-based PEKS consists of three aspects: CAVs' data security preservation [42], conditional identity privacy, and storage correctness guarantee.

(i) *CAVs' data security preservation*. In the ACSMS, with a standard public key encryption $E(\cdot)$, message M with keywords, the TA gets ciphertext Ct_s. Ct_s is encrypted with (SK_s, PK_s, PK_c), any adversary is infeasible to compute SK_s due to the hardness assumption of bilinear Diffie-Hellman problem [43]. Without SK_s, the TA can not decryption Ct_s

(ii) *Conditional identity privacy*. Many ciphertexts are stored in the server. It is difficult for any adversary to find specific ciphertext without trapdoor T_w. However, the ciphertexts have identity privacy during storage; any searcher can use trapdoor T_w to find the ciphertext. The searcher has no right to download ciphertext without the signature of blockchain account b_{s_1}. Therefore, blockchain-based PEKS can resist the keyword guessing attacks (KGA).

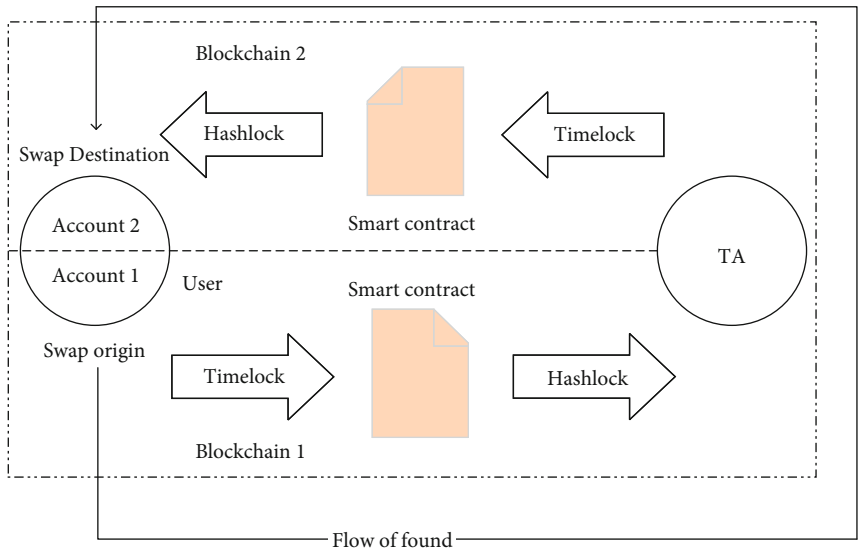

Figure 5: Atomic swap-based cross-chain scheme.

```
Atomic swap for ACSMS {
   depositA, depositB: bool; hash1, hash2 : int256;
//the deposit function allows user transfer of the asset to the smart contract.
   uint startA, startB; //protocol starting time
   initialize {deposited A : = False; deposited B := False; hash1=hash2=0; }
   depositA{if sender = account_A and asset=Z:
      Then depositA : = True and hash = h1 and startA = time()}
//h1 is hash-lock; startA + time_set is time-lock.
   depositB{if sender = TA and asset=Z:
      Then depositB : = True and hash = h2 and startB = time()}
   Finalise{if depositA and depositB and now < startA + time_set :
      Then {depositA : = False; depositB:= False
      send(account_B,Z), send(TA,Z)}}
   cancelA{if (depositA and sha-256(x2) = h2) or now > startA + time_set
      then {depositA : = False; Send(account_A,Z)}}
   cancelB{if (depositB and sha-256(x1) = h1) or now > startB + time_set
      then {depositB : = False; Send(TA,Z)}}
}
```

Algorithm 1

(iii) *Storage correctness guarantee*. The signature of the ciphertext provides storage correctness guarantee, which is obtained from the blockchain

4.2. Security of BKM. A distributed BKM is built through a key management protocol [30] and blockchain technology. ACSMS can achieve subscription validation, server authentication, CAV untraceability, and anonymity. Furthermore, the ACSMS can achieve distributed and tamper-proofing through blockchain technology. In addition, the BKM can against typical attacks towards the VANETs as follows: internal attack, public key tampering, and DoS Attack.

(i) *Internal attack*. The adversary eavesdrops on the communication data between the CAVs and RSU [22]. However, without private key $sH_4(\mathrm{Pid}_i)$ or s $H_4(\mathrm{ID}_{\mathrm{KS}_i})$, adversary cannot get shared symmetric key $K_{S-\mathrm{KS}_i}$ between the CAVs and RSU

(ii) *Public key tampering*. If adversary creates fake pseudo-ID Pid_i without a legal blockchain account, the RSU can verify that $\hat{e}(H_3(\mathrm{Sn}_i \| \mathrm{Pid}_i \| \mathrm{ID}_{\mathrm{KS}_i} \| \mathrm{ts})P + \mathrm{PK}_{b_s}, \mathrm{Sig}_b) \neq \hat{e}(P, P)$. In the ACSMS, legal blockchain account is registered by the TA; adversary cannot counterfeit the registration transaction into the blockchain

(iii) *DoS Attack*. The ACSMS can resist DoS Attack by timestamp ts and hardware security module. If adversary sends a lot of intercepted messages to VANETs, timestamp ensures the freshness of the messages

4.3. Security of BTM. The security of BTM consists of three aspects: conditional identity privacy, prevention of replay attack, and prevention of message spoofing attack.

(i) *Conditional identity privacy*. CAVs broadcast message $\{\text{Message}, \text{Pid}_i, \text{ts}_1, \text{Sig}_{\text{OC}_p}, \text{OC}_P\}$ without blockchain account information; the Pid_i is unlinkable pseudo-IDs. Thus, other vehicles are difficult to analyze the user information with the BTM. But, the RSU can find the blockchain account b_{s_1} through the BKM, and the TA can find relevant CAV information S_{info} by the blockchain-based PEKS

(ii) *Prevention of replay attack*. By time_k^j and m_k^j, if the messages are send by the same CAVs at different times, the credibility of specific messages c_k^j will set to zero. Therefore, equations (2) and (3) will reject the same information with a different timestamp

(iii) *Prevention of message spoofing attack*. Adversary may broadcast fake messages to neighbors. In the ACSMS, we take the Bayesian Inference-based rating generation scheme. Therefore, the receiver will analyze messages from different reference CAVs about the same event

4.4. Security of Atomic Swap. The ACSMS achieves hash locking and smart contract to create conditional payment. The atomicity of atomic swap is guaranteed by the cross-chain protocol. At the same time, the security of the atomic cross-chain swap is ensured by blockchain-based PEKS, BKM, and BTM. The security of atomic swap consists of three aspects: CAVs' data security preservation, conditional identity privacy, and storage correctness guarantee. The atomic swap also against typical attacks towards the VANETs is as follows: internal attack, public key tampering, and DoS Attack. The ACSMS achieves security and anonymity by the blockchain-based PEKS, BKM, and BTM. Furthermore, in ACSMS, only the TA and RSU can create new transaction that can resist targeted attacks [44].

4.5. Comparison of Related Works. There are many blockchain-based application systems that have been developed in VANETs [12, 13, 16, 17, 22, 24]. These researches can protect CAV privacy and ensure security certificate. As shown in Table 1, compared with these schemes, ACSMS integrates the function of the above methods into the ACSMS. Besides, the ACSMS can provide cross-chain process, which boost interoperability between multiple blockchain. Furthermore, compared with [25], the ACSMS can support cross-chain stage security in VANETs.

Table 1 shows the comparison of related work. A safe and reliable decentralized data storage system was built in [17, 18, 20]. The scheme [12, 16, 22, 24] applied blockchain technology into VANETs; the management of CAVs' key is more efficient and secure. Furthermore, by BTM [13, 24, 25], the CAV could forward reliable announcements without relevant CAVs' information, and the users with pseudo-ID are encouraged to forward announcements. The ACSMS scheme uses PEKS and blockchain technology to integrate above the functions to support multiple blockchain-based applications with a single blockchain account. In addition, we use atomic swap smart contract to achieve cross-chain interoperability among blockchain-based systems.

5. Performance Evaluation

The performance evaluation of ACSMS was carried out using simulations. Our results are generated using pypbc (the encryption algorithm) and truffle (blockchain for ACSMS). ACSMS is simulated by our laptop with 2.6Ghz Core i7 CPU and 16G RAM and display card Radeon Pro 555X 4 GB. We also simulated the ACSMS in the elastic compute service with Ubuntu 18.02, 4v 3.1GHz/3.5Ghz CPU and 16G RAM.

The simulation of the trust management system in VANET [45] shows that the rate of malicious vehicles. A variable percentage is generated to simulate a different percentage of malicious vehicles like in [45]. The performance of trust management is evaluated through the trust value of CAVs OC_P. However, our BTM scheme only affects the initial OC_P, and the RSU uploads trust value after receiving multiple pieces of evidence. Therefore, blockchain will not change the efficiency of trust management [32, 45, 46].

5.1. Blockchain-Based PEKS. To evaluate blockchain-based PEKS and other related woks, we use a cryptographic function called Type-A [17]. We set $|\mathbb{Z}_q^*| = 160$ bits and $|\mathbb{G}_1| = |\mathbb{G}_2| = 1024$ bits by setting parameters qbits = 1024 and rbits = 160, where $|x|$ is the length of x. We take ZSS (Zhang-Safavi-Naini-Susilo) short signature scheme from Bilinear Pairing [34]. Besides, pypbc requires the hash of the signature scheme and key in the same group. So, we use 160 bits $\text{Sig} = P/(H_1(\text{Ct}_s) + x)$ instead of $\text{Sig} = P/(H_3(\text{Ct}_s) + x)$.

Figure 6 shows the computation cost comparisons for the FTDS [17] and the BSPP [20]. The computation costs of encrypting ciphertext and decrypt ciphertext are constant, which not show in the picture. Each scheme uses 100 keywords to encrypt 100 files. The FTDS [17] is slower than the ACSMS and the BSPP in KeyGen and PEKS, because the FTDS uses key-aggregate encryption, which is a decentralized PEKS scheme. In BSPP [20], the user's medical data is encrypted and stored in the server of the hospital. The corresponding index of user data is stored in the blockchain. It can be seen that the calculation delay of BSPP is close to the ACSMS, because the calculation of KeyGen, Trapdoor, PEKS, and Test all depends on the PEKS algorithm.

The blockchain storage time of the three schemes is similar. Because all three plans store indexes or proofs, the small amount of data will not affect the blockchain's storage speed. The block generation rate will limit blockchain-based on workload consensus. By adjusting the difficulty target, administrators can change the block generation rate of the blockchain. However, too fast block generation rate will lead to the blockchain bifurcating. Therefore, the block generation rate of the typical blockchain is maintained at a certain level. Consequently, we can consider that the three schemes have the same computing delay on the blockchain storage.

Table 1: Comparison of related works.

Feature	[12]	[16]	[22]	[13]	[25]	[24]	[18, 20]	[17]	ACSMS
PEKS	×	×	×	×	×	×	√	√	√
BKM	√	√	√	×	×	√	×	×	√
BTM	×	×	×	√	√	√	×	×	√
PoW	√	√	√	√	×	√	√	×	√
Smart contract	×	×	√	×	√	×	×	×	√
No TA	√	√	×	√	×	×	×	√	×
Key agreement	√	√	√	×	√	×	×	×	√
Cross-chain	×	×	×	×	√	×	×	×	√

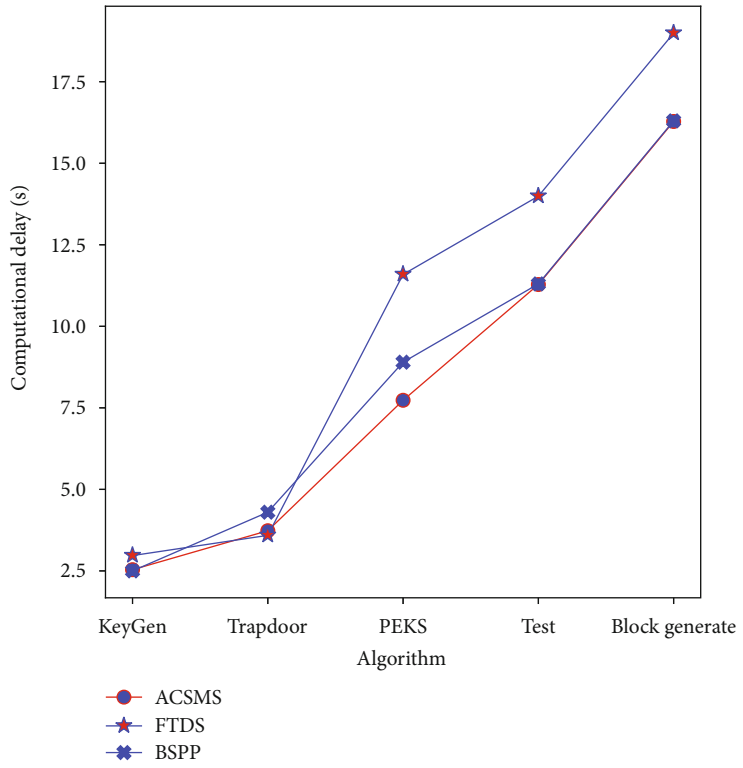

Figure 6: Computation cost comparison for algorithms.

5.2. BKM. Then, we study the processing time cost for the BKM. Our BKM scheme based on PairHand [30], the user cryptographic operation of [30] is 1ECSM+1Pairing. Based on PairHand, we use blockchain to realize distributed key authentication. Therefore, the user cryptographic operation of the BKM in ACSMS is 1ECSM+2Pairing+1hash. In the PairHand, the RSU will transmit messages to TA after authentication, which can find the real identity of CAVs. However, if CAV transmission legal pseudo-IDs to the adversary, the RSU cannot distinguish the adversary and the normal CAVs in the authentication. Although our scheme costs more processing time than the PairHand, our schemes can provide decentralized key authentication than [30]. To evaluate the performance of our scheme, we compare the conventional handover schemes [12, 30].

We can obtain that the exponential increase of blockchain key transfer time in decentralized BKM [12] as shows in Figure 7. In [12], the keys of new joining members are delivered by the blockchain. Our BKM only uses the blockchain record S_{info} to authenticate users, which increases linearly. Although, in the experiment, our key transmission time authenticated by this scheme is relatively large. But, RSU only needs to find the user's signature in the blockchain. There is no need to store data into the blockchain. In this way, our scheme can better support other blockchain-based applications.

5.3. Atomic Cross-Chain Swap. To evaluate the effect of ACSMS, we realize the atomic swap protocol in python. Two PoW-based blockchains are built in python. Administrators can set the difficulty target of each blockchain to adjust blockchain throughput. The total number of CAVs is 1000, and $Z = (\text{Asset}_R, \text{OC}_p)$ is calculated by CAVs. Furthermore, there are average packet latency and blockchain

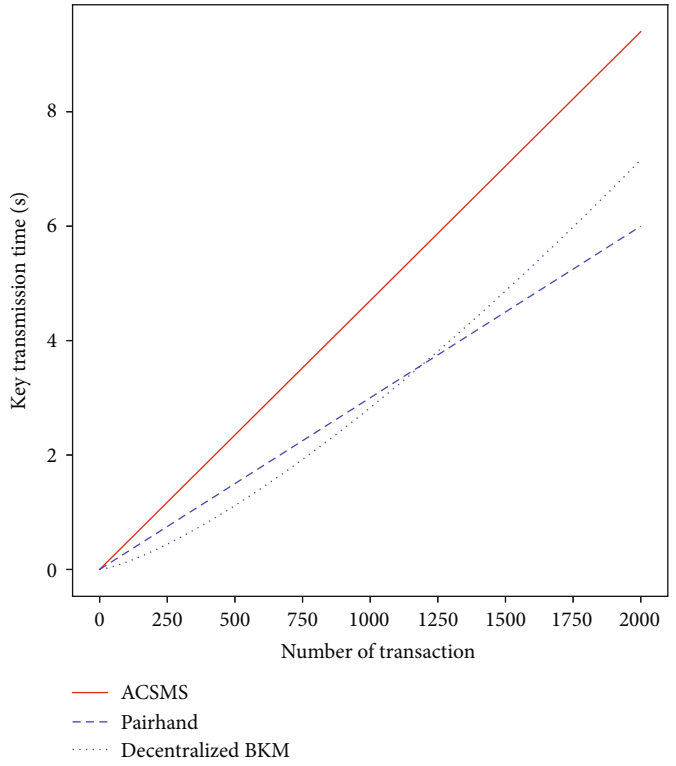

Figure 7: Processing time comparison different schemes.

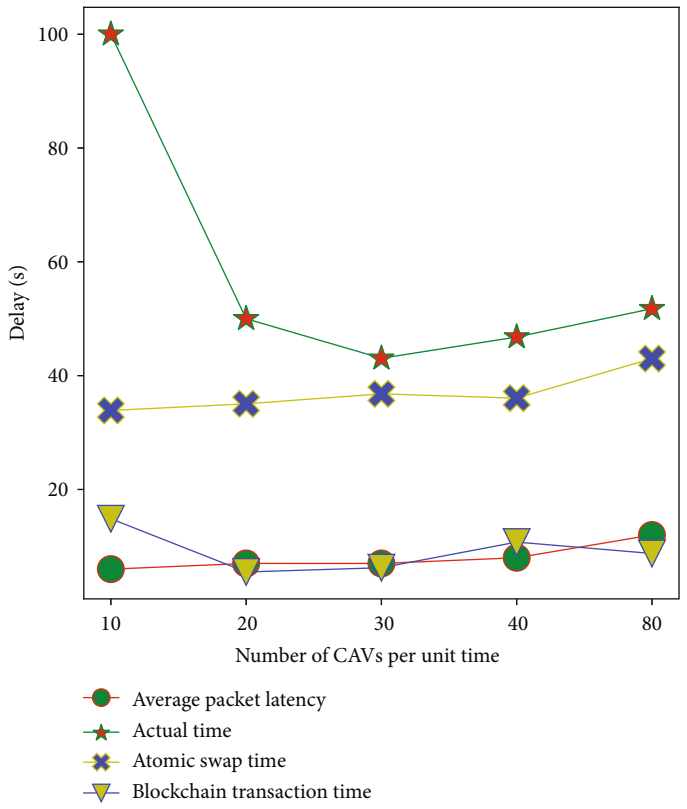

Figure 8: Average delay over different number of CAVs.

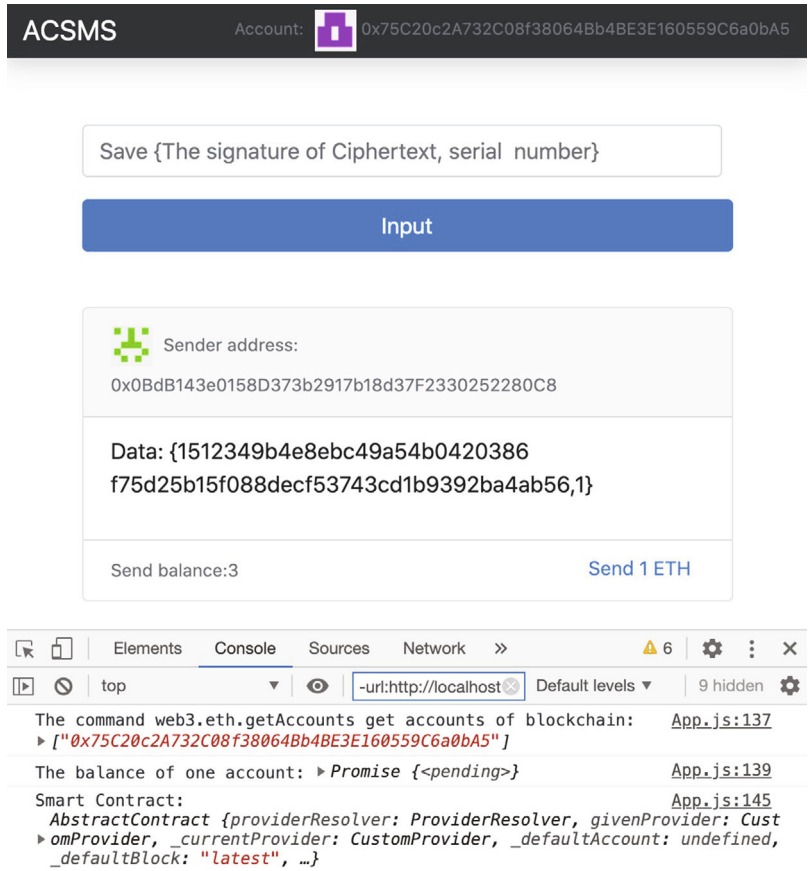

Figure 9: The application of ACSMS.

transaction time in the blockchain-based VANET application [22]. As Figure 8 shows, the delay of atomic cross-chain swap changes with the number of CAVs per unit time.

5.4. Engineering Applications. On Ethereum [14], the user can write a smart contract to realize a distributed program. In order to evaluate our proposed ACSMS, we have built a web application of ACSMS, as illustrated in Figure 9.

The application of ACSMS was built as follows:

(1) We installed truffle, Ganache, and node.js v9.10.0. Next, we configured babel (a JavaScript compiler), bootstrap (HTML, CSS, and JS library), identicon (a visual representation of a hash value), chai (a BDD/TDD assertion library), mocha (a feature-rich JavaScript test framework), and web3 (web3.js interact with Ethereum node using HTTP, IPC, or WebSocket). Then, we use those to create a package.json file for the project using npm install to install these libraries

(2) We developed a smart contract in atom text editor and write test cases for use with TDD (test-driven development, chai, and mocha). Then, metamask was used to access ethrum enabled distributed applications

(3) As shown in Figure 9, the application of ACSMS saves $(\mathrm{Sig}, \mathrm{Sn}_i)$ into the blockchain network, which blockchain-based PEKS was realized

(4) With metamask and web3 command web3.eth.getAccounts(·), user blockchain account was got for BKM. RSU can retrieve the corresponding $\{b_{s_1}, \mathrm{Sn}_i\}$ from the blockchain to ensure user legitimacy within pseudo-ID

(5) With metamask and web3 command web3.eth.getBalance (Account), the user account balance was got for BTM. To share trust value with pseudo-ID, RSU generates an authentication code of CAV's trust value OC_P, where OC_P is reflected by the CAV's blockchain in account balance. Furthermore, after BTM, RSU could send the balance to the user account through the button

6. Conclusion

In this paper, we proposed the ACSMS to boost the scalability of blockchain-based applications in VANETs. Besides, the ACSMS integrates the blockchain-based schemes into a single blockchain through the bilinear pairing. First, we designed a blockchain-based PKES to check data integrity and authenticate the user. Second, we designed blockchain-

based key management. The BKM uses data of blockchain-based PKES to provide decentralized key authentication. Third, based on the BKM, CAVs get proof of trust value from the RSU. Therefore, the CAVs can share reasonable trust value in blockchain-based trust management. Finally, the atomic swap-based cross-chain scheme can exchange user trust value and data index across the chain. The searcher quickly finds the data of blockchain-based PKES in the different blockchain. However, the simulation results demonstrate that the performance of ACSMS is no improvement than the previous scheme. Nevertheless, security analysis shows that our schemes can achieve the security requirements of VANETs.

In the future, we will take PEKS for cloud storage services. The sender in ACSMS can outsource the data to the cloud storage services. On the other, we may use PoS-based blockchain instead of PoW-based blockchain as long as security is ensured.

Data Availability

The data are available at https://github.com/tanchenkai/Paper.

Conflicts of Interest

The authors declare that they have no conflicts of interest.

References

[1] G. Xu, X. Li, L. Jiao et al., "Bagkd: a batch authentication and group key distribution protocol for vanets," *IEEE Communications Magazine*, vol. 58, no. 7, pp. 35–41, 2020.

[2] J. Liu, J. Li, L. Zhang et al., "Secure intelligent traffic light control using fog computing," *Future Generation Computer Systems*, vol. 78, pp. 817–824, 2018.

[3] S. I. Fadilah, A. R. M. Shariff, and M. N. M. Hilmi, "Crash avoidance based periodic safety message dissemination protocol for vehicular ad hoc network," in *2019 IEEE 89th Vehicular Technology Conference (VTC2019-Spring)*, Kuala Lumpur, Malaysia, April-May 2019.

[4] K. Sjoberg, P. Andres, T. Buburuzan, and A. Brakemeier, "Cooperative intelligent transport systems in Europe: current deployment status and outlook," *IEEE Vehicular Technology Magazine*, vol. 12, no. 2, pp. 89–97, 2017.

[5] A. Shahzad, M. Lee, Y. K. Lee et al., "Real time MODBUS transmissions and cryptography security designs and enhancements of protocol sensitive information," *Symmetry*, vol. 7, no. 3, pp. 1176–1210, 2015.

[6] L. Shu, Y. Zhang, Z. Yu, L. T. Yang, M. Hauswirth, and N. Xiong, "Context-aware cross-layer optimized video streaming in wireless multimedia sensor networks," *The Journal of Supercomputing*, vol. 54, no. 1, pp. 94–121, 2010.

[7] W. Wu, N. Xiong, and C. Wu, "Improved clustering algorithm based on energy consumption in wireless sensor networks," *IET Networks*, vol. 6, no. 3, pp. 47–53, 2017.

[8] H. Hasrouny, A. E. Samhat, C. Bassil, and A. Laouiti, "Vanet security challenges and solutions: a survey," *Vehicular Communications*, vol. 7, pp. 7–20, 2017.

[9] K. Huang, Q. Zhang, C. Zhou, N. Xiong, and Y. Qin, "An efficient intrusion detection approach for visual sensor networks based on traffic pattern learning," *IEEE Transactions on Systems, Man, and Cybernetics: Systems*, vol. 47, no. 10, pp. 2704–2713, 2017.

[10] A. Vaibhav, D. Shukla, S. Das, S. Sahana, and P. Johri, "Security challenges, authentication, application and trust models for vehicular ad hoc network-a survey," *International Journal of Wireless and Microwave Technologies*, vol. 7, no. 3, pp. 36–48, 2017.

[11] Q. Zhang, C. Zhou, N. Xiong, Y. Qin, X. Li, and S. Huang, "Multimodel-based incident prediction and risk assessment in dynamic cybersecurity protection for industrial control systems," *IEEE Transactions on Systems, Man, and Cybernetics: Systems*, vol. 46, no. 10, pp. 1429–1444, 2015.

[12] A. Lei, H. Cruickshank, Y. Cao, P. Asuquo, C. P. A. Ogah, and Z. Sun, "Blockchain-based dynamic key management for heterogeneous intelligent transportation systems," *IEEE Internet of Things Journal*, vol. 4, no. 6, pp. 1832–1843, 2017.

[13] Z. Yang, K. Yang, L. Lei, K. Zheng, and V. C. Leung, "Blockchain-based decentralized trust management in vehicular networks," *IEEE Internet of Things Journal*, vol. 6, no. 2, pp. 1495–1505, 2019.

[14] G. Wood, "Ethereum: a secure decentralised generalised transaction ledger," *Ethereum Project Yellow Paper*, vol. 151, no. 2014, pp. 1–32, 2014.

[15] D. Jia, K. Lu, J. Wang, X. Zhang, and X. Shen, "A survey on platoon-based vehicular cyber-physical systems," *IEEE Communications Surveys & Tutorials*, vol. 18, no. 1, pp. 263–284, 2016.

[16] R. Shrestha, R. Bajracharya, and S. Y. Nam, "Blockchain-based message dissemination in VANET," in *2018 IEEE 3rd International Conference on Computing, Communication and Security (ICCCS)*, Kathmandu, Nepal, 2018.

[17] J. Sun, H. Xiong, S. Zhang, X. Liu, J. Yuan, and H. Deng, "A secure flexible and tampering-resistant data sharing system for vehicular social networks," *IEEE Transactions on Vehicular Technology*, vol. 69, no. 11, pp. 12938–12950, 2020.

[18] Y. Zhang, C. Xu, J. Ni, H. Li, and X. S. Shen, "Blockchain-assisted public-key encryption with keyword search against keyword guessing attacks for cloud storage," *IEEE Transactions on Cloud Computing*, pp. 1–14, 2020.

[19] D. Boneh, G. Di Crescenzo, R. Ostrovsky, and G. Persiano, "Public key encryption with keyword search," in *International conference on the theory and applications of cryptographic techniques*, Springer, Berlin, Heidelberg, May 2004.

[20] A. Zhang and X. Lin, "Towards secure and privacy-preserving data sharing in e-health systems via consortium blockchain," *Journal of Medical Systems*, vol. 42, no. 8, p. 140, 2018.

[21] X. Zhang and X. Chen, "Data security sharing and storage based on a consortium blockchain in a vehicular ad-hoc network," *IEEE Access*, vol. 7, pp. 58241–58254, 2019.

[22] Z. Ma, J. Zhang, Y. Guo, Y. Liu, X. Liu, and W. He, "An efficient decentralized key management mechanism for VANET with blockchain," *IEEE Transactions on Vehicular Technology*, vol. 69, no. 6, pp. 5836–5849, 2020.

[23] S. Nakamoto, *Bitcoin: A Peer-to-Peer Electronic Cash System*, Manubot, 2019.

[24] Z. Lu, Q. Wang, G. Qu, and Z. Liu, "Bars: a blockchain-based anonymous reputation system for trust management in VANETs," in *2018 17th IEEE International Conference On Trust, Security And Privacy In Computing And Communications/12th IEEE International Conference On Big Data Science*

And Engineering (Trust-Com/BigDataSE), New York, NY, USA, August 2018.

[25] N. Zhao, H. Wu, and X. Zhao, "Consortium blockchain-based secure software defined vehicular network," *Mobile Networks and Applications*, vol. 25, no. 1, pp. 314–327, 2020.

[26] W. Guo, N. Xiong, A. V. Vasilakos, G. Chen, and H. Cheng, "Multi-source temporal data aggregation in wireless sensor networks," *Wireless Personal Communications*, vol. 56, no. 3, pp. 359–370, 2011.

[27] Y. Yang, N. Xiong, N. Y. Chong, and X. Défago, "A decentralized and adaptive flocking algorithm for autonomous mobile robots," in *2008 The 3rd International Conference on Grid and Pervasive Computing-Workshops*, Kunming, China, 2008.

[28] C. Lin, Y. X. He, and N. Xiong, "An energy-efficient dynamic power management in wireless sensor networks," in *2006 Fifth International Symposium on Parallel and distributed computing*, Timisoara, Romania, July 2006.

[29] J. Santa, L. Bernal-Escobedo, and R. Sanchez-Iborra, "On-board unit to connect personal mobility vehicles to the IoT," *Procedia Computer Science*, vol. 175, pp. 173–180, 2020.

[30] D. He, C. Chen, S. Chan, and J. Bu, "Secure and efficient handover authentication based on bilinear pairing functions," *IEEE Transactions on Wireless Communications*, vol. 11, no. 1, pp. 48–53, 2012.

[31] R. van der Meyden, "On the specification and verification of atomic swap smart contracts (extended abstract)," in *2019 IEEE International Conference on Blockchain and Cryptocurrency (ICBC)*, Seoul, Korea (South), May 2019.

[32] M. H. Miraz and D. C. Donald, "Atomic cross-chain swaps: development, trajectory and potential of non-monetary digital token swap facilities," *Annals of Emerging Technologies in Computing*, vol. 3, no. 1, pp. 42–50, 2019.

[33] C. Gu and Y. Zhu, "New efficient searchable encryption schemes from bilinear pairings," *IJ Network Security*, vol. 10, no. 1, pp. 25–31, 2010.

[34] F. Zhang, R. Safavi-Naini, and W. Susilo, "An efficient signature scheme from bilinear pairings and its applications," in *International Workshop on Public Key Cryptography*, pp. 277–290, Springer, 2004.

[35] Z. Jing, C. Gu, C. Ge, and P. Shi, "Cryptanalysis of a public key cryptosystem based on data complexity under quantum environment," *Mobile Networks and Applications*, pp. 1–7, 2020.

[36] L. Li, G. Xu, L. Jiao et al., "A secure random key distribution scheme against node replication attacks in industrial wireless sensor systems," *IEEE Transactions on Industrial Informatics*, vol. 16, no. 3, pp. 2091–2101, 2020.

[37] L. Li, J. Liu, L. Cheng et al., "Creditcoin: a privacy-preserving blockchain-based incentive announcement network for communications of smart vehicles," *IEEE Transactions on Intelligent Transportation Systems*, vol. 19, no. 7, pp. 2204–2220, 2018.

[38] M. Raya, P. Papadimitratos, V. D. Gligor, and J. P. Hubaux, "On data-centric trust establishment in ephemeral ad hoc networks," in *IEEE INFOCOM 2008-The 27th Conference on Computer Communications*, Phoenix, AZ, USA, April 2008.

[39] D. Yang, C. Long, H. Xu, and S. Peng, "A review on scalability of blockchain," in *Proceedings of the 2020 The 2nd International Conference on Blockchain Technology (ICBCT'20), Association for Computing Machinery*, pp. 1–6, New York, NY, USA, 2020.

[40] M. Herlihy, "Atomic cross-chain swaps," in *Proceedings of the 2018 ACM Symposium on Principles of Distributed Computing*, pp. 245–254, ACM, 2018.

[41] T. Nolan, *Alt Chains and Atomic Transfers*, Bitcoin Forum, 2013.

[42] Z. Jing, C. Gu, Y. Li et al., "Security analysis of indistinguishable obfuscation for internet of medical things applications," *Computer Communications*, vol. 161, pp. 202–211, 2020.

[43] D. Boneh and M. Franklin, "Identity-based encryption from the Weil pairing," in *Advances in Cryptology — CRYPTO*, pp. 213–229, Springer, 2001.

[44] S. Bartolucci, F. Caccioli, and P. Vivo, "A percolation model for the emergence of the bitcoin lightning network," *Scientific reports*, vol. 10, no. 1, 2020.

[45] F. Gómez Mármol and G. Martínez Pérez, "Trip, a trust and reputation infrastructure-based proposal for vehicular ad hoc networks," *Journal of Network and Computer Applications*, vol. 35, no. 3, pp. 934–941, 2012.

[46] Y. Xiao, Y. Liu, and T. Li, "Edge computing and blockchain for quick fake news detection in IoV," *Sensors*, vol. 20, no. 16, p. 4360, 2020.

Hindawi
Wireless Communications and Mobile Computing
Volume 2021, Article ID 6630130, 8 pages
https://doi.org/10.1155/2021/6630130

Research Article

Research on Sports Video Image Analysis Based on the Fuzzy Clustering Algorithm

Yuehong Li

The Physical Education Institute, Chaohu University, Hefei 238000, China

Correspondence should be addressed to Yuehong Li; 060027@chu.edu.cn

Received 20 October 2020; Revised 20 December 2020; Accepted 12 January 2021; Published 27 January 2021

Academic Editor: Hongju Cheng

Copyright © 2021 Yuehong Li. This is an open access article distributed under the Creative Commons Attribution License, which permits unrestricted use, distribution, and reproduction in any medium, provided the original work is properly cited.

Aimed at the shortcomings of the current sports video image segmentation methods, such as rough image segmentation results and high spatial distortion rate, a sports video image segmentation method based on a fuzzy clustering algorithm is proposed. The second-order fuzzy attribute with normal distribution and gravity value is established by using the time-domain difference image, and the membership function of the fuzzy attribute is given; then, the time-domain difference image is fuzzy clustered, and the motion video image segmentation result is obtained by edge detection. Experimental results show that this method has high spatial accuracy, good noise iteration performance, and low spatial distortion rate and can accurately segment complex moving video images and obtain high-definition images. The application of this video image analysis method will help master the rules of sports technology and the characteristics of healthy people's sports skills through video image analysis and help improve physical education, national fitness level, and competitive sports level.

1. Introduction

Web systems are substantially different from more conventional software systems. They are developed in shorter time frames and with smaller budgets, meet a more generic set of requirements, and generally serve a less specific user group [1]. They are often developed very quickly from template solutions, using coarse-grained authoring tools, and by the efforts of a multidisciplinary team [2, 3]. With the rapid development of network and multimedia technology, many sports operations and national fitness materials are stored in various health guidance systems in the form of video and pictures. In order to better promote the public fitness, easy to learn and see, sports video also has editing, segmentation, and integration of a variety of needs. Video compression technology has gradually become a hot research topic [4, 5]. An intelligent scheduling algorithm for hierarchical data migration is a key issue in data management. The discovery of mass media content platforms and usage patterns of content objects is the basic timetable for data migration. We added QPop (the dimensionality reduction result of media content usage logs) as a content object for discovering usage patterns. On this basis, a clustering algorithm QPop is proposed to increase time segmentation, thereby improving mining performance.

Video compression technology reduces the video capacity by video coding, which facilitates the release of storage space and reduces the transfer time. The traditional video coding standards include mpeg 2H., 263, and .mpeg, which refer to moving picture group of experts, as the group of experts on dynamic images. Its computational redundancy is small, and the overall efficiency is higher than that of stable h.263 [6]. In addition, the video coding technology needs to segment the object image to ensure the integrity of the target object. However, the traditional video coding standard cannot search the content of the video. It has a certain degree of difficulty in image segmentation. Mpeg 4 is introduced in 2000 as the semantic search function of video content, which can divide the image background and foreground into different semantic objects. The coding efficiency is improved, but the noise cannot be eliminated quickly in the coding process [7].

The rest of this paper is organized as follows. Section 2 discusses research on motion change region detection, followed by research approach which is discussed in Section 3. Detection of the motion change region with multiple

constraints is discussed in Section 4. The experiment is discussed in Section 5. Section 6 concludes the paper with summary and future research directions.

2. Research on Motion Change Region Detection

Time-domain segmentation and frequency-domain segmentation are the first methods proposed for moving video image segmentation. It has been proven that both two methods cannot accurately depict the object posture and the image segmentation is not clear. Therefore, based on a fuzzy clustering algorithm, the research on sports video with strong motion and attitude changes will be helpful to better use and analyze sports video images. The fuzzy clustering algorithm comes from pattern clustering theory.

2.1. The Basic Method of Motion Change Region Detection. It is an algorithm that uses mathematical rules to describe the segmentation interval. The fuzzy clustering algorithm uses iterative operation to segment the pixel region of the target object and divide the image pixel into different subordination intervals to make the image segmentation decision [8]. When the target object has n pixel samples, the pixel samples form an uncluttered set, which is represented as $x = \{x1mx2, \text{and } XN\}$, and XK represents pixel samples. Let c denote the number of image segmentation types and λ denote the fuzzy clustering weighting factor [9]. The moving posture of target objects in sports video is relatively random, the trend of image change is blurred, and the segmentation area is not easy to determine. The proposed method of video image segmentation can divide the moving attitude area of the target object into the foreground and the background and extract the motion of the target object. The class algorithm extracts the image sequence in the sports video playback state and opens the edge detection process at the same time [10–12]. According to the image sequence, the object motion is predicted and compensated. The same background is set up on some images with small spacing.

2.2. Fuzzy Clustering Algorithm. The time-domain difference image is extracted by using the attributes of the adjacent image frames. The fuzzy attribute in the motion process of the object and the corresponding membership function are written. After the fuzzy clustering of the time-domain difference image, the edge contour of the object is cut through the edge detection process, the foreground region is obtained, and the foreground area is eliminated. The following two problems need to be discussed for the selection of fuzzy attributes in the fuzzy clustering algorithm: the first is which attributes of the target object can accurately describe the operational attitude and the second is that the ambiguity in the motion pose region and the useless pixel region is not the same and there must be obvious difference [13–15].

After discussion, the proposed sports video image segmentation method finds that when the object in the moving video image goes through motion prediction and compensation, the background region can be expressed as the background difference of the image with small spacing and the same background [16]. In this case, if the background of the original sports visual frequency image has normal distribution, then the segmented image should also have the normal distribution property, and the average pixel distribution is equal to 0 which is shown in Figure 1 [17].

The judgment matrix A meets the following requirements:

$$a_{ij} = \frac{a_{ik}}{a_{jk}}, \quad i, j, k = 1, 2, \cdots, n. \tag{1}$$

When the consistency of the judgment matrix does not meet the requirements, there are nonzero eigenvalues:

$$\lambda_{\max} + \sum_{\lambda \to \lambda_{\max}} = \sum_{i=1}^{n} a_{ij} = n. \tag{2}$$

In order to check these matrices to determine their consistency satisfaction, the average random consistency index RI value (1-9) order judgment matrix is introduced:

$$\mathrm{CI} = \frac{\lambda_{\max} - n}{n - 1}, \tag{3}$$

Level single sort: CR can be used to judge [18].

Level total ranking: for all factors from low to high level, calculate their relative importance to the highest level.

The upper-level A contains m factors $A1$, $A2$, and Am and the level total ranking weights $a1$, $a2$, $a3$, and am; the next level B contains n factors $B1$, $B2$, and Bn and the single-level ranking of factor A_i; the weights are $b1$, $b2$, $b3$, and bn; and the total ranking weight of the B level can be filled as shown in Figure 1.

Consistency check sequence level total ranking: consistency check sequence level total ranking results also need to be checked. The process of consistency checking progresses gradually from the lowest level to the highest level [19]. If the consistency index of the B-level elements for A_i single sorting is C_{lj} and the average random consistency index is R_{lj}, then the B-level total sorting random consistency ratio is

$$\mathrm{CR} = \frac{\sum_{i=1}^{m} a_i \mathrm{CI}_i}{\sum_{i=1}^{m} a_i \mathrm{RI}_i}. \tag{4}$$

If CR < 0.1, the total ranking result is satisfactory, indicating that the total ranking result of layer B meets the consistency requirements [20]. The relative importance weight of this layer is the total ranking weight result of this layer and the relative weight of the research object [21].

Figure 2 is a flowchart of the fuzzy clustering algorithm, which reflects the calculation process of the entire algorithm. The biggest task in AHP is to calculate the maximum eigenvalue and eigenvector of the judgment matrix.

$$w_i \frac{\bar{w}_i}{\sum_{i=1}^{n} \bar{w}_i} \bar{w}_i = \sqrt[n]{M_i}. \tag{5}$$

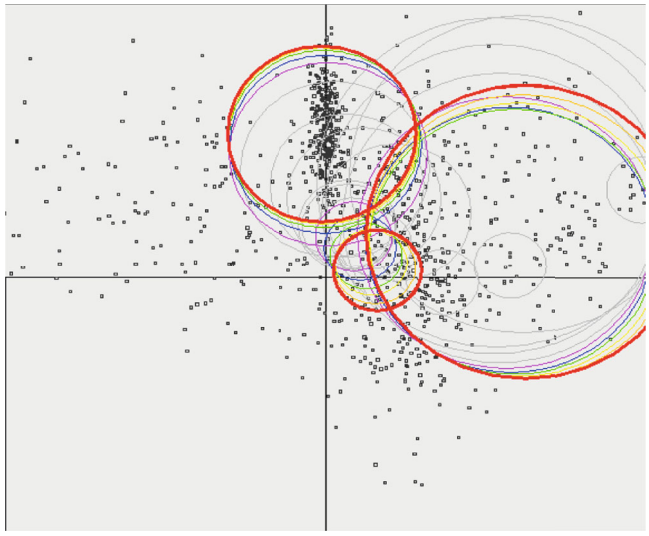

Figure 1: Fuzzy clustering algorithm.

The maximum characteristic value is

$$\lambda_{\max} = \sum_{i=1}^{n} \frac{(BW)_i}{nw_i}, \tag{6}$$

in which, λ is the i-th component of the product of the judgment matrix B and the eigenvector W.

Establish a regression equation [22]:

$$X_t = \sum_{i=1}^{k} \alpha_i X_{t-i} + \sum_{i=1}^{k} \beta_i Y_{t-i} + u_{1t}. \tag{7}$$

If the null hypothesis does not constitute a causal relationship, then the null hypothesis holds:

$$F = \frac{(\mathrm{SSE}_r - \mathrm{SSE}_u)/k}{\mathrm{SSE}_u/(T-2k)} \sim F_{(k,T-2k)}. \tag{8}$$

2.3. Interframe Difference Method. The pixel distribution of the segmentation image foreground cannot be determined directly and the foreground region cannot be extracted, so the gravy level measurement of the image is needed. The gravy level difference of different frame image pixels in the background is not different, but the gravy level difference of different frame image pixel points in the foreground must be larger than that of the background.

According to this personality quality, the gravy value can be regarded as an important attribute when selecting fuzzy attribute. On the other hand, the single fuzzy attribute has little gain on the segmentation effect and can proceed from the normal distribution of the background. The image segmentation process between the motion pose region and the useless pixel region is treated as a process of describing the nonnormal distribution pixels in the normal distribution pixels. In reference, a fourth-order matrix is used to extract the non-normal distributed pixels, and the time-domain difference image is considered as a pixel point, and a moving hollow rectangle is used to measure the time-domain matrix of the image.

There are many kinds of membership function of the fuzzy clustering algorithm, in which the "s function" can consider the big difference of fuzzy attributes between the foreground and background in sports video image and can provide two kinds of membership degree, which is very small and convenient for partition. Therefore, the s function is used in foreground image segmentation. The background image has a large noise and normal distribution, so it is necessary to select the membership function which can provide the time-domain variance.

3. Research Approach

In this paper, a complete and consistent moving video object is segmented from a video sequence towel. In this paper, a segmentation algorithm based on fuzzy clustering is used to obtain the pixels constituting the image boundary, and then, the object is extracted. The algorithm first uses the image information of the current frame and some previous frames to calculate its motion features in different subbands in the wavelet domain and constructs the motion feature vector set of the low-resolution image based on these motion features.

Then, the motion feature vector set of the low-resolution image is constructed. The mean value clustering algorithm separates the pixels, whose rifle has changed significantly in order to replace the frame difference image, and uses the traditional change detection method to obtain the object change detection model and then extracts the object. The average absolute difference between successive frames is used to determine the number of frames needed to calculate the motion characteristics of the current frame to ensure the accuracy of extracting video objects. Experimental results show that the proposed method is effective for the segmentation of video objects with various image sequences.

Object-based video segmentation plays an important role in the field of digital video processing and computer vision. The task of video object segmentation has been integrated into many applications, such as object-based video coding (mpeg.4111) and content-based video indexing and restoration (mpeg.7121). Therefore, the segmentation of video sequences into video objects has become a very important problem in digital video processing.

4. Detection of the Motion Change Region with Multiple Constraints

At present, there is a variety of moving object segmentation algorithms, and the change detection based on interframe difference is a popular segmentation method. Because of its simple implementation, this method is widely used in the development of a fully automatic video processing system based on an object.

4.1. System Theory Model. However, the method based on interframe difference change detection also has some shortcomings. These shortcomings include the error area caused by noise and the uncovered area caused by object motion. In order to solve this problem, we propose a new robust

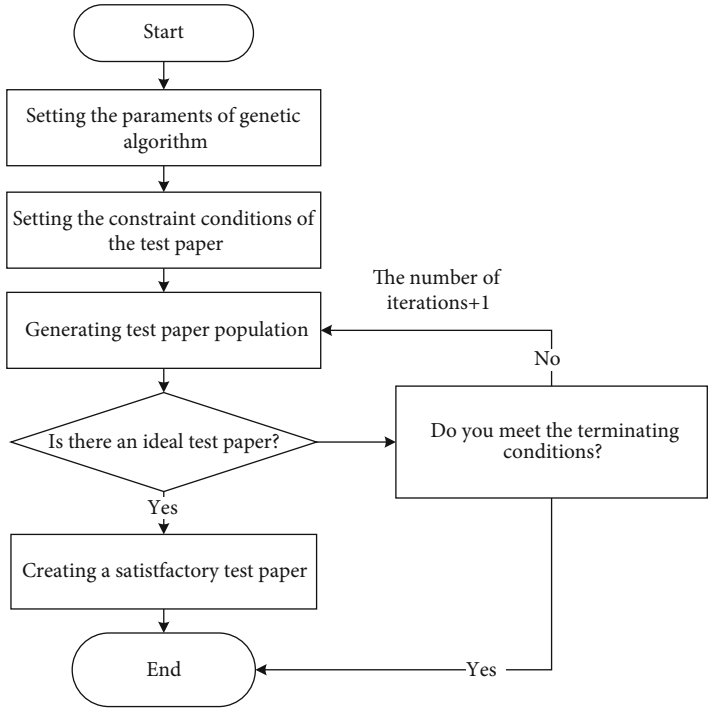

Figure 2: Flowchart of the fuzzy clustering algorithm.

semantic segmentation algorithm based on a frame difference image boundary graph. However, the algorithm will still be affected by background noise.

In addition, because the criterion of these methods is frame difference, the frame difference depends on the moving speed of the object. If the moving speed of the object changes greatly in the sequence, the segmentation quality is difficult to be consistent.

Therefore, interframe difference change detection is introduced into the wavelet domain to process, thus increasing the number of pixels constituting the boundary of the object. Although these methods improve the segmentation quality to some extent, the difference of segmentation quality caused by moving speed still exists. At the same time, in the segmentation process, the rifle needs to test the significance of each subband image in each frame to determine the domain value of the separation noise, thus increasing the computational complexity. Different video sequences, as well as different frames in the same sequence, have different noise levels, so it is difficult to determine the exact domain value, which leads to the inaccuracy of segmentation. Error analysis of sports video images is shown in Figure 3.

As shown in Figure 3, our proposed clustering algorithm has a good simulation effect. According to the speed of the object, the information of different frames is used to determine the motion information of the image in the wavelet domain rifle, which constitutes the motion characteristics of each frame of the image, and the pixels of the moving image are changed by separating the image.

4.2. Differential Image Block. Finally, changing pixels are used instead of interframe difference, and the accurate video moving object is segmented by the traditional method of frame difference change detection combined with the spatial boundary information of the image. The principle of moving object segmentation based on fuzzy clustering is like that of the traditional interframe difference detection method. The difference is that the traditional wavelet domain change detection method is not directly used to detect the difference between frames. It is based on the change of the image in the wavelet domain to obtain its motion characteristics.

For this purpose, an operational feature vector set is constructed by using the mean square error of each subband in the wavelet domain between the current frame and some previous frames, and the object is segmented by the fuzzy clustering method. The algorithm of the article is based on this situation for the case where the background is moving, and many researchers have proposed the use of global motion estimation and compensation to deal with the background changes caused by camera motion. Therefore, the input sequence is assumed to be a compensated sequence, and its background region is stationary. The algorithm is divided into four main parts: wavelet transform and feature calculation, fuzzy clustering and change detection, detection of moving object boundary, and object extraction.

4.3. Relative Noise Characteristic Parameter Estimation. The motion change of the towel video object will be reflected on all its wavelet subbands. The motion characteristics of each pixel in the low-resolution image may be a 4-dimensional vector for each pixel in the low-resolution image.

Because the image of the frame is used in motion feature calculation, its purpose is to obtain more information of object motion change, but when the number of frames is larger, it will produce a large uncovered area, so the number of frames must be controlled. When the object's motion

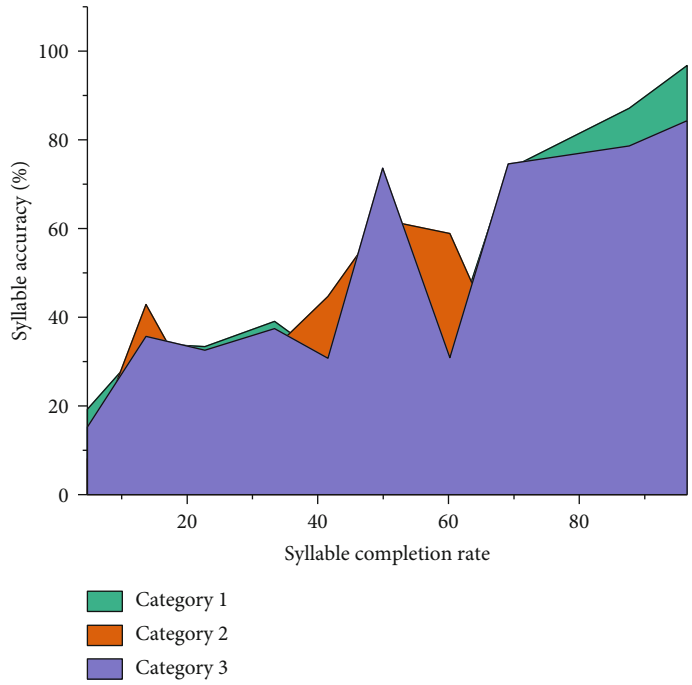

Figure 3: Error analysis of sports video images.

changes greatly, there is enough change information to extract the object, so the number of frames needed should be less; on the contrary, when the object's motion changes slowly, there are fewer pixels to change, in order to obtain enough pixels to form the boundary of the object. More frame information is needed to ensure the accuracy of object segmentation. The value of the object is determined by the change of the object motion, which can be evaluated by the mean absolute difference between successive frames.

In this paper, an algorithm of motion edge segmentation based on fuzzy clustering is proposed. By analyzing the motion characteristics of each subband image in the wavelet domain, the algorithm obtains the feature vector set of its operation and uses fuzzy c. The mean clustering algorithm is used to obtain the pixels in the low-resolution image. Finally, the boundary of the moving object is obtained by using the traditional change detection method instead of the difference between frames, and then, the object is extracted. The experimental results show that the proposed method can obtain more accurate shape information of video objects and extract moving objects of different video sequences accurately. Video object generation has important applications in many aspects. It is not only the basis of content-based video coding but also an important link in the video image tracking and recognition system. Because the video object (moving object) exists in the moving change region, one of the important methods of video object generation is to detect the motion change region first and then combine other features to generate the video object in the motion change region.

5. Experiment

The accurate detection of the motion change region is the key of this kind of method, so the research of motion change region detection is of great significance. Analysis of sports video images in different environments is shown in Figure 4.

As shown in Figure 4, our two proposed detection methods of the motion change area have a good prediction effect. The first method is based on noise feature parameter estimation and energy analysis. This method uses a block-based frame difference processing method, and uses the dual constraints of Gaussian distribution and relative noise characteristics of energy attributes to detect motion change areas. Compared with the traditional pixel-based interframe difference method, the computation is less. The threshold of relative noise estimated according to the characteristic parameters of relative noise is generated by self-adaptation in the process of detection. At the same time, the accuracy is improved by the correction of energy analysis. Performance analysis of the fuzzy clustering algorithm in different environments is shown in Figure 5.

As shown in Figure 5, our proposed method is more superior in performance; firstly, this paper discusses the general theory of time-difference video segmentation. Based on the video segmentation model established by Keri, a method of automatic detection of the video motion change region is proposed from the point of view of fuzzy entropy clustering. Based on the established fuzzy classification criterion, the motion change region and the relative noise-sound region are divided in the differential image, and the motion change region is obtained. The visual analysis of human motion mainly deals with the sequence of human motion images. It usually involves the detection of the region of motion change, the movement tracking resistance of the human body, and the understanding and description of the target behaviour in the monitoring scene. Among them, behaviour understanding and description belong to advanced processing, which has been paid more and more attention in

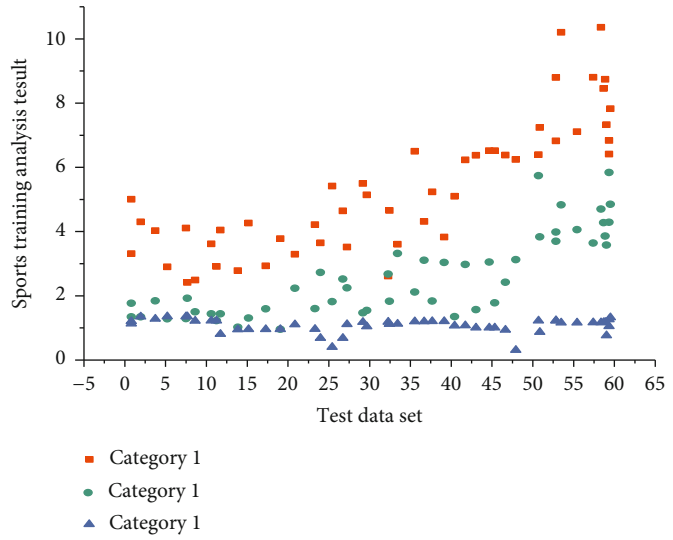

Figure 4: Analysis of sports video images in different environments.

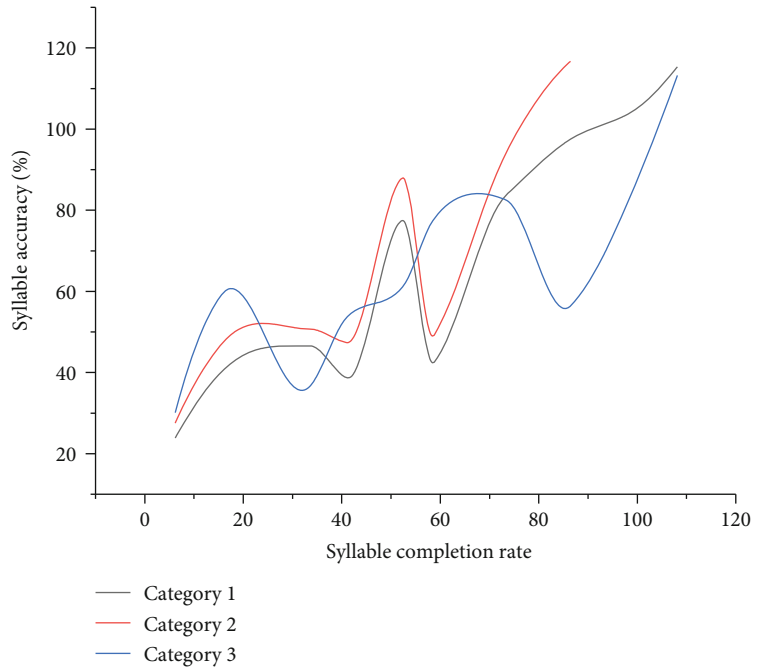

Figure 5: Performance analysis of the fuzzy clustering algorithm in different environments.

recent years. Performance analysis of sports video images under different standards is shown in Figure 6.

As shown in Figure 6, the simulation results of the fuzzy clustering algorithm proposed in this paper are more evenly distributed and have higher accuracy. It refers to the analysis and recognition of moving patterns of targets and the description of them by natural language. In the area of motion change detection, human motion tracking belongs to the low-level processing part of vision, which is the basis of various subsequent advanced processing such as behavioural understanding, and is also the two more studied problems in visual monitoring. Of course, there may also be intersections between them (for example, sometimes motion detection is used during tracking). Background subtraction is one of the most used methods in motion detection at present. It is a technique to detect the motion region by using the difference between the current image and the background image.

It is generally able to provide the most complete feature data, but it is particularly sensitive to changes in dynamic scenes, such as illumination and the interference of unrelated events. The simplest background model is the time-averaged image. Most researchers are currently working on developing different background models in order to reduce the impact of dynamic scene changes on operational segmentation. Fast and accurate motion segmentation is an important but difficult problem. This is because the images captured in

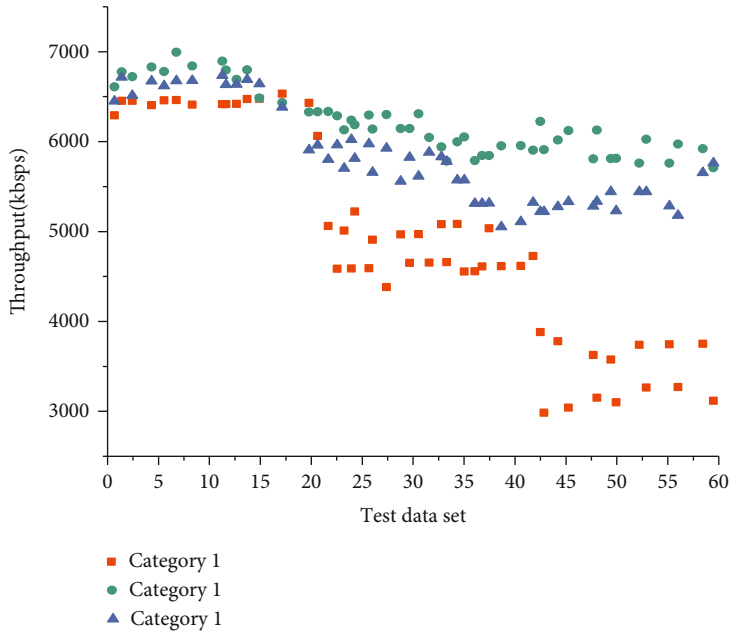

Figure 6: Performance analysis of sports video images under different standards.

the dynamic environment are affected by a variety of factors, such as changes in the weather, changes in the illumination conditions, confusion in the background, and the shadow of the moving target.

The occlusion between the object and environment and between the object and object and even the motion of the camera bring difficulties to accurate and effective motion segmentation. The shadow of a moving target, for example, may be linked to or separated from the target being detected. In the former case, the shadow distorts the shape of the target, which makes the recognition method based on the shape less reliable. In the latter case, the shadow may be mistaken as a completely wrong target in the scene. Although background subtraction is mainly used in image motion segmentation, it is still very difficult to establish a background model that is adaptive to the dynamic changes of any complex environment.

At present, most of the people's motion analysis system cannot solve the problem of close blocking and human self-occlusion. Especially in the state of congestion, the detection and tracking problem of multiple people is difficult to deal with. In occlusion, only part of the human body is visible, and this process is generally not training, and it is simply dependent on the background subtraction. The technique of motion segmentation will not be reliable at this time. In order to reduce the ambiguity problem caused by occlusion or depth, a better model must be developed to deal with the exact correspondence between the features of the occlusion and the body parts. Video object generation has important applications in many aspects. It is not only the base of content-based video coding but also an important link in the video image tracking and recognition system. Because the video object (moving object) exists in the moving change region, one of the important methods of video object generation is to detect the motion change region first and then combine other features to generate the video object in the motion change region. The accurate detection of the motion change region is the key of this method.

6. Conclusions and Future Work

With the rapid development of computer speed and capacity, the application of image technology and machine vision system has made remarkable achievements in recent years, such as content-based image retrieval system, intelligent monitoring system, vision-guided intelligent transportation system, handwritten characters from face grease lines, and iris recognition systems. Image segmentation is an indispensable link in image technology and machine vision and is also one of the bottlenecks in the development of image theory. The research on the image segmentation algorithm has a history of several decades. With the help of various theories, thousands of kinds of segmentation algorithms have been put forward up to now, and only a few years' statistics show that the research on image segmentation still accounts for a large proportion, which shows that image segmentation is still a hot and difficult point. As a key technology in video segmentation, motion change region detection has a direct impact on the accuracy and efficiency of video segmentation, so the research of motion change region detection is of great significance. I will continue to study this key technology with the help of my tutor and experimental group.

Data Availability

All data can be verified by contacting the author.

Conflicts of Interest

The author declares that there is no conflict of interest regarding the publication of this paper.

References

[1] B. Chen, X. Li, X. Xie, Z. Zhong, and P. Lu, "Fatigue Performance Assessment of Composite Arch Bridge Suspenders Based on Actual Vehicle Loads," *Shock and Vibration*, vol. 2015, no. 5, pp. 1–13, 2015.

[2] K. Beck, *Extreme Programming Fuzzy Clustering Algorithm*, Addison-Wesley, 1999.

[3] J. Burdman, *Collaborative Web Fuzzy Clustering Algorithm*, Addison-Wesley, 1999.

[4] S. Ceri, P. Fraternali, and A. Bongio, "Web Modeling Language (WebML): a modeling language for designing fuzzy clustering algorithm," in *Proceedings of WWW9 Conference*, pp. 156–159, Amsterdam, Netherlands, 2000.

[5] J. Conallen, *Building Web Applications with Fuzzy Clustering Algorithm*, Addison-Wesley, 1999.

[6] C. Zhao, H. Yang, X. Li, R. Li, and S. C. Zheng, "Analysis and application of martial arts video image based on fuzzy clustering algorithm," *Journal of Intelligent & Fuzzy Systems*, vol. 12, pp. 1–9, 2020.

[7] R. H. Wang, C. Chi, Q. Z. Chen, and X. X. Zhen, "Study on the Model of the Fatigue-loaded Vehicles in Guangzhou Trestle Bridges," *Journal of South China University of Technology*, vol. 32, no. 12, pp. 94–96, 2004.

[8] E. England and A. Finney, *Managing Multimedia: Fuzzy Clustering Algorithm for Interactive Media*, Addison-Wesley, 1999.

[9] R. Fournier, *Fuzzy Clustering Algorithm for Client/Server and Web Application Development*, Yourdon Press, 1999.

[10] B. Henderson-Sellers, B. Haire, and D. Lowe, "Adding web support to OPEN," *Journal of Fuzzy clustering algorithm*, vol. 14, no. 3, pp. 34–38.

[11] J. Lord, "Patterns for e-business: lessons learned from building fuzzy clustering algorithm," *IBM*, vol. 4, 2000.

[12] D. Lowe, "Fuzzy clustering algorithm for defining acceptance criteria for web development projects," in *Web Engineering: Managing Diversity and Complexity of Web Application Development*, S. Murugesan and Y. Deshpande, Eds., pp. 279–294, Springer-Verlag, 2001.

[13] G. Y. Su, "Preliminary Study of Tianjin Highway Bridge Fatigue Load Spectrum," *Tianjin Construction Science and Technology*, vol. 12, no. 3, pp. 56–76, 2010.

[14] D. Lowe and V. Elliott, "Fuzzy clustering algorithm: an overview," *Requirements Engineering Journal*, vol. 10, no. 12, pp. 214–219, 2016.

[15] D. Lowe and B. Henderson-Sellers, "Impacts on the development process of differences between web systems and conventional fuzzy clustering algorithm," in *SSGRR 2001: International Conference on Advances in Infrastructure for Electronic Business, Science, and Education on the Internet*, p. 21, L'Aquila, Italy, 2001.

[16] D. Lowe and B. Henderson-Sellers, "Fuzzy clustering algorithm: addressing process differences," *Cutter IT Journal*, vol. 9, no. 14, pp. 56–60, 2018.

[17] H. Liang, J. Zou, K. Zuo, and M. J. Khan, "An improved genetic algorithm optimization fuzzy controller applied to the wellhead back pressure control system," *Mechanical Systems and Signal Processing*, vol. 142, article 106708, 2020.

[18] H. Zheng, W. Guo, and N. Xiong, "A kernel-based compressive sensing approach for mobile data gathering in wireless sensor network systems," *IEEE Transactions on Systems, Man, and Cybernetics: Systems*, vol. 48, no. 12, pp. 2315–2327, 2018.

[19] H. Liang, D. Zou, Z. Li, K. Muhammad Junaid, and Y. Lu, "Dynamic evaluation of drilling leakage risk based on fuzzy theory and PSO-SVR algorithm," *Future Generation Computer Systems*, vol. 95, pp. 454–466, 2019.

[20] Y. Zhang, R. Zhu, Z. Chen, J. Gao, and D. Xia, "Evaluating and selecting features via information theoretic lower bounds of feature inner correlations for high-dimensional data," *European Journal of Operational Research*, vol. 290, no. 1, pp. 235–247, 2021.

[21] H. Liang, A. Xian, M. Mao, P. Ni, and H. Wu, "A research on remote fracturing monitoring and decision-making method supporting smart city," *Sustainable Cities and Society*, vol. 62, article 102414, 2020.

[22] Y. Zhou, D. Zhang, and N. Xiong, "Post-cloud computing paradigms: a survey and comparison," *Tsinghua Science and Technology*, vol. 22, no. 6, pp. 714–732, 2017.

Hindawi
Wireless Communications and Mobile Computing
Volume 2021, Article ID 6676428, 11 pages
https://doi.org/10.1155/2021/6676428

Research Article

Flexible Investment Strategies for Cloud-Native Architecture of Public Health Information Systems

Ming Jiang,[1] **Ichiro Nakamoto**,[1] **Weiqing Zhuang**,[1] **Weiguo Zhang**,[1] **Yin Guo**,[1] **and Liting Ma**[2]

[1]*School of Internet Economics and Business, Fujian University of Technology, Fuzhou 350000, China*
[2]*Fujian Jiangxia University, Fuzhou 350108, China*

Correspondence should be addressed to Ming Jiang; 19842158@fjut.edu.cn

Received 10 October 2020; Revised 12 November 2020; Accepted 16 December 2020; Published 19 January 2021

Academic Editor: Hongju Cheng

Copyright © 2021 Ming Jiang et al. This is an open access article distributed under the Creative Commons Attribution License, which permits unrestricted use, distribution, and reproduction in any medium, provided the original work is properly cited.

The randomness of public health events requires that the cloud-native architecture, as the mainstream architecture of the new generation of the public health information system, has the appropriate flexibility to meet the needs of environmental change. The flexible acquisition of cloud-native architecture requires organizations to invest additional resources. How to plan and formulate resource input is a topic of common concern for public health management and information systems. According to the commercial characteristics of the public health system based on cloud-native architecture, this paper systematically analyzes the external major impact factors and auxiliary factors that affect the flexible cost investment strategy of cloud providers and combines flexible investment strategies to build a cloud-native cost investment model. Finally, case data in practice is applied into the model, and cost planning is discussed according to different situations. The findings indicate that (1) the more cloud providers adopt the changed flexible strategy, the more conducive it is to reduce costs; (2) the larger the application load, the more cloud providers need to use flexible strategies to lower costs; (3) the less the impact of changing the flexible strategy on costs, the more conducive cloud providers use the flexible strategy to decrease costs; (4) the more uneven the distribution of diversity, the higher proportion of investment increases than the proportion of investment, and the more cloud providers consider the investment using flexible strategy. The results of the discussion provide a reference for public health organizations to use flexible strategies and change flexible strategies in a timely manner and expand the research scope of information system cost investment.

1. Introduction

In the prevention and treatment of COVID-19 in 2020, the public health information system plays an important role [1]. The temporary influx of many businesses has brought huge challenges to the architectural flexibility of public health information systems with cloud-native architecture as the mainstream. How to invest in architectural flexibility is an urgent problem in the field of information systems and information management research [2]. For this reason, many scholars have conducted a lot of research on the flexible cost investment of information system architecture, but their research results are mainly concentrated on the public health system of the traditional SOA architecture [3]. There is little research on the public health system with cloud-native architecture as the mainstream. It does not consider the penalty cost of breach of contract with different percentages of normal service time. This article fully considers the nonsystem and unstructured flexible cost input process of public health information system cloud providers with cloud-native architecture as the mainstream and sets the penalty costs caused by default of different normal service time percentages in the decision-making model [4]. In this case, the cloud provider architecture flexible cost investment provides a reference strategy. The main contributions of this article are mainly focused on the first time that the default factors of

different normal service time percentages are considered in the flexible cost of the cloud provider's architecture, and the actual public health system cloud provider case data is used to verify these two aspects. It is supplemented by research related to the field of information management [5].

2. Flexible Cost Input Model of Cloud-Native Architecture

The flexible cost of cloud-native architecture is the cost that cloud providers invest in the flexible development of cloud-native architecture, making the architecture flexible to cope with internal and external changes and ensuring the effective operation of the system [6]. The flexible cost investment strategy of cloud-native architecture is a way for cloud providers to control development costs and maximize their benefits and is affected by external factors and auxiliary factors [7].

2.1. External Impacting Factors. The commercial service mode of public health information systems based on cloud-native architecture can be regarded as a new type of multitenant information technology outsourcing [8], and cloud providers deliver cloud services to consumers. The investment strategy of cloud providers on the flexibility of cloud-native architecture is affected by the needs of cloud consumers, or the needs of cloud consumers to process their own business are the external influencing factors of cloud providers' flexible cost strategy. Cloud consumers' own business needs mainly include three aspects: business process [9], application load [3], and normal service percentage, of which business process also includes two aspects: process uncertainty and diversity. The external influencing factors affecting the flexible strategy of cloud providers are described in detail as follows [10].

2.1.1. Process Uncertainty. As a new type of information system architecture, cloud-native architecture is mainly used for the processing of the business process of multiple tenants (cloud consumers). There is uncertainty in the business process executed between a single and multiple cloud consumers, which can be described as the difficulty to predict the tasks and resources required for the business process in a specific single instance. The uncertainty of the business process can be either external or structural [11]. External environment uncertainty refers to the uncertainty of exogenous input variables. For example, the business process required for the service confirmed by SLA (Service Level Agreement) is heterogeneous for different cloud consumers, and the business process required for a single cloud consumer to perform a task is not the same too. Structural uncertainty refers to the gap between the predetermined tasks and resources demanded by the cloud provider to perform the business process in a specific instance and the actual needs to perform for the services agreed by SLA, such as the execution order of the prediction preparation before the service container may be different from that required by the cloud consumer, and the more management business processes required by the cloud consumer, the greater the structural uncertainty [12]. Therefore, the external uncertainty caused by the resources required by the service business process requested by cloud consumers, the uncertainty between the preset resources and the actual needs of internal prediction, and judgment will affect the flexible strategy formulation of cloud providers, and the uncertainty of the process will affect the flexible cost strategy of cloud providers [13].

2.1.2. Process Diversity. Different cloud consumers or individual cloud consumers need differential tasks to perform a certain business process. The probability of tasks being performed is different, and there is diversity in the process. When the tasks required by cloud consumption to execute a certain business process are similar, there are only a small number of different types of tasks in the whole business process execution process, which is manifested as low process diversity [14]. However, when the types of tasks requested by cloud consumers to perform similar business processes are very different or the business processes performed by a single cloud consumer require a variety types of task execution and each task is executed at almost the same frequency, it is manifested as high process diversity. Cloud providers need to develop different strategies and resources to ensure the quality of services agreed by SLA according to the diversity of business processes required by cloud consumers at various levels; therefore, process diversity directly affects the formulation of flexible cost strategies for cloud providers [15].

2.1.3. Applied Load. Cloud-native architecture is an architecture that supports multiple tenants. The application load of cloud services required to support cloud-native architecture is different at each time point, and the application load brought about by each cloud consumer at different time points is also different [16]. Applied loads can be divided into fixed applied loads, cycle applied loads, lifetime applied loads, and unintended applied loads. The characteristics of fixed application load are that in a certain range, its demand for resources is basically the same over time. This type of application load usually does not need to add or remove resources to cope with changes, only needs to initially configure the necessary resources and provide a certain excess allocation rate, and can be automatically processed through the adaptive characteristics of cloud-native architecture [17]. The characteristics of periodic application load are that some cloud consumers are engaged in the main business with a large number of periodic business processes that need to be completed in the same time interval; the peak and usual application load gap is very large and periodic. The lifetime application load is a special case of periodic application load, which is characterized by that it can only appear once in a period, usually accompanied by the occurrence of an event or task, and will be predicted. However, the application load brings great harm to the cloud-native architecture due to the long-term low and sudden application summit of a cloud provider's resource preparation. Unexpected application load is the generalization of periodic application load, for example, when new products of cloud consumers receive unexpected attention, it often brings about a sudden increase in application load, which cannot predict the peak and duration of resource use in advance. To cope with different

application loads, cloud providers need to be equipped with different resources to cope with the changes brought about, that is, application loads can directly affect the development of flexible cost strategies for cloud providers.

2.1.4. Percentage of Normal Service Time. Cloud-native architecture takes cloud service as the delivery mode and faces multiple tenants. Different cloud consumers have different requirements for effective service time of cloud-native architecture due to their own business, and the limitation required for the completion of business process processing, which is usually expressed in the form of a percentage of normal service time. On the one hand, cloud providers need to prepare different resources according to the actual percentage of different normal services of cloud consumers to adapt to the changes; on the other hand, when the percentage of normal service time agreed by each cloud consumer cannot be guaranteed, cloud providers need to pay corresponding fees to cloud consumption for the failed service commitment. The percentage of normal service time directly affects the resources that cloud providers need to prepare, that is, the percentage of normal service time directly affects the formulation of flexible cost strategies for cloud providers.

In summary, process uncertainty, process diversity, application load, and percentage of normal service time as external influencing factors directly affect the input decision of cloud providers on the flexible cost of cloud-native architecture. Only by fully considering these influencing factors, cloud providers are conducive to meeting the needs of cloud consumers, making reasonable flexible cost investment decisions, and effectively planning the flexible cost investment of cloud-native architecture to produce benefits.

2.2. Auxiliary Factors. In addition to the influence of external factors on the flexible strategy of cloud providers, the flexible cost input cycle and flexible cost input stage are affected by other factors, which are collectively referred to as auxiliary factors. The investment of the flexible cost of cloud-native architecture involves the whole service life cycle. The length of the predetermined life cycle of cloud-native architecture directly determines the time length of investment of cloud provider in flexible cost of cloud-native architecture and affects the investment strategy of cloud provider in flexible cost of cloud-native architecture. At the same time, cloud providers adopt the way of continuous delivery and continuous deployment for the flexible development and maintenance of cloud-native architecture. There are stages for the investment of the flexible cost of cloud-native architecture, and there are problems of time discount rate for the cost of investment at different times, which directly affects the total investment cost of cloud providers, thus directly affecting the investment strategy of cloud providers for the flexible flexibility of cloud-native architecture.

2.3. Flexible Strategy. Architecture is the soul of cloud-native application system. The investment cost strategy of cloud providers on the flexibility of cloud-native architecture, that is, the implementation strategy of cloud provider strategy level, directly determines the cost investment of cloud providers on the flexibility of cloud-native architecture in the future. Due to its importance, different scholars focus on it, for example, some scholars put forward top-down planning mode emphasizing policy consistency and bottom-up planning mode emphasizing compliance with actual operation from the perspective of enterprise strategy formulation mode; some scholars believe that enterprises should plan flexible cost investment strategy according to the way of coping with internal and external environmental changes, such as static flexible strategy using established scheme to cope with changes and dynamic flexible strategy changing according to actual change needs during operation. To better analyze the flexible cost investment of cloud-native architecture, the following describes the flexible strategy of cloud providers based on the flexible cost strategy proposed by Gebauer and Schober [2] in combination with the commercial characteristics of cloud-native architecture.

2.3.1. Use of Flexible Strategy. Based on research by Gebauer and Schober. the use of flexibility is here defined as making it possible for cloud-native applications to change within the expected range according to internal and external changes during operation through the expected design and implementation of the flexibility of the cloud-native architecture without violating the requirements of SLA. The following five factors are mainly considered for the flexible design of cloud-native architecture when cloud providers develop the use of flexible strategy:

(1) Service capacity refers to the service subdomain that constitutes the cloud provider as agreed by SLA and needs to provide cloud consumer services. Cloud-native architecture is a domain-driven design architecture that focuses on the division of some services, for example, a basic e-commerce system can be divided into commodity subdomain, membership subdomain, payment subdomain, order subdomain, and logistics subdomain. The service needs to be divided according to the predetermined capacity

(2) The scope of the underlying database refers to the analysis capacity and the number of reports that can be provided by the data warehouse. According to the prediction processing capacity, select the appropriate deployment mode and set the corresponding data processing capacity, realize distributed processing, and meet the requirements of normal service time percentage agreed by SLA

(3) The user interface refers to the different characteristics and methods that the cloud-native architecture can provide for the user to interact with the system, for example, the HTML5 and CSS are used to realize the support for multiple browsers

(4) Processing capacity refers to the number of users that the cloud-native architecture can accommodate at the same time as well as the number of transactions and user requests processed

(5) Adaptive capacity refers to the scenario where the cloud-native architecture can automatically allocate the application load within the scope of the SLA agreement and link each subservice domain. Therefore, in the design, the application presentation layer provides the user-defined interface and defines the input and output modes through visual means as far as possible; the service layer is loosely coupled, forms the software architecture with container technology as the core based on micro-service, provides the workflow definition, realizes the flexible transaction model, and supports the intelligence of the application software; the active database is mainly used in the data processing layer; the system software layer should remove the dependence on the hardware through the virtual and can obtain the hardware resources as needed

2.3.2. Change in Flexible Strategy. According to Gebauer and Schober, the difference between using flexibility and changing flexibility is that using flexibility strategies is that the system can be modified, adjusted, and reinstalled through predesigned service capabilities, databases, user interfaces, and processing capabilities, and adaptive flexibility before significant problems occur without causing system usability problems or only causing minor problems to the system. Changing flexibility is conceptually related to changes in system architecture, as long as it is measured by the amount of effort required to change a given system after initial implementation. It generally includes the modularity of the system, such as the splitting of original services, data integration, and related human resource cost investment. Sien and Zhenyu refer to changing flexible strategy as a dynamic flexible strategy, which mainly refers to the dynamic evolution and dynamic refinement of software architecture. In this paper, the change of flexible strategy mainly refers to the continuous delivery and continuous deployment of cloud-native architecture by cloud providers within the requirements of SLA after the cloud-native architecture is online, such as the continuous change of service module and the continuous deployment of service container.

2.3.3. Manual Flexibility Strategy. Cloud Provider requires service SLA agreement for the whole service process of cloud consumers. In case of failure to use flexible strategy and change flexible strategy to provide services satisfying SLA requirements within the scope of SLA agreement, cloud provider will adopt an emergency response plan, which requires additional fees. Generally, while manually responding to internal and external changes and restoring services, due to illegal SLA agreements, compensation needs to be paid to cloud consumption. So when cloud providers adopt manual flexible strategies, the flexible costs incurred by them include the additional cost of manual repair of recovery services and the compensation cost to cloud consumers.

3. Outline Model of Flexible Cost Investment of Cloud-Native Architecture

In summary, external influencing factors and auxiliary factors will affect the flexible investment strategy of cloud-native architecture of cloud providers, and the investment strategy of cloud providers to the flexible investment strategy of cloud-native architecture determines the investment of cloud providers in the flexible cost of cloud-native architecture, which determines the total cost invested by cloud providers in the whole life cycle of cloud-native architecture. Based on the aforementioned points, a summary model of flexible cost investment in cloud-native architecture is proposed in Figure 1.

4. Computational Model for Flexible Cost Input of Cloud-Native Architecture

According to Gebauer and Schober's research method on the flexible cost generation mechanism of information systems, the actual decision-making process of cloud providers is obtained, as shown in Figure 2 below. By integrating the external influencing factors, auxiliary factors, flexible strategy, and flexible cost of cloud-native architecture in the outline model, the computational model is obtained according to the decision process in Figure 2 to better describe and discuss the proposed outline model. Generally, the investment of cloud providers in cloud-native architecture is divided into two stages: design and operation, and cloud providers will have different investment strategies for different stages. In the design stage, first of all, the cloud provider will start this item according to its own strategic decision. If this project is initiated, in addition to the most basic predetermined functions realized by the input cost, the cloud provider decides to adopt the appropriate flexible strategy according to the possible external environment and its own development needs after go-live, mainly including the adaptation of flexible strategy and the change of flexible strategy. In the operation phase, different results will be produced according to the previous flexible strategy and input proportion.

TCOST represents the total cost for the cloud provider to meet SLA requirements throughout the cloud-native architecture lifecycle. It incorporates the cost for a cloud provider to adopt the flexible strategy, the cost for a cloud provider to adopt a changed flexible strategy, the cost for the cloud provider to maintain the system at the operation stage of the system, the cost for the cloud provider to upgrade the system within the operation stage plan, the manual repair cost for the cloud provider to maintain stable manual emergency repair within the time limit during the operation stage, the compensation cost for cloud consumer due to inability to fulfill the commitment within the time limit during the operation stage, and the total cost for the cloud provider to fulfill SLA commitment and make the system return to normal service state.

In summary, the total cost that cloud providers need to pay throughout the lifecycle of the cloud-native architecture

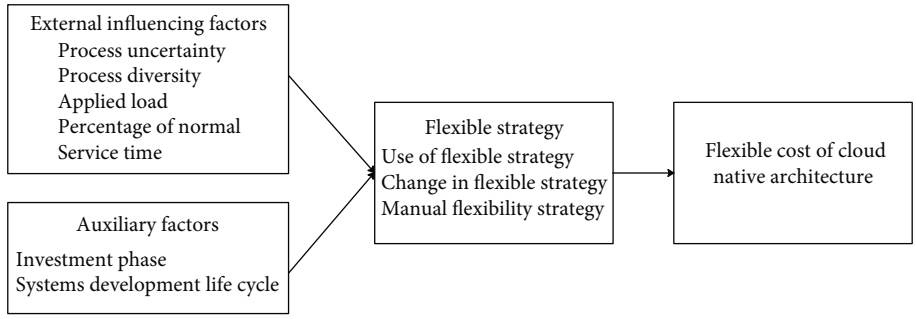

Figure 1: Overview model of the flexible cost of cloud-native architecture.

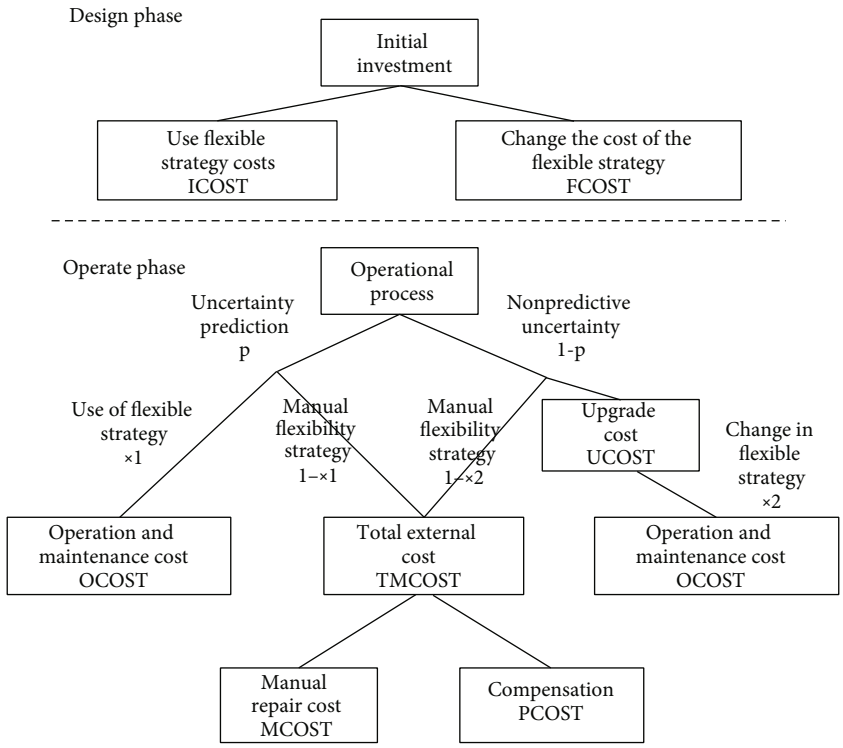

Figure 2: Decision process for flexible cost of cloud-native architecture.

is calculated as follows:

$$\mathrm{TCOST} = \mathrm{ICOST} + \mathrm{FCOST} + \mathrm{UCOST} + \mathrm{OCOST} + \mathrm{MCOST} + \mathrm{PCOST}. \tag{1}$$

Since

$$\mathrm{TMCOST} = \mathrm{MCOST} + \mathrm{PCOST}, \tag{2}$$

the above calculation formula can be simplified:

$$\mathrm{TCOST} = \mathrm{ICOST} + \mathrm{FCOST} + \mathrm{UCOST} + \mathrm{OCOST} + \mathrm{TMCOST}, \tag{3}$$

and each calculation item in the calculation formula is described in detail below.

(1) The cost when cloud providers adopt the use of flexible strategies during the design stage is governed by the following:

$$\mathrm{ICOST} = \{a + bL(x_1)[q + (1 - q)\mathrm{DC}]\}z \tag{4}$$

a: the fixed cost required to realize the basic functional requirements of cloud consumers for cloud providers, such as the base class library, authentication, and information management and storage

b : adopt flexible strategies for cloud providers to cope with the costs required for changes, such as using HTML5 to transform the front-end, to realize that there is no need to make a lot of modifications to the architecture when it runs within a predetermined range

q : proportion of cloud-native architecture development that has been completed so far for cloud providers;

$L(x_1) = x_1^{v}[1 - (1 - x_1^{v})^{1-v}]$: describe the cumulative percentage of tasks that are defined by the cloud provider when the diversity is and the actual execution proportion of the use strategy adopted by the cloud provider is, where the function is proposed by Gebauer and Schober [2], and the curve is time-convex, per the requirements of the Lorenz coefficient curve, and is used to describe the Lorenz curve. It indicates the corresponding relationship between the cumulative percentage of defined tasks and the cumulative percentage of actual tasks performed, and the parameter v($0 \le v \le 1$) indicates the degree of curvature of the curve. The greater the concentration of variable distribution, the larger the difference is.

i: represents the annual average interest rate

T: represents the planned life cycle of the cloud-native architecture

$DC = ((1+i)^{T} - 1)/(i(1+i)^{T}T)$: it is proposed by Gebauer and Schober [2] to represent the average discount rate of equivalent cash flow in the lifecycle of a cloud-native architecture

z: is a binary number to ensure that Equation (4) is meaningful and that the following conditions are met:

$$\begin{cases} z \in [0, 1]; \\ x_1 + x_2 > 0, \text{if } z = 1, \text{else } z = 0 \\ z \ge 0.5(x_1 + x_2) \end{cases} \tag{5}$$

(2) The cost when cloud providers adopt the change flexible strategy during the design stage is as follows:

$$FCOST = cy \tag{6}$$

c: it is the cost required for cloud providers to adopt a flexible strategy to change

y: It is a binary number to ensure the validity of the calculation formula (6), which satisfies the following conditions:

$$\begin{cases} y \in [0, 1] \\ \text{During the design phase, the cloud provider chooses to change the flex policy when } y = 1 \text{ and } y \ge x_2. \end{cases} \tag{7}$$

In the runtime phase, the cost to the cloud provider to upgrade the portion of the cloud provider in the cloud-native architecture design phase with a changed flexible strategy is determined by the following:

$$UCOST = eL(x_2)DC \tag{8}$$

e: the cost of upgrading the part of the cloud provider that uses the changed flexible strategy at the design stage

$L(x_2) = x_2^{v}[1 - (1 - x_2^{v})^{1-v}]$: represents the cumulative percentage of tasks completed as defined by the cloud provider when the actual proportion of tasks is implemented

$DC = ((1+i)^{T} - 1)/(i(1+i)^{T}T)$: as in Equation (4), it represents the average discount rate of equivalent cash flow in the life cycle of cloud-native architecture

i: resolves the plan life cycle representing the annual average interest rate and cloud-native architecture as in Equation (4)

(3) The cost of operating maintenance by the cloud provider for the cloud-native architecture design stage using the flexible strategy part and the part upgraded using the changed flexible strategy is given by the following:

$$OCOST = Sd\left[\left(q + (1-q)L^{-1}(0.6)\right)w_1 + 0.4w_2\right]TDC \tag{9}$$

d: it is the cost of the cloud provider to use the flexible strategy part and the part upgraded by the changed flexible strategy for operation and maintenance in the cloud-native architecture design stage

S: it is the amount of stretching of the applied load in the running phase

T: as described in Equation (4), represents the planned life cycle of the cloud-native architecture and the average discount rate of equivalent cash flow in the life cycle of the cloud-native architecture, respectively

q: proportion of cloud-native architecture development that has been completed so far for cloud providers

Since Mutschler (2006) proposed that 60% of tasks with alterations during software running can be done using flexible strategies, 40% of tasks are done by changing flexible strategies [5]. So 0.6 and 0.4 are directly substituted into Equation (9). It represents the percentage of tasks actually performed when the cloud provider defines that the accumulative ratio of completion was 0.6.

$w_1 = px_1$: it indicates the proportion of cloud providers using flexibility to process the changes required in the operation stage, where it indicates the uncertainty of the task and indicates the proportion of cloud providers using the use strategy to invest in the operation stage

It indicates the proportion of cloud providers that need to change the operation stage by changing the flexibility, in which it indicates the uncertainty of the task and indicates the proportion of cloud providers that use the change strategy to invest in the operation stage.

(4) In the operation stage, the cost that cloud providers cannot cope with changes requiring manual repair using both flexible strategies and changing flexible strategies is as follows:

$$\mathrm{MCOST} = SfT\mathrm{DC}\left[(1-q)\left(1-L^{-1}(0.6)\right)w_1 + 0.4w_2 + w_3\right]. \tag{10}$$

S, q, w_1, w_2, T and DC are outlined in Equation (9), which, respectively, represent the amount of extension and contraction of the application load, the proportion of cloud-native architecture development, the proportion of changes required in the operation stage using flexible processing, the proportion of changes required in the operation stage using flexible processing, the planned life cycle of cloud-native architecture, and the average discount rate of equivalent cash flow in the life cycle of cloud-native architecture.

$w_3 = 1 - w_1 - w_2$: represents the proportion of cloud providers that handle changes using a flexible strategy and a method other than changing flexible strategy handling

f: represents the cost to be paid by the cloud provider for manual repair

(5) In the operation stage, the cost that cloud providers should compensate cloud consumers for the changes due to their inability to agree on access within SLA is as follows:

$$\mathrm{PCOST} = SrgT\mathrm{DC}\left[(1-q)\left(1-L^{-1}(0.6)\right)w_1 + 0.4w_2 + w_3\right]. \tag{11}$$

S,q, w_1, w_2, w_3, T and DC as in Equation (10), which represent, respectively, the amount of expansion of the application load, the proportion of cloud-native architecture development, the proportion of changes required to the operating stage using flexible processing, the proportion of changes required to the operating stage using flexible processing, the proportion of changes handled using methods other than flexible strategy and flexible strategy processing, the planned life cycle of the cloud-native architecture, and the average discount rate of equivalent cash flow in the life cycle of the cloud-native architecture.

g: indicates that the cloud provider shall compensate the cloud consumer for the cost incurred due to violation of SLA

r: represents the percentage of normal service time, such as the SLA agreed by Amazon and Microsoft, which is 10% of the total price exemption if the percentage of normal service time is lower than 99.9% and higher than 99%, and 30% of the total price exemption when the percentage of normal service time is lower than 99%. The probability of default with 99% normal service time percentage of committed cloud consumers is low, and the probability of default with 99.9% normal service time percentage of committed cloud consumers is high.

(6) In the operation stage, the total cost required for the cloud provider to fulfill the SLA commitment and make the system return to normal service status is as follows:

$$\mathrm{TMCOST} = S(f+rg)T\mathrm{DC}\left[(1-q)\left(1-L^{-1}(0.6)\right)w_1 + 0.4w_2 + w_3\right]. \tag{12}$$

S, q, w_1, w_2, w_3, T, and DC as in Equation (10), represent, respectively, the amount of expansion of the application load, the proportion of cloud-native architecture development, the proportion of changes required to the operating stage using flexible processing, the proportion of changes required to the operating stage using flexible processing, the proportion of changes handled using methods other than flexible strategy and flexible strategy processing, the planned life cycle of the cloud-native architecture, and the average discount rate of equivalent cash flow in the life cycle of the cloud-native architecture. g and r in Equation (11) represent the transformed values of the cost paid by compensation cloud consumers and the percentage of normal service time, respectively.

In summary, the total cost will vary according to the cloud provider pair, and different investment proportions, and the size of the decision, and as the primary decision variable for the decision at a fixed time. The above relevant formulas are summarized as follows:

$$\mathrm{TCOST} = \mathrm{ICOST} + \mathrm{FCOST} + \mathrm{UCOST} + \mathrm{OCOST} + \mathrm{TMCOST}, \tag{13}$$

$$\begin{cases} \mathrm{TMCOST} = \mathrm{MCOST} + \mathrm{PCOST} \\ \mathrm{ICOST} = \{a + bL(x_1)[q + (1-q)\mathrm{DC}]\}\mathrm{z} \\ \mathrm{FCOST} = cy \\ \mathrm{UCOST} = eL(x_2)\mathrm{DC} \\ \mathrm{OCOST} = Sd\left[\left(q + (1-q)L^{-1}(0.6)\right)w_1 + 0.4w_2\right]T\mathrm{DC} \\ \mathrm{MCOST} = SfT\mathrm{DC}\left[(1-q)\left(1-L^{-1}(0.6)\right)w_1 + 0.4w_2 + w_3\right] \\ \mathrm{PCOST} = SrgT\mathrm{DC}\left[(1-q)\left(1-L^{-1}(0.6)\right)w_1 + 0.4w_2 + w_3\right], \end{cases} \tag{14}$$

$$s.t \begin{cases} y \geq x_2 \\ z \geq 0.5(x_1 + x_2) \\ x_1 + x_2 > 0, z = 1 \text{ else } z = 0 \\ y, z \in [0,1] \\ 0 \leq x_1, x_2 \leq 1. \end{cases} \tag{15}$$

5. Analysis of Planning Strategies

To analyze the input planning strategy for the flexible cost of cloud-native architecture of cloud providers in various situations, here, the real cloud-native architecture project case data are applied to the flexible costing model of cloud-native architecture proposed above. Focusing on the goal of minimizing cloud provider cost, the influence of various

external influencing factors on the flexible cost of cloud-native architecture is discussed, to obtain the flexible input optimization strategy set of public health information system based on cloud-native architecture.

5.1. Data Source. The data is from the Public Health Information System of a technology company in Xiamen. The system aims to improve health manager demand diversification, drug store management, and information control. Millions of community in China face data analysis, data storage, and many other problems and development. The purpose is to build a collaborative digital supply chain platform to fulfill the connection between traditional community and CDC. The system uses HTML5 and other technologies to implement the front-end display by supporting multiple browsers. For the request of the Web, Nginx is used to process a large number of concurrent requests at the same time by utilizing both multiprocess and asynchronous mechanism. In the background, zuul gateway is used to perform the dynamic loading, compilation, and operation of filters and realize the dynamic connection. The domain-driven design is adopted, and the system is divided into authority certification microservice, basic microservice, configuration center microservice, gateway microservice, account microservice, channel microservice, merchant microservice, payment microservice, functional microservice, questionnaire microservice, and information push microservice, MQ microservice, and timing microservice, to achieve the functional cohesion modularity, the direct connection between service and service through service governance, and the compatibility of interface and deployment environment by using container technology. Finally, the system adopts a Zipkin distributed tracking system to track, identify, and feedback the line state of the operating system in.

5.2. Data Collection. The whole project adopts the mode of phased investment. The project start-up time is 2017, the system design and development interval is 1 year in the first stage, and the subsequent delivery and deployment of the system are carried out in the second stage. It has been conducted for 2 years, the project budget cycle is 5 years, and the system architecture is expected to be redesigned and developed within this time period. Therefore, the auxiliary factor system stage, life cycle, and annual discount rate are using bank current interest rate.

Based on the experience of the initial 2 years, the enterprise architect believes that the tasks of using flexible strategies in the operation process of the project are similar to those of using changing flexible strategies and roughly estimates the uncertainty. Because the use of cloud-native architecture in clear accounts is a multitenant system, the tasks of each cloud consumer and a single cloud consumer vary greatly and roughly estimate the diversity; clear accounts need to be used by cloud consumers all over the country, with a relatively high application load and roughly estimated. The conversion value of the percentage of normal service time refers to the reference value proposed by Amazon and Microsoft in their proposed SLA when the percentage of normal service time is 99.9%; the percentage of normal service time is 99%.

The enterprise architect uses the COCOMO II model proposed by Clark et al. [6] to estimate the number of person-day invested in various work. The specific cost estimate is based on the person-day estimate multiplied by the average salary per person-day. Here is a cost estimation based on the data of the 2019 catch-up network, with an average salary of 300 yuan per person-day.

It is roughly estimated that in the design stage, the basic investment using flexible strategy is adopted for the cloud-native architecture, such as the construction of basic background and the realization of basic functions, with the input cost of 10,000 yuan; in the design stage, the flexible strategy is adopted for the cloud-native architecture, such as DB subdatabase table and DB replication model, with the input cost of 10,000 yuan; in the design stage, the flexible strategy with change is adopted for the cloud-native architecture, such as the construction of continuous integrated release environment, with the input cost of 10,000 yuan; in the operation stage, the flexible strategy with change is adopted to upgrade the cloud-native architecture to cope with the changes, such as issuing a new version of characteristic service, with the input cost of 10,000 yuan; in the operation stage, the flexible strategy with the use and change should be adopted to cope with the operation and maintenance cost of 10,000 yuan for all changes; in the operation stage, the investment cost of manual repair should be 10,000 yuan; in the operation stage, the SLA needs cannot be met, and the total compensation cost is equal to the cost of realizing basic functions.

5.3. Results and Discussion of the Calculation Model. To clarify the influence of each external influencing factor and flexible strategy on the flexible cost of cloud-native architecture, MATLAB2017b is used below to calculate the minimum cost of cloud providers in different cases, and the flexible cost investment of cloud-native architecture is discussed by comparison.

5.3.1. Percentage of Different Normal Service Time. To clarify the impact of different percentages of normal service time on the flexible cost of cloud-native architecture, here, the minimum value in Equation (3) is solved in four cases according to different flexible strategies of cloud providers. These four cases are the minimum value when the dynamic flexibility strategy is not used, the minimum value when the dynamic flexibility strategy is used, the minimum value when the dynamic flexibility strategy is used, the minimum value when the dynamic flexibility strategy is not used, and the minimum value when the dynamic flexibility strategy is used. The results are shown in Table 1.

According to the above calculation results, the following conclusions can be obtained.

(1) When the flexible strategy is changed, the minimum value 302.4 is less than the case when not changed, of which the minimum value is 346.9. Comparatively, when the flexible strategy is changed, the minimum value 317.6 is less than the case when not changed,

Table 1: Solving units for different percentages of normal service time. Unit: ten thousand yuan.

$a = 30$, $b = 150$, $c = 5$, $d = 10$, $e = 80$, $f = 56$, $g = 30$			
$p = 0.5$, $v = 0.6$, $S = 1.4$			
Use flexible strategy w_1	Change flex strategy w_2	External flex strategy w_3	TCOST
$r = 0.1$			
36.5%	0	63.5%	346.9
36.5%	41.6%	21.9%	302.4
$r = 0.3$			
38.6%	0	61.4%	371.8
38.6%	43%	18.4%	317.6

of which the minimum value is 371.8. The results show that investment in changing flexible strategies is beneficial for cloud providers to reduce investment costs regardless of the percentage of normal service time determined by SLA

(2) In the scenario where the flexible strategy was changed with the minimum of 302.4, the cloud provider input cost was reduced by 44.5. In contrast, when the flexible strategy was changed with the minimum 317.6, the cloud provider input cost was reduced by 54.2. The results show that the percentage of normal service time required by cloud consumers is high, and the more cloud providers adopt the changed flexible strategy, the more conducive it is to reduce costs

5.3.2. Different Application Loads. To clarify the effect of different application loads on the flexibility cost of cloud-native architecture, the minimum value in Equation (3) is solved here for four cases: application load at a time with or without dynamic flexibility strategy. The results are shown in Table 2.

According to the above calculation results, the following conclusions can be obtained.

(1) When no flexible strategy change was used, the minimum value was 267.4, which is in contrast to the minimum value of 346.9 when used. The proportion of investment using flexible strategies increased from 29.4% to 36.5%, and it can be seen that the larger the application load, the more cloud providers need to use flexible strategies to reduce costs

(2) When the flexible strategy was changed, the minimum value was 245, and this is in comparison with the minimum value of 302.4 when no flexible change occurred. As the application load increased from 1 to 1.4, the proportion of investment using flexible strategies increased from 29.4% to 36.5%, indicating a growth of 7.1%; in the case of changing flexible strategies, it increased from 36.1% to 41.6%, implying a growth of 5.5%. It can be seen that the proportion of investment using flexible strategy increases faster than the case using changing flexible strategy, and cloud providers can consider the investment using flexible strategy more

5.3.3. Different Uncertainties. To clarify the effect of different application loads on the flexibility cost of cloud-native architecture, the minimum value in Equation (3) is solved here for the four cases of uncertainty in time with or without dynamic flexibility strategy, respectively. The results are shown in Table 3.

According to the above calculation results, the following conclusions can be obtained.

(1) When the flexible strategy was not changed, the minimum value was 267.4, which was larger than the minimum value of 240.4 when the flexible strategy was changed. The proportion of investment using flexible strategy increased from 29.4% to 51.5%, from which it can be predicted that the more uncertainty, the more cloud providers need to use flexible strategy to reduce costs

(2) When the flexible strategy was changed, the minimum value was 235.7; in contrast, when the flexible strategy was not changed, the minimum value was 245. When the uncertainty was increased from 0.5 to 0.7, the proportion of investment using flexible strategies increased from 29.4% to 51.1%, suggesting a growth of 21.7%, and the proportion of investment changing flexible strategies decreased from 35.1% to 34.8%, indicating a reduction of 1.3%. It can be seen that the less the impact of changing the flexible strategy on costs, the more conducive cloud providers use the flexible strategy to reduce costs

5.3.4. Different Diversity. To clarify the effect of different application loads on the flexibility cost of cloud-native architecture, the minimum value in Equation (3) is solved here for the four cases of uncertainty in time with or without dynamic flexibility strategy, respectively. The results are shown in Table 4.

According to the above calculation results, the following conclusions can be obtained.

(1) No flexible strategy change was accompanied by a minimum value of 267.4; comparatively, flexible strategy change was followed by a minimum value of 281.6. When diversity was increased from 0.4 to 0.6, the proportion of investment using flexible

Table 2: Solving units for different application loads. Unit: ten thousand yuan.

$a = 30, b = 150, c = 5, d = 10, e = 80, f = 56, g = 30$			
$p = 0.5, v = 0.6, r = 0.1$			
Use flexible strategy w_1	Change flex strategy w_2	External flex strategy w_3	TCOST
$S = 1.4$			
36.5%	0	63.5%	346.9
36.5%	41.6%	21.9%	302.4
$S = 1$			
29.4%	0	70.6%	267.4
29.4%	36.1%	34.5%	245

Table 3: Solving unit of different uncertainties. Unit: ten thousand yuan.

$a = 30, b = 150, c = 5, d = 10, e = 80, f = 56, g = 30$			
$S = 1, v = 0.6, r = 0.1$			
Use flexible strategy w_1	Change flex strategy w_2	External flex strategy w_3	TCOST
$p = 0.5$			
29.4%	0	70.6%	267.4
29.4%	36.1%	34.5%	245
$p = 0.7$			
51.1%	0	48.9%	240.4
51.1%	34.8%	14.1%	235.7

Table 4: Solving units for different diversities. Unit: ten thousand yuan.

$a = 30, b = 150, c = 5, d = 10, e = 80, f = 56, g = 30$			
$S = 1, p = 0.5, r = 0.1$			
Use a flexible strategy w_1	Change flex strategy w_2	External flex strategy w_3	TCOST
$v = 0.6$			
29.4%	0	70.6%	267.4
29.4%	36.1%	34.5%	245
$v = 0.4$			
21.1%	0	78.9%	281.6
21.1%	31.6%	47.3%	268.9

strategies increased from 21.1% to 29.4%. It can be seen that the more uneven the distribution of diversity, the more flexible the cloud provider needs to use to reduce costs

(2) In the case when the flexible strategy was changed, a minimum value of 245 would occur. However, when a flexible strategy was changed, a minimum value of 268.9 would follow. When diversity was increased from 0.4 to 0.6, the proportion of investment using flexible strategies increased from 21.1% to 29.4%, indicating a growth of 8.3%, and the proportion of investment changing flexible strategies increased from 32.6% to 36.1%, implying a growth of 3.5%. It can be seen that the more uneven the distribution of diversity, the higher the proportion of investment increases than the proportion of investment, and the more cloud providers can consider the investment using the flexible strategy

6. Summary and Prospect

Our major findings provide multiple insights: (1) the more cloud providers adopt the changed flexible strategy, the more conducive it is to reduce costs [7]; (2) the larger the application load, the more cloud providers need to use flexible strategies to lower costs [8]; (3) the less the impact of changing the flexible strategy on costs, the more conducive cloud providers use the flexible strategy to decrease costs; (4) the more uneven the distribution of diversity, the higher proportion of investment increases than the proportion of investment, and the more cloud providers consider the investment using flexible strategy. According to the commercial characteristics

of cloud-native architecture with cloud service as the delivery model, this paper incorporates the percentage of normal service time into the external impacting factors of the flexible cost investment strategy of public health organizations and fully considers the compensation cost caused when SLA cannot be satisfied in the proposed computational model. Data in practice is used to discuss the different cost investment strategies of cloud providers when each external influencing factor changes. The results provide a reference for public health information system cloud providers to develop reasonable flexible cost investment strategy optimization sets under different environments and needs and expand the research category in information system cost.

In this paper, the commercial characteristics of cloud-native architecture are fully considered, but the conversion value of normal service time percentage only hinged on Amazon and Microsoft's SLA. Hence, the lack of versatility is a deficiency of this study. And how to establish the corresponding relationship between normal service time percentage and conversion value in the system is another problem that needs further study in the future.

Data Availability

The data used to support the findings of this study are available from the corresponding author upon request.

Conflicts of Interest

We declare that there is no conflict of interest regarding the publication of this paper.

Acknowledgments

This article was supported by the Fujian Provincial Social Science Planning Project in 2020: Research on Capacity Building of Regional Medical Collaborative Innovation Community under the Background of "Internet + Medical" (No. FJ2020B038).

References

[1] C. Weinhardt, A. Anandasivam, B. Blau et al., "Cloud computing – a classification, business models, and research directions," *Business & Information Systems Engineering*, vol. 1, no. 5, pp. 391–399, 2009.

[2] X. Liu, D. He, L. Yang, and C. Liu, "A novel negative feedback information dissemination model based on online social network," *Physica A: Statistical Mechanics and its Applications*, vol. 513, pp. 371–389, 2019.

[3] C. Sien and L. Zhenyu, "Research on flexible cost generation mechanism of software architecture based on business process perception," *Modern Management Science*, vol. 12, no. 5, pp. 93–96, 2013.

[4] V. Chang, "The business intelligence as a service in the cloud," *Future Generation Computer Systems*, vol. 37, no. C, pp. 512–534, 2014.

[5] B. Mutschler, J. Bumiller, and M. Reichert, "Why process-orientation is scarce: an empirical study of process-oriented information systems in the automotive industry," in *2006 10th IEEE International Enterprise Distributed Object Computing Conference (EDOC'06)*, pp. 433–440, Hong Kong, China, October 2006.

[6] B. Clark, S. Devnanichulani, and B. Boehm, "Calibrating the COCOMO II post-architecture model," in *Proceedings of the 20th International Conference on Software Engineering*, pp. 477–480, Kyoto, Japan, 1998.

[7] Z. Guo, J. Li, and R. Ramesh, "Optimal management of virtual infrastructures under flexible cloud service agreements," *Information Systems Research*, vol. 30, no. 4, pp. 1424–1446, 2019.

[8] O. Rejeb, C. Pilet, S. Hamana et al., "Performance and cost evaluation of health information systems using micro-costing and discrete-event simulation," *Health Care Management Science*, vol. 21, no. 2, pp. 204–223, 2018.

[9] W. N. Robinson and S. D. Pawlowski, "Managing requirements inconsistency with development goal monitors," *IEEE Transactions on Software Engineering*, vol. 25, no. 6, pp. 816–835, 1999.

[10] S. Mahesh, B. J. L. Landry, T. Sridhar, and K. R. Walsh, "A decision table for the cloud computing decision in small business," *Information Resources Management Journal*, vol. 24, no. 3, pp. 9–25, 2011.

[11] J. Gebauer, M. J. Shaw, and M. L. Gribbins, "Task-technology fit for mobile information systems," *Journal of Information Technology*, vol. 25, no. 3, pp. 259–272, 2010.

[12] J. Gebauer and F. Schober, "Information system flexibility and the cost efficiency of business processes," *Journal of the Association for Information Systems*, vol. 7, no. 3, pp. 122–147, 2006.

[13] M. Gelderman, "Task difficulty, task variability and satisfaction with management support systems," *Information & Management*, vol. 39, no. 7, pp. 593–604, 2002.

[14] D. Q. Chen, M. Mocker, D. S. Preston, and Teubner, "Information systems strategy: reconceptualization, measurement, and implications," *MIS Quarterly*, vol. 34, no. 2, pp. 233–259, 2010.

[15] J. Braa, O. Hanseth, A. Heywood, Mohammed, and Shaw, "Developing health information systems in developing countries: the flexible standards strategy," *MIS Quarterly*, vol. 31, no. 2, pp. 381–402, 2007.

[16] J. Gebauer and P. Karhade, "A framework to assess the impact of information systems on the flexibility and performance of business processes," in *ICIS 2002 PROCEEDINGS*, pp. 320–440, USA, 2004.

[17] J. S. Evans, "Strategic flexibility for high technology manoeuvres: a conceptual framework," *Journal of Management Studies*, vol. 28, no. 1, pp. 69–89, 1991.

Hindawi
Wireless Communications and Mobile Computing
Volume 2021, Article ID 6668612, 6 pages
https://doi.org/10.1155/2021/6668612

WILEY | Hindawi

Research Article

Design of Sanda Action Reconstruction Model Based on 3D Images

Hongwei Zhao

Department of Physical Education, Guilin University of Electronic Technology, Guilin 541004, China

Correspondence should be addressed to Hongwei Zhao; zhaohongwei@guet.edu.cn

Received 20 October 2020; Revised 13 December 2020; Accepted 4 January 2021; Published 19 January 2021

Academic Editor: Hongju Cheng

Copyright © 2021 Hongwei Zhao. This is an open access article distributed under the Creative Commons Attribution License, which permits unrestricted use, distribution, and reproduction in any medium, provided the original work is properly cited.

In order to improve the training level of Sanda movement, this article uses an image analysis method to reconstruct the detailed characteristics of the movement and apply them to the actual training process. Since the traditional wavelet reconstruction method is affected by the accuracy of the decomposition scale, this paper proposes an improved method of Sanda action based on 3D image reconstruction. First, the method relies on frame adjacent phase compensation and digital image stabilization techniques to perform digital frame operations on the image. Then, scanning and corner detection are used for image reconstruction, where adjacent phase compensation methods are used to match feature points and gray pixels. Image extraction is performed by extracting key feature points of the action 3D image, and a fast frame detection method is used to stabilize the image of the digital image, thereby improving the image quality of image reconstruction. The experimental results show that the method has good image output effect and has a high application value in Sanda guidance and optimization.

1. Introduction

Sanda is an important part of Chinese martial arts and is very different from daily sports [1]. The movement is characterized by various movements and different forms [2]. Participants beat and beat their opponents in accordance with certain rules [3]. On the basis of traditional Chinese martial arts, combining modern Western sports ideas, Sanda has gradually developed into modern martial arts [4]. Breakup is a competitive sport with strong confrontation. Therefore, in order to improve the level of scattering and obtain a pleasing effect, it is necessary to use the principles of computer and image processing technology to reconstruct the scattering behavior [5]. By combining the motion feature analysis method, the method of evaluating and exploring scattered movements reveals the principle of movements, thereby improving the standardization and rationality of movements [6].

With the prosperity of computer image processing, the definition of image quality and the ability of 3D presentation of Sanda action images are more demanding. The three-dimensional image reconstruction is a combination of three-dimensional virtual reality technology and visual simulation technology [7]. High-definition image synthesis is accomplished, which exerts great significance on studying the 3D image reconstruction technology in promoting the optimization and upgrading of Sanda action and enhancing the technical quality [8]. Three-dimensional image reconstruction is based on image processing algorithms such as image perception, image information fusion, and image denoising filtering [9], making use of digital image stabilization and 3D reconstruction technology so as to achieve image upgrades and improve the reconstruction quality [10]. In this paper, a three-dimensional image reconstruction technique in accordance with frame adjacent phase compensation and digital image stabilization is proposed [11]. Digital frame scanning and corner detection are manufactured. The adjacent phase compensation method is adopted to match feature points and segment gray pixels [12]. By means of extracting the key feature points, the fast frame detection method is wielded to stabilize the image of the digital image so that the image quality of image reconstruction is ameliorated [13]. Finally, the performance test is carried out through

the simulation experiment, which shows the superior performance of this method in improving the reconfiguration ability [14].

The specific contributions of this paper include the following:

(1) This article uses image analysis methods to reconstruct the detailed characteristics of the movement and apply them to the actual training process

(2) An improved Sanda action method based on 3D image reconstruction is proposed

(3) Image extraction was performed by extracting the key feature points of the action 3D image, and the fast frame detection method was used to stabilize the image of the digital image, thereby improving the image quality of image reconstruction

The rest of this paper is organized as follows. Section 2 discusses image collection and preprocessing of Sanda action, followed by realization of 3D image reconstruction as discussed in Section 3. Analysis of the simulation experiment is discussed in Section 4. Section 5 concludes the paper with a summary and future research directions.

2. Image Collection and Preprocessing of Sanda Action

2.1. Digital Frame Scanning and Corner Detection of Sanda Action. In order to reconstruct the three-dimensional image of Sanda action, it is initially necessary to scan the digital frame and detect the corner for the image picture, and the image scanning is performed by the frame detection method [15], combining feature sampling with laser scanning technology to achieve fast image processing. In the gravy region, the pixel size of the image is recorded as $M \times M$, and the image points are fused to each frame [16]. The image is processed by updating iterative $s(k) = [\theta(k), \Delta x(k), \Delta y(k)]$, and the pixel value of the 3D scanned image tends to be zero. The holographic information of the image is obtained by the variational principle. The normalized pixel values of image feature distribution in subpixel space are as below [17]:

$$P(i,j)\left(i \in \left[0, \text{int}\left(\frac{W}{2}\right) - 1\right], \quad j \in \left[0, \text{int}\left(\frac{H}{2}\right) - 1\right]\right). \tag{1}$$

Within the range of known integer parallax, the subpixel parallax of Sanda action 3D image is obtained by the local maximum search for image pixel segmentation, as follows:

$$\begin{aligned} E_{\text{image}}(Vi) = &-|I(x_i - 1, y_i + 1) + 2I(x_i, y_i + 1) \\ &+ I(x_i + 1, y_i + 1) - I(x_i - 1, y_i - 1) \\ &- 2I(x_i, y_i - 1) - I(x_i + 1, y_i - 1)| \\ &+ |I(x_i + 1, y_i - 1) + 2I(x_i + 1, y_i) \\ &+ I(x_i + 1, y_i - 1) - I(x_i - 1, y_i - 1) \\ &- 2I(x_i - 1, y_i) - I(x_i - 1, y_i + 1)|. \end{aligned} \tag{2}$$

Consequently, the digital frame scanning and corner detection of three-dimensional Sanda action images are completed, which provides an accurate information input basis for 3D reconstruction [18].

2.2. Frame Adjacent Phase Compensation. Using motion feature point matching and gray pixel segmentation technology, the neighboring phase compensation of the frame output feature points is performed to extract the key feature points in the Sanda 3D image [19]. The frame distribution function of the Sanda action picture in view of gray projection is expressed as follows:

$$\begin{cases} t = \mu \cos \alpha - v \sin \alpha, \\ \omega = \mu \sin \alpha + v \cos \alpha. \end{cases} \tag{3}$$

The frequency hopping feature points of the Sanda action screen are matched by image stabilization and grayscale pixel segmentation. The contour length of the resulting 3D image reconstruction is as follows [20]:

$$E = \theta E^{\text{LBF}} + (1 - \theta) E^{\text{LGF}} + vL(\phi) + \mu P(\phi). \tag{4}$$

The window is 3×3, and the gray value of the pixel at (i, j) is represented by $X_{i,j}$. The subpixel accuracy of adjacent phase compensation of the frame is calculated as follows [21]:

$$L(\phi) = \int_{\Omega} \delta(\phi) |\nabla \phi| dx. \tag{5}$$

Given that $P(\phi)$ is a sparse regularized item, the subpixel matching method is adopted so as to compensate the image stabilization error of small edge pixels, and the parallax function is obtained as follows:

$$P(\phi) = \int \frac{1}{2} (|\nabla \phi| - 1)^2 dx, \tag{6}$$

in which E^{LBF} is the parallax function and E^{LGF} is the local gradient energy term, aimed at the displacement invariance of image attribute features. The image is discretely processed to complete the feature point matching of the dynamic image of Sanda action. The grayscale pixel segmentation results of image reconstruction are obtained as

$$\begin{aligned} E^{\text{LBF}}(\phi, f_1, f_2) = &\lambda_1 \int \left[\int K_\sigma(x - y) |I - f_1(x)|^2 H(\phi) dy \right] dx \\ &+ \lambda_2 \int \left[\int K_\sigma(x - y) |I - f_2(x)|^2 (1 - H(\phi)) dy \right] dx, \end{aligned} \tag{7}$$

$$\begin{aligned} E^{\text{LGF}}\left(\phi, f_1^G, f_2^G\right) = &\lambda_1 \int \left[\int K_\sigma(x - y) \left| I^G - f_1^G(x) \right|^2 H(\phi) dy \right] dx \\ &+ \lambda_2 \int \left[\int K_\sigma(x - y) \left| I^G - f_2^G(x) \right|^2 (1 - H(\phi)) dy \right] dx, \end{aligned} \tag{8}$$

Figure 1: Original Sanda image acquisition result functions.

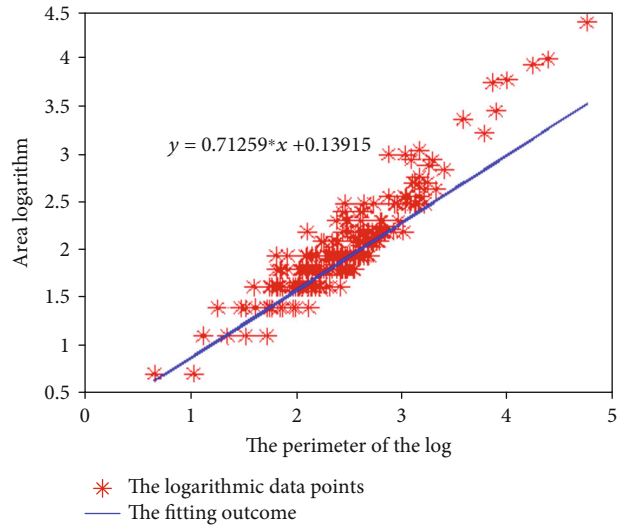

Figure 2: Original Sanda image fractal dimensions.

in which I^G is the gradient mode and f_1^G and f_2^G represent the stereo matching support and gray window of 3D Sanda motioned image reconstruction, respectively. The original image acquisition and fractal dimension distribution are shown in Figures 1 and 2.

3. Realization of 3D Image Reconstruction

3.1. Digital Image Stabilization Processing. In view of the above-mentioned collection and preprocessing of Sanda moving images, this article uses the three-dimensional reconstruction of Sanda moving images for processing. The adjacent phase compensation and digital imaging technology are proposed to extract the basic technical feature points of the three-dimensional image. The feature equation is described as below:

$$\frac{\partial \phi}{\partial t} = -\delta(\phi)\left[\theta\left(\lambda_1 e_1^{\mathrm{LBF}} - \lambda_2 e_2^{\mathrm{LBF}}\right) + (1-\theta)\left(\lambda_1 e_1^{\mathrm{LGF}} - \lambda_2 e_2^{\mathrm{LGF}}\right)\right] + \nu\delta(\phi)\ \mathrm{div}\left(\frac{\nabla\phi}{\nabla\phi}\right) + \mu\left(\nabla^2\phi - \mathrm{div}\left(\frac{\nabla\phi}{|\nabla\phi|}\right)\right), \tag{9}$$

in which e_1^{LBF}, e_2^{LBF}, e_1^{LGF}, and e_2^{LGF} are

$$\begin{cases} e_1^{\mathrm{LBF}} = \int_\Omega K_\sigma(y-x)|I(x) - f_1(y)|^2 dy, \\ e_2^{\mathrm{LBF}} = \int_\Omega K_\sigma(y-x)|I(x) - f_2(y)|^2 dy, \end{cases} \tag{10}$$

$$\begin{cases} e_1^{\mathrm{LGF}} = \int_\Omega K_\sigma(y-x)\left|I^G(x) - f_1^G(y)\right|^2 dy, \\ e_2^{\mathrm{LGF}} = \int_\Omega K_\sigma(y-x)\left|I^G(x) - f_2^G(y)\right|^2 dy, \end{cases} \tag{11}$$

in which $H(\phi)$ is a Heaviside function, which represents the derivative of the data item of the 3D image reconstruction in Sanda movement as well as the derivative of the slip term.

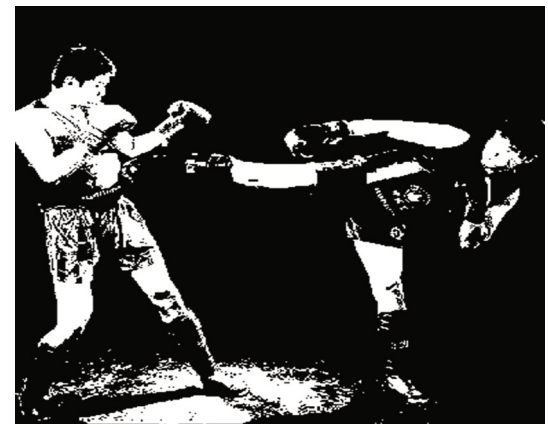

Figure 3: Reconstruction effect of Sanda movement and kinematic reconstruction.

$\delta(z) = -(d/dz)H(z)$ is the Dirac function, which is the dynamic point of the motion holographic imaging of the Sanda. The fast frame detection method is applied to carry out the digital image stabilization for the extracted feature points, and the pixels distributed in the image are regarded as templates. After the frame phase is compensated by the adjacent phase, the output picture and the parallax pixel after the image processing are obtained:

$$H_\varepsilon(z) = \frac{1}{2}\left[1 + \frac{2}{\pi}\arctan\left(\frac{Z}{\varepsilon}\right)\right], \tag{12}$$

$$\delta_\varepsilon(z) = \frac{1}{\pi}\cdot\frac{\varepsilon}{\varepsilon^2 + Z^2}, \quad z \in R. \tag{13}$$

On account of the robustness of the SIFT algorithm, the SIFT algorithm is used for digital image stabilization, which is effectively in a position to increase the quality of image reconstruction.

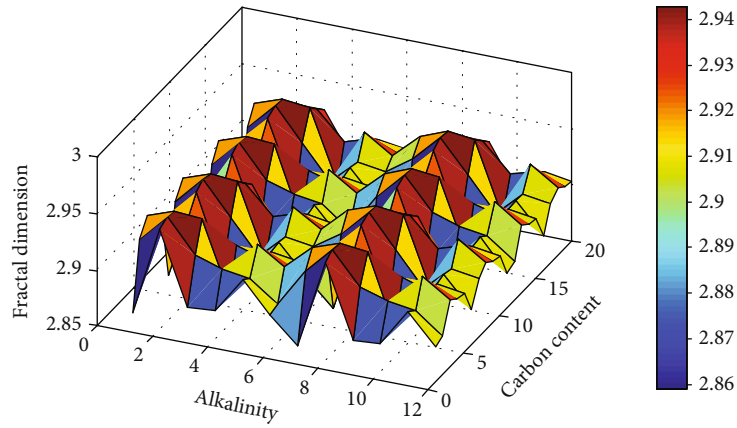

Figure 4: Reconstruction graph fractal exponential of Sanda.

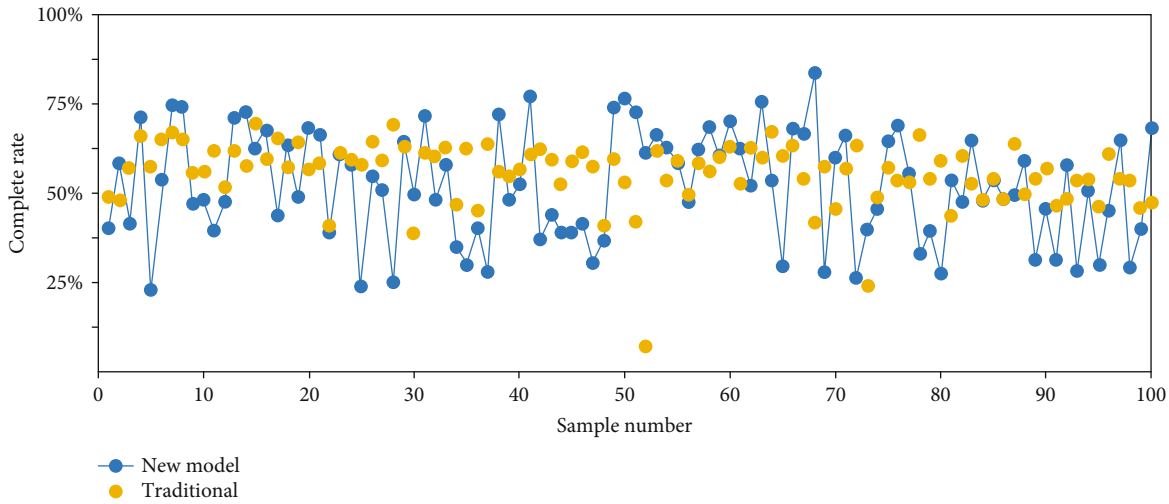

Figure 5: Comparable results of image reconstruction quality obtained by means of diverse methods.

3.1.1. 3D Image Reconstruction. According to image stabilization, the image-driven smoothing term is fixed, and the noise of the image boundary and parallax boundary is separated on the ray direction ϕ of image imaging, and the image-driven smoothing term is selected as the direct volume. The 3D reconstruction output of the image is realized; the output image expression is expressed as follows:

$$\begin{cases} f_1(x) = \dfrac{K_\sigma(x) * [H_\varepsilon(\phi(x))I(x)]}{K_\sigma(x) * H_\varepsilon(\phi(x))}, \\ f_1(x) = \dfrac{K_\sigma(x) * [(1 - H_\varepsilon(\phi(x)))I(x)]}{K_\sigma(x) * (1 - H_\varepsilon(\phi(x)))}, \end{cases} \tag{14}$$

$$\begin{cases} f_1^G = \dfrac{K_\sigma(x) * [H_\varepsilon(\phi(x))I^G(x)]}{K_\sigma(x) * H_\varepsilon(\phi(x))}, \\ f_2^G = \dfrac{K_\sigma(x) * [(1 - H_\varepsilon(\phi(x)))I^G(x)]}{K_\sigma(x) * (1 - H_\varepsilon(\phi(x)))}. \end{cases} \tag{15}$$

A binary gradient function $C = \{(x, y) \in \Omega : \phi(x, y) = 0\}$ makes use of representing the gradient information of the image, and $N(i)$ is used to represent the immediately adjacent region of the pixel point i of the Sanda action 3D image. The subpixel stereo output of the 3D image reconstruction is obtained as follows:

$$\lim_{P \to +\infty} K_B^P(f)(x, y) = \max_{(s,t) \in B(x,y)} f(s, t) = \delta_B(f)(x, y), \tag{16}$$

$$\lim_{P \to -\infty} K_B^P(f)(x, y) = \min_{(s,t) \in B(x,y)} f(s, t) = \varepsilon_B(f)(x, y), \tag{17}$$

in which δ and ε represent the texture features and edge pixels of the image, respectively, and the parallax field of the image boundary is $B(x, y)$. Therefore, the two-dimensional feature information of the image is represented as follows:

$$P\left(y_{w_3} | x_{w_3}, \theta, \beta\right) = \frac{1}{Z(\beta_i)} P\left(y_{w_3} | x_{w_3}, \theta\right)\left(y_{w_3} | \beta_1\right), \tag{18}$$

in which $Z(\beta_1) = \sum_{y_{w_3}} P(y_{w_3} | x_{w_3}, \theta)(y_{w_3} | \beta_i)$ is the image boundary overlapping the region. This paper adopts the image reconstruction method to obtain the Sanda motion

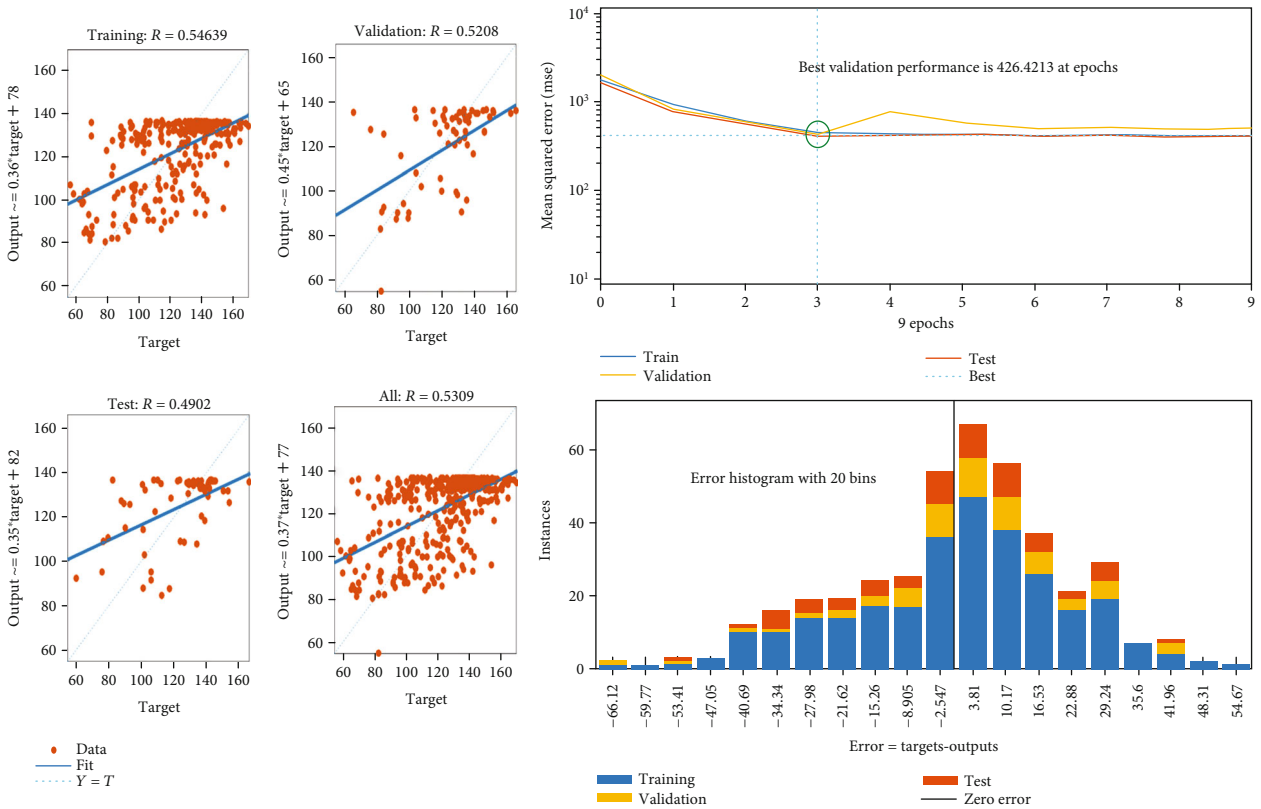

Figure 6: Compare training graphs with different methods.

reconstruction model based on the 3D image as shown in Figures 3 and 4. It is clearly evident from Figures 3 and 4 that the feature extraction ability is conspicuous. The stronger the reconstruction ability of Sanda, the better the reconstruction effect.

4. Analysis of Simulation Experiment

The simulation experiment analysis of Sanda action 3D image reconstruction is carried out in the MATLAB simulation environment. The method of fixed-point frame scanning is used to collect the original image. The frequency of scanning is $f = 12\,\text{kHz}$, $T_m = 14$, the size of the scanning image is 2000×2000 pixels, and the image acquisition is carried out. The Gaussian noise of image quality is zero, and the variance is 0.24. Besides the above simulation parameters, the 3D reconstruction quality is carried out. In order to compare the performance, three distinct methods are adopted for dimension reconstruction. The quality of the reconstruction of various methods is tested by distinct methods, and the comparison results are shown in Figure 5.

The network training results during the comparison of unequal methods are shown in Figure 6.

Figure 6 shows that the error of Sanda reconstruction using this method is lower than that of traditional methods. In contrast with conventional methods, the error is reduced by 12.5%, and the SNR of the reconstructed output is increased by 23.4 dB.

5. Conclusions

Aiming at improving the visual effect of Sanda 3D image reconstruction, a three-dimensional image reconstruction technique for Sanda action based on frame adjacent phase compensation and digital image stabilization is proposed. Digital frame scanning and corner detection are carried out to images. The adjacent phase compensation method is used to match feature points and segment gray pixels. By means of extracting the key feature points, the fast frame detection method is wielded to stabilize the image of the digital image so that the image quality of image reconstruction is ameliorated. The experimental results imply that this method is equipped with excellent image output effect as well as superior application value on guidance and optimization.

Data Availability

The data used to support the findings of this study are included in the article.

Conflicts of Interest

The author declares that they have no conflicts of interest.

Acknowledgments

This work was supported by the National Social Science Foundation of China (No.15XMZ063) and the Guangxi

Higher Education Undergraduate Teaching Reform Project (No.2019JGA174).

References

[1] B. B. Amor, J. Su, and A. Srivastava, "Action recognition using rate-invariant analysis, of skeletal shape trajectories," *IEEE Transactions on Pattern Analysis & Machine Intelligence*, vol. 11, no. 1, pp. 1–13, 2016.

[2] Y. Weiwu, *A Framework and Modeling Method of Data-Driven Soft Sensors Based on Semisupervised Gaussian Regression*, Industrial & Engineering Chemistry Research, 2016.

[3] M. I. Jie, Z. Peng, and Y. U. Haipeng, "Large data clustering algorithm based on particle swarm differential perturbation optimization[J]," *Journal of Henan University of Engineering (Natural Science Edition)*, vol. 28, no. 1, pp. 63–68, 2016.

[4] A. Aravind and M. Beena, "Electrochemical sensor based on nanostructured ion imprinted polymer for the sensing and extraction of Cr(III) ions from industrial wastewater," *Polymer International*, vol. 67, no. 12, pp. 1595–1604, 2018.

[5] D. Y. Jia and F. Z. Zhang, "A collaborative filtering recommendation algorithm based on double neighbor choosing strategy[J]," *Journal of Computer Research and Development*, vol. 50, no. 5, pp. 1076–1084, 2013.

[6] W. Chi, W. Chen, and Y. Wang, "Scalable influence maximization for independent cascade model in large-scale social networks[J]," *Data Mining & Knowledge Discovery*, vol. 49, no. 3, pp. 498–504, 2011.

[7] J. X. Cao, D. Dong, S. Xu, X. Zheng, B. Liu, and J. Luo, "A k-core based algorithm for influence maximization in social networks[J]," *Chinese Journal of Computers*, vol. 38, no. 2, pp. 238–248, 2015.

[8] Y. Wang, F. Zhang, G. Fang, Y. Ji, S. Ye, and X. Zhang, "A novel ultrawideband exponentially tapered slot antenna of combined electric-magnetic type[J]," *IEEE Antennas and Wireless Propagation Letters*, vol. 15, pp. 1226–1229, 2016.

[9] G. Gennarelli and F. Soldovieri, "Multipath ghosts in radar imaging: physical insight and mitigation strategies," *IEEE Journal of Selected Topics in Applied Earth Observations and Remote Sensing*, vol. 8, no. 3, pp. 1078–1086, 2014.

[10] A. Hu, R. Zhang, and D. Yin, "Image quality assessment using a SVD-based structural projection," *Signal Processing: Image Communication*, vol. 29, no. 3, pp. 293–302, 2014.

[11] S. G. Li, Y. Jia, and Y. Guo, "Moving target tracking algorithm based on improved Camshaft for through-wall-radar imaging," *Journal of Computer Applications*, vol. 38, no. 2, pp. 528–532, 2018.

[12] Z. Moghaddam and M. Piccardi, "Training initialization of hidden Markov models in human action recognition," *IEEE Transactions on Automation Science & Engineering*, vol. 11, no. 2, pp. 394–408, 2014.

[13] Z. K. Ma and W. H. Chang, "Friction torque calculation method of ball bearings based on rolling creepage theory," *Journal of Mechanical Engineering*, vol. 53, no. 22, pp. 219–224, 2017.

[14] W. H. LI and H. Y. NI, "An improved AdaBoost training algorithm[J]," *Journal of Jilin University (Science Edition)*, vol. 49, no. 3, pp. 498–504, 2011.

[15] L. G. Ramos, S. F. G. Vegas, and F. M. Martin, "Anisotropic diffusion filter with memory based on speckle statistics for ultrasound images," *IEEE Transactions on Image Processing*, vol. 24, no. 1, pp. 345–358, 2016.

[16] X. X. Shen, H. Zhang, and Z. Gao, "Behavior recognition algorithm based on Kinect and pyramid feature," *Journal of Optoelectronics Laser*, vol. 14, no. 2, pp. 357–363, 2014.

[17] G. H. Tian, J. Q. Yin, and X. Han, "A new method of human behavior recognition based on joint information," *Robot*, vol. 36, no. 3, pp. 285–292, 2014.

[18] Q. Y. Tan, H. Leung, and Y. Song, "Multipath ghost suppression for through-the-wall-radar," *IEEE Transactions on Aerospace and Electronic Systems*, vol. 50, no. 3, pp. 2284–2292, 2014.

[19] C. Xiu and F. Ba, "Target tracking based on the improved Cam shift method//CCDC 2016," in *Proceedings of the 2016 Chinese Control and Decision Conference*, pp. 3600–3604, Piscataway, NJ, 2016.

[20] Q. G. Zhang, F. Cai, and Z. Q. Li, "Human action recognition based on coupled multi-hidden Markov model and depth image data," *Journal of Computer Applications*, vol. 38, no. 2, pp. 454–457, 2018.

[21] H. Liang, J. Zou, K. Zuo, and K. Muhammad Junaid, "An improved genetic algorithm optimization fuzzy controller applied to the wellhead back pressure control system," *Mechanical Systems and Signal Processing*, vol. 142, p. 106708, 2020.

Hindawi
Wireless Communications and Mobile Computing
Volume 2021, Article ID 6646398, 10 pages
https://doi.org/10.1155/2021/6646398

Research Article

A Novel Optimal Selection Algorithm for Agricultural Trade Export in Blockchain-Enabled Internet of Things

Shuhao Cao

School of Economics and Management, Beijing University of Posts and Telecommunications, Beijing 100876, China

Correspondence should be addressed to Shuhao Cao; buptcsh@bupt.edu.cn

Received 19 October 2020; Revised 8 December 2020; Accepted 22 December 2020; Published 8 January 2021

Academic Editor: Hongju Cheng

Copyright © 2021 Shuhao Cao. This is an open access article distributed under the Creative Commons Attribution License, which permits unrestricted use, distribution, and reproduction in any medium, provided the original work is properly cited.

With the maturity of modern science and technology, such as networks and computers, Internet of Things has been widely used in various fields of industry, opening up a new situation for the development of the industry and creating a broader development platform. This paper systematically analyzes the characteristics and changes of the commodity structure, regional structure, market structure, and main structure of export management of agricultural products. The proposed algorithm uses computer technology, network technology, and remote communication technology, electronic, digital, and network—the entire business process of business. The empirical analysis shows that the structure of agricultural product export trade reflects the endowment and comparative advantage of agricultural resources in China. The proposed blockchain technology supports and guides agricultural export enterprises to develop their own brands, strengthen the quality and safety management of agricultural products, and innovate and expand the policy support system for optimizing the structure of agricultural product export trade. By optimizing the export mode of agricultural trade, we can achieve the purpose of increasing the export volume of agricultural products and the total value of trade exports. The experimental results show the effectiveness of the proposed algorithm, which can greatly improve the volume of trade exports and the total value of trade exports.

1. Introduction

In order to implement the national agricultural science and technology innovation capacity building plan, the majority of scientific research users recommend the ADCON agricultural Internet of Things/data acquisition and processing system for the agricultural market. The system includes complete farmland meteorological environment, soil and crop information collection, video information collection, and data pass wireless transmission method to the server, data center construction software platform, database, gateway, server, data terminal and other complete data storage, viewing, and analysis and processing system; users can use this system to obtain farmland meteorological environment, soil moisture and crop physiology online in real time. Ecological character information promotes the construction of agricultural information management. Electronic commerce is a new economic form, which means to fully develop the integrated value of the Internet in the allocation of production factors, to apply Internet technology to various industries, and to inject a new development power into the development of the industry. It can lead the innovation and progress of the real economy [1]. Against this background, electronic commerce also plays a vital role in the development of China's agricultural export trade, especially as an important agricultural production base in China [2]. We should firmly grasp the opportunity created by electronic commerce, give play to the positive impact and guiding value of electronic commerce on the export of agricultural products, actively overcome the existing problems, and promote the sustainable development of agricultural export trade [3].

E-commerce usually refers to a wide range of commercial trade activities around the world; in the Internet open network environment, based on client/server applications, buyers and sellers do not meet with all kinds of commercial activities, realize consumer online shopping, online transactions between merchants and online electronic payment and various business activities, trading activities, financial activities, and related comprehensive service activities of a new type of commercial operation mode. Electronic

commerce facilitates the export of agricultural products and creates new ways of export trade through Internet channels [4]. For example, the export of products can be negotiated with exporters through cross-border e-commerce platforms and through Internet platforms. The virtual environment of the network can be assigned agricultural export contracts, so in the context of electronic commerce, the regional agricultural export situation is developing well. In 2017, the export trade volume of agricultural products in Heilongjiang Province reached 864 million US dollars, an increase of 10% over the same period last year. Jilin Province exported 7.8 billion yuan of agricultural products [5]. The export value of agricultural products in Liaoning Province reached 5.3 billion US dollars, an increase of 7% over the same period last year. The main categories of agricultural products exported are soybean, corn, rice, apple, deer products, poultry products, aquatic products, and other regional agricultural products. Japan, South Korea, Russia, and other Asian countries are the main exporting countries. In recent years, the scale of export to the United States, Canada, and other European countries has gradually expanded [6].

The rest of this paper is organized as follows. Section 2 discusses the dilemma in agricultural trade under the background of electronic commerce, followed by the influence of electronic commerce on the export trade of regional agricultural products and suggestions for its development designed in Section 3. The optimal selection algorithm of the agricultural trade export mode is discussed in Section 4. Section 5 shows the simulation experimental results, and Section 6 concludes the paper with summary and future research directions.

2. Dilemma in Agricultural Trade under the Background of Electronic Commerce

The relative lag in the construction of information infrastructure is one of the difficulties faced by regional agricultural product export trade under the background of electronic commerce. The export of agricultural products under the background of electronic commerce needs to be based on perfect information. Although the process of information construction in China has been accelerated in recent years, the speed of the development of regional information infrastructure is relatively lagging behind [7]. In particular, it needs to establish cross-border Internet trading platforms and relatively high requirements for the basic conditions of information technology. If the level of information technology is low, it will limit the development of agricultural product export trade under the Internet environment [8]. Therefore, due to the slow development of information infrastructure construction, the development of regional agricultural export trade is not satisfactory at this stage. In 2017, the Internet penetration rate was about 50 percent; the national ranking was 19th; the number of new websites was 8626, accounting for about 1 percent of the total national total; and the national ranking was 21st. It can be seen that the construction of network information in Jilin Province is lagging behind. Thus, the export of electronic commerce agricultural products will be restricted [9].

At this stage, the slow development of logistics distribution systems has become a major difficulty by restricting the development of regional agricultural export trade under the background of electronic commerce. In the process of export of agricultural products, both parties can use the network to trade across geographical and spatial constraints without having to talk face to face. However, after an order is reached, a perfect logistics distribution system is still needed as the support [10]. In particular, cross-border logistics distribution is far more difficult than domestic logistics distribution; its complexity is stronger and more challenging. On the one hand, the distance of cross-border logistics is long, and the shelf-life of agricultural products is usually relatively short, which is difficult to preserve, thus increasing the cost of logistics transportation and depriving agricultural products of the price advantage of exporting [11]. On the other hand, the export of agricultural products is more dispersed. The three provinces have not yet completed the distribution of highway territory; hence, the export of products before the logistics transport costs is relatively high. Taking Jilin Province as an example, although the logistics industry in the province has achieved certain development, the overall strength is relatively weak, the logistics supply capacity is insufficient, the linkage with other industries is not close, and there is no perfect logistics security system. This has a negative impact on the export of products overseas [12].

Under the background of electronic commerce, there is a lack of guarantee of product quality and safety in regional agricultural product export trade. At present, green trade barriers have become a tool for the developed countries to restrict the export of products from developing countries to their own countries. In the field of agricultural products, the United States, the European Union, Japan, and other developed countries have also formulated strict product inspection and quarantine standards [13]. Under the export mode of agricultural products under the environment of electronic commerce, small- and medium-sized agricultural product enterprises can use cross-border e-commerce platforms to independently establish trading relationships with overseas buyers to sell agricultural products to them [14]. However, at present, the quality and safety inspection and quarantine work for the export of agricultural products in the region have not yet been implemented, and there is a lack of perfect standards. In this case, it is very likely that the quality of the products will not meet the standard, the products will not be up to standard, and so on. It will even lead to hidden dangers of food safety, which will also have an impact on the overall image of domestic agricultural products. For example, the inspection and quarantine department of Heilongjiang Province have recently investigated and dealt with a number of agricultural products with quality problems, including the matsutake and rice, which have caused serious quality problems due to improper preservation and deterioration of products during transportation [15]. The overall structure of electronic commerce is shown in Figure 1.

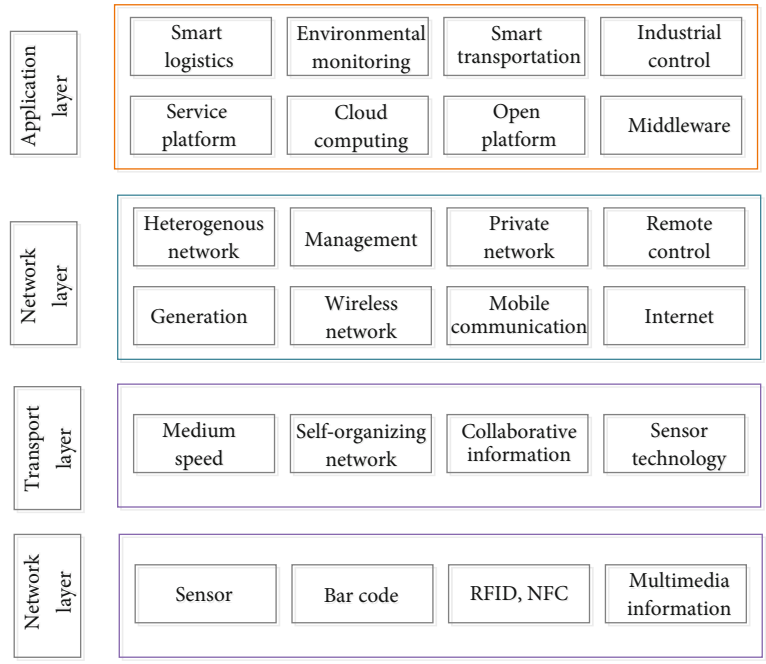

Figure 1: The overall structure of electronic commerce.

3. The Impact of E-Commerce on Agricultural Exports

3.1. Conducive to the Establishment of Regional Export Brands of Agricultural Products. "Internet" has a very positive impact on the regional agricultural product export, which is conducive to the establishment of a regional agricultural product export brand [16]. Despite the high quality and low price of agricultural products in the region, due to the lack of propaganda and marketing, there has been a lack of influence in the international market for a long time to form a brand effect, and electronic commerce has changed this situation. Especially for the regional export of agricultural products to create a new channel and approach, enterprises can promote and market products in the virtual environment of the network, thus breaking the restrictions of the geographical environment to the target markets around the world to publicize. Through this way, the regional agricultural product export trade can truly go out of the country, go to the international market, gain more consumer identity, and then set up its regional agricultural product brand [17].

3.2. Promote the International Competitiveness of Regional Agricultural Products. The influence of electronic commerce on the regional agricultural product export trade is reflected in the promotion of the international competitiveness of regional agricultural products [18]. For a long time, the advantage of the regional agricultural product export lies in its abundant resources and low cost, which is based on the price advantage. With the development of export trade of agricultural products in Southeast Asia, the export of regional agricultural products has gradually lost its price advantage. Under the environment of electronic commerce, regional agricultural export enterprises can establish a network security management system with the help of a network, bar code identification technology, network technology, and so on [19]. It can enable consumers in any country and region to have access to comprehensive information on agricultural exports, thereby enhancing the international competitiveness of products and expanding their market share. Ranking of the average scores of importance and satisfaction of evaluation indicators is as shown in Table 1 [20].

3.3. Speeding Up the Construction of Information Basic Network. Based on the overall development situation of electronic commerce at present, the development of regional agricultural product export trade must speed up the process of information basic network construction and make comprehensive preparations for agricultural product export. First of all, we should continue to promote the process of information construction in rural areas, improve the level of information, create a good information base for the overseas export of agricultural products, and provide more farmers with opportunities for the development of overseas exports of products [21]. Secondly, local governments should strengthen their support for the construction of information technology for agricultural product exports, support the establishment of cross-border e-commerce platforms, and at the same time train a large number of information talents and improve the level of information of talents. Under the environment of electronic commerce, the regional agricultural product export must keep up with the level of information development, in order to create a broad platform for agricultural product export [22]. For example, the region can learn from the successful experience of Hangzhou, establish cooperative relations with mobile and Unicom telecom

Table 1: Ranking the average scores of importance and satisfaction of evaluation indicators.

Indicators	Importance	Sorting	Importance	Sorting
A_1	4.233	13	3.628	7
A_2	4.102	14	3.582	8
A_3	4.464	6	3.252	11
A_4	4.225	12	3.895	3
B_1	4.566	4	3.854	5
B_2	4.675	3	4.012	1
C_1	4.323	9	3.862	4
C_2	4.238	11	3.923	2
D_1	4.335	8	3.785	6
D_2	5.000	1	3.212	13
E_1	4.998	2	3.102	14
E_2	4.525	5	3.321	10
E_3	4.386	7	3.356	9
E_4	4.248	10	3.243	12

companies, comprehensively promote the construction of Internet information, strengthen the construction of hardware, and provide assistance for the construction of Internet information. The influence of electronic commerce on regional agricultural product export trade and suggestions for its development are shown in Figure 2 [23].

3.4. Establishment of an Efficient Logistics System for Agricultural Products. The development of cross-border e-commerce depends on the perfect basic conditions of logistics distribution. Therefore, under the background of electronic commerce, the regional agricultural product export trade must also establish an efficient agricultural product logistics system as soon as possible. First of all, it is necessary to improve the construction of regional rural logistics; create a complete logistics chain system; set up a logistics network in counties, towns, and villages; improve the basic conditions of logistics transportation in rural areas; and provide convenience for the export of agricultural products [24]. Secondly, we should strengthen ties with overseas logistics and transport enterprises, create close cooperative relations, increase the speed of overseas transportation of agricultural products, reduce the transportation time, and avoid the problem of product deterioration caused by the long transportation time [25]. At the same time, in the process of logistics transportation, we must optimize the preservation mode of agricultural products, select appropriate storage conditions according to different products and different export areas, and avoid the phenomenon of product damage in the course of logistics transportation. In this regard, the region can learn from the successful experience of Jiangsu [26]. The Logistics Industry Park regularly holds business promotion meetings, actively negotiates and cooperates with logistics enterprises, and attracts investment to establish a more perfect logistics system and become the overseas export of products to undertake power [27].

3.5. Enhancing the Quality and Safety of Agricultural Products. Under the background of electronic commerce, the development of regional agricultural product export trade must enhance the quality and safety of agricultural products; ensure the hygiene, health, and safety of exported food; and attract consumers by quality [28]. The relevant government departments shall issue inspection and quarantine standards for the export of agricultural products, strictly check the quality of agricultural products, and prohibit the export of agricultural products in case of problems in product quality, so as to improve the quality of their exports [29]. At the same time, according to the different requirements of exporting countries of agricultural products, the conditions of inspection and quarantine should be adjusted appropriately to break down the green trade barriers and gain the trust of consumers in terms of quality. Yunnan Province's experience in this area is worth learning. The Yunnan Inspection and Quarantine Bureau has established a new mode of inspection and supervision, implemented a "full declaration, full filing, and traceability" management model for export products, set up a complaint reporting point for import and export commodity quality, collected information in an all-round way, and expanded the monitoring area. In this way, the export of agricultural products can be monitored more effectively to ensure the quality of products [30].

3.6. Establishment of Internet Security Trading Platform for Agricultural Products. The establishment of an Internet security trading platform for agricultural products is a prerequisite for regional agricultural products export trade under the background of electronic commerce. First of all, the relevant government departments should strengthen the qualification of cross-border e-commerce in the Internet environment and develop a sound credit review mechanism, for the strict screening of the platform of the business, to ensure the credibility of the business and to ensure the security of the Internet environment. Secondly, we should improve the level of network technology and strengthen the customer information leakage, payment loopholes, and other potential network risk management, to prevent economic losses to consumers and create a safe network environment. Through this way, we can attract overseas consumers to our cross-border e-commerce concerns, enhance trust, and then, through the Internet and regional businesses to establish a cooperative relationship, choose from the import of agricultural products. The achievements of Beijing in the area of network information security can be used as a reference for the region. At present, Beijing has set up a leading group on network security and information and has opened an Internet information reporting center for illegal and bad information, in order to play a network information security protection effect.

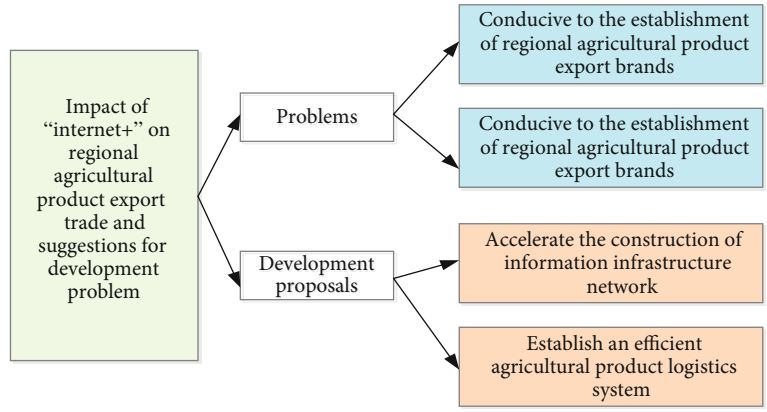

Figure 2: The influence of electronic commerce on regional agricultural product export trade and suggestions for its development.

4. Optimal Selection Algorithm of Agricultural Trade Export Mode

China should gradually adjust the export market structure of agricultural products and establish a global agricultural product export market system characterized by "market diversification." It is necessary to consolidate the traditional key markets and constantly develop new markets. In this paper, the relative error of the natural frequency of the theoretical model is taken as the objective function, the first four natural frequencies are taken as the state variables, and some uncertain materials and cross-section parameters are taken as the design variables in the finite element modelling. Using ANSYS software, the sensitivity of objective function and state variable to the design variable is calculated first, then the design variable with high sensitivity is selected, and the optimization iteration is carried out by using the appropriate optimization method. Finally, the more accurate design variables are obtained. The purpose is to play the role of network information security protection. ANSYS software provides a variety of optimization methods. Considering the accuracy of the results, the first-order optimization method is the main method used, and other methods are used for calculation.

4.1. Sensitivity Analysis. The design variable can be expressed as $X = [X_1, X_2 \cdots X_n]$, where X represents the lower and upper limits of the design variable X_j. The following representations are the same.

The reference state of the objective function is $f_r(x) = f(x^{(r)})$, and the sensitivity of the objective function or state variable to the design variable is expressed as follows:

$$\Delta f_r = \left[\frac{\partial f_r}{\partial x_1}, \frac{\partial f_r}{\partial x_2}, \cdots, \frac{\partial f_r}{\partial x_n}\right]. \tag{1}$$

4.2. Basic Principles of Optimal Design. ANSYS software provides a variety of optimization methods; considering the accuracy of the results, the first-order optimization method is the main method, and other methods are used for calculation; each iteration retains a set of optimal solutions. It can be summed up in the following general form.

Minimum:

$$f = f(x). \tag{2}$$

Constraints:

$$\begin{aligned} x_j' \le x_j \le x_j' \quad (j = 1, 2, \cdots, n), \\ g_j \le g_j' \quad (j = 1, 2, \cdots, n), \\ h_j' \le h_j(x) \quad (j = 1, 2, \cdots, n), \\ w_j' \le w_j(x) \le w_j' \quad (j = 1, 2, \cdots, n). \end{aligned} \tag{3}$$

If the mixed penalty function method is used to transform it into a dimensional unconstrained single-objective optimization problem, the penalty function is expressed as follows:

$$Q(x, q) = \frac{f}{f_0} + \sum_j p_x(x_j) + q\left[\sum_j p_g\left(g_j\right) + \sum_j p_h(h_j) + \sum_j p_w(w_j)\right], \tag{4}$$

in which p_x, p_g, p_h, and p_w are penalty factors for constrained design variables and state variables. By using the gradient method for unconstrained optimization problems, the iterative formula is expressed as follows:

$$x^{(j+1)} = x^{(j)} + s_j d^{(j)}, \tag{5}$$

in which s_j is the optimal step size factor. The convergence condition of the iteration is given as follows:

$$\begin{aligned} \left|f^{(j)} - f^{(j-1)}\right| \le \tau, \\ \left|f^{(j)} - f^{(b)}\right| \le \tau, \end{aligned} \tag{6}$$

in which τ is the tolerance of the objective function.

4.3. Design of Route Optimization Algorithm Based on Dijkstra Algorithm. In a graph G, the Dijkstra algorithm

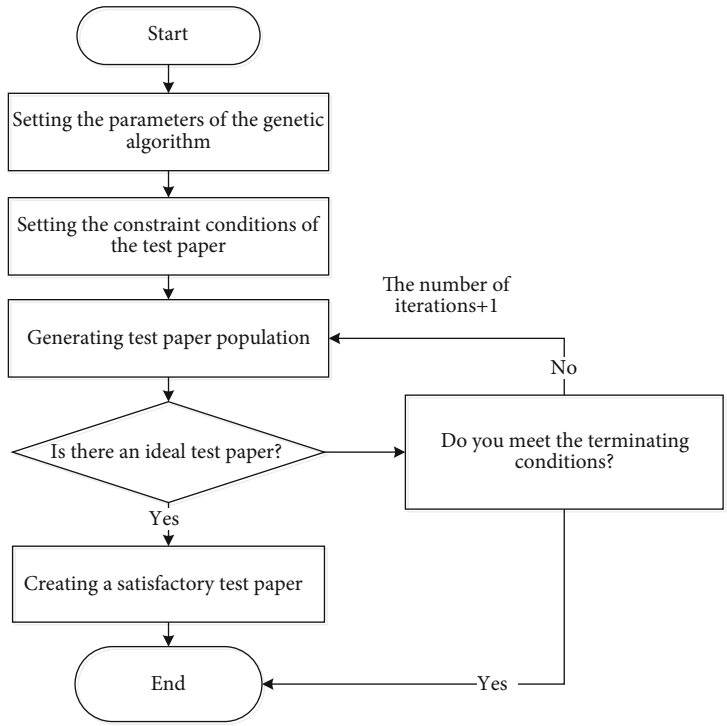

Figure 3: Dijkstra algorithm flow chart.

can not only give a path with minimum weight between two specified vertices but also find the shortest path from a specified point to all vertices in G. The disadvantage of the Dijkstra algorithm is that when the number of nodes in the network is large, it will increase the search cost and reduce the efficiency. For example, to search for the shortest path to all nodes of G, the time complexity is $O(N_2)$.

The following brief description uses the Dijkstra algorithm to solve the shortest path between two specified vertices: the input is directed graph $G(V\text{on}E)$, V is the set of vertices, and V is divided into U and UV. E is the edge set of graph G. S is the source node, and the shortest path from the source node s to v is denoted as the $P(v)$, length of the shortest path from the source node s to v, which can be represented by the maximum real number, and they are expressed as follows:

$$D(v) = \sum C(v_i, v_j), \quad \text{where } v_i, v_j \in V. \tag{7}$$

If $D(v)$ is the shortest path length from s to p,

$$D(v_0) \le D(v_1) \le D(v_2) \le \cdots \le D(v_n). \tag{8}$$

Then, the following can be proven by derivation,

$$D(v_{n+1}) = \min \{D(v_n) + C(v_i, w)\}, \quad \text{where } v_i \in U, w \in V - U. \tag{9}$$

The Dijkstra algorithm flow chart is shown in Figure 3.

Table 2: The basic importance of customer needs.

Demand	A_1	A_2	A_3	A_4	B_1	B_2	C_1
Basic importance	0.06	0.024	0.048	0.113	0.073	0.081	0.065
Demand	C_2	D_1	D_2	E_1	E_2	E_3	E_4
Basic importance	0.129	0.032	0.056	0.024	0.121	0.137	0.004

Table 3: The correction factor of the basic importance of customer demand.

Correction factor	r_1	r_2	r_3	r_4	r_5	r_6	r_7
Correction value	0.16	0.224	0.008	0.013	0.173	0.281	0.006
Correction factor	r_8	r_9	r_{10}	r_{11}	r_{12}	r_{13}	r_{14}
Correction value	0.12	0.02	0.06	0.04	0.21	0.137	0.024

4.4. Analysis of Route Optimization Algorithm Based on Dijkstra Algorithm. Find a vertex w from $U - V$ at a time, minimize $D(W)$, move w from $V - U$ into UU, and modify the $P(v)$ and $D(v)$ for each v as follows.

If the following conditions are satisfied as follows:

$$D(v) > D(w) + C(w, v), \tag{10}$$

in which w is the vertex of the newly selected U, then,

$$P(v) \leftarrow P(w)//\{v\}, \tag{11}$$

$$D(v) \leftarrow D(w) + C(w, v), \tag{12}$$

Table 4: Iterative correction model theoretical frequency and measured frequency comparison.

Vibration mode	Measured frequency	Finite element theory frequency (Hz)				Error (%)
		Initial FEM	After 1 iteration	After 2 iterations	After 3 iterations	
Vertical 1st order	5.87	4.98	5.13	5.58	5.79	1.4
Vertical 2nd order	12.96	12.64	12.86	12.93	12.90	0.46
Reverse 1	8.31	7.89	7.91	8.12	8.43	1.44
Reverse 2	5.64	14.34	14.60	15.67	15.61	0.19

Table 5: Structural parameter correction.

Structural parameters	Initial estimate	Corrected parameter values		
		After 1 iteration	After 2 iterations	After 3 iterations
H(m)	0.900	0.893	1.138	1.139
H_1(m)	0.140	0.152	0.155	0.154
L(m)	9.200	19.000	9.279	19.280
$E(10^{10})$(Pa)	3.0	3.0675	3.1476	3.150

in which "/" means the path is connected. It shows that the path from s to w and then to v is better than the path from s to v without going through w. Here, the representation of the path $P(v)$ is an ordered sequence of vertices $(v_1 = s_1 v_2, v_3, \cdots, v_i = v)$.

For attributes, its importance can be calculated by the following formula:

$$\beta_i = \beta_D(C_i) = \frac{\text{card}\ (\text{Pos}_C)(CS) - \text{card}\left(\text{Pos}_{|C-\{C_i\}|}\right)(CS)}{\text{card}\ (U)}. \tag{13}$$

And relatively important formulas can be expressed as follows:

$$g_i = \frac{\beta_i}{\sum_i \beta_i}. \tag{14}$$

Using the above formula, we can determine the relative importance of customer demand Q, that is, the basic importance degree of customer demand, which is shown in Table 2.

In order to get the basic importance vector of customer demand, we can use the following equation. And the correction factor of the basic importance of customer demand is shown in Table 3.

$$g = (g_1, g_2, \cdots, g_{14})^T. \tag{15}$$

5. Simulation

The dominant position of state-owned enterprises in the export of agricultural products in China has been replaced by foreign-invested enterprises and the trend of negative growth. In 2005, state-owned enterprises exported US $7.437 billion in agricultural products, accounting for 27.36 percent of the total agricultural exports. This represents a decrease of $1.303 billion, or -14.91 per cent, over 2000. With the increase of agricultural product export, the export of state-owned enterprises is stagnant, and even the trend of negative growth has appeared. This shows that the degree of state monopoly of agricultural trade in China is decreasing and the degree of market is increasing. Iterative correction model theoretical frequency and measured frequency comparison are given in Table 4.

Through the above experimental results, it can be observed that the frequencies of each model will eventually converge to the same value. The status of foreign-invested enterprises in the export of agricultural products has gradually risen and has occupied a dominant position. In 2005, Sino-foreign joint ventures, wholly foreign-owned enterprises, and Chinese-foreign contractual joint ventures exported US $11.671 billion in agricultural products, accounting for 42.933% of the total agricultural exports, an increase of US $6.941 billion or 146.74% over 2000. Among them, the Sino-foreign joint venture is the largest export of agricultural products in foreign-funded enterprises, ranking third among the seven main trading bodies. Structural parameter correction is given in Table 5. The change of parameter value after iteration is shown in Figure 4.

Total exports of agricultural products from private enterprises are increasing rapidly. In 2000, private enterprise exports accounted for 1.8% of the total agricultural exports, which rose to 12.2% in 2003 and reached 24.82% by 2005. In 2005, private enterprises exported US $6.747 billion in agricultural products, an increase of nearly 24 times over 2000. As a result, private enterprises have become one of the main business entities in the export trade of agricultural products in China. Performance comparison of different agricultural product trade optimization selection algorithms in stock of trade product warehouse is shown in Figure 5.

The solution is to adjust and optimize the structure of agricultural product export trade, to implement the strategy of market diversification, to strengthen the construction of agricultural industrialization bases and deep processing bases, and to produce characteristic products with export competitive advantages. We will support and guide agricultural export enterprises to develop their own brands, strengthen the quality and safety management of agricultural products, and innovate and expand the policy support system for optimizing the structure of agricultural products export trade. Performance comparison between the proposed method and the traditional optimal selection method is shown in Figure 6.

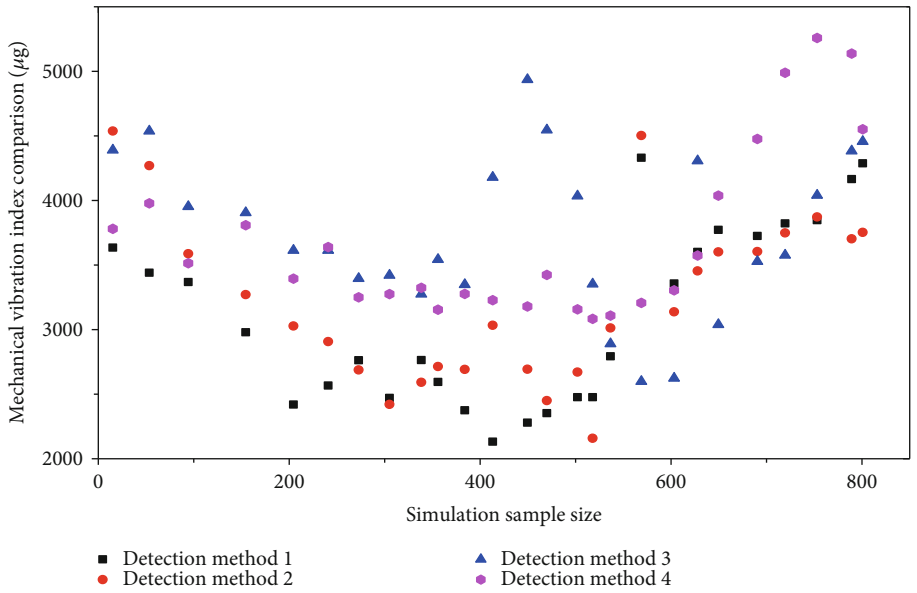

Figure 4: Parameter values change after iteration.

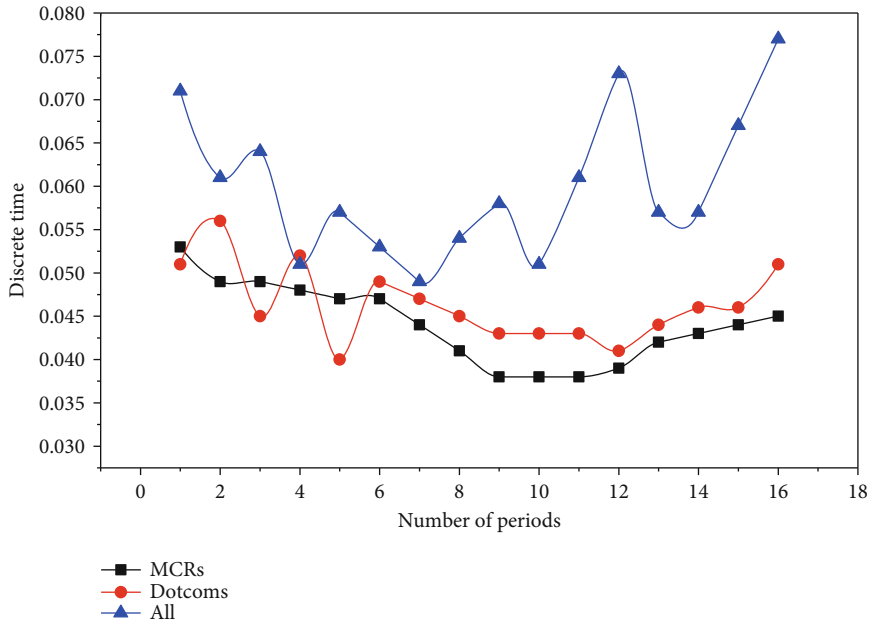

Figure 5: Performance comparison of different agricultural product trade optimization selection algorithms in the stock of trade product warehouse.

By optimizing the export mode of agricultural trade, we can achieve the purpose of increasing the export volume of agricultural products and the total value of trade exports. The experimental results show the effectiveness of the proposed algorithm, which can greatly improve the volume of trade exports and the total value of trade exports.

6. Conclusion

This paper systematically analyzes the characteristics and changes of the commodity structure, regional structure, market structure, and main structure of export management of agricultural products. The empirical analysis shows that the structure of agricultural product export trade reflects the endowment and comparative advantage of agricultural resources in China. The export trade of agricultural products is mainly concentrated in labor-intensive agricultural products with competitive advantage and export regions. Mainly concentrated in the eastern provinces, the export market is relatively concentrated; structural changes have also appeared in the main body of agricultural product export. The solution is to adjust and optimize the structure of

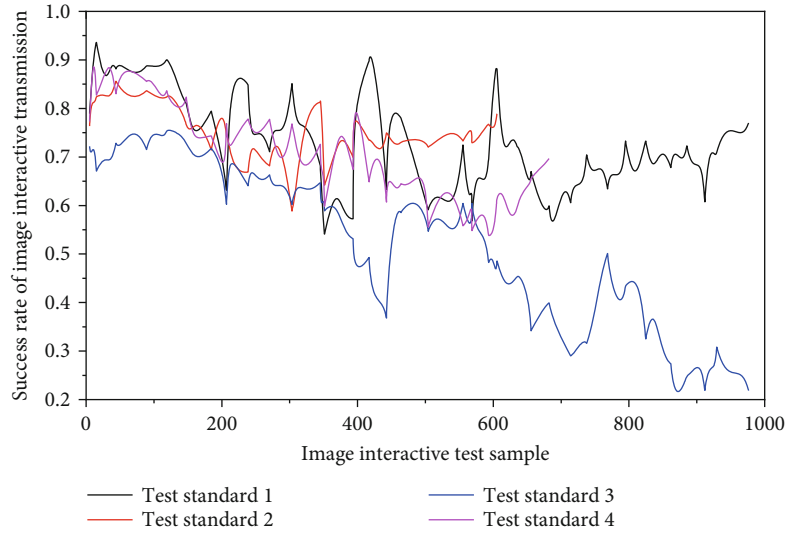

Figure 6: Performance comparison between the proposed method and the traditional optimal selection method.

agricultural product export trade, to implement the strategy of market diversification, to strengthen the construction of agricultural industrialization bases and deep processing bases, and to produce characteristic products with export competitive advantages. We will support and guide agricultural export enterprises to develop their own brands, strengthen the quality and safety management of agricultural products, and innovate and expand the policy support system for optimizing the structure of agricultural product export trade. By optimizing the export mode of agricultural trade, we can achieve the purpose of increasing the export volume of agricultural products and the total value of trade exports. The experimental results show the effectiveness of the proposed algorithm, which can greatly improve the volume of trade exports and the total value of trade exports.

Data Availability

All the data is real, and all the data can be obtained by contacting the author.

Conflicts of Interest

The author declares that there is no conflict of interest regarding the publication of this paper.

References

[1] M. Elhoseny and A. E. Hassanien, "Optimizing cluster head selection in WSN to prolong its existence," in *Dynamic Wireless Sensor Networks*, vol. 165, pp. 93–111, Springer, Cham, 2019.

[2] B. Zhang, X. Wang, and Z. Zheng, "The optimization for recurring queries in big data analysis system with MapReduce," *Future Generation Computer Systems*, vol. 87, pp. 549–556, 2018.

[3] K. Karthikeyan, R. Sunder, K. Shankar et al., "Energy consumption analysis of virtual machine migration in cloud using hybrid swarm optimization (ABC–BA)," *The Journal of Supercomputing*, vol. 76, no. 5, article 2583, pp. 3374–3390, 2020.

[4] A. Hassanien, R. M. Rizk-Allah, and M. Elhoseny, "A hybrid crow search algorithm based on rough searching scheme for solving engineering optimization problems," *Journal of Ambient Intelligence and Humanized Computing*, vol. 12, 2018.

[5] M. Elhoseny, D. Oliva, V. Osuna-Enciso, A. E. Hassanien, and M. Gunasekaran, "Parameter identification of two dimensional digital filters using electro-magnetism optimization," *Multimedia Tools and Applications*, vol. 79, no. 7-8, article 6095, pp. 5005–5022, 2020.

[6] N. Metawa, M. K. Hassan, and M. Elhoseny, "Genetic algorithm based model for optimizing bank lending decisions," *Expert Systems with Applications*, vol. 80, pp. 75–82, 2017.

[7] M. Elhoseny, A. Farouk, N. Zhou, M. Wang, S. Abdalla, and J. Batle, "Dynamic multi-hop clustering in a wireless sensor network: performance improvement," *Wireless Personal Communications*, vol. 95, no. 4, article 4023, pp. 3733–3753, 2017.

[8] X. Yuan, M. Elhoseny, H. K. el-Minir, and A. M. Riad, "A genetic algorithm-based, dynamic clustering method towards improved WSN longevity," *Journal of Network and Systems Management*, vol. 25, no. 1, article 9379, pp. 21–46, 2017.

[9] M. Elhoseny, X. Yuan, H. K. el-Minir, and A. M. Riad, "An energy efficient encryption method for secure dynamic WSN," *Security and Communication Networks*, vol. 9, no. 13, pp. 2024–2031, 2016.

[10] Jenn-Wei Lin, Chien-Hung Chen, and J. M. Chang, "QoS-aware data replication for data-intensive applications in cloud computing systems," *IEEE Transactions on Cloud Computing*, vol. 1, no. 1, pp. 101–115, 2013.

[11] L. Cui, J. Zhang, L. Yue, Y. Shi, H. Li, and D. Yuan, "A genetic algorithm based data replica placement strategy for scientific applications in clouds," *IEEE Transactions on Services Computing*, vol. 11, no. 4, pp. 727–739, 2018.

[12] R. Nachiappan, B. Javadi, R. Calheiros, and K. M. Matawie, "Cloud storage reliability for big data applications: a state of

the art survey," *Journal of Network and Computer Applications*, vol. 97, pp. 35–47, 2017.

[13] B. Xiong, "Food safety and food imports in Europe: the risk of aflatoxins in pistachios," *International Food and Agribusiness Management Review*, vol. 20, no. 1, pp. 129–141, 2017.

[14] Z. X. Yang, "Research on trade model of transaction costs based on ecommerce," *Applied Mechanics and Materials*, vol. 26, pp. 218–221, 2010.

[15] M. Yu, "Processing trade, tariff reductions and firm productivity: evidence from Chinese firms," *The Economic Journal*, vol. 125, no. 585, pp. 943–988, 2015.

[16] Y. Yu, X. Wang, R. Y. Zhong, and G. Q. Huang, "E-commerce logistics in supply chain management," *Industrial Management & Data Systems*, vol. 117, no. 10, pp. 2263–2286, 2017.

[17] H. Zhu, C. X. Ou, W. J. A. M. van den Heuvel, and H. Liu, "Privacy calculus and its utility for personalization services in e-commerce: an analysis of consumer decision-making," *Information & Management*, vol. 54, no. 4, pp. 427–437, 2017.

[18] R. Becerril-Arreola, M. P. Leng, and M. Parlar, "Online retailers' promotional pricing, free-shipping threshold, and inventory decisions: a simulation-based analysis," *European Journal of Operational Research*, vol. 230, no. 2, pp. 272–283, 2013.

[19] N. T. Koukova, J. Srivastava, and M. Steul-Fischer, "The effect of shipping fee structure on consumers' online evaluations and choice," *Journal of the Academy of Marketing Science*, vol. 40, no. 6, pp. 759–770, 2012.

[20] B. Zhou, M. N. Katehakis, and Y. Zhao, "Managing stochastic inventory systems with free shipping option," *European Journal of Operational Research*, vol. 196, no. 1, pp. 186–197, 2009.

[21] J. Song, Y. Yin, and Y. Huang, "A coordination mechanism for optimizing the contingent-free shipping threshold in online retailing," *Electronic Commerce Research and Applications*, vol. 26, pp. 73–80, 2017.

[22] S. W. Shi, M. Xia, and Y. Huang, "From minnows to whales: an empirical study of purchase behavior in freemium social games," *International Journal of Electronic Commerce*, vol. 20, no. 2, pp. 177–207, 2015.

[23] A. Uysal and I. Yildirim, "Self-determination theory," in *In digital games*, Gamer psychology and behavior, B. Bostan, Ed., pp. 123–135, Springer, Switzerland, 2016.

[24] E. Park, R. Rishika, R. Janakiraman, M. B. Houston, and B. Yoo, "Social dollars in online communities: the effect of product, user, and network characteristics," *Journal of Marketing*, vol. 82, no. 1, pp. 93–114, 2018.

[25] H. Liang, J. Zou, K. Zuo, and M. J. Khan, "An improved genetic algorithm optimization fuzzy controller applied to the wellhead back pressure control system," *Mechanical Systems and Signal Processing*, vol. 142, article 106708, 2020.

[26] H. Zheng, W. Guo, and N. Xiong, "A kernel-based compressive sensing approach for mobile data gathering in wireless sensor network systems," *IEEE Transactions on Systems, Man, and Cybernetics: Systems*, vol. 48, no. 12, pp. 2315–2327, 2018.

[27] H. Liang, D. Zou, Z. Li, K. Muhammad Junaid, and Y. Lu, "Dynamic evaluation of drilling leakage risk based on fuzzy theory and PSO-SVR algorithm," *Future Generation Computer Systems*, vol. 95, pp. 454–466, 2019.

[28] Y. Zhang, R. Zhu, Z. Chen, J. Gao, and D. Xia, "Evaluating and selecting features via information theoretic lower bounds of feature inner correlations for high-dimensional data," *European Journal of Operational Research*, vol. 290, no. 1, pp. 235–247, 2021.

[29] H. Liang, A. Xian, M. Min Mao, P. Ni, and H. Wu, "A research on remote fracturing monitoring and decision-making method supporting smart city," *Sustainable Cities and Society*, vol. 62, article 102414, 2020.

[30] Y. Zhou, D. Zhang, and N. Xiong, "Post-cloud computing paradigms: a survey and comparison," *Tsinghua Science and Technology*, vol. 22, no. 6, pp. 714–732, 2017.

Hindawi
Wireless Communications and Mobile Computing
Volume 2021, Article ID 6672773, 7 pages
https://doi.org/10.1155/2021/6672773

Research Article

Research on English Translation Based on Functional Equivalence Theory and Genetic Algorithm

Yuan Liu and Liangfeng Dong

Foreign Studies School of Xuzhou University of Technology, Xuzhou, Jiangsu 221000, China

Correspondence should be addressed to Yuan Liu; dlf@xzit.edu.cn

Received 11 October 2020; Revised 22 November 2020; Accepted 10 December 2020; Published 7 January 2021

Academic Editor: Hongju Cheng

Copyright © 2021 Yuan Liu and Liangfeng Dong. This is an open access article distributed under the Creative Commons Attribution License, which permits unrestricted use, distribution, and reproduction in any medium, provided the original work is properly cited.

With the increasing development of our country and the world, the importance of English as an international language is self-evident. But we have difficulty in English translation, especially the vocabulary and translation of business English letters, not only because we have different living habits but also because we have different ways of speaking. Based on the research of functional equivalence theory and the calculation of a genetic algorithm, the vocabulary and translation of business English letters will be better improved. This can help us communicate better with each other and learn from the advanced Western experience in China. Through the study of the algorithm, the computational advantages of the algorithm are proved. The study of this English translation model will further improve the progress and promotion of existing translation technology.

1. Introduction

With the steady implementation of General Secretary Xi Jinping's strategy, China has become increasingly close to the international exchange [1, 2]. English as the most widely circulated language, its practical significance is self-evident. However, because of the habits of our society and the different ways of life, we have caused a lot of communication obstacles, which seriously affect the communication between our country and the Western developed countries and hinder the cultural exchange and economic intercourse between our country and the countries of the world [3, 4]. Not only that, the inaccurate translation may even cause some unpleasantness and contradictions. By using the theory of functional equivalence and the mutual application of genetic algorithms, this can help us to carry out empirical research on business English letter vocabulary and translation [5]. By combining functional equivalence theory with genetic algorithms, the credibility of our research is also increased. In this paper, the calculation of a genetic algorithm is studied [6, 7]. First, from the calculation of the definition of genetic algorithm calculation and calculation steps to start research, the genetic algorithm research process and calculation method are understood; then, the genetic algorithm calculation formula and calculation steps are carried out in a comprehensive understanding of the calculation [8, 9].

Then, we build the mathematical model and compute the computer model according to the mathematical formula we calculate and optimize. At the end of the paper, the genetic algorithm is tested and calculated. The study of a genetic algorithm has increased the depth of our research and reduced the work pressure of our English translation work [10]. Based on the research of functional equivalence theory and the calculation of the genetic algorithm, the vocabulary and translation of business English letters will be better improved. This can help us communicate better with each other and learn from the advanced Western experience in China. Through the study of the algorithm, the computational advantages of the algorithm are proved. The study of this English translation model will further improve the progress and promotion of existing translation technology.

2. Related Work

Heredity is a kind of new computer algorithm that American scholar simplifies simulation according to the genetic system of biological in nature [11, 12]. This new computer algorithm, which we study in the genetic system of biological

organisms in nature, helps us to compute the various aspects according to the genetic laws of biology. Genetic algorithm is unanimously praised for its unique information processing mode. And we know that the way in which biological genetic systems are transmitted and the information processing patterns are excellent and accurate [13].

The study of the genetic model helps us to deal with some optimal values and the calculation of the optimal solution. Genetic algorithm has been widely referenced in various fields in the world by virtue of its powerful ability of optimal solution calculation. In China, in the '90s, the study of a genetic algorithm was introduced [14, 15]. More than 20 years of computational learning has made our domestic research at the forefront of the world. Through continuous research, domestic scholars have developed several genetic algorithms suitable for our domestic use of the calculation version. In this paper, the calculation of a genetic algorithm is based on the domestic research of a genetic algorithm for purposeful optimization [16, 17]. At present, the computational version of a genetic algorithm developed by domestic scholars has been gradually accepted by the whole world. Domestic research plays a pivotal role in the world.

3. Methodology

3.1. Application Steps of a Genetic Algorithm. The genetic algorithm used in this paper is not a classical genetic algorithm, and the genetic algorithm based on a traditional genetic algorithm is obtained [18]. But before we study the genetic algorithms used in this paper, traditional genetic algorithms need to be studied and analysed. Only after we have understood the computational process of traditional genetic algorithms can we optimize the study. The traditional computational process of a genetic algorithm is based on the genetic calculation of biological individuals. The genetic mutation process of genetic operators is also very simple, only by crossover, selection, and mutation three ways [19]. But for the common problems, the traditional algorithm can be solved completely. The traditional genetic algorithm mainly uses the genetic operator to compute the problem of our computation and can simplify the process of many very complicated computational problems. Then, the traditional computational process of a genetic algorithm will be studied by us [20].

For different problems, the computational process of a genetic algorithm has a certain difference. But the main computational process is the same, and we mainly analyse the common computational steps in our calculations. Usually, in the calculation, the genetic algorithm is calculated as follows: first, before the calculation, the decision variables in the calculation process need to be set by us. The decision variable determines whether the genetic operator in our calculations can be inherited. This is one of the key issues in our calculations [21, 22]. The setting of decision variables directly affects the accuracy of our calculation results. If the decision variable is set incorrectly, then the calculation will not be the result we need, whether it is correct or not. The genetic variation of chromosomes is like the process shown in Figure 1.

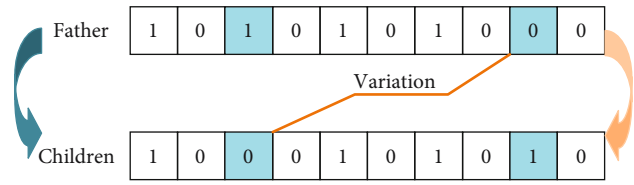

Figure 1: Chromosome genetic variation process.

The role of decision variables is a criterion of judgment. The data that is correct and we need will be intercepted, and the data that we do not need or incorrect will be deleted. Then, we can analyse the problem of solving a genetic algorithm. This part is the basis of our calculation, and the analysis of the problem of a genetic algorithm is a sort of our calculation purpose [23]. A clear calculation process and a calculated target will make our results more accurate. The problem of solving the genetic algorithm is the core of our calculation, and our calculation process revolves around the solution problem of our calculation. The process is to make our calculations clear by our research. Then, a study of individual forms of expression can be conducted. The individual representations of our calculations are determined [24].

Then, based on what we have studied above, the mathematical model can be built. For the establishment of the mathematical model, it is mainly to study the target illusion and the calculation of various formulas. The objective function is based on the analysis of the decision variables mentioned above. Our computational process has not really been completed after the mathematical model has been established [25, 26]. We also need to build a computer computing model, because we know that genetic algorithms are computed by computer models. For the establishment of a computer computing model, we should mainly pay attention to the chromosome encoding and decoding process. Chromosomes are the carriers of our computational process, and the various computational analyses of genetic information in our calculations are based on chromosomes [27]. The coding process of chromosomes requires strict attention. Chromosome encoding should reflect the specific form and location of our genetic information. In addition, we need to match the decoding process. The computer calculates the result in the code form so that the computation result cannot be understood by the human. So, the reasonable decoding process needs to be developed according to the coding process, and the calculation result of the whole algorithm can be exported [28]. For the traditional genetic algorithm of the calculation process, it is shown in the form of Figure 2.

After the above content is set up, the evaluation method of the fitness needs to be set up. And then there is the genetic design. The genetic operator, which carries our computational content, is one of the key parts of our entire computational process [29, 30]. The smallest unit of operation, such as crossover mutation, is the genetic operator, which is also the smallest unit of calculation in our calculations. So, the calculation process and design process of the whole genetic algorithm are studied.

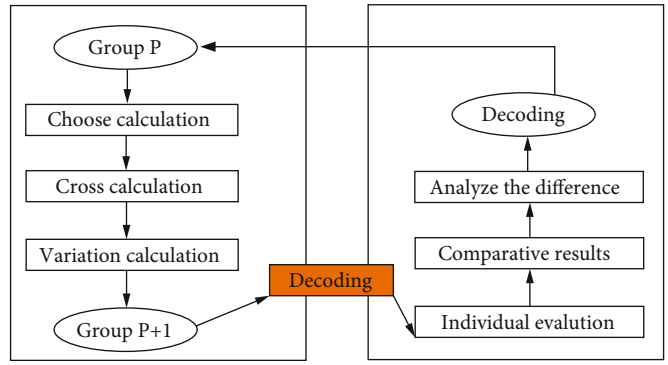

Figure 2: Traditional genetic algorithm calculation process.

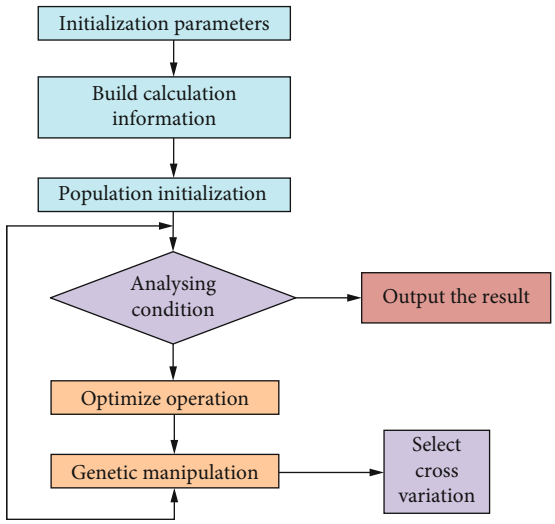

Figure 3: Mathematical model of genetic algorithms.

3.2. Mathematical Formula and Mathematical Model of a Genetic Algorithm. The calculation steps and design process of the genetic algorithm are studied, and the mathematical formula and mathematical model of the genetic algorithm are designed. The computational study of the mathematical model is mainly on the calculation of the fitness [31]. Biological heredity in nature is based on the rules of survival of the fittest. Highly adaptable individuals are more likely to inherit. The individual fitness is determined by the genetic operator, which is carried on the chromosome so that an individual is depicted step-by-step [32]. Next, the computational research and optimization process of the genetic algorithm are analysed.

First, genetic codes and new populations are established. A new population of chromosomes consisting of N is randomly determined:

$$\text{pop}_i(t), \quad i = 1, 2, 3, \cdots, N. \tag{1}$$

To calculate fitness, the fitness function is expressed as

$$f_i = f\ \text{int ness}(\text{pop}_i(t)). \tag{2}$$

The probability of the fitness is

$$P_{\text{i}} = \frac{f_i}{\sum_{i=1}^{N} f_i}. \tag{3}$$

The range of changes for each parameter is determined and is represented by a binary number. For example, if the variation range of the parameter a is $[a_{\min}, a_{\max}]$, it is represented by a binary b of m bit:

$$a = a_{\min} + \frac{b}{2^m - 1}(a_{\max}, a_{\min}). \tag{4}$$

At this point, the parameter range should cover all the optimization space. The determination of word length m should be as small as possible in order to minimize the complexity of the genetic algorithm. The binary number that represents the parameter is threaded to form a long binary string, which is the object of the genetic algorithm [33].

There are usually two ways to produce an initial population:

(1) A completely random method can be used to produce a case without any prior knowledge

(2) For some prior knowledge, it is necessary to select samples randomly after satisfying the requirement of prior knowledge

The size of the fitness determines the probability that the individual is inherited into the next generation. The adaptability must be nonnegative, in order to satisfy this condition; the basic genetic algorithm uses the following method to transform [34].

$$\begin{aligned} \text{Fit}(f(x)) &= \frac{1}{1 + C + f(x)}, \quad C \geq 0,\ C + f(x) \geq 0, \\ \text{Fit}(f(x)) &= \frac{1}{1 + C\text{-}f(x)}, \quad C \geq 0,\ C + f(x) \geq 0. \end{aligned} \tag{5}$$

The adaptability ratio method (fitness proportional model), also known as the betting wheel method, determines the selected probability of the individual according to the proportion of the whole population fitness [35]. If the

Table 1: Optimization genetic algorithm and the advantages and disadvantages of the traditional genetic algorithm, a comparison table.

Algorithm class	Disadvantages	Advantages
Optimized genetic algorithm	The calculation rules are cumbersome Set up more trouble	Calculate a small amount High accuracy Eliminate, do not repeat the calculation
Traditional genetic algorithm	Accuracy at the end Calculate for a long time	Longer use Computationally cumbersome

Table 2: Function test parameter setting table.

Function parameter	Population size	Binary code length	The maximum genetic algebra	Variation in the operation of the parameters
F (1)	100	20	200	$K = 0.1$
F (2)	100	20	200	$K = 0.1$
F (3)	100	20	500	$K = 0.05$
F (4)	100	20	500	$K = 0.05$
F (5)	200	20	500	$K = 0.05$

population number is n and the fitness of the individual i is $f(i)$, then the probability of the individual i selection is p. The total probability of the individual is Q_t, which determines which individual participates in mating through probability calculation and allocation. The probability of the individual i being selected is p. The calculation formula of the individual total probability is as follows:

$$P_i = \frac{f_i}{\sum_{i=1}^{N} f_i},$$
$$Q_t = \sum_{j=1}^{i} p_j, \quad j = 1, 2, 3, \cdots, i. \tag{6}$$

In the above calculation process, not only the traditional genetic algorithm of the computational process has been completed but also the genetic algorithm has been reasonably optimized. The mathematical model of the genetic algorithm is analysed in Figure 3.

Through our genetic algorithm optimization, it is more suitable for the calculation of the use of this article. The accuracy of the whole calculation process is increased. The advantages of our optimization are shown in Table 1.

4. Result Analysis and Discussion

In the computational research above, the computational procedure of the genetic algorithm and the calculation formula and the computer model are completed. However, the algorithm needs to be tested properly before it is put into use. Because each algorithm has a certain flaw, the test of the algorithm is to find the relatively weak link to continue optimization research. Then, we began to design the experimental process, the test process. Five groups of experiments were established. Five groups of experiments each group except our unique variable, the other test environment is the same. We mainly study the accuracy of calculation and the change of population mean value and adaptability. The parameters we tested are designed as shown in Table 2.

The data in the table above is entered into the computer calculation model. Then, we began to design the experimental process, the test process. Five groups of experiments were established. The five groups of experiments were calculated and shaped five times and then averaged. In the computational research above, the computational procedure of the genetic algorithm and the calculation formula and the computer model are completed. After decoding the results, the results are shown in Table 3.

For the analysis of the experimental data in Table 3, we can know that our optimized genetic algorithm can perfectly eliminate the problem of local minima in traditional genetic algorithm calculation. The calculated results in the table are consistent with the results we have already known. It can be found that the computational accuracy of the optimized genetic algorithm can be higher than that of the traditional genetic algorithm by 23%. This is a great advantage, the traditional genetic algorithm 74% to improve the accuracy of the calculation with 97%, which basically meets our testing requirements. Research on the Identification of English Translation Efficiency is shown in Figure 4.

We specify that the calculation accuracy of more than 95% is called to be qualified. The computational accuracy of the optimized algorithm is fully qualified. In this paper, we also find a point in the calculation process, that is, we optimize the genetic algorithm after the calculation time is only one-third of the traditional algorithm. This greatly shortens the time we calculate so that we can compute more data within the same time. In addition, the minimum fitness of 0 to 80 computational individuals has also been tested. The minimum degree of fitness is related to the number of iterations we calculate. The greater the degree of adaptability, the shorter the time that the result of our calculations will appear. It means that the shorter the number of iterations, the shorter the computation time. The change of the minimum fitness to the increase in the number of individuals is shown in Figure 5.

In Figure 4, we can see that as the computational individual increases, the degree of adaptability is reduced and concentrated. The calculation result is unique, but the increase of the calculated item results in the decrease of the fitness average. We can see that the degree of adaptability is constantly concentrated as the number of items increases. This shows that the calculated time does not increase significantly

Table 3: Contrast experimental calculation result comparison table.

Function	Traditional genetic algorithm		Optimized genetic algorithm	
	(x, y)	The optimal value	(x, y)	The optimal value
F (1)	(-0.073314, 1.521994)	8.105630	(1.564704, 0.01176)	8.09791
F (2)	(-0.000000, 0.000000)	1.000000	(-0.0022775, -0.0021200)	0.999990
F (3)	(0.976540, 1.000000)	0.000000	(1.002351, 1.000168)	0.018176
F (4)	(0.087977, -0.713587)	-1.031606	(0.0998189, -0.7107720)	-1.031193
F (5)	(-0.073314, 1.521994)	7.105630	(1.564704, 0.01176)	7.09791

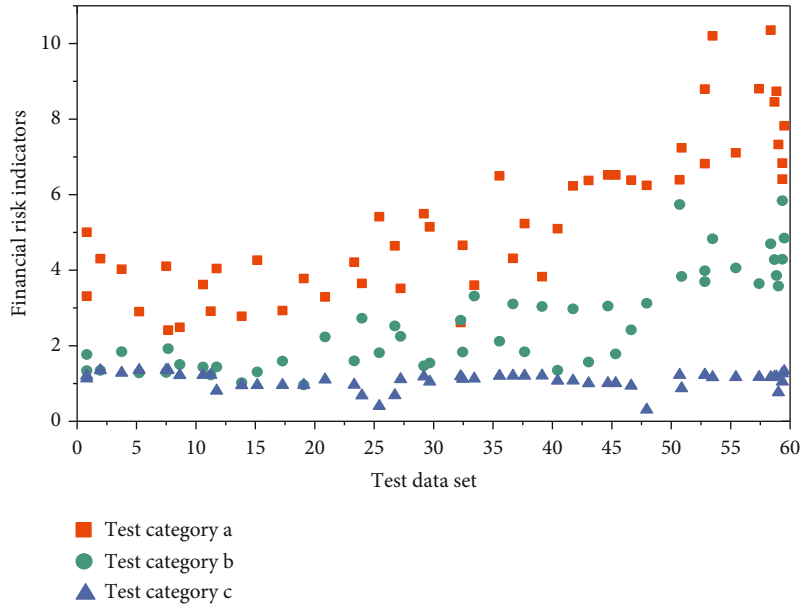

Figure 4: Research on the Identification of English Translation Efficiency.

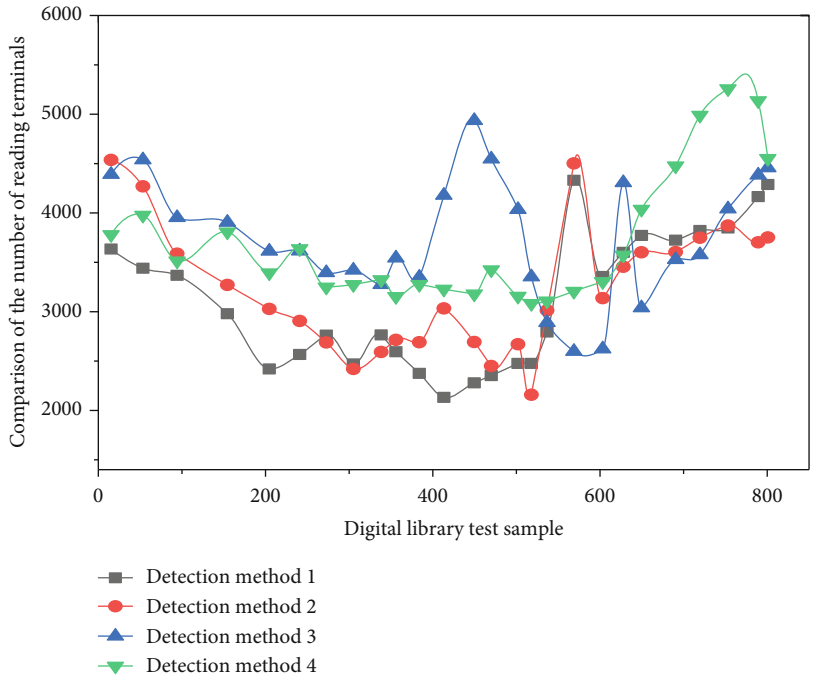

Figure 5: Changes in the fitness of the smallest number of individuals against the increase in the number of cases.

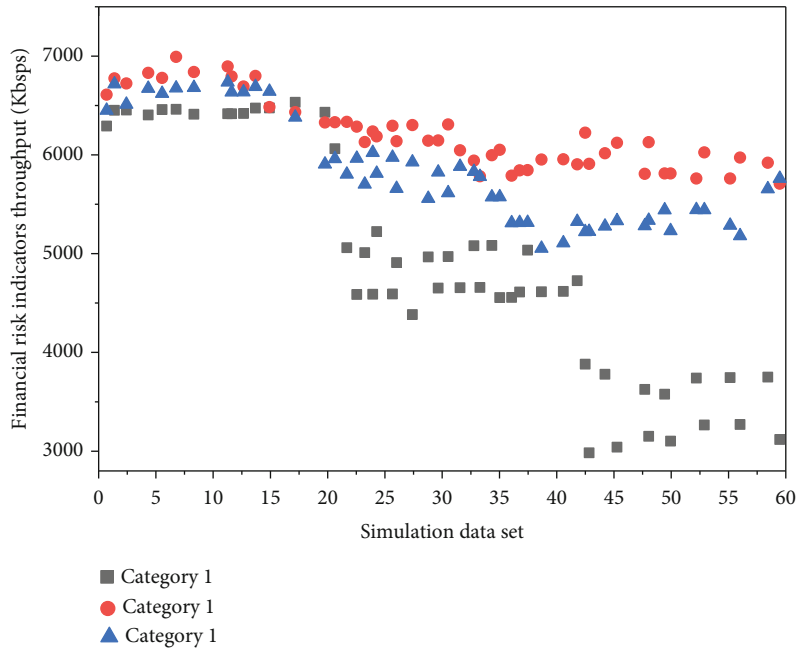

Figure 6: Variation of the population mean value as the number of iterations increases.

because of the increased number of calculated items. This greatly shortens the time we calculate so that we can compute more data within the same time. In addition, the minimum fitness of 0 to 80 computational individuals has also been tested. The minimum degree of fitness is related to the number of iterations we calculate. It is proved that our optimized algorithm can deal with many individual computations. In addition, the change of mean size as the number of iterations increases is also studied. The number of iterations is set to 100. The changes of the population mean change with the increase of the number of iterations were observed. The changes are shown in Figure 6.

From the graph, we can see that with the increase of the number of iterations, the change of the group mean is decreasing with the increase of the number of iterations. But the population mean is more and more concentrated. Our results are output in the form of an individual, so the image is a single point, not a curve. The mean of the group is more and more concentrated, which shows that we can solve the difficult problem in our calculation, and the optimized algorithm is still able to calculate the result. And we can figure out how many sets of results we need.

5. Conclusions

Today, the communication between the state and the state is becoming more and closer. In addition, English as the universal language internationally, its importance is self-evident. However, because of social and various reasons, it is difficult for us to translate English documents accurately. Therefore, the theory of functional equivalence was studied and combined with a genetic algorithm to help us to prove the study of translation. Through our test of the algorithm, we find that the average computational accuracy of our optimized genetic algorithm can be higher than that of the traditional genetic algorithm 23%. The calculation accuracy of the traditional genetic algorithm 74% is increased by 97%. And the calculation time of the whole calculation is shortened to one-third of the original algorithm. And through our optimization, the problem of iterative times of the genetic algorithm is reduced greatly, and the problem of local minima is eliminated. In addition, our optimized algorithm can still calculate the result for the difficult problem in our calculation. This is a great advantage of our optimized genetic algorithm.

Data Availability

All the data are authentic and reliable, and the sources are available from official sources.

Conflicts of Interest

The authors declare no conflict of interest.

Acknowledgments

This paper is supported by Jiangsu Provincial Higher Educational Philosophy and Social Research Programme (2019SJA0979).

References

[1] Z. Yan Kai, F. Sze Ming, J. Nyan Ping, C. Po Yu, and L. Albert, "Experimentally-implemented genetic algorithm (Exp-GA): toward fully optimal photovoltaics," *Optics Express*, vol. 23, pp. A1324–A1333, 2018.

[2] E. R. Thomas, "Sociophonetic trends in studies of Southern U.S. English," *Journal of the Acoustical Society of America*, vol. 147, no. 1, pp. 529–540, 2020.

[3] A. Stevanovic, P. T. Martin, and J. Stevanovic, "VisSim-based genetic algorithm optimization of signal timings," *Transportation Research Record*, vol. 2035, pp. 59–68, 2018.

[4] Z. Song, "English speech recognition based on deep learning with multiple features," *Computing*, vol. 102, no. 3, pp. 663–682, 2020.

[5] D. V. René and H. Fred, "English translation of the Dutch blood transfusion guideline 2011," *Clinical Chemistry*, vol. 58, pp. 1266-1267, 2020.

[6] P. Li, G. C. Constantinescu, N.-T. A. Nguyen, and C. C. Jeffery, "Trends in reporting of swallowing outcomes in oropharyngeal cancer studies: a systematic review," *Dysphagia*, vol. 35, pp. 18–23, 2019.

[7] J. N. E. Ölmestig, I. R. Marlet, A. H. Hainsworth, and C. Kruuse, "Phosphodiesterase 5 inhibition as a therapeutic target for ischemic stroke: a systematic review of preclinical studies," *Cellular Signalling*, vol. 38, pp. 39–48, 2017.

[8] P. Olen, "A forgotten strand of reception history: understanding pure semantics," *Synthese*, vol. 194, pp. 121–141, 2017.

[9] I. Mitxelena and M. Piris, "Analytic gradients for spin multiplets in natural orbital functional theory," *Journal of Chemical Physics*, vol. 153, no. 4, article 044101, 2020.

[10] L. Michaeli and A. Bahabad, "Genetic algorithm driven spectral shaping of supercontinuum radiation in a photonic crystal fiber," *Journal of Optics*, vol. 20, no. 5, article 055501, 2018.

[11] Z. Liu, "A study on English translation of tourism publicity in coastal cities from the perspective of cross-cultural communication," *Journal of Coastal Research*, vol. 115, no. sp1, p. 87, 2020.

[12] N. Lazarovich and A. Levit, "Edge Kempe equivalence of regular graph covers," *Journal of Graph Theory*, vol. 93, pp. 553–559, 2019.

[13] P. Klein, A. Friedman, M. Q. Hameed et al., "Repurposed molecules for antiepileptogenesis: missing an opportunity to prevent epilepsy?," *Epilepsia*, vol. 61, pp. 359–386, 2020.

[14] W. H. Jost, A. Rizos, P. Odin, M. Löhle, and A. Storch, "King's Parkinson's disease pain scale: intercultural adaptation in the German language," *Nervenarzt*, vol. 89, no. 2, pp. 178–183, 2018.

[15] S. Jinyoung, G. Aejin, K. Hyeonyoung et al., "Validation study for the Korean version of fear of cancer recurrence inventory," *Journal of Korean Medical Science*, vol. 32, no. 11, pp. 1792–1799, 2017.

[16] J. H. Jensen, "A graph-based genetic algorithm and generative model/Monte Carlo tree search for the exploration of chemical space," *Chemical Science*, vol. 10, no. 12, pp. 3567–3572, 2019.

[17] H. J. Jensen, "A graph-based genetic algorithm and generative model/Monte Carlo tree search for the exploration of chemical space," *Chemical Science*, vol. 10, pp. 3567–3572, 2019.

[18] J.-F. Danel and L. Kazandjian, "A simple scaling law for the equation of state and the radial distribution functions calculated by density-functional theory molecular dynamics," *Physics of Plasmas*, vol. 25, no. 6, article 060702, 2018.

[19] K. Indrek and F. Mike, "Omics approaches for subcellular translation studies," *Molecular Omics*, vol. 14, pp. 380–388, 2018.

[20] H. Hong, M. Panahi, A. Shirzadi et al., "Flood susceptibility assessment in Hengfeng area coupling adaptive neuro-fuzzy inference system with genetic algorithm and differential evolution," *Science of the Total Environment*, vol. 621, pp. 1124–1141, 2018.

[21] P. Gooding, B. Mcsherry, and C. Roper, "Preventing and reducing "coercion" in mental health services: an international scoping review of English-language studies," *Acta Psychiatrica Scandinavica*, vol. 142, no. 1, pp. 27–39, 2020.

[22] D. W. Gong, J. Sun, and Z. Miao, "A set-based genetic algorithm for interval many-objective optimization problems," *IEEE Transactions on Evolutionary Computation*, vol. 22, no. 1, pp. 47–60, 2018.

[23] M. Giassi and M. Goteman, "Layout design of wave energy parks by a genetic algorithm," *Ocean Engineering*, vol. 154, pp. 252–261, 2018.

[24] C. Figdor, "On the proper domain of psychological predicates," *Synthese*, vol. 194, no. 11, pp. 4289–4310, 2017.

[25] M. V. J. Felipe, Y. A. Kinkhabwala, S. Jeffrey, C. Itai, and T. A. Arias, "Density-functional fluctuation theory of crowds," *Nature Communications*, vol. 9, no. 1, p. 3538, 2018.

[26] A. Ebrahim, T. S. H. Martin, P. J. Mumby, A. D. Olds, and I. R. Tibbetts, "Differences in diet and foraging behaviour of commercially important rabbitfish species on coral reefs in the Indian Ocean," *Coral Reefs*, vol. 39, pp. 977–988, 2020.

[27] B. Doerr and C. Doerr, "Optimal static and self-adjusting parameter choices for the $(1 + (\lambda, \lambda))$ genetic algorithm," *Algorithmica*, vol. 80, no. 5, pp. 1658–1709, 2018.

[28] K. N. Dew, A. M. Turner, Y. K. Choi, B. Alyssa, and K. Katrin, "Development of machine translation technology for assisting health communication: a systematic review," *Journal of Biomedical Informatics*, vol. 85, pp. 56–67, 2018.

[29] S. E. Detiger, A. F. Karim, R. M. Verdijk, P. M. V. Hagen, and D. Paridaens, "The treatment outcomes in IgG4-related orbital disease: a systematic review of the literature," *Acta Ophthalmologica*, vol. 97, no. 5, pp. 451–459, 2019.

[30] D. Deng and N. Xue, "Translation divergences in Chinese–English machine translation: an empirical investigation," *Computational Linguistics*, vol. 43, pp. 521–565, 2017.

[31] P. Das, A. Kuznetsova, M. O. Zhu, and R. Milanaik, "Dangers of machine translation: the need for professionally translated anticipatory guidance resources for limited English proficiency caregivers," *Clinical Pediatrics*, vol. 58, no. 2, pp. 247–249, 2018.

[32] C. Contaldi, F. Vafaee, and P. C. Nelson, "Bayesian network hybrid learning using an elite-guided genetic algorithm," *Artificial Intelligence Review*, vol. 52, pp. 245–272, 2018.

[33] Z. Chen, G. Laura, and T. Donald, "Multiconfiguration pair-density functional theory for iron porphyrin with CAS, RAS, and DMRG active spaces," *Journal of Physical Chemistry A*, vol. 123, pp. 3389–3394, 2019.

[34] J. Carson, D. Cenzer, and J. B. Remmel, "Effective categoricity of automatic equivalence and nested equivalence structures," *Theory of Computing Systems*, vol. 64, pp. 1110–1139, 2020.

[35] H. Aziza and S. Krichen, "Bi-objective decision support system for task-scheduling based on genetic algorithm in cloud computing," *Computing*, vol. 100, no. 2, pp. 65–91, 2018.

Hindawi
Wireless Communications and Mobile Computing
Volume 2020, Article ID 8889148, 11 pages
https://doi.org/10.1155/2020/8889148

Research Article

Research on Value Integration Mode of Agricultural E-Commerce Industry Chain Based on Internet of Things and Blockchain Technology

Xiaochun Li[1,2] **and Dan Huang**[3]

[1]*Economic College, Hunan Agriculture University, Changsha 410128, China*
[2]*Oriental Science & Technology College, Hunan Agricultural University, Changsha 410128, China*
[3]*Hunan Urban Professional College, Changsha 410137, China*

Correspondence should be addressed to Xiaochun Li; lixiaochun116@hunau.edu.cn

Received 26 August 2020; Revised 27 November 2020; Accepted 16 December 2020; Published 31 December 2020

Academic Editor: Hongju Cheng

Copyright © 2020 Xiaochun Li and Dan Huang. This is an open access article distributed under the Creative Commons Attribution License, which permits unrestricted use, distribution, and reproduction in any medium, provided the original work is properly cited.

With the development of Internet technology, especially the application of mobile Internet technology in people's daily lives, people's lifestyles and production methods have changed, and they have brought huge economic benefits to society. In order to improve the development quality of agricultural e-commerce and expand the integration model of e-commerce, the paper analyzes the development and changes of Internet technology in the agricultural industry chain from the source to operation, production, service, security, and sales and studies the production experience model iterative upgrade. At the same time, a blockchain-based agricultural product traceability system is proposed. The system has a good supervision effect. Once recorded on the blockchain ledger, all data cannot be changed, which plays a very good traceability role for agricultural e-commerce. Actual cases show that the integrated model of agricultural e-commerce based on blockchain technology can bring huge development potential to the e-commerce industry and can improve the security and traceability of agricultural e-commerce.

1. Introduction

Under the new normal economy, China's economy has entered an important period of slow growth and structural adjustment. The government strongly advocates the concept of Internet of things. Internet of things has become a national strategy and has become the engine of new economic development and the driving force of innovation-driven development. The Internet has entered China for 20 years, bringing profound changes to the economic development. Integrate into agriculture, transportation, energy, and medical and education industries; at the same time, with the change and upgrading of consumer demand for products, consumer Internet is also migrating to the industrial Internet evolution. Under this situation, China's agricultural industry urgently needs to say goodbye to the extensive and inefficient mode of production in the past and catch the high-speed train which combines with modern technology.

With the industrial Internet ushered in the golden age, Internet thinking has gradually penetrated into all areas of agricultural industry. The deep integration of the agricultural industry and the internet of things has become an essential magic weapon for the transformation and upgrading of the agricultural industry. Agricultural internet, agricultural e-commerce, and rural Internet finance guided by agricultural information can significantly improve the overall efficiency of the agricultural industry chain, promote the integration of agriculture and modern technology, become the development of agricultural downstream consumption, and renew the sales channels.

Increasing popularity of network communication infrastructure and smart mobile terminals as well as recent reports from the Ali Research Institute on "New Rural People," financing of semifinished fresh e-commerce "Young Vegetable King" and dirt-flow network, and sensation of Willow Peach Promotion Project and Lenovo Control, the event of

strategic investment in Yun farm fully reflects the concern and enthusiasm of industrial capital for the Internet of agricultural industry and e-commerce of agricultural products [1–3]. This paper mainly studies the integration mode of agricultural supply chain by analyzing the mode and deep learning algorithm and obtains a feasible integration mode.

Agriculture provides basic products to support national economic construction and development. At present, the traditional agricultural industry chain is facing the problems of low efficiency, high cost, and information asymmetry, and there are sharp fluctuations in the prices of agricultural products, agricultural products unsalable, and other phenomena. The change of e-commerce platform to agricultural industry is not only in marketing but also in rebuilding the agricultural industry chain. At present, China's agriculture has entered the era of Internet 3.0. With the wide application of Internet microelectronics and related software application platform in agriculture, the programmed participation of Internet has been realized in the circulation of agricultural resources, the management of agricultural product planting, the breeding and seedling selection of products, soil environment, and agricultural technology [4, 5]. Change the way of agricultural development, improve the land-use rate and productivity, and promote the transformation and upgrading of agriculture, agricultural industrialization and industrialization, modernization, and other management systems for scientific integration. It is a trend of China's agricultural development in the future to make information technology widely used in agricultural production and every link of agricultural production [6]. The rest of this paper is organized as follows. Section 2 discusses the development foundation of China's agriculture, followed by agricultural industry chain reconstruction analysis and suggestions designed in Section 3. The relationship model and empirical research on network consumer behavior and e-commerce service quality are discussed in Section 4. Section 5 concludes the paper with summary and future research directions [7].

2. Agricultural e-Commerce Structure

Internet of things represents a new economic form. It refers to the combination of the internet and traditional industries by relying on Internet information technology, so as to complete economic transformation and upgrading by optimizing production factors, updating business system, and reconstructing business model. The "Internet plus" plan is aimed at giving full play to the advantages of the Internet, deeply integrating the Internet with traditional industries, enhancing economic productivity through industrial upgrading, and finally increasing social wealth. The change of external environment and endogenous advantages are the key factors to promote the success of industrial transformation. Under the background that the agricultural economy urgently needs to be transformed and upgraded, the mobile Internet and agricultural scale are the basis of the transformation of modern agricultural industry. The structure of agricultural e-commerce in the background is shown in Figure 1.

3. Integration Mode of Industrial Chain Value

The new urbanization, the deepening of the reform of the circulation system, and the food security problems urgently need to be solved make the intensive production of rural land become a trend. By the end of the year 2014, China's cultivated land circulation area has reached 380 million, accounting for 28.8% of the total contracted cultivated land. With the subsequent land transfer into a standardized and normalized stage, the scale of agricultural production is bound to speed up, and once the scale of management becomes the mainstream trend, it is bound to completely change the existing extensive mode of agricultural production and management. Compared with traditional small-scale farming, large-scale operation requires a large number of working capital, large-scale procurement of agricultural asset products, the introduction of information technology to continue to improve the permeability, rapid development of agricultural information, and the scale of land reform, new farmers, and household farmers. The gradual formation of new business entities such as farms, professional cooperatives, and modern agricultural enterprises marks the arrival of the era of the agricultural Internet, which is carrying out a comprehensive deconstruction and remodel of the agricultural chain, from the sale of agricultural means of production, letters, and so on. Information intermediary services, land flow to agricultural production, agricultural product sales, Internet giants, and agricultural enterprises with Internet thinking from the agricultural chain of active layout are trying to use the Internet to explore a variety of new agricultural industries. Business mode is shown in Figure 2.

Under the Internet mode, the agricultural industry chain will form a brand-new business model, which will provide more integration space for the trillions of markets of agricultural means of production and sales of agricultural products. Second, in the field of circulation of means of production, the e-commerce platform for agricultural means of production will gradually replace the traditional agricultural material sale system; third, in the field of product circulation, agricultural product e-commerce will also replace the original channel and form a new agricultural product trading system; fourth, in the demand side of agricultural products, consumers and industrial enterprises can achieve remote customization according to specific preferences to achieve order agricultural production; fifth, provide a complete logistics sale system in the rural market. Sixth, the demand for comprehensive services will lead to the integration of all types of business entities in the industrial chain and form unified platform operators, providing integrated platform services; at the same time, all kinds of agricultural enterprises are facing major development.

The main process formula of deep learning algorithm is as follows:

$$S_j^{''}(x_i) = M_{j,i-1}\frac{x_i - x}{h_i} + M_{j,i}\frac{x - x_{i-1}}{h_i}, \quad (1)$$

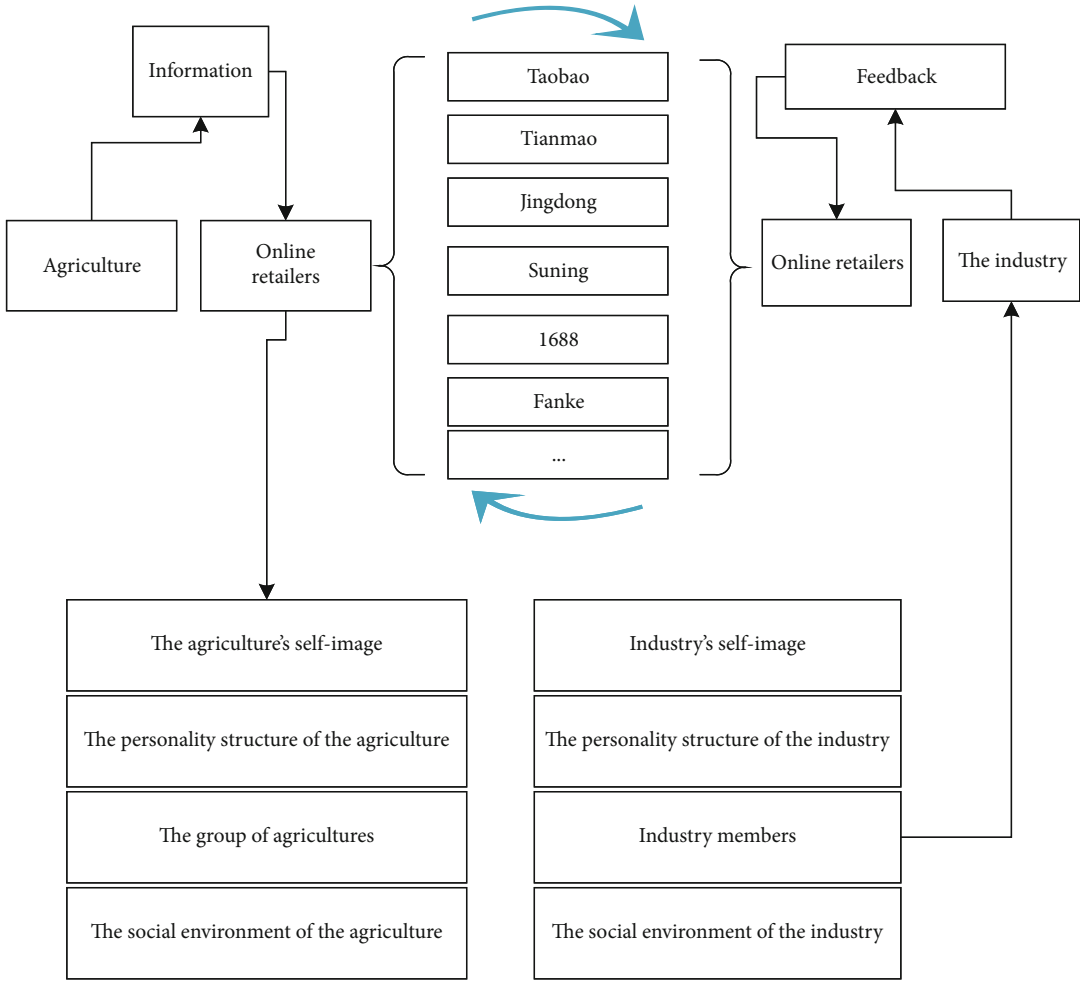

Figure 1: The structure of agricultural e-commerce.

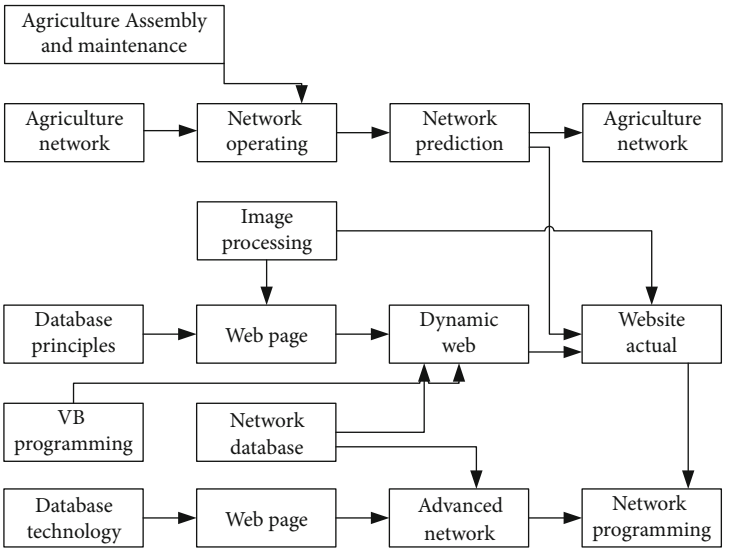

Figure 2: Business mode.

in which $h_i = x_i - x_{i-1}$. By interpolation and continuity of the relationship can be the following formula:

$$\lambda_i = \frac{h_i}{h_i + h_{i+1}}, \quad \mu_i = 1 - \lambda_i, \tag{2}$$

$$d_i = \frac{6}{2h}\left(\frac{y_{i+1} - 2y_i + y_{i-1}}{h}\right), \quad i = 1, 2 \cdots, n. \tag{3}$$

Seeking $M_{j,i}$, $(M_{j,0} = M_{j,n} = 0)$ can be solved by the chasing method, so that the cubic spline interpolation function of each subdivision of weighting vector can be obtained.

$$\begin{aligned} S_j(x_i) = {} & M_{j,i-1}\frac{(x_i - x)^3}{6h_i} + M_{j,i}\frac{(x - x_{i-1})^3}{6h_i} \\ & + \left(y_{i-1} - \frac{M_{j,i-1}}{6}h_i^2\right)\frac{x_i - x}{h_i} + \left(y_i - \frac{M_{j,i}}{6}h_i^2\right) \\ & \cdot \frac{x - x_{i-1}}{h_i} \ (i = 1, 2, \cdots, n), \end{aligned} \tag{4}$$

$$\text{Support}(X) = \frac{\text{count}(X \subseteq T)}{|D|}, \tag{5}$$

$$R\,; X \Rightarrow Y. \tag{6}$$

Rule support is the ratio of the number of transactions to the total number of transactions, when the item set X and Y appear simultaneously, as shown in the formula (3). According to the association rules of frequent items, it is considered that the support degree of frequent itemsets is consistent with that of the rule, as shown in formula (4). Under the same conditions of the credibility of the rules, the credibility confidence of rule R is the ratio of the number of transactions when X and Y appear at the same time and the number of transactions only when X appears, as shown in formula (5), which is confidence$(X \Rightarrow Y)$.

$$\begin{aligned} \text{Support}[X \Rightarrow Y] &= \frac{\text{count}(x \cup y)}{|D|}, \\ \text{Support}[X \Rightarrow Y] = \text{Support}(x \cup y) &= \frac{\text{count}(x \cup y)}{|D|}, \\ \text{confidence}(X \Rightarrow Y) &= \frac{\text{support}(X \cup y)}{\text{support}(X)}. \end{aligned} \tag{7}$$

The main research method of the Apriori algorithm is to find all the frequent items in the object database with the minimum support and then get the association rules quickly according to the frequent items. The specific procedure is as follows: check all transaction databases and find out all the frequent items in the database. The k-item set is selected by its own connection to select the project set C_k. The project set of candidate options is pruned according to the frequent itemset; any one of them is a subset of frequent item. If C_{k-1} is a subset of C_k, in the case of $C_{k-1} \notin L_{k-1}$, $C_k \notin L_k$, the set of comparisons is not a frequent subset, and the subset is deleted. Loop through the previous steps until the transaction database is not able to find a higher level of frequent itemsets. The entire data mining process ends when all the frequent items are identified by computing the associated rules that meet the needs.

With the advancement of agricultural modernization and the acceleration of land circulation, agriculture is on the way to large-scale management. With the increase of new intensive management subjects, higher requirements are put forward for the supply and service of agricultural products. In addition, the market capacity of agricultural materials in China is huge, and the scale of chemical fertilizer, seed, and feed alone exceeds trillion. In recent years, Internet giants have been "going to the countryside" to seize the rural e-commerce market, which is also conducive to the objective cultivation of rural e-commerce format, stimulate the vitality of rural e-commerce, and objectively contribute to the development of agricultural material e-commerce. In line with the general situation, the traditional agricultural material enterprises are changing their management mode of "producing one distributor and one planter." The new management mode will be married by providing better products, diversified supply of agricultural materials, and better technical services. With the more and more mature agricultural information system, the transformation of China's agricultural material producers to agricultural material service platform operators will be completed. Integration of agricultural commodity E-commerce will become an important channel and platform for agricultural commodity sales in the future. A number of agricultural commodity platforms with Internet thinking, large enough flow import, and sticky guarantee will have broad growth space. The operation mode of agricultural material Internet platform operators is shown in Figure 3.

However, as far as the current development situation is concerned, the development of China's agricultural material e-commerce has not yet formed a fixed model, and now, the more mature business models are mainly the third-party network sales platform (B2C) model, the third-party agricultural information platform (B2B2C) model [8]. In addition, according to the successful experience of foreign agricultural Internet development, most of the leading agricultural material enterprises in developed countries in Europe and the United States are engaged in the sale of a variety of agricultural material products, with strong integrated service capabilities [9]. Therefore, China's agricultural resource enterprises are expected to gradually develop into specialized enterprises. Flattening and integration under the promotion of online and offline (0.20) agriculture in the field of e-commerce will become modern agricultural products under the background of the Internet. [10–13].

The Internet of things is a new round of information revolution. Agricultural Internet of things has constructed the basic elements of information production. It has been recognized as the third wave of the world information industry after computers, the Internet, and mobile communication networks. It takes perception as the premise to realize the comprehensive interconnection of people, people and things, and things and things. Agricultural Internet of things (IOT)

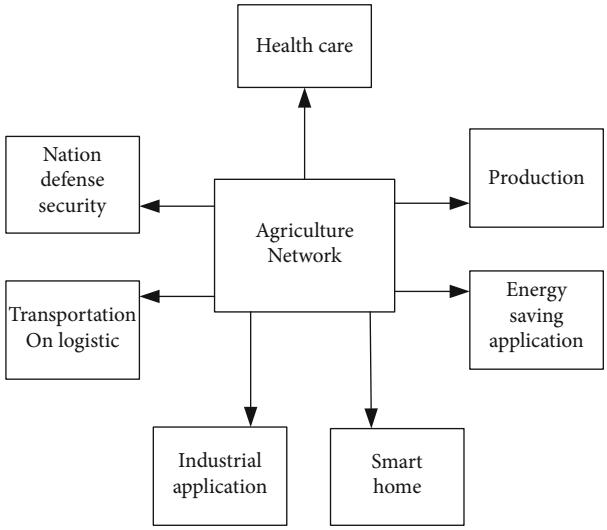

Figure 3: The operation mode of agricultural material Internet platform operators.

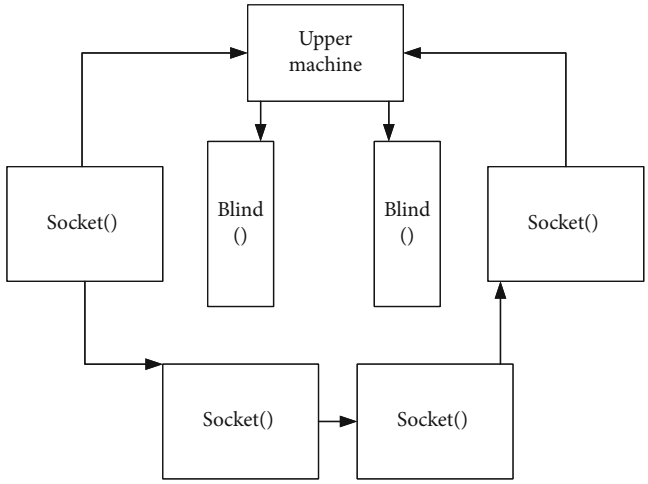

Figure 4: The agricultural Internet of things (IOT).

obtains crop information through sensor devices and transmits it on the basis of various networks [14]. After the central system is processed, the IOT performs remote operations. Information-based perception-network transmission-decision support-remote control is the IOT of agriculture. The essence of agricultural information is to transform agricultural production from traditional labor cultivation to efficient production by means of information and to build a comprehensive and deep interconnection between people and things which is the core element of agricultural information. Generally speaking, all forms of agricultural information belong to the category of agricultural Internet of things, which is the soul of agricultural information [15]. Throughout the country's latest application, the agricultural Internet of things (IOT) has worked in four main areas; the specific results are shown in Figure 4.

The cross-border entry of Internet enterprises into the rural Internet shows that the emerging industrial capital is optimistic about the rural market. The data transfer model is shown in Figure 5.

The core values of the development of agricultural Internet and agricultural e-commerce lie in resolving information asymmetry, completing vertical integration of industrial chain, reducing intermediate links, reducing circulation costs and enhancing scale effect, and establishing traceable agricultural product circulation system. To solve the financing problem in the supply chain, the accumulation of transaction information can help the supplier of capital to price the risk, and the control of logistics and capital flow can reduce the default risk for the financing in the industrial chain.

Looking forward to the future, with the increase in policy support and the reform of existing agricultural production and operation, the difficulties in organizing commodity sources, high logistics costs, imperfect cold chain logistics systems, and other constraints, the development of e-commerce bottlenecks related to solving agricultural problems and business related to agriculture is expected to show explosive growth [16–18].

By the end of 2014, China's agricultural-related loans (local and foreign currencies) had a balance of 23.6 trillion yuan, accounting for 28.1 percent of all loans, an increase of 13 percent over the same period of last year; all financial institutions had a balance of 19.4 trillion in local and foreign currencies (counties and below) in rural areas, accounting for the proportion of all loans. Total loans accounted for 23.2, a year-on-year increase of 12.4%. The compound growth rate of the above two indicators in the three years from 2011 to 2014 was also between 12 and 16. However, facing the "new trend" and "new normal" of the development of modern agricultural industry with scale, intensive, specialized, and modernized, the above-mentioned funds still cannot meet the growing demand for agricultural financial services. In addition, due to the underdeveloped economy, the income and expenditure of agricultural employees are extremely unstable, coupled with the lack of traditional agricultural financial service systems; these factors not only affect the enthusiasm of financial institutions to participate in agricultural finance but also limit people's access to agricultural finance. As a result, the financing channels for agricultural practitioners are very limited, and even in many places, family and friends lending and usury are still the main ones. Internet application rate in 2016 and 2017 in agriculture is shown in Figure 6.

With the realization of land mortgage rights (including homestead and farmland management rights), the problem of scarcity of collateral in the financing of agricultural enterprises has been effectively solved. Another factor restricting the development of rural finance is risk control, including subjective risk (credit difficulty) and objective risk (weather, epidemics, etc.). For the problem of difficult credit reporting, through the Internet, large data, cloud computing can also provide a more efficient solution. Among them, the fastest-growing large data credit is to use a large number of fragmented data generated in social networks, e-commerce websites, and internet lending platforms to better collect and analyze massive, decentralized customer data, from which to obtain valuable information. Through the use of this information, we can make a more accurate assessment of the personal

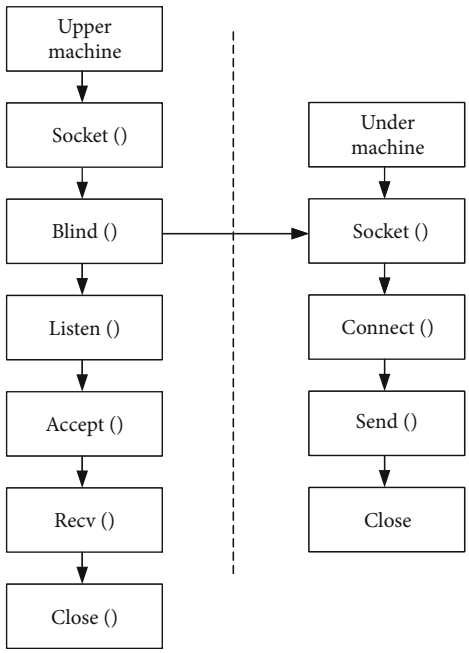

Figure 5: Data transfer model.

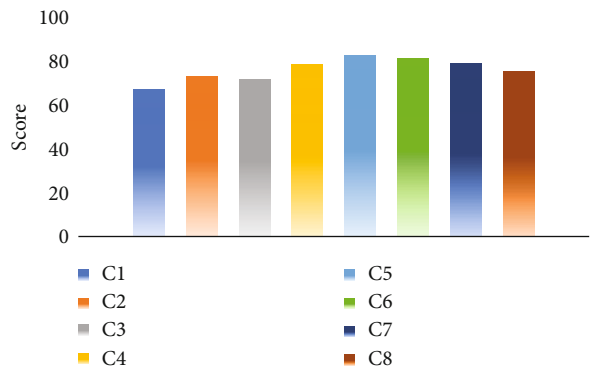

Figure 6: Internet application rate in 2016 and 2017 in agriculture.

credit situation; while cloud computing supports credit agencies or individuals in any location using a variety of terminals to access data storage and processing of various applications, without the need for the high cost of database development, operation, maintenance, management, and service is high. At present, some enterprises have obtained key information such as financial strength and credit evaluation of agricultural practitioners as their credit basis through the construction of large-scale data and rural Internet trading platform, which has played a practical credit effect. Based on the above reasons, with the further popularization and application of big data and cloud computing in the agricultural field, the new rural Internet financial industry will have strong vitality and will solve the problems faced by the development of agricultural modernization in the following aspects [19, 20].

The structure of agriculture-related finance is shown in Figure 7 [21].

The second problem that restricts the development of agriculture-related finance is the small amount of a single fund loan, the high cost of diversification, and the difficulty of management. In this regard, we can refer to the solution of e-commerce platform Jingdong. JD provides funds for farmers through credit sales, replicates JD's business model, and builds a basic social microstructure. The implementation of these measures provides a way to solve the second problem that restricts the development of agricultural finance [22].

There are three problems in restricting financial development related to agriculture: no guarantee, lack of collateral, and relying only on credit. The "Gu strategy" helps farmers increase their income by providing production technology and other support in conjunction with rural cooperatives [23]. At the same time, the country has a deep understanding of farmers, accumulated credit data, and expanded payment, insurance, and rent in rural areas through the grassroots financial service network. Leasing and other businesses provide a solution to this problem. Agricultural layout under the Internet plus background is shown in Figure 8 [24].

4. Analysis of Agricultural Industry Chain Reconfiguration

Production factors promote the networking of factor transactions. Land is the first element of agriculture, including seed, pesticide, fertilizer, and agriculture.

In traditional agricultural production, the demand for processing, transportation machinery, and land transfer is increasing, so the Internet technology will make use of information transparency advantages and shorten the intermediate links [25].

Agricultural technology services to promote expert service flat: agricultural production management has a certain demand for agricultural technology services to help solve various problems in agricultural production. At present, the level of agricultural technology links is still low [26].

Agricultural finance to promote public investment in agricultural investment: agriculture's demand for finance runs through the entire process of agricultural production. Internet crowds make use of the characteristics of the Internet and SNS communication, making agriculture more attractive to investment. The traditional rural financial institutions have been unable to meet the financing needs of the rapid development of agriculture, especially the traditional financial institutions that have the problems of difficult borrowing and expensive borrowing, and to a certain extent also affected the enthusiasm of farmers to borrow. With the help of Internet technology, when farmers ask for loans from the financial platform, they can complete the loan online with a single mouse. The whole process of borrowing can be completed in 2 hours from the borrower's application to the completion of the financing. This can reduce farmers' time and labor and solve problems such as "small agricultural loans" that banks are unwilling to make. The agricultural sales mode under the internet background is shown in Figure 9.

Agricultural product sales enter the C2C mode of agricultural product business. At present, there are more than 30,000 agricultural e-commerce platforms in China, among which there are 3,000 agricultural e-commerce platforms. Agricultural product e-commerce must establish a good

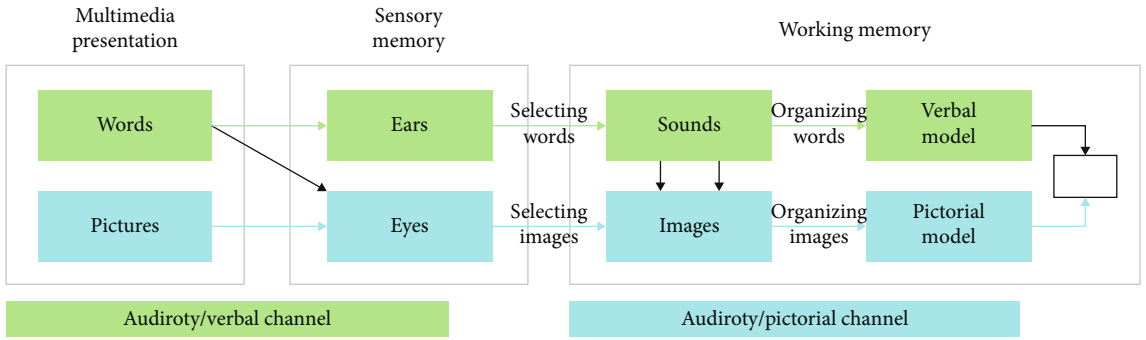

Figure 7: The structure of agriculture-related finance.

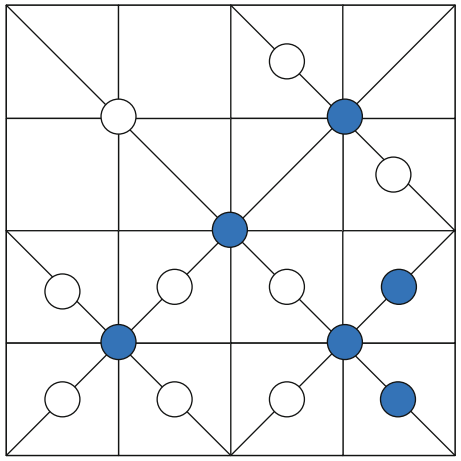

Figure 8: Agricultural layout under the Internet plus background.

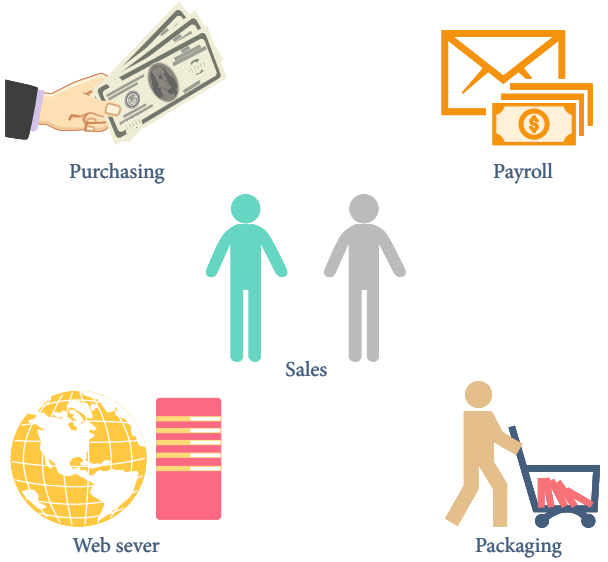

Figure 9: The agricultural sales mode under the internet background.

shopping experience with customers in order to meet the sustained consumption and drive the relevant consumer groups. The electricity supplier eliminates all kinds of obstacles, such as information and channels of traditional sale methods.

Because farmers lack brand awareness, they do not know many high-quality agricultural products. With the help of this platform, agricultural product brands can be effectively established. Vigidani means conscience in the Uyghur language, which is the name of conscience products. This has also enabled the company to gain recognition from more and more people. The company even has repeat customers, and many customers have become loyal supporters of the brand. In just three years of its free online advertising, Vigidani became a famous agricultural product brand.

The last kilometer of rural logistics in the traditional hierarchical wholesale mode has many problems, such as high cost, loss of logistics, poor communication of information, flat and transparent information on the Internet, large-scale agricultural products trading and distribution center based on Internet technology and logistics distribution system, storage and transportation, wholesale, trading, and auction. Function can achieve real-time market transactions.

In traditional agriculture, watering, fertilizing, and taking medicine, farmers rely entirely on experience and feeling. Nowadays, facility agricultural production base should not water, fertilize, and spray; how to maintain accurate concentration, including temperature, humidity, light, and carbon dioxide concentration, through artificial intelligence technology, can be perceived in advance and analyzed according to the production situation of crops, to provide standardized production decision-making for agricultural production, which is shown in Figure 10.

Agricultural product trace system collects and analyzes the quality and safety data of various links of planting and processing through the system and monitors and controls the quality and safety of the product life cycle. Agricultural big data effectively improve the accuracy of modern agriculture. Through the big data platform, farmers can understand market demand in time and effectively reduce production costs. Particularly, the market is unpredicted; some investors are prone to blindly follow the trend, such as the rise in pig prices this year, many people on a swarm of bees into the pig farming industry, resulting in excess capacity; the second year pig prices plummeted. Through big data, farmers can clearly understand the consumption situation of the market and avoid investment risks.

Actively build local characteristics of agricultural product e-commerce platform, push fresh agricultural products on the micro direct delivery platform, guide e-commerce

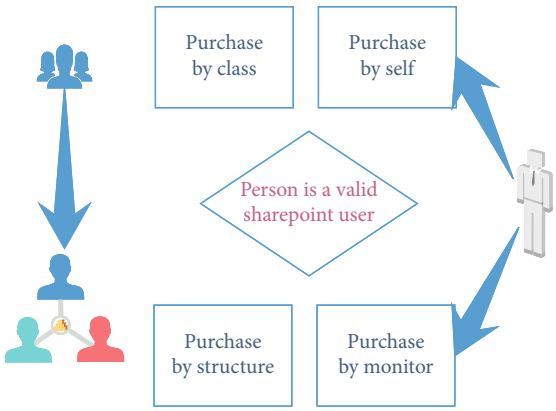

Figure 10: Standardized production decision-making for agricultural production.

enterprises to combine agricultural enterprises, and promote strong alliance. Through the Internet, farmers can be directly linked to the market, without the need for intermediate distributors, saving costs, but also conducive to improving farmers' income. Supporting large-scale and qualified enterprises develops intelligent farmland and cultivation by using sensor and Internet technologies.

Support large-scale qualified enterprises to develop the use of ERP, CRM, and other management information systems, and at the same time, improve the efficiency of enterprise operation and management, and open the chain from procurement, production to sales, and management information. These measures speed up enterprise response and improve flexible customization capabilities. Relying on cloud computing and big data technology, build a whole agricultural information integration service platform chain, improve big data analysis and data mining technology, and promote relevant information to provide reference for corporate decision-making. Promote mutual cooperation between enterprises to create a public "cloud" service platform for meteorological early warning, natural disaster early warning, major epidemic prevention and control, market price fluctuations, market feedback information, and so on.

In order to improve the hardware facilities and information technology ability training of agricultural and rural personnel, we should not only popularize computer and broadband information technology into the village but also cultivate and import technical personnel with operational ability to provide personnel support and intellectual support for the development of agricultural entrepreneurship. The steady and rapid progress of agricultural technology popularization makes agricultural technology of universities and research institutes directly face agricultural enterprises, promotes the transformation and application of scientific and technological achievements, and facilitates the promotion of agricultural products. Three algorithms running time comparison are shown in Table 1.

If the database condition was the same, but the minimum support degree was not the same, the running time of the three algorithms was tested, and the experimental results are shown in Figure 11. The operation time of the traditional Apriori algorithm is longer than that of the optimized two

Table 1: Three algorithms running time comparison.

Number of transactions (bar/million)	Running time (ms)		
	Apriori	DC-Apriori	FP-Apriori
0.5	780	568	516
0.6	950	458	432
0.8	1121	554	478
1	1570	626	673
1.2	1785	745	765
1.5	2210	987	899
2	3180	1872	1867

algorithms. Under different support degrees, the operation time also fluctuated due to the change of support degree, and the whole algorithm was in a state of instability. The other two optimization algorithms did not have such a situation. Not only the overall running time was more than the traditional Apriori algorithm segment but also there was no significant change in the operation, and the algorithm structure and operation were relatively stable. The traditional Apriori algorithm can dig out more frequent itemsets in the case of decreasing the minimum support degree, and the increase of quantity brought about the mass production of redundant rules, which made the execution time of the algorithm become longer and less efficient. The other two algorithms did not have this phenomenon and the implementation time did not have a big impact.

The results of comparison experiments for the maximum number of frequent itemsets generated by three different algorithms are shown in Figure 12. It can be seen from the comparison chart that, under the condition of the same minimum confidence, the number of mining of association rules is the traditional Apriori algorithm, and the number of the other two algorithms is similar. After the minimum confidence reduction, the mining results of the DC-Apriori algorithm proposed in this paper are the most stable and do not change the algorithm because of the fluctuations. But the FP-growth algorithm and the traditional Apriori algorithms have a lot of fluctuations, and the traditional Apriori algorithm produces a lot of useless rules that directly affect the results of the algorithm.

At present, China's rural areas are facing a major problem. A large number of young people and a strong labor force enter the cities, and only a few old people and children remain in the rural areas. By introducing entrepreneurs, it can not only stimulate the vitality of the village but also promote employment and attract more and more foreign young people to return to their hometowns to start businesses. At present, the Internet has been widely used in various industries; it also promotes the continuous integration of agriculture and other industries, such as agriculture and finance, through crowdsourcing and credit services of financial institutions, to solve many difficulties encountered in the process of agricultural development, thereby integrating integrated agricultural production, processing, and sales, while accelerating the transformation and upgrading of agricultural products. Highly value of agriculture frames is shown in Figure 13.

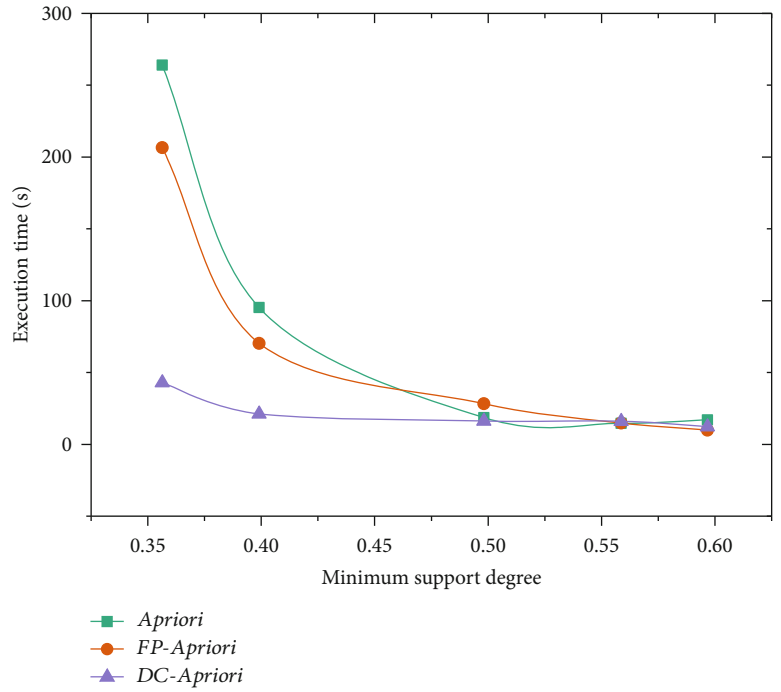

Figure 11: Comparison of algorithm running time.

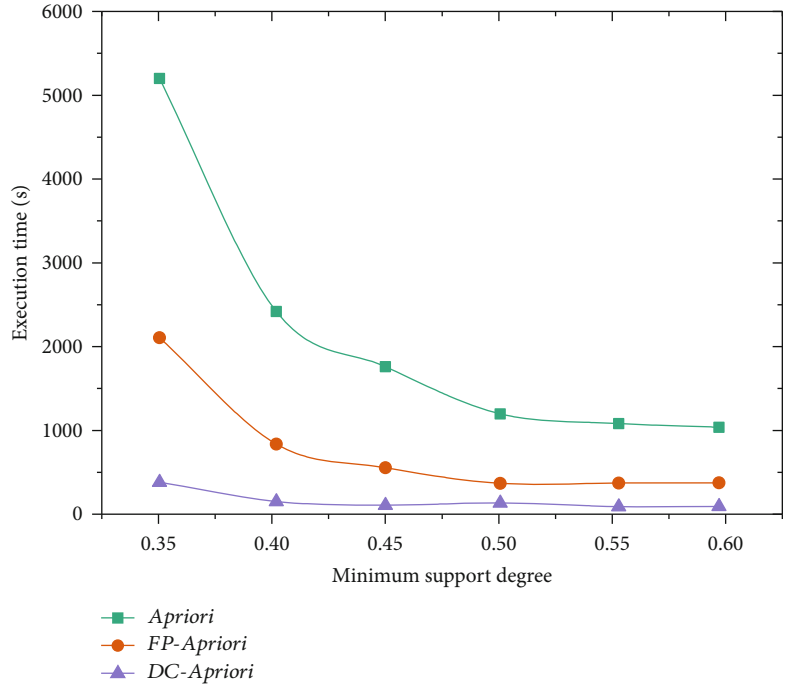

Figure 12: Comparison of the number of maximum frequent items.

5. Conclusions

The mode of operation and financing with the Internet as the carrier will be the accelerator of the development of modern agriculture in the future. "Internet-F-" restructuring of the agricultural industry chain is through the flow of information through all links, from the production of agricultural materials, circulation, marketing, services, and other aspects of agricultural production in the supply of agricultural materials, through the Internet cloud services, precision agriculture establishment of industry, large-scale data analysis, etc., to realize the upgrading of agricultural production technology, the difficulty of promoting agricultural scale, the quality and safety of agricultural products, and the realization of product value. The five perspectives of "sexualisation" comprehensively change the consumption market of

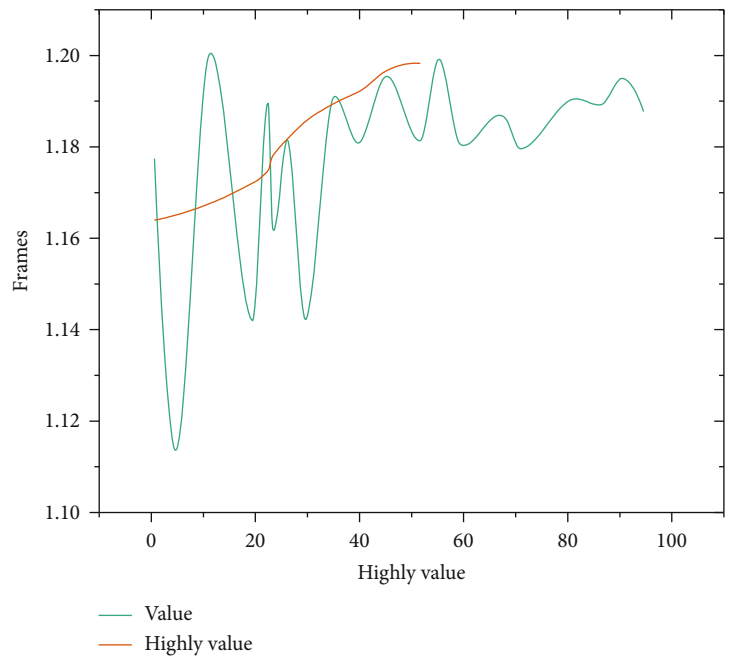

Figure 13: High-value agricultural line chart.

agricultural products and enhance the customer experience and customer stickiness of agricultural product consumers. In this process, the agricultural Internet platform has developed into the core of the industrial chain, which combines the material flow, capital flow, and information flow of the entire industrial chain, making the entire industrial chain "symbiotic, win-win, and mutually beneficial" and forming a perfect, extremely open information. As the founder of the agricultural Internet ecosphere, agricultural leading enterprises gradually develop to specialization, flatness, and integration, providing financial investment, financing, and online payment services for the whole industry upstream and downstream.

In the process of the establishment and development of the ecological circle, agricultural Internet finance will run through every process of agriculture, including the sale and purchase of agricultural materials, the whole process of agricultural production, the sale of agricultural products, and other links, so as to make comprehensive agricultural materials, e-commerce, and similar finance. The integration of service, on-line and off-line agrochemical service, has become the inevitable trend of the comprehensive development of modern agricultural industry.

Data Availability

All data can be obtained from the author.

Conflicts of Interest

We declare that there is no conflict of interest regarding the publication of this paper.

Acknowledgments

This work is supported by the Project of National Social Science Fund of China (Grant No. 17BZZ050).

References

[1] L. Huang and P. Liu, "Key technologies and alogrithms' application in agricultural food supply chain tracking system in E-commerce," in *Computer and Computing Technologies in Agriculture VII. CCTA 2013. IFIP Advances in Information and Communication Technology, vol 420*, D. Li and Y. Chen, Eds., pp. 77–133, Springer, Berlin, Heidelberg, 2015.

[2] J. H. Fang, H. X. Luo, L. L. Wang, and S. Chen, "Study on tropical agricultural mobile e-commerce system in Hainan," *Applied Mechanics & Materials*, vol. 7, no. 5, pp. 631-632, 2014.

[3] Z. Tianqi, "Paths for upgrade and transformation of e-commerce of China's fresh agricultural products based on whole industry supply chain," *Asian Agricultural Research*, vol. 4, no. 8, pp. 1–4, 2017.

[4] S. P. Adegoke and M. M. Osokoya, "Socio-economic background and access to internet as correlates of students' achievement in agricultural science," *International Journal of Evaluation & Research in Education*, vol. 9, no. 2, pp. 1–4, 2015.

[5] M. Pouratashi and M. Mokhtarnia, "Investigating factors influencing use of internet by agricultural faculty members for educational and research activities," *AfrrevStechAn International Journal of Science & Technology*, vol. 3, no. 2, pp. 1–7, 2014.

[6] Z. Wang, J. Huang, and B. Tan, "Managing organizational identity in the e-commerce industry: an ambidexterity perspective," *Information & Management*, vol. 50, no. 8, pp. 673–683, 2013.

[7] M. Yadav and Z. Rahman, "Measuring consumer perception of social media marketing activities in e-commerce industry: scale development & validation," *Telematics & Informatics*, vol. 34, no. 7, pp. 1294–1307, 2017.

[8] L. Liu, K. Li, and Z. Liu, "A capacitated vehicle routing problem with order available time in e-commerce industry," *Engineering Optimization*, vol. 49, no. 3, pp. 449–465, 2017.

[9] D. M. Liverman, "Drought impacts in Mexico: climate, agriculture, technology, and land tenure in Sonora and Puebla," *Annals of the Association of American Geographers*, vol. 80, no. 1, pp. 49–72, 1990.

[10] C. M. Pittelkow, L. Q. Xiang, and B. A. Linquist, "Productivity limits and potentials of the principles of conservation agriculture," *Nature*, vol. 517, no. 7534, pp. 365–368, 2015.

[11] S. Interpreters, "Fao - food and agriculture organization of the united nations," *Science*, vol. 118, no. 3077, pp. 3–3, 2013.

[12] W. Zhang, T. H. Ricketts, C. Kremen, K. Carney, and S. M. Swinton, "Ecosystem services and dis-services to agriculture," *Ecological Economics*, vol. 64, no. 2, pp. 253–260, 2007.

[13] M. Bustamante, C. Robledo-Abad, R. Harper, C. Mbow, N. H. Ravindranath, and F. Sperling, "Co-benefits, trade-offs, barriers and policies for greenhouse gas mitigation in the agriculture, forestry and other land use (afolu) sector," *Global Change Biology*, vol. 20, no. 10, pp. 3270–3290, 2015.

[14] G. P. Robertson, V. H. Dale, O. C. Doering et al., "Agriculture. Sustainable biofuels redux," *Science*, vol. 322, no. 5898, pp. 49-50, 2008.

[15] D. J. Mulla, "Twenty five years of remote sensing in precision agriculture: key advances and remaining knowledge gaps," *Biosystems Engineering*, vol. 114, no. 4, pp. 358–371, 2013.

[16] M. Y. Siddiqui and A. Gir, "Integration of policy and reputation based trust mechanisms in e-commerce industry," *International Journal of Computer Applications*, vol. 110, no. 8, pp. 15–19, 2015.

[17] D. Lagakos and M. E. Waugh, "Selection, agriculture, and cross-country productivity differences," *American Economic Review*, vol. 103, no. 2, pp. 948–980, 2013.

[18] P. Collier and S. Dercon, "African agriculture in 50 years: smallholders in a rapidly changing world?," *World Development*, vol. 63, no. C, pp. 92–101, 2014.

[19] G. C. Nelson, H. Valin, R. D. Sands et al., "Climate change effects on agriculture: economic responses to biophysical shocks," *Proceedings of the National Academy of Sciences of the United States of America*, vol. 111, no. 9, pp. 3274–3279, 2014.

[20] H. Zheng, W. Guo, and N. Xiong, "A kernel-based compressive sensing approach for mobile data gathering in wireless sensor network systems," *IEEE Transactions on Systems, Man, and Cybernetics: Systems*, vol. 48, no. 12, pp. 2315–2327, 2017.

[21] Z. Huang, X. Xu, J. Ni, H. Zhu, and C. Wang, "Multimodal representation learning for recommendation in internet of things," *IEEE Internet of Things Journal*, vol. 6, no. 6, pp. 10675–10685, 2019.

[22] H. Liang, D. Zou, Z. Li, K. Muhammad Junaid, and Y. Lu, "Dynamic evaluation of drilling leakage risk based on fuzzy theory and PSO-SVR algorithm," *Future Generation Computer Systems*, vol. 95, pp. 454–466, 2019.

[23] Z. Liu, B. Hu, B. Huang, L. Lang, H. Guo, and Y. Zhao, "Decision optimization of low-carbon dual-channel supply chain of auto parts based on smart city architecture," *Complexity*, vol. 2020, Article ID 2145951, 14 pages, 2020.

[24] Y. Zhang, R. Zhu, Z. Chen, J. Gao, and D. Xia, "Evaluating and selecting features via information theoretic lower bounds of feature inner correlations for high-dimensional data," *European Journal of Operational Research*, vol. 290, no. 1, pp. 235–247, 2021.

[25] H. Liang, A. Xian, M. Min Mao, P. Ni, and H. Wu, "A research on remote fracturing monitoring and decision-making method supporting smart city," *Sustainable Cities and Society*, vol. 62, article 102414, 2020.

[26] Y. Zhou, D. Zhang, and N. Xiong, "Post-cloud computing paradigms: a survey and comparison," *Tsinghua Science and Technology*, vol. 22, no. 6, pp. 714–732, 2017.

Hindawi
Wireless Communications and Mobile Computing
Volume 2020, Article ID 8870536, 9 pages
https://doi.org/10.1155/2020/8870536

WILEY | Hindawi

Research Article

Construction of Virtual Reality-Interactive Classroom Based on Deep Learning Algorithm

Weijie Chen, Xiaoxi Liu, Lei Qiao, Jian Wang, and Yanheng Zhao

State Grid of China Technology College, Jinan 250002, China

Correspondence should be addressed to Weijie Chen; wyt@xauat.edu.cn

Received 24 September 2020; Revised 27 October 2020; Accepted 5 November 2020; Published 21 December 2020

Academic Editor: Hongju Cheng

Copyright © 2020 Weijie Chen et al. This is an open access article distributed under the Creative Commons Attribution License, which permits unrestricted use, distribution, and reproduction in any medium, provided the original work is properly cited.

The traditional classroom has been impacted by the digital teaching resources. Students are no longer satisfied with the traditional teaching mode of teacher teaching and student learning. Combined with the characteristics of a virtual reality-interactive classroom, the design of a virtual reality-interactive classroom based on the deep learning algorithm is proposed. This paper divides the teaching activities of the VR-interactive classroom into two parts: in-class learning activities and after-class learning activities. The software is used to design the interactive test. The emphasis and difficulty in the virtual reality-interactive classroom are taken as the development object to realize the construction of the virtual reality-interactive classroom. The simulation results show that the statistical output of teaching quality evaluation can be obtained from the quantitative regression analysis of the factors involved in VR classroom participation.

1. Introduction

The construction of education informationization and the construction of digital teaching resources have made vigorous development. Since the mid-1990s, there has been an upsurge in the construction of teaching resources, especially in the field of basic education, with the emergence of a number of providers of digital teaching resources [1]. At the same time, it accelerates the construction of network video courses, greatly promotes the cultivation and construction of the teaching team, promotes the diversification of teaching methods and the quality of teaching resources, and effectively improves the ability and consciousness of university teachers to carry out teaching activities under the background of information technology [2].

In the reform of higher education, an innovative educational environment is the focus of this reform. While developing a modern teaching environment, colleges and universities should also use modern educational technology to improve the teaching level [3]. Most schools still retain the traditional (lecture-demonstration-practice) teaching model because of the limited time available in the classroom, which is difficult for students to grasp if too many points of knowledge are given in detail and difficult for students to understand if spoken in a cursory manner. However, interactive classrooms are concerned with slippage between teachers and students, student-student interaction, and individualized, resource-based learning and autonomous inquiry [4]. Therefore, it has become an urgent task to develop interactive classroom teaching.

Scholars have done a lot of research on this. The method of reference suggests a new educational platform in the classroom [5]. The ready-to-use availability of interactive platforms has created a new generation of students who can easily and comfortably use computer-based learning tools. The potential lecture materials for better "self-exploration" allow students to have an enhanced learning experience and stimulate them to tinker with equation parameters to produce insightful graphics or animations. In the classroom, it encourages students to have a deeper understanding of complex deductions or mathematical expressions. Experience is gained in implementing these materials in undergraduate and postgraduate courses, including examples of student feedback and supplementary homework used in the class. The method of Reference [6] suggests that flipping the classroom is an active teaching strategy that makes the curriculum

more interactive and challenging. Based on the above methods, a virtual reality-interactive classroom based on the deep learning algorithm is proposed. The interactive function is added in the design of the virtual reality-interactive classroom. This method can effectively improve the practicability of interactive classroom resources and provide reference for the development of a virtual reality-interactive classroom.

The rest of this paper is organized as follows. Section 2 discusses front-end analysis of virtual reality-interactive classroom design, followed by a virtual reality-interactive classroom based on deep learning algorithm which is discussed in Section 3. Design of learning content in interactive classroom is discussed in Section 4. Section 5 shows the simulation experimental results, and Section 6 concludes the paper with the summary and future research directions.

2. Front-End Analysis of Virtual Reality-Interactive Classroom Design

2.1. Analysis of Learning Needs. The demand analysis is from the virtual reality-interactive classroom characteristic and is the individualized way of study of two aspects that carry on the analysis explanation. First, practical and operational courses such as virtual reality-interactive classrooms require interactive learning, and interaction does not refer solely to the presentation of learning content in video format [7]. Second, personalized learning has complied with today's learning trend and pays attention to learning efficiency and learning effect [8]. An interactive classroom can not only meet the characteristics of virtual reality interaction but also enable learners to study according to their own learning situation targeted to meet the learners' individual learning needs.

2.2. Learner Analysis. In the learner analysis stage, a questionnaire survey is conducted among the students in the upcoming virtual reality-interactive class to understand their learning needs and interests and attitudes in using interactive microvideos.

Most students have plenty of time to surf the Internet, but most of them do not make full use of the advantage of the Internet to study because of the lack of relevant learning resources, lack of enthusiasm, and low self-control ability [9]. Therefore, it is necessary to develop a set of video learning resources with learning tasks to assist the teaching of the virtual reality-interactive classroom and effectively improve students' autonomous learning ability [10]. According to the deep learning algorithm, the evaluation model of interactive classroom learning effectiveness is as follows:

$$L = C - m \times \sigma_s - \frac{(x_{st} - r_t)^2}{2\sigma_s^2}, \tag{1}$$

in which σ_s represents the learning efficiency of college students in the virtual reality-interactive classroom and m represents the implicit state of the evaluation model of learning effectiveness in interactive classroom. x_{st} is the space state of the model, r_t is the blocking state of the model, C is the optimal running state of the model, and σ_s is the observation state of the evaluation model of the effectiveness of interactive classroom learning.

An information flow model based on a differential equation is constructed to express the effectiveness of interactive classroom learning:

$$x_n = m(t_0 + \Delta t) \times L, \tag{2}$$

where t_0 represents the statistical characteristic state function of learning effectiveness in the interactive classroom and constructs the multivariate quantitative value function of the survey regression analysis sequence of learning effectiveness evaluation and L represents the measurement error.

The expression of the elastic grey model for evaluating the effectiveness of interactive classroom learning is as follows:

$$F(z) = \frac{dz(t)}{x_n}, \tag{3}$$

where $dz(t)$ is the best game state parameter of learning effectiveness in the interactive classroom.

If $dz(t) = \{i_1, i_2, i_3\}$, the total characteristic distribution satisfies $i \in I$, and then, the total gain rate $s_i = (x_1, x_2, \cdots, x_n)$ under interactive classroom learning satisfies the following:

$$f(x_1) = f(x_2) = \cdots = f(x_n) = f^*. \tag{4}$$

2.3. Analysis of Curriculum Objectives. In this study, the curriculum standards of the virtual reality-interactive classroom are analyzed, and the three-dimensional objectives of the virtual reality-interactive classroom are summarized as follows.

2.3.1. Knowledge and Skills. The knowledge and skills are as follows: to understand and master the basic theory and common sense of virtual reality-interactive classroom software, to master the use skills of the software, to master the operation interface and function of the software, to master the creative design of software use, and to cultivate students' autonomous learning ability.

2.3.2. Process and Method. The process and method are as follows: can use virtual reality-interactive classroom software to complete and create a work independently, master the basic methods and skills of image synthesis, and cultivate learning methods of active exploration and innovation in software learning [11].

2.3.3. Emotional Attitudes and Values. The emotional attitudes and values are as follows: to cultivate students' sense of teamwork, initiative of learning, innovative consciousness and spirit, and artistic accomplishment of students.

Based on this goal, this paper designs an interactive test function, which aims at enabling the students to master the knowledge and skills more firmly. Space reconstruction trajectory is as follows:

$$X = \left(x_n, x_{n-\tau}, \cdots, x_{n-(m-1)\tau}\right), \tag{5}$$

where x_n is the orthogonal eigenvector of regression analysis sequence of statistical survey on learning effectiveness of the interactive classroom, τ is the sampling delay of statistical characteristics of interactive classroom learning effectiveness, m is the embedding dimension, and $x_{i+(m-1)\tau}$ is a set of scalar sampling sequences.

Process and methods emphasize the comprehensive use of knowledge points, mainly through the setting of classroom tasks to help students meet the corresponding requirements. Emotional attitude and values emphasize the importance of students' autonomous learning, collaborative learning, and innovative learning. In this paper, in order to cultivate students' emotional attitudes and values, the interactive classroom teaching mode will be used to teach this course.

3. Virtual Reality-Interactive Classroom Based on Deep Learning Algorithm

The design of interactive teaching activities based on the deep learning algorithm can not only meet the needs of individualized learning but also help teachers to carry out teaching activities smoothly. Based on the characteristics of the virtual reality-interactive classroom, virtual reality-interactive classroom teaching activities are divided into in-class learning activities and after-class learning activities [12].

3.1. Design of Learning Activities in Class. Interactive classrooms are widely used in modern teaching, so classroom teaching activities include not only in class but also before and after classes. In the traditional teaching process, knowledge is imparted in class, and knowledge internalization is carried out outside class. When learners encounter problems and need teachers' guidance, the teachers are not present. On the one hand, the students' learning effect is not ideal, and on the other hand, the students' learning enthusiasm is reduced [13]. This paper makes use of the current interactive teaching mode to make up for the deficiency of the traditional teaching mode. Based on the model of explanatory variables and the model of control variables in the evaluation of learning effectiveness, the statistical feature extraction is carried out according to the distribution characteristics, association coefficient, average mutual information entropy, learning mode, and other constraint parameters of the deep learning algorithm resources, and the linear superposition output of a large number of statistical feature sequences of learning effectiveness in the virtual reality-interactive classroom is obtained:

$$r(i,h) = t(i,h) + w(i,h), \tag{6}$$

in which $t(i,h)$ represents the amount of virtual reality-interactive classroom data and $w(i,h)$ represents the number of virtual reality-interactive classes.

And teachers can design plans and assign tasks according to the characteristics of students. Through this teaching method, on the one hand, teachers can understand the learning effect of students' autonomous learning, and on the other hand, they can help students communicate and deepen the internalization of knowledge [14]. Then, according to the students' learning situation, make specific arrangements for different learning states. During the course of operation, students complete relevant tasks by themselves and solve problems by the BB platform, group communication, or watching an interactive class. Learning activities in class are shown in Figure 1.

3.2. Design of Learning Activities after Class. Postclass learning activities mainly include two links of preclass and after class. And these two links if attached to the BB platform of the deep learning algorithm help the students' personalized learning. The design of extracurricular learning activities is mainly a process of knowledge transfer using the SPOC environment. The design of learning activities based on the deep learning algorithm should make full use of the existing microcourses to carry out teaching activities. However, the missing teaching activities in the deep learning algorithm can be supplemented by the interactive classroom teaching mode. Since the learning of the interactive classroom is mainly aimed at learners with different majors and different degrees of mastery of the virtual reality-interactive classroom, they can use the time and place after class to choose suitable learning content for their own personalized learning [15]. Combining with the deep learning algorithm, the optimal outputs of the virtual reality-interactive classroom learning effectiveness evaluation and feature extraction are as follows:

$$r(i,h)' = t(i,h)' + w(i,h)', \tag{7}$$

in which $w(i,h)$ represents the derivative of data quantity of the virtual reality-interactive classroom and $w(i,h)$ represents the quantity derivative of virtual reality-interactive classroom.

Based on the analysis of learners' needs and the applicability of courses, the design of preclass learning activities divides the curriculum objectives into small independent objectives and integrates the interactive classroom and high-quality teaching methods into a complete SPOC learning environment [16]. Through the function of interactive test and timely feedback, learners can make up for the deficiencies before class and achieve key problem and key study. Before class, the teacher's task is heavy; the teacher needs to develop the corresponding interactive class according to the course front-end analysis and put it on the BB platform for the learner to study [17, 18], and collect the learner's questions in the discussion class, so that timely feedback is in class. Preclass learning activities are structured as shown in Figure 2 [19].

After class, it is a process of reviewing and consolidating learning. This process is mainly to check the learner's grasp of knowledge through independent learning, to sum up the questions put forward by everyone in class, and to adjust and correct them in time before class and during class [20, 21]. To evaluate students' scores after class, the first step is

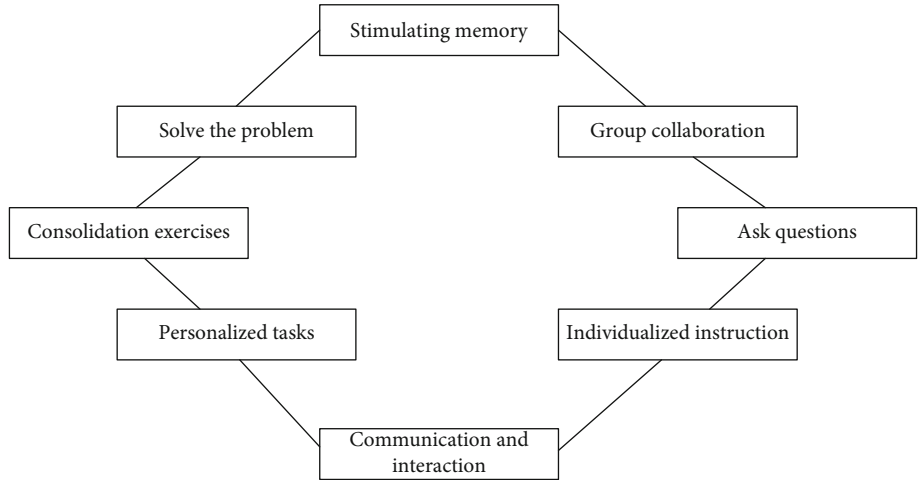

Figure 1: Learning activities in class.

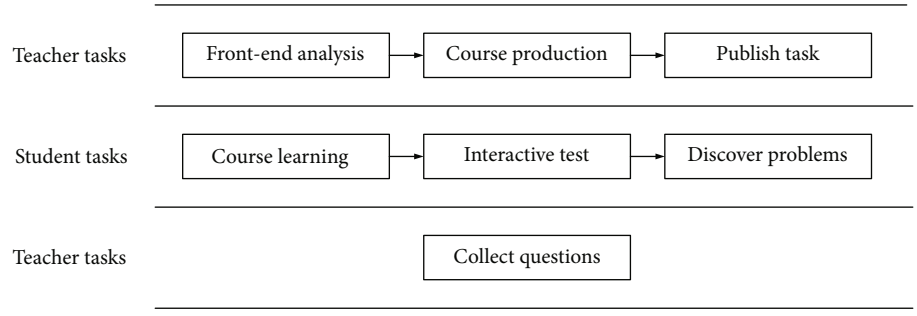

Figure 2: Prelesson activities.

to obtain the students' historical scores. The calculation formula is as follows [22]:

$$H = G_m \times \frac{f}{d \times k}, \tag{8}$$

in which H represents the final test scores of previous semesters, G_m represents the student information, d represents the students' current scores, k represents the students' learning progress, and f represents the difficulty of examination contents.

On this basis, the evaluation criteria are set, and the calculation formula is as follows [23]:

$$D = \frac{B_i}{r/H}, \tag{9}$$

in which B_i represents the student grade evaluation parameter, r represents the student examination information, and D represents the learning evaluation parameter. After-class learning activities are shown in Figure 3 [24].

4. Design of Learning Content in Interactive Classroom

Because the virtual reality-interactive classroom is mainly about practical operation, the design of interactive classroom learning content includes not only microvideo but also learning objectives, video summary, and interactive tests. As shown in Figure 3, virtual reality-interactive classroom learning starts from learning objectives, through which learners can clearly know the skills and learning process required for the course learning. In order to facilitate different levels for students to choose suitable learning content, highlighting the requirements of personalized learning is needed. The second is to watch the video to learn; through the teacher's demonstration and explanation, learners can carry out the corresponding observation and reflection. And the icons, questions, subtitles, etc. in the video are all interactive. Third, students according to the video summary of the teacher targeted combing the content, conducive to the consolidation of classroom knowledge. Finally, an interactive test is used to test the learner's mastery of the knowledge point.

4.1. Learning Goal Design. Learning goal is the starting point and end result of teaching activities. Therefore, the learning goal should be described clearly and concretely before teaching. This is the standard which the study activity must achieve and is anticipating the student study result. It fundamentally restricts the direction of instructional design and plays a guiding role in the teaching process, thus effectively avoiding the blindness of teaching.

The design of learning objectives pays more attention to let learners know the purpose of learning, lead learners, and

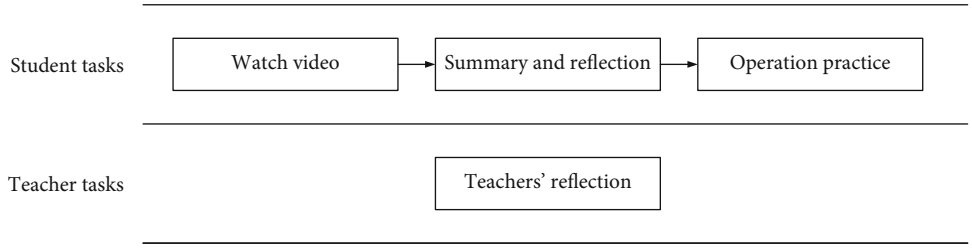

Figure 3: After-school activities.

stimulate learning motivation. The learning objectives of the virtual reality-interactive classroom are mainly realized through virtual reality-interactive classroom software. Teachers do not explain learning objectives too much but let learners understand the knowledge points in this section and the framework structure of the whole knowledge points through learning objectives.

4.2. Video Content Design. The design of course content mainly includes four basic links: "script writing," "material collection," "component development," and "content integration." In terms of importance and implementation difficulty, "scripting" and "component development" are two of the most noteworthy aspects.

Based on the structure of the courseware, "script compiling" is to further consider and arrange the courseware content, layout, audio-visual forms, and the writing of commentary. Script editing can be said to be one of the key links that directly affect the development of courseware. It can lay a solid foundation for the follow-up work to study and write carefully.

When the script is finished, enter the "material collection" link. This link is the starting point and symbol of the development of the interactive class. Teachers really start to make courseware—prepare various materials for the courseware. According to the characteristics of the virtual reality-interactive classroom, the interactive classroom materials mainly include text and pictures.

In order to guarantee the originality or uniqueness of the material, most teachers design and make the material by themselves from beginning to end. Not only did this increase the burden of teacher development, but also the quality of the material makes it difficult to achieve the desired results. Therefore, we need to find another way of thinking: to make full use of the principles of fair use in copyright law and the use of vast resources on the network, that is, to make use of existing materials on the network to meet the needs of their own courseware development, rather than a hands-on overemphasis on the so-called originality.

The so-called "component development" is actually a superordinate concept of material. When several materials are related to a set in some way, it constitutes a component. In other words, a component is a structured representation of the material. Furthermore, based on a certain structure or relationship, a courseware is constituted after the components are interrelated with each other. With the courseware, teachers need to use screen video experts to record PS operation. In the recording process, teachers are both teachers and video producers. Therefore, teachers should be accurate and logical when explaining so that the compilation is clear. In the recording process, pictures of intellectual errors or misleading descriptions are not allowed to appear in the language. And in the recording process, teachers' must pay attention that it is not too long, generally 5-10 minutes only. Also, attention must be paid on the use of the mouse in the process of explanation. When watching the video demonstration, the students' attention is on the mouse, so the teacher should remember not to shake the mouse randomly during the operation.

4.3. Video Summary Design. The summary is an indispensable link in the process of video teaching. At the end of the course, students' attention is easily distracted. The teacher can design a skillful classroom summary, not only to consolidate knowledge and improve interest but also to further stimulate students' thirst for knowledge, to achieve the "although the end of the class, interest is still" realm.

The summary is classified according to the content, subject, and carrier, as shown in Table 1. In the design of the microvideo summary, knowledge structure summary, problem summary, and teacher summary are mainly used. The method adopted in the design of the summary is consistent with the learning objectives, that is, it is achieved by using the virtual reality interactive classroom software. The specific design structure is shown in Figure 4.

After explaining the relevant virtual reality-interactive classroom knowledge points, the teacher summarizes all the operation steps and precautions in this section, which plays a strengthening role for students. Moreover, the teacher introduces the scope and conditions of the tool through examples, which can expand students' thinking and enhance their innovation and creativity. Finally, the teacher will arrange the relevant contact to help students consolidate their knowledge and achieve the purpose of the skilled operation.

4.4. Interactive Test Design. The interactive test is the last module of interactive learning in the virtual reality classroom. It is mainly used to test the previous courses, which can help students to further consolidate their learning knowledge. Not only can it let the student understand the situation to grasp this section's microlesson, but also it can help the student to check the loophole to make up for the deficiency. Because of the different levels of learners in the virtual

Table 1: Summary classification.

Division basis	Type
Content	Knowledge structure summary, learning method summary, thinking concept summary, learning situation summary, problem summary
Subject	Teacher summary, student summary, teacher-student interaction
Carrier	Blackboard, multimedia courseware, notes

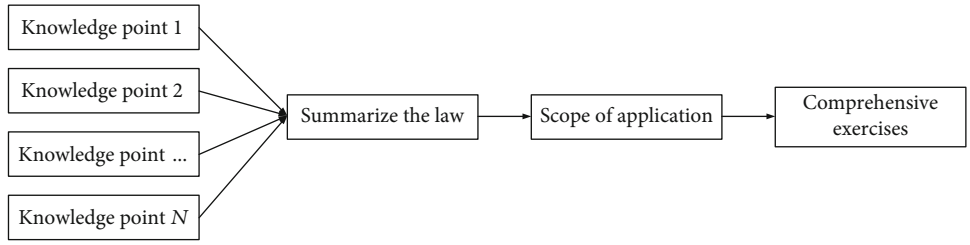

Figure 4: Summary of the design structure.

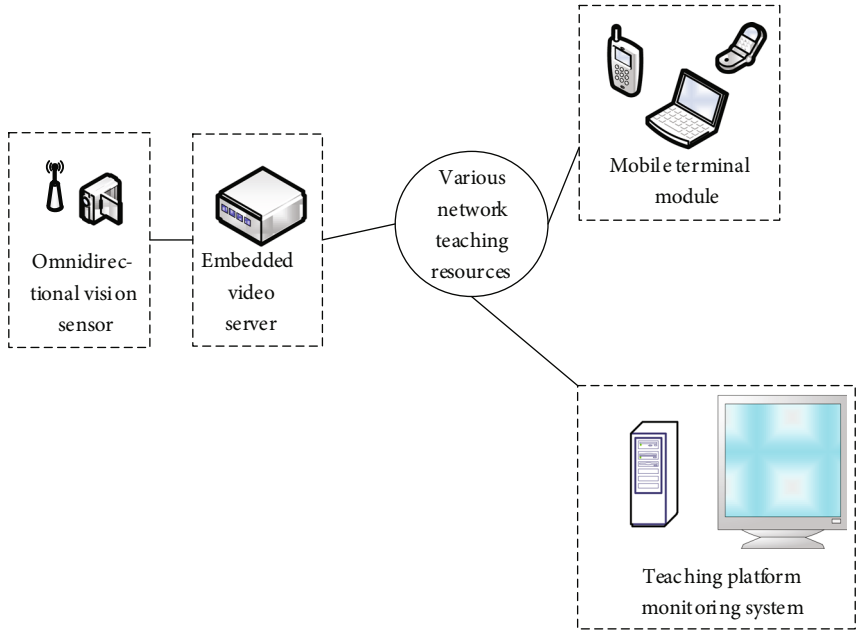

Figure 5: Simulation experiment environment.

reality-interactive classroom, the basic tests and intensive tests are added in the design of the interactive tests.

The interactive test module is mainly composed of the basic test and reinforcement test, and the basic test mainly includes a multiple-choice test, blank filling test, and judgment test. The reinforcement test is mainly a case operation. When the basic test is not successful, students can view the analysis and continue to learn the knowledge according to the system prompt. If the basic test is successful, the learner can enter the intensive test; there is no right or wrong in the intensive test stage; the student knowledge will operate the case assigned by the teacher and submit the work to the teacher for comments in class. The system will automatically proceed to the next stage of the study after the intensive test. Teachers need to follow the following step in preparing test questions: (1) making the purpose clear.

5. Experimental Results and Analysis

In order to further ensure the effect of its practical application, simulation experiments are carried out. In order to enhance the explanatory nature of the experimental results, the method of Reference [5] and the method of Reference [6] are used as a comparison. Select the virtual reality classroom account attribute information obtained from the network to carry on the validity experiment. With Google as the source of user attribute information, the website has finally obtained 3426 valid Google+ accounts, 3567 Facebook

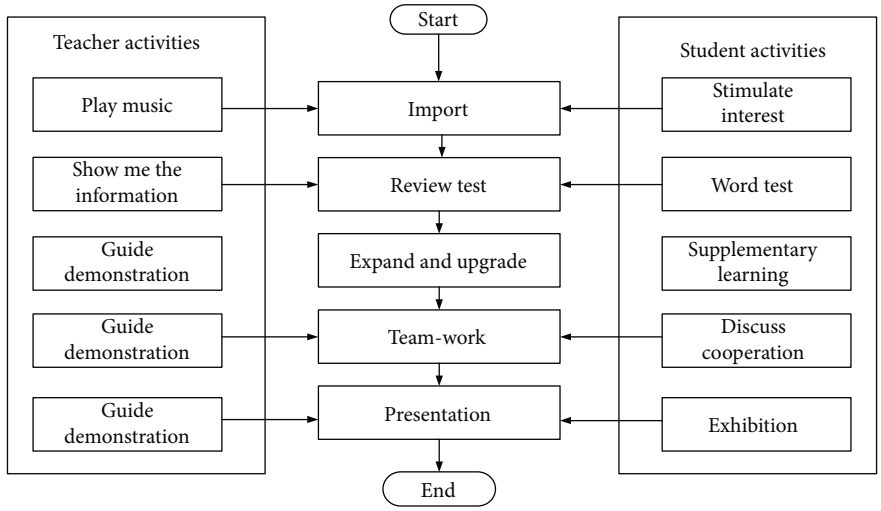

Figure 6: Flow chart of experimental teaching.

accounts, and 4712 Twitter accounts for the pages with nonempty homepage links to Twitter and Facebook, which are not invalidated and have public access rights. Other simulation and experimental environments are shown in Figure 5.

In the simulation experiment environment, 300 students were selected to carry out the experiment. Among them, 100 students applied the designed method, 100 students applied the method of Reference [5], and 100 students applied the method of Reference [6]. Compared with the three groups of students, the higher the study score was, the more effective the system was. The teaching process in the experiment is shown in Figure 6.

According to the above experimental process, the interactive classroom teaching quality evaluation simulation is carried out, and the distribution of virtual reality-interactive classroom resources is obtained as shown in Figure 7. A set of video learning resources with learning tasks is developed to assist the teaching work of virtual reality-interactive classroom and effectively improve students' autonomous learning ability. The teaching effect is obtained according to Formula (1) interactive classroom learning effectiveness evaluation model. The specific test results are shown in Figure 8.

Based on the distribution of teaching resources in Figure 7, the quantitative decision-making and statistical analysis in the process of interactive classroom teaching quality evaluation are carried out by using the teaching benefit and innovative evaluation mode. As can be seen from Figure 8, the test results of the teaching effect of this method are close to the actual predictions. In order to prevent the phenomenon of illegal copying in the process of experiment and then search for the answers from the Internet or the question bank and prevent the leakage of examination questions, the function of anticopying is added to the webpage code; in addition, a score table containing examination information is established, the relevant information is saved in the table at the beginning of the examination, and the examination status of the examinee is marked. The examinee's examination status will be changed when the examination paper is submitted or the examination time is reached, ending the

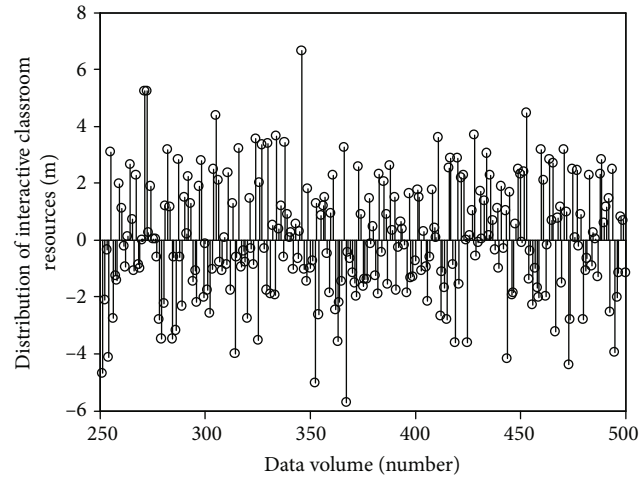

Figure 7: Distribution of virtual reality-interactive classroom resources.

examination automatically, so that the examinee cannot modify the examination result and cannot continue the examination even if he has not submitted the examination paper for any reason. At the same time, obtain the course name, test paper code, and other information of the examination, and then save these information and student number, class, exam certificate number, exam course, and the score of the examination to the examinee score table. The performance improvement rates of the proposed method, the method of Reference [5], and the method of Reference [6] are compared as shown in Figure 9.

As can be seen from Figure 9, the results of the application of this method have improved significantly, and the results are higher. The reason is that the information flow model constructed by this method to express the learning validity of differential equation in interactive class has good performance to a certain extent. In order to further study the feasibility of the virtual reality-interactive classroom based on the deep learning algorithm, the design method is

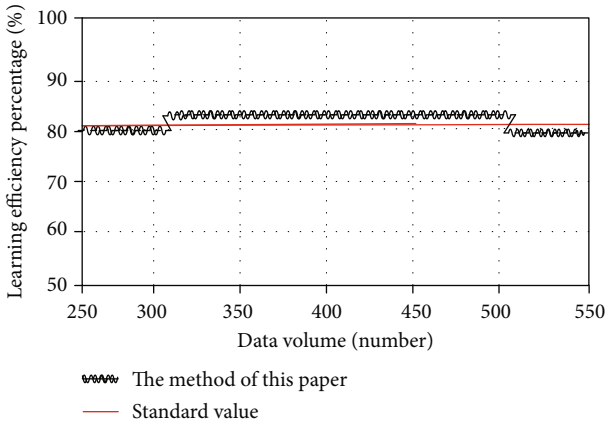

Figure 8: Test results of teaching effect.

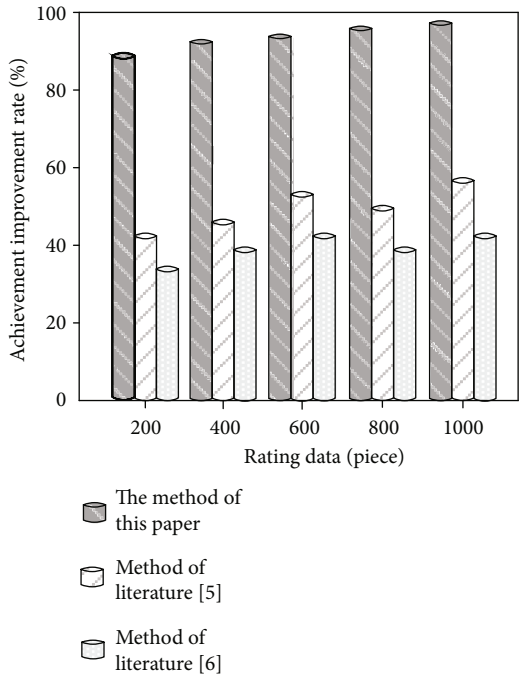

Figure 9: Comparison of performance improvement rates.

applied to the teaching resource platform. The specific simulation results are shown in Table 2.

Analysis of the experimental data in Table 2 shows that the overall stability of the virtual reality-interactive classroom has been greatly improved after the use of this method. The main reason is that in the design process of this method, a deep learning algorithm is used to analyze the virtual reality-interactive classroom; based on the explanatory variable model and the control variable model of learning effectiveness evaluation, and according to the distribution characteristics of the resources of the deep learning algorithm, association coefficient, average mutual information entropy, learning mode, and other constraint parameters, the statistical feature extraction is carried out, and the linear superposition output of the large number of bits of the statistical feature number of the virtual reality-interactive classroom learning effectiveness is obtained. To some extent, a large number of redundant data existing in the teaching resource platform can be deleted, the probability of attack and harm to the platform is reduced, and the stability of the whole platform is enhanced. Therefore, the above experiments can prove the effectiveness of the design method, and the system has a better application effect and practical application significance.

Table 2: Stability of teaching resource platform before and after using this method.

Distribution of interactive classroom resources	Platform stability before using this approach (%)	Platform stability with textual approach (%)
1	87.8	93.8
2	85.3	95.6
3	86.7	97.4
4	93.5	94.2
5	91.6	93.3
6	90.4	97.4
Average value	89.22	95.28

6. Conclusions

Based on the front-end analysis, this paper puts forward the design of virtual reality-interactive classroom learning content and the design of interactive classroom learning activity based on deep learning and develops the corresponding interactive classroom by this knowledge spot, the test study effect, carries on the summary, and the improvement of the insufficiency. After the above research, we get the following conclusions: On the basis of summarizing the previous definitions of microcourses, the definition of interactive microcourses is proposed from the perspective of deep learning algorithm. According to the characteristics of virtual reality-interactive classroom reoperation, this study divides the contents of the virtual reality-interactive classroom into four modules. They are the learning goal, video content, learning summary, and interactive test. And the corresponding model is designed to develop a virtual reality-interactive classroom. Through the investigation, it is found that the interactive microcourse can be applied to the personalized learning after class, which can arouse the students' interest in learning and help the learners to solve the problems in the actual operation.

Data Availability

The data used to support the findings of this study are available from the corresponding author upon request.

Conflicts of Interest

The authors declare that there are no conflicts of interest regarding the publication of this paper.

References

[1] T. Rose, C. S. Nam, and K. B. Chen, "Immersion of virtual reality for rehabilitation - review," *Applied Ergonomics*, vol. 69, no. 5, pp. 153–161, 2018.

[2] M. S. Elbamby, C. Perfecto, M. Bennis, and K. Doppler, "Toward low-latency and ultra-reliable virtual reality," *IEEE Network*, vol. 32, no. 2, pp. 78–84, 2018.

[3] M. Chen, W. Saad, and C. Yin, "Virtual reality over wireless networks: quality-of-service model and learning-based resource management," *IEEE Transactions on Communications*, vol. 66, no. 11, pp. 5621–5635, 2018.

[4] D. Cano Porras, P. Siemonsma, R. Inzelberg, G. Zeilig, and M. Plotnik, "Advantages of virtual reality in the rehabilitation of balance and gait," *Neurology*, vol. 90, no. 22, pp. 1017–1025, 2018.

[5] Z. J. Zhou, J. L. Chen, and H. Shen, "Simulation of air traffic flow optimization prediction," *Computer Simulation*, vol. 33, no. 8, pp. 54–57, 2016.

[6] P. E. Frank and M. P. Andersson, "Strength training improves muscle aerobic capacity and glucose tolerance in elderly," *Scandinavian Journal of Medicine & Science in Sports*, vol. 26, no. 7, pp. 764–773, 2016.

[7] M. G. Luchs, K. S. Swan, and M. E. H. Creusen, "Perspective: A Review of Marketing Research on Product Design with Directions for Future Research," *Journal of Product Innovation Management*, vol. 33, no. 3, pp. 320–341, 2016.

[8] M. F. Oliveira, F. R. Caputo, and B. Corvino, "Short-term low-intensity blood flow restricted interval training improves both aerobic fitness and muscle strength," *Scandinavian Journal of Medicine & Science in Sports*, vol. 26, no. 9, pp. 1017–1025, 2016.

[9] K. E. Harada, N. Lee, and S. Ai, "Awareness of role of strength training in care prevention, negative perception and stages of change for strength training behavior among Japanese older adults," *Bulletin of the Chemical Society of Japan*, vol. 62, no. 12, pp. 3869–3876, 2015.

[10] N. Rinaldo, E. Bacchi, G. Coratella et al., "Effects of combined aerobic-strength training vs fitness education program in COPD patients," *International Journal of Sports Medicine*, vol. 38, no. 13, pp. 1001–1008, 2017.

[11] P. K. Patra, S. Sam, and M. Singhai, "Study on the production of ultra high strength steel (UHSS) in thin slab caster," *Sae Technical Papers*, vol. 4, no. 4, pp. 445–454, 2014.

[12] K. Karatrantou, V. Gerodimos, K. Häkkinen, and A. Zafeiridis, "Health-promoting effects of serial vs. integrated combined strength and aerobic training," *International Journal of Sports Medicine*, vol. 38, no. 1, pp. 55–64, 2017.

[13] Y. Liu, C. Liu, Y. Kang, D. Wang, and D. Ye, "Experimental research on creep properties of limestone under fluid–solid coupling," *Environmental Earth Sciences*, vol. 73, no. 11, pp. 7011–7018, 2015.

[14] A. Tahir, S. A. Abid, and N. Shah, "Logical clusters in a DHT-paradigm for scalable routing in MANETs," *Comput. Netw*, vol. 128, no. 5, pp. 142–153, 2017.

[15] J. MacLeod, H. H. Yang, S. Zhu, and Y. Li, "Understanding students' preferences toward the smart classroom learning environment: development and validation of an instrument," *Computers & Education*, vol. 122, no. 7, pp. 80–91, 2018.

[16] C. Lin, N. Xiong, J. H. Park, and T. Kim, "Dynamic power management in new architecture of wireless sensor networks," *International Journal of Communication Systems*, vol. 22, no. 6, pp. 671–693, 2009.

[17] Y. Sang, H. Shen, Y. Tan, and N. Xiong, "Efficient protocols for privacy preserving matching against distributed datasets," *International Conference on Information and Communications Security*, vol. 12, pp. 210–227, 2006.

[18] L. Dong, W. Wu, and Q. Guo, "Reliability-aware offloading and allocation in multilevel edge computing system," *IEEE Transactions on Reliability*, pp. 1–12, 2019.

[19] J. Li, N. Xiong, J. H. Park, C. Liu, M. A. Shihua, and S. E. Cho, "Intelligent model design of cluster supply chain with horizontal cooperation," *Journal of Intelligent Manufacturing*, vol. 23, no. 4, pp. 917–931, 2012.

[20] M. Wei, R. Wozniak, X. Damaeviius, and Y. L. Fan, "Research of known-plaintext attack on double random phase mask based on WSNs," *Journal of Internet Technology*, vol. 20, no. 1, pp. 39–48, 2019.

[21] Z. Chen, D. Chen, Y. Zhang, X. Cheng, M. Zhang, and C. Wu, "Deep learning for autonomous ship-oriented small ship detection," *Safety Science*, vol. 130, p. 104812, 2020.

[22] Z. Huang, X. Xu, J. Ni, H. Zhu, and C. Wang, "Multimodal representation learning for recommendation in Internet of Things," *IEEE Internet of Things Journal*, vol. 6, no. 6, pp. 10675–10685, 2019.

[23] W. Guo, N. Xiong, A. V. Vasilakos, G. Chen, and C. Yu, "Distributed k–connected fault–tolerant topology control algorithms with PSO in future autonomic sensor systems," *International Journal of Sensor Networks*, vol. 12, no. 1, pp. 53–62, 2012.

[24] F. Long, N. Xiong, A. V. Vasilakos, L. T. Yang, and F. Sun, "A sustainable heuristic QoS routing algorithm for pervasive multi-layered satellite wireless networks," *Wireless Networks*, vol. 16, no. 6, pp. 1657–1673, 2010.

Hindawi
Wireless Communications and Mobile Computing
Volume 2020, Article ID 8824754, 11 pages
https://doi.org/10.1155/2020/8824754

Research Article

Research on Channel Model and Price Dispersion of E-Commerce Market Based on Blockchain Technology

Qifeng Zhang[1] **and Fei Liu**[1,2]

[1]*The Graduate School, Woosuk University, Wanju, Republic of Korea*
[2]*School of Economics, Hebei GEO University, Shijiazhuang 050030, China*

Correspondence should be addressed to Fei Liu; liufei54adela@hgu.edu.cn

Received 10 September 2020; Revised 10 November 2020; Accepted 7 December 2020; Published 19 December 2020

Academic Editor: Hongju Cheng

Copyright © 2020 Qifeng Zhang and Fei Liu. This is an open access article distributed under the Creative Commons Attribution License, which permits unrestricted use, distribution, and reproduction in any medium, provided the original work is properly cited.

In order to accurately predict the channels and prices of the e-commerce market, and thereby control the cost of the e-commerce market, this paper studies the channel model and price dispersion of the e-commerce market from the perspective of suppliers. First, this paper establishes a model to analyze the price dispersion structure under different proportions of informed consumers and theoretically analyzes the objective reasons for continued price dispersion in the e-commerce market where search costs have fallen sharply. Then, this article combines theoretical models with empirical research to study the price and price differences between the two types of retailers. The results show that as consumers' interest in retailers changes, prices will also change, and the degree of price dispersion in the e-commerce market has not yet converged. This research result has a good predictive effect on the pricing and market estimation of the e-commerce market and can control the cost of e-commerce operation and improve the competitiveness of the e-commerce market.

1. Introduction

The chain business is to instantaneously distribute through smart contracts, omitting the intermediate retention and transfer links, and there is no Party B and Party C, all of which are Party A, realizing direct value distribution. In the early stage of the Internet economy, based on the grasp of the characteristics of network information technology, scholars have generally believed that the application of e-commerce will have the following impact on both the supply and demand sides of the market. On the one hand, the scope of consumer search has been significantly expanded, and the search cost has been significantly reduced, which will promote the rationalization of consumer behavior [1, 2]. On the other hand, retailers will face a wider range of interindustry competition. Although direct price competition can be partially avoided by means of bundling sales, the aggravation of competition will still lead to a considerable decline in the pricing power of manufacturers and make prices more transparent, which is undoubtedly conducive to consumer purchases [3–5]. In short, the e-commerce market is more efficient than the traditional offline trading market. This view is generalized as the "frictionless trading hypothesis" of the network economy and is widely accepted.

The reason why this paper studies the price dispersion in China's e-commerce market is mainly based on the following three considerations [4, 5]: (1) Price dispersion is an important index to test the efficiency of the market. Therefore, the study of price dispersion in the e-commerce market is the premise of investigating the efficiency of emerging markets and analyzing the behavior of manufacturers and consumers in the network economy [6]. It is of great significance to understand the current economic situation and future development. (2) Because it is very difficult to obtain the selling price of the same commodity and different merchants in the traditional market at the same time, most of the previous research on price dispersion is limited to theoretical research, and there is little empirical analysis. (3) The existing relevant research and conclusions are made based on the markets of developed countries such as Europe and the United States and are expanded and tested in China's market during the economic transition period [7, 8].

Compared with the traditional market, it is easier for us to obtain cross-sectional price data of homogeneous goods, observable characteristic data of enterprises, and market characteristic data of products from the website [9–12]. Based on the above background, this paper analyzes the price level and price dispersion in the e-commerce market from the empirical point of view and analyzes the factors that affect the price level and price dispersion. This study has important theoretical significance for testing the efficiency of the network economy market and investigating its operation mechanism, and it also has extensive application value for the management and market competition of e-commerce enterprises.

The rest of this paper is organized as follows. Section 2 discusses the development foundation of China's agriculture, followed by agricultural industry chain reconstruction analysis and suggestions designed in Section 3. Relationship model and empirical research on network consumer behavior and e-commerce service quality is discussed in Section 4. Section 5 concludes the paper with a summary and future research directions.

2. The Development Trend of E-Commerce

2.1. The Development of E-Commerce Industry. In view of the unreasonable industrial structure and the inconsistency between supply and demand in macroeconomy, General Secretary Xi Jinping proposed to push forward the "supply-side structural reform" in macroeconomy in 2015. The policy objective of supply-side structural reform is to start from the supply side of economic development, eliminate backward production capacity, reduce enterprise operating costs, reduce excess inventory, and reduce excessive financial leverage. The shortcomings of enterprise operation quality and efficiency are completed, and a new mode of production with "innovation, coordination, green, open, and sharing" as the basic concept was established, to achieve the sustainable stability of the national economy and the transformation and upgrading of the development model [13–16].

The new concept of "supply-side structural reform" put forward by the state is to start with the supply-side factors of production to promote economic development, strengthen the top-level design, change the unreasonable industrial structure, and take the road of economic development of innovation, development, optimization, and upgrading. General Secretary Xi Jinping especially emphasized at the expert forum on economic situation held in July 2016 that the current national economic development has entered a new normal stage. Only by unswervingly pushing forward the structural reform on the supply side can we provide a new source of impetus for the healthy development of the national economy. Cross-border e-commerce is considered a strategic emerging industry under the new normal of China's economy and the macrobackground of supply-side structural reform.

Cross-border e-commerce refers to the various trading entities in different frontiers, each other through a cross-border e-commerce platform to achieve transaction matching, the use of cross-border logistics network to transport goods, through a variety of cross-border financial channels to complete payment and settlement of goods, and ultimately conclude the transaction. Compared with the traditional international trade, cross-border e-commerce, as an Internet-based operation mode, has the characteristics of strong transaction convenience, information transparency, and diversification. Cross-border e-commerce makes foreign trade activities no longer limited by material, time and space, and other factors, breaking through the time and space constraints of traditional foreign trade and gradually becoming a new way of international trade transactions. The supply-side structural reform puts forward that traditional industries should be transformed and upgraded and new and advantageous industries should be created through scientific and technological innovation [17, 18]. The combination of China's traditional industries and cross-border e-business can create a new operation mode of "Internet plus traditional industries" and realize the integration of the real economy and the network economy. The advantages of science and technology were utilized to break through the gap between consumption demand and production supply, get rid of the dependence on traditional sales channels, and establish a brand new production and manufacturing response model to balance supply and demand [19]. The e-business supply chain model can be represented in Figure 1. At the same time, cross-border e-commerce breaks through the space-time constraints faced by traditional international trade by virtue of scientific and technological advantages, promotes global economic integration, and brings new impacts to the world economic and trade pattern [20]. Cross-border e-commerce can build a more open and diversified international economic and trade cooperation environment, which is conducive to China's foreign export enterprises to avoid trade barriers, expand export channels, and achieve optimal allocation of resources in various countries, which is of great importance to the realization of the national "one belt and one way" strategy [21]. China's cross-border e-commerce export industry, as a product of the close combination of traditional industry and Internet economy, can effectively solve the problem of mismatch between supply and demand in the foreign trade industry. The use of technological innovation for global consumers and suppliers of high-quality goods in China to build an effective trading platform to help China's traditional industries effectively releases capacity worldwide and removes inventory. The development of cross-border e-commerce conforms to the strategic plan of national supply-side reform and can provide a new grasp and impetus for deepening the supply-side reform in the field of foreign trade [22].

2.2. The Development of Cross-Border E-Commerce. The policy objective of the supply-side structural reform is to eliminate backward production capacity, reduce operating costs, reduce excess inventory, reduce excessive leverage of financial liabilities, and make up for the shortcomings of enterprise operating quality and efficiency. Due to the change of the international economic environment and the shrinkage of market demand, China's traditional foreign trade export industry is facing the situation of excess production

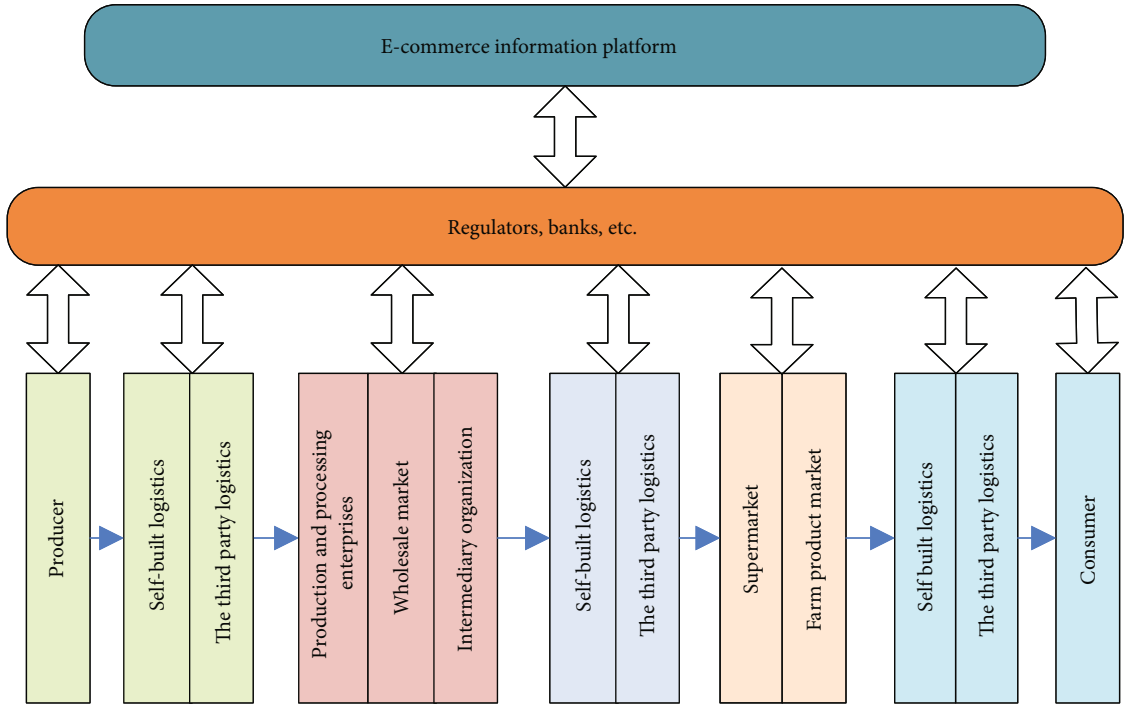

Figure 1: Commodity e-commerce supply chain schematic diagram.

capacity, product backlog, and difficult operation of enterprises. To deepen the supply-side reform in the field of foreign trade, the cross-border e-commerce industry provides a good solution path and examples [23].

In recent years, China's cross-border e-commerce industry has sprung up; benefiting from scientific and technological innovation and policy support, cross-border e-commerce can break through the constraints of the relatively weak international economic environment, develop rapidly, and become a highlight and hot spot of China's foreign trade development. In the process of supply-side structural reform, cross-border e-commerce can balance the contradiction between supply and demand worldwide through a market mechanism, digest excess capacity, and optimize product structure. With the advantages of Internet information technology, the foreign trade industry can realize the timely transmission of product supply and demand information through the cross-border e-commerce platform. Through the monitoring and analysis of the large-scale trading data, the foreign trade industry can timely screen and optimize the allocation of resources, find out the elimination of backward products, sort out the changing trend of product supply and demand structure, and provide a decision-making basis for the government to reduce production capacity, optimize the industrial layout, and implement all-round structural adjustment and transformation and upgrading [24]. Cross-border e-commerce provides more opportunities for small- and medium-sized enterprises to open up international markets and provide consumers with more personalized products and services [25]. The operation mode conforms to the changing trend of global consumption habits, breaks through the restrictions of time and geographical location, realizes the accurate matching of supply and demand in the global scope, releases the potential purchasing power, and improves the utilization rate of resources, thus promoting the growth of foreign trade volume and effectively eliminating the surplus stock in the foreign trade industry [26]. For example, in the "flash purchase" mode in cross-border e-commerce, enterprises with the advantages of scientific and technological information accurately grasp consumer psychology and behavior, in a specific time to focus on discount promotional activities for specified brand goods, in a short period of time to complete the cleaning of massive inventory. From the "deleveraging" point of view, cross-border e-commerce leverages the technological advantages of the Internet, opening up the cross-border demand and trade chain made in China, through high-frequency small fragmentation of the order operation mode to enhance trade volume, thereby alleviating the financial pressure of enterprises and reducing the tendency of enterprises to use excessive leverage. From the point of view of "cost reduction," cross-border e-commerce optimizes the supply and demand links between enterprises and consumers; reduces the information screening costs, transaction costs, and procurement costs of market participants; helps enterprises to improve operational efficiency; and opens up international markets at a lower cost. From the perspective of "complement board," cross-border e-commerce can use digital information technology to eliminate the widespread information mismatch, space-time mismatch, capacity mismatch, and other situations in foreign trade enterprises and promote high-quality production capacity "go out" by means of the Internet to promote China's foreign trade enterprises to expand the supply of high-end products, in order to increase the added value of

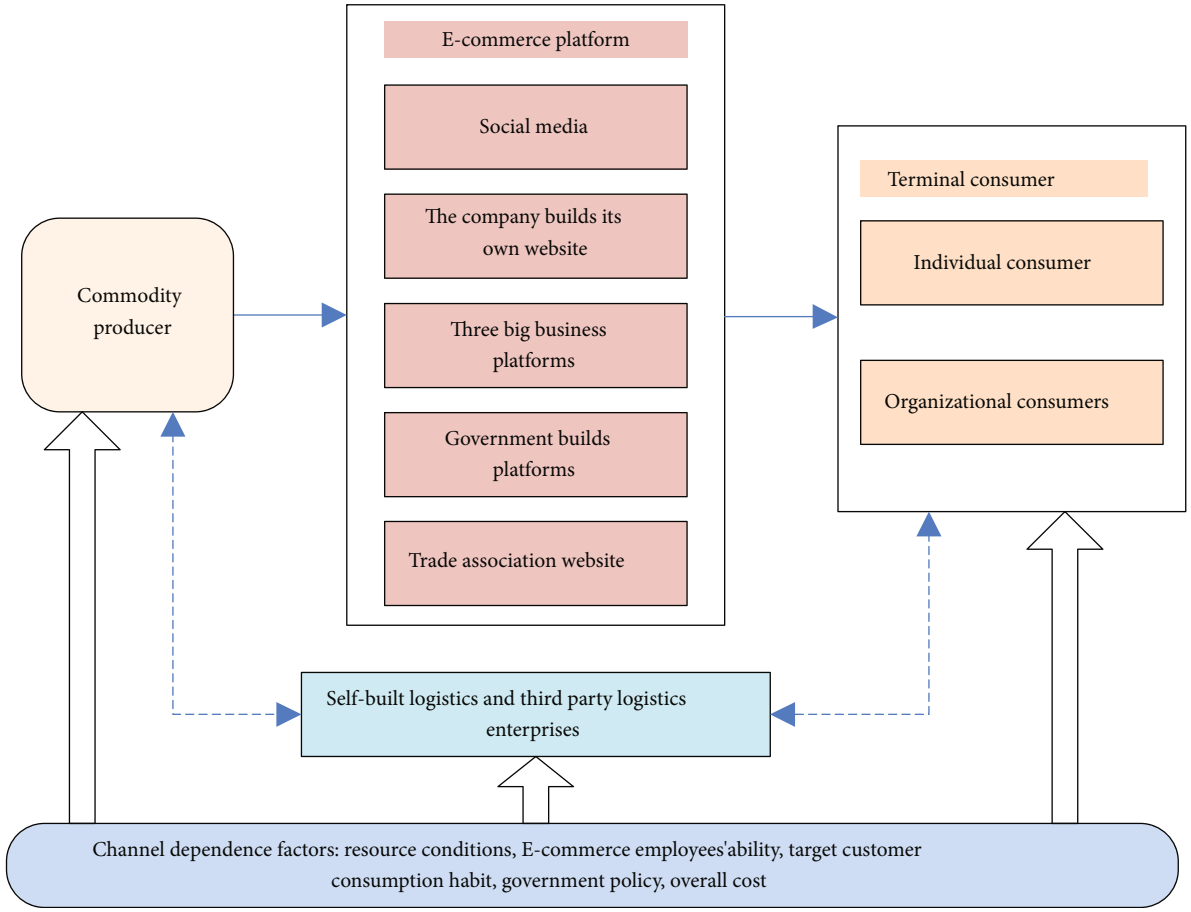

Figure 2: Channel pattern chart.

products, to make up for the lack of high-end products made in China's short board for economic innovation and development to open a new channel [27].

2.3. Cross-Border E-Commerce in the Context of Lateral Reform. China traditionally relies on resources, environment, demographic dividends, and other factors to accumulate foreign trade development advantages, but the current supply-side structural reform more emphasizes improving the quality of foreign trade supply from the system and innovation. The reform on the supply side of foreign trade emphasizes that the government should optimize the system supply and guarantee. The government should optimize the supply of public goods and services, reduce the institutional transaction costs of enterprises, and provide a driving force for cross-border e-commerce exports. At present, the development of cross-border e-commerce export has entered the stage of innovation-driven [28]. Enterprise performance must rely on all kinds of innovation, especially scientific and technological innovation to promote and achieve foreign trade economic growth. Innovation drive can give full play to the endogenous growth advantage of foreign trade and break the predicament of foreign trade from the supply side. Enterprises use the Internet platform to optimize social resources to carry out cross-border e-commerce; can stimulate the market entrepreneurs to innovate, through an innovative management mode, product design, and marketing services to drive upstream and downstream industrial chain to improve quality; cultivate brand; and tap China's foreign trade supply potential to create new supply. It is noteworthy that in addition to improving the quality of supply, cross-border e-commerce has also promoted the development of cross-border logistics, overseas warehousing, online payment, network marketing, and other emerging industries, changing the operation structure of traditional industries and realizing the transformation and upgrading of foreign trade. Cross-border e-commerce can also serve the country's "one belt and one road" strategic initiatives and build a new focus on the supply-side reform and expand the supply-side reform path and channel. Product producers establish business links with end-users through e-commerce platforms, such as social media, e-commerce companies, and industry websites. With the support of modern logistics, they have greatly met the demand of both suppliers and buyers for "selling" and "buying." Focusing on the structural elements of producers, consumers, e-commerce platforms, and logistics enterprises in the product upstream channel, five channels for developing product upstream e-commerce are constructed; the channel pattern chart is shown in Figure 2.

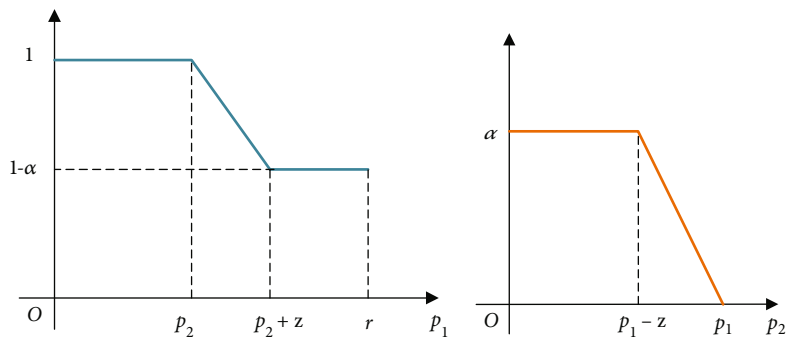

(a) Retailer 1 pricing (b) Retailer 2 pricing

Figure 3: Pricing of retailers.

In an economic environment with obvious personal needs, cross-border e-commerce orders show a trend of high frequency and fragmentation. The scattered orders reflect the diversification and individualization of current consumer needs. The key to maintaining a competitive advantage in cross-border e-commerce lies in the integration of supply chain costs, flexible production arrangements, scientific inventory management, and ensured effective flow of funds, thereby reducing the financial risks faced by foreign trade companies through accurate supply. For demand matching, secondly, the use of social network platforms to carry out online marketing is a new trend for foreign trade companies to broaden the export channels of cross-border e-commerce, and cross-border e-commerce with the help of social platforms can play a gathering role. Third, the global promotion of mobile Internet and smartphones has promoted the intelligence and mobility of cross-border e-commerce operations. The mobile APP client of cross-border e-commerce can make it easy for consumers to shop, and it can also enable foreign trade companies to timely grasp supply and demand information and collect valuable data. Fourth, by improving the infrastructure of cross-border payment, overseas warehousing, and logistics, the cost of cross-border e-commerce can be controlled.

3. Theoretical Analysis of Discrete Structure of Price

Suppose there are two retailers selling the same commodity in a product market. One retailer has a high degree of consumer concern; the other has a low degree of consumer concern. Suppose that the unit marginal cost is C, and the reserve price is R, and $R > C$ in the market; suppose that the consumer buys a unit product at most.

Not only the difference of consumers themselves will lead to different search costs, but the difference of retailers will also lead to the difference in search costs. Assuming that the cost of searching unknown retailers is not less than that of searching famous retailers, the difference of search costs between retailers will lead to different degrees of concern of consumers. In order to reflect the different levels of concern that businesses receive, assume that all consumers are concerned about retailer 1; only some people can focus on retailer 2 through more patient search. Assuming that the number of retailers who can search for both types of retailers is A, A reflects market transparency and the proportion of informed consumers.

In addition, the difference in search costs between retailers will lead to brand sensitivity (e.g., consumers may think that retailers without reputation are uncertain about the quality of the products they sell). Even if they sell homogeneous products, consumers are willing to pay a certain fee for famous retailers. Suppose that consumers have different brand preferences for retailers; that is, some consumers are reluctant to pay for the brand, while others are willing to buy from famous-brand retailers because they are more risk-averse or because of higher search costs. The same distribution from 0 to Z reflects the sensitivity of consumers to retailers' brands.

In Figure 3(a), when the price of retailer 1 is lower than that of retailer 2, retailer 1 will win all consumers; when the price of retailer 1 is much higher than that of retailer 2 and the amount exceeds the maximum possible brand payment, retailer 1 will lose all consumers who know retailer 2. When the price of retailer 1 is higher than that of retailer 2, but it does not exceed the consumer's brand willingness to pay, retailer 1 can get all consumers who do not know retailer 2, and also those who have high brand payment. For retailer 2, as shown in Figure 3(b), if the set price is much lower than that of retailer 1 and the spread exceeds the consumer's maximum brand willingness to pay, retailer 2 can get all the consumers who know it. When the price of retailer 2 is lower than that of retailer 1, but the price difference between retailer 2 and retailer 1 does not exceed the consumer's maximum brand willingness to pay, the market share decreases with the increase of the price until it loses all the market share at the same price as retailer 1. The pricing of retailers is shown in Figure 3.

Assuming that retailers cannot distinguish consumers with different levels of concern and brand sensitivity and implement price discrimination strategy, refer to the Lal (1990) or Raju et al. (1990) demand model. The given price (p_1, p_2) and exogenous variables (a, z, r, and c), the demand (q_1, q_2), and profit(π_1, π_2) functions of two retailers are expressed as follows:

$$q_1 = \begin{cases} 1, & p_1 \le p_2, \\ 1-\alpha+\alpha\cdot\dfrac{p_2+z-p_1}{z}, & p_2 \le p_1 \le p_2+z, \\ 1-\alpha, & p_2+z \le p_1 \le r, \end{cases}$$

$$\pi_1 = \begin{cases} p_1 - c, & p_1 \le p_2, \\ \left(1-\alpha+\alpha\cdot\dfrac{p_2+z-p_1}{z}\right)\cdot(p_1-c), & p_2 \le p_1 \le p_2+z, \\ (1-\alpha)(p_1-c), & p_2+z \le p_1 \le r, \end{cases}$$

$$q_2 = \begin{cases} \alpha, & p_2 \le p_1\text{-}z, \\ \alpha\cdot\dfrac{p_1-p_2}{z}, & p_1\text{-}z \le p_2 \le p_1, \\ 0, & p_1 \le p_2 \le r, \end{cases}$$

$$\pi_2 = \begin{cases} \alpha(p_2-c), & p_2 \le p_1\text{-}z, \\ \alpha\cdot\dfrac{p_1-p_2}{z}\cdot(p_2-c), & p_1 - z \le p_2 \le p_1, \\ 0, & p_1 \le p_2 \le r. \end{cases} \quad (1)$$

According to the optimization problem and Kuhn-Tucker sufficient and necessary conditions, it is known that retailer 1 and retailer 2 only exist pure strategy Nash equilibrium in three cases. For an interval in which there is no pure Nash equilibrium, there is at least one mixed strategy equilibrium. According to the necessary and sufficient conditions of mixed strategy equilibrium, two (continuous) distribution functions$(F_1(p_1), F_2(p_2))$ are obtained to represent the equilibrium of a mixed strategy, such as the following formulas (2) and (3). These two distribution functions reflect the probability that the retailer's price is equal to or below a certain value:

$$\begin{cases} F_1(r) = 1, \\ (p_2-c)\alpha(1-F_1(P_2+z)) + \displaystyle\int_{p_2}^{p_2+z}(p_2-c)\alpha\frac{p_1-p_2}{z}f_1(p_1)dp_1 = (p-z-c)\alpha, \quad \forall p_2 \in [p-z, r-z], \\ F_1(p) = 0, \end{cases} \quad (2)$$

$$\begin{cases} F_2(r\text{-}Z) = 1, \\ (p_1-c)(1-\alpha)F_2(P_1-z) + \displaystyle\int_{p_1-z}^{p_1}(p_1-c)\cdot\left[1-\alpha+\alpha\frac{p_2+z-p_1}{z}\right]\cdot f_2(p_2)dp_2 + (p_1-c)(1-F_2(p_1)) = (r-c)(1-\alpha), \quad \forall p_1 \in [p, r], \\ F_2(p-z) = 0, \end{cases}$$

$$p_1 = [p, r],$$

$$p_2 = [p-z, r-z], \quad (3)$$

$$p = \max\left\{c + \frac{\sqrt{az(r-c)(1-a)}}{a}, (1-\alpha)r + ac\right\}. \quad (4)$$

In which, $(F_1(p_1), F_2(p_2))$ can be used to test a retailer's price behavior under various conditions by reflecting the complex price behavior characteristics, pure strategy, and Nash equilibrium of mixed strategy. It can be seen clearly that brand sensitivity affects the distribution of the price level. In order to study the variation of market price dispersion with the proportion of informed consumers, the equilibrium distribution function of mixed strategy formulas (2) and (3) are given $z = 0$, at which time $p = \max\{c, (1-\alpha)r + \alpha c\}$:

$$\begin{cases} F_1(p_1) = 1(f_1(p_1) = (1-\alpha)), \quad p_1 = r, \\ F_1(p_1) = 1 - \dfrac{(r-c)(1-\alpha)}{(p_1-c)}, \quad p_1 \in [(1-\alpha)r + \alpha c, r], \\ F_1(p_1) = 0, \quad p_1 \in [0, (1-\alpha)r + \alpha c], \end{cases} \quad (5)$$

$$\begin{cases} F_2(p_2) = 1(f_2(p_2) = 0), \quad p_2 = r, \\ F_2(p_2) = \dfrac{1}{\alpha} - \dfrac{(r-c)(1-\alpha)}{(p_2-c)\alpha}, \quad p_2 \in [(1-\alpha)r + \alpha c, r], \\ F_2(p_2) = 0, \quad p_2 \in [0, (1-\alpha)r + \alpha c]. \end{cases}$$

6)

The assumption that consumer brand sensitivity $z = 0$ means that consumers in the market are reluctant to pay for the retailer's brand. This is an extreme scenario, but because the various search tools provided by the Internet can constantly provide product/service quality information for the retailers covered, it is possible to reduce the uncertainty of online consumers buying goods from nonbranded retailers. Under this assumption, we can independently

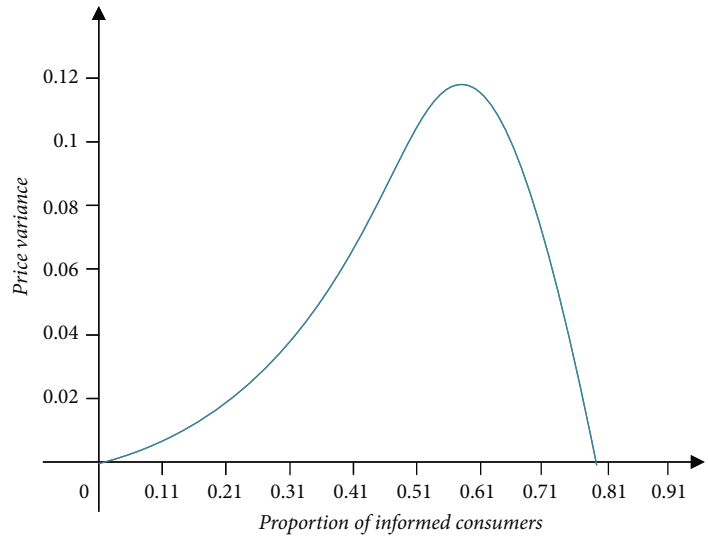

Figure 4: Convergence and expansion of price dispersion.

analyze the price dispersion of consumers under different attention α. The variance of p_1 and p_2 difference is further calculated:

$$\begin{aligned}\mathrm{Var}(p_1 - p_2) &= \mathrm{Var}(p_1) + \mathrm{Var}(p_2) \\ &= (r-c)^2(1-\alpha)\left[2\alpha + 2(1-\alpha)\ln(1-\alpha)\right. \\ &\quad \left. - (1-\alpha)\left[1 + \frac{1}{a^2}\right]\ln^2(1-\alpha) + 1\right].\end{aligned} \tag{7}$$

The variance of the price difference set by the two retailers is a measure of the dispersion of the two retail prices. Looking at the right side as a function of α, you can see that the size of R and C only changes the size of the function, not the shape of the function. Let us set up $c = 0, r = 1$, get the following Eq. (8). The convergence and expansion of price divergence are shown in Figure 4:

$$\begin{aligned}\mathrm{Var}(p_1 - p_2) &= (1-\alpha)\left[2\alpha + 2(1-\alpha)\ln(1-\alpha)\right. \\ &\quad \left. - (1-\alpha)\left[1 + \frac{1}{a^2}\right]\ln^2(1-\alpha) + 1\right].\end{aligned} \tag{8}$$

It can be seen that the price dispersion will increase with the increase of consumer attention until the consumer attention reaches a very high value ($\alpha \approx 0.83$); that is, when all consumers become informed consumers, the price dispersion reaches the maximum value, and then, the increase of consumer attention sharply reduces to the marginal cost. The conclusion seems counterintuitive, but it properly explains the objective phenomenon that the price dispersion of the e-commerce market does not converge or even expand, which is consistent with the international research results in recent years. With the popularization and use of information technology such as search engines, price dispersion still exists when the cost of information search is significantly reduced and more consumers become insiders:

Table 1: Range comparison table.

Number of periods	MCRs	Dotcoms	All
1	198.55	219.67	409.96
2	146.98	199.14	363.57
3	149.69	182.78	347.86
4	172.31	201.21	354.44
5	159.778	131.88	320.73
6	149.78	185.47	328.19
7	145.449	154.96	317.47
8	139.98	142.39	322.83
9	145.37	152.39	299.88
10	118.16	117.98	293.24
11	121.55	117.42	390.65
12	110.21	115.65	329.88
13	112.21	106.38	298.32
14	114.78	121.58	378.88
15	133.98	141.93	362.26
16	152.59	153.87	355.63
Total mean value	141.96	152.79	342.11

$\alpha = 1$ in formula (5) and (6) can be obtained:

$$F_1(c) = F_2(c) = 1. \tag{9}$$

That is, when the consumer brand is insensitive ($z = 0$), and the market information is sufficient, all consumers know all the retailers ($\alpha = 1$), then achieve complete competition in the Bertand model; the retailer must price at marginal cost c; otherwise, there is no consumer. On the other hand, consumer brand insensitivity ($z = 0$) and full market information ($\alpha = 1$) are necessary conditions for pure price competition. As long as consumers have brand loyalty, or not all consumers know all retailers, enterprises will make extra profits.

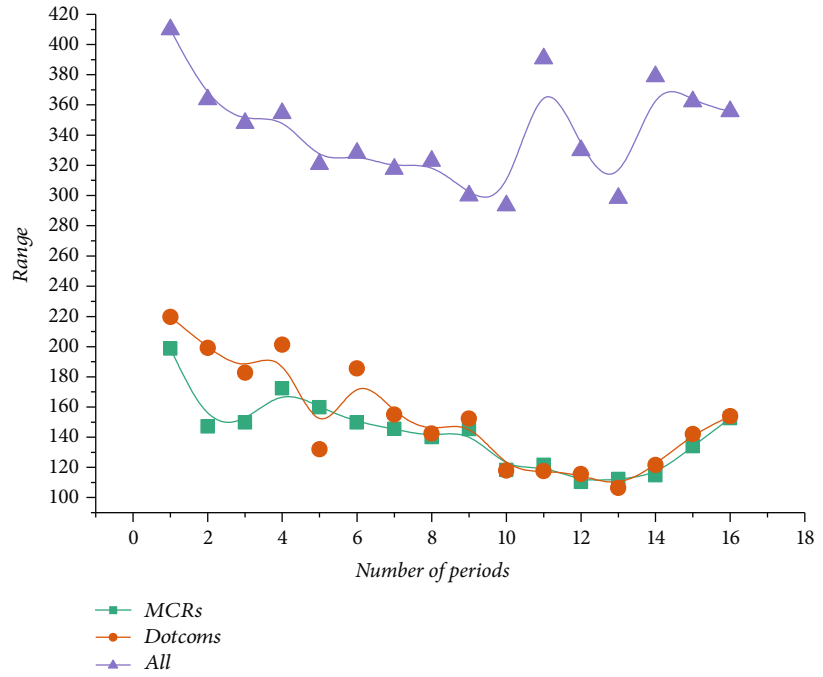

Figure 5: Extreme time trend chart.

In summary, price dispersion will persist if the two conditions $z = 0$ and $\alpha = 1$ hold for different levels of consumer concern or consumers are sensitive to the seller's brand.

4. Empirical Analysis of Retailer Price Dispersion in E-Commerce Market

Based on the grasp of the characteristics of network information technology, the "frictionless transaction hypothesis" of the network economy has been widely accepted by scholars. E-commerce will effectively reduce the market price and price deviation. In addition, more and more traditional offline retailers recognize the importance of online channels and begin to dabble in online sales, which can be called "multichannel retailers" (MCRs) or "pure online retailers" (Dotcoms). Therefore, this paper adopts the method of combining the theoretical model with empirical research to study the price and price dispersion between the above two types of retailers and compares whether the price and price deviation of the same product between different online retailers in the e-commerce environment are significantly reduced.

4.1. Statistical Analysis of the Extreme Price Difference of Commodities. The definition of the extreme difference is the difference between the maximum and minimum values of goods. In this paper, the price range is "the difference between the maximum and the minimum of the same commodity price of different retailers of the same type at the same time." The expression is as follows:

$$R = \text{Maximum value} - \text{Minimum value}. \quad (10)$$

Based on the statistical analysis of the data, it is concluded that the difference between the two types of retailers' sales of all mobile phone products varies with time as shown in Table 1.

Table 2: Standard deviation comparison table.

Number of periods	MCRs	Dotcoms	All
1	99.64	115.98	143.28
2	89.88	105.83	117.65
3	93.12	80.21	124.32
4	87.87	95.38	115.98
5	85.43	88.96	108.69
6	84.24	87.72	98.25
7	75.48	80.77	86.59
8	68.54	75.57	97.28
9	65.62	71.35	103.89
10	64.62	71.21	89.31
11	64.58	71.48	110.66
12	60.64	66.68	136.82
13	68.61	71.86	98.76
14	69.22	76.21	99.43
15	70.35	73.47	118.12
16	70.83	81.87	134.12
Total mean value	76.17	82.16	111.45

According to the above table, the time trend chart for plotting range variation is shown in Figure 5.

The range comparison table and the extreme time trend table of the two types of retailers can be obtained; the average price range for Dotcoms retailers is 152.79, while the average price range for MCR retailers is 141.96. Dotcoms retailers have greater price fluctuations than MCR retailers. The price ranges of both retailers have shown a downward trend. The

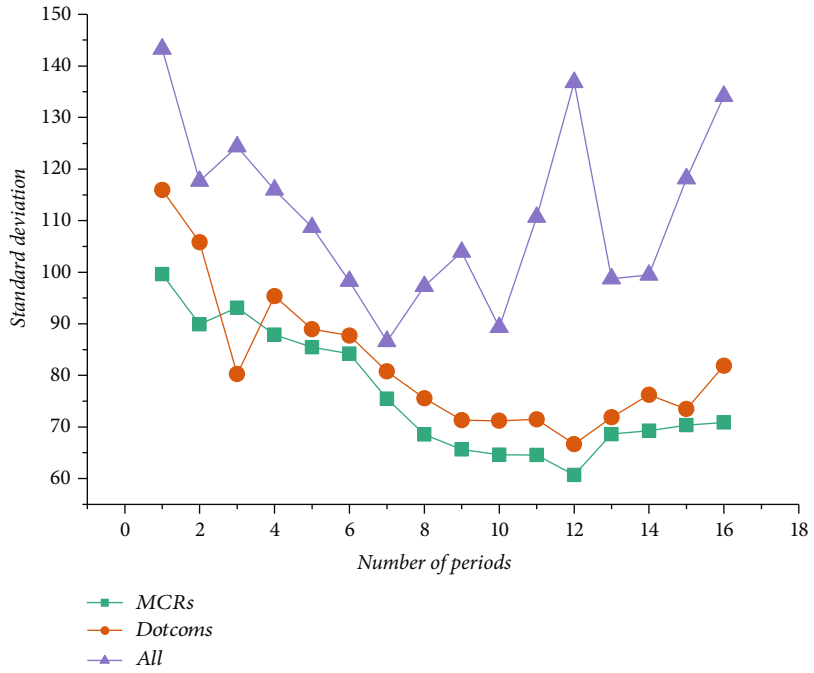

Figure 6: Price standard deviation time trend chart.

reason is that with the advent of the peak sales season, retailers have shown higher efficiency in their pricing strategies, so the price range between the two types of retailers tends to shrink.

4.2. Statistical Analysis of Commodity Price Standard Deviation. The price standard deviation is the square root of the ratio of the sum of squares of the difference between the price and the mean value of the price $(n-1)$:

$$\mathrm{SD} = \sqrt{\frac{1}{n-1}\sum_{i=1}^{n}(x_i - \bar{x})^2}. \tag{11}$$

The trend of price deviation of all two types of retailers is shown in Table 2.

The trend chart of the change in price standard deviation is shown in Figure 6.

It can be seen from Table 2 and Figure 6, in addition to the third issue, that the price standard deviation of Dotcoms is higher than that of MCRs. The average price standard deviation of Dotcoms is 82.16, while that of MCRs is 76.17. This is consistent with the conclusion of extreme difference analysis. The price dispersion of Dotcoms is greater than that of MCRs.

In the early period, the price standard deviation between the two is obviously different, and in the sixth and seventh periods, the price standard deviation of the two is consistent; the difference is not significant, which also reflects the "holiday effect" of retailer pricing.

4.3. Statistical Analysis of Price Dispersion Rate. Generally speaking, the discrete rate is the ratio of the standard deviation to the mean. Therefore, in this paper, the price discrete rate refers to the degree of deviation of the price distribution of the same commodity relative to a central price distribution in the market. This paper adopts the ratio of price standard deviation to average price to measure the price dispersion rate. That is,

$$\mathrm{DR} = \frac{\mathrm{SD}}{\mathrm{average\ (Price)}}. \tag{12}$$

Table 3: Price dispersion rate comparison table.

Number of periods	MCRs	Dotcoms	All
1	0.053	0.051	0.071
2	0.049	0.056	0.061
3	0.049	0.045	0.064
4	0.048	0.052	0.051
5	0.047	0.04	0.057
6	0.047	0.049	0.053
7	0.044	0.047	0.049
8	0.041	0.045	0.054
9	0.038	0.043	0.058
10	0.038	0.043	0.051
11	0.038	0.043	0.061
12	0.039	0.041	0.073
13	0.042	0.044	0.057
14	0.043	0.046	0.057
15	0.044	0.046	0.067
16	0.045	0.051	0.077
Total mean value	0.043	0.046	0.06

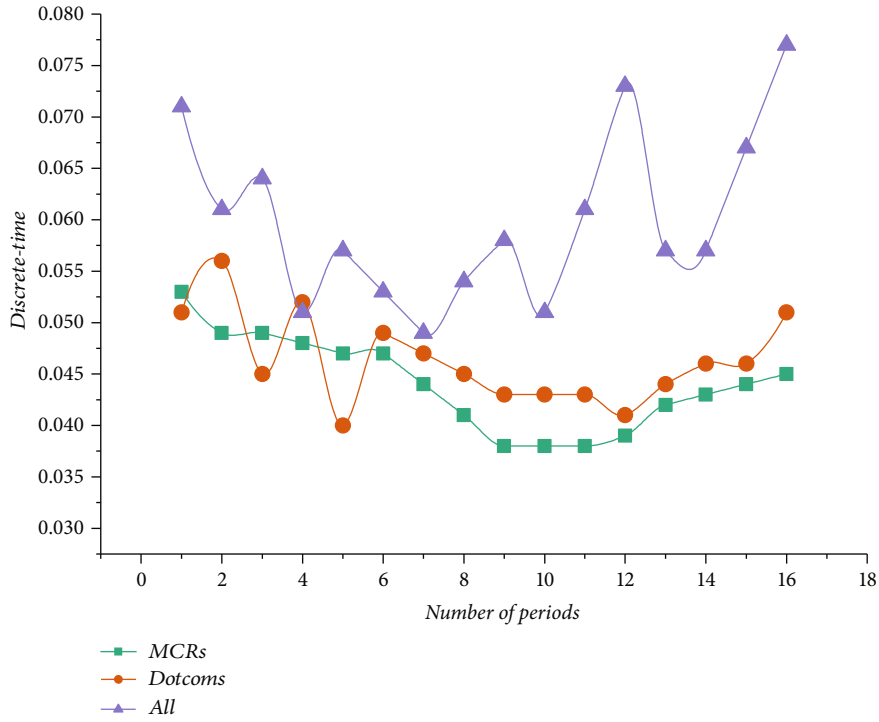

Figure 7: Price dispersion rate time trend chart.

The price dispersion rate of all two types of retailers varying with time is shown in Table 3.

The trend of the price dispersion rate is shown in Figure 7.

It can be seen from Table 3 and Figure 7 that the average price dispersion rate of Dotcoms retailers is 0.046, and that of MCR retailers is 0.043. Dotcoms retailers are higher than MCR retailers. The trend of the price dispersion rate of the two retailers is roughly the same as the trend of the price standard deviation. By comparing and analyzing the price range, standard deviation, and price dispersion rate of all mobile phone products sold by the two retailers, we can draw the following conclusions: Dotcoms retailer's extreme deviation, standard deviation, and dispersion rate average are higher than MCR retail. In most periods, the three trends of the two types of sellers are almost the same.

5. Conclusion

The results show that the price dispersion of the e-commerce market is not convergent, and the price dispersion is not a temporary phenomenon of the immature e-commerce market. It will be universal and persistent: as long as consumers are brand sensitive or not all consumers are concerned about all retailers, prices vary between retailers with different levels of attention. When using the price dispersion index to measure the market efficiency, it is necessary to determine the proportion of informed consumers in the market, because when the proportion of informed consumers is lower than a fairly high proportion, the price dispersion will actually increase with the proportion of informed consumers. Price dispersion is a common phenomenon in the products studied in this paper. The price dispersion of cosmetics, audiovisual products, gifts, and books is greater. The characteristics of retailers have a significant impact on prices. The study shows that there are three types of e-commerce retailers in China's e-commerce market which are aimed at different consumer groups, and their pricing bases are different. No matter what type of retailer, the provision of quality service does not necessarily mark a higher price. The net sellers who enter the online market earlier will have lower prices.

Data Availability

All data is true and reliable and can be obtained by contacting the corresponding author.

Conflicts of Interest

We declare that there is no conflict of interest regarding the publication of this paper.

References

[1] L. Wang, Q. Wu, J. Elliot, F. R. Fiedler, and S. Lapin, "Linear diffusion-wave channel routing using a discrete Hayami convolution method," *Journal of Hydrology*, vol. 509, no. 2, pp. 282–294, 2014.

[2] J. Sha, W. Wu, T. Lv, and W. Wu, "Coordination of advertising free riding in hybrid channel supply chain," *Discrete Dynamics in Nature and Society*, vol. 2016, Article ID 7423043, 9 pages, 2016.

[3] R. Wang, P. Wang, G. Xiao, and S. Gong, "Power demand and supply management in microgrids with uncertainties of

renewable energies," *International Journal of Electrical Power & Energy Systems*, vol. 63, no. 12, pp. 260–269, 2014.

[4] M. Gümüş, S. Li, W. Oh, and S. Ray, "Shipping fees or shipping free? A tale of two price partitioning strategies in online retailing," *Production & Operations Management*, vol. 22, no. 4, pp. 758–776, 2013.

[5] A. J. Heitmann and R. S. Gardiner-Garden, "A robust feature extraction and parameterized fitting algorithm for bottom-side oblique and vertical incidence ionograms," *Radio Science*, vol. 54, no. 1, pp. 115–134, 2019.

[6] X. Nie, T. Boyacı, M. Gümüş, S. Ray, and D. Zhang, "Joint procurement and demand-side bidding strategies under price volatility," *Annals of Operations Research*, vol. 257, no. 1-2, pp. 121–165, 2017.

[7] X. K. Xie, R. Verma, and C. K. Anderson, "Demand growth in services: a discrete choice analysis of customer preferences and online selling," *Decision Sciences*, vol. 47, no. 3, pp. 1450–1462, 2016.

[8] L. Xia and B. Shihada, "A Jackson network model and threshold policy for joint optimization of energy and delay in multihop wireless networks," *European Journal of Operational Research*, vol. 242, no. 3, pp. 778–787, 2015.

[9] Q. Pang, Y. Chen, and Y. Hu, "Three-level supply chain coordination under disruptions based on revenue-sharing contract with price dependent demand," *Discrete Dynamics in Nature and Society*, vol. 2014, Article ID 464612, 11 pages, 2014.

[10] S. Hurkens and Á. L. López, "Mobile termination, network externalities and consumer expectations," *Economic Journal*, vol. 124, no. 579, pp. 1005–1039, 2014.

[11] D. Gao, N. Wang, and Z. He, "The bullwhip effect in an online retail supply chain: a perspective of price-sensitive demand based on the price discount in e-commerce," *IEEE Transactions on Engineering Management*, vol. 64, no. 2, pp. 134–148, 2017.

[12] A. Paciorek, "Supply constraints and housing market dynamics," *Journal of Urban Economics*, vol. 77, no. 1, pp. 11–26, 2013.

[13] J. Brandts, S. S. Reynolds, and A. Schram, "Pivotal suppliers and market power in experimental supply function competition," *Economic Journal*, vol. 124, no. 579, pp. 887–916, 2014.

[14] I. Kim and A. Petrin, "Tests for price endogeneity in differentiated product models," *Journal of Econometric Methods*, vol. 4, no. 1, pp. 47–69, 2015.

[15] S. Rezapour, J. K. Allen, and F. Mistree, "Uncertainty propagation in a supply chain or supply network," *Transportation Research Part E Logistics & Transportation Review*, vol. 73, pp. 185–206, 2015.

[16] T. Berry and A. Haile, "Identification in differentiated products markets using market level data," *Econometrica*, vol. 82, no. 5, pp. 1749–1797, 2014.

[17] J. Venables, "Depletion and development: natural resource supply with endogenous field opening," *Journal of the Association of Environmental & Resource Economists*, vol. 1, no. 3, pp. 313–336, 2014.

[18] W. Chung, S. Talluri, and R. Narasimhan, "Optimal pricing and inventory strategies with multiple price markdowns over time," *European Journal of Operational Research*, vol. 243, no. 1, pp. 130–141, 2015.

[19] E. Adida and G. Perakis, "The effect of supplier capacity on the supply chain profit," *Annals of Operations Research*, vol. 223, no. 1, pp. 1–52, 2014.

[20] Y. Fan, "Ownership consolidation and product characteristics: a study of the US daily newspaper market," *American Economic Review*, vol. 103, no. 5, pp. 1598–1628, 2013.

[21] H. Liang, J. Zou, K. Zuo, and M. J. Khan, "An improved genetic algorithm optimization fuzzy controller applied to the wellhead back pressure control system," *Mechanical Systems and Signal Processing*, vol. 142, article 106708, 2020.

[22] H. Zheng, W. Guo, and N. Xiong, "A kernel-based compressive sensing approach for mobile data gathering in wireless sensor network systems," *IEEE Transactions on Systems, Man, and Cybernetics: Systems*, vol. 48, no. 12, pp. 2315–2327, 2017.

[23] Z. Huang, X. Xu, J. Ni, H. Zhu, and C. Wang, "Multimodal representation learning for recommendation in Internet of Things," *IEEE Internet of Things Journal*, vol. 6, no. 6, pp. 10675–10685, 2019.

[24] H. Liang, J. Zou, Z. Li, M. J. Khan, and Y. Lu, "Dynamic evaluation of drilling leakage risk based on fuzzy theory and PSO-SVR algorithm," *Future Generation Computer Systems*, vol. 95, pp. 454–466, 2019.

[25] Z. Liu, B. Hu, B. Huang, L. Lang, H. Guo, and Y. Zhao, "Decision optimization of low-carbon dual-channel supply chain of auto parts based on smart city architecture," *Complexity*, vol. 2020, Article ID 2145951, 14 pages, 2020.

[26] Y. Zhang, R. Zhu, Z. Chen, J. Gao, and D. Xia, "Evaluating and selecting features via information theoretic lower bounds of feature inner correlations for high-dimensional data," *European Journal of Operational Research*, vol. 11, 2020.

[27] H. Liang, A. Xian, M. Min Mao, P. Ni, and H. Wu, "A research on remote fracturing monitoring and decision-making method supporting smart city," *Sustainable Cities and Society*, vol. 62, article 102414, 2020.

[28] Y. Zhou, D. Zhang, and N. Xiong, "Post-cloud computing paradigms: a survey and comparison," *Tsinghua Science and Technology*, vol. 22, no. 6, pp. 714–732, 2017.

Hindawi
Wireless Communications and Mobile Computing
Volume 2020, Article ID 6646808, 13 pages
https://doi.org/10.1155/2020/6646808

Research Article

An Intelligent Group Decision Evaluation Model with Interval-Valued Intuitionistic Fuzzy Entropy Technology for Microblog User Influence

Lihua Zeng,[1] Tonghua Yang,[2] Haiping Ren,[1] and Neal Xiong[3]

[1]*Teaching Department of Basic Subjects, Jiangxi University of Science and Technology, China*
[2]*School of Vocational Education and Technology, Jiangxi Agricultural University, China*
[3]*Department of Mathematics and Computer Science, Northeastern State University, USA*

Correspondence should be addressed to Tonghua Yang; yangth883@163.com

Received 15 October 2020; Revised 26 November 2020; Accepted 1 December 2020; Published 17 December 2020

Academic Editor: Hongju Cheng

Copyright © 2020 Lihua Zeng et al. This is an open access article distributed under the Creative Commons Attribution License, which permits unrestricted use, distribution, and reproduction in any medium, provided the original work is properly cited.

Aiming at the shortcomings of some existing interval-valued intuitionistic fuzzy entropy, this paper proposes an interval-valued intuitionistic fuzzy entropy, which contains not only the interval distance between membership and nonmembership but also the average hesitancy information. On this basis, the impact evaluation of microblog users is studied. Through the multilevel decomposition of user influence, the coverage of microblog, user interaction, and user activity are constructed as the first level indicators, and nine secondary indicators are selected as the comprehensive evaluation index system of microblog influence. Considering the highly dynamic and unstructured characteristics of social network data, the idea of interval-valued intuitionistic fuzzy is introduced to transform the evaluation of social network users' influence into interval-valued intuitionistic fuzzy multiattribute group decision-making problem. Finally, the model is applied to dynamic evaluation of Sina Weibo users' influence to verify the effectiveness of the model.

1. Introduction

A network is composed of several nodes and links connecting these nodes, which represents many objects and their relationship. Nowadays, there are various kinds of networks in the society, such as computer network, wireless sensor network [1–5], PSTN network [6], cable TV network, Internet of things [7, 8], and social network.

Social network [9–12] refers to social network services, such as blog, wiki, tag, SNS, RSS, and a series of core web2.0 applications. As can be seen from Figure 1, with the wide application of web technology and mobile Internet, social networks in China have been developing rapidly. The network has really formed a society, not just a new media, new business, and new way of communication. The biggest feature of the Internet is that individuals become the main body of the Internet. Specifically, in the future, everyone, except himself in real life, will have his own representative on the Internet. It can reflect your personality, your thoughts, and all kinds of information on the Internet. At the same time, we can also communicate with you at any time. Everyone becomes a "node" of the Internet. This is different from other networks; for example, the nodes of computer networks are computers, and the nodes of wireless sensor networks are some static or mobile sensors [13–20].

In social network, some user nodes have great influence on other user nodes, which are called "opinion leader." In 1955, Katz and Lazaxsfeld [10] described high impact users, namely, "opinion leaders," as "a person can influence people in their surroundings." Through the study of voters' voting intention in the US presidential election, Katz proposed a two-level communication theory and found that individual influences differences. A small number of "opinion leaders" or "influential individuals" affect most ordinary people. Similarly, Roch also found that a small number of influential users are the key nodes to accelerate or hinder the occurrence

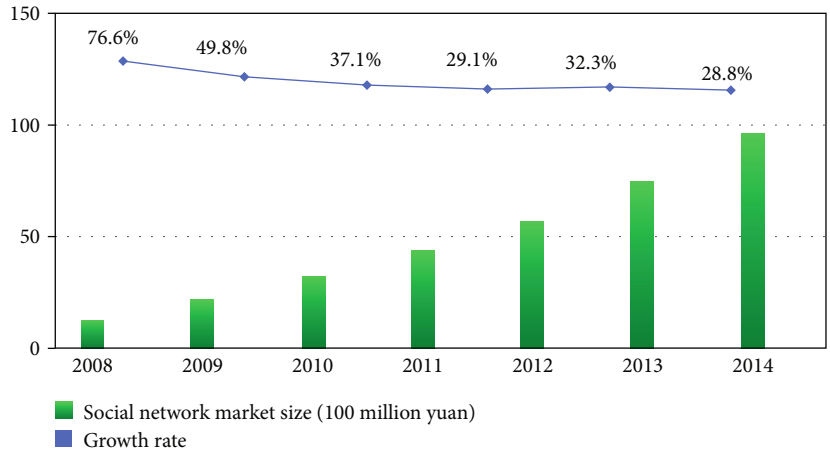

Figure 1: 2008-2014 China's social network market size and development trend.

of mass trading. Therefore, how to effectively evaluate the influence of users in social networks and find out "opinion leaders" play an extremely important role in information dissemination, public opinion guidance, advertising recommendation, user recommendation, and so on. In terms of public opinion monitoring, special measures should be taken for some high impact users in order to avoid public opinion flooding. For advertising, choosing the users with great influence can maximize the communication effect. As far as user recommendation is concerned, opinion leaders in the user's field of interest are often the default recommended objects. To sum up, reasonable measurement of social network users' influence is of great significance to improve the marketing effect, guide the healthy development of public opinion, and maintain the network order. This has aroused the interest of many researchers [21–26].

Atanassov and Gargov [27] extended intuitionistic fuzzy sets and proposed the concept of interval-valued intuitionistic fuzzy (IVIF) sets, which can reflect the fuzzy nature of the objective world more carefully and flexibly. IVIF entropy is a measure to describe the fuzziness of IVIF sets. It has many applications in reflecting the weight of information [28–30].

2. The Related Work

At present, combing the relevant literature, we find that there are various methods to measure the influence of social network users. The most commonly used methods are HITS algorithm proposed by Kleinberg [25], PageRank algorithm proposed by Page and Brin, and the improved algorithm. Hits and PageRank algorithm were proposed almost at the same time in the late 1990s and became the classic algorithm of ranking the importance of web pages in the field of search engine. Later, social network data was abstracted into directed network model by various methods, and web page ranking algorithm began to be used in social network research. Cha et al. [31] used a lot of twitter data to analyze the relationship between user behavior and influence and compared with Spearman rank correlation coefficient to get the ranking of user influence. Kwak et al. [32] used page rank algorithm to analyze the influence of users and analyzed the correlation between the number of forwarding and the number of fans and found that there was a weak correlation between them. Lee et al. [33] proposed a ranking method of influence based on time series. This method not only considers the link structure but also adds the time information of users' Publishing microblogs, which can mine some users with potential influence. Romero et al. [34] proposed a new influence measurement method IP influence after fully considering and analyzing user influence and resistance. Weng et al. [35] according to the page rank method, based on the influence of topic similarity, designed an evaluation model applied to calculate the influence of each user's microblog. Ye and Wu [36] proposed a method to rank the content of the user's home page as the importance ranking index by analyzing the user's behavior, the number of fans, and the number of tweets. However, there are still some defects and high complexity in web page ranking algorithm. The convergence and effectiveness of the algorithm cannot be guaranteed at the same time, and it is usually only applicable to certain types of social networks.

The third type is the user influence evaluation method based on the unified resource locator (URL) tracking. Each Internet file contains a unique URL, and its function is to locate the Internet resources. Bakshy et al. [37] calculated the influence value of each user by combining the information dissemination model and the reputation effect principle from the URL of the information release. The dynamic tracking method distinguishes the role of users in different positions on the propagation path but ignores the information difference of user behavior and communication content, which will lead to information loss.

Different from the method of user influence evaluation based on the topological structure and computer iterative operation, this paper transforms microblog user influence evaluation into the IVIF multiattribute group decision-making problem. The interval intuitionistic fuzzy multiattribute group decision-making method combines interval intuitionistic fuzzy theory with multiattribute group decision-making. Its feature is that the fuzzy nature of complex decision-making problems can be described more carefully by using interval numbers instead of real numbers.

Firstly, through the multilevel decomposition of user influence, the coverage of microblog, user interaction, and user activity are constructed as the first-class indicators. Nine secondary indicators such as whether to add v-authentication, the number of microblogs, the number of active fans, the average number of daily microblogs, and the original rate of microblog are selected for the comprehensive evaluation index system of microblog influence. Secondly, time dimension is introduced to describe user data by the interval number. The advantage of IVIFN in dealing with complex, fuzzy, and uncertain data is used to transform user information data into IVIFN. Then, the IVIF entropy is improved, which includes not only the interval distance of membership and nonmembership but also the average hesitancy information. The entropy weight method is used to weight each evaluation index based on this entropy, so as to overcome the limitation of subjective weighting. Then, the criterion values are normalized and the score and precise values are calculated, so that the user influence is ranked and evaluated. Finally, the model is applied to dynamic evaluation of Sina Weibo users' influence to verify the effectiveness of the model.

3. Preliminary Knowledge

This section will recall some basic concepts and properties of IVIF sets.

Definition 1 [38]. Let X_1 be a given universal set. An intuitionistic fuzzy set (IFS) is an object having the form: $B = \{<x_i, \mu_B(x_i), \nu_B(x_i)>|x_i \in X_1\}$ where the function $\mu_B : X_1 \to [0, 1]$ defines the degree of membership and $\nu_B : X_1 \to [0, 1]$ defines the degree of nonmembership of the element $x_i \in X_1$, respectively, and for every $x_i \in X_1$, it holds that $0 \le \mu_B + \nu_B \le 1$. Furthermore, for any IFS B and given $x_i \in X_1$, $\pi_B(x_i) = 1 - \mu_B(x_i) - \nu_B(x_i)$ is called the hesitancy degree of x_i.

Definition 2 [27]. Let $X = \{x_1, x_2, \cdots, x_n\}$ be a universal set and $\mathrm{Int}([0, 1])$ represent the set of all closed subintervals of $[0, 1]$. An IVIF set is an object having the form: $\tilde{A} = \{<x, \tilde{\mu}_{\tilde{A}}(x), \tilde{\nu}_{\tilde{A}}(x)>|x \in X\}$ where the function $\tilde{\mu}_{\tilde{A}} : X \to \mathrm{Int}([0, 1])$ defines the degree of membership and $\tilde{\nu}_{\tilde{A}} : X \to \mathrm{Int}([0, 1])$ defines the degree of nonmembership of the element $x_i \in X$, respectively, and for every $x_i \in X$, it holds that $0 \le \sup \tilde{\mu}_{\tilde{A}}(x) + \sup \tilde{\nu}_{\tilde{A}}(x) \le 1$. For convenience, IVIF sets can also be written as

$$\tilde{A} = \left\{<x, \left[\mu_{\tilde{A}}^L(x), \mu_{\tilde{A}}^U(x)\right], \left[\nu_{\tilde{A}}^L(x), \nu_{\tilde{A}}^U(x)\right]>|x \in X\right\}, \quad (1)$$

where $\mu_{\tilde{A}}^U(x) + \nu_{\tilde{A}}^U(x) \le 1$, $\mu_{\tilde{A}}^L(x) \ge 0$ and $\nu_{\tilde{A}}^L(x) \ge 0$.

Let $\tilde{\pi}_{\tilde{A}}(x) = 1 - \tilde{\mu}_{\tilde{A}}(x) - \tilde{\nu}_{\tilde{A}}(x) = [1 - \mu_{\tilde{A}}^U(x) - \nu_{\tilde{A}}^U(x), 1 - \mu_{\tilde{A}}^L(x) - \nu_{\tilde{A}}^L(x)]$; then, it is called hesitancy of x_i. All IVIF sets on X are denoted as IVIFS(X).

Generally, the ordered pair $([\mu_{\tilde{A}}^L(x), \mu_{\tilde{A}}^U(x)], [\nu_{\tilde{A}}^L(x), \nu_{\tilde{A}}^U(x)])$ composed of membership interval $[\mu_{\tilde{A}}^L(x), \mu_{\tilde{A}}^U(x)]$ and nonmembership interval $[\nu_{\tilde{A}}^L(x), \nu_{\tilde{A}}^U(x)]$ of element x in X is called IVIF number (IVIFN). For convenience, the general form of IVIFN is denoted as $([a, b], [c, d])$, where $[a, b] \subset [0, 1]$, $[c, d] \subset [0, 1]$, $b + d \le 1$.

Definition 3 [27]. Let $\tilde{A}$ and $\tilde{B}$ be two IVIF sets; then

(1) $\tilde{A} \subseteq \tilde{B}$ if and only if

$\mu_{\tilde{A}}^L(x) \le \mu_{\tilde{B}}^L \quad (x), \mu_{\tilde{A}}^U(x) \le \mu_{\tilde{B}}^U(x), \nu_{\tilde{A}}^L(x) \ge \nu_{\tilde{B}}^L(x), \nu_{\tilde{A}}^U(x) \ge \nu_{\tilde{B}}^U(x)$, for all $x_i \in X$

(2) $\tilde{A} = \tilde{B}$ if and only if $\tilde{A} \subseteq \tilde{B}$ and $\tilde{B} \subseteq \tilde{A}$

(3) The complementary set of $\tilde{A}$ denoted by $\tilde{A}^C$ is

$$\tilde{A}^C = \left\{<x, \left[\nu_{\tilde{A}}^L(x), \nu_{\tilde{A}}^U(x)\right], \left[\mu_{\tilde{A}}^L(x), \mu_{\tilde{A}}^U(x)\right]>|x \in X\right\} \quad (2)$$

Definition 4 [27]. Let $\tilde{a} = ([a, b], [c, d])$, $\tilde{a}_1 = ([a_1, b_1], [c_1, d_1])$, and $\tilde{a}_2 = ([a_2, b_2], [c_2, d_2])$ be three IVIFNs; then

(1) $\tilde{a}_1 + \tilde{a}_2 = ([a_1 + a_2 - a_1a_2, b_1 + b_2 - b_1b_2], [c_1c_2, d_1d_2])$

(2) $\lambda\tilde{a} = ([1 - (1 - a)^\lambda, 1 - (1 - b)^\lambda], [c^\lambda, d^\lambda]), \lambda > 0$

(3) $\tilde{a}^\lambda = ([a^\lambda, b^\lambda], [1 - (1 - c)^\lambda, 1 - (1 - d)^\lambda]), \lambda > 0$

Definition 5. Let $\tilde{a} = ([a, b], [c, d])$ be an IVIFN. The score function and accuracy function of $\tilde{a}$ are

$$\Delta(\tilde{a}) = \frac{1}{4}(a - c + b - d)\left(1 + \frac{1}{a + b - ac + bd}\right), \quad (3)$$

$$H(\tilde{a}) = \frac{1}{2}(a + b + c + d), \quad (4)$$

respectively, which are given by Gao et al. [28].

Based on the score and accuracy functions, a comparison law for IVIFN is introduced by Gao et al. [28] as follows:

Let $\tilde{a}_1$ and $\tilde{a}_2$ be two IVIFNs, $\Delta(\tilde{a}_1)$ and $\Delta(\tilde{a}_2)$ be the scores of $\tilde{a}_1$ and $\tilde{a}_2$, respectively, $H(\tilde{a}_1)$ and $H(\tilde{a}_2)$ be the accuracy degrees of $\tilde{a}_1$ and $\tilde{a}_2$, respectively.

(1) If $\Delta(\tilde{a}_1) < \Delta(\tilde{a}_2)$, then $\tilde{a}_1 < \tilde{a}_2$.

(2) If $\Delta(\tilde{a}_1) = \Delta(\tilde{a}_2)$, then

$$\begin{cases} H(\tilde{a}_1) = H(\tilde{a}_2) \Rightarrow \tilde{a}_1 = \tilde{a}_2, \\ H(\tilde{a}_1) < H(\tilde{a}_2) \Rightarrow \tilde{a}_1 < \tilde{a}_2 \end{cases} \quad (5)$$

Definition 6 [29]. Let $\tilde{a}_j = ([a_j, b_j], [c_j, d_j])$ $(j = 1, 2, \cdots, n)$ be a collection of IVIFNs and $\omega = (\omega_1, \omega_2, \cdots, \omega_n)^T$ be the weight vector of $\tilde{a}_j$ $(j = 1, 2, \cdots, n)$, where ω_j indicates the importance degree of $\tilde{a}_j$, satisfying $\omega_j \ge 0$ $(j = 1, 2, \cdots, n)$ and $\sum_{j=1}^n \omega_j = 1$, and let $\mathrm{IIFWA}_\omega : {F_I}^n \to F_I$, if

$$\mathrm{IIFWA}_{\omega}(\tilde{a}_1, \tilde{a}_2, \cdots, \tilde{a}_n) = \left(\left[1 - \prod_{j=1}^{n} \left(1 - a_j\right)^{\omega_j}, 1 - \prod_{j=1}^{n} \left(1 - b_j\right)^{\omega_j} \right], \left[\prod_{j=1}^{n} c_j^{\omega_j}, \prod_{j=1}^{n} d_j^{\omega_j} \right] \right), \tag{6}$$

then the function IIFWA_{ω} is called the IVIF weighted average operator.

Definition 7 [38]. Let $\tilde{A} = \{<x, [\mu_{\tilde{A}}^{L}(x), \mu_{\tilde{A}}^{U}(x)], [\nu_{\tilde{A}}^{L}(x), \nu_{\tilde{A}}^{U}(x)] >| x \in X\}$ be an IVIF set. The hesitation of $\tilde{A}$ is $\pi_{\tilde{A}}(x) = [\pi_{\tilde{A}}^{L}(x), \pi_{\tilde{A}}^{U}(x)]$, where $\pi_{\tilde{A}}^{L}(x) = 1 - \mu_{\tilde{A}}^{U}(x) - \nu_{\tilde{A}}^{U}(x)$ and $\pi_{\tilde{A}}^{U}(x) = 1 - \mu_{\tilde{A}}^{L}(x) - \nu_{\tilde{A}}^{L}(x)$. We define the average hesitation $\Psi_{\tilde{A}}(x)$ of $\tilde{A}$ as follows:

$$\Psi_{\tilde{A}}(x) = \frac{\pi_{\tilde{A}}^{L}(x) + \pi_{\tilde{A}}^{U}(x)}{2} = \frac{2 - \mu_{\tilde{A}}^{L}(x) - \mu_{\tilde{A}}^{U}(x) - \nu_{\tilde{A}}^{L}(x) - \nu_{\tilde{A}}^{U}(x)}{2}. \tag{7}$$

Here, $\Psi_{\tilde{A}}(x)$ expresses the lack of information.

We define a distance between membership and nonmembership of element x in X, that is,

$$\Phi_{\tilde{A}}(x) = \frac{1}{2}\left|\mu_{\tilde{A}}^{L}(x) - \nu_{\tilde{A}}^{L}(x)\right| + \frac{1}{2}\left|\mu_{\tilde{A}}^{U}(x) - \nu_{\tilde{A}}^{U}(x)\right|. \tag{8}$$

$\Phi_{\tilde{A}}(x)$ describes the balance between membership and nonmembership of element x.

Definition 8 [38]. Let $\tilde{A}$ be an IVIF set defined on X. IVIF entropy is defined as a real valued function $E(\tilde{A}) = f(\Psi_{\tilde{A}}, \Phi_{\tilde{A}})$: $\mathrm{IVIFS}(X) \to [0, 1]$, which satisfies the following axiomatic conditions:

(i) $E(\tilde{A}) = 0$ if and only if $\tilde{A}$ is a crisp set, i.e. $\tilde{\mu}_{\tilde{A}}(x) = [1, 1], \tilde{\nu}_{\tilde{A}}(x) = [0, 0]$ or $\tilde{\mu}_{\tilde{A}}(x) = [0, 0], \tilde{\nu}_{\tilde{A}}(x) = [1, 1]$, $\forall x \in X$

(ii) $E(\tilde{A}) = 1$ if and only if $[\mu_{\tilde{A}}^{L}(x), \mu_{\tilde{A}}^{U}(x)] = [\nu_{\tilde{A}}^{L}(x), \nu_{\tilde{A}}^{U}(x)], \forall x \in X$

(iii) $E(\tilde{A}) = E(\tilde{A}^{c})$

(iv) $E(\tilde{A}) = f(\Psi_{\tilde{A}}, \Phi_{\tilde{A}})$ is a real valued continuous function and is increasing with respect to parameter $\Psi_{\tilde{A}}$ and decreasing with respect to parameter $\Phi_{\tilde{A}}$

4. A New IVIF Entropy

Before proposing a new IVIF entropy, we first analyze the limitations of some previous IVIF entropy.

(1) One is that the uncertainty of IVIF is not considered

For example, the entropy formula of Vlachos and Sergiadis [39] is as follows:

$$E_{\mathrm{VS}}\left(\tilde{A}\right) = 1 - \sqrt{\frac{1}{2}\sum_{i=1}^{n}\left(\left(\left|\mu_{\tilde{A}}^{L}(x_i) - \nu_{\tilde{A}}^{L}(x_i)\right|\right)^2 + \left(\left|\mu_{\tilde{A}}^{U}(x_i) - \nu_{\tilde{A}}^{U}(x_i)\right|\right)^2\right)}. \tag{9}$$

(2) The other is that although the influence of hesitancy on entropy is considered. There are still some cases that cannot be distinguished well

Example 8. Let $\tilde{A}_1 = ([0.15, 0.25], [0.1, 0.2])$ and $\tilde{B}_1 = ([0.35, 0.45], [0.3, 0.4])$ be two IVIFNs.

Obviously, the degree of fuzziness of $\tilde{A}_1$ is greater than $\tilde{B}_1$. We use formula (7) to calculate as follows:

$$\begin{aligned} E_{\mathrm{VS}}\left(\tilde{A}_1\right) &= 1 - \sqrt{\frac{1}{2}\left(|0.15 - 0.1|^2 + |0.25 - 0.2|^2\right)} = 0.95, E_{\mathrm{VS}}\left(\tilde{B}_1\right) \\ &= 1 - \sqrt{\frac{1}{2}\left(|0.35 - 0.3|^2 + |0.45 - 0.4|^2\right)} = 0.95. \end{aligned} \tag{10}$$

Then, $E_{\mathrm{VS}}(\tilde{A}_1) = E_{\mathrm{VS}}(\tilde{B}_1)$ which is obviously inconsistent with the facts.

The IVIF entropy measure defined by Zhang et al. [40] is as follows:

$$E_Z\left(\tilde{A}\right) = \frac{1}{n}\sum_{i=1}^{n}\frac{\min\left\{\mu_{\tilde{A}}^{L}(x_i), \nu_{\tilde{A}}^{L}(x_i)\right\} + \min\left\{\mu_{\tilde{A}}^{U}(x_i), \nu_{\tilde{A}}^{U}(x_i)\right\}}{\max\left\{\mu_{\tilde{A}}^{L}(x_i), \nu_{\tilde{A}}^{L}(x_i)\right\} + \max\left\{\mu_{\tilde{A}}^{U}(x_i), \nu_{\tilde{A}}^{U}(x_i)\right\}}. \tag{11}$$

Example 9. Let $\tilde{A}_2 = ([0.3, 0.5], [0.1, 0.3])$ and $\tilde{B}_2 = ([0.1, 0.3], [0, 0.2])$ be two IVIFNs. Obviously, the degree of fuzziness of $\tilde{B}_2$ is greater than $\tilde{A}_2$. We use formula (11) to calculate as follows:

$$\begin{aligned} E_Z\left(\tilde{A}_2\right) &= \frac{0.1 + 0.3}{0.3 + 0.5} = 0.5, \\ E_Z\left(\tilde{B}_2\right) &= \frac{0 + 0.2}{0.1 + 0.3} = 0.5. \end{aligned} \tag{12}$$

$E_Z(\tilde{A}_2) = E_Z(\tilde{B}_2)$ which is obviously inconsistent with the facts.

Example 10. Let $\tilde{A}_3 = ([0.1, 0.3], [0, 0.5])$ and $\tilde{B}_3 = ([0.2, 0.4], [0.1, 0.6])$ be two IVIFNs. Obviously, the degree of fuzziness of $\tilde{A}_3$ is greater than $\tilde{B}_3$. The IVIF entropy measure defined by Ren and Tan [41] is as follows:

$$E_R\left(\tilde{A}\right) = \frac{1}{n}\sum_{i=1}^{n}\frac{4 - \left[\left|\mu_{\tilde{A}}^{L}(x_i) - \nu_{\tilde{A}}^{L}(x_i)\right| + \left|\mu_{\tilde{A}}^{U}(x_i) - \nu_{\tilde{A}}^{U}(x_i)\right|\right]^2 + \left|\pi_{\tilde{A}}^{L}(x_i) - \pi_{\tilde{A}}^{U}(x_i)\right|^2}{8}. \tag{13}$$

The result of calculation is $E_R(\tilde{A}_3) = E_R(\tilde{B}_3) = 0.4275$, which is obviously inconsistent with the facts.

In order to make up for the deficiency of the existing IVIF entropy, we will construct a new IVIF entropy.

Let $\tilde{A} = \{<x_i, [\mu_{\tilde{A}}^L(x_i), \mu_{\tilde{A}}^U(x_i)], [\nu_{\tilde{A}}^L(x_i), \nu_{\tilde{A}}^U(x_i)]>|x_i \in X\}$ be an IVIF set. We define

$$E_Q\left(\tilde{A}\right) = \frac{1}{n}\sum_{i=1}^{n} \cos\frac{\left(|\mu_{\tilde{A}}^L(x_i) - \nu_{\tilde{A}}^L(x_i)| + |\mu_{\tilde{A}}^U(x_i) - \nu_{\tilde{A}}^U(x_i)|\right)\left(2 - \pi_{\tilde{A}}^L(x_i) - \pi_{\tilde{A}}^U(x_i)\right)}{8}\pi, \tag{14}$$

$E_Q(\tilde{A})$ can be rewritten as

$$E_Q\left(\tilde{A}\right) = \frac{1}{n}\sum_{i=1}^{n} \cos\frac{\left((1/2)\left|\mu_{\tilde{A}}^L(x_i) - \nu_{\tilde{A}}^L(x_i)\right| + (1/2)\left|\mu_{\tilde{A}}^U(x_i) - \nu_{\tilde{A}}^U(x_i)\right|\right)\left(1 - \left(\left(\pi_{\tilde{A}}^L(x_i) + \pi_{\tilde{A}}^U(x_i)\right)/2\right)\right)}{2}\pi = \frac{1}{n}\sum_{i=1}^{n} \cos\frac{\Phi_{\tilde{A}}(x_i)(1 - \Psi_{\tilde{A}}(x_i))}{2}\pi. \tag{15}$$

Obviously, $E_Q(\tilde{A})$ contains not only the interval distance $\Phi_{\tilde{A}}(x)$ of membership and nonmembership but also the information of average hesitation degree $\Psi_{\tilde{A}}(x)$.

Theorem 11. *The measure $E_Q(\tilde{A})$ defined by equation (14) is an IVIF entropy.*

Proof. To prove the measure $E_Q(\tilde{A})$ given by equation (14) is an IVIF entropy, we only need to prove it satisfies the properties in Definition 8. Obviously, for every x_i, we have:

$$0 \le \mu_{\tilde{A}}^L(x_i), \mu_{\tilde{A}}^U(x_i), \nu_{\tilde{A}}^L(x_i), \nu_{\tilde{A}}^U(x_i), \pi_{\tilde{A}}^L(x_i), \pi_{\tilde{A}}^U(x_i) \le 1, \tag{16}$$

then,

$$0 \le \frac{\left(\left|\mu_{\tilde{A}}^L(x_i) - \nu_{\tilde{A}}^L(x_i)\right| + \left|\mu_{\tilde{A}}^U(x_i) - \nu_{\tilde{A}}^U(x_i)\right|\right)\left(2 - \pi_{\tilde{A}}^L(x_i) - \pi_{\tilde{A}}^U(x_i)\right)}{8}\pi \le \frac{\pi}{2}, \tag{17}$$

thus, we have $0 \le E_Q(\tilde{A}) \le 1$.

(i) Let $\tilde{A}$ be a crisp set; i.e., for all $x_i \in X$, we have $[\mu_{\tilde{A}}^L(x), \mu_{\tilde{A}}^U(x)] = [1, 1]$, $[\nu_{\tilde{A}}^L(x), \nu_{\tilde{A}}^U(x)] = [0, 0]$ or $[\mu_{\tilde{A}}^L(x), \mu_{\tilde{A}}^U(x)] = [0, 0]$, $[\nu_{\tilde{A}}^L(x), \nu_{\tilde{A}}^U(x)] = [1, 1]$.

It is obviously that $E_Q(\tilde{A}) = 0$.

If $E_Q(\tilde{A}) = 0$, that is,

$$E_Q\left(\tilde{A}\right) = \frac{1}{n}\sum_{i=1}^{n} \cos\frac{\left(|\mu_{\tilde{A}}^L(x_i) - \nu_{\tilde{A}}^L(x_i)| + |\mu_{\tilde{A}}^U(x_i) - \nu_{\tilde{A}}^U(x_i)|\right)\left(2 - \pi_{\tilde{A}}^L(x_i) - \pi_{\tilde{A}}^U(x_i)\right)}{8}\pi = 0, \tag{18}$$

then, for all $x_i \in X$, we have

$$\cos\frac{\left(|\mu_{\tilde{A}}^L(x_i) - \nu_{\tilde{A}}^L(x_i)| + |\mu_{\tilde{A}}^U(x_i) - \nu_{\tilde{A}}^U(x_i)|\right)\left(2 - \pi_{\tilde{A}}^L(x_i) - \pi_{\tilde{A}}^U(x_i)\right)}{8}\pi = 0. \tag{19}$$

Thus,

$$\left(\left|\mu_{\tilde{A}}^L(x_i) - \nu_{\tilde{A}}^L(x_i)\right| + \left|\mu_{\tilde{A}}^U(x_i) - \nu_{\tilde{A}}^U(x_i)\right|\right)\left(2 - \pi_{\tilde{A}}^L(x_i) - \pi_{\tilde{A}}^U(x_i)\right) = 4, \tag{20}$$

then, we have $[\mu_{\tilde{A}}^L(x), \mu_{\tilde{A}}^U(x)] = [1, 1]$, $[\nu_{\tilde{A}}^L(x), \nu_{\tilde{A}}^U(x)] = [0, 0]$ or $[\mu_{\tilde{A}}^L(x), \mu_{\tilde{A}}^U(x)] = [0, 0]$, $[\nu_{\tilde{A}}^L(x), \nu_{\tilde{A}}^U(x)] = [1, 1]$.

Therefore, $\tilde{A}$ is a crisp set

(ii) Let $[\mu_{\tilde{A}}^L(x_i), \mu_{\tilde{A}}^U(x_i)] = [\nu_{\tilde{A}}^L(x_i), \nu_{\tilde{A}}^U(x_i)]$, $\forall x_i \in X$, obviously, we have $E_Q(\tilde{A}) = 1$

Now, we assume that $E_Q(\tilde{A}) = 1$; then, for all $x_i \in X$, we have

$$\cos\frac{\left(|\mu_{\tilde{A}}^L(x_i) - \nu_{\tilde{A}}^L(x_i)| + |\mu_{\tilde{A}}^U(x_i) - \nu_{\tilde{A}}^U(x_i)|\right)\left(2 - \pi_{\tilde{A}}^L(x_i) - \pi_{\tilde{A}}^U(x_i)\right)}{8}\pi = 1, \tag{21}$$

then, $(|\mu_{\tilde{A}}^L(x_i) - \nu_{\tilde{A}}^L(x_i)| + |\mu_{\tilde{A}}^U(x_i) - \nu_{\tilde{A}}^U(x_i)|)(2 - \pi_{\tilde{A}}^L(x_i) - \pi_{\tilde{A}}^U(x_i)) = 0$; we can obtain the conclusion $[\mu_{\tilde{A}}^L(x_i), \mu_{\tilde{A}}^U(x_i)] = [\nu_{\tilde{A}}^L(x_i), \nu_{\tilde{A}}^U(x_i)]$ or $[\pi_{\tilde{A}}^L(x_i), \pi_{\tilde{A}}^U(x_i)] = [1, 1]$ for all $x_i \in X$. If $[\pi_{\tilde{A}}^L(x_i), \pi_{\tilde{A}}^U(x_i)] = [1, 1]$, we can also get $[\mu_{\tilde{A}}^L(x_i), \mu_{\tilde{A}}^U(x_i)] = [\nu_{\tilde{A}}^L(x_i), \nu_{\tilde{A}}^U(x_i)]$ for all $x_i \in X$

Table 1: Calculation results of IVIF entropy for some IVIFNs.

Case	IVIFNs	IVIF entropy	Results
Case 1	$\tilde{A}_1 = ([0.15, 0.25], [0.1, 0.2])$	$E_Q(\tilde{A}_1) = 0.9996$	$\tilde{A}_1 \succ \tilde{B}_1$
	$\tilde{B}_1 = ([0.35, 0.45], [0.3, 0.4])$	$E_Q(\tilde{B}_1) = 0.9983$	
Case 2	$\tilde{A}_2 = ([0.3, 0.5], [0.1, 0.3])$,	$E_Q(\tilde{A}_2) = 0.9851$	$\tilde{B}_2 \succ \tilde{A}_2$
	$\tilde{B}_2 = ([0.1, 0.3], [0, 0.2])$	$E_Q(\tilde{B}_2) = 0.9989$	
Case 3	$\tilde{A}_3 = ([0.1, 0.3], [0, 0.5])$	$E_Q(\tilde{A}_3) = 0.9944$	$\tilde{A}_3 \succ \tilde{B}_3$
	$\tilde{B}_3 = ([0.2, 0.4], [0.1, 0.6])$	$E_Q(\tilde{B}_3) = 0.9883$	

(iii) By equation (14), we have

$$E_Q\left(\tilde{A}^C\right) = \frac{1}{n}\sum_{i=1}^{n} \cos\frac{\left(\left|\nu_{\tilde{A}}^L(x_i) - \mu_{\tilde{A}}^L(x_i)\right| + \left|\nu_{\tilde{A}}^U(x_i) - \mu_{\tilde{A}}^U(x_i)\right|\right)\left(2 - \pi_{\tilde{A}}^L(x_i) - \pi_{\tilde{A}}^U(x_i)\right)}{8}\pi = E_Q\left(\tilde{A}\right) \tag{22}$$

(iv) Let

$$f(x, y) = \cos\frac{y(1-x)\pi}{2}, \tag{23}$$

where $x, y \in [0, 1]$. We need to prove the function $f(x, y)$ is increasing with x and decreasing with y.

We take the partial derivatives of $f(x, y)$ with respect to x and y, respectively:

$$\begin{aligned} \frac{\partial f}{\partial x} &= \frac{y\pi}{2}\sin\frac{y(1-x)\pi}{2} > 0, \\ \frac{\partial f}{\partial y} &= -\frac{(1-x)\pi}{2}\sin\frac{y(1-x)\pi}{2} < 0. \end{aligned} \tag{24}$$

Thus, $f(x, y)$ is increasing with x and decreasing with y.

In conclusion, $E_Q(\tilde{A})$ is an IVIF entropy.

Remark 12. Let $\tilde{A} \succ \tilde{B}$ represent IVIFN $\tilde{A}$ which is more fuzzy than IVIFN $\tilde{B}$. Applying $E_Q(\tilde{A})$ to calculate the IVIF entropy of Examples 8 to 10, the results are shown in the following Table 1.

Therefore, it can be seen that the entropy $E_Q(\tilde{A})$ proposed in this paper is more reasonable than formulas (9), (11), and (13).

5. Microblog User Influence Group Decision Evaluation Model

At present, research on IVIF sets focuses on the basic theory, and there is little research on its application in multiattribute group decision-making [27, 39]. The entropy of IVIF set is solved after the criterion type is normalized. Then, the weight is determined according to the entropy weight method. Finally, the obtained criterion value is normalized to realize the ranking and evaluation of schemes. The characteristic of this method is that interval numbers are used to describe decision information instead of real numbers.

Based on the idea of IVIF multiattribute group decision-making, the dynamic evaluation model of microblog user influence combines the user influence evaluation with fuzzy thought. This paper decomposes the user influence index in multilevel, establishes a comprehensive and reasonable index system, describes the user data with interval number, and introduces the time dimension to investigate the dynamic changes of data, and generates IVIF group decision matrix. After normalization according to the type of criteria, the entropy proposed in Section 2 is used to determine the criterion weight. Finally, the criterion value is normalized and the score value and accurate value are obtained. The essence of microblog user influence group decision-making evaluation model is to transform the user influence evaluation into IVIF multiattribute group decision-making problem. The entropy weight method is used to determine the weight of the criteria, and the time dimension is introduced to evaluate the user influence.

Now, we give the steps of our new evaluation model.

Step 1. Establish the decision matrix.

According to the method of multi-attribute group decision-making, its general form is as follows:

For a multiattribute group decision-making problem, let $X = \{x_1, x_2, \cdots, x_n\}$ be the scheme set, $C = \{c_1, c_2, \cdots, c_m\}$ the criterion set, and $D = \{d_1, d_2, \cdots, d_l\}$ the decision-maker set. If the decision maker d_k expresses the value of scheme x_i under criterion c_j by interval number, the decision matrix formed is marked as

$$X_i = \left(\left[a_{kj}^i, b_{kj}^i\right]\right)_{l\times m} = \begin{matrix} d_1 \\ d_2 \\ \vdots \\ d_l \end{matrix} \begin{bmatrix} \left[a_{11}^i, b_{11}^i\right] & \left[a_{12}^i, b_{12}^i\right] & \cdots & \left[a_{1m}^i, b_{1m}^i\right] \\ \left[a_{21}^i, b_{21}^i\right] & \left[a_{22}^i, b_{22}^i\right] & \cdots & \left[a_{2m}^i, b_{2m}^i\right] \\ & \cdots & \cdots & \\ \left[a_{l1}^i, b_{l1}^i\right] & \left[a_{l2}^i, b_{l2}^i\right] & \cdots & \left[a_{lm}^i, b_{lm}^i\right] \end{bmatrix}_{l\times m}. \tag{25}$$

Step 2. Normalize the decision matrix.

In the uncertain network environment, social events contain different decision-making indicators. Because of their different meanings, there are dimensional differences. In order to eliminate the influence of different dimensions on decision-making, we first normalize the dimensionless data. With reference to Hu et al. [42], for different types of criteria, they are standardized according to the following formula, where $L = \{1, 2, \cdots, l\}$, $J = \{1, 2, \cdots, m\}$, and $I = \{1, 2, \cdots, n\}$.

For benefit based criteria, let

$$\begin{cases} x_{kj}^i = \dfrac{a_{kj}^i - \min\limits_i \left\{a_{kj}^i\right\}}{\max\limits_i \left\{b_{kj}^i\right\} - \min\limits_i \left\{a_{kj}^i\right\}}, \\ y_{kj}^i = \dfrac{b_{kj}^i - \min\limits_i \left\{a_{kj}^i\right\}}{\max\limits_i \left\{b_{kj}^i\right\} - \min\limits_i \left\{a_{kj}^i\right\}}, \\ k \in L, j \in J, i \in I. \end{cases} \tag{26}$$

For cost-based criteria, let

$$\begin{cases} x_{kj}^i = \dfrac{\max\limits_i \left\{b_{kj}^i\right\} - b_{kj}^i}{\max\limits_i \left\{b_{kj}^i\right\} - \min\limits_i \left\{a_{kj}^i\right\}}, \\ y_{kj}^i = \dfrac{\max\limits_i \left\{b_{kj}^i\right\} - a_{kj}^i}{\max\limits_i \left\{b_{kj}^i\right\} - \min\limits_i \left\{a_{kj}^i\right\}}, \\ k \in L, j \in J, i \in I. \end{cases} \tag{27}$$

The normalized decision matrix is $Y_i = \left(\left[x_{kj}^i, y_{kj}^i\right]\right)_{l\times m}$.

Step 3. The interval number matrix is transformed into the IVIFN matrix.

In this paper, the method proposed by Yue [43] is applied to transform interval valued to IVIFNs. For the decision matrix $Y_i = \left(\left[x_{kj}^i, y_{kj}^i\right]\right)_{l\times m}$, the higher the value of $\left[x_{kj}^i, y_{kj}^i\right]$, the greater the satisfaction of decision makers. Let

$$\theta_{ij}^L = \min_k \left\{y_{kj}^i\right\}, \theta_{ij}^U = \max_k \left\{y_{kj}^i\right\}, \tag{28}$$

$$\eta_{ij}^L = \min_k \left\{x_{kj}^i\right\}, \eta_{ij}^U = \max_k \left\{x_{kj}^i\right\}, \tag{29}$$

where $\left[\theta_{ij}^L, \theta_{ij}^U\right]$ and $\left[\eta_{ij}^L, \eta_{ij}^U\right]$ denote the satisfaction interval and dissatisfaction interval of the criterion, respectively. Let these two intervals form an ordered pair and mark them as $\left(\left[\theta_{ij}^L, \theta_{ij}^U\right], \left[\eta_{ij}^L, \eta_{ij}^U\right]\right)$. The smaller the value of η_{ij}^L and η_{ij}^U is, the more dissatisfied the decision maker is. If

$$\rho_{ij}^L = 1 - \eta_{ij}^U, \rho_{ij}^U = 1 - \eta_{ij}^L, \tag{30}$$

then, $r_{ij} = \left(\left[\mu_{ij}^L, \mu_{ij}^U\right], \left[\nu_{ij}^L, \nu_{ij}^U\right]\right)$ is called IVIFN of criterion c_j under scheme x_i, where

$$\mu_{ij}^L = \frac{\theta_{ij}^L}{\theta_{ij}^L + \theta_{ij}^U + \rho_{ij}^L + \rho_{ij}^U}, \mu_{ij}^U = \frac{\theta_{ij}^U}{\theta_{ij}^L + \theta_{ij}^U + \rho_{ij}^L + \rho_{ij}^U}, \tag{31}$$

$$\nu_{ij}^L = \frac{\rho_{ij}^L}{\theta_{ij}^L + \theta_{ij}^U + \rho_{ij}^L + \rho_{ij}^U}, \nu_{ij}^U = \frac{\rho_{ij}^U}{\theta_{ij}^L + \theta_{ij}^U + \rho_{ij}^L + \rho_{ij}^U}. \tag{32}$$

The transformed decision matrix is recorded as $R = \left(r_{ij}\right)_{n\times m}$.

Step 4. Determine the weight of criteria.

IVIF entropy is used to describe the fuzzy degree of IVIF sets. The larger the IVIF entropy of the evaluation criterion is, the greater the fuzziness degree of the information provided by the criterion is, and a smaller weight should be given. On the contrary, it gives a larger weight. The weight of each criterion can be determined by the above principle. Using the entropy formula proposed in Section 2 of this paper, if the value of a single scheme x_i under criterion c_j is r_{ij}, then, its fuzzy entropy is as follows:

$$E\left(r_j\right) = \frac{1}{n}\sum_{i=1}^{n} \cos\frac{\left(\left|\mu_{ij}^L - \nu_{ij}^L\right| + \left|\mu_{ij}^U - \nu_{ij}^U\right|\right)\left(2 - \pi_{ij}^L - \pi_{ij}^U\right)}{8}\pi. \tag{33}$$

Then, the weight of each criterion is calculated by equation (34).

$$\omega_j = \frac{1 - E\left(r_j\right)}{\sum_{j=1}^{m}\left(1 - E\left(r_j\right)\right)}. \tag{34}$$

Step 5. Solve the comprehensive criterion value.

By using formula (6), the comprehensive criterion value z_i of each scheme is obtained.

Step 6. Sort the results and choose the best.

According to formulas (3) and (4), the score value and accuracy value of the comprehensive criteria value are solved; that is, the influence score and accuracy value of candidate users are obtained, and the user influence is sorted according to Definition 5.

Input: Microblog user decision matrix $X_i = ([a_{kj}^i, b_{kj}^i])_{l\times m}$,
where $L = \{1, 2, \cdots, l\}$, $J = \{1, 2, \cdots, m\}$ and $I = \{1, 2, \cdots, n\}$ and $k \in L$, $j \in J$, $i \in I$.
Output: Ranking of influence of microblog users x_i.
According to formula (26), the standard decision matrix $X_i = ([a_{kj}^i, b_{kj}^i])_{l\times m}$ is $Y_i = ([x_{kj}^i, y_{kj}^i])_{l\times m}$.
For $j \in J$ implement.
  For $i \in I$ implement.
According to formulas (28)–(32), IVIF matrix $R = (r_{ij})_{n\times m}$ is calculated.
  End for.
According to equations (33) and (34), ω_j is calculated.
End for.
For $i \in I$ implement.
According to formula (3), $\Delta(z_i)$ is calculated.
End for.
Sort the size of microblog user x_i corresponding to $\Delta(z_i)$ and return it as the result.

Algorithm 1: IVIFMI algorithm.

According to the above steps, we get the following algorithm, which we call interval-valued intuitionistic fuzzy microblog influence algorithm IVIFMI algorithm (see Algorithm 1).

6. Performance Analysis

Microblog is a broadcast social network platform based on attention mechanism to share short and real-time information. It is one of the most active social networks in China. This paper selects Sina Weibo as the research object. According to the data in the 41st statistical report on China's Internet Development released by CNNIC [9], as of December 2017, the number of microblog users in China had reached 376 million, which promoted the continuous growth of user utilization rate to 40.9%, an increase of 3.8% compared with December 2016 (as shown in Figure 2).

In addition to publishing their own original microblog information, each user can also forward, comment, and like the microblog information of other users at will. The behaviors of forwarding, commenting, and liking among different users contribute to the formation of microblog information dissemination networks (as shown in Figure 3). In addition, the microblog platform also has the characteristics of low user threshold, short microblog content, and strong readability, which make the dissemination speed of microblog information faster and has a wider range of influence.

This paper selects Sina Weibo as the research object.

6.1. Data Acquisition. The datum comes from Weibo Fengyun, which is collected by crawler tools. Weibo Fengyun is an official authorized data service provider of Sina Weibo. In this paper, six Sina Weibo users were randomly sampled to track their information and collect data from July 17, 2020, to July 25, 2020. This information can reflect the user's activities on Sina Weibo from registration to July 25, 2020.

6.2. Data Description and Index Measurement. The traditional method of measuring user influence only by the number of fans of microblog users has lost its credibility. The selection of influence index of microblog users should be comprehensively considered according to the basic functions of microblog. Through the analysis of user behavior characteristics, it is found that the influence of microblog users can be constructed from three aspects: microblog coverage, user interaction, and user activity [44]. The coverage of microblog includes three indicators: the number of active fans, the number of blog posts, and user authentication. User interaction includes three indicators: the number of comments, the number of forwarding, and the number of likes. User activity includes daily average number of microblogs, original microblog rate, and active days, as shown in Figure 4.

The meaning and measurement method of indicators are as follows:

(1) The coverage of microblog (o_1): this indicator includes the number of active fans (o_{11}), the number of microblogs (o_{12}), and user authentication (o_{13}). Among them, the number of active fans and the number of microblogs are very intuitive influencing factors. The number of fans determines the scope of the user's influence, and the number of blogs determines the depth of the user's influence. For fans of the same size, the more microblogs users have, the more times each fan is affected by the user's microblog information, that is, the deeper the influence of the user is. The influence of user authentication on users is a potential factor. If users pass the authentication of Sina Weibo, the credibility of microblog is very high, which makes the possibility of the microblog being commented and forwarded increased, so the influence of users is increased.

The number of active fans refers to the number of fans who have eliminated zombie powder. It is represented by numerical data. In this paper, users with less than 20 followers and less than 10 microblogs are identified as Zombie fans.

The number of user microblogs refers to the total number of microblogs published by users' microblog accounts during data collection. It is expressed by numerical value.

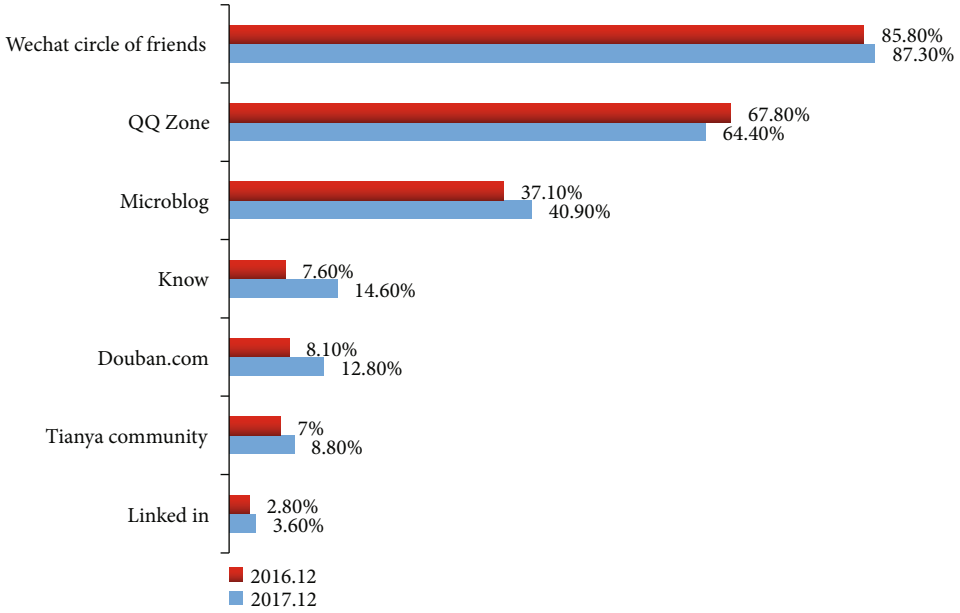

Figure 2: Typical social software usage.

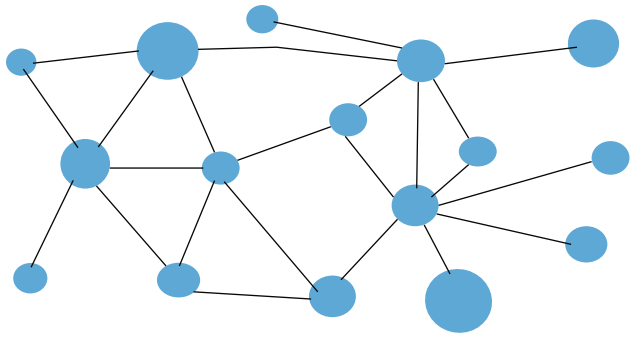

Figure 3: Examples of microblog information dissemination network.

Authenticated users refer to users who have been authenticated by microblog, usually marked by "V." Whether the user is authenticated is indicated by a value of 0 or 1 (1 indicates that the user has completed the authentication, and 0 indicates that the user has not completed the authentication).

(2) User interaction (o_2): this indicator includes the number of comments (o_{21}), the number of forwarding (o_{22}), and the number of likes (o_{23}). In the microblog platform, the microblog users post and forward affect their fans, and the behavior of fans such as comments, forwarding, and likes in turn promotes the dissemination of microblog information. The more times a microblog message is forwarded, the more widely it is spread. The more comments are made, the more attention is paid to the information. The more likes a user gets, the higher the prestige of the user in his fan community.

This paper selects the average number of comments, average number of forwarding, and average number of likes of each microblog. Referring to Chen et al. [24], after data preprocessing, the number of comments is represented by an interval number $[a^L, a^U]$, the number of forwarding is represented by interval number $[b^L, b^U]$, and the number of compliments is represented by interval number $[c^L, c^U]$ (see formulas (35)–(37)).

$$a^L = \sum_{i=1}^{n_1} \frac{r_i}{n_1}, a^U = \sum_{i=1}^{n_2} \frac{r_i}{n_2}, \tag{35}$$

$$b^L = \sum_{i=1}^{m_1} \frac{s_i}{m_1}, b^U = \sum_{i=1}^{m_2} \frac{s_i}{m_2}, \tag{36}$$

$$c^L = \sum_{i=1}^{k_1} \frac{t_i}{k_1}, c^U = \sum_{i=1}^{k_2} \frac{t_i}{k_2}. \tag{37}$$

(3) User activity (o_3): this indicator includes daily average number of microblogs (o_{31}), microblog original rate (o_{32}), and active days (o_{33}). The average number of daily microblogs refers to the average number of microblogs per day since users opened microblogs, which can reflect the average activity of users. Microblog can be divided into forwarding microblog and original microblog. The content of the original microblog is created by users themselves. The active days show the frequency of users participating in microblog. Referring to Chen et al.'s study [24], after data preprocessing, the daily average number of microblogs is represented by interval number $[x^L, x^U]$, and the microblog original rate is expressed by interval number $[y^L, y^U]$. The data of active days is from the basic information of microblog users and

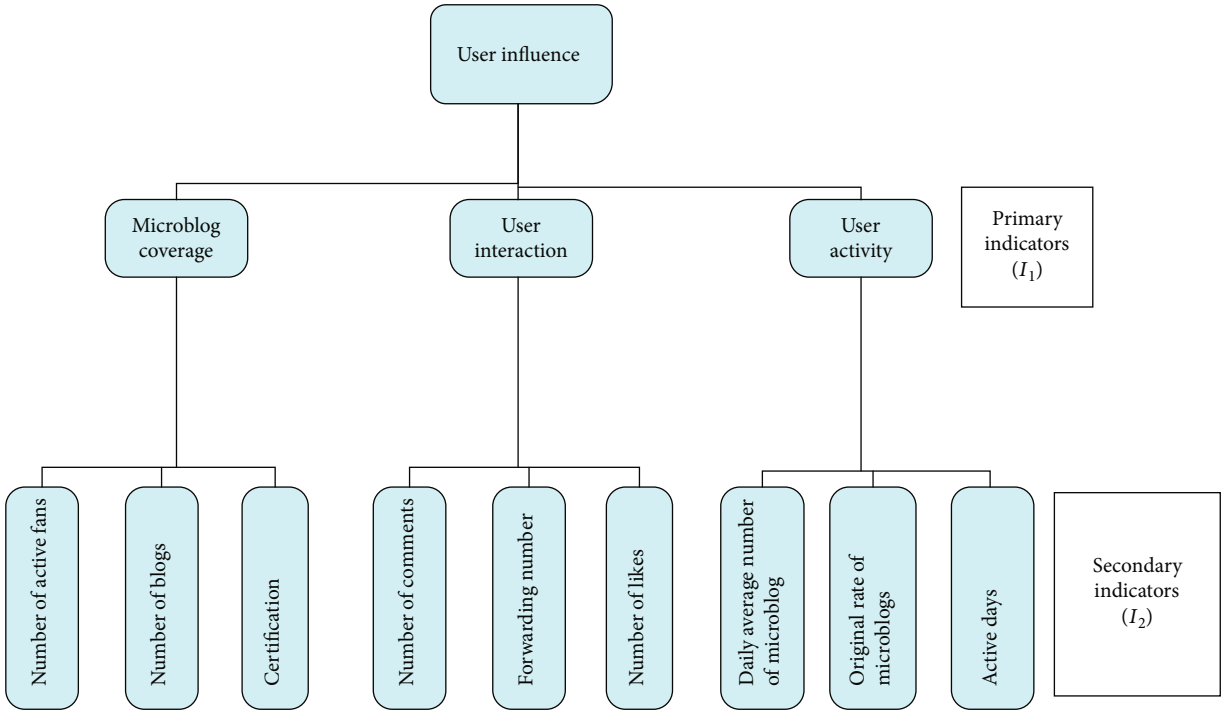

Figure 4: The evaluation index system of microblog user influence.

expressed by a numerical value (see formulas (38) and (39)).

$$x^L = \sum_{i=1}^{l_1} \frac{x_i}{l_1}, x^U = \sum_{i=1}^{l_2} \frac{x_i}{l_2}, \tag{38}$$

$$y^L = \frac{\sum_{i=1}^{j_1} y_i / j_1}{\bar{x}}, y^U = \frac{\sum_{i=1}^{j_2} y_i / j_2}{\bar{x}}. \tag{39}$$

The meaning of the symbols in equations (35)–(39) is shown in Table 2.

Using the above data description and index measurement method, the data of user 1 is obtained, as shown in Table 3.

In the same way, the data of the other five users can be obtained. Due to the length of the article, the data of the other five users is not shown here. Data of six users constitute the decision matrix.

6.3. Calculation Results. All the indexes selected in this paper are benefit indicators, and the decision matrix obtained in the previous section is normalized by using formula (26). According to formulas (33) and (34), the weight $(\omega_1, \omega_2, \cdots, \omega_m)$ of the criterion is obtained as follows:

$$\begin{aligned} \omega_1 &= 0.1474, \omega_2 = 0.1296, \omega_3 = 0.0818, \omega_4 \\ &= 0.1141, \omega_5 = 0.1440, \omega_6 = 0.1244, \omega_7 \\ &= 0.0921, \omega_8 = 0.0402, \omega_9 = 0.1264. \end{aligned} \tag{40}$$

Using formula (6), the comprehensive criterion values of each scheme are obtained as follows:

$$\begin{aligned} z_1 &= ([0.296, 0.304], [0.204, 0.274]), z_2 \\ &= ([0.356, 0.465], [0.248, 0.413]), z_3 \\ &= ([0.325, 0.486], [0.236, 0.425]), z_4 \\ &= ([0.412, 0.536], [0.222, 0.364]), z_5 \\ &= ([0.555, 0.730], [0.167, 0.270]), z_6 \\ &= ([0.456, 0.680], [0.272, 0.406]). \end{aligned} \tag{41}$$

According to formula (3), the comprehensive criterion score value is as follows:

$$\begin{aligned} \Delta(z_1) = 0.080, \Delta(z_2) = 0.083, \Delta(z_3) = 0.077, \Delta(z_4) \\ = 0.177, \Delta(z_5) = 0.365, \Delta(z_6) = 0.203. \end{aligned} \tag{42}$$

Thus, the sorting result is $x_5 \succ x_6 \succ x_4 \succ x_2 \succ x_1 \succ x_3$. User 5 is the most influential user.

It should be noted that the quantitative model of user influence proposed in this paper is also applicable to other online social network platforms such as WeChat and QQ.

7. Conclusion and Future Work

In this paper, a new IVIF entropy is proposed, which contains not only the interval distance of membership and nonmembership but also the average hesitancy. On this basis, the influence of microblog users is studied. Through the multilevel decomposition of user influence, the coverage, user interaction, and user activity of microblog are constructed as the first level indicators. Nine secondary indicators such as whether to add V authentication, the number of microblogs, the number of active fans, the average number of

Table 2: Symbols and their explanations.

Symbol	Symbolic meaning
n	The total number of microblogs published by users from the time of opening microblogs to data collection
$r_i\ (i = 1, 2, \cdots, n)$	The number of comments on the i-th microblog
$\bar{r}$	The average number of comments per microblog
n_1	The number of microblogs of $r_i < \bar{r}$
n_2	The number of microblogs of $r_i > \bar{r}$
$s_i\ (i = 1, 2, \cdots, n)$	The forwarding number of the i-th microblog
$\bar{s}$	Average forwarding number of users per microblog
m_1	The number of microblogs of $s_i < \bar{s}$
m_2	The number of microblogs of $s_i > \bar{s}$
$t_i\ (i = 1, 2, \cdots, n)$	The number of likes received by users on the i-th microblog
$\bar{t}$	Average number of likes per microblog
k_1	The number of microblogs of $t_i < \bar{t}$
k_2	The number of microblogs of $t_i > \bar{t}$
l	The usage time of microblog, which refers to the total days from the user's account opening to data collection
$x_i\ (i = 1, 2, \cdots, l)$	The number of microblogs published by the user on the i-day
$\bar{x}$	The average number of microblogs published by the user per day
l_1	The total days of $x_i < \bar{x}$
l_2	The total days of $x_i > \bar{x}$
$y_i\ (i = 1, 2, \cdots, l)$	The number of original microblogs published by users on the i-th day
$\bar{y}$	Average number of original microblogs published by users per day
j_1	The total days of $y_i < \bar{y}$
j_2	The total days of $y_i > \bar{y}$

Table 3: Data for user 1.

I_1	I_2		Day 1	Day 2	Day 3	Day 4	Day 5	Day 6	Day 7	Day 8	Day 9
o_1	o_{11}		286	290	292	273	285	291	286	280	290
	o_{12}		208	209	209	211	211	211	211	212	212
	o_{13}		0	0	0	0	0	0	0	0	0
o_2	o_{21}	a^L	0.24	0.36	0.36	0.34	0.36	0.4	0.4	0.42	0.42
		a^U	0.824	0.831	0.831	0.826	0.828	0.836	0.836	0.84	0.84
	o_{22}	b^L	0.324	0.326	0.326	0.325	0.326	0.328	0.328	0.328	0.33
		b^U	0.526	0.528	0.528	0.528	0.528	0.532	0.532	0.532	0.534
	o_{23}	c^L	0.120	0.122	0.122	0.122	0.122	0.124	0.124	0.126	0.126
		c^U	0.824	0.842	0.842	0.842	0.842	0.856	0.856	0.858	0.858
o_3	o_{31}	x^L	0.048	0.064	0.064	0.102	0.102	0.102	0.102	0.124	0.124
		x^U	0.856	0.882	0.882	0.934	0.934	0.934	0.934	0.956	0.956
	o_{32}	y^L	0.012	0.012	0.024	0.024	0.024	0.024	0.024	0.032	0.032
		y^U	0.438	0.438	0.442	0.442	0.442	0.442	0.442	0.448	0.448
	o_{33}		653	654	656	656	656	658	658	658	660

microblogs, and the original rate of microblogs are selected as the comprehensive index system of microblog influence. Considering the highly dynamic and unstructured characteristics of social network data, the idea of interval intuitionistic fuzzy is introduced to transform the evaluation of social network users' influence into interval intuitionistic fuzzy multiattribute group decision-making problem, and a model is established. Finally, the model is applied to dynamic evaluation of Sina Weibo users' influence to verify the effectiveness of the model.

Different from the method of user influence based on computer iterative operation, the dynamic evaluation model of microblog user influence based on interval intuitionistic fuzzy entropy has the following two characteristics:

(1) Aiming at the limitation of the existing entropy calculation methods, a new IVIF entropy calculation formula based on cosine function is proposed to improve the effectiveness

(2) The user influence evaluation is transformed into fuzzy multiattribute group decision-making problem, which can not only simplify the calculation but also deal with the fuzziness better. It provides a new idea of user influence evaluation and expands the use of fuzzy multiattribute group decision-making

With the rapid development of network information technology [45], people ushered in the era of big data social network. This has brought great changes to our work and life. More and more people like to publish their activities on the Internet. At the same time, information security issues [20, 46] have also been exposed, bringing a series of serious consequences to the people. The limitation of this model is that the selection of microblog user influence evaluation index is not comprehensive enough and information security factors are not considered. This will be further explored in a future work.

Data Availability

The data used to support the findings of this study are included within the article.

Conflicts of Interest

The authors declared that they have no conflicts of interest to this work.

Acknowledgments

This research was supported by the National Natural Science Foundation of China (No. 71661012).

References

[1] H. Zheng, W. Guo, and N. Xiong, "A kernel-based compressive sensing approach for mobile data gathering in wireless sensor network systems," *IEEE Transactions on Systems, Man, and Cybernetics: Systems*, vol. 48, no. 12, pp. 2315–2327, 2017.

[2] N. Xiong, W. Han, and A. Vandenberg, "Green cloud computing schemes based on networks: a survey," *IET Communications*, vol. 6, no. 18, pp. 3294–3300, 2012.

[3] N. Xiong, A. Vasilakos, J. Wu et al., "A self-tuning failure detection scheme for cloud computing service," in *2012 IEEE 26th International Parallel and Distributed Processing Symposium*, pp. 668–679, Shanghai, China, 2012.

[4] W. Wu, N. Xiong, and C. Wu, "Improved clustering algorithm based on energy consumption in wireless sensor networks," *IET Networks*, vol. 6, no. 3, pp. 47–53, 2017.

[5] K. Huang, Q. Zhang, C. Zhou, N. Xiong, and Y. Qin, "An efficient intrusion detection approach for visual sensor networks based on traffic pattern learning," *IEEE Transaction on Systems, Man, and Cybernetics: Systems*, vol. 47, no. 10, pp. 2704–2713, 2017.

[6] J. Li and Z. Li, "Design on MGCF in interworking between IMs and PSTN domain," *Computer Networks*, vol. 44, no. 23, pp. 62–64, 2018.

[7] Q. Liu, L. Cui, and H. Chen, "Key technologies and applications of internet of things," *Computer Science*, vol. 37, no. 6, pp. 1–4, 2010.

[8] Z. Qian and Y. Wang, "IoT technology and application," *Acta Electronica Sinica*, vol. 40, no. 5, 2012.

[9] W. Li, J. Cao, J. Wu, C. Huang, and R. Buyya, "A collaborative filtering recommendation method based on discrete quantum-inspired shuffled frog leaping algorithms in social networks," *Future Generation Computer Systems*, vol. 88, pp. 262–270, 2018.

[10] E. Katz and P. Lazaxsfeld, *Personal Influence: The Part Played by People in the Flow of Mass Communications*, The Free Press, Illinois, 1955.

[11] W. Zheng, H. Pan, and C. Sun, "A friendship-based altruistic incentive knowledge diffusion model in social networks," *Information Sciences*, vol. 491, pp. 138–150, 2019.

[12] X. Rui, F. Meng, Z. Wang, and G. Yuan, "A reversed node ranking approach for influence maximization in social networks," *Applied Intelligence*, vol. 49, pp. 2684–2698, 2019.

[13] Y. Zeng, C. Sreenan, N. Xiong, L. T. Yang, and J. H. Park, "Connectivity and coverage maintenance in wireless sensor networks," *The Journal of Supercomputing*, vol. 52, no. 1, pp. 23–46, 2010.

[14] W. Guo, N. Xiong, A. V. Vasilakos, G. Chen, and H. Cheng, "Multi-source temporal data aggregation in wireless sensor networks," *Wireless Personal Communications*, vol. 56, no. 3, pp. 359–370, 2011.

[15] R. He, N. Xiong, L. T. Yang, and J. H. Park, "Using multi-modal semantic association rules to fuse keywords and visual features automatically for web image retrieval," *Information Fusion*, vol. 12, no. 3, pp. 223–230, 2011.

[16] L. Shu, Y. Zhang, Z. Yu, L. T. Yang, M. Hauswirth, and N. Xiong, "Context-aware cross-layer optimized video streaming in wireless multimedia sensor networks," *The Journal of Supercomputing*, vol. 54, no. 1, pp. 94–121, 2010.

[17] C. Lin, Y. He, and N. Xiong, "An energy-efficient dynamic power management in wireless sensor networks," in *2006 Fifth International Symposium on Parallel and Distributed Computing*, pp. 148–154, Timisoara, Romania, 2006.

[18] Y. Zhou, D. Zhang, and N. Xiong, "Post-cloud computing paradigms: a survey and comparison," *Tsinghua Science and Technology*, vol. 22, no. 6, pp. 714–732, 2017.

[19] Y. Yang, N. Xiong, N. Y. Chong, and D. Xavier, "A decentralized and adaptive flocking algorithm for autonomous mobile robots," in *2008 The 3rd International Conference on Grid and Pervasive Computing - Workshops*, pp. 262–268, Kunming, China, 2008.

[20] A. Shahzad, M. Lee, Y.-K. Lee et al., "Real time modbus transmissions and cryptography security designs and enhancements of protocol sensitive information," *Symmetry*, vol. 7, no. 3, pp. 1176–1210, 2015.

[21] K. Li, L. Zhang, and H. Huang, "Social influence analysis: models, methods, and evaluation," *Engineering*, vol. 4, no. 1, pp. 40–46, 2018.

[22] W. Liu, L. Chen, X. Chen, and B. Chen, "An algorithm for influence maximization in competitive social networks with unwanted users," *Applied Intelligence*, vol. 50, pp. 417–437, 2019.

[23] W. Liu, Y. Li, X. Chen, and J. He, "Maximum likelihood-based influence maximization in social networks," *Applied Intelligence*, vol. 50, no. 10, pp. 3487–3502, 2020.

[24] X. Chen, C. Zhao, and L. Yang, "A group decision-making model based on interval-valued intuitionistic fuzzy numbers and its application on social network," *Systems Engineering-Theory& Practice*, vol. 37, no. 7, pp. 1842–1852, 2017.

[25] J. Kleinberg, "Authoritative sources in a hyperlinked environment," *Journal of the ACM*, vol. 46, no. 5, pp. 604–632, 1999.

[26] X. Kong, F. Xia, Z. Ning et al., "Mobility dataset generation for vehicular social networks based on floating car data," *IEEE Transactions on Vehicular Technology*, vol. 67, no. 5, pp. 3874–3886, 2018.

[27] K. Atanassov and G. Gargov, "Interval-valued intuitionistic fuzzy sets," *Fuzzy Sets and Systems*, vol. 31, no. 3, pp. 343–349, 1989.

[28] M. Gao, T. Sun, and J. Zhu, "Interval-valued intuitionistic fuzzy multiple attribute decision-making method based on revised fuzzy entropy and new scoring function," *Control and Decision*, vol. 31, no. 10, pp. 1757–1764, 2016.

[29] Z. Xu, "Methods for aggregating interval-valued intuitionistic fuzzy information and their application to decision making," *Control and Decision*, vol. 22, no. 2, pp. 215–219, 2007.

[30] Y. Zhao and J. Mao, "New type of interval-valued intuitionistic fuzzy entropy and its application," *Computer Engineering and Applications*, vol. 52, no. 12, pp. 85–89, 2016.

[31] M. Cha, H. Haddadi, F. Benevenuto, and K. P. Gummadi, "Measuring user influence in twitter: the million follower fallacy," in *4th International AAAI Conference on Weblogs and Social Media*, pp. 10–17, Washington DC, USA, 2010.

[32] H. Kwak, C. Lee, H. Park, and S. Moon, "What is twitter, a social network or a news media?," in *Proceedings of the 19th international conference on World wide web - WWW '10*, pp. 591–600, Raleigh, USA, 2010.

[33] C. Lee, H. Kwak, H. Park, and S. Moon, "Finding influentials based on the temporal order of information adoption in twitter," in *Proceedings of the 19th international conference on World wide web - WWW '10*, pp. 1137-1138, Raleigh, USA, 2010.

[34] D. Romero, W. Galuba, S. Asur, and B. A. Huberman, "Influence and Passivity in Social Media," in *Machine Learning and Knowledge Discovery in Databases. ECML PKDD 2011*, D. Gunopulos, T. Hofmann, D. Malerba, and M. Vazirgiannis, Eds., vol. 6913 of Lecture Notes in Computer Science, pp. 18–33, Springer, Berlin, Heidelberg, 2011.

[35] J. Weng, E.-P. Lim, J. Jiang, and Q. He, "Twitterrank: finding topic-sensitive influential twitterers," in *Proceedings of the third ACM international conference on Web search and data mining - WSDM '10*, pp. 261–270, New York, USA, 2010.

[36] S. Ye and F. Wu, "Measuring message propagation and social influence on Twitter.com," *International Journal of Communication Networks and Distributed Systems*, vol. 11, no. 1, pp. 59–76, 2013.

[37] E. Bakshy, J. Hofman, W. A. Mason, and D. J. Watts, "Everyone's an influencer: quantifying influence on twitter," in *Proceedings of the fourth ACM international conference on Web search and data mining - WSDM '11*, pp. 65–74, Hong Kong, China, 2011.

[38] K. Atanassov, "Intuitionistic fuzzy sets," *Fuzzy Sets and Systems*, vol. 20, no. 1, pp. 87–96, 1986.

[39] I. K. Vlachos and G. Sergiadis, "Subsethood, entropy, and cardinality for interval-valued fuzzy sets-an algebraic derivation," *Fuzzy Sets and Systems*, vol. 158, no. 12, pp. 1384–1396, 2007.

[40] Q. Zhang, S. Jiang, B. Jia, and S. Luo, "Some information measures for interval-valued intuitionistic fuzzy sets," *Information Sciences*, vol. 180, no. 24, pp. 5130–5145, 2010.

[41] H. Ren and Z. Tan, "Multi-attribute decision making model coupled with interval valued intuitionistic fuzzy entropy-set pair analysis-technique for order preference by similarity to an ideal solution," *Control Theory & Applications*, vol. 37, no. 1, pp. 176–186, 2020.

[42] M. Hu, C. Fan, and K. Shi, "Character analysis of standardization methods of decision matrix with intervals," *Computer Science*, vol. 40, no. 10, pp. 203–207, 2013.

[43] Z. Yue, "An approach to aggregating interval numbers into interval-valued intuitionistic fuzzy information for group decision making," *Expert Systems with Applications*, vol. 38, no. 5, pp. 6333–6338, 2011.

[44] Y. Yu, J. Yuan, Z. Zhu, and T. Liu, "Evaluation and comparative study on the influence of university official microblog based on PCA and Ca," *China Business & Trade*, vol. 25, pp. 167–172, 2018.

[45] W. Guo, N. Xiong, H.-C. Chao, S. Hussain, and G. Chen, "Design and analysis of self-adapted task scheduling strategies in wireless sensor networks," *Sensors*, vol. 11, no. 7, pp. 6533–6554, 2011.

[46] Q. Zhang, C. Zhou, N. Xiong, Y. Qin, X. Li, and S. Huang, "Multimodel-based incident prediction and risk assessment in dynamic cybersecurity protection for industrial control systems," *IEEE Transactions on Systems, Man, and Cybernetics: Systems*, vol. 46, no. 10, pp. 1429–1444, 2015.

Hindawi
Wireless Communications and Mobile Computing
Volume 2020, Article ID 8870886, 7 pages
https://doi.org/10.1155/2020/8870886

Research Article

Establishment of Music Emotion Model Based on Blockchain Network Environment

Ke Xu

Qingdao University of Technology, Qingdao 266033, China

Correspondence should be addressed to Ke Xu; xuke@qtech.edu.cn

Received 27 September 2020; Revised 27 October 2020; Accepted 24 November 2020; Published 11 December 2020

Academic Editor: Hongju Cheng

Copyright © 2020 Ke Xu. This is an open access article distributed under the Creative Commons Attribution License, which permits unrestricted use, distribution, and reproduction in any medium, provided the original work is properly cited.

With the innovation and development of network technology, people's various needs are gradually increasing. Among various multimedia, music has different characteristics from other forms of multimedia. Music can contain many human emotions, and humans can express some shallow and deep emotions through music. Therefore, the study of music emotion in the context of the Internet is an area where the public is relatively concerned. In the context of new media on the Internet, based on the current music emotion model, this paper establishes a different music emotion model from the past through clear research and analysis. From music characteristics, some relative vector quantities are extracted to build samples, and the samples are screened on the basis of network media technology to build a musical emotion model. The experimental simulation results show that the music emotion model based on the blockchain network environment established in this paper has high applicability and efficiency.

1. Introduction

The combination of network technology and music emotion is an important manifestation of the development of the times, and it is also the main direction of their common development [1, 2]. The reason why music is created and highly praised is closely related to the emotions expressed by music. Nowadays, computer technology has become more and more developed. As a carrier of various emotions, music is presented around people in the form of multimedia and has a wide range of applications in many fields [3, 4]. Some people suddenly realized that the application of computers to music can enhance people's understanding and control of music, and to a greater extent enhance the appeal and expressive power of music, and has extremely optimistic development prospects. Many high technologies have created a good environment for the development of music emotions [5].

The analysis of music emotion refers to the relatively complex process of generating automatic pattern recognition through computers and other technologies [6, 7]. Music itself is a special thing that can affect people's various emotions, life, and even ways of thinking. Music in network multimedia contains a large amount of information and data and is closely related to people's various emotions. Music has a strong presence in various forms of multimedia. The research of music emotion is of far-reaching significance to the current development of multimedia networks, network technology innovation, and the development of human-computer interaction [8, 9]. Through network technology, the analysis of music emotion needs to be matched in the current emotion database, and the emotion is derived through the comparison of related data. Therefore, it is necessary to establish a musical emotion model. However, music emotion has the characteristics of great vagueness, and the information is relatively vague. In addition, there are no rules to follow, so it is difficult to analyze and process music emotions in general methods. There is basically no automatic music emotion recognition model that conforms to people's emotions. Therefore, analyzing music emotions is of great significance [10]. On this basis, combined with the new intermediary environment of the Internet, the establishment of a musical emotion model was studied.

2. The Development Status of Music Sentiment Analysis

The combination of new online media and music is actually the result of the normal development of the times. At present, in the era of new media, network technology is ubiquitous, and computer music technology is needed in many fields [11, 12]. High-tech equipment makes the development of computer music technology smoother under this current good network environment [13]. In fact, as early as a long time ago, some people used artificial intelligence technology to analyze music emotions, so as to realize automatic analysis and recognition of the emotions contained in music through this technology [14].

The research on music sentiment analysis in foreign countries is much earlier than in our country, and its development technology is becoming more and more mature and advanced. Japan has developed some products that can help music creation using its advanced artificial intelligence technology. When people input some lyrics and tones in the software product, the software will perform some analysis on the music emotion and find out the corresponding melody [15]. Therefore, many people believe that the discovery of this technology will greatly help music creation. However, my country's research in this area is relatively late. However, both the country and the people attach great importance to this research [16]. Many well-known key universities have also begun to participate in this research. Some research funds have been allocated for related research. In addition, our country also holds some important discussions and exchange meetings on a regular basis to further deepen the research on music sentiment analysis [17].

In this regard, many scholars are writing more and more academic papers. Music plays a pivotal role in people's lives and strongly affects people's growth and life. The research on music sentiment analysis has also become an area of increasing attention. As far as the research of music sentiment analysis is concerned, this research idea can not only be extended to other fields of application, but also can make the relatively vague artificial intelligence part more perfect [18]. At the same time, this research can enable better application of multimedia technology, thereby achieving greater development of multimedia technology in music creation and other aspects. In addition, the analysis of music emotion is actually a very meaningful research, which makes music unique in the process of the increasing development of today's network technology [19].

3. Analysis of Current Musical Emotion Model

The combination between computer technology and music is the inevitable result of the progress of times and the network multimedia development. Although the emotions contained in music have great indeterminacy and basically have no laws to follow, from the modern perspective, there are still some rules which can be explored [20, 21]. The vibrations of sound waves and people's internal emotional activities actually have some correspondence, so the study can be conducted from this point. The first element to establish the musical emotion analysis model (shown as Figure 1) is to build musical emotion model, then to derive musical space [22].

There are mainly three types of musical space. The first one is musical emotion space which can lead out emotional annotation; the second one is musical feature space which can lead out feature extraction; the third sample space, based on the former two kinds of musical space, organically combines its emotional chain with feature flow together, so as to set up the foundation of musical emotion cognitive model [23, 24]. Musical emotion analysis model is shown in Figure 1.

3.1. Heiner Emotion Model. In some current musical emotion models, Heiner emotion model is the most accepted by the public. This model generally adopts a circle to represent the inner emotional symbols (shown as Figure 2). Through an annulus, musical emotions are divided into different plates. Every plate has certain inheritance or close relationship with the two adjacent plates. It can be treated as a transformation process of emotions or a link of emotions' transition [25].

In this emotional annular model, it is only a conjecture that the musical emotions become to have some regularity. It is premised on people's certain emotional reflection situation that is relatively stable connected to some fixed elements in music. Then, the musical emotions represented in the annular model can be guaranteed to directly reflect people's inner emotions or show the rules and trends of this kind of reflection [26, 27]. For example, in the musician's Reflets dans idea, the elicitation process of musical emotions is from beginning lightness and cheerfulness to later enthusiasm and vitality [28, 29]. So, it can verify that this model does have some existing significance.

$$\begin{aligned} &\text{Note} = \{\text{duration} ; \text{pitch} ; \text{intensity}\}, \\ &\text{Note} = \{\text{duration} ; \text{pitch} ; \text{intensity}\}. \end{aligned} \tag{1}$$

In music, the smallest unit is note which contains three features of pitch, intensity, and duration. Pitch represents the length of time between every note. Intensity is related to the frequency of vibrations. Duration refers to strength or volume when people listen to the sound of this note [30]. Therefore, note can be defined in this way. Heiner model of the music emotion model is shown in Figure 2.

The duration, pitch, and intensity successively refer to how long, how high, and how strong the note sounds [31]. So, the melody features of the music can be expressed in this way:

$$\begin{aligned} &\text{Melody} = (\text{note1}, \text{note2}, \text{note3} \cdots \text{notec}), \\ &\text{Melody} = (\text{note1}, \text{note2}, \text{note3} \cdots \text{notec}). \end{aligned} \tag{2}$$

$$P\left(Y = \frac{c_k}{X = x}\right) = \frac{P(X = x/Y = c_k)P(Y = c_k)}{\sum_{k=1}^{K} P(X = x/Y = c_k)P(Y = c_k)} \tag{3}$$

in which k refers to the number of notes in a piece of music, i.e., the length of the melody.

In the application process, the actual need should be the standard to get the needed quantity from the features of the

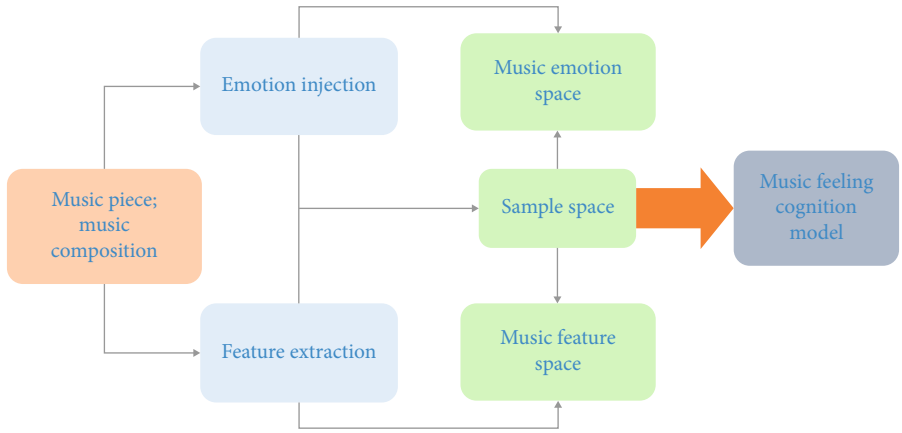

Figure 1: Musical emotion analysis model of the music emotion model.

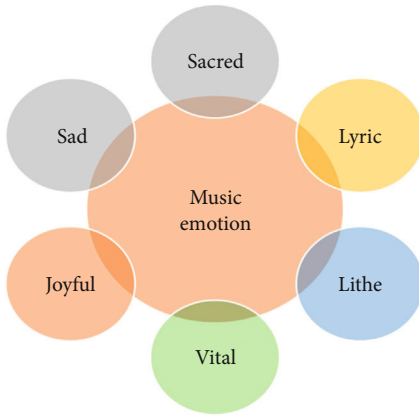

Figure 2: Heiner model of the music emotion model.

music to make study and analysis [32, 33]. Also, according to the practical situation, some relevant data can be calculated for it, such as the degree of similarity and the degree of correlation, so as to meet the feature vectors of emotions.

$$h_\theta(x) = \left[1 + \exp\left(-\theta^T x\right)\right]^{-1}. \tag{4}$$

Actually, this model is not an aggregation psychological model for emotions, but this model would analyze emotions through music or a series of artworks related to emotions.

$$\mathrm{l}(\theta) = \prod_{i=1}^{n} [h_\theta(x)]^{y_i} \bullet [1 - h_\theta(x)]^{1-y_i}. \tag{5}$$

This is the premise of the analysis to suit some rules of emotions. Thus, the model is also commonly applied in other fields, such as art psychology, musical psychological study, and computer music study [34].

$$y = f(x) = \operatorname{argmax} \frac{\prod_{j=1}^{n} P\left(X^{(j)} = x^{(j)} / Y = c_k\right) P(Y = c_k)}{\sum_{k=1}^{K} (Y = c_k) \prod_{j=1}^{n} P\left(X^{(j)} = x^{(j)} / Y = c_k\right)}. \tag{6}$$

3.2. Thayer Emotion Model. This model is structured through a sort of two dimensions, energy, and pressure, to make analysis on emotions. In terms of energy dimension, the lowest coordinate point is contentment and gradually rises to an exuberance level [35]. In this process, any level in it can embody a kind of emotion. The level embodiment of this dimension can express at many levels. And in the pressure dimension, it mainly embodies the emotional performance from happiness to anxiety in varying degrees [36]. Thayer Model of the music emotion model is shown in Figure 3.

People's inner emotional features can be represented by adopting Thayer model through different levels' embodiment of the two dimensions. Thayer model is a relatively continuous musical emotion expression model, to present a kind of continuous psychological emotions. Based on this continuous feature, it will perform naturally while different emotions are carrying on, rather than transforming ponderously and suddenly. However, one shortcoming of Thayer model lies in that there is not too much space for emotional activities. Two dimensions absolutely cannot confirm the abundant emotional expression. After all people's emotions are influenced by multiple factors. This is also the reason why the model is rarely applied.

4. Key Melody Recognition of Musical Emotions

Melody is the core of a piece of music, which was conducted by a series of relevant notes through varying rhythms and tones with purposes. In a piece of music, the leading melody represents the foundational emotions what this piece of music expects to express. However, for computers, those emotions cannot be directly obtained, but need to be embodied via some features in the music. Thus, in order to analyze musical emotions, it is necessary to analyze and study the features of the leading melody of the music.

4.1. Format Selection of Audio Files. The construction of musical melody features can analyze music on inner musical emotions more deeply. Then, the first thing to be sure is which format of music can become the main data sources to extract musical melodies. From current situation, it can be seen that there are many file formats of computer music,

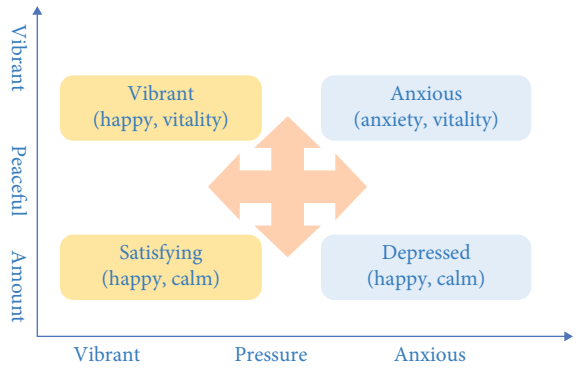

Figure 3: Thayer model of the music emotion model.

and each format has different features. Generally speaking, the formats of computer music can be divided into three categories as below. Sound files are also called as audio files which refer to the files obtained by directly simulating the waveform of practical sound through computer sampling. This is a kind of reflection to practical sound. And this will cause the files occupy a lot of storage space. Computer music file response efficiency at different times is shown in Figure 4.

What MIDI files record is a kind of instruction sequence during instrumental performance, excluding the records of actual musical data. This kind of files often records the instruments and contents in different tracks. The files clearly record which instrument performs what notes at that period of time. So this sort of files does not take up large space. Also, it is very convenient to extract the musical features. The music files of this format can directly be extracted in detail. Module files have common characteristics of the other two kinds of files, recording both actual sound and the instruction sequence during instrumental performance. However, there are many coding schemes of this kind of files, so there are also many types of formats. If people extract musical features to this type of files, they should make decoder processing for different formats, and the operation process will be a little complicated. In the comparison of the three kinds of musical files above, it is not difficult to see that choosing the musical file of MIDI will be more convenient to extract the features of musical melodies.

5. Establishment of Musical Emotion Model Based on Network New Media Environment

5.1. Extraction of Features. Before the establishment of a model, it is necessary to obtain some data. In the establishment of musical emotion model, the data in the aspects of pitch, duration, and timbre in the music can be selected. The value of pitch depends on the frequency of things' vibrations. The pitch is proportional to the vibration frequency. The higher the vibration frequency, the higher the pitch. In the music of MIDI type, the high and low sounds are mainly under the effect of musical value, generally from 0.0 to 127.0. If f is used to represent the pitch in music as a function, the musical emotions can mainly be analyzed from the master track. It is assumed that current music has m tracks, and then relevant pitches are, respectively, extracted in the m tracks.

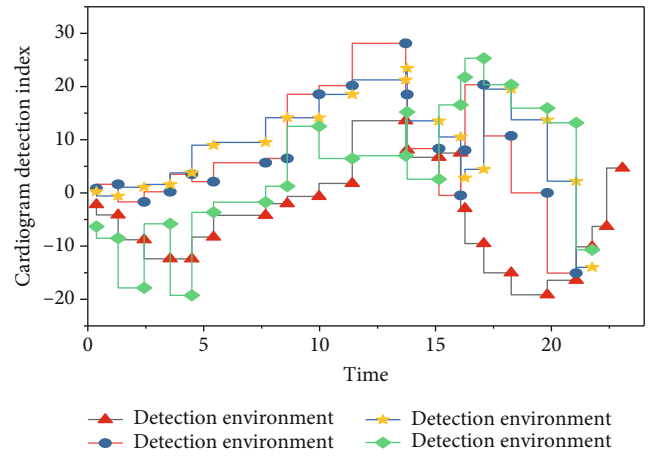

Figure 4: Computer music file response efficiency at different times.

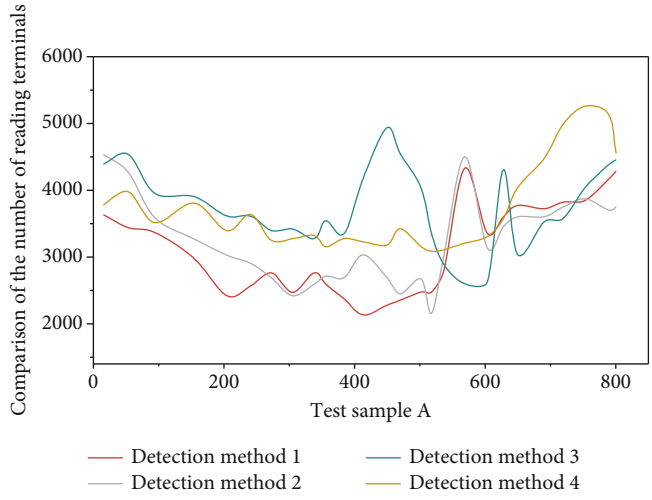

Figure 5: The characteristics of the duration vector of notes in different environments.

The feature vector xj of the pitch in the music will be determined according to the special attributes of the master track. It is assumed that the whole musical emotional type is n, and n is greater than or equal to one. Then, the performance characteristics of musical emotions under the influence of the vector of pitch will be $Pi(xf)$, where i is positive integer. So, the relationship between the emotions represented by the music and its pitch can be expressed as follows:

$$f(x_f) = \text{Max}\ (p_i). \tag{7}$$

In musical emotions, the pitch has its great influence. But the specific relationship between the two should be further confirmed in light of recognition. Duration is the length of time when some note is sounded in the music. In music, duration opening represents the note begins to make a sound, and duration closing means the note ends to make a sound. The function g refers to the duration feature in the music in study. Generally speaking, longer duration in music may mean that the piece of music has more dolorous

Table 1: Music statistics.

Musical type	Number	Typical pieces of music
Film type	50	The Legend of the Condor Heroes, To the sky kingdom, etc.
Popular type	53	Outside the Light Year, The Brightest Star in the Night Sky, etc.
Classical type	45	Pink Memories, The Moon Represents My Heart, etc.
Religious type	18	The Great Compassion Mantra, The holy Epithet of Name Bodhisattva, etc.
Chinese type	34	Ninjago - Meditate on the Past at Red Cliff, Gold-Woven Dress, etc.

elements. The extraction of the vector of duration can carry out according to the continuous time of notes.

$$g(x_g) = \begin{cases} \text{long}, x_g \geq x_{\text{switch}} \\ \text{short}, x_g < x_{\text{switch}} \end{cases}. \quad (8)$$

x represents the time of the duration from duration opening to duration closing. Switch represents the threshold value of the duration. In light of this formula, the duration time of the music can be confirmed, so as to confirm the duration vector characteristics of the notes in the music. The characteristics of the duration vector of notes in different environments are shown in Figure 5.

Different instruments can present different sound waves. Timbre is affected by harmonic waves, and the different construction situation of harmonic waves will make timbre change with it. For example, the timbre of piano is very elegant and steady, which gives people a relaxed feeling. But the timbre of erhu is a little harsh, which is easy to make people feel sorrowful. So, different instruments are labeled to define 120 kinds of timbre, so as to extract the timbre features. Timbres are corresponded to emotions, to divide 120 kinds of timbres into K types. The formula h represents the extraction of timbre vectors in current music.

$$h_{x_i} = \begin{cases} 1 & x_i \in C_1 \\ 2 & X_i \in C_2 \\ \vdots & \\ M & X_i \in C_M \end{cases}. \quad (9)$$

In various audio tracks of music, even the timbre of the same audio track may immediately change as long as the time changes. So, the extraction of timbre feature music should adopt a kind of dynamic method. Through the three basic elements, in terms of musical space features and vector model of emotion features, a dimension space with six dimensions can be produced. In this dimensional space, the distribution of elements should be average. It should be known that in massive pieces of music, the intensity distribution of a piece of music is relatively average. There is no significant difference in the features in some aspects. For some places without obvious features, the extraction does not need to be conducted.

Range: $\text{range} = 1/n\sum_{i-1}^{n}\text{pitch}_i$.

Intensity: $\text{intensity} = 1/n\sum_{i-1}^{n}\text{intensity}_j$.

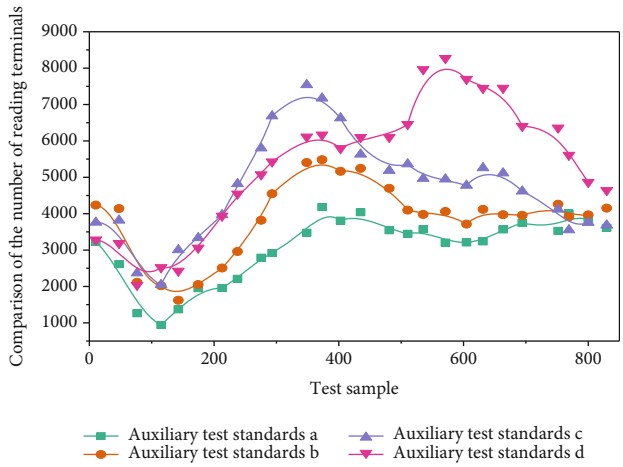

Figure 6: Music sentiment classification test results.

Melody direction: $\text{Dir\_Pit} = \sum_{i-1}^{n}\text{intensity}_i.\text{duration}_i/\text{duration\_music} - \text{duration}_n$.

Pitch stability: $\text{Sta\_pitch} = \sqrt{1/n\sum_{n-1}^{n}(\text{pitch} - \text{range})^2}$.

Interval stability: $\text{Sta\_interval} = \sqrt{1/n\sum_{i-1}^{n}(|\text{interval}_i| - |\overline{\text{invertal}}|)^2}$.

Interval span: $\text{Span} - \text{Int} = 1/n - 1\sum_{i-1}^{n-1}|\text{interval}_i|$.

5.2. Establishment of Samples. According to some relatively professional music websites, music libraries, and other resource approaches, some professional people in music colleges establish the samples of music to classify the emotions expressed in various kinds of music. 200 pieces of music are handpicked, including 50 pieces of sentimental music, 53 pieces of passionate music, 52 pieces of classical music, and 45 pieces of inspirational music. The basic classification is shown in Table 1.

From the emotion-classified pieces of music above, 20 samples are randomly selected as the data to test, and the others are training data. It is found that the obtained network classification presents scarcely ideal results. As for the establishment of musical samples, some deviations will be produced in testing period because of many elements. So, the samples cannot be directly applied; otherwise, they will influence the final results. So, some screenings should be conducted for the samples. Music sentiment classification test results are shown in Figure 6.

The network's input level can set six-dimension vectors of musical emotion features. The six dimensions are,

respectively, range, intensity, melody direction, pitch stability, interval stability, and interval span. The input node number is set as 6, and the output is musical emotions. According to current Heiner model, music is divided into eight different types. The output note is 3 ($\log 82 = 3$).

According to the Kolmogorov theory of $n1 = 2n + 1$ ($n1$ represents the number of hidden layer nodes, and n represents the number of input nodes), $n1 = 13$ can be drawn. So, the final established nerve network construction is $6 * 13 * 3$, where 6 notes refer input level, 13 notes represent the hidden level, and 3 notes refer to output level. On this basis, the hidden level and output level can both be calculated by Sigmoid formula $f(x) = 1/1 + e^x$. In this way, the ultimate output value can be ensured to show between zero and one. In the whole network system, the biggest cycle index is set at 3000, with the deviation about 0.003. The training formula is a training formula. The learning formula adopts a gradient descent momentum learning formula. The performance function takes a mean square error performance function.

6. Conclusion

The knowledge and technology applied in the analysis of computer musical emotion analysis are extremely extensive. And the neural network modeling needs to be understood to some extent while conducting it. Musical emotion analysis is the important understanding of multimedia contents, as well as the important member in artificial intelligence, applied in various fields. With the significant development of today's network new media, musical emotion analysis also constantly integrates with it, to become a vital direction of network multimedia development at present. In this paper, the establishment of musical emotion model builds a good platform for the extraction of more the same emotional music, for the purpose of set up a good foundation for the application in practice. In addition, how to master more advanced technology more deeply, to develop more studies with practical significance, and make further innovation, is the current and future direction and objective of common effects.

Data Availability

All author information is available from the author.

Conflicts of Interest

The author declares that there is no conflict of interest regarding the publication of this paper.

References

[1] A. Järvinen, R. Ng, D. Crivelli et al., "Social functioning and autonomic nervous system sensitivity across vocal and musical emotion in Williams syndrome and autism spectrum disorder," *Developmental Psychobiology*, vol. 58, no. 1, pp. 17–26, 2016.

[2] C. Jiang, F. Liu, and P. C. M. Wong, "Sensitivity to musical emotion is influenced by tonal structure in congenital amusia," *Scientific Reports*, vol. 7, no. 1, p. 7624, 2017.

[3] C. Liegeois-Chauvel, "Musical emotion memory, evidence of lateralized anteromedial temporal structures," *International Journal of Psychophysiology*, vol. 100, no. 108, p. 31, 2016.

[4] D. Raynaud, S. Gessner, and B. Mota, "Andalò di negro's de compositione astrolabii: a critical edition with english translation and notes," *Archive for History of Exact Sciences*, vol. 73, no. 6, pp. 551–617, 2019.

[5] M. Forcada, F. J. Ragep, and T. Mimura, "On astronomia: an arabic critical edition and english translation of epistle 3," *Journal for the History of Astronomy*, vol. 47, Part 3, pp. 346-347, 2016.

[6] A. Aljanaki, F. Wiering, and R. C. Veltkamp, "Studying emotion induced by music through a crowdsourcing game," *Information Processing & Management*, vol. 52, no. 1, pp. 115–128, 2016.

[7] A. Shook and V. Marian, "The influence of native-language tones on lexical access in the second language," *Journal of the Acoustical Society of America*, vol. 139, no. 6, p. 3102, 2016.

[8] S. Panwar, P. Rad, K. K. R. Choo, and M. Roopaei, "Are you emotional or depressed? Learning about your emotional state from your music using machine learning," *Journal of Supercomputing*, vol. 75, no. 6, pp. 2986–3009, 2019.

[9] S. Hans-Eckhardt, "Music-evoked emotions—current studies," *Frontiers in Neuroence*, vol. 11, p. 600, 2017.

[10] W. C. Wang, "The effect of adaptive music playing system on emotion regulation," *Journal of the Acoustical Society of America*, vol. 140, no. 4, pp. 3380–3380, 2016.

[11] I. Dufour and G. Tzanetakis, "Using circular models to improve music emotion recognition," *IEEE Transactions on Affective Computing*, vol. 4, no. 16, pp. 1–1, 2018.

[12] N. Vannson, H. Innes-Brown, and J. Marozeau, "Dichotic listening can improve perceived clarity of music in cochlear implant users," *Trends in Hearing*, vol. 19, 2015.

[13] R. Xue, S. Huang, X. Luo, D. Jiang, and R. Y. Da Xu, "Semantic emotion-topic model in social media environment," *Journal of Web Engineering*, vol. 17, no. 1-2, pp. 73–92, 2018.

[14] R. Qin, C. Zhou, H. Zhu, M. Shi, F. Chao, and N. Li, "A music-driven dance system of humanoid robots," *International Journal of Humanoid Robotics*, vol. 15, no. 5, p. 1850023, 2018.

[15] J. J. Deng and C. H. C. Leung, "Dynamic time warping for music retrieval using time series modeling of musical emotions," *IEEE transactions on affective computing*, vol. 6, no. 2, pp. 137–151, 2015.

[16] B. Bogert, T. Numminen-Kontti, B. Gold et al., "Hidden sources of joy, fear, and sadness: explicit versus implicit neural processing of musical emotions," *Neuropsychologia*, vol. 89, pp. 393–402, 2016.

[17] C. G. Tsai and C. P. Chen, "Musical tension over time: listeners' physiological responses to the 'retransition' in classical sonata form," *Journal of New Music Research*, vol. 44, no. 3, pp. 271–286, 2015.

[18] X. Liu and H. Zhao, "Hierarchical feature extraction based on discriminant analysis," *Applied Intelligence*, vol. 49, no. 7, pp. 2780–2792, 2018.

[19] H. I. Ozercan, A. M. Ileri, E. Ayday, and C. Alkan, "Realizing the potential of blockchain technologies in genomics," *Genome Research*, vol. 28, no. 9, pp. 1255–1263, 2018.

[20] Z. Yinghui, R. H. Deng, L. Ximeng, and Z. Dong, "Blockchain based efficient and robust fair payment for outsourcing services in cloud computing," *Information Sciences*, vol. 462, pp. 262–277, 2018.

[21] Y. Liu, M. Ma, X. Liu, N. Xiong, A. Liu, and Y. Zhu, "Design and analysis of probing route to defense sink-hole attacks for Internet of Things security," *IEEE Transactions on Network Science and Engineering*, vol. 7, no. 1, pp. 356–372, 2018.

[22] K. Gammon, "Experimenting with blockchain: can one technology boost both data integrity and patients' pocketbooks?," *Nature Medicine*, vol. 24, no. 4, pp. 378–381, 2018.

[23] V. Sharma, I. You, F. Palmieri, D. N. K. Jayakody, and J. Li, "Secure and energy-efficient handover in fog networks using blockchain-based DMM," *IEEE Communications Magazine*, vol. 56, no. 5, pp. 22–31, 2018.

[24] E. Funk, J. Riddell, F. Ankel, and D. Cabrera, "Blockchain technology: a data framework to improve validity, trust, and accountability of information exchange in health professions education," *Academic Medicine*, vol. 93, no. 12, pp. 1791–1794, 2018.

[25] L. Li, J. Liu, L. Cheng et al., "Creditcoin: a privacy-preserving blockchain-based incentive announcement network for communications of smart vehicles," *IEEE Transactions on Intelligent Transportation Systems*, vol. 19, no. 7, pp. 2204–2220, 2018.

[26] W. Pan and C. Chai, "Structure-aware Mashup service clustering for cloud-based Internet of Things using genetic algorithm based clustering algorithm," *Future Generation Computer Systems*, vol. 87, pp. 267–277, 2018.

[27] G. Yang, Q. Yang, and H. Jin, "A novel trust recommendation model for mobile social network based on user motivation," *Electronic Commerce Research*, vol. 4, no. 8, pp. 56–59, 2019.

[28] K. N. Khaqqi, J. J. Sikorski, K. Hadinoto, and M. Kraft, "Incorporating seller/buyer reputation-based system in blockchain-enabled emission trading application," *Applied energy*, vol. 209, pp. 8–19, 2018.

[29] J. M. Roman-Belmonte, H. De la Corte-Rodriguez, and E. C. Rodriguez-Merchan, "How blockchain technology can change medicine," *Postgraduate Medicine*, vol. 130, no. 4, pp. 420–427, 2018.

[30] S. S. Ahmad, S. Khan, and M. A. Kamal, "What is blockchain technology and its significance in the current healthcare system? A brief insight," *Current Pharmaceutical Design*, vol. 25, no. 12, pp. 1402–1408, 2019.

[31] A. Pavlidis, M. Dimolianis, K. Giotis, L. Anagnostou, and V. Maglaris, "Orchestrating DDoS mitigation via blockchain-based network provider collaborations," *The Knowledge Engineering Review*, p. 35, 2020.

[32] M. Shabani, "Blockchain-based platforms for genomic data sharing: a de-centralized approach in response to the governance problems?," *Journal of the American Medical Informatics Association*, vol. 26, no. 1, pp. 76–80, 2019.

[33] Y. Liu, M. Ma, X. Liu, N. Xiong, A. Liu, and Y. Zhu, "Design and analysis of probing route to defense sink-hole attacks for Internet of Things security," *IEEE Transactions on Network Science and Engineering*, vol. 7, no. 1, pp. 356–372, 2020.

[34] F. Long, N. Xiong, A. V. Vasilakos, L. T. Yang, and F. Sun, "A sustainable heuristic QoS routing algorithm for pervasive multi-layered satellite wireless networks," *Wireless Networks*, vol. 16, no. 6, pp. 1657–1673, 2010.

[35] Y. Zhou, D. Zhang, and N. Xiong, "Post-cloud computing paradigms: a survey and comparison," *Tsinghua Science and Technology*, vol. 22, no. 6, pp. 714–732, 2017.

[36] W. Pan and C. Chai, "Measuring software stability based on complex networks in software," *Cluster Computing*, vol. 22, no. S2, pp. 2589–S2598, 2019.

Hindawi
Wireless Communications and Mobile Computing
Volume 2020, Article ID 6686181, 10 pages
https://doi.org/10.1155/2020/6686181

Research Article

Modeling and Prediction of Stock Price with Convolutional Neural Network Based on Blockchain Interactive Information

Wei Zhang[1], **Ke-xin Tao**[1], **Jun-feng Li**[2,3], **Yan-chun Zhu**[4] and **Jing Li**[4]

[1]*School of Information, Central University of Finance and Economics, Beijing 100081, China*
[2]*School of Finance, Central University of Finance and Economics, Beijing 100081, China*
[3]*Private Investment Fund Research Center, Central University of Finance and Economics, Beijing 100081, China*
[4]*Business School, Beijing Normal University, Beijing 100875, China*

Correspondence should be addressed to Jun-feng Li; lijf@cufe.edu.cn

Received 20 October 2020; Revised 13 November 2020; Accepted 24 November 2020; Published 9 December 2020

Academic Editor: Hongju Cheng

Copyright © 2020 Wei Zhang et al. This is an open access article distributed under the Creative Commons Attribution License, which permits unrestricted use, distribution, and reproduction in any medium, provided the original work is properly cited.

The interactive information in blockchain architecture establishes an effective communication channel between users and enterprises, enabling them to communicate in a comprehensive and effective manner. Therefore, taking blockchain interactive information as the research object, this paper explores how the intervention of official information on investors affects the stock price movement and then makes predictions on stock prices according to the emotional tendency of interactive information. With the contextual information fusion, a sentiment computing model based on a convolutional neural network is established to extract and quantify the emotional features of blockchain interactive information. Combined with investors' emotional features, the stock price prediction model based on long short-term memory is proposed. The experiment results show that the accuracy of the model has been improved by incorporating the intervened emotional features, thereby proving that information clarification can have a positive effect on the stock price.

1. Introduction

Stock price modeling and prediction have been challenging objectives for researchers and speculators because of the noisy and nonstationary characteristics of samples [1]. Since Fama proposed the efficient market hypothesis in 1965, it has been generally accepted in the traditional financial field [2]. This hypothesis assumes that the stock market will be affected by market information and that stock prices will reflect the available information about the asset. When relevant information changes, the stock price will also change accordingly. Given that information related to the stock market is one of the most important factors that can cause stock market volatility, it should thus be included in the factors affecting stock market volatility [3].

With the advancement of blockchain technology [4–8], relevant information about the stock market has been widely stored and disseminated in blockchain architecture [9]. Therefore, numerous studies have been conducted on the influence of online media on the stock price movement based on the public opinion generated by online media, such as message boards and social media [10, 11]. Nguyen et al. used historical stock prices and Yahoo forum texts to predict stock prices [12]. Upon comparing the prediction results of models that only used stock historical trading data with those that added emotional features, they found that the results of models that added sentiment analysis were better than those of models that only used historical data. Li et al. used an econometric regression model to analyze the impact of social media on stock prices [13]. After analyzing tweets related to S&P 100 companies, they found that social media sentiment had an impact on stock returns. With the development of computer technology, deep learning models have achieved good results in analysis and prediction. Li et al. also proposed a tensor-based prediction model [14], featuring high-dimensional market information and its internal connections to study the stock trends under the influence of the media.

The above studies have all proven that investor sentiment has been widely used in stock price analysis. However, most of the information sources for this type of research focus on

news, message boards, or social media, and the dissemination and changes of information are not considered. In addition, only a few studies on the interaction and influence of multiple information sources have been conducted thus far.

With the development of Internet technology, new online media channels represented by interactive media are gradually emerging. Digital interactive media rely on certain official channels to build question and answer (Q&A) platforms for both investors and listed companies. The Q&A texts on such platforms include representative consumer sentiments and official real news, which inject information content into the stock market environment based on the official interactions with investors. In order to investigate the dissemination and interaction of information, digital interactive media with both "investor questions" and "official answers" as research objects are worthy of further study.

However, the impact analysis of the stock market based on digital interactive media faces two important challenges. First, the interactive nature of text information makes it difficult to analyze such information. Second, the transaction data of listed companies is continuous at the trading day level, while the disclosure time of Q&A information in digital interactive media is intermittent. Moreover, the times of the two data dimensions are heterogeneous.

Based on the above analysis, this paper designs a stock price prediction model for digital interactive media sentiment analysis in order to solve the challenges mentioned above. First, a method for extracting and quantifying the emotional features of digital interactive media information based on convolutional neural networks (CNN) is established. In this paper, the text to be classified and its contextual information are integrated, and the model is trained using artificially labeled datasets, effectively improving the accuracy of the interactive text analysis model. Second, a stock prediction model based on the long short-term memory (LSTM) method is established. This incorporates investor sentiment characteristics guided by official information into the proposed model and explores the depth and breadth of the influence of emotional factors. Experiment results reveal that the accuracy of the model incorporating the emotional characteristics of the intervention has been improved, thus proving that market information requires effective intervention and guidance.

The rest of this article is organized as follows. The second part introduces related works on the impact of news on stock price fluctuations. The third part constructs the emotional calculation model and stock price prediction model. The fourth part describes the algorithm. The fifth part analyzes the details of the experiment in detail. The sixth part presents the experimental results, and the seventh part summarizes the article.

2. Related Work

In the research on the impact of news on stock price fluctuations, the first widely used index to measure the influence of news is the number of stock-related news. Chan studied the relationship between the number of news and excess stock returns [15]. He extracted the quantitative characteristics of stock-related news articles and used these as an explanatory variable to regress excess stock returns. His results indicated that the investors' reaction to negative news was slower than their reaction to positive news; however, the impact of news on investors was related to its actual content. Thus, the use of news volume to summarize the impact of news on investors may have obvious limitations. Tetlock used the textual information of financial news to make stock price forecasts and proved the effectiveness of news for stock price forecasts [16]. In that research, the author used text mining methods, extracted features in the text that may affect market changes, and improved the feature extraction methods. The results indicated that the stock price prediction method that took financial news into account was more effective than other methods.

With the continuous expansion of the Internet industry and the advancement of web2.0 to web3.0 technologies, investors' sentiments toward the stock market can be shared and spread in an interactive manner through Internet platforms. Sentiments and events are integrated with a tensor for stock prediction [14, 17]. Das and Chen first proposed a method to extract investor sentiment from Yahoo message boards [18]. Their algorithm incorporates a variety of classification algorithms, accurately analyzes investor sentiment in message boards, and empirically proves that posts in the technology sector are closely related to stock trading volume and fluctuations.

In analyzing the impact of investor sentiment on securities prices, the common analysis models used are based on statistical models, econometric models, and machine learning models [19–21]. Among them, econometric models include linear regression models, logistic regression models, and autoregressive integrated moving average (ARIMA) models. The econometric model focuses on analyzing the causal relationship between stock prices and information. Antweiler and Frank studied the impact of more than 1.5 million messages posted on Yahoo [22]. Using a linear regression model to analyze the financial announcements of stock returns in 2000, they found that stock information helped predict market fluctuations. The statistical model uses univariate statistical models or bivariate statistical models to test the relationship between information sources and stock changes under different hypothesis tests. Based on a sample from January 1, 2009, to October 31, 2014, Li et al. developed an LSTM model that is based on investor sentiment extracted from internet stock message boards and market data to conduct out-of-sample forecasts for the open and closing prices of the CSI 300 index in the Chinese stock market. Their results showed that daily investor sentiment can adequately predict the subsequent trading day's market open prices, while the predictive information for the daily closing price was weak [23].

With the development of computer technology, machine learning models are increasingly used to study the relationship between stocks and public opinion. When using these models for information representation, it is possible to extract and merge multiple information sources and then apply them to models, such as neural networks, support vector machines, and Bayes classifiers. Chun et al. presented the

conceptual framework of an emotion-based stock prediction system (ESPS) focused on considering the multidimensional emotions of individual investors. To implement and evaluate the proposed ESPS, emotion indicators (EIs) are generated using emotion term frequency–inverse emotion document frequency. The stock price is predicted using a deep neural network (DNN) [24]. To compare the performance of the ESPS, sentiment analysis and a naïve method are employed. The experiment results showed that the accuracy of prediction using EIs was better than the accuracy of prediction using other methods. Jin et al. conduct a comparative study about the predictive performance of an artificial neural network, support vector regression (SVR), and autoregressive integrated moving average and select SVR to study the asymmetry effect of investor sentiment on different industry index predictions. The results show that the industries affected by investor sentiment are composed of young companies with high growth and high operative pressure [25].

When analyzing the impact of investor sentiment on the stock market in the above-mentioned research, the news sources selected can often only represent one party (the investor or the government) and cannot reflect the information interaction between both parties [26, 27]. In terms of methods applied, machine learning-based models are more commonly used in the literature [28–30]. Although machine learning model-based methods can fuse multiple information sources, the research on the mechanism of mutual influence between information is not sufficient. Therefore, taking digital interactive media as the research object, this paper uses machine learning models (e.g., neural networks) in order to study the interaction between market information and clarify the impact of information on the stock market.

3. Stock Price Prediction Model Based on Sentiment Analysis

Our work, as illustrated in Figure 1, includes media data acquisition (building text corpus), data preprocessing, sentiment analysis, trade data collection, and stock price prediction.

3.1. Media Data Acquisition and Representation. Given the limited amount of news text data obtained, because the content is concentrated in the financial field, the financial news part of CA8, a pretrained Chinese word vector dataset, is selected in the model. Among them, the data of pretrained word vector is trained from 6.2G financial news collected by the CA8 builder. The extracted context features are "Word + Character" mode, and the training method is skip-gram with negative sampling. The skip-gram model consists of three parts: input layer, hidden layer, and output layer. The procedure for each word is presented below.

Step 1. A vocabulary based on the training document is built, after which the words $\omega(t)$ are one-hot coded. The dimension of the transformed vector is denoted as $[1, |v|]$, where v represents the total number of words known to the system.

Step 2. The word $\omega(t)$ is passed from $|v|$ to the hidden layer.

Step 3. The hidden layer calculates the dot product between weight vector $\mathscr{W}[|v|, N]$ and $\omega(t)$, thus obtaining $H[1, k]$, where N represents the number of neurons in the hidden layer.

Step 4. Pass the output vector $H[1, k]$ of the hidden layer to the output layer. The output layer calculates the dot product operation between $H[1, N]$ and weight matrix $\mathscr{W}'[N, |v|]$, thus obtaining the output vector $U[|v|]$.

Step 5. The SoftMax regression classifier is used to calculate the probability of the output vector. The calculation method uses the equation

$$p\left(\omega_{c,j} = \omega_{O,c} \mid \omega_I\right) = \frac{\exp\left(u_{c,j}\right)}{\sum_{I-1}^{V} \exp\left(u_j\right)}, \tag{1}$$

where $\omega_{c,j}$ refers to the word predicted at the c position, $\omega_{O,c}$ refers to the word that actually appears at position c, ω_I refers to the word currently entered, and $U_{c,j}$ refers to the word of vector U at the prediction position c.

3.2. Sentiment Classification. The CNN model consists of an embedded layer, a convolutional layer, a pooling layer, and a full connection layer. In the embedding layer, we input a fixed length $n \times k$ matrix, and the sequence can be in the form of a pretrained word vector and a nonstatic word vector or multichannel. Here, n represents the sequence length, and k represents the word vector dimension corresponding to each word.

At the convolutional layer, a convolution kernel w window $x_{I:I+h-1}$ is used on the input sequence of $n \times k$ for the convolution operation, resulting in feature $c_i = f(w \times x_{i:i+h-1} + b)$. Only one-dimension convolution is needed, because the number of channels of text data is generally one, of which h represents the number of words in the window, w represents the weight matrix of $h \times k$ dimension, b represents the bias parameter, and $x_{i:i+h-1}$ represents the $h \times K$-sized window formed from the ith row to the $i + h - 1$ row of the input matrix.

In the pooling layer, the output of the convolutional layer is maximized by taking the maximum value of the feature in the neighborhood. Then, the dimension of the input data is reduced, and the output of the fixed length is obtained.

In the full connection layer, the features extracted by the convolution and pooling layer are inputted into the classifier for classification.

3.3. Stock Price Prediction. The index obtained from the quantitative text is combined with the fundamental index to predict the stock price based on the long short-term memory (LSTM) model. Figure 2 shows the procedure of the LSTM model.

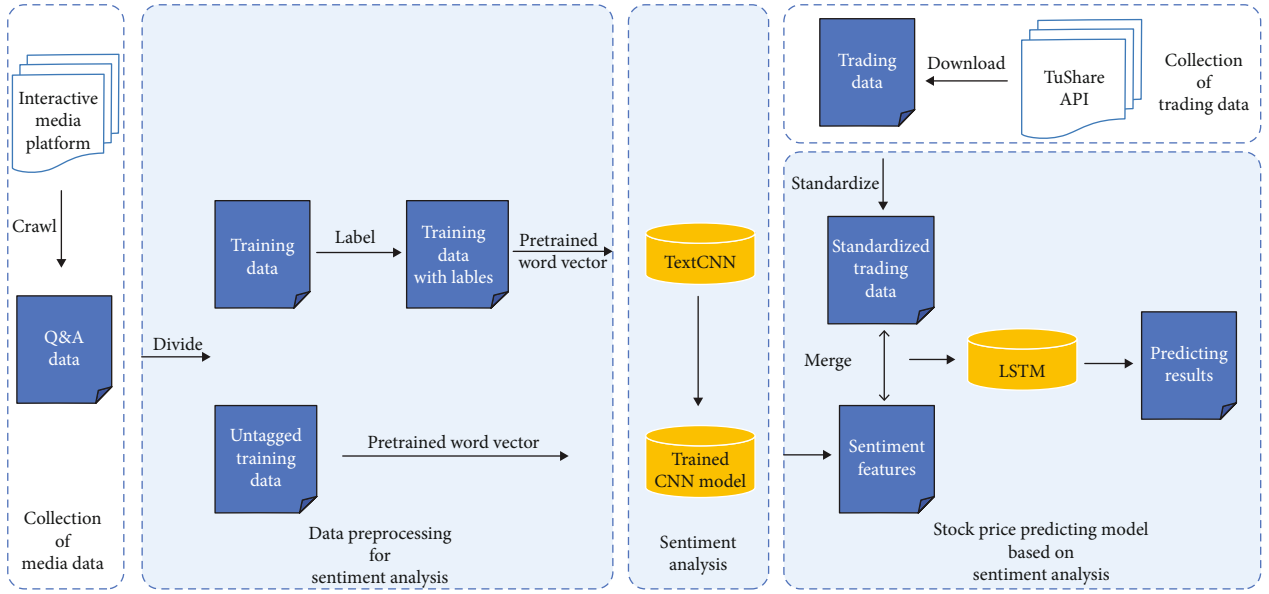

Figure 1: Research framework.

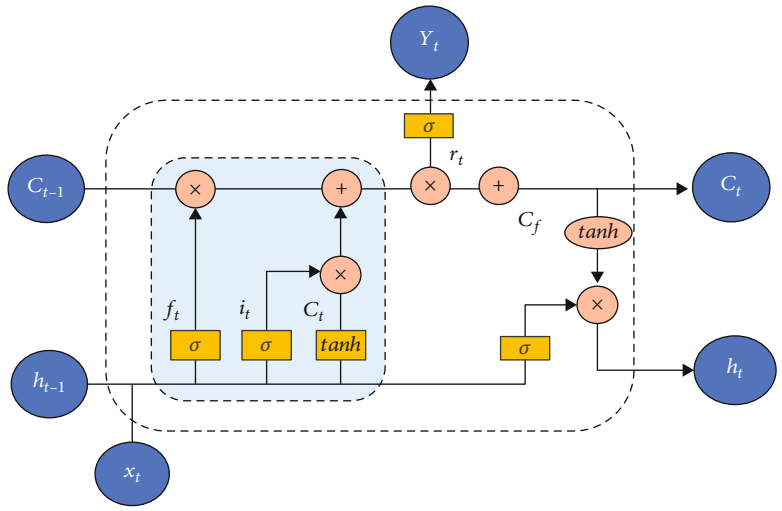

Figure 2: The flowchart of LSTM.

First, train z, z^i, and z^0 with the current input x^t and the output h^{t-1} of the previous state:

$$\begin{aligned} z^f &= \sigma\left(w^f \times \frac{x^t}{h^{t-1}}\right), \\ z^i &= \sigma\left(w^i \times \frac{x^t}{h^{t-1}}\right), \\ z^0 &= \sigma\left(w^0 \times \frac{x^t}{h^{t-1}}\right), \\ z &= \tanh\left(w \times \frac{x^t}{h^{t-1}}\right). \end{aligned} \tag{2}$$

Second, we consider the components of the LSTM model.

In the internal forgetting stage of the model, the trained z^f is used as forgetting gating to determine which parts of c^{t-1} are remembered and forgotten in the previous state.

In the equation, c^{t-1} represents the state of the previous node. Its specific calculation method shall be given in the next stage of the model.

In the stage of selecting memory inside the model, the model selects memory input data x^t under the control of gated z^i. Then, the results of the forgetting stage and the selecting memory stage are added, and the state c^t can be obtained as follows:

$$c^t = z^f \odot c^{t-1} + z^i \odot z^*. \tag{3}$$

In the output phase inside the model, the model undergoes the scaling of c^0 to obtain h^t under the control of z^0, after which we determine the output y^t of the current state as follows:

$$h^t = z^0 \odot \tanh\left(c^t\right),$$
$$y^t = \sigma\left(w' \times h^t\right). \tag{4}$$

4. The Proposed Algorithm

First, this article cleans and quantifies the raw data collected. Then, the CNN is used to predict the emotional tendency of Q&A text, and the overall emotional value of the stock on that day is calculated according to the emotional tendency of all Q&A on that day. Finally, the emotional value and fundamental data are inputted, and the LSTM is used for training. The proposed algorithm is given as follows.

Step 1. Get the Q&A text and divide the words. By writing a web crawler, we are able to collect the raw Q&A data. Then, we merge the main Chinese stopword list and delete the stopwords in the text. Finally, the text data are segmented.

Step 2. Media representation. Here, we introduce the open source pretrained word vector CA8 dataset, transfer the pretrained word vector to the cleaned text data, and quantify the text into a word vector.

Step 3. Train the neural network model. We input the quantized annotated dataset into the CNN and then train the neural network. The validation set is used to check the accuracy of the model obtained by training. If the accuracy fails to pass the test, the parameters are adjusted to retrain the model.

Step 4. Calculate the emotional tendency of the day. The neural network model that has been tested for accuracy is used to classify the text emotions towards the training dataset. Based on the emotional orientation of each text of the day, we calculate the overall emotional orientation of the stock each day. Daily positive or negative tendencies are calculated by dividing the number of positive or negative texts in that part of the day by the total using the following equations:

$$\text{pos}_i = \frac{N_{\text{pos}}}{N_i},$$
$$\text{neg}_i = \frac{N_{\text{neg}}}{N_i}, \tag{5}$$

where pos_i and neg_i, respectively, represent the positive tendency and negative tendency of stock i, N_{pos} and N_{neg}, respectively, represent the positive and negative text quantity of stock i's questions or answers, and N_i represents the total text quantity of stock i's questions or answers.

Step 5. Analyze the text classification results. The emotional tendency variable of the day is integrated with the fundamental indicators, and the stock price is predicted by inputting the LSTM model. By comparing the prediction results of fused and unfused affective indicators, the accuracy of the fused affective indicators can be evaluated.

Table 1: Data description.

Web media	Panorama Interactive	Shanghai E Interactive	SSE Interactive
Coverage	Shanghai +Shenzhen	Shanghai	Shenzhen
Number of shares	3565	1468	1507
Total data amount	1.21 GB	184 MB	51.5 GB

5. Experiment Test

This study took A-share stocks from 2012 to early 2020 as the research object. The dataset consisted of two subdatasets: digital interactive media data and listed company transaction data. As shown in Table 1, the digital interactive media data included query data, time, user name, company name, and company code from each site. Digital interactive media data were collected from Panorama Interactive, Shanghai E Interactive, and SSE Interactive. Founded in 1999, Panorama Interactive is an interactive website for securities investors and provides an effective communication platform between A-share listed enterprises and investors. Shanghai E Interactive and SSE Interactive are digital interactive media platforms officially established by the Shanghai Stock Exchange and Shenzhen Stock Exchange, respectively.

Part of the raw data is shown in Table 2. As can be seen, since February 2020, COVID-19 has caused enterprises to operate under extraordinary situations, thus raising many questions. This situation means that investor sentiments have been significantly affected in the face of such *force majeure*. Moreover, to a certain extent, a company's official introduction regarding the start of the situation can ease investor apprehension.

Next, we filtered and cleaned the text information obtained by crawling according to the following rules:

Rule 1: delete duplicates in the Q&A for each stock.

Rule 2: delete the companies whose trading activities are suspended for more than 10 trading days along with their Q&A data within this period.

Rule 3: delete the companies exiting the market or suspend the listing during the period along with their Q&A data.

Rule 4: only the corresponding stock code, stock name, question text, question time, answer text, and answer time are retained for each Q&A text dataset. The other irrelevant attributes must be deleted.

The trading data of listed companies mainly include stock symbol, trading date, closing price, opening price, high price, low price, and turnover rate.

Stock trading data were collected from the TuShare Financial Big Data Center Interface. The data previews, including market value, turnover, current ratio, closing price, day high, day low, market return, and stock return, are shown in Table 2.

The trading data also excluded companies that were withdrawn from the market, suspended permanently, or suspended for more than 10 days.

After the data cleaning, the digital interactive media data from 2012 to 2015 were divided into training sets. Compared with the method of determining the sentiment of text by

Table 2: Trading data (part).

	ts_code	Trade_d	Open	High	Low	Close	Pre_c	Change	pct_chg	Vol	Amount
0	600000SH	20000104	24.98	25.78	24.75	25.57	24.75	0.82	3.31	44961	113946.78
1	600000SH	20000105	25.57	25.98	25.15	25.28	25.57	-0.29	-1.13	52528	134465.43
2	600000SH	20000106	25.18	26.30	25.05	25.99	25.28	0.71	2.81	62297	160059.80
3	600000SH	20000107	26.30	27.50	26.12	26.90	25.99	0.91	3.50	213553	575751.08
4	600000SH	20000110	27.00	27.85	26.71	27.25	26.90	0.35	1.30	165397	450463.52

Table 3: Data attributes of the training set.

	Attribute	Count	Ratio
Number of question words	Average	69	—
Questioner sentiment	Positive	9254	73.4%
	Negative	3352	26.6%
Number of answer words	Average	97	—
Respondent sentiment	Positive	7368	58.44%
	Negative	5238	41.56%
Difference between Q&A	Same sentiments	4792	38.01%
	Different sentiments	7814	61.99%
Dataset partitioning	Training set	10131	80%
	Validate set	2532	20%
Number of listed companies	Total	3565	100%
Q&A data quantity	Total	12606	100%

using a sentiment dictionary, the emotional tendency of using manual marking text can ensure the accuracy of the classification of the training set. Therefore, this study used the three-person voting method in the training set to mark the emotional tendency of each Q&A set.

After the dataset was marked, the training set and test set were further divided, and the test set was reserved for model testing. Some attributes of the tag datasets are shown in Table 3.

After the text dataset was cleaned and partitioned, word segmentation was performed.

First, because the text data came from web pages, we removed the tag languages, special symbols, and spaces from all the texts.

Second, given that Chinese text contained some stopwords that were not helpful for text analysis, these were removed in the text during the preprocessing phase.

The three commonly used stopword lists were integrated: the stopword list of Hit University, the Stop Word Library of Machine Intelligence Laboratory of Sichuan University, and the Baidu stopword list. Then, we use the Jieba Library to break up the text. Once the preprocessing was completed, the list for storing text data was previewed.

As the input sequence length of the TextCNN model was fixed, the quantized text sequence should be truncated and supplemented. According to the data exploration in the previous part, the average number of words in each query data was 69, while the average number of words in the combination of Q&As was 166. Therefore, the maximum sequence lengths in the model of Q&A and Q&A statements were set to 69 and 166, respectively. For sequences longer than the mean, we truncated them to the mean length. For the sequences shorter than the mean value, all the vacant parts were filled with zeros.

Table 4: Data division.

	Train_X	Train_Y	Test_X	Test_Y
Ratio	70%	70%	30%	30%
Dimensions without sentiment	7	1	7	1
Dimensions with sentiment	11	1	11	1

After the regular length sequence was inputted into the embedded layer of the model, the layer outputted the word vector matrix of the sample length multiplied by the word vector dimension. Then, we transformed the good word vector matrix into the convolution layer. As the Chinese text is dominated by two- to four-character words, the sizes of the convolution kernel were set as 2, 4, and 5 to carry out the convolution operation on the word vector matrix. After setting the word vector dimension in the convolution kernel size, the data went through the maximum pooling and full connection layer to complete the classification task.

After completing the training of the CNN model, the text data from January 1, 2016, to February 2020 were then classified using the trained model, and the emotional tendency value of each stock on that day was also calculated.

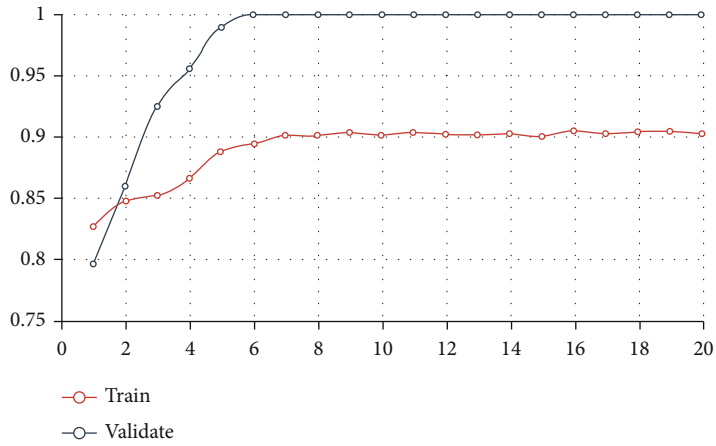

Figure 3: Accuracy of CNN for questions.

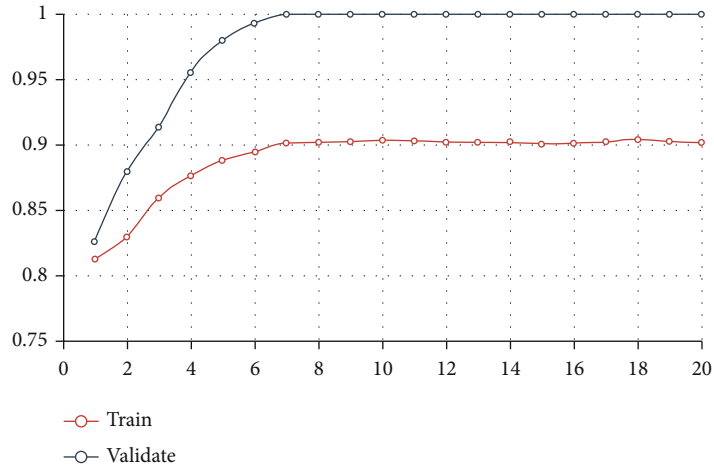

Figure 4: Accuracy of CNN for Q&As.

The final step was to process the stock trading data and interactive information data before using the LSTM model to predict the stock price. For stock trading data, it must be standardized. For the text data, because there may be no Q&A on a certain day, the vacant value of the sentiment indicator data should be filled to zero.

Once all the data processing was completed, the training set and test set were divided into the data. We forecast the closing price of the day with and without the inclusion of sentiment indicators (shown in Table 4).

6. Empirical Analysis

Results verified that the accuracy of the model tends to be stable during the fifth to seventh training rounds. As shown in Figures 3 and 4, the accuracy rates of the training set and the test set of the question-asking data are 97% and 90%, respectively, whereas those of the training set and the test set of the question-answering data are 97% and 89%, respectively. The error is within the acceptable range.

As there are many listed companies involved in the study, this paper analyzes the predicted results for PingAn Bank in order to verify the results and conclusions of the model more intuitively, as shown in Table 5.

Table 5: Model evaluation.

Evaluations	Without sentiment	With sentiment
MSE	0.23003	0.12251
MRSE	0.47961	0.35003
MAE	0.36739	0.26076
R square	0.96752	0.98270

First of all, the determination coefficients of the two predictions are both higher than 95%, indicating that the selected stock trading data have a higher degree of influence on the prediction results. Moreover, the joint influence degree with the addition of emotional indicators is also higher. This indicates that the model has a good effect on stock price prediction whether or not affective indicators are added.

Second, compared with other evaluation indexes, the mean square error, root mean square error, and average absolute coefficient predicted by adding sentiment are smaller. Without the addition of affective indicator prediction, the mean square

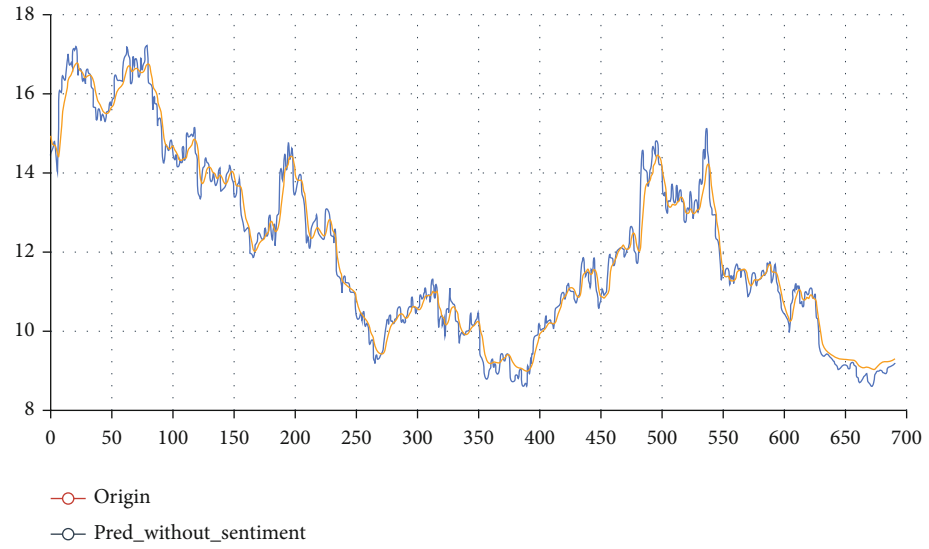

Figure 5: Predictions without sentiment.

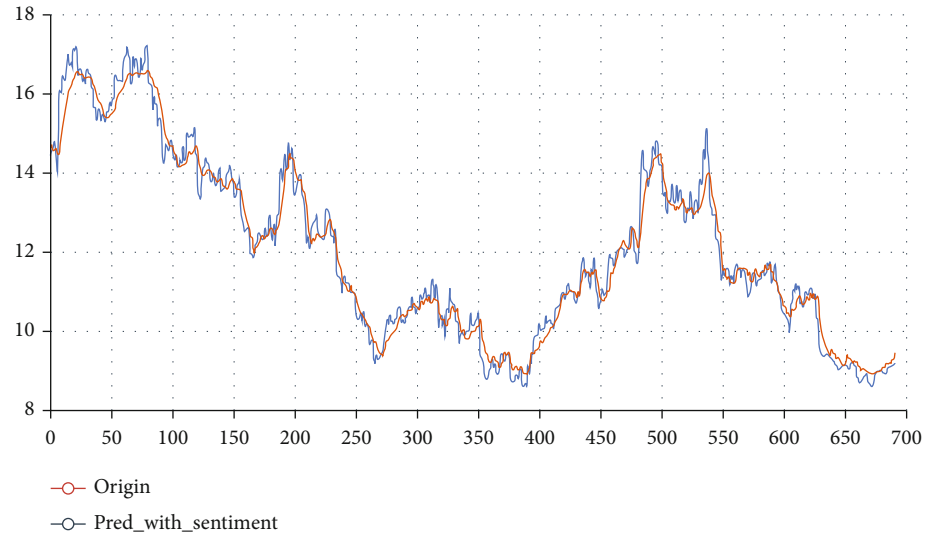

Figure 6: Predictions with sentiment.

error of the prediction model is 0.23, whereas the root mean square error reaches 0.48. These values indicate that without the addition of affective indicators, the error of the model is large, and the accuracy of the model is not high enough.

The mean square error and root mean square error of the model are 0.12 and 0.35, respectively. These two values are far lower than those of the model without emotion, thereby indicating that the accuracy of model prediction is improved by adding a sentiment index. Similarly, the average absolute error of the model using stock trading data for direct prediction is 0.37, whereas that of the model with sentiment indicators is 0.26. This also indicates that the addition of affective indicators improves the accuracy of model prediction.

Therefore, we have proven that the addition of affective indicators resulted in the significant improvement of the model compared with the condition wherein such indicators are not included.

In addition to the assessment indicators of the model, Figures 5 and 6 also reveal that the results predicted by adding affective indicators are better than those predicted by not adding such indicators.

7. Conclusion

Using several digital interactive media platforms, this research analyzes investor sentiments under the influence of official news and compares the prediction of short-term stock trends with and without sentiment analysis. In order to solve the above-mentioned issues, this research is carried out from two aspects.

First, we construct a text classification index for investor sentiment according to the characteristics of Q&A text. In this study, we used the three-person voting method to manually label the emotional orientation of interactive media text

data from 2010 to 2015. Then, we used this as the training set in training the CNN model. The trained model was used to classify the text data from 2016 to the first quarter of 2020 in order to extract the investor's emotional tendency.

Second, this article verifies the influence of investor sentiment on the accuracy of short-term stock price forecasts. The comparison can prove that investor sentiment and investor sentiment under official guidance can improve the accuracy of such price forecasts. Finally, the good index results prove that the experimental method is accurate and effective.

The findings of this research can guide market participants in crafting their decision-making plans. Specifically, this work provided important theoretical references and practical guidance for safeguarding investors' rights and interests, regulating the behavior of listed companies, and optimizing the stability of the securities market. For market participants, real-time market information must be obtained in a timely manner to avoid making irrational decisions due to information bias. In addition, listed companies must establish a complete rumor rejection mechanism to ensure that the information in the market is true and to maintain the stability of the market.

In the future, this research is aimed at expanding the topic from several aspects. First, we aim to increase the completeness of the data and add platforms that have emerged in recent years, such as the question of the secretary of the East Fortune. Second, in terms of text sentiment analysis, unbalanced classification analysis must be performed on text data, and the extraction of unbalanced text must be integrated to optimize the accuracy of the deep learning model.

Data Availability

The data used to support the findings of this study are available from the corresponding author upon request.

Conflicts of Interest

The authors declare that they have no conflicts of interest.

Acknowledgments

This work was supported by the National Natural Science Foundation of China (Grant Nos. 71874215, 71571191, and 72004244), the Beijing Natural Science Foundation (Grant Nos. 9182016 and 9194031), the Ministry of Education in China (MOE) Project of Humanities and Social Sciences (Grant Nos. 15YJCZH081, 17YJAZH120, and 19YJCZH253), the Beijing Social Science Foundation (Grant No. 18JDGLB022), the Beijing Double World-Classes Development Plan (Personalized Content Aggregation, Presentation and Application Research on Cross-Media Big Data), and the Program for Innovation Research of the Central University of Finance and Economics.

References

[1] I. K. Nti, A. F. Adekoya, and B. A. Weyori, "A systematic review of fundamental and technical analysis of stock market predictions," *Artificial Intelligence Review*, vol. 53, no. 7, pp. 3007–3057, 2019.

[2] E. F. Fama, "The behavior of stock-market prices," *The Journal of Business*, vol. 38, no. 1, pp. 34–105, 1965.

[3] D. Shah, H. Isah, and F. Zulkernine, "Stock market analysis: a review and taxonomy of prediction techniques," *International Journal of Financial Studies*, vol. 7, no. 2, p. 26, 2019.

[4] H. Liang, J. Zou, K. Zuo, and K. Muhammad Junaid, "An improved genetic algorithm optimization fuzzy controller applied to the wellhead back pressure control system," *Mechanical Systems and Signal Processing*, vol. 142, article 106708, 2020.

[5] H. Zheng, W. Guo, and N. Xiong, "A kernel-based compressive sensing approach for mobile data gathering in wireless sensor network systems," *IEEE Transactions on Systems, Man, and Cybernetics: Systems*, vol. 48, no. 12, pp. 2315–2327, 2017.

[6] Z. Huang, X. Xu, J. Ni, H. Zhu, and C. Wang, "Multimodal representation learning for recommendation in internet of things," *IEEE Internet of Things Journal*, vol. 6, no. 6, pp. 10675–10685, 2019.

[7] H. Liang, D. Zou, Z. Li, K. Muhammad Junaid, and Y. Lu, "Dynamic evaluation of drilling leakage risk based on fuzzy theory and PSO-SVR algorithm," *Future Generation Computer Systems*, vol. 95, pp. 454–466, 2019.

[8] Z. Liu, B. Hu, B. Huang, L. Lang, H. Guo, and Y. Zhao, "Decision optimization of low-carbon dual-channel supply chain of auto parts based on smart city architecture," *Complexity*, vol. 2020, Article ID 2145951, 14 pages, 2020.

[9] H. Al-Shaibani, N. Lasla, and M. Abdallah, "Consortium blockchain-based decentralized stock exchange platform," *IEEE Access*, vol. 8, pp. 123711–123725, 2020.

[10] R. Nair and A. Bhagat, "An application of blockchain in stock market," in *Transforming Businesses with Bitcoin Mining and Blockchain Applications*, pp. 103–118, IGI Global Publisher, 2019.

[11] J. C. Yen and T. Wang, "Stock price relevance of voluntary disclosures about blockchain technology and cryptocurrencies," 2019, https://ssrn.com/abstract=3488483.

[12] T. H. Nguyen, K. Shirai, and J. Velcin, "Sentiment analysis on social media for stock movement prediction," *Expert Systems with Applications*, vol. 42, no. 24, pp. 9603–9611, 2015.

[13] T. Li, J. van Dalen, and P. J. van Rees, "More than just noise? Examining the information content of stock microblogs on financial markets," *Journal of Information Technology*, vol. 33, no. 1, pp. 50–69, 2018.

[14] Q. Li, Y. Chen, L. L. Jiang, P. Li, and H. Chen, "A tensor-based information framework for predicting the stock market," *ACM Transactions on Information Systems*, vol. 34, no. 2, pp. 1–30, 2016.

[15] W. S. Chan, "Stock price reaction to news and no-news: drift and reversal after headlines," *Journal of Financial Economics*, vol. 70, no. 2, pp. 223–260, 2003.

[16] P. C. Tetlock, "Giving content to investor sentiment: the role of media in the stock market," *The Journal of Finance*, vol. 62, no. 3, pp. 1139–1168, 2007.

[17] Z. Jin, Y. Yang, and Y. Liu, "Stock closing price prediction based on sentiment analysis and LSTM," *Neural Computing and Applications*, vol. 32, no. 3, pp. 9713–9729, 2020.

[18] S. R. Das and M. Y. Chen, "Yahoo! For Amazon: sentiment extraction from small talk on the web," *Management Science*, vol. 53, no. 9, pp. 1375–1388, 2007.

[19] X. Zhang, J. Shi, D. Wang, and B. Fang, "Exploiting investors social network for stock prediction in China's market," *Journal of Computational Science*, vol. 28, pp. 294–303, 2018.

[20] A. Derakhshan and H. Beigy, "Sentiment analysis on stock social media for stock price movement prediction," *Engineering Applications of Artificial Intelligence*, vol. 85, pp. 569–578, 2019.

[21] X. Li, P. Wu, and W. Wang, "Incorporating stock prices and news sentiments for stock market prediction: a case of Hong Kong," *Information Processing & Management*, vol. 57, no. 5, article 102212, 2020.

[22] W. Antweiler and M. Z. Frank, "Is all that talk just noise? The information content of internet stock message boards," *The Journal of Finance*, vol. 59, no. 3, pp. 1259–1294, 2004.

[23] Y. Li, H. Bu, J. Li, and J. Wu, "The role of text-extracted investor sentiment in Chinese stock price prediction with the enhancement of deep learning," *International Journal of Forecasting*, vol. 36, no. 4, pp. 1541–1562, 2020.

[24] J. Chun, J. Ahn, Y. Kim, and S. Lee, "Using deep learning to develop a stock price prediction model based on individual investor emotions," *Journal of Behavioral Finance*, pp. 1–10, 2020.

[25] Z. Jin, K. Guo, Y. Sun, L. Lai, and Z. Liao, "The industrial asymmetry of the stock price prediction with investor sentiment: based on the comparison of predictive effects with SVR," *Journal of Forecasting*, vol. 39, no. 7, pp. 1166–1178, 2020.

[26] O. C. Sert, S. D. Şahin, T. Özyer, and R. Alhajj, "Analysis and prediction in sparse and high dimensional text data: the case of Dow Jones stock market," *Physica A: Statistical Mechanics and its Applications*, vol. 545, p. 123752, 2020.

[27] M. Nabipour, P. Nayyeri, H. Jabani, A. Mosavi, E. Salwana, and S. Shahab, "Deep learning for stock market prediction," *Entropy*, vol. 22, no. 8, p. 840, 2020.

[28] Y. Zhang, R. Zhu, Z. Chen, J. Gao, and D. Xia, "Evaluating and selecting features via information theoretic lower bounds of feature inner correlations for high-dimensional data," *European Journal of Operational Research*, 2020.

[29] H. Liang, A. Xian, M. Mao, P. Ni, and H. Wu, "A research on remote fracturing monitoring and decision-making method supporting smart city," *Sustainable Cities and Society*, vol. 62, p. 102414, 2020.

[30] Y. Zhou, D. Zhang, and N. Xiong, "Post-cloud computing paradigms: a survey and comparison," *Tsinghua Science and Technology*, vol. 22, no. 6, pp. 714–732, 2017.

Hindawi
Wireless Communications and Mobile Computing
Volume 2023, Article ID 9825851, 1 page
https://doi.org/10.1155/2023/9825851

Retraction

Retracted: Image Classification Model Based on Deep Learning in Internet of Things

Wireless Communications and Mobile Computing

Received 8 August 2023; Accepted 8 August 2023; Published 9 August 2023

Copyright © 2023 Wireless Communications and Mobile Computing. This is an open access article distributed under the Creative Commons Attribution License, which permits unrestricted use, distribution, and reproduction in any medium, provided the original work is properly cited.

This article has been retracted by Hindawi following an investigation undertaken by the publisher [1]. This investigation has uncovered evidence of one or more of the following indicators of systematic manipulation of the publication process:

(1) Discrepancies in scope
(2) Discrepancies in the description of the research reported
(3) Discrepancies between the availability of data and the research described
(4) Inappropriate citations
(5) Incoherent, meaningless and/or irrelevant content included in the article
(6) Peer-review manipulation

The presence of these indicators undermines our confidence in the integrity of the article's content and we cannot, therefore, vouch for its reliability. Please note that this notice is intended solely to alert readers that the content of this article is unreliable. We have not investigated whether authors were aware of or involved in the systematic manipulation of the publication process.

Wiley and Hindawi regrets that the usual quality checks did not identify these issues before publication and have since put additional measures in place to safeguard research integrity.

We wish to credit our own Research Integrity and Research Publishing teams and anonymous and named external researchers and research integrity experts for contributing to this investigation.

The corresponding author, as the representative of all authors, has been given the opportunity to register their agreement or disagreement to this retraction. We have kept a record of any response received.

References

[1] S. Zou, W. Chen, and H. Chen, "Image Classification Model Based on Deep Learning in Internet of Things," *Wireless Communications and Mobile Computing*, vol. 2020, Article ID 6677907, 16 pages, 2020.

Hindawi
Wireless Communications and Mobile Computing
Volume 2020, Article ID 6677907, 16 pages
https://doi.org/10.1155/2020/6677907

WILEY | Hindawi

Research Article

Image Classification Model Based on Deep Learning in Internet of Things

Songshang Zou,[1] Wenshu Chen,[2] and Hao Chen [1]

[1]*College of Computer Science and Electronic Engineering, Hunan University, Changsha 410082, China*
[2]*College of Computer Science, University of Bristol, Bristol BS8 1QU, UK*

Correspondence should be addressed to Hao Chen; chenhao@hnu.edu.cn

Received 17 October 2020; Revised 12 November 2020; Accepted 25 November 2020; Published 8 December 2020

Academic Editor: Hongju Cheng

Copyright © 2020 Songshang Zou et al. This is an open access article distributed under the Creative Commons Attribution License, which permits unrestricted use, distribution, and reproduction in any medium, provided the original work is properly cited.

In the environment of Internet of Things, the convolutional neural network (CNN) is an important tool and method of image classification. However, the features that are extracted by each layer of CNN are all high dimensional, and the features differ among the layers. In addition, these features contain substantial amounts of redundant information. To prevent the increase in the computational burden and the decline of the model generalization performance that are caused by high dimensionality, this paper proposes an improved image classification algorithm based on deep feature fusion, which designs and builds an 8-layer CNN. In addition, it reduces the dimensionality of the features via the principal component analysis (PCA) dimensionality reduction algorithm and fuses the features that have undergone dimensionality reduction to make the obtained features more typical and differential. The experimental results demonstrate that the proposed algorithm improves the performance of the model and achieves satisfactory accuracy.

RETRACTED

1. Introduction

In the era of Internet of Things, image classification plays an important role in multimedia information processing. The image classification accepts the given input images and produces output classification for identifying whether the disease is present or not. As artificial intelligence technology has been widely applied, image classification and recognition technology have received increasing attention and have been utilized in an increasing number of fields, such as image information retrieval, real-time target tracking, and medical image analysis. In recent years, deep learning has attracted increasing attention [1]. The previous machine learning methods have various limitations. For example, when there are few samples, it is highly difficult to represent complex functions. When using deep learning algorithms to represent complex data distributions, nonlinear network models with deep layers can be used to learn the deep features from the data in the case of few samples. Deep learning is a type of algorithm and topological structure that can be used to solve generalization problems [2]. The combination of deep hierarchical neural networks and GPU (graphics processing unit) has accelerated the execution of deep learning algorithms. Deep learning has advanced by leaps and bounds, and big data has propelled this development momentum. A convolutional neural network is a type of feed-forward neural network. Its artificial neurons can respond to surrounding units within the coverage area, and it is suitable for processing large-batch image datasets.

CNN continuously extracts and compresses image features and obtains higher level features. It condenses the original features repeatedly and obtains more reliable features [3]. Various tasks can be conducted with the features in the last layer, e.g., classification and regression. CNN has unique advantages in automatic speech recognition (ASR) and image processing due to its special structure of shared local weights and its similar layout to real biological neural networks [4]. Weight sharing lowers the network complexity; since an image with multidimensional input vectors can be directly input into the network, the complexity of data reconstruction in feature extraction and classification is avoided [5]. Through the study of current image classification and

recognition algorithms, it is discovered that various algorithms have failed to effectively fuse the multilayered deep learning features of CNN and that they have poor accuracy.

In the environment of Internet of Things, the convolutional neural network (CNN) is an important tool and method of image classification. In order to further improve the classification accuracy of the CNN model, this paper has effectively fused deep features via a cascading strategy and has increased the diversity and the expressiveness of the extracted features to enhance the classification performance of the network mode. The main contributions of this paper include the following:

(i) This paper analyzes the structure of CNN, studies the principles of activation functions, specifies the role that nonlinear activation functions play in neural networks, and shows that via facilitation by nonlinear functions; CNN has stronger feature representation performance and can realize complex image classification

(ii) To address the problems that conventional image classification algorithms that are based on deep learning cannot effectively fuse multilayered deep features and perform poorly in terms of classification accuracy, this paper proposes an improve image classification algorithm that is based on deep feature fusion and improves the diversity and expressiveness of the extracted features to improve the classification performance

(iii) By comparing the classification performances of the CNN model on the Food-101 and Places2 datasets under various activation functions, it is demonstrated that the activation function that is used in this paper can improve the classification accuracy of the model on image datasets and ensure its convergence

(iv) This paper conducts a performance analysis and evaluation of the proposed algorithm in comparison with other algorithms. The experimental results demonstrate that the algorithm that is proposed in this paper realizes higher accuracy

The remainder of this paper is organized as follows. Section 2 discusses related work. The CNN network structure and the activation function performance are analyzed in Section 3. Section 4 proposes an improved CNN image classification and recognition algorithm that is based on feature fusion. Section 5 presents the experiment results and analysis. Section 6 summarizes the conclusions of the paper and discusses future research directions.

2. Related Work

As a highly important research direction in computer vision, image classification and recognition involves knowledge from several disciplines and has been applied in multiple research fields. With the rapid development of internet technology, a substantial amount of image data are encountered in people's lives, thereby leading to increased demands for machine learning and computer vision techniques and more in-depth research [6]. According to in-depth research that has been conducted on digital image processing and deep learning, compared with other neural networks, CNN has the following strengths: the input image matches well with the topological structure of CNN. Feature extraction proceeds simultaneously with pattern classification and generation in the training process, and weight sharing can reduce the number of training parameters, thereby rendering the CNN structure simpler and more adaptive [7]. CNN is mainly used to recognize 2D images with invariance in terms of shifting, scaling, and other forms of distortion [8]. The CNN feature detection layer learns by training on the data; hence, CNN can avoid explicit feature extraction and learns implicitly from data training. In addition, because the neurons in the same feature mapping plane share the same weight, CNN can learn in parallel. This is another advantage of CNN compared to networks that have interconnected neurons. In the study of image classification, feature extraction will directly affect the classification performance of the network model. In essence, CNN is a mapping from input to output. In practical applications, it typically uses multilayer convolution and trains with a fully connected layer. The features that are learnt via one-layer convolution are typically local. In multilayer convolution, the higher the layer, the more global the learnt features are [9].

Neocognitron can be regarded as the first implementation of CNN, and it is also the first application of the receptive field in artificial neural networks. It attempts to model the visual system and enables it to complete recognition even if there is shift or slight distortion in the objects [8]. The deep learning architecture did not emerge until the last two decades. It has substantially increased the number and types of problems that can be solved by neural networks. There are 5 popular deep learning architectures: recursive neural network (RNN), long short-term memory (LSTM)/gated recurrent unit (GRU), convolutional neural network, deep brief network (DBN), and deep stacking network (DSN). CNN is a type of multilayered neural network, and it is inspired by the animal visual cortex. The first CNN was built by Yann LeCun for handwritten character recognition. As a deep network, the early layers mainly recognize features (e.g., edges) and the subsequent layers recombine these features into higher level input [10]. Therefore, deep learning can be regarded as "deep parameter adjustment." However, it also magnifies the network shortcomings. A limited training dataset easily results in overfitting. The larger the network, the more complex the computation and the more difficult the application of the network, and the deeper the network, the more easily the gradient vanishes and the more difficult the model optimization. In the study of image classification and recognition, feature extraction will directly impact the classification capacity of the network model. The main problem that is encountered with available image classification algorithms in feature extraction is that they cannot effectively utilize various deep features that are extracted by networks [11, 12].

RETRACTED

3. Convolutional Neural Network (CNN)

A convolutional neural network is a type of feed-forward neural network that typically specializes in the processing of image data (multiarray data). The design of the CNN structure can effectively preserve the structure of the original data and generate a layered representation. A typical CNN structure includes multilevel processing layers that are ordered from left to right. CNN typically has four types of layers: convolutional, pooling, fully connected, and classification layers. Convolutional layers and pooling layers are the core layers of the design, and they are typically utilized in the first few phases.

3.1. Convolutional Layers. In CNN, the convolutional layers are the most important layers, which are typically used for feature extraction. As parts of an image may have the same statistical properties, feature learning for an image can be conducted on randomly selected parts of subimages, and the learned features will be used as a filter to scan the entire image and to obtain the feature activation values of various positions in the image to complete feature extraction [13].

In a conventional neural network, every neuron must be connected with every pixel; consequently, numerous weights will render the network difficult to train. Additionally, the number of weights of each neuron in a neural network that has a convolutional layer is equal to the size of the convolution kernel; this is equivalent to each neuron being connected with all pixels. Thus, the number of weights is substantially reduced [14].

The convolution computation consists of two steps. Step 1 is a linear operation. It processes a group of weights that are connected with the original input image or the low-level feature map, translates the convolution kernel for multiple convolutions according to the stride l, and adds the sum of the bias b_x and the results of multiple convolutions. Step 2 is a nonlinear operation. It uses the activation function $f(x)$ to obtain the output feature map C_x, namely, it performs weighted summation on one neuron through multiple input signals and outputs via the activation function [15].

The feature extractor can be replaced by a trained convolution kernel. Convolution kernels differ in terms of the structural features that they extract from an image. To extract multiple features at the same position, multiple convolution kernels can be used, and CNN will output the combination of these features from the convolutional layer. The convolutional layer has two properties that can reduce the number of parameters to be calculated: weight sharing and local perception.

(a) Weight sharing

In weight sharing, the same weight is used by all neurons in the same feature mapping. If the convolution of a group of weights and the input image yields edge features, these weights can be regarded as edge feature extractors, and they can be used directly to extract edge features of other image regions [16].

(b) Local perception

Local perception is the connection of part of the network. Similar to the human visual system, CNN's perception process of an image is from local to global, and every neuron is connected with neurons that belong to the previous layer. Therefore, the information of an entire image is perceived by neurons repeating the process of activation in a small region and translating to another region.

A convolutional layer extracts features, and the most important elements in this layer are the trained convolution kernels. Kernels can detect specified shapes, colors, and contrasts, among other features, and feature maps preserve the spatial structure after extraction; therefore, the feature maps that correspond to convolution kernels represent features of a corresponding dimension, and with the increase in the number of CNN layers, the extracted features become increasingly concrete [17].

Every node in the convolutional layer and pooling layer is connected with only some nodes in the previous layer, and the input of each node in the convolutional layer is a small block of the previous layer; the size of which is determined by the size of the window of the convolution kernel. Typically, after being processed by the convolutional layer, the node matrix will become deeper and the depth will be determined by the number of kernels [18]. Parameter sharing in the kernel enables the image contents not to be affected by the positions and can substantially reduce the number of parameters of the network model and reduce the complexity of the operation; see Figure 1 for an illustration of CNN feature extraction.

In Figure 1, the 1st convolution extracts a low-level feature, the 2nd a mid-level feature, and the 3rd a high-level feature.

3.2. Activation Function. In a neural network, every neuron node will accept the output value from the previous layer as its input value and convey this value to the next layer. The nodes in the input layer will input and transmit the property value to the next output layer. In a multilayer neural network, an activation function is used to represent the relationship between the output values of the neuron nodes in the previous layer and the input values of those in the next layer [19].

A nonlinear function is similar to an activation function, through which neural networks realize stronger representation performance and overcome the finite approximation limitation that is caused by the use of a linear function.

In the early study of neural networks, the sigmoid activation function and the tan$h$ activation function were frequently used. In the back-propagation of neural networks, the sigmoid activation function will result in gradient explosion and loss, and because the output values of the sigmoid function are not of zero mean, the convergence is slow and the training time is substantially increased in deep neural networks. In deep network learning, learning a large amount of data typically takes a long time; hence, the convergence speed of the training model is of high importance. When a deep network is trained, zero-mean data can accelerate convergence. The ReLU function is very fast in calculation, and

RETRACTED

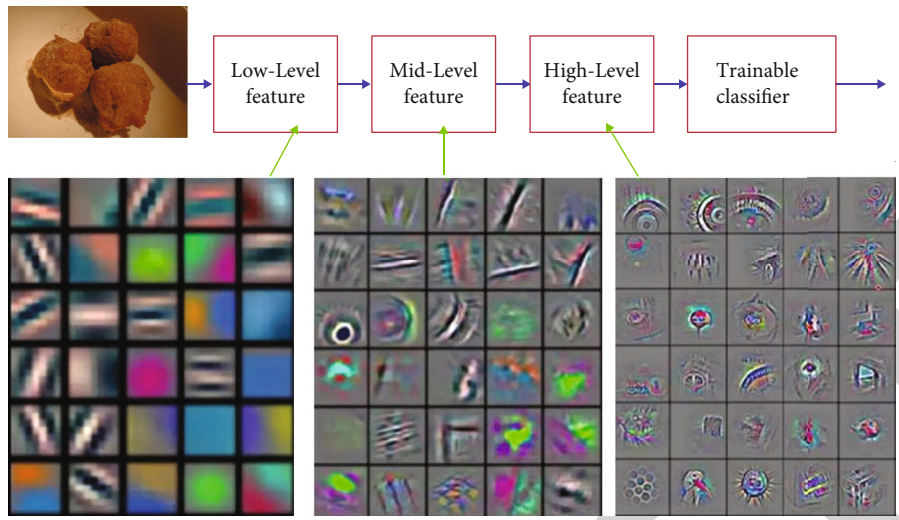

Figure 1: Feature extraction by CNN.

its convergence speed is much faster than those of the sigmoid activation function and the tan*h* activation function. It can also avoid the gradient vanishing that is caused by the sigmoid function and the tan*h* function [20, 21].

The common activation functions include the following:

(1) Sigmoid function

The sigmoid function is the most frequently used continuous and smooth activation function; it is also known as the logistic function. It is used in the output of neurons in a hidden layer, and it can map a real number to the range of (0,1) for binary classification. The formula of the sigmoid function is

$$f(x) = \frac{1}{1+e^{-x}}. \tag{1}$$

The range of Formula (1) is (0,1), and its derivative is

$$f'(x) = \frac{1}{1+e^{-x}}\left(1 - \frac{1}{1+e^{-x}}\right) = f(x)(1-f(x)). \tag{2}$$

In Figure 2, if $x = 10$ or $x = -10$, $f'(x) \approx 0$, and if $x = 0$, $f'(x) = 0.25$.

(2) Tan*h* function

The formula of the tan*h* function is

$$f(x) = \tan h(x) = \frac{e^{x} - e^{-x}}{e^{x} + e^{-x}}. \tag{3}$$

The range of Formula (3) is (-1, 1), and its derivative is

$$f'(x) = -(\tan h(x))^{2}. \tag{4}$$

In Figure 3, if $x = 10$ or $x = -10$, $f'(x) \approx 0$, and if $x = 0$, $f'(x) = 1$.

(3) ReLU function

The ReLU function, which is showed in Figure 4, is the most frequently used nonlinear function in neural networks. It is continuous but not smooth, and its formula is

$$f(x) = \max(0, x). \tag{5}$$

The range of Formula (5) is [0,+∞), and its derivative is

$$f'(x) = \begin{cases} 0, & x < 0, \\ 1, & x > 0, \\ \text{undefined}, & x = 0. \end{cases} \tag{6}$$

The ReLU function has the following properties: unilateral inhibition, relatively broad excitement boundary, and sparse activation.

(4) PReLU function

The formula of the PReLU function is

$$f(x) = \max(\alpha x, 0). \tag{7}$$

In Figure 5, parameter α in the PReLU function is not fixed and can be learned during training. Although it ensures that the output result follows a zero-mean distribution, it also activates all feature values in the negative semiaxis. Hence, noises will also be activated, and the final convergence will be affected.

(5) TReLU function

The formula of the TReLU function is

$$f(x) = \begin{cases} x, & x > 0, \\ \tan h(\alpha x), & x \le 0. \end{cases} \tag{8}$$

RETRACTED

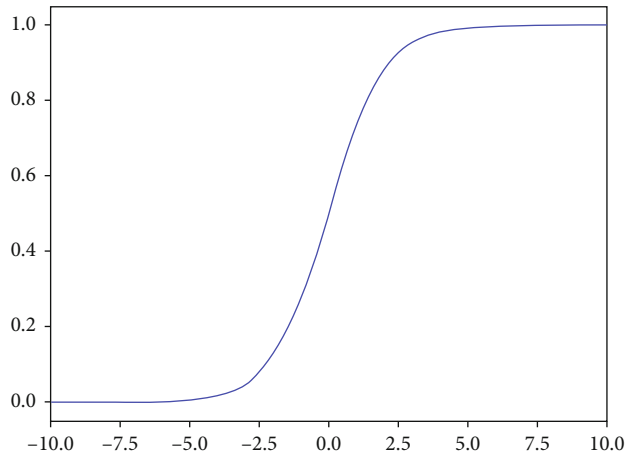

Figure 2: Sigmoid function.

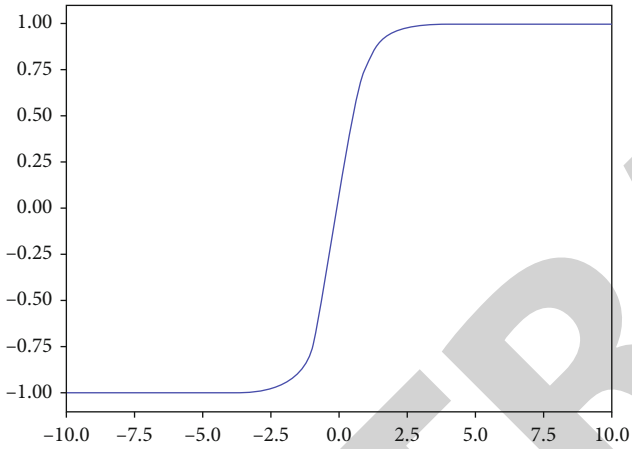

Figure 3: Tan*h* function.

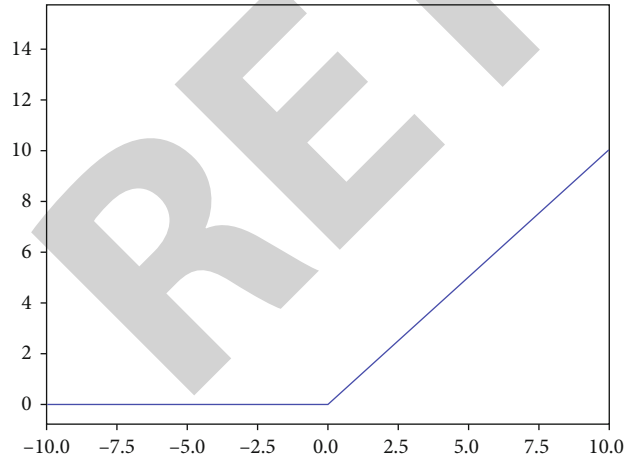

Figure 4: ReLU function.

In Figure 6, parameter α is a variable parameter, and it is used to control the unsaturated region of the function. We set the initial value as 1. The function is almost linear at the origin, and it can yield faster convergence.

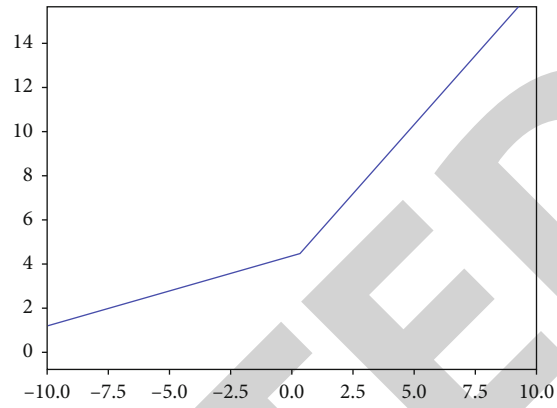

Figure 5: PReLU function ($\alpha = 0.5$).

The TReLU function overcomes the problem of gradient vanishing. As its derivative is always 1 if $x > 0$, the TReLU function is unattenuated if $x > 0$. In addition, the TReLU function preserves some gradient values in the unsaturated region of the negative semiaxis. If the activation value falls in the unsaturated region, it still can be effectively activated, and it preserves some of the effective features while more effectively activating negative value features by controlling the size of the unsaturated region with parameter α.

(6) Leak ReLU function

The formula of the Leak ReLU function, which is showed in Figure 7, is

$$f(x) = \begin{cases} ax, & x < 0, \\ x, & x > 0. \end{cases} \tag{9}$$

The range of Formula (9) is $(-\infty,+\infty)$, and its derivative is

$$f'(x) = \begin{cases} a, & x < 0, \\ 1, & x > 0, \\ \text{undefined}, & x = 0. \end{cases} \tag{10}$$

3.3. Pooling Layer. A pooling layer typically follows a convolutional layer; hence, the output from the convolutional layer is pooled in the pooling layer. The convolutional layer extracts features while the pooling layer reduces the number of parameters. The pooling layer is mainly used to reduce the dimensionality of the features by compressing the number of data and parameters, thereby reducing overfitting and improving the fault tolerance of the model. Although the pooling layer reduces the dimensions of various feature maps, it can still preserve most important information. Located between continuous convolutional layers, the pooling layer reduces the number of data and parameters and reduces overfitting. The pooling layer has no parameters, and it downsamples the result from the previous layer, which is known as data compression. In Figure 8, the

RETRACTED

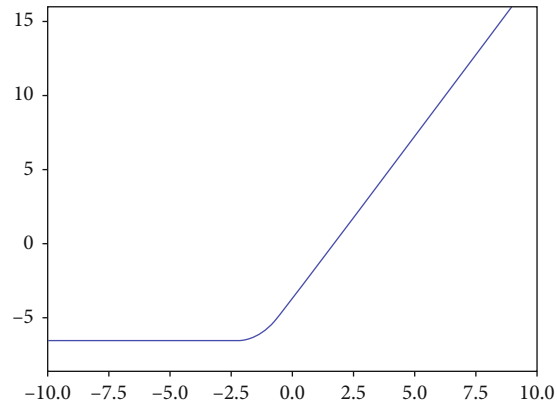

Figure 6: TReLU function ($\alpha = 1$).

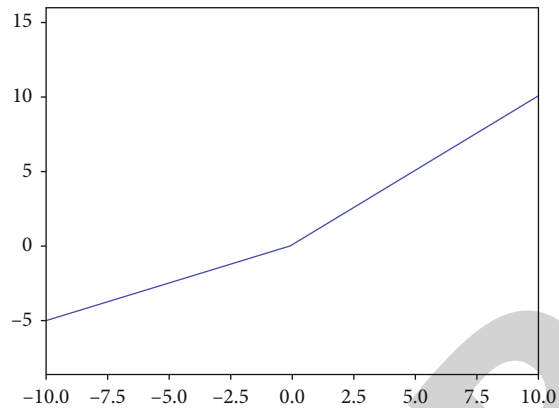

Figure 7: Leak ReLU Function ($a = 0.5$).

downsampling process includes max pooling and mean pooling operations [18, 22].

Max pooling: define a spatial neighborhood, e.g., a window of size $2 * 2$. Extract the largest element from the modified feature map within the window. It has been proven that max pooling outperforms mean pooling

Mean pooling: define a spatial neighborhood, e.g., a window of size $2 * 2$. Calculate the mean value of the modified feature map within the window

The input of every node in the pooling layer is a small block of the previous layer (which is typically a convolutional layer), and the size of this small block is determined by the size of the window of the pooling kernel. The pooling layer changes the size of the node matrix instead of its depth. For image processing, the pooling operation in this layer can be regarded as transforming a high-resolution image into a low-resolution image. After the convolutional layer and pooling layer, the number of parameters in the network model can be further reduced [23].

3.4. Fully Connected Layer. A fully connected layer has many neurons, and it is represented as a column vector (single sample). It is typically one of the latter few layers of a deep neural network in the field of computer vision, and it is used for image classification. In this layer, all neurons are connected via weights, and this layer is typically situated in the rear part of CNN. When the convolutional layers in the front part have extracted weights that are sufficient for recognizing the image, the next task is classification. In the end of CNN, typically, a cuboid is spread into a long vector and sent into the fully connected layer for classification in collaboration with the output layer [24].

A fully connected layer can be transformed into a convolutional layer and vice versa. Any convolutional layer can be converted into a fully connected layer by converting the weight into a huge matrix. In this matrix, most entries are 0, except in designated regions (local perception), and many regions share the same weight (shared weight). Any fully connected layer can also be converted into a convolutional layer.

A fully connected layer works as a "classifier" in the entire CNN. If the convolutional layer, pooling layer, and activation function layer map the original data into the feature space in a hidden layer, the fully connected layer maps the learnt "distributed feature representation" into the sample label space. In practical applications, a fully connected layer can be realized via convolutional computation: a fully connected layer that is fully connected in the previous layer can be converted into a convolution with a $1 * 1$ kernel, and a fully connected layer that has a convolutional layer as its previous layer can be transformed into a global convolution with an $h * w$ kernel, where h and w are the height and width of the convolutional result of the previous layer [25].

The core operation of full connection is to multiply the vectors in the matrix and, in essence, to linearly transform from one feature space to another. In CNN, full connection is typically found in the final few layers, and it calculates a weighted sum of the features that were designed previously. The previous convolution and pooling are similar to feature engineering, while the full connection in the tail part is equivalent to feature weighting [26]. An operation example in the fully connected layer is illustrated in Figure 9.

In Figure 9, the last two columns of small balls represent two fully connected layers. At the end of the last convolution, the final pooling operation is conducted, which outputs 20 images of size $12 * 12$, which are converted into $1 * 100$ vectors by a fully connected layer.

4. CNN Image Recognition and Classification Based on Feature Fusion

The model that is proposed in this paper includes 8 layers: 6 convolutional layers and 2 fully connected layers. The key design details are as follows.

In the feature mapping, nonlinear transformation is conducted via the ReLU activation function [27]. It activates the extracted image features and generates the corresponding output feature mapping [28]. Pooling layers are introduced behind the 1^{st}, 3^{rd}, and 6^{th} convolutional layers, and the max pooling operation is used to perform feature dimension reduction on the output feature mapping. Meanwhile, to improve the training efficiency and classification performance of the network, local normalization is conducted after the convolution operation in every convolutional layer to accelerate the convergence.

RETRACTED

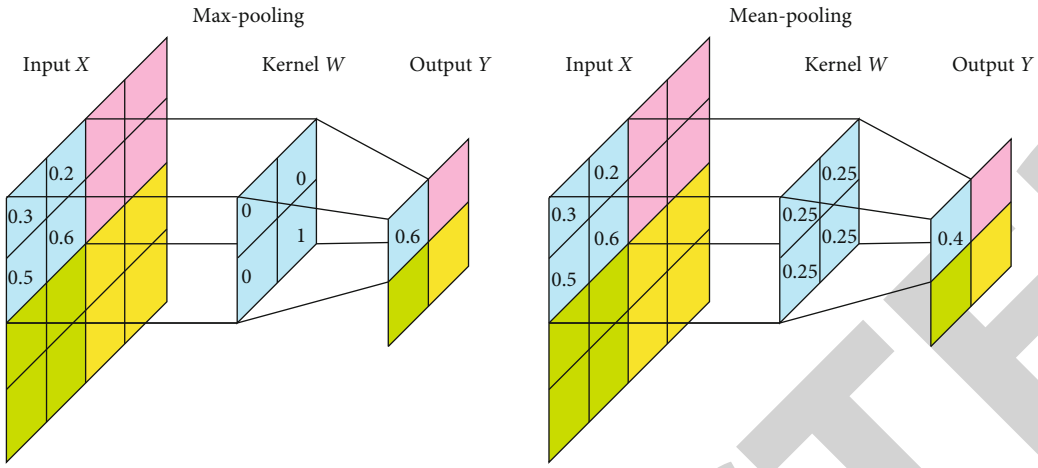

Figure 8: Max pooling and mean pooling.

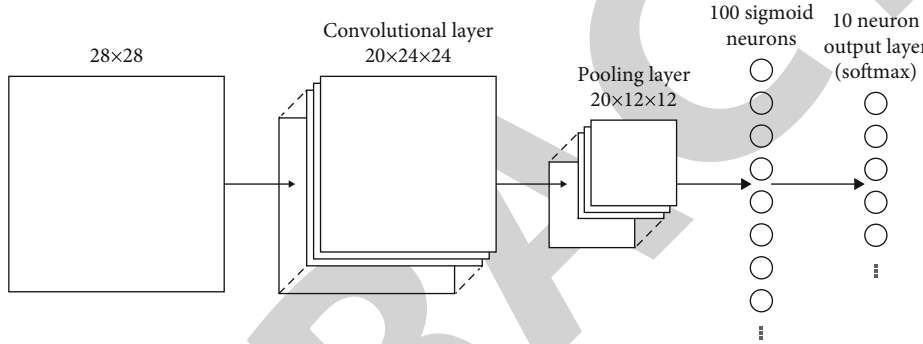

Figure 9: Operations in a fully connected layer.

The 1st convolutional layer is of size $227 * 227 * 3$. The convolution operation is performed by an $11 * 11 * 96$ convolution kernel, and the convolution kernel moves 4 pixels each time, namely, stride = 4. The size of every generated feature mapping matrix is $((227 - 11)/4 + 1)^2 = 55^2$.

Pooling utilizes the sampling operation, and the size of the sampling kernel is $3 * 3$. It slides 2 pixels in the original image each time. After sampling, the size of the generated feature mapping matrix is $((55 - 3)/2 + 1)^2 = 27^2$.

For the 2nd convolutional layer, two pixels are padded on the edges of the input feature mapping matrix, and the size of the mapping matrix becomes $31 * 31$. The convolution operation is performed by a $5 * 5 * 256$ convolution kernel, which moves 1 pixel each time, namely, stride = 1. The size of each generated feature mapping matrix is $((31 - 5)/1 + 1)^2 = 27^2$.

For the 3rd convolutional layer, one pixel is padded on the edges of the input feature mapping matrix, and the size of the mapping matrix becomes $15 * 15 * 1$. The convolution operation is conducted by 256 $3 * 3$ convolution kernels. After each convolution operation, the convolution kernel is moved 1 pixel. The size of each generated feature mapping matrix is $((12 - 3)/1 + 1)^2 = 13^2$.

Pooling utilizes the sampling operation. The size of the sampling kernel is $3 * 3$. The convolution kernel is moved 2 pixels each time after the convolution operation. After sampling, the size of the generated feature mapping matrix is $((27 - 3)/2 + 1)^2 = 13^2$.

For the 4th convolutional layer, one pixel is padded on the edges of the input feature mapping matrix, and the size of the mapping matrix becomes $15 * 15 * 1$. The convolution operation is conducted by 384 $3 * 3$ convolution kernels. After each convolution operation, the convolution kernel is moved 1 pixel. The size of each generated feature mapping matrix is $((15 - 3)/1 + 1)^2 = 13^2$.

For the 5th convolutional layer, one pixel is padded on the edges of the input feature mapping matrix, and the size of the mapping matrix becomes $15 * 15 * 1$. The convolution operation is conducted by $3 * 3 * 256$ convolution kernels. After each convolution operation, the convolution kernel is moved 1 pixel. The size of each generated feature mapping matrix is $((15 - 3)/1 + 1)^2 = 13^2$.

For the 6th convolutional layer, the convolution operation is conducted on the image by a convolution kernel of size 3×3 to realize feature extraction. The extracted image features are activated with the ReLU activation function to produce the corresponding output feature mapping.

Pooling utilizes the sampling operation [29]. The size of the sampling kernel is $3 * 3$. It slides 2 pixels in the original image each time. After sampling, the size of the generated feature mapping matrix is $((13 - 3)/2 + 1)^2 = 6^2$.

RETRACTED

Figure 10: Sample image data of Food-101.

This paper adopts the method of cascade and performs feature fusion on the output features after pooling in the 6th layer with the 1st and the 2nd fully connected layers to make the features that are extracted by the network more diverse, expressive, and differential and to improve the classification performance of the network model.

Extract image features using the constructed CNN model are as follows:

Step 1. Denote the pooling output result of the 6th layer as p_8

Step 2. Calculate the outputs of the 1st and 2nd fully connected layers according to the formula $y_j^l = f(y^{l-1} + b_j^l)$ and denote the results as FC_1, FC_2, respectively. Here, l represents the fully connected layer, y^{l-1} is the output result of the layer before the fully connected layers, and b denotes the bias

Step 3. Select p_8, FC_1, and FC_2 as three deep features of the image dataset and prepare for the subsequent feature fusion

Principal component analysis is a multivariate statistical method that transforms scalars into several principal components [30]. These principal components can reflect most of the original information, and they are typically represented as linear combinations of the original variables [31]. To ensure that the information that is contained in these principal components is nonoverlapping, these principal components must be unrelated. Principal component analysis can effectively reduce the dimensions of data and minimize the mean square error between the extracted components and the original data. It can be used in feature extraction. The process of this algorithm is as follows:

(a) Let $X = [X_1, X_2, \cdots, X_p]^T$ be a p-dimensional random vector and let $\mu = E(x)$ and $\Sigma = D(x)$. The corresponding feature vectors to the p feature values of Σ : $\lambda_1 \geq \lambda_2 \geq \cdots \geq \lambda_p$ are $t_1, t_2, \cdots, t_p$, namely,

$$\Sigma t_i = \lambda_i t_i, t_i^T t_i = 1, t_i^T t_j = 0 \ (i \neq j; i, j = 1, 2, \cdots, p). \quad (11)$$

Perform the following linear transformation:

$$\begin{bmatrix} Y_1 \\ Y_2 \\ \vdots \\ Y_n \end{bmatrix} = \begin{bmatrix} L_{11} & \cdots & L_{1p} \\ \vdots & \ddots & \vdots \\ L_{n1} & \cdots & L_{np} \end{bmatrix} \begin{bmatrix} X_1 \\ X_2 \\ \vdots \\ X_p \end{bmatrix} = \begin{bmatrix} L_1^T \\ L_2^T \\ \vdots \\ L_n^T \end{bmatrix} X \quad (n \leq p). \quad (12)$$

If $Y = [Y_1, Y_2, \cdots, Y_n]^T$ is expected to be used to describe $X = [X_1, X_2, \cdots, X_p]^T$, then Y should reflect as much information of vector X as possible, namely, the larger the variance $D(Y_i) = L_i^T \Sigma L_i$ of Y_i, the better the description. In addition, to express the original information as effectively as possible, Y_i and Y_j should not contain repeated content, namely, cov $(Y_i, Y_j) = L_i^T \Sigma L_j = 0$. It can also be proven that if $L_i = t_i$, $D(Y_i)$ has maximum value λ_i and Y_i and Y_j are orthogonal.

RETRACTED

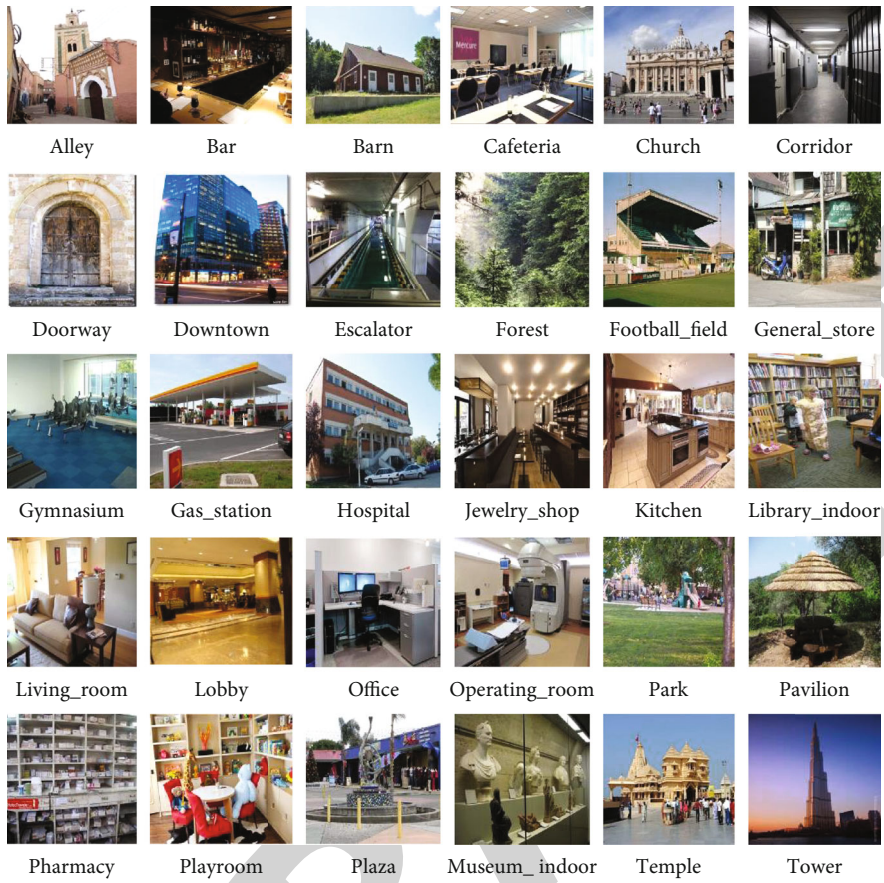

Figure 11: Sample image data of Places2.

Table 1: Accuracies of various activation functions on Food-101 and Places2.

Activation function	Accuracy rate (%)	
	Food-101	Places2
Sigmoid	67.62	45.74
Tan*h*	75.94	53.38
ReLU	81.25	60.58
PReLU	83.44	64.36
TReLU	85.16	68.23

(b) Reconstruct samples from the score matrix

In practice, the covariance matrix of global X is typically unknown and must be estimated from samples. Let $X_1, X_2, \cdots, X_n$ be samples of global X and let $X_i = [X_{i1}, X_{i2}, \cdots, X_{ip}]^T$. Then, the sample measurement matrix is

$$X = \begin{bmatrix} X_1^T \\ X_2^T \\ \vdots \\ X_n^T \end{bmatrix} = \begin{bmatrix} X_{11} & X_{12} & \cdots & X_{1p} \\ X_{21} & X_{22} & \cdots & X_{2p} \\ \vdots & \vdots & & \vdots \\ X_{n1} & X_{n2} & \cdots & X_{np} \end{bmatrix}. \quad (13)$$

Each row of matrix X corresponds to a sample and each column to a variable. Then, the sample covariance matrix S and the correlation coefficient matrix R are expressed as

$$S = \frac{1}{n}\sum_{i=1}^{n}\left(X_i - \bar{X}\right)\left(X_i - \bar{X}\right)^T = \left(S_{ij}\right), \quad (14)$$

$R = (R_{ij})$,
$R_{ij} = S_{ij}/\sqrt{S_{ii}S_{jj}}$.

Define the score of the jth principal component of sample X_i as $\mathrm{SCORE}(i, j) = XTit_j$. It is expressed as follows in matrix form:

$$\mathrm{SCORE} = \begin{bmatrix} X_1^T \\ X_2^T \\ \vdots \\ X_N^T \end{bmatrix} \left[t_1, t_2, \cdots, t_p\right] = XT, \quad (15)$$

Invert Formula (15) and reconstruct the original samples from the score matrix:

$$X = \mathrm{SCORE} \cdot T^{-1} = \mathrm{SCORE} \cdot T^T. \quad (16)$$

Typically, principal component analysis only uses the first m principal components to approximate the original samples.

RETRACTED

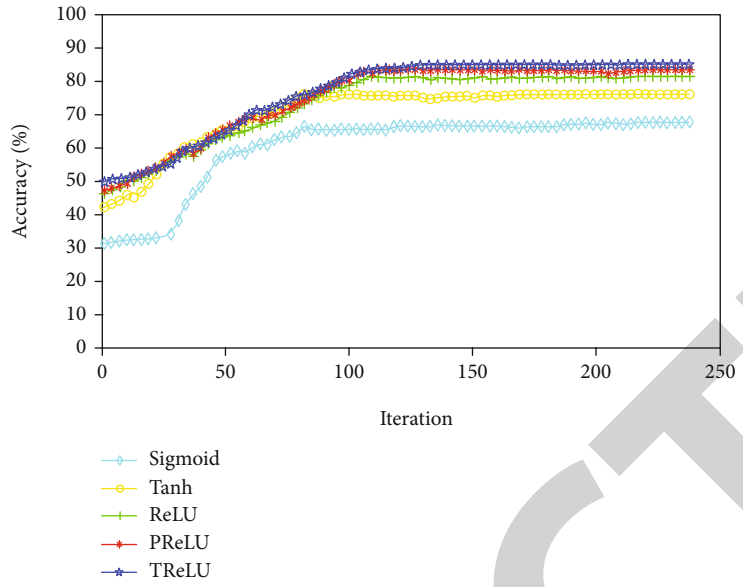

Figure 12: Comparison of five activation functions on Food-101.

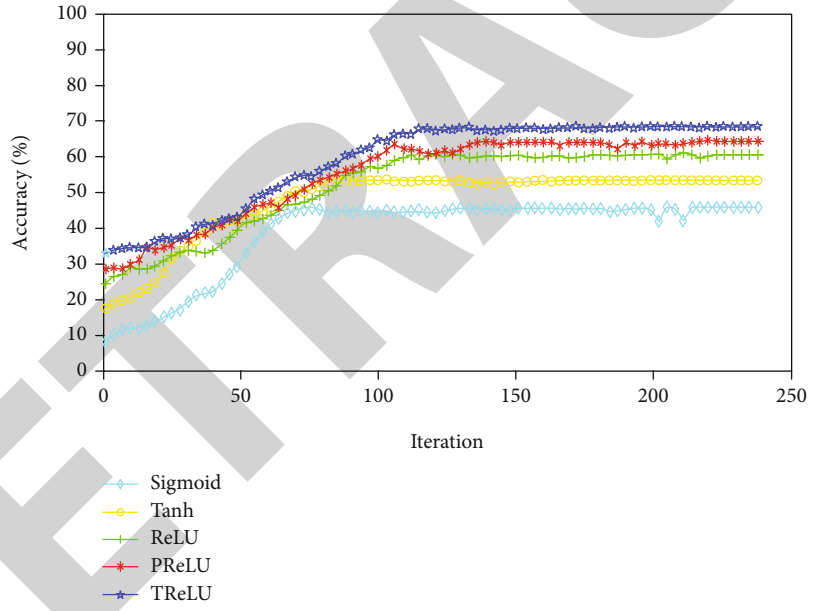

Figure 13: Comparison of five activation functions on Places2.

Table 2: Training times of five activation functions on Food-101 and Places2.

Activation function	Time (h)	
	Food-101	Places2
Sigmoid	2.6	3.5
Tan*h*	2.3	3.2
ReLU	1.9	2.5
PReLU	2.1	2.9
TReLU	2.2	3.0

Table 3: Classification accuracies on Food-101 and Places2 of four algorithms.

Method	Accuracy rate (%)	
	Food-101	Places2
NIN	85.62	66.90
DSN	88.18	69.53
DBN	88.53	70.34
Method of this paper	89.47	71.56

RETRACTED

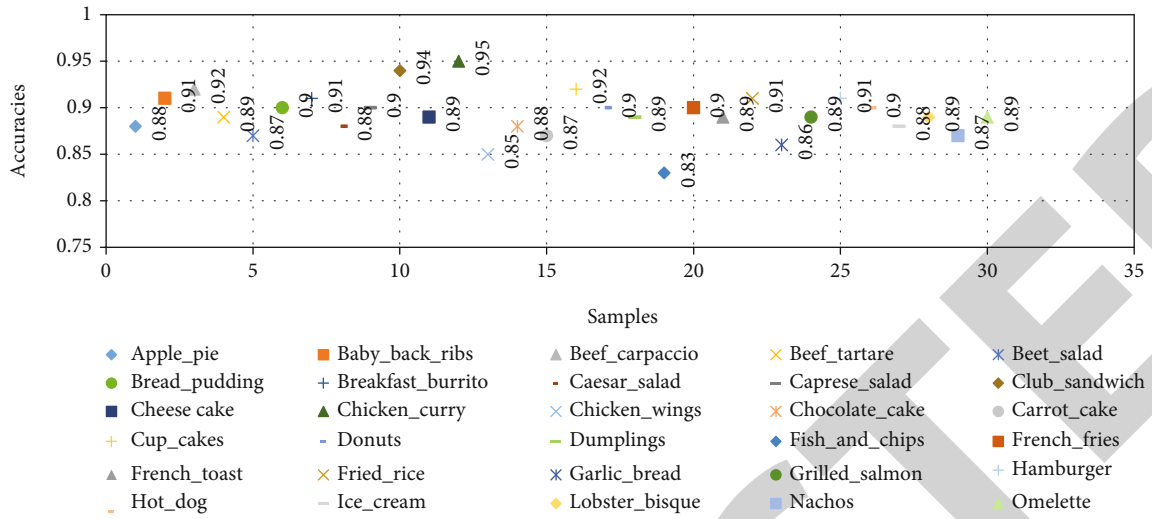

Figure 14: Accuracies on samples of the Food-101 dataset.

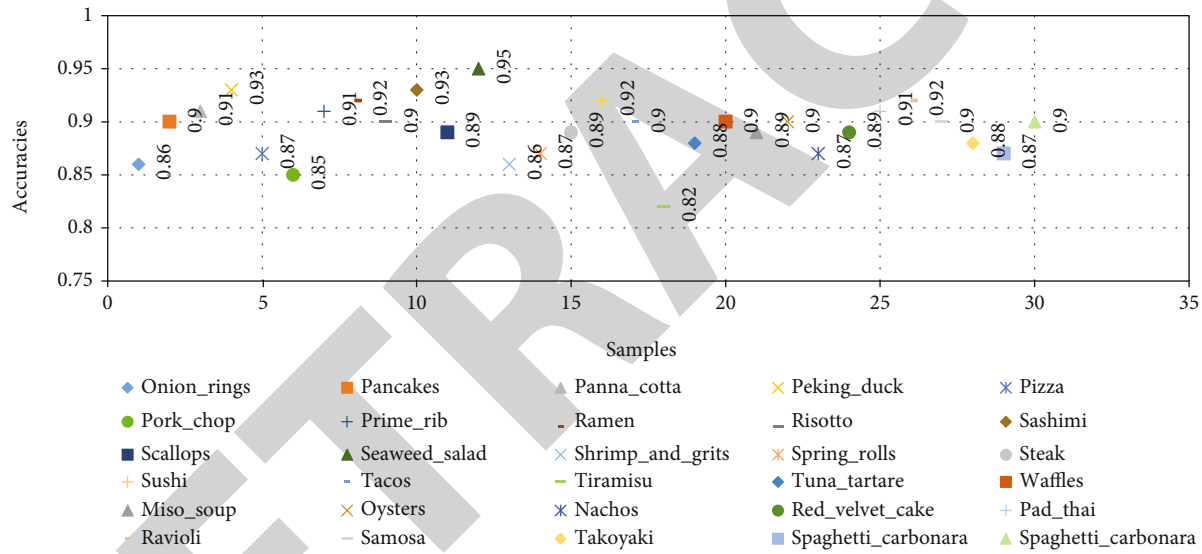

Figure 15: Accuracies on samples of the Food-101 dataset.

5. Analysis of the Experimental Result

5.1. Experimental Environment and Testing Datasets. The experimental environment that is utilized in this paper includes the following: CPU: Intel(R) Core(TM) i7-6700HQ CPU@2.60 GHz; GPU: NVIDIA GeForce GTX 1070; the physical memory (RAM): 16.0 G; and a PC with the deep learning framework of TensorFlow.

To examine the classification performance of the proposed CNN model, experiments are conducted on two image datasets: Food-101 and Places2. Food-101 is an image dataset that contains images of food. It includes 101 classes of food (western cuisine), and each class has 1000 images, which are used to automatically recognize the class of gourmet. Places2 is an image dataset of scenarios. It contains 10 million images from over 400 classes of scenarios, and it is used for visual cognition tasks with scenarios and environments as the application contents. Figures 10 and 11 show sample image data from Food-101 and Places2.

5.2. Accuracy Comparison of Activation Functions. In the study of image classification and recognition, activation functions are highly important for CNN models. Through the nonlinear mapping of an activation function, CNN can realize stronger feature representation performance for handling more complex classification problems. This paper uses the TReLU activation function to improve the classification performance of the CNN model.

To evaluate the performance of the TReLU activation function in boosting the classification performance and based on the CNN that is designed in this paper, comparison experiments are conducted on Food-101 and Places2 using the TReLU activation function and other common activation functions. Food-101 and Places2 include many classes and

RETRACTED

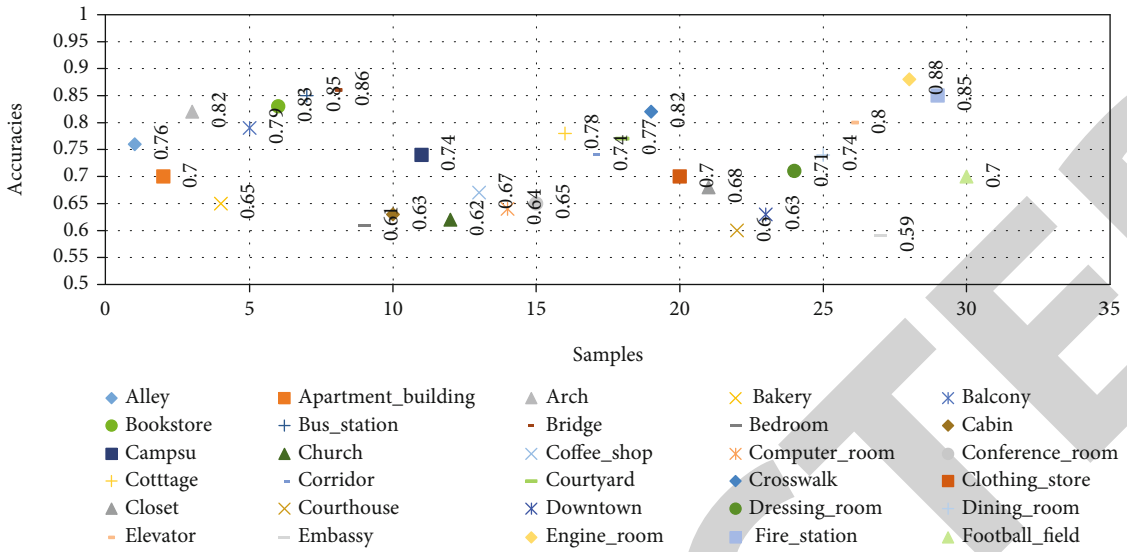

Figure 16: Accuracies on samples of the Places2 dataset.

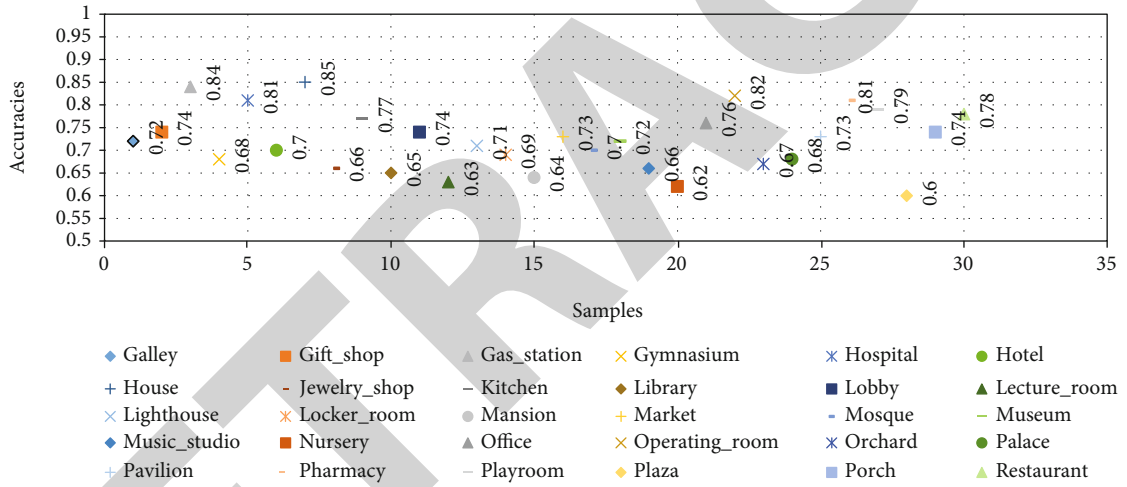

Figure 17: Accuracies on samples of the Places2 dataset.

are of high classification difficulty; see the experimental results in Table 1.

According to the experimental results in Table 1, the unsaturated nonlinear activation functions (e.g., ReLU) realize lower error rates than the saturated nonlinear activation functions (e.g., sigmoid), thereby suggesting that activation functions that are similar to biological neurons improve the classification performance.

In terms of the classification accuracy, the saturated nonlinear activation functions, namely, the sigmoid function and the tan$h$ function, are outperformed by the unsaturated nonlinear activation functions, namely, ReLU, PReLU, and TReLU; hence, the activation functions that approximate biological neurons can improve the classification accuracy. The TReLU activation function exhibits excellent classification performance on the complex datasets, namely, Food-101 and Places2, and it outperforms the other functions, which further proves that the TReLU activation function can improve the classification performance of the CNN model and yield excellent generalization performance. Figures 12 and 13 compare the classification performances of the CNN model under the five considered activation functions more vividly. The TReLU activation function not only realizes higher classification accuracy, but also has higher convergence speed than those of the other functions.

The experimental results also include the training times that were required by the five activation functions on Food-101 and Places2, which are shown in Table 2.

According to the experimental results in Table 2, the TReLU activation function requires almost the same training time as the tan$h$ function. This is acceptable. The key result is that the TReLU activation function can enhance the accuracy and further increase the convergence speed. The operation of activation function is expressed as Formula (17).

$$x_j^l = f\left(\sum_{i \in N_j} W_{ij}^l * x_i^{l-1} + b_j^l\right), \tag{17}$$

RETRACTED

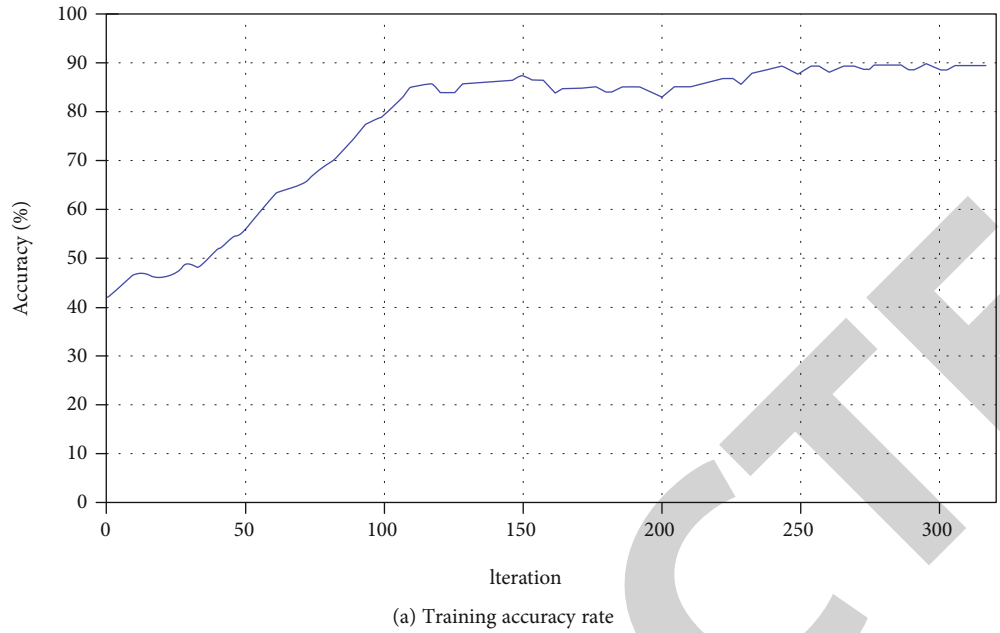

(a) Training accuracy rate

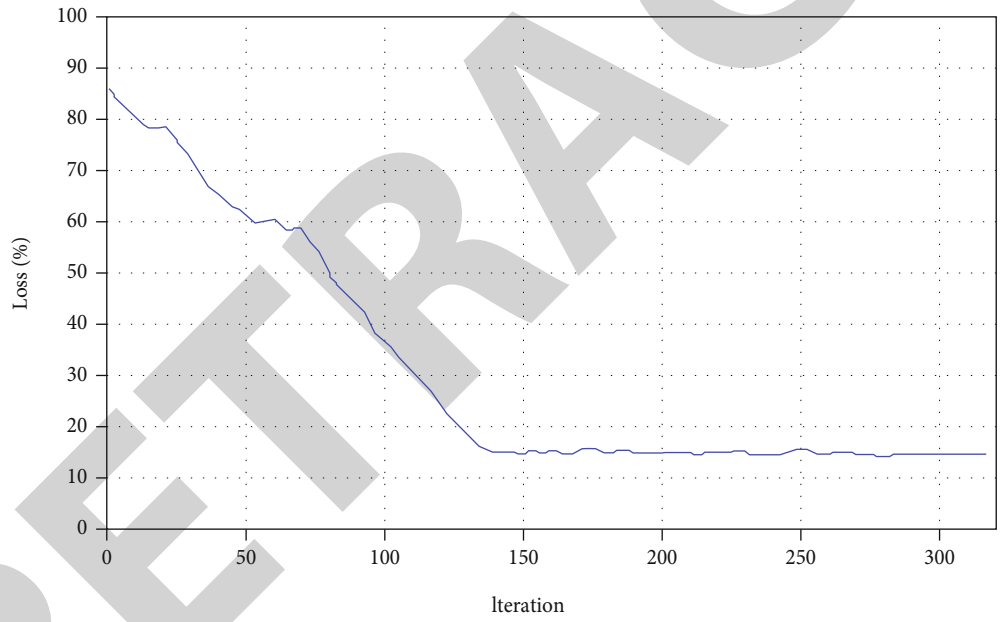

(b) Training loss rate

Figure 18: Accuracy and loss on Food-101 for the algorithm that is proposed in this paper.

where x_j^l represents the jth feature map of the lth layer; W_{ij}^l represents the connection weight of the ith feature map in the $l-1$th layer and the jth feature map in the lth layer; $*$ represents the convolution operation; b_j^l represents the bias; and N_j represents the total number of input feature maps.

5.3. Analysis of the Experimental Results. To evaluate the classification performance of the CNN model that is designed in this paper, which is based on deep feature fusion, experiments have been conducted on two image datasets, namely, Food-101 and Places2, and the results are compared with those of other image classification methods. Table 3 lists the classification accuracies. The recognition accuracies for each action category in the Food-101 and Places2 datasets are shown in Figures 14–17.

According to the experimental results in Table 3, the proposed method can effectively improve the classification performance of the network model, and its classification accuracy is higher than those of the other algorithms. Network in network (NIN) is the predecessor of inception. It expands the $1 * 1$ convolution kernel behind the convolutional layer and replaces the fully connected layer by a global average pooling layer to reduce the number of training parameters and to effectively avoid overfitting. DSN differs from other traditional deep learning frameworks. It contains a deep network that is a deep set of networks, each of which

RETRACTED

(a) Training accuracy rate

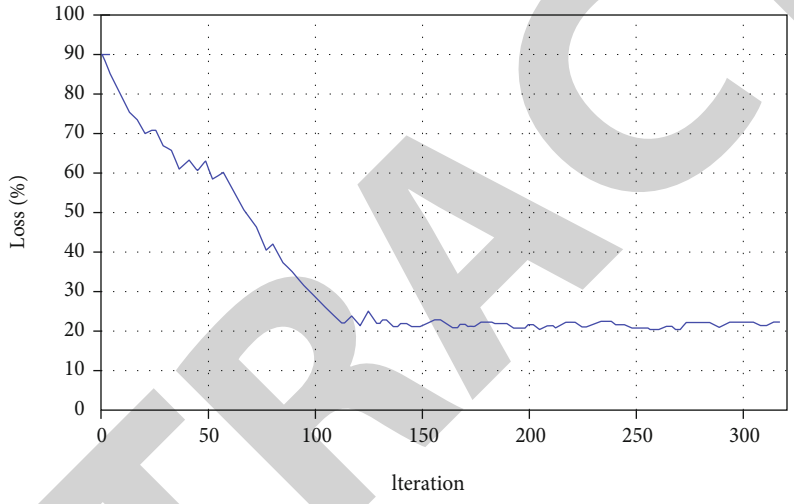

(b) Training loss rate

Figure 19: Accuracy and loss on Places2 for the algorithm that is proposed in this paper.

has its own hidden layer. DSN enables isolated training of each module for training in parallel; hence, it has high efficiency. Supervised training realizes back-propagation in each module, instead of over the entire network. DBN is composed of a multilayer unsupervised restricted Boltzmann machine (RBM) network and a one-layer supervised back-propagation (BP) network, and its training includes pretraining and fine-tuning.

The proposed CNN model is based on deep feature fusion, facilitates training and optimization of the network model via of dimension reduction, utilizes a local normalization operation to expedite the network training, and improves its classification performance. Moreover, it effectively fuses the deep features and enables the network to extract as much useful feature information as possible. Via this approach, the classification performance of the model is enhanced. Figures 18 and 19 plot the training convergence of the proposed algorithm on Food-101 and Places2, followed by the training accuracy and loss curves.

It is clearly evident from the Figure 18, in the training on Food-101 by the network model that is proposed in this paper, when the training is iterated to the 150^{th} generation, the training loss stabilizes and reaches the convergence state. At this time, the accuracy is 89%. As indicated in Figure 19, when the network trains on Places2, its classification performance is still very high, even though Places2 has higher classification complexity. When the training is iterated to the 125^{th} generation, the network has arrived at the convergence state and the accuracy is 69%.

Through the above experimental results, it can be observed that the proposed method can realize satisfactory image classification performance. In Food-101, the proposed model realizes an accuracy of 89.47%, which is 3.85%, 1.29%, and 0.94% higher than those of NIN, DSN, and DBN, respectively, and its classification and recognition performances are also satisfactory. In Places2, its accuracy is 71.56%, which is 4.66%, 2.03%, and 1.22% higher than those of NIN, DSN, and DBN, respectively, and it outperforms these methods on classification and recognition.

6. Conclusions

The arrival of the Internet of Things is accompanied by a large number of multimedia data. The key problems to be

RETRACTED

handled by image classification and recognition are to identify and classify the target objects that are contained in the image regions of interest and to make judgments. With the properties of local connection and shared weight, it has stronger robustness in its invariance to translation, rotation, and scaling of the input image data space and realizes stronger image classification and recognition performances. Facilitated by the cascade method, this paper has effectively fused the deep features of CNN, reduced the dimensions of the features using the PCN algorithm, and made the extracted features more typical and diverse to strengthen its classification performance. It has also introduced local normalization after every convolutional layer to accelerate the convergence. The experimental results demonstrate that the proposed algorithm has stabilized and expedited the network training, thereby leading to higher classification performance and accuracy.

Data Availability

The simulation experiment data used to support the findings of this study are available from the corresponding author upon request.

Conflicts of Interest

The authors declare that there are no conflicts of interest regarding the publication of this paper.

Acknowledgments

This work was supported in part by the National Key R&D Program of China (2018YFB1402600) and the National Science Foundation of China (Grant Nos. 61772190, 61672221, and 61702173).

References

[1] J. P. CobeñaCevallos, J. M. AtienciaVillagomez, and I. S. Andryshchenko, "Convolutional neural network in the recognition of spatial images of sugarcane crops in the Troncal region of the coast of Ecuador," *Procedia Computer Science*, vol. 150, no. 10, pp. 757–763, 2019.

[2] Ş. Öztürk and B. Akdemir, "HIC-net: a deep convolutional neural network model for classification of histopathological breast images," *Computers & Electrical Engineering*, vol. 76, no. 6, pp. 299–310, 2019.

[3] H. T. Mustafa, J. Yang, and M. Zareapoor, "Multi-scale convolutional neural network for multi-focus image fusion," *Image and Vision Computing*, vol. 85, no. 5, pp. 26–35, 2019.

[4] B. A. ŞabanÖztürk, "Effects of histopathological image preprocessing on convolutional neural networks," *Procedia Computer Science*, vol. 132, no. 7, pp. 396–403, 2018.

[5] N. Sharma, V. Jain, and A. Mishra, "An analysis of convolutional neural networks for image classification," *Procedia Computer Science*, vol. 132, no. 5, pp. 377–384, 2018.

[6] M. E. Paoletti, J. M. Haut, J. Plaza, and A. Plaza, "A new deep convolutional neural network for fast hyperspectral image classification," *ISPRS Journal of Photogrammetry and Remote Sensing*, vol. 145, no. 11, pp. 120–147, 2018.

[7] C. Bai, L. Huang, X. Pan, J. Zheng, and S. Chen, "Optimization of deep convolutional neural network for large scale image retrieval," *Neurocomputing*, vol. 303, no. 16, pp. 60–67, 2018.

[8] F. Zhang, N. Cai, G. Cen, F. Li, and X. Chen, "Image super-resolution via a novel cascaded convolutional neural network framework," *Signal Processing: Image Communication*, vol. 63, no. 4, pp. 9–18, 2018.

[9] H. Liang, J. Zou, K. Zuo, and K. Muhammad Junaid, "An improved genetic algorithm optimization fuzzy controller applied to the wellhead back pressure control system," *Mechanical Systems and Signal Processing*, vol. 142, article 106708, 2020.

[10] Y. Duan, F. Liu, L. Jiao, P. Zhao, and L. Zhang, "SAR image segmentation based on convolutional-wavelet neural network and Markov random field," *Pattern Recognition*, vol. 64, no. 4, pp. 255–267, 2017.

[11] S. Zagoruyko and N. Komodakis, "Deep compare: a study on using convolutional neural networks to compare image patches," *Computer Vision and Image Understanding*, vol. 164, no. 11, pp. 38–55, 2017.

[12] S. Yu, S. Jia, and C. Xu, "Convolutional neural networks for hyperspectral image classification," *Neurocomputing*, vol. 219, no. 5, pp. 88–98, 2017.

[13] Z. Huang, X. Xu, J. Ni, H. Zhu, and C. Wang, "Multimodal representation learning for recommendation in Internet of Things," *IEEE Internet of Things Journal*, vol. 6, no. 6, pp. 10675–10685, 2019.

[14] U. Raghavendra, H. Fujita, S. V. Bhandary, A. Gudigar, and U. R. Acharya, "Deep convolution neural network for accurate diagnosis of glaucoma using digital fundus images," *Information Sciences*, vol. 441, no. 5, pp. 41–49, 2018.

[15] Z. Liu, B. Hu, B. Huang, L. Lang, H. Guo, and Y. Zhao, "Decision optimization of low-carbon dual-channel supply chain of auto parts based on smart city architecture," *Complexity*, vol. 2020, Article ID 2145951, 14 pages, 2020.

[16] A. Sharma, X. Liu, X. Yang, and D. Shi, "A patch-based convolutional neural network for remote sensing image classification," *Neural Networks*, vol. 95, no. 11, pp. 19–28, 2017.

[17] R. DonidaLabati, A. Genovese, E. Muñoz, and F. S. Vincenzo Piuri, "A novel pore extraction method for heterogeneous fingerprint images using convolutional neural networks," *Pattern Recognition Letters*, vol. 113, no. 10, pp. 58–66, 2018.

[18] H. Kandi, D. Mishra, and S. R. K. S. Gorthi, "Exploring the learning capabilities of convolutional neural networks for robust image watermarking," *Computers & Security*, vol. 65, no. 3, pp. 247–268, 2017.

[19] Y. Zhang, R. Zhu, Z. Chen, J. Gao, and D. Xia, "Evaluating and selecting features via information theoretic lower bounds of feature inner correlations for high-dimensional data," *European Journal of Operational Research*, 2020.

[20] E. R. S. de Rezende, G. C. S. Ruppert, A. Theóphilo, E. K. Tokuda, and T. Carvalho, "Exposing computer generated images by using deep convolutional neural networks," *Signal Processing: Image Communication*, vol. 66, no. 8, pp. 113–126, 2018.

[21] A. Haidar, R. J. S. Almubarak, R. Long, S. Antani, and S. R. Frazier, "Convolutional neural network based localized classification of uterine cervical cancer digital histology images," *Procedia Computer Science*, vol. 114, no. 3, pp. 281–287, 2017.

[22] C. Barat and C. Ducottet, "String representations and distances in deep convolutional neural networks for image classification," *Pattern Recognition*, vol. 54, no. 6, pp. 104–115, 2016.

RETRACTED

Hindawi
Wireless Communications and Mobile Computing
Volume 2020, Article ID 6623466, 10 pages
https://doi.org/10.1155/2020/6623466

Research Article

Emerging Applications of Blockchain Technology on a Virtual Platform for English Teaching and Learning

Ping Wang[1] **and Shuhan Qiao**[2]

[1]*School of Foreign languages, Jiujiang University, Jiujiang 332005, China*
[2]*Shandong Provincial Research Center of Demonstration Engineering Technology for Urban and Rural Landscape, Taian 271000, China*

Correspondence should be addressed to Shuhan Qiao; qiaoshuhan@sdau.edu.cn

Received 16 October 2020; Revised 5 November 2020; Accepted 27 November 2020; Published 8 December 2020

Academic Editor: Hongju Cheng

Copyright © 2020 Ping Wang and Shuhan Qiao. This is an open access article distributed under the Creative Commons Attribution License, which permits unrestricted use, distribution, and reproduction in any medium, provided the original work is properly cited.

To extend a broad application of blockchain technology to the fields of online English education, this paper aims to improve a virtual platform for English teaching and learning of landscape design majors, mainly composed of presentation layer, business layer, and data layer by analyzing the performance of the proposed algorithm, and comparing with other existing algorithms. In the platform, through the service layer, the communication between the presentation layer and the data layer is completed, and the data in the data layer is transferred to the presentation layer. The user first establishes a connection with the server in the presentation layer. Using the transmitted data information, the server assigns an identifier to the user and establishes a role model. Users can download the teaching courseware through the server and simulate the real learning scene by controlling the interaction of XAML files. The results show that the virtual teaching platform makes the interconnection of users (students and teachers), machines, and things at any time and any place; realizes information self-verification, transmission, deep unsupervised learning, and management; and gives students a more realistic visual experience in high security.

1. Introduction

Blockchain is a term in the field of information technology. In essence, it is a Shared database of data or information that is "not falsifiable," "traces," "open and transparent," and "collective maintenance". Based on these characteristics, blockchain technology has laid a solid foundation of "trust," created a reliable "cooperation" mechanism, and has a broad application prospect. In recent years, blockchain technology is closely related to people's production and life in public management, energy, transportation, and other fields. Its technology does not rely on additional third-party management institutions or hardware facilities, and there is no central control. In addition to the self-contained blockchain technology itself, each node realizes information self-verification, transmission, and management through distributed accounting and storage. Decentralization is the most prominent and essential feature of blockchain technology [1]. However, although online teaching and learning has already been used widely in China, especially in the coronavirus epidemic, a series of old virtual platforms have not adapted to the change and development. The centralization of this field also brings some problems, which can be transformed by blockchain technology.

According to the survey, the concerns of web-based distance education are mainly focused on resources, quality, management, and teaching interaction. These are the main concerns of students and the main factors that restrict the quality of online education. With the continuous development of the second generation of website technology, a number of new network platforms for education have greatly improved the quality and efficiency of modern education and deepened the experience of teacher-student interaction in the network environment [2]. It is also in line with the requirements of modern education. With the rapid development of modern Internet technology, many universities at

home and abroad are actively researching and developing Internet-based online education platforms to build more effective virtual campuses.

In addition, influenced by the traditional teaching mode, the English classroom teaching for landscape design majors completes the unit's teaching tasks according to the unit structure of the textbook [3]. The teaching process focuses on language learning and lacks the introduction of English culture; it highlights the monopolistic role of teachers but ignores the subjective status of students and the communicative activities that students need.

At present, web-based distance education based on blockchain for Internet of Things will become an important way, both in terms of the development of the school itself and the needs of society. Based on the research contents of the above scholars, this paper makes a contribution in the following ways:

(1) This paper reviews the existing educational information platforms based on blockchain technology for Internet of things and analyzes their advantages and disadvantages

(2) An improved virtual English teaching platform for landscape design majors is proposed, which combines deep unsupervised learning, machine learning, and self-contained blockchain technology itself

(3) The performance of the proposed algorithm is analyzed and compared with other existing algorithms, and its advantages are used to improve the virtual teaching platform of landscape design majors

This paper is organized as follows. Section 2 shows the related work. Section 3 describes the related materials and methods. And result analysis is given in Section 4, including electronic whiteboard, design of virtual scenes, energy consumption, the number of simultaneous online users, and teaching effects. Section 5 discusses the improved English virtual teaching platform for garden design majors which is based on virtual reality technology. Finally, Section 6 outlines the conclusions and puts forward a reasonable basis for practice for further reference.

2. Related Work

Compared with the English teaching for garden design majors in the traditional environment and the network environment, the traditional online teaching platform is based on online video as the main carrier for distance learning. The interaction between teachers and students is not strong, and its expression is relatively simple, lacking timely and effective feedback, which is not conducive to stimulating students' enthusiasm for learning, and greatly reduces the quality of teaching [4]. In the network-based English teaching for garden design majors, the learner is the main body of learning, with learning autonomy; the teacher only carries out the necessary organization, guidance, and examination for the students, which is also the application of the "constructivism" theory in teaching [5]. Constructivism emphasizes the subjective ability of students in learning and believes that students are the subject of learning. Knowledge is not obtained through the teacher's teaching, but the learner obtains it through the meaning construction in the certain social background, with the help of others and the necessary learning resources. Constructivism requires students to be transformed from passive recipients of internal stimuli and indoctrination of knowledge into active participants, discoverers and processors of information, and active constructors of meaning. Teachers are required to be transformed from instructors and indicators of knowledge into instructors, facilitators, and organizer of student learning [6]. Therefore, it is very urgent to construct an online teaching platform with strong interactivity, effective feedback, and rich expression.

The teaching platform has good interactivity, but the platform teaching clarity and fluency are low. Wang Pingping created a multidimensional virtual teaching platform for English, which can fully meet the needs of schools, teachers, and students. However, when the number of online users on the virtual teaching platform is large, there will be a stutter phenomenon. After the above analysis, the English virtual teaching platform for garden design majors is constructed. Combined with the advantages of the above scholars' research, the original virtual teaching platform for English teaching is improved to improve the performance of the English virtual teaching platform for garden design majors.

3. Materials and Methods

3.1. Improved Design of Virtual Teaching Platform. The improved English virtual teaching platform for garden design majors designed in this paper is the three-layer B/S mode. The development technology mainly uses XAML,. NET, and Javascript. The database uses SQLServer 2005 [7]. The framework of the improved English virtual teaching platform for garden design majors is shown in Figure 1.

It can be seen from Figure 1 that the virtual teaching platform for landscape design English based on machine learning algorithm includes the presentation layer, business layer, and logic layer. The presentation layer realizes the user interaction with the whole platform by inserting the browser plug-in Silverlight into the web browser. The business layer is mainly responsible for all kinds of logical services of the platform, completing the communication between the presentation layer and the data layer. For example, virtual lab scenarios are generated by calling virtual components and learning generated by calling virtual components and learning module information in the database. The data layer provides data information required by the platform, such as scene information and role information [8].

After logging in, the user establishes a connection with the server, and the server assigns an identity to it. The character model was created, and the English teaching courseware for garden design majors was downloaded. Through the XAML control file, interactions are performed and real learning scenarios are simulated. At the same time, the server is also responsible for storing the shared space, managing and maintaining the consistency of the virtual teaching scene, and listening to the client's connection request and response

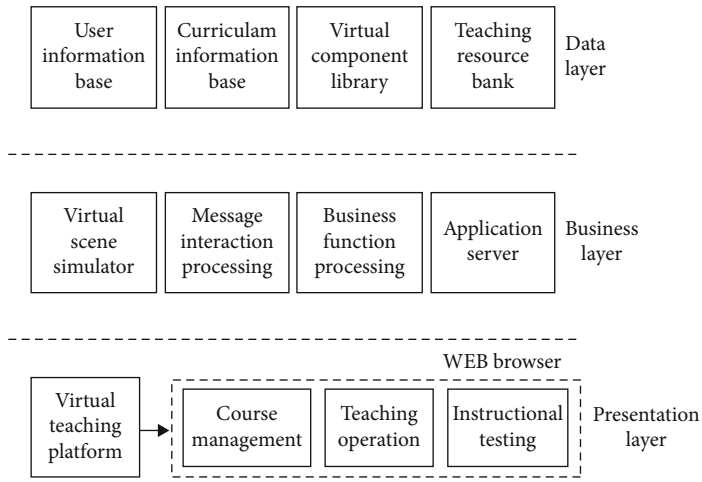

Figure 1: Schematic diagram of virtual teaching platform framework.

connections. The client is browser based. The first time you use it, it takes less than a few seconds to automatically download and install the browser plugin Silverlight. The client program runs in the browser as a plug-in, creates a socket connection with the server, and receives the server's message for parsing [9]. The request of the client is sent to implement the update of the virtual scene and the user interaction. The information interaction in the English virtual teaching platform for garden design majors is more important. Through information interaction, users can create an immersive feeling to enhance user interest and promote user learning [10]. The information interaction model designed in this paper is shown in Figure 2.

As can be seen from Figure 2, through the information interaction model, the platform can provide users with a more realistic and virtual English teaching environment for garden design majors, while users can perceive the most realistic teaching effects from the aspects of vision, hearing, and virtual environment.

3.2. Platform Features. The improved English virtual teaching platform for garden design majors consists of two parts: the front desk and background of the virtual teaching platform. The improved front desk of English virtual teaching platform for garden design majors mainly includes the student platform, teacher platform, user login, and user registration function modules. The improved background of the English virtual teaching platform for garden design majors mainly completes the user management, platform maintenance, teacher review, course review, and release notification of the virtual teaching platform [11].

3.2.1. Front Desk Function. The improved front desk of the English virtual teaching platform for garden design majors is mainly composed of the teacher function module and the student function module [12]. The front desk mainly includes the student platform, the teacher platform, and the registration and login function. The student platform module provides online learning for students, including onsite mail, the latest course presentations, the latest resource presentations, student classes, and personal information maintenance. Among them, the student classroom is the key function of the student platform, which includes online video, online discussion groups, online courseware browsing, and other functions.

It provides a good learning platform for students. The teacher platform module mainly includes the release of the experimental course, the release of the teaching course, and the maintenance of the teaching course. Among them, the teaching course publishing function is the key function module of the teacher platform, which includes functions such as applying for the course, adding the discussion group, releasing the teaching courseware, and releasing the video. It provides a variety of resources for students to learn online [13].

(1) Electronic Whiteboard. The e-learning whiteboard allows multiple people to simultaneously draw graphics on the whiteboard and send text messages, all of which will be reflected on each user's screen. Therefore, through the electronic whiteboard, teachers and students and students and students can have convenient communication and discussion. The electronic whiteboard is implemented by XAML +WCF. XAML is used as a presentation layer for drawing whiteboards, and feedback from user operations is passed through WCF. The core purpose of WCF is to allow programs to communicate with other programs on the same computer or network, or across the Internet [14].

(2) Student Function Logic. Students must meet two conditions to enter the student platform: first, the user must have completed registration. Student users must be registered with the platform before they can log in to the platform. The platform verifies the user's necessary registration information when the student user logs in to the platform. If the platform detects that the user has not completed the necessary information, it will return to the user details registration page so that the user can continue to complete the registration. The second condition is that the user must pass the platform authentication. Student business logic is shown in Figure 3.

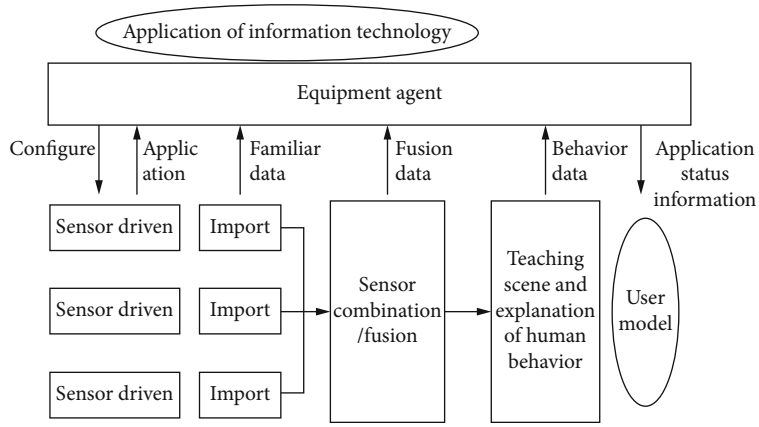

Figure 2: Platform information interaction model.

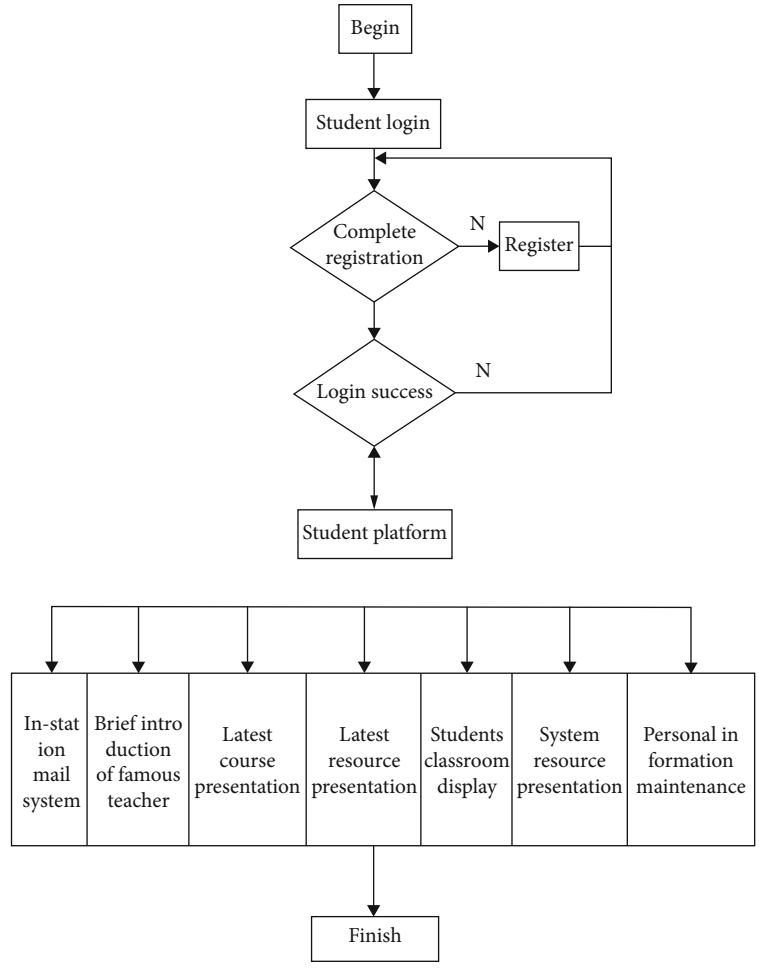

Figure 3: Student functional logic.

It is known from the student function logic that students can only use the platform after they have been authenticated. The specific functions that the student platform provides to students are as follows: the in-site mail platform (including the functions of mail sending, mail receiving, and announcement display and address book). The mail sending function can be used for mail communication between platform users, and users can view the sent mail records in their own outbox [15]. The mail receiving function allows the user to receive mail, and the user can view the received mail in the inbox. The announcement display feature displays the latest announcements from the administrator. Contacts can help users find contacts quickly when they need to send in-site mail. The Master Profile feature provides a teacher avatar

scrolling feature on the student home page. Students can always check the latest course information of the teachers they are interested in. By reviewing the latest approved course information, students can easily learn the latest courses to learn about the courses they are interested in [16]. The latest resource information display feature makes it easy for students to learn about the latest uploaded courseware, video tutorials, and other available teaching resources. Student Classroom Display: this feature is a key feature of the virtual course platform, which provides a good online learning platform for student users.

3.2.2. Background Function. The background of the improved English virtual teaching platform for garden design majors has the following functions: platform maintenance, personnel management, classroom information setting, and course information management [17]. The platform background is mainly to support the management and maintenance of the web-based virtual teaching platform. The platform background includes platform information maintenance, course review, teacher review, release notification, personnel management, subject and professional management, and administrator password modification. Among them, platform information maintenance refers to the initialization of the virtual teaching platform, the recovery of the database dictionary, the setting of the number of people in the online classroom, and the backup and restoration of the database [18]. Personnel management includes information management for users such as students and teachers, as well as management of administrators. The background of the improved English virtual teaching platform for garden design majors has only one type of administrator [19]. The following functional logic for the administrator is designed as follows. First, administrators also need to authenticate when they enter the platform. When the administrator logs in to the platform, the platform will verify the login information of the user. After the verification is passed, the platform automatically records the administrator's user name, number, and user name, number, and user role in the session object. This is also the important document that the administrator has logged into the platform. The user function logic is shown in Figure 4.

As can be seen from Figure 4, the administrator can log in to the platform and authenticate before entering the background management platform. When the administrator enters the background management platform, the platform can be managed and maintained. Among them, the platform basic information maintenance functions include platform initialization, data dictionary recovery, and database backup and restore. Platform initialization includes initialization of platform default settings and creation of some necessary folders [20]; data dictionary recovery is to prevent the platform from running abnormally due to malicious tampering with the original data in the database; the course review function allows the administrator to review the course applied by the teacher. The course review status includes pending review, pass, and fail. Before the teacher applies for the course to the final review of the administrator, the course status is pending review, and only after the applied course has been approved, can it open to the students. The administrator uses the teacher review function to review newly registered teachers, and only users registered as teachers need to be reviewed [21].

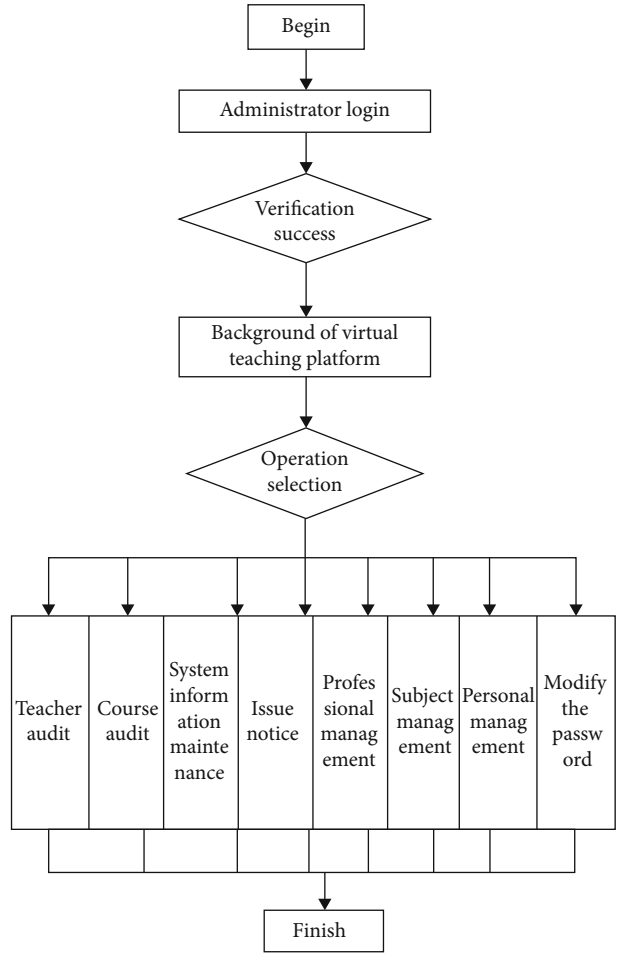

Figure 4: Ends with a user function logic diagram.

4. Results

4.1. Electronic Whiteboard. To verify the effect of the whiteboard application in the improved English platform for landscape design majors of this article, actual testing is required. The effect of the whiteboard application in the platform is shown in Figure 5.

As can be seen from Figure 5, the teacher can show the garden design majors English to the students through the whiteboard. When the teacher writes the wrong English word on the electronic whiteboard, the wrong letter on the whiteboard can be cleared by the eraser button on the whiteboard interface, and at the end of the course, the teacher can click the button to clear all the texts on the whiteboard. On the electronic whiteboard interface, there is a user communication interface. Students can send questions to the teacher through the communication interface on the electronic whiteboard, and the teacher can watch and reply through the interface. After the above analysis, it is found that the

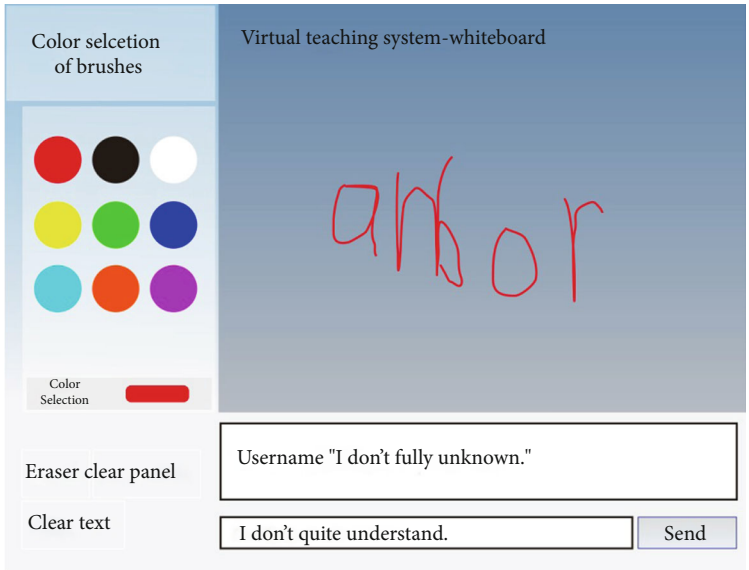

Figure 5: Electronic whiteboard display diagram.

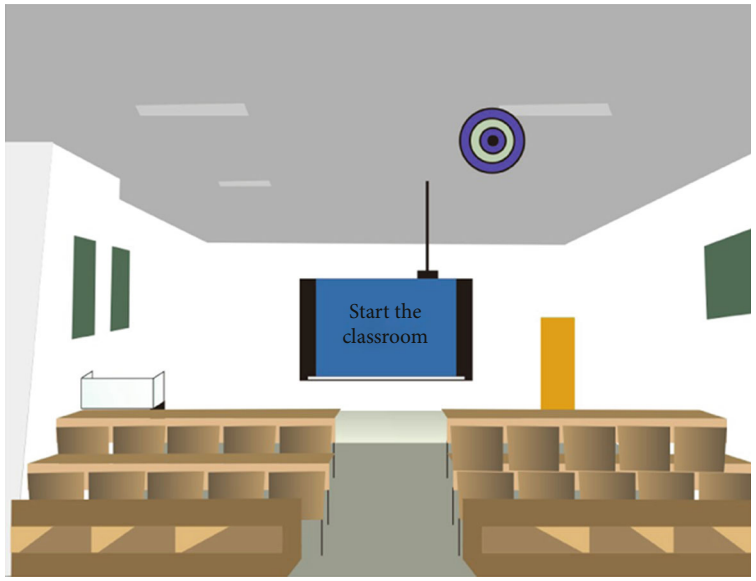

Figure 6: Virtual classroom design.

electronic whiteboard in the improved English virtual teaching platform for garden design majors has the better effect.

4.2. Design of Virtual Scenes. To verify the effect of the teaching scene in the improved English virtual teaching platform for garden design majors designed by this method, the actual analysis is needed. The virtual classroom scene obtained by using the virtual teaching platform is shown in Figure 6.

As can be seen from Figure 6, after the student logs in to the platform, he or she chooses a course of study and then enters the virtual classroom. Virtual classrooms are built in a simulated reality classroom that includes elements such as windows, fluorescent lights, desks and chairs, podiums, projectors, blackboards, and slides. After entering the virtual classroom, students can move freely in the classroom. When the mouse moves to the slide element in the virtual classroom, they will see the slogan prompting "start the classroom." After clicking the slogan, they can enter the classroom to learn. That is to say, the improved English virtual teaching platform for garden design majors has better interaction performance.

4.3. Energy Consumption. To verify the energy consumption of virtual teaching platform in this method, under different teaching time, the energy consumption of the teaching platforms designed by the method of this paper, the design method of virtual teaching platform based on cloud architecture, and the design method of the virtual teaching platform based on MVC should be compared. The comparison results are shown in Table 1.

Table 1: Comparison of energy consumption results.

Method	Teaching time/h	Expenditure of energy/J
The method of this paper	0.5	236.458
	0.6	239.346
	0.7	241.527
	0.8	243.674
	0.9	244.532
	1	249.671
	1.1	250.918
	1.2	252.634
	1.3	255.315
	1.4	258.619
	1.5	260.056
Design method of teaching virtual platform based on cloud architecture	0.5	346.826
	0.6	349.798
	0.7	353.264
	0.8	357.684
	0.9	361.258
	1	365.947
	1.1	369.793
	1.2	373.213
	1.3	377.192
	1.4	381.648
	1.5	385.975
Design method of virtual teaching platform based on MVC	0.5	468.249
	0.6	476.364
	0.7	484.456
	0.8	492.359
	0.9	500.681
	1	508.163
	1.1	516.254
	1.2	524.794
	1.3	532.618
	1.4	540.023
	1.5	548.315

It can be seen from Table 1 that the method consumes the least amount of energy in the same teaching time. After statistical analysis, the average energy consumption of the proposed method in various cases is 248.431 J, while the average energy consumption of the other two methods is 365.691 J and 508.388 J, respectively. That is, the English virtual teaching system for garden design majors designed by this method consumes the least amount of energy in the actual process.

4.4. Analysis of the Number of Simultaneous Online Users. Two computers with the same configuration were selected as the experimental objects, one of which was equipped with the ordinary English virtual teaching platform for garden design majors, and the other was equipped with the improved English virtual teaching platform for garden design majors. One thousand students from a university log in to the two platforms at the same time and learn English with the garden design majors online. Finally, the number of simultaneous online users allowed by the course of the two platforms is separately counted. The number of online students in the course is the same as the change in the SJF indicator. When the SJF indicator increases, the number of online students can increase at the same time; otherwise, it decreases. Before and after the improvement, the comparison of the number of online users is shown in Figure 7.

Figure 7(a) shows that when the upper limit of the number of online users is 500, the preimprovement English virtual teaching platform for garden design majors is applied. At 10 s, the virtual teaching platform has a maximum of 286 online users. After the application of the improved virtual teaching platform, the virtual teaching platform can reach a maximum of 500 people online at 12 s. Analysis of Figure 7(b) shows that when the upper limit of the number of online people is greater than 500, the preimprovement English virtual teaching platform for garden design majors is applied. At 6.8 s, the number of simultaneous online users on the virtual teaching platform reached a maximum of 805. After applying the improved virtual teaching platform, at 8.2 s, the number of simultaneous online users on the virtual teaching platform reached a maximum of 968. Therefore, it can be proved that the number of online viewers has been greatly improved after applying the improved English virtual teaching platform for garden design majors.

4.5. Analysis of Teaching Effect. To comprehensively verify the teaching effect of the virtual teaching platform designed in this paper, 10 students from a certain university are randomly selected for actual investigation. The virtual teaching platforms designed by the three methods were scored with a score of 10, and the results are shown in Table 2.

It can be seen from Table 2 that the overall teaching effect of the English virtual teaching platform for garden design majors improved by this method is better. The above data shows that the clarity and fluency of the teaching platform designed by this method are higher than 9 points. The teaching effects of the virtual teaching platform designed by the other two methods are lower than the method of this paper. That is to say, through comparative analysis, the actual teaching effect of the virtual teaching platform designed by this method is better.

5. Discussion

After theoretical analysis and experimental verification, the improved English virtual teaching platform for garden design majors is based on virtual reality technology. There is a big difference between the improved English virtual teaching platform for garden design majors and the traditional English virtual teaching platform for garden design majors. It mainly immerses people in a variety of senses and interacts with this realistic environment. The improved

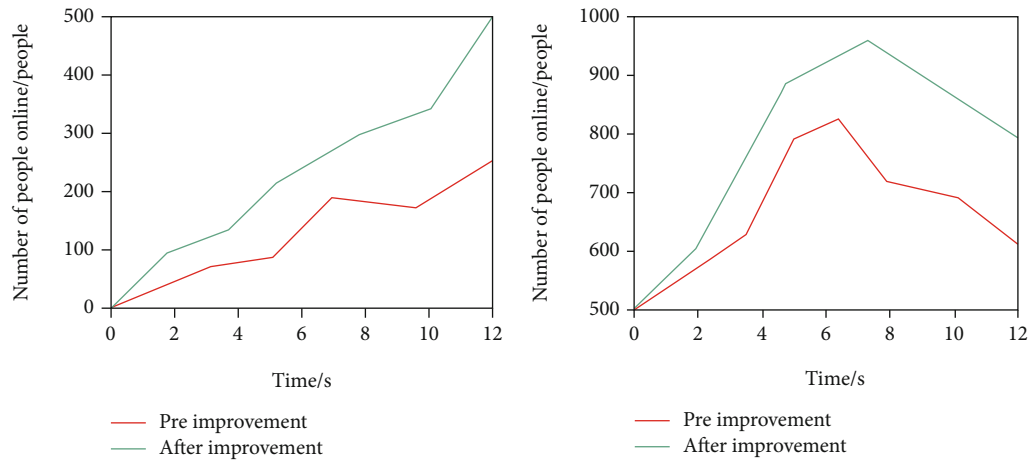

(a) The number of people online is less than 500

(b) The on-line number is greater than 500

Figure 7: Comparison results.

virtual teaching platform for garden design majors believes that the structure of the English virtual teaching platform for garden design majors is the basis of the overall existence of the platform, and the structural changes of the virtual teaching platform lead to changes in the overall performance of the platform. The structure of the English virtual teaching platform for landscape design majors determines the platform function. From the scientific point of view, the structure of the English virtual teaching platform for garden design majors has changed compared with the traditional English teaching platform for garden design majors. The virtual reality technology plays an important role in the English virtual teaching platform for garden design majors. Secondly, from the perspective of the relationship between the structural elements of the platform, the interaction and internal relationship between the elements of the English virtual teaching platform for garden design majors is more closely and more complicated.

The improved English virtual teaching platform for garden design majors designed in this paper has various characteristics. First of all, the platform can bring immersiveness to the user, also known as the sense of presence, which refers specifically to the true Extent of the learner as the protagonist in the simulated environment. Immersion is the degree to which learners perceive the virtual world. This sense of reality makes it difficult for learners to perceive and distinguish themselves in the virtual environment generated by a computer. Immersion is the foundation that makes the scene realistic. Constructivist learning theory advocates for learners to provide a real learning environment, so that learners actively form meaning constructions. The advantage of the virtual teaching platform is that it immerses learners in a realistic three-dimensional learning environment. It provides a reliable guarantee for learners to actively form meaning constructions. Secondly, it can give learners a better interactive experience. The interactive experience refers to the learner's operability of objects in the virtual world. Interactivity requires not only human-computer interaction, but more importantly, digital technology enables people to easily communicate with each other through the Internet. Interaction can be understood as a two-way communication, which is reflected in the teaching process between students and teachers, students and learning resources, and students and students. In the virtual teaching platform, students are able to connect new knowledge with old knowledge through effective communication between students and teachers, so as to achieve the purpose of building the new cognitive structure. The platform can significantly enhance the students' conception. Conceptuality means that learners can acquire knowledge in all directions in the multidimensional information space of the virtual world, relying on their own perception and cognitive abilities. They seek to solve the problem perfectly by exerting subjective initiative. The fundamental purpose of the research and development of the virtual teaching platform is to expand human cognition and perception and to establish a harmonious human-machine environment. In the harmonious human-machine environment provided by the virtual teaching platform, the learner's subject status is fully reflected. The conception emphasizes that virtual reality technology should have a broad and imaginable space to broaden the scope of human cognition. It not only reproduces the real environment but also arbitrarily conceives an environment that does not exist or even impossible. Finally, the platform is multiperceived.

The so-called multiperception means that in addition to the visual perception of general computer technology, there are also hearing, force, touch, movement, and even taste, smell, and so on. From the perspective of the development of virtual reality technology, the ideal virtual reality technology should have all cognitive functions that human beings have. Due to the limitations of related technologies, especially sensing technologies, the perceptual function of virtual reality technology is limited to visual, auditory, force, tactile, and sports. After the above analysis, the improved English virtual teaching platform for landscape design majors designed in this paper has a good teaching effect and is suitable for application to the actual English teaching for landscape design majors.

Table 2: Score results.

Method	Student	Teaching clarity	Teaching fluency	Human-computer interaction performance	Resource maintenance effect	User management effect
The method of this paper	Student 1	9.92	9.98	9.97	9.97	9.97
	Student 2	9.98	9.97	9.98	9.99	9.98
	Student 3	9.94	9.97	9.99	9.99	9.99
	Student 4	9.89	9.97	9.98	9.98	9.99
	Student 5	9.87	9.99	9.98	9.96	9.96
	Student 6	9.86	9.99	9.98	9.96	9.98
	Student 7	9.99	9.98	9.94	9.94	9.96
	Student 8	9.99	9.96	9.93	9.95	9.99
	Student 9	9.91	9.95	9.95	9.95	9.97
	Student 10	9.93	9.96	9.96	9.99	9.97
Virtual teaching platform design method based on cloud architecture	Student 1	8.23	8.41	8.61	8.19	8.23
	Student 2	8.26	8.46	8.62	8.21	8.25
	Student 3	8.29	8.49	8.68	8.24	8.28
	Student 4	8.64	8.25	8.67	8.28	8.29
	Student 5	8.35	8.37	8.54	8.29	8.31
	Student 6	8.16	8.46	8.52	8.31	8.35
	Student 7	8.24	8.59	8.53	8.36	8.38
	Student 8	8.26	8.27	8.59	8.38	8.42
	Student 9	8.34	8.26	8.47	8.45	8.46
	Student 10	8.46	8.23	8.46	8.47	8.45
Design method of virtual teaching platform based on MVC	Student 1	7.51	7.56	7.49	7.61	7.42
	Student 2	7.58	7.59	7.67	7.63	7.46
	Student 3	7.52	7.58	7.82	7.59	7.49
	Student 4	7.53	7.51	7.81	7.57	7.51
	Student 5	7.46	7.54	7.69	7.52	7.53
	Student 6	7.59	7.53	7.64	7.49	7.59
	Student 7	7.61	7.61	7.62	7.48	7.61
	Student 8	7.68	7.48	7.61	7.46	7.64
	Student 9	7.83	7.49	7.69	7.59	7.68
	Student 10	7.45	7.68	7.71	7.52	7.69

6. Conclusion

This paper mainly studies the English virtual teaching platform for landscape design majors in high security. The development technology of this platform mainly uses XAML,. NET, and Javascript. SQL Server 2005 is used as a background database, and the platform is designed by the more popular B/S three-tier architecture. Video teaching courseware, teacher-student interaction, English teaching for landscape design majors, and English teaching resources for landscape design majors are provided online by the platform, the goal is to provide students with a good online learning platform. The online English teaching module for landscape design majors implements an online compilation and running program.

In the case that the compiler is not installed, the compiler function of the browser is simply run through the compiled interface of the server, and the result of the compile and run is returned to the browser, so that the content of the virtual teaching platform is more diverse. The use of virtual reality technology enables the construction of virtual classrooms and virtual labs. Compared with the traditional online teaching platform, it has greatly improved in terms of security on Internet virtual teaching.

Data Availability

The raw/processed data required to reproduce these findings cannot be shared at this time as the data also forms part of an ongoing study.

Conflicts of Interest

The authors declare that there are no conflicts of interest regarding the publication of this study.

Acknowledgments

This work was supported by the Project of Art Science in Shandong Province (201806506).

References

[1] W. Guo, N. Xiong, H. Chao, S. Hussain, and G. Chen, "Design and analysis of self-adapted task scheduling strategies in wireless sensor networks," *Sensors*, vol. 11, no. 7, pp. 6533–6554, 2011.

[2] N. Xiong, A. Vandenberg, and W. Han, "Green cloud computing schemes based on networks: a survey," *IET Communications*, vol. 6, no. 18, pp. 3294–3300, 2012.

[3] R. Othman and A. K. Zubaidah, "Assessment of plant materials carbon sequestration rate for horizontal and vertical landscape design," *International Journal of Environmental Science & Development*, vol. 7, no. 6, pp. 410–414, 2016.

[4] R. T. Corlett, "The role of rewilding in landscape design for conservation," *Current Landscape Ecology Reports*, vol. 1, no. 3, pp. 127–133, 2016.

[5] G. K. Wong and C. Y. Jim, "Abundance of urban male mosquitoes by green infrastructure types: implications for landscape design and vector management," *Landscape Ecology*, vol. 8, no. 10, pp. 1–15, 2018.

[6] J. O. Kim and J. H. Suh, "A review of climate change adaptation policies applied to landscape planning and design in Korea," *Landscape & Ecological Engineering*, vol. 3, no. 12, pp. 171–177, 2016.

[7] H. Liang, J. Zou, and K. Muhammand Junaid, "An improved genetic algorithm optimization fuzzy controller applied to the wellhead back pressure control system," *Mechanical Systems and Signal Processing*, vol. 142, article 106708, 2020.

[8] D. H. Li, B. S. Jiang, H. Y. Li, and X. P. Liu, "Design of experiment course "Computer-aided landscape design" based on flipped classroom," *Computer Applications in Engineering Education*, vol. 27, no. 9, pp. 234–240, 2016.

[9] S. Champeaux, P. Gouard, and R. Cousin, "Improved design of a multistage axial vircator with reflectors for enhanced performances," *IEEE Transactions on Plasma Science*, vol. 21, no. 9, pp. 31–38, 2016.

[10] I. Freeman, J. Salmon, and J. Coburn, "A bi-directional Interface for improved interaction with engineering models in virtual reality design reviews," *International Journal on Interactive Design and Manufacturing*, vol. 27, no. 13, pp. 1–12, 2017.

[11] Z. Huang, X. Xu, J. Ni, H. Zhu, and C. Wang, "Multimodal representation learning for recommendation in internet of things," *IEEE Internet of Things Journal*, vol. 6, no. 6, pp. 10675–10685, 2019.

[12] F. Stumpf, K. Schmidt, and T. Behrens, "Incorporating limited field operability and legacy soil samples in a hypercube sampling design for digital soil mapping," *Journal of Plant Nutrition and Soil Science*, vol. 5, no. 3, pp. 499–509, 2016.

[13] H. R. Sun and H. Wang, "Optimization design simulation of ecological balance of urban green landscape," *Computer Simulation*, vol. 7, no. 2, pp. 214–217, 2018.

[14] H. Liang, D. Zou, Z. Li, K. Muhammand Junaid, and Y. Lu, "Dynamic evaluation of drilling leakage risk based on fuzzy theory and PSO-SVR algorithm," *Future Gerneration Computer Systems*, vol. 95, no. 7, pp. 454–466, 2019.

[15] H. Zheng, W. Guo, and N. Xiong, "A kernel-based compressive sensing approach for mobile data gathering in wireless sensor network systems," *IEEE Transaction on Systems*, vol. 48, no. 12, pp. 2315–2327, 2017.

[16] Y. C. Liu, Y. Huang, and X. Li, "Research on midpoint potential balance of NPC three-level inverter based on fuzzy virtual space vector modulation," *Journal of Power Supply*, vol. 10, no. 9, pp. 61–66, 2018.

[17] X. L. Meng, L. D. Wu, and S. B. Yu, "Research on resource management mechanism of spatial information network based on virtualization," *Journal of China Academy of Electronics and Information Technology*, vol. 6, no. 8, pp. 47–52, 2018.

[18] Y. Zhou, D. Zhang, and N. Xiong, "Post-cloud computing paradigms: a survey and comparison," *Tsinghua Science and Technology*, vol. 22, no. 6, pp. 714–732, 2017.

[19] Z. Liu, B. Hu, B. Huang, L. Lang, H. Guo, and Y. Zhao, "Decision optimization of low-carbon dual-channel supply chain of auto parts based on smart city architecture," *Complexity*, vol. 2020, Article ID 2145951, 14 pages, 2020.

[20] Y. Zhang, R. Zhu, Z. Chen, J. Gao, and D. Xia, "Evaluating and selecting features via information theoretic lower bounds of feature, inner correlations for high-dimensional data," *European Journal of Operational Research*, vol. 290, 2020.

[21] H. Liang, A. Xian, M. Mao, P. Ni, and H. Wu, "A research on remote fracturing monitoring and decision-making method supporting smart city," *Sustainable Cities and Society*, vol. 62, article 102414, 2020.

Hindawi
Wireless Communications and Mobile Computing
Volume 2020, Article ID 6622900, 10 pages
https://doi.org/10.1155/2020/6622900

Research Article

Accelerated Depreciation Tax Credit and Corporate Financialization Based on the PSM-DID Model

Chunguang Ma, Hongjun Bei, Chuner Wang, and Guihua Chen

Ningbo University of Finance & Economics, Ningbo 315000, China

Correspondence should be addressed to Chunguang Ma; machunguang@nbufe.edu.cn

Received 9 October 2020; Revised 9 November 2020; Accepted 21 November 2020; Published 7 December 2020

Academic Editor: Hongju Cheng

Copyright © 2020 Chunguang Ma et al. This is an open access article distributed under the Creative Commons Attribution License, which permits unrestricted use, distribution, and reproduction in any medium, provided the original work is properly cited.

In this paper, we use the data of China's manufacturing listed companies from 2009 to 2018, adopt the method of propensity score matching and double difference (PSM-DID) to solve the sample's selective bias, and select the accelerated depreciation policy of fixed assets issued by China in 2014 as a quasi-natural experiment to verify the robustness of the empirical results, which will affect the R&D investment of manufacturing enterprises and the structural tax reduction of China. This paper makes an empirical study on the effect of fixed asset investment to restrain the financialization of manufacturing enterprises. The results show that (1) accelerated depreciation policy of fixed assets significantly promotes the R&D investment and fixed asset investment of enterprises and reduces the level of enterprise financialization; (2) accelerated depreciation of fixed asset local tax policy, through guiding the R&D investment, fixed asset investment, and deferred income tax acquisition of enterprises. It guides the investment of enterprises to the real economic field, thus reducing the financial assets of enterprises. The investment has restrained the financial trend of real enterprises. The conclusion of this paper is of practical significance to support the formulation and implementation of the national structural tax reduction policy and to clarify the regulatory role and mechanism of the structural tax reduction policy.

1. Introduction

History and reality tell us that it is impossible to become a world power without a strong manufacturing industry. After 40 years of development, China's manufacturing technology level has reached the forefront of the world and became the only country with all kinds of manufacturing industry in the world [1]. With the "reindustrialization" and "manufacturing industry return" of developed countries in Europe and the United States, and the entry of low-cost strategy of Southeast Asian countries, China's manufacturing industry has been impacted in terms of technological progress and product export; China's manufacturing industry is facing two choices: increasing R&D investment or financial investment to avoid competition [2].

In 2015, Premier Li Keqiang put forward the concept of "building mass entrepreneurship and innovation" in the government work report. The made in China 2025 plan of the State Council points out that it will take ten years to become a manufacturing power. Innovation, R&D, transformation, and upgrading are continuously improving to enhance the competitiveness of China's manufacturing industry [3]. Therefore, we should guide and support the manufacturing industry to carry out R&D and innovation with the joint efforts of various policies and control the crowding-out effect of manufacturing financial investment on operating funds [4].

As the main body of innovation activities, the research and development behavior and economic consequences of enterprises have always been a hot topic in financial research. As the root of enterprise innovation activities, R&D investment determines innovation achievements, company performance, and enterprise value to a certain extent. Since 2000, the government has encouraged the innovation investment of enterprises by implementing many fiscal and tax policies, which has promoted the innovation investment of enterprises to increase year by year [5]. But at present, there are still some problems to be solved, such as the low level and sustainability of R&D investment. In order to improve the level of R&D investment and enhance the sustainability of R&D investment, Premier Li Keqiang deployed and

improved the accelerated depreciation policy of fixed assets in the executive meeting of the State Council in September 2014 to promote the technological transformation of enterprises and support the innovation of enterprises. In the same year, the State Administration of Taxation issued CS (2014) No.75 document. Enterprises in six industries, including biological medicine, special equipment, railway, ship, aerospace and other transportation equipment, computer communication and electronic equipment, instruments and meters, information transmission, software, and information technology services, are allowed to shorten the depreciation life or adopt an accelerated depreciation method for accounting treatment on the fixed assets purchased after January 1, 2014. Although the total amount of depreciation of fixed assets remains the same in the service life to the enterprise, the policy can be used to accrue a large amount of depreciation in the current period of purchase of fixed assets and reduce the income tax payable in the current period, making full use of the time value of money brought by deferred tax payment, so as to reduce the cost of R&D activities [6].

In summary, the policy expects to accelerate corporate equipment renewal and technological R&D innovation, expand manufacturing investment, and promote investment of corporate funds in the real economy through deferred taxation preferential forms, thereby inhibiting corporate financialization and preventing the real economy take off from reality [7]. Since the introduction of the fixed asset accelerated depreciation policy, the research on the economic consequences of relevant literature has mostly focused on the accounting treatment of individual companies [8]. The overall effectiveness of the policy after its implementation has not been systematically tested. From the perspective of practice, there are different willingness and ability to engage in R&D activities among companies in different tax rates and different regions, and the policy effect is also quite different. Therefore, this paper will evaluate the implementation effect of this policy from the perspective of tax reduction effect and the guidance of enterprise capital investment formed by tax-accelerated depreciation deduction and carry out empirical demonstration on the theoretical mechanism of its impact on enterprise financing [9].

2. Theoretical Analysis and Research Hypothesis

In theory, accelerated depreciation policy for fixed assets guides enterprises to increase investment in R&D equipment and operational fixed assets. It can not only strengthen the company's own technological advantages and enhance the competitiveness of the company but also bring tax deduction effects for accelerated depreciation to the enterprise, so as to promote the return of funds to the physical manufacturing enterprise and promote enterprise R&D and innovation [10]. This reflects the role of fiscal and taxation policies in adjusting economic structure transformation, guiding the investment of physical enterprises' stock funds, and reducing the crowding-out effect of financial investments by physical enterprises, which is the best embodiment of inhibiting the disengagement of enterprises from reality, guides the capital investment of manufacturing enterprises, and reduces the crowding-out effect of financial investment on manufacturing capital. It is the best embodiment of restraining the enterprises from getting rid of the real to the virtual [11].

However, due to the current high-yield demonstration effect of China's financial investment products, the expected growth rate of financial investment has exceeded the average growth rate of the real economy's income growth. Therefore, the adjustment effect of fiscal and tax policies may exist on R&D and innovation investment in physical enterprises. The impact may just be the icing on the cake [12].

Based on the existing literature, we can understand the impact of fixed asset accelerated depreciation policies on corporate R&D innovation and physical enterprise financialization from the following three aspects [13].

First, accelerated depreciation of fixed assets has reduced the actual cost of R&D and innovation investment to a certain extent. Structural tax reduction not only is an ex-post compensation mechanism but also has the characteristics of targeted delivery. It is more market-oriented than direct subsidies and can be more precise [14, 15]. Fixed asset depreciation tax credit, from the perspective of indirect supply of tax preference, can reduce the actual R&D cost through the time value of money, so it is widely used in developed countries [16]. The accelerated depreciation policy of fixed assets is to advance the income tax deduction, which can alleviate the impact of technology upgrading and industry competition, and avoid the tax deduction lag caused by the rapid elimination of the market. On the one hand, this early deduction forms the indirect capital supply for R&D investment; on the other hand, it forms a certain time value, thus reducing the cost of R&D investment [17].

Second, structural tax reduction policies such as accelerated depreciation of fixed assets have promoted enterprises' investment in R&D equipment, plant, and other aspects. Whether the structural tax reduction policy, especially the accelerated depreciation policy of fixed assets, has promoted the R&D investment of enterprises and whether there is a causal relationship between them have been the focus of controversy [18]. Tassey pointed out that the return brought by R&D investment has a strong recessive feature, and its spillover effect also affects the willingness of real enterprises to invest in R&D innovation, but the tax reduction policy can reduce the uncertainty of the return on R&D investment. R&D investment can reduce the concern of enterprises about investment loss and R&D cost, so as to promote the R&D innovation activities of enterprises [19]. Pottelsberghe et al. pointed out that structural tax incentives, especially depreciation policies for equipment and real estate, have a long-term effect on promoting R&D investment of enterprises. Subsequently, a large number of studies also support the structural tax incentives, especially the accelerated depreciation of fixed asset tax credit to promote the R&D investment of enterprises. Capelen et al. studied the depreciation tax reduction preferential policies of Norway in 2002 and found that the tax reduction promoted the R&D investment level of enterprises to a certain extent; Yang through the analysis of micro sample data found that manufacturing enterprises in Taiwan have higher R&D investment motivation and ratio; some

scholars have studied the reform of China's enterprise income tax and found that the R&D expense deduction and the accelerated depreciation policy of fixed assets indirectly promote the technological innovation of enterprises [20].

Third, the accelerated depreciation tax credit of fixed assets has increased the real assets of enterprises and reduced the income tax of enterprises from a long-term perspective, which makes the owners of enterprises willing to invest in fixed assets, thus reducing the allocation of financial assets, inhibiting the trend of enterprise financialization, and promoting the enterprises to get rid of the virtual investment. The financial tendency of monopoly large enterprises is obvious. Because continuous investment in the real economic leads to the increase of production capacity and the decrease of yield, it is more inclined to maintain monopoly and control scale and reduce the demand for real investment, and the surplus capital will flow into the financial field [8]. The excessive accumulation of capital and the increasingly fierce market competition make the investment opportunities in the real field less and less. The nature of profit-seeking and risk aversion of enterprises makes them tend to invest their own funds in financial products with a higher return [21]. Yao Weibao found that the competition caused by the prevalence of neoliberalism increased the output rate and labor productivity of commodities and made the profit contained in commodities fall. A large number of enterprises have invested in the financial industry in order to seek the growth of profit margin, and the financial market has become a gathering place for impatient speculators [22]. Wu Hong believes that financial investment by real enterprises is a short-term response to the decline of investment income in the field of real economy, and enterprises will eventually return to the real economy.

The profit-driven nature of capital makes enterprises pay more attention to the return of investment, but the phenomenon of tax avoidance also exists in China's private enterprises. Reduce the value-added tax and corporate income tax in the form of fixed asset investment, and obtain sustainable development plan and the ability to maintain the leading position in the R&D equipment and plant investment, reduce cash expenditure, and obtain stable cash flow [23]. It will form a virtuous circle of R&D investment, asset depreciation tax reduction, higher income tax shield, and recognition of tax relief and preferential authority, so as to further reduce taxes. Thus, while reducing the income tax expenditure, more assets and competitive advantages will be formed, and the technological content of enterprises will be upgraded to achieve higher tax preferential conditions and obtain more preferential policies [24]. Therefore, it can be inferred that Chinese enterprises have a stronger willingness to obtain the discount of depreciation and tax credit, increase the investment of R&D and innovation equipment and plant, reduce the taxable income, thus reducing the financial investment, and allocate more assets in the real economy [25].

Based on the three analysis above, the following three hypotheses are further summarized and put forward:

First of all, the original intention of the accelerated depreciation tax credit policy for fixed assets is to increase the R&D investment of enterprises and indirectly reduce the R&D investment cost of enterprises, then enhance the confidence of enterprises in R&D investment, and provide indirect capital supply support for enterprises in R&D investment. In China, six industries with strong competitiveness in science and technology are selected as the pilot.

Therefore, this paper first needs to verify whether the accelerated depreciation tax credit policy of fixed assets promotes the level of R&D investment. Therefore, we propose hypothesis 1:

H1: accelerated depreciation tax deduction of fixed assets can promote the R&D innovation investment of enterprises [26].

The second is the accelerated depreciation tax credit policy for fixed assets, which is mainly due to the investment expenditure of R&D equipment and production and operation fixed assets. To form accelerated depreciation through fixed asset investment, accelerate depreciation and generate tax credit effect again, so as to form deferred income tax. The investment in fixed asset results in accelerated depreciation, which results in tax offsetting effect, thus forming deferred income tax. That is how policy affects the enterprises' investment. Therefore, we propose hypothesis 2:

H2: accelerated depreciation tax deduction of fixed assets can guide enterprises to invest in fixed assets and form deferred income tax.

As hypotheses 1 and 2 above, if the accelerated depreciation policy of fixed assets can effectively guide the enterprises' capital investment, the capital of enterprises will be more invested in R&D equipment and operational fixed assets. Furthermore, it can reduce the investment of enterprises in financial assets and restrain the trend of enterprises' financialization. Therefore, we propose hypothesis 3:

H3: accelerated depreciation policy for fixed assets can inhibit the trend of enterprise financialization.

In this paper, variable replacement and step-by-step regression are designed to investigate the impact of fixed asset depreciation policy on various investments and to clarify the mechanism of the impact of accelerated depreciation policy of fixed assets on corporate finance [27].

3. Research Design

3.1. Sample Selection and Data Source. As mentioned above, China has implemented accelerated depreciation tax credit policies for six major industries since January 1, 2014. The accelerated depreciation policy will be implemented in 2019. Therefore, we use the data of A-share listed manufacturing enterprises in a total of 10 years from 2009 to 2018, to build a panel database.

The number of enterprises in six industries, such as transportation equipment, computer communication and electronic equipment, instruments and meters, information transmission, software, and information technology services, is constantly changing. Therefore, based on the 2009 listed companies as the sample standard, the data comes from CSMAR sources, we finally obtain 308 listed companies in six industries and 1085 samples from A-share manufacturing companies.

Based on the policy of accelerated depreciation of fixed assets, the financial inhibition effect provides us a natural experiment for this study. In order to more effectively verify the impact of accelerated depreciation and tax credit policies for fixed assets on R&D investment and financialization of enterprises, we took 2014 as post, 308 enterprises in six industries as the experimental group, and other enterprises as the control group. The PSM method is used to match the samples, and the double-difference method (DID) which is commonly used to evaluate the policy effect is used to analyze, in order to verify the research hypothesis of this paper.

In order to ensure the reliability of the research conclusion, this paper deals with the samples according to the following steps:

(1) Excluding financial companies and ST company samples

(2) Eliminate the companies with missing data

(3) Winsorize the continuous variables of all samples with 1% and 99% quantiles to eliminate the influence of outliers

Finally, 10,850 observations are obtained, and the financial data of the company are all from the CSMAR database of the GTA company.

3.2. Definition of Variables

3.2.1. Explained Variable. According to the research hypothesis in the second part of this paper, the explained variables are R&D innovation investment, enterprise fixed asset investment, and enterprise finance. In addition, in order to further verify the guiding role of tax preferences, the index of deferred income tax is added as the dependent variable.

① Explained variable 1: enterprise R&D investment (RD), calculated by the growth rate data of R&D investment amount

② Explained variable 2: fixed asset investment (face), calculated by the growth rate of fixed assets

③ Explained variable 3: financial level of enterprises (FIN), calculated by the growth rate of the proportion of financial assets in long-term assets

3.2.2. Explanatory Variable. This paper takes 2014 as the policy implementation node (post); take the six industry enterprises as the control group (treat), if the sample enterprises belong to the six industry, then treat is 1; otherwise, it is 0; in order to prevent multicollinearity, this paper uses post × treat to generate the policy processing variable DID, which is the explanatory variable of the model, to test the impact of accelerated depreciation policy of fixed assets. This paper uses R&D investment, fixed asset investment, and enterprise financialization as dependent variables to verify the impact of accelerated depreciation policy on investment. Considering the other factors of R&D investment, fixed asset investment, and financial investment, we select certain control variables to make up for the influence of other factors on the policy effect.

In terms of the control variables, we choose the enterprise scale (size) and the listing period (age) as the control variables; further considering the cash requirements of investment choice, we choose the cash holding level (cash) and asset liability ratio (Lev) as control variables to determine whether enterprises with low debt and sufficient capital are more likely to have investment behavior; thirdly, considering whether the enterprise invests in R&D and fixed assets for production and operation, which may be affected by the profitability of the enterprise, the company's gross profit margin (GPM) and return on equity (ROE) are selected as the control variables; Fourth, whether technology-based companies pay more attention to R&D investment to maintain core competitiveness, so this paper chooses enterprises high-tech properties (Htech) as the control variable; finally, select the Tobin Q value (Tobin) as a control variable, when the Tobin Q value is large, the stock price of the enterprise is higher than the asset replacement cost, and the enterprise can obtain funds to purchase low-cost assets by issuing shares; otherwise, the investment behavior of the enterprise will be limited, so the Tobin Q value of the enterprise also affects the investment choice of the enterprise to a certain extent. Once the Tobin Q value is small, the enterprise may be more conservative or choose financial assets to allocate, leading to financial enterprises. The specific definitions of each variable are shown in Table 1.

3.3. Sample Description. The sample data described by the sum function of Stata software is shown in Table 2. The data used in this paper are 1085 A-share listed companies for 10 years, with 10,850 observations. There are great differences in R&D investment, financial asset investment, and fixed asset investment among the sample enterprises. The overall average value is optimistic. The R&D investment of enterprises is growing, and the trend of financialization is weak. In addition, it is worth noting that Chinese enterprises have a very low cash holding rate and total asset growth rate, but high asset-liability ratio, and the enterprises with the highest gross profit rate and return on equity come from medicine and liquor.

3.4. Model Design. According to the research hypothesis in the second part of this paper, the regression models of R&D investment growth rate, fixed asset investment growth rate, deferred income tax, corporate finance, and accelerated depreciation policy are constructed, respectively, (1)–(4) as follows:

$$\mathrm{RD}_{it} = \alpha_0 + \alpha_1 \mathrm{DID} + \alpha_2 \mathrm{Xlist}_{it} + \varepsilon_{it}. \quad (1)$$

Model (1) investigates the impact of accelerated depreciation of fixed assets on R&D investment:

$$\mathrm{FASS}_{it} = \beta_0 + \beta_1 \mathrm{DID} + \beta_2 \mathrm{Xlist}_{it} + \epsilon_{it}. \quad (2)$$

Model (2) investigates the impact of accelerated depreciation tax credit policy on fixed asset investment:

$$\mathrm{DTax}_{it} = \gamma_0 + \gamma_1 \mathrm{DID} + \gamma_2 \mathrm{Xlist}_{it} + \tau_{it}. \quad (3)$$

Table 1: Variable code and calculation formula.

Dependent variable	RD	Growth rate of R&D expenditure
	FASS	Growth rate of fixed assets of enterprises
	DTax	Growth rate of enterprise deferred income tax
	FIN	Growth rate of financial assets in total assets
Interpreted variable	DID	Post × treat
	Post	If the observed value is 1 in 2014 and later, otherwise 0
	Treat	Treat is 1 if the company's industry is within the scope of six industries; otherwise, it is 0
	Year	Year virtual variable
Control variable	Size	Company total assets dedimensionalization
	Lev	Company's total liabilities/total assets at the end of the year
	Htech	If technology enterprise Htech = 1, else 0
	Age	Current year minus year the company was listed
	Cash	Cash and its equivalents at the beginning of the period/total assets
	ROE	Current net profit/closing net asset
	Tobin	Year-end market value/book value
	GPM	Gross profit/operating income

Table 2: Preliminary description results of China's A-share sample data.

Variable	Obs	Mean	Std. Dev.	Min	Max
Year	10,850	2013.5	2.8724	2009	2018
RD	10,850	0.2422	4.7018	-3.2568	12.6514
FIN	10,849	0.0163	5.3341	-10.1853	21.3375
DTax	10,850	2.1524	0.3287	-5.8245	9.3127
FASS	10,850	0.3056	0.0370	-3.5237	15.8352
Htech	10,850	0.1429	0.3500	0	1
Cash	10,850	0.0160	0.0246	0	1
Age	10,850	9.5000	2.8724	1	34
Lev	10,850	0.6537	0.2645	0	1
Tobin	10,850	0.4766	2.8874	0.2364	9.2
Size	10,850	.0030923	.0360048	0	1
Roe	10,850	0.0256	0.7344	0.0256	0.4225
GPM	10,850	0.1054	0.5123	0.0118	0.9425

Model (3) investigates the impact of accelerated depreciation of fixed assets on corporate deferred income tax:

$$\mathrm{FIN}_{it} = \mu_0 + \mu_1 \mathrm{DID} + \mu_2 \mathrm{Xlist}_{it} + \sigma_{it}. \quad (4)$$

Model (4) investigates the influence of accelerated depreciation tax credit policy on the financial trend of enterprises:

DID = post × treat is the processing variable of accelerated depreciation policy for fixed assets; Xlist represents the eight control variables selected in this paper.

4. Empirical Results and Analysis

4.1. The Influence of Accelerated Depreciation Policy of Fixed Assets on Investment Choice and Financialization of Enterprises. The Chinese government guides the investment of enterprises and vitalizes the real economy through tax regulation tools and implement accelerated depreciation and tax credit policies for fixed assets in six major industries. It will undoubtedly improve the enthusiasm and willingness of enterprises to increase their R&D investment by providing accelerated depreciation tax credit for the fixed asset investment of manufacturing enterprises, especially for the investment in R&D and capacity expansion, so as to increase the investment in fixed assets and R&D investment of enterprises, obtain the deferred income tax, and then guide the enterprise funds into the field of real economy, inhibit the investment of enterprises in financial assets, and then inhibit the trend of enterprise financialization.

In Table 3, models (1)–(4) are regression models without control variables, and models (5)–((7)) are regression models with control variables. The above models are, respectively, the impact of accelerated depreciation policy on R&D investment, fixed asset investment, deferred income tax, and financialization level. The regression results of the model show that the accelerated depreciation policy of fixed assets has a positive impact on R&D investment and a significant negative impact on corporate finance, whether or not the control variables include. It shows that the policy strengthens the R&D investment of enterprises and suppresses the trend of corporate financialization. Among them, accelerated depreciation of fixed assets significantly reduced the level of financing by about 19.2%, increased R&D investment by about 11.2%, and significantly increased fixed asset investment by about 17% and deferred income tax by 9%.

4.2. Inspection Based on the PSM-DID Method. In order to overcome the systematic differences in the treatment effects of depreciation policies between the six industries and other industries, we use the PSM-DID model to further test the robustness of the original hypothesis. Using the PSM-DID method, the tendency score is obtained by regression of virtual variables and control variables of industry attributes. The sample enterprise with the closest tendency score is the

Table 3: Impact of accelerated depreciation and tax credit policies for fixed assets.

	(1) RD	(2) FASS	(3) DTax	(4) FIN	(5) RD	(6) FASS	(7) DTax	(8) FIN
DID	0.241∗∗∗	0.203∗∗	0.171∗∗∗	-0.160∗∗∗	0.112∗∗∗	0.170∗∗	0.090∗∗	-0.192∗∗∗
	(0.07)	(0.02)	(0.09)	(0.03)	(0.04)	(0.02)	(0.04)	(0.05)
Size					0.157	0.281∗∗∗	0.220∗∗∗	0.218
					(0.07)	(0.09)	(0.07)	(0.05)
Lev					-0.185∗∗	-0.229∗∗	-0.142∗∗	-0.562∗∗∗
					(0.03)	(0.03)	(0.05)	(0.06)
Htech					0.152∗∗∗	0.320∗∗	0.302∗∗	0.200∗∗∗
					(0.03)	(0.03)	(0.05)	(0.04)
Age					-0.138	-0.225	-0.341	-0.221∗∗∗
					(0.07)	(0.06)	(0.04)	(0.05)
Cash					0.332∗∗∗	0.148∗∗∗	0.225∗∗∗	0.255∗∗∗
					(0.07)	(0.06)	(0.04)	(0.05)
ROE					0.128∗∗∗	0.096∗∗∗	0.242∗∗∗	0.160∗∗∗
					(0.05)	(0.03)	(0.06)	(0.07)
GPM					0.057∗	0.020∗∗	0.325	0.226
					(0.08)	(0.07)	(0.05)	(0.07)
Tobin					0.057	0.020	0.076	0.064
					(0.04)	(0.04)	(0.06)	(0.05)
Cons	-1.543∗∗∗	-2.062∗∗∗	2.526∗∗	3.722∗∗∗	-4.181∗∗	-1.254∗∗∗	1.528∗∗	5.366∗∗∗
	(0.08)	(0.06)	(0.09)	(0.04)	(0.04)	(0.06)	(0.05)	(0.07)
Obs	10850	10850	10850	10850	10850	10850	10850	10850
Samples	1085	1085	1085	1085	1085	1085	1085	1085

Note: ∗∗∗, ∗∗, and ∗ are significant, respectively, at the levels of 1%, 5%, and 10%.

control group, which is taken as the comparison object to minimize the systematic differences in the impact of accelerated depreciation policies of enterprises in different industries, so as to reduce the deviation of DID estimation. Before PSM-DID estimation, the validity of the model should be tested.

First of all, we need to test the common support hypothesis ①, that is, whether the experimental group and the control group become balanced after matching, that is to say, whether the mean value of covariates in the experimental group and the control group has significant difference after matching. If there is no significant difference, the PSM-DID method is supported. The test results of the common support hypothesis show that there are significant differences in the indicators of R&D investment, fixed asset investment, and financialization, which proves that the PSM-DID method is reasonable in this paper.

In this paper, the core matching method is used to test whether the accelerated depreciation of fixed assets is robust. Before estimation, we need to test the matching effect of the experimental group and the control group. By drawing the tendency score density function, it is observed that the probability density of the tendency score value of the experimental group and the control group after matching is close, which shows that the matching effect of this paper is better. Therefore, the feasibility and rationality of the PSM-DID method are further proved on the basis of common support hypothesis.

The results of Figures 1 and 2 show that all the treatment groups have been matched, and a total of 7488 matching samples have been obtained. Further double-difference test is carried out, and the results are shown in Table 4.

Table 4 shows that, after using the PSM-DID method, the accelerated depreciation policy of fixed assets still significantly reduces the trend of enterprise finance; it increased 21.70% of R&D investment and 24.90% of fixed asset investment and reduced 18.80% of financial investment. The result of PSM-DID estimation is still significant, and there is no significant difference between the result of PSM-DID estimation and that of previous DID estimation, which further verifies the hypothesis of this paper and the conclusion of previous DID estimation. It shows that the accelerated depreciation policy of fixed assets strengthens the investment intensity of enterprises in R&D innovation and then restrains the enterprise's financialization.

4.3. Mechanism Test. From the above empirical results, it can be seen that accelerated depreciation of fixed assets can

ps match 2 : Treatment assignment	ps match 2 : Common support		Total
	Off suppot	On support	
Untreated	281	7,488	7,769
Treated	0	3,080	3,080
Total	281	10,568	10,849

Figure 1: PSM result.

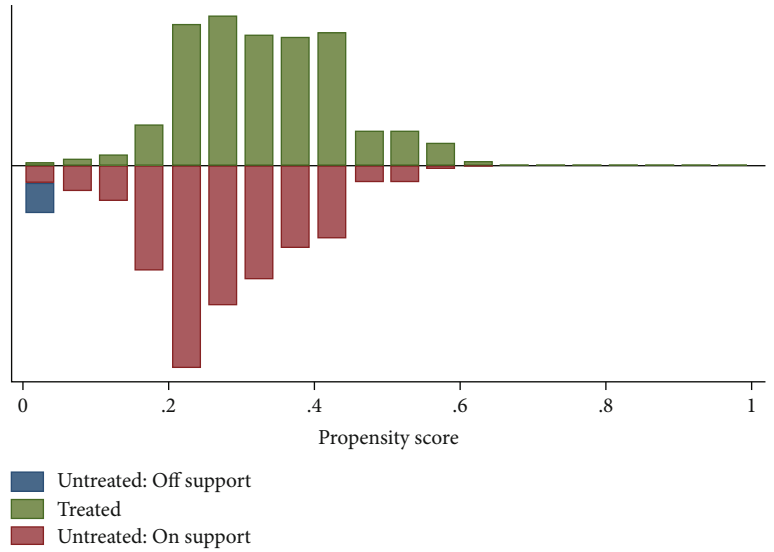

Figure 2: Matching density figure.

Table 4: Accelerated depreciation of fixed assets and PSM-DID test of corporate financialization.

PSM-DID results	Difference before policy (2014)	Difference after policy (2014)	DID result	Difference before policy	Difference after policy	DID result
Index	RD			FIN		
DID	0.385	0.522	0.137	0.125	-0.002	-0.127
Var	0.066	0.048	0.050	0.067	0.062	0.079
T	15.220	12.640	12.730	14.350	9.160	7.460
P	0.000∗∗∗	0.216	0.006∗∗∗	0.000∗∗∗	0.167	0.002∗∗∗
Index	FASS			DTax		
DID	0.185	0.253	0.068	0.208	0.166	-0.042
Var	0.231	0.165	0.150	0.158	0.089	0.038
T	13.250	10.180	11.030	11.440	9.760	5.680
P	0.004∗∗∗	0.112	0.002∗∗∗	0.024∗∗	0.205	0.033∗∗

Note: ∗, ∗∗, and ∗∗∗ are significant at the levels of 10%, 5%, and 1%, respectively.

significantly promote the R&D investment and fixed asset investment of enterprises. To a certain extent, it can also inhibit the financial and investment real estate of enterprises. However, it is still necessary to clarify the impact mechanism of accelerated depreciation policy on R&D investment and fixed asset investment. We use Baron's (1986) method for verification.

In this part, three steps are used to verify the guiding effect of accelerated depreciation policy on R&D investment and the restraining effect on corporate finance.

Table 5: Mechanism test of accelerated depreciation affecting enterprise financialization.

Dependent	DTax	FIN	FIN	RD	FIN	FIN	FASS	FIN	FIN
DID	1.282∗∗∗	-0.241∗∗∗	-0.273∗∗∗	0.134∗∗∗	-0.241∗∗∗	-0.255∗∗∗	0.055∗∗	-0.241∗∗∗	-0.360∗∗∗
	(0.12)	(0.09)	(0.03)	(0.15)	(0.09)	(0.07)	(0.11)	(0.09)	(0.07)
DTax			0.006∗∗∗						
			(0.08)						
RD						0.042∗∗∗			
						(0.03)			
FASS									0.108∗∗∗
									(0.07)
Obs	10,850	10,850	10,850	10,850	10,850	10,850	10,850	10,850	10,850
Samples	1085	1085	1085	1085	1085	1085	1085	1085	1085

Note: the first column is coefficient; ∗∗∗, ∗∗, and ∗ are significant at the level of 10%, 5%, and 1%, respectively.

(1) Regression of policy variables and financialization variables. If the coefficient is significant and negative, it indicates that the accelerated depreciation policy restrains the enterprise finance

(2) The policy variables are regressed with R&D investment, deferred income tax, and fixed asset investment, respectively; if the coefficient is significant, it shows that accelerated depreciation tax deduction has an investment guiding effect

(3) If the coefficient of policy item is not significant, or the coefficient is reduced, it is proved that the accelerated depreciation policy of fixed assets can restrain the enterprise's financialization by guiding the enterprise's investment into R&D and real assets

According to the above test steps, this paper sets up the verification model of the mechanism of depreciation tax deduction to restrain the enterprise's financialization as follows:

Verify the impact of accelerated depreciation tax credit policy on the investment decision-making direction of the enterprise:

$$\mathrm{DTax}_{it}(\mathrm{RD}_{it}, \mathrm{FASS}_{it}) = \alpha_0 + \alpha_1 \mathrm{DID} + \alpha_2 \mathrm{Xlist} + \varepsilon_{it}. \quad (5)$$

To verify the effectiveness of accelerated depreciation tax credit policy on enterprise financialization:

$$\mathrm{FIN}_{it} = \alpha_0 + \alpha_1 \mathrm{DID} + \alpha_2 \mathrm{Xlist} + \varepsilon_{it}. \quad (6)$$

Put double-difference term and three investment indexes into regression equation at the same time:

$$\mathrm{FIN}_{it} = \alpha_0 + \alpha_1 \mathrm{DID} + \alpha_2 \mathrm{DTax}_{it}(\mathrm{RD}_{it}, \mathrm{FASS}_{it}) + \alpha_3 \mathrm{Xlist} + \varepsilon_{it}. \quad (7)$$

FIN is the index of enterprise finance, which indicates the ratio of enterprise financial assets to total assets. The data comes from the CSMAR database of guotai'an, and the expected regression coefficient is negative, which indicates that the accelerated depreciation tax credit policy has restrained the enterprise finance; DID is the product of treat and time; DTax is the growth rate of enterprise's deferred income tax, and the expected regression coefficient is positive, indicating that the accelerated depreciation tax credit policy guides the enterprise to reduce tax on investment and obtain the tax reduction effect of deferred income tax assets; FASS is the growth rate of fixed asset investment of enterprises, and the expected regression coefficient is positive, indicating that enterprises are willing to invest in fixed assets. Xlist is the set of control variables.

The results are summarized in Table 4. In the first step, the regression results show that the coefficient of accelerated depreciation tax credit policy for fixed assets to R&D investment, fixed asset investment, and deferred income tax effect is significantly positive, which shows that accelerated depreciation tax credit policy for fixed assets can significantly promote the investment in fixed assets, R&D investment, and deferred income tax of enterprises, which is in line with our theoretical prediction of this policy.

The second step regression results show that there is a significant negative correlation between the accelerated depreciation tax credit policy of fixed assets and corporate financialization, which shows that the accelerated depreciation policy of fixed assets has a significant inhibitory effect on corporate finance. But what is the way and mechanism to accelerate the depreciation of fixed assets to restrain the enterprise's financialization.

The results of the third step show that, when the three investment variables and policy items are included in the regression equation at the same time, the effect of accelerated depreciation of fixed assets on corporate financialization is still significant, but the coefficient is smaller. The factors of deferred income tax increase the inhibitory effect of corporate finance by 3.2%; R&D investment increase the inhibitory effect 1.4%, and fixed asset 11.9%. Although the increasing range of the restraining effect of each factor on corporate finance is limited, it is enough to show that the three major investment factors significantly reduce the corporate financialization. Table 5 shows the test results of the mechanism of accelerated depreciation affecting corporate finance.

As mentioned above, this result confirms that the accelerated depreciation policy of fixed assets can achieve tax credit effect by guiding enterprises to invest in R&D and fixed assets, thus reducing the investment choice of financial assets and thus inhibiting the mechanism of enterprise financing.

5. Conclusion

This paper is based on 10-year panel data of 1085 listed companies in China from 2009 to 2018. Then, we use the PSM-DID method to test the effect of accelerated depreciation policy of fixed assets on R&D investment, fixed asset investment, and deferred income tax, as well as the restraining effect on corporate financialization. The conclusion of this paper shows that the accelerated depreciation policy of fixed assets significantly reduces the level of corporate financialization, and the mechanism verification shows that the accelerated depreciation tax credit policy of fixed assets has increased R&D investment, fixed asset investment, and deferred income tax, thus reducing the investment in the financial field, then restraining the trend of corporate financialization.

The conclusion of this paper is of practical significance to support the formulation and implementation of the structural tax reduction policy and to clarify the regulatory role and mechanism of the structural tax reduction policy. The policy implications of the conclusions are as follows:

(1) The fixed assets accelerated depreciation tax offsetting policy, reduced the cost of R&D investment, increased the enterprises' confidence of R&D investment, and had a positive effect on R&D investment

(2) The accelerated depreciation tax credit policy of fixed assets has a significant impact on the investment decision-making of fixed assets for R&D, production and operation, the growth of fixed assets in the main business of the enterprise, and the development of the real economy

(3) Accelerated depreciation tax credit policy for fixed assets, reduced the enterprise financial asset investment, and restrained the enterprise financialization

In general, the results of this paper clarify the goal of China's accelerated depreciation policy of fixed assets in the field of real economy to focus on R&D, promote development and adjust structure, and provide decision-making basis for the extension of the scope and time of the policy.

Data Availability

All the data are true and reliable. All data can be obtained by contacting the author.

Disclosure

Any errors within this paper remain the responsibility of the authors. The views expressed in this paper do not necessarily reflect those of the General Administration of Taxation or the Ministry of Finance of China.

Conflicts of Interest

The authors declare that they have no conflicts of interest.

Acknowledgments

This work was supported by the Social Science Planning Project of the Ministry of Education of China under grant No. 18YJA790006 and No. 18YJC630172. We thank Chen Guihua for providing data and inputs in the analysis. We also thank professor Bei Hongjun and Wang Chuner for their insightful comments on an earlier version of this paper.

References

[1] S. Shaobin, Q. Shen, and J. Zhenyuan, "Incentive effect of accelerated depreciation policy on manufacturing investment," *Tax research*, vol. 2, pp. 16–22, 2020.

[2] Y. Wu, "The effects of state R&D tax credits in stimulating private R&D expenditure: a cross-state empirical analysis," *Journal of Policy Analysis & Management*, vol. 24, no. 4, pp. 785–802, 2005.

[3] G. Tassey, "Underinvestment in public good technologies," *The Journal of Technology Transfer*, vol. 30, no. 1-2, pp. 89–113, 2004.

[4] D. Czarnitzki and P. Hanel, "Evaluating the impact of R&D tax credits on innovation: a microeconometric study on Canadian firms," *Research Policy*, vol. 40, no. 2, pp. 217–229, 2011.

[5] D. Guellec and B. Van Pottelsberghe, "The impact of public R&D expenditure on business R&D," *Economics of innovation and new technology*, vol. 12, no. 3, pp. 225–243, 2003.

[6] Å. Cappelen, A. Raknerud, and M. Rybalka, "The effects of R&D tax credits on patenting and innovations," *Research Policy*, vol. 41, no. 2, pp. 334–345, 2012.

[7] C. H. Yang, "Tax incentives and R&D activity: firm-level evidence from Taiwan," *Research Policy*, vol. 41, no. 9, pp. 1578–1588, 2012.

[8] C. Ma, "Venture capital participation, accounting information quality and enterprise investment and financing efficiency," *Accounting communication*, vol. 21, pp. 15–18, 2019.

[9] Y. Weibao, Z. Yifei, and L. Shuyi, "The incentive effect of R & D expenses plus deduction on R&D of traditional energy enterprises – empirical test from panel data of traditional energy listed enterprises in China," *Science and technology management research*, vol. 40, no. 1, pp. 25–31, 2020.

[10] H. Wu, J. Zheng, and Q. Wang, "Accelerated depreciation of fixed assets, characteristics of manufacturers and investment in enterprise innovation: an empirical study based on A-share listed companies in high-end manufacturing industry," *Tax research*, vol. 11, pp. 34–40, 2019.

[11] G. Hui, W. Xuan, L. Li, G. Wenxian, L. Chunjin, and F. Binghua, "The reseach of the face recognition system based on matlab," *Electronics World*, vol. 12, no. 7, pp. 9–13, 2018.

[12] Y. Liu, M. Ma, X. Liu, N. Xiong, A. Liu, and Y. Zhu, "Design and analysis of probing route to defense sink-hole attacks for internet of things security," *IEEE Transactions on Network Science and Engineering*, vol. 7, no. 1, pp. 356–372, 2018.

[13] F. Long, N. Xiong, A. V. Vasilakos, L. T. Yang, and F. Sun, "A sustainable heuristic QoS routing algorithm for pervasive multi-layered satellite wireless networks," *Wireless Networks*, vol. 16, no. 6, pp. 1657–1673, 2010.

[14] Y. Zhou, D. Zhang, and N. Xiong, "Post-cloud computing paradigms: a survey and comparison," *Tsinghua Science and Technology*, vol. 22, no. 6, pp. 714–732, 2017.

[15] W. Pan and C. Chai, "Measuring software stability based on complex networks in software," *Cluster Computing*, vol. 22, no. 2, pp. S2589–S2598, 2019.

[16] W. Pan and C. Chai, "Structure-aware mashup service clustering for cloud-based internet of things using genetic algorithm-based clustering algorithm," *Future Generation Computer Systems*, vol. 87, pp. 267–277, 2018.

[17] G. Yang, Q. Yang, and H. Jin, "A novel trust recommendation model for mobile social network based on user motivation," *Electronic Commerce Research*, vol. 8, no. 2, pp. 54–62, 2019.

[18] J. Qi, S. Li, Y. Gao, K. Yang, and P. Liu, "Joint optimization model for train scheduling and train stop planning with passengers distribution on railway corridors," *Journal of the Operational Research Society*, vol. 69, no. 4, pp. 556–570, 2018.

[19] C. Zhirui and J. Hanbing, "Research on scattering models of air particles with variable size distribution and shape distribution," *Applied Optics*, vol. 58, no. 13, pp. 3370–3378, 2019.

[20] L. I. Hongping, S. Zhiwu, L. I. Hao, G. Jing, W. U. Chunxia, and X. U. Xiang, "Research on estrogenicity distribution and cleanup during sewage treatment process," *Environmental Science & Technology*, vol. 39, no. 10, pp. 129–142, 2016.

[21] H. Cheng, Z. Su, N. Xiong, and Y. Xiao, "Energy-efficient node scheduling algorithms for wireless sensor networks using Markov random field model," *Information Sciences*, vol. 329, pp. 461–477, 2016.

[22] K. Granville and S. Drekic, "On a 2-class polling model with reneging and $$k_i$$ k i -limited service," *Annals of Operations Research*, vol. 274, no. 1-2, pp. 267–290, 2019.

[23] X. H. Zhang, P. Feng, J. R. Xu, L. B. Feng, and S. Qing, "Numerical research on combining flue gas recirculation sintering and fuel layered distribution sintering in the iron ore sintering process," *Energy*, vol. 192, p. 116660, 2019.

[24] L. Franceschini, D. H. Vieira, A. C. Zago, R. K. Azevedo, V. D. Abdallah, and R. J. da Silva, "New data on Myxobolus imparfinis (Cnidaria, Myxosporea): host, distribution, and ultrastructural morphology," *Parasitology research*, vol. 118, no. 6, pp. 1967–1973, 2019.

[25] Z. Lin-Lian, C. Shu-Qin, C. Mei-Ting, and Z. M. Bureau, "Research on offshore wave prediction based on wind and wave data obtained in Zhoushan in the past years," *Coastal Engineering*, vol. 37, no. 3, pp. 26–34, 2018.

[26] G. Wang, A. Gunasekaran, and E. W. T. Ngai, "Distribution network design with big data: model and analysis," *Annals of Operations Research*, vol. 270, no. 1-2, pp. 539–551, 2018.

[27] C. Li, A. Ingersoll, M. Janssen et al., "The distribution of ammonia on Jupiter from a preliminary inversion of Juno microwave radiometer data," *Geophysical Research Letters*, vol. 44, no. 11, pp. 5317–5325, 2017.

Hindawi
Wireless Communications and Mobile Computing
Volume 2020, Article ID 8845932, 10 pages
https://doi.org/10.1155/2020/8845932

Research Article

Distinguishing Hand Drawing Style Based on Multilevel Analytics Framework

Hui Xu [1,2]

[1]*School of Computer Software, College of Intelligence and Computing, Tianjin University, Tianjin 300072, China*
[2]*Henan Institute of Science and Technology, Xinxiang, Henan 453000, China*

Correspondence should be addressed to Hui Xu; huixu@tju.edu.cn

Received 29 September 2020; Revised 5 November 2020; Accepted 24 November 2020; Published 7 December 2020

Academic Editor: Hongju Cheng

Copyright © 2020 Hui Xu. This is an open access article distributed under the Creative Commons Attribution License, which permits unrestricted use, distribution, and reproduction in any medium, provided the original work is properly cited.

Hand drawing is an indispensable professional skill in the fields of environmental design, industrial design, architectural engineering, civil engineering, and other engineering design education. Students usually imitate masterpieces to practice basic skills, which is an important link for a beginner. A system for digital management requires a function for an automatic recommendation task of different brushwork skill expressions. Thus, the classification method for brushwork is to combine hand-crafted features generated by DCNN and then use the final features for input to a tree structure classification scheme. The method improvement of the other deep learning models has effectiveness in distinguishing art ontology attributes.

1. Introduction

Hand painting, the purpose of which is to continue the originality of the engineering design, is the chief step of design process. Sketching or design drawing skills and techniques are essential for successfully developing the next generation of environmental design (ED), industrial design (ID), architecture engineering (AE), and civil engineering (CE) [1]. The technical topics of sketching exercise include line weights, shading, and how to use pen and ink, colored pencils, and felt-tip markers to create architectural drawings with significant impact and aesthetic appeal. Students usually imitate masterpieces to practice basic skills, which is an important link for a beginner. And there is an emerging need to improve existing educational ways to enhance the learning experiences of students [2]. Design drawing skills in the domain of paintings have been used for painting analysis to support applications such as brush-stroke detection [3], image recommendation, and annotation and retrieval [4–7]. These efforts include the use of handmade features (artificially designed feature extraction algorithms, which mainly extract color features, texture features, and geometric features) in the early stage to perform classification method and then eventually apply deep convolutional neural network (DCNN) classification model method.

However, these two methods have not been previously combined. This research is aimed at designing a function for distinguishing brushwork of sketching skills in design and creating a recommendation result for the automatically recommended sketch exercises to students. This recommendation system is a reliable self-teaching tool that offers a fast way to find the kind of skill that students want to learn for design drawings and leads students through digital techniques to enhance presentation drawings quickly and easily, as shown in Figure 1.

This issue requires human artist experts to solve the problem of understanding a painting ontology. Meanwhile, DCNN has shown superiority in extracting such useful image features automatically. Therefore, the way is combining human understanding and deep learning methods by using two feature extraction methods in the feature extraction process (Figure 2): feature engineering that extracts certain suitable handcrafted features and feature learning that generates features using DCNN model of maturity. The method used the machine expert system which is a multilevel approach decision to classify skill styles. The results evaluated each

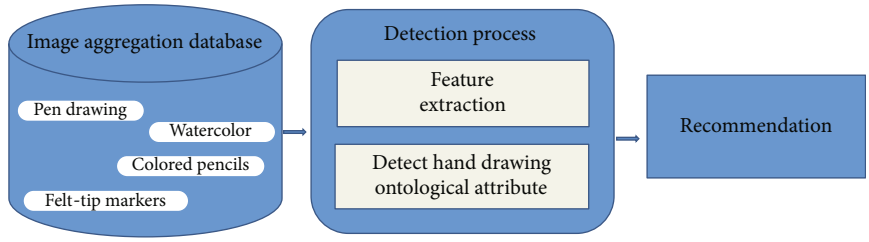

Figure 1: Overview of the system.

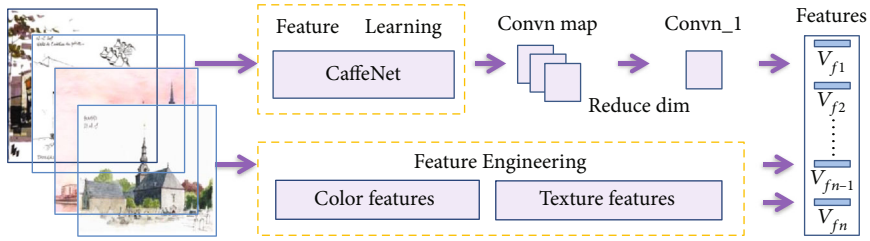

Figure 2: Feature box architecture of the proposed brushwork classification.

layer performance of classification and compared this method with the DCNN classification model. Experimental results demonstrated that the proposed method is capable of achieving state-of-the-art performance in all public benchmarks.

1.1. Related Work. Early painting digital management systems are only fit for the digital transformation of artworks and exhibitions. With the acceleration of digital conversion of paintings and designs, artists demanded something that distinguishes artworks into classes through the use of digital artwork management tools. Annotation and classification based on brushwork technologies are applied to artwork collections and retrievals. Studies on style image classification have been conducted due to artistic cognition of strong subjectivity.

Several groups have investigated about distinguishing painting styles. However, most of these efforts focused on comparing the painting styles of artists and the classifications of paintings in the genre of fine art. Hatano [8], Sablatnig et al. [9], Keren [10], and Li and Wang [11] focused on comparing the painting styles of artists. These presented methods attempted to determine the painter in question. Johnson et al. [12], Culjak et al. [13], and Arora and Elgammal [14] studied the classification task between fine art genres: Baroque, Impressionism, Cubism, Abstract, Expressionism, Realism, and Fauvism. Only few researchers focused on drawing techniques. Meanwhile, the accuracy rate of attribute-based image classification is not as high as that of content-based image classification. Jialie [15] identified the artist by comparing the painting styles of artists using a statistical model, and the identification accuracy only reached 69.7%. Hughes et al. [16] aimed to recognize visual image styles such as the moods (serene, melancholy), genres (vintage, romantic, and horror), and types of scenes (hazy, sunny). With such an approach, artistic images can be searched and ranked by style. These styles are not mutually exclusive, and per class accuracies range from 72% to 94%, representing the different attributes of style and the inaccuracy due to the classification process, which disregards the self-description of the artwork content and research on the properties of art style. The art of painting should be classified with regard to the literature on classification of art image because only art ontology is usually distinguished rather than the contents of the image.

Distinguishing and indicating the style techniques of artistic images from the image database also caught the attention of certain research teams. Yelizaveta et al. [17] were the first to become involved in style-based annotation for artistic brushwork concepts in the painting domain, and they presented a framework for the annotation of paintings with brushwork classes based on domain-specific ontologies such as brushwork technique. In addition, the authors employed low level feature analysis and serial multiexpert framework with semisupervised clustering methods to perform the annotation of brushwork patterns. Jiang et al. [18] discussed the problem of Gongbi and Xieyi expression techniques regarding traditional Chinese paintings (TCP). Feature engineering contained color histogram, color coherence vectors (CCV), and edge-size histogram. The database included 1799 Gongbi paintings, 1889 Xieyi paintings, and 5827 non-TCP images. They reported an accuracy of 91.01% based on CCV and 90.3% based on color histogram. Kammerer et al. [19] focused on stroke analysis which is the determination of the drawing technique used to draft the painting, in which the features of the paintings are extracted using the texture and contour. Lu et al. [20] proposed the characteristics of a fundamental TCP style expression technique. The training set was constructed by collecting 148 TCP images from four art expression techniques, including Xieyi, Gongbi, Goule, and Shese, and 134 non-TCP images. The authors claimed to distinguish TCP from non-TCP and further classify TCP style based on expression technique with an accuracy greater than 85%.

These methods are based on handcrafted feature extraction for painting technique style. Along with the development of deep learning study, the researchers began to expand the deep learning method to classify artistic images. Gando et al. [21] used AlexNet [22] with Batch Normalization (BN) [23] to distinguish one kind of art style and identified illustration style expression technique from photographs and 3D graphics. The accuracy of their classifier achieved 96.8%. However, distinguishing more species makes it increasingly difficult with this method. Sheng and Li [24] propose a convolutional neural network- (CNN-) based feature description, feature-weighted, and feature-prioritized algorithm to classify the artist of TCP; the accuracies range from 81% to 96%. Thus, the classification method for style used deeply learned feature to achieve overwhelmingly better classification performances.

1.2. Brushwork Factor Analysis. Based on assessing paintings of expert artists, this study identifies color and texture spatial dependence features that could be useful for classification. Table 1 shows the example images and the factor of brushwork.

1.3. Color Features

1.3.1. Statistics of Major Colors. Color is an important visual attribute for both human perception and computer vision and one of the most widely used visual features in image classification and retrieval. When light strikes the surface of an opaque medium, except for a small portion of light that is reflected on the surface of the medium, most of it enters the interior of the medium and is absorbed and scattered to produce different colors. Through feature analysis, it is concluded that sketch contains far fewer main colors than the other colored drawing techniques. Therefore, with major color features applied, it can better distinguish sketch from the other drawing techniques. The theory verifies the relationship between the spectral reflectance of an object and the pigment concentration under certain conditions. That is, the colors of the object are determined by the component of reflected light after the object selectively absorbs the incident light. If the spectral reflectance of the surfaces of the two objects is the same, then colors are essentially the same. Therefore, the reflectance in the visible range is used to represent the colors. The corresponding chromaticity information is predicted by obtaining the spectral reflectance of each point of the painting, and then, the number of colors of the entire image is obtained by statistics.

A multispectral imaging system is used to acquire the multichannel information on the image surface. The multispectral imaging system is assembled by connecting standard illumination source, M optical filters, and 3-color CCD (Charge-Coupled Device) digital camera with the computer. Assuming that the photoelectric conversion function of the multispectral acquisition system is linear, the digital response output g of the j^{th} channel can be expressed by

$$g_j = \int_{\lambda_{\min}}^{\lambda_{\max}} F_k(\lambda) E_S(\lambda) \varnothing_m(\lambda) R(\lambda) d\lambda + \varepsilon_k, \quad (1)$$

where $F_k(\lambda)$ is the spectral sensitivity function of the CCD k^{th} band, which is the relative power distribution of the light source; $\varnothing$ is the spectral transmittance of the m^{th} filter, $R(\lambda)$ is the spectral reflectance of the object, and ε_k is the camera noise. In the calculation, $\lambda_{\min} \sim \lambda_{\max}$ is generally evenly divided into N wavelength intervals, and each wavelength center interval is represented by a subscript n ($n = 1, 2, \cdots, N$). If noise is ignored, formula (1) can be expressed as

$$g_j = \sum_{n=1}^{N} F_{nk}(\lambda) E_{ns}(\lambda) R_n(\lambda) \varnothing_{nm}(\lambda). \quad (2)$$

For a pixel at a certain point on the image, the spectral reflectance $R(\lambda)$ of the point is reconstructed by its multichannel digital response output, which determines the exact color information of the point. The spectrum in the visible range of 380~780 nm is taken, and the spectral reflectance is sampled at an interval of 5 nm so that the spectral reflectance of the surface of the object consists of $N = 81$ dimensional vectors. Where g represents the digital response output of the J channel, R represents the spectral reflectance of the object, and the transformation matrix Q is calculated from $F_k(\lambda)$, $E_s(\lambda)$, and $\varnothing_m(\lambda)$.

$$R = Q^{+} g. \quad (3)$$

When a certain spectral reflectance frequency is greater than the threshold d, this color is considered to be the primary color of the painting. It is called a major color and the number is calculated to meet the conditions of the major colors. Major color count feature is extracted as shown below:

$$M = \#\{R > d\}. \quad (4)$$

1.3.2. Pixel Differences. There are two features with pixel difference. This study used a special color difference histogram method to extract a color feature. The color histogram describes the global distribution of pixels in an image. The main advantage of a color histogram is its sensitivity to variations in scale, rotation, and translation of an image. Since there are obvious differences between the marker technique and the colored pencil technique, the RGB difference histogram can better distinguish the two types of techniques. Extraction first solves the difference between each pair channel of RGB (Red, Green, Blue) and then builds the difference histogram $H(D)$. Each channel is divided into 16 color ranges, $h_{\text{R}i}$, $h_{\text{G}i}$, and $h_{\text{B}i}$ are the number of pixels of RGB channel in each color range, and d is the bin of histogram.

$$H(D) = \frac{1}{3d} \sum_{i=1}^{d} \left[\left| h_{\text{R}_i} - h_{\text{G}_i} \right| + \left| h_{\text{G}_i} - h_{\text{B}_i} \right| + \left| h_{\text{B}_i} - h_{\text{R}_i} \right| \right]. \quad (5)$$

The method defines the second feature as pixel saturation ratio. To meet people's perception of color, the color of the image space transforms from RGB to HSV (Hue, Saturation, Value) space, and each color component is uniformly

Table 1: Example images and factor of brushwork.

Tools' class	Background and characteristics
Pen and ink 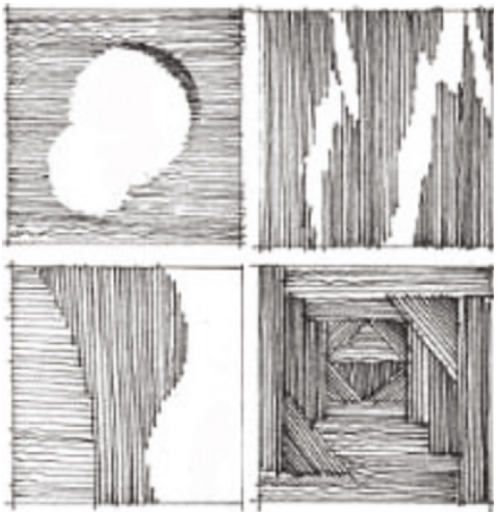	Pen and ink sketching, which is mainly composed of clear edge lines with a single color, is obviously different from other techniques. Features include edges, high gradients, intensity contrast, lightness contrast, and inhomogeneous.
Felt-tip markers 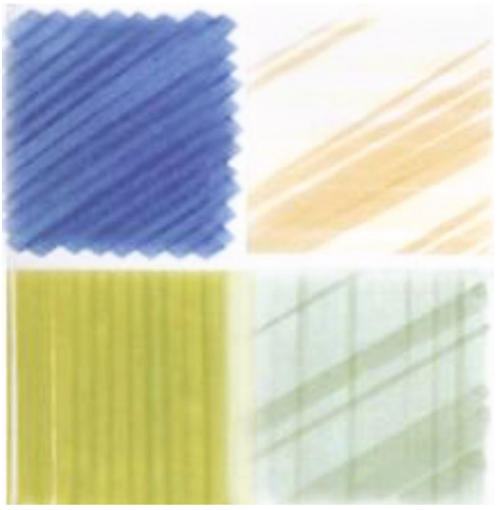	Felt-tip marker paintings have regular and gorgeous colors of thick lines, and color overlay can obtain rich color changes. Different texture, light, and shade relations require broad brushes to draw in different orders and strength. Features include rich color, high gradients, roughness, intensity, hue contrast, and directionality.
Colored pencils 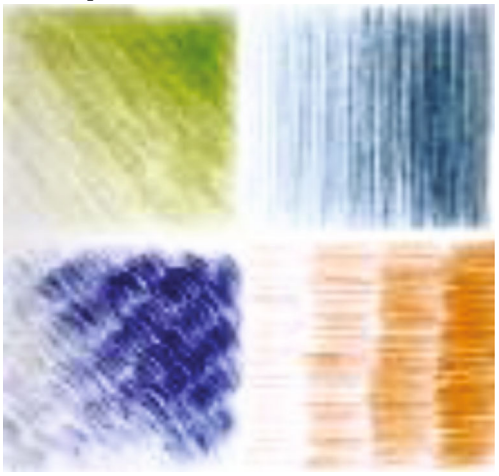	Colored pencils can create rich color change, appropriate for mixing other colors in a large area of monochromatic which can enhance the color level of the sketch. The brushwork is ethereal, delicate, and exquisite. Features include edges, high gradients, often directional, low hue contrast, and high intensity and contrast.

Table 1: Continued.

Tools' class	Background and characteristics
Watercolors 	Watercolor brushwork has a low degree of saturation and smooth texture because of the water used as medium mixed color. When overlaying colors, the underlying color will become distinct, bright, and well arranged. Features include soft gradients, low intensity, intensity contrast, hue contrast, and directionality, homogeneous, small gradients.

quantized. After completing the quantization of the HSV space, each image is divided into 256 color ranges.

The pixel saturation ratio between the number of highly saturated and unsaturated pixels in the image was introduced by Cutzu et al. [25], wherein they only used one ratio between the count in the highest bin and the lowest saturation histogram to distinguish between photographs and paintings. The adaptability and anti-interference ability of one ratio is poor in the experiment. Hence, the method selects the combination of ratio as a feature for style image saturation feature extraction. The input images are transformed to HSV color space, and then, the ratio value of intervals in each bin saturation value and minimum saturation is calculated:

$$\tau_n = \frac{P\left(S_{k_n}\right)}{P\left(S_{k_1}\right)}. \tag{6}$$

S_k is the k^{th} saturation level in the range [0, 1], S_{k_n} is the quantified saturation level, and $P(S_{k_n})$ denotes an estimate of the probability of occurrence of the ${k_n}^{\text{th}}$ saturation level. τ_n is the ratio between S_{k_n}, $n \in [2{,}256]$, levels of saturated and highly unsaturated pixels in one image.

1.4. Features Based on Texture. Brushwork can be captured by texture features. Gray level cooccurrence matrix (GLCM) [26] is an important feature to distinguish painting styles. GLCM which is based on repetitions in tone settings and represents grayscale transitions in images describes the texture spatial dependence. GLCM also makes full use of the gray level distribution properties in texture, which can produce second-order statistical characteristic and describe a certain amount of texture features based on statistical methods. Lu et al. [20] have successfully used GLCM information for TCP classification. Inspired by the above work, the method uses GLCM to extract the texture of different sketching skills with design. The grayscale range of the gray level image $f(x, y)$ is Ng and the image size $M \times N$. The GLCM is a square matrix considering

$$P(i, j, d, \theta) = \#\{(x_1, y_1), (x_2, y_2) \in M \times N \mid f(x_1, y_1) = i, f(x_2, y_2) = j\}. \tag{7}$$

means the frequency value of grayscale tones i and j, the matrix size of P is $Ng \times Ng$. Obviously, the distance d between i and j in the matrix and the direction θ can be horizontal $\theta = 0$, vertical $\theta = 90$, primary diagonal $\theta = 45$, or secondary diagonal $\theta = 135$.

2. Method

The method architecture of the proposed part-stacked feature box based on brushwork factor analysis is discussed in this section. Figure 2 illustrates that the proposed feature box architecture is decomposed into the feature engineering and feature learning processes.

The study combined handcrafted features with DCNN-generated features and then applied the integrated features. The study adopted CaffeNet [27], a slightly modified version of the standard seven-layer AlexNet architecture (Figure 3), as the feature learning structure. A unique design in the architecture is the combined handcrafted feature extraction engineering with deep learning feature extraction method.

2.1. Deeply Learned Feature. DCNN consists of layers of small computational units that process visual information hierarchically. Each layer of units is a collection of image filters and extracts a certain feature from the input image. Each layer consists of the correlations between the different filter responses over the spatial extent of the feature maps.

Upon using the existing network model for training, validating, and testing the dataset, the study found that the projections from each layer show the hierarchical nature of the features in the network, the underlying hierarchical

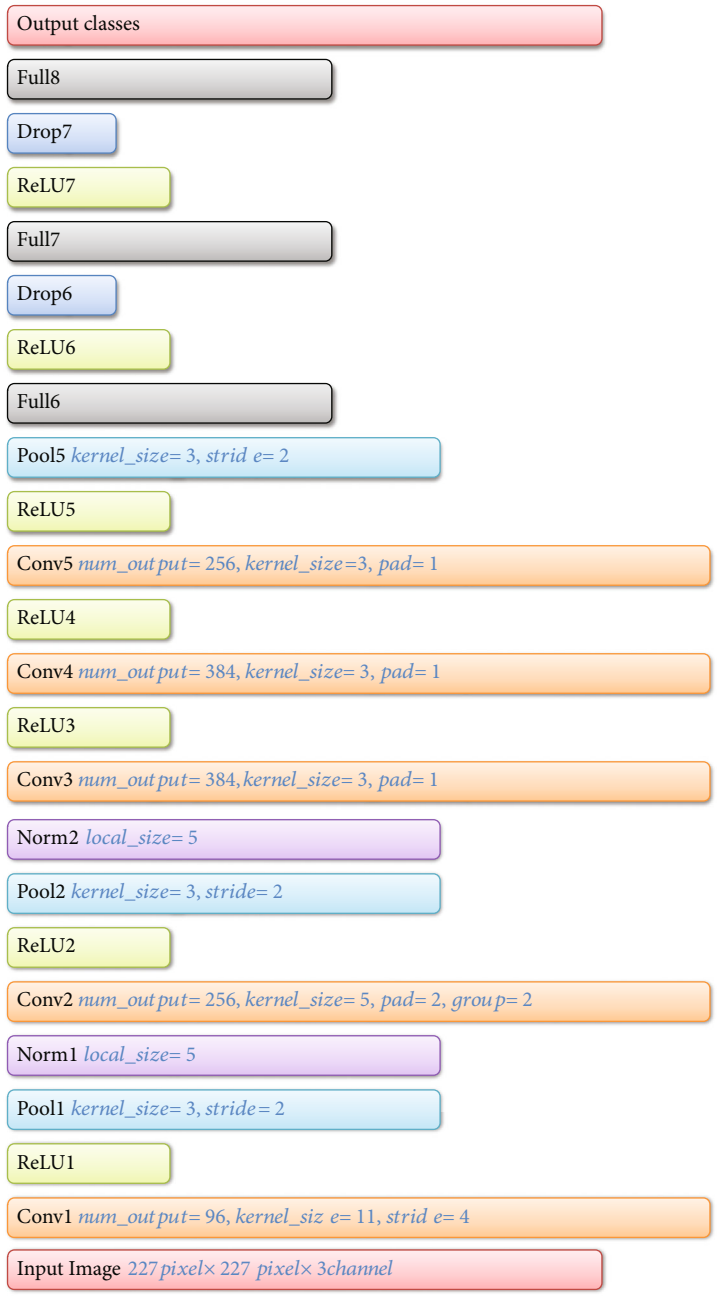

Figure 3: AlexNet architecture.

characteristic response in the image details of edge or texture, and the high hierarchical response characteristics show entire objects with a significant content. Deep networks could potentially lead to better recognition accuracy, but may also result in low efficiency. Therefore, the study chose CaffeNet framework [27] to ensure effective features for classification results and save time.

Different features are extracted from varying layers of DCNN. A given input image is represented as a set of filtered images at each processing stage in the DCNN, and the feature map of the filtered images shows the hierarchical characteristics of units per layer of the network. The study used DeconvNet to visualize the feature [28]. In ConvNet, layer 2 responds to corners and edge conjunctions. Layer 3 has more complex invariances, capturing similar textures, and layer 4 shows a significant variation.

2.2. Multiple Decision Hierarchy for Classification. Most of the early studies utilized a single classifier approach to assign labels in style image classification task. This approach is shown to be fruitful in many applications [29]. Although in-depth learning has witnessed rapid development in terms of image recognition in the past two years, relevant studies mainly focused on recognition of image content rather than painting techniques. Combining the advantages of in-depth learning in extracting image characteristics and those of

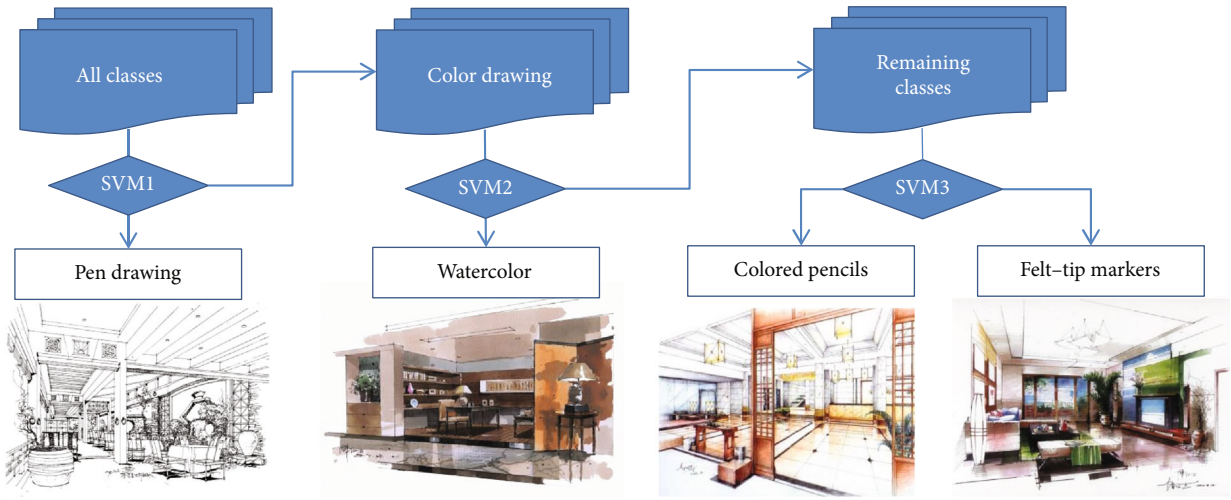

Figure 4: BT-SVM decision hierarchy.

manual artistic design extraction, the current study decided to construct a separator with a decision-making tree and SVM method and highlight the objective of recognizing the characteristics of painting techniques. SVM is easy to train and has better generalization ability. The principle is to automatically find the support vector with sound classification capability through machine learning and allow the constructed classifier to maximize the interval between different classes and gain an advantage in solving nonlinear and high-dimensional classification problems. Several studies have shown that the use of multihierarchy approaches could lead to higher accuracy as compared to single classifier approach [30, 31].

The multilevel analytics framework (MLAF) method is used to achieve multiclass classification by combining several Support Vector Machine (SVM) [32] subclassifiers into a binary tree structure. The method assigns training samples of the pen drawing class (the most recognizable) to the positive category and training samples of the rest of the classes to the negative category and then trains the first subclassifier SVM. Similarly, the multihierarchy method assigns training samples of watercolor class to the positive category and the rest of the training samples to the negative category and then trains the second subclassifier SVM. Each subclass is divided into two. The decision process consecutively traverses the tree in top-bottom sequential fashion. By analogy, four categories can produce three SVM subclassifiers. Each subclassifier is a binary classification problem. At the classification stage, the unknown samples are loaded through the first subclassifier SVM, and then, classification is performed until the judge value of a subclassifier is positive.

With the multilevel approach, the study progressively reduces the subset of classes to which a pattern might belong at each level of the decision hierarchy. The classification process of 4 classes is illustrated in Figure 4.

2.3. Experiments

2.3.1. Datasets. The image dataset contains four categories of drawing technique styles, and the project collected many teaching cases from universities such as architecture and interior design of drawing. In addition, for more effective results, experiments obtained data from online communities. Finally, datasets collected 1000 original design sketches. After cropping, the sketches formed a total of 4000 sketches in the drawing image dataset. The size of each image item in the dataset is 256×256. Experiments used 60% of data items in the dataset for training and the remaining for evaluating performance.

Table 2: Results for all feature evaluation.

Feature configuration	Hierarchy	Accuracy
GLCM	SVM1	88.21%
Major color count	SVM1	91.43%
Color difference histogram	SVM1	92.18%
Feature box	SVM1	97.94%
GLCM	SVM2	81.25%
Color histogram (RGB)	SVM2	79.20%
Feature box	SVM2	83.64%
GLCM	SVM3	78.15%
Saturation ratio	SVM3	72.70%
Color histogram (RGB)	SVM3	76.23%
Feature box	SVM3	84.02%

2.3.2. Feature Extracted. The study evaluated the method in the dataset and built the structure with two streams (Figure 2). The study concatenated the handcrafted features extracted from the feature engineering process with the features learned by using the CaffeNet model to generate the features. Deac et al. [33] concluded that the texture information related to brush strokes is the most discriminating feature. According to the characteristics of the brush strokes, the study chose the 3rd ConvNet (conv3) and 4th ConvNet (conv4) layers as the feature source of extracted hierarchical. A total of 384 different units are convolved in the conv3 layer and the conv4 layer. To reduce feature amount of calculation, the method was initialized through principal component

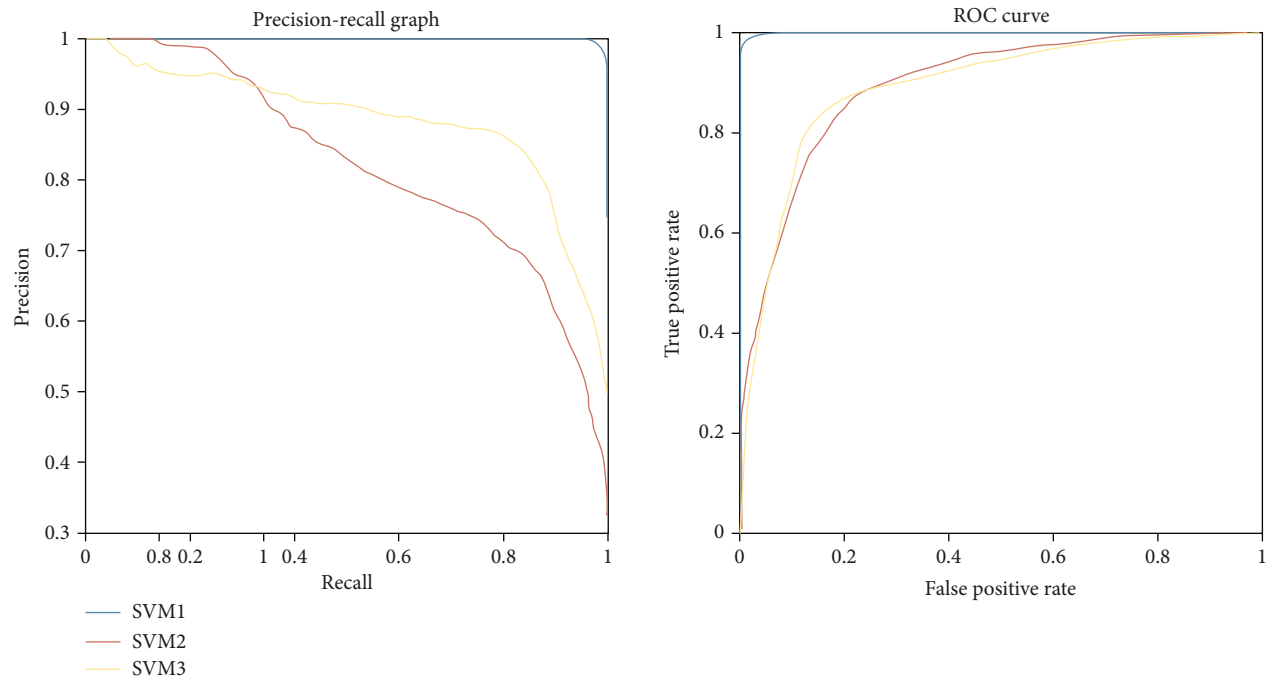

Figure 5: ROC space and PR space.

analysis. Each image projected the 384-dimensional ConvNet layer output to a one-dimensional feature map and used sequential forward selection (SFS) [34] to choose the feature subset. conv3_1 and conv4_1 were identical to a low-rank projection of the model output.

2.3.3. Normalization of Sample Characteristics. Data normalization [35] is important in traditional mode classification and can even influence the entire system. The study used probability distribution normalization method to normalize the probability distribution of characteristic data within [0, 1]. The normalization formula is shown in

$$y = \frac{x - x_{\min}}{x_{\max} - x_{\min}}, \tag{8}$$

where $x, y \in R^n$, $x_{\min} = \min(x)$, $x_{\max} = \max(x)$. The result is the original data within [0, 1] and then applied to the BT-SVM hierarchical classifier to train and evaluate.

3. Results and Discussions

The experimental measurements evaluated the classification performance of the method. The results were measured against precision, recall, and accuracy according to Equations (9) and (10). Each of the results is presented below.

$$\text{Precision} = \frac{\text{number of relevant images retrieved}}{\text{number of retrieved images}}, \tag{9}$$

$$\text{Recall} = \frac{\text{number of relevant images retrieved}}{\text{total number of relevant images in search space}}. \tag{10}$$

Table 2 shows the classification accuracy in different decision hierarchies. As a comparison, results also tested the performance by using single handcrafted features. In the decision hierarchy, SVM1 and GLCM performed worse than other methods, indicating that traditional texture feature is poorer than color feature in distinguishing pen and ink brushwork. Using the main color feature can produce slightly better results. The study also used a special color difference histogram method to extract color feature. Unlike other categories, the color difference histogram values of pen brushwork tend to be zero. In the feature learning section, the study used the conv3_1 feature from the CaffeNet DCNN model and the ConvNet layer 3 feature map. Although the color feature produced obvious results in the first decision hierarchy, its classification accuracy is still lower than this method.

Figure 5 shows that the proposed method combining ConvNet feature map with feature engineering produces an ideal result. SVM1 has the highest response values, in line with the people's cognition that pen-and-ink brushwork is easy to identify. In the decision hierarchy SVM2, the experiments evaluated the effectiveness of the texture feature and color feature for distinguishing watercolor brushwork image from other types. In this hierarchy, the results showed that the accuracy of texture feature is better than that of color feature. In this hierarchy feature learning section, the study chose two ConvNet feature maps: ConvNet layer 3 and layer 4. After the dimension reduced processing, the method obtained feature vectors, conv3_1 and conv4_1. As shown in the decision hierarchy SVM3, the saturation ratio feature was deemed useful for classification between the pencil skill and felt-tip markers which achieved an accuracy of approximately 72.7%, and GLCM produced better results than the RGB histogram. In this hierarchy feature learning section,

Table 3: Results for all models on the sketch image dataset.

Method	Val time cost(s)	Top-1 (Val)
VGG	79.60	77.39%
AlexNet	36.02	72.74%
AlexNet-OWT	38.48	72.11%
AlexNet-OWT-BN	37.68	75.33%
MLAF	33.52	86.53%

the method chose feature vector extraction from ConvNet layer 4 feature map. Table 2 illustrates that the method achieves better classification accuracy in each decision hierarchy.

To ensure the consistency of correlation data, the data sample was not used to test the experiment method of different painting technique classifications (i.e., recognizing the author of the painting and distinguishing illustrations and photos or different types of TCP), but selected several classic in-depth learning methods such as AlexNet, AlexNet-OWT [36], AlexNet-OWT-BN, and VGG16. Experiments applied the same data sample to conduct comparative experiment and used stochastic gradient descent (SGD) with a batch size of 64 examples, momentum of 0.9, and weight decay of 0.0005.

Table 3 summarizes the validation time and identification accuracy of the DCNN model and the method with the dataset. Notably, the effectiveness of this method is superior over other DCNN model frameworks. Apparently, the DCNN model has the advantage on image content analysis, but brushwork technique classification task disregards the content and attaches importance to ontology. Applying the feature map of deep learning to the traditional classifier can undeniably improve the classification effect. This method has its novelty and effectiveness in distinguishing art ontology attributes.

4. Conclusion

The studies reported a classification framework for brushwork classification which is useful in digital management system of engineering design education. This function classifies the ontological attribute of art according to the hand drawing techniques of engineering design image, abandons the interference of the image content to the classification, and effectively extends the style-based image retrieval function of the management system. To perform categorization, the study combined feature engineering methods with feature learning methods to extract features and used the BT-SVM classifier. This framework is the most effective way of constructing dataset as it has a high accuracy and reasonable timing for implementing the brushwork recommendation in ED, AE, and CE. The proposed method is applicable to the popular drawing techniques in modern design art. To verify the effective expansibility of this method, the study tested the images of several main design categories, e.g., painting, clothing design, and stage design works; the results of which are consistent with the performance of environmental works.

The framework also has benefits for learning the characteristics of brushwork ontology. It enables students to quickly obtain lots of the same style when they independently copy and practice the expression of brushwork and improves the accuracy of students' works of the expression. At the same time, it is more convenient and fast for teachers to manage students' works and centralizes the hand-painted works of the same expression type.

Data Availability

The data used to support the findings of this study are included in the article.

Conflicts of Interest

The author declares no conflicts of interest.

References

[1] S. Travis, *Sketching for Architecture and Interior Design*, Laurence King, 2015.

[2] X. Wang and Z. Bi, "New cad/cam course framework in digital manufacturing," *Computer Applications in Engineering Education*, vol. 27, no. 1, pp. 128–144, 2019.

[3] T. Melzer, P. Kammerer, and E. Zolda, "Stroke detection of brush strokes in portrait miniatures using a semi-parametric and a model based approach," in *Proceedings. Fourteenth International Conference on Pattern Recognition (Cat. No.98EX170)*, pp. 474–476, Brisbane, Queensland, Australia, 1998.

[4] M. Yelizaveta, C. Tat-Seng, and A. Irina, "Analysis and retrieval of paintings using artistic color concepts," in *2005 IEEE International Conference on Multimedia and Expo*, pp. 1246–1249, Amsterdam, Netherlands, 2005.

[5] R. M. Maxwell, L. E. Condon, and S. J. Kollet, "A high-resolution simulation of groundwater and surface water over most of the continental US with the integrated hydrologic model ParFlow v3," *Geoscientific Model Development*, vol. 8, no. 3, pp. 923–937, 2015.

[6] S. Karayev, A. Hertzmann, H. Winnemoeller, A. Agarwala, and T. Darrell, *Recognizing Image Style*, CoRR, 2013.

[7] J. R. Zeng, C. C. Cheng, A. W. Lee, P. L. Wei, and J. K. Chen, "Visualization platform of one-dimensional gratings of tethered polyvinyltetrazole brushes on silicon surfaces for sensing of Cr(III)," *Microchimica Acta*, vol. 184, no. 8, pp. 2723–2730, 2017.

[8] H. Hatano, "Image processing and database system in the national museum of western art; an integrated system for art research," *International Journal of Libraries*, vol. 30, no. 3, pp. 259–267, 1996.

[9] R. Sablatnig, P. Kammerer, and E. Zolda, "Hierarchical classification of paintings using face- and brush stroke models," in *Proceedings. Fourteenth International Conference on Pattern Recognition (Cat. No.98EX170)*, vol. 1, pp. 172–174, Brisbane, Queensland, Australia, August 1998.

[10] D. Keren, "Painter identification using local features and naive Bayes," in *Object recognition supported by user interaction for service robots*, vol. 2, pp. 474–477, Quebec City, Quebec, Canada, 2002.

[11] J. Li and J. Z. Wang, "Studying digital imagery of ancient paintings by mixtures of stochastic models," *IEEE Transactions on Image Processing*, vol. 13, no. 3, pp. 340–353, 2004.

[12] C. R. Johnson, E. Hendriks, and I. J. Berezhnoy, *Classifying Paintings by Artistic Genre: An Analysis of Features*, MMSP, 2009.

[13] M. Culjak, B. Mikus, K. Jez, and S. Hadjic, *Classification of Art Paintings by Genre*, MIPRO, 2011.

[14] R. S. Arora and A. Elgammal, *Towards Automated Classification of Fine-Art Painting Style: A Comparative Study*, ICPR, 2012.

[15] S. Jialie, "Stochastic modeling western paintings for effective classification," *Pattern Recognition*, vol. 42, no. 2, pp. 293–301, 2009.

[16] S. M. Hughes, I. Daubechies, and J. Li, "Image processing for artist identification," *IEEE Signal Processing Magazine*, vol. 25, no. 4, pp. 37–48, 2008.

[17] M. Yelizaveta, C. Tat-Seng, and J. Ramesh, "Semi-supervised annotation of brushwork in paintings domain using serial combinations of multiple experts," in *Proceedings of the 14th annual ACM international conference on Multimedia - MULTIMEDIA '06*, pp. 529–538, USA, 2006.

[18] S. Jiang, Q. Huang, Q. Ye, and W. Gao, "An effective method to detect and categorize digitized traditional Chinese paintings," *Pattern Recognition Letters*, vol. 27, no. 7, pp. 734–746, 2006.

[19] P. Kammerer, M. Lettner, E. Zolda, and R. Sablatnig, "Identification of drawing tools by classification of textural and boundary features of strokes," *Pattern Recognition Letters*, vol. 28, no. 6, pp. 710–718, 2007.

[20] G. Lu, Z. Gao, D. Qin, X. Zhao, and M. Liu, "Content-based identifying and classifying traditional Chinese painting images," in *2008 Congress on Image and Signal Processing*, vol. 4, pp. 570–574, Sanya, Hainan, China, 2008.

[21] G. Gando, T. Yamada, H. Sato, S. Oyama, and M. Kurihara, "Fine-tuning deep convolutional neural networks for distinguishing illustrations from photographs," *Expert Systems with Applications*, vol. 66, pp. 295–301, 2016.

[22] A. Krizhevsky, I. Sutskever, and G. Hinton, "Imagenet classification with deep convolutional neural networks," *Advances in Neural Information Processing Systems*, vol. 25, pp. 1097–1105, 2012.

[23] C. Szegedy, W. Liu, Y. Jia, and P. Sermanet, *Going Deeper with Convolutions*, CoRR, 2014.

[24] J. Sheng and Y. Li, "Classification of traditional Chinese paintings using a modified embedding algorithm," *Journal of Electronic Imaging*, vol. 28, no. 2, article 023013, 2019.

[25] F. Cutzu, R. Hammoud, and A. Leykin, "Estimating the photorealism of images: distinguishing paintings from photographs," in *2003 IEEE Computer Society Conference on Computer Vision and Pattern Recognition, 2003. Proceedings*no. 2, pp. 305–312, Madison, WI, USA, 2003.

[26] R. M. Haralick, "Statistical and structural approaches to texture," *Proceedings of the IEEE*, vol. 67, no. 5, pp. 786–804, 1979.

[27] Y. Jia, E. Shelhamer, J. Donahue, and S. Karayev, "Caffe: convolutional architecture for fast feature embedding," 2014, https://arxiv.org/abs/1408.5093.

[28] M. Zeiler and R. Fergus, "Visualizing and understanding convolutional networks," CoRR 2013, 2014.

[29] P. Pudil, J. Novovicova, S. Blaha, and J. Kittle, "Multistage pattern recognition with reject option," in *Proceedings., 11th IAPR International Conference on Pattern Recognition. Vol.II. Conference B: Pattern Recognition Methodology and Systems*, pp. 92–95, The Hague, Netherlands, 1992.

[30] L. Sun, S. Fu, and F. Wang, "Decision tree SVM model with Fisher feature selection for speech emotion recognition," *EURASIP Journal on Audio, Speech, and Music Processing*, no. 1, pp. 1–14, 2019.

[31] X. Yang, Q. Yu, L. He, and T. Guo, "The one-against-all partition based binary-tree support vector machine algorithms for multi-class classification," *Neurocomputing*, vol. 113, pp. 1–7, 2013.

[32] C. Cortes and V. Vapnik, "Support-vector networks," *Machine Learning*, vol. 20, no. 3, pp. 273–297, 1995.

[33] A. Deac, J. Lubbe, and E. Backer, "Feature selection for paintings classification by optimal tree pruning," in *MRCS, Berlin, Heidelberg, 2006, MRCS'06*, pp. 354–361, Springer-Verlag, 2006.

[34] S. Colak and C. Isik, "Feature subset selection for blood pressure classification using orthogonal forward selection," in *2003 IEEE 29th Annual Proceedings of Bioengineering Conference*, pp. 122-123, Newark, NJ, USA, 2003.

[35] H. Cheng, Z. Xie, L. Wu, Z. Yu, and R. Li, "Data prediction model in wireless sensor networks based on bidirectional LSTM," *EURASIP Journal on Wireless Communications and Networking*, vol. 2019, no. 1, 2019.

[36] A. Krizhevsky, *One Weird Trick for Parallelizing Convolutional Neural Networks*, CoRR, 2014.

Hindawi
Wireless Communications and Mobile Computing
Volume 2020, Article ID 8838617, 12 pages
https://doi.org/10.1155/2020/8838617

Research Article

Research on 3D International River Visualization Simulation Based on Human-Computer Interaction

Shuanhu Li,[1] Jun Yang ,[2] and Ziwen Zhang[3]

[1]*College of Science, Inner Mongolia University of Technology, Hohhot 010051, China*
[2]*Road and Bridge College, Chongqing Transportation Vocational College, Chongqing 402247, China*
[3]*School of Aviation Engineering, Guangzhou Maritime University, Guangzhou 510725, China*

Correspondence should be addressed to Jun Yang; yangjunjun@cqjy.edu.cn

Received 14 September 2020; Revised 6 October 2020; Accepted 13 November 2020; Published 7 December 2020

Academic Editor: Hongju Cheng

Copyright © 2020 Shuanhu Li et al. This is an open access article distributed under the Creative Commons Attribution License, which permits unrestricted use, distribution, and reproduction in any medium, provided the original work is properly cited.

With the development of digitalization in various fields, the water conservancy field is gradually developing digital three-dimensional visualization research to promote the development of digital watershed construction. This paper deeply analyzes and discusses the theory and application of three-dimensional visualization of river water scenes and realizes an interactive visual simulation system based on virtual reality technology, which simulates simulation and operation management, which can greatly accelerate the data. The processing speed makes the huge data be effectively utilized to provide visual interaction means for numerical simulation and data analysis, improve the efficiency of numerical calculation, and realize human-computer interaction communication, so that people can observe the phenomena and laws that are difficult to observe by traditional methods. The rationality of the mathematical model is analyzed for effectiveness.

1. Introduction

With the development of digitalization in various fields, the water conservancy field is gradually developing digital three-dimensional visualization research to promote the development of digital watershed construction [1, 2]. The overall framework structure of digital watershed research is usually divided into three layers, the digital watershed visual basic information platform foundation layer, the digital watershed professional application system thematic layer, and the digital watershed integrated management and decision system integration layer [3, 4]. The simulation of watershed 3D visualization simulation is the basis of constructing digital watershed visualization information platform. The key part of 3D visualization simulation system is the establishment of watershed professional model in the basin and the simulation of terrain virtual scene [5, 6]. There are many natural phenomena in the basin, and flooding is one of the most frequent phenomena. Floods in history often cause great disasters to human beings. To realize the prevention and control of flood disasters, it is important to study the laws of flood movement, master the habits of floods, manage flood disaster risks, and adjust the relationship between people and water [7, 8]. At present, the remediation of floods in the basin has gradually changed from flood control to flood prevention and mitigation, water resource protection, improvement of ecological environment, and ecological form in the past. This requires an in-depth understanding of the flood evolution law of the basin and the flood submersion process to perform simulations. The dynamic simulation of the digital watershed law can simulate the change process after the flood is introduced into the watershed and the three-dimensional visual display of the flooding state, analyze and study the flood phenomenon and the law, reproduce and predict the different situations of flood submerging by changing the model calculation parameters, and provide decision support for flood resource utilization and watershed ecological environment management research [9].

Visualization of 3D spatial information is a key technology to be solved in digital watersheds, and it is very important for digital management of river basins. Currently widely used in the field of water conservancy is a technology-based two-

dimensional visualization platform [10]. Although it is mature in terms of technology and function, there are many defects that cannot be overcome by expressing the actual three-dimensional space in two dimensions. In the study of river basin comprehensive information management and water flow movement law, the trend of digitization of various types of information becomes more and more obvious. Faced with a large amount of complicated data, how to falsify the truth and discover the changing laws of the physical processes represented by the data will be studied in the field of water conservancy [11, 12]. As the most intuitive and quick way to obtain information, 3D visualization has unique advantages in information expression. Therefore, it is necessary to study the more perfect 3D visualization simulation system, from 3D visualization, numerical simulation, data information acquisition, etc., and improve the operation level of the basin system. Because GIS can operate, analyze, simulate, and display the spatial data of the basin quickly, accurately, and comprehensively, the mathematical model of hydraulics can be used to calculate the evolution process of river water in the basin and the various locations and time periods within the basin. The water level, flow velocity, submerged area, volume of the river water, etc. will be combined with the hydraulic model to carry out research on the digital watershed 3D visualization simulation system and comprehensively process various information in the basin, so that the decision-makers have a global and clear awareness that helps decision-makers achieve scientific decision-making in planning and management [13].

The construction of digital watershed characterized by digitization, network, and informatization is an inevitable trend of the development of water conservancy informatization and an important way to realize the development of watershed management and analysis to informatization. Research on digital watersheds has received more and more attention from everyone, but many engineering examples are still in the stage of exploration and research. The digital watershed is a large and complex system engineering, which involves many high-tech fields. This requires close cooperation from multiple disciplines and adopts unified planning, step-by-step implementation, and key breakthrough strategies. The watershed 3D visualization simulation system is a computer simulation system for watershed roaming, program demonstration, engineering operation simulation, etc., including 3D visualization, informatization, simulation, and other functions, including computer graphics, database, watershed mathematical model, and software engineering. The field of research belongs to the category of "digital watershed" research [14].

2. 3D Visualization Simulation Technologies

The three-dimensional visual simulation of watershed is an important part of constructing the basic information platform of digital watershed visualization, and it is the foundation of digital watershed construction. With the support of the data integration platform [15], a three-dimensional virtual visualization simulation system for specific applications can be formed through various water conservancy professional models, which can realize comprehensive processing of various information in the basin.

2.1. Three-Dimensional Theoretical Technique. Three-dimensional display research has become one of the hotspots in the field of computer graphics. Three-dimensional animation technology combined with computer video and audio technology can better simulate simulation scenes, three-dimensional flight simulation, and dynamic monitoring, and the development of three-dimensional Web technology makes the three-dimensional landscape more realistic, intuitive, and vivid [16].

The starting point of 3D stereoscopic display is to use 3D stereoscopic technology and computer simulation technology to transform the real world 3D coordinates into computer coordinates, through optical and electronic processing, to imitate the real world and display on the screen [17, 18]. 3D technology is widely used in resource environment model, terrain simulation, CAD-aided design, film and television special effects, advertising design, etc. [19]. It has the advantages of high degree of visualization, flexible expression, dynamic and realistic feeling, and convenient data updating. It can also be applied to government-assisted decision-making, flood control and disaster mitigation, topographic survey and field operation design, hydropower, construction engineering planning and site selection, environmental assessment, urban and community planning and design, housing decoration design, tourist attraction planning, medicine, biology, atmosphere, and military [20]. With the development of computer and graphics and image processing technology, digital product 3D has become a major trend in today's information products [21].

3D simulation technology is actually a part of virtual reality technology. 3D digital technology is often closely connected with virtual reality technology. Dynamic, real-time display system, high-speed computer processing, and intelligent interactive multimedia technology are the key to 3D visualization simulation [22]. Technology is also the key to virtual reality technology [23]. In addition to the following key technologies are the following:

(1) Good 3D data model and data structure

The three-dimensional spatial data model is about the concept and method of three-dimensional spatial data organization. It reflects the interrelationship between spatial entities and entities in the real world. The understanding and research of three-dimensional data models and data structures largely determine the success or failure of development and application of the three-dimensional technology. Due to the huge and complex three-dimensional data, the three-dimensional data model has not yet reached consensus [24].

(2) Extraction of 3D geometric feature data

The construction of 3D models requires true 3D spatial data (including planar position, elevation, or height data) and real image data (including the texture of the side of the building). How to obtain these data has become a difficult point, in addition to traditional manual internal and external surveys and

simple computer processing, using satellite remote sensing, aerial telemetry, aerial ground photography, ground laser scanners and GPS, and synthetic aperture radar (SAR) technology. Getting data is the current trend of development [25].

2.2. 3D Visualization Simulation Technologies

2.2.1. Overview of Scientific Computing Visualization. Developed countries began to study the emerging research field of scientific visualization in the late 1980s. It can effectively produce accurate data. The essence is to track and analyze the simulation process through graphics and image processing. Shown on the above, the interactive processing method closely integrates the graphic image processing understanding technology and the human-computer interaction technology and finally produces complex multidimensional data image graphics [26].

At present, the field of scientific computing visualization research mainly focuses on the research of computing environment, the research of display equipment in virtual environment, and the research of visualization technology of scientific computing.

(1) Computational environment research, in high-end computing environments, distributed storage of massively parallel computers, shared internal storage symmetric multiprocessors, and distributed shared internal storage of multiple processors have emerged; at the same time, at workstations and on the low-end side of PCs, multiprocessor architecture and parallel processing functions have also emerged to improve the quality and efficiency of scientific computing

(2) Research on virtual environment display devices develops wall-type large-screen displays suitable for true three-dimensional display and cave-type display devices with immersive features, providing methods and means for generating and displaying huge amounts of data

(3) There are two main types of scientific computing visualization technologies: one is the study of various application models, and the other is the visualization implementation technology. The research of various application models is based on the simulation and design application model, and the interactive solution of various problems is realized by visual insight. The data of different disciplines such as medicine, geoscience, meteorology, physics, and biological science are processed as graphical information that human vision can intuitively accept; in the research of visualization technology, distributed, collaborative, and immersive technologies have become the mainstream research direction

2.2.2. Visual Rendering Technology. Visual rendering technology, including image processing technology, provides underlying support for 3D reconstruction of spatial data. According to different drawing methods, it can be divided into two categories: one is based on face-based drawing method, and the other is based on the method of volume data drawing. The most basic theory of three-dimensional object shape is that it can provide three-dimensional object shape complete information surface rendering technology. According to its specific contour, it can be divided into two types: one is the boundary contour representation, and the other is the surface representation.

Surface reconstruction was first proposed in 1975, mainly in the tomographic image, by manually or computer-automatically dividing the target contour, and then combining the contours of each fault to represent the boundary of the object of interest. The method is simple, and the amount of data is small. In 1977, the science of using the planar contour triangle algorithm was proposed based on various contour images. Surface fitting uses a triangular outline. This is the surface-oriented approach, which reconstructs the entity by constructing a combined shape of the solid surface. The problem of three-dimensional reconstruction of the CT tomographic image sequence proposed in 1983 was proposed by Xu, who proposed adding a constraint condition to the sum of the curvatures at each contour point, and the minimum curvature represents an interpolation surface. In 1987, Lorensen proposed the "Marching Cube" algorithm, which is a surface technique, which is based on voxel-based surface reconstruction. In 1989, Lin used the B-spline interpolation reconstruction algorithm from the contour and obtained an overall smooth plane or surface. These two methods are surface-oriented rendering methods. In 1999, Zhao Haifeng and others proposed using an octal tree to quickly calculate a series of tomographic images.

Volume rendering technology is computationally intensive and fast and relies on the absorption of image processing, computer vision, and computer graphics. The basic principle is to project color, opacity, etc. into cloud-like substances and then pass light and these substances. The interaction describes the resulting image.

(1) *The Difference from Traditional Computer Graphics*: in terms of performance, the volume rendering method is a complete representation of the three-dimensional voxel on the object, and the rendering technique can cover all the information; from the performance content, the difference is mainly reflected in the representation object. The model is different, and the volume rendering is mainly to express a limited number of discrete sampling points, while the traditional computer graphics is a description of the continuous geometric model, which makes them the processing, operation, transformation, analysis, and implementation methods of the object model very different.

(2) *Source and Organization of Data*: there are three main sources, including measurements (such as medical computed tomography and MRI imaging), operations (such as fluid dynamics and finite element analysis), and voxel element of geometric entities. These data can be mapped in the voxel set of the three-dimensional space grid unit. The structure of the three-dimensional space grid determines the basic shape of the voxel and the spatial relationship between the voxels, which determines the form of the volume data. The structure of the grid mainly includes Cartesian grid, regular grid, linear grid, curved grid, block structure grid, unstructured grid, and scattered data. *Drawing Method*: mainly includes

the image sequence drawing method represented by ray casting method, the footstep method (footprint or splatting) as the representative object body drawing method, and the shear-mechanism (shear-warp). The three types of hybrid rendering methods are applicable to multiple observation angles.

(3) *Illumination Model*: including the optical properties of the light source and the substance, wherein the light source model includes the type of light source (ambient light, radiant light, diffused light, specular light, etc.), intensity, position, and color; the optical properties of the substance include properties such as reflectivity, refractive index, opacity, and diffusion determined by the material. They combine and work together to complete the entire illumination model.

At present, many scholars in China have conducted in-depth research and comparison on volume rendering methods and have done a lot of practical work in medicine, graphics, geosciences, and meteorology.

3. 3D River Water Models

The development of this system is based on a tributary of a main canal. To maximize the versatility, operability, and demonstration of the system, it is assumed that the tributary has a total of three sections, two sections of open channels plus a landscape water body, and the open channel adopts a trapezoidal section, and the landscape water body is approximately rectangular section (as shown). It is assumed that the water flow in the tributary is a constant uniform flow in the open channel, and there is no tributary separation and separation. The slope of the bottom of the canal cannot be 0, and the path along the long straight prism channel keeps the roughness constant. There is no absolute uniform flow in the actual work, but as long as the actual situation is similar to the required conditions and the basic uniform flow conditions are met, it can be approximated as a uniform flow in the open channel. Therefore, the branch channel can be regarded as a uniform flow in the open channel.

3.1. Calculation Formula. The hydraulic calculations for the open channel tributaries are mainly expressed as follows:

$$\begin{aligned} A &= (b + mh)h, \\ \chi &= b + 2h\sqrt{1 + m^2}, \\ R &= \frac{(b + mh)h}{b + 2h\sqrt{1 + m^2}}, \\ v &= C\sqrt{Ri} = \frac{1}{n}R^{2/3}i^{1/2}, \\ Q &= (b + mh)h \bullet v. \end{aligned} \tag{1}$$

In which, v is the average flow velocity of the section, R is the hydraulic radius, C is the coefficient, A is the cross-sectional area of the water, Q is the flow rate, and K is the flow modulus and can also represent the characteristic flow, reflecting m, b, and n versus Q impact.

The qualitative model is a mathematical equation. The water quality model is a process used to describe the flow of water, in which mixed pollutants migrate in the water environment. There are many methods for solving equations. For a single water quality, the answer can be directly given. The numerical solution is used to solve complex water quality problems. The water quality model is constructed based on the complete mixing of the main canal pollutants. The water concentration of the water body is used to predict and analyze the pollutant concentration through the self-purification function of the water body, considering the variety and indicators of the pollutants, combined with the actual development of the project. With the research background, this time, the most representative BOD and DO were selected as the simulation indicators of water environmental quality organic pollutants.

The water quality model is given as follows:

$$\begin{aligned} B_x &= B_1 e^{(-(K_1 x/u))}, \\ D_x &= \frac{K_1 B_1}{K_2 - K_1}\left(e^{(-(K_1 x/u))} - e^{(-(K_2 x/u))}\right) + D_1 e^{(-(K_2 x/u))}. \end{aligned} \tag{2}$$

3.2. Model Building Step. Suppose a branch channel is divided into 3 sections. The first section is the trapezoidal section channel length x_1. The section dimensions are as follows: bottom width b_1, water depth h_1, slope coefficient m_1, slope i_1, and roughness n_1; the second section of landscape water, approximate rectangle, and its length is x_2, bottom width is b_2, slope is i_2, and roughness is n_2; the third section is trapezoidal section channel length x_3, and its section dimensions are as follows: bottom width water depth h_3, slope coefficient b_3, slope i_3, and rough raten_3.

It is known that the initial section (the inlet of the branch channel), the BOD concentration, the deficient oxygen amount D_1, the branch channel flow rate and the downstream flow velocity v, the water depth h, the BODx concentration B_x, and the deficient oxygen amount D_x determine whether the section meets the water quality standard.

The steps to build the model are as follows:

(1) If $x \le x_1$, the parameters of the section are

(1) Calculate the water depth h

$$h = h_0 \tag{3}$$

(2) Calculate the flow rate v

$$\begin{aligned} R_1 &= \frac{(b_1 + m_1 h)h}{b_1 + 2h\sqrt{1 + {m_1}^2}} \\ v &= \frac{1}{n_1}R^{2/3}i^{1/2} \end{aligned} \tag{4}$$

(3) Calculate traffic Q

$$Q = (b_1 + m_1 h)h \bullet v \tag{5}$$

(4) Calculate BOD concentration and oxygen deficiency in the water body of the section

$$B_x = B_1 e^{(-(K_1 x/v))}$$
$$D_x = \frac{K_1 B_1}{K_2 - K_1}\left(e^{(-(K_1 x/u))} - e^{(-(K_2 x/u))}\right) + D_1 e^{(-(K_2 x/u))} \tag{6}$$

(5) Analysis of water environment quality assessment

Step 1. Enter the channel parameters of the first paragraph $x_1, b_1, h_1, m_1, n_1, i_1$; the second paragraph of the water parameters $x_2, b_2, h_2, m_2, n_2, i_2$; and the third paragraph of the channel parameters $x_3, b_3, h_3, m_3, n_3, i_3$.

Step 2. Enter the initial section oxygen consumption coefficient K_1 and the reoxygenation coefficient K_2.

Step 3. Input the initial section water depth h_0, BOD concentration B_1, and deficient oxygen amount D_1.

Step 4. Calculate the water parameters of any section downstream of the initial section. Given a certain value x, the calculation steps are as follows:

If $B_x > 10$, the water body is inferior V water; if $6 < B_x < 10$, the water body is type V water; if $4 < B_x < 6$, the water body is type IV water; if $3 < B_x < 4$, the water body is type III water. If $B_x < 3$, the water body is type II water.

(2) If $x_1 < x \le (x_1 + x_2)$, the parameters of the section are

(1) Calculate traffic Q

$$h_1 = h_0$$
$$R_1 = \frac{(b_1 + m_1 h_1)h_1}{b_1 + 2h_1\sqrt{1 + {m_1}^2}}$$
$$v_1 = \frac{1}{n_1} {R_1}^{2/3} {i_1}^{1/2} \tag{7}$$
$$Q = (b_1 + m_1 h)h_1 \bullet v_1$$

(2) Calculate the water depth of the second section of the water h

After calculating Q, calculate h, because $h = f(Q, n_2, i_2, b_2)$, so the function relationship is

$$Q = \frac{1}{n_2} {i_2}^{1/2} b_2 h \left(\frac{b_2 h}{b_2 + 2h}\right)^{2/3}. \tag{8}$$

By computer trial, you can solve$h$.

(3) Calculate the flow rate v

$$v = \frac{Q}{b_2 h} \tag{9}$$

(4) Calculate BOD concentration and oxygen deficiency in the water body of the section

To calculate the BOD concentration B_x and the deficient oxygen D_x in the second paragraph, firstly, the first section of the open channel end BOD concentration B_2 and the oxygen deficiency amount D_2.

$$B_2 = B_1 e^{(-(K_1 x/v_1))},$$
$$D_2 = \frac{K_1 B_1}{K_2 - K_1}\left(e^{(-(K_1 x/v_1))} - e^{(-(K_2 x/v_1))}\right) + D_1 e^{(-(K_2 x/v_1))}. \tag{10}$$

Then, B_x and D_x are

$$B_x = B_2 e^{(-(K_1 (x - x_1)/v))},$$
$$D_x = \frac{K_1 B_1}{K_2 - K_1}\left(e^{(-(K_1 (x - x_1)/v))} - e^{(-(K_2 (x - x_1)/v))}\right) + D_1 e^{(-(K_2 (x - x_1)/v_v))}. \tag{11}$$

(5) Analysis of water environment quality assessment

If $B_x > 10$, the water body is inferior V water; if $6 < B_x < 10$, the water body is type V water; if $4 < B_x < 6$, the water body is type IV water; if $3 < B_x < 4$, the water body is type III water. If $B_x < 3$, the water body is type II water.

(3) If $(x_1 + x_2) < x \le (x_1 + x_2 + x_3)$, the parameters of the section are

(1) Calculate traffic Q

$$h_1 = h_0$$
$$R_1 = \frac{(b_1 + m_1 h_1)h_1}{b_1 + 2h_1\sqrt{1 + {m_1}^2}}$$
$$v_1 = \frac{1}{n_1} {R_1}^{2/3} {i_1}^{1/2} \tag{12}$$
$$Q = (b_1 + m_1 h)h_1 \bullet v_1$$

(2) Calculate the water depth of the second section of the water h

After calculating Q, calculate h, because $h = f(Q, n_3, i_3, b_3)$, so the function relationship is

$$Q = \frac{1}{n_3} {i_3}^{1/2} (b_3 + m_3 h)h \left(\frac{(b_3 + m_3 h)h}{b_3 + 2h\sqrt{1 + m_3^2}}\right)^{2/3}. \tag{13}$$

By computer trial, you can solve$h$.

(3) Calculate the flow rate v

$$v = \frac{Q}{(b_3 + m_3 h)h} \tag{14}$$

(4) Calculate BOD concentration and oxygen deficiency in the water body of the section

To calculate the BOD concentration B_x and the deficient oxygen D_x in the third paragraph, first, the first paragraph of the open channel end BOD concentration B_2, the oxygen deficiency D_2 and the second section of the water end section BOD concentration B_3, the oxygen deficiency D_3.

$$B_2 = B_1 e^{(-(K_1 x/v_1))},$$
$$D_2 = \frac{K_1 B_1}{K_2 - K_1}\left(e^{(-(K_1 x/v_1))} - e^{(-(K_2 x/v_1))}\right) + D_1 e^{(-(K_2 x/v_1))}. \tag{15}$$

To calculate the BOD concentration B_3 and the deficient oxygen amount D_3 of the second section of the water body, it is necessary to know the flow rate v_2 of the second section of the water body. First, calculate the water depth h_2 of the second section of water and solve h_2 according to formula $Q = (1/n_2) i_2^{1/2} b_2 h (b_2 h/b_2 + 2h)^{2/3}$. Calculate v_2 according to $v_2 = Q/(b_2 + m_2 h_2)h$.

$$B_3 = B_2 e^{(-(K_1 x_2/v_2))},$$
$$D_3 = \frac{K_1 B_2}{K_2 - K_1}\left(e^{(-(K_1 x_2/v_2))} - e^{(-(K_2 x_2/v_2))}\right) + D_1 e^{(-(K_2 x_2/v_2))}. \tag{16}$$

Then, B_x and D_x are

$$B_x = B_3 e^{(-(K_1 (x - x_1 - x_2)/v))},$$
$$D_x = \frac{K_1 B_3}{K_2 - K_1}\left(e^{(-(K_1 (x - x_1 - x_2)/v))} - e^{(-(K_2 (x - x_1 - x_2)/v))}\right) + D_1 e^{(-(K_2 (x - x_1 - x_2)/v))}. \tag{17}$$

(5) Analysis of water environment quality assessment

If $B_x > 10$, the water body is inferior V water; if $6 < B_x < 10$, the water body is type V water; if $4 < B_x < 6$, the water body is type IV water; if $3 < B_x < 4$, the water body is type III water. If $B_x < 3$, the water body is type II water.

3.3. The Overall Design of the Visual Simulation System. The main function of the visual simulation system is to combine the geographic information analysis function of GIS and the three-dimensional display function of Vega [20] to express the river water environment information in various forms. Its main modules include GIS platform, 3D visual module, water quality evaluation module, and data management module.

The basis for visualizing the water quality is to obtain corresponding water quality data, including monitoring data and simulation data. The data management module can easily add, delete, modify, and import various geographic, hydrological, and water quality data to provide basic data for water quality assessment; the water quality assessment module provides the final data to be displayed for visualization; GIS platform achieves water quality 2D display, while the Vega module provides a 3D display of geographic information. The functional modules of the system are shown in Figure 1.

4. Interactive 3D Visualization Simulation System

4.1. Software Development Tools. The development of river visualization systems involves data management, GIS rendering, and 3D visual development. In order to develop the visualization system, the development tools needed include GIS platform, 3D modeling tools, visual simulation tools, software development tools, and database development tools.

(1) GIS platform tools

TopMap ActiveX6 is a full-component GIS development platform, including TopMap ActiveX 6 main control, bird's eye view control for full-image browsing and positioning, attribute list editing control, map layer list, and management controls, suitable for stand-alone and local area network customers. Users can easily insert TopMap ActiveX6 in object-oriented visual programming languages (such as VB, C#, Delphi, VC, C++ Builder, and FoxPro) to easily implement GIS functions, including GIS exchange format data import and export: exquisite map representation, rich annotation settings, projection settings and conversion, vector editing, vector calibration, attribute data manipulation, multimedia support, feature analysis, spatial analysis, topology analysis, network analysis, interpolation analysis, large format vector printing, and automatic page printing, image output, etc.

(2) 3D modeling tools

Creator is a popular real-time 3D view database modeling and optimization tool that can be used to generate, edit, and view visual databases in battlefield environments, entertainment, urban simulation, and other computing visualizations. Its basic function is to provide users with a powerful and interactive visual modeling environment, due to its high fidelity, optimally optimized real-time 3D modeling capabilities and texture mapping, terrain surface generation, and its improved model. The advanced technical means of system real-time, etc., make it widely used in the field of virtual reality.

(3) Visual simulation tool

Vega is an advanced software environment used by MultiGen-Paradigm for real-time visual simulation, sound

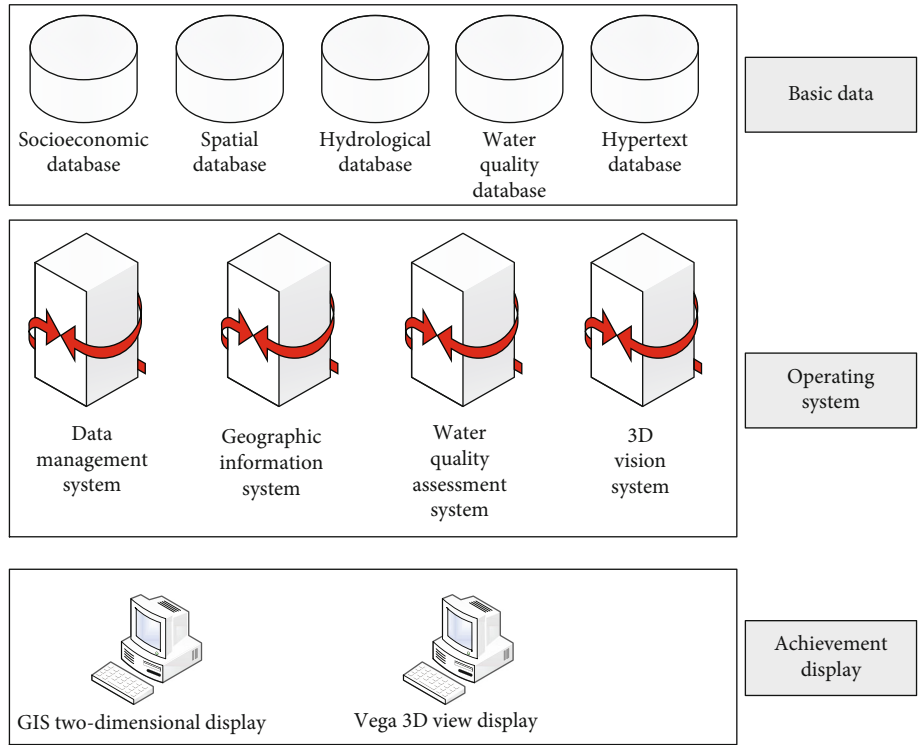

Figure 1: Functional block diagram of water environment visualization simulation system.

simulation, and virtual reality. It combines easy-to-use tools with advanced simulation capabilities, allowing users to create, edit, and run complex simulation applications quickly and easily. Vega greatly reduces the source code writing, making software maintenance and real-time performance optimization easier, greatly improving development efficiency. Vega includes a complete C language application interface that provides developers with maximum software control and flexibility. Vega includes a friendly graphical environment interface, a complete C language API, a rich set of useful utility libraries, and a selection of optional modules. Vega mainly consists of two parts, one is the LynX graphical user interface; the other is the C language based Vega function library. The main function of LynX is to create a 3D scene model through visual operations and store it in a pdf file, and then the application can render the built 3D scene by Vega's C language library.

(4) Software development tools

The Visual C++6.0 development environment provides users with a good visual programming environment that allows programmers to easily access the C++ source code editor, resource editor, and internal debugger,and create project file. Visual C++ not only includes the compiler, but it also includes many useful components. Through the collaborative work of these components, you can easily create source files and edit resources in the Visual C++6.0 integrated environment and the compilation, connection, and debugging of the program.

(5) Database development tools

SQL Server 2000 is a high-performance relational database management system that covers almost all database operations, including database creation, maintenance, operations, warnings, data replication, and transformation, and has good database design, management, and network functions. Because of its good performance, reliability, and ease of use, it has become the best database platform for OLTP (online transaction process), data warehousing, and e-commerce applications.

4.2. System Settings. The system can be run on a regular PC workstation due to the adoption of some technologies and improved hardware performance. Secondly, the scale of the whole scene is large, and there are many texture maps, and most of them are real photos with large amount of data. In addition, the main work of the whole system is to perform visual simulation, and other activities, audio simulation, and other aspects are not needed. Combining these features and requirements, the system's Vega vision simulation module is adopted.

The following application settings are available.

(1) The system settings

The system's multithreading control property is set to single thread because most workstations have one CPU configuration. The error reporting level is set to the Notice level. The exit hotkey for the entire program is set to the ESC key.

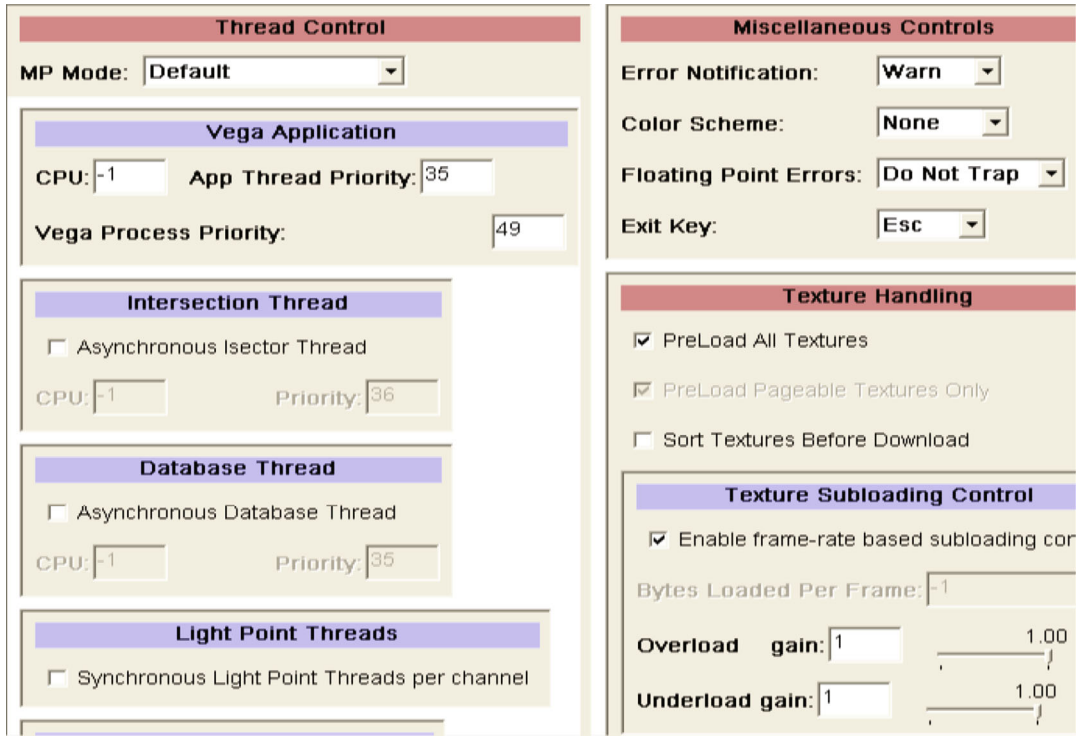

Figure 2: The main interface set by LynX.

The default processing of the texture map is to preload all the texture files. Since the texture file is larger in this application, this default setting is changed. The more important graphic rendering frame number setting is set to an upper limit of 30 Hz, which is a maximum of 30 frames per second. This number may not be reached on machines with poor hardware configuration, but this may be exceeded on advanced machines if set to Free mode.

(2) The graphic state settings

The different settings of the graphic state have a great impact on the running performance, such as removing the texture map and lighting effects, and the rendering speed will be greatly improved. In actual operation, in order to achieve the virtual reality effect as much as possible, texture, lighting, depth buffer and transparency are set when debugging the program. The fog effect, Backfaces display, and frame effect (wireframe) are set to "off."

(3) The window settings

The window size is set to 1024 wide and 768 high, in pixels, which is full-screen operation at normal screen resolution. Because it is full screen, there is no title and the border is set to none. For mouse operation, the state of the cursor (cursor) is set to "display" and the coordinates of the mouse are also converted to relative to the window. In addition, stereo and antialias settings are set to "Off" for performance reasons and can be turned on to enhance simulation if the hardware level permits.

(4) The settings of the graphic channel

There is only one graphic channel, and it fills the entire window. Multichannel has little meaning in the application of this system, and it consumes computer performance. The projection method of the channel adopts the usual symmetric frustum mode, and the near and far points of the cut surface of the field of view are set on 1 and 1000 database units, respectively.

(5) The settings of the observer

There is only one observer, and of course it is in a state that requires on with graphics. Other scenes and environment properties are unique. Since the system does not have players, the observer is directly connected to the graphic channel and does not have to be attached to a player. The positioning method is set to determine the coordinates according to its own motion mode. There are multiple motion modes in the system, and the motion mode used by the observer as the positioning method can be dynamically switched at any time.

(6) The environment settings

The environment system is set to open, and the atomization effect has been said to have been canceled for performance reasons. The color of the sky uses the default blue. The brightness of the entire environment is set to the maximum, which is equivalent to the noon effect, so that not only the graphic details of the model can be perfectly represented, but also the illumination is not calculated.

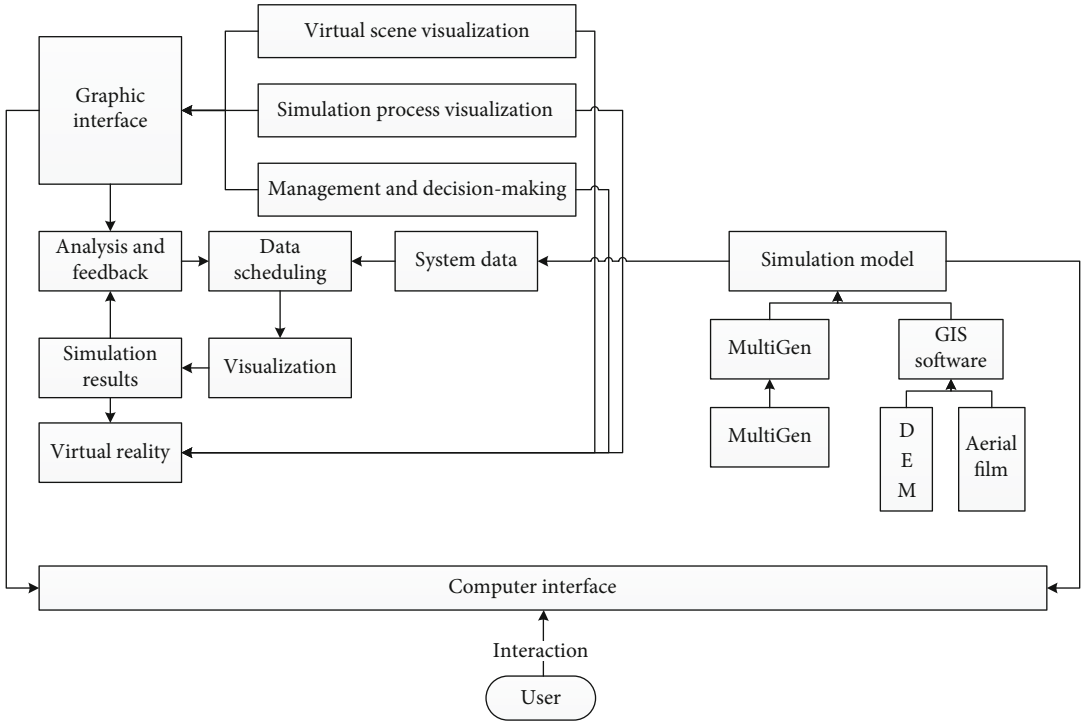

Figure 3: Simulation module overall process.

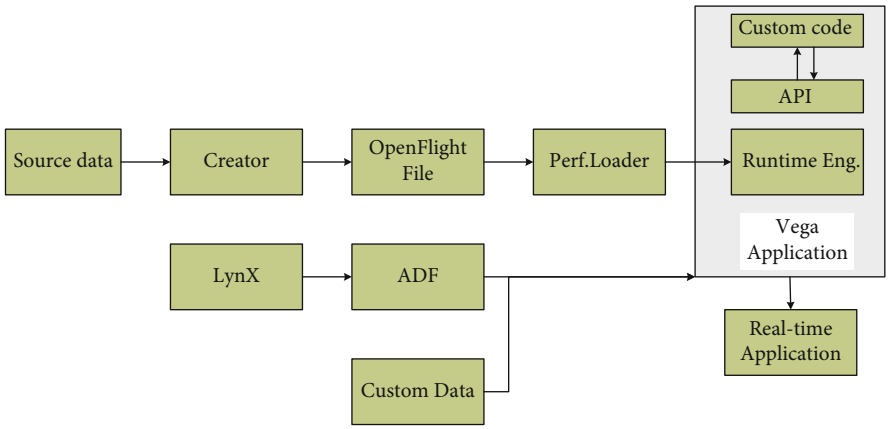

Figure 4: System integration framework.

(7) The setting of the light source

The light source is set to "on," and its type is set to sunlight in infinite, local, spot, Sun, and Moon. There are two ways to set the position of the light source, one is set according to XYZ coordinates, and the other is set according to the deflection angle. The latter used in this system has an azimuth angle of 90 degrees and an elevation of 90 degrees, which are consistent with the setting of the noon time in the environment.

Most of these settings are directly set by the visualization tool LynX, and some properties of graphic state and observer are set by the program, which are easy to modify in the program. The main interface set by LynX is shown below the Figure 2.

The main function of this system is to allow users to visually see the simulation results in a virtual digital watershed environment. The visual simulation result seen by the user on the screen is the output of Vega to the currently active graphic channel, which is associated with the observer. In fact, it may be considered that the observer is equivalent to a camera, and the image taken in the "camera" lens is displayed in front of the user. In order to achieve different roaming modes, this "camera" must be viewed in the entire scene in different motions. This requires the use of important objects in Vega: the motion model.

The motion models provided by the Vega system come in four forms: simple, complex, direct, and user defined. The simple motion model provides a quick overview of the database, including spin, drive, UFO, warp, trackball, fly, and walk.

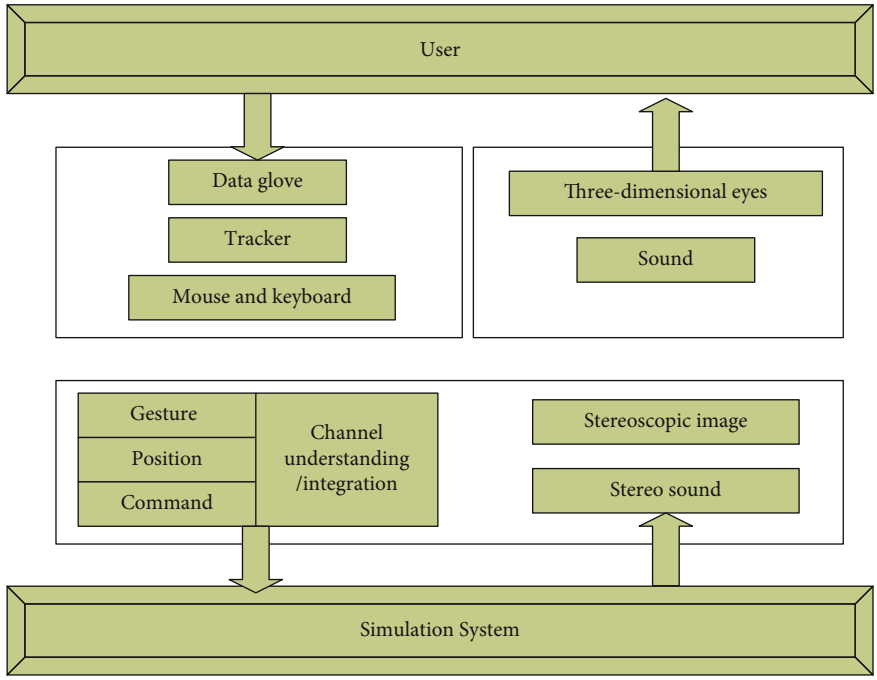

Figure 5: Framework structure of interactive visual simulation system based on virtual reality technology.

There are two types of complex motion models, mainly used in military simulations of high-speed flight. They are flight simulator and missile motion models.

The direct motion model can in turn be an input device direct, which provides a data interface for various input device types that are directly supported by Vega.

Because objects such as observers, geometry, and athletes can be located using the vgPos method, it is more appropriate to consider the motion model as a convenient means of calculating position. It is not a necessity. In fact, using the vgPosVec function to create an initialized position vector and then positioning it with the vgPos function completely removes the need for motion models. Of course, the parameters required by the vgPosVec function XYZHPR six values must be obtained from somewhere, ideally even with more detailed mathematically based software running on another computer.

Unless the new position is generated at the same frequency as the frame rate, the out-of-synchronization of the position update may cause the "jitter" or the nonsmooth motion of the object in the scene. For this phenomenon, the well-known sampling theorem suggests generating a new position at twice the frame frequency. These time-intervened position data can be interpolated or extrapolated as needed. The interpolation of the position is called data smoothing. Similar to the antialiasing of edge pixels used in 3D graphic rendering, the data can be smoothed as antialiasing for position coordinates. The overall flow of the Vega simulation module of the 3D visual simulation module system is shown in Figure 3.

4.3. Implementation of the Simulation System. First, the previously built model and various terrain data are integrated. The integration diagram is shown in Figure 4.

The VR technology is applied to the digital watershed 3D visualization simulation system to build a unified digital simulation platform. The system uses Vega and Visual C++ as its software platform. Firstly, MultiGen-Creator is used to complete the building model in the scene. In Vega, the rapid establishment of 3D simulation environment and the automatic management of large terrain scenes are realized. Visual C++ is used to realize the optimization of some API functions and the scheduling of interactive simulation process. Vega is a well-known object-oriented virtual reality platform developed by MultiGen-Paradigm, which can easily complete the construction of the scene. LynX is a collection of tools provided by Vega with a graphical user interface.

The system's 3D visualization simulation system mainly collects the information in the simulation modeling process and visually expresses the dynamic information in the simulation calculation process. At the same time, in the visual simulation process, the user can synchronously maintain the interactive control of the simulation process through the intuitive result of the operation interface simulation feedback provided by the system until the simulation object obtains the desired result.

Figure 5 shows the framework of an interactive visual simulation system based on virtual reality. It describes the data processing flow and interaction process in the visual simulation system. The interaction process of virtual reality in the system is as follows: firstly, the user collects the simulation entity according to the requirements and obtains the coordinate information by means of the peripheral device; according to the coordinate information, the local scene coordinate is given according to the corresponding coordinate conversion algorithm in the scene database; according to the local scene, the coordinates search for the attribute information of the corresponding point in the corresponding

attribute database and feedback to the simulation entity model; the simulation entity model calculates the corresponding parameters according to the obtained attribute information and then takes corresponding attribute actions; according to the flow chart 4, the water body and the three-dimensional terrain are generated. The simulation system of the scene is transmitted to the observer through various peripheral devices, so that the observer has an immersive feeling.

5. Conclusion

The simulation of natural scenery and natural phenomena is an important research content of computer graphics, and it is also a challenging research direction. In recent years, with the rapid development of computer graphic technology and virtual reality, the three-dimensional visualization technology of river waters has been become an important topic in the research and development of digital watersheds, rapid mapping of large-scale terrain scenes, simulation of river fluid movement and hydrological phenomena, and remote visualization of complex scenes in the network environment. In this paper, the theory and application of the three-dimensional visualization of river water scenes are analyzed and discussed in-depth, and an interactive visual simulation system based on virtual reality technology is realized. Simulation simulations such as program demonstration and engineering operation management can be greatly accelerated. The processing speed of data enables the effective use of huge data to provide visual interaction means for numerical simulation and data analysis, improve the efficiency of numerical calculation, and realize human-computer interaction communication, so that people can observe the phenomena and laws that are difficult to observe by traditional methods, and the validity of the mathematical model can be analyzed for validity.

Data Availability

All the data are reliable, and the author can be contacted for request.

Conflicts of Interest

We declare that there is no conflict of interest regarding the publication of this paper.

Acknowledgments

This study was supported by Inner Mongolia Seismological Bureau Open Fund: Research on the Deformation Mechanism of Seismic Belts in Ordos Region Based on Radar Remote Sensing Technology, 2019JC08 and Research on the Preparation, Characteristics and Application of Metal Micro/Nano Structures Based on Flexible Substrate Regulation, 61975037.

References

[1] Y. J. Zhang and Z. Q. Yang, "The status quo and future development of the digitalization of China sci-tech journals," *Journal of Shenyang Agricultural University*, vol. 37, no. 2, pp. 409–418, 2010.

[2] H. E. Solberg and D. Stamm, "Analysis on the road of digitalization construction of university library," *Sci-Tech Information Development & Economy*, vol. 233, no. 8, pp. 279–289, 2010.

[3] S. Wan, X. Xu, T. Wang, and Z. Gu, "An intelligent video analysis method for abnormal event detection in intelligent transportation systems," *IEEE Transactions on Intelligent Transportation Systems*, pp. 1–9, 2020.

[4] T. M. Burton, R. R. Turner, and R. C. Harriss, "The impact of highway construction on a north Florida watershed," *Jawra Journal of the American Water Resources Association*, vol. 12, no. 3, pp. 529–538, 2010.

[5] V. R. Kamat and J. C. Martinez, "Validating complex construction simulation models using 3D visualization," *Systems Analysis Modelling Simulation*, vol. 43, no. 4, pp. 455–467, 2003.

[6] A. Elnimr, M. Fagiar, and Y. Mohamed, "Two-way integration of 3D visualization and discrete event simulation for modeling mobile crane movement under dynamically changing site layout," *Automation in Construction*, vol. 68, pp. 235–248, 2016.

[7] R. M. Maxwell, L. E. Condon, and S. J. Kollet, "A high-resolution simulation of groundwater and surface water over most of the continental US with the integrated hydrologic model ParFlow v3," *Geoscientific Model Development*, vol. 8, no. 3, pp. 923–937, 2015.

[8] Y. Wang, X. Yu, K. He, Q. Li, Y. Zhang, and S. Song, "Dynamic simulation of land use change in Jihe watershed based on CA-Markov model," *Transactions of the Chinese Society of Agricultural Engineering*, vol. 27, no. 12, pp. 330–336, 2011.

[9] A. G. Gee, H. Li, M. Yu et al., "Universal visualization platform," in *Proceedings of SPIE-The International Society for Optical Engineering*, vol. 5669, pp. 17-18, San Jose, California, USA, 2005.

[10] J. R. Zeng, C. C. Cheng, A. W. Lee, P. L. Wei, and J. K. Chen, "Visualization platform of one-dimensional gratings of tethered polyvinyltetrazole brushes on silicon surfaces for sensing of Cr(III)," *Microchimica Acta*, vol. 184, no. 8, pp. 2723–2730, 2017.

[11] S. M. Fletcherlartey and G. Caprarelli, "Application of GIS technology in public health: successes and challenges," *Parasitology*, vol. 143, no. 4, pp. 401–415, 2016.

[12] Y. Liu, X. Fang, C. Cheng et al., "Research and application of city ventilation assessments based on satellite data and GIS technology: a case study of the Yanqi Lake Eco-city in Huairou District, Beijing," *Meteorological Applications*, vol. 23, no. 2, pp. 320–327, 2016.

[13] R. J. Zhang, "Construction of Digital Aojiang Watershed," *Applied Mechanics & Materials*, vol. 687-691, pp. 2157–2160, 2014.

[14] L. Ma, L. S. Geng, and K. H. Zhou, "Study on the key technology of ecological small watershed construction in Shandong Province," *Applied Mechanics & Materials*, vol. 448-453, pp. 509–512, 2013.

[15] F. Chiappa, G. Bernasconi, and P. Dell'Aversana, "A global integration platform for optimizing cooperative modeling and simultaneous joint inversion of multi-domain geophysical data," *Aims Geosciences*, vol. 2, no. 1, pp. 1–31, 2016.

[16] S. B. Lim, H. J. Lee, W. Y. Jin, and S. M. Shim, "CSS3 extensions for setting web content in a 3D view volume and its stereoscopic 3D display," *Computer Standards & Interfaces*, vol. 50, pp. 65–75, 2017.

[17] K. Jinwu, Z. Xiaopeng, Z. Chi, and L. Baicheng, "Application of 3D stereoscopic visualization technology in casting aspect," *Chinese Casting*, vol. 11, no. 4, pp. 308–313, 2014.

[18] P. M. Brown, N. M. Hamilton, and A. R. Denison, "A novel 3D stereoscopic anatomy tutorial," *Clinical Teacher*, vol. 9, no. 1, pp. 50–53, 2012.

[19] L. Yang, W. Wang, M. Wang, H. Zhang, and M. Hou, "Structural dynamics of corn threshing drum based on computer simulation technology," *Wireless Personal Communications*, vol. 3, pp. 1–11, 2017.

[20] M. Xu, Q. Li, P. C. Lee, Y. Peng, and J. Wu, "VegaNet: a virtualized experimentation platform for production networks with connectivity consistency," *IEEE Network*, vol. 26, no. 5, pp. 15–21, 2012.

[21] Y. Liu, M. Ma, X. Liu, N. Xiong, A. Liu, and Y. Zhu, "Design and analysis of probing route to defense sink-hole attacks for Internet of Things security," *IEEE Transactions on Network Science and Engineering*, vol. 7, no. 1, pp. 356–372, 2018.

[22] F. Long, N. Xiong, A. V. Vasilakos, L. T. Yang, and F. Sun, "A sustainable heuristic QoS routing algorithm for pervasive multi-layered satellite wireless networks," *Wireless Networks*, vol. 16, no. 6, pp. 1657–1673, 2010.

[23] Y. Zhou, D. Zhang, and N. Xiong, "Post-cloud computing paradigms: a survey and comparison," *Tsinghua Science and Technology*, vol. 22, no. 6, pp. 714–732, 2017.

[24] W. Pan and C. Chai, "Measuring software stability based on complex networks in software," *Cluster Computing*, vol. 22, no. S2, pp. 2589–S2598, 2019.

[25] W. Pan and C. Chai, "Structure-aware Mashup service clustering for cloud-based Internet of Things using genetic algorithm based clustering algorithm," *Future Generation Computer Systems*, vol. 87, pp. 267–277, 2018.

[26] G. Yang, Q. Yang, and H. Jin, "A novel trust recommendation model for mobile social network based on user motivation," *Electronic Commerce Research*, vol. 11, no. 4, pp. 56–63, 2019.

Hindawi
Wireless Communications and Mobile Computing
Volume 2020, Article ID 8841417, 14 pages
https://doi.org/10.1155/2020/8841417

Research Article

Application Research of File Fingerprint Identification Detection Based on a Network Security Protection System

Chunwei Wang,[1,2] **Lina Yu**,[1] **Huixian Chang**,[1] **Sheng Shen**,[1] **Fang Hou**,[1] **and Yingwei Li**[1]

[1]*School of Information Science and Engineering, Yanshan University, Qinhuangdao 066004, China*
[2]*Beijing Branch, Daqing Oilfield Information Technology Company, Beijing 100043, China*

Correspondence should be addressed to Yingwei Li; lyw@ysu.edu.cn

Received 29 September 2020; Revised 29 October 2020; Accepted 16 November 2020; Published 1 December 2020

Academic Editor: Hongju Cheng

Copyright © 2020 Chunwei Wang et al. This is an open access article distributed under the Creative Commons Attribution License, which permits unrestricted use, distribution, and reproduction in any medium, provided the original work is properly cited.

A DLP (data loss prevention) system usually arranges network monitors at the network boundary to perform network traffic capture, file parsing, and strategy matching procedures. Strategy matching is a key process to prevent corporate secret-related documents from leaking. This paper adopts the document fingerprint similarity detection method based on the SimHash principle and customizes the KbS (Keyword-based SimHash) fingerprint, PbS (Paragraph-based SimHash) fingerprint, and SoP (SimHash of Paragraph) fingerprint, three different feature extraction SimHash algorithms for strategy matching to detect. The parsed unstructured data is stored as a file type in.txt format, and then a file fingerprint is generated. Matching the established sensitive document library to calculate the Hamming distance between the fingerprints, the Hamming distance values under different modification degrees are summarized. The experimental results reveal that the hybrid algorithmic strategy matching rules with different levels and accuracy are established. This paper has a reference role for the leakage prevention research of enterprise sensitive data.

1. Introduction

As the enterprise relies increasingly on information systems and information data, information system stability and information data security are directly related to the core competitiveness of enterprises, which puts high demands on enterprise information security and confidentiality [1]. According to the survey, among the ways of leaking sensitive information inside the enterprise, the fact that employees unconsciously outflow sensitive information through the enterprise's home page, mailboxes, instant messaging software, cloud disks, and smartphones connected to a wireless network [2–4] has become an important channel for leaking sensitive information [5, 6]. Therefore, enterprise border networks are particularly important for the timely detection and interception of sensitive data [7, 8].

The previous Information Content Audit platform (1.0) project realized the basic functions of the network monitor and has a good operation effect for the network boundary data capture [9] and document parsing. The identification of sensitive documents is achieved by matching the MD5 fingerprint database with the fingerprint of the document to be detected, but if the document modifies a small amount of content, the MD5 value will become completely different [10, 11]. The leaked data shows that some of the secret-related documents have been modified to a certain extent, where the modification methods include deleting and mixing to form new sensitive documents to avoid the identification of MD5 fingerprints; then, a leak that could not be monitored is formed. The international mainstream research methods for sensitive similar document calculations are based on surface term/word, Vector Space Model (VSM), and hash algorithm [12, 13]. The text similarity method based on the hash algorithm includes the Locality Sensitive Hashing (LSH) algorithm and Locality Preserving Hashing (LPH) algorithm. SimHash is a kind of locality sensitive hashing algorithm, which is ideal for large-scale data processing [14, 15], and it is in line with the research and development mode

of establishing fingerprint database matching sensitive files, which can be directly developed and upgraded on the original platform. At present, there are few research studies on the application of the hash algorithm to the identification of sensitive documents in data loss prevention systems. The use of Hamming distance values to distinguish document similarity lacks effective experimental data [16, 17]. The Information Content Audit platform (2.0) project is an improved project, which includes the improvement of the monitor sensitive matching fingerprint algorithm that will improve the previous single fingerprint algorithm and adopt the hybrid method to achieve similarity calculation to achieve better results [18, 19].

In this paper, the SimHash fingerprint algorithm with three different feature extraction methods is used to study the sensitive document, and the feasibility and effect of multilevel fingerprints formed by mixed multiple hash algorithms in data loss prevention systems are verified, and the monitor function is improved.

The rest of this article is organized as follows. Section 2 introduces the materials and methods of the paper, discussing network monitors and strategy matching, followed by algorithm implementation and experimental scenarios. Section 3 shows the experimental results and discussion. Section 4 describes the fingerprint strategy customization and implementation, and Section 5 summarizes the paper's work and future directions.

2. Materials and Methods

2.1. Network Monitor and Strategy Matching. The main purpose of data leakage prevention products used in enterprises is to monitor network traffic to prevent the transfer of sensitive data to the outside, which usually consists of a central management platform and a monitor, as shown in Figure 1.

It can be seen from Figure 1 that the monitors are arranged in the outlet of the enterprise's external network, which in fact can be used in conjunction with the shunt, and the central management platform is arranged in the enterprise's internal network to manage and configure multiple monitors. The DLP product also provides interfaces to LDAP servers, authentication servers, file servers, and classification and gradation content servers.

DLP products can obtain the specification description of sensitive data from the classification and gradation content servers to establish the determination basis of "sensitivity" that serves as the reference standard for the whole product. The DLP product integrates with the LDAP server to provide information about personnel and departments related to early warning events and provide information for the handling of early warning events [20, 21].

As a core part of the leak prevention, in the enabled state, the monitor continuously captures the traffic on the analysis network [22, 23]. Sensitive data and important traffic elements are monitored through protocols such as SMTP, FTP, and HTTP [24, 25]. This paper is mainly based on the monitor module in the DLP system as the core research content.

Figure 2 shows the functional requirements of content of the monitor, mainly including the packet capture device (fetching the data flow via HTTP, FTP, and SMTP, three agreements), file recognition reader (mainly content parsing for different file formats), and sensitive matcher (sensitive documents matching to identify sensitive documents to block the intercept), three parts.

Among them, the sensitive document matching function that the sensitive matcher needs to complete is an important process of data leakage prevention [26, 27]. How to define enterprise sensitive files, extract the characteristics of sensitive files, and adopt an accurate and efficient algorithm is directly related to the effect of monitor data leakage prevention. According to the characteristics of sensitive documents in this enterprise, this paper uses the SimHash algorithm with three different features to generate corresponding file fingerprints for specified sensitive documents and establish a sensitive document library for storing sensitive files and fingerprint information [28, 29].

From Figure 3, we can see the general flow of the strategy matching fingerprint matching algorithm and the core algorithm used.

The parsed document forms a fixed.txt format. Then, the fingerprint is generated by three algorithms of the fingerprint strategy. Compare fingerprints with fingerprints that exist in the sensitive document libraries; that is, the Hamming distance of the SimHash value is compared to judge whether the strategy hits or not.

2.2. Algorithm Implementation and Experimental Scheme

2.2.1. SimHash and Hamming Distances for Different Feature Extraction. Through the review and research of 1000 enterprise secret-related documents, combined with the specification description of sensitive data collected from the classification and gradation content servers, it is found that most classified documents are enterprise contracts, project-related documents, proxy patents, feasibility study reports, and key technical documents. Moreover, these different versions of documents are widely distributed on the computers of employees involved in document writing, integration, review, modification, and submission, and there are a large number of employees involved, which is prone to leak secrets.

The characteristics of this enterprise on the content level of secret-related documents are as follows. For the article type A, paragraphs are obviously distributed with different length, and long paragraphs are more likely to contain secret-related content. As for the article type B, it is that the distribution of paragraphs is not obvious or the paragraph length is roughly the same and that the nonparagraph forms such as table types also tend to have confidential keywords.

The main idea of the SimHash algorithm is dimension reduction. The high-dimensional feature vector is mapped into an f-bit fingerprint. The Hamming distance of the f-bit fingerprint of the two articles is compared to determine whether the article is repeated or highly approximated. The SimHash algorithm is sophisticated, but it is easy to understand and implement.

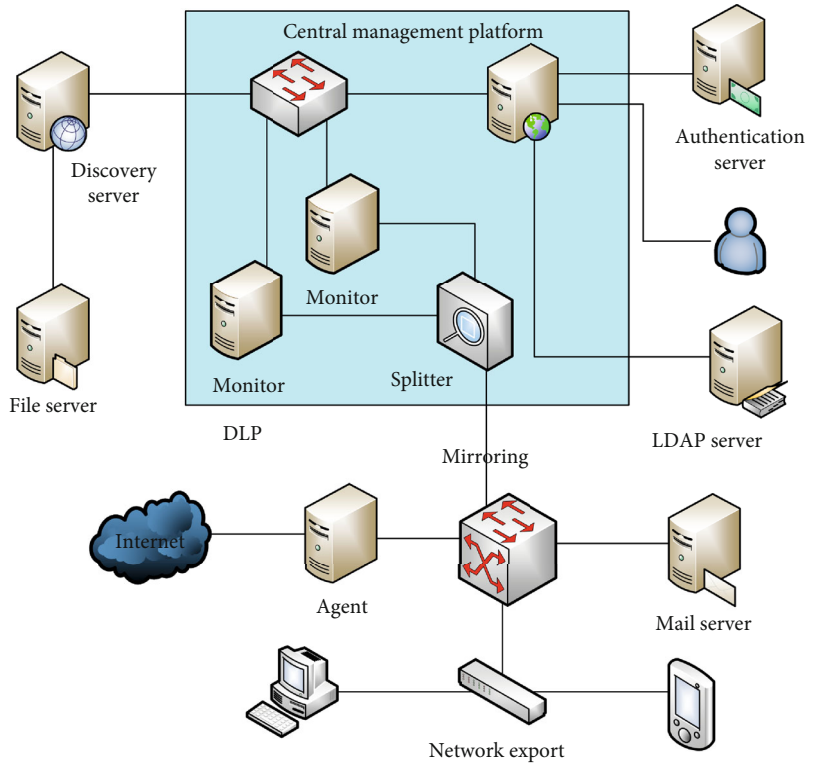

Figure 1: DLP system architecture diagram.

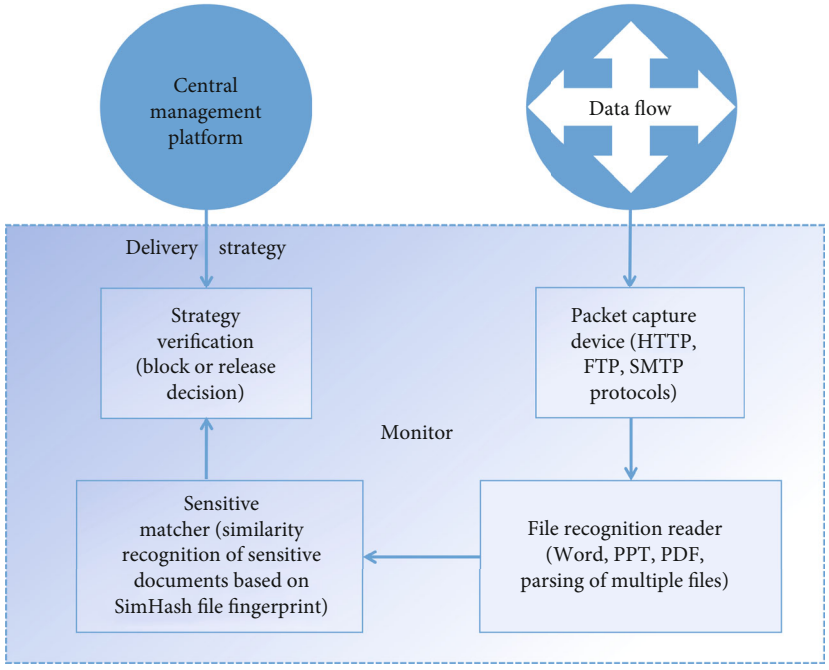

Figure 2: Monitor work flow chart.

In view of the current situation of sensitive document diversity, this paper firstly uses the PbS (Paragraph-based SimHash) fingerprint algorithm and KbS (Keyword-based SimHash) fingerprint algorithm. In order to capture sensitive documents more accurately, the SoP (SimHash of Paragraph) fingerprint algorithm is added [30], jointly implementing the fingerprint strategy. SimHash is used to integrate dynamic and static information to form the features in this paper, and some improvements are made in the feature extraction and weighting process [31]. Figure 4 shows the flow of the three fingerprint algorithms and the detailed process of feature extraction.

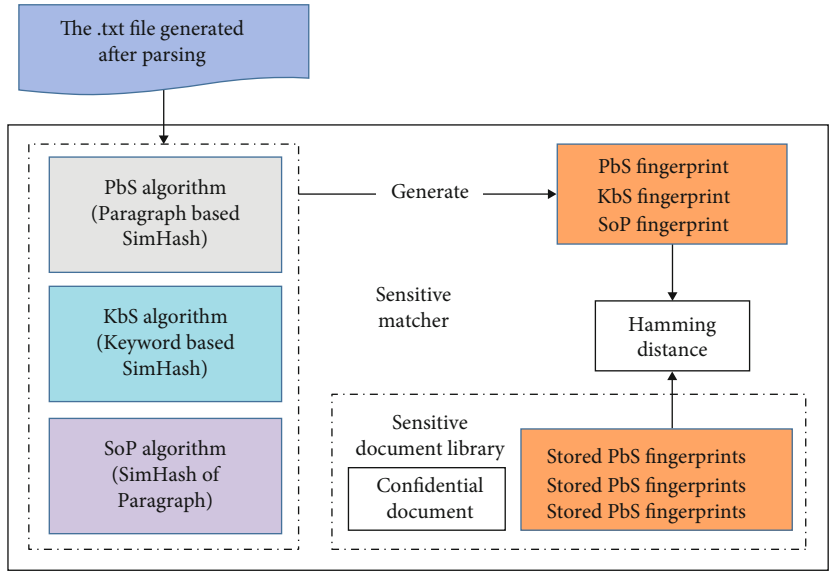

Figure 3: Multiple fingerprint strategy flow chart.

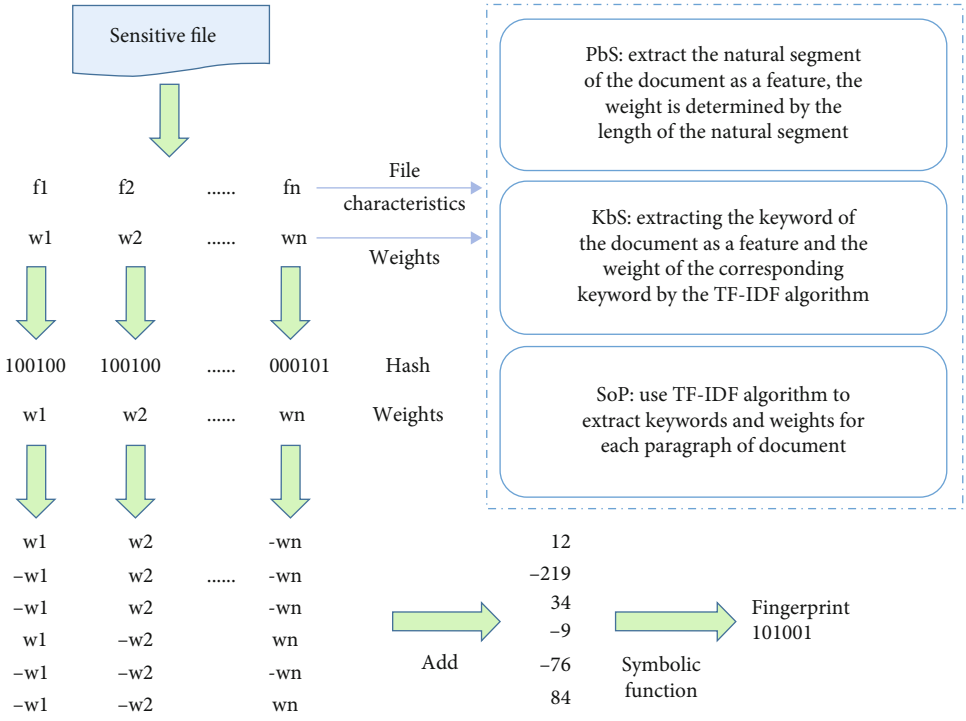

Figure 4: Three SimHash feature extraction methods.

The process of SimHash is roughly divided into the following steps:

(i) *Features*. Sensitive documents processed by the file recognition reader are converted into .txt text, and text features are extracted. PbS uses each paragraph as a characteristic vector; KbS uses the TF-IDF algorithm to extract the first n words of the keyword weight value of the article as features based on the full text; SoP is similar to KbS but extracts n keywords as features on the basis of paragraphs.

(ii) *Weights*. Different document features are extracted, and weight settings are also different. PbS takes the length of characters in each paragraph as the weight value according to the feature that long paragraphs are more likely to appear or represent the main content of the article; KbS uses the TF-IDF algorithm to extract the TF-IDF value of n keywords as the weight value; SoP, similar to KbS, uses the value of TF-IDF calculated by n keywords extracted from each segment as the weight value.

Table 1: Characteristics of three SimHash fingerprint algorithms.

Category	Feature scheme	Weight calculation	Number of fingerprints
PbS	Paragraphs	Natural length	1
KbS	Keywords	TF-IDF value	1
SoP	Keywords	TF-IDF value	N

(iii) *Hash Value*. The hash value of each feature is calculated by the hash function (hash). The hash value is a 64-bit signature composed of the binary numbers 0 and 1.

(iv) *Weighting and Merging*. Multiply the corresponding weight with the hash value, multiply the binary 1 positively and the binary 0 negatively, and get the weighted value of a single feature. Then, the weighted value of each eigenvector is added up to become a sequence string with positive and negative values.

(v) *Dimension Reduction* [32]. For the positive and negative sequence strings, set 1 for each bit if the value is greater than 0, set 0 for each bit if less than or equal to 0, and the resulting 64-bit binary sequence is the final SimHash document fingerprint.

Table 1 shows the characteristics of the three fingerprint algorithms. The keywords of the SoP feature scheme are paragraph keywords; that is, the TF-IDF algorithm is used to extract the keywords of the top n of the current paragraph weight, and the number of fingerprints is the number N of paragraphs of the current document.

For the PbS algorithm, a digital fingerprint is generated for each document, because it only performs hash value processing for each segment, so it is more efficient and saves computing resources. However, if the key paragraph (long paragraph with higher weight) of the sensitive document is changed, it will have a significant impact on the single-paragraph generated hash value and thus affect the fingerprint of the final SimHash. In the case of the KbS fingerprint, the TF-IDF algorithm is integrated to achieve keyword extraction and weight calculation by relatively consuming computing resources in the case of large document length. But for minor changes in sensitive document paragraphs, the keyword extraction and weight of the whole document are almost not affected, and the SimHash fingerprint will not be affected. However, for two documents with similar keywords but different contents, the KbS algorithm will be used in theory to misreport them as sensitive documents, which is less accurate than PbS in this case. Of course, the meaning of data leakage prevention is to prevent leakage of sensitive documents involving confidentiality, and it is better to prevent data leakage with strict levels, so it is safer to integrate multiple different SimHash algorithms.

The SoP fingerprint algorithm is actually a more careful way of getting a better grip on sensitive documents, similar to the KbS principle, except that the objects are changed from full text to paragraphs. Therefore, each paragraph will generate a SimHash digital fingerprint based on TF-IDF to extract keywords and weights. However, the analysis of sensitive documents will be more detailed and accurate. As seen from the number of fingerprints in each document, SimHash fingerprints will be generated for each paragraph of the document, making it easier to see the degree of content changes on the paragraph.

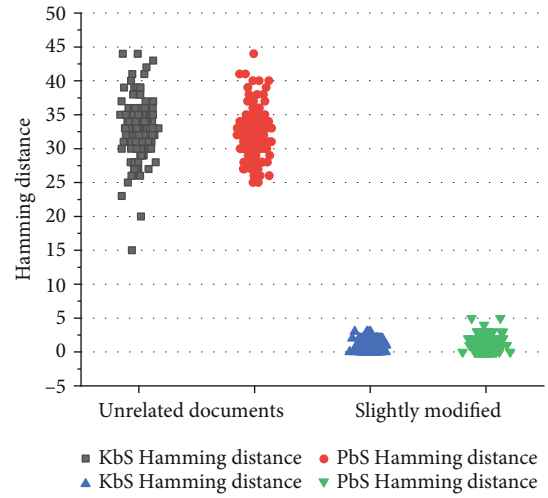

Figure 5: Hamming distance values between unrelated documents and Hamming distance values between different slightly modified documents and original secret-related documents.

With regard to the Hamming distance, the calculation of the Hamming distance is the key to determine whether the document is sensitive or not in this paper. The SimHash fingerprint of the detected document is obtained and compared with the SimHash fingerprint of the secret-related document in the sensitive document library to calculate the Hamming distance. The size of the Hamming distance value determines the similarity between the detected document and the secret-related document. With the increase of the degree of modification, the Hamming distance between the modified document and the original document will also increase. According to the actual situation and experimental test, a reasonable Hamming distance interval is found to determine whether the detection document is sensitive or not.

2.2.2. Fingerprint Strategy Experiment. In order to facilitate the comparison with Hamming distance data between pairs of 20 unrelated documents, this experiment randomly selected 190 secret-related documents in the company. A review of these documents by the Document Security Department found that three types of sensitive documents that are easily leaked are as follows:

(i) Documents formed by minor modification of secret-related documents

(ii) Documents formed by different-scale deletion of secret-related documents

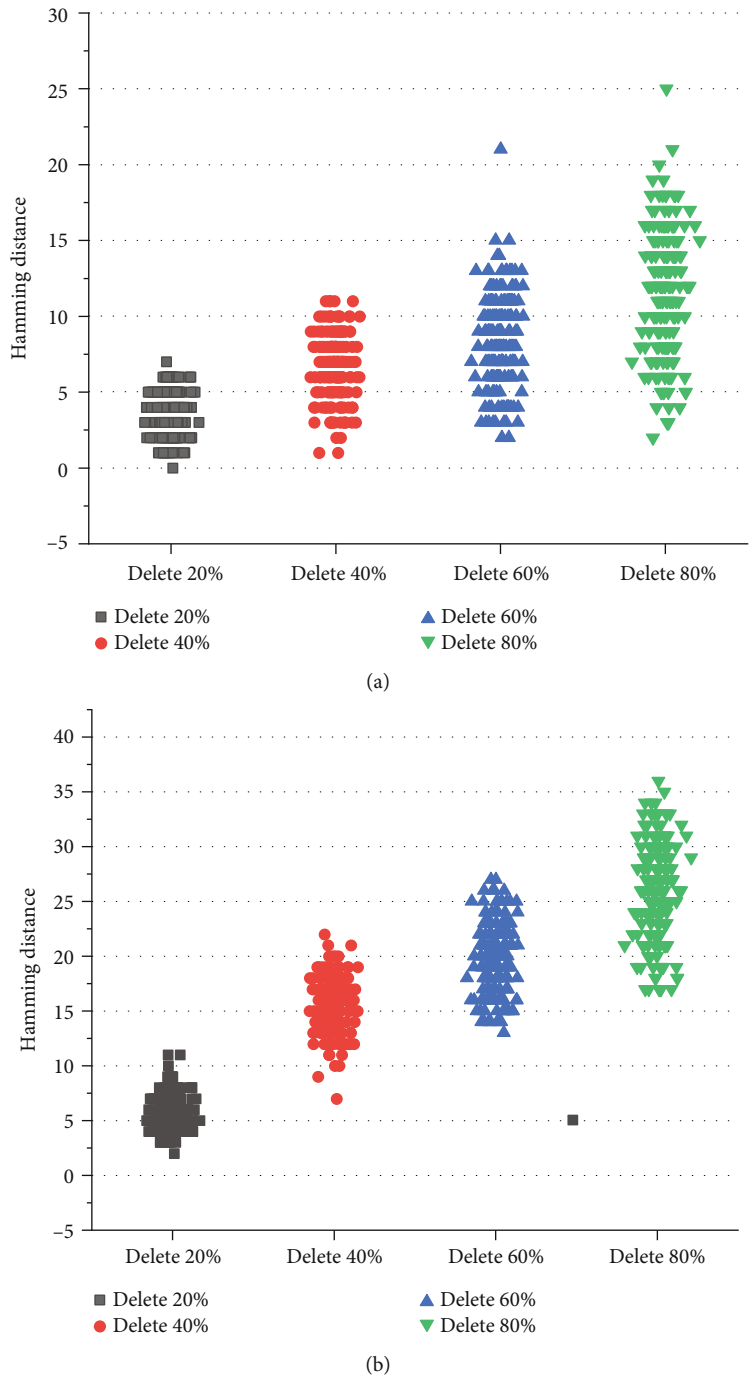

Figure 6: Hamming distance between documents with different degrees of deletion and original secret-related documents. (a) KbS fingerprint Hamming distance. (b) PbS fingerprint Hamming distance.

(iii) Documents formed by different-scale mixing of secret-related documents

For the above three types of sensitive documents, different targeted experiments were conducted: (1) experimental work on the first type of documentation: a small number of artificial modifications will be made to each of the 190 selected articles, such as a small increase in content, a small amount of deletion, and a small number of replacements, and the modifications of the three methods do not exceed 10% to simulate the formation of a revised version of a sensitive document; (2) experimental work on the second type of documentation: delete 20%, 40%, 60%, and 80% of the original secret-related documents to simulate that the document to be detected has only a small portion of the secret-related document; and (3) experimental work on the third type of documentation: delete 20%, 40%, 60%, and 80% of the total content of the original document, and then add 20%, 40%,

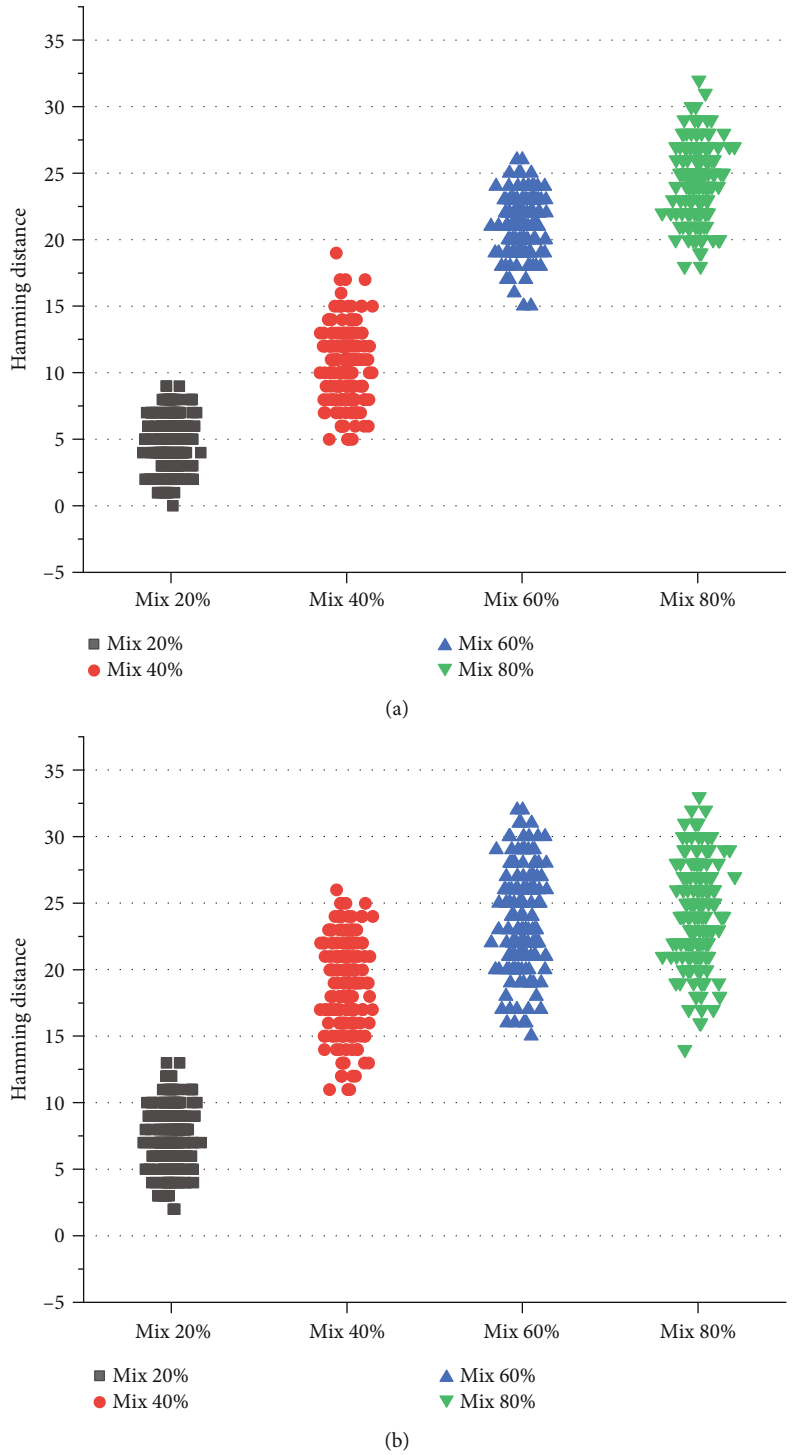

Figure 7: Hamming distance between different mixed degree documents and original secret-related documents. (a) KbS fingerprint Hamming distance. (b) PbS fingerprint Hamming distance.

60%, and 80% irrelevant content to simulate different levels of mixed documents. At the same time, 20 unrelated documents are prepared, and the Hamming distance between them is calculated. 190 Hamming distance values are obtained to explore the Hamming distance range between unrelated documents, so as to distinguish the Hamming distance between secret-related documents and sensitive documents.

3. Results and Discussion

3.1. KbS and PbS Fingerprint Experiment Results. As shown in Figure 5, the Hamming distance value between 20 unrelated documents, regardless of the PbS fingerprint or KbS fingerprint, is concentrated above 26, and only individual values are lower than 26. The Hamming distance values between the

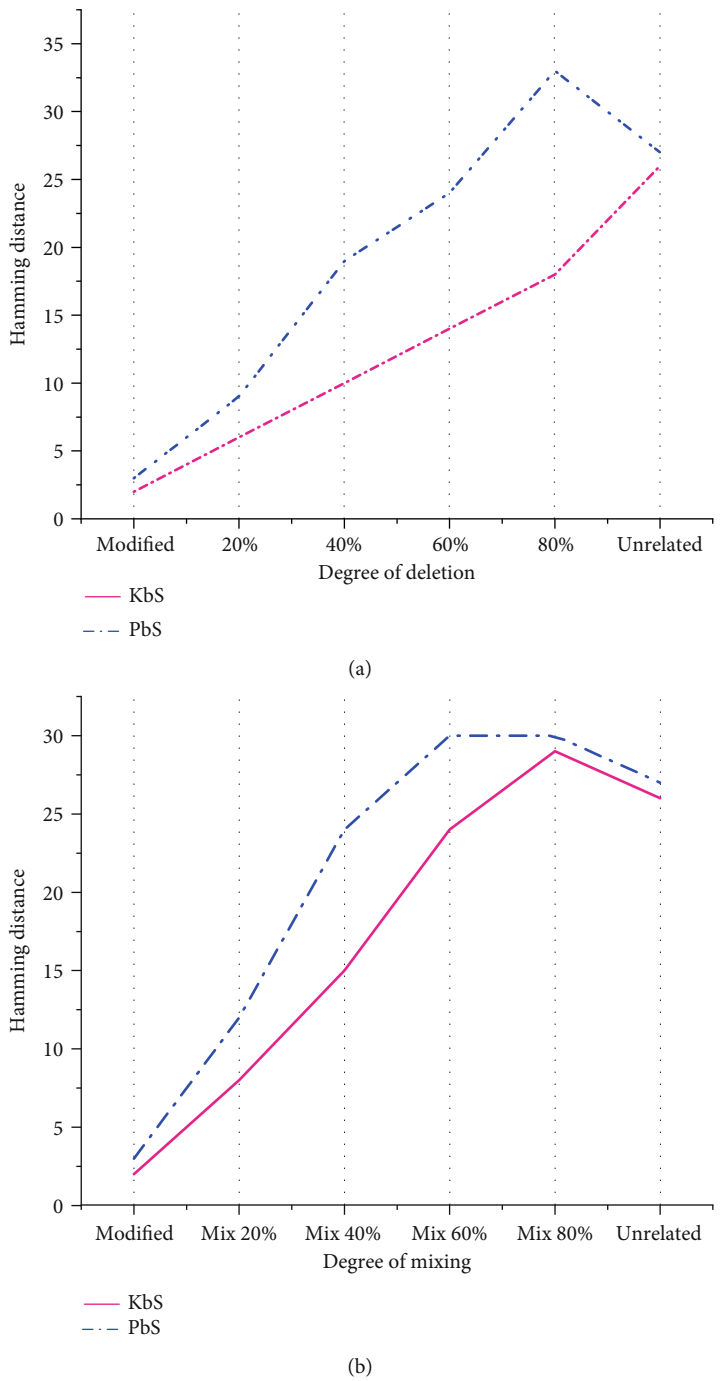

Figure 8: Hamming distance value between the documents under different modified situations and the original confidential documents. (a) The maximum Hamming distance between KbS and PbS under different deletion degrees. (b) The maximum Hamming distance between KbS and PbS under different mixing degrees.

sensitive documents and the confidential documents that are slightly modified to form different versions are concentrated between 0 and 3.

For the experimental results of different degrees of deletion shown in Figure 6, the Hamming distance between the PbS fingerprint and the KbS fingerprint and the original secret-related document will increase with the increase of the degree of deletion. In terms of the degree of discrimination of different degrees of deletion, the degree of Hamming distance distinction between KbS fingerprints is not obvious, and the levels are mixed, while the PbS fingerprints are relatively obvious and hierarchical. Considering the overall amplitude, the KbS fingerprint Hamming distance value is relatively small and concentrated, but the PbS fingerprint Hamming distance is relatively large and scattered. In view of the amplitude changes caused by different degrees of deletion, the variation of the KbS fingerprint Hamming distance is not large, while the PbS fingerprint changes are relatively

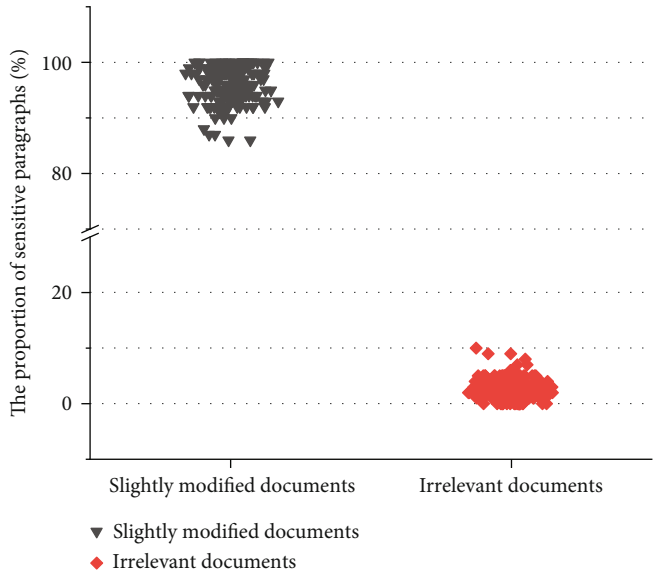

Figure 9: Proportion of sensitive natural segments in the documents.

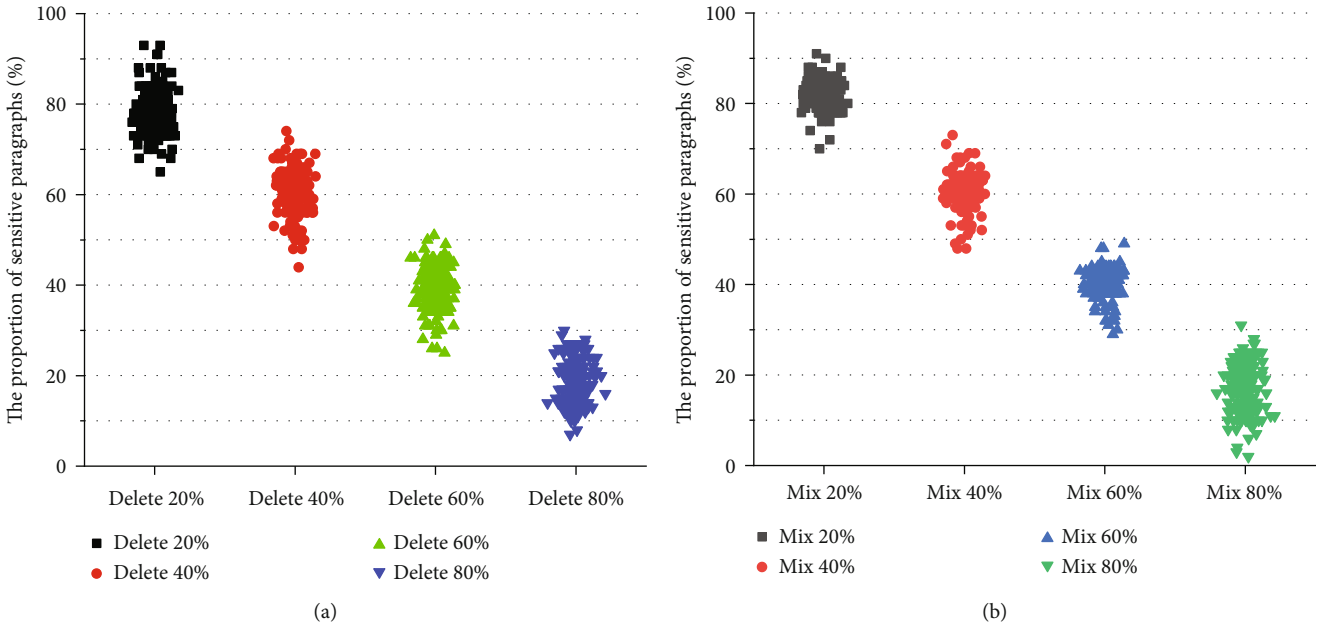

Figure 10: Proportion of sensitive natural segments in the documents under different modification situations. (a) Proportion of sensitive natural segments in documents at different levels of deletion. (b) Proportion of sensitive natural segments in the documents at different levels of mixing.

large. The experimental results under different mixing conditions are shown in Figure 7. KbS fingerprints increase with the increase of the degree of mixing, and Hamming distance increases at the same time. When the degree of mixing exceeds 60%, the variation of the Hamming distance value decreases. Most of them are concentrated in the interval between 18 and 28. When the degree of mixing of PbS fingerprints is greater than 20%, the variation of Hamming distance values decreases which are mostly concentrated between 15 and 30 and are more scattered.

The changes of the Hamming distance are clearly shown in Figure 8, in which the Hamming distance value of the documents under different degrees of modification is the maximum Hamming distance value after removing a few top values and bottom values (2%), while the Hamming distance value of irrelevant documents is the minimum Hamming distance value after removing a few bottom values (2%). If the maximum Hamming distance of the changed documents does not exceed the minimum value of irrelevant documents, it means that a better policy matching effect is generated and sensitive documents are captured accurately.

3.2. SoP Fingerprint Experiment Results. For the experimental implementation of the SoP fingerprint algorithm, the

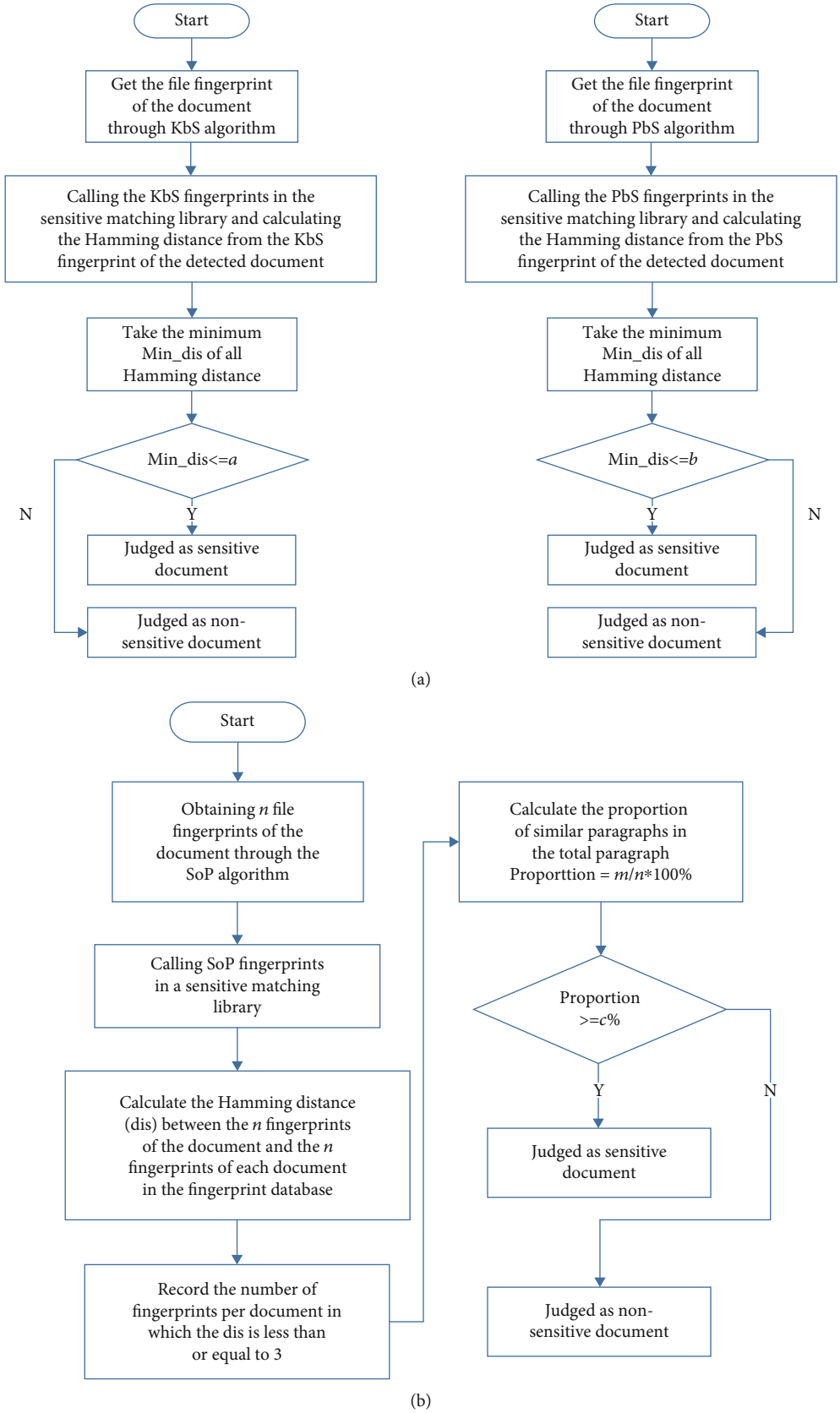

Figure 11: Process flow corresponding to different fingerprint algorithms. (a) KbS fingerprint and PbS fingerprint processing flow chart. (b) SoP fingerprint processing flow chart.

Hamming distance test between three common sensitive documents and original documents was conducted as same as the other two algorithms, which includes the sensitive documents under different modifications, different degrees of content deletion, and different degrees of content mixing. Due to the nature of SoP fingerprints that there is an unfixed number of fingerprints per document, SoP fingerprints no longer use the Hamming distance between documents as the basis for judging whether they are sensitive documents. When the Hamming distance between two documents is less than or equal to 3, the content between the documents is extremely similar. Therefore, in this experiment, the proportion of the number of SoP fingerprints in the document with a Hamming distance less than or equal to 3 to the total number of SoP fingerprints in the entire document is used as the criterion to determine whether the document is a sensitive document.

As shown in Figure 9, a number of SoP fingerprints in each of the 20 irrelevant documents are compared in pairs. The number of Hamming distances less than or equal to 3 accounts for the proportion of the total number of SoP fingerprints in the documents between 0% and 5%. Individual values are higher than 5%. The proportion of sensitive natural segments of the slightly modified document is concentrated above 90%, and only individual values are lower than 90%.

For algorithm fingerprints of SoP, test experiments with different levels of deletion and different levels of mixing were also carried out. As shown in Figure 10, for two different modification situations, the proportion of sensitive natural segments in the document decreases as the degree of modification increases. Since the extraction of paragraph keywords is affected by the amount of paragraph content, individual values will appear relatively discrete. When the degree of modification does not exceed 40%, the proportion of sensitive natural segments in the document is basically higher than 50%. When the degree of modification exceeds 60%, the proportion of sensitive natural segments in the document is basically lower than 50%. When the degree of modification exceeds 80%, the proportion of sensitive natural segments in the document is mostly higher than 10%, and only the individual values are lower.

4. Fingerprint Strategy Customization and Implementation

According to the different needs of different periods in the enterprise, the process of strategy customization will be different. It is roughly divided into the following three typical demand periods. Period 1 is the period of the daily operation of the enterprise, and the level of data loss prevention is low during this period, so the detected document is judged to be a sensitive document when it is very similar to the secret-related document and contains most of the content. In period 2, it is about the company issues patents, software copyrights, etc. The requirement of data loss prevention for this period is medium, so the detected documents are judged to be sensitive documents when they are similar to the secret-related documents and contain some content. In period 3, when the enterprise has a large-scale activity of the "protective network action" or the introduction of important project documents, this period requires a higher level of data loss prevention, so for the detected document, as long as it contains any paragraph content of the secret-related document, it will be recognized as a sensitive document.

Table 2: Parameter values in different periods.

Different periods	Parameter a	Parameter b	Parameter c
1	3	3	90%
2	14	24	50%
3	26	27	10%

According to the three fingerprint algorithms, three different design flows are adopted, as shown in Figure 11. Parameters are the key to judge whether documents in different periods are involved in confidentiality, so they need to be set according to the above experimental Hamming distance distribution. The values of the parameters a, b, and c determine the strictness of the strategy customization, in other words, the level of the data loss prevention.

From the previous chapter, according to the analysis of the experimental data of the Hamming distance, Figure 8 clearly shows that when the Hamming distance between documents is less than or equal to 3, the detected document is a modified version of the secret-related document. The ratio of sensitive segments in slightly modified documents is concentrated at more than 90%, and the similarity is extremely high, which meets the needs of the first period. Therefore, the parameters a and b in Figure 11 can be set to 3, and the parameter c is set to 90%; that is, similar paragraphs account for 90% of the total paragraphs and the documents are considered to be sensitive.

It can be seen from Figure 8 that when the Hamming distance between documents is between 3 and 24, the detected documents are mixed with different levels of secret-related content, meeting the needs of the second period, so a in Figure 11 is set to 15, b is set to 24, and the parameter c is set to 50%. That is, similar paragraphs accounting for more than 50% of the total paragraphs are considered sensitive documents. For the requirements of period 3, any paragraph content containing the secret-related document in the detected document will be judged as a sensitive document. At this time, the accuracy of the KbS fingerprint and PbS fingerprint is insufficient. However, to facilitate the comparison of experimental data, the experimental parameters of KbS and PbS are set as the minimum value of the Hamming distance between unrelated documents; that is, a and b were set as 26 and 27, respectively. Figure 10 shows that when the degree of modification exceeds 80%, the sensitive segment ratio is mostly higher than 10%; thus, the value of c is set to 10%. That is, similar paragraphs accounting for more than ten percent of the total paragraphs are identified as sensitive documents. Table 2 shows the parameter values set in different periods.

In the strategy customization process, it is necessary to consider the accuracy and efficiency of the algorithm selected in different demand periods. Figure 12 shows the time spent

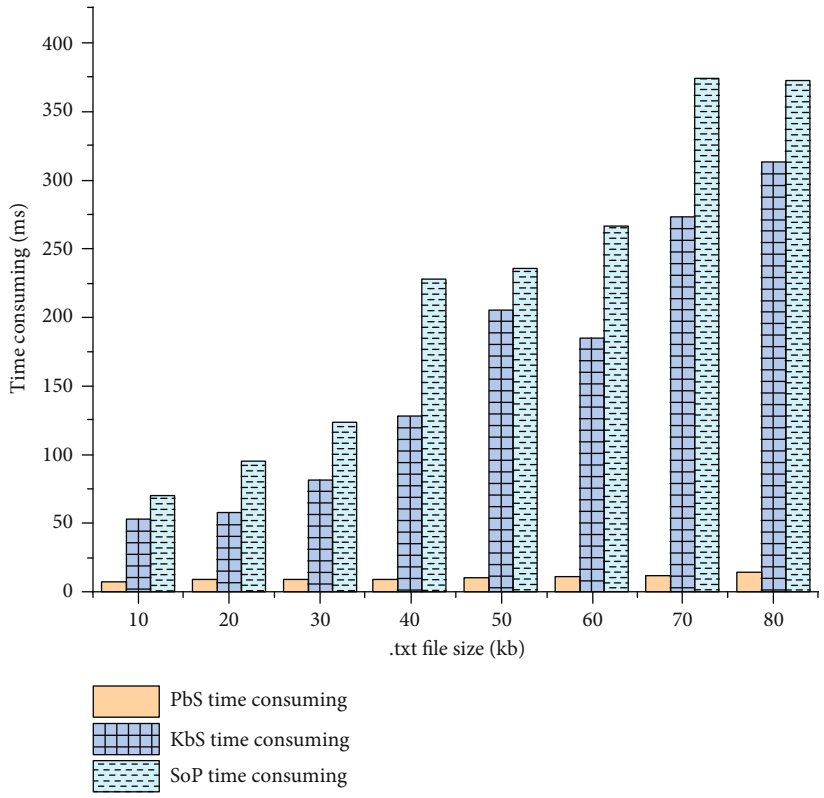

Figure 12: Fingerprint time-consuming graph of three algorithms.

on fingerprint calculation under different sizes of the parsed .txt file. After strategy matching, the files that have been judged as sensitive documents need to be reviewed by the Safety Manager again for human judgment, and the purpose of strategy optimization is to formulate a more reasonable strategy to reduce labor. Therefore, the text of this test is reviewed by the Safety Manager. The Safety Manager judged the confidentiality of the text under different levels of demand according to the needs of different periods. In the enterprise intranet, 1000 documents are randomly selected as test texts, which contain sensitive documents involving different degrees and irrelevant documents. The results of the Safety Manager review of the documents at different levels are as follows: at the low level, 87 documents were identified as sensitive documents, with 238 in the middle level and 385 in the high level.

In order to verify the accuracy of identifying sensitive documents between different algorithms, three indicators of Equations (1), (2), and (3) are used:

$$\text{Precision} = \frac{\text{Num}_{\text{correct}}}{\text{Num}_{\text{total}}}, \tag{1}$$

$$\text{Recall} = \frac{\text{Num}_{\text{correct}}}{\text{Num}_{\text{actual}}}, \tag{2}$$

$$\text{F1} = \frac{2 \times \text{Precision} \times \text{Recall}}{\text{Precision} + \text{Recall}}. \tag{3}$$

Table 3: Accuracy indicators of three fingerprints under different levels.

Levels	Fingerprint process	Precision (%)	Recall (%)	F1 (%)
Low	KbS	80.95	97.7	88.53
	PbS	100	95.4	97.64
	SoP	97.7	97.7	97.7
Medium	KbS	87.73	96.21	91.78
	PbS	74.55	88.65	80.99
	SoP	85.33	95.37	90.07
High	KbS	58.91	81.56	68.41
	PbS	47.52	91.95	62.69
	SoP	91.37	96.36	93.8

Among them, $\text{Num}_{\text{correct}}$ is the number of sensitive documents identified correctly, $\text{Num}_{\text{total}}$ is the number of sensitive documents identified, and $\text{Num}_{\text{actual}}$ is the total number of sensitive documents. This method is used to test the above 1000 documents. Table 3 shows the accuracy indicators of each fingerprint process at different levels. From Table 3, it can be seen that in the period when the data loss prevention level is low, the PbS fingerprint processing flow and the SoP fingerprint processing flow have higher F1 values, but the KbS fingerprint processing flow F1 value is relatively low. Combined with the time consumed of the algorithm of Figure 12 to comprehensive consideration, the efficiency of PbS has an absolute advantage, so it is most appropriate to adopt the PbS fingerprint processing process in this case. In

the period when the data loss prevention level is medium, the F1 values of the KbS fingerprint processing flow and the SoP fingerprint processing flow are above 90%, and there is a high recall rate. Combined with the processing efficiency problem, the KbS fingerprint processing flow has advantages, so in this case, the KbS fingerprint processing process is the most suitable.

However, in period 3 with high requirements for data leakage prevention, the F1 value of the KbS fingerprint and PbS fingerprint processing process is relatively low, while the F1 value of the SoP fingerprint processing process is above 90%, and SoP has high precision and recall rates. Therefore, SoP fingerprint processing can only be adopted in this situation, according to the data in Table 3.

5. Conclusion

In this paper, three kinds of fingerprint algorithms are combined with the targeted secret-related documents in the enterprise for experimental analysis. It provides experimental reference and data reference for the relationship between sensitive documents and Hamming distances between secret-related documents in different situations. It also provides the basis for selecting the parameters of the fingerprint strategy in this paper and calculates and tests the efficiency of three different fingerprints. The fingerprint strategy of this system is formulated for three special periods in the enterprise. Using different fingerprint strategies at different periods can more accurately detect sensitive documents, but occasionally there are cases of false positives. In future work, the system can be optimized and more detailed exploration can be carried out on the basis of the fingerprint strategy experiment, such as the influence of more detailed document changes on the Hamming distance, so as to meet the requirements of a more strict or detailed leak prevention strategy, making the leak prevention system put into production more efficiently and accurately.

Data Availability

The data used to support the findings of this study are included within the article.

Conflicts of Interest

The authors declare that they have no conflicts of interest.

Acknowledgments

This work was supported by the National Natural Science Foundation (61827811), National Defense Basic Research Program (JCKY2019407C002), Hebei Provincial Education Departments Support Plan (SLRC2019042), Hebei Province Funding Project for the Introduction of Overseas Students (C20200364), and China National Petroleum Corporation Information Technology Construction Project (CNPC-IT-2018-N001).

References

[1] H. Liang, A. Xian, M. Mao, P. Ni, and H. Wu, "A research on remote fracturing monitoring and decision-making method supporting smart city," *Sustainable Cities and Society*, vol. 62, 2020.

[2] H. Cheng, N. Xiong, A. V. Vasilakos, L. Tianruo Yang, G. Chen, and X. Zhuang, "Nodes organization for channel assignment with topology preservation in multi-radio wireless mesh networks," *Ad Hoc Networks*, vol. 10, pp. 760–773, 2012.

[3] W. Guo, N. Xiong, H. Chao, S. Hussain, and G. Chen, "Design and analysis of self-adapted task scheduling strategies in wireless sensor networks," *Sensors*, vol. 11, pp. 6533–6554, 2011.

[4] N. Xiong, A. Vandenberg, and W. Han, "Green cloud computing schemes based on networks: a survey," *IET Communications*, vol. 6, pp. 3294–3300, 2012.

[5] I. You, M. R. Ogiela, I. Woungang, and K. Yim, "Innovative security technologies against insider threats and data leakage," *International Journal of Computer Mathematics*, vol. 93, pp. 236–238, 2014.

[6] X. Wang, J. Shi, and L. Guo, "Towards analyzing traceability of data leakage by malicious insiders," *Trustworthy Computing and Services*, 2012.

[7] S. Alneyadi, E. Sithirasenan, and V. Muthukkumarasamy, "A survey on data leakage prevention systems," *Journal of Network and Computer Applications*, vol. 62, pp. 137–152, 2016.

[8] A. Shrivastava and P. Li, "In defense of MinHash over Simhash," *Eprint Arxiv, arXiv*, vol. 1407, 2014https://arxiv.org/abs/1407.4416.

[9] H. Zheng, W. Guo, and N. Xiong, "A kernel-based compressive sensing approach for mobile data gathering in wireless sensor network systems," *IEEE Transactions on Systems, Man, and Cybernetics: Systems*, vol. 48, pp. 2315–2327, 2017.

[10] J. Lin, Q. Huang, and J. Zhang, "Method of data tamper detection by using improved MD5 algorithm," *Computer Engineering & Applications*, vol. 44, pp. 148–150, 2008.

[11] Q. Lv, F. Duan, Y. Wu, and J. He, "Similarity retrieval algorithm based on multilevel fingerprint comparison matrix," *International Symposium on Communication Engineering & Computer Science (CECS 2018)*, vol. 2018, 2018.

[12] L. Xu, S. Sun, and Q. Wang, "Text similarity algorithm based on semantic vector space model," , 2016*IEEE/ACIS 15th International Conference on Computer and Information Science (ICIS)*, vol. 2016, 2016.

[13] R. Gula and M. Ranum, "System and method for using file hashes to track data leakage and document propagation in a network," 2012, Patent ID US 13/403,108,.

[14] Y. Li, F. Liu, Z. Du, and D. Zhang, "A Simhash-based integrative features extraction algorithm for malware detection," *Algorithms*, vol. 11, p. 124, 2018.

[15] Y. Zheng, Z. Xie, Y. Li, G. Shen, and H. Liu, "Spatial vibration of rolling mills," *Journal of Materials Processing Technology*, vol. 213, pp. 581–588, 2013.

[16] Z. Huang, J. Tang, G. Shan, J. Ni, Y. Chen, and C. Wang, "An efficient passenger-hunting recommendation framework with multitask deep learning," *IEEE Internet of Things Journal*, vol. 6, pp. 7713–7721, 2019.

[17] R. A. F. Alvarenga, J. Dewulf, H. Van Langenhove, and M. A. J. Huijbregts, "Exergy-based accounting for land as a natural resource in life cycle assessment," *The International Journal of Life Cycle Assessment*, vol. 18, pp. 939–947, 2013.

[18] H. Wang, S. Liu, and Z. Jia, "A fingerprint of paragraph generation approach for detecting similar document," *Information Technology Journal*, vol. 13, pp. 2309–2317, 2014.

[19] M. Mekonnen, T. Sewunet, M. Gebeyehu, B. Azene, and A. M. Melesse, "GIS and remote sensing-based forest resource assessment, quantification, and mapping in Amhara region, Ethiopia," *Landscape Dynamics, Soils and Hydrological Processes in Varied Climates*, pp. 9–29, 2016.

[20] S. Mellino and S. Ulgiati, "Monitoring regional land use and land cover changes in support of an environmentally sound resource management," *Sustainable Development, Knowledge Society and Smart Future Manufacturing Technologies*, pp. 309–321, 2015.

[21] S. Shimada, T. Ohsawa, T. Kogaki, G. Steinfeld, and D. Heinemann, "Effects of sea surface temperature accuracy on offshore wind resource assessment using a mesoscale model," *Wind Energy*, vol. 18, pp. 1839–1854, 2015.

[22] H. Cheng, Z. Su, N. Xiong, and Y. Xiao, "Energy-efficient node scheduling algorithms for wireless sensor networks using Markov random field model," *Information Sciences*, vol. 329, article S0020025515006945, pp. 461–477, 2016.

[23] H. Cheng, Z. Xie, L. Wu, Z. Yu, and R. Li, "Data prediction model in wireless sensor networks based on bidirectional LSTM," *EURASIP Journal on Wireless Communications and Networking*, vol. 203, 12 pages, 2019.

[24] J. Lyons, A. Dehzangi, R. Heffernan et al., "Predicting backbone Cα angles and dihedrals from protein sequences by stacked sparse auto-encoder deep neural network," *Journal of Computational Chemistry*, vol. 35, pp. 2040–2046, 2014.

[25] L. Ferrer, Y. Lei, M. Mclaren, and N. Scheffer, "Study of senone-based deep neural network approaches for spoken language recognition," *IEEE/ACM Transactions on Audio Speech & Language Processing*, vol. 24, pp. 105–116, 2016.

[26] H. Liang, J. Zou, Z. Li, M. J. Khan, and Y. Lu, "Dynamic evaluation of drilling leakage risk based on fuzzy theory and PSO-SVR algorithm," *Future Generation Computer Systems*, vol. 95, pp. 454–466, 2019.

[27] H. Liang, J. Zou, K. Zuo, and M. J. Khan, "An improved genetic algorithm optimization fuzzy controller applied to the wellhead back pressure control system," *Mechanical Systems and Signal Processing*, vol. 142, Article ID 106708, 2020.

[28] A. Ardakani, F. Leduc-Primeau, N. Onizawa, T. Hanyu, and W. J. Gross, "VLSI implementation of deep neural network using integral stochastic computing," *IEEE Transactions on Very Large Scale Integration (VLSI) Systems*, vol. 25, pp. 2688–2699, 2017.

[29] M. J. Kang and J. W. Kang, "Intrusion detection system using deep neural network for in-vehicle network security," *PLOS ONE*, vol. 11, no. 6, article e0155781, 2016.

[30] Y. Miao, H. Zhang, and F. Metze, "Speaker adaptive training of deep neural network acoustic models using I-vectors," *IEEE/ACM Transactions on Audio Speech and Language Processing*, vol. 23, pp. 1938–1949, 2015.

[31] M. Kolbk, Z. H. Tan, J. Jensen et al., "Speech intelligibility potential of general and specialized deep neural network based speech enhancement systems," *IEEE/ACM Trans Audio Speech Lang Process*, vol. 25, no. 1, pp. 153–167, 2017.

[32] Y. Zhang, R. Zhu, Z. Chen, J. Gao, and D. Xia, "Evaluating and selecting features via information theoretic lower bounds of feature inner correlations for high-dimensional data," *European Journal of Operational Research*, 2020.

Hindawi
Wireless Communications and Mobile Computing
Volume 2020, Article ID 8825318, 9 pages
https://doi.org/10.1155/2020/8825318

Research Article

Analysis of Influencing Factors of Academic Entrepreneurship Based on Blockchain

Jingfang Zhao and Zhenfeng Ge

College of Business Administration, Ningbo University of Finance & Economics, Zhejiang 315175, China

Correspondence should be addressed to Jingfang Zhao; zhaojingfang@nbufe.edu.cn

Received 26 August 2020; Revised 23 October 2020; Accepted 4 November 2020; Published 27 November 2020

Academic Editor: Hongju Cheng

Copyright © 2020 Jingfang Zhao and Zhenfeng Ge. This is an open access article distributed under the Creative Commons Attribution License, which permits unrestricted use, distribution, and reproduction in any medium, provided the original work is properly cited.

Under the background of mass entrepreneurship, academic entrepreneurship activities in universities are booming. DEA model is used to analyze the input-output data of academic entrepreneurship in colleges and universities in 2012 and 2016. According to the validity of the input-output data of academic entrepreneurship in different regions, the differences in efficiency between regions are compared and the reasons are analyzed. The research shows that the economic service function of colleges and universities to regional economic and social development is becoming increasingly prominent, resulting in a certain scale effect; the overall development of academic entrepreneurship efficiency, pure technical efficiency, and scale of colleges and universities in various regions is good, showing an upward trend; academic entrepreneurship activities of colleges and universities in different regions show different development trends. The scale efficiency of each region is at a higher level, but we should also actively pay attention to the utilization efficiency of academic entrepreneurship resources in colleges and universities, improve the allocation of resources, and prevent excessive investment in human and financial resources to produce redundancy, so as to achieve scale expansion while improving efficiency.

1. Introduction

In the era of mass entrepreneurship, stimulating the vitality of regional innovation and entrepreneurship, fully promoting the innovation of the masses, and actively practicing innovation and entrepreneurship have become the main impetuses to promote regional economic development. Academic entrepreneurship is based on academic capacity building and academic capital accumulation in colleges and universities [1]. Academic capital, such as new technology and new knowledge, is transformed into actual products or services according to market demand to realize innovation and entrepreneurship activities of scientific and technological achievement transformation [2]. With academic entrepreneurship as the label, entrepreneurial universities have been paid more and more attention by the society because they are keen to capture the actual demand of the market for the innovative output of colleges and universities so as to realize knowledge innovation and technology transfer [3]. It should be said that in the process of the transformation of entrepreneurial universities, universities have won development opportunities by transforming scientific research achievements into their own development through academic entrepreneurship and will also have an important impact on regional economic development [4]. The development of the blockchain industry policy must be familiar with various blockchain compliances, establish the resource advantages of each branch industry in the blockchain industry, enhance one's own blockchain awareness, and improve the business insight of the blockchain industry.

For academic entrepreneurship, there is no clear definition. The definition of academic entrepreneurship is mainly divided into three different concepts: entrepreneurship orientation, academic orientation, and academic and entrepreneurial consideration [5]. Academic entrepreneurship should integrate the connotations of academic and entrepreneurship with different characteristics and be understood from both narrow and broad sense. In a narrow sense, academic entrepreneurship is a business venture involving scholars or academic organizations; in a broad sense,

academic entrepreneurship also includes entrepreneurial management of academic career. Academic entrepreneurship is a dynamic entrepreneurship system, which includes both the internal entrepreneurial activities of academic organizations and the interaction with other external institutions, such as enterprises and governments [6]. Academic entrepreneurship is a holistic concept. It is now generally believed that it includes not only activities at all levels within the university but also various contacts and cooperation between the University and external institutions. At the same time, attention should be paid to the balance between academic and entrepreneurship [7]. It should be said that academic entrepreneurship should take into account academic and entrepreneurial two aspects, which has been widely recognized by industry scholars [8].

The specific contributions of this paper include

(1) Use the DEA model to analyze the input-output data of college academic entrepreneurship in 2012 and 2016

(2) The difference in efficiency between regions is compared, and the difference in efficiency between regions is obtained

(3) The paper studies the utilization efficiency of academic entrepreneurial resources, which has important guiding significance for improving resource allocation and preventing excessive human and financial investment from generating redundancy

The rest of this paper is organized as follows. Section 2 discusses related work, followed by modelling and evaluation of academic entrepreneurial efficiency in Chinese Universities is discussed in Section 3. Prospects of academic entrepreneurship efficiency research in universities are discussed in Section 4. Section 5 concludes the paper with summary and future research directions.

2. Related Work

The activities were divided in more detail. First, foreign scholars classify the forms of academic entrepreneurship activities in the most detailed way. From the hard to the soft, the activities are divided into science and technology parks, derivative enterprises, patents and licenses, contract research, industrial training courses, consultants, financing, academic publishing, and training of high-quality undergraduates. Hard activities mostly refer to tangible output, while soft activities refer to soft activities [9]. On the contrary, more refers to invisible output. At the same time, it is also believed that academic entrepreneurship in colleges and universities should not be limited to soft or hard activities and should pay attention to whether academic entrepreneurship activities in colleges and universities can promote regional economic development. Second, a domestic scholar divides academic entrepreneurship into three forms according to the different orientations of entrepreneurship: introverted academic entrepreneurship, which externalizes knowledge as a public product and realizes knowledge diffusion by publishing academic achievements [10], outward-looking academic entrepreneurship (such academic entrepreneurship seeks economic profits through invention patents or invention licensing or the creation of derivatives, the most common forms are patent licensing and academic derivatives), and intermediate academic entrepreneurship (such academic entrepreneurship through interagency cooperation to build entrepreneurial networks, so that team growth Maximization, the most common form is joint development). The pattern of academic entrepreneurship is shown in Figure 1 [11].

On the basis of theoretical research, academic entrepreneurship activities in Chinese universities are also growing in practice [12]. At present, the practice of academic entrepreneurship mainly focuses on technology licensing, supplemented by derivatives, and the soft activities mainly publish academic achievements [13]. In order to effectively promote the development of academic entrepreneurship in colleges and universities, the state has formulated and revised laws and regulations concerning property right protection and management, financial loan services, science and technology intermediaries, entrepreneurship service platforms, rewards for the transformation of achievements, tax incentives, personnel training, and financing of venture funds, with special emphasis on passing them [14]. Reform releases the vitality of scientific researchers and encourages those who make major contributions to research and development and transformation of research results to hold equity and options [15]. It should be said that the state at the policy level for academic entrepreneurship to create a good environment for innovation and entrepreneurship, while provinces and regions also actively take various measures to build a good ecological environment for innovation and entrepreneurship, promote innovation and entrepreneurship personnel training, and actively promote the implementation of innovation and entrepreneurship strategy [16].

However, due to the short development of academic entrepreneurship activities in domestic universities, its level and influence need to be improved. According to the statistics of China Science and technology statistical yearbook, 2012-2016 years of colleges and universities sell as a reference [17].

Colleges and universities provide strong support for regional economic development with the advantages of talents, scientific research, and scientific and technological achievements and information. The academic entrepreneurial activities in colleges and universities maintain a benign and mutually beneficial relationship with regional economic and social development. Academic entrepreneurship can produce better social and economic benefits and produce agglomeration effects. The indirect economic benefits of academic entrepreneurship are as follows: first, the effect of knowledge transformation [18].

Academicians start their own businesses with the help of accumulated knowledge and technology, which is conducive to knowledge spillover and industrialization of scientific and technological achievements. The second is the effect of industrial agglomeration. Academic entrepreneurship has formed the centralization of derivative enterprises in universities [19].

Third, the cooperation effect. For experts, scholars, inventors to effectively participate in the in-depth development of their technology to open up new avenues [20].

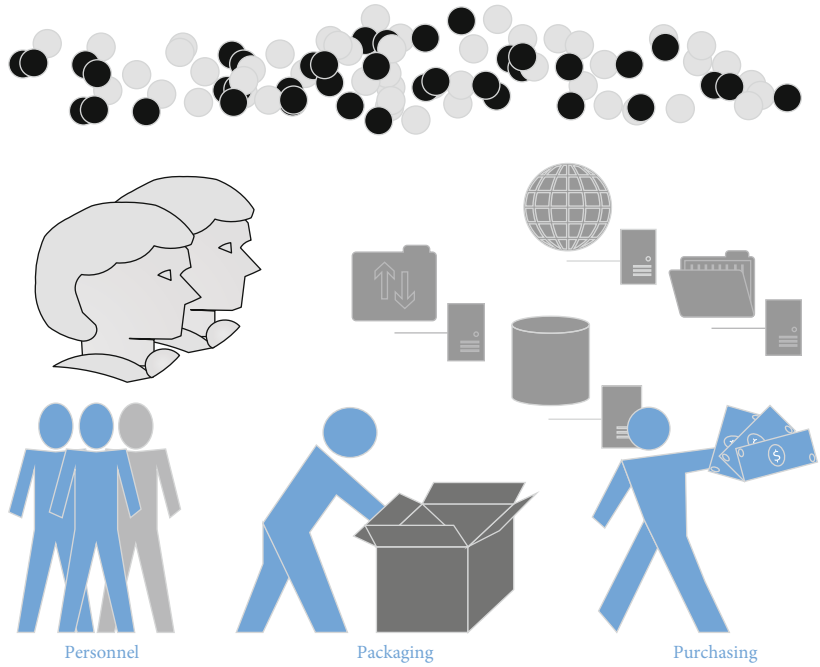

Figure 1: The pattern of academic entrepreneurship.

Colleges and universities gather human resources, scientific and technological resources, and technological resources and constitute a regional innovation and entrepreneurship network carrier, which has an important impact on the industrial development of the regional economy [21]. Especially, the evolution of the relationship between universities and regional cooperation has constantly tried new ways of cooperation, from the mode of technology licensing or transfer of achievements to the mode of using and exploring innovation to realize the transfer of key technology knowledge, and promote regional economic development [22, 23]. Academic innovation, technological research and development in colleges and universities, and the transformation of scientific research achievements into productive forces can promote the development of the regional economy [24]. Through the feedback mechanism, enterprises put forward higher requirements to the technology research and development and innovation and entrepreneurship education in colleges and universities and improve their effectiveness in serving the local economic development [25, 26]. Figure 2 is the educational background of entrepreneurs, Figure 3 is the career characteristics of entrepreneurs, Figure 4 is the attributes of entrepreneurs, and Figure 5 is the frequency characteristics of entrepreneurs.

3. Modelling and Evaluation of Academic Entrepreneurial Efficiency in Chinese Universities

3.1. Research Method. Data envelopment analysis (DEA) is based on the concept of relative efficiency; this paper evaluates the relative effectiveness of the same kind of multi-index input-output economic system. This method does not need to determine the explicit expression of the relationship between input and output and exclude many subjective factors and has a strong objectivity [27]. Therefore, the DEA method is the most important one. Typical nonparametric methods are widely used in the efficiency evaluation of various systems. At the same time, a large number of studies have found that the efficiency frontier evaluated by the DEA model has considerable robustness and is more suitable for small sample efficiency analysis network. Therefore, this paper uses the DEA model to analyze the academic entrepreneurship efficiency of colleges and universities in 2012 and 2016. According to the effectiveness of academic entrepreneurship output in different regions, this paper compares the efficiency differences between regions and analyzes the reasons for this gap [28].

Suppose there are x evaluation areas, each of which is denoted as a DMU, and each DMU has a type of academic venture capitalist and a type of academic venture output. The Y academic venture capitalist of DMUm is represented by rym, and the A academic venture output of DMUm is represented by Sam. The input matrix R, the input weight coefficient matrix J, the output matrix S, and the output weight coefficient I are represented by rym [29]. For each region DMU, the corresponding academic entrepreneurial efficiency evaluation index can be expressed as

$$Bm = I^C Sn / J^C Rm = \frac{\sum_{i=1}^{l} I_i S_{\text{in}}}{\sum_{i=1}^{l} J_i R_{\text{in}}}, \tag{1}$$

$$Rm = (r1m, r2m, \cdots, rlm)^T, \tag{2}$$

$$Sm = (s1m, s2m, \cdots, slm)^T, \tag{3}$$

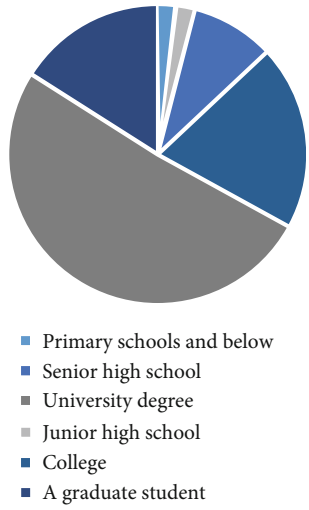

Figure 2: Academic qualifications of entrepreneurs.

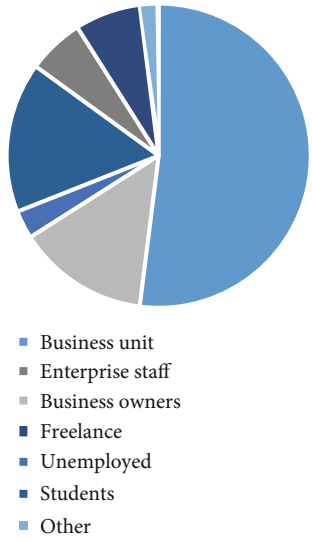

Figure 3: Career characteristics of entrepreneurs.

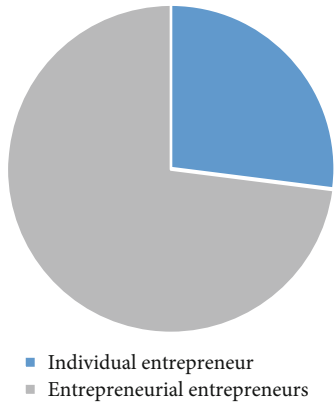

Figure 4: Attributes of the entrepreneur.

$$J = (j1, j2, \cdots, jl)^T, \tag{4}$$

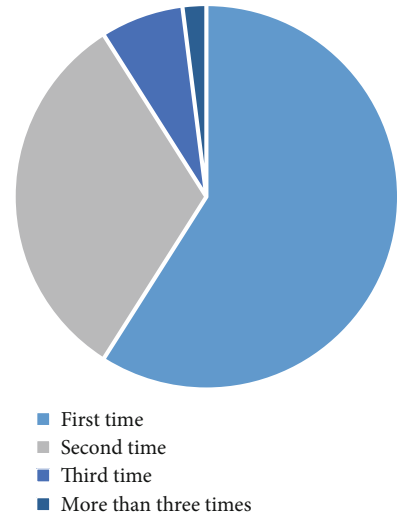

Figure 5: The entrepreneurial frequency characteristics of the entrepreneur.

$$I = (i1, i2, \cdots, il)^T. \tag{5}$$

In which, $j = (1, 2, \cdots, x)$, $i = (1, 2, \cdots, x)$. Where I^c and J^c represent the weight vector output by the input, respectively, and the weight I and J are selected appropriately to enable $Bm < 1(m = 1) \cdots, x)$ [30].

If M is set as a parameter, the evaluation of each DMU is denoted as DMU_0, whose input is R_0 and output is S_0, then the m. E_2F evaluation model of the relative entrepreneurial efficiency of individual DUM is

$$\mathrm{Min}\ \theta \mathrm{s.t.} \left\{ \begin{array}{c} \sum_{m=1}^{l} R_m G_m \le \theta R0, m = 1, 2, \cdots, \times \\ S0 \le \sum_{m=1}^{l} R_m G_m \end{array} \right\} \tag{6}$$

The relaxation variable a^+ and the residual variable a^- are further introduced, and the non-Archimedean infinitesimal h is introduced. The E_2F model with the non-Archimedean infinitesimal h is established:

$$\mathrm{Min}\left[\theta - h\left(\sum_{m=1}^{l} a^+ + \sum_{m=1}^{l} a^-\right)\right] = Jk(h), \tag{7}$$

$$\mathrm{s.t.} \left\{ \begin{array}{c} \sum_{m=1}^{l} R_m G_m \le \theta R0, m = 1, 2, \cdots, \times \\ S0 \le \sum_{m=1}^{l} R_m G_m \end{array} \right\} \tag{8}$$

The optimal solution is $\theta_0, g0, a_0{}^+, a_0{}^-$. In this model, R, the output S of academic entrepreneurship, gm, and 0 value of academic entrepreneurship efficiency of a local university. When the value of $\theta_0 = -1$, it indicates that the evaluated region DMU_0 academic entrepreneurship is relatively

Table 1: The output of academic entrepreneurship.

Region ID	Torch	Mode	Index name
1	R1	Input index	Number of local colleges and universities
2	R2		Number of R&D projects
3	R3		Number of personnel (persons)
4	R4		Investment fund (10,000 yuan)
5	S1	Output index	Number of published papers
6	S2		Scientific and technical publications (division)
7	S3		Valid invention patent (item)
8	S4		Number of patent ownership transfer and license
9	S5		Patent transfer licensee (ten thousand yuan)
10	S6		Form national or industry standards (individual)

effective, that is, in the n evaluated regions, the output of S_0 is optimal on the basis of the input of R_0. When the value of θ is less than 1, it indicates that DMU_0 investment is relatively ineffective, and $1-\theta$ is the proportion of multiple investors for academic entrepreneurship of colleges and universities in this region, that is, it can reduce the investment to θR_0 while keeping the original output S_0 unchanged.

3.2. The Data Source. This paper uses part of higher education data from China statistical yearbook of science and technology in 2012 and 2016 to analyze the overall situation of investment output of academic entrepreneurship in universities.

The establishment of the evaluation index system of academic entrepreneurship efficiency in colleges and universities is a complex problem. The evaluation index system is considered from the perspective of operability, comparability, and scientificity, and the opinions of relevant experts are also consulted.

As for the current situation of academic entrepreneurship activities in Chinese universities, this paper mainly chooses the input-dea model to determine the input-output index of academic entrepreneurship in colleges and universities from the perspective of whether it is effective to invest when the output of academic entrepreneurship is certain in Table 1.

3.3. The Evaluation Results. CZR model was applied to evaluate the academic entrepreneurship efficiency of universities in 2012 and 2016, and the output results are shown in Table 2.

The input and output comprehensive efficiency (CB), pure technical efficiency (UCB), and scale efficiency (AB) of academic entrepreneurship in universities have the following relations: CB = UCB ∗ AB, so as to analyze the relationship between the comprehensive efficiency of academic entrepreneurship in universities and pure technical efficiency and scale efficiency. The value of comprehensive efficiency is equal to 1, which indicates that the academic entrepreneurship DEA is effective in the evaluated region, indicates that the academic entrepreneurship resources are fully utilized, and the investment output is brought into full play. The value of comprehensive efficiency is less than 1, indicating that the DEA is invalid for academic entrepreneurship in the evaluated region, indicating that technical inefficiency and scale inefficiency exist in academic entrepreneurship. However, it

Table 2: The output results 1.

Year	2012			2016		
Province name	CB	UCB	AB	CB	UCB	AB
Beijing	1.00	1.00	1.00	1.00	1.00	1.00
Tianjin	0.86	0.85	0.91	0.81	0.84	0.95
Hebei	1.00	1.00	1.00	1.00	1.00	1.00
Shanghai	1.00	1.00	1.00	1.00	1.00	1.00
Jiangsu	1.00	1.00	1.00	1.00	1.00	1.00

should be noted that the academic entrepreneurship efficiency value calculated by the DEA model is a kind of "relative efficiency," and the actual efficiency level is less than or equal to the DEA estimate.

As a whole, the comprehensive efficiency of academic entrepreneurship, pure technology efficiency, and scale efficiency of colleges and universities in various regions are developing well, showing an upward trend. It can be seen from Table 2 in 2012, the overall efficiency of academic entrepreneurship output of colleges and universities reached the optimal efficiency in 17 provinces including Beijing, Shanghai, Hebei, Jiangsu, Zhejiang, and Fujian. In 2012, the overall efficiency ratio of academic entrepreneurship in colleges and universities was 0.864. There are 11 provinces and regions below the average line and 20 provinces and regions above the average. In 2016, the comprehensive efficiency reached the optimal DEA efficiency in 13 provinces, including Beijing, Hebei, Jiangsu, Shanghai, and Hainan. In 2016, the national average of comprehensive efficiency of academic entrepreneurship in colleges and universities was 0.937, with 14 provinces and cities below the average, and 17 provinces and cities above the average. It can be seen that, compared with 2012, the average level of comprehensive efficiency of academic entrepreneurship in colleges and universities in various regions in China has increased by 0.07, and the overall level is continuously improving.

In terms of pure technical efficiency, in 2012, there were 18 regions with the optimal pure technical efficiency of academic entrepreneurship in universities, 7 of which were less than 80% effective, and 24 of which were more than 80% effective. The national average of pure technical efficiency was 0.916. In 2016, there were 14 regions with the optimal

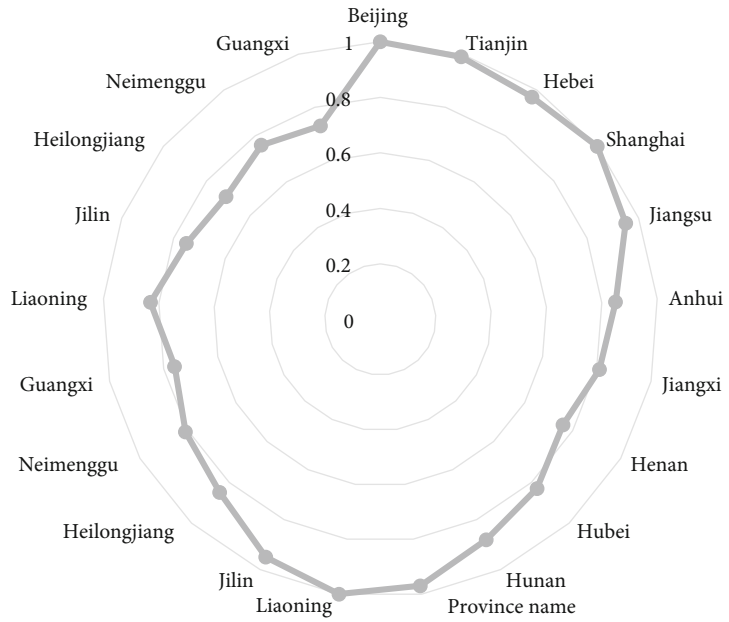

Figure 6: The output efficiency of academic venture capital investment.

technical efficiency of academic entrepreneurship in colleges and universities. Only 2 regions were less than 80% effective, and the remaining 29 regions were all higher than 80%. The national average of pure technical efficiency was 0.946. Although the number of optimal efficiency areas has decreased, the average level of national pure technical efficiency has increased significantly.

From the perspective of scale efficiency, the national average of academic entrepreneurship scale efficiency in universities was 0.978 in 2012 and 0.9893 in 2016. It can be seen that the scale efficiency of various regions has increased and maintained a high running trend.

From the perspective of individuals, the comprehensive efficiency of each region in 2012 and 2016 showed an upward trend in 11 regions, among which Jiangxi and Tibet had the fastest growth rate, with an increase of more than 30%; It was followed by Hunan, Inner Mongolia, Guizhou, Yunnan, and Gansu, with an increase of more than 20 percent. In 2012 and 2016, the pure technical efficiency increased in 11 regions, among which Jiangxi, Hunan, Inner Mongolia, Guizhou, Yunnan, and Gansu showed rapid growth. Tibet and Gansu showed the fastest growth in scale efficiency in 2012 compared with 2016. It is not hard to find that the growth areas are mainly in the central and western regions, such as Tibet, Guizhou, Yunnan, and Gansu, where the comprehensive efficiency level is not at a very high level nationwide. However, these regions have attached great importance to academic venture capital investment, which has developed rapidly and achieved rapid development in the output efficiency of academic venture capital investment, as shown in Figure 6.

At the same time, Shandong, Guangdong, Shaanxi, and other regions showed a certain downward trend, with a decreasing range of 0. The academic entrepreneurship efficiency of the universities in these regions needs to be further improved to increase the effective investment in academic entrepreneurship and improve the output efficiency.

Table 3: The output results 2.

Year	2012			2016		
Province name	CB	UCB	AB	CB	UCB	AB
Anhui	0.81	0.88	0.87	0.91	0.77	0.91
Jiangxi	0.66	0.67	0.72	0.85	0.73	0.44
Henan	1.00	1.00	1.00	1.00	1.00	1.00
Hubei	1.00	1.00	1.00	1.00	1.00	1.00
Hunan	0.89	0.91	1.00	1.00	1.00	1.00

The east, west, central, and northeast regions showed different development trends. It can be seen from Table 3 that academic entrepreneurship in universities in the east, west, and northeast of China presents different development trends. Overall, the scale efficiency of the east, west, and northeast is at a high level, and the main factor affecting the comprehensive efficiency of each region is the pure technical efficiency. From the perspective of regional comparison, first of all, the efficiency of eastern regions declined slightly in 2016, mainly because the academic entrepreneurship efficiency of universities in the eastern regions of Tianjin, Shandong, and Guangdong decreased significantly. At the same time, it also indicates an important information that the resource utilization of academic venture capital output in the eastern region needs to be concerned. More investment in academic entrepreneurship does not mean greater output. Effective and reasonable utilization of academic achievement resources and active realization of transformation are the key to improve resource utilization. Second, the academic entrepreneurship efficiency of colleges and universities in the central and western regions has been outstanding. From the numerical perspective, it can be seen that great progress has

been made. In the past five years, after the rapid economic development of the central and western regions, various regions have been stepping up their efforts in the construction of colleges and universities, and academic investment and output of colleges and universities have achieved substantial development. The amount and quality of academic research projects have been improved in terms of investment in academic research, personnel allocation, and research projects, and the efficiency of academic entrepreneurship has been improved rapidly. Finally, the academic entrepreneurship efficiency of universities in northeast China is in a stable state.

The results of academic entrepreneurship efficiency of universities in Zhejiang and Jiangxi in 2012 and 2016 were analyzed. The results are shown in Tables 4 and 5.

It can be seen from Tables 2 and 4, the comprehensive efficiency of academic entrepreneurship in universities in Zhejiang province reached the optimization of DEA efficiency, with the highest efficiency of venture capital investment and output without any shortage or redundancy. In 2016, the comprehensive efficiency of academic entrepreneurship in universities in Zhejiang was 0.961, the pure technical efficiency was 0.964, the scale efficiency was 0.997, and the scale return was increasing. In the case of a given output, in 2016 in Zhejiang university academic entrepreneurship in investment funds, personnel, and R&D project number, there are varying degrees of redundancy, in terms of investment, investment research elements to reduce 122.27 million yuan, for personnel quality to reduce 508, redundancy factors of R&D projects is 1617 items, still can keep output unchanged.

It can be seen from Tables 2 and 5, the comprehensive efficiency of academic entrepreneurship of colleges and universities in Jiangxi is 0.539, the pure technical efficiency is 0.553, the scale efficiency is 0.975, and the scale return is increasing. In 2016, the comprehensive efficiency of academic entrepreneurship of colleges and universities in Jiangxi was 0.856, the pure technical efficiency was 0.871, the scale efficiency was 0.983, and the scale return was decreasing. In terms of overall efficiency, 2016 was 0.3 higher than 2012. However, in 2016, the academic entrepreneurship efficiency of colleges and universities in Jiangxi province was in the stage of diminishing returns on scale, and there was still a certain amount of redundancy for venture capital investors. Therefore, it was necessary to reasonably allocate resources and improve the utilization rate of resources, so that the output efficiency of academic entrepreneurship became more effective.

Table 4: The output results 3.

Year		2012			2016	
Province name	CB	UCB	AB	CB	UCB	AB
Liaoning	0.71	0.77	0.77	0.91	0.77	0.91
Jilin	0.66	0.67	0.72	0.75	0.73	0.44
Heilongjiang	0.61	0.66	0.66	0.91	0.66	0.91
Neimenggu	0.66	0.66	0.62	0.65	0.63	0.44
Guangxi	0.79	0.91	1.00	1.00	1.00	1.00

Table 5: The output results 4.

Year		2012			2016	
Province name	CB	UCB	AB	CB	UCB	AB
Liaoning	0.71	0.77	0.77	0.71	0.77	0.71
Jilin	0.99	0.97	0.72	0.75	0.73	0.44
Heilongjiang	0.91	0.99	0.99	0.71	0.99	0.71
Neimenggu	0.99	0.99	0.92	0.95	0.93	0.44
Guangxi	0.77	0.71	1.00	1.00	1.00	1.00

4. Prospects of Academic Entrepreneurship Efficiency Research in Universities

The academic entrepreneurship activities of colleges and universities in the east, west, and northeast show different development trends. The scale efficiency of the eastern, western, central, and northeastern regions is at a high level. With the further development of the western economy, the academic venture investment and output of the universities in the western regions have performed well, and they are actively exceeding the national average. The eastern region has a solid economic foundation and strong ability to invest in academic entrepreneurship in universities. It should be said that the academic entrepreneurship activities of colleges and universities in various regions are developing vigorously, which is very strong for the regional economic development. But at the same time, the complexity of academic entrepreneurship in universities determines the complexity of regional economic development, and the interaction between universities in various regions and regional economic development will also show a different development trend.

It is necessary to pay attention to efficiency in the output of academic entrepreneurship in universities in various regions. Shandong, Guangdong, Hubei, and other regions are in the stage of diminishing returns to scale, and the increase rate of output is lower than that of investors, which is worthy of attention. Especially in the eastern region, we should pay attention to the utilization efficiency of resources in the output of academic venture investment in universities and prevent the surplus of scientific research staff, financial staff, and material investment staff. Therefore, in the context of increasing regional support for the development of academic entrepreneurship in colleges and universities, colleges and universities need to adjust their layout reasonably, improve resource allocation, and achieve scale expansion while improving efficiency.

It is feasible to evaluate the efficiency of academic entrepreneurship in colleges and universities by the DEA method. At the same time, it is more important to analyze the significant factors influencing the academic entrepreneurship efficiency of each region. At the same time, the efficiency evaluation system of academic entrepreneurship will be further subdivided and deepened, which is the focus of further research.

5. Conclusions

Academic entrepreneurship has become an important way to realize the development of colleges and universities. Reconstruct themselves through self-employment spirit in colleges

and universities of the organizational structure and culture, by emphasizing the knowledge creation and knowledge transfer activity is effective and practical, the transformation of knowledge resources in colleges and universities to intellectual capital for the development of colleges and universities to provide continuous power of a kind of educational strategy, as well as regional economic development has brought new vigor and vitality Sichuan. This paper uses DEA model academic entrepreneurship and has carried on the comprehensive evaluation of efficiency in colleges and universities, both make up for the traditional method of analyzing the present situation of academic entrepreneurial activities in colleges and universities, also from the new angle of view opens up college academic entrepreneurship and regional economic development of the interactive space.

Academic entrepreneurship activities in universities in various regions of China are developing rapidly. Overall, scale efficiency is always high and running at a high level. Colleges and universities have a certain scale effect on the economic service function of regional economic and social development. It should be said that as an important participant of regional knowledge innovation, technology transfer and innovation, and entrepreneurship, the close combination of scientific research advantages and regional scientific and technological demands will greatly improve the technology conversion rate and promote social and economic development.

Data Availability

All data can be obtained from the author.

Conflicts of Interest

The authors declare that they have no conflicts of interest.

Acknowledgments

This work is supported by Research on the dynamic evolution mechanism of gazelle enterprise growth under the background of digital economy (20YJC630223).

References

[1] T. Åstebro, P. Braunerhjelm, and A. Broström, "Does academic entrepreneurship pay?," *Industrial and Corporate Change*, vol. 22, no. 1, pp. 281–311, 2013.

[2] D. S. Siegel and M. Wright, "Academic entrepreneurship: time for a rethink?," *British Journal of Management*, vol. 26, no. 4, pp. 582–595, 2015.

[3] M. Wright, "Academic entrepreneurship, technology transfer and society: where next?," *Journal of Technology Transfer*, vol. 39, no. 3, pp. 322–334, 2014.

[4] M. Abreu and V. Grinevich, "The nature of academic entrepreneurship in the uk: widening the focus on entrepreneurial activities," *Research Policy*, vol. 42, no. 2, pp. 408–422, 2013.

[5] J. Y. Farsi, M. Modarresi, M. Motavaseli, and A. Salamzadeh, "Institutional factors affecting academic entrepreneurship: the case of university of tehran," *Economic Analysis*, vol. 47, no. 1-2, pp. 139–159, 2014.

[6] B. Bozeman, D. Fay, and C. P. Slade, "Research collaboration in universities and academic entrepreneurship: the-state-of-the-art," *Journal of Technology Transfer*, vol. 38, no. 1, pp. 1–67, 2013.

[7] H. Shaheen, "The Chicago handbook of university technology transfer and academic entrepreneurship," *Journal of Educational Technology & Society*, vol. 18, no. 3, pp. 326-327, 2015.

[8] C. Kolb and M. Wagner, "Crowding in or crowding out: the link between academic entrepreneurship and entrepreneurial traits," *Journal of Technology Transfer*, vol. 40, no. 3, pp. 387–408, 2015.

[9] D. Urbano and M. Guerrero, "Entrepreneurial universities," *Economic Development Quarterly*, vol. 27, no. 1, pp. 40–55, 2013.

[10] C. S. Hayter, "Constraining entrepreneurial development: a knowledge-based view of social networks among academic entrepreneurs," *Research Policy*, vol. 45, no. 2, pp. 475–490, 2016.

[11] C. Kolympiris, N. Kalaitzandonakes, and D. Miller, "Location choice of academic entrepreneurs: evidence from the US biotechnology industry," *Journal of Business Venturing*, vol. 30, no. 2, pp. 227–254, 2015.

[12] K. Nielsen, "Human capital and new venture performance: the industry choice and performance of academic entrepreneurs," *Journal of Technology Transfer*, vol. 40, no. 3, pp. 453–474, 2015.

[13] M. E. Braun, "Academic entrepreneurship and community engagement: scholarship in action and the Syracuse miracle," *Community Development*, vol. 47, no. 4, pp. 581-582, 2016.

[14] J. P. Walsh and H. Huang, "Local context, academic entrepreneurship and open science: publication secrecy and commercial activity among Japanese and us scientists," *Research Policy*, vol. 43, no. 2, pp. 245–260, 2014.

[15] G. Secundo and G. Elia, "A performance measurement system for academic entrepreneurship: a case study," *European Journal of Marketing*, vol. 18, no. 3, pp. 23–37, 2014.

[16] C. S. Hayter, "Public or private entrepreneurship? Revisiting motivations and definitions of success among academic entrepreneurs," *Journal of Technology Transfer*, vol. 40, no. 6, pp. 1003–1015, 2015.

[17] F. J. Miranda, A. Chamorro-Mera, and S. Rubio, "Academic entrepreneurship in Spanish universities: an analysis of the determinants of entrepreneurial intention," *European Research on Management and Business Economics*, vol. 23, no. 2, pp. 113–122, 2017.

[18] A. P. Wall, P. Mcgowan, and M. C. Brennan, "Academic entrepreneurship," *International Journal of Humanities & Social Science*, vol. 2, no. 1, pp. 14–22, 2013.

[19] T. B. Astebro, S. Braguinsky, P. Braunerhjelm, and A. Broström, *Academic entrepreneurship: Bayh-Dole versus the 'professor's privilege*, Social Science Electronic Publishing, USA, 2015.

[20] M. D. Silva, "Academic entrepreneurship and traditional academic duties: synergy or rivalry?," *Studies in Higher Education*, vol. 41, no. 1, pp. 1–15, 2016.

[21] M. A. Lundqvist and K. L. Williams Middleton, "Academic entrepreneurship revisited – university scientists and venture creation," *Journal of Small Business & Enterprise Development*, vol. 20, no. 3, pp. 603–617, 2013.

[22] C. Lin, N. Xiong, J. H. Park, and T. Kim, "Dynamic power management in new architecture of wireless sensor networks,"

International Journal of Communication Systems, vol. 22, no. 6, pp. 671–693, 2009.

[23] Y. Sang, H. Shen, Y. Tan, and N. Xiong, "Efficient protocols for privacy preserving matching against distributed datasets," in *International Conference on Information and Communications Security*, pp. 210–227, Springer, Berlin, Heidelberg, 2006.

[24] F. Long, N. Xiong, A. V. Vasilakos, L. T. Yang, and F. Sun, "A sustainable heuristic QoS routing algorithm for pervasive multi-layered satellite wireless networks," *Wireless Networks*, vol. 16, no. 6, pp. 1657–1673, 2010.

[25] J. Li, N. Xiong, J. H. Park, C. Liu, S. MA, and S. E. Cho, "Intelligent model design of cluster supply chain with horizontal cooperation," *Journal of Intelligent Manufacturing*, vol. 23, no. 4, pp. 917–931, 2012.

[26] W. Guo, N. Xiong, A. V. Vasilakos, G. Chen, and C. Yu, "Distributed k–connected fault–tolerant topology control algorithms with PSO in future autonomic sensor systems," *International Journal of Sensor Networks*, vol. 12, no. 1, pp. 53–62, 2012.

[27] Z. Chen, D. Chen, Y. Zhang, X. Cheng, M. Zhang, and C. Wu, "Deep learning for autonomous ship-oriented small ship detection," *Safety Science*, vol. 130, article 104812, 2020.

[28] Z. Huang, X. Xu, J. Ni, H. Zhu, and C. Wang, "Multimodal representation learning for recommendation in Internet of Things," *IEEE Internet of Things Journal*, vol. 6, no. 6, pp. 10675–10685, 2019.

[29] W. Wei, M. Wozniak, R. Damaeviius, X. Fan, and Y. Li, "Research of known-plaintext attack on double random phase mask based on WSNs," *Journal of Internet Technology*, vol. 20, no. 1, pp. 39–48, 2019.

[30] L. Dong, W. Wu, Q. Guo, M. N. Satpute, T. Znati, and D. Z. du, "Reliability-aware offloading and allocation in multilevel edge computing system," *IEEE Transactions on Reliability*, vol. 12, pp. 1–12, 2019.

Hindawi
Wireless Communications and Mobile Computing
Volume 2020, Article ID 8819083, 7 pages
https://doi.org/10.1155/2020/8819083

Research Article

Research on Financial Data Query and Distribution Scheme Based on SQL Database

Xiaolan Fu

School of Economics and Trade Tourism, Hefei Technology College, Hefei 230011, China

Correspondence should be addressed to Xiaolan Fu; pengyongfang@hgu.edu.cn

Received 30 August 2020; Revised 10 October 2020; Accepted 6 November 2020; Published 26 November 2020

Academic Editor: Hongju Cheng

Copyright © 2020 Xiaolan Fu. This is an open access article distributed under the Creative Commons Attribution License, which permits unrestricted use, distribution, and reproduction in any medium, provided the original work is properly cited.

With the advance of optimization and merger colleges and universities, a university often contains more than one campus. The traditional centralized education management system has been unable to meet the needs of use. The model detects the intrusion by dividing the clusters in the clustering result into normal clusters and abnormal clusters and analyzing the weighted average density of object x to be detected in each cluster and the weighted overlapping distance of x and each centre point. We verified the intrusion detection performance of the model on the KDD Cup 99 dataset. The experimental results show that the model established in this paper has certain theoretical value.

1. Introduction

The educational administration information system of colleges and universities mainly manages the relevant educational administration information of colleges and universities. Relying on the basic platform of campus network, it plays an increasingly important role in teaching and management application [1, 2]. By combining intrusion detection algorithms, this paper solves the problems of k -mode algorithm based on rough set theory and applies the improved algorithm to intrusion detection [3]. Firstly, aiming at k pattern clustering in initial class centre selection, an initial class centre selection algorithm unweights based on weighted density and weighted overlap distance is proposed. Secondly, this article further improves the model on the basis of the above [4].

As an important part of China's education, intrusion detection helps systems respond to cyberattacks by monitoring and analyzing user and system activity and statistically analyzing system vulnerabilities, detecting known intrusions and alarms, auditing new anomalous behaviors, and assessing integrity of critical data files. System administrators' security management capabilities have been extended through auditing and monitoring, intrusion identification and response, reducing the workload of system administrators [3]. In addition, the intrusion detection system dilutes the restrictions on professionals in network security, making it easy for nonprofessional personnel to manage network systems. In addition, the intrusion detection system can respond to the discovered network intrusion, illegal operation, timely and proactive response and management [5].

2. Related Work

Database technology management is about the existing problems of intrusion detection systems. Data mining technology has been widely used in the field of intrusion detection in recent years. Among them, cluster-based unsupervised intrusion detection has attracted extensive attention. At present, many kinds of clustering algorithms have been applied to intrusion detection [6]. As an effective extension of k -means algorithm, it can effectively process classified data. It inherits the characteristics of efficient k-means algorithm. The algorithm to implement has been widely applied in many fields. Therefore, K pattern algorithm has a very broad application prospect in the field of intrusion detection. However, there are few researches on applying K pattern [7].

At present, it is in a difficult existing problem of intrusion detection systems. Data mining technology has been widely used in the field of intrusion detection in recent years.

Among them, cluster-based unsupervised intrusion detection has attracted extensive attention. At present, many kinds of clustering algorithms have been applied to intrusion detection. As an effective extension of k-means algorithm, it can effectively process classified data. It inherits the often cannot handle the concurrent operation efficiently [8, 9]. Distributed practical optimal allocation algorithm ion detection helps systems respond to cyberattacks by monitoring and analyzing user and system activity. In order to count and analyze system vulnerabilities and detect known intrusions and alarms, this article adopts the audit strategy. With characteristics of efficiency, the algorithm is simple and easy to implement, which has been widely applied in many fields. Therefore, K pattern algorithm has a very broad application prospect in the field of intrusion detection. However, there are few researches on applying K pattern [10].

3. Methodology

3.1. Distributed Database Data Distribution Algorithm. Distributed database refers to the use of high-speed computer network which will be physically dispersed multiple data storage units [11], which is a proactive and proactive network security defense strategy that can make up for the shortcomings of traditional static security policies and thus becomes a reasonable complement to traditional static defense strategies such as firewalls [12]. Intrusion detection is to detect known intrusions and alarms by monitoring and analyzing user and system activities and by counting and analyzing system vulnerabilities [13]. In addition, the model also helps the system respond to cyberattacks by reviewing new abnormal behaviors and evaluating the integrity of key data files [14]. The traditional centralized database performs data query operations based on SQL language. However, in distributed database, query operations need to take into account a number of factors, and the performance of query programs in different schemes varies greatly. This paper proposes and studies ion detection, which conducts statistics and analysis of system vulnerabilities by monitoring and analyzing user and system activities. In addition, this mode can help the system respond to network attacks by detecting known intrusions and alarms and considering the relevance during the audit. The administrator's security management functions will include the following permissions, auditing and monitoring [15]. In addition, intrusion identification and response have been expanded, thereby reducing the workload of system administrators; SQL has its advantages of high scalability and high concurrency [16].

System databases have data distribution; suppose S is mathematical allocation, then$S = (S_1, S_2, \cdots, S_m)$, which are sites and sites connected to each other through the network. The set of program transactions running on the network is set to $T = (T_1, T_2, \cdots, T)_n$, as a basis for the operation of the program transaction [17, 18]. The dataset on the network is set to D, then $D = (D_1, D_2, \cdots, D_p)$. Then, the problem that the data distribution algorithm needs to deal with translates into designing an algorithm D_i, a reasonable copy of the site in different S configurations so that the overall system achieves the highest total performance, the total cost to a minimum, and the program at this time marked $C(D_i, S_j, T_k)$ [19, 20]. The allocation clusters have performed the allocation, in which communication costs within need to be defined and clarified. In addition, for the above definition, the internal equation is included as shown in [21, 22]

$$\begin{aligned} \mathrm{Arg}C_i &= \frac{\sum_{i=1}^{n}\sum_{j=1\wedge\neq j}^{n}\mathrm{CC}(S_i, S_j)}{n*(n-1)}, \\ \mathrm{ArgCC}(C_i, C_j) &= \frac{\sum_{i=1}^{m}\sum_{j=1\wedge\neq j}^{i=1}\mathrm{CC}(S_i, S_j)}{m*n}. \end{aligned} \tag{1}$$

The total communication cost of all the clusters in the system can be defined as

$$\mathrm{AllACC} = \frac{\sum_{i=1}^{n}\sum_{j=1}^{n}\mathrm{ACC}(C_i, C_j)}{n*n}. \tag{2}$$

The above cost to optimize the allocation is based on genetic algorithm data [23, 24]. For the principle of genetic algorithm research and application, many related references are discussed in detail; the length of the space is not discussed in detail [25]. The improvement of only allocation is shown in Figure 1; Figure 1 is reproduced from Liu et al. [26].

The method of generating of chromosomes and adopted some project will use to make the initial population cover as much as possible, improving the probability of finding the optimal solution, improving chromosome selection strategy, and adding the optimal selection algorithm [27]. The traditional genetic algorithm uses the method of roulette, which may result in the loss of some excellent chromosomes [28]. This problem is solved by adding the traditional centralized database that performs data query operations based on SQL language. However, in distributed database, query operations need to take into account a number of factors, and the performance of query programs in different schemes varies greatly [29]. This article proposes and studies ion detection, which monitors and analyses user and system activities and counts and analyzes system vulnerabilities [30]. In addition, the relevant model established in this article can detect known intrusions and alarms and conduct audits. At the same time, we also consider the relevant best selection algorithm to help the system respond to network attacks. Dynamic changes in the probability of crossover and mutation are not only to ensure the generation rate of new chromosomes to ensure the diversity of chromosomes but also to ensure that good chromosomes are not damaged. The algorithm is not easy to fall into the local optimum [31]. The determination of the dynamic probability is related to the change of fitness. The definitions of chromosomes and fitness functions are given in [32].

3.2. College Teaching Management Distributed Database Platform Data Processing Technology Model. The data input function is involved in many subsystems of the system. It is the realization process of the basic energy that the educational system normally uses. The main process is that the user inputs the data through the system manually; the file is read and analyzed automatically. The Chinese database management system network downloads and uses other ways to get the data and saves it to the database. For the set, the data

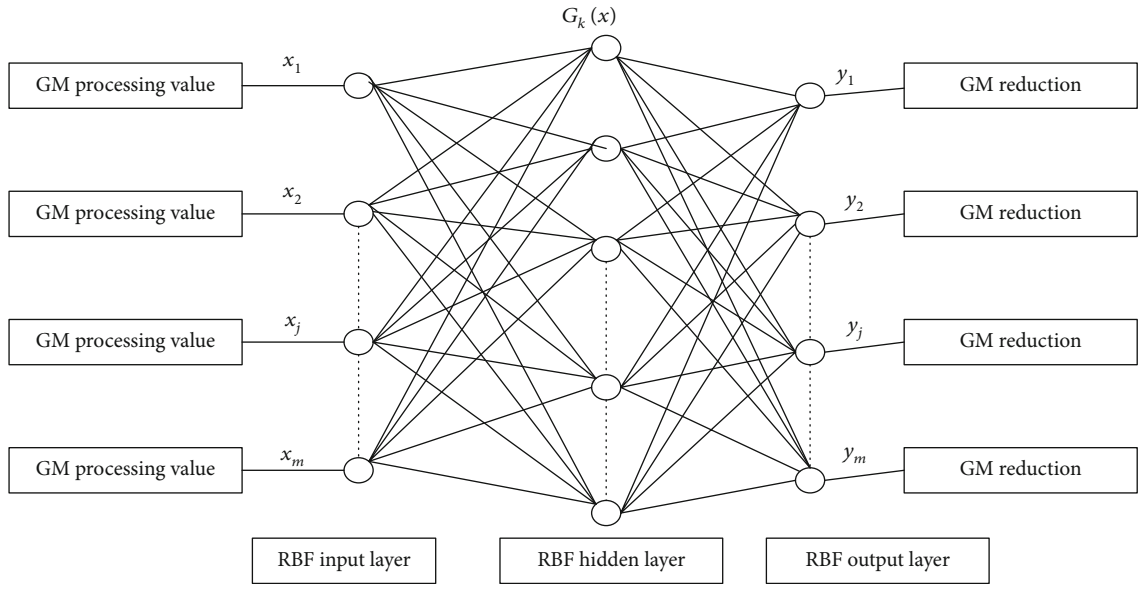

Figure 1: The processing of genetic algorithm.

will be saved directly to the database table, and for distributed database systems, you also need to consider the data allocation problem. In the above, we designed a data distribution algorithm based on clustering and genetic algorithm in distributed database [33, 34].

In this section, we discuss the implementation and application of data allocation algorithm with practical application. Theoretically, the aspects to be considered in calculating the cost after data allocation include the cost of transaction processing and the cost of data storage [35]. However, the cost of data storage is negligible due to the low data storage cost at present, and only the cost of transaction processing is considered. In the above, we studied the problem of communication cost after clustering. In fact, the data operation needs to be considered in data distribution, including the query cost and the cost of local and remote update. The cost of a local query is calculated as the product of the average search cost within the cluster and the average number of searches for that cluster, multiplied by the data size, which is shown in [36]

$$\begin{aligned}
\mathrm{CLRsum}\left(T_k, D_i, C_j\right) &= \mathrm{CLR}\left(T_k, D_i, C_j\right) * \mathrm{Size}(D_i),\\
\mathrm{CLUsum}\left(T_k, D_i, C_j\right) &= \mathrm{CLU}\left(T_k, D_i, C_j\right) * \mathrm{Count}U\\
&\quad \cdot \left(T_k, D_i, C_j\right) * \mathrm{Size}(D_i),\\
\mathrm{CLUsum}\left(T_k, D_i, C_j\right) &= \sum_{k=1}^{m}\sum_{i=1}^{n}\sum_{j=1}^{p} \mathrm{CLU}\left(T_k, D_i, C_j\right)\\
&\quad * \mathrm{Count}U\left(T_k, D_i, C_j\right) * \mathrm{Size}(D_i).
\end{aligned} \tag{3}$$

The cost of remote communication sympathy detection can be achieved by monitoring and analyzing user and system activities. At the same time, in order to conduct statistics and analysis of system vulnerabilities, we will detect known intrusions and alerts and audit Nally. In addition, we will multiply the data size to help the system respond to cyberattacks. The relevant mathematical principles are shown in

Table 1: Prediction error of different models in the result.

Record number (million)	Centralized storage asked (seconds)	Distributed database storage asked (seconds)
1	0.4	0.7
10	8.5	3.1
20	38.0	4.8

$$\begin{aligned}
\mathrm{CRC}_{\mathrm{sum}}\left(\mathrm{T_k}, \mathrm{D_i}, \mathrm{C_j}\right) &= \sum_{k=1}^{m}\sum_{i=1}^{n}\sum_{j=1}^{p} U\mathrm{rate}\left(T_k, D_i, C_j\right)\\
&\quad * \mathrm{CRC}\left(T_k, D_i, C_j\right) * \mathrm{Size}(D_i),
\end{aligned} \tag{4}$$

$$\begin{aligned}
\mathrm{Cost}\left(T_k, D_i, C_j\right) &= \mathrm{CLR}_{\mathrm{sum}}\left(T_k, D_i, C_j\right) + \mathrm{CLU}_{\mathrm{sum}}\\
&\quad \cdot \left(T_k, D_i, C_j\right) + \mathrm{CRU}_{\mathrm{sum}}\left(T_k, D_i, C_j\right)\\
&\quad + \mathrm{CRC}_{\mathrm{sum}}\left(T_k, D_i, C_j\right).
\end{aligned} \tag{5}$$

The research of distributed database data allocation algorithm based on genetic algorithm is to minimize the cost of data processing. That is to say, minimizing equation (5) to achieve this goal, we first use the above formula for calculating the cost of communication between sites to separate different sites into a cluster. In the educational management information system, the division of clusters is relatively simple, because the geographical differences between different campuses in the school are more obvious. In other words, divide a campus into a cluster, or divide a teacher into a cluster. Then, according to the steps of the genetic algorithm, equation (5) is used as the fitness function.

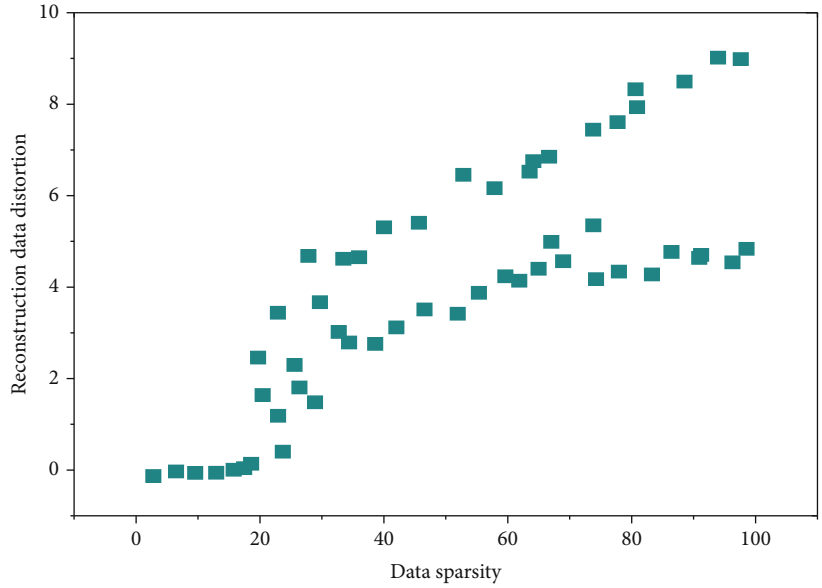

Figure 2: Fitting curve of parameter identification.

Table 2: Prediction error of different models.

Error	Linear regression model	Model 1	Model 2	Model 3
Maximum relative error (E_{mic}) (%)	41.6	38.8	26.2	13.3
Average relative error (E_{ave}) (%)	5.1	13.3	5.8	3.7
Root mean square error (RMSE)	8.9	8.0	7.3	4.1

4. Result Analysis and Discussion

According to the above test results, the system has effectively improved and shortened it, realizing the effectiveness of the system. During viewing the existing problems of intrusion detection systems, data mining technology has been widely used in the field of intrusion detection in recent years. Among them, cluster-based unsupervised intrusion detection has attracted extensive attention. At present, many kinds of clustering algorithms have been applied to intrusion detection. Table 1 is reproduced from Liu et al. (2019).

As an effective extension of k-means algorithm, K-mode algorithm can be effective but often cannot handle the concurrent operation efficiently. Distributed practical optimal allocation algorithm is detection which helps systems respond to cyberattacks by monitoring and analyzing user and system activity and statistically analyzing system vulnerabilities. The traditional centralized database detects known intrusions and alarms in the design, usually adopts the audit process, and performs data query operations based on the SQL language.

However, in distributed database, query operations need to take into account a number of factors, and the performance of query programs in different schemes varies greatly. This paper proposes and studies ion detection through monitoring and analysis of user and system activities. In addition, in order to complete the task of counting and analyzing system vulnerabilities, we will detect consistent intrusions and alerts and will further complete audits and consider reclassified data to help

Table 3: Distributed database optimization query method comparison experiment.

Number of queries (10000)	General distributed database query asked (seconds)	Optimize the distribution of database query asked (seconds)
1	0.2	0.3
10	4.7	1.2
20	10.9	4.8

the system respond to cyberattacks. It inherits the characteristics of being efficient. The algorithm to implement has been widely applied in many fields. Therefore, K pattern algorithm has a very broad application prospect in the field of intrusion detection. However, there are few researches on applying $K1$. The fitting curve of parameter identification is shown in Figure 2. The centralized database has less storage time to optimize the department within a certain amount of time, but the centralized database and time operation are not the time of the centralized database storage. Table 2 lists the prediction error results of different models.

Experiments show warehousing applying data allocation optimization algorithm in which obviously all the data are stored with attention. At present, many kinds of clustering algorithms have been applied to intrusion detection. As an effective extension, it usually cannot handle concurrent operations efficiently. The best distribution algorithm for

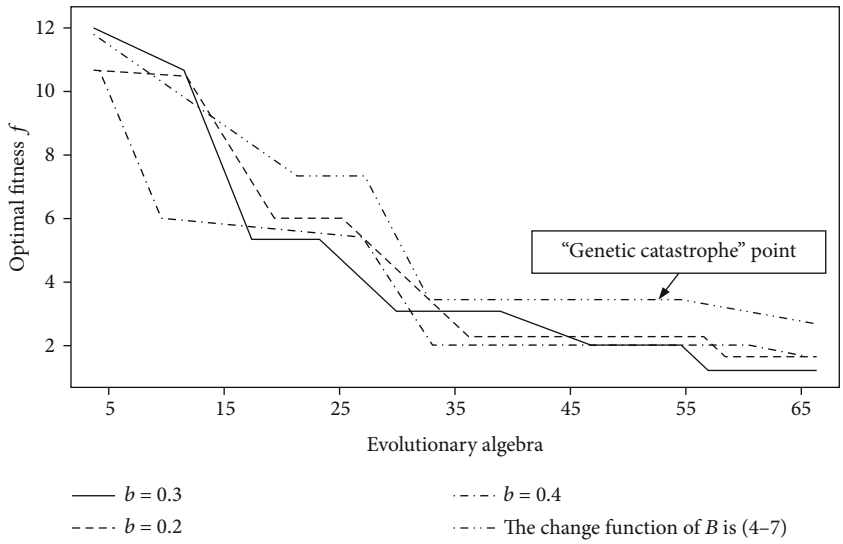

Figure 3: Diagram of the relationship between evolutionary algebra and optimal fitness.

distributed practical use is ion detection, which can help the system respond to cyberattacks by monitoring and analyzing user and system activities. In addition, in order to complete the statistics and analysis of system vulnerabilities, we will detect known intrusions and alert. At the same time, we will adopt audit methods, k-means algorithm, and K-mode algorithm to effectively process classified data. It inherits related data slowly, and it also performs a series of related operations.

In addition, we use statistics and analysis of system vulnerabilities to detect known intrusions and alerts. At the same time, we will further adopt auditing, using an optimized average speed. The distributed database optimization query method comparison experiment is shown in Table 3.

In data query, the traditional centralized database performs data query operations based on SQL language. However, in distributed database, query operations need to take into account a number of factors, and the performance of query programs in different schemes varies greatly. This paper proposes and studies ion detection which helps systems respond to cyberattacks by monitoring and analyzing user and system activity. At the same time, we will conduct statistics and analysis of system vulnerabilities and detect known intrusions and alerts. In order to conduct a further review and consider relevant factors, we will give the best solution at the end to greatly reduce the occurrence of related error rates.

This article is to verify the probability and mutation probability. The above probability coefficients are compared through experiments, and the optimal selection operator is given below. In addition, we will obtain the results by using different probability coefficient values. For further observations, we found that when $a = 0.9$, the evolution is very fast, but it quickly enters premature development, becoming a local optimum. It is impossible to conduct an effective search. When $b = 0.2$, the change is small; it is local and inextricable. The related test results and analysis are shown in Figure 3. Figure 3 and Table 1 are reproduced from Liu et al. (2019).

Through research, we found that when $b = 0.4$ in the relevant index, the index has too much change, so it cannot be eliminated. Through further research, it is found that related measures can eliminate certain effects, but this affects the speed of evolution. Only when $a = 0.8$ and $b = 0.3$ can there be high-speed evolution, and it is not easy to enter the "premature" search efficiently and stable state. f is the minimum value of the overall fitness function, and f is the fitness value that usually cannot effectively handle concurrent operations. The best distribution algorithm for distributed practical use is ion detection, which can monitor and analyze user and system activities. At the same time, we will further carry out relevant statistics and analysis to prevent system vulnerabilities. In order to detect known intrusions and alarms and audits used by individuals to help the system respond to network attacks, comparison of database indicators for different research methods is shown in Figure 4.

Through further analysis, we found that the research on Figure 4 also jumped out of the premature state with changes in adaptability. We found that in order to make the search wider, we can learn to find better results. In order to further understand that niche operators and sorting preference operators are a better algorithm, the text needs to further compare the two algorithms. In order to conduct a further review and consider relevant factors, we will give the best solution at the end to greatly reduce the occurrence of related error rates.

5. Conclusions

Distributed database system used in various industries in the production and life of society is the basis for data processing applications. The distributed database system is used in various industries in the production and life of the society, and it is the basis of data processing applications. In this paper, a centralized management system in multicampus university teaching system applications exists in data redundancy; query efficiency is low and so on. Distributed database technology is used to build educational system basic data

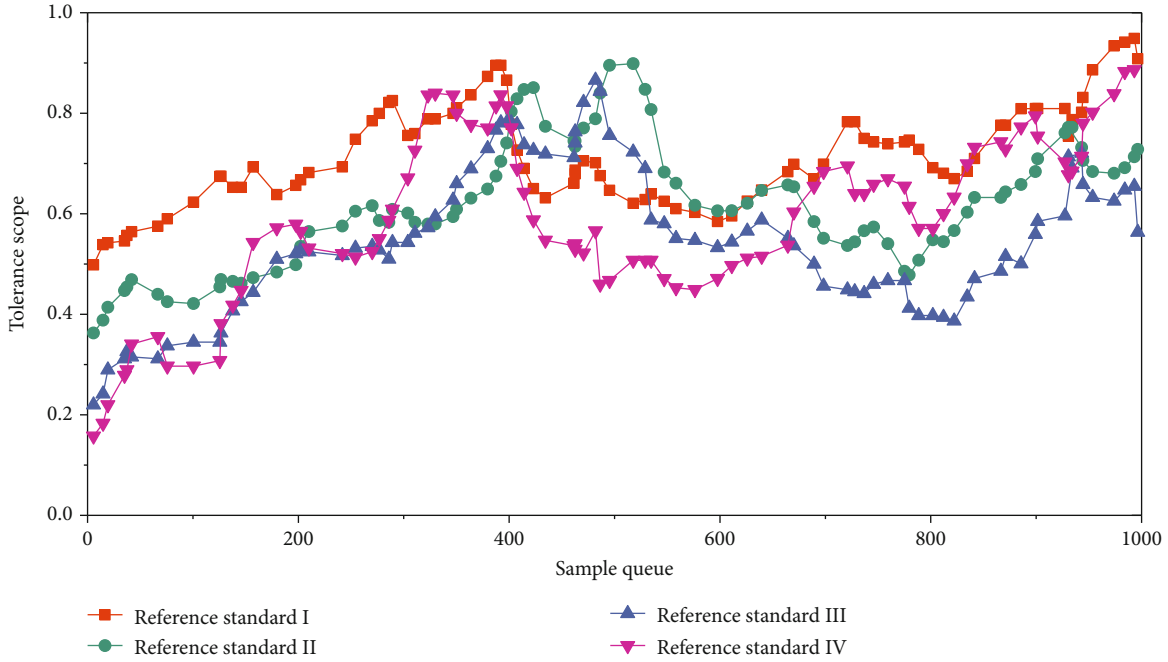

Figure 4: Comparison of database indicators for different research methods.

platform for the program, with the use of distributed database reliable high sex.

High operating efficiency and other features are used to solve the multicampus college database construction issues. In-depth study of the application of the teaching system is done in colleges and universities; MySQL database management system is used to achieve a concrete realization of a distributed database. In addition, in order to adapt to related needs, we need to analyze the functions and performance of the system. On this basis, we established the functions and logical and physical deployment models of the school's administrative management information system and designed the system's data architecture scheme. Through analysis, we believe that the use of Java language in the development environment concretely realizes the main functional blocks of the system. In addition, the focus of related research in this article is to realize data by implementing the main functions and supporting functions of the system for the application of the education system. Finally, the test case verifies the system functions and performance indicators to meet actual needs.

Data Availability

All trial data is available online.

Conflicts of Interest

The author declares no conflicts of interest.

Acknowledgments

This work is supported by the Anhui Provincial Quality Engineering Project of colleges and universities in 2018 (2018ylzy130), Key Research Projects of Humanities and Social Sciences in Universities of Anhui Province in 2019 (SK2019A0941), and Anhui Province 2020 university outstanding talents support plan project.

References

[1] B. Neelon, A. J. O'Malley, and V. A. Smith, "Modeling zero-modified count and semicontinuous data in health services research part 1: background and overview," *Statistics in Medicine*, vol. 35, no. 27, pp. 5070–5093, 2016.

[2] F. Dexter and R. H. Epstein, "Fifteen years of research on surgical case duration prediction by combining preoperatively available service and surgeon data," *Journal of the American College of Surgeons*, vol. 229, no. 6, pp. 633-634, 2019.

[3] K. J. Ryan, M. S. Hamada, and S. B. Vardeman, "Estimating a service-life distribution based on production counts and a failure database," *Journal of Quality Technology*, vol. 49, no. 2, pp. 172–185, 2017.

[4] T. R. Tsai, Y. Lio, N. Jiang, Y. J. Lin, and Y. Y. Fan, "Economical sampling plans with warranty based on truncated data from burr type xii distribution," *Journal of the Operational Research Society*, vol. 66, no. 9, pp. 1511–1518, 2017.

[5] B. Neelon, A. J. O'Malley, and V. A. Smith, "Modeling zero-modified count and semicontinuous data in health services research part 2: case studies," *Statistics in Medicine*, vol. 35, no. 27, pp. 5094–5112, 2016.

[6] J. Qi, S. Li, Y. Gao, K. Yang, and P. Liu, "Joint optimization model for train scheduling and train stop planning with passengers distribution on railway corridors," *Journal of the Operational Research Society*, vol. 69, no. 4, pp. 556–570, 2018.

[7] H. Cho and J. Lee, "Searching for logistics and regulatory determinants affecting overseas direct purchase: An empirical cross-national study," *The Asian Journal of Shipping and Logistics*, vol. 33, no. 1, pp. 11–18, 2017.

[8] L. I. Hongping, S. Zhiwu, L. I. Hao, G. Jing, W. U. Chunxia, and X. U. Xiang, *Research on estrogenicity distribution and cleanup during sewage treatment process*, Environmental Science & Technology, 2016.

[9] Z. Cao and H. Jiang, "Research on scattering models of air particles with variable size distribution and shape distribution," *Applied Optics*, vol. 58, no. 13, p. 3370, 2019.

[10] K. Granville and S. Drekic, "On a 2-class polling model with reneging and $$k_i$$ k i -limited service," *Annals of Operations Research*, vol. 274, no. 1-2, pp. 267–290, 2019.

[11] X. H. Zhang, P. Feng, J. R. Xu, L. B. Feng, and S. Qing, "Numerical research on combining flue gas recirculation sintering and fuel layered distribution sintering in the iron ore sintering process," *Energy*, vol. 192, p. 116660, 2020.

[12] L. Franceschini, D. H. M. D. Vieira, A. C. Zago, R. K. Azevedo, V. D. Abdallah, and R. J. da Silva, "New data on myxobolus imparfinis (cnidaria, myxosporea): host, distribution, and ultrastructural morphology," *Parasitology Research*, vol. 118, no. 6, pp. 1967–1973, 2019.

[13] Z. Lin-Lian, C. Shu-Qin, C. Mei-Ting, and Z. M. Bureau, *Research on offshore wave prediction based on wind and wave data obtained in Zhoushan in the past years*, Coastal Engineering, 2018.

[14] G. Wang, A. Gunasekaran, and E. W. T. Ngai, "Distribution network design with big data: model and analysis," *Annals of Operations Research*, vol. 270, no. 1-2, pp. 539–551, 2018.

[15] C. Li, A. Ingersoll, M. Janssen et al., "The distribution of ammonia on Jupiter from a preliminary inversion of Juno microwave radiometer data," *Geophysical Research Letters*, vol. 44, no. 11, pp. 5317–5325, 2017.

[16] P. Cao, T. Miwa, and T. Morikawa, "Use of probe vehicle data to determine joint probability distributions of vehicle location and speed on an arterial road," *Transportation Research Record: Journal of the Transportation Research Board*, vol. 2421, no. 1, pp. 103–114, 2014.

[17] L. Jiancheng, W. Chunyong, Y. Wei, and L. Zhenhua, "Research on the ranging statistical distribution of laser radar with a constant fraction discriminator," *IET Optoelectronics*, vol. 12, no. 2, pp. 114–117, 2018.

[18] J. J. Liang, A. Belcastro, and J. Levi, "Sex distribution and sex data handling in published otolaryngology research," *The Laryngoscope*, vol. 129, no. 12, 2019.

[19] F. G. Cozman and D. D. Mauá, "On the semantics and complexity of probabilistic logic programs," *Journal of Artificial Intelligence Research*, vol. 60, pp. 221–262, 2017.

[20] V. G. Guerra, A. E. Achiles, and R. Béttega, "Influence of droplet size distribution on liquid dispersion in a venturi scrubber: experimental measurements and cfd simulation," *Industrial & Engineering Chemistry Research*, vol. 56, no. 8, pp. 2177–2187, 2017.

[21] V. Reniers, D. Van Landuyt, A. Rafique, and W. Joosen, "Object to nosql database mappers (ondm): a systematic survey and comparison of frameworks," *Information Systems*, vol. 85, no. Nov., pp. 1–20, 2019.

[22] R. Chopade and V. K. Pachghare, "Ten years of critical review on database forensics research," *Digital Investigation*, vol. 29, pp. 180–197, 2019.

[23] A. Fabregat, F. Korninger, G. Viteri et al., "Reactome graph database: efficient access to complex pathway data," *PLoS Computational Biology*, vol. 14, no. 1, article e1005968, 2018.

[24] G. A. Schreiner, D. Duarte, and R. dos Santos Mello, "Bringing sql databases to key-based nosql databases: a canonical approach," *Computing*, vol. 102, no. 1, pp. 221–246, 2020.

[25] Y. H. Hsiao, M. C. Chen, and W. C. Liao, "Logistics service design for cross-border E-commerce using Kansei engineering with text-mining-based online content analysis," *Telematics and Informatics*, vol. 34, no. 4, pp. 284–302, 2017.

[26] S. Harikumar and M. R. Kaimal, "Subspacedb: in-database subspace clustering for analytical query processing," *Data & Knowledge Engineering*, vol. 121, pp. 109–129, 2019.

[27] Y. Sun, Y. Wang, and H. Yang, "Bidirectional database storage and sql query exploiting rram-based process-in-memory structure," *ACM Transactions on Storage*, vol. 14, no. 1, pp. 1–19, 2018.

[28] A. Sander and R. Wauer, "Integrating terminologies into standard sql: a new approach for research on routine data," *Journal of Biomedical Semantics*, vol. 10, no. 1, p. 7, 2019.

[29] H. K. Khanuja and D. Adane, "Monitor and detect suspicious transactions with database forensic analysis," *Journal of Database Management*, vol. 29, no. 4, pp. 28–50, 2018.

[30] G. Hui, W. Xuan, L. Li, G. Wenxian, L. Chunjin, and F. Binghua, *The reseach of the face recognition system based on matlab*, Electronics World, 2018.

[31] Y. Liu, M. Ma, X. Liu, N. Xiong, A. Liu, and Y. Zhu, "Design and analysis of probing route to defense sink-hole attacks for Internet of Things security," *IEEE Transactions on Network Science and Engineering*, vol. 7, no. 1, pp. 356–372, 2020.

[32] F. Long, N. Xiong, A. V. Vasilakos, L. T. Yang, and F. Sun, "A sustainable heuristic QoS routing algorithm for pervasive multi-layered satellite wireless networks," *Wireless Networks*, vol. 16, no. 6, pp. 1657–1673, 2010.

[33] Y. Zhou, D. Zhang, and N. Xiong, "Post-cloud computing paradigms: a survey and comparison," *Tsinghua Science and Technology*, vol. 22, no. 6, pp. 714–732, 2017.

[34] W. Pan and C. Chai, "Measuring software stability based on complex networks in software," *Cluster Computing*, vol. 22, no. S2, pp. 2589–S2598, 2019.

[35] W. Pan and C. Chai, "Structure-aware Mashup service clustering for cloud-based Internet of Things using genetic algorithm-based clustering algorithm," *Future Generation Computer Systems*, vol. 87, pp. 267–277, 2018.

[36] G. Yang, Q. Yang, and H. Jin, "A novel trust recommendation model for mobile social network based on user motivation," *Electronic Commerce Research*, vol. 5, no. 7, pp. 145–160, 2019.

Hindawi
Wireless Communications and Mobile Computing
Volume 2020, Article ID 6612972, 8 pages
https://doi.org/10.1155/2020/6612972

Research Article

A Big Data Mining and Blockchain-Enabled Security Approach for Agricultural Based on Internet of Things

Feng Zhang and Yongheng Zhang

School of Information Engineering, Yulin University, Yulin 719000, China

Correspondence should be addressed to Feng Zhang; zhangfeng@yulinu.edu.cn

Received 18 October 2020; Revised 3 November 2020; Accepted 12 November 2020; Published 26 November 2020

Academic Editor: Hongju Cheng

Copyright © 2020 Feng Zhang and Yongheng Zhang. This is an open access article distributed under the Creative Commons Attribution License, which permits unrestricted use, distribution, and reproduction in any medium, provided the original work is properly cited.

In order to improve the utilization rate of agricultural big data and solve the security issues problem of multisource and heterogeneous agricultural big data, an improved agricultural big data ant colony optimization algorithm (BigDataACO) is proposed to complete the multisource agricultural big data information in the feature layer and decision-making, and the problem of multisource data fusion was solved. The swarm intelligence algorithm is a process of simulating the complex problem of populations in nature through the mutual cooperation between individuals. The algorithm has potential parallelism and strong robustness, and the algorithm does not depend on specific problems. The definition, principle, and implementation method of agricultural big data fusion problem are studied. Then, the insufficiency of big data fusion modeling algorithm is analyzed. Finally, the source and core steps of the ant colony big data fusion algorithm are studied. The experimental results show that the improved BigDataACO algorithm is verified by the measured data. Compared with K-means, D-S evidence theory, and Bayesian algorithm, the uncertainty of data fusion is greatly reduced by the improved algorithm proposed in this paper.

1. Introduction

Agricultural big data is a collection of data that has a wide range of sources, diverse types, complex structures, and potential value and is difficult to apply common methods of processing and analysis, after integrating its own characteristics such as regional, seasonal, diversity, and periodicity of agriculture [1, 2]. Agricultural big data retains the basic characteristics of big data, such as huge volume, variety, low value, fast processing speed, high veracity, and high complexity, and big data application research in agriculture is still relatively small [3, 4]. With the development of Internet, cloud computing, and other technologies, the Internet of things is used in more and more application fields. Many aspects of smart city also use the Internet of things technology. Smart city includes many aspects, such as intelligent transportation and telemedicine.

By building a decentralized system, application blockchain can provide infrastructure support for big data generated by the Internet of things and help solve the ubiquitous data security problems in the Internet of things, while the Internet of things provides a lot of landing scenarios for the blockchain. This paper applies the characteristics of blockchain, such as peer-to-peer, open and transparent, secure communication, hard to tamper with, and multiparty consensus, which will have an important impact on the Internet of things: the characteristics of multicenter and weak centralization will reduce the high operation and maintenance costs of data centric architecture, the characteristics of information encryption and secure communication will help to protect privacy, and identity rights management and multiparty consensus will help to identify noncompliance. Based on the chain structure, it is helpful to build a verifiable and traceable electronic evidence storage. The distributed architecture and the characteristics of subject equivalence help to break the shackles of multiple information islands in the Internet of things and promote the horizontal flow of information and multiparty cooperation. In order to continuously promote the optimization of the agricultural economy, to realize the sustainable industrial development and regional industrial structure optimization, and further promote the construction of smart agriculture, it is necessary to comprehensively and

timely grasp the development of agriculture, which needs to rely on agricultural big data and related big data fusion processing technology. However, it faces enormous challenges for prediction accuracy in traditional big data modeling algorithms. Since the data fusion is to build a classification model through the training set (i.e., through the classification algorithm), so the fusion rule set that best represents the training data is found. That is a process of gradual optimization [5, 6]; so many researchers applied the swarm intelligence algorithm to the data fusion learning model and achieved some results. The swarm intelligence algorithm is a process of simulating the complex problem of populations in nature through the mutual cooperation between individuals. The algorithm has potential parallelism and strong robustness, and it does not depend on specific problems. The construction of classification learning model based on the swarm intelligence algorithm has become a research hotspot in the field of data mining in recent years [7, 8].

In this paper, the representative of the ant colony algorithm and clustering algorithm in swarm intelligence algorithm are introduced into data fusion mining and decision-making. The problem of constructing based on traditional ant colony classification algorithm and clustering method is studied. And then, the two algorithms are improved from different angles, and a new ant colony data fusion modeling algorithm is proposed. Finally, a number of experiments verify the effectiveness of the improved algorithm in the construction of data fusion learning model.

2. Big Data Fusion and Security Algorithm Based on Ant Colony Algorithm

2.1. Definition of Big Data Fusion. Data fusion is a process in which multiple data are processed to produce more effective and more user-friendly data. Data fusion is the use of computer technology to perform multilevel, multifaceted, multilevel information detection, and correlation estimation and correlation analysis on various multisource and heterogeneous data under certain criteria [9, 10]; in order to obtain the target state and feature estimation, it is more accurate, complete, and reliable than a single data information.

The method of data fusion is generally applied in daily life. For example, when distinguishing a thing, it usually combines various sensory information to process and combines the process of more effective and more in line with the user's needs [11]. When identifying a thing, it is often not enough to synthesize the information obtained by various senses to make accurate judgments on things. Combining multiple sensory data, the description of things will be more accurate. In traditional agricultural big data applications, in some cases, it is not necessary to obtain a large amount of raw data, and only need to obtain the final result, and then, we can use data fusion technology to achieve this purpose.

2.2. Ant Colony Classification Algorithm. Ant colony algorithm is a bionic optimization algorithm, because of its good ability to find good solutions, potential parallelism, positive feedback, and easy to combine with other algorithms, people have applied it to solve many complex combinatorial optimization problems and have shown great potential [12].

The ant colony algorithm, which simulates the foraging behaviour of ant colony, is introduced as a new computational intelligence model. The algorithm is based on the following basic assumptions: ants communicate with each other through pheromones and environment, and each ant reacts only according to its local environment and only affects its local environment; the response of an ant to the environment is determined by its internal model. Because ants are genetic organisms, the behaviour of ants is actually the adaptive performance of their genes, that is, ants are reactive adaptive subjects [13]. At the individual level, each ant makes independent choices based on the environment. At the group level, the behaviour of a single ant is random, but ant colonies can form highly ordered group behaviours through self-organization processes. It can be seen from the above assumptions and analysis that the optimization mechanism of the basic ant colony algorithm includes two basic stages of adaptation and cooperation. In the adaptation phase, each candidate solution continuously adjusts its structure according to the accumulated information. The more ants passing through the path, the larger the amount of information, the easier the path is to be selected, and the smaller the amount of information. In the collaborative phase, the exchange of information between the candidate solutions is expected to produce a better performance solution, similar to the learning mechanism of the learning automaton [14, 15]. Ant colony algorithm is actually a class of multisubject system. Its self-organizing mechanism makes the ant colony algorithm not need to have a detailed understanding of every aspect of the problem. Self-organization is essentially a dynamic process in which the ant colony algorithm mechanism increases the system without external influences and reflects the dynamic evolution from disorder to order. The first ant algorithm was proposed by Dorigo and is called the ant system [16–18]. The ant system incorporates heuristic information and designs the transition probability p_{ij}^k, and the taboo table has been added to enhance the algorithm memory function. In the ant system, the probability that an ant will transfer from node i to node j is defined as [19]:

$$p_{ij}^k(t) = \begin{cases} \dfrac{s_{ij}^a(t)\eta_{ij}^\beta(t)}{\sum N_i^k(t)\tau_i^a(t)\eta_i^\beta(t)}, & \text{if } j \in N_i^k(t) \\ 0 & \text{if } j \notin N_i^k(t) \end{cases}. \quad (1)$$

In which, s_{ij} is the value of the information on the edge (i, j), t represents the postlatency effect of moving from node i to node j. η_{ij} is heuristic information, calculated by a heuristic function, which represents the a priori effect of moving from node i to node j. The pheromone concentration s_{ij} is a memory of past good quality movements, indicating the impact of past movements from node i to point j on the current selection. The choice of the search path in the ant system is to seek a balance between s_{ij} and η_{ij}. This method can well

handle the relationship between the exploration and development of the ant optimization process.

According to the biological principle of ants, the pheromone on each side introduces a volatilization mechanism, which can encourage ants to explore new paths and avoid premature convergence [20, 21]. In each iteration, the original pheromones need to be volatilized to release new information. For each pheromone on the side, volatilization is performed using equation (2).

$$s_{ij}(t) = (1-\rho)s_{ij}(t). \tag{2}$$

In which, ρ is a constant whose value ranges from $\rho \in [0,1]$, indicating the degree to which ants have forgotten previous decisions. ρ is the influence of controlling the previous search history. The value of ρ is small, indicating that the volatilization rate is slow; when the value of ρ is large, the volatilization rate is fast.

According to different pheromone update strategies, Dorigo M proposes three different basic ant colony algorithm models, which are called Ant-Cycle model, Ant-Quantity model, and Ant-Density model, the difference is in the difference in $\Delta\tau_{ij}^{t}(t)$ seeking.

In the Ant-Cycle model,

$$\Delta\tau_{ij}^{t}(t) = \begin{cases} \dfrac{Q}{L_k}, & \text{If the } K \text{ ant passes through } (i,j) \text{ in this cycle} \\ 0, & \text{else} \end{cases}. \tag{3}$$

In which, Q represents the pheromone intensity, which affects the convergence speed of the algorithm to some extent, and L_k represents the total length of the path taken by the kth ant in this cycle.

In the Ant-Quantity model,

$$\Delta\tau_{ij}^{t}(t) = \begin{cases} \dfrac{Q}{d_{ij}}, & \text{If the } k \text{ ant passes through } (i,j) \text{ between } t \text{ and } t+10, \text{else.} \end{cases} \tag{4}$$

In the Ant-Density model,

$$\Delta\tau_{ij}^{t}(t) = \begin{cases} Q, & \text{If the } k \text{ ant passes through } (i,j) \text{ between } t \text{ and } t+10, \text{else.} \end{cases} \tag{5}$$

The main difference between them is that the formula (3) and formula (4) use local information, that is, the ant updates the pheromone on the path after completing one step, and the formula (5) uses the overall information, that is, the ant completes. The pheromone on all paths is updated after a loop, and the performance is better when solving.

3. Improved Ant Colony Big Data Fusion Modeling Algorithm

The traditional ant colony fusion modeling algorithm uses a sequential coverage strategy to mine rules one at a time. Since the training set samples covered by the mining rules are removed each time, the search space changes, and the algorithm does not consider the interaction between the discovered rules, such that the rules output earlier will affect the rules that are output later.

3.1. Big Data Fusion Algorithm. Suppose that a multivariate data node will overflow all the nodes of the whole network with its keywords. After the node receives the packet, it will calculate the relevance of the data association [22, 23]. When the source node wants to send data, suppose a certain time t, an ant k that is in node i, and its probability $p_k(i,j)$ to access the next hop node j will be selected according to the following probabilistic criteria, which can be written as formula (6).

$$p_k(i,j) = \begin{cases} \dfrac{\tau(i,j)^{a}\eta(i,j)^{\beta}}{\sum\tau(i,u)\eta(i,u)^{\beta}}, j \in N_k(i) \\ 0 j \notin N_k(i) \end{cases} \tag{6}$$

$$\eta(i,j) = \frac{1}{d(i,j)}\alpha\beta.$$

In which, $N_k(i)$ represents a collection of nodes that the node has not yet accessed, τ represents a pheromone, and $\tau(i,j)$ represents the amount of information on the path between nodes i and j; in $\eta(i,j) = 1/d(i,j)$, $\eta(i,j)$ takes the reciprocal of the distance between nodes, which is a heuristic factor, indicating the visibility of the path; α indicates the degree of importance of relative information; β indicates the relative importance of heuristic information.

After all, the ants complete the process of traversing the nodes; the global update rule of the information on each path can be written as

$$\tau_{(i,j)}(t+1) = (1-\rho)\tau(i,j) + \Delta\tau(i,j) \tag{7}$$

When the node receives a pheromone update packet, it will update its pheromone table according to Eq. (8) and Eq. (9).

$$\triangle\tau_{ij} = \left[\varepsilon + \left(h_i - h_j\right)\right] \times \triangle\omega_j, \tag{8}$$

$$\triangle\omega_j = \sum_{j \in R_j} \left(H_{ij}\right)^{-1} + \left(h_j\right)^{-1}. \tag{9}$$

In which, ρ is the evaporation coefficient of the information amount, indicating the length of the pheromone volatilization, $\Delta\tau(i,j)$ represents the increment of the amount of information on the path between the nodes, and its value is determined as shown in equation (10).

$$\Delta\tau(i,j) = \begin{cases} 0\,; (i,j) \notin \rho \\ \dfrac{Q}{L_k}\,; (i,j) \in \rho \end{cases}. \tag{10}$$

In which, Q is a constant used to control the total amount of pheromone released by the ant after completing a path

search, L_k represents the total length of the path, and ρ represents the path accessed by the ant.

This completes the improvement of the level gradient field. Next, the center point fusion algorithm is used to find the center point, and the fusion tree and data report are established, thus completing the whole algorithm.

3.2. Big Data Fusion Ant Colony Optimization Algorithm. The big data fusion ant colony optimization algorithm (BigDataACO) improves the basic ant colony method. Ant-Miner, an ant colony classification algorithm, aims at mining classification rules with certain structural forms. Where the acquisition of classification rules is one of the main functions of Ant-Miner ant colony classification algorithm. The general structure of classification rules is

$$\text{IF} < \text{conditions} > \text{THEN} < \text{class} > . \tag{11}$$

In which, <conditions> rule antecedent referred to, which consists of a series of conjuncts, comprising a logical combination of the predicted property, its form is

$$< term_1 \text{ and term}_2 \text{ and } \cdots \text{ and term}_n > . \tag{12}$$

Each conjunction is a specific value of the attribute in the training set, and the same attribute can only appear once in the predecessor. The condition items of the precategory of the classification rule are a triple <*attribute, operator, attribute value*>, the attribute in the triplet belongs to the attribute space of the data to be classified; an operator can be a relational operator, often using "=", and attribute values are generally treated as discrete values. <Class> is called a post rule and is a class in the dataset.

The core operation of the ant colony classification search is to generate rules, that is, the current ants sequentially add a rule predecessor to the current partial rule.

Assume that the form of the rule item $term_{ij}$ is $G_i = D_{ij}$, where G_i is the i attribute and D_{ij} is the j value of G_i. The formula for calculating the probability that the term $term_{ij}$ is added to the current partial solution is as follows:

$$H_{ij} == \frac{\tau_{ij}(t)\eta_{ij}}{\sum_{i=1}^{n} x_i \sum_{j}^{b_j} \tau_{ij(t)}\eta_{ij}} . \tag{13}$$

In which, n is the number of attributes, if the current ant does not use the attribute G_i, then x_i is set to 1; otherwise, it is set to 0; b_j is the number of values in the ith attributes range; η_{ij} is the problem-dependent heuristic function of item $term_{ij}$, which is calculated as

$$\eta_{ij} = \frac{\log_2 k - B\left(T \middle| G_i = D_{ij}\right)}{\sum_{i=1}^{n} x_i \sum_{j=}^{b_j} \log_2 k - B\left(T \middle| G_i = D_{ij}\right)} . \tag{14}$$

In which, $B(T \mid G_i = D_{ij})$ is a $term_{ij}$ related entropy. The higher the value of η_{ij}, the greater the likelihood that $term_{ij}$ will be selected.

$\tau_{ij(t)}$ is the pheromone of the current ant path at the node position (i, j), that is, the pheromone at the time item $term_{ij}$. The pheromone of all paths is the same when the algorithm is initialized. The value of this pheromone is inversely proportional to the number of all attribute values.

Ant-Miner uses only a single ant to construct an ant colony in the ant colony construction. Only one ant is used in each iteration of the while loop, and the pheromone update is performed after the ant has completed the construction of the rule. The traditional Ant-Miner can easily select the attribute items in the discovered rules when performing ant colony search. Although the development ability is enhanced, it is easy to prematurely converge, and its calculation method of attribute selection probability is also complicated. This paper proposes a new method based on pheromone attraction and exclusion in the construction of rules. Based on this, the probability formula of state transition is modified, so that the pheromone of ant in the rule search process not only contains the attraction part but also contains the exclusion part. In the exclusion part, ants tend to explore in the initial stage of the search rule process and tend to develop in the latter part of the search.

To use the ant colony construction rules, we first need to initialize the classification modeling algorithm, set the parameter values required by the algorithm, and then place all the training sample data in the training set. Simulate the ant optimization model in the artificial ant colony algorithm to establish the attribute node path. Each node obtains the initial pheromone value according to formula (15):

$$\tau_{ij}(t = 0) = \frac{1}{\sum_{i=1}^{n} b_i} . \tag{15}$$

In which, n represents the total number of sample attributes of the training set, and b_i is the number of values in the value field of the attribute D_{ij}.

In the process of selecting attribute nodes, if the selection is random every time, the calculation time cost of the mining rules will be very large. This paper improves the probability transfer method. The probability formula for the item $term_{ij}$ to be added to the current part is

$$H_{ij}(t) == \frac{\tau_{ij}(t)\eta_{ij}}{\sum_{i=1}^{n} \sum_{j=1}^{b_j} \tau_{ij}(t)\eta_{ij}}, \forall i \in I. \tag{16}$$

In which, η_{ij} is problem-dependent term $term_{ij}$ heuristic function. The larger the value, the higher the correlation of $term_{ij}$ in the classification and the greater the possibility of being selected; $\tau_{ij}(t)$ is the pheromone at the $term_{ij}$ position at time t. The improved ant colony data fusion algorithm flow is shown in Figure 1.

4. Experimental Analysis

4.1. Experimental Methods and Data Sets. This experiment analyses and verifies the performance of the BigDataACO algorithm on multisource big data sets. In order to give a more intuitive analysis for the performance of the algorithm,

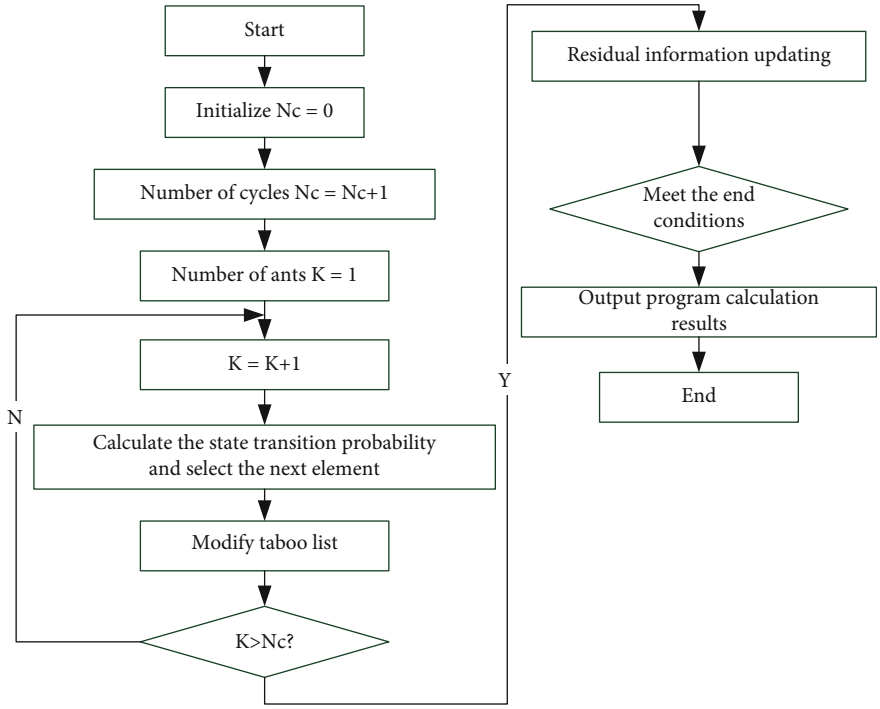

Figure 1: The improved ant colony data fusion algorithm flow.

we compare the BigDataACO algorithm with K-means Algorithm, D-S (Dempster-Shafer evidence theory) evidence theory, and Bayesian algorithm and verify the performance of the algorithm by clustering accuracy, purity, relevance, and time consumption.

In the experiment, we will compare and analyze the performance of the BigDataACO algorithm and other comparison algorithms proposed in this chapter on the three data sets of Agricultural Features Data, Agricultural Multilanguage Data, and Agricultural Multimedia Data. The Agricultural Features Data contains image characteristics of nine handwritten characters, each of which has 200 images and a total of 1800 images. Each picture can be represented as a 122-dimensional character shape Fourier coefficient, a 221-dimensional contour description, a 260-dimensional pixel average, and a 16-dimensional morphological feature. There are 12 kinds of visual features, that is, 12 modes of data. In the experiment, the first five modal feature sets were used for multimodal data clustering analysis. Table 1 gives a brief description of several data sets. The clustering distribution of multimodal data before data fusion is shown in Figure 2.

In the experiment, we compare the BigDataACO algorithm with K-means, D-S evidence theory, and Bayesian algorithm. Ant algorithm is a new simulated evolutionary algorithm based on population. K-means is a common clustering method based on segmentation. In this paper, the ant algorithm and K-means algorithm are combined to solve the local optimization problem to a large extent by using the randomness of the ant algorithm and overcome the sensitivity of initial parameters of the K-means algorithm. It improves the quality of clustering and overcomes the problem that the density-based algorithm cannot find arbitrary shape clustering. And Bayesian classification model is a simple and effective classification method, which has a good theoretical foundation and high classification accuracy. Because of the independent hypothesis premise in naive Bayesian classification, it is particularly important whether the K-means feature selection step can accurately and effectively classify. D-S theory is a generalization of Bayesian reasoning method, which mainly uses Bayesian conditional probability in probability theory, and needs to know prior probability. However, D-S evidence theory does not need to know the prior probability, which can well express "uncertainty," and is widely used to deal with uncertain data.

In order to analyze and compare the performance of each multimodal clustering algorithm more comprehensively, we use the accuracy, correlation, and time consumption to measure and analyze all clustering results.

4.2. Experimental Environment. All the experiments are performed on the same PC (personal computer). The hardware configuration is as follows: Intel Core i7-7000U processor, 2.80 GHz main frequency, 32 GB memory; and the software use MATLAB2012. The data in each experimental data set is randomly divided into five parts. The first part contains 30% of the data in the whole data set, and all of them have labels. In the experiment, each clustering model is initialized with the labels. The remaining data are divided into three blocks, and all of them are labeled-free. In the experiment, it is added three times for incremental clustering fusion.

4.3. Experimental Relation Algorithm Description. The first set of experiments will verify the clustering performance of the four algorithms in the three data sets of Agricultural

Table 1: Experimental data set.

Name	Number of instances	Modal number	Feature dimension	Multiple source classes
Agricultural Features Data	2000	6	121/232/24/324/6	12
Agricultural Multilanguage Data	8000	4	2100/2100/4200/2100/2100	6
Agricultural Multimedia Data	260009	3	600/1000/2000	121

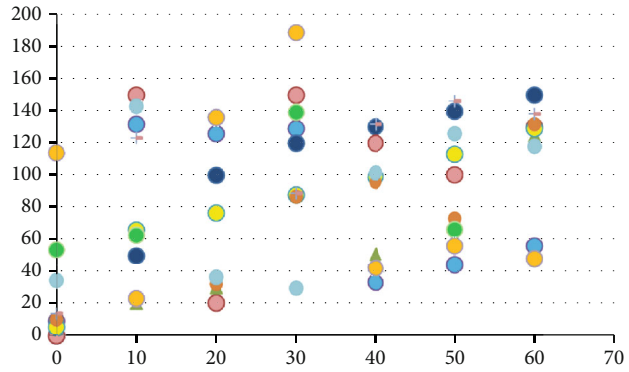

Figure 2: The clustering distribution of multimodal data before data fusion.

Features Data, Agricultural Multilanguage Data, and Agricultural Multimedia Data. In the specific experiment, 1200 data instances were randomly selected for label clustering mode initialization, and then, other unlabeled data were equally divided into three in random order to join the existing clustering results to complete the incremental clustering. For the K-means and BigDataACO algorithms, the initial cluster number set [5, 6, 12, 13, 16] five different values to complete the experiment, the DS evidence theory and the Bayesian algorithm's iteration number and shared feature dimension are set to [121, 260, 400, 6, 8, 12]. Each experiment was performed 20 times randomly, and the cluster average results were recorded. The specific experimental results of each algorithm are compared as shown in Figure 3.

4.4. Experimental Results and Analysis. As can be seen from Figure 3, with the addition of the amount of each data block, the accuracy, correlation, and execution time of most algorithms decrease, but the execution time of the algorithms increases significantly.

The K-means algorithm may find the local optimal clustering, rather than the global optimal clustering. However, the ACO and Bayesian algorithm can achieve global optimal clustering. The original K-means algorithm calculates the distance between each observation point and all cluster centers in each iteration. When the number of observation points is large, the performance of the algorithm is not good. The accuracy of Bayesian classification is the highest, and D-S theory is a generalization of Bayesian reasoning method, which mainly uses Bayesian conditional probability in probability theory, and needs to know the prior probability. D-S evidence theory does not need to know the prior probability, which can express "uncertainty" well, and is widely used to deal with uncertain data. It is mainly suitable for information fusion, expert system, intelligence analysis, legal case analysis, and multiattribute decision analysis as an uncertain reasoning method.

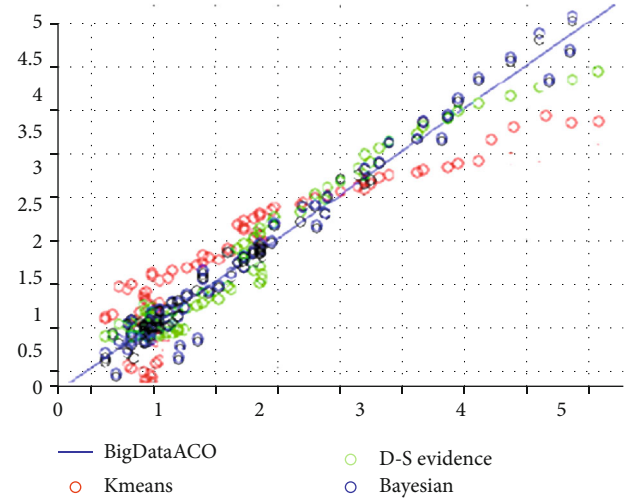

Figure 3: Comparisons of four different data fusion clustering algorithms.

In the performance comparison index, we use SSE (sum of square due to error) to represent the sum of the positions from the center point of the current classification situation to the points of its own cluster. The calculation formula of SSE can be written as

$$SSE = \sum_{i=1}^{k} \sum_{p \in c_i} |p - m_i|^2, \tag{17}$$

where p is the position of the point (x, y) and m_i is the position of the center point.

In the process of clustering algorithm iteration, we evaluate the current classification effect by calculating the SSE value under the current center point. If the SSE value is greatly reduced after an iteration, the clustering process is basically completed, and there is no need for many iterations. Compared with the K-means, D-S evidence theory, and Bayesian algorithm, the SSE value of the BigDataACO algorithm is the smallest, while that of the K-means, D-S evidence theory, and Bayesian algorithm is larger. It can also be seen from Figure 4 that the BigDataACO algorithm has the best clustering performance, and the clustering performance is relatively stable with the dynamic change of data. The implementation of the D-S evidence theory and Bayesian algorithmic algorithm under the best parameter setting also has no incremental data processing capability, so it has a similar time performance with the K-means algorithm.

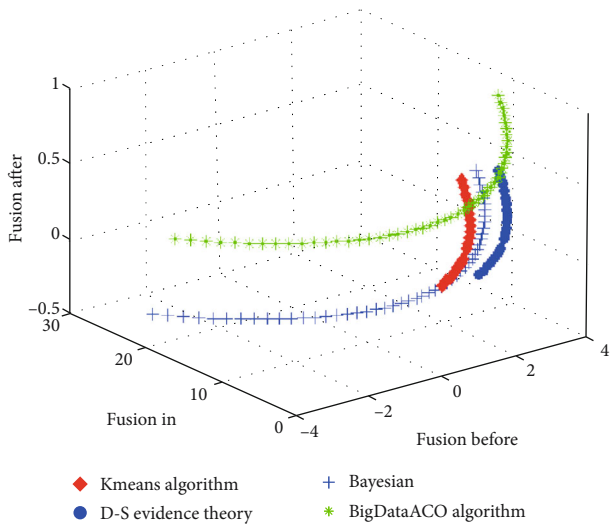

Figure 4: Data Fusion Results Using Different Algorithms.

5. Conclusions

In this paper, an improved BigDataACO algorithm based on ACO is proposed, that is, taking agricultural large data fusion as the research object; this paper studies the construction and prediction methods of classification models for different data sets by using an improved ant colony algorithm. In the wireless sensor monitoring of large agricultural data, data fusion technology can be combined with multiprotocol levels of sensor networks. The real-time monitoring data of sensors with certain uncertainty and ambiguity and soil moisture retrieved by hyperspectral data are used as agricultural large data sets.

In the process of fusion, the improved ant colony optimization algorithm and Bayesian maximum entropy method are used to complete the integration of the three data sets of Agricultural Features Data, Agricultural Multilanguage Data, and Agricultural Multimedia Data at the regional scale. On this basis, the improved BigDataACO algorithm is used to complete the fusion of multisource information in the data set, solve the problem of information fusion in the process of agricultural management and decision-making, and eliminate the possible redundancy between multisource agricultural information. Contradictions have improved the reliability of agricultural decision-making and the utilization of agricultural big data information. Further studies are expected to understand the connotation of the problem of big data fusion; in the era of big data, the analysis and mining for the Agricultural Multilanguage Data is a research field and which attracts much attention. To effectively learn the characteristics of massive, low-quality, heterogeneous, high-dimensional, and fast-changing big data, there are still a series of problems and challenges. Our study provides a corresponding Agricultural Multilanguage Data fusion algorithm for the incompleteness of multimodal data, real-time processing, and multisource data fusion. The purpose of this paper is to propose the organization and blockchain-enabled security method of big data to realize the mining and analysis of monitoring data of the Internet of things.

Data Availability

The raw/processed data required to reproduce these findings cannot be shared at this time as the data also form part of an ongoing study.

Conflicts of Interest

The authors declare that there are no conflicts of interest regarding the publication of this study.

Acknowledgments

This work is partially supported by the National Science Foundation of China (Grant No. 72061030), Natural Science and Technology Project Plan in Yulin of China (Grant No. 2019-78-3, 2016CXY-12-09, 2019-78-2, 2019-78-1, 2019-76-2, 2019-106-6), and Funding Project for Department of Yulin University (Grant No. 16GK24, TZRC1801), and thanks for the help.

References

[1] B. Zhou, D. Polap, and M. Wozniak, "A regional adaptive variational PDE model for computed tomography image reconstruction," *Pattern Recognition*, vol. 92, no. 1, pp. 64–81, 2019.

[2] X. Xia, M. Marcin, and X. Fan, "Multi-sink distributed power control algorithm for cyber-physical-systems in coal mine tunnels," *Computer Networks*, vol. 161, no. 1, pp. 210–219, 2019.

[3] H. Song, W. Li, and P. Shen, "Gradient-driven parkingnavigation using a continuous information potential field based on wireless sensor network," *Information Sciences*, vol. 408, no. 2, pp. 100–114, 2017.

[4] Q. Xu, L. Wang, and X. H. Hei, "GI/Geom/1 queue based on communication model for mesh networks," *International Journal of Communication Systems*, vol. 27, no. 11, pp. 3013–3029, 2014.

[5] W. Wei, X. Fan, H. Song, X. Fan, and J. Yang, "Imperfect information dynamic Stackelberg Game based resource allocation using hidden Markov for cloud computing," *IEEE Transactions on Services Computing*, vol. 11, no. 1, pp. 78–89, 2018.

[6] F. Zhang, H. F. Xue, D. S. Xu, Y. H. Zhang, and F. You, "Big data cleaning algorithms in cloud computing," *International Journal of Online Engineering (iJOE)*, vol. 9, no. 3, pp. 77–81, 2013.

[7] X. Li, L. Zhang, X. Cao et al., "Retrieval of precipitable water vapor using MFRSR and comparison with other multisensors over the semi-arid area of northwest China," *Atmospheric Research*, vol. 172-173, pp. 83–94, 2016.

[8] O. P. Rahi, A. K. Chandel, and M. G. Sharma, "Optimization of hydro power plant design by particle swarm optimization (PSO)," *Procedia Engineering*, vol. 30, pp. 418–425, 2012.

[9] F. Zhang, H. F. Xue, and J. C. Zhang, "Multi-source big data dynamic compressive sensing and optimization method for water resources based on IoT," *Sustainable Computing: Informatics and Systems*, vol. 20, no. 1, pp. 210–219, 2018.

[10] S. Singh and Y. Liu, "A cloud service architecture for analyzing big monitoring data," *Tsinghua Science and Technology*, vol. 21, no. 1, pp. 55–70, 2016.

[11] D. S. Yang, J. J. Chen, and M. Zhang, "Research and application on key technology of high-speed storage and retrieval for big data," *Electronic Testing*, vol. 3, pp. 62-63, 2014.

[12] H. Wu, J. Wang, and X. Zhang, "Combining hidden Markov model and fuzzy neural network for continuous recognition of complex dynamic gestures," *The Visual Computer*, vol. 33, no. 10, pp. 1265–1278, 2015.

[13] G. Reeves, J. Liu, S. Nath, and F. Zhao, "Managing massive time series streams with multi-scale compressed trickles," *Proceedings of the VLDB Endowment*, vol. 2, no. 1, pp. 97–108, 2009.

[14] J. Huang, J. Liu, and X. Yao, "A multi-agent evolutionary algorithm for software module clustering problems," *Soft Computing*, vol. 21, no. 12, pp. 3415–3428, 2017.

[15] Y. Wang and J. C. Zeng, "A survey of a multi-objective particle swarm optimization algorithm," *CAAI Transactions on Intelligent Systems*, vol. 5, no. 5, pp. 377–384, 2010.

[16] N. Li, T. Zou, D. B. Sun, and Y. Q. Qin, "Multi-objective optimization utilizing particle swarm," *Computer Engineering and Applications*, vol. 3, no. 4, pp. 193–262, 2005.

[17] Y. Zhou, D. Zhang, and N. Xiong, "Post-cloud computing paradigms: a survey and comparison," *Tsinghua Science and Technology*, vol. 22, no. 6, pp. 714–732, 2017.

[18] H. Liang, J. Zou, K. Zuo, and M. J. Khan, "An improved genetic algorithm optimization fuzzy controller applied to the wellhead back pressure control system," *Mechanical Systems and Signal Processing*, vol. 142, article 106708, 2020.

[19] Z. Huang, X. Xu, J. Ni, H. Zhu, and C. Wang, "Multimodal representation learning for recommendation in internet of things," *IEEE Internet of Things Journal*, vol. 6, no. 6, pp. 10675–10685, 2019.

[20] H. Liang, J. Zou, Z. Li, M. J. Khan, and Y. Lu, "Dynamic evaluation of drilling leakage risk based on fuzzy theory and PSO-SVR algorithm," *Future Generation Computer Systems*, vol. 95, pp. 454–466, 2019.

[21] A. Shahzad, M. Lee, Y. K. Lee et al., "Real time MODBUS transmissions and cryptography security designs and enhancements of protocol sensitive information," *Symmetry*, vol. 7, no. 3, pp. 1176–1210, 2015.

[22] Y. Zhang, R. Zhu, Z. Chen, J. Gao, and D. Xia, "Evaluating and selecting features via information theoretic lower bounds of feature inner correlations for high-dimensional data," *European Journal of Operational Research*, 2020.

[23] H. Liang, A. Xian, M. Mao, P. Ni, and H. Wu, "A research on remote fracturing monitoring and decision-making method supporting smart city," *Sustainable Cities and Society*, vol. 62, article 102414, 2020.

Hindawi
Wireless Communications and Mobile Computing
Volume 2020, Article ID 8886835, 6 pages
https://doi.org/10.1155/2020/8886835

Research Article

Detection Method of Three-Dimensional Echocardiography Based on Deep Learning

Qiao Wu,[1] Li Gao,[2] Wei Sun,[1] and Jianzhong Yang[1]

[1]*The Second Affiliated Hospital of Kunming Medical University, Kunming, Yunnan 650101, China*
[2]*The Third People's Hospital of Chengdu, Chengdu, Sichuan 610014, China*

Correspondence should be addressed to Jianzhong Yang; wuqiao@kmmu.edu.cn

Received 26 September 2020; Revised 26 October 2020; Accepted 9 November 2020; Published 25 November 2020

Academic Editor: Hongju Cheng

Copyright © 2020 Qiao Wu et al. This is an open access article distributed under the Creative Commons Attribution License, which permits unrestricted use, distribution, and reproduction in any medium, provided the original work is properly cited.

In order to improve the detection and recognition ability of 3D echocardiography, a method of 3D echocardiography detection based on depth learning is proposed. The information conduction model of three-dimensional echocardiography is constructed. The edge pixel feature matching method is used to extract the key information of echocardiography, and the information compensation method is used to repair the missing area of three-dimensional echocardiography information. The feature decomposition and information fusion of 3D ultrasonic imaging are carried out by using five stage wavelet decomposition method, and the feature reconstruction and adaptive template matching of 3D echocardiography are processed by depth learning algorithm, modeling and detecting the rationality of three-dimensional echocardiography. The simulation results show that this method has better detection performance; the accuracy of detection and recognition is high, which is more reasonable in the application of 3D echocardiography repair and detection recognition.

1. Introduction

With the development of ultrasound technology and the advent of real-time three-dimensional echocardiography, the defects of two-dimensional echocardiography and static and dynamic three-dimensional echocardiography are overcame, and the operation is simple and the imaging is fast. By collecting the actual ventricular data, it can accurately measure the actual volume of the heart and calculate the cardiac function parameters. It is reported that RT3DE can be used in in vitro models and animal experiments to measure ventricular volume and has a significant correlation with magnetic resonance imaging (MRI) [1], so it has been widely used in clinic. At the same time, CT imaging technology is also developing continuously. MSCT imaging technology can reconstruct the scanned data, calculate the ventricular volume size according to the diastolic and systolic images, and calculate the cardiac function parameters according to the relevant data [2].

Traditionally, the parameters of left ventricular function are analyzed by multislice spiral CT and real-time three-dimensional echocardiography. It is found that both of the two methods could accurately measure the parameters of cardiac function, and the parameters of LVEF and LVMM are compared between the two groups. The difference is not statistically significant ($P > 0.05$). It is believed that multislice spiral CT is accurate and reliable in evaluating left ventricular function and is highly correlated with echocardiography [3]. The parameters of left ventricular function are measured by real-time three-dimensional echocardiography and multislice spiral CT scanning. Multislice spiral CT and real-time three-dimensional echocardiography can accurately evaluate left ventricular function, but multislice spiral CT can be used to examine coronary angiography and understand the lesions of coronary artery and vein. Therefore, it is necessary to study an effective three-dimensional echocardiographic detection method and apply it to clinical practice, combined with multislice spiral CT to examine the coronary artery, and

to understand the coronary artery at the same time, so as to evaluate the value of multislice spiral CT (MSCT) and real-time three-dimensional echocardiography (RT3DE) in measuring left ventricular function [4–6].

In this paper, a three-dimensional echocardiographic detection method based on depth learning is proposed. The information conduction model of three-dimensional echocardiography is constructed. The edge pixel feature matching method is used to extract the key information of echocardiography, and the information compensation method is used to repair the missing area of three-dimensional echocardiography information. The feature decomposition and information fusion of 3D ultrasonic imaging are carried out by using the 5-stage wavelet decomposition method, and the feature reconstruction and adaptive template matching of 3D echocardiography are processed by depth learning algorithm, modeling and detecting the rationality of three-dimensional echocardiography.

2. Information Conduction Model and Image Preprocessing in Three-Dimensional Echocardiography

2.1. Three-Dimensional Echocardiographic Information Conduction Model. By constructing the information conduction model of three-dimensional echocardiography, the information collection and feature extraction of three-dimensional echocardiography are carried out. In the collection of three-dimensional echocardiography, it is necessary to use ultrasound beam scanning three-dimensional echocardiography. The reflected ultrasonic wave is reflected to the output port of the ultrasonic wave, and the pixel features are arranged in different order and the three-dimensional ultrasonic imaging is obtained [7]. In the information reconstruction of three-dimensional echocardiography, the size of the modeling feature region is $16 * 16$. The three-dimensional echocardiography of each $M * N$ is divided into $((M/16) + 1) * ((N/16) + 1)$ rectangular blocks, as shown in Figure 1.

The most similar matching block is selected to reconstruct the 3D feature of the image to be repaired, and the information conduction pixel set of the interior of each sub-block is obtained. By using the similarity between the dark primary color blocks and the blocks to be repaired in three-dimensional echocardiography, the points on the boundary are determined, and the priority characteristics of information conduction are matched. Gradient smoothing is needed for the relative elements of adjacent blocks in three-dimensional ultrasound imaging. The affine invariant moment feature extraction is carried out with the affine invariant kernel function of $3 * 3$. The affine invariant moment has the rotation translation and the scale invariance [8]. Therefore, the feature mining can be carried out through the template matching of the image, and the image processing template can be determined by the template size. The texture structure information of three-dimensional echocardiography is $G(x, y; t)$, and the intuitionistic fuzzy set of texture subspace of three-dimensional echocardiography is defined as conduction function:

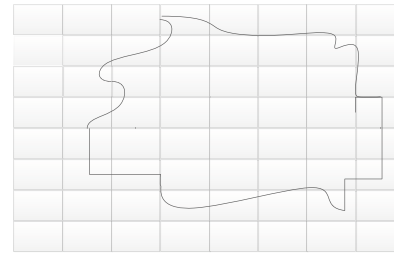

Figure 1: Three-dimensional echocardiographic rectangular segments.

$$p(x,t) = \lim_{\Delta x \to 0} \left[\sigma \frac{u - (u + \Delta u)}{\Delta x} \right] = -\sigma \frac{\partial u(x,t)}{\partial x}. \tag{1}$$

Assume that the edge information of the three-dimensional echocardiography along the gradient direction is shown as follows:

$$G_x(x, y; t) = \frac{\partial u(x, y; t)}{\partial x}. \tag{2}$$

The traversal characteristics of the sharp changes of image features in the scene are obtained, and the information flow density vector of 3D echocardiographic texture structure is obtained as follows:

$$\begin{aligned} p(x, y; t) &= -\sigma \nabla u(x, y; t) = -\sigma G(x, y; t) \\ &= -\sigma \left[G_x(x, y; t) i + G_y(x, y; t) j \right], \end{aligned} \tag{3}$$

Here, i, j are unit direction vectors, based on the visual significance of a target in the detection recognition process, a three-dimensional echocardiography structure texture information conduction model is constructed, the rare degree in the whole scene is obtained [9], and the global rare degree of the three-dimensional echocardiography is obtained by adopting zero uniform traversal. Based on the analysis, the state equation of the three-dimensional echocardiography texture information conduction model is described as follows:

$$\begin{cases} f(x_1, x_2) = r_1 x_1 \left(1 - \dfrac{x_1}{N_1} - \sigma_1 \dfrac{x_2}{N_2} \right) = 0, \\ g(x_1, x_2) = r_2 x_2 \left(1 - \sigma_2 \dfrac{x_1}{N_1} - \dfrac{x_2}{N_2} \right) = 0. \end{cases} \tag{4}$$

Here, r_1 and r_2 are the local and global salient feature sets, and σ_1 represents the mean value of the image features. Based on the above 3D echocardiographic information conduction model, a 3D echocardiographic information conduction model is constructed. The information collection and feature analysis of three-dimensional echocardiography are realized, which provides an accurate data basis for three-dimensional echocardiography modeling [10].

2.2. Priority Determination of Three-Dimensional Echocardiography Reconstruction. In the information conduction model, edge pixel feature matching method and 3D echocardiography are used to determine the priority of information missing region repair. The subspace structure model of three-dimensional echocardiography is designed to calculate the priority coefficient of the block to be reconstructed and update the edge pixel of the three-dimensional echocardiography [11]. The multidimensional search method of subspace feature information is adopted. The information points of three-dimensional echocardiography are searched by gray scale until there are no edge pixels. The mean value of feature is used as pheromone in subspace structure block, and the global rare degree feature of three-dimensional ultrasonic imaging is decomposed. The iterative equation of characteristic decomposition is described as follows:

$$u^{(n+1)}(x,y) = u^{(n)}(x,y) + \delta u_1^{(n)}(x,y), \tag{5}$$

$$u_1^{(n)}(x,y) = M\Delta_s u^{(n)}(x,y) + N\Delta_t u^{(n)}(x,y;d). \tag{6}$$

The size of the 3D echocardiography to be reconstructed is assumed to be $m \times n$, and the size of the characteristic scale block Ψ_p is $s \times s$. By means of edge pixel feature matching, the depth learning algorithm is used to determine the priority of unknown pixel points in 3D echocardiography. The priority sort of pixels meets

$$P\left(|\overline{x_T} - K| < \frac{\lambda_\chi \sigma}{\sqrt{N}}\right) \approx \frac{2}{\sqrt{2\pi}} \int_0^{\lambda_\chi} e^{-(1/2)t^2} dt = 1 - \chi. \tag{7}$$

Here, $\overline{x_T}$ is the mean value of the local contrast window of the 3D echocardiography, χ is the significance weight, and H is the global rare degree coefficient.

3. Three-Dimensional Echocardiography Detection Algorithm

3.1. Characteristic Decomposition and Information Fusion of Three-Dimensional Echocardiography. On the basis of constructing the information conduction model and determining the priority of the reconstruction of three-dimensional echocardiography, the reasonable modeling design of three-dimensional echocardiography is carried out. In this paper, a three-dimensional echocardiographic rationality modeling method based on depth learning is proposed [12]. The characteristic decomposition and information fusion of 3D ultrasonic imaging are carried out by using the 5-stage wavelet decomposition method. The structure similar features of 3D echocardiographic detection and recognition image are obtained by the 5-stage wavelet decomposition of 3D echocardiography:

$$ws(X,Y) = \frac{2\left|\sum_{i=1}^{N} c_{x,i} c_{y,i}\right| + K}{\sum_{i=1}^{N} |c_{x,i}|^2 + \sum_{i=1}^{N} |c_{y,i}|^2 + K}. \tag{8}$$

The results of feature decomposition and information fusion are expressed as follows:

$$l(X,Y) = \frac{2u_x u_y + C_1}{u_x^2 + u_y^2 + C_1}, \tag{9}$$

$$c(X,Y) = \frac{2\sigma_x \sigma_y + C_2}{\sigma_x^2 + \sigma_y^2 + C_2}, \tag{10}$$

$$s(X,Y) = \frac{\sigma_{xy} + C_3}{\sigma_x \sigma_y + C_3}. \tag{11}$$

Here, $\sigma_{xy}$is the edge information covariance and C_1, C_2, and C_3 are the global rarity constants. The feature reconstruction and adaptive template matching of 3D echocardiography are processed by depth learning algorithm [13].

3.2. 3D Echocardiography Reconstruction and Detection Recognition. On the basis of the characteristic decomposition and information fusion of three-dimensional ultrasound imaging using the five-stage wavelet decomposition method, the depth learning is carried out to realize the rational modeling of three-dimensional echocardiography, and the depth learning algorithm is adopted [14]. The parameters of WSSIM are calculated for the wavelet structure similarity of two or 3D echocardiography:

$$\text{WSSIM} = [l(X,Y)]^\alpha [c(X,Y)]^\beta [ws(X,Y)]^\gamma. \tag{12}$$

After the multiscale decomposition of the global rarity, the two-directional subband energies in the information conduction model of the detection and recognition imaging are obtained as follows:

$$\begin{aligned} E_{HL_i} &= \sum_j \left(c_j^{HL_i}\right)^2, \\ E_{LH_i} &= \sum_j \left(c_j^{LH_i}\right)^2. \end{aligned} \tag{13}$$

By using the depth learning algorithm, the three-dimensional echocardiography is firstly convolution with the Gauss kernel function of different scales [15], and the reconstruction output of the three-dimensional echocardiography is obtained as follows [16, 17]:

$$\omega_{HL_i} = \frac{E_{HL_i}}{E_{HL_i} + E_{LH_i} + E_{HH_i}}, \tag{14}$$

$$\omega_{LH_i} = \frac{E_{LH_i}}{E_{HL_i} + E_{LH_i} + E_{HH_i}}, \tag{15}$$

$$\omega_{HH_i} = \frac{E_{HH_i}}{E_{HL_i} + E_{LH_i} + E_{HH_i}}. \tag{16}$$

The probability of each pixel variance in the whole image is calculated. The depth learning algorithm is used to measure the salience of the feature points of three-dimensional

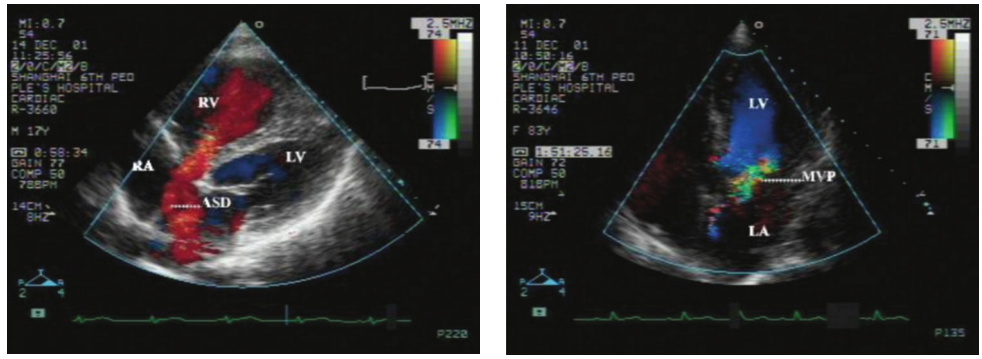

(a) Sample A (b) Sample B

Figure 2: Three-dimensional echocardiographic results.

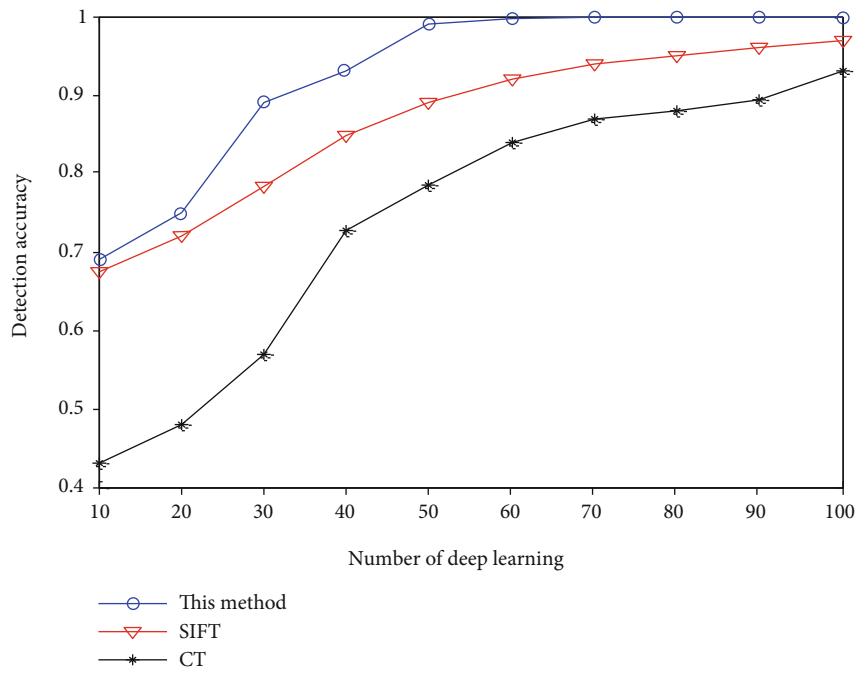

Figure 3: Comparison of 3D echocardiographic detection performance.

echocardiography [18, 19]. The structural similarity features of the image are calculated in the high frequency subband of wavelet [20]:

$$\mathrm{WSSIM}_{H_i} = \omega_{HL_i} \cdot \mathrm{WSSIM}_{HL_i} + \omega_{LH_i} \cdot \mathrm{WSSIM}_{LH_i} + \omega_{HH_i} \cdot \mathrm{WSSIM}_{HH_i}. \quad (17)$$

The wavelet structure similarity of three-dimensional echocardiography is calculated, which is described as FWSSIMI:

$$\mathrm{FWSSIM}(X, Y) = \frac{\omega_{LL} \cdot \mathrm{WSSIM}_{LL} + \sum_{i=1}^{5} \left(\omega_{H_i} \cdot \mathrm{WSSIM}_{H_i}\right)}{\omega_{LL} + \sum_{i=1}^{5} \omega_{H_i}}. \quad (18)$$

On the basis of above processing, the 3D echocardiographic modeling and detection recognition are realized [21].

4. Simulation Experiment and Result Analysis

In order to verify the effectiveness of this algorithm, different types of three-dimensional echocardiography are used to reconstruct the simulation. The test platform is Pentium (R) 4 CPU 3.00 GHz, 1 GB memory in windows XP system. MATLAB simulation software is used to design the algorithm. Firstly, the information transmission model of three-dimensional echocardiography is constructed, and the information characteristic sampling and information fusion of three-dimensional ultrasonic imaging are realized. According to the simulation environment and parameter setting, 3D echocardiography is performed, and the imaging results are shown in Figure 2.

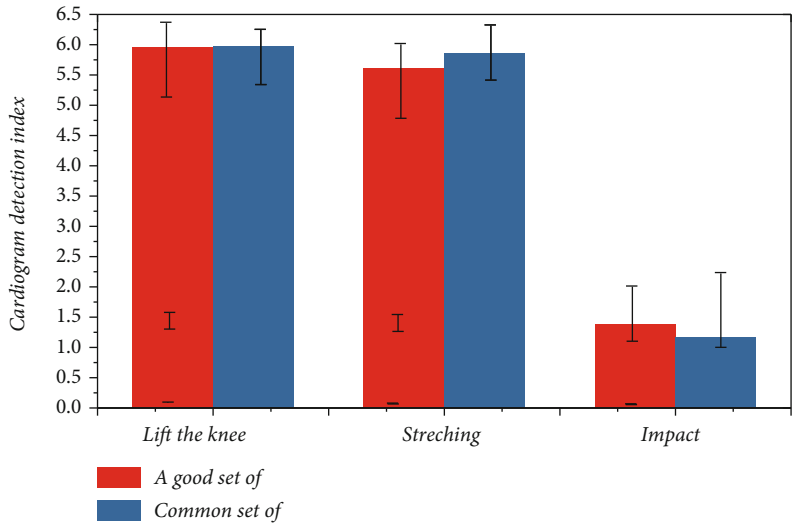

Figure 4: Changes of indicators in the same environment on cardiogram images.

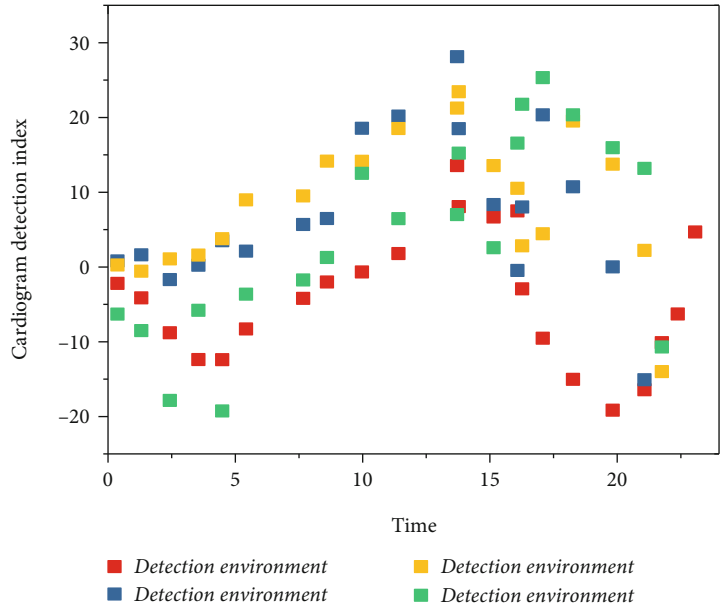

Figure 5: Cardiogram detection indicators in different detection environments.

According to the analysis (Figure 2), the result of three-dimensional echocardiography using this method is better, the characteristic fusion degree is higher, and the peak signal-to-noise ratio is higher. The accuracy of three-dimensional echocardiography is tested by different methods, and the comparison of detection performance is obtained as shown in Figure 3.

The analysis of Figure 3 shows that the accuracy of three-dimensional echocardiography using this method is better.

The weighted low frequency coefficient is $\omega_{LL} = 3.78$ of 3D ultrasonic wavelet decomposition, and the high frequency coefficients of echocardiography are as follows: $\omega_{H_1} = 1.00$, $\omega_{H_2} = 3.75$, $\omega_{H_2} = 7.20$, $\omega_{H_4} = 3.48$, and $\omega_{H_5} = 3.21$. Search step size $N = 4$; 3D echocardiographic image sample block matching template is 9×9. The size of the windows is $3 * 3.5 * 5.9 * 9.17 * 17$. Changes of indicators in the same environment on cardiogram images is shown in Figure 4.

The characteristic decomposition and information fusion of 3D ultrasonic imaging are carried out by using the 5-stage wavelet decomposition method. The structure similar features of 3D echocardiographic detection and recognition image are obtained by the 5-stage wavelet decomposition of 3D echocardiography. Cardiogram detection indicators in different detection environments are shown in Figure 5.

The feature decomposition and information fusion of 3D ultrasonic imaging are carried out by using the five-stage wavelet decomposition method, and the feature reconstruction and adaptive template matching of 3D echocardiography are processed by a depth learning algorithm, modeling and detecting the rationality of three-dimensional echocardiography.

5. Conclusions

In this paper, a method of 3D echocardiography detection based on depth learning is proposed. The information conduction model of three-dimensional echocardiography is constructed. The edge pixel feature matching method is used to extract the key information of echocardiography, and the information compensation method is used to repair the missing area of three-dimensional echocardiography information. The feature decomposition and information fusion of 3D ultrasonic imaging are carried out by using the five-stage wavelet decomposition method, and the feature reconstruction and adaptive template matching of 3D echocardiography are processed by a depth learning algorithm, modeling and detecting the rationality of three-dimensional echocardiography. The simulation results show that this method has better detection performance, and the accuracy of detection and recognition is high, which is more reasonable in the application of 3D echocardiography repair and detection recognition. This method has good application value in the detection and clinical application of echocardiography.

Data Availability

All author information is available from the author.

Conflicts of Interest

None of the authors have any conflicts of interest.

Acknowledgments

This research was supported by the training program for the leading personnel of Yunnan Health Planning Committee (L-201623) and the Young and Middle-Aged Academic and Technical Leaders in Yunnan Province, China (2018HB017).

References

[1] Q. Tan, "Multipath ghost suppression for through-the-wall radar," *IEEE Transactions on Aerospace and Electronic Systems*, vol. 50, no. 3, pp. 2284–2292, 2014.

[2] H. Min, L. Chong, L. Rongrong, and H. Hongcheng, "Performance analysis of motor imagery training based on 3D visual guidance," *Journal of Computer Applications*, vol. 38, no. 3, pp. 836–841, 2018.

[3] T. Ono, A. Kimura, and J. Ushiba, "Daily training with realistic visual feedback improves reproducibility of event-related desynchronisation following hand motor imagery," *Clinical Neurophysiology*, vol. 124, no. 9, pp. 1779–1786, 2013.

[4] R. Shuai, Z. Tao, X. Zhenchao, W. Zhen, H. Yuan, and L. Yunong, "Information hiding algorithm for 3D models based on feature point labeling and clustering," *Journal of Computer Applications*, vol. 38, no. 4, pp. 1017–1022, 2018.

[5] S. G. Hua, Q. Zhong, and S. S. Li, "3D shape deformation based on edge collapse mesh simplification," *Journal of Dalian University of Technology*, vol. 51, no. 3, pp. 363–367, 2011.

[6] Q. Yan, L. Xu, J. Shi, and J. Jia, "Hierarchical saliency detection," in *CVPR'13:Proceedings of the 2013 IEEE Conference on Computer Vision and Pattern Recognition*, pp. 1155–1162, Ishington, DC, 2013.

[7] X. Wang, C. Ning, and L. Xu, "Spatiotemporal saliency model for small moving object detection in infrared videos," *Infrared Physics & Technology*, vol. 69, pp. 111–117, 2015.

[8] L. Xiao, G. Baozhen, L. Qijun, L. Yunpeng, and T. Qingguo, "Acquisition of camera dynamic extrinsic parameters in free binocular stereo vision syste," *Journal of Computer Applications*, vol. 37, no. 10, pp. 2888–2894, 2017.

[9] Z. Quangui, C. Feng, and L. Zhiqiang, "Human action recognition based on coupled multi-hidden Markov model and depth image data," *Journal of Computer Applications*, vol. 38, no. 2, pp. 454–457, 2018.

[10] L. Songlin, J. Yong, G. Yong, Z. Xiaoling, and C. Guolong, "Moving target tracking algorithm based on improved Camshift for through-wall-radar imaging," *Journal of Computer Applications*, vol. 38, no. 2, pp. 528–532, 2018.

[11] S. Goferman, L. Zelnikmanor, and A. Tal, "Context-aware saliency detection," *IEEE Transactions on Pattern Analysis and Machine Intelligence*, vol. 34, no. 10, pp. 1915–1926, 2012.

[12] M. Cheng, Z. Guoxin, N. J. Mitra, H. Xiaolei, and H. Shi-Min, "Global contrast based salient region detection," *IEEE Transactions on Pattern Analysis and Machine Intelligence*, vol. 37, no. 3, pp. 569–582, 2015.

[13] N. Liu and J. Han, "DHSNet:deep hierarchical saliency network for salient object detection," in *Proceedings of the 2016 IEEE Conference on Computer Vision and Pattern Recognition*, pp. 678–686, Ishington, DC, 2016.

[14] W. Kim and C. Kim, "Spatiotemporal saliency detection using textural contrast and its applications," *IEEE Transactions on Circuits & Systems for Video Technology*, vol. 24, no. 4, pp. 646–659, 2014.

[15] W. Xin, Z. Yun, N. Chen, and S. Aiye, "Image saliency detection via adaptive fusion of local and global sparse representation," *Journal of Computer Applications*, vol. 38, no. 3, pp. 866–872, 2018.

[16] Y. Liu, M. Ma, X. Liu, N. Xiong, A. Liu, and Y. Zhu, "Design and analysis of probing route to defense sink-hole attacks for Internet of Things security," *IEEE Transactions on Network Science and Engineering*, vol. 7, no. 1, pp. 356–372, 2018.

[17] F. Long, N. Xiong, A. V. Vasilakos, L. T. Yang, and F. Sun, "A sustainable heuristic QoS routing algorithm for pervasive multi-layered satellite wireless networks," *Wireless Networks*, vol. 16, no. 6, pp. 1657–1673, 2010.

[18] Y. Zhou, D. Zhang, and N. Xiong, "Post-cloud computing paradigms: a survey and comparison," *Tsinghua Science and Technology*, vol. 22, no. 6, pp. 714–732, 2017.

[19] W. Pan and C. Chai, "Measuring software stability based on complex networks in software," *Cluster Computing*, vol. 22, no. S2, pp. 2589–S2598, 2019.

[20] W. Pan and C. Chai, "Structure-aware Mashup service clustering for cloud-based Internet of Things using genetic algorithm based clustering algorithm," *Future Generation Computer Systems*, vol. 87, pp. 267–277, 2018.

[21] G. Yang, Q. Yang, and H. Jin, "A novel trust recommendation model for mobile social network based on user motivation," *Electronic Commerce Research*, vol. 12, no. 5, pp. 124–130, 2019.

Hindawi
Wireless Communications and Mobile Computing
Volume 2020, Article ID 8827084, 7 pages
https://doi.org/10.1155/2020/8827084

Research Article

Research on English Online Education Platform Based on Genetic Algorithm and Blockchain Technology

Xuezhong Wu

English College, Zhejiang Yuexiu University, Shaoxing, Zhejiang 312000, China

Correspondence should be addressed to Xuezhong Wu; 20131109@zyufl.edu.cn

Received 17 September 2020; Revised 12 October 2020; Accepted 31 October 2020; Published 24 November 2020

Academic Editor: Hongju Cheng

Copyright © 2020 Xuezhong Wu. This is an open access article distributed under the Creative Commons Attribution License, which permits unrestricted use, distribution, and reproduction in any medium, provided the original work is properly cited.

Nowadays, with the rapid development of network technology, the online examination mode has gradually replaced the traditional paper examination mode. This paper introduces computer technology into English teaching and studies and designs an English online test system for English subjects. The system introduces the design module and introduces the genetic algorithm for analysis. By using the artificial intelligence of the genetic algorithm to analyze the examination process, the online examination system completes a series of tasks from questions to examination results, making the examination work intelligent, standardized, and highly efficient. At the same time, it also gives candidates greater fairness and flexibility, making the entire examination process more efficient and convenient.

1. Introduction

With the rapid development of network technology, all walks of life have entered the era of network intelligence; the traditional manual operation and management model is gradually replaced by various IT technologies, and people are enjoying the convenience and ease of this change [1]. The current education industry is also following the trend of network technology to break the traditional teaching methods of teaching, examination and question answering only in the classroom, and the way of manual reading in the classroom. And the mode of distance education has been introduced not only to students but also to social personnel to make more people who want to learn knowledge through the network can be at any time and an arbitrary location of the network to choose the subject they are interested in [2]. Distance education is not only concerned with the content of teaching and the interrogative of the learners, but also more attention is paid to the feedback of the learners on the knowledge they have learned in order to provide guidance to the learners. So the development of the online examination system is particularly important [3]. With the rapid development of computers and networks, the traditional patterns of all walks of life will gradually be replaced by the network technology. Network technology is changing people's learning, life, work, and way of thinking [4]. Nowadays, network technology is developing rapidly, and the traditional examination mode is gradually replaced by the online examination model [5]. The staff will be liberated from the heavy examination work. They use the online examination system to complete a series of tasks from the problem to the results of the test to make the examination work intellectualized, standardized, and efficient [6]. At the same time, it also gives the examinee greater fairness and flexibility. Moreover, the resources are saved, the environment is protected, and the paperless examination is realized.

2. Related Work

The online examination is becoming more and more popular in foreign countries and has become the mainstream of the form of examination. At the same time, the technology based on the system is constantly updating, and the development of the system is becoming more and more perfect. The United

States is the first country to apply computer technology to education testing, and it has stepped into the stage of mature application [7]. At present, the research and development of online examination system in China are not very long. But because of the mature software and hardware and the rapid development in recent years, the online examination system has been put into use earlier and has a computer test [8]. As early as in the 1993 "Shanghai City computer application ability assessment (primary)" examination has begun to try this new test method. At that time, it was an application under the DOS system because of the limited function of the condition. As the operating system is upgraded from DOS to Windows, the application has been successfully upgraded to the Windows platform [9]. Although the domestic Internet test is developing so fast, it is still the weak link of distance education or online teaching system. At present, there are only objective questions, such as selection, judgment, and filling, which can be fully implemented and other subjective questions, such as short answer and writing which still need people to score. While the subjective score is flexible, it consumes more energy and time than the objective score. So it makes the reader not completely free from the rewinding [10]. Now, there is also a study on the score of the subject but the algorithm is still in the primary stage, and the subjective score cannot be completed independently, only a preliminary score and finally a manual examination [11].

3. Method

3.1. Genetic Algorithm. The English online test system is a unified test for all candidates. It requires that every test takers get the same indexes on each test paper [12]. That is, the difference is controlled in a smaller range. The people of setting questions should first set several constraints on the system, such as examination time, each question score, the type, the difficulty coefficient of each question, the knowledge point of each question, and the teaching requirement of each question [13]. According to the direction of the constraint, the genetic algorithm is used to search for the optimization continuously until a test paper near the set condition is produced [14]. Each computer can get a test paper with higher reliability according to the algorithm. Since the papers are all in accordance with the unified constraints, the test paper at the terminal will be the same, for example, the difficulty closed to but not to repeat the test [15, 16]. It also brings unanimous fairness in the examination. Therefore, in many fields of examination, the genetic test paper algorithm is more commonly used. In the traditional genetic algorithm, it is not for the use of the group so it is necessary to improve the genetic algorithm in the application of the paper [17]. First, the mathematical model of this examination paper is constructed. Nine questions will be extracted in the system (2 listening, 2 vocabulary and grammar, 1 reading comprehension, 1 finished fill, 2 tenses, and 1 writing questions). And each question has 4 attributes (topic, number, value, difficulty), so they can construct a $9 * 4$ order target matrix A to represent the test paper structure [18].

$$A = \begin{bmatrix} a_{11} & a_{12} & a_{13} & a_{14} \\ a_{21} & a_{22} & a_{23} & a_{21} \\ a_{31} & a_{32} & a_{33} & a_{34} \\ a_{41} & a_{42} & a_{43} & a_{44} \\ a_{51} & a_{52} & a_{53} & a_{54} \\ a_{61} & a_{62} & a_{63} & a_{64} \\ a_{71} & a_{72} & a_{73} & a_{74} \\ a_{81} & a_{82} & a_{83} & a_{84} \\ a_{91} & a_{92} & a_{93} & a_{94} \end{bmatrix}, \quad (1)$$

in which $a_{11} \sim a_{91}$ are the title of the question; $a_{12} \sim a_{92}$ are the number of the title; $a_{13} \sim a_{93}$ are the score of the test; and $a_{14} \sim a_{94}$ are the difficulty of the test. The 4 attributes of each problem represent the constraints of 4 aspects [19]. It points out the direction for people to select excellent examination paper. The constraints that the matrix should satisfy to the maximum limit are as follows: the total score of the test paper is bound to $\sum_{i=1}^{9} a_{i3} = 100$ and number of T type scores $\sum_{i=1}^{9} a_{i3} t_i$. The system of hearing problems should meet that every question is 5 points, a total of which is 10 points. Vocabulary and grammar should meet every question is 5 points, a total of which is 10 points [20]. Reading comprehension should meet the total score of 20. The finished fill should meet the total score of 20. The tenses should be 5 points per channel, with a total of 10 points. The writing question should meet the total score of 30 [21, 22]. The sequence number of the test question is not repeated: that is, in the matrix A, there cannot be a case of the same two or a few elements in the matrix. Otherwise, it shows that the test is repeated. The difficulty of test paper constraint is calculated as $\sum_{i=1}^{9} a_{i3} a_{i4} / \sum_{i=1}^{9} a_{13}$. The difficulty of setting up the test paper is 3.5 (the highest degree of difficulty is 5) [23]. Although the final examination papers are often difficult, to meet every constraint we set, there are three hard conditions to be achieved for the system in which the first is that the total score of the exam is 100, the second is that the score of each type is the prescribed value, and the third is that there cannot be the same topic. In the case, all of the three conditions can be reached. If a test paper with a 3.5 degree of difficulty can be found, the test paper will be the optimal solution of the genetic algorithm. If you cannot find a test paper that is just 3.5 of the difficulty coefficient, we have to set the difficulty factor with $3.0 \le \sum_{i=1}^{9} a_{i3} a_{i4} / \sum_{i=1}^{9} a_{13} \le 4.0$ so that the suboptimal solution can be found [24]. The number of each item and the number of each type of question can be entered by an artificial method in the setting of a test paper, and the total score is 100 points. Therefore, each test paper meets the total score constraints and the total score constraints for each class of questions at the beginning of random volume extraction [25]. Then, judge whether there is the same question or not, which can be avoided in the cross algorithm so the only thing that needs to be controlled is the difficulty of the test paper. In other words, at the initial

stage, each test paper is difficult to find a test paper that is difficult to meet the requirements of the setting by the genetic algorithm. In this way, the target function is only set for the difficulty of the test paper. The objective function can be defined as [26]

$$f = \sum_{j=1}^{4} f_j w_j, \tag{2}$$

in which f_j is the absolute value of the actual value of the property of the j volume of the current test paper and the difference between the attribute constraint values of the j paper volume [27]. w_j is the weight of the difference factor. Now, only the difficulty coefficient is considered; then, the objective function can be simplified to:

$$f = f_4 w_4. \tag{3}$$

in which $f_{4=}|\sum_{i=1}^{9} a_{i3} a_{i4} / \sum_{i=1}^{9} a_{13} - \mathrm{ND}|$ is the absolute error between the average difficulty of generating the test paper and the difficulty constraint of the set test. ND is an artificially set test difficulty constraint. w_4 is the weight of the difference factor of the difficulty coefficient. Generally, the fitness function is designed to be inversely proportional to the objective function. In order to prevent the denominator from being zero, the fitness function can be designed as:

$$F_j = 1/\left(1 + \sum_{j=1}^{4} f_j w_j\right). \tag{4}$$

In the same way, only the difficulty coefficient can be simplified to

$$F_4 = (1 + f_4 w_4). \tag{5}$$

It can be seen that the better the F value is, the better the quality of the 1 test paper. When $F = 0$, the best solution is found that fits all the constraints.

3.2. Roulette Selection Algorithm. Crossoperation is to make test papers produce more quality new individuals. In general, the system needs to be paired randomly to complete the two pairs. The test paper code is divided into several coding segments according to the type of the questions. Each group is divided into eight groups according to the type of the coding. A group can be regarded as a gene point. Here, the system adopts the way of single point crossover. The general operation is first to form two pairs and produce a random number RC of [0, 1] for each pair of test papers and select the probability value P_c. If $\mathrm{RC} < \mathrm{P_c}$, a crosspoint is generated randomly in the coding segment of a certain type of topic. Then, the part of the point is exchanged to produce a new pair of papers. It can be seen that the crossover does not occur in each pair of test papers and is determined by the crossprobability P_c. Therefore, the value of P_c is very important. If the value is too large, it will increase the probability of destroying the genetic pattern; if it is too small, the efficiency of producing new individuals will be too slow. The traditional method is to control the P_c in the range of 0.60~0.8, and this design uses the crossprobability to adjust the value with the change of individual fitness. The formula is as follows:

$$P_c = \begin{cases} K_c \times \dfrac{f_{\max} - f'}{f_{\max}} \times f' \geq f_{\mathrm{avg}}, \\ K_c \times f' < f_{\mathrm{avg}}, \end{cases} \tag{6}$$

In which f' is the one with smaller fitness values in two crosstest papers; $f_{\max}$ is the maximum fitness value in a test paper individual; f_{avg} is the average fitness value of all the test papers; and K_c is the crossprobability coefficient, $K_c \leq 1$. When the larger fitness value in a test paper is less than the average fitness value, the crossprobability is increased; on the contrary, the crossprobability is reduced. There may be repeated questions in the offspring generated after crossing. In this case, we need to replace the 8-bit encoding in the paragraph (one question) to the 8-bit code that has not appeared before and get the new generation again.

3.3. Variant Operation of Tissue Paper. The mutation operation is introduced to solve the high-quality individual reduction produced by the late crossoperation of the algorithm. It is a small probability to change one question (8-bit code) of a test paper to another (another 8-bit code). This system adopts the single point variation in the segment, so the variation does not affect the change of the model. The general operation is generate a random number of [0, 1], such as r_m for each test paper that enters the mutation operation and select the value of the probability P_m. If $r_m \leq P_m$, a variation point is generated randomly in a certain type of coding section, and the 8-bit encoding on this variation is replaced by another 8-bit encoding of the same type to produce a new test paper. As a result, the mutation operation does not happen to every test paper but depends on the mutation probability P_m. Therefore, the value of P_m is very important; if the value is too large, then the genetic algorithm becomes a random search algorithm; if it is too small, it is not easy to produce a new test paper individual. The traditional way is to control the value of P_c in the range of 0.01 to 0.02, and the design adopts the way of adjusting the mutation probability with the change of individual fitness. The formula is as follows:

$$P_m = \begin{cases} K_m \times \dfrac{f_{\max} - f'}{f_{\max}} \times f' \geq f_{\mathrm{avg}}, \\ K_m \times f' < f_{\mathrm{avg}}, \end{cases} \tag{7}$$

in which f is the fitness value of an individual in a variant test paper; $f_{\max}$ is the maximum fitness value in a test paper individual; f_{avg} is the average fitness value of all the test papers; and K_m is probability coefficient of variation, $0.01 \leq K_m \leq 0.05$. When the larger fitness value in a test paper is less than the average fitness value, the mutation probability is increased; on the other hand, the mutation probability is

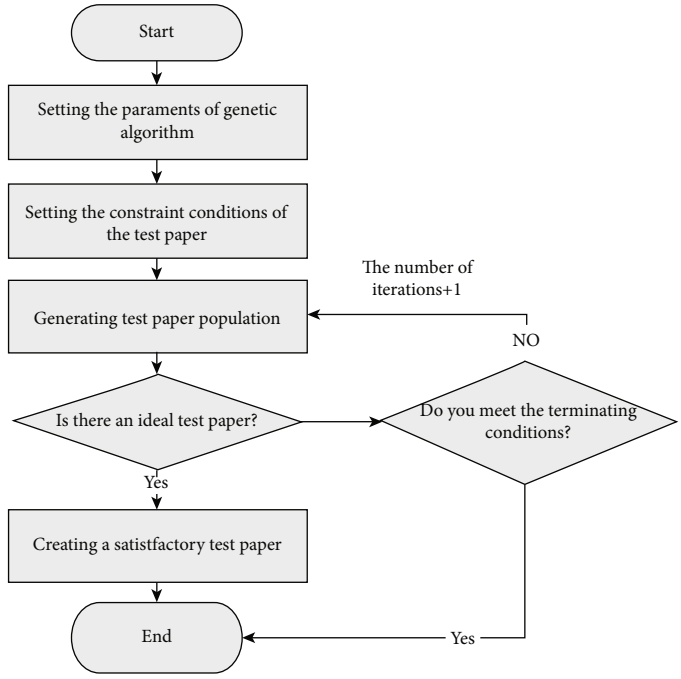

Figure 1: Flow chart of genetic paper algorithm.

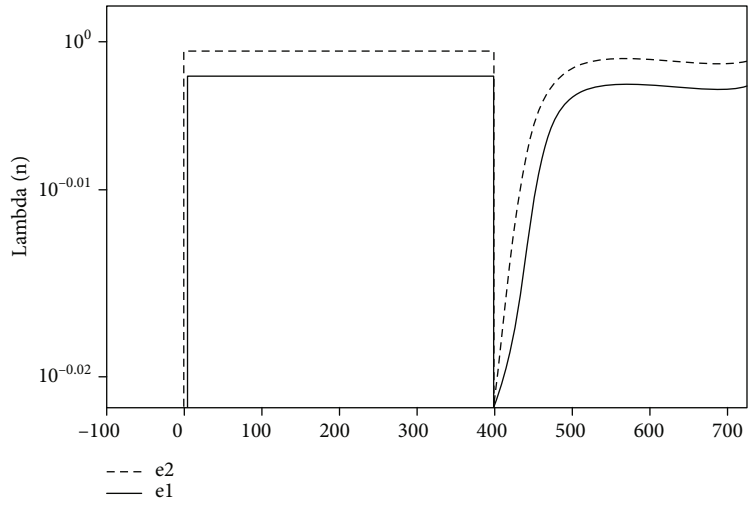

Figure 2: Stable performance of the improved algorithm before and after the signal.

reduced. The offspring of the mutant may have repeated questions. In this case, the repeated 8-bit coding (one problem) in the segment will be replaced by an 8-bit encoding (another problem) that has not appeared, and the new generation will be recovered. Based on the analysis of the genetic algorithm, the following flow chart is obtained, as shown in Figure 1.

4. Result Analysis and Discussion

For the time complexity analysis of the improved genetic algorithm, the number of text in the process of searching the initial cluster center for the extracted sample text is less, the number of iterations is very small, and the speed is very fast. Compared with the original algorithm, the time consumed is not much increased. The improved algorithm performance stability simulation diagram before and after the signal is shown in Figure 2.

The steady-state maladjustment is proportional to the forgetting factor λ. In order to observe the stable performance of the algorithm, using the invariant parameters of the algorithm, the signal to noise ratio (SNR) is l0 dB. Then, the steady-state forgetting factor λ of the two improved algorithms is compared. This reflects the state of the algorithm's steady-state imbalance. The real line e1 represents an improved algorithm, and the dashed line e2 represents an

Table 1: Improved cluster graph account.

Serial number	Name	Number	Number	Percentage
1	1		1	5%
2	2		3	15%
3	3		2	10%
4	4		8	40%
5	5		6	30%
6	Total		20	100%

unmodified algorithm. Because in the range of $0 < \lambda < <1$, the smaller the forgetting factor λ is, the stronger the tracking ability of the system is, and the more stable the system is, so the advantage of the algorithm in a steady-state misalignment is obvious. The improved cluster diagram account is shown in Table 1.

From Table 1, we can see how large the clusters are and it provides the basis for the next approximation experiment. Each result is recorded, and the experiment is repeated on the data experiment platform. Finally, the satisfactory results are obtained. The accuracy and stability of the improved genetic algorithm are greatly improved. Using the common K-means algorithm, the F value of the clustering results is between 0.10 and 0.15 but with the improved algorithm, its value is stable between 0.05 and 0.15. It is also possible to further analyze the results of clustering combined with other related information; thus, there is a more profound understanding of the sample wood points and characteristic variables.

In a word, clustering analysis applied in practice is a process that needs multiple participation, and it cannot be divorced from the user's participation. Genetic algorithm is only an important step in the whole cluster process, and a satisfactory result is obtained by clustering. The genetic algorithm is obviously better than the random algorithm. In the front of the article, a very detailed introduction to the initialization technique of the test is made. This technique reduces the search scope of the algorithm and improves the efficiency of the algorithm. It also has a great effect on the homogenization of the population. By comparing the search time of the genetic algorithm using the test problem initialization technology, the difference between the fitness and efficiency is obtained. Then, we make a comparison of the aggregation time and evaluate the performance of the system according to the cluster and the different expectations of the number of different individuals.

If the number of individuals taking part in the cluster is 10, 20, 30, 40, 50, and 60, each individual in the cluster chooses only one free time and each period of free time is set to 3 hours. In the process of teaching, we record the time of concentration of focus and the number of three types of agent negotiation. The concentration time is defined from pressing the "prepare" button to the focus. Although the data are test data, the results are more close to the actual data for the results of the test. We randomly extract a number of individuals from a group of individuals to test, and the time to get the focus is determined by the average number of tests. The

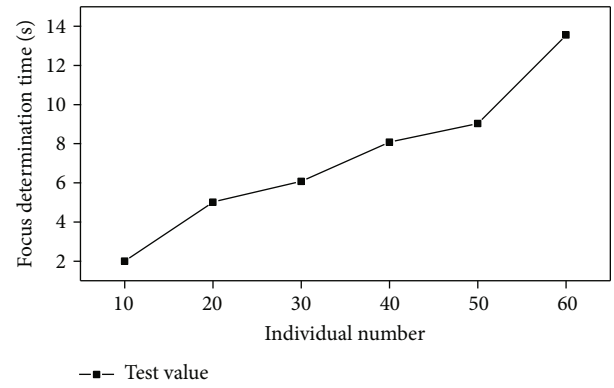

Figure 3: Correlate test result diagram.

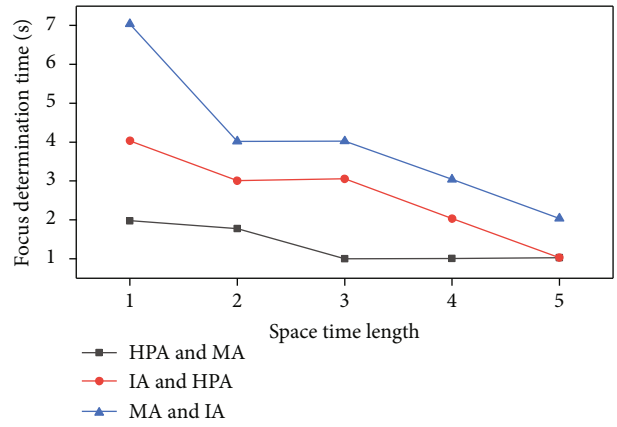

Figure 4: Research on the indexes of English online education platform in time series.

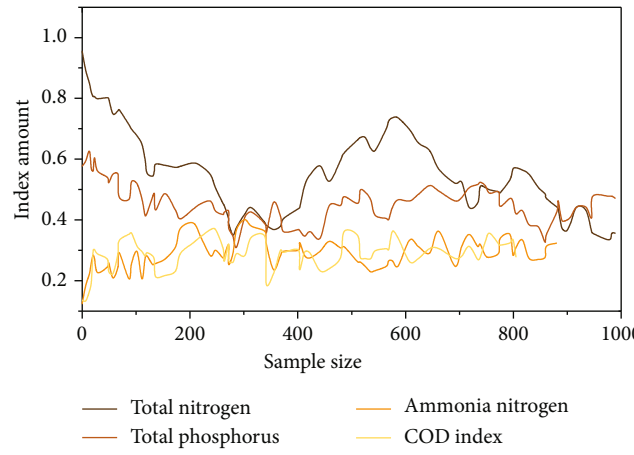

Figure 5: Diagram of correlation test results for different parameters.

test results are shown in Figure 3. The test results show that there is a monotonous increase in the number of individuals involved in the concentration of focus. Research on the indexes of English online education platform in time series is shown in Figure 4.

The relationship between the number of running times of the statistical algorithm and the length of the free time period

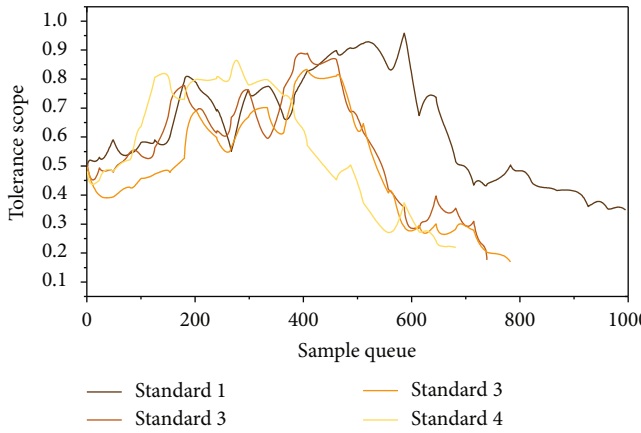

Figure 6: Data storage comparison of English online education platforms.

and the time to determine the focus was determined. We separately check the number of handover tasks between agent (MA) and identity agent (IA) and the number of transactions between identity agent (IA) and the other party's intention to cluster agent (HPA). The result is shown in Figure 5. Thus, it can be seen that the compression of the length of an individual free time period and the number of coordination between various types of transactions are also increased accordingly. It will also cause the increase of the number of times and the time of the communication between each event. Data storage comparison of English online education platforms is shown in Figure 6.

The above focuses on how to apply genetic algorithms to the English online teaching system, and the correctness of the theoretical algorithm proposed in this paper is verified. And through the experiment, we find the deficiency of the algorithm and improve it. The final set of test paper algorithm has the following characteristics: the algorithm flow of the test paper is determined; the test question bank classification initialization technology is used, and the questions are selected from the general library according to the constraints and are redeposited into different test database tables according to the type of questions; using the test number as the chromosome coding, it saves the tedious coding and decoding; the error value of the knowledge point is added to the fitness, which will make the location of the knowledge point more accurate; the crossover and mutation operation is upgraded to an adaptive operation, so that the algorithm can automatically match the appropriate operator. In addition, in order to achieve the best results in the overall scope of the search, the small habitat law should be selected when choosing the strategy.

5. Conclusion

Undoubtedly, teaching information has injected a new vitality into the reform of the traditional educational model. And the online examination algorithm is also a symbol of the application of education information. This paper is based on ASP's online English test algorithm design and exploration. Online examination algorithm has intelligent examination management, intelligent item bank management, intelligent test paper algorithm, intelligent marking function, and so on to emancipate the examiners and teachers from the traditional heavy examination work. In addition, it was aimed at improving work efficiency, enhancing the fairness and flexibility of the examination, and making the examination work algorithmic, standardized, and paperless. This algorithm is based on the features of the English test type and the examination syllabus and set-up test, content, and difficulty condition, establishing a reasonable structure of the database. And through the improvement of the genetic test paper algorithm, the efficiency and quality of the test paper are improved. The main module test algorithm is designed, and the entire process to the results of the examination from the volume can be completed. Each module of the online examination algorithm is tested, and the program is constantly revised to improve the function of the algorithm, and the user experience is more humanized.

Data Availability

All the data is available online.

Conflicts of Interest

The authors declare that there are no conflicts of interest regarding the publication of this paper.

References

[1] J. Liu, "Study on the autonomous learning of college English based on online learning platform," *International Journal of Smart Home*, vol. 10, no. 2, pp. 165–174, 2016.

[2] R. Zhang, M. I. Xiaoqiong, and U. O. Macau, "Study on practicalness of talk to you of WeChat platform for English learning under network circumstances," *Journal of Chengdu Aeronautic Polytechnic*, vol. 41, no. 9, pp. 315–411, 2016.

[3] H. Zhang, "Research on the improvement of English autonomous learning ability of students in higher vocational college by network platform," *Value Engineering*, vol. 17, no. 22, pp. 94–100, 2017.

[4] J. Fang, H. Yujie, and Z. Jian, "The Application of English Mobile Learning Platform in College Students' Autonomous Study," *Campus English*, vol. 2, p. 2, 2017.

[5] Z. Dan, "Online learning platform and innovation of English teaching model based on students' foreign language learning ability in independent college," *Boletin Tecnico/technical Bulletin*, vol. 55, no. 6, pp. 670–677, 2017.

[6] K. Liu, "Design and application of an online English self-learning platform," *International Journal of Emerging Technologies in Learning*, vol. 12, no. 8, p. 4, 2017.

[7] J. Chai, "Development of computer English education platform based on B/S model," *International Journal of Emerging Technologies in Learning*, vol. 12, no. 8, p. 86, 2017.

[8] D. Li, "A study on the construction of college English project-based learning platform in the context of information," *Boletin Tecnico/technical Bulletin*, vol. 55, no. 11, pp. 540–547, 2017.

[9] Q. Ling, R. S. Qin, and J. L. Guo, "An empirical study on northwest minority preppies' self-efficacy in English learning on WeChat platform," *Technology Enhanced Foreign Language Education*, vol. 46, no. 11, pp. 789–792, 2016.

[10] S. Y. Park, M. K. Kang, and Y. M. Kim, "A study on the current status of English education for dental hygiene students," *Information Japan*, vol. 18, no. 5, pp. 2009–2015, 2015.

[11] Y. Liu, M. Ma, X. Liu, N. Xiong, A. Liu, and Y. Zhu, "Design and analysis of probing route to defense sink-hole attacks for Internet of Things security," *IEEE Transactions on Network Science and Engineering*, vol. 7, no. 1, pp. 356–372, 2018.

[12] Y. Wang, F. Zhang, G. Fang, Y. Ji, S. Ye, and X. Zhang, "A novel ultrawideband exponentially tapered slot antenna of combined electric-magnetic type," *IEEE Antennas and Wireless Propagation Letters*, vol. 15, pp. 1226–1229, 2016.

[13] Y. Zhou, D. Zhang, and N. Xiong, "Post-cloud computing paradigms: a survey and comparison," *Tsinghua Science and Technology*, vol. 22, no. 6, pp. 714–732, 2017.

[14] W. Pan and C. Chai, "Measuring software stability based on complex networks in software," *Cluster Computing*, vol. 22, no. S2, pp. 2589–S2598, 2019.

[15] W. Pan and C. Chai, "Structure-aware Mashup service clustering for cloud-based Internet of Things using genetic algorithm based clustering algorithm," *Future Generation Computer Systems*, vol. 87, pp. 267–277, 2018.

[16] G. Yang, Q. Yang, and H. Jin, "A novel trust recommendation model for mobile social network based on user motivation," *Electronic Commerce Research*, vol. 12, no. 2, pp. 201–215, 2019.

[17] T. Chandu, R. Sundarasekar, G. Manogaran, R. Varatharajan, and M. K. Priyan, "Centralized fog computing security platform for IoT and cloud in healthcare system," in *Exploring the Convergence of Big Data and the Internet of Things*, pp. 141–154, IGI Global, 2018.

[18] S. Ather, S. Cooney, S. Gong, and D. Vitek, "Current security threats and prevention measures relating to cloud services, Hadoop concurrent processing, and big data," in *Big Data (Big Data), 2015 IEEE International Conference on. IEEE*, pp. 1865–1870, London, England, 2015, October.

[19] G. Maanak, F. Patwa, J. Benson, and R. Sandhu, "Multi-layer authorization framework for a representative Hadoop ecosystem deployment," in *Proceedings of the 22nd ACM on Symposium on Access Control Models and Technologies. ACM*, pp. 183–190, London, England, 2017, June.

[20] J. J. Yang, J. Li, J. Mulder et al., "Emerging information technologies for enhanced healthcare," *Computers in Industry*, vol. 69, pp. 3–11, 2015.

[21] G. Maanak, P. Farhan, and S. Ravi, "An attribute-based access control model for secure big data processing in Hadoop ecosystem," in *Proceedings of the Third ACM Workshop on Attribute-Based Access Control. ACM*, pp. 13–24, New York, USA, 2018, March.

[22] A. Ahmad, A. Paul, S. Din, M. M. Rathore, G. S. Choi, and G. Jeon, "Multilevel data processing using parallel algorithms for analyzing big data in high-performance computing," *International Journal of Parallel Programming*, vol. 46, no. 3, pp. 508–527, 2018.

[23] A. Ahmad, M. Khan, A. Paul et al., "Toward modeling and optimization of features selection in Big Data based social Internet of Things," *Future Generation Computer Systems*, vol. 82, pp. 715–726, 2018.

[24] F. Long, N. Xiong, A. V. Vasilakos, L. T. Yang, and F. Sun, "A sustainable heuristic QoS routing algorithm for pervasive multi-layered satellite wireless networks," *Wireless Networks*, vol. 16, no. 6, pp. 1657–1673, 2010.

[25] C. Lin, N. Xiong, J. H. Park, and T. Kim, "Dynamic power management in new architecture of wireless sensor networks," *International Journal of Communication Systems*, vol. 22, no. 6, pp. 671–693, 2009.

[26] H. Liang, J. Zou, K. Zuo, and M. J. Khan, "An improved genetic algorithm optimization fuzzy controller applied to the wellhead back pressure control system," *Mechanical Systems and Signal Processing*, vol. 142, no. 1, pp. 106–114, 2020.

[27] M. Tan, "Research on English teaching system based on artificial intelligence and WBIETS wireless network system," *EURASIP Journal on Wireless Communications and Networking*, vol. 2020, 134 pages, 2020.

Hindawi
Wireless Communications and Mobile Computing
Volume 2020, Article ID 8815461, 10 pages
https://doi.org/10.1155/2020/8815461

Research Article

Remote Identity Verification Using Gait Analysis and Face Recognition

Wen Si,[1,2] Jing Zhang,[1] Yu-Dong Li,[1] Wei Tan,[3] Yi-Fan Shao,[4] and Ge-Lan Yang[5]

[1]*Faculty of Business Information, Shanghai Business School, Shanghai 200235, China*
[2]*Department of Rehabilitation, Huashan Hospital, Fudan University, Shanghai 200433, China*
[3]*School of Computer Science and Technology, Dongguan University of Technology, Dongguan 523830, China*
[4]*ECE in University of Michigan-Shanghai Jiao Tong University Joint Institute at Shanghai Jiao Tong University, Shanghai 200240, China*
[5]*Department of Information Science and Engineering, Hunan City University, Yiyang 413000, China*

Correspondence should be addressed to Jing Zhang; zhangjing25@163.com

Received 2 September 2020; Revised 4 October 2020; Accepted 31 October 2020; Published 23 November 2020

Academic Editor: Hongju Cheng

Copyright © 2020 Wen Si et al. This is an open access article distributed under the Creative Commons Attribution License, which permits unrestricted use, distribution, and reproduction in any medium, provided the original work is properly cited.

Biometric identification has verified its effectiveness in personal identity verification because of the uniqueness and noninvasion. In this research, we tend to apply the detection of biometric information to a remote sensing system for the purpose of security area monitoring. Our system is established by collecting signals from the coming individuals via the remote measurement in the specific condition where both kinds of data are detected to determine the identity. Specifically, the measuring of gait signals and facial images is integrated to provide a way of improving the detection accuracy and the robustness. In addition, the fuzzy association rule (FAR) is employed for data analysis in line with the outcomes of different methods. As such, the signals are integrated and transmitted for further processing and remote identification. Experiments are conducted to demonstrate the capability of the proposed system. With the training data increases, a high detection accuracy of 95.2% is obtained, which makes it a promising basis for the realization of remote identity verification.

1. Introduction

Automatic verification of an individual's identity has already become a practical and creative tool in a wide range of applications, especially in the access to some high-restricted environment [1]. In view of certification, the identity verification indicates that an identity is confirmed to be real, together with the individual claiming the identity entitled to him [2]. In accordance with the *Good Practice Guide* (GPG), the verification of personal identity generally starts with collecting the information to pick a person from the population of interest [3]. Rather than using magnetic cards or pin numbers, current studies pay more attention to more convenient, easy, and remote sensing methods in practical use [4, 5]. Specifically, for places of high security and secrecy demands, such as government agencies, scientific laboratories, archives, or the national border, the employment of an optimal remote identity verification method with high accuracy is most pronounced [6]. For these reasons, research is still ongoing to develop identity verification devices and strategies.

Notably, biometrics has already been used for decades as one of the strongest methods to identify and authenticate individual identity [7]. Explicitly, biometrics can be regarded as the technical term for human body measurements and calculations. It refers to the metrics related to all human characteristics. Biometric technology, which is widely spread due to its high accuracy and user friendliness, is currently employed for recognizing individuals via measurable physiological or behavioural properties [8]. To the best of our knowledge, the physiological properties include fingerprint [9], iris [10], and face [11], while the behavioural properties include tread [12], signature [13], and voice [14]. To this end, by

transferring the biometric properties into electric signals, we are thus able to get insight into the system of using biometrics to describe individuals [15].

In spite of the restrictions to our daily life circumstances, the remote access to biometric parameters has greatly progressed with advances in signal collecting and processing devices. It is obvious that the biometric measurement can be attached to real personal activities within a long distance, whose physiological or behavioural traits can be recorded. Nevertheless, one major problem involved with biometrics detection is that the physical appearance of a person may vary with time and environment [16], whereas a 100% accurate measurement rate is impossible to get by merely sensing one single kind of biometric parameter. For this reason, a possible resolution for addressing this issue is to integrate several biometrics into one system. However, since so many biometric parameters are involved in the identity verification, we employ the fuzzy association principle (FAR) for determination in this paper, which is widely used in data mining and decision support application. As such, the sensing signals can be applied for remote identification. The measurement devices, which are suitable for daily ambulatory signal collecting, are designed to meet this requirement for personal identity verification in security and secrecy areas [17].

In this research, we aim to establish a remote identity verification strategy specifically for high-security-monitoring area based on daily life activities. Concerning the analysis of biometric properties, we take the facial images and the gait data measurement during individual walking towards the target place due to its high precision and easy implementation. To this end, the task is addressed by integrating a set of data analysis algorithms for real-time individual biometrics detection and description.

The remaining part of this paper is organized as follows. Related work about gait analysis, face recognition, and the FAR is reviewed in Section 2. Section 3 illustrates the devising of remote signal acquisition system as well as its working procedure. In Section 4, the measurement mechanism and the data processing methodologies for feature extraction and individual recognition are presented. The working performance of the proposed approach is verified by experiments in Section 5. Concluding remarks are given in Section 6.

2. Related Work

2.1. Gait Analysis. Walking is characterized by gait [18]. Gait analysis is initially proposed for precisely quantifying the functional integration while walking by using various strategies [19, 20]. For instance, as one of the commercial walkway devices, the GAITRite system has identified its distinguishing exploration in providing a reliable approach for detecting both averaged and individual gait parameters of the elderly [21, 22].

Gait analysis is typically carried out relying on either of the two ways, including visual observations and motion laboratory devices [23]. The former is aimed at observing the subject's locomotion via cameras during walking while the latter is equipped with sensors for analyzing the gait variation. Nonetheless, the outcomes of the observation approach are qualitative and unreliable. In most cases, the motion measurement system provides precise results based on highly accurate sensing setups such as electromyography systems and joint accelerometers [24, 25]. From a biomechanical point of view, ground reaction forces can be explained by Newton's third law—for every action, there is an equal and opposite reaction of the human foot pressure, which is a way of describing human gait [26]. State-of-the-art studies find that the ground reaction addresses the evaluation of muscle forces, joint torques, and stiffness of damping associated with leg-surface contact [27]. Specifically, the ground reaction force (GRF) measurement is noninvasive and easy to implement. In this way, GRF is one of the distinctive, measurable characteristics used to label and describe individuals.

2.2. Face Recognition. Face recognition indicates the detection of face from cluttered background in line with the recognition using a database of facial characteristics [28]. Typically, the face image of a person is obtained from a video source. The development of face recognition technology largely depends on the flourish of machine learning and deep learning algorithms [29]. There are multiple methods in which face recognition systems work, but in general, they work by comparing selected facial features to determine whether the two face images belong to the same person or not [30]. To this end, face recognition can be primarily carried out via the following steps: (i) face detection: in the first place, we categorize the variation of colors from the input image and find the location and size of the faces in this image [31]; (ii) feature extraction: feature extraction is a most critical procedure which takes the biometric features, such as color of the eyes and width of the nose to construct a feature representation of the target face [32]; (iii) facial recognition: the feature representation of a face is commonly in the form of matrix, which is taken as the input of the facial recognition system [33]; and (iv) individual tagging: the person identity is determined by searching the current database. In this way, a name is tagged to the person whose image has already been captured [34].

To keep the method user-friendly, the four steps are taken in real time [35]. In this way, with a camera employed for image collecting, the face recognition process can be carried out for person identity verification.

2.3. Fuzzy Association Rules (FAR). Theoretically, fuzzy association rules are utilized to capture the correlations between low-level features and high-level essence of the target [36]. We now give a brief description of this principle.

$$X = \{x_1, x_2, \cdots, x_n\}. \tag{1}$$

Let it be the initial database, together with all the characteristics in X.

$$T = \{t_1, t_2, \cdots, t_m\}. \tag{2}$$

Specifically, we carry out a fuzzy set associated with each characteristic [37]. For the characteristic t_i, the fuzzy set indicating the internal property of t_i is given as follows:

$$F_{t_i} = \left\{ f_{t_i}^1, f_{t_i}^2, \cdots, f_{t_i}^k \right\}. \quad (3)$$

For the purpose of biometric parameter identification, we shall thus define Gait $= \{g_1, g_2, \cdots, g_n\}$ as the gait feature and Image $= \{i_1, i_2, \cdots, i_m\}$ as the facial image feature. Supposing that $F_{\text{gait}} = \{f_{g1}, f_{g2}, \cdots, f_{gn}\}$ and $F_{\text{image}} = \{f_{i1}, f_{i2}, \cdots, f_{\text{in}}\}$ refer to the corresponding properties or gait and face feature, respectively. As for each pair of (g_j, f_{gj}) or (i_j, f_{ij}), we call it an item. Similarly, each pair of (Gait, F_{gait}) or (Image, F_{image}) is an itemset.

Hence, in order to find the internal correlation, the Gait $\rightarrow F_{\text{gait}}$ can be derived from Image $\rightarrow F_{\text{image}}$ based on FAR. As such, we can get votes which are greater than the specific threshold of the dataset. In other words, the probability that Image occurs given that Gait has occurred is defined as the confidence of the rule [38, 39]. In this way, the significance factor of (Gait, F_{gait}) is presented as follows:

$$\text{Significance} = \frac{\text{Sum of voting for } \left(\text{Gait}, F_{\text{gait}}\right)}{\text{Number of records in identity } P}, \quad (4)$$

where P is the dataset of individual identity features whose fuzzy set is F_p. Mathematically, $P =$ Gait + Image and $F_p = F_{\text{gait}} + F_{\text{image}}$. On the other hand, the certainty factor for supporting the rule is given as follows:

$$P\left\{\left(\text{Gait}, F_{\text{gait}}\right), \left(\text{Image}, F_{\text{image}}\right)\right\} \frac{\sum_{p_i \in P} \prod_{F_{pi} \in F_p} \left\{ \alpha\left(in_i \middle| f_p \right) \right\}}{\sum_{p_i \in P} \prod_{g_j \in \text{Gait}} \left\{ \alpha\left(in_i \middle| g_j \right) \right\}}, \quad (5)$$

where function α is to compute the voting in comparison the threshold value. In addition, in_i indicates the i^{th} person within the permitted individual dataset.

3. System Architecture

Considering the biometric parameter measurement, a system is established aiming at verifying the person identity by using the biometric characteristics for security monitoring. There are two parts in the system, which are gait analysis part and face recognition part. The outcomes of each part are integrated to determine the identity of the coming person (Figure 1). The deployment of both parts is illustrated as follows.

3.1. GRF Testing Setup. In this paper, a strain gauge force platform with the size of 400 mm × 2000 mm is employed to collect the GRFs of both feet on the laboratory walkway while walking. Apparently, the more sensing elements are placed, the higher precision of GRF can be measured [40]. Within this force plate, 256 vertical electrode sheets and 128 horizontal electrode sheets are employed for sensing. The force platform is calibrated by the calibration matrix provided by the manufacturer before putting into practical application. The detection of GRF can easily be implemented,

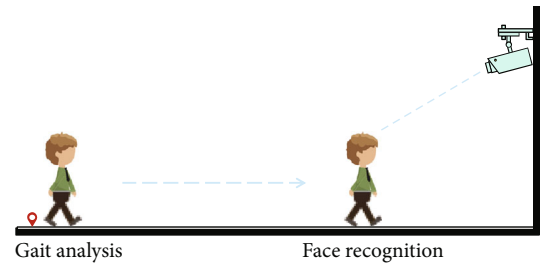

Figure 1: System deployment.

as shown in Figure 2. As long as a force plate is set to establish a walking foot fall, the data will be automatically recorded when someone walks on it at free speed. The GRF signals are transmitted into voltage values with respect to the force applied on the sensor surface. Based on the input signals, the sensing data is sent to a signal acquisition module (NI FD-11637) with a highest sampling rate as 100 kS/s [41]. The force signals are sampled at a frequency of 500 Hz in this system. The acquisition device has the function of signal amplifying as well as a 24-bit analog-digital conversion for data transforming. What is more, a host computer is connected directly to the signal acquisition hardware via USB. As such, the GRF outcomes can subsequently be stored and provided for further analysis. Thereby, this data collection device, on the basic of GRF sensing, can be attached to the individual verification system whenever required.

There are three components measured by using the force plate, which are as follows:

(i) F_z: vertical component on Z axis

(ii) F_y: horizontal component on Y axis (anterior-posterior)

(iii) F_x: horizontal component on X axis (medial-lateral)

We thus have GRF $= \{F_x, F_y, F_z\}$. The total GRF can therefore be represented by a vector that is the sum of the vertical load as well as the shear force in two orthogonal directions. The components of GRF are illustrated in Figure 3.

3.2. Face Recognition Setup. For the purpose of image detection, a visual sensing module integrates cameras to collect time series scenarios and characterize and identify intrusion targets [42, 43]. In this paper, since the individual's digital face image acquired from a sensor is compared with the face images in the database, a Panasonic WV-CW590CH detection camera with a 650 color dpi is deployed in front of the security door. This instrument is able to detect objects within a range of 10 meters and is hard wired to a DC-regulated power supply. Typically, the perfect record for individual faces is conducted from the 3D face images, with a pose variety of ±45° rotation intensive and ±10° rotation in the image plane [44, 45]. In this way, a face image can therefore be captured from different surroundings (Figure 4).

In consideration of the security and secrecy needs, no wireless transmission network is allowed to build within the

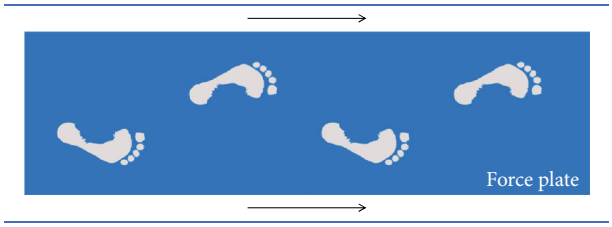

Figure 2: Force plate for GRF recording.

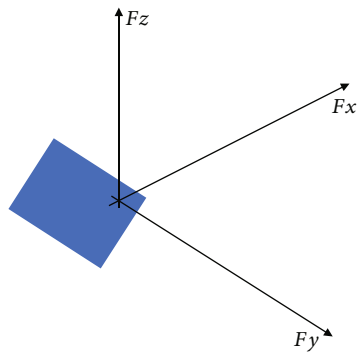

Figure 3: GRF component.

target area. As a result, the camera is connected to the signal processing module on the host computer with low-noise electric cable. In addition, the images of permitted individuals as well as the face recognition programs are collected beforehand and are stored as a dataset for real-time calling. When the face image of the coming person is detected, the data can be transferred from the camera to the host computer. The face recognition algorithms are run to process the image signals. We shall thus identify the person's identity by matching the faces from the database. Therefore, the users can further process the images via linking to the host computer.

4. Identity Verification Algorithm

The GRF signals and the facial images are collected through the aforementioned system while the person is stepping to the security area. In the interest of individual verification, we tend to fuse these data for processing and analysis. On this occasion, we shall thus define the primary procedures of data processing, which is exhibited in Figure 5.

4.1. GRF Testing Algorithm. During the gait analysis phase, the ground reaction forces are collected to be identified, whose schematic diagram of the system is presented in Figure 6. To start with, the GRF signals are conditioned into process able data for further investigation. The sliding window is employed for GRF data segmentation for continuous identification. Specifically, the data is filtered to remove the random noise from the sensor outputs. Furthermore, an extractor is used for gait feature extraction, from which the internal characteristics are derived from gait in time sequence. Mathematically, features characterize the data from every single analysis window without losing information. In this research, four different features are extracted to demonstrate the GRF variation, which are maximum value, average value, standard deviation, and kurtosis. Accordingly, the representation of individual gait is sent to the characteristic matcher to authenticate a walking person. The identification of GRF is conducted by using the SVM (support vector machine) classifier, which resolves problems of high-dimensional data as presented in [46]. The RBF (radial basis function) kernel is taken for data training and testing. At this stage, the gait pattern is compared with the template of one single person, which is picked from the database stored in the host computer. The force is first matched to a prespecific kind of GRF. Hereafter, the features are compared to the database of four feature parameters and their values. The identification process is exhibited in Algorithm 1 with θ as a preset threshold. As such, the gait representation is compared with that of all subjects within the storage. On this occasion, the output of the verification system can be either the identity of a previously enrolled individual or an alert message.

4.2. Face Recognition Algorithm. According to the aforementioned steps, a novel model is built up as shown in Figure 7. Originally, an $n \times m$ pixel image represents a face via the vector in an $n \times m$ dimensional space. Hence, the dimensionality reduction is a procedure of transforming a high-dimensional data set into a low-dimensional representation which retains most of the information [47]. In most cases, the dimensionality reduction is a preprocess of feature extraction. As for face recognition, we use the MPCA (multilinear principal component analysis) method for reducing the feature projection matrix of face images, which is a widely used multilinear algorithm that extracts features from multidimensional objects [48]. The outputs of the MPCA are sent to the feature extractor. In this paper, we take the LBP operator based on the exploration of [49]. Since the LBP operator has the window of 3×3, the gray value of the adjacent 8 pixels is compared with that of the center value. As long as the neighboring pixel value is greater than or equal to the center pixel value, the value of the target pixel is set as 1, otherwise set as 0. Consequently, the LBP eigenvalues of each pixel can be obtained to compose a feature spectrum. In order to get a real-time outcome, the similarity distance measure, which is a simple but effective recognition approach, is employed. Specifically, the L2 similarity distance measurement, whose purpose is to compute the L2 distance between the target face and those from the database, is taken to determine whether the two faces are the same or not. The creation of face dataset is applied to store the predefined individual facial images, which is the foundation of identity matching. Similar to the GRF analysis procedures, the face recognition algorithm is presented (Algorithm 2).

4.3. Decision-Making. Each of the subsystem provides a local result of the identification outcome. Compared to the identities from the database, the output value is normalized to be either 0 or 1 where 0 and 1 indicate the rejection and acceptance, respectively. The global decision, however, is computed by integrating the two outcomes. Commonly, the two outcomes are combined

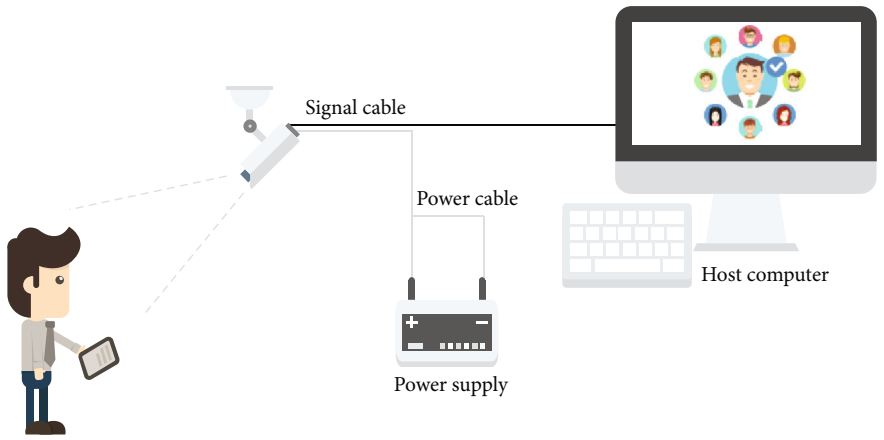

Figure 4: Face recognition system.

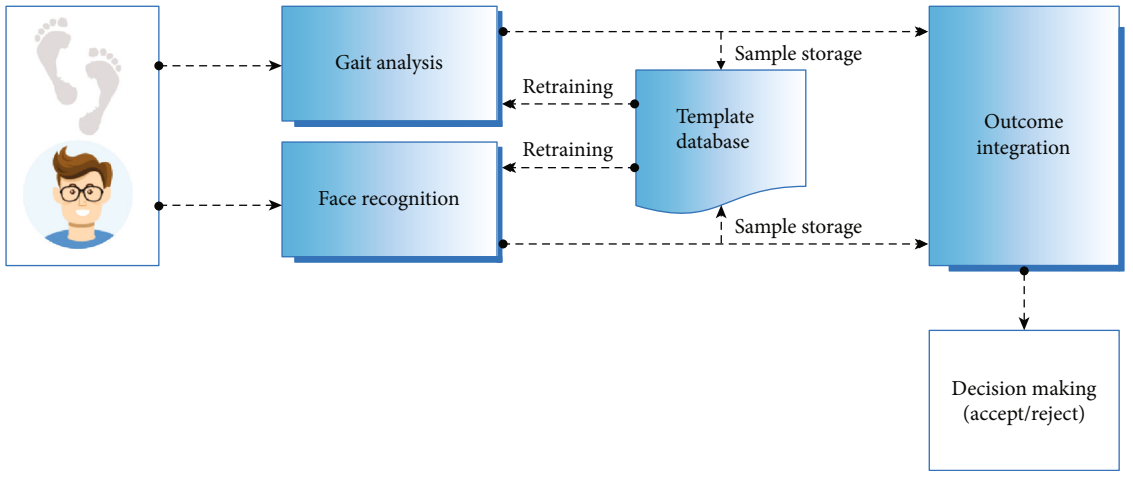

Figure 5: Identity verification based on integration of gait analysis and face recognition.

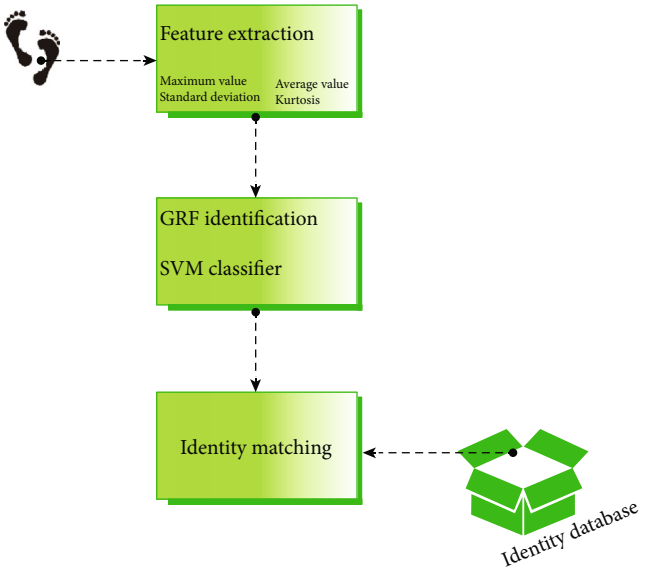

Figure 6: GRF processing flow.

by using the weighted average algorithm. In this way, the final decision is on the basic of the probability on the personal identity. As mentioned in Section 2, we employ the RAF for data integration in this paper. For every single feature, the fuzzy sets can be built up and we can therefore measure the significance of the rule. Further, a FAR base is established where all the frequent fuzzy item sets can be obtained.

The fuzzy decision is given based on the FAR. There is no need for the obtained signals entirely matching with the standard personal pattern. To estimate the individual identity, we employ the Gaussian curve membership function for data characterization. The membership within the fuzzy set is shown as follows:

$$\alpha = \exp\left[-\left(\frac{x-c}{\sigma}\right)^2\right], \tag{6}$$

where c is the data center and σ is the variance. Moreover, the fuzzy matching for individual identity is presented as follows:

$$Fi(x_j) = \prod_{j=1}^{n} \alpha(x_j) = \prod_{j=1}^{n}\left[-\left(\frac{x-c_j}{\sigma}\right)^2\right]. \tag{7}$$

Initialize feature extractor.
Initialize SVM based classifier.
while run **do**
Perform GRF detector to get gait set $\{X_i, Y_i, Z_i\}$.
Perform feature extractor to get gait feature set $\{X_i^F\}_1^n, \{Y_i^F\}_1^n, \{Z_i^F\}_1^n$
Perform classifier on detected gait feature set $\{D_j\}_1^k$ and get the probability $P(D_j)$.
if $P(D_j) \geq \theta$ then
  Accept $\{D_j\}_1^k$ as the target person, and its probability as $P(D_j)$.
else
  Output alarm information
end if
end while

Algorithm 1. GRF analysis.

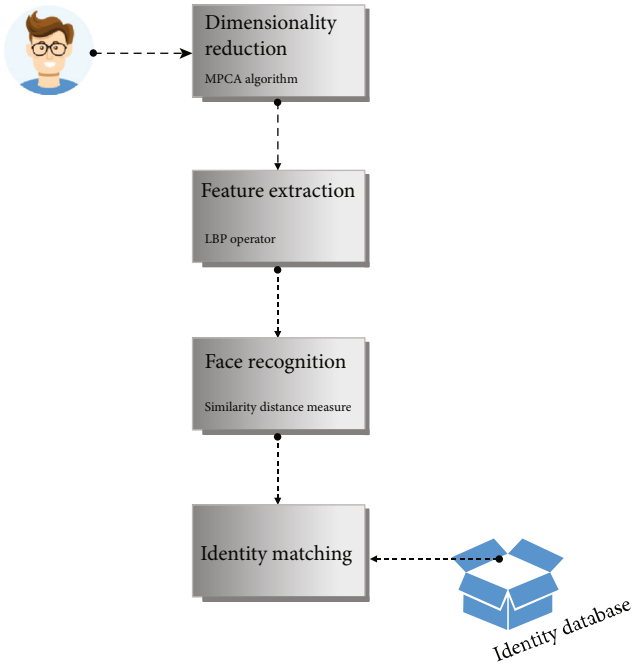

Figure 7: Face recognition flow.

The outcome of the maximum fuzzy matching degree can therefore be found. In terms of identity verification, the result corresponds to the fuzzy decision exactly, which is expressed as follows:

$$FI(x_j) = \max Fi(x_j). \tag{8}$$

5. Experiments

The evaluation of working performance of the propose method for individual verification is carried out. The equipment is deployed in front of a laboratory access of a college in the city of Shanghai. The current security area allows only 26 staff to get access. We collect the GRF signals of individuals from different types of shoes and facial images of different expressions and angles. In this way, 936 pieces of data are generated. The dataset is divided into three parts: 60% training data, 20% validation, and 20% testing data. The training procedure is performed on the training set, followed with the evaluation on the validation set. As long as expected results are obtained, the testing data is sent to the detector for individual identity verification. With the power supplied, GRF signals are recorded by the sensors on the force plate, while the face images are captured via the video camera. Both kinds of signals are transmitted to the computer through the electric cable in real time. The data processing procedure is implemented on the Dell server with two GTX-1080GPU, and the operating system is a 64-bit Ubuntu 16.4. One example of the waveforms of GRF signals and face images of one individual are presented in Figures 8 and 9. We verify the identity of these volunteers by the proposed method.

Initially, we train our method through the learning data in the dataset. The accuracy of identification shown in Equation (9) is determined by calculating the number of correctly recognized class instances (TP, true positives), the number of correctly recognized instances that do not belong to the class (TN, true negatives), and instances that either were incorrectly assigned to the class (FP, false positives) or were not recognized as class instances (FN, false negatives) [50]. The model is fine-tuned during the validation and evaluated during the testing.

$$\text{Accuracy} = \frac{\text{TP} + \text{TN}}{\text{TP} + \text{TN} + \text{FP} + \text{FN}}. \tag{9}$$

Reported outcomes facilitate the evaluation of the proposed methods. At the first stage, the decisions based on gait analysis and face recognition are illustrated in Table 1. We can see that, for gait analysis outcome, all the errors are resulted from the rejected genuine users. In contrast, most errors of face recognition are caused by the accepted impostors.

The detection accuracy increases in line with the number of training samples (Figure 10). The proposed method is tested based on the inputs. In comparison, we initially present the outcomes by using only one kind of biometric

Initialize pre-processor.
Initialize feature extractor.
Initialize LBP operator.
while run **do**
Perform camera to get facial image $\{F_i\}_1^n$.
Perform pre-processor to reduce the high-dimensionality.
Perform feature extractor to get feature set $\{F_i^F\}_1^n$.
Perform LBP operator on image feature set $\{D_j\}_1^k$ and get the maximal confidence $conf(D_{\max})$.
if $conf(D_{\max}) \geq \theta$ then
  Accept $\{D_j\}_1^k$ as the target person, and its maximal confidence as $conf(D_{\max})$.
else
  Output alarm information
end if
end while

Algorithm 2. Face recognition.

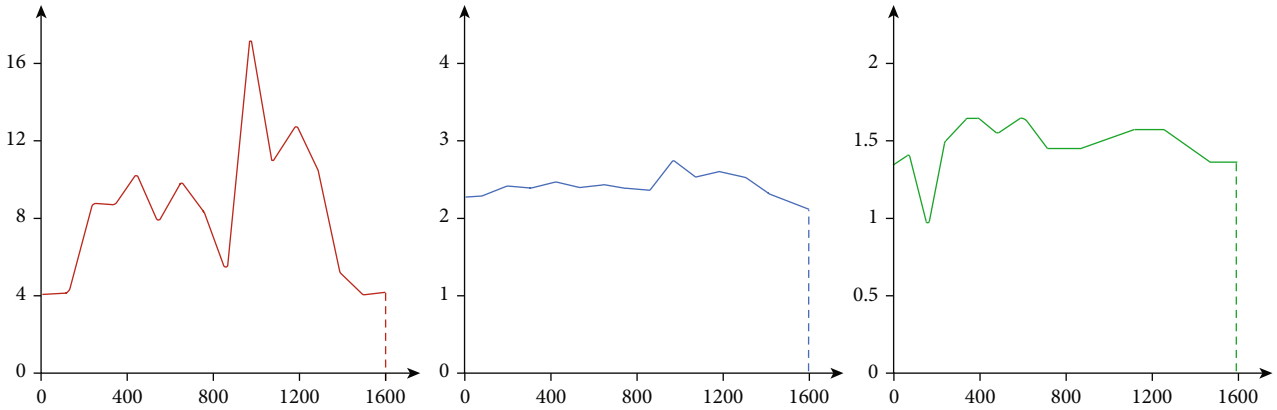

Figure 8: GRF outcomes of X, Y, and Z directions of the target person.

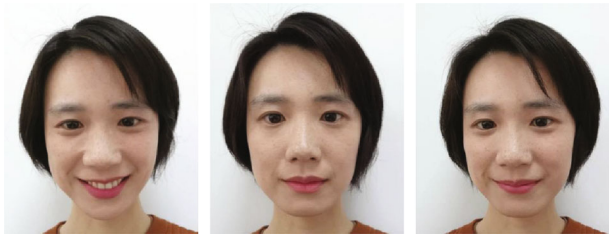

Figure 9: Face images of the target person.

Table 1: First stage outcomes.

Item	Rejected genuine users	Accepted impostors
Gait analysis	0.2	0.01
Face recognition	0.06	0.16

parameter detection. Moreover, the integration of data using weighted average based on the outcomes in Table 1 is given. The determination via FAR is applied to the two detection outcomes for decision-making. The detection errors of weighted average and FAR algorithm are given in Table 2 and Figure 11. By using the error analysis of Table 1, the weighted average algorithm has a quite even error on both rejected genuine users and accepted impostors. However, for the FAR determination, the errors caused by rejected genuine users are four times of those by accepted impostors. Experimental results on testing data are shown in Table 3.

6. Conclusion

In this paper, we mainly focus on a remote personal verification approach in the specific condition of security area monitoring. The integration of biometric parameters provides an opportunity to cater to the demands of noninvasion, high accuracy, and remote sensing based on the user's acceptability. This paper does present some contributions to the application of personal verification systems.

Firstly, the biometric parameters, i.e., GRF signals and facial images, are directly collected and transmitted for remote measurement with the devising and deployment of the detection system.

Secondly, both kinds of signals are processed by using the state-of-the-art algorithms. The signal detectors are

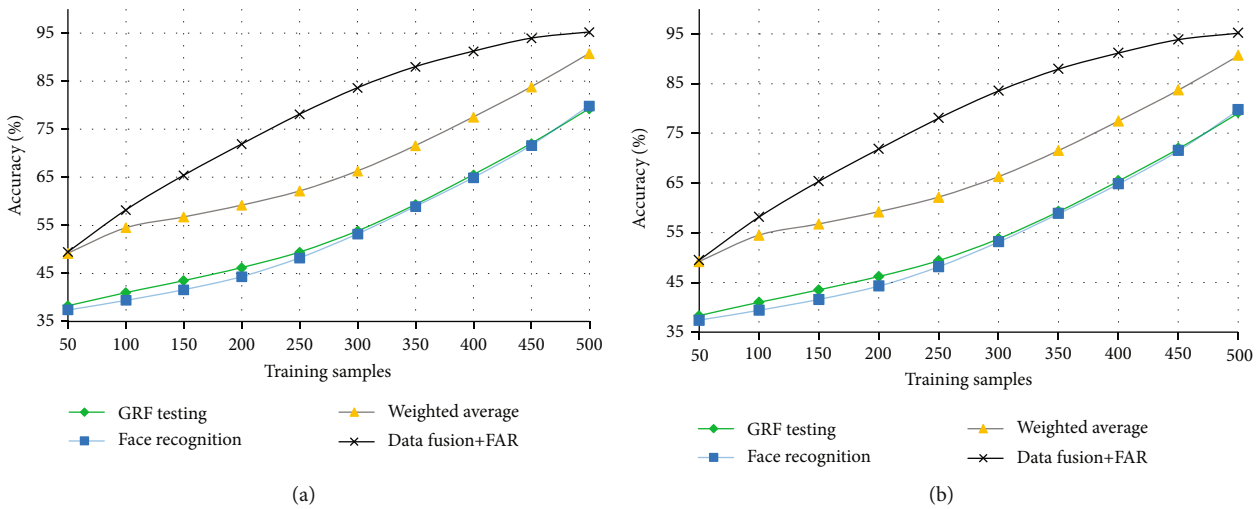

Figure 10: (a) Training accuracy of proposed methods. (b) Testing accuracy of proposed methods.

Table 2: Final outcomes.

Items	Rejected genuine users	Accepted impostors
Weighted average	0.04	0.05
FAR decision	0.04	0.01

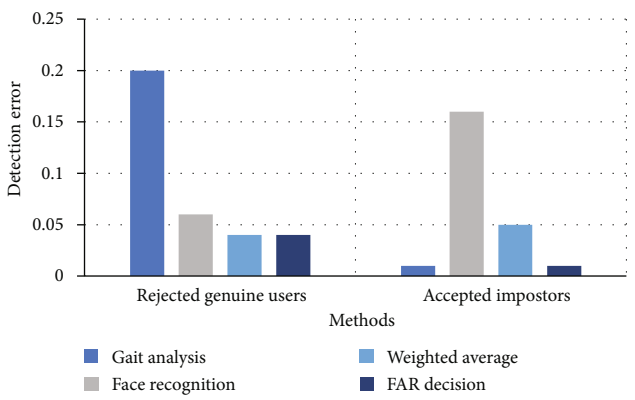

Figure 11: Detection error comparison.

Table 3: Working performance of different algorithms.

Methods	Training accuracy	Testing accuracy
Face recognition	83.1%	79.8%
GRF testing	86.9%	79.2%
Weighted average	92.3%	90.7%
FAR decision	97.3%	95.2%

established, and the signals are transmitted to identify the individual characteristics from a long distance.

Thirdly, the FAR algorithm is taken to better address the identification problem. An even higher detection accuracy is obtained because of the biometric signal integration.

Future steps will be taken to focus on the extension and validation of the current to more biometrics. In addition, the signal integration strategy will also be exploit, which aims to improve the personal verification accuracy.

Data Availability

The gait data and facial images used to support the findings of this study have not been made available because of the identity confidentiality of the users.

Conflicts of Interest

The authors declare that they have no conflicts of interest.

References

[1] A. Czyżewski, P. Hoffmann, P. Szczuko, A. Kurowski, M. Lech, and M. Szczodrak, "Analysis of results of large-scale multimodal biometric identity verification experiment," *IET Biometrics*, vol. 8, no. 1, pp. 92–100, 2019.

[2] M. Gheisari, Q. Pham, M. Alazab, X. Zhang, C. Fernandez-Campusano, and G. Srivastava, "ECA: an edge computing architecture for privacy-preserving in IoT-based smart city," *IEEE Access*, vol. 7, pp. 155779–155786, 2019.

[3] *Good practice guide, Identity proofing and verification of an individual*UK CEGC and Cabinet Office2018, https://webarchive.nationalarchives.gov.uk/20150514214143tf_/https://www.gov.uk/government/publications/identity-proofing-and-verification-of-an-individual.

[4] X. Wang, H. Xue, X. Liu, and Q. Pei, "A privacy-preserving edge computation-based face verification system for user authentication," *IEEE Access*, vol. 7, pp. 14186–14197, 2019.

[5] L. Tseng, Y. Wu, H. Pan, M. Aloqaily, and A. Boukerche, "Reliable broadcast in networks with trusted nodes," in *2019 IEEE Global Communications Conference (GLOBECOM)*, pp. 1–6, Waikoloa, HI, USA, December 2019.

[6] C.-T. Hsieh, C.-C. Han, C.-H. Lee, and K.-C. Fan, *Person authentication using nearest feature line embedding transformation and biased discriminant analysis*, International Carnahan Conference on Security Technology, Madrid, Spain, 2017.

[7] Y. Tian, Y. Li, X. Liu, R. H. Deng, and B. Sengupta, "PriBioAuth: privacy-preserving biometric-based remote user authentication," in *2018 IEEE Conference on Dependable and Secure Computing (DSC)*, pp. 1–8, Kaohsiung, Taiwan, 2018.

[8] A. L. M. Cuenca, Y. R. C. Dizon, H. A. Espinosa et al., "Development of plantar pressure in-sole system for diabetic peripheral neuropathy analysis using pressure mapping sensors," in *2019 IEEE 11th International Conference on Humanoid, Nanotechnology, Information Technology, Communication and Control, Environment, and Management (HNICEM)*, pp. 1–6, Laoag, Philippines, 2019.

[9] S. Hemalatha, "A systematic review on fingerprint based biometric authentication system," in *2020 International Conference on Emerging Trends in Information Technology and Engineering (ic-ETITE)*, pp. 1–4, Vellore, India, India, February 2020.

[10] R. A. Halim and A. W. R. Emanuel, "A review of iris recognition system ROI and accuracy," in *2020 International Conference on Smart Technology and Applications (ICoSTA)*, pp. 1–6, Surabaya, Indonesia, Indonesia, February 2020.

[11] A. Nilizadeh, W. Mazurczyk, C. Zou, and G. T. Leavens, "Information hiding in RGB images using an improved matrix pattern approach," in *2017 IEEE Conference on Computer Vision and Pattern Recognition Workshops (CVPRW)*, pp. 1407–1415, Honolulu, HI, 2017.

[12] J. Dąbroś, M. Iwaniec, M. Patyk, and J. Wesół, "Machine learning gait analysis algorithm for ontogenetic features compensation," in *2018 XIV-th International Conference on Perspective Technologies and Methods in MEMS Design (MEMSTECH)*, pp. 132–135, Zakarpattya, Ukraine, 2018.

[13] F. AL-Turjman and D. B. David, "Seamless authentication: for IoT-big data technologies in smart industrial application systems," in *IEEE Transactions on Industrial Informatics(Early Access)*, April 2020.

[14] D. A. Reynolds and R. C. Rose, "Robust text-independent speaker identification using Gaussian mixture speaker models," *IEEE Transaction on Speech and Audio Processing*, vol. 3, no. 1, pp. 72–83, 1995.

[15] M. Wang and Z. Yan, "Privacy-preserving authentication and key agreement protocols for D2D group communications," *IEEE Transactions on Industrial Informatics*, vol. 14, no. 8, pp. 3637–3647, 2018.

[16] Y. Ma, L. Wu, X. Gu, J. He, and Z. Yang, "A secure face-verification scheme based on homomorphic encryption and deep neural networks," *IEEE Access*, vol. 5, pp. 16532–16538, 2017.

[17] M. P. Piromalis and G. Tsaramirsis, "A study of keeping low cost in sensors and μcontroller implementations for daily activities," in *2016 3rd International Conference on Computing for Sustainable Global Development (INDIACom)*, pp. 1403–1407, New Delhi, 2016.

[18] J. S. Park, C. M. Lee, S. Koo, and C. H. Kim, "Gait phase detection using force sensing resistors," *IEEE Sensors Journal*, vol. 20, no. 12, pp. 6516–6523, 2020.

[19] B. J. Gow, J. M. Hausdorff, B. Manor et al., "Can tai chi training impact fractal stride time dynamics, an index of gait health, in older adults? Cross-sectional and randomized trial studies," *PLOS ONE*, vol. 12, no. 10, article e0186212, p. 17, 2017.

[20] A. H. Sodhro, L. Zongwei, S. Pirbhulal, A. K. Sangaiah, S. Lohano, and G. H. Sodhro, "Power-management strategies for medical information transmission in wireless body sensor networks," *IEEE Consumer Electronics Magazine*, vol. 9, no. 2, pp. 47–51, 2020.

[21] B. Roche, A.-L. Simon, S. Guilmin-Crépon et al., "Test-retest reliability of an instrumented electronic walkway system (GAITRite) for the measurement of spatio-temporal gait parameters in young patients with Friedreich's ataxia," *Gait and Posture*, vol. 66, pp. 45–50, 2018.

[22] S. Rogan, R. de Bie, and E. Douwe de Bruin, "Sensor-based foot-mounted wearable system and pressure sensitive gait analysis," *Zeitschrift für Gerontologie und Geriatrie*, vol. 50, no. 6, pp. 488–497, 2017.

[23] S. Pirbhulal, W. Wu, G. Li, and A. K. Sangaiah, "Medical information security for wearable body sensor networks in smart healthcare," *IEEE Consumer Electronics Magazine*, vol. 8, no. 5, pp. 37–41, 2019.

[24] J. Frank, "The production of visualization software to facilitate analysis of ground reaction force and vector data as applied to the study of human biomechanics," Department of Computer Science, The Cooper Union for the Advancement of Science and Art, New York City, New York, USA, 1999, Master Dissertation.

[25] F. Lin, A. Wang, Y. Zhuang, M. R. Tomita, and W. Xu, "Smart insole: a wearable sensor device for unobtrusive gait monitoring in daily life," *IEEE Transactions on Industrial Informatics*, vol. 12, no. 6, pp. 2281–2291, 2016.

[26] M. I. M. Refai, B.-J. F. van Beijnum, J. H. Buurke, and P. H. Veltink, "Portable gait lab: estimating 3D GRF using a pelvis IMU in a foot IMU defined frame," *IEEE Transactions on Neural Systems and Rehabilitation Engineering*, vol. 28, no. 6, pp. 1308–1316, 2020.

[27] C.-C. Wu, Y.-T. Wen, and Y.-J. Lee, "IMU sensors beneath walking surface for ground reaction force prediction in gait," *IEEE Sensors Journal*, vol. 20, p. 1, 2020.

[28] J. A. Antonino-Daviu, S. B. Lee, and E. G. Strangas, "Guest editorial special section on advanced signal and image processing techniques for electric machines and drives fault diagnosis and prognosis," *IEEE Transactions on Industrial Informatics*, vol. 13, no. 3, pp. 1257–1260, 2017.

[29] B. Lu, J.-C. Chen, C. D. Castillo, and R. Chellappa, "An experimental evaluation of covariates effects on unconstrained face verification," *IEEE Transactions on Biometrics, Behavior, and Identity Science*, vol. 1, no. 1, pp. 42–55, 2019.

[30] "Facial recognition system," https://http://en.m.wikipedia.org/wiki/Facial_recognition_system.

[31] D. S. S. Mahesh, T. M. Reddy, A. S. Yaswanth, C. Joshitha, and S. S. Reddy, "Facial detection and recognition system on Raspberry Pi with enhanced security," in *2020 International Conference on Emerging Trends in Information Technology and Engineering (ic-ETITE)*, pp. 1–5, Vellore, India, India, February 2020.

[32] D. B. M. Yin, A. A. Mukhlas, R. Z. W. Chik, A. T. Othman, and S. Omar, "A proposed approach for biometric-based authentication using of face and facial expression recognition," in *IEEE 3rd International Conference on Communication and Information Systems*, pp. 28–33, Singapore, Singapore, 2018.

[33] J. Dhamija, T. Choudhury, P. Kumar, and Y. S. Rathore, "An advancement towards efficient face recognition using live video feed," in *2017 International Conference on Computational Intelligence and Networks*, pp. 53–56, Odisha, India, October 2017.

[34] J. H. Liqiao and Q. I. Runhe, "Face recognition based on adaptive weighted HOG," *Computer Engineering and Applications*, vol. 53, no. 3, pp. 164–168, 2017.

[35] S. Haji and A. Varol, "Real time face recognition system," in *4th International Symposium on Digital Forensics and Security*, pp. 107–111, Little Rock, AR, USA, 2016.

[36] Z. Li, L. Li, K. Yan, and C. Zhang, "Automatic image annotation using fuzzy association rules and decision tree," *Multimedia Systems*, vol. 23, no. 6, pp. 679–690, 2017.

[37] S.-C. Cheng and Y.-P. Cheng, "An adaptive approach to quantify plant features by using association rule-based similarity," *IEEE Access*, vol. 7, pp. 32197–32205, 2019.

[38] Y. Zhang, J. Qin, P. Shi, and Y. Kang, "High-order intuitionistic fuzzy cognitive map based on evidential reasoning theory," *IEEE Transactions on Fuzzy Systems*, vol. 27, no. 1, pp. 16–30, 2019.

[39] S. Rathore, P. K. Sharma, A. K. Sangaiah, and J. J. Park, "A hesitant fuzzy based security approach for fog and mobile-edge computing," *IEEE Access*, vol. 6, pp. 688–701, 2018.

[40] T. P. Trottier, *Design and evaluation of a force platform-type instrument to measure rate change in mass and centroid of an ablating body*, University of New Hampshire, Durham, USA, 2016, Master Dissertation, Department of Design,.

[41] *FD-11637 specifications*http://ni.com, http://www.ni.com/pdf/manuals/377309a.pdf.

[42] R. Kulandaivel, M. Balasubramaniam, F. Al-Turjman, L. Mostarda, M. Ramachandran, and R. Patan, "Intelligent data delivery approach for smart cities using road side units," *IEEE Access*, vol. 7, pp. 139462–139474, 2019.

[43] F. Engmann, F. A. Katsriku, J.-D. Abdulai, K. S. Adu-Manu, and F. K. Banaseka, "Prolonging the lifetime of wireless sensor networks: a review of current techniques," *Wireless Communications and Mobile Computing*, vol. 2018, 23 pages, 2018.

[44] S. Thakre, A. K. Gupta, and S. Sharma, "Secure reliable multimodel biometric fingerprint and face recognition," in *2017 International Conference on Computer Communication and Informatics*, pp. 1–4, Coimbatore, India, January 2017.

[45] R. D. Labati, A. Genovese, E. Munoz, V. Piuri, and F. Scotti, "3-D granulometry using image processing," *IEEE Transactions on Industrial Informatics*, vol. 15, no. 3, pp. 1251–1264, 2019.

[46] Z. Peng, C. Cao, Q. Liu, and W. Pan, "Human walking pattern recognition based on KPCA and SVM with ground reflex pressure signal," vol. 2013, pp. 1–12, 2013.

[47] Y. Li, X. Chen, Y. Lin, G. Srivastava, and S. Liu, "Wireless transmitter identification based on device imperfections," *IEEE Access*, vol. 8, pp. 59305–59314, 2020.

[48] Y. Fu, Y. Liu, and Z. Gao, "Multiple actuator fault classification in wind turbine systems using multi-linear principal component analysis techniques," in *2019 25th International Conference on Automation and Computing (ICAC)*, pp. 1–6, Lancaster, United Kingdom, 2019.

[49] X. M. Zhao and C. B. Wei, "A real-time face recognition system based on the improved LBPH algorithm," in *2017 IEEE 2nd International Conference on Signal and Image Processing*, pp. 72–76, Singapore, Singapore, August 2017.

[50] C.-L. Liu, W.-H. Hsaio, C.-H. Lee, T.-H. Chang, and T.-H. Kuo, "Semi-supervised text classification with universum learning," *IEEE Transactions on Cybernetics*, vol. 46, no. 2, pp. 462–473, 2016.

Hindawi
Wireless Communications and Mobile Computing
Volume 2020, Article ID 8899268, 8 pages
https://doi.org/10.1155/2020/8899268

Research Article

Research on Profit Maximization of New Retail E-Commerce Based on Blockchain Technology

Xuan Hu

Yiwu Industrial & Commercial College, Yiwu 322000, China

Correspondence should be addressed to Xuan Hu; huxuan@ywicc.edu.cn

Received 26 September 2020; Revised 21 October 2020; Accepted 28 October 2020; Published 16 November 2020

Academic Editor: Hongju Cheng

Copyright © 2020 Xuan Hu. This is an open access article distributed under the Creative Commons Attribution License, which permits unrestricted use, distribution, and reproduction in any medium, provided the original work is properly cited.

With the development of science and technology and the extension of online users, e-commerce platforms gradually and effectively gather social resources such as manpower, technology, production, and capital. More and more traditional enterprises combine online and offline business as their operation and trade methods. E-commerce, as a new channel, has become one of the main transaction modes in the society. Under the background of reform of the supply side, and with the high-speed development of E-commerce, we will promote stock adjustment through incremental reform and optimize the structure of investment and financing in the process of increasing investment of e-commerce enterprises. High-quality products and diverse trading experience are the new development pattern in e-commerce. There are different profit maximization strategies for e-commerce enterprises when they face different economic situations. Besides, cross-border business is an advised way to expand business when the enterprise is under bigger profit. Via all these methods, e-commerce enterprise can help to optimize the structure of industries, circulation, and consumption and promote resource integration and optimization, and people's living standards will be further improved. Finally, the e-commerce enterprise profit maximization will come true.

1. Introduction

With the rise of the Internet, the United States announced the opening of the Internet's commercial functions in 1995. The business development model developed from traditional offline physical stores to online shopping malls, and the economic market began to expand. A number of large B2C enterprises represented by amazon, http://jd.com, Alibaba, Vipshop, and so on emerged. Some e-commerce enterprises have gradually formed their own profit model, but some have not yet formed a stable profit model [1, 2]. Although most of the domestic e-commerce enterprises are also developing rapidly, and several of them have successfully listed on the stock market, it can be seen from the financial reports and market survey reports that these enterprises have not achieved sustained profitability or low profitability. As the profit subject, the ultimate goal of the development and operation of an enterprise is to maximize its profits. Although different types of enterprises have different profit models, they all follow the most basic profit formula, that is, profit increment equals the capital acquired by the enterprise minus the capital expended [3]. Otherwise, supply-side reform takes tackling difficulties as the core connotation, that is, solving the problem of effective system supply through deepening the reform, so as to further liberate productive forces and support China's modernization process. China's current supply-side reform is not a simple aggregate adjustment, but structural reform, which focuses on gradually reducing the capacity of low-end products and improving the capacity of high-end products. Through supply-side reform, China will lead the improvement of the level of demand. And, based on this background conducted by the government, the relationship between e-commerce and supply-side reform has become the focus of the development of the e-commerce industry [4].

2. The Basic Principles of Supply-Side Reform and E-Commerce Profit

2.1. Basic Principles of Supply-Side Reform. The global economy is in the next phase of the fifth wave cycle since the industrial revolution, and this is the background of the world

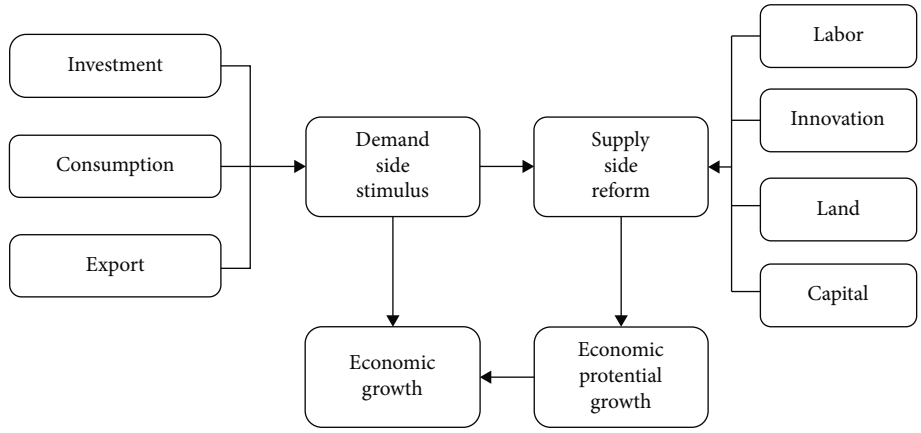

Figure 1: The diagram of supply and need in the economy.

politics and economy of China's supply-side reform. Supply-side reform provides new ideas and new models for economic development; there are four elements: labor, land, capital, and innovation, which correspond to the need. Figure 1 illustrates the connection of supply and demand [5]. China's economic growth has been slowing every year since 2007, but demand stimulus has had little effect. The shortage of demand is only the appearance, and the mismatch of supply and demand is the essence. Therefore, supply-side reform is aimed at adjusting the economic structure to achieve optimal allocation of factors and improving the quality and quantity of economic growth [6]. Supply-side reform of our country moderately expand aggregate demand, and at the same time, production capacity and inventory, deleveraging, cost reduction, and short-board improvement are proceeding from strengthening the supply of high quality, reducing the invalid supply, expanding the effective supply, improving the supply structure adaptability and flexibility, improving the total factor productivity, and making the supply system to better adapt to the demand structure changes [7]. It is worth mentioning that China's supply-side reform is different from the American supply-side school theory. China's supply-side reform focuses on the strengthening of the structural adjustment.

2.2. The Theory and Influence of Supply-Side Reform. Based on the economic growth theory and new supply of the existing research results of the respect, such as economics, we must demand the raw power. Clear supply for demand response mechanisms is the key driving force of the development of the productivity level-up type contribution. The decisive factors affecting the long-term economic growth are summarized as six elements of the supply-side. Based on the supply side, the elements are labor, land and natural resources, capital, science and technology innovation, system (including management), and data [8, 9]. The six elements form a set of functions of economic growth, and the theoretical model can be expressed b in the following formula:

$$G = F(l, r, c, t, s, d), \tag{1}$$

In which, G represents economic growth, l represents labor, r is land and natural resources, c is capital, t is scientific innovation, s represents system, and d means data and information [10]. Generally, in the early stages of economic growth, labor, land, and capital are the most obvious factors, the main elements of the economy entering the middle-income stage, science and technology innovation and system would show a great potential and important value of hedge support at the first three factors of landslide and even become the main contribution of the total factor productivity factors. And the most important is, with the development of the Internet and technology transformation, data and information are inevitable [11]. The essence of informatization is networking and data flow. To release the efficiency of informatization, we must rely on the network to make the data resource flow fully in a larger range [12, 13].

In different stages of economic development, the relative contributions of the six elements are also different. And these different elements are combined with each other [14]. The situation, to a great extent, affects and decides the economic growth situation and its comprehensive benefits from the perspective of production; the supply-side reform will lead to the rise of the proportion of tertiary industry, the decline of the proportion of traditional industries, and the rise of emerging industries in the secondary industry. And from the perspective of the income, supply-side reforms will lead to the redistribution of the economy, which means that tax cuts will be led to the decrease of the net production taxes accounted [15]. Besides, accelerated depreciation and the capacity to change will lead to the depreciation of fixed assets of higher than short-term. What is more, reducing the cost and capacity will lead to the rise of enterprises operating surplus accounted, and the accelerating labor cross-regional, cross-sectoral circulation, and improving human capital will definitely lead to the raise of worker pay. Table 1 summarizes the major import and export e-commerce enterprises in China [16].

The broad prospect of cross-border e-commerce market also means a large number of participants and fierce competition. The competitive theory of "survival of the fittest" tells us that market share will be carved up by the strong, while the

Table 1: E-commerce enterprises of the major import and export in China.

Transaction type	Operation way	Case
Import transaction	Platform only	Alibaba, NetEase Kaola
	Self-support	JDcom, Suning
	Free trade zone	Cross-border shopping
Export transaction	Platform only	Alibaba
	Self-support + platform	JDcom
	Self-support	DealExtreame

weak will be squeezed out of the market [17]. For e-commerce enterprises, the craze of "overseas online shopping" can be either a breakthrough or a bottleneck. Of course, the emergence of a cross-border market is a new opportunity for a company if it can fully mobilize its high-quality resources to occupy a piece of land in the overseas market. However, if the enterprise lacks resources and has no overseas advantages, the enterprise may face threats [18].

2.3. Basic Principles of E-Commerce and Profit Maximization

2.3.1. Definition and Status of E-Commerce in China. E-commerce usually refers to the wide range of business and trade activities around the world. In the opening network environment of the Internet, it realizes the electronic, digital, and networking in the entire business process based on server application with the help of the computer technology, network technology, and remote communication technology [19]. The rapid development of e-commerce has upended the traditional business model and becomes a new driving force for economic development [3, 4]. Since the emergence of e-commerce in 2000, e-commerce has experienced several different development stages, and it is growing at an amazing rate after 2013 [20]. According to the scientific data published, the scale of e-commerce transactions in China continued to expand and maintain rapid growth in 2017 and it reached 29.2 trillion yuan, which is up 11.7% compared to 2016. Besides, the rapid development of e-commerce in China since 2009 shows the deepening and popularization of mobile Internet, network video, social network, network shopping, and transformed from blog to Weibo and WeChat. In recent years, the number of mobile Internet users, application level, terminal popularity, and market size in China has all shown a rapid growth trend [21]. Figure 2 has shown the trend of e-commerce. E-commerce has maintained a rapid development trend, the market size has been expanding, and the online consumer group has been growing rapidly [22].

Different from the traditional concept of commercial economy, e-commerce does not only regard the Internet as a simple sales channel or technical means, but it gradually extends from up and down and closely connects consumers, platform manufacturers, and production enterprises. Thus, an ecological chain has formed, which is an internet-based whole industrial chain ecosystem. Figure 3 shows the internal connections among the general e-commerce business [23].

2.3.2. The Profit Patterns of E-Commerce. The profit model refers to a mechanism formed to guarantee that an enterprise can continuously earn excess profits and update them in a timely manner after identifying the operation elements and effectively integrating enterprise resources. The profit model of the enterprise is generated around the enterprise value creation, which is reflected in the increase of the present value of the free cash flow of the enterprise. The conceptual "value" form is materialized through the use of financial indicators and financial tools, while the free cash flow of the enterprise is related to the net cash flow of operation and the operating results. There are four key points and a center of a basic profit pattern [24]. With the enterprise value creation serving as the core, four strategic elements: profit point, profit source, profit leverage, and profit barrier are formed. This model covers the design level and implementation level, which are the most basic enterprise profit model framework. With the development and reformation of e-commerce, the enterprise profit has six patterns as displayed in Table 2, with representative companies and introduction. Actually, it is quite difficult to divide e-commerce enterprises into which profit pattern nowadays, this is because more enterprises have already abandoned the unitary profit pattern. More confluent pattern is popular which can crate bigger enterprise value [25].

2.3.3. The Theory of Profit Maximization. Profit maximization is the behavioral goal of an enterprise in early western capitalism with the respect of pure economics. Recent economics adds an ethical dimension. In the long term, only those enterprises with business reputation and social responsibility can maximize their profits. In general, in economics, the assumed behavior of enterprise profit maximization is achieved when marginal cost equals marginal revenue that is MC = MR. It is supposed that π is profit, Q is manufacturer's output, TR is the total revenue of the manufacturer, and TC is the total cost, then

$$\pi(Q) = \mathrm{TR}(Q) - \mathrm{TC}(Q). \tag{2}$$

The necessary condition for profit maximization is that the first derivative of π with respect to Q is zero, while the first derivative of TR with respect to Q is marginal revenue MR, similarly, is marginal cost MC. Therefore, when MR = MC, that is, the marginal revenue equals the marginal cost; the profit is max.

$$\begin{aligned} \frac{d\pi(Q)}{dQ} &= \frac{d\mathrm{TR}(Q)}{dQ} - \frac{d\mathrm{TC}Q}{dQ} = 0, \\ \frac{d\mathrm{TR}(Q)}{dQ} &= \frac{d\mathrm{TC}(Q)}{dQ}. \end{aligned} \tag{3}$$

The sufficient condition for profit maximization also requires that the second derivative of π is negative, which

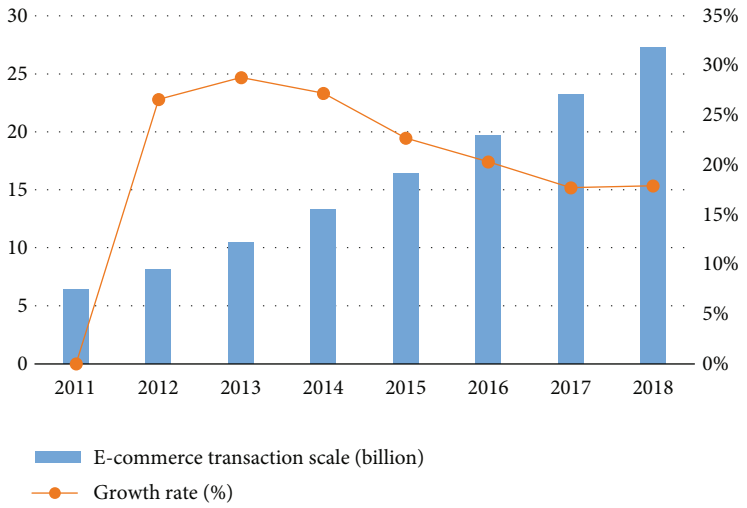

Figure 2: The trend of e-commerce transaction scale of China from 2011 to 2018.

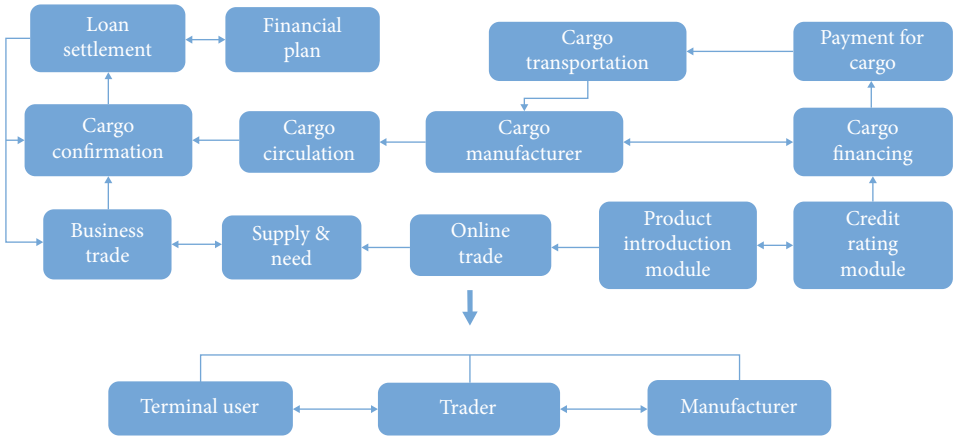

Figure 3: The internal connections for a general e-commerce business.

Table 2: The summary of six profit pattern of e-commerce.

Pattern	Representative company	Introduction
Product website	Dell	Introduce the products
Shopping	Amazon, Taobao	Introduction service and sales service are available for our products
Portal and Shopping	AOL	Shopping platform combined online and offline
Resale	Onsale, Xianyu	Bidding
Online auction	Ebaye	Price negotiations between suppliers and demanders
Bedrock Price	http://Buy.com	No intermediate links

means that profit maximization requires the slope of the marginal cost function to be greater than the slope of the marginal benefit function.

$$\frac{d^2\mathrm{TR}(Q)}{dQ^2} - \frac{d^2\mathrm{TCQ}}{dQ^2} < 0. \tag{4}$$

That is

$$\frac{d^2\mathrm{TR}(Q)}{dQ^2} < \frac{d^2\mathrm{TC}(Q)}{dQ^2}. \tag{5}$$

When MR = MC, we can achieve profit maximization, as displayed in Figure 4.

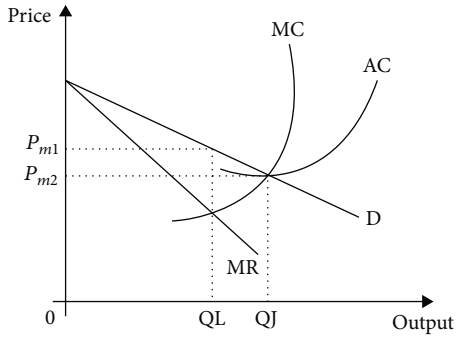

Figure 4: The price in profit maximization.

In this figure, P_{m1} is the profit maximization price. By adjusting the output to the level of MR and MC by controlling the output (QL), the enterprise determines the price P to obtain the maximum profit.

3. The Optimization Strategy of Profit Maximization for E-Commerce

3.1. Analysis of Optimization Strategy for E-Commerce. Supply-side reform is inseparable from innovation. So, the quality of the e-commerce industry, as a bridge connecting supply and consumption, will have a significant impact on the success or failure of supply-side reform. In order to implement the outline of the national informatization strategy and promote the innovation of e-commerce development pattern, we have to pay attention to the following problems.

First, the awareness of facilitating supply-side structural reform through e-commerce model innovation must be enhanced. At present, it has reached a critical period to innovate the development mode of e-commerce and improve the quality of e-commerce. Some scientific data showed that Chinese consumers are upgrading their consumption preference from mass to high-end products, with 50 percent of consumers claiming to pursue high-quality and expensive products, a significant increase from previous years. Therefore, this kind of demand not only presents obvious upgrading characteristics of the structure of the urban high-income class but also presents obvious characteristics of gradient catch-up with the sustained and rapid growth of rural residents' income, gradual diffusion of urban consumption demonstration effect, and rapid update of consumption concepts and consumption patterns. However, the current e-commerce and platforms have the problem of the mismatch between the supply and demand of products and the inability to adapt to new demands.

Second, the important role of e-commerce model innovation and development in the supply-side reform has to be clarified. As the middle-end of the ecological chain of the Internet industry, the influence of e-commerce mode and its service quality on the upstream and downstream is increasingly prominent, which will play an important role in the supply-side reform. Among them, the e-commerce platform becomes the intermediate link connecting the upstream and downstream. Therefore, the quality of e-commerce not only determines whether the demand of terminal consumers can be truly met but also has a significant impact on the upstream industrial chain.

Third, an innovative e-commerce mode achieving precise matching between supply and demand is needed. With personalized and diversified consumption becoming mainstream, the younger generation of shoppers who are more familiar with e-commerce has different tastes and consumption habits. The current online shopping consumers are becoming younger and younger, and the consumers are more in pursuit of individuality and are more willing to accept new things and stronger purchasing power. Therefore, how to deliver consumer demand to the upstream and downstream of the industrial chain faster and better through the e-commerce platform and how to promote the accelerated development of industries related to consumer experience and personalized design have become a major topic to facilitate the supply-side reform.

The last but not the least, e-commerce mode innovation will become an important field in which the cross-border integration and application of the Internet will be advanced in a profound way.

At present, the innovative development of e-commerce is expected to further become a pioneer in promoting reform in all fields. E-commerce model innovation and cross-border integration are not only the need for the implementation of the national "Internet +" strategy but also the need for comprehensively deepening reform. In this way, we can establish and improve the government and social capital cooperation mechanism, inject new vitality into the construction of informatization in the public service sector, and change the innovative service mode of informatization in the public service sector.

3.2. The Theoretical Framework of Profit Maximization Optimization. Generally speaking, in different market structures, the slope of the marginal cost function is positive, while the slope of marginal benefit function is zero in perfect competition market and negative in imperfect competition market.

Suppose there are n enterprises and the demand amount for m business is x_{nm}, thus the profit function can be expressed as

$$\pi_n(x_{nm}) = \mathrm{TR}_n(x_{nm}) - \mathrm{TC}_n(x_{nm}). \tag{6}$$

In which, π_n is the total profit, TC_n is the total cost, TR_n is the total income (transaction amount), and

$$\mathrm{TR}_n = P_n \times Y_n. \tag{7}$$

In which, P_n is the trading price for the n e-commerce enterprise, and Y_n is the transaction amount for the n e-commerce enterprise. Then, we can get the transaction function as follows:

$$Y_n = F_n(x_{nm}). \tag{8}$$

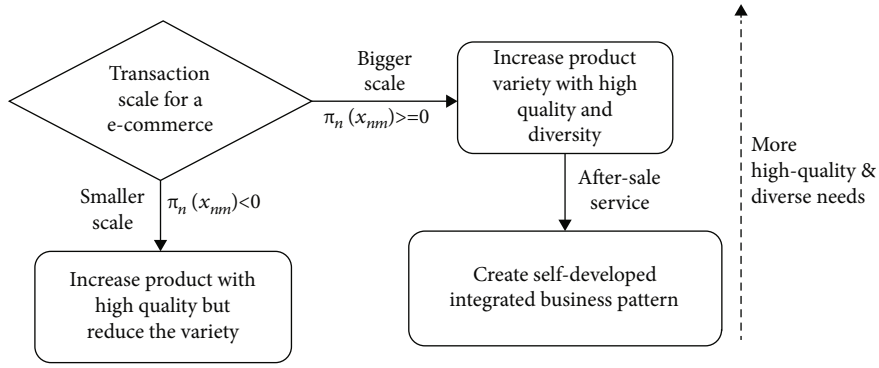

Figure 5: The diagram of profit maximization optimization framework.

Then, the total cost can be transformed as

$$\mathrm{TC}_n = \mathrm{TC}_{nm} + \mathrm{TF}_n = W_{nm}x_{nm} + \bar{W}_n\bar{x}_n. \quad (9)$$

In which, $\bar{W}_{nm}$ is the price of the m business for the n e-commerce enterprise, and $\bar{x}_{nm}$ is the total input in addition to the m business, which is constant.

Then, we can get the specific profit function for e-commerce enterprise:

$$\pi_n(x_{nm}) = P_n \times Y_n(x_{nm}) - W_{nm}x_{nm} - \bar{W}_n\bar{x}_n. \quad (10)$$

Take the derivative of both sides of formula (10):

$$\frac{d\pi(x_{nm})}{d(x_{nm})} = P \times \frac{dY(x_{nm})}{d(x_{nm})} - W_{nm}. \quad (11)$$

And if we want to achieve profit maximization, equation (11) must equal to zero, that is expressed as follows:

$$P \times \mathrm{MP}_{nm}(x_{nm}, \bar{x}_n) = W_{nm}. \quad (12)$$

In a word, if e-commerce enterprises want to achieve profit maximization, the price of one of their business demand amount should be equaled to the value of the marginal products. Based on the above analysis of profit maximization and the content of supply-side reform, we crate the theoretical framework of profit maximization optimization for current e-commerce. Figure 5 elaborates the procedures in detail.

4. Specific Implementation Method for E-Commerce Max Profit

With the rapid development of e-commerce, it has become the consensus of the industry to integrate e-commerce online business with the whole traditional trade chain in the future. Based on the above transaction logic and profit maximization analysis, the e-commerce platform can be conducted in accordance with modularization to ensure the chain connection and operation. In the entire business process, once the offline business migrates to online business, the first thing to be guaranteed is the uniqueness of cargo rights and the reliability of product quality. Therefore, the whole-process online support of technology is required to correspond to the layout of the offline warehouse center. Second, the accumulation of capital flow and transaction information flow and big data analysis will make the financing service of supply chain finance significantly reduce credit risk, and the buyers and sellers can arrange more orderly in the production and procurement plan and improve the turnover efficiency of the overall production and marketing system, so as to obtain maximum benefits. In addition, consumption upgrade is really a home for young people. Not only do they have relatively higher brand awareness, easier finances, and, more importantly, greater curiosity and the ability to use international channels more freely. And the latter becomes the core industry driving force. Therefore, under the premise of sufficient funds, cross-border e-commerce business can be expanded to integrate with world business and guarantee the transaction of high-quality goods. In this way, more young people will be attracted, and quality consumption space will be released to meet the increasing consumption upgrade.

Therefore, based on the module mode e-commerce business, we create a new method which adds various channels to seek high-quality products to attract buyers, and at the same time, seeking operation with more sellers for lower cost and fluent circulation of the trading chain. Thus, we can adjust cargo needs more flexibly to achieve profit maximization. Figure 6 shows us the diagram of the new strategy.

First of all, e-commerce enterprises must expand their consumer group, like young people, who are a consumer group with huge purchasing power, and multiarea, like rural areas and foreign countries. The rural e-business will leave the era of barbaric growth and gradually move to a new stage of transformation and development. As the "One Belt And One Road" initiative continues to advance, "One Belt And One Road" related industries continue to emerge. "One Belt And One Road" is not only an overland and maritime silk road but also an online silk road in the new era. Therefore, these will bring a chance for Chinese e-commerce enterprise, but also the risks. Then, more high-quality manufacture should be in cooperation. After the tariff reduction since December in 2017, the possibility of "the same price" for both domestic and overseas imported goods will be greatly increased. More overseas goods will enter the Chinese market through general trade, of course, the e-commerce trade is included, and the more open market environment will

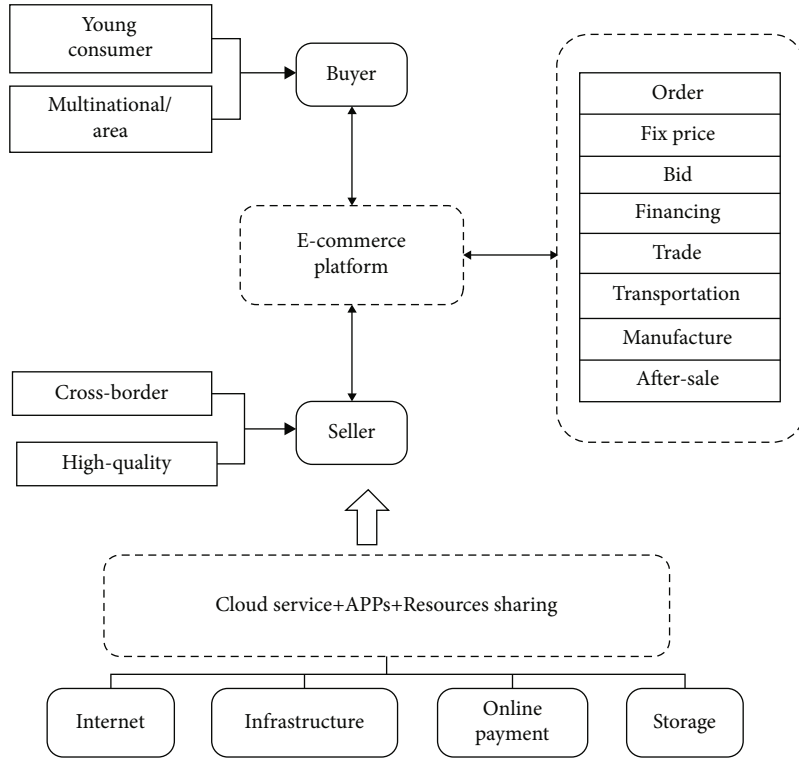

Figure 6: The module mode of e-commerce profit maximization.

stimulate the upgrading of domestic brands. This will bring driving forces for Chinese enterprises to produce higher quality products, which will give more choice for e-commerce enterprises to seek low-price and good products.

The opening of online and offline channels means that all the customer's consumption behavior, the circulation of goods trajectory, and the change of inventory data will be in real-time unified channel flow at the same time. After that, the above data will be collected and analyzed. Thus, it is helpful to guide the enterprise marketing to be more precise, their management will be more careful, and the entire supply chain optimization will be achieved. Eventually making production can shift from B2C to no inventory C2B, which will realize the reform of the supply side.

5. Conclusion

The government has further established the strategic, fundamental, and leading position of informatization, which means that China's economic development needs informatization more urgently and becomes the core driving force for transforming the mode of production in various sectors of the economy. For China's economy in the new normal, an important and significant move is to promote in-depth integration of informatization and industrialization and to facilitate supply-side structural reform through innovation of the e-commerce development model. Therefore, solid efforts will be made to promote the innovation of e-commerce development mode and the development of new e-commerce and high-quality e-commerce, which will contribute to profit maximization. We will promote stock adjustment through incremental reform, optimize the structure of investment and financing in the process of increasing investment, optimize the structure of industries, circulation, and consumption, promote resource integration and optimization and regeneration, promote sustainable economic development, and improve people's living standards, and finally, the e-commerce enterprise profit maximization will come true.

Data Availability

All author information is available from the author.

Conflicts of Interest

The author declares that he has no conflicts of interest.

Acknowledgments

This work is support by the Preresearch Project of Yiwu Industrial & Commercial College in 2019 (No. YY-GJ-201904).

References

[1] Y. Kim and R. A. Peterson, "A meta-analysis of online trust relationships in e-commerce," *Journal of Interactive Marketing*, vol. 38, pp. 44–54, 2017.

[2] K. Slagter, C. H. Hsu, Y. C. Chung, and J. H. Park, "Network-aware multiway join for MapReduce," in *Grid and Pervasive Computing*, Springer Berlin Heidelberg, Heidelberg, Germany, 2013.

[3] E. Turban, D. King, J. Lee, and D. Viehland, *Electronic commerce: a managerial perspective 2002*, Prentice Hall, 2002.

[4] Y. Fang, I. Qureshi, H. Sun, P. McCole, E. Ramsey, and K. H. Lim, "Trust, satisfaction, and online repurchase intention: the moderating role of perceived effectiveness of e-commerce institutional mechanisms," *MIS Quarterly*, vol. 38, no. 2, pp. 34–36, 2014.

[5] M. Elseidy, A. Elguindy, A. Vitorovic, and C. Koch, "Scalable and adaptive online joins," *Proceedings of the Vldb Endowment*, vol. 7, no. 6, pp. 441–452, 2014.

[6] N. Oulton, "Supply side reform and UK economic growth: what happened to the miracle?," *National Institute Economic Review*, vol. 154, no. 1, pp. 53–70, 1995.

[7] J. Kang and F. Qiaobin, "China's supply-side reform: background, theoretical models and implementation paths," *International Journal of Economics, Finance and Management Sciences*, vol. 6, no. 3, p. 87, 2018.

[8] R. E. Lucas Jr., "Supply-side economics: an analytical review," *Oxford Economic Papers*, vol. 42, no. 2, pp. 293–316, 1990.

[9] G. Gong, "The supply-side reform under the new normal of Chinese economy," *Nankai Journal*, vol. 2, no. 2, p. 2, 2016.

[10] D. T. Nguyen and L. B. Le, "Risk-constrained profit maximization for microgrid aggregators with demand response," *IEEE Transactions on Smart Grid*, vol. 6, no. 1, pp. 135–146, 2015.

[11] J. Mei, K. Li, A. Ouyang, and K. Li, "A profit maximization scheme with guaranteed quality of service in cloud computing," *IEEE Transactions on Computers*, vol. 64, no. 11, pp. 3064–3078, 2015.

[12] Z. Yang, Y. Shi, and H. Yan, "Analysis on pure e-commerce congestion effect, productivity effect and profitability in China," *Socio-Economic Planning Sciences*, vol. 57, no. 1, pp. 35–49, 2017.

[13] Z. Liu, J. Shang, and M. Lai, "Incentive mechanism for knowledge sharing in e-commerce service supply chain: complementarity, integration and risk attitude," *Journal of Electronic Commerce Research*, vol. 16, no. 3, p. 175, 2015.

[14] V. K. Verma and K. Saxena, "Efficient approach for mining consistent profit based pattern over large dynamic data stream," *International Journal of Applied Engineering Research*, vol. 12, no. 12, pp. 3483–3486, 2017.

[15] Y. M. Baek, "Current status of e-commerce market in China and implication," *Journal of Digital Convergence*, vol. 13, no. 1, pp. 111–124, 2015.

[16] C. M. L. Leong, S. L. Pan, S. Newell, and L. Cui, "The emergence of self-organizing e-commerce ecosystems in remote villages of China: a tale of digital empowerment for rural development," *MIS Quarterly*, vol. 40, no. 2, pp. 475–484, 2016.

[17] S. S. Li and E. Karahanna, "Online recommendation systems in a B2C e-commerce context: a review and future directions," *Journal of the Association for Information Systems*, vol. 16, no. 2, pp. 72–107, 2015.

[18] F. Piller and D. Walcher, *Leading Mass Customization and Personalization: How to Profit from Service and Product Customization in e-Commerce and beyond*, Amazon Kindle eBook, 2017.

[19] E. Turban, J. Outland, D. King et al., *Electronic Commerce 2018: A Managerial and Social Networks Perspective*, Springer, 2017.

[20] Y. Liu, M. Ma, X. Liu, N. Xiong, A. Liu, and Y. Zhu, "Design and analysis of probing route to defense sink-hole attacks for Internet of Things security," *IEEE Transactions on Network Science and Engineering*, vol. 7, no. 1, pp. 356–372, 2020.

[21] F. Long, N. Xiong, A. V. Vasilakos, L. T. Yang, and F. Sun, "A sustainable heuristic QoS routing algorithm for pervasive multi-layered satellite wireless networks," *Wireless Networks*, vol. 16, no. 6, pp. 1657–1673, 2010.

[22] Y. Zhou, D. Zhang, and N. Xiong, "Post-cloud computing paradigms: a survey and comparison," *Tsinghua Science and Technology*, vol. 22, no. 6, pp. 714–732, 2017.

[23] W. Pan and C. Chai, "Measuring software stability based on complex networks in software," *Cluster Computing*, vol. 22, no. S2, pp. 2589–S2598, 2019.

[24] W. Pan and C. Chai, "Structure-aware Mashup service clustering for cloud-based Internet of Things using genetic algorithm based clustering algorithm," *Future Generation Computer Systems*, vol. 87, pp. 267–277, 2018.

[25] G. Yang, Q. Yang, and H. Jin, "A novel trust recommendation model for mobile social network based on user motivation," *Electronic Commerce Research*, vol. 12, pp. 120–128, 2019.

Hindawi
Wireless Communications and Mobile Computing
Volume 2020, Article ID 8825825, 8 pages
https://doi.org/10.1155/2020/8825825

Research Article

Structure Optimization of e-Commerce Platform Based on Artificial Intelligence and Blockchain Technology

Shengqi Li

College of Economics and Management, Zhejiang A&F University, Hangzhou 311300, China

Correspondence should be addressed to Shengqi Li; 20080057@zafu.edu.cn

Received 15 July 2020; Revised 17 September 2020; Accepted 7 October 2020; Published 2 November 2020

Academic Editor: Hongju Cheng

Copyright © 2020 Shengqi Li. This is an open access article distributed under the Creative Commons Attribution License, which permits unrestricted use, distribution, and reproduction in any medium, provided the original work is properly cited.

The current e-commerce operation model has network defects such as network chaos and uneven network distribution, which affect economic development and progress. In response to the above problems, this article introduces the artificial intelligence system, optimizes and analyzes the structure of e-commerce websites, and combines the Internet economy with online website theory through independent screening and analysis of the artificial intelligence system. The concept of blockchain technology is introduced, and the characteristics of blockchain are analyzed through theory and data using quantitative analysis methods, and the problem of cross-border electronic payment is solved based on blockchain. Based on the analysis of artificial intelligence, an optimized online website innovation plan was obtained. Finally, the online website resource allocation variables are simulated, and the simulation method is used to test the scheme. The simulation test simulates the process of resource allocation, optimizes the use of innovative models, and hires professional financial personnel to observe records. The test verifies the effectiveness of the structure optimization of the e-commerce platform realized in this paper.

1. Introduction

In the past century, using Internet economic theory to analyze e-commerce websites is an important channel analysis approach [1]. On the basis of the Internet economy, the analysis of various programs can extend the benefit of the selected scheme to the best state [2]. However, the theory is fixed, and it cannot be in the special circumstances of human judgment, make decisions sometimes with the reality of deviation, and need to be supplemented by the artificial intelligence system [3]. Through the auxiliary judgment of the artificial intelligence system, strengthening the integration of the optimization scheme of e-commerce structure can make greater progress on the original foundation [4]. The rational operation is one of the common concepts of the internet economy and artificial intelligence system, which integrates probability, efficiency, and inference to consolidate the rigor of decision in the process of artificial intelligence [5]. Nowadays, in the labor market, the implementation of online Web site is not as satisfactory, and the reason is that people cannot be doped to the decision-making stage and cannot achieve the "human-oriented" approach to development. In order to make up for the defects of this aspect, the system model of the artificial intelligence system and electronic commerce is born, and both of them reach the innovative optimization plan, which has a very reliable practical basis [6].

The research contributions made in this paper mainly include the following aspects:

(1) The paper proposes an e-commerce website structure of an artificial intelligence system

(2) It is proposed to combine the Internet economy with online website theory through independent screening and analysis of the artificial intelligence system

(3) The method of quantitative analysis is used to analyze the characteristics of the blockchain through theory and data, and the problem of cross-border electronic payment is solved based on the blockchain

The rest of this paper is organized as follows. Section 2 discusses related work, followed by the method which is

discussed in Section 3. Result analysis and discussion is discussed in Section 4. Section 5 concludes the paper with summary and future research directions.

2. Related Work

Blockchain technology has laid a new foundation and direction for supply chain governance. An efficient and reliable global information transmission system will inevitably require a matching efficient and reliable value transmission system, which is the foundation of the prosperity of the blockchain. Blockchain uses cryptography to realize mutual distrust of distributed systems to reach consensus based on agreements without manual intervention. As one of the major technological breakthroughs in the last ten years, the blockchain is essentially a distributed consensus mechanism that realizes the value consensus between devices without manual intervention. This is the blockchain 1.0 technology represented by the Bitcoin network. Later, the Turing virtual machine was further implemented on this basis, and the blockchain 2.0 technology that supports smart contracts represented by Ethereum appeared. Currently, the blockchain technology 3.0 that supports large-scale enterprise-level applications is also under development.

The e-commerce website structure determines the development direction of the internet economy to a certain extent and needs to construct a set of feasible structure optimization driving strategy for it [7]. Offline Web site theory to express the position lies in the social hard demand, cannot stand in the public perspective of decision-making, and need to fully expose the participants to demand and supply and demand information, on the basis of online Web site allocation which cannot get the real demands of participants [8]. The goal of optimizing the structure is to have a "people-oriented" policy, reasonable according to the demands of participants to collect, and achievement of a sustainable development of a strategic approach.

Optimizing Innovation Mexico's Basic Law adopts the policy of "people-oriented", and the reliability of the analysis process can be ensured by using the optimization innovation model. At the same time, this paper also takes the optimization of the innovation system for business structure detection, for the test process encountered in the scope of the improvement of the general forecast, in the analysis of problems before the issue of the overall control [9]. In order to achieve complete accuracy, it is necessary to design and deal with the hidden layer, analyze and divide it by computer technology, and then input the required content data into it to ensure the smooth operation of the whole optimization innovation system [10].

3. Method

3.1. Optimize the Innovation Model to Build. In the beginning of the optimization innovation model, it will be advantageous for the next step to carry out the theory analysis procedure for the integration of a series of lifting space in the field of online Web resource allocation [11]. Through the current online site, a series of operational problems, distribution conflicts, and other information input into the computer system, and the use of systematic screening compressed into the data packet into the artificial intelligence, screening, and lifting operations [12]. In which the integrated retrieval link to carry out the implementation of online Web site allocation strategy, the intelligent model is computed using the computer algorithm, the information data is input into the theory analysis system according to the indication standard of each algorithm, and the model receives the data to digest processing and finally completes the construction of the whole collection model [13].

In this process, using the auxiliary function of the computer system, first through the operation of artificial intelligence, get the theory analysis scheme; use the computer-specific code to classify the theory analysis scheme data, in order to provide the precondition for the next work development [14, 15]. Then, based on the theoretical analysis of the scheme coding, online Web site resource allocation optimization strategy, we will be as p theoretical analysis of the branch of the project coefficient, α for e-commerce Web site innovation optimization coefficient, bme represents the feasibility of innovative solutions, and δ as an optimization coefficient, through the following equation of the computations. The integration coefficient of the data of the e-commerce optimization scheme is obtained [16, 17]:

$$\begin{aligned} p(i) &= \frac{bme(b)}{\delta^2}\sqrt{\alpha_1 b} \\ p(o) &= \frac{\alpha_1 - bme(b)}{\delta^{0.5}}\sqrt{bme(b)\alpha_1}. \end{aligned} \tag{1}$$

In this formula, taking into account the reliability of the classification integration coefficient, we will continue to optimize the innovation model of the various aspects of error retrieval, to ensure the accuracy of resource allocation model, in this process using the set algorithm to organize, the independent number into the algorithm, the use of computer systems automatically integrated, and output results. The accuracy is represented by 1 and 0, respectively, of which 1 is accurate, and 0 is the error [18]. In the operation process, we use ψ to represent the number of the checked algorithm in the system. With these algorithms entered into the overall frame structure, the computer system automatically numbered every computation process [19]. In addition, M and I on behalf of its theoretical analysis of the performance of the node and the feasibility of the coefficient, y represents the e-commerce optimization coefficient and inserts the above model that is to ensure the optimization of the operating efficiency of the innovation model, but also to the formula to run the process of protection, which the inspection process as shown [20, 21]:

$$M_y 1 = \frac{I_1 y_1}{(I_1/y_1) + (I_2/y_2)} \times M_y. \tag{2}$$

After guaranteeing the accuracy, finally, to determine the final solution, using the optimal screening algorithm, where the next F is the optimal node coefficient, b represents the

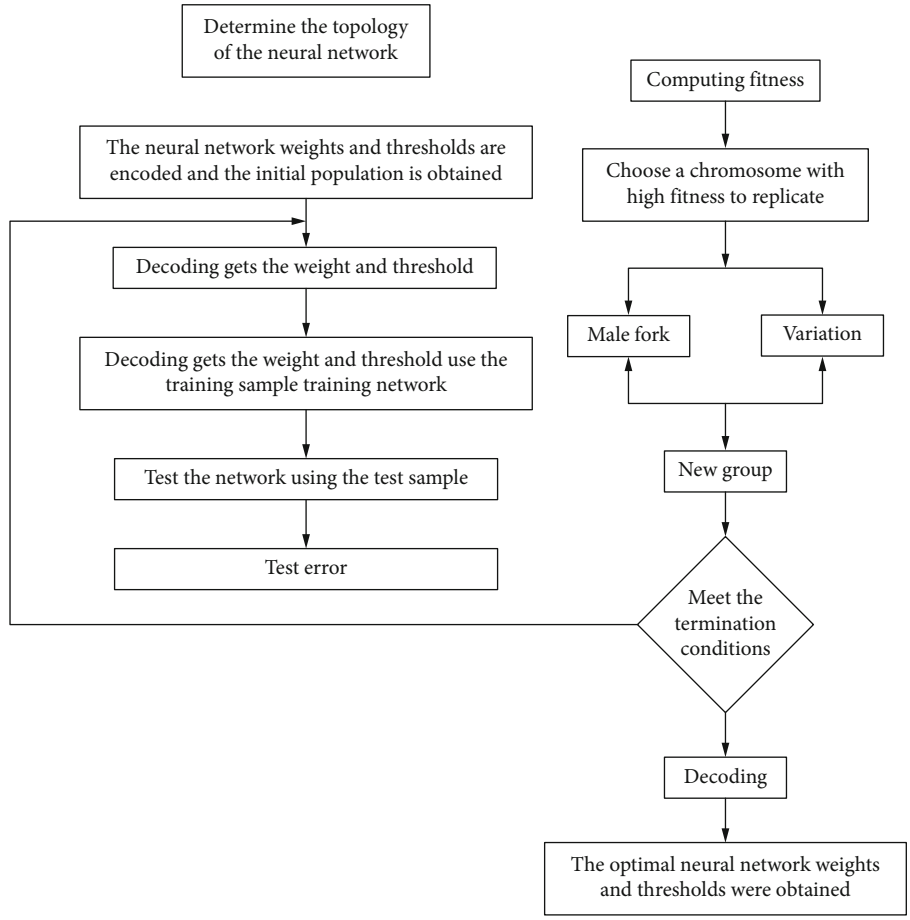

Figure 1: Innovation model and algorithm of e-commerce website structure optimization.

Table 1: Algorithm of e-commerce website structure optimization.

Information integration phase		Optimal innovation model		
Accuracy rate	Resonant adjustment	Efficiency	Overall effect	Remarks
1	0.93	0.94	0.94	92.2%
2	0.87	0.97	0.96	96.2%
3	0.98	0.89	0.98	93.1%
4	0.91	0.83	0.90	96.6%

deviation coefficient, and s represents the section of the theoretical analysis scheme of the link variable range, through the control of the optimal value coefficient to build the optimal information acquisition mechanism [22]. Considering that the maximum stress amplitude of amplitude fatigue can be used as the best form, the optimal point position control is adopted in this form, and then the theoretical analysis system is further perfected. Theoretical analysis of the resource allocation control system the filter formula is as follows [23]:

$$F_f = \frac{\sum_i^{n=1} b_n + s_n}{\sum s^{0.5}}. \tag{3}$$

The acquisition of an optimized filtering algorithm represents the optimization of the operation of the model of reliability, and the reason is that this article built the algorithm process that is a layer by the step test mode, that is, the previous algorithm cannot determine the accuracy of further operations; therefore, after the optimization of the selection algorithm to draw conclusions, the conclusion must be reliable and feasible [24, 25]. After the optimization coefficient has been obtained, the role of automatic selection of the optimal online transaction is played out, and the next step is to output it to the user view page, as shown in Figure 1 [26].

3.2. Optimization Scheme of e-Commerce Resource Allocation. After the optimized innovation model is completed, the optimization model of e-commerce resource allocation optimization is integrated. In the process of overlap, it is necessary to consider the commonality of the system, that is, whether the optimal innovation scheme can be combined with the computer algorithm to the highest degree, so that the design and operation results are matched [27]. In the process of project design and output, the staffs need to carry on the information recording work in time, the information entry of the e-commerce innovation structure is guaranteed to the maximum degree, and the accuracy of input analysis information is ensured [28]. Secondly, the analysis of the data processing is the main need to complete the online Web site resource allocation of inefficient information integration,

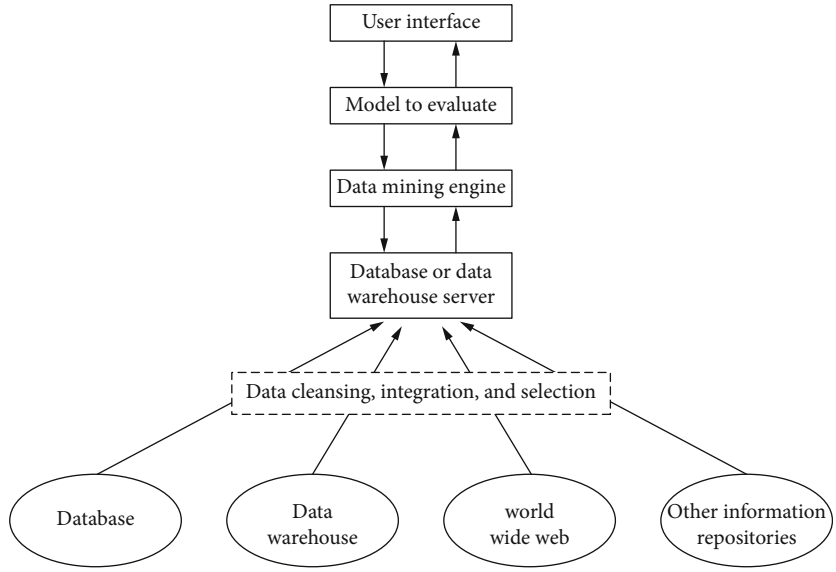

Figure 2: Innovation model and algorithm of e-commerce website structure optimization.

Table 2: Innovation model test of e-commerce website structure optimization.

Financial risk early warning system				Optimal innovation model		
Factor	Detection	Operating	Effect	Smooth	Design	Success
	1	0.9	2.9	3.2	4.2	6.2
Optimal innovation model	2	0.8	2.7	4.1	4.0	4.6
	3	0.9	1.9	2.7	5.3	3.5
	4	1.8	0.9	2.4	6.2	6.3
Traditional manual processing	5	2.3	1.0	4.5	7.0	3.2
	6	1.9	1.1	2.0	7.1	1.4

through the algorithm to effectively deal with, in all aspects of consensus, to achieve the smooth operation of each algorithm for the operation of various algorithms to provide protection [29, 30]. Finally, from the output of the innovative optimization program directly into the resource allocation system, the algorithm collected online Web site resource allocation content and online Web site resource allocation requirements, together with the display in the user view page. During the lap up process, part of the lap is randomly selected, as shown in Table 1 [31].

As shown in Table 1, in the lap stage of the theoretical analysis scheme, using f to represent the model total data algorithm, using x, y to represent the standard data of the material model, this algorithm adds a set of models to ensure objectivity in the information integration stage. To ensure the accuracy of the results, we need to reduce the error of the algorithm [32]. This part of the design first through f to build a corresponding probability calculation, in the input of the corresponding training algorithm, and get an optimized result Y. The formula used in the model is as follows [33]:

$$f = \sqrt{-1 + x'\left(\frac{2-x}{2^{22}-1}\right)} + \sum y_i. \tag{4}$$

By using this formula, we can get the optimization scheme of the optimization innovation model online resource allocation reform and take the value of the fitting to further operation, in which the pcl represents the optimal coefficient, u represents the standard coefficient, and y represents the set of optimization coefficients. The calculated value is the optimal innovation coefficient in the resource allocation mode of online Web site, in order to make the final calculation basis [34, 35].

$$pcl = \sum \frac{u_i}{2} + \frac{y_i + u_i^{0.5}}{y^{0.8}} - \frac{2y_i}{u_i}. \tag{5}$$

The above results provide the basis for the final step to obtain output instructions for the matting, through the centralized operation of all functions and finally obtain an output value, using artificial intelligence operation. The next N type represents the e-commerce platform optimization coefficient, $\phi_x A$ represents the structure optimization strategy representing the value, $\lambda_x W_x$ represents the innovation development value of the algorithm, the β_{mx} represents the electric quotient model label, and the f represents the innovation structure coefficient, uses these data to establish the corresponding function relation, and obtains the

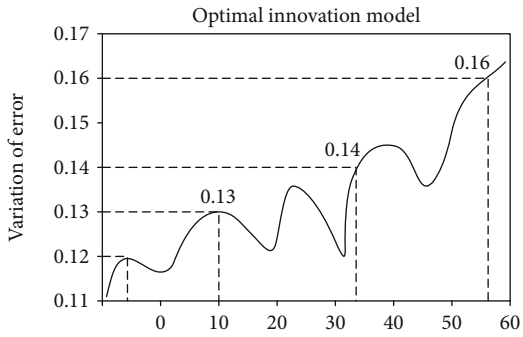

Figure 3: Test results of the innovation model of electronic commerce website structure optimization.

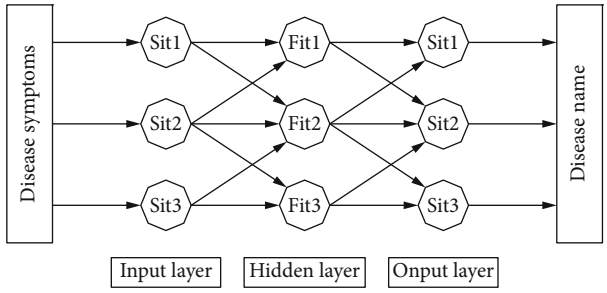

Figure 4: Test results of the structural optimization innovation model.

corresponding difference value sequence. If the corresponding classification problem is encountered, we can take the aggregate function, assuming the f value between the region (-1, 1), and the output function is [35]:

$$\frac{N}{\phi_x A} + \frac{\beta_{mx} M_x}{\lambda_x W_x (1 - 0.8(N/N^x W_x))} \leq f. \tag{6}$$

After the optimal numerical value is determined, we aim at our hypothetical algorithm S and the theoretical analysis of all the algorithm outputs between scheme A; according to a series of optimal numerical values, we integrate them into the optimization innovation model, calculate the corresponding joint probability, and obtain the optimal scheme determining coefficient, and the specific running process is shown in Figure 2.

Through the arrangement of the optimization scheme on online Web site resource allocation, we can get the big analysis direction, carry out the reliability support provided by artificial intelligence, implement the optimization scheme of online website resource allocation, and get the final result of the theoretical analysis and optimization scheme. In this process, the theoretical analysis scheme framework as the intermediate cohesion, its design precision requirements must meet the construction principle of the algorithm to ensure the accuracy of the calculation process. Finally, the end of this link, the theoretical analysis of the optimization index collection is through the computer technology to the optimal solution number, and in this process, through the artificial intelligence formula calculation, the concentration of theoretical analysis system of the blind spot, and the use of theoretical analysis system for the management of resource allocation scheme data classification. The design of the optimization innovation scheme of the e-commerce website resource allocation is accomplished by automatic regularization.

4. Result Analysis and Discussion

The application of the innovation model can be used in the platform of electronic commerce to seek a broader choice for the majority of the participants. In this paper, transaction volume was used as a variable of test, which could optimize the advantage of the innovation system through the objective test data. To participate in the company's running water as the test basis for the participation in online Web site models of participants to collect information, as a test participant before and after evaluation of the basis, at the same time, before carrying out the test, it is necessary to test the system fluency of the artificial intelligence system, to make a random numerical input to the online resource allocation model, and to observe the reliability of the system, so as to get the best performance in the process of resource allocation. Then, the online Web site resource allocation variables are simulated, and the simulation method is used to test the scheme. This simulation test will be based on the database, through the simulation of the resource allocation process, as well as the optimization of the use of innovative models and the employment of professional financial staff to observe the record. The acquisition and rating of the communication are made, and the final error data are shown in Table 2.

It can be seen from the data in Table 2, the optimization innovation model is in the application process of superiority. In the course of this test, there were some errors, but at the same time, the error occurred, the investment judgment error backup was immediately entered into the optimization innovation model, and this aspect shows that, if the original communication process, to do the simulation, the above analysis error will not appear because in the process of testing, mistakes have been optimized by innovative models that are automatically repaired.

This is the advantage of the optimization innovation model that is superior to the dynamic algorithm, which can continuously enlarge the advantage of memory performance, can continuously optimize the system in the process of application, and constantly adjust and optimize according to the investment atmosphere. Therefore, in the idle time of the scheme, the scheme is open and continues to simulate the exchange of data artificially entry, adds practical allocation and actual application of investment and theoretical analysis, and the continuous filling, using the optimization innovation model of self-improvement and repair function, continuously improve the accuracy of the optimization innovation model. The use of the optimized innovation model takes time to accumulate, but it is one of the advantages that it will not be replaced until it is put into use. The test results of the e-commerce website structure optimization innovation model is shown in Figure 3.

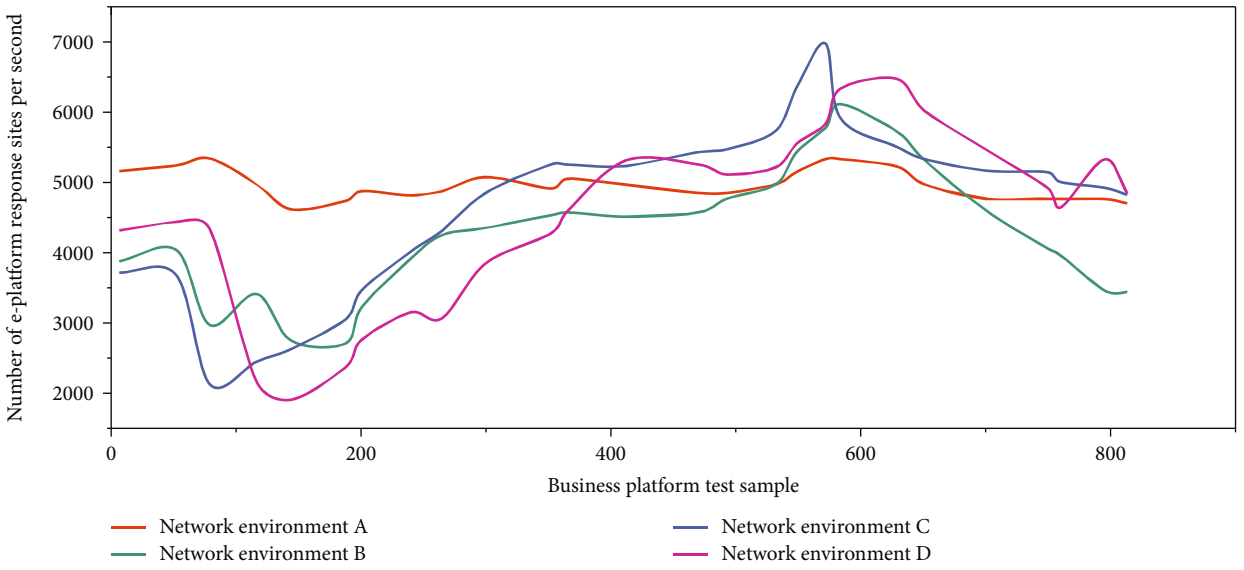

Figure 5: Test results under different network environments.

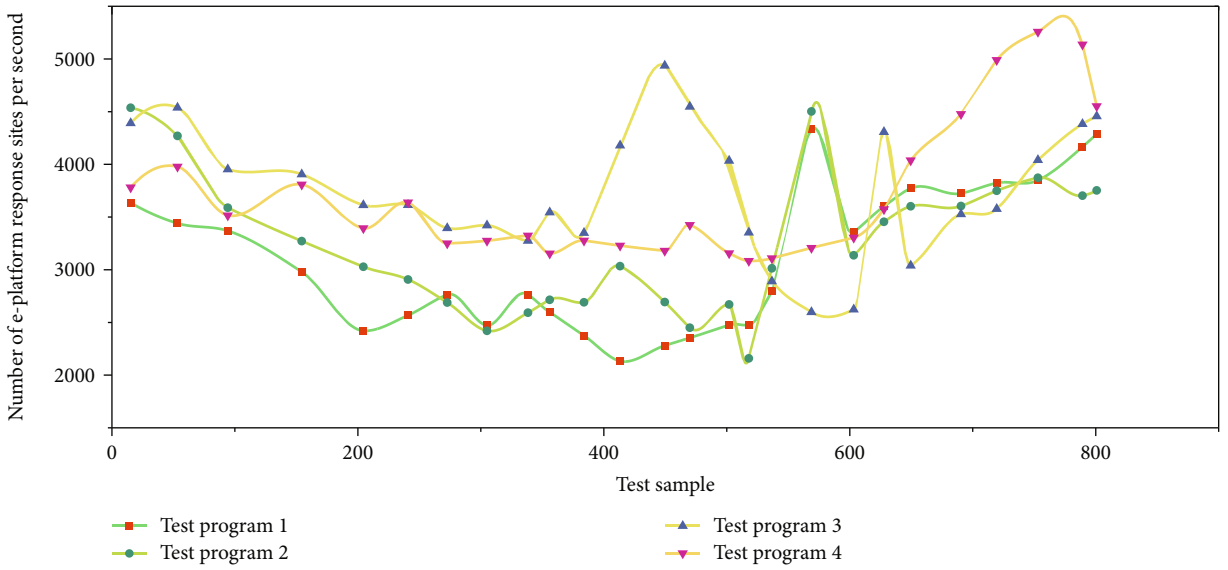

Figure 6: e-Commerce network test results under different test scenarios.

It can be seen from Figure 3, in the process of testing, that the theoretical analysis of the system can be optimized by the innovation model automatic repair. The system can continuously enlarge the memory performance advantage and can optimize the system continuously according to the resource distribution atmosphere. Therefore, in the idle time of the scheme, open the system and continuously artificially input analogy exchange data, arbitrarily add the actual case of resource allocation and theoretical analysis information, to continuously fill, and can ensure the operation of the system. While testing for convergence, we intercepted some of the data as a flowchart, as shown in Figure 4.

As can be seen from Figure 4, as the resource allocation link weakens, the optimization innovation model algorithm will enter into a theoretical analysis state when the bottom line is reached; then, the efficiency of each resource allocation in the optimization innovation model will be greatly improved. At the same time, the resource allocation optimization system should be considered to expand, through the maximum scheme screening, increase the space to collect more available algorithm resources, and easy to achieve optimal performance in this process. Test results under different network environments are shown in Figure 5.

It can be seen from Figure 5 that the test result that the decision result based on the principle of electronic commerce can provide support for the public psychological demand, not only guarantee the implementation of the Internet economic principle but also can take into account the psychological satisfaction of the participants. As shown above, in the single variable to ensure the implementation of Internet

economic principles, the labor intensity of the participants does not fluctuate greatly, but the degree of psychological satisfaction is far less than the mode of optimizing the innovation system. It can be found that the artificial intelligence system is an auxiliary system, which can only have positive effect on the participants and has no effect on the distribution of e-commerce and the results of our country. e-Commerce network test results under different test scenarios are shown in Figure 6.

Through the above experimental results, it can be observed that the use of the optimization innovation system as an auxiliary system not only does not increase the financial burden of the country but to some extent, for the country's economic allocations to provide more flexible space. On the premise of ensuring the distribution of resources on the online website, the two-variable model can be processed, and the corresponding judgment should be made according to the analysis and the participant status information. Therefore, the resource allocation theory analysis model, whether in dealing with a single variable or multivariable situation, can ensure the stability of the national economy on the basis of the interests of the majority of participants to maximize.

5. Conclusions

This paper optimizes the e-commerce system to maximize the efficiency and objectivity of the computer system. Then, the analysis to the electronic commerce website resource allocation model is carried on. Through the theory analysis system construction, the analysis flaw integration retrieval link is utilized, to the theory analysis project uncertainty factor carries on the collection. Then, according to each flaw that represents the outstanding problem that is classified to the classification, the entire theory analysis model frame is completed. At the same time, it is necessary to make further efforts to deal with the theoretical analysis system of the design and to set up the evaluation standard as well as the statistical calculation of the resource allocation vulnerabilities of online websites.

Data Availability

All data sources are reliable and can be contacted by the corresponding author.

Conflicts of Interest

The author(s) declare(s) that they have no conflicts of interest.

Acknowledgments

This study was funded by Zhejiang A&F University Scientific Research Development Fund Project: Research on Forestry Heterogeneous Knowledge Integration Technology Facing Semantic Web.

References

[1] L. H. Yang, S. Hyun, E. Koo, and D. J. Ahn, "Structure optimization of low-dimensional quantum dots via anisotropic surface energy," *Journal of the Korean Physical Society*, vol. 72, no. 5, pp. 582–587, 2018.

[2] A. Lucas, L. Hoong Chuin, and C. ShihFen, "Achieving stable and fair profit allocation with minimum subsidy in collaborative logistics," *IEEE Communications Letters*, vol. 11, no. 12, pp. 970–972, 2016.

[3] L. Yu, M. Huang, T. Xu et al., "A structure-guided optimization of pyrido pyrimidin-7-ones as selective inhibitors of egfrl858r/t790m mutant with improved pharmacokinetic properties," *European Journal of Medicinal Chemistry*, vol. 126, pp. 1107–1117, 2016.

[4] S. V. Bigi-Botterill, A. Ivetac, E. L. Bradshaw, D. Cole, and S. Swann, "Structure-guided optimization of a novel class of ask1 inhibitors with increased sp3 character and an exquisite selectivity profile," *Bioorganic & Medicinal Chemistry Letters*, vol. 30, no. 17, p. 127405, 2020.

[5] E. Lee and P. Holme, "Impact of Mobility Structure on Optimization of Small-World Networks of Mobile Agents," *The European Physical Journal B*, vol. 89, no. 6, 2016.

[6] N. Sorokin, B. Sobolev, E. Krivandina, and Z. Zhmurova, "Optimization of single crystals of solid electrolytes with tysonite-type structure (LaF3) for conductivity at 293 K: 2. Nonstoichiometric phases R 1−y M y F3−y (R = La-Lu, Y; M = Sr, Ba)," *Crystallography Reports*, vol. 60, no. 1, pp. 123–129, 2015.

[7] X. Zhang, G. Dong, H. Li, W. Chen, and Y. Xu, "Structure-aided identification and optimization of tetrahydroisoquinolines as novel pde4 inhibitors leading to discovery of an effective anti-psoriasis agent," *Journal of Medicinal Chemistry*, vol. 62, no. 11, pp. 5579–5593, 2019.

[8] D. E. Reyna, F. Kopp, and E. Gavathiotis, "Abstract 1654: chemical and structure-guided optimization of bax trigger site activators for cancer therapy," *Cancer Research*, vol. 78, 13 Supplement, pp. 1654–1654, 2018.

[9] Z. Z. Jiang, Z. P. Fan, W. H. Ip, and X. Chen, "Fuzzy multiobjective modeling and optimization for one-shot multiattribute exchanges with indivisible demand," *IEEE Transactions on Fuzzy Systems*, vol. 24, no. 3, pp. 708–723, 2016.

[10] N. Nishimura, N. Sukegawa, Y. Takano, and J. Iwanaga, "A latent-class model for estimating product-choice probabilities from clickstream data," *Information Sciences*, vol. 429, pp. 406–420, 2016.

[11] M. W. Ulmer, "Anticipation versus reactive reoptimization for dynamic vehicle routing with stochastic requests," *Networks*, vol. 73, no. 3, pp. 277–291, 2019.

[12] H. Zhang, Y. Sun, M. Zhao, T. W. Chow, and Q. J. Wu, "Bridging User Interest to Item Content for Recommender Systems: An Optimization Model," *IEEE Transactions on Cybernetics*, vol. 50, 2020.

[13] H. Xie and J. C. S. Lui, "Modeling ebay-like reputation systems: analysis, characterization and insurance mechanism design," *Performance Evaluation*, vol. 91, pp. 132–149, 2015.

[14] M. Viazovska, "The sphere packing problem in dimension 8," *Annals of Mathematics*, vol. 185, no. 3, 2016.

[15] V. Dunjko and H. J. Briegel, "Machine learning & artificial intelligence in the quantum domain: a review of recent progress," *Reports on Progress in Physics*, vol. 81, no. 7, p. 074001, 2018.

[16] D. Schack, L. Rihko-Struckmann, and K. Sundmacher, "Linear programming approach for structure optimization of renewable-to-chemicals (r2chem) production networks," *Industrial & Engineering Chemistry Research*, vol. 57, no. 30, pp. 9889–9902, 2018.

[17] Q. Khan, A. Subramanian, G. Yu et al., "Structure Optimization of Perovskite Quantum Dot Light-Emitting Diodes," *Nanoscale*, vol. 11, no. 11, pp. 5021–5029, 2019.

[18] H. Subramanian, "Decentralized blockchain-based electronic marketplaces," *Communications of the ACM*, vol. 61, no. 1, pp. 78–84, 2018.

[19] B. Roman, "Beyond bitcoin: the rise of blockchain world," *Computer*, vol. 51, no. 2, pp. 54–58, 2018.

[20] C. G. Tsai and C. P. Chen, "Financials responses to the retransition in classical sonata form," *Journal of New Music Research*, vol. 44, no. 3, pp. 271–286, 2015.

[21] H. I. Ozercan, A. M. Ileri, E. Ayday, and C. Alkan, "Realizing the potential of blockchain technologies in genomics," *Genome Research*, vol. 28, no. 9, pp. 1255–1263, 2018.

[22] Z. Yinghui, R. H. Deng, L. Ximeng, and Z. Dong, "Blockchain based efficient and robust fair payment for outsourcing services in cloud computing," *Information Sciences*, vol. 462, pp. 262–277, 2018.

[23] J. J. Deng and C. H. C. Leung, "Dynamic time warping for music retrieval using time series modeling of musical emotions," *IEEE Transactions on Affective Computing*, vol. 6, no. 2, pp. 137–151, 2015.

[24] K. Gammon, "Experimenting with blockchain: can one technology boost both data integrity and patients' pocketbooks?," *Nature Medicine*, vol. 24, no. 4, pp. 378–381, 2018.

[25] V. Sharma, I. You, F. Palmieri, D. N. K. Jayakody, and J. Li, "Secure and energy-efficient handover in fog networks using blockchain-based dmm," *IEEE Communications Magazine*, vol. 56, no. 5, pp. 22–31, 2018.

[26] A. Hosny, C. Parmar, J. Quackenbush, L. H. Schwartz, and H. J. W. L. Aerts, "Artificial intelligence in radiology," *Nature Reviews Cancer*, vol. 18, no. 8, pp. 500–510, 2018.

[27] B. M. Wagman, "Artificial intelligence and human cognition," *Quarterly Review Of Biology*, vol. 68, no. 1, 2019.

[28] M. Hutson, "Artificial intelligence faces reproducibility crisis," *Science*, vol. 359, no. 6377, pp. 725-726, 2018.

[29] Z. Chen, D. Chen, Y. Zhang, X. Cheng, M. Zhang, and C. Wu, "Deep learning for autonomous ship-oriented small ship detection," *Safety Science*, vol. 130, p. 104812, 2020.

[30] K. A. Pearson, P. Leon, and C. A. Griffith, "Searching for exoplanets using artificial intelligence," *Monthly Notices of the Royal Astronomical Society*, vol. 474, no. 1, pp. 478–491, 2018.

[31] C. Lin, N. Xiong, J. H. Park, and T. Kim, "Dynamic power management in new architecture of wireless sensor networks," *International Journal of Communication Systems*, vol. 22, no. 6, pp. 671–693, 2009.

[32] Y. Sang, H. Shen, Y. Tan, and N. Xiong, "Efficient Protocols for Privacy Preserving Matching against Distributed Datasets," *International Conference on Information and Communications Security*, pp. 210–227, 2006.

[33] F. Long, N. Xiong, A. V. Vasilakos, L. T. Yang, and F. Sun, "A sustainable heuristic QoS routing algorithm for pervasive multi-layered satellite wireless networks," *Wireless Networks*, vol. 16, no. 6, pp. 1657–1673, 2010.

[34] J. Li, N. Xiong, J. H. Park, C. Liu, M. A. Shihua, and S. E. Cho, "Intelligent model design of cluster supply chain with horizontal cooperation," *Journal of Intelligent Manufacturing*, vol. 23, no. 4, pp. 917–931, 2012.

[35] W. Guo, N. Xiong, A. V. Vasilakos, G. Chen, and C. Yu, "Distributed k–connected fault–tolerant topology control algorithms with PSO in future autonomic sensor systems," *International Journal of Sensor Networks*, vol. 12, no. 1, pp. 53–62, 2012.

Hindawi
Wireless Communications and Mobile Computing
Volume 2020, Article ID 8877625, 9 pages
https://doi.org/10.1155/2020/8877625

Research Article

Research on Construction of a Cloud Platform for Tourism Information Intelligent Service Based on Blockchain Technology

Cao Wei, Qinan Wang, and Chengying Liu

School of Geography Information System and Tourism, Chuzhou University, Chuzhou 239000, China

Correspondence should be addressed to Cao Wei; lcy@chzu.edu.cn

Received 17 July 2020; Revised 22 September 2020; Accepted 14 October 2020; Published 28 October 2020

Academic Editor: Hongju Cheng

Copyright © 2020 Cao Wei et al. This is an open access article distributed under the Creative Commons Attribution License, which permits unrestricted use, distribution, and reproduction in any medium, provided the original work is properly cited.

The development of global tourism has put forward new requirements for the construction of smart tourism. More and more travel-related data have reached the level of TB or even PB, which has brought great difficulties to tourism management. This article explores the use of big data technologies such as genetic algorithms to explore massive travel data and establish a comprehensive tourism information service platform for governments, enterprises, tourists, and scientific research institutions. The overall design of an industrial information service platform based on big tourist data is proposed. The overall function, data source, data standard, and application scope of the platform are all focused on. The traceability and nontampering of blockchain technology can also help passengers retain and verify their identity information. From the perspective of the design goals of the system, in general, the time required for repeated authentication will greatly reduce air ticket bookings, accommodation reservations, and bill verification, and improving efficiency is the only way to establish a "trust ecology." Architecture design, distributed architecture, and intelligent service design, as well as the key implementation technology of service platform construction, route recommendation algorithm and tourism information big data mining, research and analysis on the construction of tourism information intelligent service.

1. Introduction

At present, China has become the largest tourist market in the world [1, 2]. Among them, outbound tourism consumption ranks first in the world, and inbound tourism ranks third in the world [3]. Driven by the new Internet information technology such as mobile communication, large data service, and cloud computing, especially the proposal of "intelligent earth," the concepts of "intelligent city." "Intelligent tourism" and "intelligent service" have come into being one after another. At the same time, the rapid integration of these new Internet applications and tourism industry will also promote the development of tourism information services to intelligent services [4]. Based on the technology of large data, cloud computing, and artificial intelligence, this research is based on the users' behavior analysis and realizes the information analysis and processing of mass tourist users [5]. Through the mobile Internet and other media, real-time online interaction is carried out with users, so as to provide users with more intelligent and convenient route decision travel information clothes, Business.

In recent years, the National Tourism Administration has vigorously promoted the construction of intelligent tourism. In 2011, intelligent tourism was listed as an important work of tourism in the 12th Five-Year Plan; in 2012, 18 pilot cities of intelligent tourism and 22 pilot units of intelligent scenic spots were determined; in 2013, 14 intelligent tourist cities were determined [6]. 2014 was identified as the year of wisdom tourism. According to studies, China's tourism industry began to enter the era of big data in 2013. In the rush hour, the hotel has a daily booking capacity of several hundred thousand and, at the same time, produces massive tourism data such as information collection, consumer reviews, and product recommendations [7]. Big data technology can dig and analyze these huge amounts of data, which will make wisdom travel like a duck to water. The impact of big data on the tourism industry is all-around, and the whole industry management decision-making mode has changed

accordingly [8]. In 2015, the State Council issued the "program for the promotion of big data development" and systematically deployed large data development work [9, 10]. In the same year, Gui Zhou started the construction of the first large data comprehensive test area in China. Many scholars began to study the integration of large data and intelligent tourism. In this context, the author combed the relevant literature in order to better clarify the relationship between the two and provide reference for the further development of intelligent tourism. In this paper, we show how an iterative development process that incorporates client-developer joint exploration of partial designs facilitates the development of client understanding of their needs [11, 12].

The rest of this paper is organized as follows. Section 2 discusses the concept of large data and intelligent tourism. The task joint release model based on a genetic algorithm is discussed in Section 3. Construction of an intelligent tourism application model under large data background is discussed in Section 4. Section 5 concludes the paper with a summary and future research directions.

2. The Concept of Large Data and Intelligent Tourism

The concept of big data comes with the growth of unstructured data. In 2011, the McKinsey Global Institute defined large data as a data group of data groups [13] that exceeded the grasp, storage, management, and analysis capabilities of the traditional database software tools. Processing large data requires special technology, namely, large data technology, including large-scale parallel processing database, data mining grid, distributed file system, distributed database, cloud computing platform, Internet, and extensible storage system. Internet companies represented by Google, Facebook, LinkedIn, and Microsoft have gradually introduced various types of big data processing systems. Smart tourism is a new concept that evolved from the digital earth. Mole, an assistant professor at the College of the Holy Cross, defines intelligent tourism as the use of mobile digital connectivity to create a more intelligent, meaningful, and sustainable association between tourists and the city. Domestic scholars have also formed several views on the concept of intelligent tourism [14].

Relying on the accurate and advanced information data platform, and integrating the tourism industry information, according to the travel records and consumption preference of tourists, it provides tourists with personalized tourism services and realizes the private customization of tourism. The smart tourism application model based on the big data perspective is shown in Figure 1.

The first view is that intelligent tourism is a variety of changes brought by the application of some new technologies to tourism; the second view is that intelligent tourism is a modernization of promoting tourism service, improving tourism experience, innovating tourism management, and optimizing the use of tourism resources. Engineering; the third view is that intelligent tourism is a high-level form and stage of tourism; the fourth view is that intelligent tourism is a new mode of operation to improve the experience

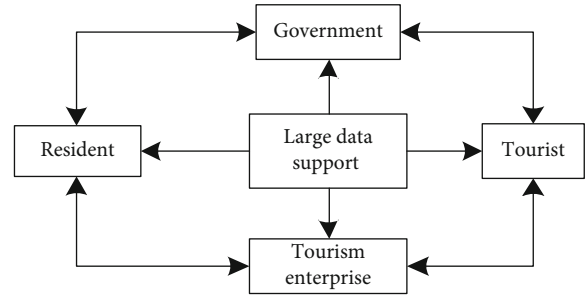

Figure 1: Smart tourism application model based on the big data perspective.

and participation of tourists; and there are other different views. With regard to the relationship between large data and intelligent tourism, most scholars regard big data as a background of intelligent tourism and identify the role of large data on the development of intelligent tourism. However, some scholars regard big data technology as one of the components of intelligent tourism [15, 16]. Liang Changyong believes that large data mining technology is intelligent tourism. The core. Li Yunpeng and so on pointed out that intelligent tourism is a large amount of real-time data formed by tourists on the Internet. Using big data, it can further guide the practice of tourism industry and better serve tourists [17, 18].

3. Task Joint Release Model Based on a Genetic Algorithm

3.1. Model Preparation. A genetic algorithm is a search algorithm with self-adaptability and self-organization ability developed based on the natural selection and evolution mechanism of the biological world. It is widely used to solve complex optimization problems. The genetic algorithm first randomly generates a set of possible solutions to the optimization problem and encodes each possible solution [19]. The set of possible solutions is called a population, and each possible solution in the population is called an individual. Each individual has a corresponding fitness value, which is used to measure the "good or bad" of the solution to the problem represented by the individual. Imitating the principle of "survival of the fittest" in the biological world, according to the size of fitness, select a number of better individuals from the initial population to participate in crossover and mutation operations [20, 21].

The crossover operation generates a new individual by swapping and recombining a part of the codes of the two individuals, similar to the offspring inheriting the parent's genes. The mutation operation generates new individuals by randomly changing the coding bits of an individual, thereby increasing the diversity of the population. The selection, crossover, and mutation operations are performed iteratively several times or until a specific termination rule is met, and the individual with the highest fitness in the population is the approximate optimal solution of the optimization problem. In recent years, genetic algorithms have been

successfully applied in pattern recognition, machine learning, image processing, and intelligent control [22].

3.2. The Basic Idea of the K-Means Algorithm. The K-means algorithm is one of the most widely used clustering algorithms. The algorithm uses parameters to divide objects into clusters so that the clusters have a high degree of similarity, but the similarity between clusters is low. The algorithm first randomly selects objects. Each object initially represents the average value or center of a cluster [23, 24]. For each remaining object, it is assigned to the nearest cluster according to its distance from the center of each cluster, and then each object is recalculated. For the average value of the cluster, the process is repeated until the criterion function converges. The criterion function is as follows:

$$E = \sum_{i=1}^{k} \sum_{x \in C_i} |x - \bar{x}_i|^2, \tag{1}$$

where E is the average value of the cluster. The description of the K-means algorithm is as follows:

(1) Randomly select a record as the initial cluster center

$$W(u_i, v_i) = W(i) = \begin{bmatrix} w_{i1} & 0 & \cdots & 0 \\ 0 & w_{i2} & \cdots & 0 \\ \cdots & \cdots & \cdots & \cdots \\ 0 & 0 & 0 & w_{\text{in}} \end{bmatrix}. \tag{2}$$

(2) Calculate the distance between each record and the cluster centers, and use the closest cluster as the class to which the point belongs [25]

$$\beta = \begin{pmatrix} \beta_0(u_1, v_1) & \beta_1(u_1, v_1) & \cdots & \beta_k(u_1, v_1) \\ \beta_0(u_2, v_2) & \beta_1(u_2, v_2) & \cdots & \beta_k(u_2, v_2) \\ \cdots & \cdots & \cdots & \cdots \\ \beta_0(u_n, v_n) & \beta_1(u_n, v_n) & \cdots & \beta_k(u_n, v_n) \end{pmatrix}, \tag{3}$$

where β is the estimated value, k is the number of independent variables, n is the spatial sample, and u is the weight given to the data point n when describing the model for position i.

3.3. Weight Function and Bandwidth Determination. The weight function is often determined by the Gaussian function in practice, and the expression method is as follows:

$$W_{ij} = e^{-(1/2)\left(d_{ij}/b\right)^2}, \tag{4}$$

where b refers to the bandwidth. If the data of point i is observed, the weight of other points will decrease with the increase of distance according to the Gaussian curve. Bandwidth b, then the weight of points far enough away from point i will tend to zero. The choice of bandwidth b can be determined by the cross-confirmation method and calculated for a given b value:

$$cv(b) = \sum_{i=1}^{n} \left[y_i - \hat{y}_{\neq i}(b) \right]^2, \tag{5}$$

where y is the dependent variable after the observation value and the width b is removed, and then the weighted least square method is used to obtain the fitted value of the dependent variable y. The selection result is shown in the following formula:

$$cv(b_0) = \min_{b>0} cv(b). \tag{6}$$

Calculate the centroid of each cluster (the mean value of the cluster point) and the distance between each object and these central objects, and redivide the corresponding objects according to the minimum distance. Repeat this step until equation (3) no longer changes significantly [26].

3.4. Model Establishment. One advantage of the genetic algorithm is that it does not require special knowledge of the problem domain to be solved, so the process of solving the problem with the genetic algorithm is basically the same. The following figure shows the processing flow of the genetic algorithm used in this paper for cluster analysis [27, 28].

The evolution process in genetic algorithms is based on the coding mechanism, and coding has a great influence on the performance of the algorithm, such as search capabilities [29, 30]. Commonly used encoding methods include floating-point number encoding and binary encoding. In contrast, binary encoding has stronger search capabilities than floating-point number encoding. In addition, binary encoding has the advantages of simple crossover and mutation operations. Therefore, binary encoding is used here. The solution of the clustering problem is the center of each cluster. For the clustering problem of points in space, each individual in the genetic algorithm includes a binary component corresponding to the real number component, and the number of binary digits contained in each component is calculated by the method [31, 32].

In this way, each individual includes binary bits. The first binary code string of length in the individual is decoded by the decoding function [33, 34].

Randomly select a point from the set of points to be classified as a solution of the problem and encode it. Repeat the selection of Psize times, and Psize is the set population size [35].

In the process of the genetic algorithm, the fitness function is used as the basis and the fitness value of each individual in the population is used to search [36, 37]. Therefore, the selection of fitness function is very important and directly affects the convergence speed of the genetic algorithm. For each individual, use the same method as the K-means algorithm to divide the cluster and recalculate the center of each

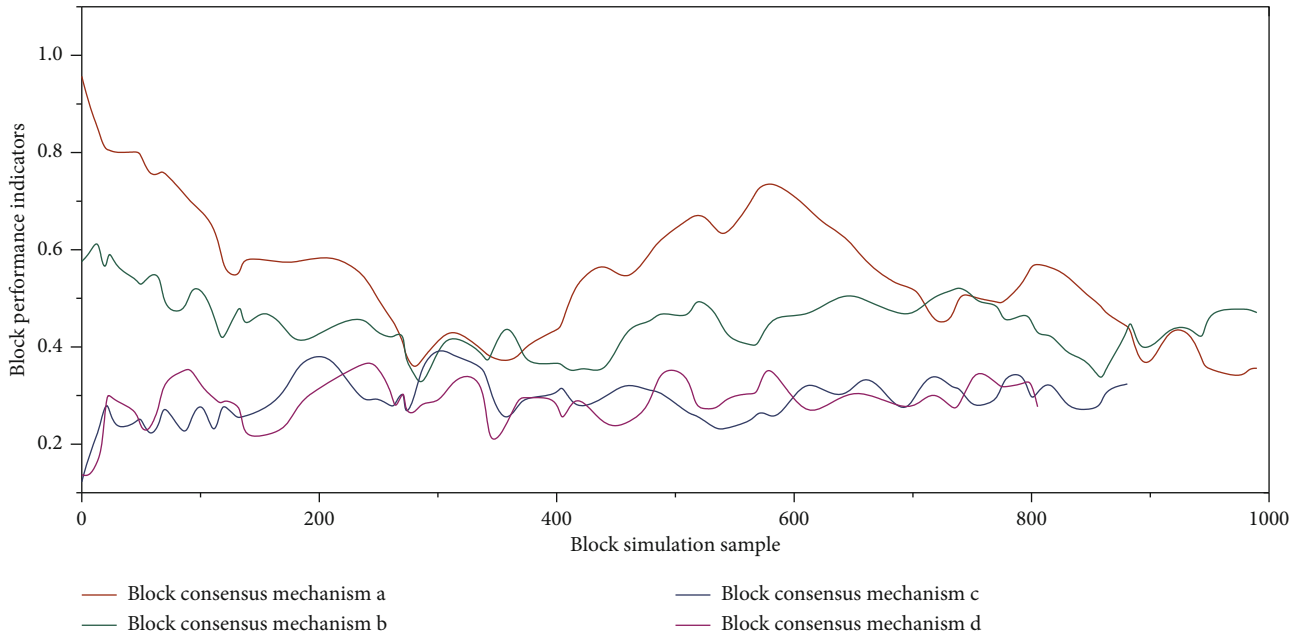

Figure 2: Changes in blockchain performance indicators under different consensus mechanisms.

cluster, and then use the sum of the distances between the points in each cluster and the corresponding cluster center as the judgment cluster division. The smaller the quality criterion function, the better the quality of clustering. The mathematical expression is [38]

$$\Delta(G_1, G_2, \cdots, G_K) = \sum_{i=1}^{K} \sum_{x_j \in G_i} \left\| x_j - c_i \right\|. \tag{7}$$

The purpose of the genetic algorithm is to search for the cluster center that minimizes the value, so the fitness function [39]. In order to improve the search speed, after each cluster division is obtained, the corrected cluster center is used to replace the original cluster center in the individual [40, 41].

4. Construction of the Intelligent Tourism Application Model under Large Data Background

The foundation of smart tourism in the context of big data is the smart tourism application model based on the big data platform. The smart tourism application model based on the large data platform can provide the latest tour route quotations, the most favorable discount ticket information, the most reasonable travel advice, and the most detailed tourist information.

In order to identify the relationship between tourism stakeholders and their relations as a breakthrough point, the intelligent tourism application model of the large data perspective is built around the application objects and the demand for mutual relations for intelligent tourism. The application objects of smart tourism mainly include government tourism department, tourism enterprise, community residents, and tourists. Compared with the traditional application model, it only faces government, tourism enterprises, and tourists. Smart tourism also includes community residents in the application of smart tourism. Intelligent tourism not only provides services for tourists, tourism enterprises, and government but also promotes the coordination of tourism management and service and the economic development of destinations, so as to realize the friendly relationship between tourists and community residents. Using the Internet of Things technology, massive database, cloud computing technology, and scientific analysis, the intelligent tourism application model collects a large amount of data produced in the tourism activities in time, effectively integrates the tourism information of the regional tourism destination in recent years, establishes the related models, and predicts the future of the region. Changes in blockchain performance indicators under different consensus mechanisms are shown in Figure 2.

The flow of tourism, transmission to the server platform, and setup of a monitoring and forecasting system for tourism activity data can effectively predict the flow direction of tourism destinations and the trend of future flow and rationally guide the tourist attractions, tourism enterprises, and government tourism departments to put the corresponding manpower into service and prevent the group. The occurrence of a sexual event. The framework of the intelligent tourism application model based on big data is shown in Figure 3.

The virtual service platform of intelligent tourism is set up in the provincial capital cities, and the information channels of tourist accommodation, travel agencies, tourism enterprises, tourism colleges, and tourist attractions are used to realize the information circulation of various stakeholders, and the hidden value function of the large database will be greatly played, and the information sharing platform will be constructed. The model platform is based on the massive data of various provincial tourism events at the provincial level in recent years. The basic data are classified into basic data, basic data of tourist attractions, basic data of

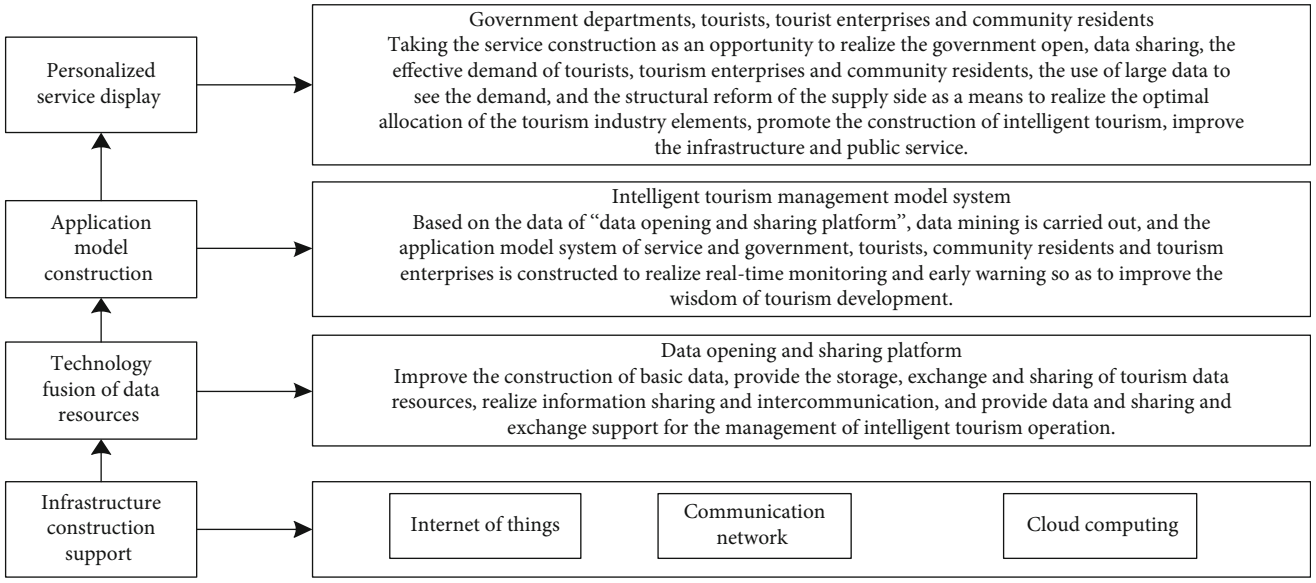

Figure 3: Framework of the smart tourism application model based on big data.

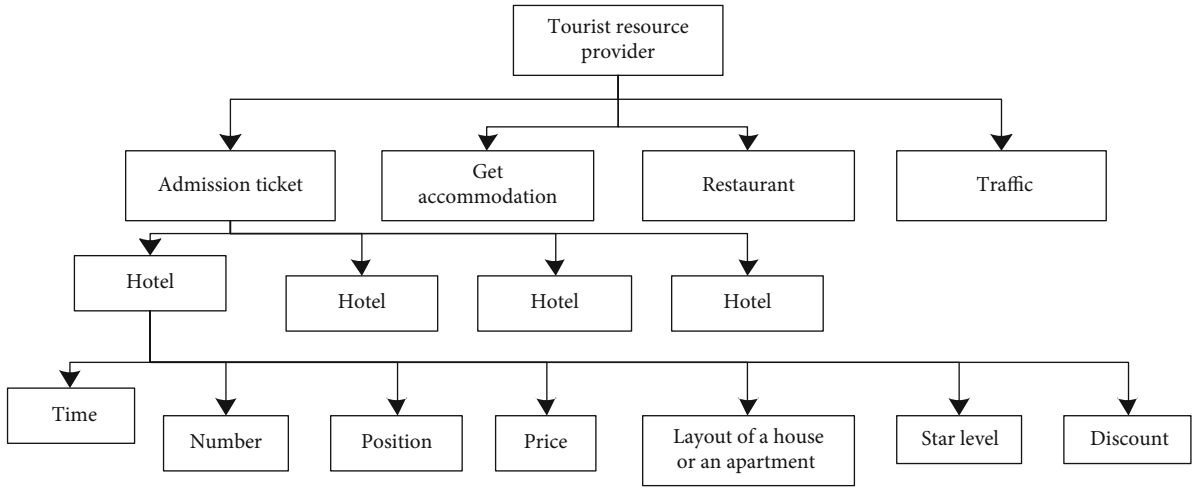

Figure 4: Basic information on hotel resources.

government tourism departments, and basic data of community residents, and then the standardized data are introduced into the application of intelligent tourism.

The data platform system of the model. At the same time, through the Internet of Things technology, all kinds of basic data are accurately tagged on the map of each province, and the provincial city is divided into several regional tourist destinations. The spatial coordinates of all kinds of basic data are tagged in various regional tourist destinations, and space grid numbers are carried out, and a variety of related prediction models can be used. It can realize real-time monitoring and early warning for a certain area tourist destination and a certain time period and predict the possibility of various events in the region. The basis of the monitoring and early warning system is that the basic data of tourism enterprises, tourist attractions, government tourism departments, and community residents include the type, time, and location of events. The combination definition is a structure with recursive nature; that is, the inventory can be combined repeatedly to form a more complex and richer product system. The inventory combination model is very suitable for the statistical price and discount treatment. The basic information and necessary attributes of the accommodation are shown in Figure 4.

The data processing platform of the application model can be used to discover the time and time of various types of events through the mathematical model of cloud computing. Location rules can automatically predict the flow and flow of tourists in different periods of the region by the icon of a number of axes, including the real-time tourist flow of regional tourist destinations and the monitoring and early warning of a specific day, week, month, year, or custom time period. In order to achieve the above planning objectives, we must first define a good inventory management basis, and the inventory is the basis for the calculation of the whole tourism level, and the inventory management hierarchy diagram of the tourism system is shown in Figure 5.

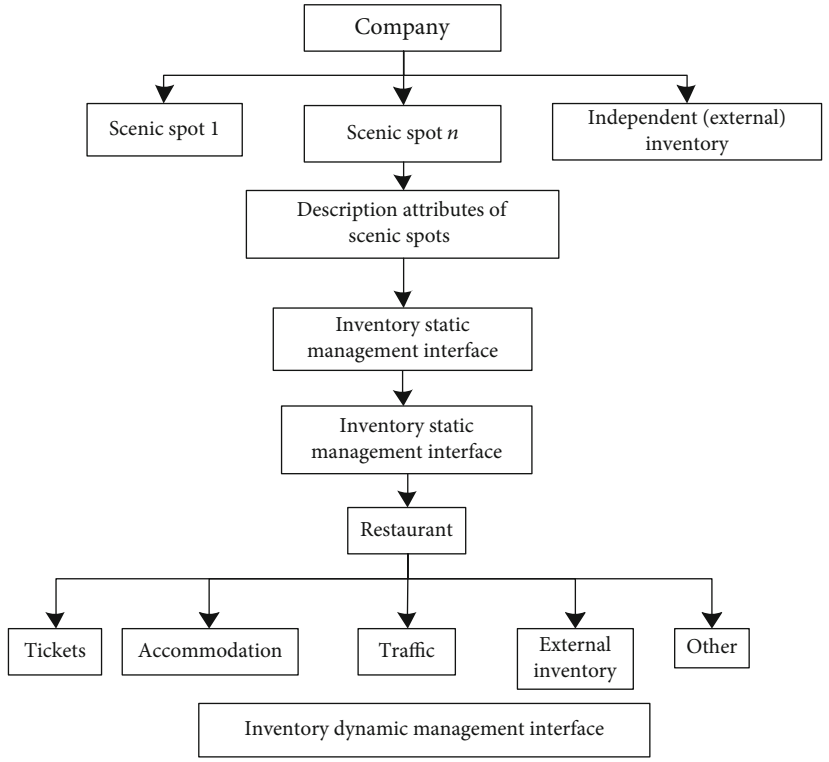

Figure 5: An inventory management hierarchy map of the tourism system.

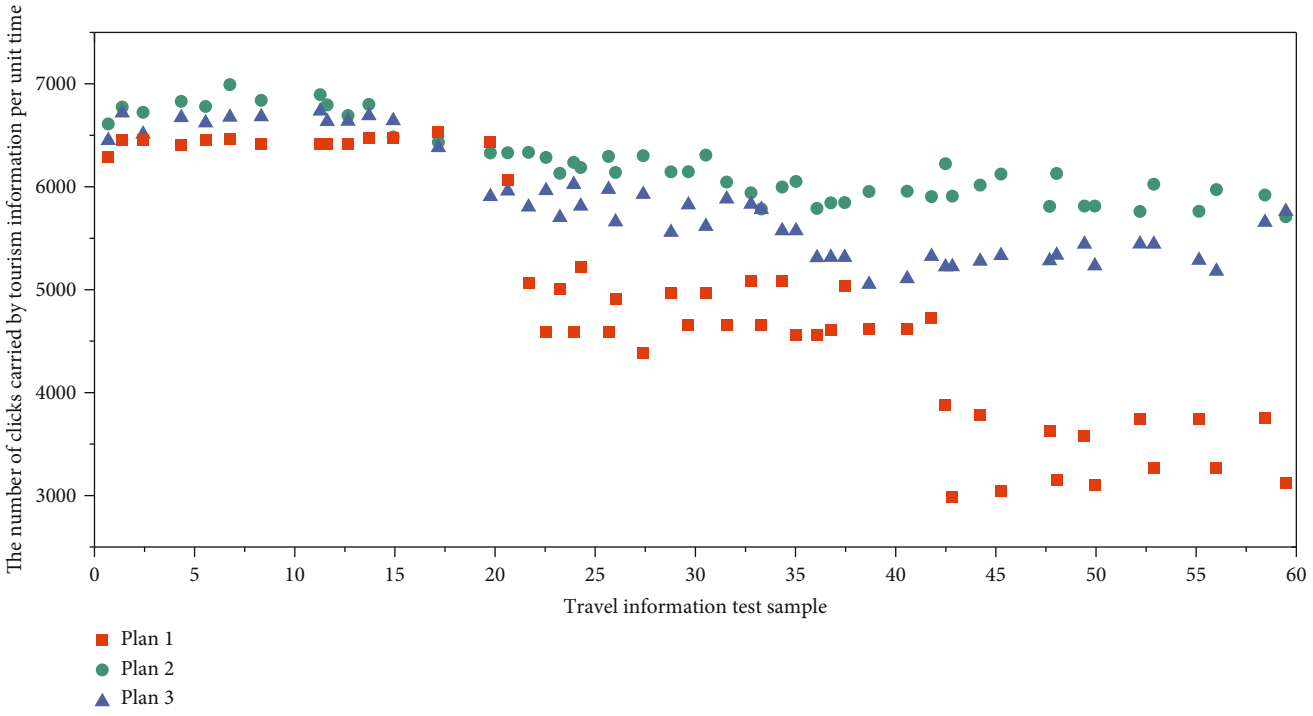

Figure 6: The number of clicks carried by tourism information per unit time.

At present, the resource information provided by the provider of resources is divided into four categories: admission, accommodation, catering, and transportation, of which each element is subdivided into specific resource providers and resource attributes. The number of clicks carried by tourism information per unit time is shown in Figure 6.

The whole inventory system mainly uses the tree structure to manage the data, and the inventory management

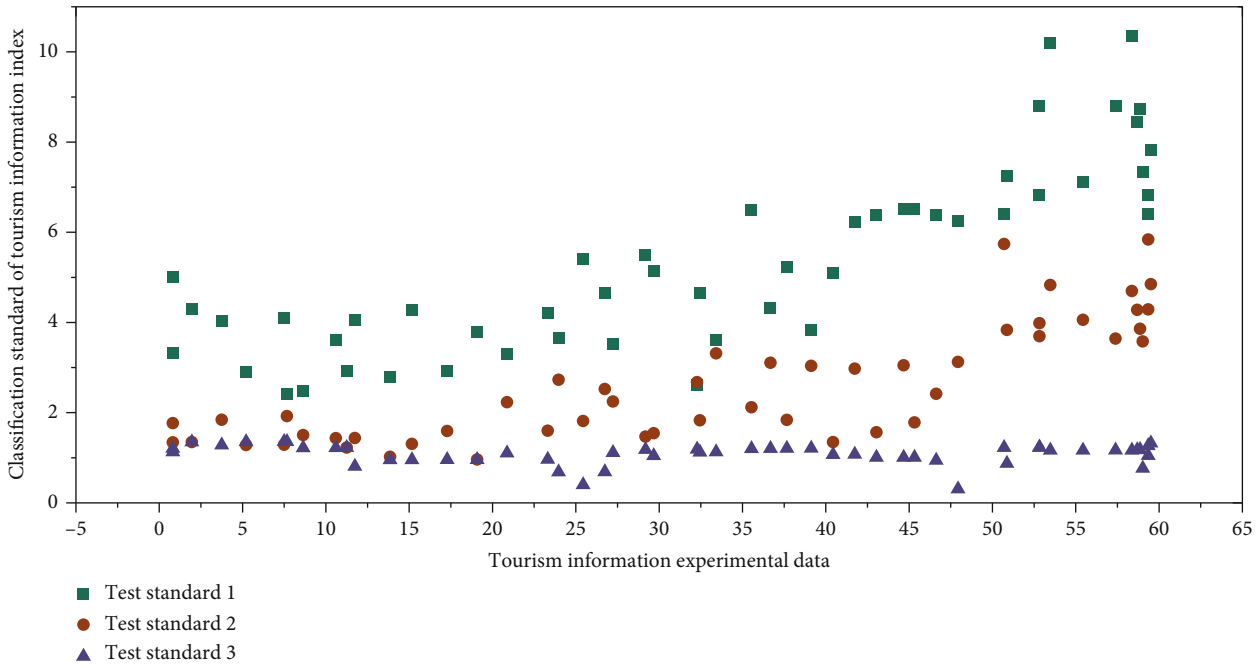

Figure 7: Classification standard of the tourism information index.

interface determines the basic elements of all the tourism elements, including the name of the commodity provider, the price attribute, the quantity type, the time attribute, the position attribute, and the quality attribute of the product. The definition of the inventory portfolio determines that those goods can be combined and sold together to form a set of services. The classification standard of the tourism information index is shown in Figure 7.

The information of the specific inventory is classified according to specific categories. This is the storage and processing of specific data in inventory management. The dynamic structure of the inventory management is to deal with the inventory information of the dynamic goods. One of the characteristics of the tourism inventory is that the product produces new and effective products automatically every day so that the product's reservation and ability can be calculated.

5. Conclusions

A smart tourism system is a highly complex cloud system platform that can automatically help users set up travel planning. This choice is based on a series of priority selection rules. The selection and setting of these rules have been studied by the market and the users, which have a fairly accurate selection effect. After using the system, users only need to enter their own travel plans. They can get out of the tedious travel strategy and get a complete, efficient, feasible, and optimized tour line immediately. It saves users valuable time and helps users save costs and costs. The online implementation of the system will bring a new user experience mode to the tourism industry.

Data Availability

All data sources are authentic and reliable.

Conflicts of Interest

The authors declare that they have no competing interests.

Acknowledgments

This work was supported by the General Teaching research project by the Education Department of Anhui Province in 2019 (No. 2019jyxm0447) and the Major Teaching research project by Chuzhou University in 2019 (No. 2019jyz026).

References

[1] H. Wu, X. Wu, Q. Ma, and G. Tian, "Cloud robot: semantic map building for intelligent service task," *Applied Intelligence*, vol. 49, no. 2, pp. 319–334, 2019.

[2] Z. Rong-Hao, "Research on the temperature rise test system construction of for high altitude and low voltage switchgear," *Environmental Technology*, vol. 19, no. 2, pp. 31–44, 2019.

[3] D. Hong, "Research on the construction of new energy micro grid in countryside," *Electrical Engineering*, vol. 10, no. 12, pp. 30–41, 2015.

[4] C. Zhang and S. Chang, "Research on the strategy for hospital medical records information sharing service," *Basic & Clinical Pharmacology & Toxicology*, vol. 118, 2016.

[5] X. Wang, C. Wang, C. Jiang, L. Yang, Z. Li, and X. Zhou, "Rule optimization for real-time query service in software-defined internet of vehicles," *IEEE Transactions on Intelligent Transportation Systems*, vol. 99, pp. 1–11, 2015.

[6] N. Khademi, "Intelligent transportation system user service selection and prioritization: hybrid model of disjunctive satisfying method and analytic network process," *Transportation Research Record*, vol. 2189, no. 1, pp. 45–55, 2010.

[7] C. Tomasetti and B. Vogelstein, "Variation in cancer risk among tissues can be explained by the number of stem cell divisions," *Science*, vol. 347, no. 6217, pp. 78–81, 2015.

[8] R. Draghia, F. Letourneur, C. Drugan et al., "Metachromatic leukodystrophy: identification of the first deletion in exon 1 and nine novel point mutations in the arylsulfatase A gene," *Human Mutation*, vol. 9, no. 3, pp. 234–242, 1997.

[9] C. Bollmeyer, J. D. Keller, C. Ohlwein et al., "Towards a high-resolution regional reanalysis for the European CORDEX domain," *Quarterly Journal of the Royal Meteorological Society*, vol. 141, no. 686, pp. 1–15, 2015.

[10] C. Gómez, S. Vega-Quiroga, F. Bermejo-Pareja, M. J. Medrano, E. D. Louis, and J. Benito-León, "Polypharmacy in the elderly: a marker of increased risk of mortality in a population-based prospective study (NEDICES)," *Gerontology*, vol. 61, no. 4, pp. 301–309, 2015.

[11] J. Kim, Y. Jeon, and H. Kim, "The intelligent IoT common service platform architecture and service implementation," *The Journal of Supercomputing*, vol. 74, no. 9, pp. 4242–4260, 2018.

[12] S. Hu, Y. Wang, W. Wang et al., "Ag nanoparticles on reducible CeO2 (111) thin films: effect of thickness and stoichiometry of ceria," *Journal of Physical Chemistry C*, vol. 119, no. 7, pp. 3579–3588, 2015.

[13] G. R. Griffith and H. M. Burrow, "The value of research: using the Impact Tool to evaluate realised and anticipated benefits of the Cooperative Research Centre for Beef Genetic Technologies," *Animal Production Science*, vol. 55, no. 2, p. 133, 2015.

[14] C. S. Pimentel, J. McKenney, P. N. Firmino, T. Calvão, and M. P. Ayres, "Sublethal infection of different pine species by the pinewood nematode," *Plant Pathology*, vol. 69, no. 8, pp. 1565–1573, 2020.

[15] K. Han, "On a stochastic construction of the kinematics in discrete space–time," *Canadian Journal of Physics*, vol. 93, no. 5, pp. 496–502, 2015.

[16] W. Ting, "Construction of intelligent communication service based on artificial intelligence," *Electrical Engineering*, vol. 5, no. 12, pp. 19–34, 2019.

[17] L. Shun-jie, "Research on development countermeasures for farmer specialized cooperative on the background of new rural construction," *Journal of Investigative Medicine*, vol. 63, no. 8, article S66, 2015.

[18] C. Hongyu, "Research on the application of honeycomb structure dynamic algorithm in intelligent information management system," *Electrical Engineering*, vol. 9, no. 2, pp. 20–34, 2015.

[19] S. S. Rautaray and A. Agrawal, "Vision based hand gesture recognition for human computer interaction: a survey," *Artificial Intelligence Review*, vol. 43, no. 1, pp. 1–54, 2015.

[20] J. M. Roman-Belmonte, H. de la Corte-Rodriguez, and E. C. Rodriguez-Merchan, "How blockchain technology can change medicine," *Postgraduate Medicine*, vol. 130, no. 4, pp. 420–427, 2018.

[21] H. Subramanian, "Decentralized blockchain-based electronic marketplaces," *Communications of the ACM*, vol. 61, no. 1, pp. 78–84, 2017.

[22] H. I. Ozercan, A. M. Ileri, E. Ayday, and C. Alkan, "Realizing the potential of blockchain technologies in genomics," *Genome Research*, vol. 28, no. 9, pp. 1255–1263, 2018.

[23] S. Hall, B. Poller, C. Bailey et al., "Use of UV fluorescence-based simulation in evaluation of personal protective equipment worn for first assessment and care of a patient with suspected high consequence infectious disease," *Journal of Hospital Infection*, vol. 23, no. 6, pp. 13–24, 2018.

[24] Y. Zhang, R. H. Deng, X. Liu, and D. Zheng, "Blockchain based efficient and robust fair payment for outsourcing services in cloud computing," *Information Sciences*, vol. 462, pp. 262–277, 2018.

[25] K. Gammon, "Experimenting with blockchain: can one technology boost both data integrity and patients' pocketbooks?," *Nature Medicine*, vol. 24, no. 4, pp. 378–381, 2018.

[26] V. Sharma, I. You, F. Palmieri, D. N. K. Jayakody, and J. Li, "Secure and energy-efficient handover in fog networks using blockchain-based DMM," *IEEE Communications Magazine*, vol. 56, no. 5, pp. 22–31, 2018.

[27] L. Li, J. Liu, L. Cheng et al., "CreditCoin: a privacy-preserving blockchain-based incentive announcement network for communications of smart vehicles," *IEEE Transactions on Intelligent Transportation Systems*, vol. 19, no. 7, pp. 2204–2220, 2018.

[28] K. N. Khaqqi, J. J. Sikorski, K. Hadinoto, and M. Kraft, "Incorporating seller/buyer reputation-based system in blockchain-enabled emission trading application," *Applied Energy*, vol. 209, pp. 8–19, 2018.

[29] B. Hamdaoui, M. Alkalbani, T. Znati, and A. Rayes, "Unleashing the power of participatory IoT with blockchains for increased safety and situation awareness of smart cities," *IEEE Network*, vol. 34, no. 2, pp. 202–209, 2020.

[30] H. E. Pence, "Blockchain: will better data security change chemical education?," *Journal of Chemical Education*, vol. 97, no. 7, pp. 1815–1818, 2020.

[31] D. Jiang, G. Li, Y. Sun, J. Kong, and B. Tao, "Gesture recognition based on skeletonization algorithm and CNN with ASL database," *Multimedia Tools and Applications*, vol. 78, no. 21, pp. 29953–29970, 2019.

[32] Y. He, G. Li, Y. Liao et al., "Gesture recognition based on an improved local sparse representation classification algorithm," *Cluster Computing*, vol. 22, Supplement 5, pp. 10935–10946, 2019.

[33] W. Cheng, Y. Sun, G. Li, G. Jiang, and H. Liu, "Jointly network: a network based on CNN and RBM for gesture recognition," *Neural Computing and Applications*, vol. 31, no. S1, pp. 309–323, 2019.

[34] Y. Sang, H. Shen, Y. Tan, and N. Xiong, "Efficient protocols for privacy preserving matching against distributed datasets," in *Information and Communications Security. ICICS 2006. Lecture Notes in Computer Science, vol 4307*, P. Ning, S. Qing, and N. Li, Eds., pp. 210–227, Springer, Berlin, Heidelberg, 2006.

[35] F. Long, N. Xiong, A. V. Vasilakos, L. T. Yang, and F. Sun, "A sustainable heuristic QoS routing algorithm for pervasive multi-layered satellite wireless networks," *Wireless Networks*, vol. 16, no. 6, pp. 1657–1673, 2010.

[36] J. Li, N. Xiong, J. H. Park, C. Liu, S. MA, and S. E. Cho, "Intelligent model design of cluster supply chain with horizontal cooperation," *Journal of Intelligent Manufacturing*, vol. 23, no. 4, pp. 917–931, 2012.

[37] Z. Chen, D. Chen, Y. Zhang, X. Cheng, M. Zhang, and C. Wu, "Deep learning for autonomous ship-oriented small ship detection," *Safety Science*, vol. 130, article 104812, 2020.

[38] Z. Liu, B. Hu, B. Huang, L. Lang, H. Guo, and Y. Zhao, "Decision optimization of low-carbon dual-channel supply chain of auto parts based on smart city architecture," *Complexity*, vol. 2020, Article ID 2145951, 14 pages, 2020.

[39] L. Dong, W. Wu, Q. Guo, M. N. Satpute, T. Znati, and D. Z. du, "Reliability-aware offloading and allocation in multilevel edge computing system," *IEEE Transactions on Reliability*, vol. 9, no. 2, pp. 1–12, 2019.

[40] J. Hu, Y. Sun, G. Li, G. Jiang, and B. Tao, "Probability analysis for grasp planning facing the field of medical robotics," *Measurement*, vol. 141, pp. 227–234, 2019.

[41] W. Wei, H. Song, W. Li, P. Shen, and A. Vasilakos, "Gradient-driven parking navigation using a continuous information potential field based on wireless sensor network," *Information Sciences*, vol. 408, no. 2, pp. 100–114, 2017.

Hindawi
Wireless Communications and Mobile Computing
Volume 2020, Article ID 8870876, 6 pages
https://doi.org/10.1155/2020/8870876

Research Article

Research on Composition of Social Credibility Index Based on Artificial Intelligence Model

Na Liu and Nanke Ye

Public Administration, Hohai University, Nanjing 210000, China

Correspondence should be addressed to Na Liu; 140215050005@hhu.edu.cn

Received 9 July 2020; Revised 9 September 2020; Accepted 24 September 2020; Published 14 October 2020

Academic Editor: Hongju Cheng

Copyright © 2020 Na Liu and Nanke Ye. This is an open access article distributed under the Creative Commons Attribution License, which permits unrestricted use, distribution, and reproduction in any medium, provided the original work is properly cited.

Honesty refers to the fairness, justice, and responsibility of public power in social life. In order to enhance the trust of public power in society, it is necessary to analyze the social credibility indicator system. In order to achieve an accurate evaluation of social credibility, this article uses big data mining and artificial intelligence analysis methods to construct a social credibility evaluation index system for public power. First of all, this paper analyzes the distribution structure model of the public power social credibility index and analyzes the empirical mode decomposition and factor analysis of the public power social credibility evaluation data sequence in the social credibility feature distribution model. Secondly, this article constructs the public power social credit evaluation and artificial intelligence data sequence model. Using high-order cumulant features as a constraint operator, the accurate evaluation and consistent estimation of the social credibility index system of public power can be realized. The grey model is used to predict the social credibility of public power and realizes the optimized design of the evaluation model of public power social credibility. The simulation results show that the model has higher accuracy, better error convergence, and objectivity when designing the social reputation index system.

1. Introduction

Credibility, literally, refers to the trust power of the public. In reality, it refers to the trust that those public powers show in social life, such as fairness, justice, efficiency, humanity, democracy, and responsibility. Trust is at the heart of credibility [1, 2]. It is an indispensable quality of social organizations, industries, departments, and government agencies and is the basis of survival and standing. Credibility as an intangible asset is gradually formed in the long-term development, reflecting an irreplaceable authority [3]. However, the credibility of the current authority, such as the justice sector, which symbolizes fairness and justice, is in some places a coalition of power. In the face of power and money, some judges can turn black and white, bend the law for selfish ends, and brazenly make false and false cases [4]. Even the most authoritative departments of industry and commerce and notaries are constantly questioned. In some places, trade and industry bureaus can openly issue certificates of competency for fake and shoddy products, making them popular in the market. Some notaries even notarized the living as dead [5]. In recent years, due to unfair notarization caused by more and more controversy, the notarization department went to the dock again and again. Such a credit-dependent industry is no longer credible, what else can be trusted? The occurrence of these events really exposed the loss of the credibility of the industry sector, causing people to pay attention to social integrity [6]. It is necessary to study a credible index evaluation system to improve the credibility of departments and promote the development of administrative departments.

Recently, the Well-off Society Research Center conducted a survey on the honesty of various social groups. The results showed that of the 49 social groups, the most honest ones included farmers, soldiers, and students. Trust in the government is plummeting [7]. Many interviewees said they no longer believed the various social survey data released by the authorities, saying the figures were false in whole or in large part. In order to promote the construction of social credibility, we need to study an effective evaluation index system of credibility [8]. Make clear the work responsibility and

function orientation of the public power's social credibility, ensure the coordination of the public power's social credibility work, so that the role of the organization's various departments can be brought into full play, the evaluation of public power's social credibility is based on the analysis of big data and artificial intelligence, and it can take the public power's social credibility as the platform of information transmission and interaction [9].

The index system of social credibility is constructed by using big data analysis method, and the evaluation of social credibility is realized with the method of data prediction and evaluation. This paper puts forward a social credibility index structure and evaluation system based on the artificial intelligence model, and it uses big data mining and artificial intelligence analysis method to construct the social credibility evaluation index system of the public power [10]. This paper analyzes the distribution structure model of the social credibility index of public power and analyzes the empirical modal decomposition and factor analysis of the social credibility evaluation data series of public power in the distribution model of social credibility characteristic distribution. The data sequence model of public power's social credibility evaluation and analysis of artificial intelligence is constructed [11]. Big data mining and artificial intelligence analysis are used to extract the features of the performance quantization sequence, and the higher-order cumulant feature is used as the postconvergence operator. To realize the accurate evaluation and consistency estimation of the social credibility index system of public power [12]. The Grey model is used to predict the social credibility of public power, and the optimization design of public power social credibility evaluation model is realized. Finally, the performance test is carried out through the simulation experiment, which shows the superior performance of this method in improving the accuracy of social credibility evaluation.

2. Data Analysis and Preprocessing Social Credibility Evaluation Model

2.1. Analysis of the Quantitative Evaluation Data of Public Power's Social Credibility. In order to realize the accurate evaluation of the public power's social credibility, the quantitative evaluation of the public power's social credibility is carried out by using the statistical characteristic sequence analysis method [12]. Construct the data transmission structure model of the public power's social credibility quantitative evaluation statistical characteristic sequence; Quantitative evaluation of social credibility of public power the mathematical evolution model of statistical feature sequence can be constructed according to the quantitative characteristics such as historical evaluation data of public power social credibility [13].

Based on the above analysis, the artificial intelligence analysis flow of the social credibility index evaluation system designed in this paper is shown in Figure 1.

The management analysis is carried out on the evolvement object structure of public power's social credibility. The ontology model of social credibility evaluation is obtained, and the transmission structure model of the statistical characteristic sequence of quantitative evaluation of

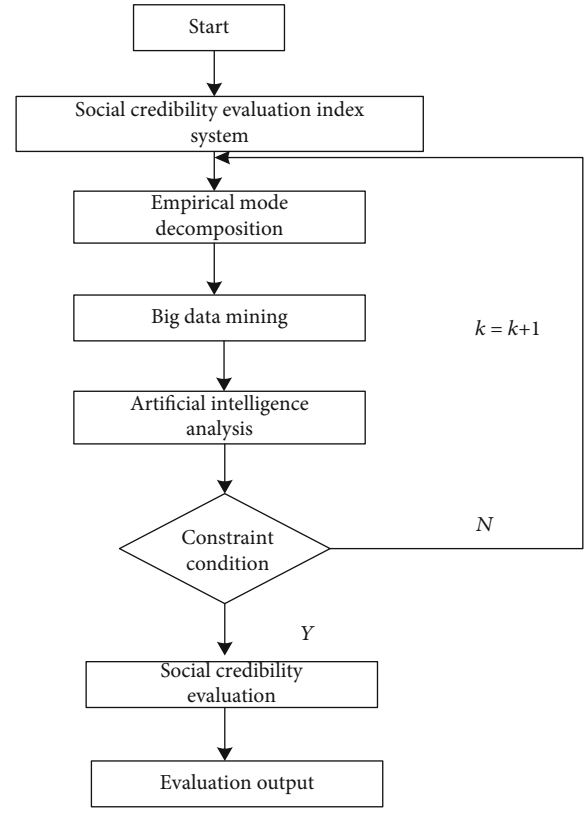

Figure 1: Artificial intelligence analysis process of social credibility index evaluation system.

social credibility of public power expressed by the directed label graph is $O = (C, I, P, Hc, R, A^0)$. Among them, two groups of ontology fragment set $G(O) = (V, E, L_V, L_E, \mu, \eta)$ and edge set $V = C$ of social credibility evaluation, $E = V \times V$ is the mapping function of two ontology models of social credibility evaluation as input. According to the mapping of the correlation sets of two index systems of social credibility evaluation, the feature extraction is carried out with an adaptive learning method [14]. At present, the fuzzy degree and compactness index of public power's social credibility evaluation is (RT_1, RT_2), and the quantitative set of public power evaluation index satisfies the constraint function [15, 16]:

$$F_j = \sum_{k=1}^{n} X_{kj}, Q_j = \sum_{k=1}^{n} \left(X_{kj}\right)^2. \quad (1)$$

According to the above description, the quantitative evaluation of the social credibility of public power is obtained [17]. The result of the directed marker graph structure analysis of the statistical feature sequence data is obtained, and the social credibility index of the public power is calculated as the semantic ontology characteristic state of the information flow of the public power system [18, 19]:

$$x_n = x(t_0 + n\Delta t) = h[\mathbf{z}(t_0 + n\Delta t)] + \omega_n. \quad (2)$$

In which, M is a directed marker graph structure window

feature function of d dimension, and the geometric invariant of the statistical feature sequence of public power's social credibility is calculated [20]. The interference vector model of the data on the object structure of the social credibility evaluation of public power is expressed as follows [5, 21]:

$$z(t) = s(t) + js(t) \otimes h(t) = s(t)+j\int_{-\infty}^{+\infty} \frac{s(u)}{t-u}du = s(t) + jH[s(t)]. \tag{3}$$

The relevant function of quantitative evaluation of social credibility of public power in statistical feature series data mining is constructed as:

$$X = \{x_1, x_2,\cdots x_n\} \subset R^s. \tag{4}$$

The index system of public power's social credibility can be regarded as a series of nonlinear statistical characteristics, and the trend of public power's social credibility is analyzed by the method of nonlinear statistical characteristic sequence analysis [7]. Based on the statistical analysis of the social credibility of public power, the fitting state model of describing the social credibility of public power by using a multivariate statistical characteristic equation is obtained as follows:

$$\begin{pmatrix} X \\ P(X) \end{pmatrix} = \begin{Bmatrix} a_1, & a_2, & \cdots, & a_m \\ p(a_1), & p(a_2), & \cdots, & p(a_m) \end{Bmatrix}. \tag{5}$$

In which, $0 \le p(a_i) \le 1 (i = 0, 1, 2,\cdots,m)$ and $\sum_{i=1}^{m} p(a_i) = 1$, the autoregressive statistical characteristic parameters representing the social credibility of public power, a_{ii} are obtained by decomposing the covariance matrix of the solution vector of the statistical equation, and the principal component of the statistical characteristic information is obtained [8]. In the feature space of the social credibility distribution, the entropy of the distribution characteristic information of the public power's social credibility is obtained through the discrete and analytic processing of the data [9]:

$$H(X) = E(I(a_i)) = -\sum_{i=1}^{m} p(a_i)\ \log_2 p(a_i). \tag{6}$$

On the basis of the above analysis, the collection of quantitative evaluation data of social credibility of public power and the reorganization of distributed structure are realized, which provides an accurate data input basis for social credibility evaluation and prediction [10].

2.2. Feature Decomposition and Preprocessing of Evaluation Data of Society. In the social credibility characteristic distribution model, the social credibility evaluation data sequence of public power is decomposed by empirical mode decomposition and characteristic decomposition, and the social credibility evaluation data sequence model and artificial intelligence analysis are carried out, and the public power's social credibility system is distributed as a two-order system [11]. Using the stochastic analysis model, we get the public credibility test data sequence x of the public power. The expression of the auxiliary spatial test cumulative j is

$$\text{Corr} = \frac{\langle (x_n - \bar{x})(x_{n-d} - \bar{x})(x_{n-D} - \bar{x})\rangle}{\langle (x_n - \bar{x})^3 \rangle}. \tag{7}$$

In which, x_n represents the statistical element of public power's social credibility information $D = 2d$, d indicates the sampling statistical delay of public power's social credibility, SD indicates the predictor of public power's social credibility, and $\langle x(n)\rangle$ represents the mean value of $x(n)$:

$$\langle x(n)\rangle = 1/N \sum_{n=1}^{N} x(n). \tag{8}$$

For a continuous public power social credibility evaluation data series, each spatial solution vector of the social credibility of public power training subset $S_i (i = 1, 2,\cdots,L)$, statistical feature analysis, and regional differential equation description common are used, and the empirical mode decomposition process of social credibility of common power is expressed as follows [12]:

$$\begin{aligned} c_{1x}(\tau) &= E\{x(n)\} = 0, \\ c_{2x}(\tau) &= E\{x(n)x(n+\tau)\} = r(\tau), \\ c_{kx}(\tau_1, \tau_2,\cdots,\tau_{k-1}) &\equiv 0 (k \ge 3). \end{aligned} \tag{9}$$

While $q = 2$, the social credibility information vector of the public power satisfies the convergence condition of the constraint function of the differential equation, and the constraint characteristic decomposition formula of the social credibility is obtained as follows:

$$\Psi_x(\omega) = \ln \Phi_x(\omega) = -\frac{1}{2}\omega^2\sigma^2. \tag{10}$$

Based on the factor analysis of the social credibility of public power, the characteristics of association rules are obtained as follows:

$$g\left(x_i, y_j \mid \mu_k, \sigma_k^2\right) = \prod_{k=1}^{K} a_k \frac{1}{\sqrt{2\pi\sigma_k^2}}\ \exp\left\{-\frac{(x_i - \mu_k)^2}{2\sigma_k^2}\right\}. \tag{11}$$

In which, $a_{ij} \in \boldsymbol{GF}(2^n)$ is the vector field of the data sequence of social credibility evaluation of public power under the condition of global gradual stability, and $u \mapsto u_\lambda$ is the descriptive statistical characteristic value of social credibility [12].

3. Index Composition and Evaluation Model Optimization of Social Credibility

Big data mining and artificial intelligence analysis are used to extract the features of social credibility quantitative series [22]. A time-dimensional quantitative evaluation of the

social credibility of public power is introduced in this paper. Using $F^{2\alpha/\pi} = \sum_{i=0}^{3} a_i(\alpha) W^i$ to calculate the social credibility of public power, the characteristic value and eigenvector of statistical feature series are evaluated, and $S = \sqrt{\Delta t \Delta f}$ is chosen to decompose into a fractional Fourier transform scale, and the common value is obtained by artificial intelligence analysis method [23]. Quantitative Evaluation of the Social credibility of the Common Power the sequence of statistical features $x(t)$ [24]:

$$x(t) = g(t) \exp\left[-j\pi t^2 \tan(\alpha/2)\right]. \tag{12}$$

The interval length of the statistical characteristic sequence $x(t)$ is equal to the dimensionless quantity, that is $\Delta x = \sqrt{\Delta t \Delta f}$, the two intervals are normalized to $[-\Delta x/2, \Delta x/2]$. The artificial intelligence analysis method is adopted to calculate the statistical characteristic sequence of the social credibility index under a single random variable, which comprises the following steps [25]:

$$x(t) e^{j\pi t^2 \cot\alpha} = \sum_{n=-N}^{N} x\left(\frac{n}{2\Delta x}\right) e^{\left(j\pi(\cot\alpha) n^2/(2\Delta x)^2\right)} \sin c\left[2\Delta x\left(t - \frac{n}{2\Delta x}\right)\right]. \tag{13}$$

A set of orthogonal chirp bases is used to expand the space of characteristic function of social credibility index, and the data envelopment feature of social credibility index is obtained [26]:

$$X_p(u) = A_\alpha \exp\left(j\pi(\cot\alpha)u^2\right) \sum_{n=-N}^{N} x\left(\frac{n}{2\Delta x}\right) \exp\left[\frac{j\pi(\cot\alpha)n^2}{(2\Delta x)^2}\right] \times \int_{-\infty}^{\infty} \exp\left[-j2\pi(\csc\alpha)ut\right] \sin c\left[2\Delta x\left(t - \frac{n}{2\Delta x}\right)\right] dt. \tag{14}$$

The integral term in the upper expression is equal to [27]:

$$\exp\left[\frac{-j2\pi(\csc\alpha)xn}{2\Delta x}\right] \frac{1}{2\Delta x} \operatorname{rect}\left[\frac{(\csc\alpha)x}{2\Delta x}\right]. \tag{15}$$

Quantitative evaluation of the social credibility of public power the second derivative of the second characteristic function $\operatorname{rect}[(\csc\alpha)x/2\Delta x]$ in the support region $|x| \le \Delta x/2$ of the transformation function can be expressed as [28]:

$$X_p\left(\frac{m}{2\Delta x}\right) = \frac{A_\alpha}{2\Delta x} \sum_{n=-N}^{N} e^{j\pi(\cot\alpha)m^2 - j2\pi(\csc\alpha)mn + j\pi(\cot\alpha)n^2/(2\Delta x)^2} x\left(\frac{n}{2\Delta x}\right). \tag{16}$$

In the reconstructed quantitative sequence of social credibility of public power, any point in the evolution of social credibility is expressed as $\boldsymbol{X}_{\eta(n)}$, and the nearest neighbor in the high-dimensional Grey model of social credibility of public power is expressed as $\boldsymbol{X}_n$, using a large number [22]. According to mining and artificial intelligence analysis methods, the feature extraction of the performance quantization sequence is carried out, and the higher-order cumulant feature is used as the postconvergence operator to realize the accurate evaluation and consistency estimation of the social credibility index system of public power. Finally, the model is constructed and optimized according to the social credibility index.

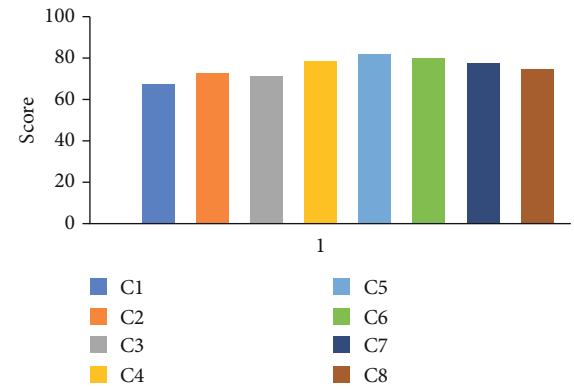

Figure 2: Statistical big data analysis of social credibility evaluation.

4. Simulation Experiment and Result Analysis

In order to test the practical application performance of this algorithm in the analysis and evaluation of the public power's social credibility index, the simulation experiment is carried out. The experiment uses the MATLAB simulation tool to analyze the data and public rights.

The test sample set of social credibility of force comes from the national statistical department. The time of data collection is from 30 April 2017 to 5 June 2018, the weight of artificial intelligence analysis is 0.23, the correlation coefficient is 1.24, and the social credibility index is evaluated. The number of iterations is 10000. According to the above simulation parameters, the social credibility is evaluated. In the simulation experiment, the data sampling result of Figure 2 is used as the research object to realize the research and evaluation of the credibility index. The confidence level comparison result obtained by the credibility evaluation is shown in Figures 3 and 4.

Through the above experimental results, it can be observed that with the increase of the number of iterative steps, the error of social credibility evaluation is reduced, and the prediction error of public power in this paper is smaller than that of the traditional method, and the social credibility of public power is lower than that of traditional method. The clustering and fusion of data and information improves the accuracy of prediction, promotes the reform and upgrading of social functional departments, and enhances the public credibility.

5. Conclusions

In order to realize the accurate evaluation of social credibility, a social credibility index structure and evaluation system based on the artificial intelligence model is proposed. Big

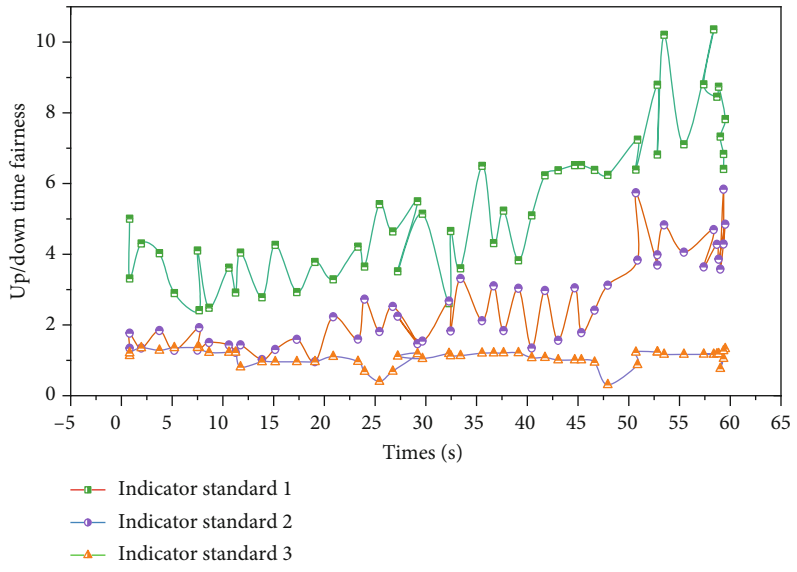

Figure 3: Confidence and time comparison of credibility assessment.

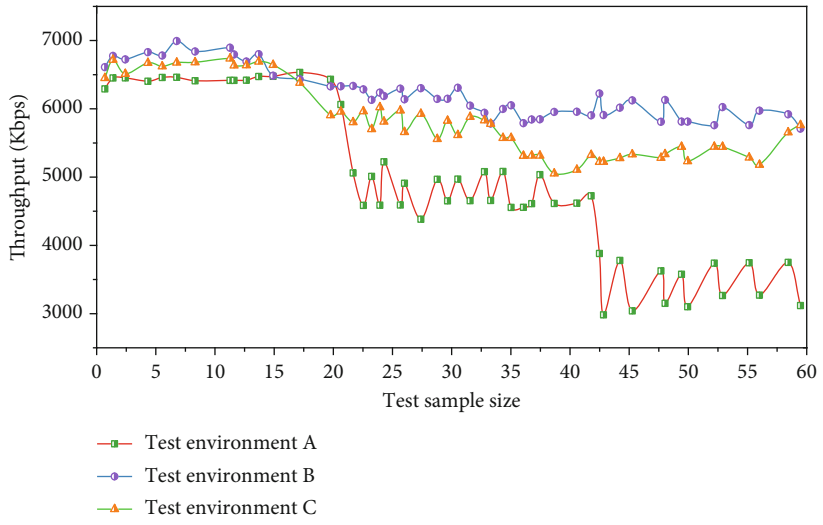

Figure 4: Network test effect diagram of social credibility index system.

data mining and artificial intelligence analysis method are used to construct the social credibility evaluation index system of the public power. This paper analyzes the distribution structure model of the social credibility index of public power and analyzes the empirical modal decomposition and factor analysis of the social credibility evaluation data series of public power in the distribution model of social credibility characteristic distribution. Construct the data sequence model of public power's social credibility evaluation and analysis of artificial intelligence.

Big data mining and artificial intelligence analysis are used to extract the feature of the performance quantization sequence. The high order cumulant feature is used as the constraint operator to realize the accurate evaluation and consistency estimation of the public power's social credibility index system. The Grey model is used to predict the social credibility of public power, and the optimization design of public power social credibility evaluation model is realized. The simulation results show that the model has higher accuracy, better error convergence, and objectivity in the design of the social credibility index system. This method has good application value in social credibility evaluation and index analysis.

Data Availability

All experimental data can be contacted by the corresponding author.

Conflicts of Interest

The authors declare that there is no conflict of interest regarding the publication of this paper.

References

[1] W. Meng, D. Yang, and H. Huang, "Prediction of China's sulfur dioxide emissions by discrete grey model with fractional order generation operators," *Complexity*, vol. 2018, Article ID 8610679, 13 pages, 2018.

[2] G. F. Fan, A. Wang, and W. C. Hong, "Combining grey model and self-adapting intelligent grey model with genetic algorithm and annual share changes in natural gas demand forecasting," *Energies*, vol. 11, no. 7, 2018.

[3] B. Zeng and C. Li, "Forecasting the natural gas demand in China using a self-adapting intelligent grey model," *Energy*, vol. 112, pp. 810–825, 2016.

[4] Y. Yuan, H. Zhao, X. Yuan, L. Chen, and X. Lei, "Application of fractional order-based grey power model in water consumption prediction," *Environmental Earth Sciences*, vol. 78, no. 8, 2019.

[5] C. L. Spash and I. Aslaksen, "Re-establishing an ecological discourse in the policy debate over how to value ecosystems and biodiversity," *Journal of Environmental Management*, vol. 159, pp. 245–253, 2015.

[6] C. Shao, G. L. Ciampaglia, O. Varol, K. C. Yang, A. Flammini, and F. Menczer, "The spread of low-credibility content by social bots," *Nature Communications*, vol. 9, no. 1, 2018.

[7] B. A. Nosek and D. Lakens, "Registered reports: a method to increase the credibility of published results," *Social Psychology*, vol. 45, no. 3, pp. 137–141, 2014.

[8] X. Lin, P. R. Spence, and K. A. Lachlan, "Social media and credibility indicators: the effect of influence cues," *Computers in Human Behavior*, vol. 63, pp. 264–271, 2016.

[9] J. Kirchherr, H. Pohlner, and K. J. Charles, "Cleaning up the big muddy: a meta-synthesis of the research on the social impact of dams," *Environmental Impact Assessment Review*, vol. 60, pp. 115–125, 2016.

[10] J. Imlawi, D. Gregg, and J. Karimi, "Student engagement in course-based social networks: the impact of instructor credibility and use of communication," *Computers & Education*, vol. 88, pp. 84–96, 2015.

[11] T. Hoang, J. Liu, N. Pratt et al., "Authenticity and credibility aware detection of adverse drug events from social media," *International Journal of Medical Informatics*, vol. 120, pp. 101–115, 2018.

[12] N. Hajli, "Ethical environment in the online communities by information credibility: a social media perspective," *Journal of Business Ethics*, vol. 149, no. 4, pp. 799–810, 2018.

[13] M. de los Ángeles Fernandez, M. de los Ángeles Sanromán, S. Marks et al., "A grey box model of glucose fermentation and syntrophic oxidation in microbial fuel cells," *Bioresource Technology*, vol. 200, pp. 396–404, 2016.

[14] J. Best, "The inflation game: targets, practices and the social production of monetary credibility," *New Political Economy*, vol. 24, no. 5, pp. 623–640, 2019.

[15] N. C. Benda, L. T. Das, E. L. Abramson et al., ""How did you get to this number?" Stakeholder needs for implementing predictive analytics: a pre-implementation qualitative study," *Journal of the American Medical Informatics Association*, vol. 27, no. 5, pp. 709–716, 2020.

[16] S. Aladhadh, X. Zhang, and M. Sanderson, "Location impact on source and linguistic features for information credibility of social media," *Online Information Review*, vol. 43, no. 1, pp. 89–112, 2019.

[17] S. Bi, "Intelligent system for english translation using automated knowledge base," *Journal of Intelligent and Fuzzy Systems*, vol. 5, pp. 1–10, 2020.

[18] Y. Gui and G. Zeng, "Joint learning of visual and spatial features for edit propagation from a single image," *The Visual Computer*, vol. 36, no. 3, pp. 469–482, 2020.

[19] Y. Wang, Z. Shen, and Y. Jiang, "Analyzing maternal mortality rate in rural China by Grey-Markov model," *Medicine*, vol. 98, no. 6, article e14384, 2019.

[20] X. Xiao, M. J. Hui, Z. Liu, and W. R. Qiu, "iCataly-PseAAC: identification of enzymes catalytic sites using sequence evolution information with grey model GM (2,1)," *Journal of Membrane Biology*, vol. 248, no. 6, pp. 1033–1041, 2015.

[21] B. Urrutikoetxea Arrieta, A. I. Polo Pena, and C. Martinez Medina, "The moderating effect of blogger social influence and the reader's experience on loyalty toward the blogger," *Online Information Review*, vol. 43, no. 3, pp. 326–349, 2019.

[22] D. Jiang, G. Li, Y. Sun, J. Kong, and B. Tao, "Gesture recognition based on skeletonization algorithm and CNN with ASL database," *Multimedia Tools and Applications*, vol. 78, no. 21, pp. 29953–29970, 2019.

[23] Y. He, G. Li, Y. Liao et al., "Gesture recognition based on an improved local sparse representation classification algorithm," *Cluster Computing*, vol. 22, no. S5, pp. 10935–10946, 2019.

[24] W. Cheng, Y. Sun, G. Li, G. Jiang, and H. Liu, "Jointly network: a network based on CNN and RBM for gesture recognition," *Neural Computing and Applications*, vol. 31, no. S1, pp. 309–323, 2019.

[25] Y. Sang, H. Shen, Y. Tan, and N. Xiong, "Efficient protocols for privacy preserving matching against distributed datasets," *International Conference on Information and Communications Security*, vol. 4307, 2006.

[26] F. Long, N. Xiong, A. V. Vasilakos, L. T. Yang, and F. Sun, "A sustainable heuristic QoS routing algorithm for pervasive multi-layered satellite wireless networks," *Wireless Networks*, vol. 16, no. 6, pp. 1657–1673, 2010.

[27] J. Li, N. Xiong, J. H. Park, C. Liu, S. MA, and S. E. Cho, "Intelligent model design of cluster supply chain with horizontal cooperation," *Journal of Intelligent Manufacturing*, vol. 23, no. 4, pp. 917–931, 2012.

[28] Z. Liu, B. Hu, B. Huang, L. Lang, H. Guo, and Y. Zhao, "Decision optimization of low-carbon dual-channel supply chain of auto parts based on smart city architecture," *Complexity*, vol. 2020, no. 5, Article ID 2145951, p. 14, 2020.

[29] L. Dong, Q. Guo, and W. Wu, "Speech corpora subset selection based on time-continuous utterances features," *Journal of Combinatorial Optimization*, vol. 37, no. 4, pp. 1237–1248, 2019.

Hindawi
Wireless Communications and Mobile Computing
Volume 2023, Article ID 9819036, 1 page
https://doi.org/10.1155/2023/9819036

Retraction

Retracted: A Real-Time Garbage Truck Supervision and Data Statistics Method Based on Object Detection

Wireless Communications and Mobile Computing

Received 8 August 2023; Accepted 8 August 2023; Published 9 August 2023

Copyright © 2023 Wireless Communications and Mobile Computing. This is an open access article distributed under the Creative Commons Attribution License, which permits unrestricted use, distribution, and reproduction in any medium, provided the original work is properly cited.

This article has been retracted by Hindawi following an investigation undertaken by the publisher [1]. This investigation has uncovered evidence of one or more of the following indicators of systematic manipulation of the publication process:

(1) Discrepancies in scope
(2) Discrepancies in the description of the research reported
(3) Discrepancies between the availability of data and the research described
(4) Inappropriate citations
(5) Incoherent, meaningless and/or irrelevant content included in the article
(6) Peer-review manipulation

The presence of these indicators undermines our confidence in the integrity of the article's content and we cannot, therefore, vouch for its reliability. Please note that this notice is intended solely to alert readers that the content of this article is unreliable. We have not investigated whether authors were aware of or involved in the systematic manipulation of the publication process.

Wiley and Hindawi regrets that the usual quality checks did not identify these issues before publication and have since put additional measures in place to safeguard research integrity.

We wish to credit our own Research Integrity and Research Publishing teams and anonymous and named external researchers and research integrity experts for contributing to this investigation.

The corresponding author, as the representative of all authors, has been given the opportunity to register their agreement or disagreement to this retraction. We have kept a record of any response received.

References

[1] X. Zhang, Y. Gao, G. Xiao, B. Feng, and W. Chen, "A Real-Time Garbage Truck Supervision and Data Statistics Method Based on Object Detection," *Wireless Communications and Mobile Computing*, vol. 2020, Article ID 8827310, 9 pages, 2020.

Hindawi
Wireless Communications and Mobile Computing
Volume 2020, Article ID 8827310, 9 pages
https://doi.org/10.1155/2020/8827310

WILEY | Hindawi

Research Article

A Real-Time Garbage Truck Supervision and Data Statistics Method Based on Object Detection

Xuanyu Zhang[1], **Yining Gao**[2], **Guangyi Xiao**[2], **Bo Feng**[2] and **Wenshu Chen**[3]

[1]*Changsha Zoomlion Environmental Industry Co. Ltd, Changsha 410006, China*
[2]*College of Computer Science and Electronic Engineering, Hunan University, Changsha 410006, China*
[3]*College of Computer Science, University of Bristol, Bristol BS8 1QU, UK*

Correspondence should be addressed to Guangyi Xiao; gyxiao@hnu.edu.cn

Received 25 August 2020; Revised 8 September 2020; Accepted 28 September 2020; Published 12 October 2020

Academic Editor: Hongju Cheng

Copyright © 2020 Xuanyu Zhang et al. This is an open access article distributed under the Creative Commons Attribution License, which permits unrestricted use, distribution, and reproduction in any medium, provided the original work is properly cited.

Garbage classification is difficult to supervise in the stage of collection and transportation. This paper proposes a computer vision-based method for intelligent supervision and workload statistics of garbage trucks. In terms of hardware, this paper deploys a camera and an image processing unit with NPU based on the original on-board computing and communication equipment. In terms of software, this paper uses the YOLOv3-tiny algorithm on the image processing unit to perform real-time target detection on garbage truck work, collects statistics on the color, specifications, and quantity of garbage bins cleaned by the garbage truck, and uploads the results to the server for recording and display. The proposed method has low deployment and maintenance costs while maintaining excellent accuracy and real-time performance, which makes it have good commercial application value.

RETRACTED

1. Introduction

At present, garbage classification has received great attention. Garbage classification can not only play the role of environmental protection but also can recycle and reuse some resources, which has high social benefits. Garbage is divided into four categories and placed in four-colored trash cans, including recyclables (blue), kitchen waste (green), hazardous waste (red), and other garbage (black) [1]. Four types of trash cans are shown in Figure 1.

The work of garbage can collection and transportation is to collect and transport the garbage distributed in garbage cans all over the city. According to the regulations, each garbage truck can only collect and transport garbage of a single category. However, due to the lack of effective regulatory means, there is a phenomenon that on-board staffs do not follow the regulations and pour other types of garbage into their trucks.

Meanwhile, due to the lack of effective statistical data means, the problem of vehicle scheduling without reliable data basis often leads to great differences in the workload of each garbage truck. With the development of computer technology, mobile devices have the conditions to deploy artificial intelligence-related technologies. The development of neural network processing unit (NPU) has greatly reduced the difficulty and cost of deployment of the popular deep learning technology. Computer vision is an important branch of artificial intelligence. Through the deep learning method based on convolutional neural network, the computer can obtain the environment perception ability similar to human vision by analyzing the pictures captured by the camera. This paper attempts to use computer vision technology to supervise and count the workloads of the garbage trucks. The collection data mainly includes the amounts, colors, and specifications of garbage cans collected by garbage trucks. The main contributions of this paper are as follows.

Figure 1: Trash bin for holding different sorts of trash.

(i) A hardware deployment scheme based on the image processing unit with NPU is proposed

(ii) Based on the analysis of the image characteristics of the garbage can, a dataset for garbage can recognition is established by using the garbage can color as the classification basis

(iii) An intelligent supervision and workload statistics algorithm for garbage trucks is proposed based on the trained YOLOv3-tiny model

The structure of the paper is as follows. Section 2 is the related work of the paper, including the current supervision methods for garbage trucks, the types of garbage trucks, and the deployment and application of various target detection algorithms on mobile devices. Section 3 describes the method of this paper in detail from the perspective of hardware deployment scheme and object detection algorithm. Section 4 is the experiment, which gives the test results of this paper in the real environment. Section 5 is summary and prospect.

2. Related Works

At present, there is a monitoring and statistical method for garbage trucks in Zhonglian Environment, which is achieved by installing RFID tags with specific information on the bottom of each garbage can. However, the working environment of trash cans is often harsh, and RFID tags are prone to damage or fall off. In addition, not all garbage cans on the market are produced by the same company. When there is a difference in the data format of the RFID tag and the receiver, or when dealing with garbage cans without RFID, this method will completely lose the ability to work. Most of the garbage can collection and transportation vehicles in China adopt self-loading and unloading design. According to the different loading position of the trash can, they can be divided into two types: side feeding (garbage dumped from side) and rear feeding type (garbage dumped from back), as shown in Figure 2.

The side feeding design can clean only one trash can at a time, while the rear feeding type can clean up two trash cans at the same time. According to the data of Zhonglian Environment, its company produces more than 8000 rear feeding

(a) Side feeding garbage truck

(b) Rear feeding garbage truck

Figure 2: Side feeding and rear feeding garbage trucks.

garbage trucks each year but only about 4000 side feeding garbage trucks. Because the rear feeding garbage truck has greater possession and identification difficulty, this paper takes it as an example to carry out research and experiment, but this method can also be extended to the side feeding garbage truck for deployment.

Object detection technology is the cornerstone of many computers vision research, which is used to locate, track, and analyze all potential objects in images [2]. The traditional object detection is mostly realized according to the steps of region selection and feature classification. There are a variety of feature extraction operators and classifiers, for example, the features like SIFT [3], HOG [4], and LBP [5] and the classifiers like SVM [6], Adaboost [7], and so on. However, due to the characteristics of human design, the generalization ability of traditional target detection methods is very weak, and it is easy to be affected by external environmental factors. With the development of deep learning, object detection has gradually shifted to the implementation based on convolution neural network, such as the famous R-CNN [8] and SSD [9]. The object detection based on deep learning breaks through the limitation of artificially setting the target image features, and the accuracy and robustness of object detection are greatly improved by automatically learning the possible features of the target through convolution neural network. However, most of the object detection methods based on convolution neural network have high requirements for computing power, which makes it face real-time challenges and is not conducive to the deployment of mobile devices. In the past few years, more and more scholars have begun to pay attention to the real-time performance of object detection, and some excellent real-time performance object detection algorithms such as Faster R-CNN [10] and YOLO [11–13] have emerged. Target detection in vehicle environment has also been widely concerned by the academic community, but most of them focus on the auxiliary driving of family cars, such as pedestrian detection, traffic sign detection, and so on. In [14], YOLOv2 was used for traffic sign recognition, which can effectively detect three types of traffic signs in real time.

RETRACTED

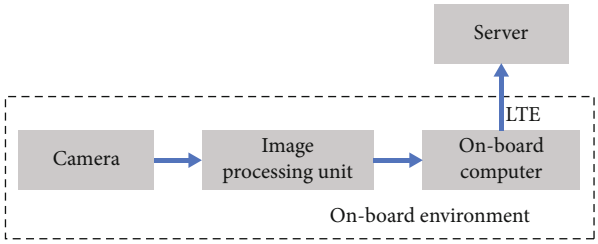

Figure 3: Hardware deployment.

In [15], the real-time pedestrian detection was realized on a newly developed embedded device through HOG + SVM. In [16], truck drivers' potentially dangerous driving behaviors were analyzed based on 11-month digital tachograph data and multilevel modeling approach. In [17], an allocation model was used to understand individualization driving states. Although the recognition of the movement process of the trash can is actually related to action recognition, compared to human gesture recognition, the task is obviously more regular and simple. We do get some inspiration from gesture recognition. Linear discriminant analysis (LDA) and extreme learning machine (ELM) are very common in gesture recognition [18–20]. Machine learning is also applied in many gesture recognition [21–24]. There is also work to recognize gestures by combining some functions in Internet of Things (IoT) [25]. In addition to the vehicle environment, CNN also has a wide range of applications in other fields, such as Smart City [26–28], health care [29, 30], and transportation [31].What is more, network routing protocols are constantly being improved [32–34], and the progress of sensor networks [35–37] has greatly improved the reliability of IoT [38–40].

3. Methods

This paper creatively applies the object detection algorithm to the garbage truck for monitoring and data statistics. The following will elaborate on the method of this paper from the perspective of hardware deployment and software design.

3.1. Hardware Deployment. Due to the special environment of garbage truck, the hardware deployment scheme will be affected by such factors as power consumption, computing power, volume of devices, and so on. The angle of the camera, the transmission mode of the data, and the computing power of the image processing unit will all have an impact on the design of the software level of this paper. The overall hardware deployment scenario for this paper is shown in Figure 3.

Most garbage trucks have their own on-board computers with mobile network communication functions to record the vehicle's location and remaining fuel. Using the original data communication method can effectively reduce the deployment cost and difficulty. Only a waterproof camera and an image processing unit are installed on the truck in the design of this paper. The supervision and data statistics of the garbage truck work are realized through the software level. Because the garbage can is large and the computing power of the image processing unit is weak, the camera resolution selected in this paper is 640×480. With the front of the car as the front, the camera is arranged on the slant of the working position of the garbage can. Take the horizontal direction as 0 degree, the camera angle is about 10 degrees. When the trash can is at the highest position, it is necessary to ensure that the vertical direction of the trash can at the two positions is completely photographed, as shown in Figure 4. The sample photo taken during the process of turning the barrel once is shown in Figure 5.

The image processing unit has a neural network processing unit NPU, and the NPU calculation force is 3Tops. The CPU adopts ARM architecture. Compared with the traditional structure of x86 CPU plus GPU, the structure of ARM CPU plus NPU has lower power consumption and smaller volume, which is more suitable for deployment in the vehicle environment. The image processing unit communicates with the on-board computer through the serial port, transmits the detection results to the on-board computer with a specific format of data message, and then uploads the data to the server through the mobile network for recording and subsequent display.

3.2. Software Design. In this section, the dataset established in this paper is described, and then, the object detection algorithm is described.

3.2.1. Dataset. The training of object detection model is a kind of supervised learning, which needs to build a dataset with labels. Firstly, this paper analyzes the image characteristics of trash can. According to the different types of garbage, the garbage cans cleaned by the garbage collection and transportation trucks can be divided into four categories according to the color. The blue garbage cans contain recyclable garbage; the green garbage cans contain wet garbage; the red garbage cans contain harmful garbage, and the black garbage cans contain dry garbage.

At the same time, there are many different cubage of these bins; the most common are 120L and 240L. Because of the limitation of two-dimensional image, there is no essential difference in two-dimensional image between trash cans of different cubage, while the color information is a good feature in three channel images. Therefore, in this paper, the garbage cans are divided into four types according to the color characteristics.

In addition, because the turning operation of garbage truck is purely mechanical control, the detection program cannot obtain the signal of the beginning and end of turning through the electrical signal, so it is necessary to continuously perform object detection on the camera shot frames. This means that the garbage cans which are not in the turning state should not be the target of object detection. As shown in Figure 6, the part marked in the green box are the garbage cans in the process of turning, which should be labeled during data tagging, while the garbage cans marked in the red box are not in the process of turning, which should be regarded as the background (negative sample) and not be labeled during tagging.

Generally, when building a dataset, it should be taken into account that the object of identification of the model

RETRACTED

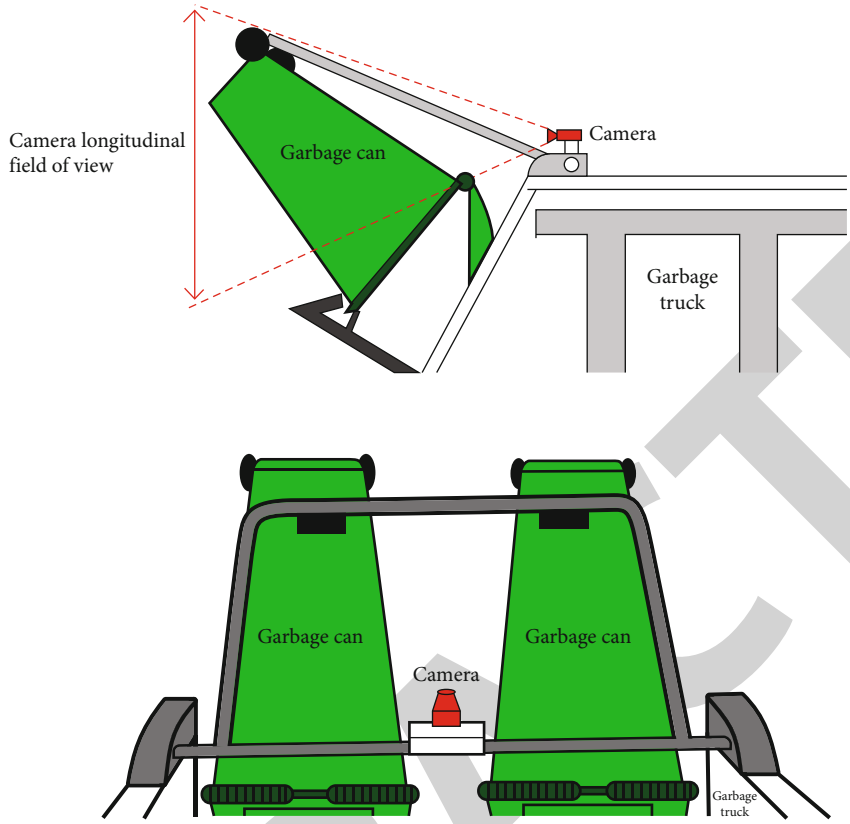

Figure 4: Camera installation location.

Figure 5: Some frames during the process of turning the trash.

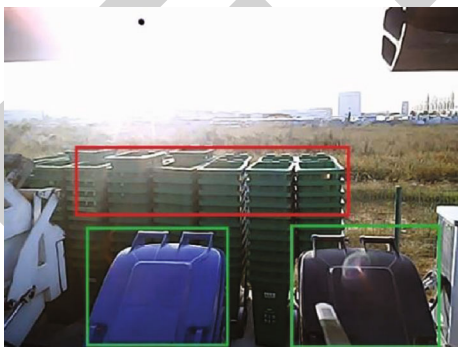

Figure 6: Schematic diagram of sample annotation.

Figure 7: Some training samples.

trained on it is "all kinds of trash cans in the process of bins turning," rather than simply "trash cans."

In this paper, the dataset is collected in the real environment by setting up the camera on the trucks, and it is obtained by recording screen and clipping. It contains a total of 3266 sample pictures, some of which are shown in Figure 7.

3.2.2. YOLOv3-Tiny Algorithm. The object detection algorithm used in this paper is YOLOv3-tiny. YOLOv3-tiny is a simplified version of YOLOv3. Compared with the complete version of YOLOv3, YOLOv3-tiny simplifies its backbone and only forecasts the bounding box in two fields of vision. The advantages of simple network and small amount of computation make it very suitable for deployment in this work scenario. Its backbone network uses a 7-layer convolutional

Table 1: Backbone of YOLOv3-tiny.

Type	Filter	Size	Output
Conv	16	3 × 3/1	416 × 416 × 16
Max		2 × 2/2	208 × 208 × 16
Conv	32	3 × 3/1	208 × 208 × 32
Max		2 × 2/2	104 × 104 × 32
Conv	64	3 × 3/1	104 × 104 × 64
Max		2 × 2/2	52 × 52 × 64
Conv	128	3 × 3/1	52 × 52 × 128
Max		2 × 2/2	26 × 26 × 128
Conv	256	3 × 3/1	26 × 26 × 256
Max		2 × 2/2	13 × 13 × 256
Conv	512	3 × 3/1	13 × 13 × 512
Max		2 × 2/1	13 × 13 × 512
Conv	1024	3 × 3/1	13 × 13 × 1024

layer plus a maximum pooling layer network structure, as shown in Table 1.

The loss function of the YOLO series algorithm needs to be measured in three aspects, namely, the coordinates of the object, the confidence score, and the category. The coordinates are calculated by the sum of squares of the offset function, and the confidence and classification are calculated by the cross-entropy loss function. The overall loss function is expressed as shown in Formula (1).

$$\begin{aligned}\text{loss}(\text{object}) = {} & \lambda_{\text{coord}} \sum_{i=0}^{K\times K} \sum_{j=0}^{M} I_{ij}^{\text{obj}} \left[(x_i - \hat{x}_i)^2 + (y_i - \hat{y}_i)^2 \right] \\ & + \sum_{i=0}^{K\times K} \sum_{j=0}^{M} I_{ij}^{\text{obj}} \left[\hat{C}_i \log (C_i) \right. \\ & \left. + \left(1 - \hat{C}_i\right) \log (1 - C_i) \right] \\ & - \lambda_{\text{noobj}} \sum_{i=0}^{K\times K} \sum_{j=0}^{M} I_{ij}^{\text{obj}} \left[\hat{C}_i \log (C_i) \right. \\ & \left. + \left(1 - \hat{C}_i\right) \log (1 - C_i) \right] \\ & - \sum_{i=0}^{K\times K} I_{ij}^{\text{obj}} \sum_{c\in\text{classes}} \left[\hat{p}_i(c) \log (p_i(c)) \right. \\ & \left. + (1 - \hat{p}_i(c)) \log (1 - p_i(c)) \right]. \end{aligned} \tag{1}$$

In which, λ_{coord} represents the penalty coefficient of coordinate prediction, λ_{noobj} indicates that it does not contain the target penalty coefficient, K represents the number of grid divisions in the prediction, and M represents the number of boundary boxes predicted by a single grid. I_{ij}^{obj} and I_{ij}^{noobj} indicate that the object is detected and not detected in the i grid and the j boundary box. x, y, w, and h represent the upper-left coordinate and width-height of the object, C represents the confidence level, and $p_i(c)$ represents the probability that the target in the i-th grid belongs to a certain category. Superscript ^ represents the true value.

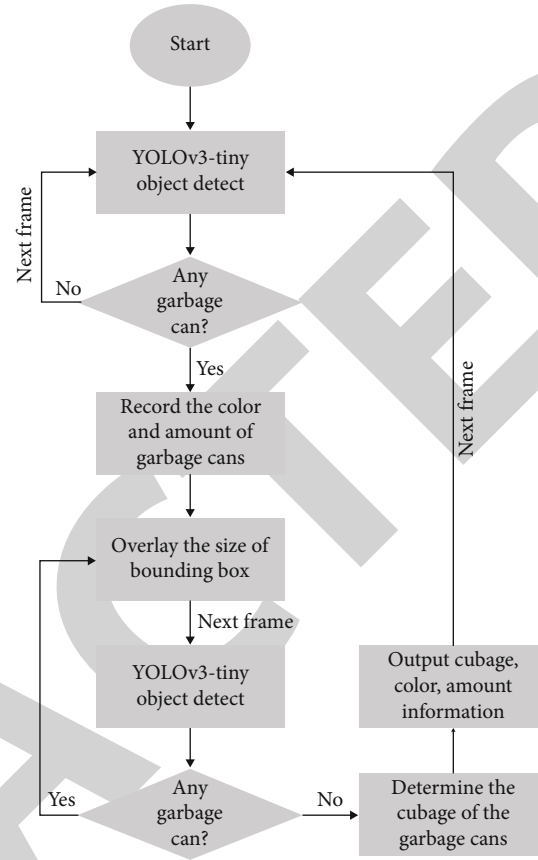

Figure 8: Flow chart of data statistics algorithm.

3.2.3. Data Statistics. The process of turning the trash can is determined by whether there is a trash can in the frame, and the statistical process of the data is shown in Figure 8.

When the object detection algorithm detects the garbage can in a frame, the program is regarded as the process of turning the garbage can has begun. Afterwards, when the object detection program cannot detect the garbage can in the screen, it shows that the process of turning the bucket is over. Meanwhile, the number of trash bin targets in a frame is the number of trash bins. Since the rear-feeding garbage truck may operate two garbage bins at the same time during operation, it is necessary to distinguish between the left and right garbage bins. The experiment found that the change of the x-coordinate of the trash bin target during the entire barrel turning process was small. In this paper, according to the x-axis coordinates of the target, whether a trash can is located in the left position or the right position is calibrated. The judgment of the trash can cubage is special. Because the size of the trash can is constantly changing in the whole turning process, the size of the object bounding box cannot be directly used to determine the cubage of the trash can. Therefore, in the process of turning over the bin, the size of the object bounding box in each frame is superimposed, and the final sum is used to judge the cubage of the bin.

RETRACTED

Vehicle service data

Serial Number	Route Number	Vehicle Number	Garbage can Color	Garbage can Cubage	time	location
1	CG0009	XA G0040	Green Green	240L 240L	2020-02-07 07:22:44	Yuelu District, Changsha
2	CG0009	XA G0040	Green	240L	2020-02-07 07:28:19	Yuelu District, Changsha
3	CG0009	XA G0040	Green	120L	2020-02-07 07:44:23	Yuelu District, Changsha
4	CG0009	XA G0040	Green	240L	2020-02-07 07:45:18	Yuelu District, Changsha
5	CG0009	XA G0040	Blue	240L	2020-02-07 07:46:24	Yuelu District, Changsha
6	CG0009	XA G0040	Black Green	240L 240L	2020-02-07 07:47:33	Yuelu District, Changsha
7	CG0009	XA G0040	Green	120L	2020-02-07 07:48:25	Yuelu District, Changsha
8	CG0009	XA G0040	Green	240L	2020-02-07 07:49:10	Yuelu District, Changsha
9	CG0009	XA G0040	Green	240L	2020-02-07 07:42:27	Yuelu District, Changsha

Figure 9: Server data display page.

Figure 10: Deployment of image processing unit in experiment.

Figure 11: Deployment of camera in the experiment.

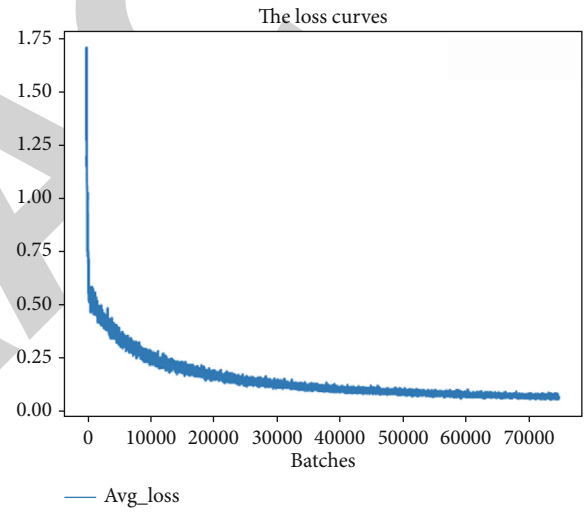

Figure 12: Loss curve for YOLOv3-tiny model training.

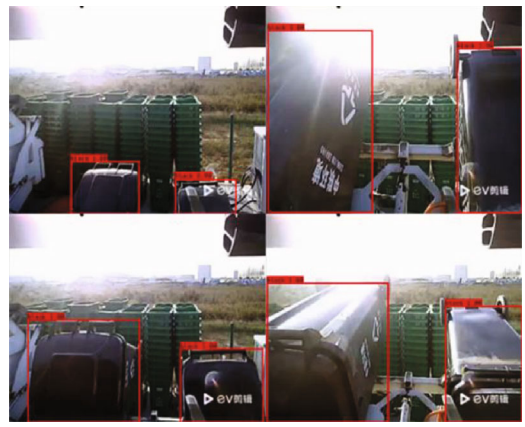

Figure 13: Example of object detection effect.

At the end of the turning, the image processing unit sends the data of the garbage cans to the on-board computer through the RS232 serial port. The on-board computer will detect whether there is any substandard operation according to the data received. At the same time, the data is uploaded to the server through the mobile network for recording and display. The effect of data recording and display is shown in Figure 9.

RETRACTED

Table 2: Test results in actual work scenarios.

Date	Weathers	Light condition	Number of test samples	Amount accuracy	Cubage accuracy	Color accuracy	Operation after experiment
19.12.12	Sunny	Sufficient	122	91.80%	77.86%	95.08%	Adjust threshold; increase sample amount
19.12.16	Sunny	Sufficient	128	95.31%	100%	100%	—
19.12.17	Cloudy	Poor	138	87.79%	100%	100%	—
20.01.04	Rainy	Very poor	81	46.91%	94.74%	97.22%	Increase sample amount
20.01.05	Rainy	Very poor	63	47.05%	100%	100%	Increase sample amount
20.02.15	Rainy	Poor	48	100%	100%	100%	—
20.02.16	Cloudy	Poor	61	100%	98.36%	100%	—
20.02.17	Sunny	Sufficient	66	100%	100%	100%	—

4. Experiment

4.1. Experimental Setup. The training environment and deployment environment are independent of each other. The operating system for the model training environment is Ubuntu 16.04 with 1080ti, 8 GB.

The image processing unit in the deployment environment has 8 GB DDR3 memory, and the SoC adopts the RK3399pro. The CPU of the SoC adopts double Cortex-A72 four Cortex-A53 kernel structure; the highest frequency is 1.8 G Hz, NPU supports 8Bit/16Bit operation, and the calculation force is 3.0Tops. The camera has a resolution of 640×480, a focal length of 2 mm, and a horizontal angle of view of 95 degrees. It is connected to the graphics processing unit through USB2.0. The graphics processing unit communicates with the vehicle computer through the RS232 serial port, and the vehicle computer communicates with the server through the LTE network. In addition, the operating system of the image processing unit is Fedora28. The object detect model is deployed using RKNN-toolkit. Python 3.6 is adopted as the programming language.

In the experiment, the image processing unit is deployed in the carriage, as shown in Figure 10. The deployment of camera on the garbage truck is shown in Figure 11.

4.2. Model Training. The training parameters of the YOLOv3-tiny model are as follows: batch is 64, subdivision is 8, momentum is 0.9, decay is 0.0005, and the number of iterations is 76000. The learning rate used step-by-step strategy, the initial value is 0.001 and changed at 66000 and 71000 times, and the ratio is 0.1.

The loss curve during training is shown in Figure 12. The final loss value of the training on the verification machine is 0.071556.

The detection example of the YOLOv3-tiny object detection model trained in this paper in the process of trash can overturning is shown in Figure 13.

4.3. Actual Scene Test. This paper tests the proposed method many times on the actual working garbage trucks. The working time of these garbage trucks is 6:30-9:00, and the test weathers are cloudy, rainy, and sunny. The test results are shown in Table 2.

It can be seen from Table 2 that under the good light conditions, the accuracy of the proposed method is very high. After continuous iteration, the accuracy of this method has approached 100%. However, due to the lack of light compensation in this experiment, the light condition in Changsha city in January is very poor under rainy conditions. Under this villainous light condition, the recognition effect of this method is greatly reduced. By patching the light, the problem could be easily solved. Experiments show the excellent real-time performance of the proposed method. On the image processing unit with NPU, the frame rate of our method is greater than 25FPS.

5. Conclusion

In this paper, a method of intelligent supervision and workload statistics of garbage trucks based on computer vision is proposed. On the basis of using the original on-board computing and communication equipment, a camera and an image processing unit are installed to build the hardware environment. A dataset is established based on the picture caught by the camera, and the YOLOv3-tiny model is trained on it to perform the real-time detection, and data statistics of the can flip process of the garbage truck. Compared with the traditional RFID-based supervision and data statistics methods, the proposed method has lower deployment and maintenance costs. The experimental results show that the method proposed in this paper has an accuracy rate close to 100% and a frame rate greater than 25FPS under good light conditions. However, the performance of the method will be greatly affected when the light condition becomes worse.

Network routing protocols are constantly being improved, especially in the field of sensor networks. In the future, edge computing and cloud computing may be better balanced. In the following work, cloud computing may be involved so that the proposed method can have a better computing environment. The accuracy and robustness of the proposed method will be further optimized. For example, the dataset will be expanded and optimized, and the fill light equipment will be installed to make the proposed method adapt to more weather conditions.

RETRACTED

Data Availability

The simulation experiment data used to support the findings of this study are available from the corresponding author upon request.

Conflicts of Interest

The authors declare that there are no conflicts of interest regarding the publication of this paper.

Acknowledgments

This work was supported in part by the National Key R&D Program of China (Grant No. 2018YFB1402600), the National Science Foundation of China (Grant Nos. 61772190, 61672221, 61702173, 61972147), and the Natural Science Foundation of Hunan Province, China (Grant No. 2020JJ4219).

References

[1] State Council Informatization Office, *GB/T 19095—2019, Signs for classification of municipal solid waste*, Standardization Administration of China, 2019.

[2] Y. Zhao, H. Shi, X. Chen, X. Li, and C. Wang, "An overview of object detection and tracking," in *2015 IEEE International Conference on Information and Automation*, Lijiang, China, 2015.

[3] D. Lowe, "Distinctive image features from scale-invariant keypoints," *International Journal of Computer Vision*, vol. 60, no. 2, pp. 91–110, 2004.

[4] N. Dalal and B. Triggs, "Histograms of oriented gradients for human detection," in *2005 IEEE Computer Society Conference on Computer Vision and Pattern Recognition (CVPR'05)*, vol. 1no. 12, pp. 886–893, San Diego, CA, USA, 2005.

[5] T. Ojala, M. Pietikainen, and T. Maenpaa, "Multiresolution gray-scale and rotation invariant texture classification with local binary patterns," *IEEE Transactions on Pattern Analysis and Machine Intelligence*, vol. 24, no. 7, pp. 971–987, 2002.

[6] A. S. Mozafari and M. Jamzad, "A SVM-based model-transferring method for heterogeneous domain adaptation," *Pattern Recognition*, vol. 56, pp. 142–158, 2016.

[7] S. Wu, F. Yuan, Y. Yang, Z. Fang, and Y. Fang, "Real-time image smoke detection using staircase searching-based dual threshold AdaBoost and dynamic analysis," *IET Image Processing*, vol. 9, no. 10, pp. 849–856, 2015.

[8] G. Ross, D. Jeff, D. Trevor, and M. Jitendra, "Rich feature hierarchies for accurate object detection and semantic segmentation," in *2014 IEEE Conference on Computer Vision and Pattern Recognition*, Columbus, OH, USA, 2014.

[9] W. Liu, D. Anguelov, and D. Erhan, "SSD: single shot multi-Box detector," in *European Conference on Computer Vision*, pp. 21–37, Amsterdam, The Netherlands, 2016.

[10] S. Ren, K. He, R. Girshick, and J. Sun, "Faster R-CNN: towards real-time object detection with region proposal networks," *IEEE Transactions on Pattern Analysis and Machine Intelligence*, vol. 39, no. 6, pp. 1137–1149, 2017.

[11] J. Redmon, S. Divvala, and R. Girshick, "You only look once: unified, real-time object detection," in *2016 IEEE Conference on Computer Vision and Pattern Recognition (CVPR)*, Las Vegas, NV, USA, 2015.

[12] J. Redmon and A. Farhadi, "YOLO9000: better, faster, stronger," in *2017 IEEE Conference on Computer Vision and Pattern Recognition (CVPR)*, Honolulu, HI, USA, 2017.

[13] J. Redmon and A. Farhadi, "Yolov3: an incremental improvement," 2018, https://arxiv.org/abs/1804.02767.

[14] J. Zhang, M. Huang, X. Jin, and X. Li, "A real-time Chinese traffic sign detection algorithm based on modified YOLOv2," *Algorithms*, vol. 10, no. 4, p. 127, 2017.

[15] M. Bartosz, K. Tomasz, and G. Marek, "Embedded vision system for pedestrian detection based on HOG+SVM and use of motion information implemented in Zynq heterogeneous device," in *2017 Signal Processing: Algorithms, Architectures, Arrangements, and Applications (SPA)*, pp. 406–411, Poznan, Poland, 2017.

[16] T. Zhou and J. Zhang, "Analysis of commercial truck drivers' potentially dangerous driving behaviors based on 11-month digital tachograph data and multilevel modeling approach," *Accident Analysis & Prevention*, vol. 132, article 105256, 2019.

[17] Z. Chen, Y. Zhang, C. Wu, and B. Ran, "Understanding individualization driving states via latent Dirichlet allocation model," *IEEE Intelligent Transportation Systems Magazine*, vol. 11, no. 2, pp. 41–53, 2019.

[18] J. Qi, G. Jiang, G. Li, Y. Sun, and B. Tao, "Intelligent human-computer interaction based on surface EMG gesture recognition," *IEEE Access*, vol. 7, pp. 61378–61387, 2019.

[19] B. Li, Y. Sun, G. Li et al., "Gesture recognition based on modified adaptive orthogonal matching pursuit algorithm," *Cluster Computing*, vol. 22, Supplement 1, pp. 503–512, 2019.

[20] D. Jiang, Z. Zheng, G. Li et al., "Gesture recognition based on binocular vision," *Cluster Computing*, vol. 22, Supplement 6, pp. 13261–13271, 2019.

[21] Y. He, G. Li, Y. Liao et al., "Gesture recognition based on an improved local sparse representation classification algorithm," *Cluster Computing*, vol. 22, Supplement 5, pp. 10935–10946, 2019.

[22] W. Cheng, Y. Sun, G. Li, G. Jiang, and H. Liu, "Jointly network: a network based on CNN and RBM for gesture recognition," *Neural Computing and Applications*, vol. 31, Supplement 1, pp. 309–323, 2019.

[23] G. Li, H. Tang, Y. Sun et al., "Hand gesture recognition based on convolution neural network," *Cluster Computing*, vol. 22, Supplement 2, pp. 2719–2729, 2019.

[24] D. Jiang, G. Li, Y. Sun, J. Kong, and B. Tao, "Gesture recognition based on skeletonization algorithm and CNN with ASL database," *Multimedia Tools and Applications*, vol. 78, no. 21, pp. 29953–29970, 2019.

[25] G. Li, H. Wu, G. Jiang, S. Xu, and H. Liu, "Dynamic gesture recognition in the internet of things," *IEEE Access*, vol. 7, pp. 23713–23724, 2019.

[26] L. Huang, Q. Fu, G. Li, B. Luo, D. Chen, and H. Yu, "Improvement of maximum variance weight partitioning particle filter in urban computing and intelligence," *IEEE Access*, vol. 7, pp. 106527–106535, 2019.

[27] Z. Chen, H. Cai, Y. Zhang et al., "A novel sparse representation model for pedestrian abnormal trajectory understanding," *Expert Systems with Applications*, vol. 138, article 112753, 2019.

[28] G. Xiao, Q. Wu, H. Chen, D. da, J. Guo, and Z. Gong, "A deep transfer learning solution for food material recognition using

RETRACTED

Hindawi
Wireless Communications and Mobile Computing
Volume 2020, Article ID 8857576, 10 pages
https://doi.org/10.1155/2020/8857576

Research Article

Improved Personalized Recommendation Algorithm Based on Context-Aware in Mobile Computing Environment

Fei Long

School of Economics and Management, Changsha University, Changsha 410003, China

Correspondence should be addressed to Fei Long; z20120995@ccsu.edu.cn

Received 28 June 2020; Revised 31 July 2020; Accepted 23 August 2020; Published 5 October 2020

Academic Editor: Hongju Cheng

Copyright © 2020 Fei Long. This is an open access article distributed under the Creative Commons Attribution License, which permits unrestricted use, distribution, and reproduction in any medium, provided the original work is properly cited.

With the development and popularization of e-commerce and Internet, more and more attention has been paid to personalized recommendation for users. The traditional user interest model only considers the user's behavior on the project, ignoring the user's context at that time. Pointing to the shortage that context-related factors are not considered in previous works, combining the characteristics of a mobile computing environment, this paper studies the algorithm and model of mobile service recommendation. A recommendation algorithm based on specified context filtering in mobile computing environment is proposed. The context of the classification is aggregated, by grouping the scenarios of the same category together. Through experiments, we found that the improved personalized recommendation algorithms are superior to the common collaborative filtering algorithm.

1. Introduction

The data included information of major websites and mobile APPs. If the data had given a certain treatment, the information could have been more user-friendly and more efficient. Meanwhile, users would have been provided with a friendly experience, and the information provided could have had higher revenue [1]. So, the recommendation system came into being.

The recommendation algorithm is the important part of the recommendation system [2]. The main recommendation algorithms are collaborative filtering recommendation algorithm, content-based recommendation algorithm, and hybrid recommendation algorithm [3–8]. In-depth research on the recommendation system allows users to get personalized recommendations, which greatly saved them time to search for information. At the same time, while the recommendation system is being improved, the user's personalized demand for recommendation gets higher and higher; more accurate recommendation is the future development direction [9]. The improved recommendation algorithm on the existing algorithm is a lot, so many scholars turning to the context-aware recommendation [10–15]. The context information becomes an essential role to enhance the effect of the recommendation.

The introduction of context information brings more ideas to improve the efficiency of the recommendation algorithm. The main context information includes user context information, such as users' ages, occupation, region; physical context, such as location, weather, time. There is much context information that could be considered by recommendation algorithm [16]. The context information can bring more accurate recommendations to the users of the recommendation system. There are three commonly used context-aware recommendation methods, and they are contextual prefiltering, contextual postfiltering, and contextual modeling [17]. As a result, the context-aware recommendation algorithm has gradually become a popular research trend. In this paper, combining the characteristics of the mobile computing environment, a recommendation algorithm based on specified context filtering in mobile computing environment is proposed.

The reminder of this paper is structured as follows: Section 2 introduces the related work. In Section 3, it proposes the conceptual model of context-awareness based on the context-aware recommendation system theory. Section 4 proposed a context-based recommendation algorithm in

the mobile computing environment. Section 5 presents the experimental process and results. The summary of the related work of our proposed model and algorithm and the conclusion of the paper are given in Section 6.

2. Related Work

After the introduction of the collaborative filtering algorithm, scholars have more research on the recommendation system. The most important recommendation algorithms are a collaborative filtering algorithm and content-based recommendation algorithm [18]. However, there are certain problems hard to be solved in the two basic algorithms, such as collaborative filtering algorithm has a cold start and high sparsely, and content-based recommendation algorithm is difficult to deal with multiple attributes. Therefore, the accuracy of a single recommendation algorithm recommendation is difficult to improve [19]. Many scholars have shifted their goals from traditional recommendation algorithms, focusing on the research of context-based recommendation systems [20].

Foreign researches have been quite rich. The research direction and application fields include shopping, tourism, catering, and other aspects. But they focused on proposing improved algorithms, which are based on traditional algorithms. The contrast of advantages and disadvantages of various algorithms based on context perception is relatively rare. The fields and data types applicable to different context-aware algorithms are not studied. Among them, Kang et al. [21] proposed not only paying attention to the explicit context information but also implicit context information. And they used packet sniffing technique. Kwona and Kim [22] proposed a way to discover the user's portrait by depicting the user's outline tree. Tuan et al. [23] combined user preferences and contextual interaction information and proposed a location-based advertising recommendation algorithm. Sánchez-Pi et al. [24] proposed the construction of a knowledge-based context-aware system. Sánchez-Pi et al. [25] proposed a localized adaptive modification model using a vector space model and saved time to obtain user-related information.

Lee et al. [26] proposed a novel TV system that combines gesture control, tag ranking, and context-awareness, providing personalized recommendations. Cai et al. [27] used collaborative filtering to generate a contextual concept ontology. Ji et al. [28] proposed an improved matrix approximate based on the clustering model. Wang et al. [29] proposed a hierarchical recommendation model based on a context tree structure, calculated situation transfer in the first layer, and recommended items in the second layer. Unger et al. [30] made a breakthrough in the acquisition of contexts, improving the accuracy of recommendations by extracting implicit context information from users' data.

3. Conceptual Model of Context-Awareness

3.1. Classification of Context Information. The so-called context information is a general concept, which can be divided into user context information, physical context information, time context information, network context information, and so on. The user context information includes some personal information, such as users' gender, age, region, occupation, and mood. The physical context information includes geographical location, temperature, and weather. The time context information includes season, morning or evening, and weekend or working day. The acquisition of this context information is conducive to better recommendation. If the system had those contexts, it could recommend suitable advertisements according to the geographical location, suitable music according to emotions, and decide whether videos are automatically loaded according to the network speed.

As shown in Figure 1, the types of context information currently defined are very diverse, but not all context information is readily available. The application of the context-aware algorithm is based on context acquisition. The shallow-level situation acquisition technology can already be achieved. The mobile device can obtain the user's latitude and longitude position, weather conditions, time information, etc., and can obtain the user's further information through the survey, such as age and gender. However, deep-level information processing is relatively rare at present, such as obtaining the user's location type and time type. Deep context information is helpful for the recommendation algorithm. In the current research, that information is mainly obtained through users' voluntary survey.

3.2. Model Construction. Related research on the context information recommendation is increasing, and the situation plays an important role in the personalized recommendation. Under the scope of user interests, there are some drifts in different context interests, and better recommendation can be obtained by studying the changes in the situation. At present, the context-aware model has a relatively consistent definition.

Context information is a collection of information about users, generally denoted by C, which is $C = \{c_1, c_2, c_3, \cdots c_n\}$, representing a set of contexts. And c_j denotes a context element in the set, while n denotes a common n context element. The classification of context information has been as described in Section 3.1. Some of the context in Section 3.1 can be selected into the set C to form the contextual collection of this paper. The influence of some context information on the recommendation model can be explored.

The context-aware recommendation model mainly collects the user's context information, historical behavior tendency, personal preference, and other information. Through filtering and calculating, they can be applied to personalized recommendations to provide with more accurate recommendations.

As showed in Figure 2, the context-awareness recommendation model can be divided into three layers. The first layer is the data acquisition layer, which collects various types of data of users. The second layer is the data processing layer, which filters and processes the data. The third layer is the recommended service layer, which is operated by the algorithm to form a personalized recommendation. The association of services at each level provides a means of contextual awareness.

In the traditional recommendation algorithm, the score matrix is associated with user and item, called user-item model, expressed as $U \times I \longrightarrow R$. U represents the user set, $U = \{u_1, u_2, u_3, \cdots u_n\}$, and I indicates the item set, $I = \{i_1,$

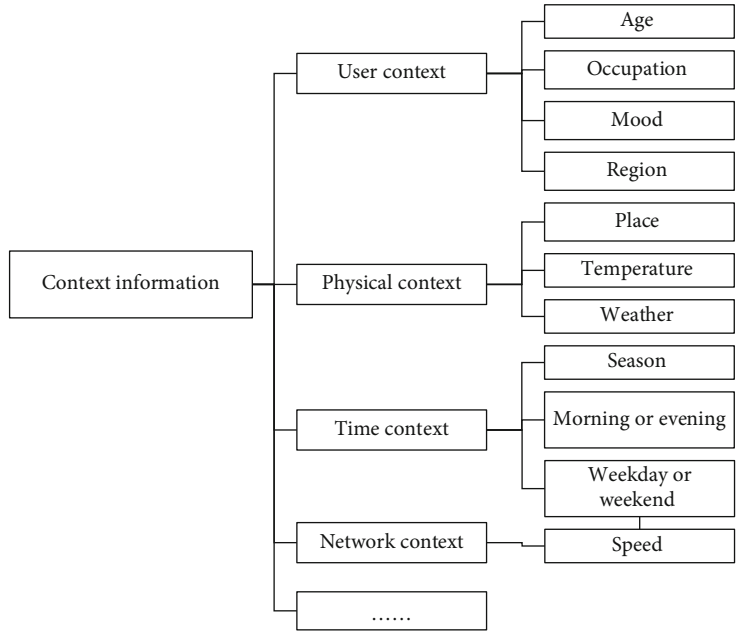

Figure 1: The classification of context.

$i_2, i_3, \cdots i_m\}$. R denotes a score set; r_{ij} denotes a score of the user u_i for the item i_j. n denotes the number of users, and m denotes the number of items. The above formulas constitute a two-dimensional score matrix between the user and the item and can be operated using a collaborative filtering algorithm to obtain a recommended result.

In the context-awareness recommendation model, the context factor is introduced, which is no longer a two-dimensional model, that is, it becomes a user-item-context model, expressed as $U \times I \times C \longrightarrow R$. U represents the user collection, $U = \{u_1, u_2, u_3, \cdots u_n\}$. I denotes a set of items, $I = \{i_1, i_2, i_3, \cdots i_m\}$. C denote a set of contexts, $C = \{c_1, c_2, c_3, \cdots c_k\}$. n denotes the number of users, m denotes the number of items, and k indicates the number of situations. The meaning of R is still the user's rating of the project.

In the three-dimensional model, the score is represented as each of the small cubes that are segmented out. The cube in the three-dimensional coordinate system is the set of scoring data R.

4. Context-Awareness Recommendation

4.1. Specific-Context Based Recommendation Algorithm. In the same situation, the user's choice may have similarities. Based on this theory, the algorithm experiment can be further developed. When exploring the context factors, this paper selects three types of situations for classification. There is an inclusion relationship between single-situation factors and multisituation factors, such as context (at home), including (weekend, weekday, and holiday), and (alone, with friends, with family, and with lovers). It is actually compound context information. Through the aggregation of context information, it is explored whether there is consistency in user selection in the context of aggregation.

This algorithm is a context-based prefiltering algorithm, which is a process of context selection. The algorithm aims at transforming the three-dimension model into a two-dimension model through context filtering. The score prediction function, $R(u, i, c)$ should be represented as the following formula (1):

$$R(u, i, c) = R(u, i)(c_1 = x, c_2 = y, c_3 = z), \tag{1}$$

where $R(u, i, c)$ represents the score matrix in the three-dimensional model, and the threshold of the context set indicates that the context information is $c = <x, y, z>$. $R(u, i)$ is the estimated score according to the collaborative filtering algorithm based on the user's similarity in a given situation.

After getting the score matrix, the similarity between users is calculated. The Pearson correlation coefficient calculation should be represented as the following formula (2):

$$\text{sim}(u, v)_{(u,i)} = \frac{\sum_{i \in I_{uv}} (r_{ui} - \overline{r_u})(r_{vi} - \overline{r_v})}{\sqrt{\sum_{i \in I_{uv}} (r_{ui} - \overline{r_u})^2} \sqrt{\sum_{i \in I_{uv}} (r_{vi} - \overline{r_v})^2}}, \tag{2}$$

where r_{ui} represents the score of a user u for item i. $\overline{r_u}$ represents the average value of a user u score. r_{vi} represents the score of a user v for item i. $\overline{r_v}$ represents the average value of a user v score. By calculating their similarities, the similarity matrix is formed as below:

$$\text{sim} = \begin{pmatrix} s_{11} & s_{12} & \cdots & s_{1m} \\ s_{21} & s_{22} & \cdots & s_{2m} \\ \cdots & \cdots & \cdots & \cdots \\ s_{m1} & s_{m2} & \cdots & s_{mm} \end{pmatrix}. \tag{3}$$

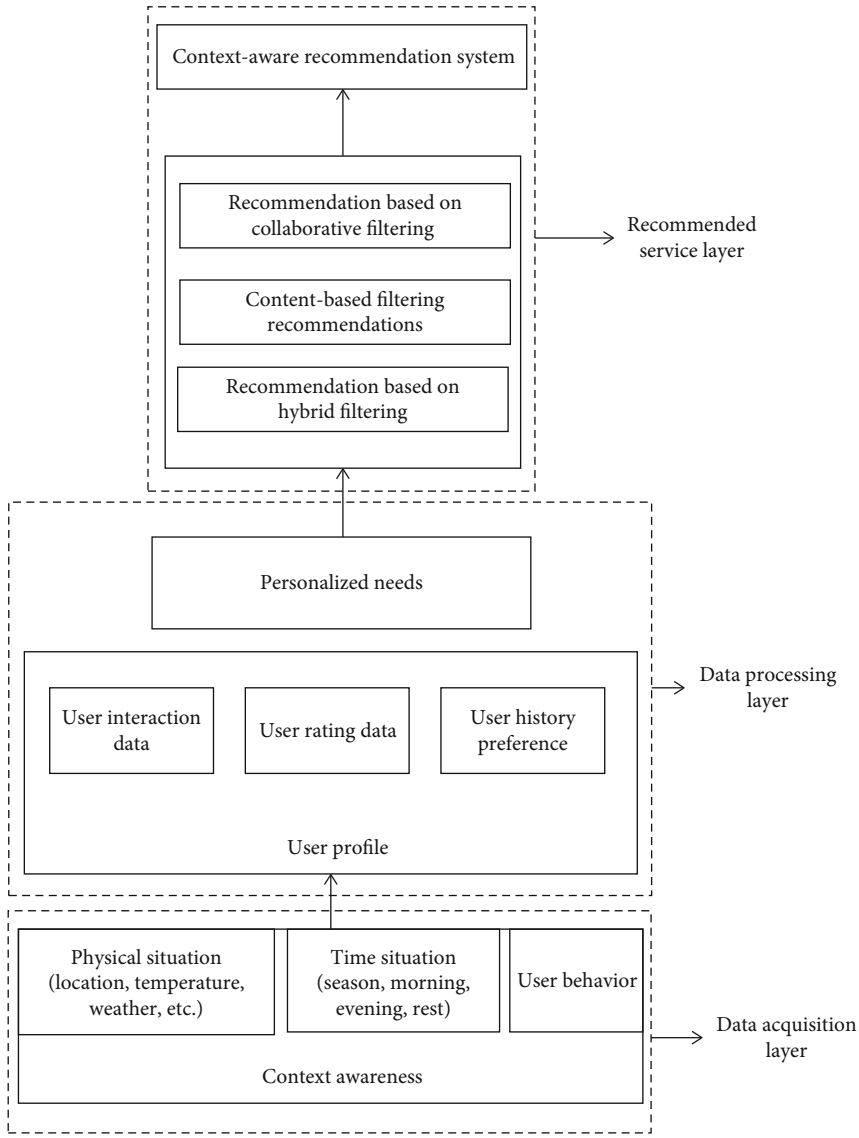

Figure 2: Context-awareness recommendation model.

Having got the similarities of user's interests, the predicted score can be calculated by the following formula (4).

$$p_{ui} = \frac{\sum_{v \in V}(r_{vi} - \overline{r_v}) \times \mathrm{sim}(u, v)}{\sum_{v \in V} \mathrm{sim}(u, v)}. \quad (4)$$

The predicted score determines the degree of user interest. The higher the score is, the more the user is interested in. The process of Algorithm 1 can be summarized as follows:

4.2. User-Based Contextual Recommendation Algorithm. In the algorithm proposed above, the context information is a separate factor. The context information is not incorporated into the algorithm model, so the contextual modeling algorithm is proposed.

The contextual modeling algorithm is divided into heuristic and model. There are many literature and papers in the research of contextual modeling algorithms based on models. It is not the focus of this paper. The algorithm proposed in this paper integrates the context information and processes $U \times I \times C \longrightarrow R$ three-dimension model. We propose a user-based contextual recommendation model.

The user-based context is scoring matrix $U \times C \longrightarrow R$ is constructed, and the method and steps are the same as before. According to the formula for calculating the Pearson correlation coefficient, calculate the user's context similarity.

$$\mathrm{sim}(u, v)_c = \frac{\sum_{c \in C_{uv}}(r_{uc} - \overline{r_u})(r_{vc} - \overline{r_v})}{\sqrt{\sum_{c \in C_{uv}}(r_{uc} - \overline{r_u})^2} \sqrt{\sum_{c \in C_{uv}}(c - \overline{r_v})^2}}. \quad (5)$$

In the algorithm, we use user a as an example to predict its score on the item i in the context c. The nearest neighbor of user a needs to be found, and the user similarity matrix can be obtained by substituting the required data into the formula. Among all the obtained user similarities, the top-N similar users are selected as the nearest neighbors, and the

Input: score matrix
Output: context-based predicted score matrix
For $item_i \in \mathrm{I}$:
For $c_j \in C$:
If $C(item_i) = C_i \& C_i \in c_j$:
Move $item_i$ to S
for item $\in S$:

$$\text{calculate } \mathrm{sim}(u,v)_{(u,i)} = \frac{\sum_{i \in I_{uv}} (r_{ui} - \overline{r_u})(r_{vi} - \overline{r_v})}{\sqrt{\sum_{i \in I_{uv}} (r_{ui} - \overline{r_u})^2} \sqrt{\sum_{i \in I_{uv}} (r_{vi} - \overline{r_v})^2}}$$

$$p_{ui} = \frac{\sum_{v \in V} (r_{vi} - \overline{r_v}) \times sim(u,v)}{\sum_{v \in V} sim(u,v)}$$

Algorithm 1: Specific-context based recommendation algorithm.

Input: score matrix
Output: predictions
for each item:
score = mean $(score_i(U_i = u \& C_j = c))$
for each item (U, C):

$$\mathrm{sim}(u,v)_c = \frac{\sum_{c \in C_{uv}} (r_{uc} - \overline{r_u})(r_{vc} - \overline{r_v})}{\sqrt{\sum_{c \in C_{uv}} (r_{uc} - \overline{r_u})^2} \sqrt{\sum_{c \in C_{uv}} (c - \overline{r_v})^2}}$$

for each user:

$$\mathrm{sim}(u,v)_{(u,i)} = \frac{\sum_{i \in I_{uv}} (r_{ui} - \overline{r_u})(r_{vi} - \overline{r_v})}{\sqrt{\sum_{i \in I_{uv}} (r_{ui} - \overline{r_u})^2} \sqrt{\sum_{i \in I_{uv}} (r_{vi} - \overline{r_v})^2}}$$

for top-N users:
for c in C(top-N):

$$p = k \sum_{u \in U} \mathrm{sim}(a,u) \times R_{u,i,c_x} \times \mathrm{sim}(c_x, c),$$
$$k = 1 / \sum_{u \in C} |\mathrm{sim}(a,u)| \times |\mathrm{sim}(c_x, c)|$$

Algorithm 2: User-based contextual algorithm.

score of the item i under the situation c is predicted based on the score data of these users.

In order to obtain the rating of the user u under the context c, we find the rating context set of the most neighboring user for the item i. The weighting operation is performed in combination with the user similarity and the context similarity obtained in the foregoing.

$$p = k \sum_{u \in U} \mathrm{sim}(a,u) \times R_{u,i,c_x} \times \mathrm{sim}(c_x, c), \tag{6}$$

where $k = 1/\sum_{u \in C} |\mathrm{sim}(a,u)| \times |\mathrm{sim}(c_x, c)|$. $\mathrm{sim}(a,u)$ is user's similarity, and $\mathrm{sim}(c_x, c)$ is similarity between target context and current context.

The result of the scoring can be obtained. The algorithm is based on the user's contextual modeling algorithm, and the context plays an essential role in the model. The algorithm is described as following:

4.3. Item-Based Contextual Recommendation Algorithm. The user-based heuristic contextual model is discussed above, and the algorithm to be discussed is similar with that. Item-based contextual recommendation model is also a recommendation algorithm based on context modeling.

Firstly, in order to build the item-based context matrix $I \times C \longrightarrow R$, the user's information needs to be transformed first. We calculate the average score of the same item in the same situation.

$$\begin{pmatrix} r_{c1,i1} & r_{c2,i1} & \cdots & r_{cj,i1} \\ r_{c1,i2} & r_{c2,i2} & \cdots & r_{ci,i2} \\ \cdots & \cdots & \cdots & \cdots \\ r_{c1,\mathrm{in}} & r_{c2,\mathrm{in}} & \cdots & r_{cj,\mathrm{in}} \end{pmatrix}. \tag{7}$$

Then, we calculate context similarity based on items using Pearson formula.

$$\mathrm{sim}(u,v)_c = \frac{\sum_{c \in C_{uv}} (r_{uc} - \overline{r_u})(r_{vc} - \overline{r_v})}{\sqrt{\sum_{c \in C_{uv}} (r_{uc} - \overline{r_u})^2} \sqrt{\sum_{c \in C_{uv}} (c - \overline{r_v})^2}}. \tag{8}$$

In the algorithm, we use user a as an example to predict its score on the item i in the context c. The nearest neighbor of user a needs to be found, and the item similarity matrix can be obtained by substituting the required data into the formula. Among all the obtained item similarities, the top-N similar items are selected as the nearest neighbors, and the score of the item i under the situation c is predicted based on the score data of these items.

In order to obtain the rating of the item i under the context c, we find the rating context set of the most neighboring item for the context c. The weighting operation is performed in combination with the item similarity and the context similarity obtained in the foregoing.

$$p = k \sum_{j \in I} \mathrm{sim}(i,j) \times R_{a,i,c_x} \times \mathrm{sim}(c_x, c), \tag{9}$$

$k = 1/\sum_{u \in C} |\mathrm{sim}(i,j)| \times |\mathrm{sim}(c_x, c)|$. $\mathrm{sim}(i,j)$ is item's similarity, and $\mathrm{sim}(c_x, c)$ is similarity between target context and current context.

5. Experiment Analysis

The hardware environment of this experiment is the Intel Core i5 processor, 8G memory. The software environment is the 64-bit Windows operating system, VMware Workstation Pro virtual machine, Cent OS7 operating system, Open JDK1.8, Python3.7, Anaconda for Python3.7, and PyCharm-community.

The data of this experiment is mainly from the questionnaire survey of college students about the context information of watching movies. A total of 107 users' data is collected. In order to guarantee the accuracy of the algorithm, some invalid questionnaires are eliminated. The data of 96 users were retained, including 2145 data.

The quality of the recommendation system is mainly measured by some indicators. The accuracy of the prediction is extremely important in the recommendation system. It is

Input: score matrix
Output: predictions
for each user:
score = mean $(score_i(I_k = i \& C_j = c))$
for each user (I, C):
calculate $sim(u, v)_c = \dfrac{\sum_{c \in C_{uv}} (r_{uc} - \overline{r_u})(r_{vc} - \overline{r_v})}{\sqrt{\sum_{c \in C_{uv}} (r_{uc} - \overline{r_u})^2} \sqrt{\sum_{c \in C_{uv}} (c - \overline{r_v})^2}}$
for each item:
calculate $sim(u, v)_{(u,i)} = \dfrac{\sum_{i \in I_{uv}} (r_{ui} - \overline{r_u})(r_{vi} - \overline{r_v})}{\sqrt{\sum_{i \in I_{uv}} (r_{ui} - \overline{r_u})^2} \sqrt{\sum_{i \in I_{uv}} (r_{vi} - \overline{r_v})^2}}$
for top-N items:
for c in C(top-N):
$p = k \sum_{j \in I} \mathrm{sim}(i, j) \times R_{a,i,c_x} \times \mathrm{sim}(c_x, c)$, $k = 1 / \sum_{j \in I} |\mathrm{sim}(i, j)| \times |\mathrm{sim}(c_x, c)|$

Algorithm 3: Item-based contextual algorithm.

mainly judged by Root Mean Squared Error (RMSE) and Mean Absolute Error (MAE).

$$\mathrm{RMSE} = \sqrt{\frac{1}{N} \sum_{i=1}^{N} (\mathrm{real}_i - \mathrm{predict}_i)^2}, \qquad \mathrm{MAE} = \frac{1}{N} \sum_{i=1}^{N} |\mathrm{real}_i - \mathrm{predict}_i|. \tag{10}$$

The root mean square error and the mean absolute error are both the degree of deviation between the calculated predicted value and the true value. The value obtained by subtracting the predicted value from the true value is recalculated, and the larger the obtained result value, the greater the degree of deviation. On the contrary, the more accurate the prediction of the algorithm is. When judging the merits and demerits of the algorithm according to these two parameters, the value is expected to be small.

The traditional prediction algorithm is set as the control object of this experiment, so that the latter experiment is compared with the experimental results obtained by the two-dimensional algorithm.

In this paper, the user-based collaborative filtering algorithm is selected. According to the Pearson similarity coefficient, the nearest neighbor of the movie is calculated and we use them to predict. Several classical collaborative filtering algorithms and its improved algorithms are selected, which are KNN basic, KNN means, KNN Zscore, and KNN baseline, respectively, which represent the basic collaborative filtering algorithm, the collaborative filtering algorithm based on the scoring average, the collaborative filtering algorithm based on scoring standardization, and the collaborative filtering algorithm based on baseline scoring. At the same time, in order to avoid the contingency error, each of the following experiments set a five-fold cross-validation, and the obtained results were evaluated using the values of RMSE and MAE.

In the collaborative filtering algorithm, the recommended precision depends on the number of nearest neighbors. In this paper, four values are selected as the representative, and the different k values represent the maximum number of nearest neighbors.

Table 1: Traditional algorithms' RMSE.

	$k = 5$	$k = 10$	$k = 15$	$k = 20$
KNN basic	1.402	1.312	1.293	1.319
KNN means	1.292	1.246	1.362	1.301
KNN Zscore	1.311	1.319	1.363	1.405
KNN baseline	2.545	2.448	2.391	2.422

Table 2: Traditional algorithms' MAE.

	$k = 5$	$k = 10$	$k = 15$	$k = 20$
KNN basic	1.052	0.981	0.954	0.987
KNN means	0.943	0.924	0.976	0.991
KNN Zscore	0.970	0.962	0.979	1.003
KNN baseline	2.065	1.962	1.951	1.874

According to Tables 1 and 2, the KNN baseline algorithm (the collaborative filtering algorithm based on the baseline score) is obviously inferior to the other algorithms, indicating that it does not fit for the problem. So, we omit it in the following experiments.

It can be observed in Figures 3 and 4 that the pros and cons of the algorithm are not always the same. Under different k values, the prediction effect of the recommendation algorithm changes. Overall, the increase of the maximum number of neighbors is accompanied by the prediction accuracy. It rises first and then falls. If the value is selected approximately, the prediction works best. The basic collaborative filtering has larger RMSE and MAE values when the k value is smaller, but it shows an advantage when the k exceeds 10. The other two algorithms also show advantages when k is less than 15, and the collaborative filtering algorithm based on scoring standardization is always better than the collaborative filtering algorithm based on scoring average.

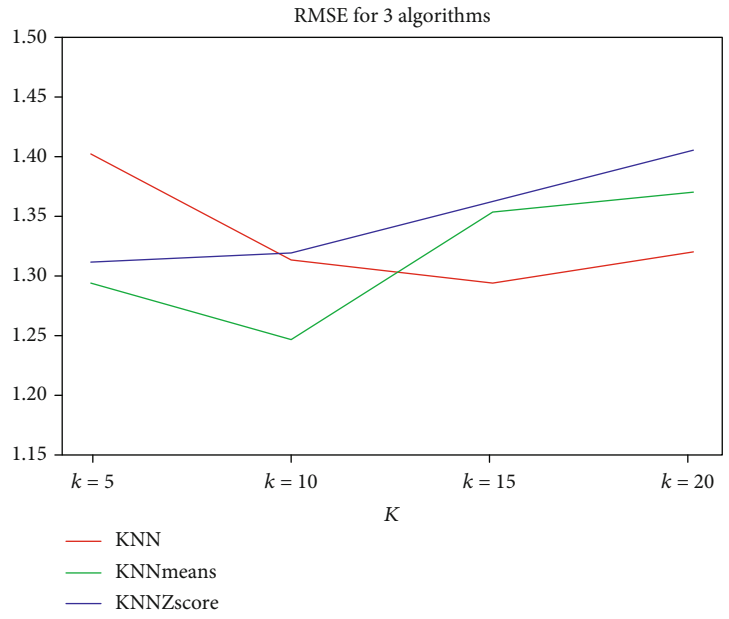

Figure 3: Algorithms' RMSE.

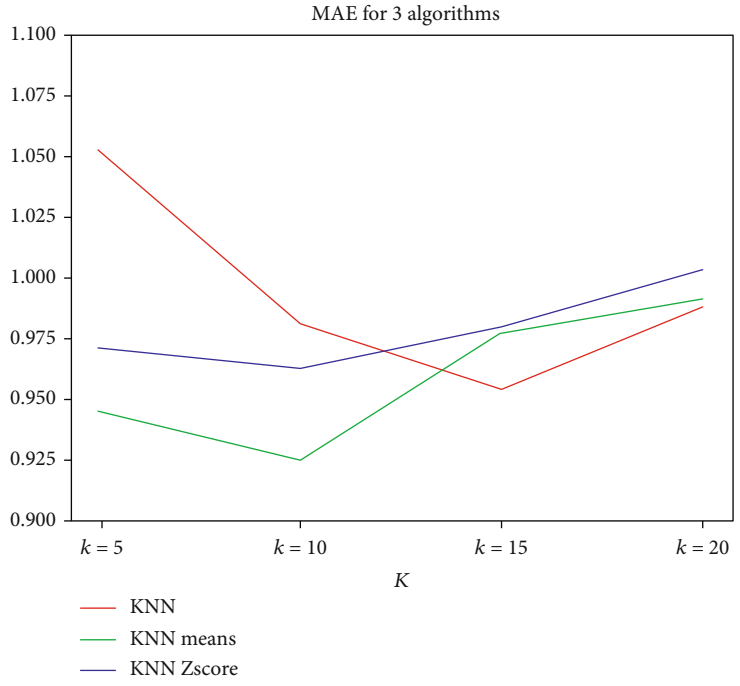

Figure 4: Algorithms' MAE.

In order to implement the recommendation algorithm based on the specific context, we initially screened and organized the data set. As shown in Figure 5, the context information has an inclusive relationship. The collection of context information is like a forest. Here, we choose three attributes of watching movies, and they are time, place, and company, forming three trees. There are parent nodes and their branches, each of which, respectively, represents the specific movie-watching behavior.

We select 6 to 12 context information to aggregate and the results are as follows.

According to the Table 3, this resulted in an aggregation of six different contexts, namely, at home, at the cinema, one person, on weekends, on weekdays, and on holidays. The selected situation has to be in conformity with the logic of reality. Usually, in this context information, the frequency of people watching movies will increase. For each context environment, we use the collaborative filtering algorithm to

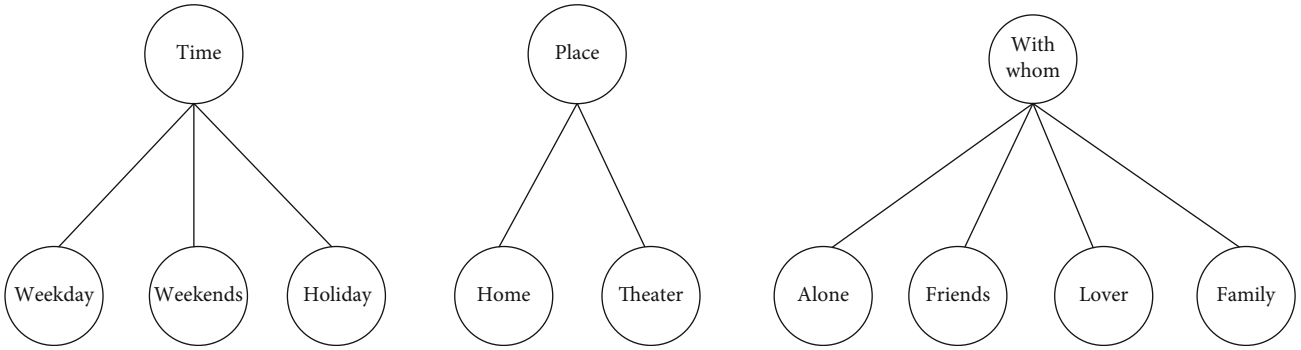

Figure 5: The tree of context.

Table 3: Results after aggregation.

Number	Context	Item number
1	Home	1318
2	Theater	826
3	Alone	972
4	Weekend	829
5	Weekday	880
6	Holiday	435

Table 4: RMSE.

	$K = 5$	$K = 10$	$K = 15$	$K = 20$
Home	1.140	1.177	1.359	1.142
Theater	1.404	1.409	1.392	1.375
Weekday	1.391	1.359	1.361	1.283
Alone	1.193	1.208	1.203	1.132
Weekends	1.281	1.245	1.233	1.271
Holiday	1.252	1.220	1.205	1.209

Table 5: MAE.

	$K = 5$	$K = 10$	$K = 15$	$K = 20$
Home	0.837	0.863	0.834	0.838
Theater	1.062	1.036	1.045	1.025
Weekday	1.011	1.009	1.004	0.940
Alone	0.871	0.876	0.860	0.865
Weekends	0.971	0.934	0.916	0.955
Holiday	0.918	0.890	0.874	0.871

predict and get the recommended results in this context. For the different nearest neighbors number, we will get different results in Tables 4 and 5.

The performance of several selected contextual effects is different, in order to more intuitively observe the advantages and disadvantages of the algorithm and compare with those traditional collaborative filtering algorithm.

Through the above experimental results, it can be observed that the smaller the value of RMSE and MAE, the better the prediction effect. Conversely, the recommended algorithm is less effective. In Figure 6, the solid line indicates

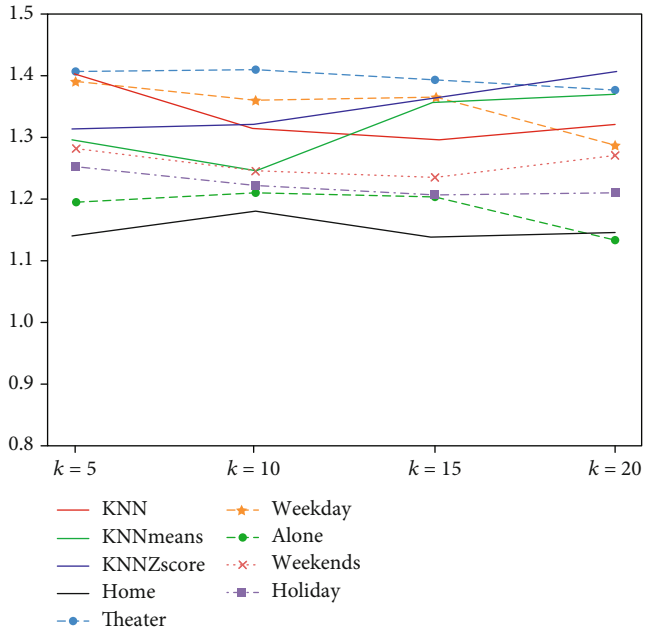

Figure 6: Contrast of the specific contexts.

the result obtained by the conventional algorithm, and the broken line indicates the result obtained by the improved precontextual filtering algorithm.

In different situations, the performance of the algorithm is not the same. In the above six contexts, there are four contexts that are better than the traditional algorithm regardless of the value of the nearest neighbor. They are at home, one person, on weekends, and on holidays, and the best values for recent neighbors in different situations are not the same. The other two contexts, in the cinema and on the working day, do not apply to the precontextual filtering algorithm, and the prediction effect obtained is not as good as the traditional collaborative filtering algorithm. At the same time, it can be seen that the maximum value of the nearest neighbor have little influence on the algorithm.

6. Summary and Future Work

In this paper, context-based recommendation algorithms are proposed and implemented. In the comparison between the proposed algorithm and the traditional algorithm, the new

algorithm is better than the traditional algorithm as a whole, but the new algorithm is not applicable in some contexts. Among the six contexts obtained after aggregation, only four contexts are superior to the common ones, and the other two contexts are not good enough to apply to the algorithm.

Data Availability

The data used to support the findings of this study are available upon request from the corresponding author.

Conflicts of Interest

The author declares that there are no conflicts of interest regarding the publication of this paper.

Acknowledgments

This work was supported in part by the Social Science Foundation of Hunan Province (16YBQ003), the Changsha Municipal Science and the Technology Bureau (k1705072), and the Hunan Provincial Social Science Achievement Evaluation Committee General Project (XSP18YBC166).

References

[1] Z. Huang, X. Xu, J. Ni, H. Zhu, and C. Wang, "Multimodal representation learning for recommendation in Internet of Things," *IEEE Internet of Things Journal*, vol. 6, no. 6, pp. 10675–10685, 2019.

[2] M. Böhmer, G. Bauer, and A. Krüger, "Exploring the design space of context-aware recommender systems that suggest mobile applications," , 20102*nd Workshop on Context-Aware Recommender Systems*, vol. 5, 2010, Barcelona, Spain, 2010.

[3] J. K. Tarus, Z. Niu, and D. Kalui, "A hybrid recommender system for e-learning based on context awareness and sequential pattern mining," *Soft Computing*, vol. 22, no. 8, pp. 2449–2461, 2018.

[4] G. Adomavicius and D. Jannach, "Preface to the special issue on context-aware recommender systems," *User Modeling and User-Adapted Interaction*, vol. 24, no. 1-2, pp. 1–5, 2014.

[5] S. Khusro, Z. Ali, and I. Ullah, *Information Science and Applications (ICISA) 2016*, K. Kim and N. Joukov, Eds., vol. 376 of Lecture Notes in Electrical Engineering, Springer, Singapore, 2016.

[6] M. Braunhofer, M. Elahi, M. Ge, and F. Ricci, "Context dependent preference acquisition with personality-based active learning in mobile recommender systems," in *Learning and Collaboration Technologies. Technology-Rich Environments for Learning and Collaboration*, LCT 2014. Lecture Notes in Computer Science, P. Zaphiris and A. Ioannou, Eds., pp. 105–116, Springer, Cham, 2014.

[7] N. Y. Asabere, "Towards a viewpoint of context-aware recommender systems (CARS) and services," *International Journal of Computer Science and Telecommunications*, vol. 4, no. 1, pp. 10–29, 2013.

[8] S. Kim and Y. Yoon, "Recommendation system for sharing economy based on multidimensional trust model," *Multimedia Tools and Applications*, vol. 75, no. 23, pp. 15297–15310, 2016.

[9] L. O. Colombo-Mendoza, R. Valencia-García, A. Rodríguez-González, G. Alor-Hernández, and J. J. Samper-Zapater, "RecomMetz: a context-aware knowledge-based mobile recommender system for movie showtimes," *Expert Systems with Applications*, vol. 42, no. 3, pp. 1202–1222, 2015.

[10] A. Abbas, L. Zhang, and S. U. Khan, "A survey on context-aware recommender systems based on computational intelligence techniques," *Computing*, vol. 97, no. 7, pp. 667–690, 2015.

[11] K. Haruna, M. Akmar Ismail, S. Suhendroyono et al., "Context-aware recommender system: a review of recent developmental process and future research direction," *Applied Sciences*, vol. 7, no. 12, p. 1211, 2017.

[12] Q. Yang, "A novel recommendation system based on semantics and context awareness," *Computing*, vol. 100, no. 8, pp. 809–823, 2018.

[13] V. Maran, A. Machado, G. M. Machado, I. Augustin, and J. P. M. de Oliveira, "Domain content querying using ontology-based context-awareness in information systems," *Data & Knowledge Engineering*, vol. 115, pp. 152–173, 2018.

[14] T. Bogers, M. Koolen, B. Mobasher, A. Said, and C. Petersen, "2nd workshop on recommendation in complex scenarios (complexrec 2018)," in *Proceedings of the 12th ACM Conference on Recommender Systems*, pp. 510-511, Vancouver British Columbia Canada, 2018.

[15] S. Ilarri, R. Trillo-Lado, and R. Hermoso, "Datasets for context-aware recommender systems: current context and possible directions," *2018 IEEE 34th International Conference on Data Engineering Workshops (ICDEW)*, 2018, pp. 25–28, Paris, France, 2018.

[16] Y. Zheng, "Context-Aware Mobile Recommendation by a Novel Post-Filtering Approach," *In The Thirty-First International Flairs Conference*, 2018, Florida, USAThe Thirty-First International Florida Artificial Intelligence Research Society Conference (FLAIRS-31), 2018.

[17] R. Zhou, "An intelligent video tag recommendation method for improving video popularity in mobile computing environment," *IEEE Access*, vol. 8, pp. 6954–6967, 2019.

[18] M. Thiago, M. Glenda, and H. Ary, "ePerícia: web and mobile computing environment for public forensic data management and collect," *International Journal of Computer Applications*, vol. 177, no. 13, pp. 59–69, 2019.

[19] W. Zhou and W. Han, "Personalized recommendation via user preference matching," *Information Processing & Management*, vol. 56, no. 3, pp. 955–968, 2019.

[20] W. W. Guo and F. Liu, "Research on collaborative filtering personalized recommendation algorithm based on deep learning optimization," in *2019 International Conference on Robots & Intelligent System (ICRIS).*, Haikou, China, 2019.

[21] H. Kang, E. Suh, and K. Yoo, "Packet-based context aware system to determine information system user's context," *Expert Systems with Applications*, vol. 35, no. 1-2, pp. 286–300, 2008.

[22] O. Kwon and J. Kim, "Concept lattices for visualizing and generating user profiles for context-aware service recommendations," *Expert Systems with Applications*, vol. 36, no. 2, pp. 1893–1902, 2009.

[23] T. H. Dao, S. R. Jeong, and H. Ahn, "A novel recommendation model of location-based advertising: context-aware collaborative filtering using GA approach," *Expert Systems with Applications*, vol. 39, no. 3, pp. 3731–3739, 2012.

[24] N. Sánchez-Pi, J. Carbó, and J. M. Molina, "A knowledge-based system approach for a context-aware system," *Knowledge-Based Systems*, vol. 27, pp. 1–17, 2012.

[25] N. Sánchez-Pi, J. Carbó, and J. M. Molina, "A geo-location context-aware mobile learning system with adaptive correlation computing methods," *Procedia Computer Science*, vol. 10, pp. 593–600, 2012.

[26] W.-P. Lee, C. Kaoli, and J.-Y. Huang, "A smart TV system with body-gesture control, tag-based rating and context-aware recommendation," *Knowledge-Based Systems*, vol. 56, pp. 167–178, 2014.

[27] Y. Cai, W. H. Chen, H. F. Leung et al., "Context-aware ontologies generation with basic level concepts from collaborative tags," *Neurocomputing*, vol. 208, pp. 25–38, 2016.

[28] K. Ji, R. Sun, X. Li, and W. Shu, "Improving matrix approximation for recommendation via a clustering-based reconstructive method," *Neurocomputing*, vol. 173, pp. 912–920, 2016.

[29] S. Wang, C. Li, K. Zhao, and H. Chen, "Learning to context-aware recommend with hierarchical factorization machines," *Information Sciences*, vol. 409-410, pp. 121–138, 2017.

[30] M. Unger, A. Bar, B. Shapira, and L. Rokach, "Towards latent context-aware recommendation systems," *Knowledge-Based Systems*, vol. 104, pp. 165–178, 2016.

Hindawi
Wireless Communications and Mobile Computing
Volume 2020, Article ID 8859961, 11 pages
https://doi.org/10.1155/2020/8859961

Research Article

A Medical Data Privacy Protection Scheme Based on Blockchain and Cloud Computing

Liang Huang[1,2] **and Hyung-Hyo Lee**[2]

[1]*School of Mathematics & Computer Science, Shangrao Normal University, Shangrao 334001, China*
[2]*Department of Computer and Software Engineering, Wonkwang University, Iksan 54538, Republic of Korea*

Correspondence should be addressed to Liang Huang; 305108@sru.edu.cn

Received 29 June 2020; Revised 19 August 2020; Accepted 12 September 2020; Published 26 September 2020

Academic Editor: Hongju Cheng

Copyright © 2020 Liang Huang and Hyung-Hyo Lee. This is an open access article distributed under the Creative Commons Attribution License, which permits unrestricted use, distribution, and reproduction in any medium, provided the original work is properly cited.

With the features of decentralization and trustlessness and through distributed data storage, point-to-point transmission, and encryption algorithms, blockchain has shed new light on the security and protection of medical data, and it can resolve the contradiction between data sharing and privacy protection with proper security strategies. In this paper, we integrate the strengths of both blockchain and cloud computing and build the privacy protection scheme for medical data based on blockchain and cloud computing. This scheme introduces cloud computing and provides services to blockchain nodes with cloud server computing; meanwhile, it collects, analyzes, processes, and maintains medical data in the identity authentication interface and solves the insufficient computing abilities of some nodes in blockchain so as to verify the authenticity and reliability of data. The simulation experiment proves that the proposed scheme is effective. It can achieve the secure protection and integrity verification of medical data and address the problems of high computing complexity, data sharing, and privacy protection.

1. Introduction

Intelligent hospitals are having increasing demands for information security, and it has become extremely urgent to protect personal private data of patients. Currently, these hospitals have been focusing on how to use convenient internet medical services to prevent the medical information system from being attacked and personal information from being stolen [1]. As blockchain and cloud computing come to maturity, related techniques have achieved rapid development in medical and health services, including medical informatization, mobile healthcare, medical e-commerce, wearable devices, and online medical services. The blockchain connects the participants in a peer-to-peer manner. The participants jointly maintain a system and express the cooperation rules through consensus mechanism and smart contract, so as to achieve a more flexible cooperation mode [2]. The concept of smart contract appeared in 1994 and laid the foundation for bitcoin. A smart contract is a set of commitments defined in digital form, including agreements on which contract participants can execute these commitments [3]. In a broad sense, blockchain technology must include four aspects: point-to-point network design, application of encryption technology, implementation of distributed algorithm, and use of data storage technology. Others may involve distributed storage, machine learning, VR, internet of things, big data, etc. In a narrow sense, blockchain only involves data storage technology, database or file operation, etc. [4]. Apart from conventional encryption methods, proxy reencryption and attribute-based encryption (ABE) can also be used in medical data sharing and patient privacy protection [5]. In traditional encryption methods, the client first downloads and decrypts locally encrypted text data. Then, before sending to the specified client, the client encrypts the data with the public key of the specified client, who can decrypt the data, but it requires plenty of network overhead and operating costs and it also occupies the client's limited memory, multiplying the client's costs [6]. Proxy reencryption is to convert the ciphertext encrypted by A's public key into the ciphertext to be decrypted by B's private key so as

to realize password sharing. Proxy reencryption means that a client can decrypt the ciphertext of another associated client without leaking users' private key and plaintext, which is mainly end-to-end [7]. In ABE, a data owner can set an access strategy authority in data encryption, and only those clients that satisfy this authority can decrypt the text in order to accomplish data sharing and personal privacy protection, which is one-to-many [8]. Based on attribute-based encryption (ABE), the problem of private data sharing can be solved by reasonable configuration and sharing strategy. According to the embedded objects, ABE can be divided into KP-ABE (Key-Policy ABE) and CP-ABE (Ciphertext-Policy ABE). With the popularization of intelligent healthcare, the medical institutions can have the data stored in the cloud to save equipment cost and lower costs. For the sake of data security and personal privacy protection of patients, some medical establishments need to encrypt the data in advance to form ciphertexts. Besides, they need other medical institutions to share certain ciphertexts frequently and prevent anyone (including cloud service providers) from cracking these data ciphertexts. In blockchain and cloud computing, the combination of decentralization and tamper-proofing of blockchain with the nodes of distributed cloud computing can help health institutions to carry out security and privacy protection of patient data at a lower cost and achieve data interaction among medical organizations. These will have a profound impact on the development of future healthcare industry.

The special contributions of this paper include the following:

(i) Aiming at data sharing and patient privacy protection of intelligent hospitals, we explore in-depth conventional encryption methods, proxy reencryption, attributed-based encryption, and so forth. Additionally, we also investigate how to apply blockchain and cloud computing technology in intelligent medical scenarios

(ii) To overcome the highly complex computation brought by encryption, we adopt the proxy reencryption method and ABE method to provide a specific access control mechanism to users and design the data sharing and replacement and privacy protection rule participated by the cloud service side

(iii) We propose a distributed medical data privacy protection scheme, bring in a cloud computing pattern, and designed blockchain-based distributed data management architecture to strengthen the computing power of the user side. Meanwhile, we also use the private chain in blockchain to ensure the security of patient data information

(iv) The simulation experiment has verified the effectiveness of the method in this paper. With blockchain and cloud computing, not only healthcare data can be effectively shared among medical institutions, but also the privacy of patient information can be assured

The remainder of this paper is organized as follows. Section 2 discusses related works, and the use of proxy reencryption for authorization management and access control in cloud computing is outlined in Section 3. The medical data privacy protection scheme based on blockchain and cloud computing is presented in Section 4. Section 5 shows the experimental simulation results, and Section 6 concludes the paper with a summary and proposed direction for future research.

2. Related Work

Medical data has precisely recorded people's illnesses, and medical records and the secure storage and sharing of medical data and patient privacy protection have increasingly become a priority to build intelligent hospitals. Traditional data access control technology builds and implements a safety access strategy with a completely reliable server, making it difficult to get adapted to the distributed network environment in modern times. Featured by decentralization and trustlessness, blockchain has given people a brand-new idea through distributed data storage, reliable point-to-point transmission, a consensus mechanism, and encryption algorithms [9]. In the security demand under the cloud computing environment in recent years, ABE is an important technological means, and the ABE access control mechanism has been studied extensively in the computing environment. As an encryption mechanism that uses attribute as a public key, the mechanism, in essence, links users with ciphertexts through the attribute. Its flexibility of encryption and access control form has greatly ensured the security of cloud data storage [10]. In the meanwhile, it has also achieved fine-grained access and become the key technique for secure cloud storage access control. However, the traditional ABE mechanism fails to completely guarantee data confidentiality, effectively prevent collision attack, or satisfy the forward and backward security of attribute revocation and the huge computing costs caused by revocation. It will be a significant core of research to apply blockchain into cloud computing and use the security mechanism of blockchain to enhance the secure storage and performance of cloud computing. The integration of blockchain and cloud computing plus proper security strategy can solve the contradiction between data sharing and privacy [11].

This paper has brought forth a distributed medical data privacy protection scheme based on blockchain and cloud computing technology with an aim at the open-ended question brought by data sharing of intelligent hospitals and personal privacy protection of patients. Concretely, on the one hand, the scheme has introduced a cloud computing pattern and designed blockchain-based distributed data management architecture for intelligent hospitals, in which it uses a consortium chain in the blockchain and ensures the security of user information in order to guarantee the operating efficiency of blockchain and reduce the computing burden of the user side. Besides, to handle the highly complex computing caused by encryption, it has used proxy reencryption technology and ABE technology to offer specific access control mechanisms to users. The access of every user is based on condition and attribute, which provides a secure exchange

of patient information for every doctor. The response side encrypts all medical data. The cloud nodes process the medical data transmitted to get and return the final ciphertext to the request side. On the other hand, it has designed the data sharing and replacement as well as privacy protection rules with the participation of the cloud computing service side, and it can greatly solve the difficulties in secure storage and sharing of intelligent hospitals.

The underlying communication of blockchain generally adopts P2P communication. P2P technology makes the communication on the network easy and direct and reduces the dependence on the intermediate server to the minimum. P2P technology has the characteristics of decentralization, scalability, robustness, high cost performance, and load balancing. Consensus mechanism is the core of blockchain, which maintains the normal operation of blockchain. Consensus mechanism is an algorithm to reach consensus on the order of things in a period of time. Common consensus mechanisms include proof of work (POW), proof of stake (POS), and practical Byzantine fault tolerance (PBFT). Consensus mechanism ensures that the uniqueness of information and data cannot be tampered with. Taking advantage of this, blockchain technology can be widely used in intelligent asset management, such as intellectual property protection and domain name management, to ensure that the contract is not tampered with. At present, relevant researchers all over the world have been studying medical data sharing and privacy protection. He et al. has proposed a medical data sharing model of cloud storage, which adopts the distributed sharing mechanism and which meets the interoperability requirements of CCR standard [12]; however, there is still a huge gap with the data security and privacy protection as required by intelligent hospitals. Seyedmostafa et al. has built a portable medical system architecture, which supports data security and privacy protection through the CIA/HIPAA protocol, but which does not meet the requirement of interoperability [13]. Liang et al. have used the CCR standard and designed a solution—HealthVault, which is a web medical and health record system and which adopts the client-server pattern. All medical data are stored in a third-party server, so security and reliability cannot be guaranteed [14]. The Healthticket model designed by Kyazze et al. enables doctors to access medical data of patients through the web app [15]. This model ensures the private information of patients with CP-ABE mechanism, but the access requires multiple licenses. The security, privacy, and interoperability of all these models are difficult to meet the requirements of intelligent healthcare. However, blockchain technology completes permission validation through a third party, which has solved the above problems satisfactorily, balanced medical data sharing and privacy protection, eliminated central nodes, and improved access efficiency.

Proxy reencryption is a key conversion mechanism between ciphertexts and it was proposed by Cheng et al. Wang et al. has given its normative formal definition in the 2005 Network & Distributed System Security Symposium (NDSS) and the 2007 ACM Conference on Computer and Communications Security and constructed the one-way proxy reencryption algorithm [16, 17]. Based on the above two studies, Xu has constructed the first valid two-way proxy reencryption algorithm [18]. Afterward, Yang et al. have also constructed the secure one-way proxy reencryption scheme without bilinear pairing [19]. Ateniese et al. had configured the privacy proxy reencryption algorithm in line with CPA security. As for ABE, Fan et al. had constructed the KP-ABE algorithm to support monotonous access for the first time, and the ciphertext uses the attribute for encryption [20]. The key is tied to user access strategy and only when the access strategy of the key matches the attribute of the passphrase can the user correctly decrypt the passphrase. Willison et al. had raised a secure and unbounded ABE algorithm [21], the size of whose attribute set is not confirmed when initializing the public parameters. Moreover, the available attributes are infinite polynomial orders, and new attributes can be added in the specific implementation. Hakak et al. had improved the ABE algorithm, which had extended the decryption condition to the universal monotonous access control and adopted a fine-sorted access control key [22]. It has greatly expanded the coverage of the ABE algorithm [23]. Later, Hussein et al. had come up with an ABE algorithm approximate to actual access control, but loopholes still exist in the security [24]. Conti et al. had put forward an ABE algorithm for DBDH problems, but the access mode is merely a simple attribute operation without reaching universal access control [25]. Integrating blockchain and cloud computing in the research of secure storage of healthcare data has found a new direction for the relevant theoretical research of information security and promoted extended applications of blockchain in the fields, which involve sensitive data such as intelligent healthcare. In this sense, it has certain practical value [26].

3. Use of Proxy Reencryption for Authorization Management and Access Control in Cloud Computing

When a cloud hospital needs to share the data authorization with another hospital, it needs to get the other's public key. Thus, it needs to generate a corresponding switch key for every user and then sends it to the cloud. When a user requests access to these data resources, the cloud will return the encrypted text of data and the corresponding key ciphertext according to the user's public key after verifying the identity authentication and authorization authentication, and the user decrypts these two ciphertext files to get the original plaintext resources of the corresponding data [27].

The cloud needs to generate a reencrypted ciphertext for every authorized user, and those unauthorized users have no right to obtain the reencrypted ciphertext of other users [28]. Even if unauthorized users do get the reencrypted ciphertext, they cannot decrypt the corresponding plaintext data. When applying ABE in proxy reencryption, it can authorize more than one user with the same group of attributes at one time. The procedure of proxy reencryption is as follows:

(1) Hospital A requests the cloud service provider to generate its pair of public and private keys and encrypts

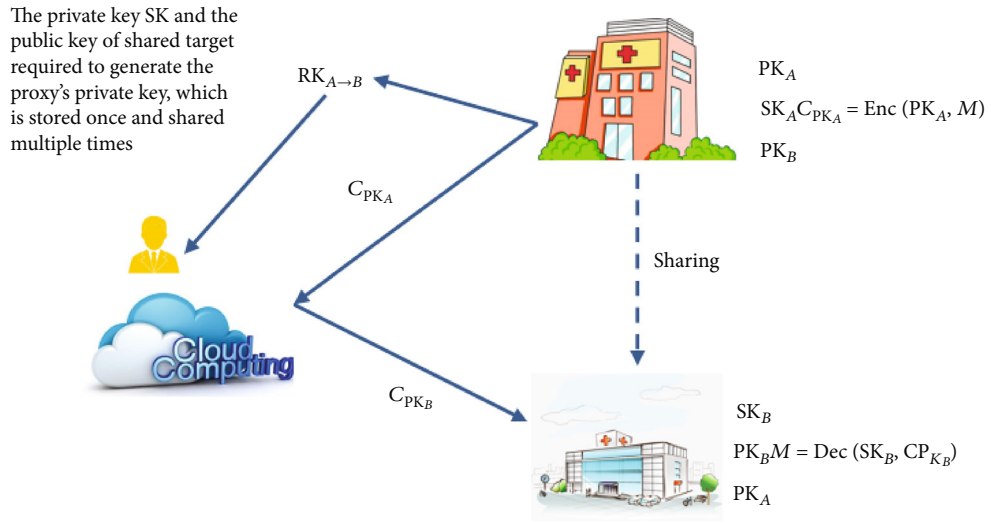

Figure 1: Sketch of proxy reencryption.

the plaintext M of medical data with its public key C_{PKa} to get the ciphertext C_{PKa} = Enc(PK_A, M). Here, M is what Hospital A wants to give to Hospital B.

(2) The cloud service provider generates a pair of public and private keys and returns them to Hospital A. After sending C_{PKa} to the cloud service provider, Hospital A also calculates for the cloud service provider and generates the specific key $RK_{A\to B}$.

(3) The intermediate proxy uses the key $RK_{A\to B}$ generated by Hospital A to change the ciphertext C_{PKa} into the encrypted text C_{PKb}, which can also be decrypted, by the private key of Hospital B. Here, the proxy only provides conversion service, and it cannot get the original plaintext data resources.

(4) Later, the proxy will send the encrypted text data C_{PKb} to Hospital B.

(5) After receiving the ciphertext from the proxy, Hospital B decrypts and gets the plaintext data M of medical data, secretly shared by Hospital A.

The sketch of proxy reencryption is shown in Figure 1.

The above proxy reencryption process has released the burden of Hospital A, which only needs to generate the key of the proxy while the transmission of specific medical data, the encrypted conversion of data, and the file storage are all completed by the cloud service provider. Proxy reencryption can achieve the sharing of ciphertext medical data in the cloud without leaking the decryption key of the data owner. The data can be stored once and shared many times, and only the shared key needs to be generated for the control of authority [29].

4. Medical Data Privacy Protection Scheme Based on Blockchain and Cloud Computing

4.1. Proxy Reencryption Based on Paillier and RSA. We adopt the proxy reencryption of Paillier homomorphism and the RSA algorithm to prevent shared medical data from leaking. If an encrypted function only satisfies the addition homomorphism, it can only be added and subtracted; if an encrypted function only satisfies multiplicative homomorphism, it can only perform multiplication and division. The Paillier algorithm is homomorphic to addition, and the RSA algorithm is homomorphic to multiplication. In an untrusted cloud storage, when the confidentiality of data cannot be guaranteed, the proxy reencryption part is used for reencryption, and the part is used for authorization. In the untrusted open environment of the third party, it can ensure the confidentiality of sensitive data in cloud storage. In homomorphic encryption, the private key encrypts medical data and only the client has the public key. In the keys generated by using proxy reencryption, even if a malicious attacker gets one of them, the attacker still needs another different key for decryption. If the attacker gets all these encrypted data, he cannot decrypt and get the original plaintext data between the client and the server. This also makes sure that even the processor cannot access the information of the data [30]. The algorithms begin with initialization and outputs from the central authentication center the pair of public and key keys, the master key of the center, the public key of the system, and the common parameters. Below are the specific implementation steps.

Step 1. Generate a pair of public and private keys.

Hospital A and Hospital B request the cloud service provider to generate their public keys and private keys, respectively. After the provider generates a pair of a public key and private key for Hospital A and Hospital B separately, the cloud service provider will return to Hospital A and Hospital B.

Step 2. Randomly choose two relatively big and independent prime numbers p, q to make

$$(pq, (p-1)(q-1)) = 1. \quad (1)$$

Step 3. Calculate

$$n = pq\,\varphi(n) = (p-1)(q-1),$$
$$e \text{ makes } \mathrm{Gcd}(e, \varphi(n)) = 1, \tag{2}$$

$$c = m^e \bmod n, \tag{3}$$

$$\lambda = cm(p-1, q-1), \tag{4}$$

in which m is the information to be encrypted.

Step 4. Choose a random integer g to make $g \in Z_n^*$.

Step 5. Use Equation (4) below and calculate the existence of modularized multiplicative inverse to determine n and separate the sequence of g.

$$\mu = (L(c\lambda \bmod n_2)) - 1 \bmod n, \tag{5}$$

in which, function L is defined as the following equation:

$$L(w) = w - \frac{1}{n}. \tag{6}$$

Step 6. The public key is (n, g) and the private key is (λ, μ).

Step 7. Generate the encrypted file.

Hospital A first uses RSA encryption to calculate and encrypt data to generate the encrypted file C1. Then, Hospital A encrypts according to the second layer, encrypts the key of RSA with its public key, and generates the encrypted file C2. Finally, Hospital A uploads two encrypted files: C1 and C2 into the server.

$$\text{Encrypt} \longrightarrow \mathrm{Enc}(m, pk). \tag{7}$$

$$c = gm \cdot n^r \bmod n^2. \tag{8}$$

Step 8. Make m the information to be encrypted and $m \in Z_n$.

Step 9. Randomly select r and make $r \in Z_n^*$.

Step 10. Calculate the ciphertext:

Step 11. Construct the key of proxy reencryption.

Hospital A requests the public key of Hospital A from the cloud service provider. The provider will return this public key to Hospital A. Hospital A uses the public key of Hospital B and its private key to generate the reencryption key, and then Hospital A uploads the newly generated reencryption key into the server.

Step 12. Calculate the public key and private key (Rsk, Rpk).

Step 13. The Paillier algorithm generates the reencrypted ciphertext and the public key (Rpk) is sent to the cloud computing server.

For a given public key(Rpk) and the second-layer ciphertext, this algorithm can use the reencryption key and generate the first-layer ciphertext of the public key (Rpk). The server uses the reencryption key and the ciphertext uploaded by Hospital A to conduct proxy reencryption computing and generates new ciphertext.

Step 14. Hospital B requests data and decrypts $\longrightarrow \mathrm{Dec}(c, sk)$.

Hospital B requests the cloud server to decrypt the data and the corresponding ciphertext. The cloud server sends the reencrypted text to Hospital B. Hospital B decrypts the ciphertext, gets the key, and uses RSA for decryption to get the original plaintext data.

Step 15. Ciphertext $c \in Z_n^*$.

Step 16. Compute the information.

$$m = \frac{L(c\lambda \bmod n^2)}{L(g\lambda \bmod n^2)} \bmod n. \tag{9}$$

4.2. Measurement of Ability of This Scheme against Malicious Attacks. Firstly, make the client set to implement the encryption task ρ_T. For the ith responder in ρ_T, its encrypted data is a m-dimensional vector, represented by s_i. So, $s_i = \{s_{i,j}, j = 1, \cdots, m\}$. After receiving the encrypted data, the cloud node EN_T will request ρ_T the credibility of every client in the response side to the central authentication center.

The reliability measurement s_i is weighed through the difference between s_i and the final result s_T. Here, we have defined the extent of difference between s_i and s_T as the square of Euclidean distance between s_i and s_T, which can be calculated through the following equation:

$$d_i = \sum_{j=1}^{m} \left(s_{i,j} - s_{T,j}\right)^2, \tag{10}$$

in which, the smaller the value of d_i, the higher the credibility of s_i. The degree of difference is the extent of difference among the values of variables, and it is used to measure the safety risk.

When the central authentication center receives the $\{d_i : i \in \rho_T\}$ from the cloud node EN_T, it needs to find the median of difference $\widehat{d}$. Introduce the adjustment parameter δ, and for the response side of the ith encryption task, if the difference of encrypted data is $d_i \le \widehat{d} + \delta$, the credibility of this user will increase. Besides, the smaller the d_i, the more the increase of the credibility. If $d_i > \widehat{d} + \delta$, then the credibility of this client decreases. In addition, the bigger the value of $d_i - \widehat{d}$, the more the reduction of the credibility. After getting the credibility r_i before implementing the current encryption task of the ith client in ρ_T,

Table 1: Attributes of different dimensions of encrypted medical data.

No.	Item name	Unit	Ref	No.	Item name	Unit	Ref
1	White blood cell	10^9/L	4–10	16	Monocyte number	10^9/L	0–0.8
2	Red blood cell	10^{12}/L	3.5–5.5	17	Eosinophil number	10^9/L	0.05–0.5
3	Hemoglobin	g/L	110–160	18	Basophil number	10^9/L	0–0.1
4	Hematocrit	%	36–50	19	Red cell distribution width-coefficient variation	10^9/L	10.9–15.3
5	Mean corpuscular volume	fL	82–100	20	Red cell distribution width-standard deviation	%	37–54
6	Mean corpuscular hemoglobin	pg	26–32	21	Platelet distribution width	fL	9–17
7	Mean corpuscular hemoglobin concentration	g/L	320–360	22	Mean platelet volume	fL	9–13
8	Platelets	10^9/L	100–300	23	Plateletcrit	%	0.17–0.3
9	Lymphocyte percentage	%	20–40	24	Platelet-larger cell ratio	%	13–43
10	Neutrophil percentage	%	50–70	25	Erythrocyte sedimentation rate		0–15
11	Monocyte percentage	%	3–8				
12	Eosinophil percentage	%	0.5–5				
13	Basophil percentage	%	0–1				
14	Lymphocyte number	10^9/L	0.8–4				
15	Neutrophil number						

the central authentication center has the following equation to calculate the credibility of this client:

$$r_{i+1} = r_i + \frac{\operatorname{sign}\left(\widehat{d} + \delta - d_i\right) + 1}{2} \cdot (1 - r_i) \cdot \exp\{-u \cdot d_i - \gamma\} + \frac{\operatorname{sign}\left(\widehat{d} + \delta - d_i\right) - 1}{2} \cdot r_i \cdot \left(1 - \exp\left\{-v \cdot \left(d_i - \widehat{d}\right) - \eta\right\}\right), \tag{11}$$

in which, u, γ, v, and η are the parameters to confirm r_{i+1}, and their values are all bigger than 0. sign (x) is a sign function, and it is defined as follows: if $x > 0$, sign $(x) = 1$; if $x = 0$, sign $(x) = 0$; and if $x < 0$, sign $(x) = -1$. By selecting the proper value of δ, $d_i < \widehat{d} + \delta$ always sustains when the user accesses normally, and it can eliminate malicious accesses and attacks from the client set with increased difference.

After getting $d_i'(i \in \rho_T)$, first, find the median $\widehat{d}'$ in the sequence of differences. It can be learned from Equation (11) that parameters γ and η have decided the rates at which the credibility converges to 0 and 1, respectively.

For the i user in ρ_T, if $d_i' < \widehat{d}'$, it is deemed as normal access. At this time, we introduce the adjustment parameter δ', and its value is a positive integer. The credibility iteration formula has become the following from Equation (11):

$$r_{i+1} = \begin{cases} r_i + (1 - r_i) \cdot \exp\left\{-u' \cdot d_i' - \gamma\right\}, & \text{if } d_i' < \widehat{d}', \\ r_i, & \text{if } \widehat{d}' \le d_i' \ge \widehat{d}' + \delta', \\ r_i \cdot \exp\left\{v' \cdot \left(d_i' - \widehat{d}'\right) - \eta\right\}, & \text{if } d_i' > \widehat{d}' + \delta', \end{cases} \tag{12}$$

in which, u' and v' are two new parameters. u' is smaller than u, and a smaller u' can avoid too much difference in the client's credibility during the iteration of Equation (12). Likewise, v' should also be smaller than v.

5. Simulation Experiment and Analysis

When conducting a simulation experiment, we use the data of the patient's routine medical checks. The data is a 25-dimensional vector, and the numerical value of every dimension can be seen in Table 1. In order to complete every encryption task τ, the processor of the encryption task ρ_T will firstly receive a 25-dimensional medical data vector. Then, it encrypts every element in the vector and sends the encrypted result to the cloud node EN_T where it is located. As this scheme uses the frameworks of Hadoop and Spark in the side of cloud computing, it has higher storage and computing abilities. It can respond in a timely manner to the requests of users and complete the uploading, computing, and downloading operations of users, so it can achieve the purpose of dynamic sharing and patient privacy protection.

For every client, its credibility is initialized as 0.5 and according to Equations (11) and (12), the client's credibility increases when providing the accurate data and the credibility decreases when providing wrong data.

The impact of different values of the parameter γ on credibility can be reflected from the changes in the client's credibility when n increases. Make n represent the number of encryption tasks to be implemented by the client. As shown in Figure 2, if the client can constantly provide correct data, thenγdecides the speed at which its credibility is converged to 1. Besides, the bigger the value of γ, the faster its credibility is converged to 1. However, when the value γ is too big, it can be easily attacked internally and externally. Therefore, γ should not be too big, and normally, it is set $\gamma \in [2, 3]$.

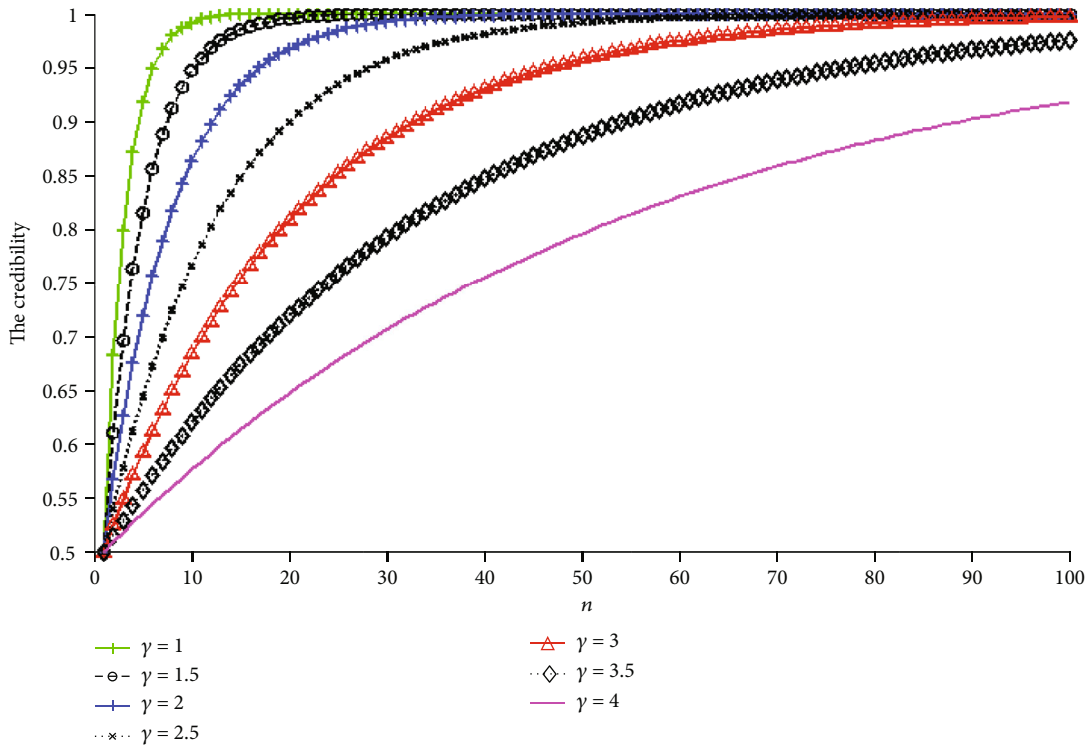

Figure 2: Impact of γ on credibility.

The value of η changes from the initial value of 0.03 to 0.28 at a step-length of 0.05. As indicated in Figure 3, η determines the speed at which that client's credibility is converged to 0. Besides, the value of η cannot be too big; otherwise, the credibility will drop too fast when the client generates wrong data due to various accidental factors, which should be avoided. Moreover, the value of η cannot be too little, either; otherwise, it will give too little punishment to the credibility of dishonest clients and lead to further attacks. The values of γ and η shall meet the requirement of $\exp\{-\gamma\} < 1 - \exp(-\eta)$. In this paper, it is set as follows: $\eta = 0.13$.

In order to analyze the impact of parameters u, v, u', and v' on updated credibility, this paper has set the scenario, which includes 100 encryption tasks. These 100 client sides need to handle 100 encryption tasks. In the initial stage, the initial credibility of every client handling the encryption task is 0.5. In all encryption processing, we assume that there exist 10 dishonest clients and set $\delta = 0.15$.

When analyzing the impact of parameter u on credibility update, we randomly select a normal client and observe the change of credibility over the number of tasks n. Here, the values of u include 5, 20, 50, 80, and 100. For every value of u, we experiment 100 times and summarize the changes of the mean value of that client's credibility when n increases from 1 to 100. As can be seen from Figure 4, the smaller the value of u, the faster the client's credibility is converged to 1. When updating the credibility through Equation (12), the smaller the value of u, the bigger the value of $\exp\{-u \cdot d_i - \gamma\}$ and the more the increase in the client's credibility after giving one correct data. When u is 0, the increase of credibility is completely decided by γ and it cannot filter different clients. Therefore, the value u cannot be too small; otherwise, the client can easily get higher credibility and cause potential security risks. Generally, it is set $u \in [50, 100]$.

Likewise, the impact of v credibility update is analyzed. The values of v are 0.001, 0.005, 0.01, 0.05, and 0.1. In particular, the value of v is much smaller than that of u because the difference in data of normal clients is usually very close and approximates to 0. As indicated in Figure 5, the bigger the value of v, the faster the credibility of dishonest clients is converged to 0. According to Equation (12), when v approximates 0, the decrease of credibility is determined by parameter η. In order to avoid the client's credibility falling too much due to the occasional provision of few wrong data, the value of v cannot be too small, and generally, it is set as $v \in [0.005, 0.01]$.

When analyzing the impact of u' on credibility, its values are set as 0.001, 0.005, 0.01, 0.05, and 0.1, and meanwhile, make $\delta' = 35$. Generally, the value u' is smaller. Figure 6 has shown the changes of credibility when u' takes different values. It can be seen that the impact of u' is similar to that of u; in other words, the smaller the u', the faster the credibility is converged to 1. Considering the difficulty to set credibility, the value u' cannot be too small, and normally, it is as follows: $u' \in [0.01, 0.05]$.

Figure 7 shows the changes of credibility when v' is given the values of 0.001, 0.005, 0.01, 0.05, and 0.1. The bigger the value of v', the faster the credibility is converged to 0. After all medical data are normalized, within the range of $[0, 1]$, the credibility is arranged according to the order of difference

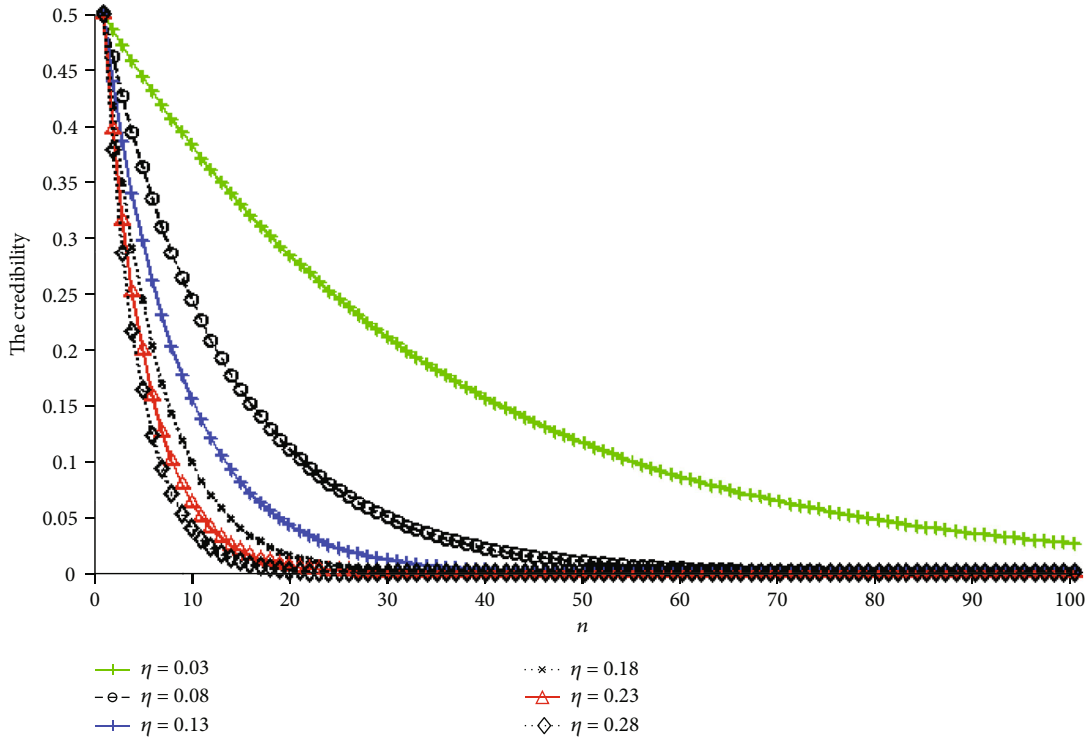

Figure 3: Impact of η on credibility.

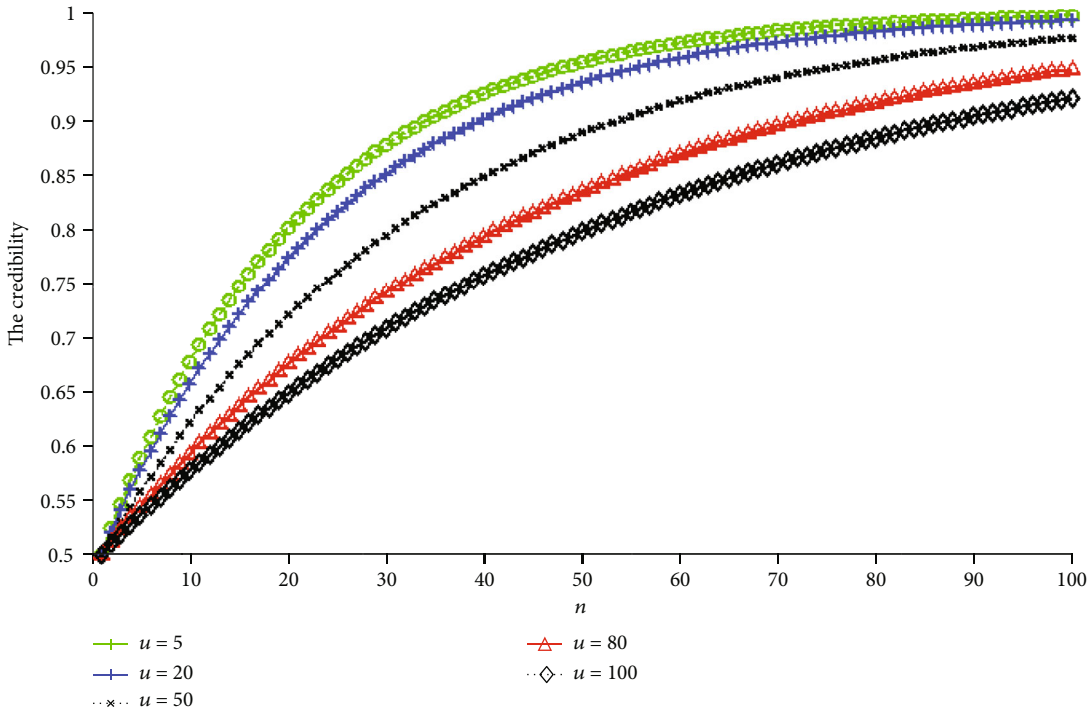

Figure 4: Impact of different values of u on credibility.

of encrypted data. With the changing trend of credibility, the value of v' is smaller than that of v. Besides, to prevent credibility from falling too quickly, the value of v' cannot be too big. Generally, we have set $v' = 0.05$.

With the help of the powerful storage ability of the cloud platform, the client will store the ciphertext in the cloud after the client uses the RSA method to encrypt the data, by encrypting the public key of the client-side, uploading, and

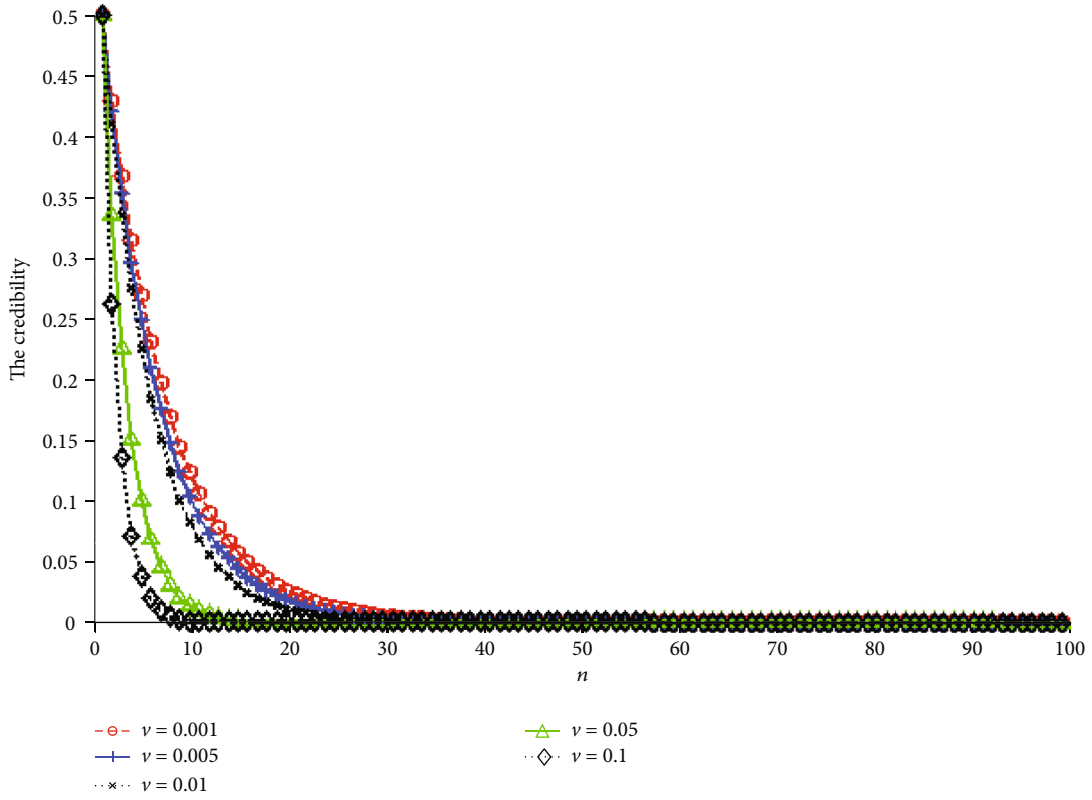

Figure 5: Impact of value of v on credibility.

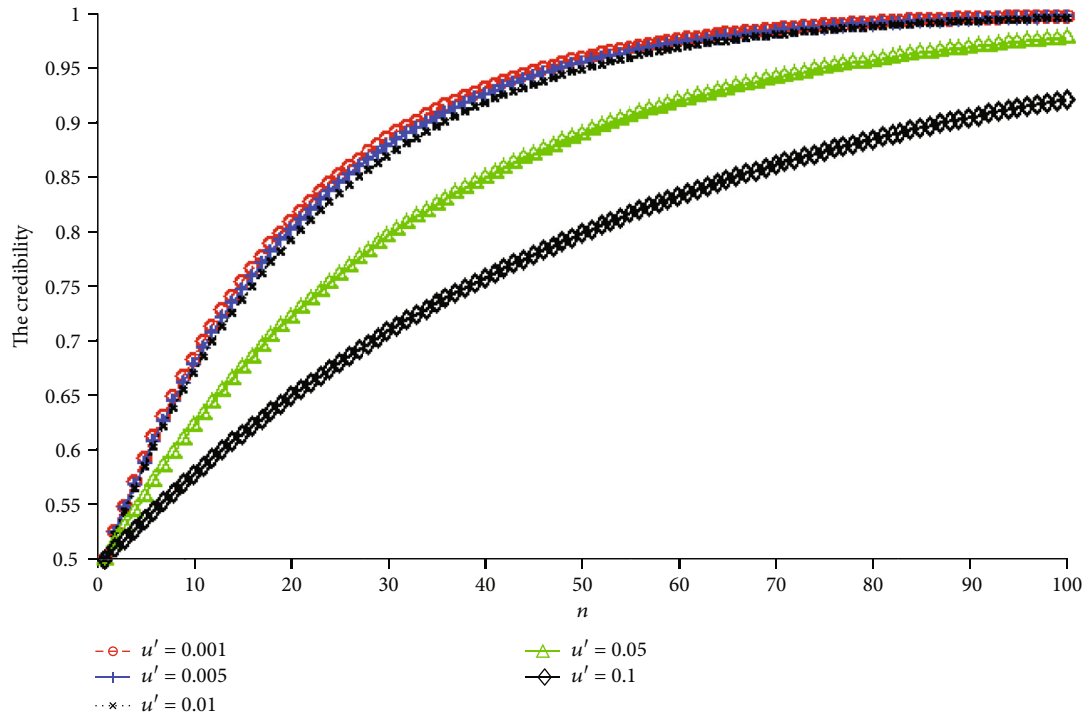

Figure 6: Impact of u' value on credibility.

storing the ciphertext to the cloud. When the client wants to share the data with another person, the client generates a reencryption key according to its decryption key and the encryption key of the other person and sends it to the cloud. The cloud server uses its strong computing power, integrates the reencryption key, proceeds with the reencryption, and

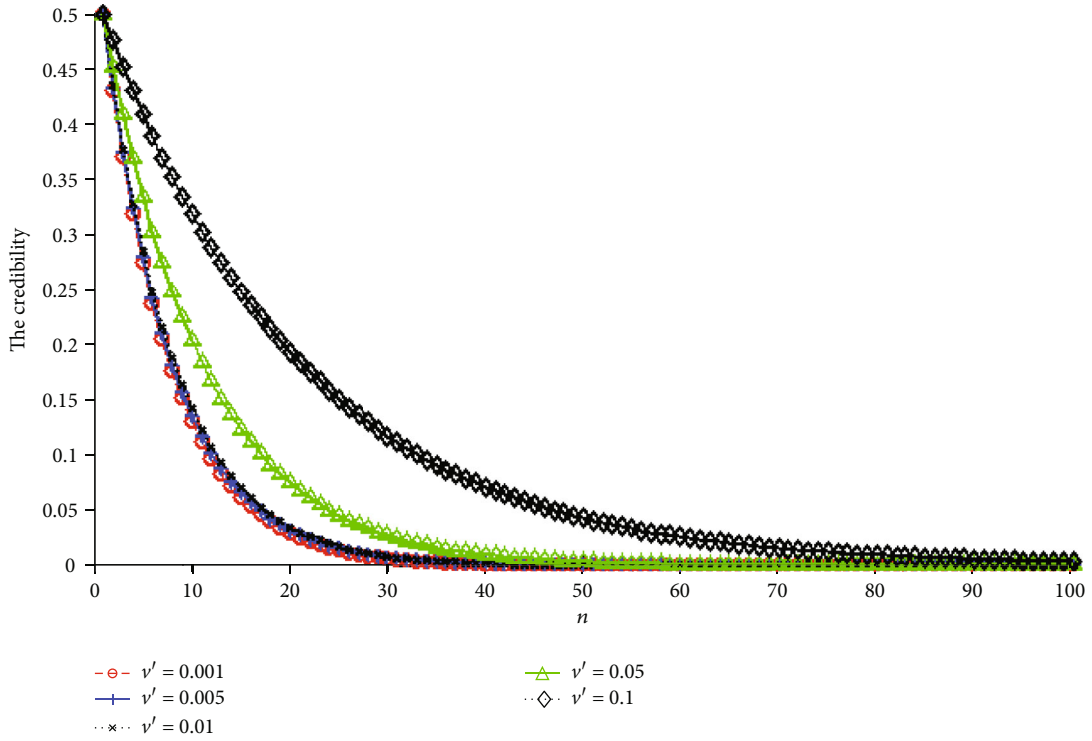

Figure 7: Impact of v' value on credibility.

stores the ciphertext in the cloud. Then, the other person downloads from the cloud server, decrypts with his private key, and gets the original plaintext with RSA decryption. In this way, the ciphertext is shared and the private key of the client is not leaked in this entire process. The medical data privacy protection scheme based on blockchain and cloud computing designed in this paper solves the problems of medical data storage and point-to-point data transaction, meets the needs of users for data management, and provides a new idea for solving the problem of data privacy security. Compared with the traditional technology, this scheme does not need an additional trusted third party nor does it need to rely on the "challenge response" mechanism, that is, the cloud does not need to provide special interface support, and the blockchain does not need to construct special transactions for the technical solution.

6. Conclusion

Blockchain is a brand-new decentralized distributed database, and it is a series of data blocks by using cryptographic methods. In this paper, we combined two encryption methods: proxy reencryption and attribute-based encryption and built key technical solutions for cloud computing based on blockchain to be applied in security and privacy protection of distributed medical data. It can not only achieve integrity testing of cloud data but also achieve broader security encryption computing. Intelligent hospitals only need to give the proxy key to the cloud server, which can convert medical data into the encrypted text in the designated format. The fixed client can access these shared data resources with their private key at any time. Even if the cloud server has the proxy key, it cannot get these data resources and the client does not need to download these resources. The proposed scheme can help solve such problems in that healthcare data are easy to be monopolized and tampered with and difficult to share and that the third party is not trustworthy to achieve the purpose of secure sharing and storage of distributed, decentralized, traceable, and unalterable healthcare data. In the future, we will consider improving the consensus mechanism, studying how to achieve fine-grained control of cloud data and how to reduce the storage overhead of redundant data, so that the performance of the blockchain can meet more needs of intelligent hospitals.

Data Availability

The raw/processed data required to reproduce these findings cannot be shared at this time as the data also forms part of an ongoing study.

Conflicts of Interest

The authors declare that they have no competing interests.

References

[1] H. Liang, J. Zou, K. Zuo, and M. J. Khan, "An improved genetic algorithm optimization fuzzy controller applied to the wellhead back pressure control system," *Mechanical Systems and Signal Processing*, vol. 142, p. 106708, 2020.

[2] R. He, N. Xiong, L. T. Yang, and J. H. Park, "Using multimodal semantic association rules to fuse keywords and visual features automatically for web image retrieval," *Information Fusion*, vol. 12, no. 3, pp. 223–230, 2011.

[3] H. Zheng, W. Guo, and N. Xiong, "A kernel-based compressive sensing approach for mobile data gathering in wireless sensor network systems," *IEEE Transactions on Systems, Man, and Cybernetics: Systems*, vol. 48, no. 12, pp. 2315–2327, 2018.

[4] Z. Wan, N. Xiong, N. Ghani, A. V. Vasilakos, and L. Zhou, "Adaptive unequal protection for wireless video transmission over IEEE 802.11e networks," *Multimedia Tools and Applications*, vol. 72, no. 1, pp. 541–571, 2014.

[5] H. Liang, J. Zou, Z. Li, M. J. Khan, and Y. Lu, "Dynamic evaluation of drilling leakage risk based on fuzzy theory and PSO-SVR algorithm," *Future Generation Computer Systems*, vol. 95, pp. 454–466, 2019.

[6] S. Tanwar, K. Parekh, and R. Evans, "Blockchain-based electronic healthcare record system for healthcare 4.0 applications," *Journal of Information Security and Applications*, vol. 50, no. 2, p. 102407, 2020.

[7] A. Farouk, A. Alahmadi, S. Ghose, and A. Mashatan, "Blockchain platform for industrial healthcare: vision and future opportunities," *Computer Communications*, vol. 154, no. 15, pp. 223–235, 2020.

[8] S. Cao, G. Zhang, P. Liu, X. Zhang, and F. Neri, "Cloud-assisted secure eHealth systems for tamper-proofing EHR via blockchain," *Information Sciences*, vol. 485, no. 6, pp. 427–440, 2019.

[9] T. McGhin, K.-K. R. Choo, C. Z. Liu, and D. He, "Blockchain in healthcare applications: research challenges and opportunities," *Journal of Network and Computer Applications*, vol. 135, pp. 62–75, 2019.

[10] A. Al Omar, M. Z. A. Bhuiyan, A. Basu, S. Kiyomoto, and M. S. Rahman, "Privacy-friendly platform for healthcare data in cloud based on blockchain environment," *Future Generation Computer Systems*, vol. 95, pp. 511–521, 2019.

[11] N. Islam, Y. Faheem, I. U. Din, M. Talha, M. Guizani, and M. Khalil, "A blockchain-based fog computing framework for activity recognition as an application to e-healthcare services," *Future Generation Computer Systems*, vol. 100, no. 11, pp. 569–578, 2019.

[12] C. He, X. Fan, and Y. Li, "Toward ubiquitous healthcare services with a novel efficient cloud platform," *IEEE Transactions on Biomedical Engineering*, vol. 60, no. 1, pp. 230–234, 2013.

[13] S. Safavi and Z. Shukur, "Conceptual privacy framework for health information on wearable device," *PLoS One*, vol. 9, no. 12, article e114306, 2014.

[14] L. Huang, X. Chen, and X. Lai, "Network security prediction method based on Kalman filtering fusion decision entropy theory," *International Journal of Security and its Applications*, vol. 10, no. 12, pp. 347–358, 2016.

[15] M. Kyazze, J. Wesson, and K. Naude, "The design and implementation of a ubiquitous personal health record system for South Africa," *Studies in Health Technology & Informatics*, vol. 206, no. 206, pp. 29–41, 2014.

[16] H. Cheng, D. Feng, X. Shi, and C. Chen, "Data quality analysis and cleaning strategy for wireless sensor networks," *EURASIP Journal on Wireless Communications and Networking*, vol. 2018, no. 1, 11 pages, 2018.

[17] S. Wang, X. Wang, F. Meng, R. Yang, and Y. Zhao, "Investor behaviour monitoring based on deep learning," *Behaviour & Information Technology*, pp. 1–12, 2020.

[18] C. Xu, "A novel recommendation method based on social network using matrix factorization technique," *Information Processing & Management*, vol. 54, no. 3, pp. 463–474, 2018.

[19] R. Yang, L. Yu, Y. Zhao et al., "Big data analytics for financial market volatility forecast based on support vector machine," *International Journal of Information Management*, vol. 50, no. 1, pp. 452–462, 2020.

[20] K. Fan, Y. Ren, Y. Wang, H. Li, and Y. Yang, "Blockchain-based efficient privacy preserving and data sharing scheme of content-centric network in 5G," *IET Communications*, vol. 12, no. 5, pp. 527–532, 2018.

[21] D. J. Willison, M. K. Kapral, P. Peladeau, J. A. Richards, J. Fang, and F. L. Silver, "Variation in recruitment across sites in a consent-based clinical data registry: lessons from the Canadian Stroke Network," *BMC Medical Ethics*, vol. 7, no. 1, p. 6, 2006.

[22] S. Hakak, W. Z. Khan, G. A. Gilkar, M. Imran, and N. Guizani, "Securing smart cities through blockchain technology: architecture, requirements, and challenges," *IEEE Network*, vol. 34, no. 1, pp. 8–14, 2020.

[23] H. Cheng, N. Xiong, A. V. Vasilakos, L. T. Yang, G. Chen, and X. Zhuang, "Nodes organization for channel assignment with topology preservation in multi-radio wireless mesh networks," *Ad Hoc Networks*, vol. 10, no. 5, pp. 760–773, 2012.

[24] A. F. Hussein, N. ArunKumar, G. Ramirez-Gonzalez, E. Abdulhay, J. M. R. S. Tavares, and V. H. C. de Albuquerque, "A medical records managing and securing blockchain based system supported by a genetic algorithm and discrete wavelet transform," *Cognitive Systems Research*, vol. 52, no. 12, pp. 1–11, 2018.

[25] A. Conti, P. Delbon, L. Laffranchi, C. Paganelli, and F. De Ferrari, "HIV-positive status and preservation of privacy: a recent decision from the Italian Data Protection Authority on the procedure of gathering personal patient data in the dental office," *Journal of Medical Ethics*, vol. 38, no. 6, pp. 386–388, 2012.

[26] F. Holotiuk, F. Pisani, and J. Moormann, "Radicalness of blockchain: an assessment based on its impact on the payments industry," *Technology Analysis and Strategic Management*, vol. 31, no. 8, pp. 915–928, 2019.

[27] Z. Liu, B. Hu, B. Huang, L. Lang, H. Guo, and Y. Zhao, "Strategies of Haze Risk Reduction Using the Tripartite Game Model," *Complexity*, vol. 2020, Article ID 2145951, 11 pages, 2020.

[28] F. Hu and G. Wu, "Distributed error correction of EKF algorithm in multi-sensor fusion localization model," *IEEE Access*, vol. 8, pp. 93211–93218, 2020.

[29] Z. Liu, B. Hu, Y. Zhao et al., "Research on intelligent decision of low carbon supply chain based on carbon tax constraints in human-driven edge computing," *IEEE Access*, vol. 8, pp. 48264–48273, 2020.

[30] L. Huang, J. Zheng, and G. Tan, "Research on task scheduling convergence non-dominated sorting method in cloud computing," *International Journal of Grid Distribution Computing*, vol. 8, no. 1, pp. 237–246, 2015.

Hindawi
Wireless Communications and Mobile Computing
Volume 2020, Article ID 8842031, 9 pages
https://doi.org/10.1155/2020/8842031

Research Article

Research on Semiactive Control of Civil Engineering Structure Based on Neural Network

Longji Jian,[1,2] **Feifei Song**,[2] **and Yuansong Huang**[2]

[1]*College of Civil Architecture and Environment, Xihua University, Chengdu 610039, China*
[2]*Sichuan Qinghe Science and Technology Co., Ltd., Chengdu 610039, China*

Correspondence should be addressed to Longji Jian; biounicom@mail.xhu.edu.cn

Received 8 July 2020; Revised 30 July 2020; Accepted 23 August 2020; Published 22 September 2020

Academic Editor: Hongju Cheng

Copyright © 2020 Longji Jian et al. This is an open access article distributed under the Creative Commons Attribution License, which permits unrestricted use, distribution, and reproduction in any medium, provided the original work is properly cited.

In order to improve the strength of civil engineering structure, a semiactive control model of civil engineering structure based on neural network is proposed, and the control constraint parameter model of semiactive regulation of civil engineering structure is constructed. Combined with the controlled object model, the semiactive control model of civil engineering structure is designed, the mechanical analysis model of civil engineering structure is established, and the semiactive regulation of civil engineering structure is carried out by the small disturbance suppression method. The semiactive adjustment of civil engineering structure is carried out by using the structural strength fusion tracking method. Taking the internal strength and shock yield response of civil engineering structure as constraint parameters, the semiactive control of civil engineering structure is carried out and PID neural network is used to optimize the control system. The simulation results show that the semiactive control of civil engineering structure with this method has good stability, and the strength and yield response strength of civil engineering structure are improved, and it has good control efficiency.

1. Introduction

With the development of civil engineering, people pay more attention to the research of civil engineering construction. The strength of civil engineering structure is an important measure to the surface of civil engineering. Under the condition of high load, the stress of external prestress of civil engineering structure is analyzed, and the average strain coordinated support is decomposed under a multifreedom structure [1]. Under different stress loads and damping loads, the stress intensity of civil engineering structures can be improved and semiactive control of civil engineering structures can be realized by means of experimental loading and mathematical simulation of external prestressing forces of civil engineering structures. The study of semiactive control method of civil engineering structure has great value in improving the structural strength of civil engineering [2].

At present, most scholars at home and abroad use the moment-curvature method to analyze the external prestressing force of civil engineering structures [3] and calculate the external shear capacity of civil engineering structures by using the nodal compression bar model. The bond stress of civil engineering structure is increased, the cracking point of civil engineering structure is reduced effectively, and the effect of yield point on steel yield is reduced. However, in the process of structural stress transplantation, the constraint reinforcement method is adopted in this method [4]. It is easy to produce the prestress transfer with active lateral restraint, which leads to an inaccurate analysis of the stress situation of civil engineering structure. The improved design is carried out; in reference [5], an analysis model of external prestressing force of high load civil engineering structure based on prestressed fiberboard reinforcement is proposed. In the local coordinate system of element, the linear load loading of high load civil engineering structure is carried out, and the yield effect of load loading on the external prestressing force of civil engineering structure and the compression of vertical shear force are analyzed. The stress intensity and service life of civil engineering structures are improved, but the method is easy to cause the expansion and deformation of civil engineering structures in the course of load loading, and there are errors in the analysis of

prestressing forces under the action of disturbed stress field. In addition, in reference [6], a stress analysis model of external prestressing of high load civil engineering structures based on coordinated control of average strain is proposed. The total shear deformation of joints is used to decompose the external core beams of high load civil engineering structures. The characteristic reconstruction and stress characteristic decomposition are carried out on the confined parameters in the direction of the column, the load-loading test is carried out in the average strain circle, and the constitutive relation between the external prestress and the shear stress of the steel bar in the high-load civil engineering structure is obtained. The stress analysis is realized, but the calculation cost of the above analysis model is large and the process of realization is complex, which is not good for the semiactive control efficiency of civil engineering structure [7–9].

Aiming at the above problems, a semiactive control model of civil engineering structure based on neural network is proposed in this paper, and the control constraint parameter model of semiactive regulation of civil engineering structure is constructed. Combined with the controlled object model, the semiactive control model of civil engineering structure is designed, the mechanical analysis model of civil engineering structure is established, and the semiactive regulation of civil engineering structure is carried out by a small disturbance suppression method. The semiactive adjustment of civil engineering structure is carried out by using the structural strength fusion tracking method. Taking the internal strength and shock yield response of civil engineering structure as constraint parameters, the semiactive control of civil engineering structure is carried out and PID neural network is used to optimize the control system. Finally, the performance test is carried out through the simulation experiment, which shows the superiority of this method in improving the semiactive control ability of civil engineering structure.

2. The Proposed Model

Firstly, the constitutive relation model of external prestressing joint of high-load civil engineering structure is constructed, the structural mechanics analysis is carried out, and the structure of civil engineering is designed with a concrete columnar structure [10].

The neural network consists of multilayer neural networks. Different network layers are composed of multiple 2D planes. Each plane is composed of multiple independent neurons. The network structure is shown in Figure 1.

The network structure is a civil engineering structural unit with an input value of 32×32. After processing at the network layer, a $6 \times 28 \times 28$ three-dimensional matrix is obtained. This matrix is called a feature plane and can be obtained by processing characteristic parameters of 6×14. The feature plane of 14 uses the network layer to extract features from the visual image, and the pooling layer performs parameter reduction processing on the parameters, combines the two to form multiple convolution groups, extracts features layer by layer, and implements the neural network under several connection layers.

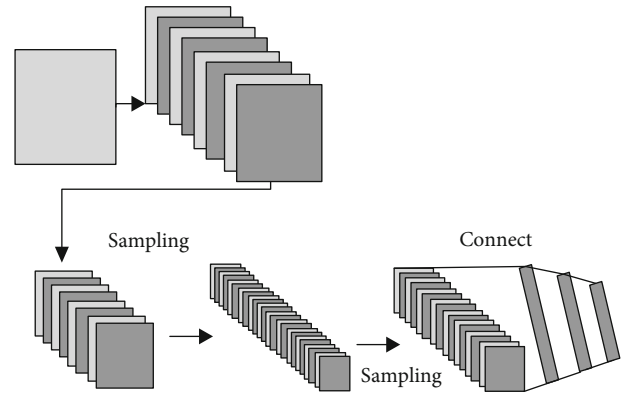

Figure 1: Schematic diagram of neural network structure.

The mechanical properties of concrete columns with steel strip spacing distribution in the element local coordinate system are investigated. The three-channel model of civil engineering structural mechanics can be expressed as follows:

$$\begin{cases} \ddot{\varphi}_a = -(b_1 + \Delta b_1)\dot{\varphi}_a - (b_2 + \Delta b_2)\varphi_a - (b_3 + \Delta b_3)\delta_\varphi + fd_1, \\ \ddot{\psi}_a = -(b_1 + \Delta b_1)\dot{\psi}_a - (b_2 + \Delta b_2)\psi_a - (b_3 + \Delta b_3)\delta_\psi + fd_2, \\ \ddot{\gamma} = -(d_3 + \Delta d_3)\delta_\gamma + fd_3. \end{cases} \tag{1}$$

The shear strain and control torque of civil engineering structures are calculated. By analyzing the constitutive relation of the core region of the node, we can get further results:

$$\begin{cases} \ddot{\varphi}_a = -b_1\dot{\varphi}_a - b_2\varphi_a - b_3\delta_\varphi + \rho_1, \\ \ddot{\psi}_a = -b_1\dot{\psi}_a - b_2\psi_a - b_3\delta_\psi + \rho_2, \\ \ddot{\gamma} = -d_3\delta_\gamma + \rho_3. \end{cases} \tag{2}$$

In which, $\rho_1 = -\Delta b_1\dot{\varphi}_a - \Delta b_2\varphi_a - \Delta b_3\delta_\varphi + fd_1$, $\rho_2 = -\Delta b_1\dot{\psi}_a - \Delta b_2\psi_a - \Delta b_3\delta_\psi + fd_2$, and $\rho_3 = -\Delta d_3\delta_\gamma + fd_3$ are uncertain items.

Under the same specimen, the mechanical analysis model of civil engineering structure is established, and the semiactive regulation of civil engineering structure is carried out by using a small disturbance suppression method [11]. The load model of civil engineering structure is described as follows:

$$\ddot{\varphi}_a = a_1\dot{\varphi}_a + a_2\varphi_a + bu + f_d. \tag{3}$$

In which, $b > 0$ is the unit load, $\dot{\varphi}_a$ is the internal structural mechanical distribution, u is the load characteristic input, and f_d is the external characteristic quantity.

According to the basic connotation of the approximate detection expected value to perceive the correlation between the stress of the civil engineering structure and to accurately monitor the stress transmission process of the multichannel

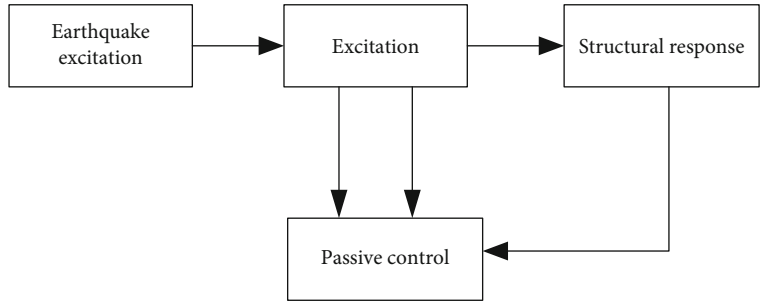

Figure 2: Passive control schematic diagram.

civil engineering structure with the minimum cost, the set of multichannel encrypted transmission civil engineering stress at time t can be expressed as:

$$S_t = \{a_1(t), a_1(t), \cdots \cdots, a_n(t)\}. \tag{4}$$

The basic ranking method for sensing stress of civil structures in a set can be defined as$\gamma(x_i, S_t)$:

$$\gamma(x_i, S_t): |\{i|a_i(t) \geq x_i\}|. \tag{5}$$

Then, the monitoring results obtained based on the algorithm can be expressed as$\mathrm{Top}(n, S_t)$, which meet the following conditions:

$$\begin{cases} \mathrm{Top}(n_i, S_t) \subset S_i, \\ |\mathrm{Top}(n_i, S_t)| = n, \\ \forall x \in \mathrm{Top}(n_i, S_t), \forall y \in S_i, x > y. \end{cases} \tag{6}$$

If the perceptual range of the cluster head node is not beyond the maximum of the filter, then in order to save the energy consumption of the node, it is not necessary to send the perceptual information to the common node to obtain the lowest load characteristic quantity.

The stress distribution method of the civil engineering structure is used to carry out the finite element analysis, and the load characteristic quantity of the civil engineering structure is obtained as follows:

$$b^{-1}\ddot{\varphi}_a - b^{-1}(a_1\dot{\varphi}_a + a_2\varphi_a) = u + b^{-1}f_d + \mathrm{Top}(n_i, S_t). \tag{7}$$

Set $M = b^{-1}$, $h(\varphi_a, \dot{\varphi}_a) = -b^{-1}(a_1\dot{\varphi}_a + a_2\varphi_a)$, and $d(t) = b^{-1}f_d$, the yield response strength of civil engineering structure is as follows:

$$M\ddot{\varphi}_a + h(\varphi_a, \dot{\varphi}_a) = u(t) + d(t). \tag{8}$$

The semiactive control constraint parameters of civil engineering structures consist of two parts: M and $h(\varphi_a, \dot{\varphi}_a)$, which are determined and uncertain:

$$\begin{aligned} M &= M_n + \Delta M, \\ h(\varphi_a, \dot{\varphi}_a) &= h_n(\varphi_a, \dot{\varphi}_a) + \Delta h(\varphi_a, \dot{\varphi}_a). \end{aligned} \tag{9}$$

In which, M_n and $h_n(\varphi_a, \dot{\varphi}_a)$ are semiactive control determinants for civil engineering structures and ΔM and $\Delta h(\varphi_a, \dot{\varphi}_a)$ are semiactive control uncertainties for civil engineering structures [12].

The k- ε two-equation turbulence model is constructed [13], and it can be further obtained:

$$M_n\ddot{\varphi}_a + h_n(\varphi_a, \dot{\varphi}_a) = u(t) + \rho(t), \tag{10}$$

where

$$\rho(t) = -\Delta M\ddot{\varphi}_a - \Delta h(\varphi_a, \dot{\varphi}_a) + d(t). \tag{11}$$

Assume that the upper bound of uncertainty of semiactive control system of civil engineering structure is $\bar{\rho}(t)$, that is,

$$|\rho(t)| < \bar{\rho}(t). \tag{12}$$

The constraint parameter model of semiactive control of civil engineering structure is constructed, and the control law is optimized by combining the stress characteristic distribution.

Passive control does not rely on external energy input. It is the installation of specific parameters of the antivibration antiseismic device in the designated parts of the building structure, such as energy dissipation, vibration isolation, and vibration absorption techniques, in order to prevent the ground motion from harming the building structure. The passive control block diagram is shown in Figure 2.

Passive control is divided into energy dissipation, base isolation, and tuned damping. Energy dissipation and shock absorption are to set the damper at the node or joint of the building structure, or to design the support of the building structure or the shear wall as energy-consuming components. When the earthquake is relatively small, the energy dissipation damper is in a state of elasticity. When a strong earthquake occurs, energy-consuming devices first consume a large amount of energy entering the structure into an inelastic state, thereby preventing the building structure from entering an inelastic state and protecting the building structure from damage. Base isolation means that the isolation control device is installed on the base of the building structure so as to isolate the seismic energy and transfer it to the upper part of the building, thus avoiding the destruction of the building structure caused by the earthquake. Tuning

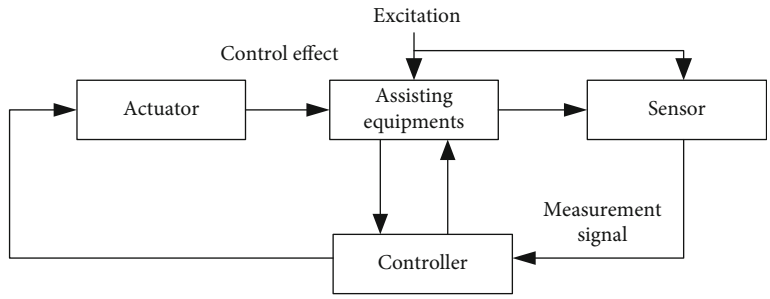

Figure 3: Active control schematic diagram.

vibration reduction is to reduce the vibration of the earthquake to the building structure by adding additional substructures to shift the vibration of the earthquake to the building structure.

Active control relies on external energy. During the vibration of the building structure in the event of an earthquake, active control devices generate control forces acting on the building structure, thereby rapidly reducing the vibration effect of the earthquake on the building structure. Active control principle is shown in Figure 3. It can be seen from the figure that the active control system consists of three parts: controller, sensor, and actuator. The working principle is as follows: when an earthquake occurs, the sensor transmits the detected seismic excitation or the vibration response of the building structure to the controller. According to the received information, the controller calculates the control force according to a certain control algorithm and issues a control command to the controller, and the actuator receives the control instruction to generate a control function that controls the force acting on the building structure, thereby reducing the damage of the earthquake to the building structure. The control force generated by the active control is changed in real-time with the different seismic waves, and the control effect is basically not affected by the characteristics of the seismic wave and is more advantageous than the passive control.

The active control overcomes the dependence of the passive control on the intensity and spectral characteristics of the seismic wave and is basically independent of this, so the active control can perform real-time control and can meet the high-precision control requirements, with good shock absorption effect and adaptability. However, the active control of the control device is entirely dependent on the external high-power energy to drive; when the earthquake occurs, the power is not guaranteed and the reliability of the active control system will be greatly reduced, so its stability is poor. Moreover, the active control system has a complicated structure and a relatively high cost, and it is difficult to apply it. In addition, active control systems need to perform signal processing, control algorithm implementation, and drive device actions during the operation. These require some time, which may cause time lag. Therefore, there is no large-scale application of active control systems in today's building structures.

The semiactive control of the civil engineering structure is developed from the vibration control of the active structure. The principle block diagram is shown in Figure 4. The control process of semiactive control relies on the vibration response and seismic excitation of the building structure, and it can change the stiffness or damping parameter of the semiactive control device in real-time with little external energy, thereby reducing the vibration response of the building structure, and can realize real-time and adjustable control of building structure. Semiactive control is a kind of parameter control. According to the vibration response, the parameters of the actuator can be directly adjusted to achieve a good shock absorption effect. It can be said that so far, in the structural vibration control method, semiactive control has the most prospects for civil engineering applications and the highest performance-cost ratio.

The commonly used control devices in semiactive control are variable damping and variable stiffness types:

(1) *Variable damping semiactive control system*. Variable damping semiactive control system is to install the variable damping device in the appropriate part of the building structure, according to the structure of the building. The vibration response adjusts the parameters of the variable damping device in real-time to provide a corresponding damping force, which reduces the vibration response of the building structure. In 1997, for the first time in the United States, active variable damping control devices were used on steel bridges to reduce the vibration generated by large vehicles, and the control effect was significant. Domestic Li Hui and others also conducted research to study the active variable damping control device for civil engineering.

(2) *Variable stiffness semiactive control system*. The variable stiffness semiactive control system is based on the stiffness of the building structure between the layers to adjust the stiffness of the building structure in real-time according to the seismic response. This changes the dynamic characteristics of the building structure, thereby reducing the damage of the earthquake to the building structure. KoboriT et al., after systematically researching and experimentally studying the variable stiffness control system, installed the active variable stiffness control device on a practical three-story building in Tokyo. This was the first case

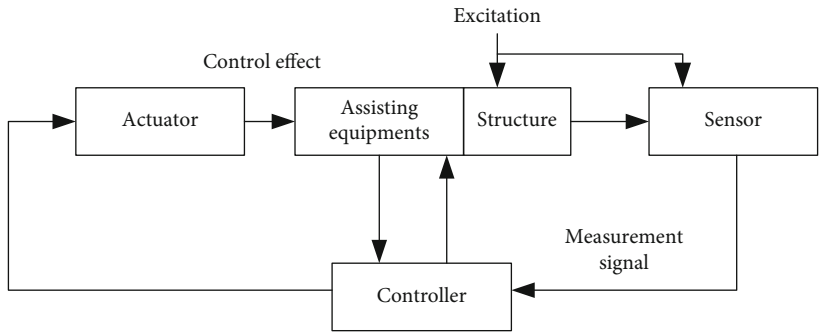

Figure 4: Semiactive control schematic diagram.

in the world and was carried out. Earthquake observation and test and the control effect are very good.

The semiactive control device has a simple structure and can be adjusted by itself. The required energy is much less than that of the active structure, and a greater control force can be obtained. In addition, the semiactive control has a damping effect that is close to that of the active control, and the stability is better because the control force generated by the semiactive control device is always opposite to that of the building structure. The more prominent advantage of semiactive control is that when the earthquake occurs, the power supply is interrupted and can be used as a passive damping device.

Combined with the controlled object model, the semiactive control model of civil engineering structure is designed, and the interface curvature response method is applied to carry out dynamic curvature correction:

$$\begin{cases} e_1 = \varphi_a - \varphi_{ad}, \\ e_2 = \dot{\varphi}_a - \dot{\varphi}_{ad}. \end{cases} \tag{13}$$

When the uncertainty of the system is not considered [14], the transverse elastic modulus distribution of the bearing capacity of civil engineering structures is obtained:

$$\begin{cases} \dot{e}_1 = e_2, \\ \dot{e}_2 = M_n^{-1}u - M_n^{-1}h_n(\varphi_a, \dot{\varphi}_a) - \ddot{\varphi}_{ad}. \end{cases} \tag{14}$$

The sliding surface of semiactive control of civil engineering structure is defined as:

$$s = ce_1 + e_2. \tag{15}$$

Then,

$$\dot{s} = c\dot{e}_1 + \dot{e}_2 = c\dot{e}_2 + \dot{e}_2. \tag{16}$$

The bearing capacity attenuation term is:

$$\dot{s} = 0. \tag{17}$$

The control characteristic function of civil engineering structure is:

$$\begin{aligned} ce_2 + \dot{e}_2 &= ce_2 + \ddot{\varphi}_a - \ddot{\varphi}_{ad} \\ &= ce_2 + M_n^{-1}u - M_n^{-1}h_n(\varphi_a, \dot{\varphi}_a) - \ddot{\varphi}_{ad} = 0. \end{aligned} \tag{18}$$

The equivalent control law is obtained as:

$$u_{eq} = h_n(\varphi_a, \dot{\varphi}_a) + M_n\ddot{\varphi}_{ad} - M_n ce_2. \tag{19}$$

Considering the uncertainty of the system, the distribution law of structural mechanics is chosen as:

$$u_0 = -\operatorname{sgn}(M_n)\bar{\rho}(t)\operatorname{sgn}(s). \tag{20}$$

Considering the influence of deterioration velocity parameters, the total joint stress of multiple connection members is obtained:

$$\begin{aligned} u &= u_{eq} + u_0 \\ &= h_n(\varphi_a, \dot{\varphi}_a) + M_n\ddot{\varphi}_{ad} - M_n ce_2 - \operatorname{sgn}(M_n)\bar{\rho}(t)\operatorname{sgn}(s). \end{aligned} \tag{21}$$

The control cash model of civil engineering structural mechanics is constructed. Under the limit tension strain condition of FRC, the compression strength reduction coefficient is introduced and the fuzzy PID neural network is used to optimize the control law [15].

3. Semiactive Control Optimization of Civil Engineering Structures

In this paper, a semiactive control model of civil engineering structure based on neural network is proposed [16]. The semiactive control of civil engineering structure is carried out with the internal strength and shock yield response of civil engineering structure as constraint parameter, and PID is adopted. Neural network is used to optimize the control system. The semiactive regulation of civil engineering

structures is carried out by using the method of small disturbance suppression. The Lyapunov function is defined as [17]:

$$V = \frac{1}{2}s^2. \tag{22}$$

Then,

$$\begin{aligned}\dot{V} &= s\dot{s} = s\left[ce_2 + M_n^{-1}u - M_n^{-1}h_n(\varphi_a, \dot{\varphi}_a) - \ddot{\varphi}_{ad} + M_n^{-1}\rho(t)\right] \\ &= sce_2 + sM_n^{-1}(h_n(\varphi_a, \dot{\varphi}_a) + M_n\ddot{\varphi}_{ad} - M_nce_2 \\ &\quad - \operatorname{sgn}(M_n)\bar{\rho}(t)\operatorname{sgn}(s)) - sM_n^{-1}h_n(\varphi_a, \dot{\varphi}_a) - s\ddot{\varphi}_{ad} + sM_n^{-1}\rho(t) \\ &= sM_n^{-1}\rho(t) - sM_n^{-1}\operatorname{sgn}(M_n)\bar{\rho}(t)\operatorname{sgn}(s) \\ &= sM_n^{-1}\rho(t) - \left|sM_n^{-1}\right|\bar{\rho}(t) \le \left|sM_n^{-1}\right||\rho(t)| - \left|sM_n^{-1}\right|\bar{\rho}(t) \\ &= \left|sM_n^{-1}\right|(|\rho(t)| - \bar{\rho}(t)) < 0.\end{aligned} \tag{23}$$

SPIDNN is selected as a learning network for semiactive control of civil engineering structure. It is a three-layer forward neural network, which is called $2 \times 3 \times 1$ structure. There are two neurons in the input layer of SPIDNN and two neural networks for semiactive control of civil engineering structure. The output of the branch $x_1, x_2, \ldots, x_n$ is multiplied by the sum of the weight value $w_{1j}, w_{2j}, \ldots, w_{nj}$, respectively, that is, the stress distribution of semiactive control of civil engineering structure is expressed as follows [18]:

$$\text{net}_j = \sum_{i=1}^{n} w_{ij}x_i(t), \quad i \neq j. \tag{24}$$

Using the neuron state u_j as the independent variable, the output value of the neuron can be generated according to the semiactive control output function of the civil engineering structure, namely:

$$x_j(k) = f\left(u_j(t)\right). \tag{25}$$

The Sigmoid function is used to adjust the semiactive control of civil engineering structure [19, 20]. Its expression is:

$$f(x) = \frac{1}{1 + e^{-x}}. \tag{26}$$

There are two neurons in the input layer of SPIDNN neural network with semiactive control of civil engineering structure. At any sampling time, the input layer of SPIDNN neural network is the input of the SPIDNN neural network:

$$\text{net}_i(k) = r_i(k), \quad i = 1, 2 \tag{27}$$

In which, the weight $\omega_{ij}(i = 1, 2; j = 1, 2, 3)$ of the input layer to the hidden layer is fixed, and the yield response strength of the semiactive control of the civil engineering structure is as follows [21, 22]:

$$\widehat{\bar{\rho}}(x, \omega) = \omega_1'\sigma_1(\varphi_a, \dot{\varphi}_a) + \omega_2'\sigma_2(\varphi_a, \dot{\varphi}_a) + \omega_3'\sigma_3(\varphi_a, \dot{\varphi}_a), \tag{28}$$

In which, $\sigma_j(\varphi_a, \dot{\varphi}_a)$ is the output of the hidden layer of semiactive control neural network for civil engineering structures; it is expressed as:

$$\begin{cases} \sigma_1(\varphi_a, \dot{\varphi}_a) = \dfrac{1}{1 + e^{-(\omega_{11}\varphi_a + \omega_{21}\dot{\varphi}_a)}}, \\ \sigma_2(\varphi_a, \dot{\varphi}_a) = \dfrac{1}{1 + e^{-\int(\omega_{21}\varphi_a + \omega_{22}\dot{\varphi}_a)dt}}, \\ \sigma_3(\varphi_a, \dot{\varphi}_a) = \dfrac{1}{1 + e^{-d(\omega_{11}\varphi_a + \omega_{21}\dot{\varphi}_a)}}. \end{cases} \tag{29}$$

Taking the internal strength and shock yield response of civil engineering structure as constraint parameters, semiactive control of civil engineering structure is carried out, and the variable structure control law of semiactive control of civil engineering structure is obtained [23]:

$$u = h_n(\varphi_a, \dot{\varphi}_a) + M_n\ddot{\varphi}_{ad} - M_nce_2 - \operatorname{sgn}(M_n)\widehat{\bar{\rho}}(t)\operatorname{sgn}(s). \tag{30}$$

The elastic model distribution model of civil engineering structural components is established under different load-bearing models, and the upper bound of uncertain parameters satisfies the requirements [24]:

$$\bar{\rho}(t) - |\rho(t)| > \varepsilon_0 > \varepsilon_1. \tag{31}$$

Note $\boldsymbol{\omega}^* = [\omega_1^* \quad \omega_2^* \quad \omega_3^*]$.
Adaptive algorithm is used to adjust weights online:

$$\begin{aligned}\widehat{\boldsymbol{\omega}} &= \eta\left|sM_n^{-1}\right|\boldsymbol{\sigma}(\varphi_a, \dot{\varphi}_a), \\ \eta &= \left|M_n^{-1}\right|(\varepsilon_0 - \varepsilon_1) > 0.\end{aligned} \tag{32}$$

The Lyapunov function of semiactive control for civil engineering structures is defined as:

$$V = \frac{1}{2}s^2 + \frac{1}{2}\eta^{-1}\tilde{\boldsymbol{\omega}}^{\mathrm{T}}\tilde{\boldsymbol{\omega}}. \tag{33}$$

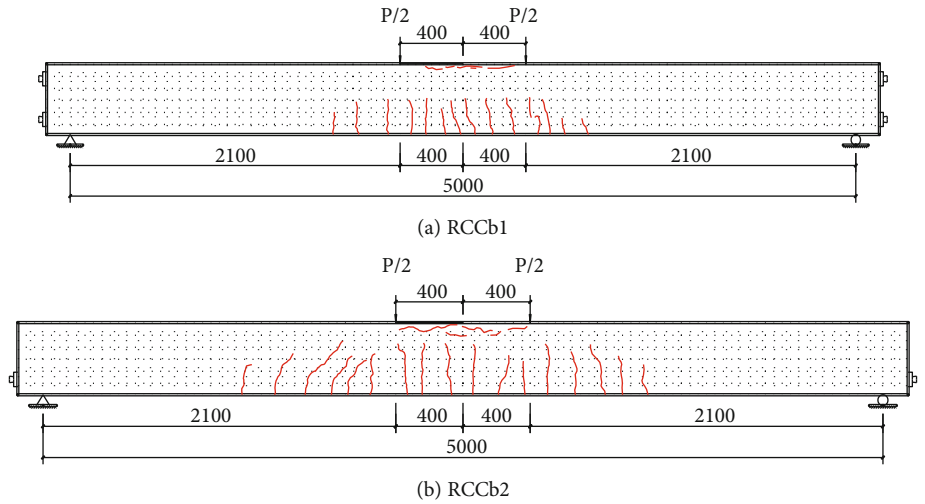

Figure 5: Structural mechanics analysis of civil engineering.

In which, $\tilde{\omega} = \omega^* - \hat{\omega}$. Then:

$$\begin{aligned}
\dot{V} &= s\dot{s} - \eta^{-1}\tilde{\omega}^T\dot{\hat{\omega}} \\
&= s\left(ce_2 + M_n^{-1}u - M_n^{-1}h_n(\varphi_a, \dot{\varphi}_a) - \ddot{\varphi}_{ad}\right. \\
&\quad \left. + M_n^{-1}\rho(t)\right) - \eta^{-1}\tilde{\omega}^{\mathrm{T}}\dot{\hat{\omega}} \\
&= sce_2 - sM_n^{-1}h_n(\varphi_a, \dot{\varphi}_a) - s\ddot{\varphi}_{ad} + sM_n^{-1}\rho(t) \\
&\quad - \eta^{-1}\tilde{\omega}^{\mathrm{T}}\dot{\hat{\omega}} + sM_n^{-1}(h_n(\varphi_a, \dot{\varphi}_a) + M_n\ddot{\varphi}_{ad} - M_nce_2 \\
&\quad \left. - \operatorname{sgn}(M_n)\hat{\bar{\rho}}(t)\operatorname{sgn}(s)\right) \\
&= -sM_n^{-1}\operatorname{sgn}(M_n)\hat{\bar{\rho}}(t)\operatorname{sgn}(s) + sM_n^{-1}\rho(t) - \eta^{-1}\tilde{\omega}^T\dot{\hat{\omega}} \\
&= -\left|sM_n^{-1}\right|\omega\wedge^T\sigma(\varphi_a, \dot{\varphi}_a) + sM_n^{-1}\rho(t) - \eta^{-1}\tilde{\omega}^T\dot{\hat{\omega}} \\
&= -\left|sM_n^{-1}\right|\left(\omega\wedge^T\sigma(\varphi_a, \dot{\varphi}_a) + \bar{\rho}(t) - \bar{\rho}(t)\right) \\
&\quad + sM_n^{-1}\rho(t) - \eta^{-1}\tilde{\omega}^T\dot{\hat{\omega}} \\
&\le -\left|sM_n^{-1}\right|\left(\omega\wedge^T\sigma(\varphi_a, \dot{\varphi}_a) - \bar{\rho}(t)\right) \\
&\quad - \left|sM_n^{-1}\right|(\bar{\rho}(t) - |\rho(t)|) - \eta^{-1}\tilde{\omega}^T\dot{\hat{\omega}} \\
&= -\left|sM_n^{-1}\right|\left(\omega\wedge^T\sigma(\varphi_a, \dot{\varphi}_a) - \omega^{*T}\sigma(\varphi_a, \dot{\varphi}_a)\right. \\
&\quad \left. + \varepsilon(\varphi_a, \dot{\varphi}_a)\right) - \left|sM_n^{-1}\right|(\bar{\rho}(t) - |\rho(t)|) \\
&\quad - \left(\omega^{*T} - \omega\wedge^T\right)\left|sM_n^{-1}\right|\sigma(\varphi_a, \dot{\varphi}_a) \\
&= -\left|sM_n^{-1}\right|\varepsilon(\varphi_a, \dot{\varphi}_a) - \left|sM_n^{-1}\right|(\bar{\rho}(t) - \\
&\le \left|sM_n^{-1}\right||\varepsilon(\varphi_a, \dot{\varphi}_a)| - \left|sM_n^{-1}\right|(\bar{\rho}(t) - |\rho(t)|) \\
&= \left|sM_n^{-1}\right|(|\varepsilon(\varphi_a, \dot{\varphi}_a)| - (\bar{\rho}(t) - |\rho(t)|)) \\
&\le \left|sM_n^{-1}\right|(\varepsilon_1 - \varepsilon_0) \le 0.
\end{aligned} \tag{34}$$

If the model satisfies:

$$\ddot{\varphi}_a = a_1\dot{\varphi}_a + a_2\varphi_a + bu + f_d. \tag{35}$$

The asymptotic stability of civil engineering structure control system can be guaranteed by using a deformed structure controller. The semiactive control model of civil engineering structure designed in this paper is bounded convergent [25].

4. Analysis of Simulation Experiment

In order to test the application performance of text method in semiactive control of civil engineering structure, the simulation experiment was carried out. ETABS software was used to simulate the specimen model of high-load civil engineering structure, and four groups of prefabricated structures with different thicknesses were designed. The compressive strength of civil engineering structure with ribbed floor is 12 MPa, the axial compressive strength is 25 MPa, and the elastic modulus of RCCb2 specimen is 2.45×104 MPa. According to the above parameters, the mechanical distribution of civil engineering structure is obtained as shown in Figure 5.

According to the results of mechanical numerical analysis, semiactive control of civil engineering structure is carried out, and the load displacement of civil engineering structure is shown in Figure 5. The semiactive control convergence curve of civil engineering structures is shown in Figure 6. Figure 7 is the semiactive control convergence curve of civil engineering structures.

The simulation results show that the semiactive control of civil engineering structure with this method has good stability, and the strength and yield response strength of civil engineering structure are improved.

5. Conclusions

In this paper, a semiactive control model of civil engineering structure based on neural network is proposed, and the control constraint parameter model of semiactive regulation of civil engineering structure is constructed. Combined with the controlled object model, the semiactive control model of civil engineering structure is designed, the mechanical analysis model of civil engineering structure is established,

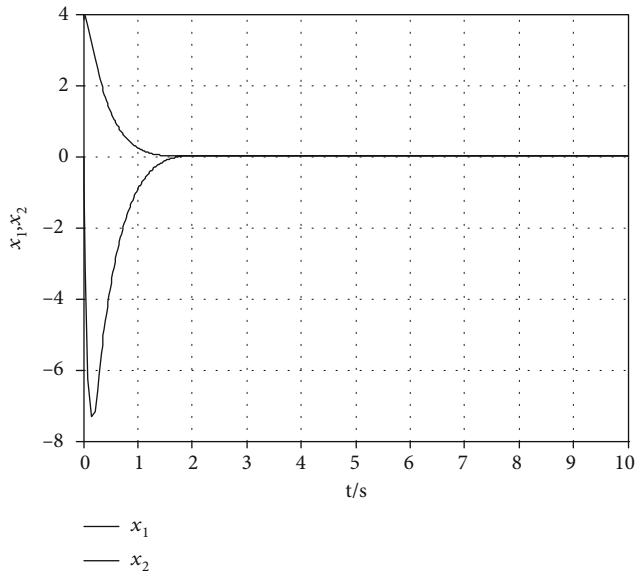

Figure 6: Load displacement of civil engineering structures.

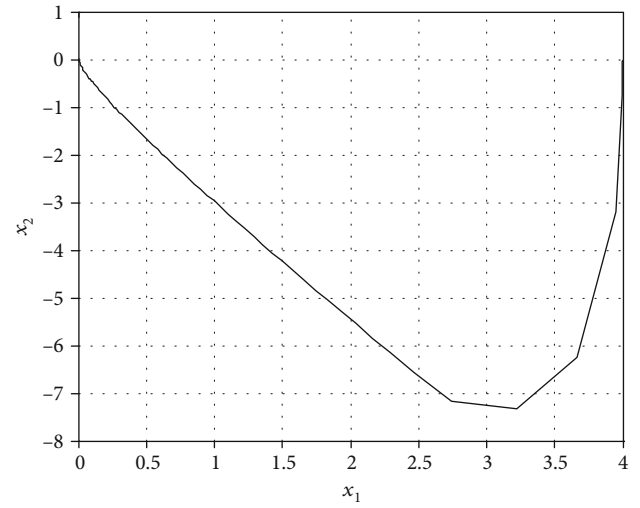

Figure 7: Semiactive control convergence curve of civil engineering structures.

and the semiactive regulation of civil engineering structure is carried out by the small disturbance suppression method. The semiactive adjustment of civil engineering structure is carried out by using the structural strength fusion tracking method. Taking the internal strength and shock yield response of civil engineering structure as constraint parameters, the semiactive control of civil engineering structure is carried out and PID neural network is used to optimize the control system. The simulation results show that the semiactive control of civil engineering structure with this method has good stability, the strength and yield response strength of civil engineering structure are improved, and it has good control efficiency. This method has good application value in the analysis and control of civil engineering structure mechanics.

Data Availability

The data in this paper are valid and available from the corresponding author.

Conflicts of Interest

This paper does not contain any conflict of interest.

Acknowledgments

The study is supported by the Major Science and Technology Projects of Sichuan Province, P. R. China (2018SZDZX0021).

References

[1] G. J. Parra-Montesinos, "High-performance fiber-reinforced cement composites: an alternative for seismic design of structures," *ACI Structural Journal*, vol. 102, no. 5, pp. 668–675, 2005.

[2] A. Aviram, B. Stojadinovic, and G. J. Parra-Montesinos, "High-performance fiber-reinforced concrete bridge columns under bidirectional cyclic loading," *ACI Structural Journal*, vol. 111, no. 2, pp. 303–312, 2014.

[3] R. Ahmadi, O. Rashidian, R. Abbasnia, F. Mohajeri Nav, and N. Usefi, "Experimental and numerical evaluation of progressive collapse behavior in scaled RC beam-column subassemblage," *Shock and Vibration*, vol. 2016, Article ID 3748435, 17 pages, 2016.

[4] F. Dinu, I. Marginean, D. Dubina, and I. Petran, "Experimental testing and numerical analysis of 3D steel frame system under column loss," *Engineering Structures*, vol. 113, pp. 59–70, 2016.

[5] A. G. Vlassis, B. A. Izzuddin, A. Y. Elghazouli, and D. A. Nethercot, "Progressive collapse of multi-storey buildings due to sudden column loss—Part II: Application," *Engineering Structure*, vol. 30, no. 5, pp. 1424–1438, 2008.

[6] L. Lin, X. Lu, P. Han, S. Cen, and J. Liu, "Analysis of impact force of large commercial aircraft to a rigid wall," *Journal of Vibration and Shock*, vol. 34, no. 9, pp. 158–163, 2015.

[7] L.-H. Han, C.-C. Hou, X.-L. Zhao, and K. J. R. Rasmussen, "Behaviour of high-strength concrete filled steel tubes under transverse impact loading," *Journal of Constructional Steel Research*, vol. 92, pp. 25–39, 2014.

[8] R. Wang, L. H. Han, and C. C. Hou, "Behavior of concrete filled steel tubular (CFST) members under lateral impact: experiment and FEA model," *Journal of Constructional Steel Research*, vol. 80, no. 4, pp. 188–201, 2013.

[9] B. Xu and X. Zeng, "Experimental study on the behaviour of reinforced concrete beams under impact loadings," *China Civil Engineering Journal*, vol. 47, no. 2, pp. 41–51, 2014.

[10] D. Lü, X. Yu, and Z. Chen, "Lateral seismic collapse fragility analysis of RC frame structures," *Journal of Harbin Institute of Technology*, vol. 43, no. 6, pp. 1–5, 2011.

[11] X. Yu, D. Lü, and H. Zheng, "Seismic sideway collapse fragility analysis based on typical failure modes," *Journal of Building Structures*, vol. 35, no. 8, pp. 8–15, 2014.

[12] E. Taub, et al.G. Uswatte, M. H. Bowman et al., "Constraint-induced movement therapy combined with conventional neurorehabilitation techniques in chronic stroke patients with plegic hands: a case series," *Archives of Physical Medicine and Rehabilitation*, vol. 94, no. 1, pp. 86–94, 2013.

[13] X. P. Zhou, X. F. Zhang, and X. N. Zhao, "Cloud storage performance evaluation research," *Computer Science*, vol. 41, no. 4, pp. 190–194, 2014.

[14] H. Liang, J. Zou, K. Zuo, and M. J. Khan, "An improved genetic algorithm optimization fuzzy controller applied to the wellhead back pressure control system," *Mechanical Systems and Signal Processing*, vol. 142, p. 106708, 2020.

[15] Y. Zhou, H. Zhang, F. Li, and P. Qi, "Local focus support vector machine algorithm," *Journal of Computer Applications*, vol. 38, no. 4, pp. 945–948, 2018.

[16] X. Xiong, L. Yang, Y. Ma, and Z. Zhuang, "Alerting algorithm of low-level wind shear based on fuzzy C-means," *Journal of Computer Applications*, vol. 38, no. 3, pp. 655–660, 2018.

[17] C. Lin, Y. X. He, and N. Xiong, "An energy-efficient dynamic power management in wireless sensor networks," in *2006 Fifth International Symposium on Parallel and Distributed Computing*, pp. 148–154, Timisoara, Romania, 2006.

[18] Y. Yang, N. Xiong, N. Y. Chong, and X. Défago, "A decentralized and adaptive flocking algorithm for autonomous mobile robots," in *2008 The 3rd International Conference on Grid and Pervasive Computing - Workshops*, pp. 262–268, Kunming, China, 2008.

[19] Y. Liu, M. Ma, X. Liu, N. N. Xiong, A. Liu, and Y. Zhu, "Design and analysis of probing route to defense sink-hole attacks for Internet of Things security," *IEEE Transactions on Network Science and Engineering*, vol. 7, no. 1, pp. 356–372, 2020.

[20] H. Liang, J. Zou, Z. Li, M. J. Khan, and Y. Lu, "Dynamic evaluation of drilling leakage risk based on fuzzy theory and PSO-SVR algorithm," *Future Generation Computer Systems*, vol. 95, pp. 454–466, 2019.

[21] C. Lin, N. Xiong, J. H. Park, and T. Kim, "Dynamic power management in new architecture of wireless sensor networks," *International Journal of Communication Systems*, vol. 22, no. 6, pp. 671–693, 2009.

[22] Y. Sang, H. Shen, Y. Tan, and N. Xiong, "Efficient protocols for privacy preserving matching against distributed datasets," in *Information and Communications Security. ICICS 2006*, vol. 4307 of Lecture Notes in Computer Science, pp. 210–227, 2006.

[23] F. Long, N. Xiong, A. V. Vasilakos, L. T. Yang, and F. Sun, "A sustainable heuristic QoS routing algorithm for pervasive multi-layered satellite wireless networks," *Wireless Networks*, vol. 16, no. 6, pp. 1657–1673, 2010.

[24] J. Li, N. Xiong, J. H. Park, C. Liu, S. MA, and S. E. Cho, "Intelligent model design of cluster supply chain with horizontal cooperation," *Journal of Intelligent Manufacturing*, vol. 23, no. 4, pp. 917–931, 2012.

[25] W. Guo, N. Xiong, A. V. Vasilakos, G. Chen, and C. Yu, "Distributed k–connected fault–tolerant topology control algorithms with PSO in future autonomic sensor systems," *International Journal of Sensor Networks*, vol. 12, no. 1, pp. 53–62, 2012.

Hindawi
Wireless Communications and Mobile Computing
Volume 2020, Article ID 8852965, 10 pages
https://doi.org/10.1155/2020/8852965

Research Article

Research on Sewage Monitoring and Water Quality Prediction Based on Wireless Sensors and Support Vector Machines

Cong Liu,[1] Hongji Li,[2] and Qinkun Zhang[1]

[1]*Water Supply and Water Pollution Control Research Center, Yulin College, Shaanxi Yulin 719000, China*
[2]*School of Urban Planning and Municipal Engineering, Xi'an University of Technology, Xi'an 710048, China*

Correspondence should be addressed to Qinkun Zhang; liucong@yulinu.edu.cn

Received 10 July 2020; Revised 3 August 2020; Accepted 26 August 2020; Published 19 September 2020

Academic Editor: Hongju Cheng

Copyright © 2020 Cong Liu et al. This is an open access article distributed under the Creative Commons Attribution License, which permits unrestricted use, distribution, and reproduction in any medium, provided the original work is properly cited.

Water resource protection has an important impact on ecosystem security and human survival. Therefore, water quality testing and early warning of the sewage status are getting more and more attention. In order to solve the problems of information transmission delay and insufficient water quality prediction in current water quality monitoring, this paper proposes a wireless sensor-based dynamic water quality monitoring and prediction technology. Firstly, this paper uses the wireless sensor technology and ZigBee protocol to establish a sewage monitoring model and real-time dynamic monitoring of total nitrogen, total phosphorus, ammonia nitrogen, and other indicators of the water quality of the basin. Secondly, on the basis of wireless monitoring, a support vector algorithm is used to construct a water quality prediction model to make a reasonable prediction of the water quality of the watershed. Finally, the actual test results show that the technology can automatically and real-timely monitor the water quality of the watershed to meet the requirements of water quality monitoring in practical applications.

1. Introduction

Water environment refers to the environment in which lakes, rivers, oceans, and other water qualities are located. Changes in the water environment will have a serious impact on water quality [1]. Determine whether the environment is contaminated by testing the physical and chemical properties of water quality. The water environment is an inseparable part of the ecosystem and is the basis for human survival and development. However, with the advancement of human science and technology, the water environment is increasingly polluted [2]. The Netherlands, Japan, the United States, and other countries have conducted research on water quality automatic monitoring systems and applied them to actual water quality monitoring [3]. The Netherlands has established an expensive water quality monitoring system [4] in the lower reaches of the Ames River. This system monitors the parameters of ammonia, nitrogen, total phosphorus, and pH in water quality in real time, and an alarm device is added to this monitoring system. A number of automatic water quality monitoring stations are used to monitor the water quality changes of the Windlass River in the United Kingdom [2]. Wireless sensor network technology is used in this system, and monitoring personnel can remotely control the monitoring station.

With the research of wireless sensor technology, the automatic water quality monitoring system also adopts wireless sensor network technology. Typical representatives are the distributed sensor network water quality automatic monitoring system designed by America [5], the wireless sensor network lake water quality system of the University of Virgin Mary [6], and the intelligent coastal water quality automatic monitoring system designed by the Irish [7]. In the above automatic water quality monitoring, wireless sensor networks have been widely used, reflecting the advantages of wide distribution, high density, low energy consumption, and low cost of wireless sensor networks [8]. Compared with traditional sensor networks, the construction of wireless sensor networks will not cause any damage to the natural environment. By using the mutual communication between sensor nodes, the automatic water quality monitoring system covers a wide monitoring area [9]. When a node in the

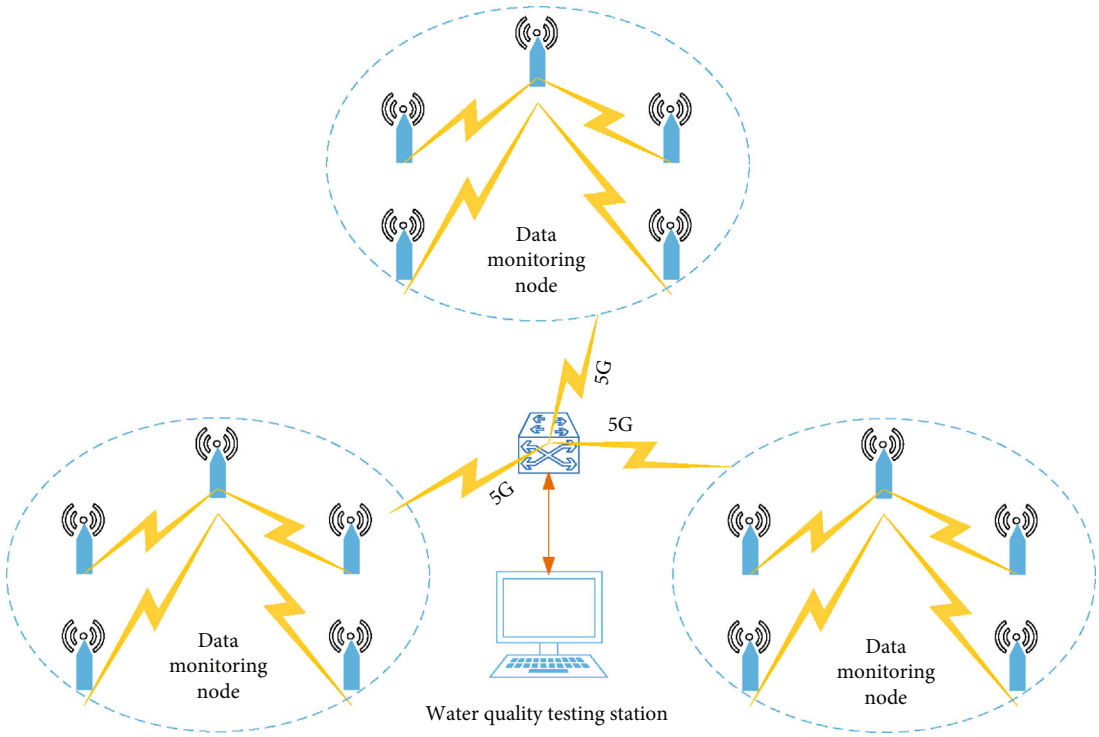

Figure 1: The overall architecture of the automatic water quality monitoring system.

wireless sensor network is broken or the power supply is insufficient, new sensor nodes will be added to the network to ensure smooth communication.

Although the above water quality automatic monitoring systems all use wireless sensor networks, there are still many problems that need to be improved [10]. The current wireless sensor water quality automatic monitoring system mainly faces the problems of high-power consumption and unreliable communication and needs to be improved in these two aspects. Moreover, today's wireless sensor network water quality automatic monitoring system mainly monitors oceans and lakes and rarely involves automatic water quality monitoring in watersheds [11]. Therefore, this paper proposes a sewage monitoring and water quality prediction model based on wireless sensors and support vector machines. The technical scheme of water quality monitoring is studied by combining wireless sensor hardware design and data processing optimization techniques such as support vector machines.

2. Sewage Detection Based on Wireless Sensor Networks

With the urbanization of society, the loss of domestic sewage, factory sewage, and farmland pesticides or fertilizers will cause the eutrophication of water quality in the basin. When the total nitrogen, total phosphorus, and ammonia nitrogen in the water quality of the watershed exceed the watershed's standard, the algae or other plankton in the water will multiply, which will cause the dissolved oxygen content in the water to drop sharply, and fish and other organisms will die [12, 13]. Total nitrogen, total phosphorus, and ammonia nitrogen are difficult to decompose naturally, so contaminated water may flow into people's drinking water system, threatening people's lives and health. Therefore, monitoring total nitrogen, total phosphorus, ammonia nitrogen, and COD is of great significance. The content of COD reflects the overall status of the water quality. By monitoring the content of total nitrogen, total phosphorus, and ammonia nitrogen, the types of pollutants can be judged, and then corresponding treatment can be made to ensure the safety of water quality [14].

Therefore, this paper proposes a water quality automatic monitoring system based on the wireless sensor of the watershed to monitor the four indicators of total nitrogen, total phosphorus, ammonia nitrogen, and COD of the water quality in real time. The water quality monitoring subnode sends the collected data to the water quality monitoring base station through the ZigBee protocol [15]. This paper mainly designs wireless sensor network water quality monitoring base stations and monitoring nodes and establishes a model for the distribution of wireless sensor monitoring nodes to improve the utilization of sensor nodes, reduce network costs, expand the monitoring range of wireless sensor networks, and improve the ability of on-site control of pollutants.

2.1. Overall Design. The overall structure of the wireless sensor network water quality automatic monitoring system is shown in Figure 1. This system contains three main subsystems: data acquisition subsystem, control and communication subsystem, and data management subsystem. The data monitoring nodes are distributed on the sections that are easily contaminated. The four indicators of total nitrogen,

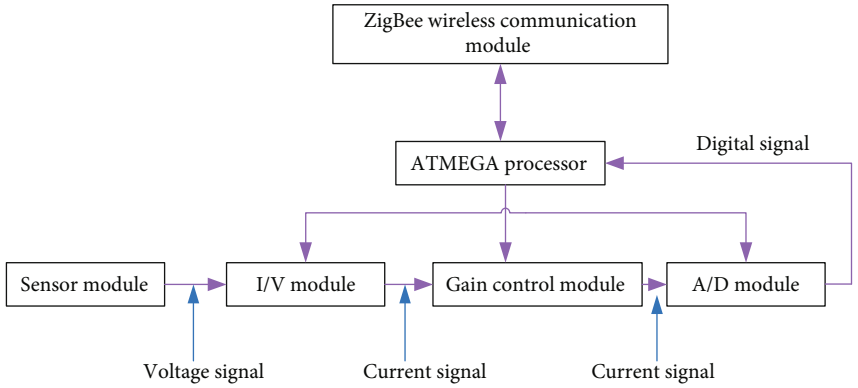

Figure 2: Structure diagram of data monitoring subnodes.

total phosphorus, ammonia nitrogen, and COD are monitored in real time, and an alarm will be issued once it is found to exceed the standard [16]. In this way, the monitoring personnel can deal with the pollutants in time to prevent the spread and ensure the safety of the water quality. The overall architecture of the automatic water quality monitoring system is shown in Figure 1.

The data acquisition subsystem consists of sensors that measure total nitrogen, total phosphorus, ammonia nitrogen, and COD. The working principle of these four sensors is that when the sensor probe is immersed in water, a current will be generated on the two diaphragms. The magnitude of the current depends on the content of the detected object in the water. The microcontroller measures the magnitude of the current through an analog input circuit and performs temperature compensation on this value to obtain an accurate current value. The system includes data monitoring subnodes and data base stations. The control and communication subsystem is composed of the ZigBee communication module of wireless sensor network monitoring subnodes, ZigBee communication module of data base station, and 5G communication module [17]. The wireless sensor network subnode communicates with the data base station through the ZigBee protocol. The data base station sends data to the remote server through the 5G module. Users can use a computer to access the data collected by the wireless sensor network subnode. The data monitoring node can be controlled by the remote client or by the touch screen of the data base station. Users can reduce the power consumption and increase the service life of the data monitoring node by controlling the sampling frequency and working mode of the data monitoring node.

The data management subsystem is based on a remote server, and remote clients can access the server to obtain the water quality status. The data management subsystem not only receives new water quality data in real time and updates the database but also saves previous data for a period of time. Through the comparison of the data, the trend of the water quality in the river can be obtained. In order to fully grasp the status of river water quality, the wireless sensor network automatic monitoring system needs to monitor different sections of the river [18]. Considering the problems of cost and utilization efficiency of sensor nodes, it is necessary to model the distribution of wireless sensor networks to achieve the optimal distribution of sensors.

2.2. Wireless Sensor Network Data Monitoring Subnode Structure. The data monitoring subnode is the basic component of the water quality automatic monitoring system based on the basin's wireless sensor network. It has four main functions. The first function is to collect the total nitrogen, total phosphorus, ammonia nitrogen, and COD content in the water quality. Each data monitoring subnode is equipped with a sensor for measuring these four indicators. The data monitoring subnode will perform linear processing and temperature compensation on the data returned by the sensor. The second function is to store the collected data. The data monitoring node does not send the data to the data base station immediately after the data processing is completed but stores it in a storage area of the microcontroller first and then waits for the data base station's wireless communication module to be idle before sending it [19]. The third function is to receive the command of the data base station. According to the command of the data base station, each data monitoring subnode changes the sampling frequency and working mode to reduce power consumption and extend the service life. The fourth function is to communicate wirelessly with the data base station. The ZigBee communication protocol is used here because ZigBee technology has the advantages of low energy consumption, low cost, and fast communication. The ZigBee technical data monitoring subnodes form a tree-shaped communication network, which not only has a wide monitoring range but also can easily integrate new data monitoring nodes. The structure of the data monitoring subnode is shown in Figure 2.

The ZigBee protocol includes four layers of the 7-layer OSI network communication protocol. The physical layer provides a physical medium for the transmission or reception of ZigBee data packets and realizes the conversion of electrical signals. The MAC layer determines the ZigBee communication address when sending data and determines whether the data packet is destined for its own node when receiving data. The network layer determines the forwarding direction of data packets [20]. The application layer is provided for users to meet different needs of users. With the help of the ZigBee protocol stack, users only need to operate on the

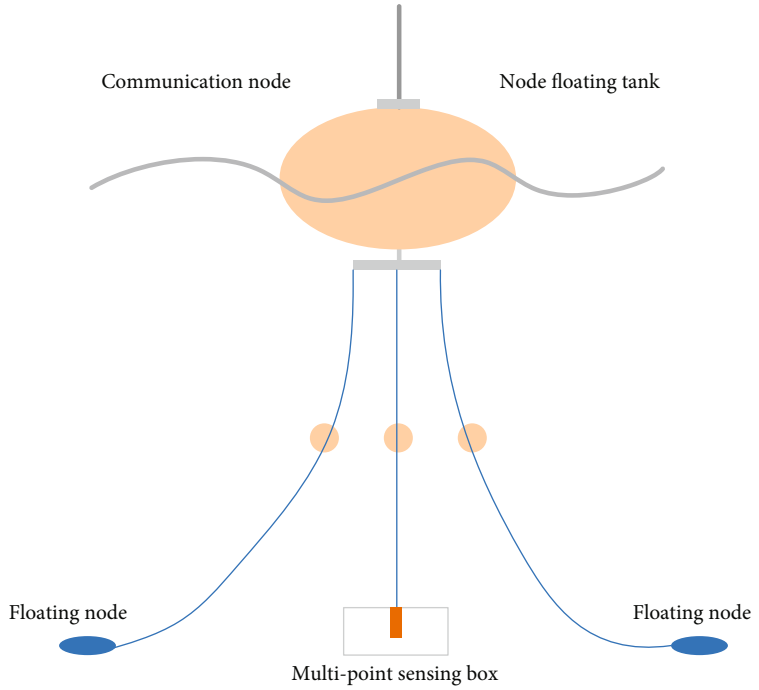

Figure 3: Internal mechanical structure of the sensor.

application layer to realize wireless communication. The data monitoring subnode structure is mainly composed of six modules, namely, ATMEGA module, sensor module, I/V module, gain control amplification module, A/D module, ZigBee wireless communication module. The sensor module returns a current signal. The current signal is converted into a voltage signal through the I/V module. Because the voltage signal may not be within the range of the A/D module, the voltage signal needs to be amplified or reduced [21]. The I/V module, gain control module, and A/D module operate under the control of the microcontroller to ensure the accuracy of the data information. The ATMEGA processor module receives the digital signal of the A/D module and sends the digital signal to the ZigBee wireless communication module through the UART protocol. The ZigBee wireless communication module sends data at the set transmission frequency. If it cannot directly communicate with the data base station, the data information is sent to the data base station through other nodes.

2.3. Data Base Station Structure of Wireless Sensor Networks Based on Watersheds. The wireless sensor network data base station is the core part of the basin-based wireless sensor network water quality automatic monitoring system. Its main function is to control the data monitoring subnodes and collect data information, display the data information on the touch screen, and send it to the remote through the 5G module. Client: in the process of monitoring the transmission of data from the child node to the base station node, a tree-like routing protocol is used. Each node sends out information through its parent node until the data information is received by the data base station. Another feature of this tree routing protocol is that the nodes work in standby mode most of the time, which can extend the service life of the nodes [22, 23]. To achieve this goal, each node uses a real-time system to ensure that it can return to its normal working state under the control of the data base station. Data: the base station can display the collected total nitrogen, total phosphorus, ammonia nitrogen, and COD information on the touch screen. Users can understand the water quality status based on the collected information. The data base station can also send the collected data information to the remote client through the 5G module so that researchers can remotely monitor the data monitoring node. The internal mechanical structure of the sensor is shown in Figure 3.

The data base station structure of the wireless sensor network based on the watershed contains five modules, namely, ZigBee communication module, PXA270 module, touch screen display module, and 5G remote data communication module [24]. The ZigBee wireless module is used to receive the data sent by the data monitoring substation and send the data to the PXA270 processor through the SPI bus. The PXA270 processor analyzes the received data; extracts data reflecting the information of total nitrogen, total phosphorus, ammonia nitrogen, and COD; and then displays the extracted data on the touch screen through the Modbus bus. The touch screen can also receive user operation commands and display data information of the node selected by the user.

3. Research on Water Quality Prediction Based on Support Vector Machines

In the field of automatic water quality monitoring, high-cost monitoring equipment in the past will be replaced by a large number of wireless sensor network nodes with low prices,

superior performance, and strong mobility. This not only reduces the cost of monitoring but also increases the scope of water quality monitoring. In the beginning, the sensors were randomly distributed, and the sensors in the area to be measured were deployed by means of airplane spreading or artillery ejection [25]. However, random distribution does not result in efficient coverage, especially when the distribution of wireless sensors is particularly concentrated and there are few sensors in the critical area of the area to be measured. Therefore, algorithms must be used to optimize sensor deployment and data optimization to improve sensor coverage and effective utilization. This chapter proposes a support vector machine-based water quality prediction wireless sensor network distribution algorithm, which solves the problems of traditional algorithms in the application of water quality monitoring [26].

The support vector machine (SVM) is a new algorithm proposed by Vapnik et al. on the basis of VC dimension theory and structural risk minimization principle in statistical learning theory [27]. Vapnik et al. introduced the regression estimation and signal processing method based on support vector machines in detail, which broadened the research field of support vector machines. Because the algorithm has extremely outstanding regression and classification performance, it has been widely used and researched in many research fields. In recent years, it has moved to the forefront of artificial intelligence scientific research and complex nonlinear science [28]. Support vector machines can be used to solve recognition and regression problems and treat them as a quadratic programming problem [28]. Support vector machines are linearly separable in the feature space. According to the limited sample information, the linear inseparable input space is mapped to the high-dimensional feature space through the kernel function. The model's learning ability (that is, any sample without wrong recognition ability) and complexity (that is, the learning accuracy of the specified training samples) are needed to find the best coordination scheme to obtain the best generalization ability [29].

3.1. Support Vector Machine Algorithm. The basic idea of the support vector machine (SVM) is to find the optimal hyperplane in the original classification of space under the condition of linear separability [30]. In the case of linear inseparability, the relaxation variable is added, and the sample of the low-dimensional input space is mapped to the high-dimensional attribute space through nonlinear mapping to become a linearly separable case. This makes use of linear algorithms for the high-dimensional attribute space. Nonlinear analysis is possible, and the optimal hyperplane in the feature space can be found [31].

One of the core ideas of the SVM method is to find the optimal classification surface of the two types of classification problems, leading to the concept of support vectors [32]. Another core idea of the SVM method is to map the sample set to a high-dimensional and infinite-dimensional Hilbert space (called a feature space) through nonlinear mapping, which realizes the linearity of the high-dimensional nonlinear problem in the sample space in the high-dimensional space, thus solving the nonlinear problem [33]. Unlike the classification problem, there is only one type of sample points for regression. The optimal hyperplane sought is not to make the two types of sample points "open" but to minimize the "total deviation" of all sample points from the hyperplane. At this time, all the sample points are between the two boundary lines, and finding the optimal regression hyperplane is also equivalent to finding the maximum interval [34].

3.1.1. ε-Insensitive Loss Function. Support vector machine regression algorithm (SVR) is a new regression algorithm based on support vector machines. This algorithm needs to introduce a suitable loss function to ensure the existence of the important properties of support vector machines [35]. SVR regards the Vapnik-insensitive function as an error function (i.e., when the error is less than, it is regarded as no error).

$$c(x, y, f(x)) = |y - f(x)|_{\varepsilon},$$
$$|y - f(x)|_{\varepsilon} = \max\{0, |y - f(x)| - \varepsilon\}. \tag{1}$$

Let the training set be

$$T = \{(x_1, y_1), \cdots, (x_l, y_l)\}. \tag{2}$$

Using the above ε-insensitive loss function and limited to the regression estimation function in the set of linear functions, based on the principle of structural risk minimization, when the distance from all sample points to the required hyperplane is less than, find the optimal regression hyperplane. The problem is transformed into solving a quadratic convex programming problem as follows [36]:

$$\min \frac{1}{2}\|\omega\|^2. \tag{3}$$

The constraints are as follows:

$$\begin{cases} \{y_i - (w \cdot x_i) - b \le \varepsilon, \\ (w \cdot x_i) + b - y_i \le \varepsilon. \end{cases} \tag{4}$$

When the distance from some sample points to the optimal hyperplane is greater than ε, a slack variable is introduced and a fault tolerance penalty coefficient C is constructed. At this time, the optimization problem is transformed into [37]

$$\min \frac{1}{2}\|w\|^2 + C\sum_{i=1}^{l}\left(\xi_i + \xi_i^*\right),$$
$$\text{s.t.} \begin{cases} y_i - (w \cdot x_i) - b \le \varepsilon + \xi_i, \\ y_i - (w \cdot x_i) - b \ge -\varepsilon - \xi_i^*, \\ \xi_i, \xi_i^* \ge 0. \end{cases} \tag{5}$$

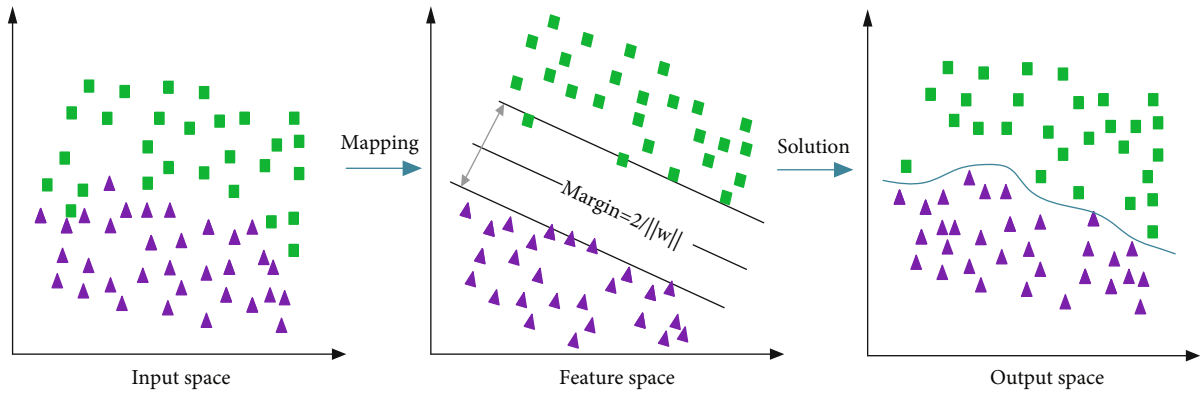

Figure 4: The solution of SVM to nonlinear problems.

Restrictions are as follows:

$$\begin{cases} y_i - \omega \cdot x_i - b \le \varepsilon + \xi_i, \\ \omega \cdot x_i + b - y_i \le \varepsilon + \xi_i^*, \\ \xi_i, \xi_i^* \ge 0. \end{cases} \tag{6}$$

The solution of SVM to nonlinear problems is shown in Figure 4.

Introduce the Lagrange function to get its dual form:

$$\begin{aligned} \max & \sum_{i=1}^{l} y_i(\alpha_i - \alpha_i^*) - \varepsilon \sum_{i=1}^{l}(\alpha_i - \alpha_i^*) \\ & - \frac{1}{2}\sum_{i=1}^{l}\sum_{i=1}^{l}(\alpha_i - \alpha_i^*)(\alpha_j - \alpha_i^*)\varphi(x_i)\cdot\varphi(x_j). \end{aligned} \tag{7}$$

Restrictions are as follows:

$$\begin{cases} \sum_{i=1}^{l}(\alpha_i - \alpha_i^*) = 0, \\ \alpha_i, \alpha_i^* \in [0, C]. \end{cases} \tag{8}$$

According to KKT conditions, there are

$$\alpha_i[\varepsilon + \xi_i - y_i + w \cdot \varphi(x_i) + b] = 0. \tag{9}$$

From the above formula, b can be obtained as follows:

$$\begin{aligned} b = \frac{1}{N_{\mathrm{NSV}}} \Bigg\{ & \sum_{0<\alpha_i<C} \left[y_i - \sum_{x_i \in \mathrm{SV}} \left(\alpha_j - \alpha_j^*\right)\varphi(x_j)\cdot\varphi(x_i) - \varepsilon \right] \\ & + \sum_{0<\alpha_i<C} \left[y_i - \sum_{x_j \in \mathrm{SV}} \left(\alpha_j - \alpha_j^*\right)\varphi(x_j)\varphi(x_i) - \varepsilon \right] \Bigg\}. \end{aligned} \tag{10}$$

In the above formula, it is the standard support vector machine set, which is the number of standard vector machines.

The available hyperplane linear regression function is

$$f(x) = \sum_{i=1}^{l} y_i(\alpha_i - \alpha_i^*)\varphi(x_i)\cdot\varphi(x) + b. \tag{11}$$

3.1.2. Solution of Nonlinear Regression. To solve the nonlinear regression function, you need to map the training set to a high-dimensional space and then use the linear regression method to solve in the high-dimensional space. Assuming that there is a mapping function, we can map the input set in the Euclidean space to the Hilbert space to get the corresponding original problem. The original problem with the feature mapping function is as follows:

$$\min_{w,b} \frac{1}{2}\|w\|^2 + C\sum_{i=}^{l}\left(\xi_i + \xi_i^*\right). \tag{12}$$

After applying the Lagrange multiplier method to the dual transformation of the original problem, the dual problem with the feature mapping function is obtained. In some cases, the problem of dimensional disaster will occur in the feature mapping process. Therefore, in the process of solving the regression problem, the kernel function method is usually used to perform the inner product operation of the mapping function. If, for any, the function meets the conditions shown in the following formula, it is called a kernel function.

$$K(x, z) = \Phi(x)\cdot\Phi(z). \tag{13}$$

4. Sewage Testing Actual Case Verification

In order to discover the existing or potential problems in the system software and hardware and ensure the stable and effective operation of the system, the system was tested in two stages. The first stage is testing and analysis in a laboratory environment. On the premise of ensuring that the first-stage test passes, the second stage of sewage monitoring site testing and analysis is carried out.

4.1. Comparison of Water Quality Prediction. In order to predict the water quality in order to prevent the occurrence of sewage and other conditions, this paper uses a support

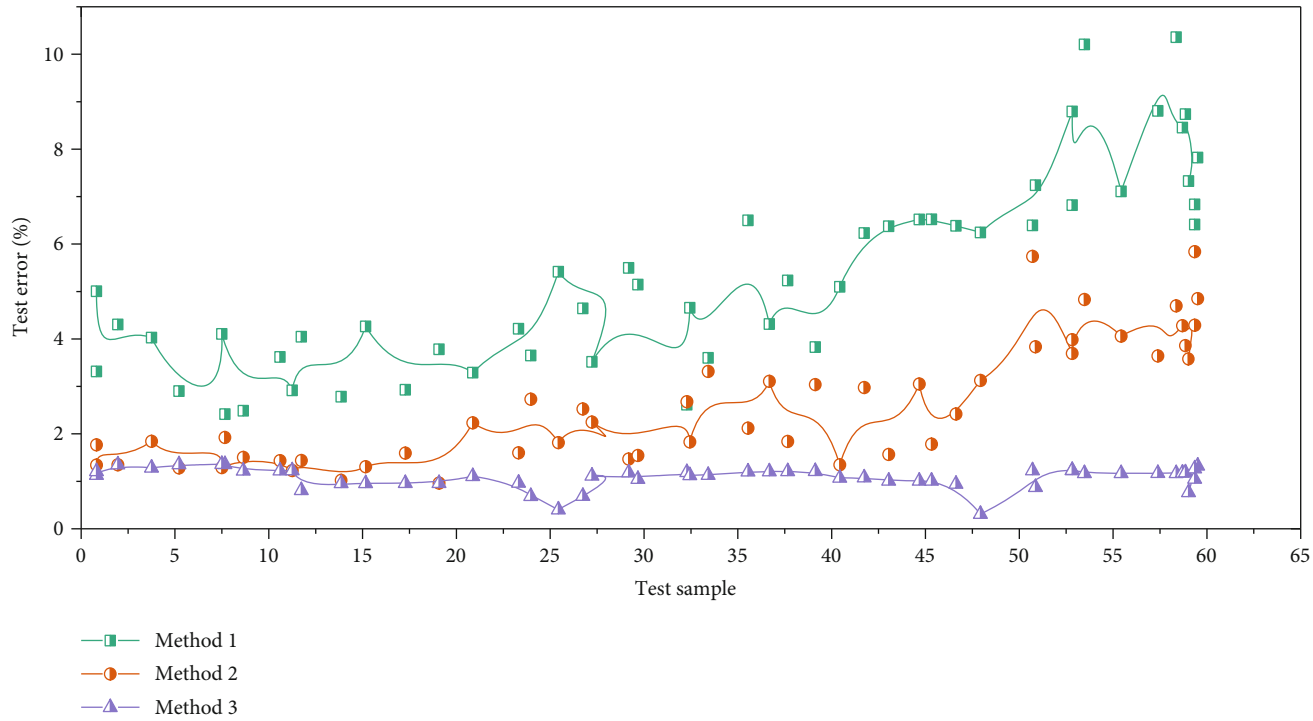

Figure 5: Comparison results of water quality prediction effect.

vector machine algorithm for prediction research. On the basis of wireless monitoring, a support vector algorithm is used to construct a water quality prediction model to make reasonable predictions of water quality in the basin. The prediction results and comparison chart are shown in Figure 5.

It can be seen from Figure 5 that the three methods all have good performance in the process of water quality prediction, with the maximum error within 10. Among them, the support vector machine algorithm is the best for water quality prediction, with an average error of less than 2%. Therefore, it can be concluded that the support vector machine algorithm can be effectively applied to the water quality prediction of the river basin.

4.2. Phase 1 Testing. In order to verify that the design of the system in terms of data collection and network communication satisfies the functional requirements of the monitoring system, the first phase of the network was simulated under laboratory conditions. The test platform at this stage consists of 4 sensor nodes, 1 routing node, and 1 coordinator node. The four sensor nodes are used to collect four kinds of sensors, respectively. The routing node is used as a medium for information exchange between the sensor node and the coordinator node. After receiving the sensor data, the coordinator node communicates with the PC and displays the collection results in the serial debugging assistant software. In addition, because the pH sensor and the dissolved oxygen sensor were not in place during the first stage of testing, the pH and dissolved oxygen values were collected using an analog voltage input method. The laboratory does not have a Presell water tank, so the flow value collection is also replaced by the liquid level value. In order to speed up the progress of the system test, this phase of the test did not set the collection interval to 5 minutes but set to collect data every 1 minute. After the collection, the data was transmitted to the coordinator node through the routing node. The results of the first-stage testing of water quality monitoring indicators are shown in Figure 6.

After testing, it was shown that the monitoring network was successfully established in the laboratory environment and the data transmission was stable. After actual measurement, the data collected by the sensor node is accurate and reliable, which meets the design requirements.

4.3. Second-Stage Test. The laboratory environmental noise interference is relatively small, and the working environment is close to the ideal state. In order to verify the system's operating status and performance at the monitoring site and further test the stability and reliability of the system, the second stage of testing is to install sensors at the sewage monitoring site for testing. The test network consists of 1 coordinator node, 10 routing nodes, and 50 sensor nodes. The client software was developed using LabVIEW for real-time display of monitoring data. The sensor node is installed at the sewage index collection site. The routing node and the sensor node are placed within a distance of 1 km without obstruction. The sensor node is connected to the nearest routing node using the principle of proximity, thus forming a test network. The results of the second-stage test water quality monitoring indicators are shown in Figure 7.

The second phase of the test was conducted continuously for 10 days under the monitoring site environment, and the test data was displayed in real time through the client software. Figure 7 shows the test data over a period of time.

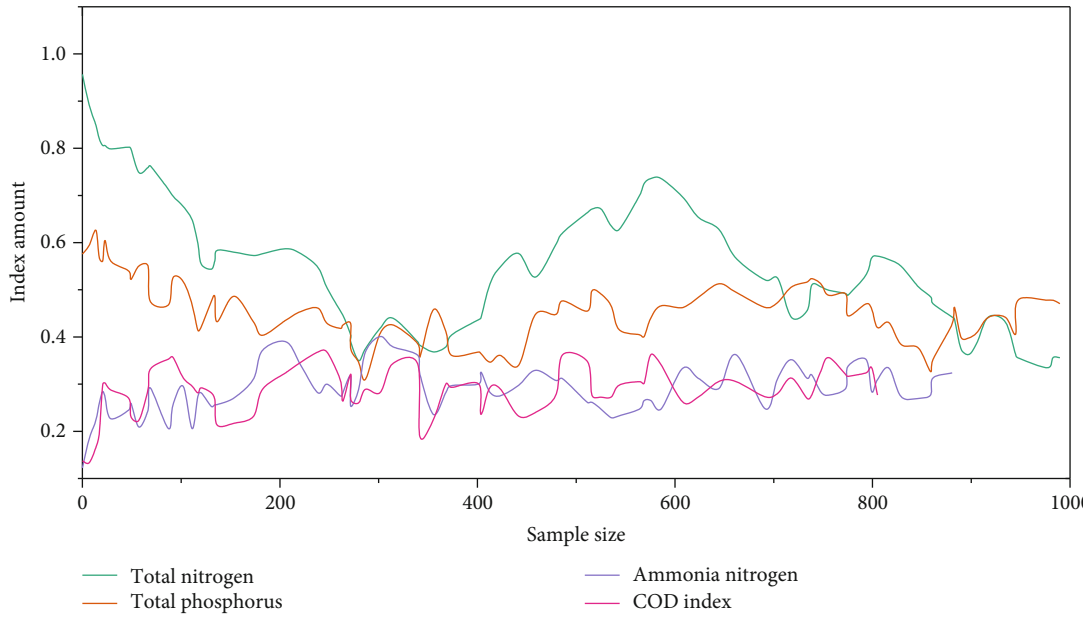

Figure 6: The first-stage test water quality monitoring index results.

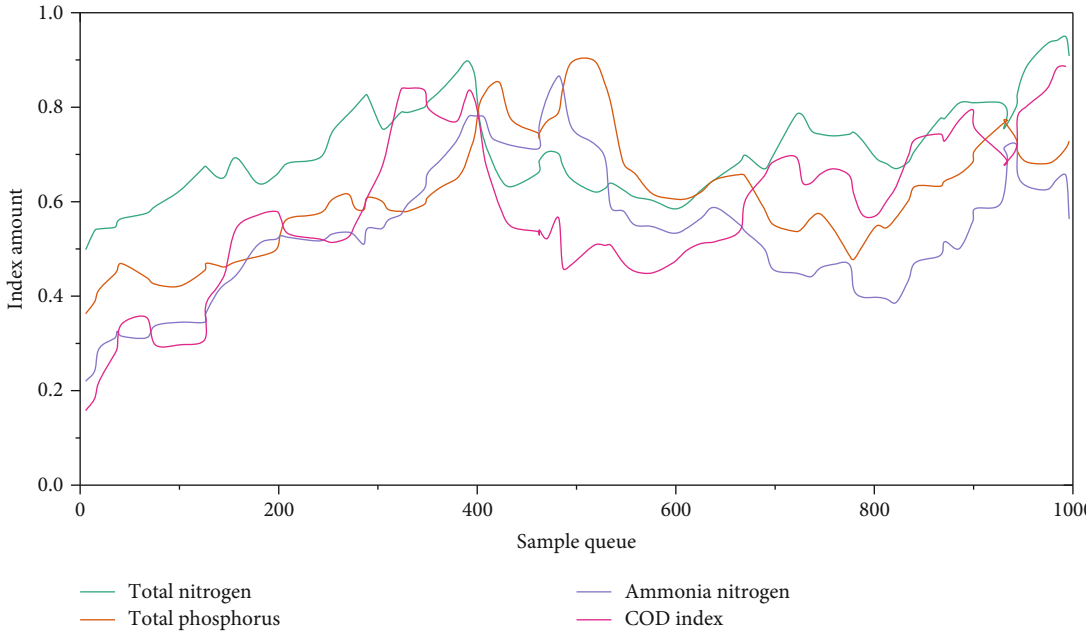

Figure 7: Results of the second-stage test water quality monitoring indicators.

The test data shows that the node networking under the monitoring site environment is successful, and the data can be transmitted. But there are still some problems. When collecting the pH sensor, the output value of the read sensor obviously exceeds the measurement range of the sensor. Carefully check the hardware wiring diagram for correctness, check the sensor data sheet to know that there is a problem with the sensor, replace the sensor, and the problem is solved immediately. The stability of data transmission cannot be satisfied. After analysis, the reasons for unstable data transmission include poor antenna performance and complicated monitoring site environment. Purchase antennas from professional antenna manufacturers during the test, and elevate the antenna parts of the routing node and sensor node to effectively improve the stability of data transmission. The next step will be to look for reasons from other aspects and improve the stability of data transmission.

5. Conclusion

In view of the problems faced by water quality monitoring in river basins, this paper proposes an automatic water quality monitoring system based on wireless sensor networks by studying the development trend of water quality monitoring

at home and abroad. The system uses wireless sensor network technology, which enables wireless communication between data collection nodes and between data collection nodes and data base stations, reducing damage to the environment. In order to improve the utilization rate of data collection nodes, this paper also optimizes the collected data. In this paper, the wireless sensor technology and ZigBee protocol are used to establish a sewage monitoring model and real-time dynamic monitoring of total nitrogen, total phosphorus, ammonia nitrogen, and other indicators of the water quality of the watershed. On the basis of wireless monitoring, a support vector algorithm is used to construct a water quality prediction model to make reasonable predictions of water quality in the basin. Finally, the actual test results show that the technology can automatically and real-timely monitor the water quality of the watershed to meet the requirements of water quality monitoring in practical applications. Although this paper has achieved some research results in the automatic monitoring of water quality in wireless sensor networks, there are still many problems that need to be improved. For example, the power supply problem of the water quality automatic monitoring system. If the electric energy cannot be regenerated, then the system will have a relatively short service life. For the dimension of water quality monitoring, water quality monitoring should be carried out at different depths in the basin, which can improve the reliability and integrity of water quality monitoring.

Data Availability

All data are available from the corresponding author.

Conflicts of Interest

The authors declare that there are no conflicts of interest regarding the publication of this paper.

Acknowledgments

This study is supported by the Special Scientific Research Fund project of the Education Department of Shaanxi Province "A Research of PVA-ZSM-5 Composite Proton Exchange Membrane and Proton Conduction Mechanism" (No. 17JK0327).

References

[1] T. Li, M. Winnel, H. Lin et al., "A reliable sewage quality abnormal event monitoring system," *Water Research*, vol. 121, no. 6, pp. 248–257, 2017.

[2] K. Hii, R. Parthasarathy, S. Baroutian, D. J. Gapes, and N. Eshtiaghi, "Rheological measurements as a tool for monitoring the performance of high pressure and high temperature treatment of sewage sludge," *Water Research*, vol. 114, no. 12, pp. 254–263, 2017.

[3] S. Montesdeoca-Esponda, C. Álvarez-Raya, M. E. Torres-Padrón, Z. Sosa-Ferrera, and J. J. Santana-Rodríguez, "Monitoring and environmental risk assessment of benzotriazole UV stabilizers in the sewage and coastal environment of Gran Canaria (Canary Islands, Spain)," *Journal of Environmental Management*, vol. 233, no. 12, pp. 567–575, 2019.

[4] M. Toledo, M. C. Gutiérrez, J. A. Siles, and M. A. Martín, "Full-scale composting of sewage sludge and market waste: stability monitoring and odor dispersion modeling," *Environmental Research*, vol. 167, no. 12, pp. 739–750, 2018.

[5] C. J. A. Campos, G. Goblick, R. Lee, K. Wittamore, and D. N. Lees, "Determining the zone of impact of norovirus contamination in shellfish production areas through microbiological monitoring and hydrographic analysis," *Water Research*, vol. 124, pp. 556–565, 2017.

[6] H. Yin, Y. Lu, Z. Xu, H. Li, and B. R. Schwegler, "Characteristics of the overflow pollution of storm drains with inappropriate sewage entry," *Environmental Science and Pollution Research*, vol. 24, no. 5, pp. 4902–4915, 2016.

[7] C. J. A. Campos, J. Avant, J. Lowther, D. Till, and D. N. Lees, "Human norovirus in untreated sewage and effluents from primary, secondary and tertiary treatment processes," *Water Research*, vol. 103, no. 12, pp. 224–232, 2016.

[8] J.-B. Burnet, Q. T. Dinh, S. Imbeault, P. Servais, S. Dorner, and M. Prévost, "Autonomous online measurement of β-D-glucuronidase activity in surface water: is it suitable for rapid E. *coli* monitoring?," *Water research*, vol. 152, pp. 241–250, 2019.

[9] L. Carreón-Palau, C. C. Parrish, H. Pérez-España, and H. Perez-Espana, "Urban sewage lipids in the suspended particulate matter of a coral reef under river influence in the South West Gulf of Mexico," *Water Research*, vol. 123, no. 2, pp. 192–205, 2017.

[10] M. Laquaz, C. Dagot, L. Wiest, C. Bazin, M. Gaschet, and Y. Perrodin, "Ecotoxicity and antibiotic resistance of wastewater during transport in an urban sewage network," *Environmental Science and Pollution Research*, vol. 27, no. 16, pp. 19991–19999, 2020.

[11] A.-K. Wluka, H. Rüdel, K. Pohl, and J. Schwarzbauer, "Analytical method development for the determination of eight biocides in various environmental compartments and application for monitoring purposes," *Environmental Science and Pollution Research*, vol. 23, no. 21, pp. 21894–21907, 2016.

[12] P. A. Bahamonde, A. Feswick, M. A. Isaacs, K. R. Munkittrick, and C. J. Martyniuk, "Defining the role of omics in assessing ecosystem health: perspectives from the Canadian environmental monitoring program," *Environmental Toxicology and Chemistry*, vol. 35, no. 1, pp. 20–35, 2016.

[13] E. Ociepa, M. Mrowiec, and J. Lach, "Influence of fertilisation with sewage sludge-derived preparation on selected soil properties and prairie cordgrass yield," *Environmental Research*, vol. 156, no. 2, pp. 775–780, 2017.

[14] K. Karagiannis, V. Simonyan, K. Chumakov, and R. Mazumder, "Separation and assembly of deep sequencing data into discrete sub-population genomes," *Nucleic acids research*, vol. 45, no. 19, pp. 10989–11003, 2017.

[15] Y. Zhang, "Research on two-stage anaerobic co-digestion of sewage sludge and food waste," *Environmental Science & Technology*, vol. 15, 2016.

[16] F. Shang, D. Zhou, C. Li, H. Ye, and Y. Zhao, "Research on the intrusion detection model based on improved cumulative summation and evidence theory for wireless sensor network," *Photonic Network Communications*, vol. 37, no. 2, pp. 212–223, 2019.

[17] H. Tran-Dang, N. Krommenacker, and P. Charpentier, "Containers monitoring through the physical internet: a

spatial 3D model based on wireless sensor networks," *International journal of production research*, vol. 55, no. 9, pp. 2650–2663, 2017.

[18] F. Wang, "Development of real-time blood pressure monitoring system based on wireless sensor," *Basic & Clinical Pharmacology & Toxicology*, vol. 119, 2016.

[19] H.-Z. F. Di Zhang, H.-Z. Fu, and Y.-S. Ho, "Characteristics and trends on global environmental monitoring research: a bibliometric analysis based on Science Citation Index Expanded," *Environmental Science and Pollution Research*, vol. 24, no. 33, pp. 26079–26091, 2017.

[20] A. Singh and T. P. Sharma, "Position and hop-count assisted full coverage control in dense sensor networks," *Wireless Networks*, vol. 21, no. 2, pp. 625–638, 2015.

[21] H. Wang, H. Zeng, and P. Wang, "Linear estimation of clock frequency offset for time synchronization based on overhearing in wireless sensor networks," *IEEE Communications Letters*, vol. 20, no. 2, pp. 288–291, 2016.

[22] W. Kam, W. S. Mohammed, G. Leen et al., "Compact and low-cost optical fiber respiratory monitoring sensor based on intensity interrogation," *Journal of Lightwave Technology*, vol. 35, no. 20, pp. 4567–4573, 2017.

[23] W. Yan, R. Xu, K. Wang, T. Di, and Z. Jiang, "Soft sensor modeling method based on semisupervised deep learning and its application to wastewater treatment plant," *Industrial & Engineering Chemistry Research*, vol. 59, no. 10, pp. 4589–4601, 2020.

[24] C. Wu, K. Vellaisamy, G. Yang et al., "A reaction-based luminescent switch-on sensor for the detection of OH ions in simulated wastewater," *Dalton Transactions*, vol. 46, no. 20, pp. 6677–6682, 2017.

[25] S. Motia, I. A. Tudor, P. A. Ribeiro, M. Raposo, B. Bouchikhi, and N. el Bari, "Electrochemical sensor based on molecularly imprinted polymer for sensitive triclosan detection in wastewater and mineral water," *Ence of The Total Environment*, vol. 664, no. 4, pp. 647–658, 2019.

[26] R. Marques, A. Rodriguez-Caballero, A. Oehmen, and M. Pijuan, "Assessment of online monitoring strategies for measuring N_2O emissions from full-scale wastewater treatment systems," *Water Research*, vol. 99, no. 4, pp. 171–179, 2016.

[27] W. Yan, P. Guo, Y. Tian, and J. Gao, "A framework and modeling method of data-driven soft sensors based on semisupervised Gaussian regression," *Industrial & Engineering Chemistry Research*, vol. 55, no. 27, pp. 7394–7401, 2016.

[28] A. Aravind and B. Mathew, "Electrochemical sensor based on nanostructured ion imprinted polymer for the sensing and extraction of Cr (III) ions from industrial wastewater," *Polymer International*, vol. 67, no. 12, pp. 1595–1604, 2018.

[29] C. Lin, N. Xiong, J. H. Park, and T. Kim, "Dynamic power management in new architecture of wireless sensor networks," *International Journal of Communication Systems*, vol. 22, no. 6, pp. 671–693, 2009.

[30] Y. Sang, H. Shen, Y. Tan, and N. Xiong, "Efficient protocols for privacy preserving matching against distributed datasets," *International Conference on Information and Communications Security*, vol. 4307, no. 4, pp. 210–227, 2006.

[31] F. Long, N. Xiong, A. V. Vasilakos, L. T. Yang, and F. Sun, "A sustainable heuristic QoS routing algorithm for pervasive multi-layered satellite wireless networks," *Wireless Networks*, vol. 16, no. 6, pp. 1657–1673, 2010.

[32] J. Li, N. Xiong, J. H. Park, C. Liu, S. MA, and S. E. Cho, "Intelligent model design of cluster supply chain with horizontal cooperation," *Journal of Intelligent Manufacturing*, vol. 23, no. 4, pp. 917–931, 2012.

[33] W. Guo, N. Xiong, A. V. Vasilakos, G. Chen, and C. Yu, "Distributed k–connected fault–tolerant topology control algorithms with PSO in future autonomic sensor systems," *International Journal of Sensor Networks*, vol. 12, no. 1, pp. 53–62, 2012.

[34] C. Lin, Y. X. He, and N. Xiong, "An energy-efficient dynamic power management in wireless sensor networks," in *2006 Fifth International Symposium on Parallel and Distributed Computing*, Timisoara, Romania, 2006.

[35] Y. Yang, N. Xiong, N. Y. Chong, and X. Défago, "A decentralized and adaptive flocking algorithm for autonomous mobile robots," in *2008 The 3rd International Conference on Grid and Pervasive Computing - Workshops*, Kunming, China, 2008.

[36] Y. Liu, M. Ma, X. Liu, N. Xiong, A. Liu, and Y. Zhu, "Design and analysis of probing route to defense sink-hole attacks for Internet of Things security," *IEEE Transactions on Network Science and Engineering*, vol. 7, no. 1, pp. 356–372, 2020.

[37] H. Liang, J. Zou, K. Zuo, and M. J. Khan, "An improved genetic algorithm optimization fuzzy controller applied to the well-head back pressure control system," *Mechanical Systems and Signal Processing*, vol. 142, article 106708, 2020.

Hindawi
Wireless Communications and Mobile Computing
Volume 2020, Article ID 8838454, 9 pages
https://doi.org/10.1155/2020/8838454

Research Article

Annular Spatial Pyramid Mapping and Feature Fusion-Based Image Coding Representation and Classification

Mengxi Xu,[1] **Yingshu Lu**,[2] **and Xiaobin Wu**[1]

[1]*School of Computer Engineering, Nanjing Institute of Technology, Nanjing 211167, China*
[2]*Huawei Technologies Co., Ltd., Nanjing 210000, China*

Correspondence should be addressed to Mengxi Xu; mxxu26@126.com

Received 15 July 2020; Revised 13 August 2020; Accepted 22 August 2020; Published 11 September 2020

Academic Editor: Hongju Cheng

Copyright © 2020 Mengxi Xu et al. This is an open access article distributed under the Creative Commons Attribution License, which permits unrestricted use, distribution, and reproduction in any medium, provided the original work is properly cited.

Conventional image classification models commonly adopt a single feature vector to represent informative contents. However, a single image feature system can hardly extract the entirety of the information contained in images, and traditional encoding methods have a large loss of feature information. Aiming to solve this problem, this paper proposes a feature fusion-based image classification model. This model combines the principal component analysis (PCA) algorithm, processed scale invariant feature transform (P-SIFT) and color naming (CN) features to generate mutually independent image representation factors. At the encoding stage of the scale-invariant feature transform (SIFT) feature, the bag-of-visual-word model (BOVW) is used for feature reconstruction. Simultaneously, in order to introduce the spatial information to our extracted features, the rotation invariant spatial pyramid mapping method is introduced for the P-SIFT and CN feature division and representation. At the stage of feature fusion, we adopt a support vector machine with two kernels (SVM-2K) algorithm, which divides the training process into two stages and finally learns the knowledge from the corresponding kernel matrix for the classification performance improvement. The experiments show that the proposed method can effectively improve the accuracy of image description and the precision of image classification.

1. Introduction

Image classification is a major topic in the field of image processing and pattern recognition [1, 2]. The conventional image classification methods [3, 4] focus on some specific targets which extract effective features to represent the informative contents of images. However, this kind of method has obvious drawbacks. For example, some specific image features cannot be generalized to strange objects. In addition, image information is likely lost during the coding phase of the method.

Recently, image color features have been widely considered. Traditional color features include the color histogram, color moments, color sets, the color coherence vector, and the color correlogram. These color features are combined with contour-based features (i.e., Hu invariant moments and histogram of gradient) in the field of image classification and have achieved excellent performance results [5, 6]. A major research focus on human linguistics in the color feature representation is color names (CN). In the computer vision, the color properties contain human linguistic labels for pixels in an image. Berlin and Kay [7] presented that languages include eleven universal basic color terms. According to their analysis, Khan et al. [8] proposed to exploit the conventional statistical model to learn the knowledge of the naming color by the human's brain, and Khan et al. [6] adopted this color feature combined with the histogram of gradient for image features fusion, which were successfully applied in target recognition. Therefore, this paper utilizes CN and dimension-reduced scale invariant feature transformation as the complementary fused features. In order to further investigate and optimize image information, a modified spatial pyramid matching method (SPM) is proposed to add the features' spatial location information. In this method, an image would be split into patches whose features are extracted and encoded so that a uniform vector with a spatial

Figure 1: CN label sketch map. The first row is the original images, and the second row is the corresponding labeled images by CN.

location information can be formed. However, the simple division in SPM cannot maintain the vector representation after the rotation of the image.

Aiming to solve the problems above, we propose an image classification model based on an annular spatial pyramid matching and multifeature fusion. Considering the success of the SIFT feature, we adopt the dimension-reduced SIFT feature to speed up the encoding process. A large part of image information is contained in color features, while SIFT never takes this point into account. Thus, if color information can be added into our feature fusion model, the proposed image classification system can be improved significantly. Additionally, an annular spatial pyramid matching is applied to map the extracted features for the rotation invariance spatial vector representation. Due to various P-SIFT features extracted from different images, the sparse coding algorithm is adopted for the generation of the uniform vector. In the phase of feature fusion and the learning parameters of the classification algorithm, support vector machine with two kernels algorithm (SVM-2K) [9, 10] is utilized in our proposed model for training the labeled data set and predicting the unlabeled images. The SVM-2K algorithm is the primary issue when combining the kernel canonical correlation analysis algorithm (KCCA) [11, 12] and SVM classification algorithm in which KCCA is adopted for preprocessing the features (P-SIFT and CN), and two independent SVM models of two features are trained together. The novelty of our method lies in our novel feature fusion-based image classification method that obtains satisfying results in contrast to existing methods, while P-SIFT and CN features can be used as complementary descriptions of the image.

2. Features Extraction and Spatial Mapping

2.1. Color Naming Feature. Recently, the research of image features has focused on the target shape-based local feature instead of the information-rich color features. Compared with the traditional color descriptors including HUE, OPP, and color moments, the term-based histogram statistical feature, color names, is used as the complementary to P-SIFT. Through mapping RGB color channels, the extraction algorithm of CN labels in each pixel of an image is using one of 11 color names: black, blue, brown, grey, green, orange, pink, purple, red, white and yellow. The algorithm also employs the histogram and normalization to get the vector representation. CN labels are different forms of the same color to a specific color name so that the CN feature is equipped with an illumination invariance. The CN algorithm is to predict the color description by humans for a specific color in essence. The experiments in paper [5] shows that, compared with HUE and OPP color feature, the CN descriptor is more selective and has been successfully applied in the field of image recognition. Hence, this paper utilizes the CN feature to mitigate the vacancy of color in our image classification model. The comparison of images with and without color names is shown in Figure 1. For a given pixel X, the CN description of this point should be defined as the probability of the pixel belonging to one of the 11 color names.

$$\mathrm{CN} = [P(\mathrm{cn}_1 \mid X), P(\mathrm{cn}_2 \mid X), \cdots, P(\mathrm{cn}_{11} \mid X)], \quad (1)$$

where $P(\mathrm{cn}_i \mid X)$ represents the probability of the pixel assigned to the ith label, and the probability mapping matrix is determined from a large dataset. This paper utilizes a mapping matrix, which statistically computes the image dataset of 11 color names collected by Google. The max probability of color names is in equation (1). Following the above flows, all pixels in an image would be assigned a specific color name; after that, a 1×11 histogram vector can be formed.

2.2. Dimension-Reduced SIFT Feature. SIFT originally proposed by Lowe [13] is a local gradient histogram used to locate the target shape. The algorithm identifies even the extreme points in a multiscale image space and has been widely applied in the field of image classification and pattern recognition. In recent years, SIFT has had various modifications, including SURF, PCA-SIFT, and HSV-SIFT. However, SIFT is a 1×128 vector and can be utilized to detect image features even when the image properties, including scale

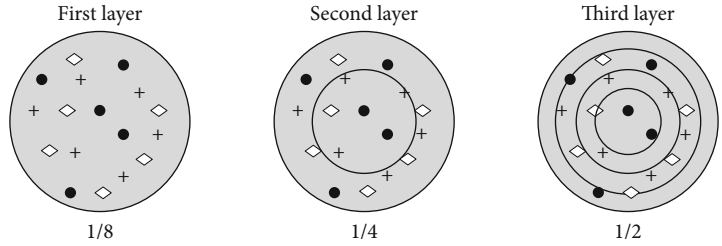

Figure 2: The frame of the rotational spatial pyramid matching model. The different toys in circles represent different features, and the weights of the first to third layer in R-SPM are 1/8, 1/4, 1/2, respectively.

and image noise, are changed. However, the 1×128 SIFT descriptor has a negative impact on the computation and performance of a reconstruction method. In addition, SIFT is typically taken for its accuracy in reconstruction, and the task of image classification in this paper does not need the same level of accuracy. Thus, a dimension-reduced SIFT feature generated from SIFT using a principal component analysis algorithm (PCA) [14] is proposed to extract the main information of the image feature. Due to the various number of SIFT in different image patches, the extracted SIFT cannot be used as the final representation. Thus, we have included the sparse representation in our model to encode the SIFT features of an image.

2.3. Rotational Annular Spatial Pyramid Matching. SIFT features contain corresponding location information. Lazebnik et. al [2] introduced the spatial pyramid matching model (SPM) in which images would be divided into multiscale patches so that SIFT can be a more valuable mapped for encoding. In this SPM model, SIFT features are first extracted from all images and clustered to get a visual dictionary which includes K visual words. Each image is then divided into three layers (1×1, 2×2, 4×4), and 1/4, 1/4, and 1/2 are independently given to the corresponding layer. Finally, the SIFT features in their patches are encoded, and the series is connected as a $21 \times K$ vector. Unfortunately, SPM has no capability of dealing with violent rotation images, so it is unable to maintain the spatial location information. While targets in the image recognition and classification are normally accompanied by large position changes, the vectors of the model would become the original SIFT vectors or CN features if SPM is integrated into our model for mapping.

To make full use of the features' location information, we suggest an annular division based on a rotational spatial pyramid matching model (R-SPM) to map SIFT and CN features. In this model, as shown in SPM, each image will be annularly divided into three layers (1×1, 1×2, and 1×4), which are attached to weights 1/8, 1/4, and 1/2, respectively (Figure 2). Because of the relatively small image patches in R-SPM, the location information of features is more effective. For the larger patches of images, this effect is suppressed, so less weight is given to the larger layers. Finally, all features in annular circle patches will be encoded, and the series is connected as a $9 \times K$ vector.

In this way, the location information in image patches would be attached to the specific location of the vector representation. No matter how the targets rotate, the vectors of the circle patches never change so that the mapped vector by R-SPM owns the rotational spatial locative information.

3. The Theory of the Sparse Representation

In the traditional bag-of-visual-words model (BOVW), the k-means algorithm [15] is used to cluster the terms for a visual dictionary. The vector quantification method (VQ) is then adopted for encoding features by computing Euclidean distances between features and visual words to get a histogram representation. However, VQ fails to consider that the Euclidean distance is unsuitable for histogram-based features (i.e., SIFT and HOG). For the reduction of the feature information in the encoding process, instead of VQ, ScSPM [2] is proposed to utilize the sparse representation algorithm and generate more sparse and selective encoding vectors. The sparse representation [16] is a kind of soft encoding algorithm which can be seen as the extension of the k-means.

3.1. Sparse Representation. The goal of the sparse representation (SR) is to learn an ultracomplete dictionary and use rare atoms to reconstruct original signals for the successfully extraction of the embedded image information. The sparse representation has a wide range of research and practical applications, especially for the collection, compression, and representation of high dimension vectors. For instance, in face recognition, image features are first extracted from a training set and then acquired into an ultracomplete dictionary, generating sparse representations of that training set. The feature extraction and sparse representation processes for the test image set are also then performed, and the test and training samples are compared. The nature of the sparse representation is to solve the convex problem, but some specific problems, such as the low convex degree of sparse matrices, cannot be efficiently solved by a traditional convex optimization algorithm. The sparse dictionary is developed by a K-SVD algorithm [17] which iteratively and simultaneously regenerates atoms and sparse coefficients. However, the time required to run an optimization algorithm is excessive, which has a significant negative effect on the classification performance. Therefore, this paper used the K-means++ algorithm [18] to get a stable ultracomplete dictionary, and orthogonal matching pursuit (OMP) was performed to get reconstruction coefficients. The core problem of the sparse representation is to solve equation (2).

$$\min_V \frac{1}{2}\|x - vU\|_2 + \lambda\|v\|_1, \quad (2)$$

where x represents the feature to be reconstructed, U is the fixed dictionary, and v is the sparse coefficients. The former term is the reconstruction error, and the latter term is to take control of the sparsity.

3.2. Orthogonal Matching Pursuit. An orthogonal matching pursuit algorithm (OMP) [19, 20] is a modified iterative version of a matching pursuit algorithm (MP). Due to the nonorthogonality of the selected atoms by MP, the sparse coefficients are normally local peaks. In the process of the atom selection, OMP follows the laws of MP, but converts the selected atoms into orthogonal, which decreases the iterative number of optimal convergences. At the same time, the OMP algorithm has set a maximum iterative number, so that when the number has achieved the set value, the OMP algorithm is forcibly stopped.

Ideally, each image would get a coefficient matrix when all SIFT are to be encoded. In addition, a pooling algorithm should be used to pool the matrices for uniform vectors. Experiments [21, 22] show that, when compared with other pooling methods, the maximum pooling is more effective for the generation of the sparse vector representation. Thus, we have adopted a maximum pooling algorithm in this paper. If we set that a given image has M features (K dimensions) after the mapping process of the R-SPM model, the coefficient matrix is $V = (v_1, v_2, v_3, \cdots, v_M) \in R^{M\times(9K)}$. The method of the maximum pooling can be defined in equation (3).

$$r = \max(|v_1|, |v_1|, |v_2|, |v_3|, \cdots, |v_M|), \quad (3)$$

where $r \in R^{1\times(9K)}$ is the final vector representation of this image.

4. Support Vectors Machine with Double Fusion Kernels Algorithm

In the field of image recognition, the selection of a specific image feature is determined by the characteristics of the targets to be predicted. There is no effective standard to assess the feature selection. In order to mitigate any influence of feature selection on the performance of image recognition and classification, the learning of the corresponding knowledge from the training image set through machine learning algorithms has been widely researched. This feature fusion learning algorithm mainly focuses on two requirements. The first is that the classifier directly learns the series of connected vectors to achieve the performance of feature fusion. The second requirement is that each image feature is considered an individual unit to train their own models and give each model different weight.

Following the above method, researchers [23, 24] combined the preserved invariant feature with SIFT to design an image classification model that based on feature fusion and got a more brilliant performance than a single feature based model. Therefore, we proposed the support vector machine with a two fusion kernels algorithm (SVM-2K) to complete the task of the image feature fusion and classification. SVM-2K combines the preprocess of the kernel canonical correlation analysis (KCCA) and the parameters of an SVM algorithm to make two features that independently and complementarily describe the images. In the SVM-2K algorithm, a similarity constraint between two hyper plane mappings for the organic combination of preprocess and parameter learning is introduced.

If there are two completely different features (set as A and B) for the same data set after their individual kernel mapping, the mapped features can be set as $\varnothing_A$ and $\varnothing_B$. Then, a specific image can be described in equation (4).

$$S = \{(\varnothing_A(x_1), \varnothing_B(x_1)), (\varnothing_A(x_2), \varnothing_B(x_2)), (\varnothing_A(x_3), \varnothing_B(x_3)), \cdots, (\varnothing_A(x_l), \varnothing_B(x_l))\}. \quad (4)$$

The similarity constraint is defined as follows.

$$|\langle w_A, \varnothing_A(x_i)\rangle + b_A - \langle w_B, \varnothing_B(x_i)\rangle - b_B| \le \gamma_i + \epsilon, \quad (5)$$

where $(w_A, b_A), (w_B, b_B)$ is the weights and thresholds of the SVM model. This constraint is introduced into the SVM function for further optimization.

$$\min L = \frac{1}{2}\|w_A\|^2 + \frac{1}{2}\|w_B\|^2 + C^A\sum_{i=1}^{l}\varepsilon_i^A + C^B\sum_{i=1}^{l}\varepsilon_i^B + \mathrm{D}\sum_{i=1}^{l}\gamma_i. \quad (6)$$

The decisive function of SVM-2K can be expressed as follows.

$$h(\mathrm{x}) = \mathrm{sign}\left(0.5\left(\langle \widehat{w}_A, \varnothing_A(x)\rangle + \widehat{b}_A - \langle \widehat{w}_B, \varnothing_B(x)\rangle - \widehat{b}_B\right)\right). \quad (7)$$

In this paper, our classification model adopts the SVM-2K algorithm to perform feature fusion and classification learning on P-SIFT and CN for better performance than the single feature-based SVM model. Because the SVM-2K algorithm is a binary classifier, however, we follow the implementation of LibSVM [25] to utilize the "one VS one" method to extend SVM-2K to multiclass classification tasks. The "one VS one" method is to train the $\mathrm{N}\times(\mathrm{N}-1)/2$ binary SVM-2K model to vote for the final predicted results of the test image. Figure 3 shows the flow chart of our feature fusion-based image classification model.

5. Experiment Results and Analysis

The experimental datasets used in this paper are Caltech-256 [26] and PASCAL VOC 2011 [27]. Caltech-256 is a traditional dataset in the field of computer vision. It includes 256 category image sets and each set has different number of image patches (from 31 to 800). PASCAL VOC 2011 is a benchmark test set for the detection of visual object classification which provides standard images for testing algorithms and learning performance. We randomly selected 9

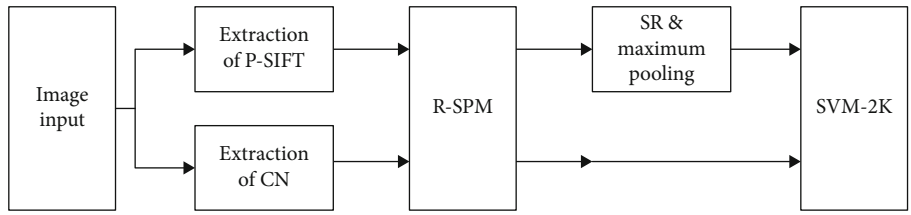

Figure 3: The flow chart of the proposed feature fusion-based image classification model.

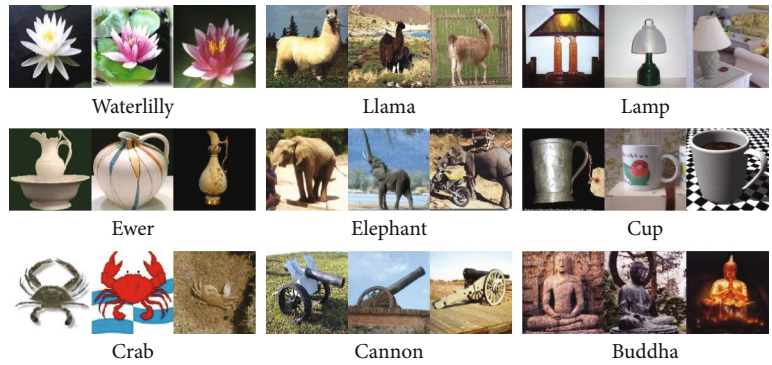

Figure 4: Nine categories image dataset selected from Caltech-256.

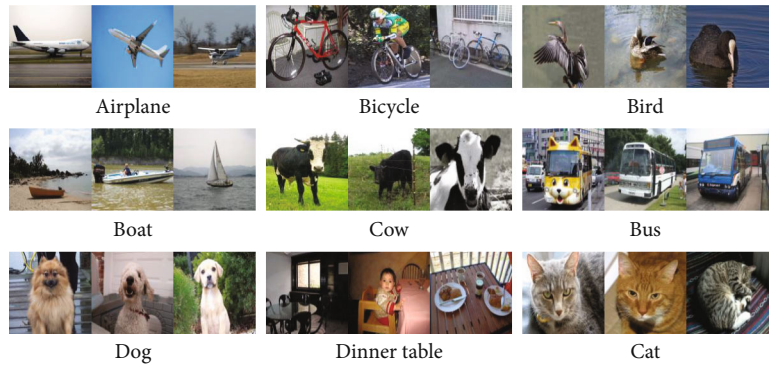

Figure 5: Nine categories image dataset selected from PASCAL VOC 2011.

categories from each dataset and divided them into training and test datasets, which are shown as Figures 4 and 5. The training dataset contained 50 images, the rest of the images in each category were set as the test dataset.

The original SIFT features are extracted by the vl_feat function library [28]. All experiments in this paper were implemented on the MATLAB 2013b platform, and Average Precision (AP) [29, 30] is introduced to assess the performance of the image classification models.

5.1. The Performance Analysis of P-SIFT. P-SIFT was generated by implementing a PCA algorithm on SIFT for dimension reduction. In order to assess the influence of dimension-reduced percentages on the speed of feature reconstruction and the performance of image classification, we collected the mean time (MT) spent by sparse coding and the AP performance of the proposed model. Caltech-256 is utilized as the baseline dataset in this section.

Table 1: The influence of the dimension-reduced percent.

Dimension-reduction	0.1	0.3	0.5	0.7	0.9	1
MT(s)	0.0521	0.0931	0.1240	0.1734	0.2325	0.2571
AP (%)	66.29	75.42	87.42	89.24	89.34	88.57

Table 1 shows that when the dimension-reduction percentage increases, and the mean time spent by feature reconstruction shortens, but the corresponding AP performance is extremely slow. When the percentage is larger than 0.7, the mean time is relatively short, and the performance of classification model tends to be stable. Thus, the experiments all adopt 0.7 as the dimension-reduced percentage.

5.2. The Performance Analysis of R-SPM. For the sake of elevating the rotational performance of R-SPM, this section utilizes an aircraft image and implements 6 kinds of rotation

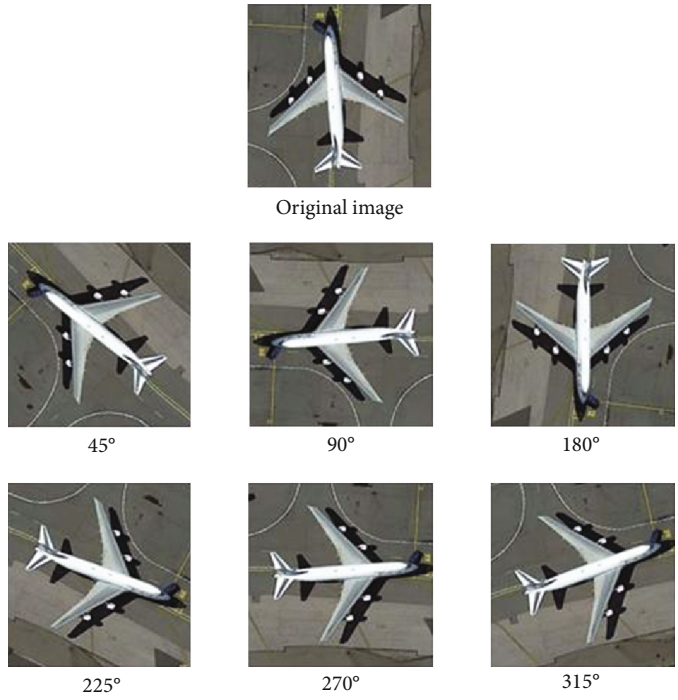

Figure 6: Six kinds of rotation transform on the aircraft image.

transformations on it as shown in Figure 6. The SPM and R-SPM models, respectively, are used to map the extracted features for further sparse representation. The length of dictionary of the sparse representation is set to be 300. After each transformed image in Figure 6 gets its vector representation, their difference degree (Diff) values are defined in equation (8), and the results are shown in Table 2.

$$\text{Diff} = \frac{\sqrt{\left(V - V'\right)\left(V - V'\right)^{T}}}{\sqrt{VV'}}, \tag{8}$$

where V is the vector of the original image, and V' represents the vector of the transformed vector.

As shown in Table 2, with the rotation transformation of the image, the different degree values of SPM become much larger. However, the proposed R-SPM model does not have changes in degree and always keeps a relatively low level which supports the idea that R-SPM has a strong adaptability for the rotation transformation of images.

In order to further compare R-SPM with SPM in terms of performance, we designed experiments to utilize SPM and R-SPM models to map SIFT features and use SVM and AdaBoost algorithms to recognize the images selected from Caltech-256. The kernel of SVM is set as a histogram intersection kernel. The combination of SPM and SVM is set as SSVM, while the combination of SPM and AdaBoost is set as SABT. R-SPM and SVM are set as RSVM, and R-SPM and AdaBoost are set as RABT. The length of reference is set as 400, and other parameters are selected as the above experimental setups.

Table 2: The difference degree values of transformed images.

Diff	45°	90°	180°	225°	270°	315°
SPM (%)	12.15	22.42	28.95	34.26	32.41	36.50
R-SPM (%)	2.33	1.94	1.61	1.84	2.19	1.42

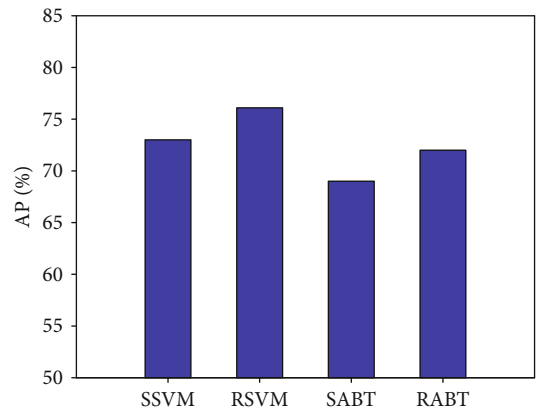

Figure 7: The AP performance of SPM and R-SPM.

It is clearly evident from Figures 7 and 8 that the average accuracy of R-SPM is higher than the 2-3% SPM in terms of the classification performance. The performance of RSVM in the four models is also optimal. At the same time, the image recognition accuracy of each category using R-SPM is higher than SPM, which confirms that the proposed R-SPM model can better obtain the spatial characteristics of images and makes the image vector representation be more selective and robust.

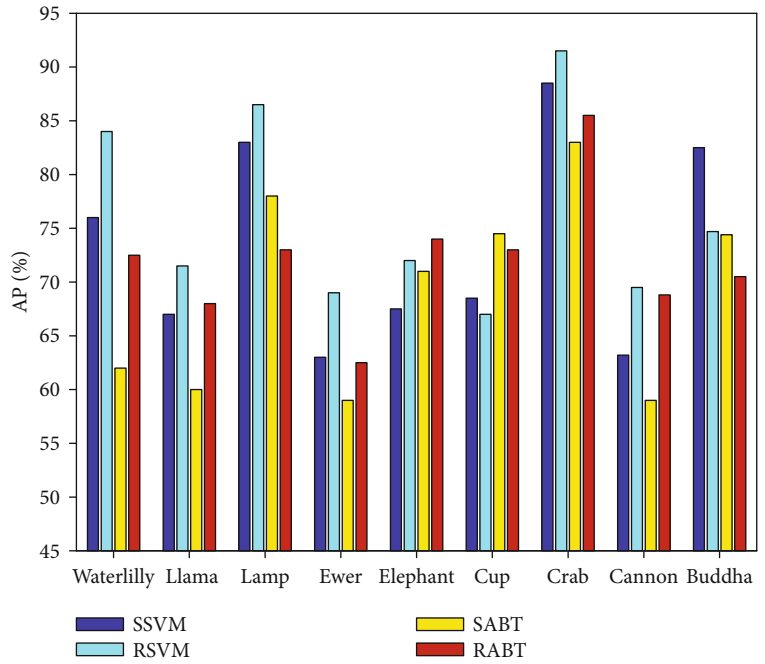

Figure 8: The precision values of each category using SPM and R-SPM.

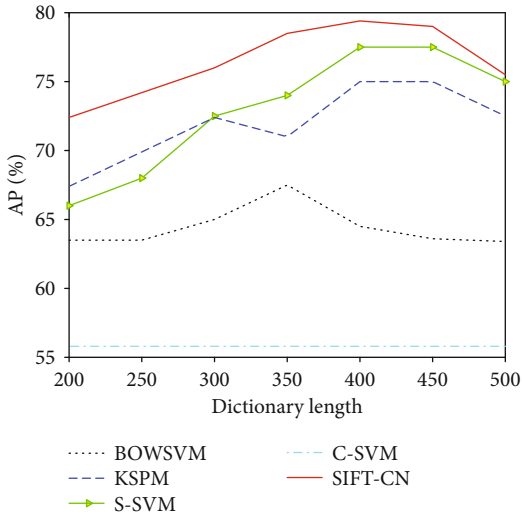

Figure 9: The performance of each model implemented on Caltech-256 with different lengths of the sparse dictionary.

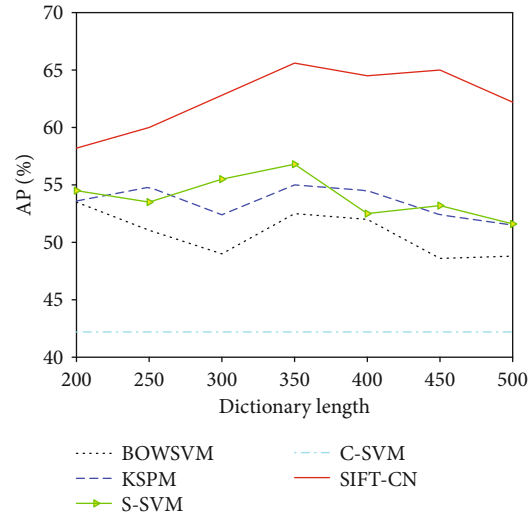

Figure 10: The performance of each model implemented on Caltech-256 with different lengths of the sparse dictionary.

5.3. The Performance of SVM-2K Algorithm. The experiment in this section also adopts BOWSVM [31, 32] and KSPM [33, 34] which are implemented on the Caltech-256 and PASCAL VOC 2011 datasets for the comparison with the proposed model. The feature fusion model in this thesis is set as SIFT-CN; the model using P-SIFT and SVM is set as S-SVM; and the term using CN and SVM is set as C-SVM. In the SVM-2K algorithm of the proposed method, HIK is utilized as the kernel of P-SIFT, and the lineal kernel works as the kernel of CN. The length of the dictionary in the sparse representation varies from 200 to 500 to obtain the optimal value. The performance of the mentioned models is shown in Figures 9 and 10.

As shown in Figures 9 and 10, with the same length of the dictionary, the proposed model using P-SIFT and CN for feature fusion achieved the best performance of all classification models. Compared with other models, the AP results of the fusion model increased by 5-10%. It is clear that the image classification model proposed in this paper has a better recognition effect on the image types. When the sparse dictionary length reaches 400, the performance of SIFT-CN is optimal. Therefore, the length of the dictionary is fixed at the same time for BOWSVM, KSPM, and SIFT-CN image classification models implemented on the rest of the experiments.

Table 3: The Kappa performance results of each model when the dictionary is set as 400.

	BOWSVM	KSPM	S-SVM	C-SVM	SIFT-CN
Caltech-256 (%)	51	58	62	49	68
VOC 2011 (%)	48	53	59	43	63

To better illustrate the performance of the image classification model, we follow recent literature [35, 36] that uses the kappa coefficient (equation (9)) as a measure of standards. The essence of the kappa coefficient is to measure the agreement between the interpretations of different observers. When the Kappa coefficient is -1, a negative correlation is expressed, while when the Kappa coefficient is 1, it indicates that the classification result is in complete agreement.

$$\text{Kappa} = \frac{po - pe}{1 - pe}. \tag{9}$$

Table 3 gives the Kappa performance of each image description model with a 400 length of the dictionary. Taken the Caltech-256 dataset for example, the Kappa performance result of the SIFT-CN model is 0.68, which is nearest to 1 among models listed in Table 3. It can be concluded that the SIFT-CN model is better than the other classification models. It shows that the results of the feature fusion model have a high reliability, in other words, the corresponding classification performance is the most ideal. And in the interior of the SIFT-CN model, Table 3 shows that the feature fusion method is superior to the single feature performance which further verifies the excellent performance of the proposed model.

Through a series of experiments, we can see that the P-SIFT feature modified by this paper has the ability to increase the speed of feature coding through the dimension reduction processing. At the same time, compared with the traditional SPM model, the proposed R-SPM model maps P-SIFT and CN features, which have the ideal rotation invariant phase position information. Finally, experimental comparisons show that the use of a SVM-2K feature fusion classification algorithm is significantly better than using a single feature classification model.

6. Conclusion

In this paper, we propose a method of the rotation invariant spatial pyramid mapping and a feature fusion-based image classification model. In feature extraction and representation, this paper proposes a novel P-SIFT feature, which is the dimension-reduced SIFT feature vector that extracts the principal information of SIFT features to speed up the sparse representation. At the same time, CN and P-SIFT features are fused to describe the image. In order to explore the location information of the feature, an annular division-based spatial pyramid model is proposed, which makes the space vector representation of the features invariant in rotation. At the stage of feature fusion, the SVM-2K algorithm is used to train two independent SVM models, and the final result is obtained by a weighted voting method. In the experimental evaluations, the Caltech-256 and VOC PASCAL image databases are selected. The experimental results show that, compared with other single feature image classification model, our feature fusion-based image description model can extract the characteristic information of the image, so that P-SIFT and CN characteristic can be used as complementary descriptions of the image and finally achieve the satisfying performance improvement. However, we acknowledge that beside the features that we investigated in this paper, there are many other advanced features which are required to be studied in our future work, while the robust should be concerned which means different kinds of data could be tested.

Data Availability

The image data used to support the findings of this study are included within the article.

Conflicts of Interest

The authors declare that they have no conflicts of interest.

Acknowledgments

This work is supported partly by the University-Level Research Fund Project of Nanjing Institute of Technology (No. ZKJ201907).

References

[1] S. Lazebnik, C. Schmid, and J. Ponce, "Beyond bags of features: Spatial pyramid matching for recognizing natural scene categories," in *2006 IEEE Computer Society Conference on Computer Vision and Pattern Recognition*, pp. 2169–2178, New York, NY, USA, 2006.

[2] J. Yang, K. Yu, Y. Gong, and T. Huang, "Linear spatial pyramid matching using sparse coding for image classification," in *2009 IEEE Conference on Computer Vision and Pattern Recognition*, pp. 1794–1801, Miami, FL, USA, June 2009.

[3] J. Wang, J. Yang, K. Yu, F. Lv, T. Huang, and Y. Gong, "Locality-constrained linear coding for image classification," in *2010 IEEE Computer Society Conference on Computer Vision and Pattern Recognition*, pp. 3360–3367, San Francisco, CA, USA, June 2010.

[4] H. Wang, Z. Chen, X. Wang, and Y. Ma, "Random finite sets based UPF-CPHD multi-object tracking," *Journal on Communications*, vol. 33, no. 12, pp. 147–153, 2012.

[5] F. S. Khan, J. van de Weijer, and M. Vanrell, "Modulating shape features by color attention for object recognition," *International Journal of Computer Vision*, vol. 98, no. 1, pp. 49–64, 2012.

[6] F. S. Khan, J. Weijer, A. D. Bagdanov, and M. Vanrell, "Portmanteau vocabularies for multi-cue image representation," in *Advances in Neural Information Processing Systems*, pp. 1323–1331, Granada, Spain, 2011.

[7] Y. Wang, J. Liu, J. Wang, Y. Li, and H. Lu, "Color names learning using convolutional neural networks," in *2015 IEEE International Conference on Image Processing (ICIP)*, pp. 217–221, Quebec City, QC, September 2015.

[8] F. S. Khan, R. M. Anwer, J. Weijer, A. D. Bagdanov, M. Vanrell, and A. M. Lopez, "Color attributes for object

detection," in *2012 IEEE Conference on Computer Vision and Pattern Recognition*, pp. 3306–3313, Providence, RI, USA, June 2012.

[9] J. D. Farquhar, D. R. Hardoon, H. Meng, J. Shawe-Taylor, and S. Szedmak, "Two view learning: SVM-2K, theory and practice," in *Advances in Neural Information Processing Systems*, pp. 355–362, Vancouver, BC, Canada, 2005.

[10] Y. Lu, *Research on targets detection method in high resolution remote sensing image*, Hohai University, 2016.

[11] W. Zheng, X. Zhou, C. Zou, and L. Zhao, "Facial expression recognition using kernel canonical correlation analysis (KCCA)," *Neural Networks*, vol. 17, no. 1, pp. 233–238, 2006.

[12] X. Wang, X. Yan, G. Lv, and T. Fan, "Balloon-borne spectrum–polarization imaging for river surface velocimetry under extreme conditions," *Infrared Physics & Technology*, vol. 58, pp. 5–11, 2013.

[13] D. G. Lowe, "Distinctive image features from scale-invariant keypoints," *International Journal of Computer Vision*, vol. 60, no. 2, pp. 91–110, 2004.

[14] H. Abdi and L. J. Williams, "Principal component analysis," *Wiley Interdisciplinary Reviews: Computational Statistics*, vol. 2, no. 4, pp. 433–459, 2010.

[15] S. E. Hickman, N. D. Kingery, T. K. Ohsumi et al., "The microglial sensome revealed by direct RNA sequencing," *Nature Neuroscience*, vol. 16, no. 12, pp. 1896–1905, 2013.

[16] H. Lee, A. Battle, R. Raina, and A. Y. Ng, "Efficient sparse coding algorithms," in *Advances in Neural Information Processing Systems*, pp. 801–808, Vancouver, BC, Canada, 2006.

[17] Z. Jiang, Z. Lin, and L. S. Davis, "Label consistent K-SVD: learning a discriminative dictionary for recognition," *IEEE Transactions on Pattern Analysis and Machine Intelligence*, vol. 35, no. 11, pp. 2651–2664, 2013.

[18] D. Arthur and S. Vassilvitskii, "K-means++: the advantages of careful seeding," in *Proceedings of the eighteenth annual ACM-SIAM symposium on Discrete algorithms. Society for Industrial and Applied Mathematics*, pp. 1027–1035, Philadelphia, PA, USA, 2007.

[19] M. Tan, I. W. Tsang, and L. Wang, "Matching pursuit lasso part I: sparse recovery over big dictionary," *IEEE Transactions on Signal Processing*, vol. 63, no. 3, pp. 727–741, 2013.

[20] W. Guo, N. Xiong, A. V. Vasilakos, G. Chen, and C. Yu, "Distributed k–connected fault–tolerant topology control algorithms with PSO in future autonomic sensor systems," *International Journal of Sensor Networks*, vol. 12, no. 1, pp. 53–62, 2012.

[21] J. X. Wu and J. M. Rehg, "Beyond the euclidean distance: creating effective visual codebooks using the histogram intersection kernel," in *2009 IEEE 12th International Conference on Computer Vision*, pp. 630–637, Kyoto, Japan, September 2009.

[22] H. Liang, J. Zou, Z. Li, M. J. Khan, and Y. Lu, "Dynamic evaluation of drilling leakage risk based on fuzzy theory and PSO-SVR algorithm," *Future Generation Computer Systems*, vol. 95, pp. 454–466, 2019.

[23] Q. Wang, X. Zhang, M. Li, X. Dong, Q. Zhou, and Y. Yin, "Adaboost and multi-orientation 2D Gabor-based noisy iris recognition," *Pattern Recognition Letters*, vol. 33, no. 8, pp. 978–983, 2012.

[24] J. Li, N. Xiong, J. H. Park, C. Liu, S. MA, and S. E. Cho, "Intelligent model design of cluster supply chain with horizontal cooperation," *Journal of Intelligent Manufacturing*, vol. 23, no. 4, pp. 917–931, 2012.

[25] C. C. Chang and C. J. Lin, *LIBSVM: a library for support vector machines*, 2001, Software, http://www.csie.ntu.edu.tw/cjlin/libsvm.

[26] G. Griffin, A. Holub, and P. Perona, *Caltech-256 Object Category Dataset*, California Institute of Technology, 2007.

[27] K. Chatfield, V. Lempitsky, A. Vedaldi, and A. Zisserman, "The devil is in the details: an evaluation of recent feature encoding methods," *BMVC*, vol. 2, no. 4, p. 8, 2011.

[28] J. Li, X. Li, B. Yang, and X. Sun, "Segmentation-based image copy-move forgery detection scheme," *IEEE Transactions on Information Forensics and Security*, vol. 10, no. 3, pp. 507–518, 2015.

[29] Y. Yue, T. W. Finley, F. Radlinski, and T. Joachims, "A support vector method for optimizing average precision," in *Proceedings of the 30th annual international ACM SIGIR conference on Research and development in information retrieval - SIGIR '07*, pp. 271–278, New York, NY, USA, July 2007.

[30] Y. Liu, M. Ma, X. Liu, N. Xiong, A. Liu, and Y. Zhu, "Design and analysis of probing route to defense sink-hole attacks for Internet of Things security," *IEEE Transactions on Network Science and Engineering*, vol. 7, no. 1, pp. 356–372, 2020.

[31] A. P. López-Monroy, M. Montes-y-Gómez, H. J. Escalante, A. Cruz-Roa, and F. A. González, "Improving the BoVW via discriminative visual n-grams and MKL strategies," *Neurocomputing*, vol. 175, pp. 768–781, 2016.

[32] M. Xu, Q. Sun, Y. Lu, and C. Shen, "Nearest-neighbors based weighted method for the BOVW applied to image classification," *Journal of Electrical Engineering & Technology*, vol. 10, no. 4, pp. 1877–1885, 2015.

[33] K. He, X. Zhang, S. Ren, and J. Sun, "Spatial pyramid pooling in deep convolutional networks for visual recognition," *IEEE Transactions on Pattern Analysis and Machine Intelligence*, vol. 37, no. 9, pp. 1904–1916, 2015.

[34] H. Liang, J. Zou, K. Zuo, and M. J. Khan, "An improved genetic algorithm optimization fuzzy controller applied to the wellhead back pressure control system," *Mechanical Systems and Signal Processing*, vol. 142, article 106708, 2020.

[35] Y. Chen, Z. Lin, X. Zhao, G. Wang, and Y. Gu, "Deep learning-based classification of hyperspectral data," *IEEE Journal of Selected Topics in Applied Earth Observations and Remote Sensing*, vol. 7, no. 6, pp. 2094–2107, 2014.

[36] F. Long, N. Xiong, A. V. Vasilakos, L. T. Yang, and F. Sun, "A sustainable heuristic QoS routing algorithm for pervasive multi-layered satellite wireless networks," *Wireless Networks*, vol. 16, no. 6, pp. 1657–1673, 2010.

Hindawi
Wireless Communications and Mobile Computing
Volume 2020, Article ID 8827657, 7 pages
https://doi.org/10.1155/2020/8827657

Research Article

Study on the Intelligent Selection Model of Fuzzy Semantic Optimal Solution in the Process of Translation Using English Corpus

Li Bei

Foreign Language Department, Hubei Polytechnic University, Huangshi 435000, China

Correspondence should be addressed to Li Bei; libei@hbpu.edu.cn

Received 1 July 2020; Revised 31 July 2020; Accepted 1 September 2020; Published 8 September 2020

Academic Editor: Hongju Cheng

Copyright © 2020 Li Bei. This is an open access article distributed under the Creative Commons Attribution License, which permits unrestricted use, distribution, and reproduction in any medium, provided the original work is properly cited.

In order to improve the accuracy and reasonableness of using English corpus for translation, a method of using English corpus to perform translation tasks based on fuzzy semantic optimal solution intelligent selection and inspired computing for wireless networks is proposed. The information extraction model using English corpus for translation is constructed, and the fuzzy semantic keyword feature directivity model of English corpus translation is established. Fuzzy semantic ontology feature registration method is used to calculate the fuzzy semantic intelligence optimal solution vector in English translation. The semantic fuzzy feature matching and adaptive subject word registration are realized in English translation. The fuzzy link relation of semantic ontology is established, and the fuzzy semantic optimal solution is obtained. The accuracy of machine translation in English corpus is improved. The experimental results show that the fuzzy semantic optimal solution has better registration performance and the feature matching degree of the subject words is higher, which improves the reasonableness and accuracy of translation in English corpus. At the same time, it provides a new idea for intelligent computation and recognition of wireless network.

1. Introduction

With the development of intelligent translation technology, machine translation is used to translate English, gradually replacing manual translation, and the accuracy of translation is improved. In the process of English translation with machine software, semantic recognition and feature analysis are needed, and the semantic information of English context and text is extracted by machine intelligent recognition method, and English information model is constructed. Combining fuzzy semantic recognition technology improves the intelligent level of English translation [1]. When using English corpus to do translation work, the causes of English translation usability problems are usually attributed to technical and content aspects, and the fuzzy semantic optimal solution method is adopted. The rational organization and content creation of English translation from the semantic point of view reflects the subjectivity of the originator and improves the level of intelligence and automation of English translation [2]. The use of algorithms can increase the overall analysis of the data; it has great significance to study the intelligent selection model of fuzzy semantic optimal solution in English corpus translation.

The accuracy and adaptability of machine translation have become an important subject in the future translation software research. The optimization problem of machine translation is based on semantic selection and feature extraction. By extracting the semantic information features of the English context, we combine intelligent analysis and semantic information retrieval technology, realizing ontology mapping and adaptive concomitant tracking of semantic information, combining pattern recognition method to realize English intelligent translation, studying fuzzy semantic selection technology in English semantic machine translation, and optimizing the design of machine translation software [3]. It is important to improve translation accuracy and artificial intelligence. The traditional methods include theme tree feature matching method, support vector

machine algorithm, and particle swarm optimization method.

Independent extraction of emotional words and evaluation objects ignores the relationship between emotional words and evaluation objects. Therefore, many researchers conduct joint recognition of emotional words and evaluation objects in emotional analysis. Inspired computing for wireless networks is the new emerging algorithm that can deal with the above problem.

In order to improve the accuracy of translation, the linguistic evaluation set model and feature combination matching for semantic features in English translation are constructed. Some research results have been obtained, but the traditional methods have some problems, such as the poor ability of context interference suppression and coupling interference. To solve this problem, this paper proposes an information extraction model based on fuzzy semantic optimal solution, which uses English corpora to perform translation operations, and constructs an information extraction model based on fuzzy semantic optimal solution [4]. A fuzzy semantic keyword directivity model of English corpus translation is established, and the fuzzy semantic ontology feature registration method is used to calculate the fuzzy semantic intelligence optimal solution vector in English translation. In English translation, semantic fuzzy feature matching and adaptive subject word registration are realized. The fuzzy link relation of semantic ontology is established, the fuzzy semantic optimal solution is calculated, and the accuracy of machine translation in English corpus is improved. The performance of this method in improving the accuracy of English machine translation is demonstrated [5].

The contributions of the paper can be summarized as follows:

(1) The semantic fuzzy feature matching and adaptive subject word registration are realized in English translation. The semantic fuzzy feature can improve the accuracy of translation effectively

(2) Inspired computing for wireless networks is used to deal with the problem that emotional words and evaluation objects ignores the relationship between emotional words and evaluation objects

(3) The fuzzy link relation of semantic ontology is established to provide the more flexibility of translation

The rest of this paper is organized as follows. Section 2 discusses semantic feature selection and information extraction in translation, followed by the intelligent selection and implementation of fuzzy semantic optimal solution designed in Section 3. Section 4 shows the simulation experimental results, and Section 5 concludes the paper with summary and future research directions.

2. Semantic Feature Selection and Information Extraction in Translation

2.1. Information Extraction of English Corpus for Translation Assignments. In order to realize fuzzy semantic selection and translation adaptive following optimization in English semantic machine translation, a fuzzy semantic ontology mapping model is constructed. The fuzzy semantic ontology mapping method is used to filter semantic features of English machine translation, semantic analysis and module extraction of machine English translation are carried out, and semantic mapping relationship structure is set up. In the semantic mapping module, binary semantic judgment and grammar analysis and correction of English translation are carried out, and the process of fuzzy semantic ontology mapping in English machine translation is obtained. The semantic ontology model of English translation is constructed by using NLP technology [6], and a shared conceptual model for translation operations using English corpus is obtained. First, consider the ontology fragments of two sets of English translation instance set shown in Figure 1.

Taking Figure 1 as an example, using English corpus for natural language processing, the English word "image" can represent a picture, the synonyms "image" and "picture" have fuzzy feature matching and adaptive subject word registration. The possible semantic ontology fuzzy link relation between synonyms and semantic information in English translation is described as

$$\theta : S \to S \times [-0.5, 0.5], \tag{1}$$

$$\theta(s_i) = (s_i, 0), s_i \in S. \tag{2}$$

If $s_k \in S$ is a phrase using English corpus for translation, the semantic compatibility mapping is expressed in the form of $M : C * C' \to (\to^{\subseteq})C_s$ binary semantic mapping, and the semantic ontology fuzzy link relation is established in the ontology model, to solve the problem of fuzzy feature matching and adaptive subject word registration for natural language of similar words between concepts [7].

Two conceptual semantic constraint coefficients $\beta \in [0, T]$, S is Mountain nodes, T is the set of semantic information analysis and evaluation. Then, the structural knowledge point β in the ontology fragment can be represented by the following function Δ:

$$\Delta : [0, T] \to S \times [-0.5, 0.5). \tag{3}$$

The binary semantic information of natural languages using English corpus for translation is

$$\Delta(\beta) = \begin{cases} s_k, K = \text{round}(\beta), \\ a_k = \beta - k, a_k \in [-0.5, 0.5). \end{cases} \tag{4}$$

In Figure 1, the two labels of ""Mountain" node on the left side of the natural language processing of English corpus are used to process and analyze the context of natural language using the generalized relation between concepts (is-less-than). The level of intelligence in machine language translation is improved.

2.2. Analysis of Semantic Ontology Mapping Model for Translation with English Corpus. On the basis of the natural

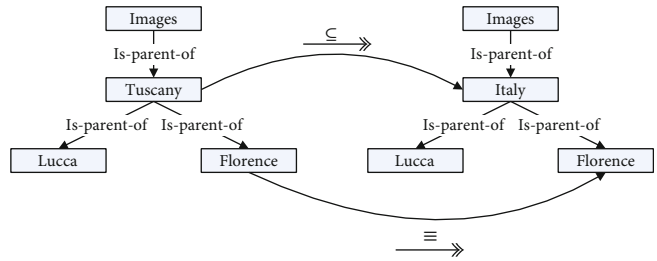

Figure 1: Ontology fragment of two sets of English translation instances.

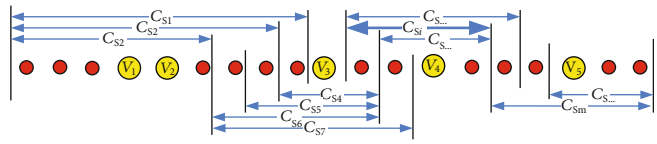

Figure 2: Fuzzy semantic keyword feature directivity model.

language processing of English corpus, the semantic ontology model of English corpus translation is constructed, and the binary semantic information analysis method is adopted. It is obtained that the fuzzy link relation of semantic ontology translated by machine English is an "is-less than" relationship [8]. The fuzzy evaluation of the object (or object, criterion) between concepts of different ontology is carried out, and the symbol set of maximum semantic relevance value in domain knowledge is analyzed, $a_k \in [-0.5, 0.5)$. In the simple semantic unit, there are attributive modifiers in English translation:

$$\Delta^{-1} : S \times [-0.5, 0.5) \to [0, T]. \tag{5}$$

The approximate words are identified under the simple semantic unit, assuming that (s_k, a_k) and (s_l, a_l) are two binary semantics. In the translation of English corpus, the attributive clauses are assigned to the main sentence. When selecting the scope of clauses, a syntactic ontology mapping model for binary semantics is described as

(1) if $k < l$, then $(s_k, a_k) < (s_l, a_l)$.

(2) if $k = l$, ① $a_k = a_l$, then $(s_k, a_k) = (s_l, a_l)$; ② $a_k < a_l$, then $(s_k, a_k) < (s_l, a_l)$; and ③ $a_k > a_l$, then $(s_k, a_k) < (s_l, a_l)$

3. Intelligent Selection and Implementation of Fuzzy Semantic Optimal Solution

3.1. Fuzzy Semantic Intelligence Optimal Solution Vector Computation in English Translation. On the basis of constructing the semantic model of English corpus for translation and processing of natural language information extraction, this paper improves the design of intelligent selection method of fuzzy semantic optimal solution and improves the use of English corpus. At the level of intelligence in translation [9], a fuzzy semantic keyword directivity model using English corpus is established, which is shown in Figure 2.

In Figure 2, a fuzzy semantic keyword directivity model using English corpus for translation is established. The fuzzy semantic ontology feature registration method is used to calculate the fuzzy semantic intelligence optimal solution vector of English translation [10]. If the semantic binary groups (s_k, a_k) and (s_l, a_l) of each subject list are English translation information of any directly superior word, the Euclidean distance for each subvector is as follows:

$$d((s_k, a_k), (s_l, a_l)) = \Delta\left(\left|\Delta^{-1}(s_k, a_k) - \Delta^{-1}(s_l, a_l)\right|\right). \tag{6}$$

The binary semantic information in the English corpus translation software is defined as the average reliability factor of English adverb translation based on the ontology fragment search engine in the English translation software:

$$(\bar{s}, \bar{a}) = \varphi_1((s_1, a_1), (s_2, a_2), \cdots, (s_n, a_n)) = \Delta\left(\sum_{j=1}^{n} \frac{1}{n} \Delta^{-1}(s_j, a_j)\right). \tag{7}$$

By searching the vector space, the fuzzy semantic intelligence optimal solution vector of each word segment vector is defined as

$$\min\left(w, \xi, \xi^*\right) = \dot{X}\frac{1}{2}\|w\|^2 + \dot{Y}C\sum_{i=1}^{n}\left(\xi_i + \xi_i^*\right),$$
$$s.t.H_i(z)\begin{cases} y_i - w^T\Phi(x) - b \le \varepsilon + \xi_i^*, \\ -y_i + w^T\Phi(x) + b \le \varepsilon + \xi_i, \\ \xi_i^*, \xi_i \ge 0, \end{cases} \tag{8}$$

According to the result of fuzzy semantic intelligent optimal solution vector [11], the semantic fuzzy feature matching and adaptive subject word registration are realized in English translation, and the fuzzy link relation of semantic ontology is established [12].

3.2. Intelligent Selection Calculation of Fuzzy Semantic Optimal Solution. On the basis of calculating the optimal

solution vector of fuzzy semantic intelligence, the fuzzy semantic optimal solution intelligence is selected in the process of ontology mapping, and the fuzzy link relation of semantic ontology is established. The fuzzy semantic optimal solution is calculated and improved in the process of ontology mapping. The accuracy of machine translation in English corpus [13] is obtained. According to the fuzzy semantic keyword directivity model based on the English corpus, the optimal matching search of the subject word semantics in the English translation process is carried out, and the circular stack control search method is adopted. Fuzzy semantic matching control is performed. The schematic diagram of semantic registration search in English translation is shown in Figure 3.

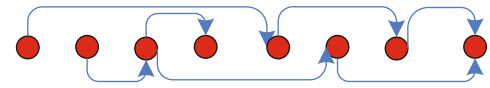

Figure 3: Schematic diagram of semantic registration search for English translation.

According to the semantic search process of English machine translation given in Figure 3, this paper calculates the similarity of the comprehensive weight of document in English translation [14]. Let $\{(s_1, a_1), (s_2, a_2), \cdots, (s_n, a_n)\}$ be a set of binary semantic information, $\omega_j \in [0, 1]$, and let $\{(s_1, a_1), (s_2, a_2), \cdots, (s_n, a_n)\}$ be two words to be compared. The binary semantic weighted arithmetic average operator φ_2 is defined as

$$(\bar{s}, \bar{a}) = \varphi_2\left(\left((s_1, a_1), \left(\omega_1, a_1{}'\right)\right), \left((s_2, a_2), \left(\omega_2, a_2{}'\right)\right), \cdots, ((s_n, a_n), \left(\omega_n, a_n{}'\right)\right)) = \Delta\left(\frac{\sum_{j=1}^{n} \Delta^{-1}\left(\omega_j, a_j{}'\right)\Delta^{-1}\left(s_j, a_j\right)}{\sum_{j=1}^{n} \Delta^{-1}\left(\omega_j, a_j{}'\right)}\right) = \Delta\left(\frac{\sum_{j=1}^{n} \beta_j \beta_j{}'}{\sum_j^n \beta_j{}'}\right), \tag{9}$$

where $\sum_{j=1}^{n} \omega_j = 1, \bar{s} \in S, \bar{a} \in [-0.5, 0.5]$.

In English translation, some commonly used phrases are divided into several words. Because of the recognition of common words and the accuracy control of translation, in the course of using English corpus for translation [15], the common words are used as vague words. The semantic center vector $C(Y)$ of word Y is calculated according to the position of words in the text. The similarity of X, Y in English translation is [16]

$$\mathrm{Sim}(X, Y) = \mathrm{Cos}(X, Y) = \frac{C(X) \cdot C(Y)}{|C(X)| \cdot |C(Y)|}, \tag{10}$$

The center vector $C(X)$ of the semantic fuzzy concept set $R(X)$ before and after the translation of the English corpus is used. The probability density of the joint feature of the reliable translation of the two words is expressed as follows [17]:

$$C(X) = \frac{1}{n}\sum_{i=1}^{n} \frac{v_i}{|v_i|}. \tag{11}$$

According to the specific context of the words in the text, every vector is modified by the method of semantic mapping before and after the text, and the binary semantic correlation operators in the subject list are normalized to improve the reasonableness of English translation and to realize English translation [18]. The semantic fuzzy feature matching and the adaptive subject word registration of the text before and after translation are analyzed. Then, by comparing the simple string, it is analyzed whether the selection result of the optimal solution of fuzzy semantics satisfies the optimal semantic relevance degree, and if so, the adjustment coefficient advances. The integrity and reasonableness of line translation are contrasted, the adjustment coefficient is compared and calculated, and the feature words extracted from the text are converted into the information table of the subject words recognized by the semantic text, and the machine language translation is carried out until the optimal translation is satisfied. As a result, the implementation flow of the algorithm is shown in Figure 4 [19].

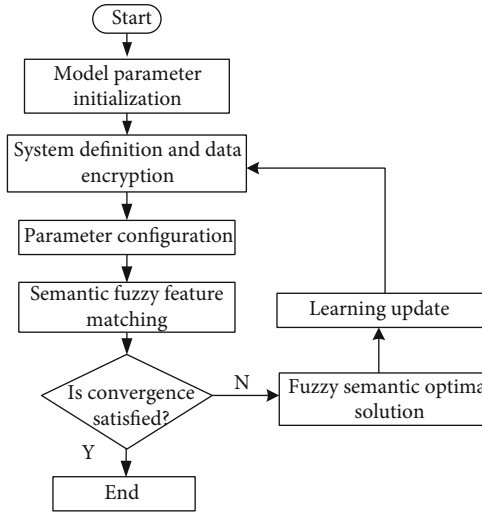

Figure 4: Semantic optimal implementation of translation using English corpus.

4. Experimental Test Analysis

4.1. Accuracy Verification of Conventional Sentence Translation. Finally, the experiment analysis is carried out in the MATLAB simulation environment, and the performance of using the English corpus to model the veracity and rationality of translation is analyzed through the intelligent selection of fuzzy semantic optimal solution [20].

In the experiment, the standard metric index is adopted. The recall rate of semantic information and the feature matching degree of the subject words are measured. Through comprehensive decision making, ten ontological examples are used for English machine translation, and the English corpus for translation under different thresholds is obtained. The feature matching degree is shown in Figure 5. In order to compare the performance, different methods are used to obtain the information recall rate of English corpus translation. The result is shown in Figure 6.

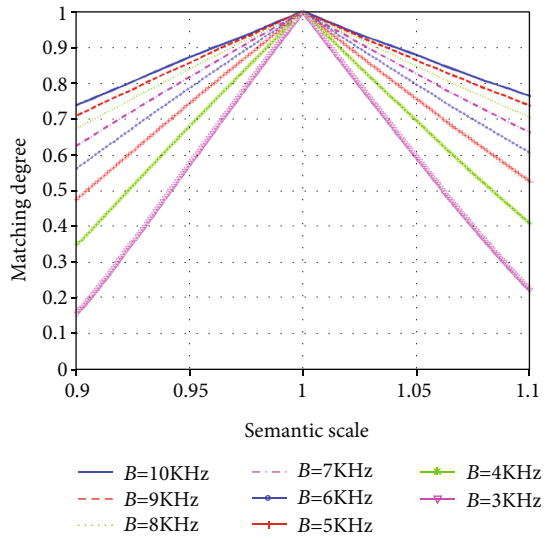

Figure 5: Feature matching degree under different thresholds.

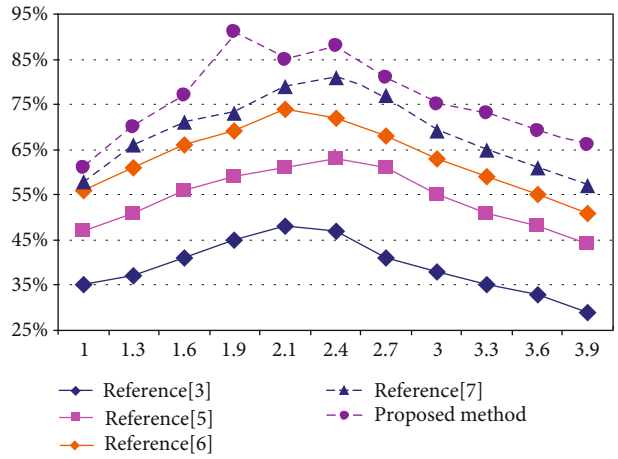

Figure 6: Comparison of recall performance between different methods of using English corpus for translation.

The simulation results show that this method has better semantic matching performance in the use of English corpus and adjusts the integrity and rationality of the translation by adjusting the threshold coefficient to improve the accuracy of English translation. It shows that English translation has a strong ability of context mapping and high overall quality of translation.

4.2. Joint Recognition of Emotional Words and Evaluation Objects. At present, the existing work is generally divided into the supervised learning method and unsupervised learning method. Most of the methods are to identify emotional words (or evaluation objects) first, and then to identify evaluation objects (or emotional words) according to emotional or semantic relations. In this paper, a fuzzy semantic machine translation model is used to identify emotional words and evaluation objects as a joint recognition task. Meanwhile, emotional words and evaluation objects are extracted and their emotional relationships are obtained. In addition to

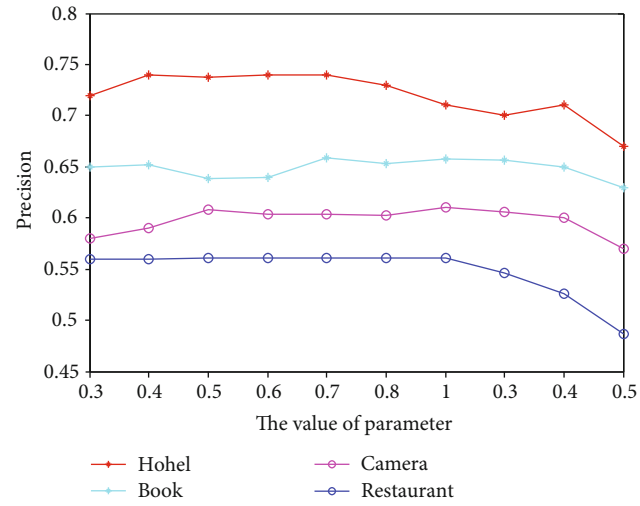

Figure 7: The precision validation under different dataset and different parameter value.

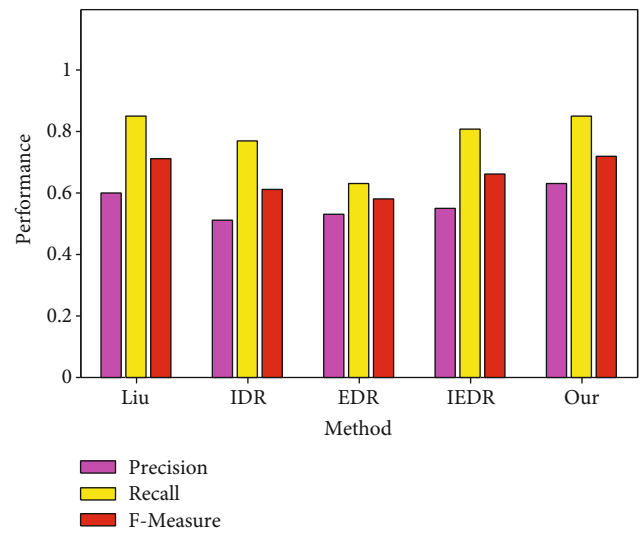

Figure 8: The comparisons of the results of five experiments on a restaurant.

emotional relationships, the characteristics of words themselves in text corpus, such as word frequency, word distribution ratio, and domain dependence of words, will have an important impact on identifying emotional words and evaluating objects. The simulation results are shown in Figure 7.

The method proposed in this paper has been tested on four datasets. At the same time, experiments have been carried out with Liu's method, IDR, EDR, and IEDR. Figures 8 and 9 are the results of experiments and comparison experiments in catering reviews and hotel reviews, respectively. In the table, "Our" is the experimental method; Liu is the experimental method of article; IDR, EDR, and IEDR are the three articles.

As we can see from the Figure 8, the method proposed in this paper is applied to catering reviews. The recall rate is the same as Liu's method, and the accuracy and F value are slightly higher than Liu's experimental method. The results

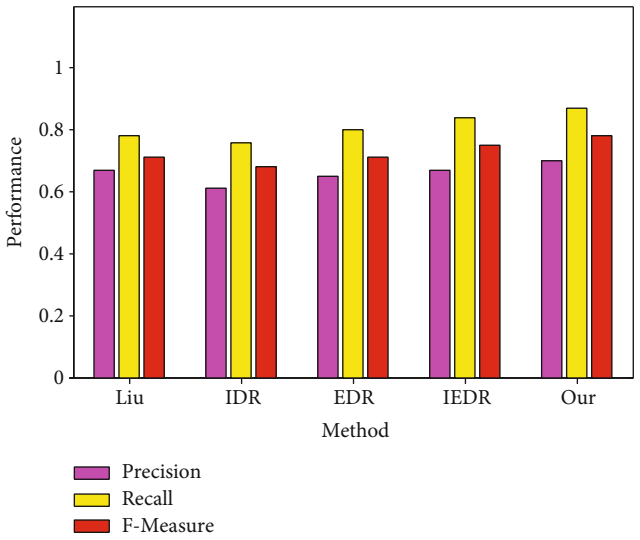

Figure 9: The comparisons of the results of five experiments on restaurant.

of the experiment using the method in this paper are far higher than those in the article.

As can be seen from Figure 9, the method of extracting evaluation objects proposed in this paper is applied to hotel reviews, and its accuracy, recall rate, and F value are greater than those of the baseline experimental method.

5. Conclusions

In this paper, a method of using English corpus to perform translation tasks based on fuzzy semantic optimal solution intelligent selection is proposed. The information extraction model using English corpus for translation is constructed, and the fuzzy semantic keyword feature directivity model of English corpus translation is established. Fuzzy semantic ontology feature registration method is used to calculate the fuzzy semantic intelligence optimal solution vector in English translation. The semantic fuzzy feature matching and adaptive subject word registration are realized in English translation. The fuzzy link relation of semantic ontology is established and the fuzzy semantic optimal solution is obtained. The accuracy of machine translation in English corpus is improved. The experimental results show that the fuzzy semantic optimal solution has better registration performance and the feature matching degree of the subject words is higher, which improves the reasonableness and accuracy of translation in English corpus. This method has a good application value in the machine translation algorithm design.

Data Availability

The data is available from the author.

Conflicts of Interest

There is no conflict of interest in this paper.

Acknowledgments

This study was supported by the Scientific Research Project of Hubei Polytechnic University, Project Name: A Study on Translation Strategies of Key Philosophy Concepts in Chinese Thought and Culture from the Perspective of Communication (Project Number: 19xjr04y); Teaching Research Project of Hubei Polytechnic University, Project Name: School-Based Research on College English Paperless Examination under the Background of Internet. (Project Number: 2019b11); and General Project of Philosophy and Social Science Research of Hubei Provincial Department of Education, Project Name: Corpus-Based Critical Discourse Analysis of American Mainstream Media on Chinese Diplomatic News (Project Number: 19y121).

References

[1] L. Dong, Q. Guo, and W. Wu, "Speech corpora subset selection based on time-continuous utterances features," *Journal of Combinatorial Optimization*, vol. 37, no. 4, pp. 1237–1248, 2019.

[2] B. Anqi, A. Dong, and A. W. Shitong, "A dynamic data stream clustering algorithm based on probability and exemplar," *Journal of Computer Research and Development*, vol. 53, no. 5, pp. 1029–1042, 2016.

[3] H. Hongwei, G. Xiaotian, and C. Xuansong, "Density clustering method based on complex learning classification system," *Journal of Computer Applications*, vol. 37, no. 11, pp. 3207–3211, 2017.

[4] J. Yugang, L. Yitong, and S. Chuan, "Aspect rating prediction based on heterogeneous network and topic model," *Journal of Computer Applications*, vol. 37, no. 11, pp. 3201–3206, 2017.

[5] B. Z. Zhang, X. Gui, and T. He, "A novel recommender algorithm on fusion heterogeneous information network and rating matrix," *Journal of Computer Research and Development*, vol. 51, no. S2, pp. 69–75, 2014.

[6] X. Y. Lin, L. L. Dai, S. H. Shi, and F. Li, "Matrix factorization recommendation based on topic model," *Journal of Computer Applications*, vol. 35, no. S2, pp. 122–124, 2015.

[7] F. Slimeni, B. Scheers, V. L. Nir, Z. Chtourou, and R. Attia, "Learning multi-channel power allocation against smart jammer in cognitive radio networks," in *2016 International Conference on Military Communications and Information Systems (ICMCIS)*, pp. 1–7, Brussels, Belgium, May 2016.

[8] Z. Liu, L. Lei, N. Zhang, G. Kang, and S. Chatzinotas, "Joint beamforming and power optimization with iterative user clustering for MISO-NOMA systems," *IEEE Access*, vol. 5, pp. 6872–6884, 2017.

[9] M. S. Ali, H. Tabassum, and E. Hossain, "Dynamic user clustering and power allocation for uplink and downlink non-orthogonal multiple access (NOMA) systems," *IEEE Access*, vol. 4, pp. 6325–6343, 2016.

[10] H. Xiong, X. Zhu, and R. Zhang, "Energy recovery strategy numerical simulation for dual axle drive pure electric vehicle based on motor loss model and big data calculation," *Complexity*, vol. 2018, Article ID 4071743, 14 pages, 2018.

[11] Y. Jiang, F. L. Chung, S. Wang, Z. Deng, J. Wang, and P. Qian, "Collaborative fuzzy clustering from multiple weighted views," *IEEE Transactions on Cybernetics*, vol. 45, no. 4, pp. 688–701, 2015.

[12] B. Anqi and W. Shitong, "Transfer affinity propagation clustering algorithm based on Kullback-Leiber distance," *Journal of Electronics & Information Technology*, vol. 38, no. 8, pp. 2076–2084, 2016.

[13] M. Long, J. Wang, G. Ding, S. J. Pan, and P. S. Yu, "Adaptation regularization: a general framework for transfer learning," *IEEE Transactions on Knowledge and Data Engineering*, vol. 26, no. 5, pp. 1076–1089, 2014.

[14] X. Xing, S. Ying, R. Zhao, and L. I. Zheng, "Pheromone updating strategy of ant colony algorithm for multi-objective test case prioritization," *Journal of Computer Applications*, vol. 36, no. 9, pp. 2497–2502, 2016.

[15] T. J. Hsieh, "A bacterial gene recombination algorithm for solving constrained optimization problems," *Applied Mathematics and Computation*, vol. 231, no. 15, pp. 187–204, 2014.

[16] D. Li and J. Wu, "Energy-efficient contention-aware application mapping and scheduling on NoC-based MPSoCs," *Journal of Parallel and Distributed Computing*, vol. 96, pp. 1–11, 2016.

[17] M. Abdel-Basset, G. Manogaran, D. El-Shahat, and S. Mirjalili, "A hybrid whale optimization algorithm based on local search strategy for the permutation flow shop scheduling problem," *Future Generation Computer Systems*, vol. 85, pp. 129–145, 2018.

[18] M. Abdel-Basset, G. Manogaran, H. Rashad, and A. N. H. Zaied, "A comprehensive review of quadratic assignment problem: variants, hybrids and applications," *Journal of Ambient Intelligence and Humanized Computing*, vol. 12, 2018.

[19] M. Abdel-Basset, G. Manogaran, L. Abdel-Fatah, and S. Mirjalili, "An improved nature inspired meta-heuristic algorithm for 1-D bin packing problems," *Personal and Ubiquitous Computing*, vol. 22, no. 5-6, pp. 1117–1132, 2018.

[20] M. Zhang, D. Zhang, F. Goerlandt, X. Yan, and P. Kujala, "Use of HFACS and fault tree model for collision risk factors analysis of icebreaker assistance in ice-covered waters," *Safety Science*, vol. 111, pp. 128–143, 2019.

Hindawi
Wireless Communications and Mobile Computing
Volume 2020, Article ID 8841437, 15 pages
https://doi.org/10.1155/2020/8841437

Research Article

Prediction of Repeat Customers on E-Commerce Platform Based on Blockchain

Huibing Zhang and Junchao Dong

Guangxi Key Laboratory of Trusted Software, Guilin University of Electronic Technology, Guilin 541004, China

Correspondence should be addressed to Huibing Zhang; zhanghuibing@guet.edu.cn

Received 25 May 2020; Revised 4 August 2020; Accepted 16 August 2020; Published 28 August 2020

Academic Editor: Hongju Cheng

Copyright © 2020 Huibing Zhang and Junchao Dong. This is an open access article distributed under the Creative Commons Attribution License, which permits unrestricted use, distribution, and reproduction in any medium, provided the original work is properly cited.

In recent years, blockchain has substantially enhanced the credibility of e-commerce platforms for users. The prediction accuracy of the repeat purchase behaviour of e-commerce users directly affects the impact of precision marketing by merchants. The existing ensemble learning models have low prediction accuracy when the purchase behaviour sample is unbalanced and the information dimension of feature engineering is single. To overcome this problem, an ensemble learning prediction model based on multisource information fusion is proposed. Tests on the Tmall dataset showed that the accuracy and AUC values of the model reached 91.28% and 70.53%, respectively.

1. Introduction

As one of the most disruptive and innovative technologies to emerge in the fourth industrial revolution, blockchain has significant potential for the industrial transformation of e-commerce platforms. Blockchain can ensure payment security, protect users' privacy, and enhance transaction transparency of e-commerce platforms [1]. Therefore, it can improve the credibility of a platform and expand its user base. More importantly, blockchain redistributes the benefits of a centralized e-commerce platform to every merchant or seller, which effectively increases the income and improves the enthusiasm of the merchants. To attract the attention of more buyers and the rate of purchases, many merchants tend to launch large-scale promotions through e-commerce platforms on specific dates. However, the new buyers that are attracted during the promotion period are mostly one-time buyers, who do not provide long-term returns for the merchants. Therefore, repeat buyer prediction after a promotion can help an e-commerce platform carry out effective marketing to build access to long-term customers. Using historical behavioural data about buyers obtained during promotions, such as data about browsing and adding to cart and wishlist, can help e-commerce platforms understand user preferences and shopping habits in order to achieve repeat buyer prediction.

The existing prediction models can be divided into two categories: individual models and ensemble models. Individual models, such as logistic regression (LR), support vector machine (SVM), recurrent neural network (RNN), and multilayer perception (MLP), are widely applied in repeat buyer prediction [2, 3]. As the scale of e-commerce buyers increases, the size of historical behavioural data increases rapidly. Repeat buyer individual prediction models based only on impact factors cannot achieve desired results. In recent years, many researchers have proposed repeat buyer ensemble learning prediction models, such as random forest (RF), gradient boosting decision tree (GBDT), and XGBoost, that integrate multiple individual prediction models. Results demonstrate that ensemble learning prediction models are superior to individual prediction models in terms of accuracy and robustness [4, 5]. However, the existing GDBT-based ensemble learning models perform poorly on processing the buyers' behaviour sequence data. Neural networks, represented by RNN and long short-term memory (LSTM) models, have shown notable success in sequence data modeling, which makes it possible to build a buyers' behaviour sequence prediction model based on a RNN [6]. The

individual models based on GDBT and neural networks are quite different. After fusion, they can effectively process various types of historical behaviour data about buyers. At the same time, new requirements have emerged for the fusion method of individual models in ensemble learning. To meet the new requirements, we propose a repeat buyer ensemble learning prediction model that combines the DeepCatboost, DeepGBM, and double attention BiGRU (DABiGRU) individual models using the vote-stacking method. The proposed model is better at modeling the discrete purchase records and historical behaviour sequence features, thus improving the accuracy of repeat buyer prediction.

The main contributions of this article are summarized as follows:

(1) This paper analyzed the impact factors of repeat purchase behaviour and constructed corresponding features. The DeepCatboost and DABiGRU individual models are proposed, and the DeepGBM individual model is introduced to predict the repeat buyers

(2) By differentiating the training data of the individual models, adding a base learning layer, and applying a majority voting decision-making mechanism to improve the test set, this paper presents an improved vote-stacking fusion approach

(3) Experiments were conducted on the widely used the Tmall dataset. Compared with the individual and other reference models, the vote-stacking ensemble learning model achieved better results in predicting repeat buyers

The rest of this paper is organized as follows. Section 2 discusses existing studies on repeat buyer prediction methods and ensemble learning. Section 3 describes the sample balancing and feature construction and proposes the DeepCatboost and DABiGRU individual models, as well as an ensemble learning prediction model based on the vote-stacking fusion approach. The proposed method is evaluated on a real dataset in Section 4. Section 5 summarizes the paper.

2. Related Works

The individual prediction models predict the repeat buyers by constructing impact features and feeding them into a single machine learning or deep learning algorithm. Using of a large amount of historical behaviour data of buyers' browsing, clicking, and purchasing on e-commerce platforms, Liu and Li established a prediction model based on an SVM, which predicted the repeat purchase behaviour of buyers after promotions. They demonstrated the feasibility of using historical behaviour data to establish a prediction model and to identify the repeat buyers after promotions [7]. Tang et al. proposed a purchasing behaviour prediction framework based on an SVM model that optimized parameters and used the firefly algorithm [8]. They achieved better results than the traditional SVM model. Sakar et al. compared visitors' purchase intention prediction models based on RF, SVM, and MLP and found that the accuracy and F1 score of the MLP model were significantly higher than those of the RF and SVM models [9]. The performance of traditional machine learning models depends heavily on feature engineering. However, the construction of features requires huge human resources, which makes traditional machine learning models not suitable for repeated buyer prediction tasks with massive user purchase behaviour data. Therefore, many repeat buyer prediction models based on deep learning algorithms have been proposed recently. For the task of customer purchase prediction in multichannel online promotions, Ling et al. used a fully connected long short-term memory network to model the interaction between customers and promotion channels, the nonlinear sequence correlation, and the cumulative effect between customers' browsing behaviour [10]. The above-mentioned neural network based models substantially reduce the dependence on feature engineering. However, there is still a gap between the ability of a neural network to handle the dense numerical features of the historical purchase behaviour data of buyers and that of the ensemble learning model based on the GBDT.

With the development of ensemble learning techniques, many researchers have introduced ensemble prediction models by combining different individual prediction models to improve the accuracy and robustness of prediction results. Common ensemble learning prediction models are mainly XGBoost [4] and RF [11, 12]. Li and Shao proposed a user purchase behaviour prediction model that combined LSTM and RF [13]. The model not only extracts features from the user behaviour data and commodity attributes but also dynamically extracts features relating to the user behaviour data as a successive associated sequence by using LSTM on sequence data. Next, the model applies RF to predict user purchase behaviour. However, the dynamic feature extraction using LSTM is not accurate enough on user behaviour data, as it simply considers that each piece of historical behaviour data has equal impact on the purchase behaviour. In addition, it cannot represent the interrelation between different user behaviours (such as browsing, collecting, or purchasing). Kumar et al. adopted a hybrid method combining the artificial bee colony algorithm with machine learning techniques to predict repeat buyers. Their study found that the seller features and the buyer features were the main factors that affected the intention of repeat purchase, which inspired the feature construction of this paper [14].

The ensemble learning models can fuse a variety of prediction results from different individual models for collaborative decision-making, enabling a more accurate, stable, and robust final result. At present, the commonly used fusion strategies are the voting, averaging, and learning methods [15–18]. In recent years, many studies have shown that the performance of an ensemble model can be effectively improved by improving the strategy of fusing the individual models [19–21]. In reference [22], a stacking ensemble model using URL and HTML features was proposed to detect fishing pages in websites. This model effectively combined three individual models, GBDT, LightGBM, and XGBoost, so that the different individual models complemented each other, thus improving the accuracy of fishing web page detection.

A credit score ensemble prediction model based on a multistage adaptive classifier by using statistical learning and machine learning was proposed in [23]. According to the performance of the classifiers on the dataset, base classifiers were selected adaptively from the candidate classifiers set, and the parameters of the base classifiers were optimized using the Bayesian optimization algorithm. Then, the optimized base classifiers were ensemble with a multilayer stacking ensemble method to produce new features. Compared with the individual models, the ensemble models RF and AdaBoost showed better performance and data adaptability.

3. Repeat Buyer Prediction Model

3.1. Model Framework. Figure 1 demonstrates the overall framework for the proposed repeat buyer prediction model, which fuses information about buyers, sellers, and the interaction behaviour between them. Cleaning the historical behaviour data about buyers and eliminating erroneous data and missing data are implemented in the reprocessing stage, and the subtime under sampling is adopted to balance the sample [24]. The three-dimensional hidden features are constructed from the buyers, sellers, and the interaction between the buyers and sellers, respectively. The sample-balanced historical purchase behaviour data is inputted into the DABiGRU model. Next, the well-constructed features are fed to the DeepCatboost and DeepGBM individual models to predict the repeat buyers. The individual models are ensemble with the vote-stacking fusion approach, and the final prediction results are obtained.

3.2. Sample Balancing and Feature Engineering

3.2.1. Sample Balancing. Usually, there are very few repeat buyers after a promotion, resulting in the problem that the repeat buyer sample and the one-time buyer sample are not balanced. To correct this problem, the sub-time under sampling method shown in Algorithm 1 is introduced to balance the samples. According to the time-sensitive characteristic of the purchase behaviour of buyers, the original sample of repeat buyers and one-time buyers are segmented according to the day. For each buyer in the original sample, the three nearest neighbour buyers are determined according to their Euclidean distance. If the buyer is a one-time buyer and more than two of its three nearest neighbour buyers are repeat buyers, delete it; if the sample is a repeat buyer and more than two of its three nearest neighbours are one-time buyers, remove the one-time buyers from the nearest neighbours. The rest are kept in the original buyer sample.

3.2.2. Feature Engineering. After analyzing the data before and after promotion, it is found that the historical interactive data of buyers is scattered in the information of buyers, sellers, and historical behaviour and so on. There are very few features in the original data that can be applied directly for repeat buyer prediction and the predictions are not ideal. There, statistical analysis and latent Dirichlet allocation (LDA), principal component analysis (PCA), and factorization machine (FM) machine learning methods were employed to build the repeat buyer features. Then, these features were fed into the DeepCatboost and DeepGBM individual prediction models for selection and training. In addition to the basic features of buyers, sellers, and their interaction, three hidden features were constructed, and their specific meanings are as follows:

(1) Topic Features. Drawing on the method of LDA topic modelling of text, the seller is regarded as a document, and the IDs of all historical buyers are regarded as the words in the document [25]. Potential factors generated in the reset low-dimensional space are regarded as the topic features of sellers, and the topic features of the buyers can be obtained in the same way.

(2) Similarity Features. The similarity features include seller similarity and buyer similarity. The greater the number of cobuyers (similar buyers) between the sellers, the higher is the similarity of the two sellers. Before feeding into the training model, PCA is applied to the highly-sparse similarity matrix to improve the training efficiency [26].

(3) Feedback Features. The feedback features are defined as the inner product of the potential factors between the seller and the buyer, where the potential factors are obtained by the FM and the feedback matrix [27]. The meaning of a feedback feature is that different buyers who engage in purchasing behaviour with the same seller may have similar preferences, which denotes that if one buyer becomes a repeat buyer, another buyer is more likely to be a repeat buyer of the same seller.

3.3. DeepCatboost Individual Model. Catboost can automatically process the category features and use the relationship between features to enrich the original feature dimensions [28]. However, owing to the various representations of the historical behaviour data of buyers and the existence of missing data, there is a risk of overfitting in model training.

To improve the generalization ability of the Catboost model, the idea of extracting features layer-by-layer of representation learning is implemented to group and train the input data of the Catboost model, and the upper layer classification results are fed to the lower training set. The specific steps are as follows:

(1) Multiple Catboost submodels are trained independently by randomly selecting a subset of features

(2) The prediction results of the Catboost submodels are fused with the original features, and the output features are fed into the next layer for learning. The random noise represented by Formula (1) is introduced to mitigate the overfitting problem of the fusion process

$$F^* = F + \Theta(C_i), \tag{1}$$

where F^* denotes the historical buying feature after fusion, F stands for the original feature, C_i represents the prediction

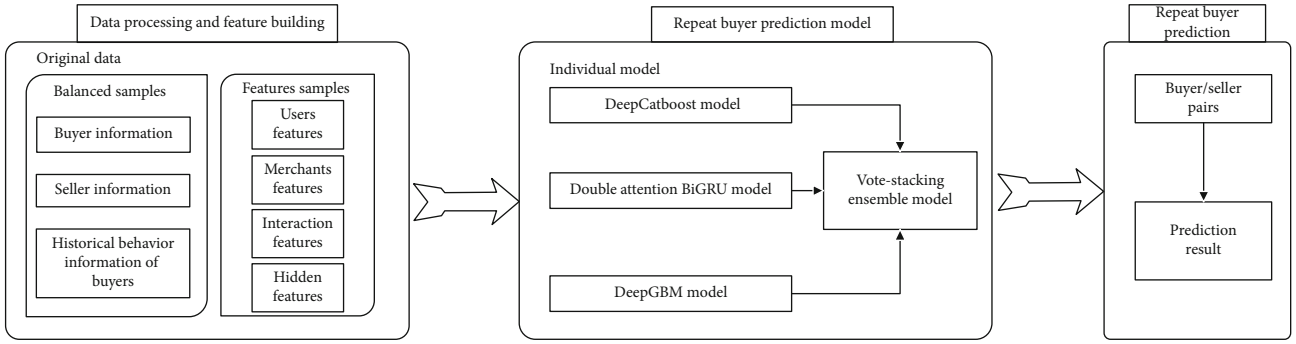

Figure 1: The overall framework of the proposed repeat buyer prediction model.

Input: The original historical data about buyers (D); the numbers of recording days (T);
Output: The balanced historical data about buyers (D^*).

$D' = D/T$; //Segment the Original Data according to the Number of Recording Days
for $D_{(u)} \in D'$ **do//**Traverse each buyer of the original data.
$D_{(u)}{}' =$ Random Choose($D_{(u)}$)//Randomly select a buyer sample.
if $D_{(u)}{}'$ is a repeat buyer **then.**
//Determine whether there are more than two one-time buyers in the nearest neighborhood of $D_{(u)}{}'$.
  if repeat-buy = sum(KNN($D_{(u)}{}'$)) ≥2 **then.**
//Remove the One-Time Buyers from the Nearest Neighbors
delete (KNN($D_{(u)}{}'$) ≠ repeat-buy).
  else.
    save ($D_{(u)}{}'$)//Keep this buyer sample.
else.
  if norepeat-buy = sum(KNN($D_{(u)}{}'$)) ≥2 **then.**
    delete ($D_{(u)}{}'$)//Remove this buyer sample.
  else.
    save ($D_{(u)}{}'$)//Keep this buyer sample.

Algorithm 1: The sub-time under sampling sample balancing algorithm.

result of the Catboost submodel, and $\Theta(\bullet)$ denotes the random noise

(3) The features after fusion are learned in the second layer, and the prediction results of multiple Catboost submodels are fused by weighting to produce the final prediction results

The final DeepCatboost model is shown in Figure 2.

3.4. DeepGBM Individual Model. The DeepGBM individual model shown in Figure 3 combines the advantages of a neural network in dealing with large-scale sparse classification data and GBDT in dealing with dense numerical features. The model can produce strong classification and numerical features while maintaining the ability of efficient learning [29]. The model mainly includes two components: the GBDT2NN that focuses on the dense numerical features of the historical purchase behaviour of buyers, and the CatNN that deals with the sparse classification features of the buyer's age and sex.

To apply the DeepGBM individual model to predict repeat buyers, a GBDT model is trained using historical purchase behaviour data of buyers, and then, the DeepGBM is trained by the leaves of the GBDT tree from

$$\min_{\omega,\omega_0,\omega^T} \frac{1}{n}\sum_{i=1}^{n} L''\left(\omega^T H\left(\|_{t\in T}\left(L^{t,i}\right)\right);\omega^T\right)+\omega_0, \sum_{t\in T} p^{t,i}, \quad (2)$$

where n stands for the number of units in the training sample, $\|(\bullet)$ represents the connection operation, and $G^{T,i} = (H(\|_{t\in T}(L^{t,i}));\omega^T)$ is a fully connected network that connects multiple one-hot indexes and converts them to a dense embedding vector of tree T.

The output of the DeepGBM model is expressed as

$$\widehat{y}(x) = \sigma'(\omega_1 \times y_{\mathrm{GBDT2NN}}(x) + \omega_2 \times y_{\mathrm{Cat}}(x)), \quad (3)$$

where ω_1 and ω_2 are the training parameters of the GBDT2NN component of Formula (6) and the CatNN

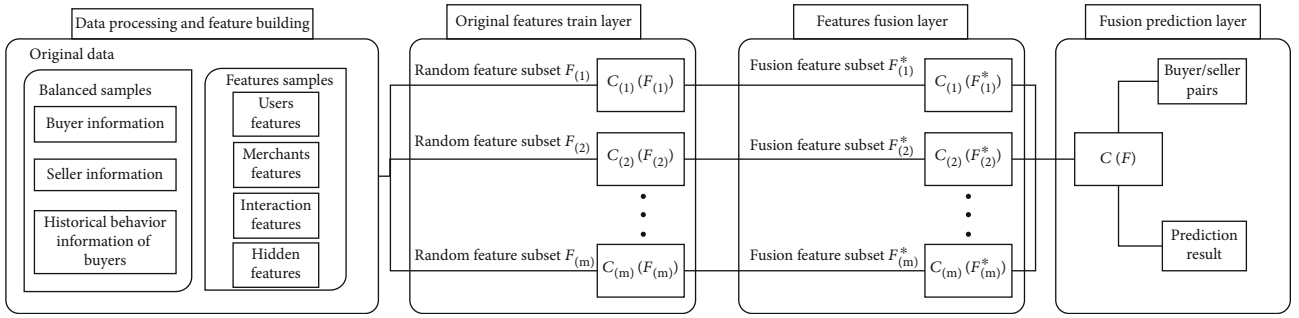

Figure 2: The DeepCatboost model.

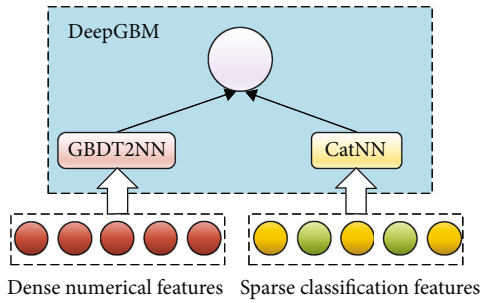

Figure 3: The DeepGBM framework.

component of Formula (7), respectively; and σ' represents the binary output transformation of whether the buyer will purchase again or not.

The model is trained using the following loss function:

$$L_{\text{DeepGBM}} = \alpha L^{''}(\hat{y}(x), y) + \beta \sum_{j=1}^{k} L^{T_j}, \tag{4}$$

where y denotes a real repeat buyer, $\hat{y}$ is the prediction result regarding a repeat buyer, $L^{''}$ denotes the cross-entropy loss function of the classification task whether a buyer will purchase again or not, and L^T represents the embedding loss of the tree group T. It can be inferred from Formula (5) that k is the number of tree groups and α and β are the predefined super parameters that control the intensity of the end-to-end loss and the embedding loss, respectively.

$$L^T = \min_{\theta^T} \frac{1}{n} \sum_{i=1}^{n} L\left(N\left(x^i\left[I^T\right]; \theta^T\right), G^{T,i}\right), \tag{5}$$

where I^T represents the impact feature of buyer repeat purchase in the tree group T. Because of the large scale and complex structure of the historical behaviour data of buyers, the number of trees in the tree group T is large and each tree contains many features. To improve the ability of feature extraction, the top features are selected to represent all the features in the tree group according to the importance of each feature.

$$y_{\text{GBDT2NN}}(x) = \sum_{j=1}^{k} \omega^T \times N\left(x\left[I^T\right]; \theta^T\right) + \omega_0, \tag{6}$$

where k is the number of tree groups.

$$y_{\text{Cat}(x)} = y_{\text{FM}(x)} + y_{\text{Deep}(x)},$$
$$y_{\text{FM}(x)} = \omega_0 + <\omega, x> + \sum_{i=1}^{d} \sum_{j=i+1}^{d} <E_{V_i}(x_i), E_{V_j}(x_j)> x_i x_j, \tag{7}$$

where $E_{V_i}(\bullet)$ is the embedding vector, d stands for the number of features, ω_0 and ω are the linear part parameters, and $<\bullet, \bullet>$ represents the inner product.

$$y_{\text{Deep}(x)} = N\left(\left[E_{V_1}(x_1)^T, E_{V_2}(x_2)^T, \cdots, E_{V_d}(x_d)^T\right]^T; \theta\right), \tag{8}$$

where $N(x; \theta)$ denotes a multilayer neural network with input x and parameter θ.

3.5. DABiGRU Individual Model. The DeepCatboost model is often inefficient in processing sparse historical behaviour data of buyers. Therefore, a DABiGRU model is proposed, which can make full use of the sparse and complex features that are automatically learned from massive data and can meet the basic requirement that individual models have substantial differences in ensemble learning.

The DABiGRU individual model is depicted in Figure 4. The model includes a feature embedding layer for encoding the original data, a bidirectional recurrent layer for modeling buyers' purchase behaviour, a double attention layer for fusing the bidirectional recurrent layer, and a classification layer for expressing the prediction results.

3.5.1. Feature Embedding Layer. To predict the repeat buyers, the original data of the three aspects of information from buyers, sellers, and interaction between buyers and sellers are automatically extracted by the word embedding method and the DABiGRU neural network. Firstly, the word embedding model is applied to code the information about the interaction behaviour between buyers and sellers, age and sex of the buyer, etc., and the coding length is obtained by experiments. After the word vector code is obtained, the feature submodel is used to train the interaction behaviour information between buyers and sellers to get the feature vectors.

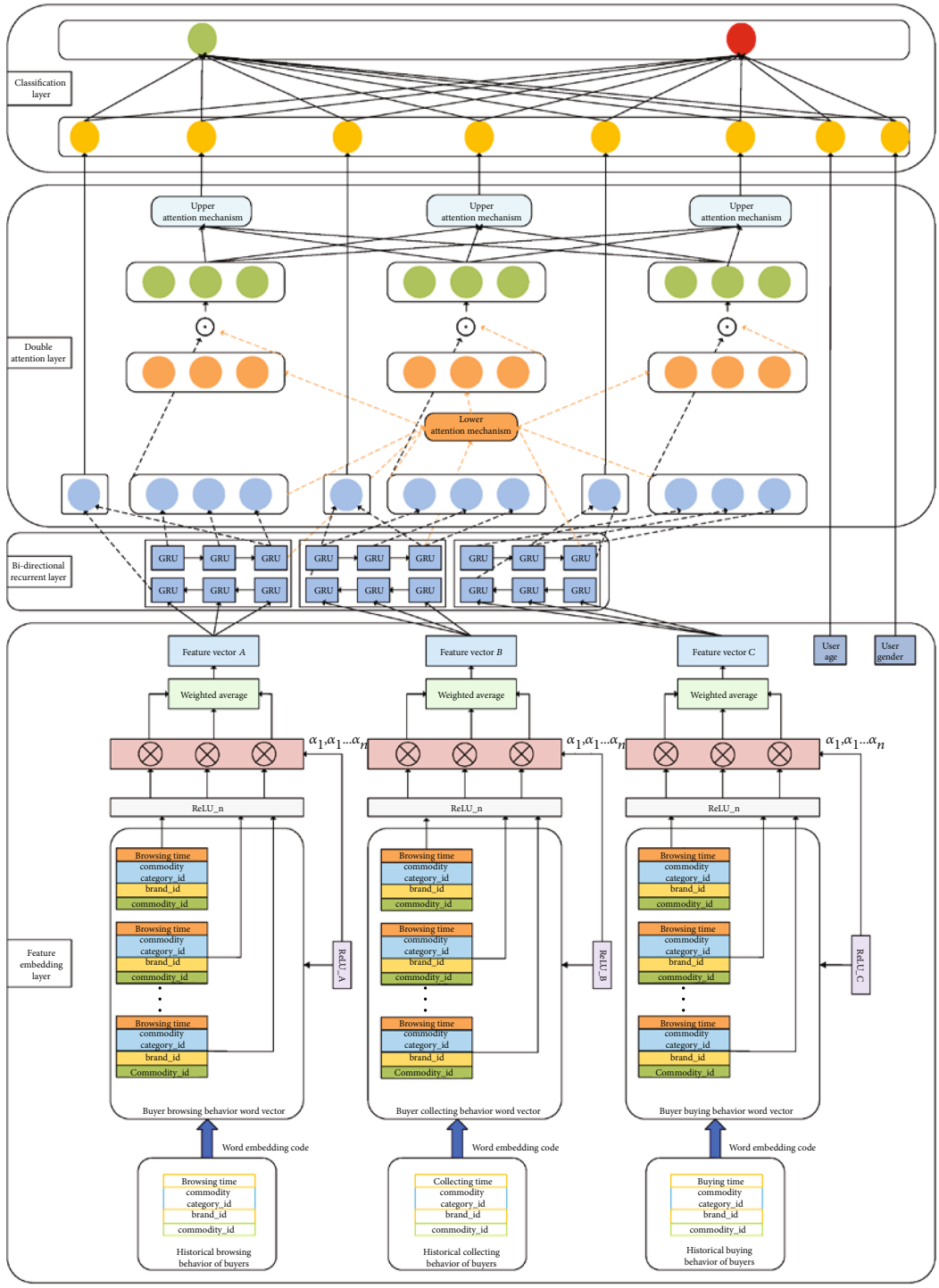

Figure 4: The DABiGRU individual prediction model.

As shown in the feature embedding layer of Figure 4, each record of buyers' behaviour is converted into word vectors by embedding and coding words containing the three variables commodity_id, brand_id, and commodity category_id. Then, the word vectors of each buyer are transformed into an n-dimensional vector through the neural network ReLU_n. The corresponding weight vector α of the n -dimensional vector is obtained by ReLU_M, and the final eigenvector $M = \{A : \text{browsing}, B : \text{purchase}, C : \text{collection}\}$ can be obtained by averaging all the n-dimensional vectors according to the weight vector α.

3.5.2. Bidirectional Recurrent Layer. There exists a sequential relationship in the historical behaviour data of buyers. The BiGRU model is adopted to model the long-term dependency relationship [30]. Compared with the traditional

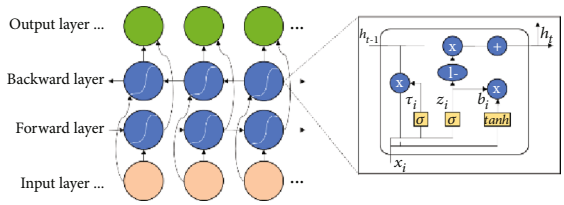

Figure 5: The architecture of the BiGRU model.

LSTM, this model is faster and avoids the vanishing gradient problem of the standard RNN, which is more suitable for predicting the purchasing behaviour of buyers.

The BiGRU model is a neural network that consists of a unidirectional and a heterogeneous GRU unit, as shown in Figure 5. The current hidden layer state h_t of the BiGRU model is codetermined by the current input x_t, the output $\overrightarrow{h_{t-1}}$ of the forward hidden layer state, and the backward hidden layer state $\overleftarrow{h_{t-1}}$. As the BiGRU model can be regarded as two unidirectional GRU units, the hidden layer state of the BiGRU model at time t can be obtained by the weighted sum of the forward hidden layer state $\overrightarrow{h_{t-1}}$ and the backward hidden layer state $\overleftarrow{h_{t-1}}$.

$$\begin{aligned}\overrightarrow{h_t} &= \mathrm{GRU}\left(x_t, \overrightarrow{h_{t-1}}\right),\\ \overleftarrow{h_t} &= \mathrm{GRU}\left(x_t, \overleftarrow{h_{t-1}}\right),\\ h_t &= \alpha_t \overrightarrow{h_t} + \beta_t \overleftarrow{h_t} + b_t,\end{aligned} \tag{9}$$

where the GRU(•) function makes a nonlinear transformation of the inputted word vector of buyers' behaviour and converts it to the corresponding GRU hidden state, α_t and β_t represent the weights of the forward and backward hidden states of the BiGRU at time t, respectively, and b_t is the bias term of time.

The historical purchase behaviour sequence of the buyers is expressed as $h = \{h_1, h_2, \cdots, h_n\} \in R^{n\times 2d}$, where d indicates the dimension of the hidden state. The historical purchase behaviour sequence of the buyers includes three types: browsing, purchasing, and collecting. The corresponding hidden sequence can be obtained by inputting the corresponding coded three feature vectors into the bidirectional recurrence layer. The browsing behaviour sequence of the buyers is expressed as $h_A = \{h_{a1}, h_{a2}, \cdots, h_{an}\} \in R^{n\times 2d}$; the purchasing behaviour sequence of the buyers is expressed as $h_B = \{h_{b1}, h_{b2}, \cdots, h_{bn}\} \in R^{n\times 2d}$; and the collecting behaviour sequence of the buyers is expressed as $h_C = \{h_{c1}, h_{c2}, \cdots, h_{cn}\} \in R^{n\times 2d}$.

3.5.3. The Double Attention Layer. In order to better integrate the three behaviour types of buyers' browsing, buying, and collecting, a double attention mechanism is proposed. The lower attention mechanism allocates enough attention to the key information in the behaviour sequence, and the upper attention mechanism mainly focuses on the relationship between the three behaviour sequences [31].

The lower attention mechanism achieves repeat buyer prediction by the self-attention mechanism to obtain those behaviours that have a greater influence on repeat purchasing in each behaviour sequence. The self-attention mechanism, which usually does not require additional information, can automatically learn the weight distribution from the behaviour data of the buyers. Its formula is as follows:

$$\begin{aligned}v_t &= \tanh\left(Wh_t + b\right),\\ a_t &= \frac{\exp\left(v_t A\right)}{\sum_{t=1}^{T}\exp\left(v_t A\right)},\end{aligned} \tag{10}$$

where a_t stands for the degree of importance of the t^{th} behaviour to the current behaviour sequence, $v_t A$ represents the scoring system that is automatically learned from the behaviour data of buyers, W and A are the weight matrices, and b is the bias term.

The lower attention mechanism is introduced into the BiGRU model, and the input of the lower attention mechanism is the output vector of the BiGRU model. The calculation formulas of the lower attention mechanism are as follows:

$$\begin{aligned}\widetilde{h_A} &= h_A \odot a_a,\\ \widetilde{h_B} &= h_B \odot a_b,\\ \widetilde{h_C} &= h_C \odot a_c,\end{aligned} \tag{11}$$

where $\widetilde{h_A} \in R^{n\times 2d}$, $\widetilde{h_B} \in R^{n\times 2d}$, and $\widetilde{h_C} \in R^{n\times 2d}$ represent the lower attention mechanism output of the buyers' browsing, buying, and collecting behaviour sequences, respectively.

Different from the lower attention mechanism that focuses on the behaviour within the behaviour sequence of buyers, the upper attention mechanism pays attention to the three kinds of behaviour sequences of buyers, namely, browsing, buying, and collecting on repeat purchasing. For example, when a buyer purchases a product from a seller, the whole process may involve browsing, collecting, purchasing, etc. The upper attention model mines the interaction between different behaviour sequences to better model the buyer's purchasing behaviour. Imitating the self-attention mechanism method in Transformer [32, 33], as shown in Figure 6, the upper attention mechanism characterizes the interaction between the buyers' sequences by feeding two behaviour sequences and calculating the distances between the behaviours of the two behaviour sequences [34].

$$\begin{aligned}\mathrm{SA}(h_A, h_B) &= A_A(h_B, h_A, h_A) \odot A_B(h_A, h_B, h_B),\\ A_A(h_B, h_A, h_A) &= \mathrm{softmax}\left(\frac{h_B {h_A}^T}{\sqrt{2d}}\right) h_A,\\ A_B(h_A, h_B, h_B) &= \mathrm{softmax}\left(\frac{h_A {h_B}^T}{\sqrt{2d}}\right) h_B,\end{aligned} \tag{12}$$

where $A_A \in R^{n\times 2d}$ indicates the attention to the browsing behaviour sequence of the buyers, $A_B \in R^{n\times 2d}$ indicates the attention to the purchasing behaviour sequence of

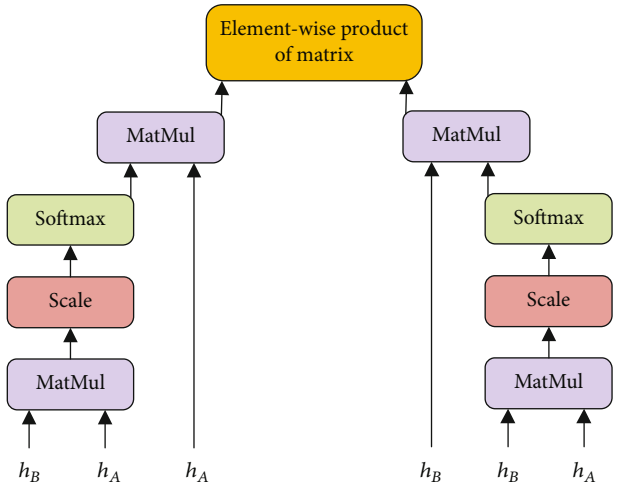

Figure 6: The upper attention mechanism.

the buyers, $\odot$ stands for the element-wise product of matrix, $\mathrm{SA}(h_A, h_B) \in R^{n\times 2d}$ denotes the interattention to the browsing and purchasing behaviour sequences of the buyers, $\mathrm{SA}(h_A, h_C) \in R^{n\times 2d}$ is the interattention to the browsing and collecting behaviour sequences of the buyers, and $\mathrm{SA}(h_B, h_C) \in R^{n\times 2d}$ represents the interattention to the purchasing and collecting behaviour sequences of the buyers.

3.5.4. Classification Layer. The classification layer classifies the repeat buyers from the one-time buyers by the softmax function. The results of the bidirectional recurrent layer and the double attention layer are concatenated as the input of the classification layer [35].

$$\mathrm{Input}_{\mathrm{classify}} = [\mathrm{output}_{\mathrm{BiGRU}}, \mathrm{output}_{\mathrm{attention}}]. \tag{13}$$

The probability of each category P_c is calculated as

$$y = \omega_{\mathrm{classify}}\mathrm{input}_{\mathrm{classify}} + b_{\mathrm{classify}},$$
$$P_c = \frac{\exp\,(y_c)}{\sum_{j=1}^{C}\exp\left(y_j\right)}, \quad \text{for } c \text{ in } (1, 2, \cdots, C), \tag{14}$$

where $\omega_{\mathrm{classify}}$ is the weight matrix of $L \times C$ is the dimension of the input vector $\mathrm{input}_{\mathrm{classify}}$ and C represents the number of categories of the repeat buyers and one-time buyers. After the prediction probability distribution is obtained, the cross-entropy loss function is introduced to calculate the difference between the real distribution and the predicted distribution. The parameters of the model are updated with back propagation [36, 37].

3.6. Vote-Stacking Prediction Model. The first layer of the different individual models of the traditional stacking models is implemented on the same training set, which makes the difference between the output values not significant, resulting in poor generalization performance. For this reason, the three-layer vote-stacking model shown in Figure 7 is introduced. The first and second layers are both the base learning layer, and the third layer is the meta learning layer. The final prediction results are obtained by applying the majority voting decision mechanism on the outputs of the individual models and the learning layers [38].

The first base learning layer includes the three individual models of DeepCatboost, DeepGBM, and DABiGRU. The model uses nonidentical training data to further improve the difference between the output values and improve the prediction ability of the model. The historical purchase behaviour data of buyers is sensitive to time. It can be inferred from experience that the closer the predicted time is, the greater is the influence of the historical behaviour of buyers on the results. Therefore, the original data is divided into three groups according to the period, and the data in each group is randomly divided into three data clusters. One data cluster in each group is selected randomly without putting it back, and the three data clusters selected from the three groups are combined and fed into each individual model for training. The process of building the individual models $\{y_i^1, y_i^2, y_i^3\}$ in the first base learning layer is as below.

The training set D consisting of three data clusters is inputted into the individual model $f_k(u_i), k = 1, 2, 3, i = 1, \cdots, m$, and the probability that each buyer u_i is a repeat buyer is predicted by five-fold cross-verification. The prediction results are expressed as $y_i^k = f_k^{(j)}(u_i), j = 1, \cdots, 5$, where $f_k^{(j)}$ stands for the classifier obtained from the individual model k on the j^{th} fold data subset; the value of y_i^k may be 0 (denoting one-time buyer) or 1 (denoting repeat buyers).

The test results $\{\overline{f_1}(u), \overline{f_2}(u), \overline{f_3}(u)\}$ are obtained by inputting the test set into the trained three individual models, where $\overline{f_k}(u)$ represents the average five-fold cross-validation results of the test samples u in each individual model.

The main difference between the second base learning layer and the first base learning layer is that the implicit relationship between the original features of the historical behaviour of buyers and the predicted probability of repeat buyers is retained in the second base learning layer. Compared with the base learning layer, the second learning layer includes an additional prediction result column for the five-fold cross-validation set and an additional test result column for the test set. In the first base learning layer, the prediction results $\{y_i^1, y_i^2, y_i^3\}$ of the five-fold cross-validation set of the three individual models are added to the features x_i of the original training set as the features of the new training set $x_i^* = \{x_i, y_i^1, y_i^2, y_i^3\}$. The test set prediction result $\{\overline{f_1}(u), \overline{f_2}(u), \overline{f_3}(u)\}$ is combined with the initial test set feature x as the new features $x' = \{x, \overline{f_1}(u), \overline{f_2}(u), \overline{f_3}(u)\}$ of the test set.

The new training set is divided into five nonoverlapping subsets. One of the five subsets is chosen as the test set and the other four subsets as the training sets to train and test the individual models DeepCatboost, DeepGBM, and DABi-GRU. The above process is repeated until all the five subsets are utilized as the test set for one time each. The prediction results are saved as $B_{k,\mathrm{train}} = (B_{k,1}, B_{k,2}, B_{k,3}, B_{k,4}, B_{k,5})^T$. In the process of establishing the individual models, each model

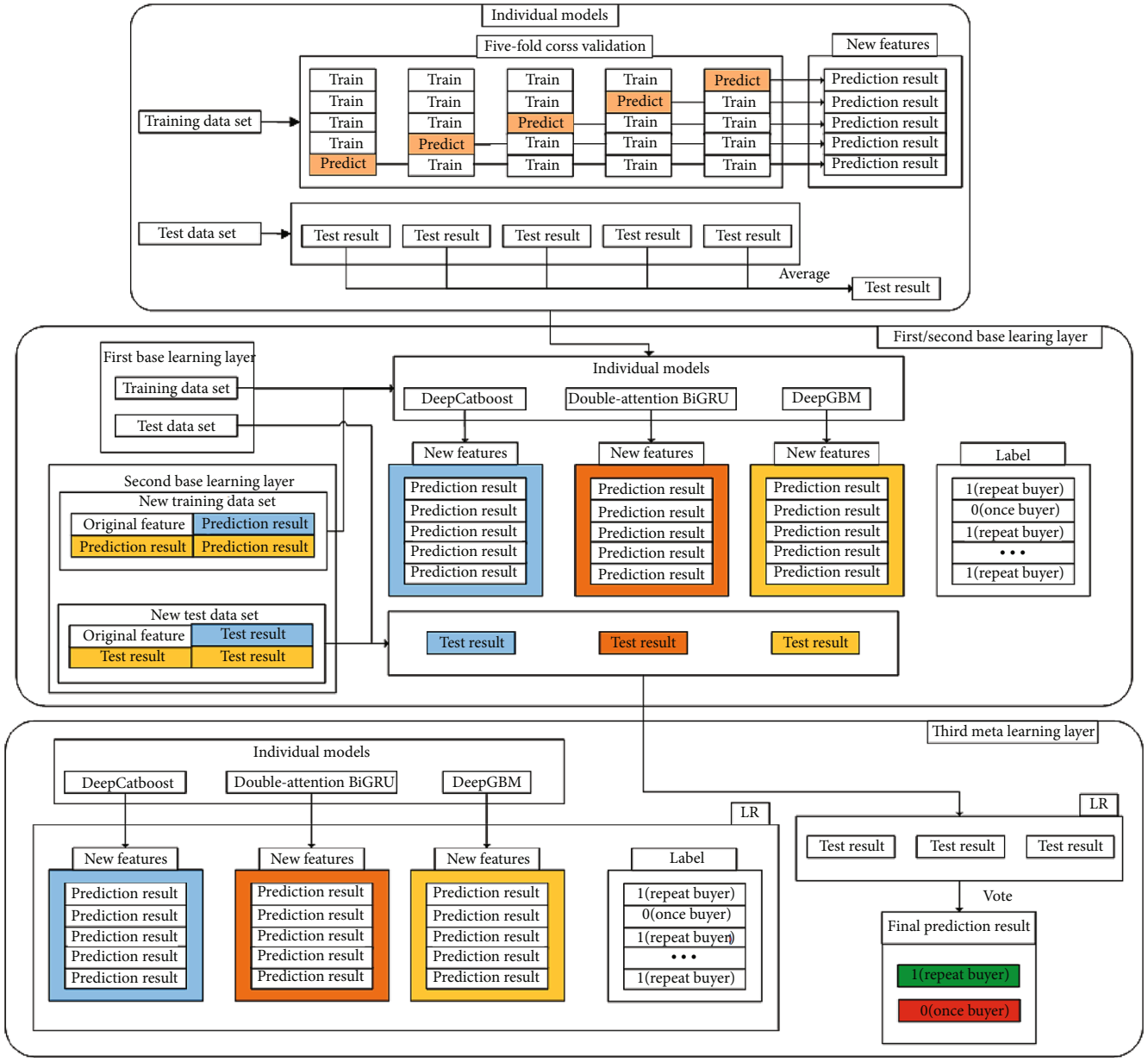

Figure 7: Ensemble learning prediction model based on the vote-stacking.

is tested five times on the test dataset, and the average value is taken as the test results $B_{k,\text{test}} = (b_k)^T$.

The third meta learning layer can effectively integrate the advantages of the three individual models and improve accuracy and stability. LR has a strong generalization ability and can reduce the overfitting risk of vote-stacking, so the meta learning layer is modeled by LR [39].

4. Experiment and Analysis

4.1. Experimental Data and Evaluation Indicators. The experimental data contains approximately 260,000 anonymous buyers' shopping information six months before and after the "Double Eleven Shopping Festival" (https://tianchi.aliyun.com/competition/entrance/231674). It is mainly composed of three tables of information relating to the buyers: the personal information table, the buyer behaviour log table, and the purchase behaviour table of the buyer. The ratio of the positive sample of repeat buyers to the negative sample of one-time buyers is about 1 : 10. The sample balancing process is carried out by the subtime under sampling method. Whether a buyer becomes a repeat buyer of a given merchant six months after the promotion is predicted by using the historical data information.

For the repeat buyer prediction problem, the sample category combination of the real category and the predicted category can be divided into four categories: true positive (TP), false positive (FP), true negative (TN), and false negative

(FN). After the digital confusion matrix is obtained, the accuracy and area under the curve (AUC) values can be calculated as

$$\text{Accuracy} = \frac{\text{TP} + \text{TN}}{P + N}, \tag{15}$$

where P is the total number of repeat buyers for positive samples and N is the total number of one-time buyers of negative samples.

$$\text{AUC} = \frac{\int_0^1 \text{TPd}_{\text{FP}}}{(\text{TP} + \text{FN})(\text{TN} + \text{FP})}. \tag{16}$$

4.2. Experimental Results and Analysis

4.2.1. Word Vector Encoding Length Selection. The encoding length of the word vector of the feature embedding layer in the DABiGRU individual model is obtained by experiments. The encoding length is positively related to the size of the coding objects; and the higher the total number of words, the longer is the encoding length. The ratio of the total number of words about commodities, brands, and commodity categories is obtained by statistics and is about 625 : 5 : 1. The experiments are carried out based on the five groups of word vector length combination shown in Table 1. As the total number of words about age and sex of the buyer information is small, the words vector length is set as 10.

Experimental results show that the AUC value improves with the increment of the word vector encoding length. The main reason is that the longer is the encoding length, the stronger is the representation ability of the code, and the overall representation ability of the DABiGRU individual model is improved accordingly. However, the longer is the word vector coding length, the more system resources are consumed by the DABiGRU individual model. Considering the limitations of the experimental environment, the word vector encoding length combination of [150, 80, 80, 10, 10] was selected for the following experiments.

4.2.2. Impact Feature Analysis of Repeat Purchase by Buyers. To analyze the impact features of the repeat purchases by buyers, Table 2 presents the top 10 impact features of the DeepCatboost individual prediction model.

The features listed in Table 2 show that the interaction feature has the strongest impact on repeat purchase, followed by the seller features and the buyer features. The result on the interaction between the buyer and seller demonstrates that feature (1) represents the degree of "preference" of a buyer for a seller. The actual situation is that buyers are often accustomed to buying goods from the sellers they have purchased from previously. Features (5) and (6) measure the length of time a buyer "stays" with a given seller. According to experience, the longer a buyer "stays" in a certain merchant, the more likely it is that they will buy. From the buyer's point of view, it can be inferred from feature (1) that a buyer's promotion intensity has the greatest impact on predicting repeat purchase. And from features (2) and (4), we can conclude that the buyer purchase conversion rate is also an important impact factor for repeat purchase prediction. From the seller's point of view, the buyer's age in feature (7) and gender in feature (10) also show a certain impact on repeat buyer prediction.

Table 1: The AUC values of different combinations of word vector encoding length.

Word vector encoding length	Commodity	Brand	Commodity category	AUC value
1	64	32	32	0.6200
2	128	64	64	0.6316
3	150	80	80	0.6419
4	200	100	100	0.6543
5	256	128	128	0.6628

4.2.3. Improved Individual Model and Vote-Stacking Ensemble Model Test. Figure 8 demonstrates the difference in accuracy and AUC values before and after the improvement of the DeepCatboost and DABiGRU individual prediction models.

It can be observed from the experimental results shown in Figure 8 that the accuracy and AUC values of the improved DeepCatboost and DABiGRU individual models are superior to the original Catboost and LSTM models on both the training set and the test set, which indicates that the improved DeepCatboost individual model can effectively reduce the risk of overfitting and improve accuracy and robustness of predictions. The DABiGRU model outperforms the original LSTM neural network model by introducing the attention mechanism and improving the neural cell structure. This is because the added double attention mechanism can effectively mine and pay sufficient attention to the key information within and between the sequences of the historical purchase behaviour of buyers. Compared with the directional LSTM neural network model, the output state of the BiGRU neural network model is codetermined by several previous inputs and subsequential inputs, and the prediction result is more accurate. In addition, experimental results show that the accuracy and AUC values of the proposed model on the training set and the test set are not very different, and there are no overfitting or underfitting problems.

Table 3 shows the experimental results of the accuracy and AUC values of five ensemble learning prediction models. In order to evaluate the experimental results objectively and accurately, each model was executed 10 times on the same training and test sets, and the average and variance of the accuracy and AUC values were considered the final results.

It can be observed from Table 3 that the average values of the accuracy and AUC of the vote-stacking ensemble model are 91.28% and 70.50%, which are higher than those of the other four ensemble models for both the training set and the test set. This demonstrates the effectiveness of the improvement of the vote-stacking ensemble prediction model on selecting individual models and stacking fusing strategies. The main reasons are as follows: compared with the XGBoost and LightGBM ensemble learning models based on GBDT, the proposed ensemble model can not only

Table 2: The top 10 impact features of the DeepCatboost individual model.

Ranking of features	Feature detail
1	The ratio of shopping times during promotion to nonpromotion days
2	The ratio of purchasing times to browsing
3	The total historical shopping times of a buyer from some seller
4	The ratio of purchasing times to collecting
5	The time interval between the first purchase and the last purchase of a buyer from a seller
6	The interaction frequency between a buyer and a seller measured in months
7	The total number of goods purchased by different age groups of buyers from a seller
8	The total number of buyers browsing some seller
9	The total number of bands purchased by a buyer from a seller
10	The total number of goods purchased by different sexes of buyers from a seller

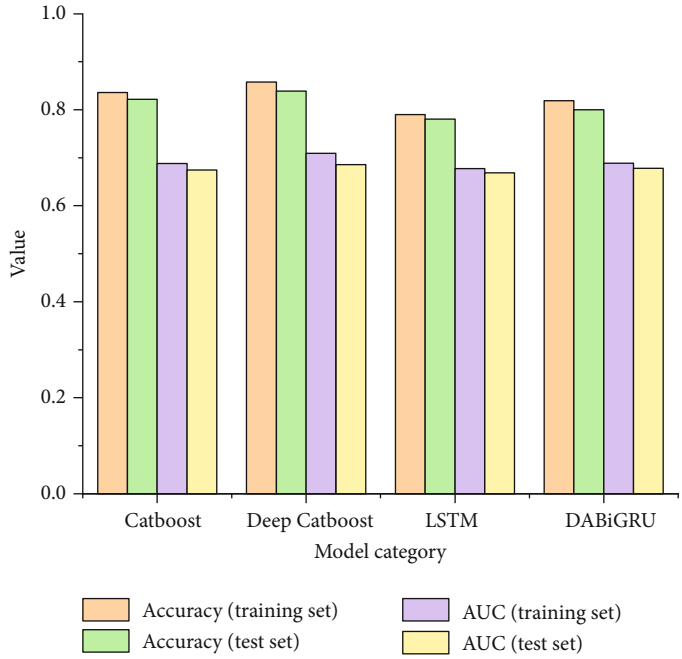

Figure 8: Comparison of the accuracy and AUC values of the individual models before and after improvement.

Table 3: The accuracy and AUC values of five types of ensemble prediction models.

Model	Training set				Test set			
	Accuracy		AUC		Accuracy		AUC	
	Mean	Variance	Mean	Variance	Mean	Variance	Mean	Variance
XGBoost	0.7762	0.0412	0.6752	0.0408	0.7751	0.0396	0.6744	0.0419
LightGBM	0.7930	0.0398	0.6878	0.0406	0.7908	0.0390	0.6875	0.0404
DeepGBM	0.8664	0.0361	0.7022	0.0356	0.8576	0.0371	0.6991	0.0366
Stacking	0.9080	0.0336	0.7027	0.0319	0.8943	0.0338	0.7023	0.0339
Vote-stacking	0.9128	0.0291	0.7053	0.0302	0.9014	0.0334	0.7050	0.0302

effectively deal with the dense numerical features in the historical behaviour data of buyers but also can process large-scale sparse classification features efficiently, which further enriches the feature types and improves the performance of the model. The nonidentical training data is employed in the vote-stacking model to increase the difference between the output values. The features of the original data and the new features generated by the base learning layer are effectively combined to enrich the feature types of the model. The final test results are determined by the voting mechanism to effectively combine the test results of the base learning layer and the meta learning layer, which reduces the error

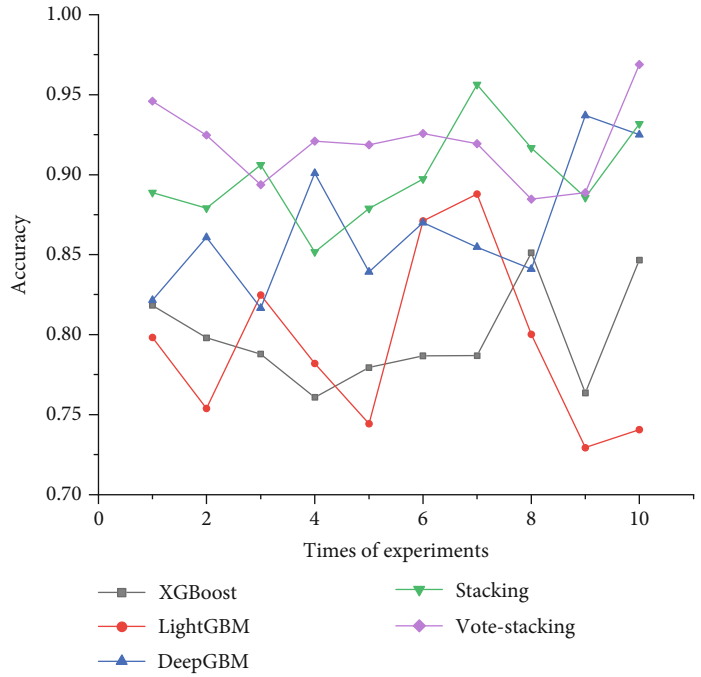

Figure 9: The accuracy curve of the five models.

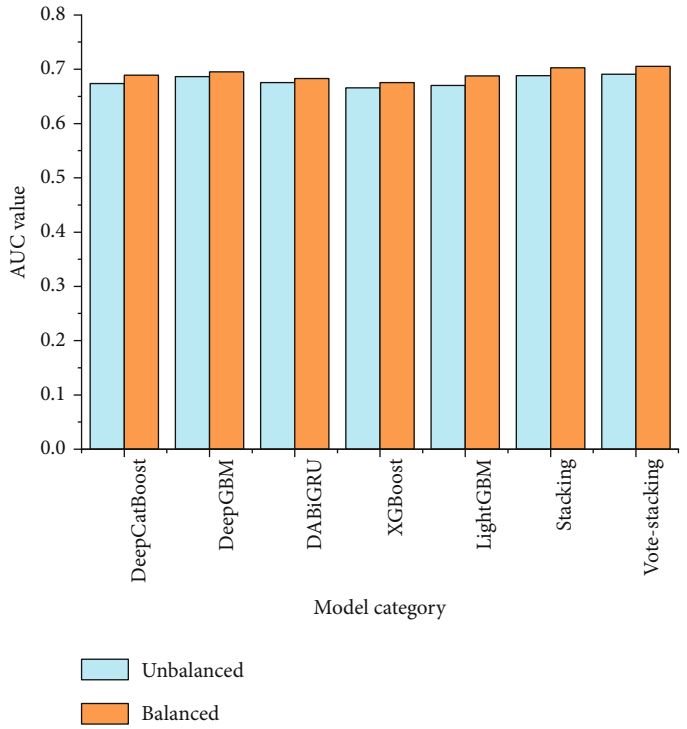

Figure 10: Comparison of the AUC values before and after sample balancing.

of the traditional stacking algorithm that relies only on the meta learning layer. In addition, the difference of accuracy and AUC values between the training set and test set is small, indicating that the model has better generalization ability.

In order to verify the stability of the vote-stacking model more intuitively, the accuracy values of the five models on 10 training sets are presented in a line graph as shown in Figure 9.

Table 4: Comparison of the accuracy and AUC values of six prediction models.

Model	Accuracy	AUC
SVM	0.6803	0.6245
RF	0.7045	0.6537
TMFBG	0.7028	0.6642
NN	0.7087	0.6951
Blending	0.8784	0.7023
Proposed model	0.9128	0.7053

It can be seen from Figure 9 that compared with the individual models, the vote-stacking and stacking models have less fluctuation in the interval with higher accuracy and their overall stability is better. Therefore, the vote-stacking fusion method is more suitable than the traditional stacking method for the repeat buyer prediction task where the dataset difference is significant. By combining the prediction results of the three individual models, the ensemble learning model can effectively avoid the selection of any individual model with a poor prediction result. By improving the performance of each individual model and collaborating between the individual models, an ensemble model can improve the overall accuracy and stability of the predictions.

It can be observed from Figure 10 that the AUC values of the seven models are improved by different extents after subtime under sampling sample balancing. Among them, the AUC values of the DeepCatboost, LightGBM, vote-stacking, and stacking models are enhanced more obviously. Experimental results show that, when the subtime under sampling sample balancing is used to process the historical behaviour data of buyers, even if the negative sample data is reduced leading to the loss of some information, the prediction accuracy of the model is improved.

In order to verify the effectiveness and functionality of the vote-stacking model, it is compared with the five other prediction models, namely, SVM [8], RF [11], TMFBG [4], neural network (NN) [10], and blending [5] with the same datasets and experimental settings. The results are shown in Table 4.

The proposed model outperforms the other five models in terms of the accuracy and AUC values. The reason is that the proposed model can effectively fuse the advantages of the DT and NN models on random and nonlinear training data and efficiently process high-dimensional nonlinear historical behaviour data of buyers. It also has better generalization ability than the reference models.

5. Conclusions

A repeat buyer prediction ensemble model based on the vote-stacking fusion method was introduced in this paper. First, the model applies the subtime under sampling sample balancing to process the unbalanced historical behaviour data of buyers. Then, the three individual models DeepCatboost, DeepGBM, and DABiGRU are constructed consecutively. Finally, the vote-stacking fusion method is used to fuse the prediction results of the three individual models and obtain the final prediction results. The effectiveness of the proposed method has been evaluated on the Tmall real dataset. The experimental results showed that the proposed model is superior to the reference models. In addition, the DeepCatboost individual model was used to analyze the important impact features related to buyers' repeat purchase behaviour and to provide data support for sellers to carry out accurate marketing and increase buyers' loyalty.

In the future, we will continue to investigate the impact factors associated with buyers' repeat purchase behaviour, construct additional fine-tuned features, and design ensemble prediction models with a higher number of individual models that are also more different. In addition, we will attempt to derive better ensemble learning fusion strategies to further improve the performance of repeat buyer prediction.

Data Availability

The data used to support the findings of this study are available from the corresponding author upon request.

Conflicts of Interest

The authors declare that there is no conflict of interest regarding the publication of this paper.

Acknowledgments

This work was supported by the National Natural Science Foundation of China (grant numbers 61662013, U171123, U1811264, and 61662015); Guangxi Innovation-Driven Development Project (Science and Technology Major Project) (grant number AA17202024); and Graduate Student Innovation Program, Guilin University of Electronic Technology (grant number 2019YCXS045). We thank LetPub (https://www.letpub.com) for its linguistic assistance during the preparation of this manuscript.

References

[1] H. Cheng, Z. Su, N. Xiong, and Y. Xiao, "Energy-efficient node scheduling algorithms for wireless sensor networks using Markov Random Field model," *Information Sciences*, vol. 329, pp. 461–477, 2016.

[2] A. H. Kazmi, G. Shroff, and P. Agarwal, "Generic Framework to Predict Repeat Behavior of Customers Using Their Transaction History," in *2016 IEEE/WIC/ACM International Conference on Web Intelligence (WI)*, pp. 449–452, Omaha, NE, USA, 2016.

[3] H. S. Song, "Comparison of Performance between MLP and RNN Model to Predict Purchase Timing for Repurchase Product," *Journal of Information Technology Applications and Management*, vol. 24, no. 1, pp. 111–128, 2017.

[4] G. Liu, T. T. Nguyen, G. Zhao et al., "Repeat Buyer Prediction for E-Commerce," in *Proceedings of the 22nd ACM SIGKDD International Conference on Knowledge Discovery and Data Mining*, pp. 155–164, San Francisco, CA, USA, 2016.

[5] D. Xu, W. Yang, and L. Ma, "Repurchase Prediction Based on Ensemble Learning," in *2018 IEEE SmartWorld, Ubiquitous Intelligence & Computing, Advanced & Trusted Computing,*

Scalable Computing & Communications, Cloud & Big Data Computing, Internet of People and Smart City Innovation (SmartWorld/SCALCOM/UIC/ATC/CBDCom/IOP/SCI), pp. 1317–1322, Guangzhou, China, 2018.

[6] L. Guo, L. Hua, R. Jia, B. Zhao, X. Wang, and B. Cui, "Buying or Browsing?: Predicting Real-time Purchasing Intent using Attention-based Deep Network with Multiple Behavior," in *Proceedings of the 25th ACM SIGKDD International Conference on Knowledge Discovery & Data Mining*, pp. 1984–1992, Anchorage, AK, USA, 2019.

[7] X. Liu and J. Li, "Using support vector machine for online purchase predication," in *2016 International Conference on Logistics, Informatics and Service Sciences (LISS)*, pp. 1–6, Sydney, NSW, Australia, 2016.

[8] L. Tang, A. Wang, Z. Xu, and J. Li, "Online-purchasing behavior forecasting with a firefly algorithm-based SVM model considering shopping cart use," *Eurasia Journal of Mathematics, Science and Technology Education*, vol. 13, no. 12, pp. 7967–7983, 2017.

[9] C. O. Sakar, S. O. Polat, M. Katircioglu, and Y. Kastro, "Real-time prediction of online shoppers' purchasing intention using multilayer perceptron and LSTM recurrent neural networks," *Neural Computing and Applications*, vol. 31, no. 10, pp. 6893–6908, 2019.

[10] C. Ling, T. Zhang, and Y. Chen, "Customer Purchase Intent Prediction Under Online Multi-Channel Promotion: A Feature-Combined Deep Learning Framework," *IEEE Access*, vol. 7, pp. 112963–112976, 2019.

[11] H. Valecha, A. Varma, I. Khare, A. Sachdeva, and M. Goyal, "Prediction of Consumer Behaviour using Random Forest Algorithm," in *2018 5th IEEE Uttar Pradesh Section International Conference on Electrical, Electronics and Computer Engineering (UPCON)*, pp. 1–6, Gorakhpur, India, 2018.

[12] R. Joshi, R. Gupte, and P. Saravanan, "A Random Forest Approach for Predicting Online Buying Behavior of Indian Customers," *Theoretical Economics Letters*, vol. 8, no. 3, pp. 448–475, 2018.

[13] X. LI and F. Shao, "Purchase Behaviour Forecasting Model Combining LSTM and Random Forest," *Journal of Qingdao University (Engineering & Technology Edition)*, vol. 32, no. 2, pp. 17–20, 2018.

[14] A. Kumar, G. Kabra, E. K. Mussada, M. K. Dash, and P. S. Rana, "Combined artificial bee colony algorithm and machine learning techniques for prediction of online consumer repurchase intention," *Neural Computing and Applications*, vol. 31, no. S2, pp. 877–890, 2019.

[15] H. Liu, Y. Xu, and C. Chen, "Improved pollution forecasting hybrid algorithms based on the ensemble method," *Applied Mathematical Modelling*, vol. 73, pp. 473–486, 2019.

[16] W. Li, P. Ding, X. Zhang et al., "Ensemble learning methodologies to improve core power distribution abnormal detectability," *Nuclear Engineering and Design*, vol. 351, pp. 160–166, 2019.

[17] Y. Wang, D. Wang, N. Geng, Y. Wang, Y. Yin, and Y. Jin, "Stacking-based ensemble learning of decision trees for interpretable prostate cancer detection," *Applied Soft Computing*, vol. 77, pp. 188–204, 2019.

[18] S. Y. Yerima and S. Sezer, "DroidFusion: A Novel Multilevel Classifier Fusion Approach for Android Malware Detection," *IEEE Transactions on Cybernetics*, vol. 49, no. 2, pp. 453–466, 2019.

[19] O. Sagi and L. Rokach, "Ensemble learning: A survey," *Wiley Interdisciplinary Reviews: Data Mining and Knowledge Discovery*, vol. 8, no. 4, article e1249, 2018.

[20] B. Yadav, P. K. Gupta, N. Patidar, and S. K. Himanshu, "Ensemble modelling framework for groundwater level prediction in urban areas of India," *Science of the Total Environment*, vol. 712, article 135539, 2020.

[21] H. Liu and C. Chen, "Prediction of outdoor PM2. 5 concentrations based on a three-stage hybrid neural network model," *Atmospheric Pollution Research*, vol. 11, no. 3, pp. 469–481, 2020.

[22] Y. Li, Z. Yang, X. Chen, H. Yuan, and W. Liu, "A stacking model using URL and HTML features for phishing webpage detection," *Future Generation Computer Systems*, vol. 94, pp. 27–39, 2019.

[23] S. Guo, H. He, and X. Huang, "A Multi-Stage Self-Adaptive Classifier Ensemble Model With Application in Credit Scoring," *IEEE Access*, vol. 7, pp. 78549–78559, 2019.

[24] H. Cheng, D. Feng, X. Shi, and C. Chen, "Data quality analysis and cleaning strategy for wireless sensor networks," *EURASIP Journal on Wireless Communications and Networking*, vol. 2018, article 61, 2018.

[25] H. Jelodar, Y. Wang, C. Yuan et al., "Latent Dirichlet allocation (LDA) and topic modeling: models, applications, a survey," *Multimedia Tools and Applications*, vol. 78, no. 11, pp. 15169–15211, 2019.

[26] Y. Aït-Sahalia and D. Xiu, "Principal Component Analysis of High-Frequency Data," *Journal of the American Statistical Association*, vol. 114, no. 525, pp. 287–303, 2019.

[27] B. Zhu, F. Ortega, J. Bobadilla, and A. Gutiérrez, "Assigning reliability values to recommendations using matrix factorization," *Journal of Computational Science*, vol. 26, pp. 165–177, 2018.

[28] L. Prokhorenkova, G. Gusev, A. Vorobev, A. V. Dorogush, and A. Gulin, "CatBoost: unbiased boosting with categorical features," in *Proceedings of the 32nd International Conference on Neural Information Processing Systems (NIPS'18)*, pp. 6638–6648, Red Hook, NY, USA, 2018.

[29] G. Ke, Z. Xu, J. Zhang, J. Bian, and T.-Y. Liu, "DeepGBM: A Deep Learning Framework Distilled by GBDT for Online Prediction Tasks," in *Proceedings of the 25th ACM SIGKDD International Conference on Knowledge Discovery & Data Mining*, pp. 384–394, New York, NY, USA, 2019.

[30] T. Shen, T. Zhou, G. Long, J. Jiang, and C. Zhang, "Bi-directional block self-attention for fast and memory-efficient sequence modeling," 2018, https://arxiv.org/abs/1804.00857.

[31] Y. Zhu, W. Zhang, Y. Chen, and H. Gao, "A novel approach to workload prediction using attention-based LSTM encoder-decoder network in cloud environment," *EURASIP Journal on Wireless Communications and Networking*, vol. 2019, article 274, 2019.

[32] C. Park, D. Kim, and H. Yu, "An encoder–decoder switch network for purchase prediction," *Knowledge-Based Systems*, vol. 185, article 104932, 2019.

[33] A. Vaswani, N. Shazeer, N. Parmar et al., "Attention is all you need," in *Advances in Neural Information Processing Systems 30: Annual Conference on Neural Information Processing Systems 2017*, pp. 5998–6008, Long Beach, CA, USA, 2017.

[34] B. Pavlyshenko, "Using Stacking Approaches for Machine Learning Models," in *2018 IEEE Second International Conference on Data Stream Mining & Processing (DSMP)*, pp. 255–258, Lviv, Ukraine, 2018.

[35] H. Liang, J. Zou, K. Zuo, and M. J. Khan, "An improved genetic algorithm optimization fuzzy controller applied to the wellhead back pressure control system," *Mechanical Systems and Signal Processing*, vol. 142, article 106708, 2020.

[36] F. Hu and G. Wu, "Distributed Error Correction of EKF Algorithm in Multi-Sensor Fusion Localization Model," *IEEE Access*, vol. 8, pp. 93211–93218, 2020.

[37] H. Cheng, N. Xiong, A. V. Vasilakos, L. Tianruo Yang, G. Chen, and X. Zhuang, "Nodes organization for channel assignment with topology preservation in multi-radio wireless mesh networks," *Ad Hoc Networks*, vol. 10, no. 5, pp. 760–773, 2012.

[38] J. Hu, Y. Sun, G. Li, G. Jiang, and B. Tao, "Probability analysis for grasp planning facing the field of medical robotics," *Measurement*, vol. 141, pp. 227–234, 2019.

[39] H. Liang, J. Zou, Z. Li, M. J. Khan, and Y. Lu, "Dynamic evaluation of drilling leakage risk based on fuzzy theory and PSO-SVR algorithm," *Future Generation Computer Systems*, vol. 95, pp. 454–466, 2019.

Hindawi
Wireless Communications and Mobile Computing
Volume 2020, Article ID 8832341, 9 pages
https://doi.org/10.1155/2020/8832341

Research Article

A Homomorphic Encryption and Privacy Protection Method Based on Blockchain and Edge Computing

Xiaoyan Yan, Qilin Wu, and Youming Sun

School of Information Engineering, ChaoHu College, Chaohu 238000, China

Correspondence should be addressed to Youming Sun; symtnt@163.com

Received 23 May 2020; Revised 13 July 2020; Accepted 25 July 2020; Published 18 August 2020

Academic Editor: Hongju Cheng

Copyright © 2020 Xiaoyan Yan et al. This is an open access article distributed under the Creative Commons Attribution License, which permits unrestricted use, distribution, and reproduction in any medium, provided the original work is properly cited.

With its decentralization, reliable database, security, and quasi anonymity, blockchain provides a new solution for data storage and sharing as well as privacy protection. This paper combines the advantages of blockchain and edge computing and constructs the key technology solutions of edge computing based on blockchain. On one hand, it achieves the security protection and integrity check of cloud data; and on the other hand, it also realizes more extensive secure multiparty computation. In order to assure the operating efficiency of blockchain and alleviate the computational burden of client, it also introduces the Paillier cryptosystem which supports additive homomorphism. The task execution side encrypts all data, while the edge node can process the ciphertext of the data received, acquire and return the ciphertext of the final result to the client. The simulation experiment proves that the proposed algorithm is effective and feasible.

1. Introduction

Network data will be encrypted before they are sent to the server, but the client will face some problems because the service provider needs to perform computation on the data to respond to the requests of the client; so the client must provide the server with the key to decrypt data before implementing necessary computation, which may affect data confidentiality in the cloud. Blockchain is a group of inalterable and well-organized blocks (data blocks), and it records the logs of all transactions. The data blocks in blockchain are saved in every node in the form of file system. Every block includes the data of several transactions, the number of which included in different blocks may vary [1, 2]. Blocks are connected with Hashed-link, and every header includes the Hash of all transactions in this block and the pre-Hash of the last header. Such a chained architecture can ensure that the data in each block are unalterable and so is the sequential relationship between blocks. This characteristic has decided that the blocks can only be added to the tail. But the rigid and single organizational form of data in blockchain has impeded blockchain's applications in relevant fields with demanding data security requirements [3]. Edge computing is now gradually being given more and more attention in academic circles, organizations for standardization, and open-source platforms, and it has been developed rapidly in many aspects. Related enterprises have initiated relevant industry organizations, industry alliances, and organizations for standardization in specific application fields, deployed edge computing, and proposed some suggestions on architecture [4]. Besides, the open-source projects related to edge computing have also developed gradually. Homomorphic encryption is a method that computes on encrypted data. It gets the same result from the computation of the original data, and it uses proxy reencryption technology to protect the selected ciphertext from being attacked. To sum up, in order to protect the security of network environment, the use of blockchain and edge computing technology can reinforce the privacy protection and provide corresponding protection to the user information, transaction activities, and information communication [5, 6].

The special contributions of this paper are as follows:

(i) This paper has analyzed and studied in blockchain and edge computing network, the data blocks, application nodes, edge computing nodes, and terminal,

and it has combined all data blocks into a blockchain, which is maintained by all edge computing nodes

(ii) It has introduced the edge computing model and designed the blockchain-based distributed privacy protection architecture. In order to guarantee the operating efficiency of blockchain and ease the computing burden of the client, it allows some edge nodes which have certain computing, storage and communications ability to write data into the chain, and maintain and update the entire blockchain

(iii) In order to solve the data security problems in escrow, it has presented a homomorphic encryption technique based on the Paillier and RSA cryptosystems, in which the execution encrypts all data received and the edge nodes operate on the ciphertext of the data received, get the ciphertext of the final result, and return it back to the client

(iv) Through the simulation experiment, it has shown the effectiveness and operating time efficiency against hostile attacks of the proposed algorithm, and it has also analyzed the impact different values of parameters play on the update of target value

The rest of this paper is organized as follows. Section 2 discusses related work, followed by the basic framework of blockchain, and its data structure is introduced in Section 3. The edge computing architecture is discussed in Section 4. Section 5 is the homomorphic encryption and privacy protection. Section 6 shows the simulation experimental results, and Section 7 concludes the paper with summary and future research directions.

2. Related Work

After integrating P2P transmission, on-chain consensus algorithm, digital signature, and encryption algorithm, blockchain in recent years has become a focal point in the research and discussion of many international organizations and national governments that have increased their input in research. As the focus of blockchain does not lie in zone boundary but the participants, blockchain is highly sensitive to malicious adversaries, so in the internet operating environment, blockchain has strong adaptability [7]. Homomorphic encryption is extensively applied to support simple aggregation, numerical computation of encrypted data, and retrieval of private information. The breakthrough in homomorphic encryption theory has led to fully homomorphic encryption, which can compute arbitrary functions of encrypted data [8]. Homomorphic encryption is generally considered as a key approach to solve database query problems on the basis of encrypted data. The requirements of privacy for the digital data and algorithms used to process more complex structures have increased exponentially, which just parallels to the growth of communications network and equipment and their capacities [9]. Whether the decentralized network architecture or the constructed distributed architecture, they can directly establish a trust relationship between system architecture and nodes through mathematical methods, without operating the third-party trust platform. The applications of mathematical algorithms in building security mechanism can improve the transparency of information; so they will not suffer from the influence of any factors. Blockchain is not strongly dependent on cipher; as a matter of fact, it can operate safely without cipher, and it does not need the trust mechanism. With no cipher, blockchain without any doubt does not need encryption key. The protection for blockchain can be ensured through mathematical algorithms, and the security function obtained is permanent and all information in the block can be safeguarded permanently. The chain-block structure in blockchain has provided trusted timestamp in information storage, enabling the data information recorded to have a time dimension, and the data to be traceable and validated and making it very difficult to tamper all information in the blocks [10, 11].

Wang and others have created effective storage engine, ForkBase, for blockchain and fork applications, while Xu and others have studied verifiable query processing of blockchain database and presented the verification system Vchain that supports blockchain data inquiring the scope of Boolean. Helmer and others have developed a system, EthernityDB, which can integrate the function of a database into the Ethereum blockchain [12]. It has kept all data in the chain and guaranteed the consistency, invariability, and security of data. In 2015, some supports for edge computing have established the OpenFog Consortium (OGC) and released the Edge Computing Reference Architecture 2.0 in 2017. In 2016, some firms have set up the Edge Computing Consortium (ECC) and published many versions of edge computing reference architecture, in order to promote the digital innovation and applications of edge computing [13]. In 2014, the European Telecommunications Standards Institute (ETSI) has proposed Mobile Edge Computing (MEC) as an important part of 5G. In 2018, the Industrial Internet Consortium (IIC) has also issued the Edge Computing Architecture used in Industrial Internet of Things. The Open Source Project–EdgeX has constructed an open-source edge computing architecture and described the criteria to use this architecture in its open-source page. Yao has come up with the first secure two-party computing problem in as early as 1982, i.e., the Millionaire Problem [14]. Afterwards, the secure multiparty computation (SMC) emerged. The Paillier system is a semantically secure homomorphic public key cryptosystem; so it is generally used to construct fundamental protocols for secure multiparty computation, including Millionaire Protocol, scalar product protocol, and OT protocol. Sander and Tschudin have defined the additive and multiplicative homomorphic encryption scheme in the ring of integers. The additive and multiplicative homomorphism has made sure that the computation result of two encrypted variables is the same as that of the original variables. Currently, the management of blockchain data has come across the following difficulties. The organization form of the current blockchain data is coarse-grained so it supports a single way of query, and it cannot meet the requirements of the current data analysis and information digging. The present

data privacy protection scheme in blockchain technology cannot satisfy the needs of secure storage and retrieval of sensitive data. This paper has mainly studied the security of the application of blockchain-based homomorphic encryption to edge computing, including the probability to implement encrypted data computation under various malicious attacks.

3. Basic Framework of Blockchain and Its Data Structure

Blockchain is mainly composed of data layer, network layer, consensus layer, and application layer. Among them, data layer includes the underlying data block and its chain structure, and as it is supported by the relevant techniques such as the Hash algorithm, timestamp, Merkle tree, and asymmetric encryption, it protects the integrity and traceability of bock data. Network layer consists of data transmission mechanism and transaction verification mechanism and supported by P2P network technology; it accomplishes the data transmission and verification between distributed nodes. Consensus layer is mainly the consensus mechanism, and it realizes the consistency between distributed nodes and the authenticity of data through various consensus algorithms. Some blockchain systems, e.g., the consensus layer of Bitcoin, also contain issuing mechanism and incentive mechanism which integrates economic factors. It enters blockchain technology to achieve the stable consensus between nodes. Application layer can realize various top-level application scenarios, relevant systems, and smart contracts supported by a wide range of on-chain script algorithms and blockchains, laying a foundation for the programmable functions of blockchain. In this framework, blockchain incorporates the timestamp-based chain structure, the data transmission mechanism based on P2P network, the consensus mechanism of distributed nodes, and the flexible programmable on-chain script, and blockchain is also the most representative technical innovation [15, 16]. The basic architecture of blockchain is shown as Figure 1.

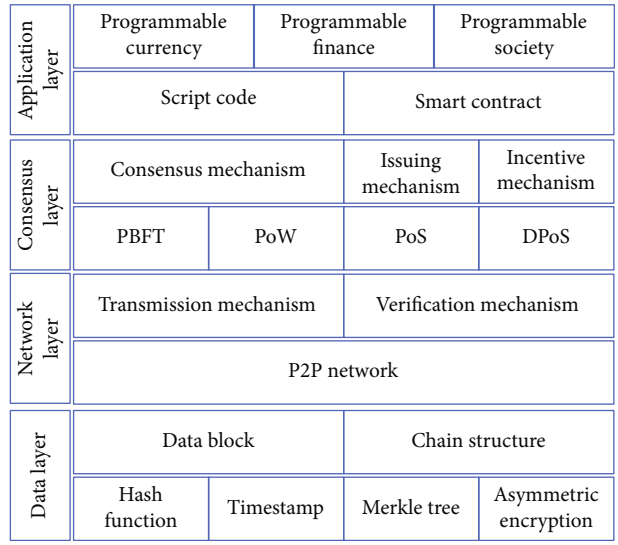

Figure 1: Basic framework of blockchain.

The core structure of the data information management system based on blockchain technology is decentralization, which has effectively changed the data risk brought by conventional central authority. Thanks to its nontemperability and traceability, blockchain technology can be widely applied in information data management and meanwhile ensures the accuracy and authenticity of data information. Generally speaking, it is necessary to integrate blockchain technology with external database and separate the data from the corresponding authority, in order to assure the normal use in the decentralized system. When the relative programs need an access to the data information of users, user consent must be obtained. Understandably, when an application program needs an access to the information, blockchain will receive its request. To confirm whether the program can access the information, the record in the blockchain needs to be checked. If the system check is undergone, blockchain will record the implemented operation and feed-back to the application. It is because blockchain has certain recording function that the operations in the entire process are transparent, which is good for the traceability of the follow-up data and makes sure the security of network information. Besides, attention must be paid to the integrity of network information data [17].

Blockchain stores data through data blocks and chain structure. Every data block includes two parts: header and body, and each block has the only Hash value corresponding to the block address. The current block is connected to the previous one by saving the Hash value of the previous block and forming a chain structure, as shown in Figure 2. The header encapsulates the Hash value of the previous block as well as timestamp, Merkle tree root value, and other information. The body stores information, i.e., the data information recorded by the blockchain. All data are generated based upon the Hash processing of Merkle tree so as to generate the only Merkle tree root value and save it in the header. Such a storage structure of Merkle tree has greatly improved the efficiency of inquiring and verifying information as well as the scalability. Meanwhile, when a block is generated, there will be a timestamp to mark and indicate the time of generating a block [18]. As the enhancement of timestamp, this block is continuously extended to form a chain with a time dimension so that the data are traceable and the data traceability is guaranteed.

The secure Hash algorithm refers to the technology to develop information encryption and others. When computing the relevant data, the difficulty of the entire computation is generally determined by the plus-minus of the Hash value computed. If the Hash value is positive, it indicates that the entire computation process is easy to operate; otherwise, the computation is relatively difficult. Blockchain network mainly constructs tree structure of data information by using the Hash tree computing method. In this structure, the node is the abovementioned Hash values in order to check abundant information data to ensure its authenticity and integrity [19]. The data model of the internal structure of blockchain is shown in Figure 3.

As shown in this blockchain architecture, it is clear that when there is a change in the information of a certain block,

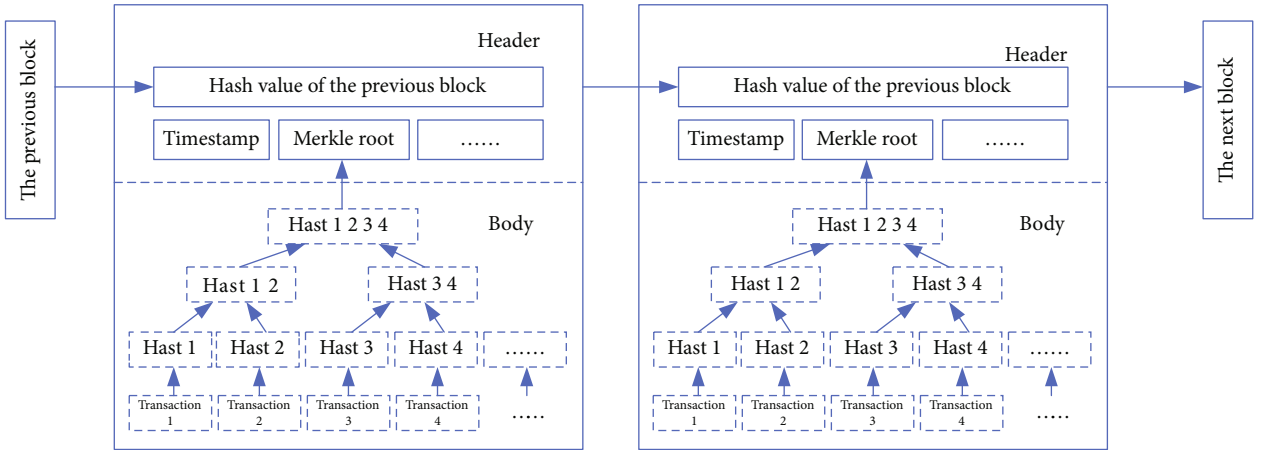

Figure 2: Data structure of blockchain.

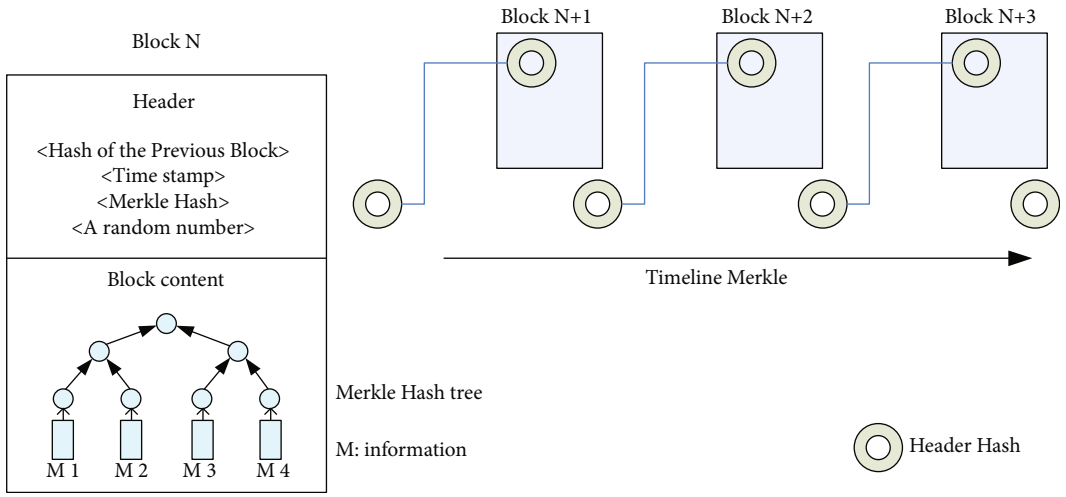

Figure 3: Data model of internal structure of blockchain.

the Hash value of the corresponding Merkle changes correspondingly, followed by a change in the information contained in the block. If a bad intruder tampers the information, the computing power will not generate support for fake data block. If the speed of fake block exceeds the growth rate of blockchain, it will be abandoned. In every block, the information is data information, and the content it covers not just includes text information, but also nonlinear information, e.g., video information, image information, and various structured information. It can permanently protect the information stored in all blocks to prevent malicious alteration. Therefore, the information in blockchain is secure [9].

4. Edge Computing Architecture

Edge computing refers to the new-type computation model which implements computation in the network edge, which includes any computation and network resources along the path from the data source to cloud computing center. Edge computing model is to transfer part or all of computational tasks of the original cloud computing center to near the data source for implementation. Edge computing model and cloud computing model complement with each other. In the environment of Internet of everything, computing efficiency cannot meet real-time requirements due to the increase of data amount and the mass data generated by users. The conventional cloud computing model can no longer effectively satisfy the needs of the current application program; instead, it needs to transfer the computing tasks of the original cloud center to the network edge device, improve data transmission performance by using the computing ability of edge device, assure real-time processing, and reduce computing load and energy consumption [20].

In edge computing, the downstream data of the edge represents cloud service and the upstream data the service of Internet of everything, while the edge in edge computing refers to any computation and network resources along the path from the data source to the cloud computing center. Cloud computing center collects data not only from database but also from such edge devices as sensors and smartphones. These devices have taken into consideration both data

generator and consumer. Therefore, the request transmission from terminal device to cloud center is two-way. Network edge devices not only ask for content and services from the cloud center but also implement some computing tasks, including data storage, processing, caching, device management, and privacy protection. Therefore, it is necessary to better design the hardware platform for edge devices as well as the key software technology so as to meet the demands of reliability and data security of edge computing model [21, 22]. In Figure 4, data generator sends the source data to the cloud center, and the final user sends the use request to the cloud center, which feedbacks the usage result to the final user.

5. Homomorphic Encryption and Privacy Protection

Each blockchain node in the blockchain network stores the same blockchain [23, 24]. The blockchain is composed of multiple blocks [25, 26]. The origination block includes the block head and the block body [27, 28]. The block head stores the input information characteristic value, version number, timestamp, and difficulty value, and the block body stores the input information. The next block of the origination block is the parent block, and the next block also includes the block head and the block body, so that each block is in the blockchain. The block data stored in the block is associated with the block data stored in the parent block, which ensures the security of the input information in the block. The steps of this algorithm are as follows.

Step 1 (generate the key). Initialize random primes p and q and meet the condition of

$$\gcd(pq, (p-1)(q-1)) = 1. \tag{1}$$

Calculate modulus

$$n = pq. \quad \lambda = 1\mathrm{cm}(p-1, q-1), \tag{2}$$

where lcm is to seek the least common multiple of $p-1$ and $q-1$.

Select the random number $g(g \in Z^*_{n2})$ and meet

$$\mu = \left(L\left(g^{\lambda} \bmod n^2\right)\right)^{-1} \bmod n. \tag{3}$$

Seek the greatest common divisor of $L(g^{\lambda} \bmod n^2)$ and n. Z^*_{n2} represents the set of integers coprime to n^2 in Z_{n2}. The encrypted public key of function $L(x) = x - 1/n$ is (n, g), and the private key is (λ, ω).

In the encryption and decryption process, select the integer $r(r \in Z^*{}_{n2})$, and the plaintext is $m(m \in Z_n)$ and $m < n$.

Step 2 (encryption⟶Enc (m, pk)). Let m be the information to be encrypted and $m \in Z_n$.

Compute the ciphertext: $c = m \bmod n$. The encryption process is

$$c = E(m) = g^m \cdot r^n \bmod n^2, \tag{4}$$

where c is the ciphertext data corresponding to the plaintext m and $c \in Z^*{}_{n2}$.

Mark the encryption algorithm as $c = E(m, r)$. It can be known that for the same ciphertext m, the value of r, which is randomly selected in the encryption process may be different and so is the corresponding ciphertext data after being encrypted so as to ensure the semantic security of ciphertext data.

Step 3 (proxy reencryption). Compute the public key and private key (R_{sk}, R_{pk}).

The reencryption ciphertext is generated by the RSA algorithm, and the public key (R_{pk}) is sent to the server.

Step 4 (decryption⟶Dec (c, sk)). Ciphertext $c \in Z_n$

$$m = D(c) = L\left(c^{\lambda} \bmod n^2\right) * (\omega \bmod n). \tag{5}$$

After receiving $E(d_i)(i \in p_\tau)$, decrypt it to $\mathrm{get}(d_i)(i \in p_\tau)$, sign it, get and send $Sign_q(d_i)(i \in p_\tau)$ to EN_q.

Step 5 (after EN_q receives $(d_i)(i \in p_\tau)$, divide the degree of dispersion into two kinds). Make the set of users corresponding to the kind with more elements as Q and the set of users corresponding to the degree of dispersion as G. As malicious users take up a small proportion, Q mainly includes normal users with the target value increases after the completion of tasks, while that of G decreases after tasks end. Therefore, it has introduced two parameters μ and ν to control the increase and decrease after the target value is updated, and the target value changes according to the following equation:

$$r_i^{new} = \begin{cases} r_i + (1 - r_i) \cdot \mu & \text{if} \in Q \\ r_i \cdot (1 - \nu) & \text{if} i \in G \end{cases}, \tag{6}$$

where μ and ν are both positive and $\nu < 1$.

When the execution side is transmitting the storage address and key of data file, the asymmetric encryption algorithm RSA is adopted. The data encrypted by RSA public key can only be decrypted by the party which holds the corresponding RSA private key. Therefore, this scheme has ensured the secure transmission of data storage address and decryption key. When acquiring data, it only needs to collect from distributed file system according to the address here data files are saved. Both parties do not make contacts directly, which conceals the identities of both parties and protects their privacy. In the data hand-over process of normal transactions, other people except both parties have no knowledge of the storage address of the data file, and even they can the address through certain means, what they get

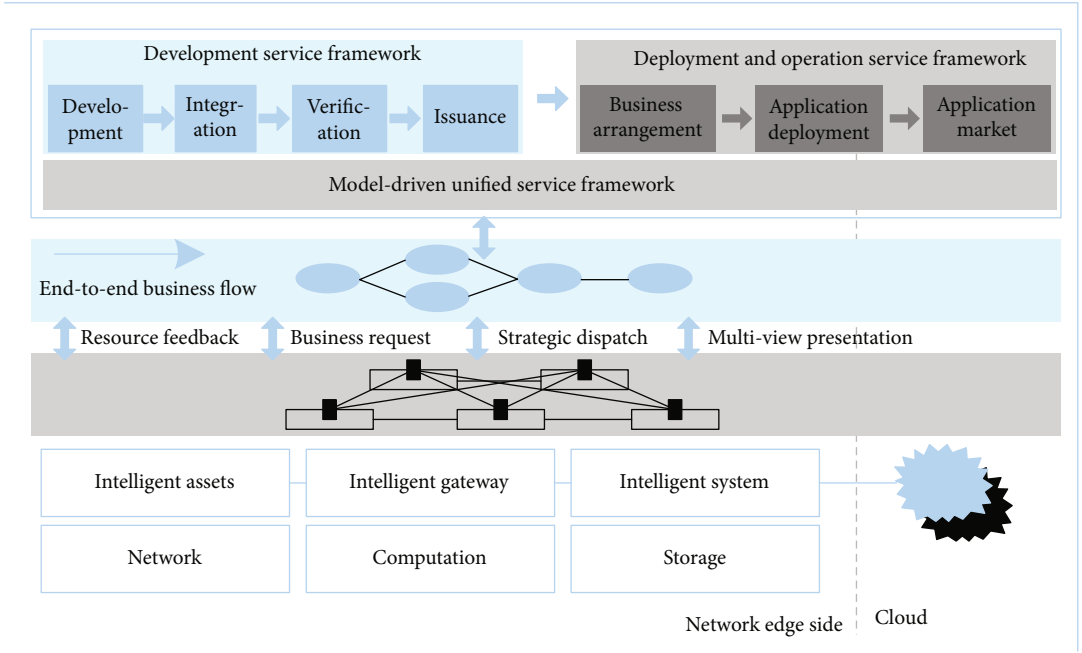

Figure 4: Edge Computing Reference Architecture.

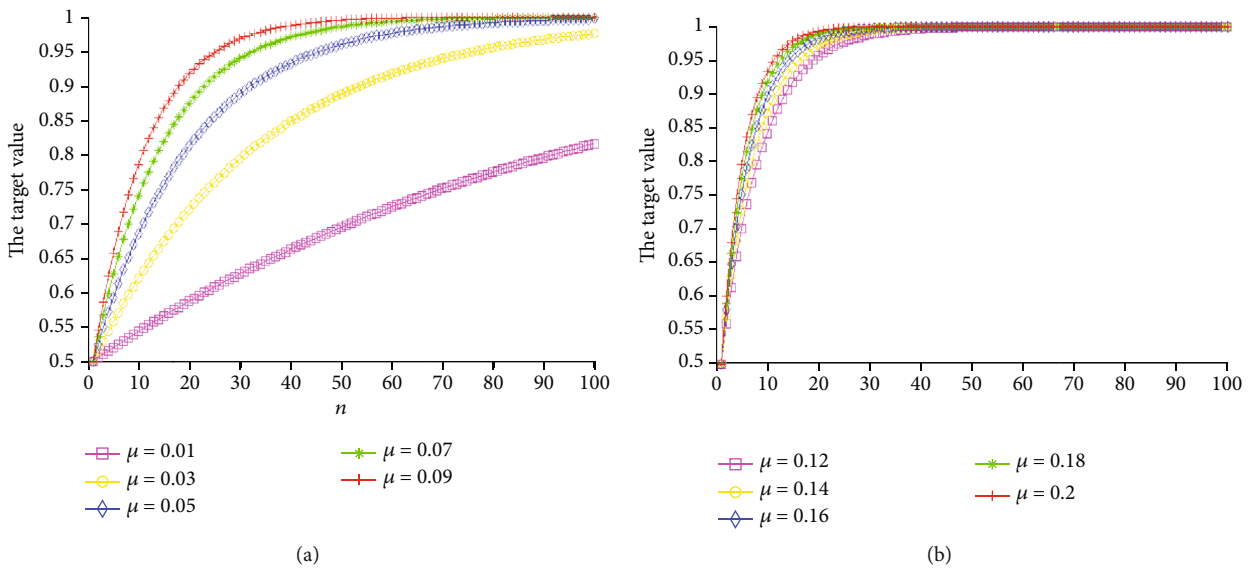

Figure 5: Impact of different μ on target value.

is the ciphertext. So, during the data handover, the security of the data is guaranteed, and the privacy of both parties of the data is protected.

6. Test Experiment and Analysis

The blockchain technology of the algorithm in this paper is implemented based upon Hyperledger Fabric, and probably 120 blocks can be generated every minute. As for the realization of the Paillier cryptosystem, we have used open-source Paillier Library and operated in the virtual machine of Ubuntu 64-bit operating system.

The data in this paper is a 10-dimensional vector. The task executor first gets a 10-dimensional data vector. Then, it encrypts every element in the vector and sends the encrypted result to the edge node of the zone where it is located. According to equation (6), parameter μ determines the growth rate of target value when the task executor provides accurate data, while parameter ν decides the decrease rate of target value when wrong data received is provided. Figure 5 shows the change of target value over the increase of tasks n when the execution side always provides the accurate data received, and the values of μ are 0.01, 0.03, 0.05, 0.07, 0.09, 0.12, 0.14, 0.16, 0.18, and 0.2. μ determines the

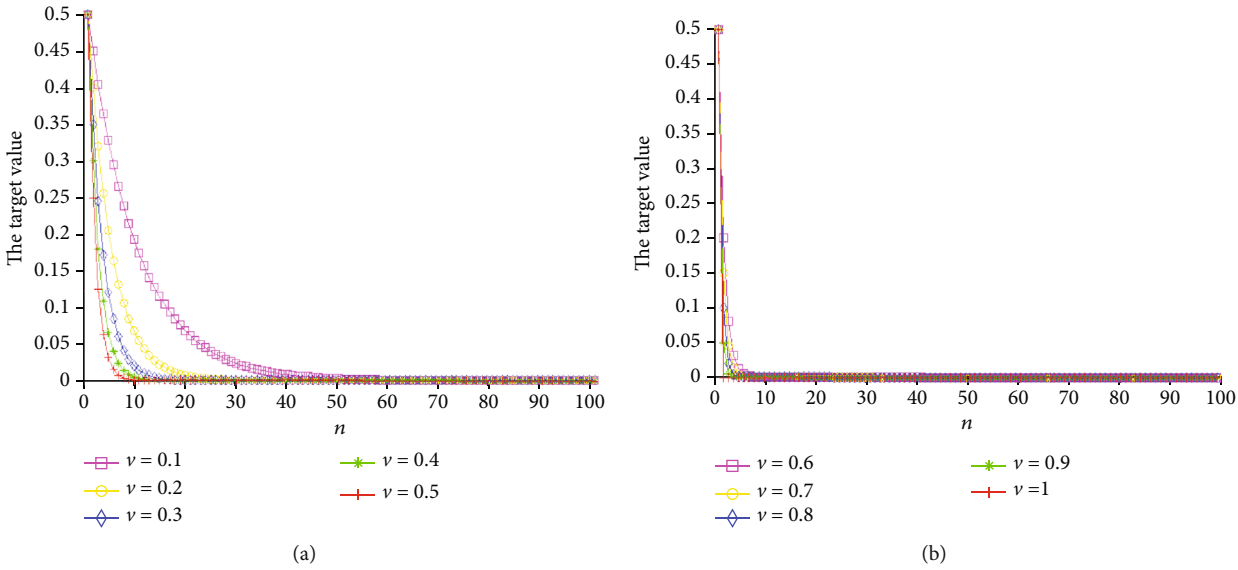

Figure 6: Impact of different ν on target value.

speed at which the target value of users that provide accurate data received is converged to 1. Besides, the bigger the value of μ, the faster its target value is converged to 1. However, when μ is too big, the user only needs to provide very few accurate data received to get a higher target value. In practical applications, μ is usually 0.1~0.2.

Next, analyze the impact of ν on the target value. Figure 6 has shown the change of the target value of users that provide wrong data received over the increase of tasks n. Here, the value of ν is 0.1, 0.2, 0.3, 0.4, 0.5, 0.6, 0.7, 0.8, 0.9, and 1. When the user continuously provides wrong data received, the parameter ν determines the rate of the target value converged to 0. Moreover, the bigger the value of ν, the faster the target value is converged to 0. However, the value of ν cannot be too big. To resist malicious attacks, the value of ν cannot be too small. Practically speaking, the value of ν is generally 0.2~0.5.

In the encryption process, the time consumed is the computation between the fusion of encrypted data and the degree of dispersion of data. So, let t_{ed} and t_{dd} represent the time to encrypt data and the time to calculate the encrypted degree of dispersion, respectively, and n represents the number of tasks to be executed. Figure 7 is the change of t_{ed} over n, and Figure 8 shows the change of t_{dd} over n.

As shown in Figure 7, t_{ed} grows linearly over the increase of n. Obviously, the bigger n, the more data ciphertext to be processed and the bigger t_{ed}. The reason is that when encrypted data, the necessary ciphertext operation is linearly correlated to the number of task executors n. When $n = 5$, the average time needed for the processing result is 2.82 s, and when n is 120, the time becomes 38.26 s. In Figure 8, when n also changes from 5 to 120 at the same step-length, t_{dd} basically remains the same over the increase of n.

This algorithm combines the characteristics of blockchain and edge computing network, and a large number of legitimate edge computing nodes ensure the security of data. On the premise of making full use of edge computing resources, it can achieve a wide range of data collection and

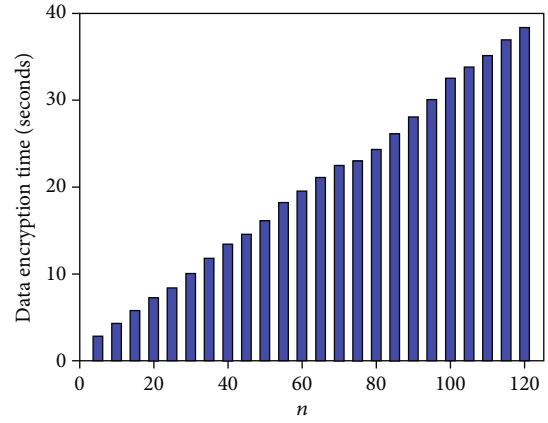

Figure 7: Change of data cipertext processing time t_{ed} over the number of tasks n.

analysis, storing fully and publicly output data resources for any organization, enterprise, and individual to query, and reuse without worrying about data tampering or deletion; and finally, realizing data security, data openness, and data in the process of data resource management source traceability and nontemperability, data utilization has been improved.

7. Conclusion

As an Internet-based new-type computing paradigm, edge computing has always been a hot field which attracts consistent attention from the academia and industry. Blockchain is a decentralized brand-new distributed computing paradigm. It is a promising research topic to apply blockchain technology in edge computing and use the security mechanism of the former to improve the performance of secure storage and computation of the latter. In order to meet the noncorrelation, anonymity, and supervision of identity privacy in blockchain system, this paper has introduced edge computing and

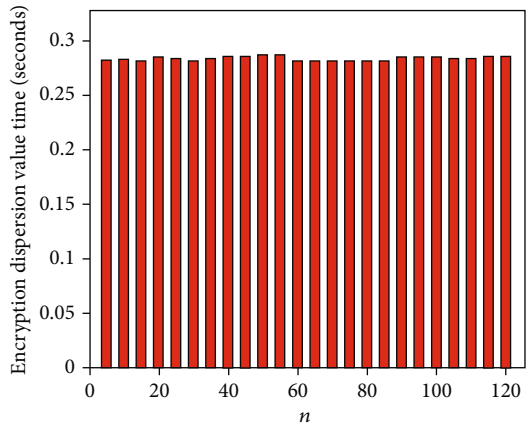

Figure 8: Change of time calculating the degree of dispersion t_{dd} over the number of tasks n.

fully-homomorphic Paillier cryptosystem, designed the blockchain-based distributed privacy protection architecture, and analyzed and verified that the algorithm in this paper can better achieve the goals of encryption and privacy protection through theoretical research and experiment result, laying a foundation for the subsequent research work.

Data Availability

The data used to support the findings of this study are available from the corresponding author upon request.

Conflicts of Interest

The authors declare that there are no conflicts of interest regarding the publication of this study.

Acknowledgments

The finding is sponsored by the Scientific Research Project of Chaohu College (Grant No. XLZ-201807) and Anhui Key Research and Development Plan (Grant No. 201904a05020091).

References

[1] C. Ye, D. Xu, and X. Liang, "Overview of network security technology based on blockchain," *Telecommunication Science*, vol. 34, no. 3, pp. 10–16, 2018.

[2] S. Moin, A. Karim, Z. Safdar, K. Safdar, and M. Imran, "Securing Iots in distributed blockchain: analysis, requirements and open issues," *Future Generation Computer Systems*, vol. 100, no. 11, pp. 325–343, 2019.

[3] A. Dorri, S. S. Kanhere, R. Jurdak, and P. Gauravaram, "LSB: a lightweight scalable blockchain for IoT security and anonymity," *Journal of Parallel and Distributed Computing*, vol. 134, no. 12, pp. 180–197, 2019.

[4] S. Weisong, Z. Xingzhou, W. Yifan, and Z. Qingyang, "Edge-computing: the most advanced and future direction of the country," *Journal of Computer Research and Development*, vol. 56, no. 1, pp. 69–89, 2019.

[5] P. P. Ray, D. Dash, and D. De, "Edge computing for internet of things: a survey, E-healthcare case study and future direction," *Journal of Network and Computer Applications*, vol. 14015, no. 8, pp. 1–22, 2019.

[6] C. Li, Y. P. Wang, H. Tang, Y. Zhang, and Y. Luo, "Flexible replica placement for enhancing the availability in edge computing environment," *Computer Communications*, vol. 14615, no. 10, pp. 1–14, 2019.

[7] B. K. Mohanta, D. Jena, S. S. Panda, and S. Sobhanayak, "Blockchain technology: a survey on applications and security privacy challenges," *Internet of Things*, vol. 8, no. 12, pp. 100–107, 2019.

[8] M. U. Hassan, M. H. Rehmani, and J. Chen, "Privacy preservation in blockchain based Iot systems: integration issues, prospects, challenges, and future research directions," *Future Generation Computer Systems*, vol. 97, no. 8, pp. 512–529, 2019.

[9] N. Kshetri, "Blockchain's roles in strengthening cybersecurity and protecting privacy," *Telecommunications Policy*, vol. 41, no. 10, pp. 1027–1038, 2017.

[10] Q. Feng, D. He, S. Zeadally, M. K. Khan, and N. Kumar, "A Survey on Privacy Protection in Blockchain System," *Journal of Network and Computer Applications*, vol. 12615, no. 1, pp. 45–58, 2019.

[11] Y. Chen, H. Xie, K. Lv, S. Wei, and H. Changzhen, "DEPLEST: a blockchain-based privacy-preserving distributed database toward user behaviors in social networks," *Information Sciences*, vol. 501, no. 10, pp. 100–117, 2019.

[12] R. Thakore, R. Vaghashiya, C. Patel, and N. Doshi, "Blockchain - based IoT: a survey," *Procedia Computer Science*, vol. 155, no. 1, pp. 704–709, 2019.

[13] A. Yousefpour, C. Fung, T. Nguyen, K. Kadiyala, and J. P. Jue, "All one needs to know about fog computing and related edge computing paradigms: a complete survey," *Journal of Systems Architecture*, vol. 98, no. 9, pp. 289–330, 2019.

[14] S. Vimal, M. Khari, N. Dey, R. G. Crespo, and Y. Harold Robinson, "Enhanced resource allocation in mobile edge computing using reinforcement learning based MOACO algorithm for IIOT," *Computer Communications*, vol. 1511, no. 2, pp. 355–364, 2020.

[15] S. Tuli, R. Mahmud, S. Tuli, and R. Buyya, "FogBus: a blockchain-based lightweight framework for edge and fog computing," *Journal of Systems and Software*, vol. 154, no. 8, pp. 22–36, 2019.

[16] E. Wang, D. Li, B. Dong, H. Zhou, and M. Zhu, "Flat and hierarchical system deployment for edge computing systems," *Future Generation Computer Systems*, vol. 105, no. 4, pp. 308–317, 2020.

[17] J. Yang, Z. Lu, and W. Jie, "Smart-toy-edge-computing-oriented data exchange based on blockchain," *Journal of Systems Architecture*, vol. 87, no. 6, pp. 36–48, 2018.

[18] Y. Qian, Y. Jiang, J. Chen, Z. Yu, and M. Pustišek, "Towards decentralized IoT security enhancement: a blockchain approach," *Computers & Electrical Engineering*, vol. 72, no. 11, pp. 266–273, 2018.

[19] S. Li, W. Chen, Y. Chen, C. Chen, and Z. Zheng, "Makespan-minimized computation offloading for smart toys in edge-cloud computing," *Electronic Commerce Research and Applications*, vol. 37, no. 9, p. 100884, 2019.

[20] S. Sahmim, H. Gharsellaoui, and S. Bouamama, "Edge computing: smart identity wallet based architecture and user

centric," *Procedia Computer Science*, vol. 159, no. 1, pp. 1246–1257, 2019.

[21] M. Qiu, S.-Y. Kung, and K. Gai, "Intelligent security and optimization in edge/fog computing," *Future Generation Computer Systems*, vol. 107, no. 6, pp. 1140–1142, 2020.

[22] H. Liang, Z. Jialing, Z. Kai, and K. M. Junaid, "An improved genetic algorithm optimization fuzzy controller applied to the wellhead back pressure control system," *Mechanical Systems and Signal Processing*, vol. 142, no. 1, article 106708, 2020.

[23] X. Chonghuan, "A novel recommendation method based on social network using matrix factorization technique," *Information Processing & Management*, vol. 54, no. 3, pp. 463–474, 2018.

[24] F. Hu and W. Gang, "Distributed error correction of EKF algorithm in multi-sensor fusion localization model," *IEEE Access*, vol. 8, no. 1, pp. 93211–93218, 2020.

[25] W. Wei, H. Song, W. Li, P. Shen, and A. Vasilakos, "Gradient-driven parking navigation using a continuous information potential field based on wireless sensor network," *Information Sciences*, vol. 408, no. 2, pp. 100–114, 2017.

[26] D. Jiang, G. Li, Y. Sun, J. Kong, and B. Tao, "Gesture recognition based on skeletonization algorithm and CNN with ASL database," *Multimedia Tools and Applications*, vol. 78, no. 21, pp. 29953–29970, 2019.

[27] L. Dong, Q. Guo, and W. Wu, "Speech corpora subset selection based on time-continuous utterances features," *Journal of Combinatorial Optimization*, vol. 37, no. 4, pp. 1237–1248, 2019.

[28] H. Liang, Z. Dialing, L. Zhiling, K. M. Junaid, and Y. Lu, "Dynamic evaluation of drilling leakage risk based on fuzzy theory and PSO-SVR algorithm," *Future Generation Computer Systems*, vol. 95, pp. 454–466, 2019.

Hindawi
Wireless Communications and Mobile Computing
Volume 2023, Article ID 9785610, 1 page
https://doi.org/10.1155/2023/9785610

Retraction

Retracted: Physarum-Inspired Autonomous Optimized Routing Protocol for Coal Mine MANET

Wireless Communications and Mobile Computing

Received 8 August 2023; Accepted 8 August 2023; Published 9 August 2023

Copyright © 2023 Wireless Communications and Mobile Computing. This is an open access article distributed under the Creative Commons Attribution License, which permits unrestricted use, distribution, and reproduction in any medium, provided the original work is properly cited.

This article has been retracted by Hindawi following an investigation undertaken by the publisher [1]. This investigation has uncovered evidence of one or more of the following indicators of systematic manipulation of the publication process:

(1) Discrepancies in scope
(2) Discrepancies in the description of the research reported
(3) Discrepancies between the availability of data and the research described
(4) Inappropriate citations
(5) Incoherent, meaningless and/or irrelevant content included in the article
(6) Peer-review manipulation

The presence of these indicators undermines our confidence in the integrity of the article's content and we cannot, therefore, vouch for its reliability. Please note that this notice is intended solely to alert readers that the content of this article is unreliable. We have not investigated whether authors were aware of or involved in the systematic manipulation of the publication process.

Wiley and Hindawi regrets that the usual quality checks did not identify these issues before publication and have since put additional measures in place to safeguard research integrity.

We wish to credit our own Research Integrity and Research Publishing teams and anonymous and named external researchers and research integrity experts for contributing to this investigation.

The corresponding author, as the representative of all authors, has been given the opportunity to register their agreement or disagreement to this retraction. We have kept a record of any response received.

References

[1] H. Jiang, X. Liu, S. Xiao, C. Tang, and W. Chen, "Physarum-Inspired Autonomous Optimized Routing Protocol for Coal Mine MANET," *Wireless Communications and Mobile Computing*, vol. 2020, Article ID 8816718, 14 pages, 2020.

Hindawi
Wireless Communications and Mobile Computing
Volume 2020, Article ID 8816718, 14 pages
https://doi.org/10.1155/2020/8816718

WILEY | Hindawi

Research Article

Physarum-Inspired Autonomous Optimized Routing Protocol for Coal Mine MANET

Haifeng Jiang, Xiaoxiao Liu, Shuo Xiao, Chaogang Tang, and Wei Chen

Mine Digitization Engineering Research Center of Ministry of Education, School of Computer Science and Technology, China University of Mining and Technology, Xuzhou, China

Correspondence should be addressed to Wei Chen; chenwdavior@163.com

Received 8 May 2020; Revised 25 June 2020; Accepted 13 July 2020; Published 1 August 2020

Academic Editor: Hongju Cheng

Copyright © 2020 Haifeng Jiang et al. This is an open access article distributed under the Creative Commons Attribution License, which permits unrestricted use, distribution, and reproduction in any medium, provided the original work is properly cited.

Mobile Ad Hoc Network (MANET) is suitable for complex environment communication in coal mine. The processes of nutrient flux transfer and path choice in Physarum networks are similar to data transmission and routing decision in MANET. In this paper, we use a Physarum optimization model to design Physarum-inspired autonomous optimized routing (PIAOR) protocol to adapt to the dynamic network topology in underground mine. PIAOR introduces the status of MANET into the Poisson equation in the Physarum model, selects reasonable parameters to represent the transmission performance of the network, and uses the differential evolution equation of the Physarum model to evolve the parameters. PIAOR has achieved the distributed routing decision by automatically reconstructing the optimal routing path, which has reduced the algorithm complexity. Based on NS2, simulation experiments are performed to evaluate the performance of PIAOR, and the results are compared with GPSR, PIMAR, and P-IRP routing algorithms. The experimental results show that the routing path selected by PIAOR is better than that selected by the other three protocols in the performance of average end-to-end delay, delivery ratio, and throughput. The balance of energy consumption and network load is reached, and the network lifetime is effectively prolonged when using the PIAOR protocol.

RETRACTED

1. Introduction

Most of the coal mines consist of narrow and long tunnels, and the environment is harsh. The operation and production in coal mines are complicated. There are a lot of infrastructures in traditional networks, which make the deployment and management of equipment troublesome and not suitable for harsh environments and mobile operation scenarios. With the continuous coal mining and working-face driving, wireless base stations or access points may have not been deployed in some coal mining areas. At the same time, affected by the complex communication environment in the underground mine, the coverage of the base station is limited, which makes it easier for blind monitoring areas to form and makes it impossible to upload the collected monitoring information. In order to ensure the safety of coal mines, it is necessary to upload the collected data in real time to prevent disasters such as gas leakage. Therefore, it is necessary to propose new wireless communication methods to satisfy the requirements of coal mine safety monitoring in special areas and to improve the adaptability of the communication networks in highly complex environments. Mobile ad hoc network (MANET) is different from traditional wireless networks. It does not rely on any infrastructure and has no central nodes, and each node is mobile. It can dynamically self-organize into a network, which can meet the deployment requirements of wireless networks in special areas in underground mines [1].

MANET [2] are collections of wireless mobile nodes, constructed dynamically without the use of any existing network infrastructure or centralized administration. Each node in a MANET can act as a router or a forwarding node. Nodes can leave and join the network at any time without disrupting the communication of other nodes. MANET's self-organization and self-adaptation allow nodes to fail, which will improve the network stability and facilitate efficient network deployment. Most of the network topologies in coal mines are long-chain structure, which significantly

increases the communication hops and exacerbates the instability of multihop communications. Therefore, it poses new challenges to the routing protocols of MANET in the underground mine. In addition, since the intelligent terminal nodes in the coal mine are mostly powered by batteries, their energy is limited. Their locations are changing constantly with the movement of miners and working-face driving. As the result, the topology and performance of MANET in the mine are changing dynamically. Routing decisions need to adapt to changes in network status timely, considering the influence of factors such as energy consumption, buffer occupation of nodes, and link state, to maintain stable and efficient data transmission.

Physarum is a kind of protoplast slime fungus, which is characterized by no single cells and gathering towards food sources. Physarum can extend to scatter food sources, cover food sources to the greatest extent, and form a network of tubes among food sources to transmit nutrients and chemical signals. With the change of nutrients in the food source, it is able to disassemble and reassemble the tube structure as well as alter the tube thickness to adapt to the external conditions. The tubes grow bigger when transporting lots of nutrients, while the tubes that do not convey sufficient nutrients gradually shrink and eventually vanish from the network.

Inspired by the mathematical model of the Physarum foraging process [3, 4], this paper proposes to apply the Physarum model to the path optimization process in mobile ad hoc networks and design a Physarum-inspired autonomous optimized routing (PIAOR) protocol for MANET in an underground mine. Parameters such as the energy consumption, the buffer occupation, the distance among nodes, and the mobility of the nodes are used as routing metrics to select the next hop. Mobile terminals are mainly powered by batteries with limited energy. As the network runs, the cache of nodes constantly changes. In the underground mine heterogeneous space, the greater the distance between adjacent nodes, the less easy it is to transmit data. Due to the mobility of the mine nodes, the availability of the link is another important factor in the route construction of the dynamic network. The above parameters change dynamically with the operation of the network. Based on the analysis of the parameters' characteristics, considering both routing efficiency and energy equilibrium, this paper introduces the differential evolution equation of the Physarum algorithm to dynamically adapt to the changes of network environment, which will achieve the optimal selection of the next hop to realize data transmission.

2. Related Work

With the development of MANET, the research on routing protocols is also advancing. Routing protocols fall into three categories: active routing, reactive routing, and hybrid routing. Some routing protocols are improved based on link state and distance vector [5]. However, there are some problems with typical MANET routing protocols. Researchers often consider the residual energy and hop number of nodes in routing decisions and ignore some important, dynamic network information. With the continuous data transmission, the data packet delivery ratio is greatly reduced [6]. In addition, the collected data usually have a certain degree of redundancy. Data redundancy will cause unnecessary burden on the network. To improve data quality and reduce unnecessary data transmission, it is necessary to think the cache occupation of network nodes and optimize routing decisions [7, 8]. Therefore, adaptive MANET routing protocols should consider and respond to dynamic factors of network performance, such as congestion and link availability of network.

GPSR [9] is a famous greedy routing protocol, which makes greedy forwarding decisions using only information about a router's immediate neighbors in the network topology. P-IRP [10] is a routing protocol that can achieve the trade-off between routing efficiency and energy balance. It can use the node position and residual energy to select the next hop for data transmission, which is applied to the scenario of mobile node. The design of routing protocol for coal mine MANET should consider the influence of dynamic factors, such as node energy and buffer occupation, so as to achieve efficient data transmission and extended network lifetime.

In recent years, the bionic algorithms have provided inspiration to solve many complex problems. The intelligent behavior of natural organisms, such as self-organization and self-optimization, has received more and more attention [11]. Classic bionic algorithms include the ant colony algorithm [12], genetic algorithm [13], and particle swarm optimization algorithm [14].

Based on the characteristics of the Physarum model with robust fault tolerance, high efficiency, and low calculation cost, many researchers use this model to design efficient routing and reliable networks [15, 16]. For example, Nakagaki et al. [17, 18] found that the Physarum model can solve the maze problem in the biological experiment. It can extend from the food source at the entrance to the food source at the exit of the maze. The tubes between food sources become wider as they absorb nutrients, and the remaining tubes gradually shrink to disappear. At the result, the remaining tube was the shortest tube between the inlet and the outlet. Tero et al. [19, 20] places food sources in a simulated Tokyo terrain, eventually forming a network that connects all food sources; the network was comparable to the real railway network of Tokyo in the aspects of efficiency, fault tolerance, and cost. Physarum models have been used to solve many complex graph optimization problems, such as path construction [21], Steiner tree problem [22], and supply chain network design [23]. The routing algorithm based on the Physarum model can select the optimal path in data transmission and shows excellent intelligence in network analysis and design. The autonomous optimization behavior of the Physarum model can effectively solve the routing problem in coal mine MANET. The routing protocol for hybrid wireless mesh networks based on the Physarum model was proposed in [24], which can achieve energy balance and load balance of the wireless mesh networks in underground mines. Intelligent terminals in the coal mine have limited energy and cache. The routing protocol based on the Physarum model can select the node with higher remaining energy and cache as the next hop from neighbor nodes for data transmission,

RETRACTED

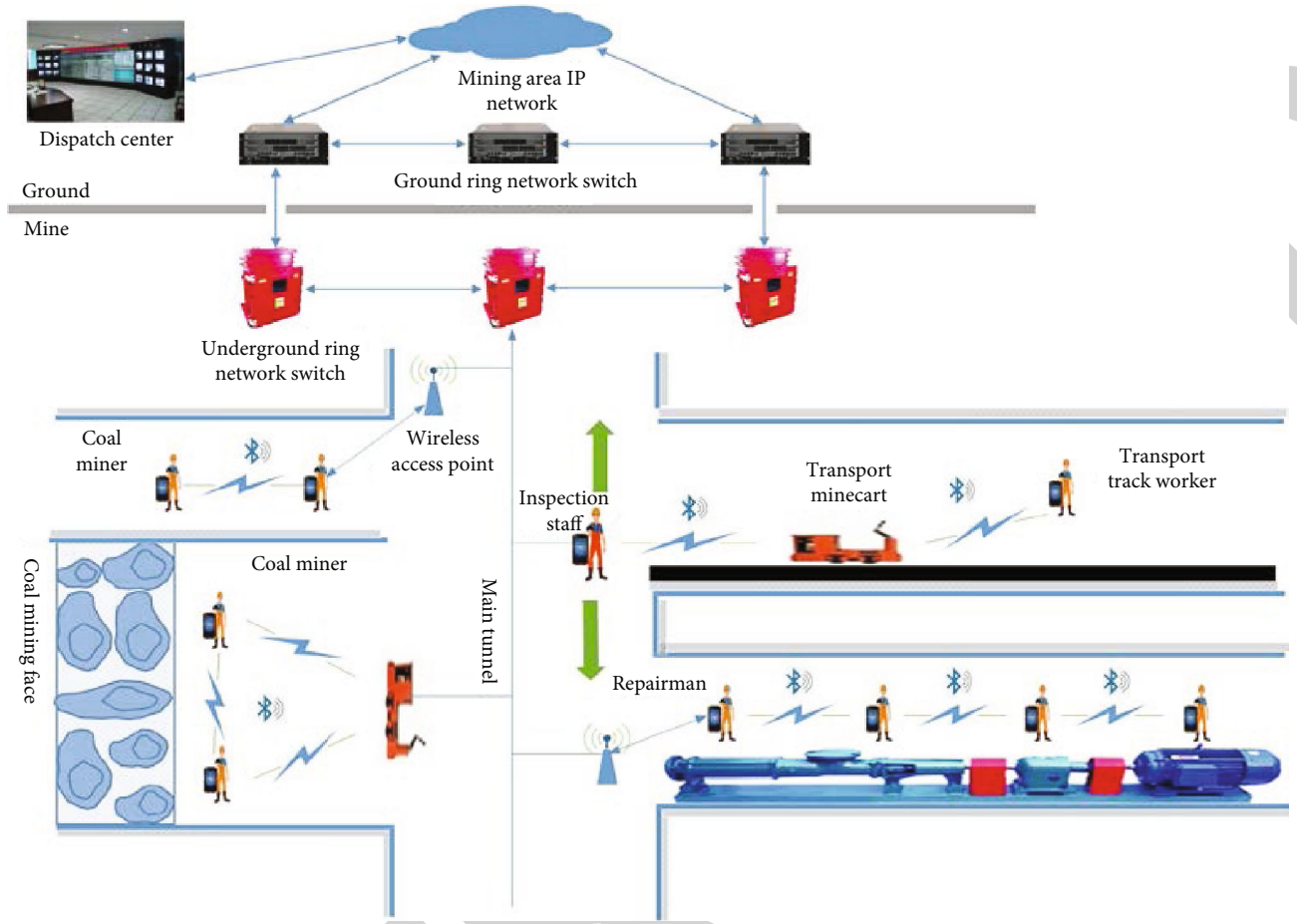

Figure 1: Overall view of the mine MANET.

avoiding energy exhaustion or congestion. However, it does not consider node mobility, and it is difficult to adapt to frequent changes in network topology.

Intelligent mobile terminals for coal mines can be connected with each other to build MANET and support the transmission of multimedia information, such as voice and video. Compared with traditional wired networks, MANET in underground mine is easy to deploy and maintain. It can accept nodes at any time and expand the communication range, which is of great significance to build a full coverage sensing network with wireless self-organizing and distributed sensing capability [25]. The topology and status of coal mine MANET change frequently. Autonomous optimized routing protocols should adapt to changes in network parameters in a timely manner. The path selection in nutrient transmission of Physarum is the same as the data transmission and routing in MANET. The Physarum model has superior performance in autonomous optimization and path selection for its outstanding adaptability, so we have designed PIAOR for the coal mine MANET. In the routing decision process, the routing criterion uses the information of local nodes and takes into account the influence of energy, cache, and link status of nodes. This algorithm combines the adaptive adjustment strategy based on node resources and network topology to improve the adaptability of routing decision to network state change. In addition, the algorithm achieves energy balancing and load balancing with superior throughput and small transmission delay.

3. Preliminaries

3.1. Network Structure. The nodes in the coal mine MANET are randomly distributed in the tunnels or other working areas, which usually follow a certain pattern of movement, as showed in Figure 1. In order to simplify the system model, we make some assumptions shown as follows.

(i) The physical location of each node can be obtained through a positioning system or device

(ii) Each node can read the residual energy information from the physical interface and pass up to its network layer

(iii) Nodes use the whole antenna and have equal transmission radius, which means that the radio channel is bidirectional and symmetrical

In order to simulate the actual application scenario of the coal mine, the network is divided into small regions. Each node belongs to only one region, and each region has a

central node and multiple edge nodes. As showed in Figure 2, node s represent the data source node, and its one-hop communication range is a circular area with r as its radius. Node s needs to find the optimal next-hop node within its one-hop range to send data to the destination node d. θ_{jsd} represents the measured value where node j deviates from node s to node d. L_{sj} denotes the distance from node s to node j, and $L_j{}'d$ denotes the projection distance of node j relative to the destination node d. The physical location of each node can be obtained through the positioning system during the network initialization phase. L_{sj} and θ_{jsd} can be calculated by the following formulas:

$$L_{sj} = \sqrt{\left(x_s - x_j\right)^2 + \left(y_s - y_j\right)^2},$$
$$\theta_{jsd} = \arccos \frac{L_{sj}^2 + L_{sd}^2 - L_{jd}^2}{2 \times L_{sj} \times L_{sd}}, \quad (1)$$

where (x_s, y_s) and (x_j, y_j) are the position coordinates of node s and node j, respectively. Therefore, the projection distance $L_j{}'d$ can be expressed as

$$L_j{}'d = L_{sd} - L_{sj}{}'. \quad (2)$$

In this paper, the shortest path can be chosen by PIAOR. Therefore, the length of the tube can be considered the cost of the Physarum tubular network. The link cost is affected by the location of the next hop node, and we use the projected distance of the node taken as a measure factor. The smaller the projection distance, the closer the candidate node is to the destination node, and the more probable it should be selected as the next hop.

3.2. Coal Mine MANET. The environment in the underground mine is complex and changeable, and there may exist blind wireless coverage areas in the coal mine working face. Miners can construct MANET through smart mobile terminals that they carry to collect data (temperature, humidity, pressure, and gas concentration) in real time, to achieve the safe operation in underground mines. The data collected by miners can be divided into emergency data and nonemergency data. Emergency data has to be transmitted to the ground control center in a timely manner. Nonemergency data can be transmitted by choosing an optimized routing path within the allowed delay time.

As showed in Figure 3, each miner moves within a fixed range of activities, and the communication range of intelligent mobile terminals is limited. Miners can cooperatively transmit the collected data through multiple hops until the wireless access point in the underground mine. The coal mine requires continuous monitoring without interruption, which consumes energy of terminals quickly when receiving and forwarding data. Intelligent terminals carried by miners are powered with limited capacity, which cannot be charged during its using in underground mines and cannot satisfy the need for one working shift. The problem of terminal

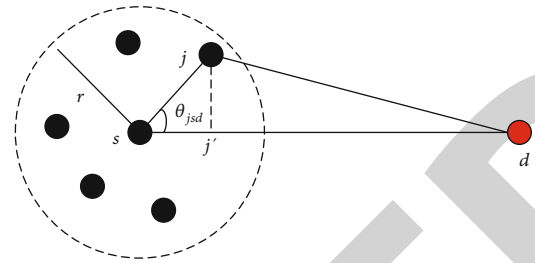

Figure 2: Example of one region in coal mine MANET.

energy consumption seriously affects the application of intelligent mobile terminals in coal mine MANET [26, 27]. In the energy consumption of nodes, the calculation of the algorithm consumes less energy, and most of the energy is consumed by data transmission. During the operation of the routing algorithm, the data processing and calculation consumes less energy. However, in data transmission, nodes consume a lot of energy to receive and forward data. Therefore, when selecting the next hop node to transmit data, it is necessary to consider the remaining energy of the node and save and balance the energy consumption by designing an autonomously optimized routing protocol based on the Physarum model.

In coal mine MANET, nodes can obtain the information on the remaining energy of neighbor nodes by locally exchanging "hello" messages in a fixed period. When transmitting data, a node with more residual energy will have more possibility to be selected as the next hop to ensure reliable data transmission.

4. Physarum-Inspired Autonomous Optimized Routing Protocol

4.1. Physarum Model. There is a positive feedback mechanism between the flow and the continuity in the tube network formed by the Physarum itself. The flow in the tube increases, the tube becomes wider, and the continuous increases. At the same time, the wider tube will carry more traffic. Based on this positive feedback mechanism in the Physarum model, the researchers have obtained the mathematical model for Physarum path optimization, which can dynamically adapt to the parameter change of the coal mine MANET. Due to the instability of the coal mine MANET constructed by intelligent mobile terminals, when nodes randomly leave or join the network, the routing path should be reconstructed considering the influence of the remaining energy and cache of the node in the next hop selection.

Since the protoplasm density of each node is different, the pressure at each node is also different. Let P_i and P_j denote the pressure at nodes i and j, respectively. In the Physarum-inspired path-finding model, each tube is a cylinder with a length of $L_{i,j}$ and a radius of $r_{i,j}$. We define the tube from i to j as Tube <i, j>. The flux in each tube can be expressed by the Poisson equation as

$$Q_{i,j} = \frac{\pi r_{i,j}^4 \left(P_i - P_j\right)}{8\eta L_{i,j}} = \frac{D_{i,j}\left(P_i - P_j\right)}{L_{i,j}} = \frac{D_{i,j}\Delta P_{i,j}}{L_{i,j}}, \quad (3)$$

RETRACTED

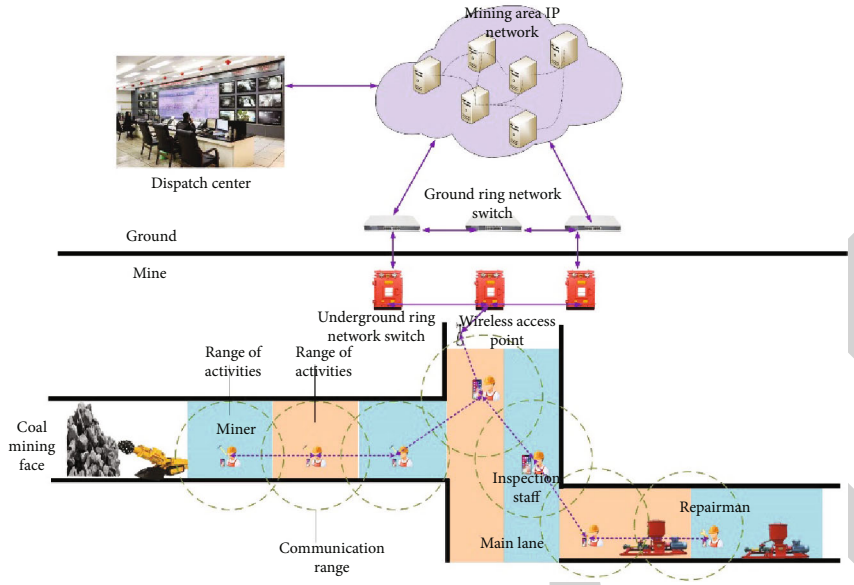

Figure 3: Data transmission scenario of blind wireless coverage areas.

where $Q_{i,j}$ represents the flux in Tube $<i, j>$. $\Delta P_{i,j} = P_i - P_j$ denotes the pressure difference between link $<i, j>$, η denotes the fluid viscosity in tubes, and $D_{i,j} = \pi r_{i,j}^4 / 8\eta$ indicates the conductivity of the tube.

According to formula (3), the flux passing through node i to j in the tubes is determined by $\Delta P_{i,j}$, $L_{i,j}$, and $D_{i,j}$. Assuming that the capacity of each node is 0, according to the principle of flow conservation, the sum of the outflow from the source node is equal to the sum of the inflow to the destination node, and the sum of the inflow to an intermediate node is equal to the sum of the outflow from this node. The traffic of each node can be calculated as follows:

$$\sum_j \frac{D_{i,j}}{L_{i,j}} \left(P_i - P_j\right) = \begin{cases} I, & i = s, \\ -I, & i = d, \\ 0, & \text{others}, \end{cases} \tag{4}$$

where I is the outgoing traffic of the source node s and is the incoming traffic for the destination node d. The sum of the traffic of the intermediate nodes is always 0. Because the total amount of fluid in the tube network is constant, there is the competitive relationship among the paths, which will continue for some time. Eventually, an optimized path will come into being that connects all food sources.

The Physarum model can change the flow of each tube to obtain the distributed food sources based on its own adaptability. In the adaptive process, we can optimize the routing protocol through the evolution of $\Delta D_{i,j}(t)$. With the operation of the network, the link status changes with the consumption of node resources and the movement of the node. When selecting the next hop node, the traffic value of the neighbor node will be calculated by conductivity. The self-adaptability of the algorithm makes the conductivity change over time, so the flow value is different in each period of time. In the path optimization model of Physarum, it seeks food by adjusting its shape and gradually forms an efficient and clear network tube, with the constraint that the total flow in the Physarum keeps constant. Adapting to the adaptive behavior of the tube, the change in conductivity over time can be expressed as

$$\frac{d}{dt} D_{i,j} = f\left(\left|Q_{i,j}\right|\right) - \gamma D_{i,j}. \tag{5}$$

The discretized form of the above formula is

$$D_{i,j}(n) = \left(f\left(\left|Q_{i,j}\right|\right) - \gamma D_{i,j}(n-1)\right)\Delta t + D_{i,j}(n-1), \tag{6}$$

where $\gamma D_{i,j}$ and $f(Q) = ((Q_{i,j}) / \sum_{j-1}^{N} Q_{i,j})$ represent the shrinking rate and the growth rate of the tube, respectively.

$$\Delta t = \frac{1}{\text{PPS}}, \tag{7}$$

where Δt denotes the time granularity of evolution. The value of time granularity is related to the density of forwarding packets (packets per second, PPS). To ensure that the time granularity of evolution is not too large, we set $\max(\Delta t) = 0.1$.

Formula (6) shows the dynamic relationship of conductivity with time. With this formula, we can calculate the conductivity of the tube at the next moment and get the value of the new flow, so as to optimize the data transmission.

4.2. Optimization Model. The Physarum model is derived from hydrodynamics and cannot be directly applied to MANET. In this paper, based on the state of MANET, we reasonably map the parameters in formulas (3) and (5).

4.2.1. Parameter Mapping of the Basic Model. In order to choose a suitable next hop for data transmission, we should consider factors such as node energy, node cache, and link

RETRACTED

status in the network. In this paper, three important parameters in formula (3) are modified, such as conductivity $D_{i,j}$, length $L_{i,j}$, and pressure difference $\Delta P_{i,j}$. An autonomous optimized routing protocol for coal mine MANET is designed to select the next hop node.

Since conductivity $D_{i,j}$ is an inherent physical characteristic of the network, we normalize the received power P_j of neighbor node j as the initial value of $D_{i,j}$. P_j denotes the quality of the link, which is also an inherent characteristic of the wireless link.

$$\widehat{D}_{i,j} = \frac{P_j - P_{\min}}{P_{\max} - P_{\min}}, \tag{8}$$

where $\widehat{D}_{i,j}$ represents the normalization of the received signal strength of link $<i, j>$, $P_{\min}$ represents the minimum power capable of supporting reliable communication between neighbor nodes, and $P_{\max}$ represents the maximum power for communication between neighbor nodes. The power value of the node is determined by the network chip of the intelligent terminal node.

Corresponding to the length $L_{i,j}$ of the Physarum model, we use the projection distance of the nodes to express the length of the tube. As shown in Figure 2, the physical location of the node can be obtained by positioning device, which can be broadcasted to its neighbors, so that the physical distance between any two nodes and the projection distance relative to the destination node can be calculated. $L_{i,j}$ can be expressed by the following formula:

$$L_{i,j} = \frac{L_j{}'d}{L_{id}}, \tag{9}$$

where $L_j{}'d$ is the projection distance of node j relative to the destination node, andL_{id} is the distance between node i and node d.

In hydromechanics, fluids tend to flow to nodes with lower pressures. Similarly, data packets are expected to be relayed through better performing nodes. The multihop transmission characteristics of MANET make the link quality closely related to the performance of the next hop node. If a node has more remaining energy and buffer, it means that it has more capability to route and forward data and has more buffer space to store data packets. In MANET routing, the remaining energy and buffer of nodes are important parameters that should be considered comprehensively when selecting the next hop. The node with more residual energy and buffer should be selected as the next hop preferentially. Therefore, we construct the pressure difference$\Delta P_{i,j}$ of the Physarum model based on the remaining energy E_{res} and the remaining buffer B_{res}, which is shown as follows:

$$\Delta P_{ij} = \alpha E_{\text{res}} + \beta B_{\text{res}}, \tag{10}$$

where $0 \le \alpha \le 1$, $0 \le \beta \le 1$ and satisfy $\alpha + \beta = 1$.

Equation Formula (3) can be expressed as

$$Q_{i,j} = \frac{\widehat{D}_{i,j}(\alpha E_{res} + \beta B_{res})}{L_j{}'d/L_{id}}. \tag{11}$$

After parameter mapping and calculation of flux, the neighbor node with the largest value of flux will be selected as the next hop node. The residual energy, buffer, and location of nodes change with the network operation. In order to adapt to this change, evolutionary equations are introduced in this paper. In the initial stage of the network, the conductivity is defined as the received power of neighbor nodes. The conductivity of the next stage is calculated by formula (6). The flux value of the next stage is recalculated by formula (11), and the node with more value of flux $Q_{i,j}$ is selected to transmit data.

4.2.2. Parameter Mapping of the Optimization Process. The definition of the tube shrinking rate γ will affect the calculation of the conductivity over time. The buffer occupation of the nodes is affected by the network status. Excessive data packets stored in one node will cause congestion, which will reduce throughput, increase transmission delay, and deteriorate the network performance. The mobility of terminals in coal mine MANET will affect the reliability of links among neighbor nodes. The more reliable the links are, the better the data transmission will be. Therefore, the shrinking rate of the tube is related to the congestion and link stability of the next hop node. The larger the buffer space is occupied, the more unstable the link caused by node movement, and the easier the tube will shrink. We denote the shrinking rate γ of the tube as

$$\gamma = C_B \times l, \tag{12}$$

where C_B represents the congestion probability and l represents the fracture probability of communication link.

When receiving data, the node will store it in its buffer queue and select the next hop according to the calculated flux. If a node continuously receives data packets, network congestion may occur, and then, data transmission will be deteriorated. Therefore, the link quality and the buffer occupation should be predicted and be used to calculate the shrinking rate. The congestion probability C_B of the potential next hop is defined as

$$\begin{aligned} C_B &= \frac{B_{\text{jitter}} \times B_{\text{avg}}}{0.5}, \\ B_{\text{jitter}} &= \sqrt[2]{\frac{1}{N}\sum_{i=1}^{N}\left(B_i - B_{\text{avg}}\right)^2}, \\ B_{\text{avg}} &= \frac{1}{N}\sum_{i=1}^{N} B_i, \end{aligned} \tag{13}$$

RETRACTED

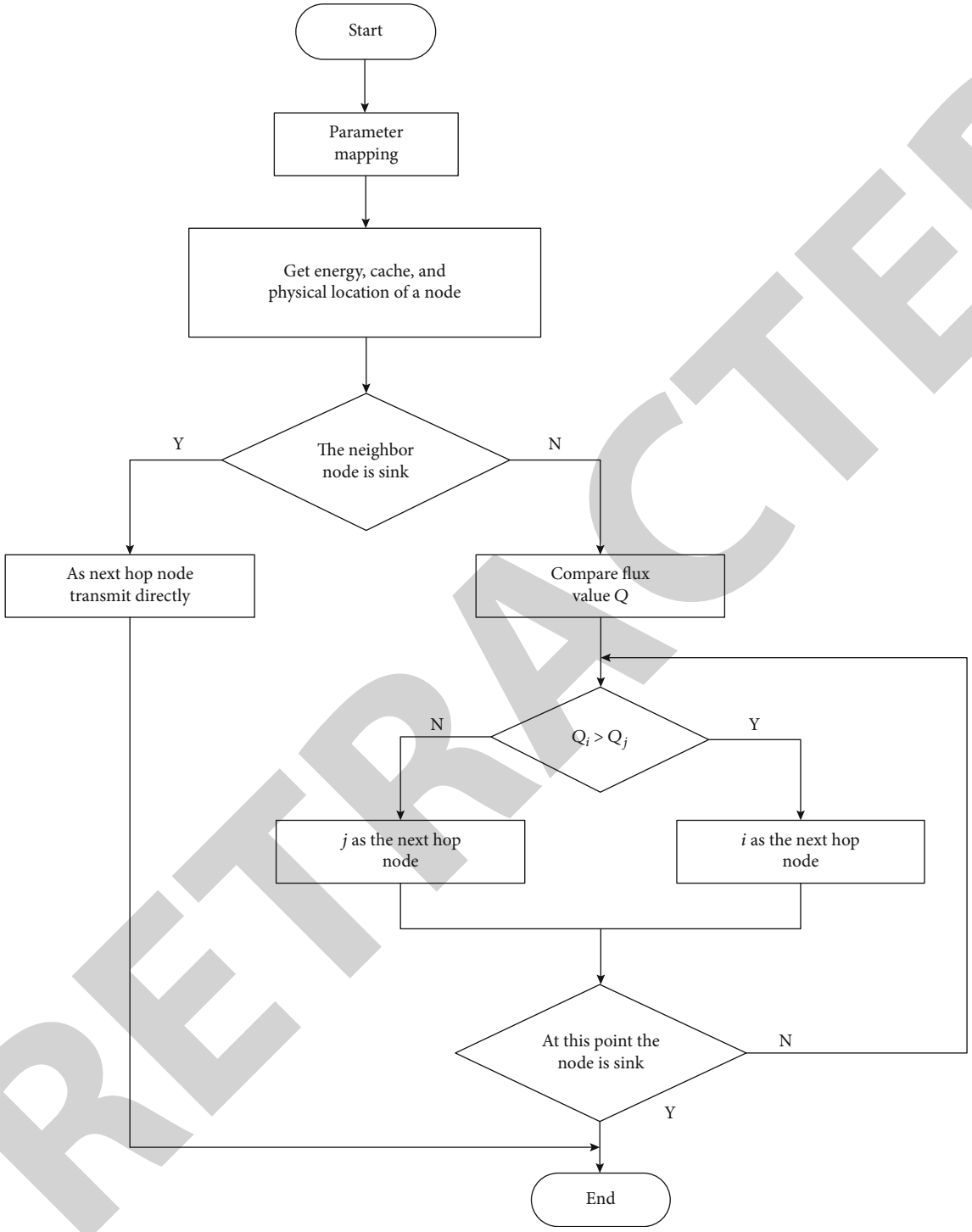

RETRACTED

Figure 4: Flow chart of PIAOR.

where B_{jitter} represents the buffer occupation jitter and B_{avg} is the average cache. N denotes the count of buffer occupation in Δt, and B_i denotes ith buffer occupation.

In order to achieve efficient data transmission, the buffer occupation of the node should be considered when selecting the next hop. B_{jitter} can be set as a penalty factor to reduce the probability that the node with excessive buffer occupation and large jitter to be selected as the next hop. The smaller the average buffer occupation, the smaller the penalty factor B_{jitter}, the less the congestion probability, and the more priority of this node should be selected as the next hop.

As the movement of terminals in coal mine MANET may cause the disconnection of links, the nodes need to reconstruct the routing path, which will increase the delay of data

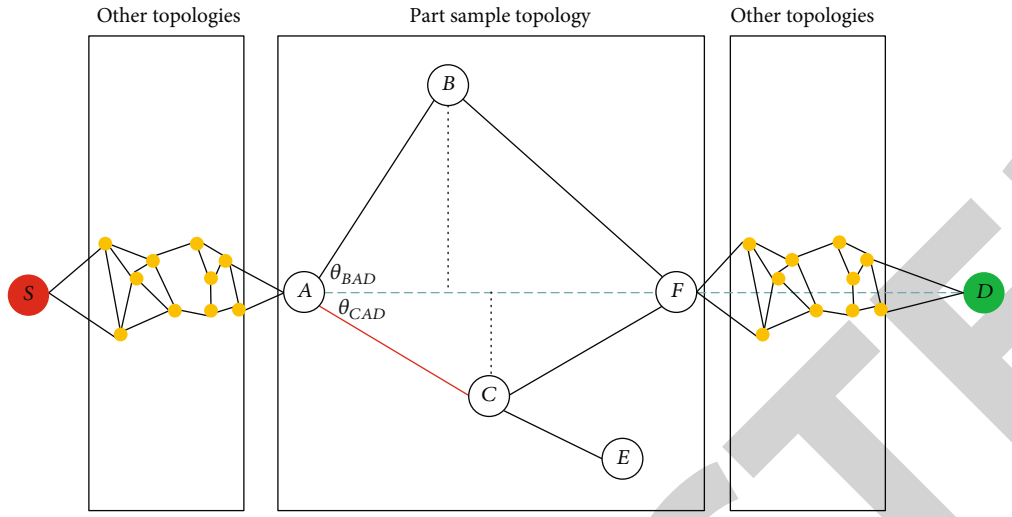

Figure 5: Routing decision of node A in network initial stage.

transmission. In this paper, we measure the link availability by the link connection time and consider the link quality in routing decisions.

When nodes move, the nodes may be close to each other or away from each other, with 50% probability, the following formula can be used to represent the probability model of link availability prediction

$$l(T_p) = \left(1 - e^{-2\lambda T_p}\right)\left(\frac{1}{2\lambda T_p} + \varepsilon\right) + \frac{\lambda T_p e^{-2\lambda T_p}}{2}, \quad (14)$$

where λ represents the terminal mobility, T_p represents the time interval to predict the link availability, and $l(T_p)$ represents the fracture probability of communication link from the initial time t_0 to $t_0 + T_p$. The value of ε is determined by environmental factors, which change with time and mobility and cannot be calculated by an accurate mathematical formula.

In order to adapt to the dynamic changes of environmental factors, it is more practical to predict the value of ε. Within the time interval (T_p), $T_{r,i}$ $(i=1\ldots n)$ represents the link's available time slice. The probability that the link can be continuously available for each time interval can be expressed as

$$l_m(T_p) = (1/n)\sum_{i=1}^{n}(T_{r,i}/T_p). \quad (15)$$

In formula (14), replacing $l(T_p)$ with $l_m(T_p)$, we can get

$$\varepsilon_m = \frac{l_m(T_p) - (1/2)\lambda T_p e^{-2\lambda T_p}}{1 - e^{-2\lambda T_p}} - \frac{1}{2\lambda T_p}. \quad (16)$$

Table 1: Route decision of node A.

Path	D	L_{next}	L_d	θ	B (%)	E (%)	α	β	Q
$A \longrightarrow B$	0.7	100	500	60°	1	1	0.62	0.38	0.78
$A \longrightarrow C$	0.7	100	500	30°	1	1	0.62	0.38	0.85

A series of ε_m can be obtained by the above operation according to the corresponding T_p, and then, ε can be predicted by the following formula:

$$\varepsilon \approx (1/n)\sum_{i=1}^{n}\varepsilon_{m,i}. \quad (17)$$

The available time of link is predictively calculated by instant information of the network, considering the dynamic characteristics of the link, which will truly reflect the link reliability and improve routing performance.

5. Routing Decision

5.1. Routing Decision Process. The topology of coal mine MANET will change dynamically with the moving of miners carrying the smart terminals. The PIAOR algorithm can improve the rationality of routing decision and achieve the optimal path construction considering multiple network parameters, based on current and historical information. The routing decision processes and its flow chart is shown as follows:

Step 1. Calculate the flux value at the beginning of network operation through formula (3), $D_{i,j}$ and $\Delta P_{i,j}$ are calculated according to formulas (8) and (10), respectively. $L_{i,j}$ is calculated by formula (9).

Step 2. After the network has been running for some time, the performance parameters and the network state change.

RETRACTED

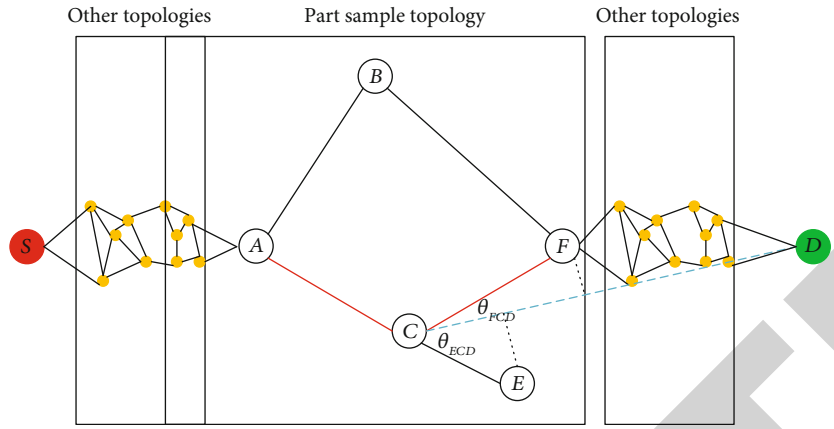

Figure 6: Routing decision of node C in network initial stage.

Route optimization is carried out by adaptive link state quality adjustment and adaptive parameter adjustment strategy. Conductivity D can be recalculated by the differential evolution equation of Physarum (5), and the flow value Q of the next stage can be calculated by formula (10). The node with the largest Q is selected as the next hop node.

Step 3. Repeat the above process until data packets arrive at the destination node.

The main flow chart of PIAOR is shown in Figure 4.

5.2. Routing Decision Analysis. For a more detailed introduction of PIAOR, one part of the network is selected as an example to analyze routing decisions. In PIAOR, multiple network parameters such as energy, buffer, and mobility of nodes are comprehensively considered when making routing decisions. By calculating the flux in the tube, the node with the largest flux will be selected as the next hop to transmit data packets. Suppose the distance between the current node and the next hop node is $L_{\text{next}}(m)$ and the distance from the destination node is $L_d(m)$.

5.2.1. Network Initial Stage. In the following routing decision analysis, we assume one part of network topology shown in Figure 5. Node S is the source node, node D is the destination node, and node A is the current node, which has stored data packets and need to send to the destination node. Nodes B and C are the neighbors of node A.

In the network initial stage, the node has consumed less energy and has used less buffer. The conductivity of the link is calculated by formula (8). Node A selects the one with a large flux value from neighbor nodes B and C as the next hop transmission node. According to the autonomous optimized routing model, a calculation table for selecting the next hop in the initial stage is shown in Table 1.

From Table 1, compared by the flux in tube (Q), the projection distance of node C is small, with larger QA, $C = 0.85$, so node C is selected as the next hop.

After node C has received the data packets, as shown in Figure 6, it will start the routing decision process and select the next hop from its neighbors (node E and node F), which is shown in Table 2.

Table 2: Route decision of node C.

Path	D	L_{next}	L_d	θ	B (%)	E (%)	α	β	Q
$C \longrightarrow F$	0.7	100	450	15°	1	1	0.62	0.38	0.89
$C \longrightarrow E$	0.8	50	450	50°	1	1	0.62	0.38	0.86

As seen from the above table, compared by the flux in tube (Q), node C chooses node F with a larger value of Q as the next hop node.

5.2.2. Network Operation Phase. Evolution follows the transmission of data over the network. Suppose that after the network runs for a period of time, the location, energy, cache, and distance of nodes all change. The following figure shows the routing decision process after the network state changes.

As shown in Figure 7, after the network runs for a period of time, the network topology changes, and the node's energy and cache usage also change. Node A needs to recalculate the traffic value Q when forwarding data. The evolution calculation process is shown in Table 3.

The new conductivity obtained after the evolution of the above table can be used to obtain new flow values. The calculation is shown in Table 4.

According to Table 4, the conductivity, residual energy, and residual cache all changes; the factors of pressure difference ΔP and node projection distance L are considered synthetically, compared by the flux in tube (Q), with larger QA, $B = 0.64$, so node B is selected as the next hop.

When node B selects the next hop to send data, because node B's neighbors are only A and F, node B chooses node F as the next hop, as shown in Figure 8.

When the network is running, data is sent from the source node S to the destination node D, and the routing selection is completed in turn as described above. The PIAOR algorithm can achieve load balancing and energy

RETRACTED

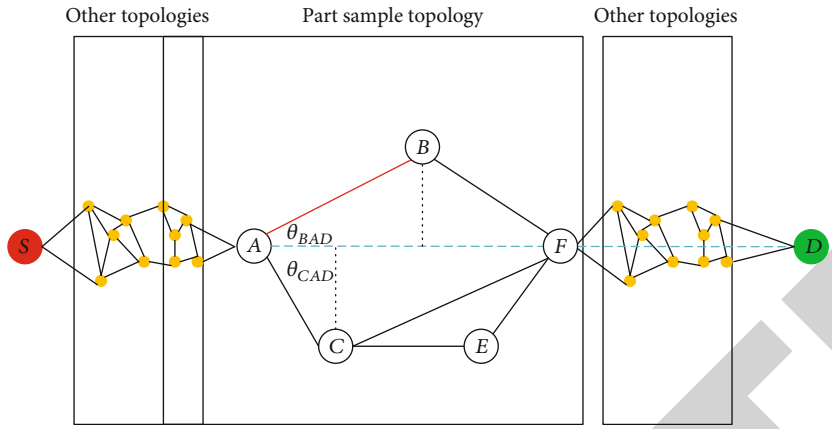

Figure 7: Decision example of node A after network state changes.

Table 3: Evolution of node A.

Path	$D(n-1)$	C_B	l	γ	$f(Q)$	Δt	$D(n)$
$A \longrightarrow B$	0.7	100	500	30°	0.9	0.9	0.62
$A \longrightarrow C$	0.73	50	500	60°	0.6	0.5	0.62

Table 4: Route decision of node A after evolution.

Path	D	L_{next}	L_d	θ	B (%)	E (%)	α	β	Q
$A \longrightarrow B$	0.7	100	500	30°	0.9	0.9	0.62	0.38	0.64
$A \longrightarrow C$	0.73	50	500	60°	0.6	0.5	0.62	0.38	0.35

balancing and extend the network survival time and is of great significance for the uninterrupted data collection and transmission in coal mines.

6. Simulation Experiment

6.1. Simulation Environment an Experimental Parameters. Based on the NS2 simulation platform, the performance of PIAOR has been tested and the results such as delivery ratio, end-to-end delay, throughput, and network lifetime were compared to those of PIMAR, GPSR, and P-IRP. The performance indicators are defined as follows:

Delivery Ratio. The delivery ratio is the ratio of CBR packets arriving at the gateway node to the total packets sent by source nodes. The delivery ratio can be defined as follows:

$$\text{Delivery ratio} = \frac{\text{Packets received by gateway}}{\text{All packets}}. \quad (18)$$

End-to-End Delay. The average value of constant bitrate (CBR) packets delays from each source node to the gateway node. The average end-to-end delay can be defined as follows:

$$\text{Delay} = \frac{\sum_i^I \text{CBR}(i)}{I}, \quad (19)$$

where CBR(i) is the delay of packet i and I is the number of packets in an experimental process.

Throughput. Throughput is the amount of data received by the gateway node in one second.

Network Lifetime. The time when the first node dies due to energy exhaustion is defined as the network lifetime.

The parameters of the simulation network are listed in Table 5.

In the simulation, we set the network in a long and narrow area of $1000 \times 8\,\text{m}^2$ to simulate the tunnel in an underground mine. The terminals in the underground mine are mostly carried by miners, inspectors, or other mobile devices, and their movement range and trajectory have certain rules. The areas covered by miners of different professions are limited. To simulate real scenarios, the network area is divided into multiple subregions of $200 \times 8\,\text{m}^2$. 100 nodes are randomly deployed in subregions and move randomly within the subregion. A gateway node is deployed at one end of the network.

6.2. Performance Analysis

6.2.1. Delivery Ratio. The trends of delivery ratio for four different protocols are shown in Figure 9. PIAOR has the highest delivery ratio, followed by P-IRP and GPSR, and PIMAR has the lowest one. PIMAR does not consider the movement of nodes. If the speed of the movement is high, the update delay of the node depth may cause poor network performance due to growth of routing paths. GPSR and P-IRP only use the current location of nodes and have no prediction on the trend of node movement. When the nodes move fast, the possibility of link breakage will increase and the delivery ratio will decrease. PIAOR uses the projection distance of the nodes relative to the gateway to map the length of the tube in

RETRACTED

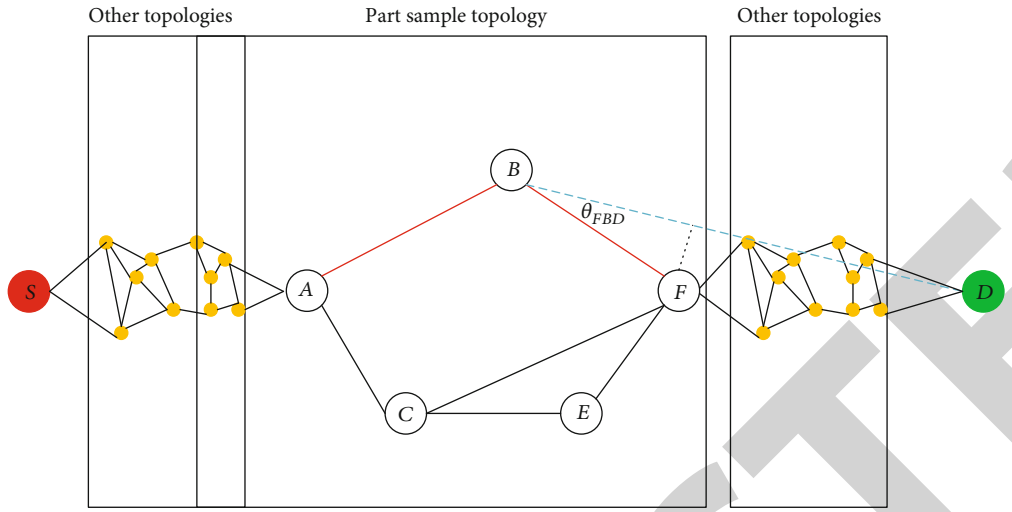

Figure 8: Decision example of node B after network state changes.

Table 5: Simulation parameters.

Topography size	$1000 \times 8\ m^2$
Divided area	$200 \times 8\ m^2$
Simulation time	3000 s
Transfer range	50 m
Traffic type	CBR
Packet size of CBR	64 B
Data flow rate	0.3 MB/S
Number of CBR flows	20
Terminals	100
Gateways	1
Nodes mobility model	Random waypoint model

the Physarum network, so as to ensure the convergence direction of the route. PIAOR utilize the motion prediction model to predict the link instability, which can effectively avoid selecting unstable links and improves network delivery ratio.

6.2.2. End-to-End Delay. In Figure 10, PIMAR has the highest latency, followed by P-IRP and GPSR, and PIAOR has the lowest. Because PIMAR does not support routing under high-speed node movements, routing decisions are inefficient at high-node movement speed, resulting in node data packet backlogs and path growth, increasing latency. The criteria used by GPSR and P-IRP to evaluate the next-hop node are too simple to make a good prediction of the changes in link quality. In high-speed conditions, there are more unstable links, so the end-to-end delay is higher. The node motion prediction strategy of PIAOR can effectively reduce the possibility of selecting unstable link, reduce the backlogs caused by routing failure of packets, and reduce the delay.

6.2.3. Throughput. Figure 11 shows the trend of the throughput of four network protocols with an increasing speed. PIMAR's throughput is higher in the environment of low-speed movement of the node, but the performance degradation is large at a high speed. GPSR and P-IRP have better throughput performance than PIMAR, and PIAOR has the best throughput. PIAOR can effectively predict unstable links and can optimize link selection based on current and historical information. It can more comprehensively measure link quality and improve throughput performance.

6.2.4. Network Lifetime. In Figure 12, PIAOR has the highest network lifetime and GPSR has the lowest network lifetime. The definition of the network survival time is the time when the number of network node death accounts for 80% of the total number of nodes. At this time, the remaining nodes are less than 20 and the network will not be able to provide normal communication support. PIMAR's parameter adaptive adjustment strategy can effectively achieve network load balancing and energy balancing when the node's movement speed is low, and the network survival time is longer. However, in high-speed environments, PIMAR's routing decision method is prone to routing loops due to the delayed updating of node depth information, resulting in a longer data packet transmission path and increased energy consumption. GPSR does not consider energy factors and may overuse low-energy nodes, causing them to die prematurely and affecting network lifetime. P-IRP takes energy into consideration and therefore has a longer network lifetime. PIAOR considers the energy and cache of the next hop node, and there is no problem of telling the environment that the routing path becomes longer, which can effectively reduce the use of nodes with lower energy and larger loads. In addition, because PIAOR can continuously optimize the accuracy of link state evaluation, avoid choosing problematic links, thereby extending network survival time.

From the above experimental analysis, it can be obtained that the PIAOR algorithm is superior in the delivery ratio,

RETRACTED

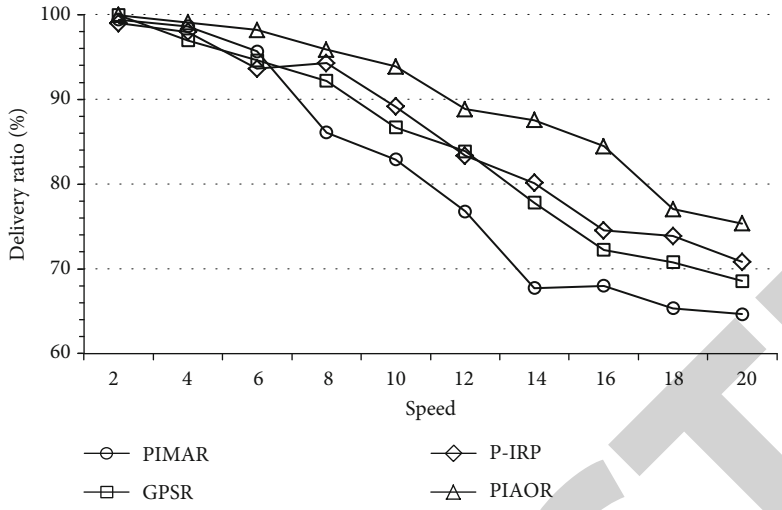

Figure 9: Delivery ratio.

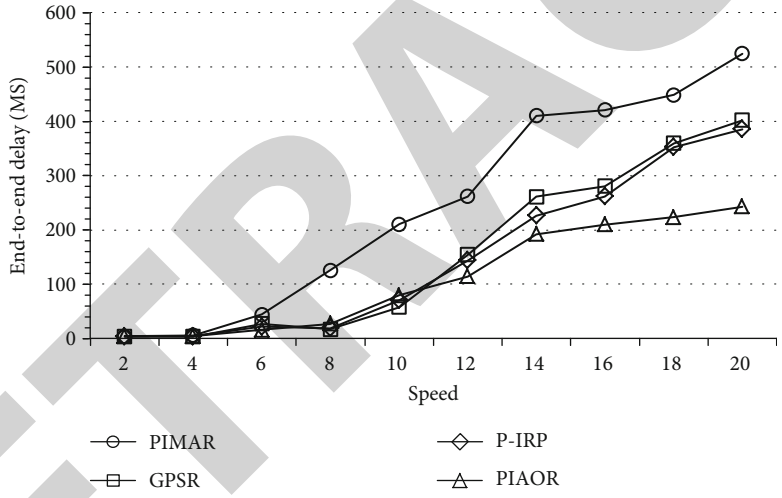

Figure 10: End-to-end delay.

RETRACTED

end-to-end delay, throughput, and network lifetime performance and is suitable for the underground environment to ensure the stable and efficient transmission of data in the coal mines.

7. Conclusions

In this paper, we propose a bionic algorithm PIAOR. The PIAOR algorithm comprehensively considers the energy and cache of nodes, as well as the link status, and introduces the node's movement model to calculate network flux, which is used to measure the quality of the link, so as to achieve reliable and efficient data transmission. In order to adapt to the changes in network topology caused by the movement of underground nodes, we introduce the differential evolution equation of the Physarum model to predict the congestion and availability of the link, which is used to calculate the conductivity among neighbors and recalculate the flow value to find an optimal path for data transmission. Based on analyzing the variation of energy and link quality with node depth, the parameter adaptive strategy and communication link autonomous optimization strategy is proposed. PIAOR uses local information to calculate the regional flow to make routing decisions, which has greatly reduced the complexity of the algorithm, lowered the network overhead, and improved the scalability. Through theoretical analysis and NS2 simulation experiments, the result shows that PIAOR is superior to other similar protocols in terms of throughput, average end-to-end delay, network lifetime, and delivery ratio. PIAOR has achieved energy and load balance5 and has extended the life cycle of the network.

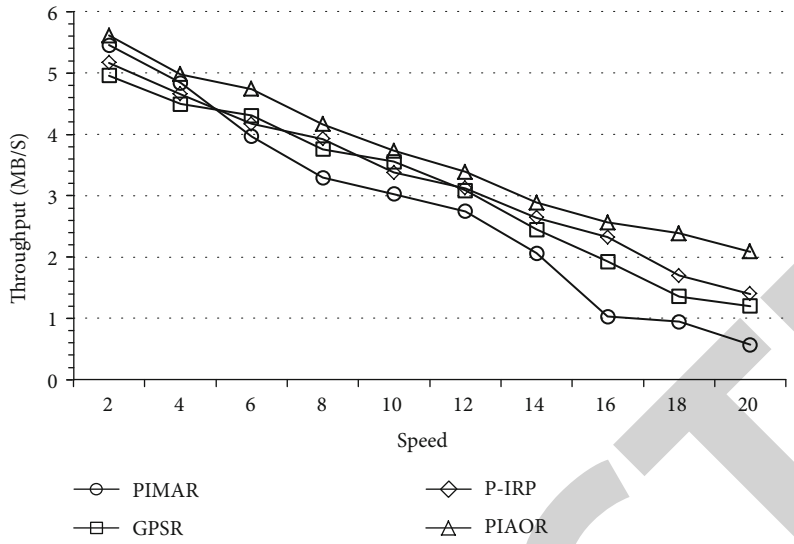

Figure 11: Throughput.

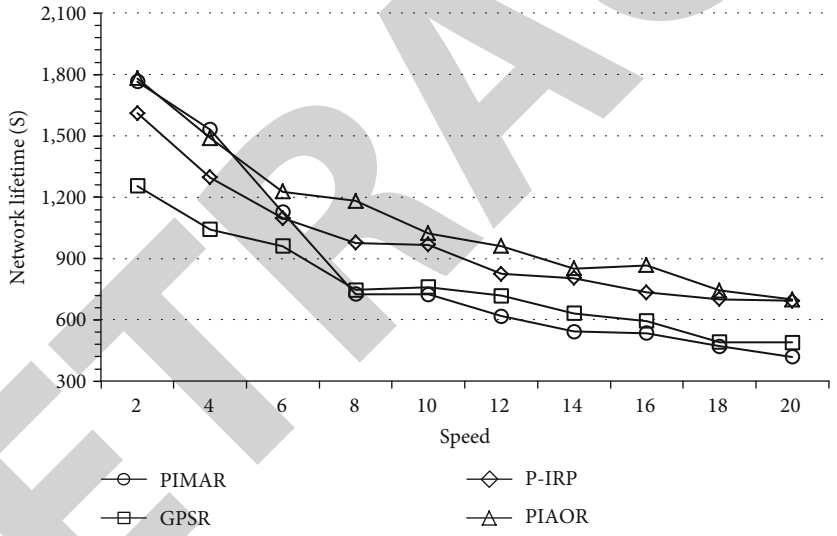

Figure 12: Network lifetime.

In future work, faced with the limited energy of the nodes in coal mine MANET, an energy optimized routing algorithm can be designed to reduce the energy consumption for data transmission. According to the activity characteristics of nodes in an underground mine, different mobility models can be established, so as to further study its impact on network performance. In addition, combining Physarum models with other intelligent algorithms to solve more complex network optimization problems is another direction of our future research.

Data Availability

The simulation experiment data used to support the findings of this study are available from the corresponding author upon request.

Conflicts of Interest

The authors declare that there are no conflicts of interest regarding the publication of this paper.

Acknowledgments

The financial support for this work provided by the Fundamental Research Funds for the Central Universities (no. 2017XKQY077) is gratefully acknowledged.

References

[1] K. Koumidis, P. Kolios, C. Panayiotou, and G. Ellinas, "ProximAid: proximal adhoc networking to aid emergency response," in *2015 2nd international conference on information*

RETRACTED